

UNCLASSIFIED

AD 434850

DEFENSE DOCUMENTATION CENTER

FOR

SCIENTIFIC AND TECHNICAL INFORMATION

CAMERON STATION, ALEXANDRIA, VIRGINIA



UNCLASSIFIED

NOTICE: When government or other drawings, specifications or other data are used for any purpose other than in connection with a definitely related government procurement operation, the U. S. Government thereby incurs no responsibility, nor any obligation whatsoever; and the fact that the Government may have formulated, furnished, or in any way supplied the said drawings, specifications, or other data is not to be regarded by implication or otherwise as in any manner licensing the holder or any other person or corporation, or conveying any rights or permission to manufacture, use or sell any patented invention that may in any way be related thereto.



**Best  
Available  
Copy**

UNCLASSIFIED  
PROCEEDINGS

INDEXED BY DDC  
AD No. 434850

434850

NINTH TRI-SERVICE CONFERENCE ON ELECTROMAGNETIC COMPATIBILITY

# NINTH TRI-SERVICE CONFERENCE ON ELECTROMAGNETIC COMPATIBILITY

Sponsored jointly by  
U.S. Army, U.S. Navy,  
and U.S. Air Force

Conducted by IIT Research Institute

In cooperation with the  
Professional-Technical Group on Electromagnetic Compatibility  
of the Institute of Electrical and Electronic Engineers

OCTOBER, 1963

DDC AVAILABILITY NOTICE

QUALIFIED REQUESTORS MAY OBTAIN COPIES  
OF THIS REPORT FROM DDC.

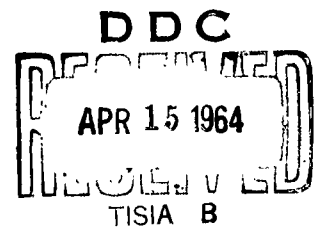
UNCLASSIFIED PROCEEDINGS  
OF THE NINTH  
TRI-SERVICE CONFERENCE  
ON ELECTROMAGNETIC COMPATIBILITY

Held at the  
Museum of Science and Industry  
Chicago, Illinois  
October 15, 16, and 17, 1963

Sponsored Jointly by  
U.S. Army  
U.S. Navy  
U.S. Air Force  
Contract No. DA 36-039 SC-89102

Conducted by  
IIT Research Institute  
Chicago, Illinois

In Cooperation with  
The Professional-Technical Group  
on Electromagnetic Compatibility  
of the  
Institute of Electrical and Electronic Engineers



## CONTENTS

Foreward		
Welcome	J. E. Bridges	1
Keynote Address	Brig. Gen. A. T. Stanwix-Hay	3
Luncheon Address	Lt. Gen. J. D. O'Connell	8

### SESSION I - GENERAL

The Western Electric Company-Wide Program for Compliance with Part 18 of the Rules and Regulations of the Federal Communications Commission	R. A. Kay	23
RFI/EMI at the Crossroads	F. J. Nichols	45

### SESSION IIA - ANALYSIS I

The Behavior of Nonlinear Mixing	R. D. Trammell, Jr. and E. W. Wood	59
Mixer Analysis and Design	R. W. Long	82
Off-Tuning Effects Produced by Interference	R. J. Mayher	101
Radio Frequency Interference in Digital Two-Phase Coherent Communication Systems	A. Krinitz	120

### SESSION IIB - CABLES AND GROUNDING

Low-Pass Transmission Lines for RFI Protection	H. G. Tobin and L. J. Greenstein	134
The Realization of Compatible Structure Grounding Systems	H. W. Ervin, D. R. Lightner and R. Powers	155

Electromagnetic Coupling Between Coaxial, Single- Wire, Two-Wire, and Shielded Twisted Pair Cables	M. Kaplit	183
Achieving Electromagnetic Compatibility by Control of the Wiring Installation	G. J. King	193

#### SESSION IIIA - MODELING AND SYNTHESIS

Compatibility Analysis Sensitivity	H. M. Sachs and T. N. Truske	205
The Analysis and Synthesis of Radar Emission Spectrums by Digital Computer Methods	R. B. Marcus	231
Advanced Reciever Model System "ARMS"	D. H. Cook, J. L. Pierzga, and F. N. Leahy	261
Computer Processing of Antenna Patterns	H. N. Kritikos and M. R. Dresp	283

#### SESSION III B - INSTRUMENTATION I

The Use of Directional Couplers as Harmonic Pads	L. Young	295
A Standard Response Indicator for Pulsed Systems	W. R. Free and L. A. Hill	310
RI/FI Instrumentation to 21 Gc.	S. Abrams and B. Leibowitz	320
Tracking Notch Filter for the Rejection of CW Interference	W. B. Warren, Jr.	326

#### SESSION IV A - ANALYSIS II

Comparison of Transmitter Spectrum Signature Data and Radiated Field Strength Data for Transmitter Emissions	P. F. Chen and C. E. Blakely	340
Analysis of Airborne Radio Frequency Interference Problems	R. E. Haydon, T. F. Barone, L. J. Grady, and T. E. Selby	358
Mutual Gain of Radar Search Antennas	R. C. Johnson	368
Probability of Interference from Randomly Dispersed Sources	P. Christopher	381

#### SESSION IV B - DESIGN FOR INTERFERENCE CONTROL

Analysis and Evaluation of Electromagnetic Compatibility Tests	W. B. McIntosh and G. D. Brosius	403
A Wide-Stop-Band Filter for a High Power S-Band Radar	J. P. Rooney and F. P. Ventolieri	432
A Technique for Determination of Filter Insertion Loss as a Function of Arbitrary Generator and Load Impedance	S. M. Vakil	445

#### SESSION IV C - ECAC INTERFERENCE PREDICTION MODEL

ECAC MSS-2 Interference Prediction Program- General	J. A. Zoellner	459
---	----------------	-----

ECAC MSS-2 Interference Prediction Program- Cull Model	J. B. Scott	469
Automatic Terrain Information Processing System	J. Iseli	493
A Propagation Model for Electromagnetic Compatibility Analysis	W. E. Frazier and D. S. Anderson	505
Spectrum Signature Synthesis for Compatibility Analysis	R. W. Fleck, F. C. Pethel and J. W. Marini	534

#### SESSION V A- SHIELDING

The Application of Absorption and Scattering Coefficients for Concentric Spheres to the Problem of EMI-Free Enclosures	R. A. Eldred, H. A. Lasitter and J. Roberts	560
Shielding Theory and Practice	R. B. Schulz, V. C. Plantz and D. R. Brush	597
Shielding a Flight Vehicle Against Electromagnetic Interference During Test	R. O. Lange	637
Propagation in Absorbent- Material-Lined Cavities	J. W. Wright and W. E. White	656



## SESSION VB - CLASSIFIED\*

### SESSION VIA - INSTRUMENTATION II

A Spectrum Analyzer with 2 Gc. Display	A. Fong, H. L. Halverson, G. C. Jung and R. W. Anderson	668
Interference Spectrum Analyzer with Automatic Frequency Scanning and Data Recording	L. Valcik, J. E. Batz, J. Faraone and D. Rees	681
Measurement Techniques with a Spectrum Signature Monitor	M. Feigenbaum and R. Sandstrom	701
Electromagnetic Compatibility Program for the McDonnell RF-4C, Phantom II Aircraft	W. D. McKerchar	709

### SESSION VIB - MEASUREMENT TECHNIQUES

A Method for Performing Transient Susceptibility Tests on Primary Power Leads	R. F. Kantner	725
MIL-E-6051 Electromagnetic Compatibility Testing Concepts and Techniques	W. A. Taylor	736
Analysis of the High Impedance Field in Susceptibility Tests	W. A. Stirrat	747
Radio Noise Considerations for Extra High Voltage Transmission 345- 1000 Kilovolts	E. R. Taylor and W. E. Pakala	775

\* U. S. Military agencies may obtain copies of the classified proceedings from DDC. Other qualified DDC users should request through Commanding Officer, USAELRDL, Fort Monmouth, N. J., Attention: SELRA/GFE. Certification of military sponsor is required.

## FOREWORD

Forty-seven technical papers were presented at this year's Ninth Tri-Service Conference on Electromagnetic Compatibility, the largest program in its history, yet barely more than half of the total number of papers submitted. Attendance topped 500, indicating the continuing need for exchange of information on compatibility problems.

The conference committee would like to extend its thanks to the authors and speakers, to the session chairmen, to Fifth Army Headquarters, and to those in attendance for their part in making this a successful conference.

### Conference Committee:

J. E. Bridges, Chairman  
IIT Research Institute

\* S. Weitz  
USAELRDL

F. Murphy  
U. S. Navy, Bureau of Ships

C. Miller  
RADC

T. Jackson  
IIT Research Institute

P. Hanen  
IIT Research Institute

\* See "In Memoriam," pp. ix - x.



**SIDNEY WEITZ**

**1914 - 1964**

### IN MEMORIAM

Sidney Weitz was born in New York, N. Y. on 7 June 1914. He received his early education in New York City, and later attended Cooper Union. Actually Sid never stopped attending school and was always taking a course or two at Monmouth College. The day before his untimely death on January 16, 1964, he studied for a final exam.

Sid was one of the pioneers in the Government in Radio Interference Reduction. He joined the USAELRDL in 1942. Since that time, with the exception of three years in the Army in World War II, he was engaged in research and development in all areas of electromagnetic compatibility. He was chief of the Interference Evaluation Branch at the time of his death.

Sid was nationally recognized as the expert in RFI instrumentation and measurement procedures. He conceived many new techniques for the measurement of broad-band voltages, currents and fields which are reflected in equipments such as the AN/URM-3, AN/URM-7, AN/URM-85 and their commercial equivalents. In addition all current Department of the Army RFI Specifications incorporate test procedures evolved by him.

Sid was a tireless worker and had many papers published, served on numerous committees, and was responsible for the annual Tri-Service Conference on Electromagnetic Compatibility. Yet, he was never too busy to help a fellow employee in the solution of a knotty problem.

Everyone concerned with electromagnetic compatibility will find the passing of this dedicated, imaginative engineer hard to accept.

## WELCOME ADDRESS

J. E. Bridges, Manager  
Electromagnetic Compatibility  
IIT Research Institute

As chairman of the Ninth Tri-Service Conference on Electromagnetic Compatibility, and on behalf of your host, IIT Research Institute, it is my pleasure to welcome each of you here today. This conference is sponsored by the United States Army, Navy, and Air Force and is held in cooperation with the PTG on Electromagnetic Compatibility of the Institute of Electrical and Electronic Engineers. I also wish to acknowledge the excellent cooperation and effort given by the people who helped implement this conference from the Three Services, the PTG on Electromagnetic Compatibility and IIT Research Institute. A most important contribution will come from the speakers and chairmen who are contributing their time and talents to this meeting. It is hoped that their papers and resulting informal discussions will provide answers to some of our current problems as well as pointing out new problem areas.

As you know, the last ten years has brought almost revolutionary changes in the Radio Frequency Interference field. Much needed recognition has been given to both the technical problems and to the early pioneers. We are now beginning to find ourselves a part of management bar graphs or PERT control charts. We now have large groups devoted exclusively to compatibility problems. Still further accomplishments will be required in both technological and management areas.

To emphasize this point, the growth of the domestic electronic industry is creating many challenging compatibility problems. In 1960 it was estimated that the total annual electronic effort in the United States amounted to some ten billion dollars and, by 1970, this would be increased to an annual rate of twenty billion dollars. This dollar estimate does not include non-electronic equipments such as motors, converters, powerline systems, household equipments and the like. Of this total investment, a very substantial portion appears as new electronic equipment. On top of

this, the old equipment, which is more susceptible to interference, is not being obsoleted or scrapped. All of these new equipments are potentially capable of creating interaction problems among themselves as well as playing havoc with the old equipments.

The demands of the increasing population of the United States for more goods, improved services, increased productivity, better defense, and reliable equipment, (such as aircraft) are rapidly using up our remaining Radio Frequency Spectrum. No part of our complex agricultural and metropolitan life remains unaffected. We cannot go to a hospital, make a telephone call, drive a car, watch television, bake a cake, or shoot the moon without affecting or being affected by the crowded and sometimes poorly used Radio Frequency Spectrum. Thus, the challenging problems of Electromagnetic Compatibility are not unique to any specific group of individuals, government agencies, or geographical areas. The management and technical solutions must, however, be provided by many of you who are now attending this conference.

It is hoped, therefore, that this Conference -- the presentations and discussions -- will provide the necessary communications, guidance and stimulation required for the future. Again on behalf of the Three Services, the PTG on Electromagnetic Compatibility, and IIT Research Institute, I extend to you a welcome to this conference.

### KEYNOTE ADDRESS

Brigadier General Allen T. Stanwix-Hay  
Deputy Chief Signal Officer  
U. S. Army

Ladies and Gentlemen:

First, I would like to thank you all for the honor you have bestowed by inviting me to make your keynote address. I am, indeed, very happy to be here with you today.

As many of you realize, I am a newcomer to these conferences. Nevertheless, I am generally familiar with your efforts -- if not through being personally acquainted with as many of you individually as I would like, then in the broader sense of being well aware of the importance of what you have -- collectively -- accomplished, the importance your work will continue to have with respect to the security of our Nation, and the many problems that must still be solved.

Though you are not -- figuratively speaking -- the halfbacks who get the limelight and receive the applause, no knowledgeable observer will deny that you are the guards and tackles who make possible the electronic touchdowns that our Armed Services must accomplish. I know there are few challenges which require so much intra- and inter-Service coordination and Service-Industry teamwork then that of obtaining and maintaining Radio Frequency Compatibility.

Those of you with whom I am acquainted know that I have spent much of my career in logistics, and that much of my time and effort have been devoted to working with industry. It is for this reason that, in considering what I should say to you today, I found it quite natural to explore some of the radio frequency compatibility relationships which exist between industry, on the one hand; and the three services, on the other; and, after thinking about this for a while, I realized that throughout this broad program -- which covers research and development, procurement and maintenance, and frequency management -- a rather unusual situation exists. There are not one, but at least three major and somewhat contradictory relationships which we in the Defense Department have with industry: first, we are your customers; second we are your clients; and third, we are your competitors.

Let's take a few minutes to examine these one at a time. We are your customers. This is the most obvious relationship, for we of the Military Services buy communications-electronic equipment from industry. And, connected with this seemingly simple relationship is a host of problems.

You of industry must design compatibility into equipment. At last year's Tri-Service Compatibility Conference, Mr. Bridges of ODDR and E suggested that compatibility will follow the successes of the reliability program, which includes such important phases -- development of techniques, standards, and specifications, and eventually the incorporation of the desired quality from the very first design concept of new equipment.

You in industry working closely with your military counterparts, have been doing a fine job in the past. It is because of your work and because of your groundwork on the components of communications-electronics equipment, that our systems work at all today -- in spite of the crowded electromagnetic environment that exists.

The services are also customers of industry for measurement equipments. These items are of critical importance, for without them, we would not know whose equipment was interfering with whom, nor whether a modification had fixed the trouble.

Consider the basic paradox that the test equipment designer must face: We ask for something -- say a communications transceiver -- to be built exploiting the very limit of the electronic art: the highest possible frequency, the highest possible sensitivity, the greatest possible stability. Then, to measure that transceiver, we ask the test instrument designer to build measuring equipment capable of even higher frequency and sensitivity, and even greater stability. Yet, in spite of this apparently impossible collection of requirements, the test instruments are designed and built, and to a large extent, do meet the needs of the compatibility program.

But, as one problem is solved, industry's customers, the Military Services, are faced with more.

Consider the problem of miniaturization. Can circuits and components be made smaller and smaller, and yet retain the ability to reject spurious responses and to suppress spurious emissions? Will simplification of circuits be possible without sacrificing interference control?

Then there are the problems involved in tactical Army communications equipment. Even when spurious and harmonic emissions and responses are completely under control, communications will still be interference-limited. They will be limited by the number of times the bandwidth of a single equipment can be divided into the available spectrum bandwidth. We are close to this limit now. Other approaches must be found.

One possibility is narrow-band frequency modulation equipment. Another, now under extensive test is Single Side Band tactical radio equipment. But conversion to either of these brings a new set of problems. For example: Wide band FM gives relative freedom from static and low-signal-level interference, all at the cost of using more spectrum space. We are considering if we should give up these advantages, because of cost in spectrum space. Can industry overcome the loss of these advantages, and overcome the other interference problems that will be generated if we do decide to shift to narrow band equipment?



Consider the problems of tropospheric and ionospheric scatter communications. Or the challenges created by the ground terminals for satellite communications systems. There is a combination of high-gain antennae, high-power transmitters, highly sensitive receivers -- a veritable nest of potential radio frequency interference.

Further, there is no lack of problems in non-communications equipment design -- ever more powerful radars need ever greater relative suppression of unwanted emission, to prevent the absolute level of out-of-band interference to rise to intolerable levels.

As I have said before, the services are industry's customers. Give us equipment which overcomes these problems and we will be fortunate customers indeed.

The Military Services are not only the customers for those of you in industry; we are also your clients. We depend on you for advice and for professional services, particularly in our new radio frequency interference analysis facilities. Progress in this field since the last Tri-Service Compatibility Conference has been significant. In these last twelve months, the Tri-Service Electromagnetic Compatibility Analysis Center has begun work on interference problems in support of specific Joint-Service needs. Also during this period, the Army's Electromagnetic Environmental Test Facility has validated its interference model, for many types of communications equipment. This facility is also being asked to solve problems of immediate military importance.

The progress in computer analyses of interference problems for future equipments and deployments has created demand for still more analyses. Our initial tasks were to validate computer models, to collect equipment data, and to collect environmental data. Field measurements, particularly around San Diego, California, and Ft. Huachuca, Arizona, have done much of the necessary validation. The Spectrum Signature Measurement Program, another Tri-Service effort, accomplished through many contracts with industry, has built up a substantial file of signature data. And just this past summer, the first collection of environmental data, covering fixed military equipment operating at above 100 Megacycles was completed throughout the Continental United States.

These analysis facilities are building a reputation for accuracy and competence. This but brings a new problem: More tasks than the facilities have computer time to accomplish. The solution isn't just rental of more equipment. First we must develop the most efficient use of the equipment now on hand. Later expansions of facilities may well become necessary, but first we must be certain that any further expansion will be used with maximum practical efficiency, not just in scheduling time, but in the efficiency of the computer models themselves. Let me expand on this somewhat.

Whereas our initial problem in development, with industry, of the analysis facilities, was the writing and validating of the computer interference models, our current problem is to increase the efficiency of

these computer programs. Computer time -- and computer cost -- are well on their way to becoming the limiting factor concerning how many interference studies we can undertake. I don't know, at this point, whether progress will be made with a series of small improvements in present model efficiency, whether progress will come from a sudden breakthrough in the concept of the interference analysis, or whether progress will come from a combination of the two. I do know we need progress.

An engineer has been defined as a man who can do with one shilling what any blunderer can do with two. By this definition, an engineer is not necessarily one who can do what no one else can do at all; the emphasis is on doing something efficiently. I suggest our great need in interference programming is for engineers, in the sense of this definition -- men who can do in one minute of computer time what someone else can do with two.

The initial breakthrough -- computer analysis of interference -- is past. The next frontier is efficiency -- or speed -- in performing these analyses.

As your clients we need certain answers -- and this comprises the advice that we in the Military Services want to buy from you in industry. We need, quantitative, not just qualitative answers. It is not enough to tell us "it won't work because of interference." We need to know, rather, how much will overall communications be degraded. We need to know in detail how well target acquisition will be accomplished despite interference. We need to have specific measures on the relative effectiveness of different possible fixes to a problem.

If industry can give us good answers to questions like these, we will be fortunate clients indeed.

I have outlined the manner in which the Military Services are the customers and clients of industry. However, in a sense, the Services are your competitors as well.

As you all know, the Radio Frequency Spectrum is a limited resource. Its bounds are not entirely under our control, but rather are dictated by the natural behavior of Radio Propagation. And, again as you all know, all users of the radio spectrum must compete with one another for this resource.

One of the most reliable of all fixes for radio communications interference is to get a cable plow, or a cable ship, and bury the communications out of reach of interference. However, this solution just isn't applicable when we consider installations which must be frequently moved. It is even less applicable to communications in mobile installations, and it won't work

at all for radars. These, unfortunately, are characteristic of most military applications. We'll use the cable plow when we can -- but by the very nature of military operations, that isn't very often.

We must realize -- we of the Military Services -- that the spectrum is not ours alone, no matter what the emergency. We share it with others who also have need for it -- in emergency, as well as in routine times. Some of these competitors are here now -- the communications industry -- the various non-military government users of radio. Many of you here represent other competitors indirectly, since they are your customers, for they buy your equipment. Inevitably, we are in competition with each other for the available radio spectrum. But this competition is closely tempered by cooperation.

Consider that every TV receiver with a spurious response is a potential complaint to the Military Services if a Service-operated emitter should land on that response. But that television receiver is as much a potential complaint to the manufacturer. In almost every case, the Defense Department has nearly as big a stake as industry has in equipment built for industry's non-military customers. Since we both must use the frequency spectrum, it is to your advantage as well as ours, that Military equipment generate as little interference as possible. Similarly, it is to the advantage of the Military that the equipment that industry builds and uses for non-Defense applications, be interference-free as well.

Therefore when we, acting as customers of industry, obtain an improvement in transmitter stability, it is to our own interest that this improvement be applied to all transmitters. When we, acting as clients of industry, obtain an improvement in interference prediction techniques, it is to our own benefit that these techniques be used by you to solve your own problems as well -- for it is then less likely that you will interfere with us in the limited radio spectrum that we compete for, and must share.

And this brings me to my final thought. Because the whole is always greater than the sum of its parts, the total relationship existing between the Services and industry consists of more than just that of customer, client and competitor.

The most important relationship we hold to one another is the sum total, and this translates directly into the single word "partnership."

It is for this reason that I see these conferences -- of which this one is the ninth -- so valuable a platform for the exchange of ideas, information, and concepts, it is also for this reason that I consider these conferences so valuable a vehicle towards the over-all goal of radio frequency compatibility.

Thank you.

## TEAMWORK IN SPECTRUM CONSERVATION

Luncheon Talk By

James D. O'Connell, Chairman  
The Joint Technical Advisory Committee

Colonel Woolwine, Mr. Chairman and Gentlemen: I want to thank our Conference Chairman, Mr. Bridges, for asking me to make this talk because it afforded me an opportunity to get more up-to-date on the Military Electromagnetic Compatibility Program before speaking to this astute and competent group. I must admit, however, that I did not realize the amount of education that would be necessary to become conversant with this program. I thought that reading material on previous meetings, several visits to the staff of the F.C.C., and a visit to the Electromagnetic Compatibility Analysis Center would bring me up to date.

I had several visits with the staff of the F.C.C.. Mr. Ralph Clark and I had a most instructive visit to ECAC. Colonel Woolwine and Mr. Stan Cohn and their colleagues presented a very interesting program, and we were much impressed with the value of the work being done at the Center.

However, when I told Mr. Henry Randall of the Department of Defense of our appreciation of the visit we had to ECAC, he said, "Now you must go to Ft. Huachuca because they are doing some very good work out there, too." So Mr. Clark and I visited Ft. Huachuca yesterday and were again very much impressed with the importance of the work being done.

It immediately became obvious that more education would be needed and that a visit to Rome Air Force Base, to the Bureau of Ships, and to the

Naval Research Laboratory were essential in order to get conversant with the programs of those two services. Furthermore, it certainly seemed to be advisable for the Joint Technical Advisory Committee to discuss the results of these visits and to determine how it can help more in this program. Again, this morning at breakfast with Rex Daniels, he recounted many new examples of interferences that are being encountered in radar and other fields. I now feel that given another three months I would be prepared to make this talk.

As a result of the visit that Mr. Clark and I made to ECAC, most of the members of JTAC now wish to hear the ECAC presentation at first hand, and Henry Randall and Colonel Woolwine have kindly arranged to have this presentation made.

It is necessary at the outset to describe briefly what is the Joint Technical Advisory Committee of the IEEE and the EIA and what are its objectives. Because it seeks to work quietly with complete objectivity in the National interest and without advertising or fanfare, possibly, it is not well known to the military.

On March 23, 1948, the late Wayne Coy, Chairman of the Federal Communications Commission, addressed the President's Luncheon at the IRE National Convention. Present were both IRE's President B. E. Shackelford and W. R. G. Baker of the Electronic Industries Association. Mr. Coy spoke of the need for assistance to the F.C.C. in arriving at adequate national allocation of television facilities; he spoke of the many other conflicting demands for spectrum space, notably those of the Land Mobile Service, and of the need of advice of a particularly disinterested and objective nature-- I would like to emphasize and stress these two words, "disinterested" and "objective," because they are the unique characteristics of this technical

committee.

JTAC was specifically conceived to meet this need. It was to be a committee of eight members. Its Charter missions were to obtain and evaluate information of a technical or engineering nature relating to the radio art for the purpose of advising government bodies and other industrial and professional groups. It was to determine what technical information is required to insure the wise use and regulation of radio facilities . . . to sift and evaluate information thus obtained so as to resolve conflicts of fact . . . to separate matters of fact from matters of opinion, and to relate the detailed findings to the broad problems presented to it . . . to present its findings in a clear and understandable manner available to the profession and to the public . . . to appear, if necessary, before government bodies or other parties to interpret the findings of the committee.

Past and present members of JTAC include five IRE Presidents, the first President of the newly merged Society of the IEEE, and more than eleven members of the IRE Board of Directors. Members are chosen on the basis of professional standing, integrity and competence to deal with the problems before the committee and without respect to the organizations of which they may be members. They are required to operate without instruction so that complete objectivity shall be achieved. And I would again like to emphasize this particular feature, "without instruction and complete objectivity."

JTAC has undertaken fourteen major studies, of which ten were requested by the F.C.C. Many of the studies resulted in more than one report, as many as six in one case. Let me give you some of the titles:

Utilization of Ultra High Frequencies for Television

Allocation Standards for VHF Television and FM Broadcasting

Proposed TV Broadcast Allocation--Monochrome and Color

Frequency F allocation of Land-Mobile Services

Consideration of Aeronautical, Broadcast, Land-Mobile and  
Marine Services

Electromagnetic Interference Problems (three reports)

Arc Welder Interference (six reports)

Desirable Allocation for Forward Scatter Propagation

Frequency Diversity Services

Frequency Allocation for Space Communication

This last study reached the important conclusion that with suitable geographic separation of ground stations, sharing of the same spectrum space by satellite and point-to-point ground communication was feasible. This finding was accepted by the F.C.C. and their present concepts of broad-band assignments and spectrum sharing were at least assisted by this study.

JTAC prepared and published in 1952 a book titled, "Radio Spectrum Conservation," and a sub-committee is now in the final stages of completing a new and up-to-date rewriting of the same book, which will be perhaps many times the content size of its predecessor because of the amount of additional knowledge that has come to hand during the past twelve years.

Recognizing the important requirements of the military forces of many nations, for the use of the radio spectrum, the importance to military operations and the military's interest in its conservation, a special section is devoted to discussion of military usage.

My subject today is "Teamwork in Spectrum Conservation." Unfortunately, in the past teamwork between the military services and JTAC has not always been close. The May 5, 1958 PROCEEDINGS of the IRE contained an article entitled, "JTAC--10 Years of Service," from which I quote a passage--"It is too much to expect that every project undertaken by JTAC would be crowned with success. For example, it became increasingly apparent to JTAC and

industry groups that there was insufficient coordination on problems of frequency utilization and conservation among the United States Government, non-government users and manufacturers. In 1954, the then Chairman of JTAC, Lloyd V. Berkner, acting for the Committee, attempted to get various government agencies interested in implementing a program of spectrum conservation. Nothing ever came of it. Then, as now, the ponderous machinery of government administration proved invincible to prodding from without."

It so happened that as a member of the Joint Communications Electronics Committee I was personally in the midst of the discussions which went on as a result of JTAC's proposal at that time and so I guess I must count myself as one of the invincibles. However, as a party to these deliberations I know something of what the problems were. I certainly know what my thoughts were on this subject, and I cannot agree that the failure of active consultative coordination was due to the ponderous machinery of Government or to lack of active interest in conservation on the part of the military. My thoughts were that the military services did not have sufficient information in hand to contribute effectively to a continuous joint committee-type of action. I know that much discussion took place as to the heavy drain which would be placed on the Services and on their scarce and over-worked frequency experts. No one of the Services felt that they had a sufficient staff of experts to engage in contributing the amount of material which would be required. The question as to where the money would come from to meet the additional requirements was a major problem, and the only answer was that the military of each Service would have to take it out of their hides, so to speak. Furthermore, another very important point was not clear to me. I did not understand that JTAC was not an industry committee with objectives of seeking more space for TV or other entertainment purposes, but was in fact a group charged with



complete objectivity in the national interest and was as much interested in the success, effectiveness and efficiency of our defense efforts as in the welfare of the industrial, and entertainment segment of the economy.

I also know that the interest and prodding of JTAC had a very significant and helpful effect on the work already under way in the Services, as a result of Rand studies, Project Monmouth and others. In fact, Dr. Baker and Dr. McRae in their consultation with Government Advisory Committees, had much to do in getting present programs under way. But I must admit that it would probably have been difficult in 1958 to predict that there would be the consistent leadership efforts of Jim Bridges and Henry Randall, and that within the three Services there would be leadership which would bring the military program to the achievements which are beginning to be realized. I wish that the members of that 1958 JTAC group had been able to make the visit to ECAC and to Ft. Huachua with Mr. Clark and myself; they would have been gratified and enthusiastic, as we were. Real accomplishments at both installations had been made. There is an understanding of the problems and how to attack them. They are actually doing problem solving. They are actually at the achievement stage of the work. They are learning their equipment deficiencies and are taking a highly critical attitude toward them.

For example, one of the points brought out at Ft. Huachua was that in order to simulate one of their transmitters, they would have to have 325 different emitters operating on 325 different frequencies just to represent the spurious emissions from that one transmitter.

There have been more recent efforts by JTAC to achieve a cooperative and understanding mode with Government programs, with those of NASA and DOD especially, and these have been increasingly successful. In 1960 Mr. Ralph Clark became Chairman of JTAC and brought to its deliberation a comprehensive

understanding of military and Government communication problems. During the studies by a JTAC Sub-committee in 1961-62 of frequency allocations for space communication, there were active Sub-committee members from NASA and the Propagation Laboratory of the Bureau of Standards. In fact the Bureau of Standards' Propagation Laboratory performed one very important aspect of the study in collaboration with Stanford Research Institute. Observers from DOD, from the Services, from their contractors, from the staff of the F.C.C. participated in the Sub-committee sessions. Only in this way was it possible to assemble the perspectives, knowledge and skills that could lead to a well-balanced report. There was unique know-how available in some defense contractors' organizations, in the Rand Corporation, and in other non-profit institutions contracting with the Government. So much for the past . . . perhaps too much, but the very essence of this talk on Teamwork depends on past relationships and on what can be done in the future to achieve a better team approach in attacking this massive and complex problem.

Big and complex the problem certainly is and I wish we could adopt the philosophy of my favorite comic strip character, Charlie Brown of Peanuts, who, as you recall, said, "There is no problem so big and so complex that you can't just walk away from it." Unfortunately, you can't just walk away from this problem because it follows you and it is growing every day in practically every way. Informal discussions with F.C.C. personnel indicate that frequency usage in the United States has increased tenfold since 1949, while personnel strength in the twenty-four districts dealing with interference has gone down to one-half. At the present time, the F.C.C. is receiving some 600,000 applications per year. Marine license applications alone are at the rate of some 3500 a month. There are some 500 applications a month

for microwave radio relay purposes. Industrial applications, telemetering and plant safety purposes appear to be major additional expansion programs for the future. In the Los Angeles area there seems to be a completely saturated condition for mobile communications. Aircraft surveys have performed some over flight noise measurements of urban versus rural areas, . . . these over-flights were a part of military R & D programs and are fallouts from such programs. These over-flights indicate major increases of broad band spectral noise over urban areas. Unfortunately, no data is available to indicate the extent to which this general spectrum smog is getting worse year by year. We do not have adequate trend information. Successive measurements have not been made of the same areas to indicate the extent to which this general spectrum noise is growing. On the other hand at the present rate of increase of spectrum usage, it seems perfectly safe to predict that usage again will increase some ten times during the next decade unless the spectrum congestion becomes so intolerable so as to prevent further growth. This could very well become the case unless advance planning is done to prevent it. It is obvious that the problem of saturation is much more difficult to solve after it occurs than well in advance before capital investments have been committed.

At the present time, the regional F.C.C. districts are doing valiantly with rather meager facilities to handle the interference cases that come to their attention on a case-by-case basis. In some districts the Citizens Interference Committees are most active in arousing public interest in spectrum noise and in interference problems. In the 6th Army area, which includes the Western States, the military and the F.C.C. are building close teamwork at this front line of the interference problem. The San Francisco chapter of the Armed Forces Communication and Electronics Association has

formed a Radio Frequency Interference Committee to work with the Citizens Interference Committee. This is teamwork at the local level, which should be recognized, commended and extended. The National Armed Forces Communications and Electronic Association might well undertake a major program nation-wide to assist in bringing this problem to the recognition of our citizens. One of the examples of interference which occurred in the San Francisco area had a somewhat humorous twist. It involved interference to an airways frequency used by light army aircraft, one of their navigation frequencies which at various times of the day or night was being blacked out. After investigation by the local F.C.C. district people, it was found that this interference originated with radio frequency garage door openers which had been installed in a new development in the vicinity. The humorous twist came when a radio station in the vicinity began interfering with the garage door installations causing them to open and close at frequent intervals!

One of the greatest problems is lack of information. It seems very difficult indeed to get reliable over-all data which can spell out the National interference problems in quantitative terms and which can indicate what the trends are. Specifically, how serious is the problem now? Of course, we know in some areas, Los Angeles for one, that there is a saturated and intolerable condition in the mobile communication field. This is receiving attention from the F.C.C. How much increase in interference is occurring from year to year, and what are the specific categories of increase? On the other hand, to what extent have interference reduction measures been effective? By a wide margin the interferences reported to the F.C.C. are radio system to radio system cases, but we have not yet obtained data which categorize these or which indicates what the trends may be. Many complaints are received from television set owners of interference from industrial

devices and other radio systems. The problems of increasing the selectivity of TV receivers brings out many of the difficulties involved in this business of spectrum conservation. The achievement of suitable over-all balance in use of the spectrum, versus cost of the equipment as limiting factors to usage, adds up to techno-economic problems of much complexity.

It is encouraging, however, that such widespread interest in this problem is growing. It is apparent that EMC has become a major career field which is rapidly expanding. A late estimate indicates that there are approximately twenty committees from many different professional associations which have been formed to study the problem as it relates to their interest. In fact, this increasing interest, the formation of additional committees, has created another major problem of coordinating the studies of the various groups that are seeking to investigate various facets of the problem and bring about improvements.

In order to try to get a hold of this problem, and because so many activities are going on in so many places and so many phases of EMC, Professor Showers and several members of the Professional Technical Group on Electromagnetic Compatibility recently held a series of meetings to review the state of the art, the groups conducting studies in this field and requirements which exist for coordinating the efforts of the many committees and individuals who are involved. They established the objective of advancing the coordination of electromagnetic compatibility through standardization, and they established panels on systems effectiveness, interference criteria, measurements techniques and instrumentation, interference sources and definitions. I am aware that participation in this effort will be representative of the major groups now active in the EMC field and will include interested Government military activities. ECAC,

Ft. Huachuca, Air Force and Navy efforts will all be represented.

Dr. A. L. Hebert of the Rand Corporation has undertaken a study of the National problem of electromagnetic compatibility. He seeks answers to questions such as: What is the magnitude of the problem? Are the efforts now going on enough to cope adequately with it? While we think we can say with certainty that the problem is growing considerably faster than are the effective efforts to contain it and control it, much more positive information is needed. Dr. Hebert's study seems most appropriate and most needed.

I understand that the Illinois Institute of Technology is undertaking a study of compatibility as an international problem. This study also fills an important need.

In Washington it appears that Government agencies or their contractors are engaged in building some five different data bases for various purposes, and probably no one of these will be all-inclusive.

Nothing has been said as yet of the dichotomy of Frequency Administration which manages allocations at the National level. A much longer talk than this could be devoted entirely to the many studies, proposals and recommendations which have sought to unify in some way the administrations of the F.C.C. and the IRAC. But it seems clear that the growing problems and growing interest will not and cannot wait for the solution of complex reorganization concepts. It took us a long time to arrive at the philosophy of organization and of management that we now have in frequency administration at the National level, and it may take many years before modifications are made in this system.

From a practical standpoint, it appears that increased teamwork and agreed upon coordination in the over-all National interest can, and, in fact,

will have to be brought to bear on the major problem areas. We cannot wait for organizational changes, which may take a very long time to come. I have real confidence that teamwork can now be made effective in a practical way and that it can get results. A very substantial part of this confidence comes from a better understanding and appreciation of the capabilities and attitudes of the Federal Communications Commission. Discussions have convinced me that the Commission staff has a comprehensive knowledge of the problems that beset our allocation policies and procedures and that their attitude is open minded, exploratory, progressive and forward looking. I have found no organization that has the comprehensive knowledge of these problems which the F.C.C. has. They recognize full well the difficulties involved in the administrative techniques of sub-allocation which have split up so many of our bands above 30 Mc into commercial, Government and further into functionalized areas such as land-mobile, fixed, fixed and mobile, common carrier and allocation divisions according to user, environment and mobility considerations.

Considering the techniques and knowledge available at the time it was instituted, this administrative technique was probably sensible and established order which would not otherwise have been established. Many predict, however, that it does not and will not provide for the maximum utilization of the spectrum which should be our established objective. This means that all of the allocator's tools, namely, frequency, time, geography, distance, must be used to the fullest advantage to make the radio spectrum available everywhere to the maximum benefit of legitimate users. It would appear that in the past there has not been enough use of the geography-distance tools in the allocation technique. The tool most used, of course, has been frequency separation. One of the basic needs has

been the establishment of systems characteristics, measurement techniques and methodology for planning in advance and for minimizing the interference and vulnerability characteristics of all radiating systems in their particular geographical environment. These new techniques and methodologies are now becoming available. The pioneering work of the Electromagnetic Compatibility Analysis Center, of the Army's Ft. Huachuca and of the other Services, deserve support and encouragement from the entire EMC community.

I find also that the staff of the Commission is highly conscious of the importance of teamwork, and their relationships with Government agencies, including the military, are growing closer. I think the time has come for the military to take specific steps to bring the Commission staff into the closest possible relationship with all of the EMC work it is doing. The money being spent to develop techniques and methods for more efficient utilization of the Government military frequencies and systems far exceeds the money spent to better utilize non-Government frequencies, and this does not include the actual cost of the equipment. If one does consider the over-all cost of equipment, one estimate postulates that some 5% of equipment costs are now going into interference and compatibility studies and the engineering of systems, sub-systems and components which will be compatible. I must admit, that data other than estimates do not seem to be available. It is certainly clear, however, that weapon system designers can no longer take chances that systems performance will be impaired, partially or catastrophically, by internal or external interference.

The point has frequently been made that military R & D, in advancing the state of the art, contributes greatly to the generation of new techniques and new products for U. S. industry. The field of electromagnetic compatibility and better spectrum utilization should provide a major case in point if effective teamwork is established. The views that JTAC holds



are these: that the electrommagnetic spectrum is a national and international natural resource which is unique. It is unique because it is wasted when it is underused or inefficiently used, and it is conserved when its total capabilities are fully used in the most efficient way for the most important purposes of mankind. Learning more about how to use this unique resource better should be a never-ending quest. Much knowledge has been gained over the past ten years and significant progress has been made in better spectrum utilization. More information is conveyed, more services performed per segment of the frequency spectrum used, than previously. But the growth of spectrum use and the growing demands of the future have outrun, and continue to outrun, the advances in spectrum utilization. More knowledge and better application of that knowledge to administrative procedures and management are needed in all areas of frequency usage.

The Department of Defense program is beginning to pay major dividends in knowledge of deficiencies, in techniques and methodologies for attacking this massive problem. The military need no longer feel that they are behind or not on top of their problem. They are certainly in a position to contribute much to the other elements of our economy, to the non-Government portion of our economy, in assisting an attack on that problem. The military electromagnetic compatibility program should be encouraged, strongly supported and enlarged. There appears to be a real need for the establishment of National leadership of this program at the highest level. It appears certain that the Director of Telecommunications, in his role as an advisor to the President, is in the best position to do this and to bring together a National team that can think in terms of our total society. No changes in any existing organization or relationships are needed to get this teamwork

going.

Now then, how and what specifically can JTAC do to help in this effort? For one thing, it can encourage and provide inputs to such study efforts as the one Dr. Al Hebert is starting at Rand. Perhaps phases of some of these studies could include testing of new concepts of allocation techniques, more sharing for example, better use of geography, distance and time, rather than predominantly the frequency separation.

Secondly, where current studies do not seem to be completely covering essential needs, JTAC can suggest additional studies and either start them or assist in getting them started. For example, how can the F.C.C. best make use of or translate into useful terms the techniques and methodologies that are now starting to come from the work at ECAC, Ft. Huachua and the other Service laboratories?

Finally, JTAC can repeatedly, never endingly if you will, persist in emphasizing the vital need of total teamwork in this program. The legitimate individual interests of every member of the team will benefit by such teamwork--and the National interest demands it.

THE WESTERN ELECTRIC COMPANY-WIDE PROGRAM FOR COMPLIANCE WITH PART 18  
OF THE RULES AND REGULATIONS OF THE FEDERAL COMMUNICATIONS COMMISSION

R. A. Kay  
Western Electric Company, Inc.  
Hawthorne Station  
Chicago 23, Illinois

Abstract.-

I. Magnitude: The Western Electric Company has 12 manufacturing Works or Plants, some of which include satellite shops. The shops may be in cities other than that of the Works location. The approximate area boundaries within which these factories are located are from Merrimack Valley, Massachusetts to Winston-Salem, North Carolina, to Oklahoma City, Oklahoma to Omaha, Nebraska. Within these manufacturing locations are approximately 1,000 machines coming under the regulation of Part 18, of the Rules and Regulations of The Federal Communications Commission, including induction heaters, dielectric heaters, ultrasonic cleaners, medical diathermy, RF stabilised arc welders, electronic discharge machines and other miscellaneous devices. The minimum power output of any machine is about 100 watts, the maximum is 50 KW and the total power out rating adds to between 5,000 and 6,000 KW. The fundamental operating frequency ranges between 15 KC/sec. and 2450 mc/sec.

II. Outline of Program: A special development case was originated at WECO, Hawthorne, to establish a uniform company-wide program for Compliance with Part 18. The program provides for three major activities: (a) Semiannual and annual routine inspections of all machines. (b) Radiation measurements as required for certifications and recertifications, and (c) Provision for an annual report by a third party to ensure the continuation of the program. During parts (a) and (b) techniques were developed for the use of the Sprague Model 500 Interference Locator for annual radiation relative measurements and for the use of Empire Devices NF105 and Stoddart NM20B Field Intensity meters for radiation measurements.

III. Administration Aids: In order to accomplish the maximum uniformity within the Company, several administration aids were created: (a) A Manufacturing Standard was written based on Part 18, which is to be kept up to date with Rules changes by Hawthorne. As Transmittals are issued by the FCC, they are interpreted and written into the Standard in terms of Western Electric Company procedure. (b) Manufacturing Division Instructions - WECO rules of procedure defining organizational responsibilities were written to assure uniformity. (c) Standard forms for: Inspection Logs, Maintenance Required, Certification Manuals, and Annual Reports were adopted for Company wide use.

IV. Measurements Program: The responsible engineers and inspectors at all plants were given specific instruction in the techniques of radiation measurements, shielding and grounding of machines, use of line filters and screen rooms. (a) Testing routines to be followed using the Sprague Model 500 for annual measurement of relative radiations. (b) Testing routines for making radiation measurements required for Certification or recertification.

V. Conclusions: It has cost the Western Electric Company in excess of \$100,000 to set up this program on a Company-Wide basis. We estimate an annual cost of approximately \$10,000 to carry on the routine inspections and recertifications. Emphasis is placed throughout the Company to procure industrial heating equipments properly certified by suppliers, in an effort to reduce the cost of compliance with Part 18 of the FCC Rules and Regulations.

## I. BACKGROUND

Western Electric Company, Hawthorne was alerted to possible FCC regulation of industrial use of high frequency electric power in July, 1945. Mr. James L. Fly, a former chairman of the FCC spoke, at the July meeting of the Chicago Chapter of the Society of Plastic Industries, of pending action by the Commission. Later in 1945, Hawthorne ordered field intensity meters from RCA and Ferris Instruments, and in 1946 began radiation measurements of induction and dielectric heaters in use within the Hawthorne Works.

In 1946, most of our attention centered on our Archer Avenue Plant (the Wartime Studebaker aircraft engine plant) located at Archer Avenue and Cicero Avenue, which was immediately adjacent Midway Airport. Many studies were made to ascertain that the 10 high frequency dielectric heaters being used there in the manufacture of the telephone handsets, were not causing interference at the airport.

Part 18 went into effect in 1947, with a 5 year "grace" period. By the end of this period, 1952, all of the industrial heating units at Hawthorne had been measured and brought within the radiation limits of Part 18. A few units, of "historic" engineering design were scrapped and replaced by better designed machines. By 1952 our electron tube manufacturing plant at Allentown, Pennsylvania was using in the neighborhood of 100 induction heaters and had purchased field intensity meters for its own use. The Hawthorne field intensity meters and engineer were sent to Western Electric Company Plants, at Kearny, New Jersey, and Baltimore, Maryland to measure and certificate induction and dielectric heaters at those locations. By 1952, all WECO electronic devices, regulated by Part 18, were tested and certificated.

As many of you know, extensive changes were made in Part 18 in 1957, 1959, and 1961. New requirements added: (a) Routine inspections to assure that Industrial, Scientific, and Medical equipments were being maintained and operated within the intent of Part 18. (b) Filing of FCC Form 724 with the Commission, which required a Company Official to go on record with the Commission and obligate the Company to comply continuously with Part 18. (c) Increased technical limitations, including measurements of harmonics 1 through 10, spurious radiations, power line conducted voltages, exclusion of distress frequency bands, and the inclusion of requirements for radio frequency stabilized arc welders.

In 1960 the Management at Hawthorne established a project, headquartered at Hawthorne, to set up a Company-Wide Program for Uniform Compliance with Part 18 of the Rules and Regulations of the FCC. A Development authorization was approved to provide funds for the estimated one and one-half years of engineering effort needed to put the program into effect. The project was introduced at a conference on April 16, 1961, at Hawthorne. Engineering representatives were called in from all Western Electric Company locations, and were briefed on the details of the Program. Preliminary plans called for the Hawthorne engineer to visit each Manufacturing location twice. The first visit would be to train inspection personnel to perform the visual

and electrical inspections. The second visit would be to perform radiation measurements, as required, and prepare the Certification Manuals and FCC Form 724's for filing with the Commission. The engineering representatives were requested to survey their areas in advance of the Conference and submit a list of all Industrial, Scientific, or Medical devices in their area, which they considered as coming under the regulation of Part 18.

## II. MAGNITUDE

The Western Electric Company has twelve manufacturing Works or Plants. Each Works or Plant may include several satellite shops, which may be located in the same or different cities. Hawthorne Works consists of the Hawthorne Shops in Cicero and Chicago, the Fullerton Avenue and Clearing Shops in Chicago, and the Montgomery Shops at Montgomery, Illinois, just South of Aurora. A separate FCC Form 724 was required for each shop, and in some cases, such as the Hawthorne Shops, three 724's were required. Our 12 locations extend from Merrimack Valley, Massachusetts, to Winston-Salem, North Carolina; to Oklahoma City, Oklahoma; to Omaha, Nebraska; including Buffalo, New York; Kearny, New Jersey; Baltimore, Maryland; Allentown and Laureldale, Pennsylvania; Columbus, Ohio; Indianapolis, Indiana; Chicago, Illinois; and Kansas City, Missouri. Within the WEC's shops we have approximately 1,000 machines coming under Part 18. We have induction heaters ranging from 500 watts to 50 KW power output, used in brazing, soldering, and heat treating applications. SLIDE NO. 1: Is an automated line for encasing cable, and includes a 50 KW induction soldering position. Our dielectric heaters range between 500 watts and 20 KW used in plastic preheating for molding, thermoplastic heat sealing, glueing and drying operations. SLIDE NO. 2: shows one of our earlier molding areas, where dielectric heaters are used to heat thermo-setting plastic preforms prior to molding. This is a manual process. SLIDE NO. 3: is an automated molding area with the preheater attached to the molding press. The process is highly automatic. Ultrasonic devices up to 2 KW are used for cleaning, welding, soldering, and mixing operations. Radio frequency stabilized arc welders; electronic discharge machines for metal cutting; and ultrasonic devices for ceramic cutting are found in many locations. Most Shops have hospital units for First Aid in case of accidents; these may have medical diathermy and ultrasonic therapy devices. Our lowest radio frequency is 15 KC and our highest is 2450 mc. Our total family of fundamental and harmonic frequencies is very large! We estimate that the total power output of all ISM machines used by the WEC is between 5,000 and 6,000 KW.

## III. OUTLINE OF PROGRAM

As I mentioned before, the Management at Hawthorne approved a special development authorization covering the effort of one engineer for about a year and a half to set up the Program. Each Works or Plant provided effort by an engineer and one or more inspectors for an amount of time equal to three or four times that spent by the Hawthorne engineer at that location, carrying out their portion of the Program. The Program was divided in three areas of effort: (1) Establishing a uniform inspection procedure whereby each machine is visually inspected semiannually for physical condition including actual operation, and annually for relative radiation measurements, (2) Radiation measurements as required for certifications and recertifications, and (3) Preparation of an annual report by a third party to ensure the continuous effectiveness of the Program.

Decisions for the administration of the Program reached high levels of Management within the Company. Legal opinion of the interpretation of Part 18 was obtained from our Legal Department. Since the authority to shut down any machine used in manufacturing operations was required, the Works or Plant Manager was asked to approve Part II of FCC Form 724 "Certificate of Compliance". This decision was relatively simple and straight forward since the Works Manager or Plant Manager has the highest authority at his location. The responsibility for Part I of 724 was not as easily determined. The Commission desires the responsibility for Part I, which, in reality, is the full responsibility for Compliance, to be with an engineer or person completely acquainted with Part 18, who assumes full responsibility for the machine, its installation, its certification, its maintenance, and continued operation. Such a man is hard to find within WECO! After much discussion, it was concluded that a member of our Plant Engineering, Electrical, would be best qualified. Plant Engineers are responsible for issuing purchase and installation requisitions for all machines, for installation drawings and instruction, for factory space, and for all relocations of machines, therefore, are the most logical to assume Part I responsibility. A Plant Engineer was selected at each Works or Plant for this function. He is assigned the responsibility for Part I by the respective Works Manager.

Assignment of the routine inspection responsibility likewise required considerable discussion. Electrical maintenance men, particularly test set maintenance, probably have the most experience related to radiation and interference problems. However, these men are usually assigned to specific areas and do not have plant wide coverage. Installation electricians are generally familiar with radio interference prevention but likewise have limited areas of operation. Our electrical plant inspectors have technical training and plant wide coverage, but have little experience with high frequency circuitry. The option was left with the individual Works or Plant, to select inspection personnel as they preferred. However, as I mentioned previously, one of the objectives of the 1st visit by the Hawthorne engineer was to train the inspectors and acquaint them with the overall problems of radio interference prevention.

The routine inspection program was established at each Works or Plant during the 1st visit by the Hawthorne engineer, and required from two to five days. The activity began with a briefing conference of an hour or so, during which the different types of devices were discussed, the inspection log forms were reviewed, and particular attention was paid to the procedure to be followed for machines that did not pass inspection. In such cases the inspector is to issue a "Maintenance Required" form to the production organization. This form identifies the machine and points out the condition to be corrected. Before completing the form the inspector is to discuss the correction with the production supervisor and mutually agree upon a reasonable time limit during which the repair can be made. Both the seriousness of the condition and the production demand are to be weighed to determine the time allowed for the repair. The agreed upon interval of time is entered on the form and a recheck date indicated. The inspector is to return at the agreed upon time and if everything is in order, a supplementary log sheet is entered and the case closed. However, should the correction not be made, the inspector will again contact the production supervisor, issue a second "Maintenance Required" form and notify the responsible Plant Engineer. The Plant Engineer will review the case and as authorized, order the shut down of the machine should the situation warrant.

Inspectors were instructed to check for proper shielding, bonding, grounding, missing panels or fastenings, and conditions in general that might result in increased radiation. A special compartment was provided, on each machine or installation, for posting the original copy of each inspection log and maintenance required form. These visual inspections are to be made at least once every six months. The annual relative radiation inspection will be discussed later.

The second phase of the Program, certification or recertification, took place a month or more after the first visit for establishing the visual inspections. During the interim, all machines requiring maintenance were repaired and in some cases altered to assure the lowest possible radiation. The Hawthorne engineer returned equipped with an Empire Devices NF105 and a Stoddart NM20B Field Intensity meters. The group certification procedure was followed and separate certification manuals and FCC Form 724's were prepared for each group. Several shops required more than one 724. The measurements procedure will be discussed in more detail later. As the measurements were made by the Hawthorne engineer, the inspector for that area took readings on a Sprague Model 500 Interference Locator, to give comparative data and become familiar with the use of the test set.

When the measurements were all taken, the certification manuals and 724's were typed locally in proper quantity. The local responsible engineer was left with the task of obtaining the approval of his local Works Manager and filing with the FCC Regional and the Secretary at Washington. He was advised to send the documents to the Secretary of the Commission at Washington by registered mail with return receipt requested. This receipt serves to establish the beginning of the 60 day period during which the Commission agrees to notify the user of any changes desired in the Certifications. After the certification manuals were completed, the inspector was instructed in the use of the Model 500 Interference Locator for making the annual relative radiation measurements, both for individual machines and groups. He was also shown how to interpret the Certification Manual in order to know when a machine measured by the Model 500 was approaching excessive radiation. Details of this procedure will be discussed later also.

The final phase was to set up a "watch dog" over the program. At first it was thought that the WECO headquarters at 195 Broadway, NYC should assume responsibility for ensuring that the Program continued to function. After some discussion, it was concluded that this function should be local, and also that it should involve a third party and take the form of an annual audit. The procedure agreed upon was that a separate group would annually audit the records of the inspection organization to determine that the proper number of inspection logs were being entered each year. Changes in location of machines and maintenance required would also be noted. A random sample of about 10% of the total number of machines would then be checked on location to determine that the logs and entries were made properly on the machines. This audit is then submitted to the Works or Plant Manager directly on a standard form which presents the report in a simplified, easily read manner. Although this entire program has been in effect only a year or two, we believe it is effective and will keep our Company in Compliance with Part 18.

#### IV. ADMINISTRATION AIDS

In a Company as large and as spread out as ours, uniformity of procedure is both of major importance and difficult to maintain. To cope with

this problem, we utilize a system of issuing Manufacturing "Division Instructions" - MDI's. When Company-Wide uniformity is required, the instruction is issued by our Business Methods organization at Headquarters, 195 Broadway, NYC. During the first few months of carrying out the Program, the Business Methods people at Hawthorne cooperated with Headquarters to prepare, approve, and issue a Company-Wide Instruction. The Instruction defined the functional responsibilities of all organizations involved in carrying out the Program continuously. Administrative but not technical procedures were defined. Subsequently, each Works or Plant has issued its own local MDI defining its local organizational responsibilities. During the period of setting up the Program, many lessons were learned, resulting in a revised MDI, with almost 60% rewrite!

Technical information was organized and issued for Company-Wide use in the form of a Manufacturing Standard. Most of the information contained in the Standard was taken directly from Part 18 of the Rules and Regulations of the FCC. It was reorganized to fit our Company procedures. A certain amount of engineering know how is also included in the Standard, to assist inspectors and certifying engineers in measurements procedures. One function of the Development Engineering group at Hawthorne, headquarters of the Program, is to maintain the Standard up to date. This group subscribes to Volume II of the Rules and Regulations and receives Transmittals when issued by the Commission. These are reviewed, and changes are made in the Standard in accordance with changes in Part 18. As new testing procedures are developed, these are included in the Standard also.

Three standard forms are used for the inspections. SLIDE NO. 4: MD 686R is an Inspection Log for Dielectric Heaters. SLIDE NO. 5: MD 686RA is used for induction heaters, ultrasonic devices, RF stabilized arc welders and miscellaneous machines. A log identifies the machine and its location.

The first three entries check the machine operation during production and expose good (or bad) habits of the operators that might effect radiation. Routine Inspections are performed without prior notice to the using shop so that actual operating practices may be observed by the inspector. The balance of the entries pertains to the physical condition of the machine, and operation is suspended while these items are checked. SLIDE NO. 7: When an entry is indicated "Bad", the inspector must issue a "Maintenance Required" form. If the inspector is uncertain about an entry, he will check "doubtful" and observe the condition carefully at the next inspection, at which time it may be "bad" or found to have been corrected by regular maintenance. All inspection logs are prepared in triplicate: the original is posted on the machine, the duplicate is sent to the "responsible Plant Engineer", the triplicate is retained in the inspection department. All logs are retained for at least 5 years. SLIDE NO. 8: When maintenance is required, Form MD 850B is issued. As mentioned before, the inspector will determine a reasonable time within which the repairs are to be made. This is generally with the agreement of the operating supervisor, however, if the condition could cause radio interference, the inspector will insist that the repair be made at once. If he needs support he can call upon the responsible Plant Engineer and an immediate shutdown can be made. When an MD 850B is issued, a follow up inspection and log are required.

Part III of FCC Form 724 is a testimonial that the machine involved is properly designed and meets the FCC requirements and has been installed so that it will be operated within the requirements. When Form 724 is issued covering a newly purchased machine, the manufacturer's certification manual, based on prototype measurements, or type approval number, is attached with Part III, and the responsible Plant Engineer who signs Part I also signs



Part III. As some of you have probably heard, the Western Electric Company has embarked on a Company-Wide program to persuade all of our suppliers to provide us with certification manuals which are acceptable to the Commission, or Type Approval numbers which they obtain from the Commission directly. This policy is very important to us for two reasons: (1) If the supplier has a Type Approval Number or an acceptable Certification Manual, we know the machine has been designed and proved to meet the radiation limits set forth by the Commission. In a few cases, we have spent several thousand dollars on poorly designed machines, or have even junked them. (2) It is expensive to obtain the data required for an acceptable Certification Manual. The supplier can obtain these on a prototype or on type approval by the Commission and the costs will be divided over all additional machines of the same model, thereby distributing this expense among several customers and not require each customer to bear the total expense of radiation measurements.

When we move our machines around, as we do at frequent intervals, or modify their application, we have to recertificate. Not infrequently, we will move an entire shop! We use a standard form SLIDE NO. 9: MD 850C-P1-13 called Certification Manual. This Manual can be used for individual or group Certifications and contains individual data pages for Polar Pattern Data SLIDE NO. 10 measured and extrapolated, rate of attenuation (4 lobes), SLIDE NO. 11, specific bands SLIDE NO. 12, of spurious frequency radiations, power line radiations, and graphs for polar pattern SLIDE NO. 13, rate of attenuation SLIDE NO. 14 (Semi-log), and frequency vs. signal strength SLIDE NO. 15 (log log). In addition, a page of general operating and installation information, and SLIDE NO. 16, a field intensity meter information sheet are included. We have found this standard form adequate to record the information required for any shop or machine. Item modifications are made when required.

Since the Commission gives us the option of posting the FCC Form 724, with the attached Certification Manual on a machine, or posting a Certificate which tells where the 724 and Manual are conveniently located, we have prepared a standard Certificate Form MD 850 CA SLIDE NO. 17. This is posted on the machine and gives the location of the full documentation.

#### V. MEASUREMENTS PROGRAM

I sincerely believe that training in measurements technique, filtering, and shielding of Industrial, Scientific, and Medical equipments could well take a whole year of College level laboratory training, and that, when the diploma is issued, it should include the admonition "never forget the "boogy" factor!" When one least expects it and apparently from nowhere can appear a signal 40 db above, and minutes later its gone - never to be found again!!

For our radiation measurements we have experimented with various equipments including the Ferris Model 22/32, the RCA Models 301B and 308B, and are now using the Empire Devices NF 105 and Stoddart NM20B. Early exasperations resulted when an 18 mc signal measured at the same location and instant on different instruments varied 40 db! Recently everything was going fine on harmonics 1 to 10 for a group, until the 21st harmonic of machine No. 10 operating on a different fundamental overrode the 3rd harmonic of machine No. 17 and ended up setting the pattern for the entire group of machines.

Time will not permit and the experiences will not interest many of you, therefore, I will limit this portion of the paper to a more general outline of the procedures we follow in taking data for Certification.

Interworks shipping of the Field Intensity Meters is a major problem. Our shipping containers grew heavier and heavier, in an effort to avoid shipping damage. Our shipping weight is now well over 1,000 lbs., and we still have damage during every shipment. When the equipment arrives we rent a station wagon SLIDE NO. 18 and mount the Field Intensity Meters and accessories on the wagon for local handling. For close range testing we often use the Tea Wagon-Setup. SLIDE NO. 19. We send our meters to the suppliers every two years for overhaul and calibration, or more frequently when damage during shipment warrants.

Most of our measurements are made for group certification. Readings are taken of the radiations from the machines on harmonics at fairly close range, 50 to 200 feet, to determine what harmonics are within the category of "maximum to 15 db down". We do not stop at 10 harmonics but may go as high as 40 or 50. The machines are operated individually, usually with maximum plate voltage and under no load, and at a time when interference from other machines is not present. If the building in which the machines are located appears to have "hidden antenna" possibilities, readings of a given machine may be taken in three or four locations to determine if there are any conducted or beamed patterns at any frequency. When all machines in the group have been tested in the above manner, their signal strengths are extrapolated to 1000', using inverse square law, so they may be compared. The maximum radiation and all radiations within 15 db. of maximum are then identified. At least all of these signals, sometimes many more, are included in the "machines operating" when the measurements required by Part 18 are made. These measurements are made with the machines in normal shop operation. When taking data for the polar pattern and rate of attenuation etc., we concentrate on the maximum radiation and all radiations that are not more than 15 db down, that is are stronger than 17.8% of the maximum. In a sense, we lose the identify of the machine or the harmonic frequency, and concentrate on the signal strength. The data recorded for polar pattern and rate of attenuation contain only those within the "maximum to -15 db" range.

Our Certification Manual has spaces for data for the maximum and three additional lobes. Frequently "additional lobes" may be at frequencies other than that of the maximum lobe, and may not even be harmonically related to the maximum, as they may come from entirely different machines. Although our certification manual is standardized, supplementary tables are often added and table legends altered to adjust for individual areas.

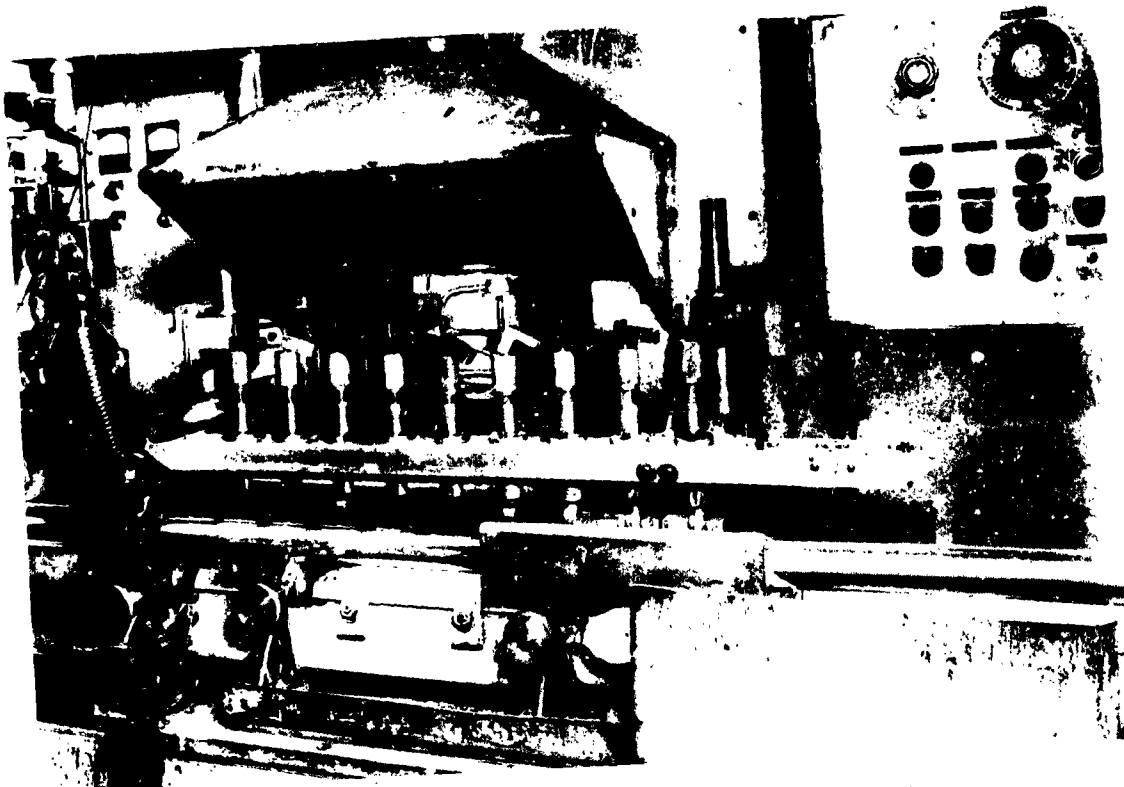
While the radiation measurements are being made, the local inspector, who is to make the annual relative radiation measurements, accompanies us with his Sprague Model 500. SLIDE NO. 20. He makes measurements with it wherever possible and can compare his readings with those taken for Certification. He is given instruction and experience in the use of the Model 500 and in particular shown how to use the instrument so that he knows when the radiation from a given machine or group of machines may be approaching the limit. Some inspectors acquire skill in using the instrument quickly, others struggle with many doubtful readings before they develop confidence in the team of "themselves plus the Model 500"! The Boulevard Model TC-2 Converter is used with the Sprague Model 500 Interference Locator to measure radiations of induction heaters below 490 KC. The frequency range of the Model 500 is 540 KC to 220 mc. The Model TC-2 has a frequency range of 200 to 400 KC when used with the Model 500 tuned to 1600 KC. We have been able to extend the coverage of the TC-2 to: 150 KC to 490 KC by adjusting the IF selected on the Model 500. As the two sets are always used at close range for relative radiation testing, there is adequate sensitivity for making the

tests. When the Certification Manual is completed, and the extrapolated levels at the limit distances are determined, the inspector is advised how much increase in relative radiation measurements can be tolerated before both he and the responsible engineer should take a careful look at the situation.

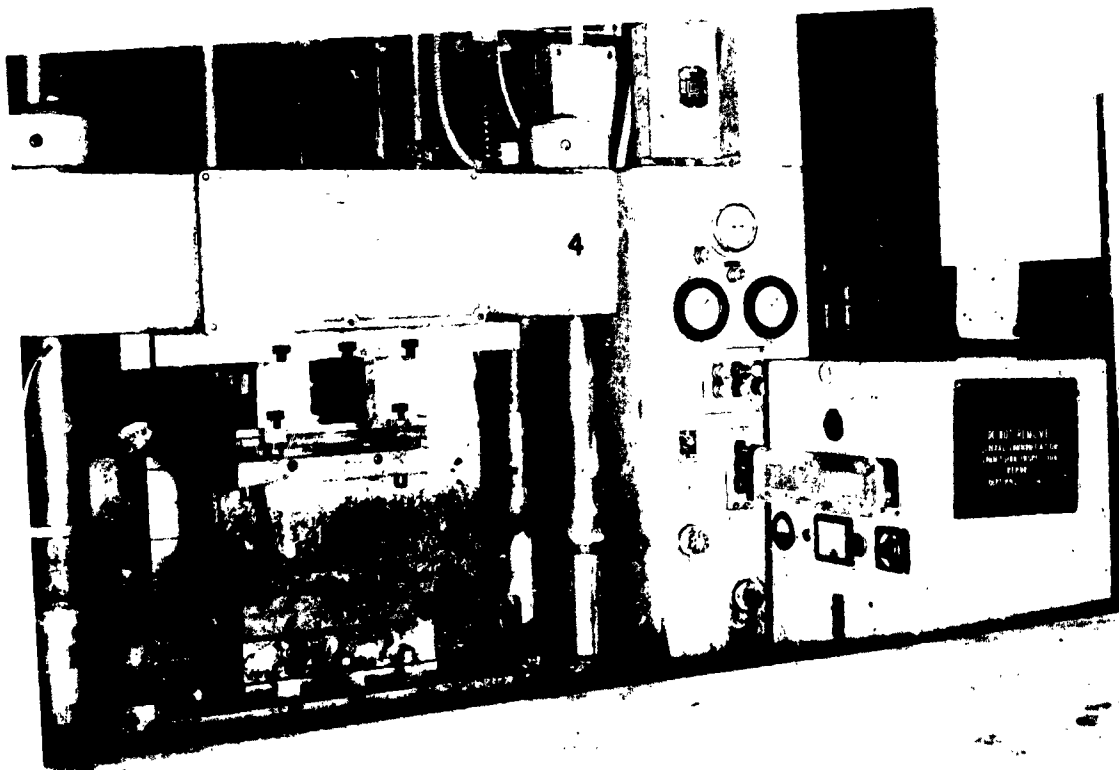
For future relative radiation measurements the following procedure is recommended to the inspector: (1) select a location along each of four 90° radials at a distance of 50 to 200 ft. Identify these locations completely and record the absolute positions of the test set. (2) Adjust the test set pickup and attenuator to give a reading on the meter scale below that at which AVC becomes effective (roughly 20%), (3) Record complete test set information and readings on the Inspection Log (Use back of page if desirable). (4) Duplicate the setup conditions very carefully when future relative radiation tests are made to eliminate all variables except the received signal.

## VI. CONCLUSIONS

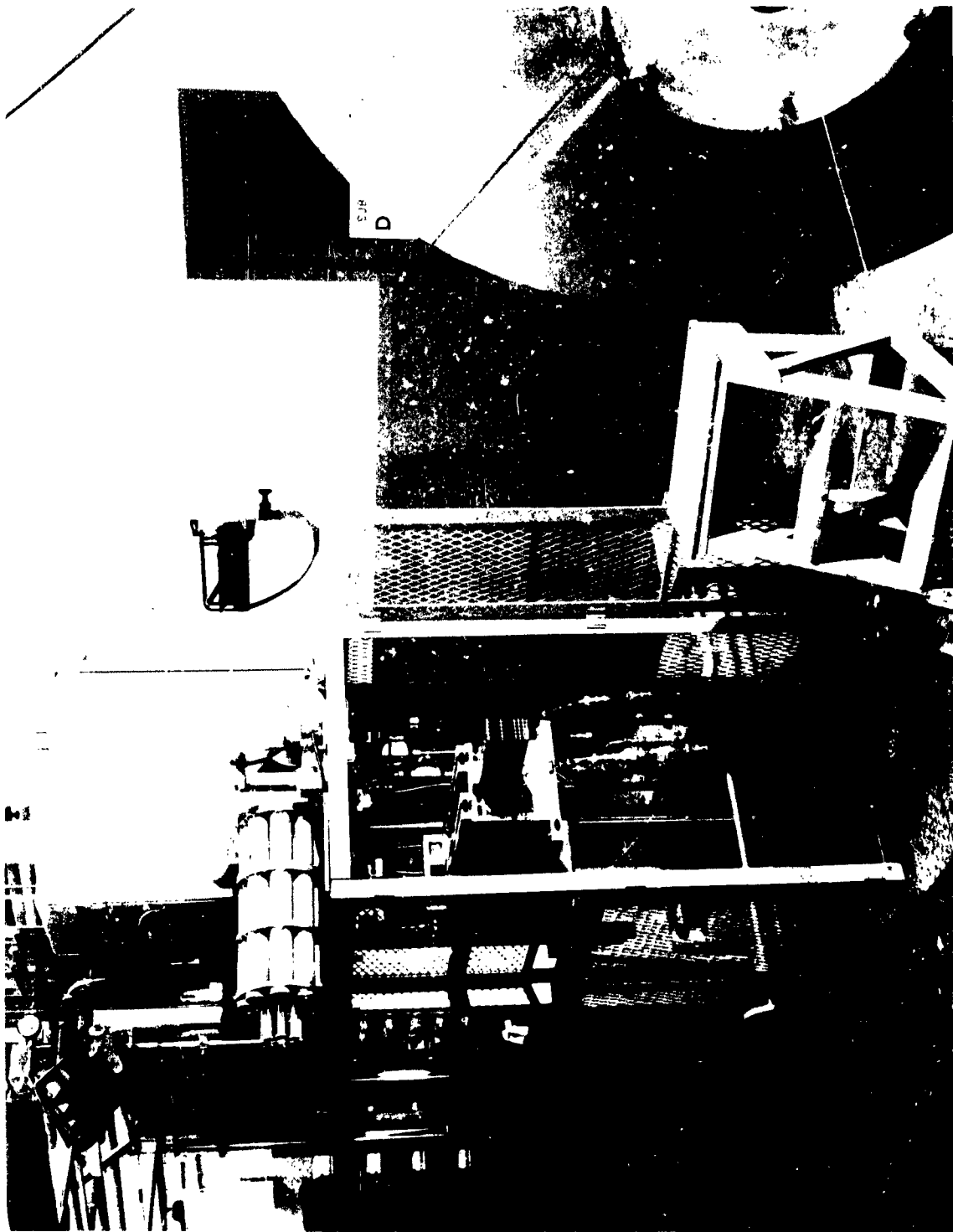
In a Company like Western, a responsibility like Part 18, is very difficult to control. New plants and new shops are frequently being established. Machines are moved among these plants and shops. Personnel is fluid, responsible persons are shifted, promoted, retired. With all of this in mind, we believe we have set up a Program that is, and will continue to be effective. We feel today that the Company house is in good order and have confidence that it will stay that way. But it has been expensive. The Hawthorne engineer responsible for the Program has devoted over 3,000 hours of engineering time to the effort. In addition, more than 6,000 hours have been invested at all Works and Plants involved by engineers and inspectors, with a result that in dollars and cents over \$100,000 was required to bring the house in order. We believe that our annual expense to keep the Compliance Program in effect, will be in the order of \$10,000. However, if this Program should, unbeknown to anyone, prevent the loss of any military or commercial jet, or a missile, or any loss of human life, due to communications interference prevention, there is no question of the economic justification.



SLIDE NO. 1 - A TYPICAL AUTOMATIC INDUCTION SOLDERING APPLICATION



SLIDE NO. 2 - A TYPICAL MANUAL TRANSFER DIELECTRIC HEATING APPLICATION



SLIDE NO. 3 - A TYPICAL AUTOMATIC DIELECTRIC HEATING APPLICATION

MD 686-R

INSPECTION LOG

(Dielectric Heating Facility)

Facility \_\_\_\_\_ Location: Bldg. \_\_\_\_\_ Floor \_\_\_\_\_ Works \_\_\_\_\_  
Manufacturers Model \_\_\_\_\_  
Manufacturers Serial No. \_\_\_\_\_ W.E. Facility No. \_\_\_\_\_

Conditions Inspected

During Operation \_\_\_\_\_  
1. Preform doors \_\_\_\_\_  
2. Conveyor access door \_\_\_\_\_  
3. Grid-Plate controls door \_\_\_\_\_

Out of Operation \_\_\_\_\_  
4. Bonding springs inside preform compartment \_\_\_\_\_  
5. Preform access door safety interlock \_\_\_\_\_  
6. Preform door bonding (hinges, locks, stripping) \_\_\_\_\_  
7. Ground plane and bonding inside preform compartment \_\_\_\_\_  
8. Conveyor access door bonding (hinges, locks, stripping) \_\_\_\_\_  
9. Grid-plate controls door bonding (hinges, locks, stripping) \_\_\_\_\_  
10. High voltage cable to oscillator (shielding and ground) \_\_\_\_\_  
11. Number of fastenings holding oscillator chassis in cabinet \_\_\_\_\_

Remarks: \_\_\_\_\_

Date: \_\_\_\_\_ Inspector \_\_\_\_\_ Dept. \_\_\_\_\_  
Signature in full \_\_\_\_\_

Original attached to facility; duplicate filed in Inspection Organization, triplicate filed in Engineering Department issuing Certification. (See MDI 1.13 092, Manufacturing Standard 18,004.)

SLIDE NO. 4 - INSPECTION LOG MD-686R - DIELECTRIC HEATERS

MD-686-RA

INSPECTION LOG

(Induction Heating or Ultrasonic Facility)

Facility \_\_\_\_\_ Location: Bldg. \_\_\_\_\_ Floor \_\_\_\_\_ Works \_\_\_\_\_  
Manufacturers Model \_\_\_\_\_ W.E. Facility No. \_\_\_\_\_  
Manufacturers Serial No. \_\_\_\_\_

Conditions Inspected

During Operation \_\_\_\_\_  
1. Access doors or removable panels \_\_\_\_\_  
2. Transmission line shields \_\_\_\_\_  
3. Work coil shields or cleaning tanks \_\_\_\_\_

Out of Operation \_\_\_\_\_  
4. Bonding stripping for doors and removable panels \_\_\_\_\_  
5. Security with which access doors, removable panels, & RF shields for transmission lines and work coils are held in place \_\_\_\_\_  
6. Grounding of RF generator (and/or RF shields) \_\_\_\_\_  
7. Condition of RF shields on transmission lines \_\_\_\_\_  
8. Condition of work coil shields or cleaning tank \_\_\_\_\_  
9. Condition of interlock switches on access doors and removable panels \_\_\_\_\_  
10. Grounding of adjacent metallic objects such as tables, transporters, supply racks, exposed electric cables, etc. \_\_\_\_\_

11. Number of fastenings holding doors and removable panels in place: \_\_\_\_\_ out of \_\_\_\_\_ required  
12. Operating frequency: Nominal \_\_\_\_\_, Measured \_\_\_\_\_

Remarks: \_\_\_\_\_

Date: \_\_\_\_\_ Inspec \_\_\_\_\_ Dept \_\_\_\_\_  
Signature in full \_\_\_\_\_

Original attached to facility; duplicate filed in Engineering Department issuing Certification, triplicate filed in Inspection Organization (See MDI 1.13 092)

SLIDE NO. 5 - INSPECTION LOG MD-686RA - INDUCTION HEATERS

(Dielectric Heating Facility)

Facility \_\_\_\_\_ Location: Bldg. \_\_\_\_\_ Floor \_\_\_\_\_ Month \_\_\_\_\_  
 Manufacturers Model \_\_\_\_\_  
 Manufacturers Serial No. \_\_\_\_\_ U.S. Facility No. \_\_\_\_\_

Conditions Inspected

Particulars	Good	Deficient	Remarks
1. Prefurn doors	_____	_____	_____
2. Conveyor access door	_____	_____	_____
3. Grid-Plate controls door	_____	_____	_____
4. Banding springs inside prefurn compartment	_____	_____	_____
5. Prefurn access door safety interlock	_____	_____	_____
6. Prefurn door banding (hinges, locks, stripping)	_____	_____	_____
7. Ground plane and banding inside prefurn compartment	_____	_____	_____
8. Conveyor access door banding (hinges, locks, stripping)	_____	_____	_____
9. Grid-plate controls door banding (hinges, locks, stripping)	_____	_____	_____
10. High voltage cable to oscillator (shielding and ground)	_____	_____	_____
11. Number of fastenings holding oscillator chassis in cabinet	_____	_____	_____

Remarks:

Date: \_\_\_\_\_ Inspector: \_\_\_\_\_ Signature in Full \_\_\_\_\_ Dept. \_\_\_\_\_

Original attached to facility; duplicate filed in Inspection Organization, triplicate filed in Engineering Department Issuing Certification. (See NMI 1.13 092, Manufacturing Standard 18,004.)

REPORT OF MAINTENANCE REPAIRS

(Facilities Operating Radio Frequency Energy)

To Proceeding Dept. \_\_\_\_\_ Date \_\_\_\_\_  
 Manufacturers Model \_\_\_\_\_ Location: Bldg. \_\_\_\_\_ Flr. \_\_\_\_\_  
 Manufacturers Serial No. \_\_\_\_\_ U.S. Facility No. \_\_\_\_\_

The machine, identified above, is in unsatisfactory condition because:

This condition must be corrected if the validity of the CERTIFICATION of the facility is to be continued. Please issue repair order and have the condition corrected by \_\_\_\_\_ 19\_\_\_\_. The facility will be checked on \_\_\_\_\_ 19\_\_\_\_ and if correction has not been made, facility will be shutdown.

Condition Serious ☒

Previously Notified On \_\_\_\_\_ Inspector: \_\_\_\_\_ Signature in Full \_\_\_\_\_ Dept. \_\_\_\_\_

Notes:

Duplicate to Engineering Department Issuing Certification. (See NMI 1.13 092, Manufacturing Standard 18,004.)





MD 850-CP6 (10-61)

PAGE \_\_\_\_\_

OF \_\_\_\_\_ PAGES

TABLE II

MAXIMUM RADIATIONS AT MEASUREMENT LOCATIONS FOR RATE OF ATTENUATION DETERMINATION OF MAXIMUM LOBE AND OTHER LOBES WITHIN 150B.

MAXIMUM LOBE			ADDITIONAL LOBE			ADDITIONAL LOBE			ADDITIONAL LOBE		
RADIAL	DIST.	E	RADIAL	DIST.	E	RADIAL	DIST.	E	RADIAL	DIST.	E

SLIDE NO. 11 - CERTIFICATION MANUAL MD-650-C PAGE 6

MD 850-CP7 (10-61)

PAGE \_\_\_\_\_

OF \_\_\_\_\_ PAGES

TABLE III

MAXIMUM RADIATIONS WITHIN FREQUENCIES SPECIFIED IN PAR. 18.109G IF OBSERVED.

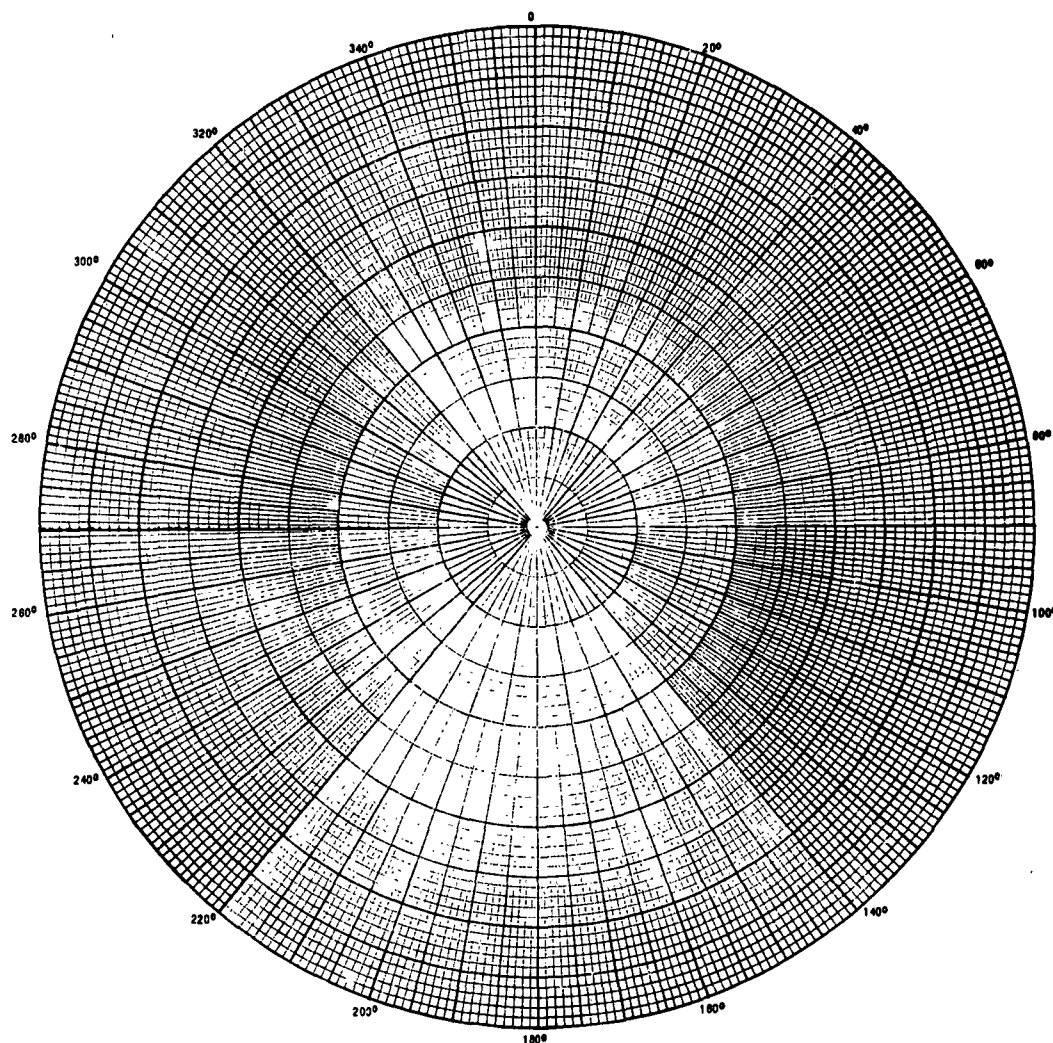
LOCATION OR RADIAL	DISTANCE	FREQUENCY (MC)						
		74.6 - 75.4	108.0 - 110.0	121.5	150.8	243.0	328.6 - 335.4	420.0 - 460.0

SLIDE NO. 12 - CERTIFICATION MANUAL MD-850-C PAGE 7

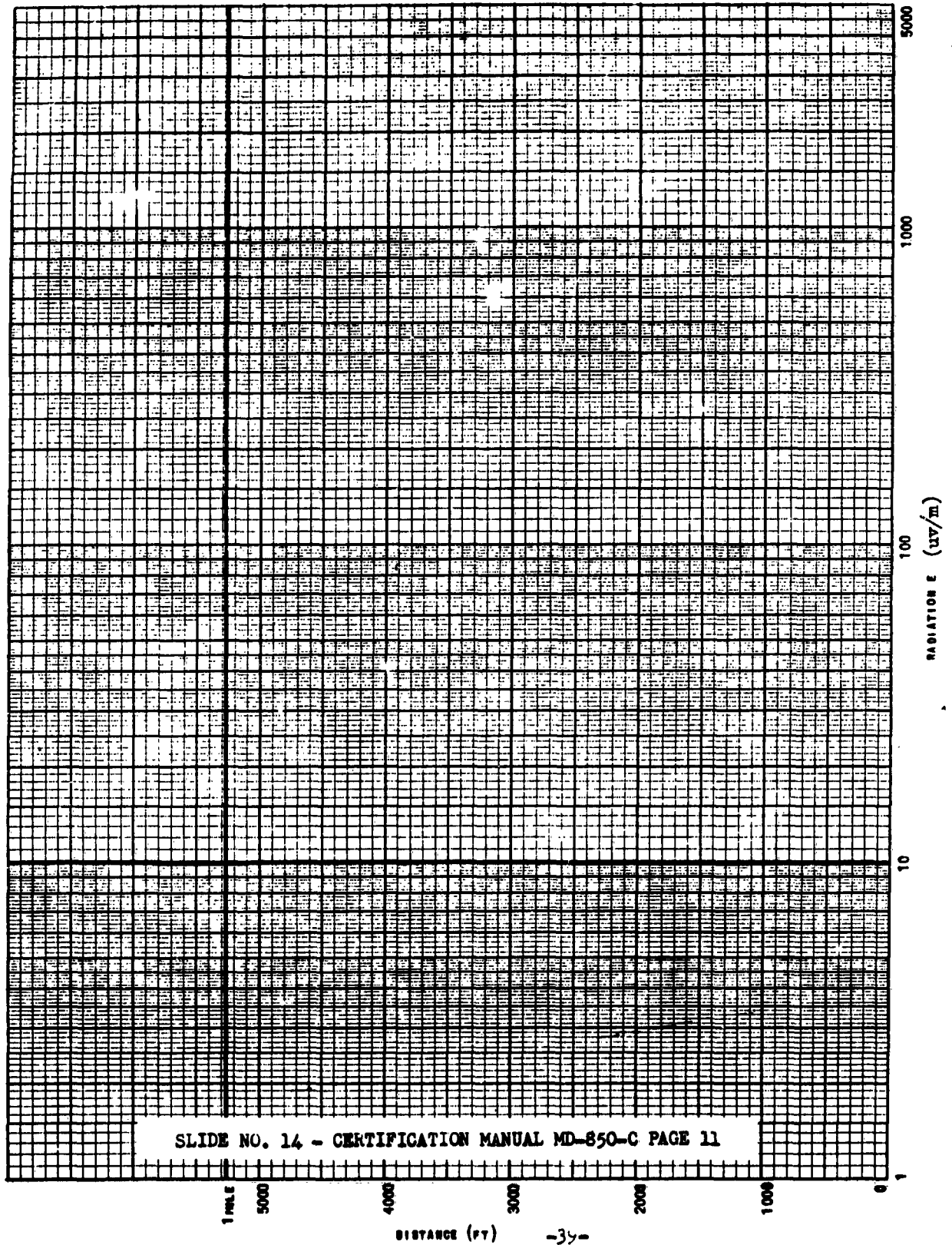
POLAR PATTERN OF RADIATIONS EXTRAPOLATED TO 1000' (SEE TABLE I)

Page \_\_\_\_\_

of \_\_\_\_\_ Pages



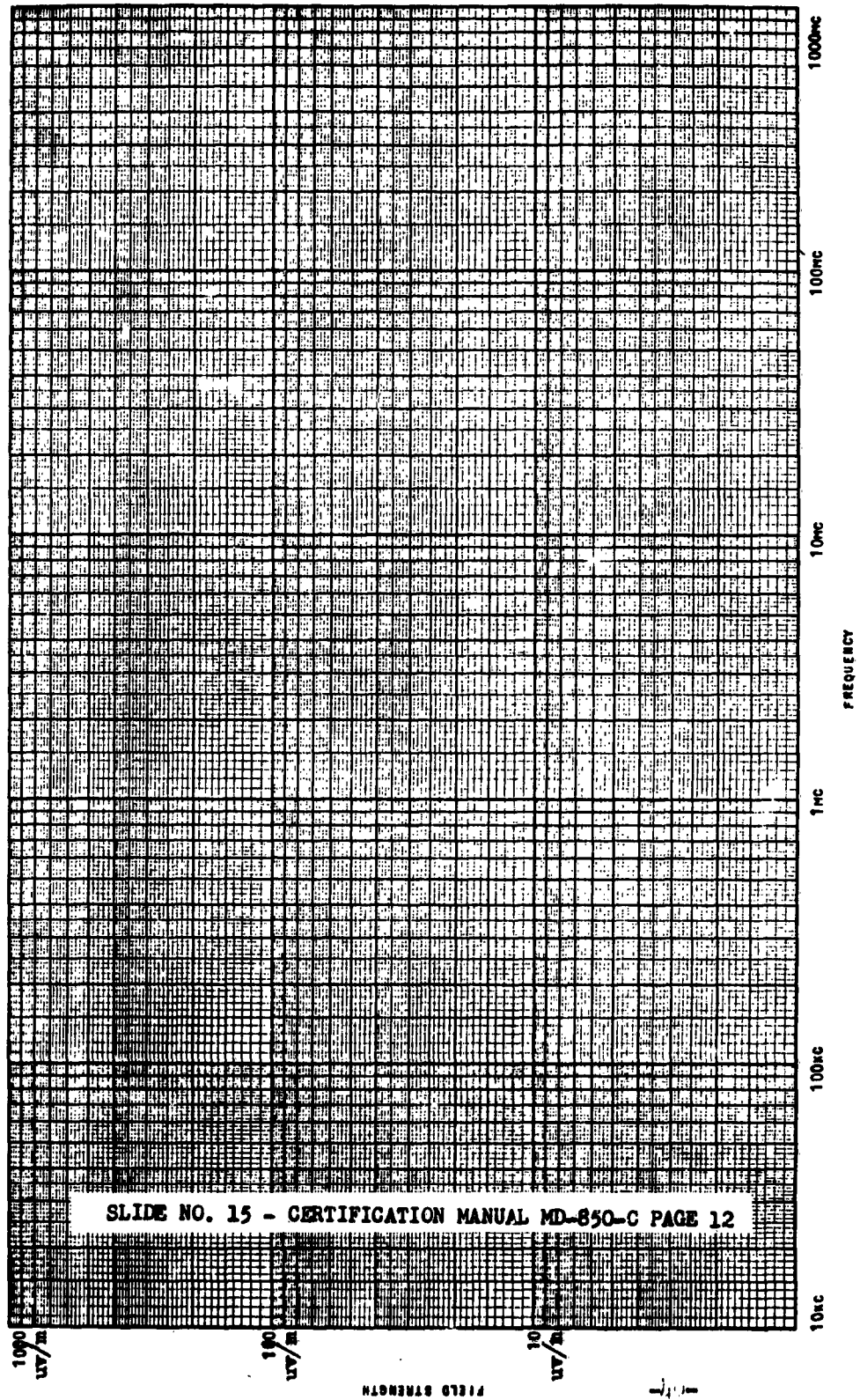
# DECAY OF SIGNAL STRENGTH WITH DISTANCE



DISTANCE (FT)

-35-

FIELD STRENGTH vs. FREQUENCY - EXTRAPOLATED VALUES FOR 1000'



1000000

Page \_\_\_\_\_  
of \_\_\_\_\_ Pages

CERTIFICATE

FOR

HIGH FREQUENCY EQUIPMENT FOR INDUSTRIAL,  
SCIENTIFIC, OR MEDICAL SERVICE

This Certificate applies to Western Electric Company Machine  
Number \_\_\_\_\_, located near Column \_\_\_\_\_, Building \_\_\_\_\_,  
Floor \_\_\_\_\_ of the \_\_\_\_\_ Plant.

The undersigned certifies that the above identified machine has  
been tested and found to meet, and may reasonably be expected to  
meet for a period of at least 3 years, the Requirements of the  
Federal Communications Commission, as set forth in Part 18 of the  
Rules and Regulations of the Commission, pertaining to said equip-  
ment.

The Certification Manual Number \_\_\_\_\_ containing the measurements  
data, graphs, and installation and operation conditions upon which  
this certificate is based is available in the office of Engineering  
Department \_\_\_\_\_ or \_\_\_\_\_.

DATE OF CERTIFICATE \_\_\_\_\_

SIGNED \_\_\_\_\_  
CERTIFYING ENGINEER

SLIDE NO. 17 - CERTIFICATE NO-850-C

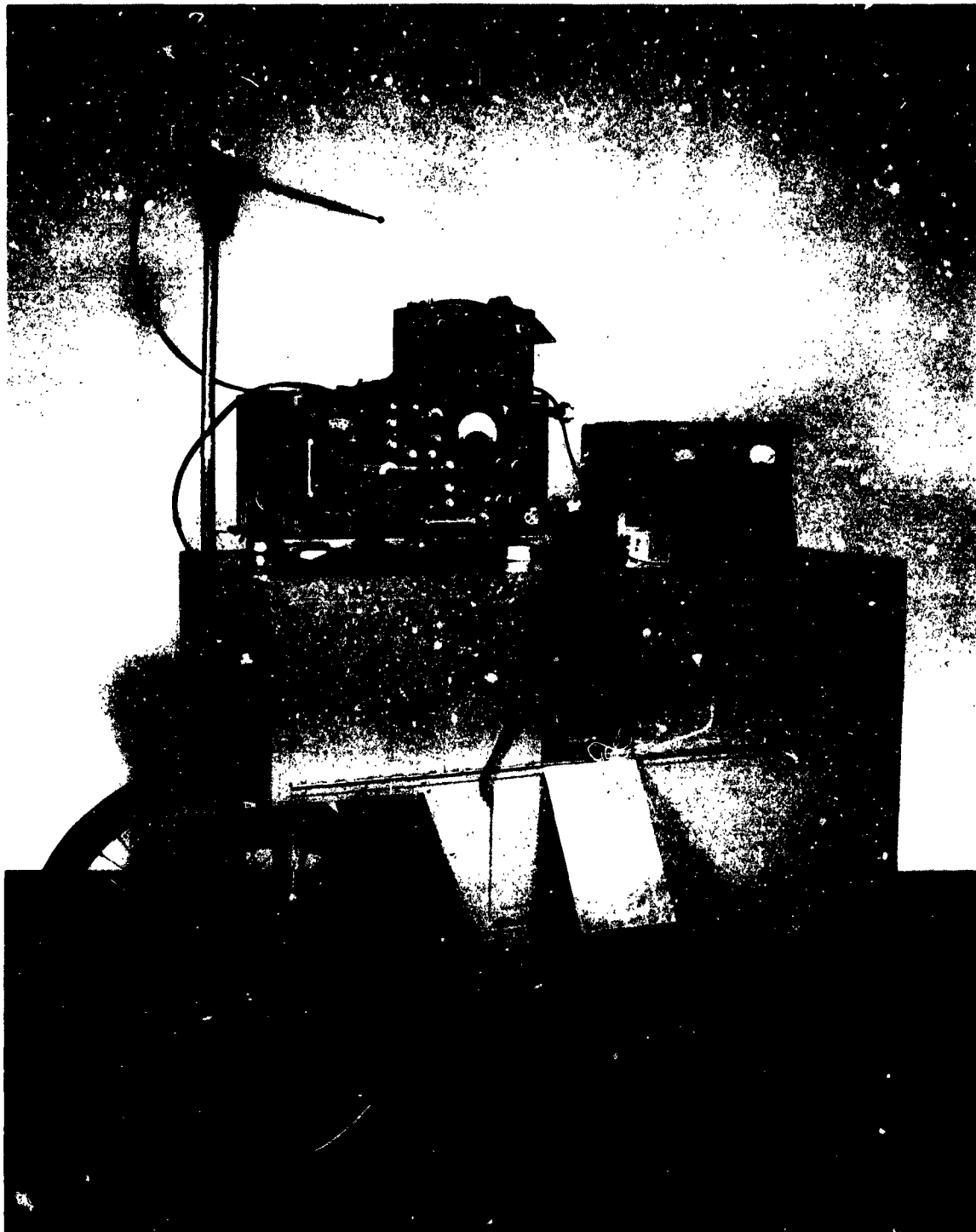
The data upon which this report is based were taken on the \_\_\_\_\_  
Model \_\_\_\_\_ Field Intensity Meter, Serial Number \_\_\_\_\_  
The date of most recent calibration of the instrument is \_\_\_\_\_ The  
data are the maximum values of radiations measured at each location. The original  
values of data taken may be found in Engineer's Notebook No. \_\_\_\_\_  
Pages \_\_\_\_\_

Date: \_\_\_\_\_ Signed: \_\_\_\_\_  
CERTIFYING ENGINEER

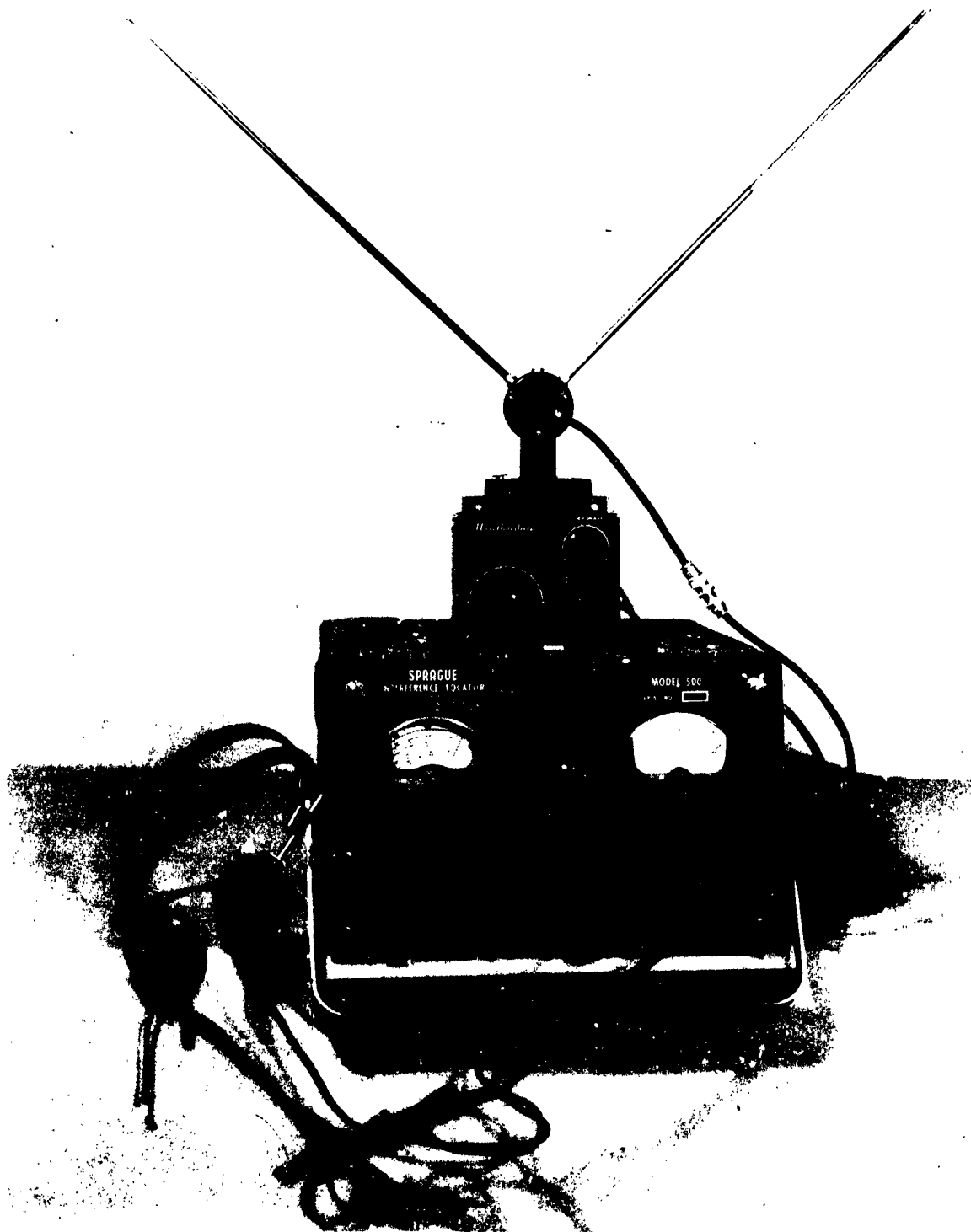
SLIDE NO. 16 - CERTIFICATION MANUAL NO-850-C PAGE 13



SLIDE NO. 18 - FIELD INTENSITY METER - STATION WAGON SETUP



SLIDE NO. 19 - FIELD INTENSITY METER - TEA WAGON SETUP



SLIDE NO. 20 - RADIATION INSPECTION TEST SETUP



## RFI/EMI AT THE CROSSROADS

Fred J. Nichols  
Genistron, Incorporated  
Los Angeles, California

Abstract. - Electromagnetic interference controls at this time are not compatible with our nation's newer electronics systems. Specifications, instrumentation, and controls are basically based on policies established for long range communications as typically used by aircraft and naval vessels. The excellent policies of these "near past" systems have not truly been upgraded into the policies required for today's electronic systems. We have examples of the necessary efforts of ECAC, the Electronic Proving Grounds at Ft. Huachuca, and the recently announced electromagnetic test facility for the Navy at the Navy Electronics Laboratory, San Diego.

These programs are aimed at defining the existing problem areas and will produce information to prevent a re-occurrence of the problems. However, these programs basically exist today because strong management policies were not established, or the existing policies of ten to fifteen years ago were not enforced.

A strong awakening is vitally needed today to prevent further collapse of existing specifications so that the output of ECAC, Ft. Huachuca and NEL is not obsolete when published. Further, strong EMI policies are immediately required at the planning stage of new electronic systems in order that they will be compatible with themselves as well as the environment in which they will be utilized.

Our modern electronic systems should be thought of in terms of full operational usage, just as a countermeasure is designed jointly with a new offensive device or system.

This paper will illustrate some typical examples of the crossroads that RFI/EMI is at and make recommendations to establish early EMI policies on a per program basis, as well as recommending EMI specifications on a per type of equipment or system basis, and on an intra and inter-system basis.

### I. INTRODUCTION

This is the Ninth Tri-Service Conference Electromagnetic Compatibility. In addition to these Tri-Service Conferences here under the sponsorship of the three military services and Armour Research Foundation, there has been a series of other radio interference and electromagnetic compatibility conferences held by Bureau of Ships, United States Navy in 1952. In the early 1950's there were several meetings on electromagnetic compatibility in regard to future weapons systems held by the United States Air Force under sponsorship of the then Air Research and Development Command. Therefore it is safe to say that we have been having nationwide conferences on electromagnetic compatibility for over ten years. In addition to those mentioned, the professional group on radio interference under IRE and most recently under IEEE has had five national symposiums on radio interference and electromagnetic compatibility, with the fifth of these meetings held this past June in Philadelphia.

With this tremendous depth of national symposia and efforts of those within the electromagnetic compatibility industry, I believe it is most appropriate that at this time we review exactly where we are, and where we are headed. I believe it is very necessary at this time because we are in a very fluid dynamic state of change in the military procurement of various weapons systems. We are in the twilight hours of weapons systems which were basically manually operated and/or manually controlled and in transition to weapons systems which are virtually automatic whether they are manned or unmanned. Also, we are on the threshold of major expansions by NASA into all forms of outer space exploration. We are, literally and figuratively speaking, at the crossroads, and from this and related conferences we will determine future policies in the direction of electromagnetic compatibility. Before we can adequately make good judgements leading to policy and operational decisions for the future, we must review our present status and prevent by design the same pitfalls that occurred in the past and are occurring at this time.

## II. REVIEW OF PRESENT STATUS

At the risk of much heated debate, it is my personal opinion that the electromagnetic compatibility program in the military and in industry at this time is not as far advanced as it was approximately three to five years ago. I realize that this may be an unpopular opinion, but let me have your attention on a few main points and we will review these and see if we are in general concurrence. Whether we are in concurrence or not as to the present status, I believe we will be in full concurrence as to future needs. The reason that I feel that our status, collectively speaking, at this time is not equivalent to three to five years ago is based on a review of history within the electronic industry from both a military and industry standpoint.

Three to five years ago, most of the large electronic prime contractors and/or their major sub-contractors were accustomed to working with specific agencies in each of the military services. For example, a given contractor could determine very easily the agency's name and the names of the personnel in these agencies in the Air Force, Navy, and Army. Most of us present could readily repeat names of these personnel and agencies and in the majority of cases on the first-name basis. Specifications at that time were more or less current, and various problems related to specifications, interpretations, or performance could be readily solved through the usual military procurement channels with these particular agencies and their personnel. The major segment of the electronic industry in this period of three to five years was on a sub-systems and component basis. Numerous companies had excellent facilities and highly proficient technical skills in the RFI and electromagnetic compatibility field. Most military weapons systems as stated were manned or manually controlled. The human element in these weapons systems was quick to spot and correct deficiencies in RFI or electromagnetic compatibility. Systems were not too complex in comparison to today's weapons and/or space systems and with the exception of some major systems it did not involve an appreciable penalty to build, measure and fix. Today the build, measure and fix approach is completely uneconomical from an engineering dollars and cents and operational viewpoint.

While we were in the midst of this electronic procurement cycle, many missile systems and other related complex electronic systems were in their very R & D stages.

This period of time was approximately seven to nine years ago from today, or some three to four years behind this three to five year period. Many military agencies set up policies for the forthcoming missile and other complex electronic systems. However, since these were R & D systems little or no recognition was given to electromagnetic compatibility. In a few years major air frame companies as well as other major electronic systems companies and/or their prime sub-contractors had established major missile and/or electronic divisions. Many well known companies who had RFI and electromagnetic compatibility capabilities in their parent plant found to their dismay that they had a complete void for electromagnetic compatibility in the growing missile and electronic system industry. Not only was there a void in many of these new major divisions but actually there were no plans in their corporate growth, corporate structure, etc. to set up electromagnetic compatibility capability. Much of this was due to lack of management familiarization with the need for electromagnetic compatibility at the design and systems integration level as well as to the lack of requirements in the procurement contracts from the military services. In many cases the contracts did reference electromagnetic compatibility specifications but the various services, on a completely independent basis among themselves and independently within a given agency, issued waivers of various types. This continued up to a point that some three to five years ago these new divisions became major identities and became the "tail that wagged the dog." These major companies by direction of the military, or through their inability to obtain successful systems integration found major problem areas in the electromagnetic compatibility areas.

These electromagnetic compatibility problems which arose were completely new problems to the electronic and/or missile systems management engineers. Many a hurried call went out to the parent company for electromagnetic compatibility help but it was then found in the parent company that the engineers who had been working on previous systems no longer in procurement had left the company of their own accord or were terminated. This happened because there was no basic policy or planning in these new complexes which called for job descriptions which could be adequately handled by electromagnetic compatibility engineers. Therefore companies which found themselves with excellent capabilities in the past now found themselves in a position with virtually no capabilities and they turned to outside contractors for assistance on a project-to-project basis. I do not feel that this is a basic fault of the industry, the military agencies or other governmental functions, or vice-versa. I feel that this was due to a collapse of communications within industry and within the military and between them. This can be readily shown as the EMI engineers in the military service were busy on their assigned tasks, and industry was more or less in the same position. The military personnel concerned with RFI as well as the industry had related problems including what they could most effectively do within a given budget. Many of these budgetary requirements came about, I feel, due to this collapse of communications between a new major segment of industry forming rapidly and the other segment of industry that was rapidly disappearing.

I feel that we can all learn something from these situations. And since "it has happened" let's examine the existing situation and look forward so that history does not repeat itself.

Considerable effort is being devoted toward today's and tomorrow's problems by the various governmental agencies. I believe that military and industry leaders have

recognized the collapse and we have seen considerable cooperation between the services to improve the status-quo and to more effectively direct our manpower and budget in the future, so that we do not have a repeat of some of the problems of the last several years. I feel the need is still great that we reach management of the governmental military and space agencies, and industry, to be given the opportunity to prove that electromagnetic compatibility is necessary, and that we can properly design, produce and deliver at cost on schedule a completely usable, functional and reliable weapon or space system, or related complex electronic system. For example, it does not benefit us to have various tight controls on an airborne weapons system and then completely relax all the controls on the ground controls and support system. This results in a compatible system only after we get the airborne weapons systems off the ground and in many cases the costs in malfunctions that occur in pre-launch and count down equipment have been so numerous that we see major areas of negligence with respect to electromagnetic compatibility, if we wish to use a little different term, complete systems integration and functional reliability. Due to a few typical areas which I will mention here, I do not feel that as a collective body, we have fully reached the respective managements within our own companies or within industry and/or the various governmental functions.

One typical example of a major step forward was that of the establishment of the Electromagnetic Compatibility Analysis Center or ECAC at Annapolis under the cognizance of DOD and the United States Air Force. The establishment of this has lead to DOD level recognition that the electromagnetic spectrum of emitters was such that the RF spectrum was over-crowded and that controls had more or less collapsed in procuring equipment that was fully compatible with other equipment. ECAC is a controversial subject among industry members and their spokesmen. I have been critical myself and have expressed my criticism in the past on ECAC. My criticism as such is not directed at ECAC itself or its people and their functions. In fact, my opinions of ECAC, and I think of others who are intimately familiar with their functional responsibility and job description are that they are exceptionally well staffed both from a military and civilian civil service standpoint with exceptionally qualified, dedicated public servants who, within their job descriptions are doing an excellent job. It must be understood that ECAC, as established by DOD, is in essence a collecting agency. As such they are collecting and reducing through computer techniques the spectrum signatures and the spurious radiation from various emitters used by the military services. The spectrum signatures are taken by the respective military services and this data is supplied to ECAC for data reduction and comparison and final presentation to military agencies and/or their contractors who have required this information. My particular criticisms and that of many others whom I have heard is that much of the work that ECAC is doing should be unnecessary. By this I mean that if the management of the military and industry had followed the policies recommended by the present ECAC management personnel, as well as the numerous authors from these stages here in Chicago, on controlling the harmonic content to the existing RFI specifications, ECAC would have a relative simple job of collecting spectrum signatures from these existing emitters.

If these existing emitters had followed the more or less simple procedures of the FCC on harmonic control, the task of making spectrum signatures and the task of reducing and analyzing data would be very simple indeed, compared to their present

activities. I think that it can be justly surmised that each of the military services and many of their contractors more or less ignored present and future compatibility problems of the given emitter. We have seen numerous cases where the requirements for control of harmonic content, or all stray emissions for that fact, have been waived or completely voided altogether on a given piece of equipment or on numerous equipments if we want to look over a period of years. If the existing emitters in the field met specifications such as MIL-I-6181, MIL-I-26600, MIL-I-1690, MIL-I-11748 or their equivalent specifications, we could have a fair degree of assurance that the second harmonic would be 60 or 80 DB below the fundamental and all other harmonics would be 80 DB or greater below the fundamental. If we had that situation today, I am sure that you could all appreciate that ECAC's task would be much simpler.

It must be pointed out that ECAC is a necessary function even if all emitters fully complied with all the military specifications, as there is still a very valid need among the various services to have a central agency that can describe the fundamental and all incidental or spurious emissions from a given emitter or emitter system. If all the equipments met all their respective specifications the data collecting systems would be much simpler, and the information more readily available at considerable cost savings to the military and industry alike. Also, the output of ECAC will always be a necessity inasmuch as there is valid need among the Tri-Services for information that will allow better frequency controls for tomorrow and the long-term future. In essence, ECAC will supply information, if this has not already been done, which type of service will lead to an equivalent of the FCC of the military services.

The electronic industry today needs to have the output of ECAC readily available, on a classified basis where necessary and on a public basis where security risks are not involved. In fact this output is needed urgently at this time so that management decisions can be made in the electronic industry so as not to produce a new generation of emitters which will completely void today's output of ECAC. Also, I feel that the results of the many spectrum signatures required to date from ECAC should result in an immediate tightening and enforcement of all existing stray radiation requirements for all existing emitters so that we are not opening new flood gates and establishing a complete second generation of emitters that will require a complete new set of RF spectrum signatures.

Many an industry spokesman has mentioned that ECAC would solve many of their major RFI and electromagnetic compatibility problems. This I believe is an erroneous feeling and its false hope of many and has led to both government and industry let down.

ECAC at the present time is working generally in the area of electromagnetic environment and I distinguish electromagnetic environment from electromagnetic compatibility as follows:

Electromagnetic environment is the RF environment that exists around any emitter or weapons system from RF energy released into/or propagated into a given area. Electromagnetic compatibility, on the other hand, is the complete set of conditions within a given weapons system that will assure that the weapons system is functional and reliable and will perform all the functions for which it was designed. We might say that electromagnetic environment

involves inter-systems problems whereas electromagnetic compatibility involves intra-systems problems. With this review of ECAC I do not feel that their immediate output is going to make any ICBM system fly any better, functionally work better in its initial test stage: It will not make the intra-systems of a submarine, ship, aircraft, etc. be any better. In fact, I feel, that ECAC at this time is working in some 10%-20% of the general total problem area in regard to the control of electromagnetic energy.

I do want to be sure that all of us collectively recognize that the intra-system electromagnetic compatibility problem is within a given military system or within a given industry. I don't see how we could establish an agency such as ECAC to be technically qualified and staffed to solve all of the intra-systems compatibility problems. Each individual agency and their contractors must take care of their intra-system compatibility problems. In other related compatibility areas such as the aerodynamics compatibility of all of the surfaces, projections, protrusions from a airborne item, we do not rely on outside areas for assistance nor do we ask for waivers for performance. Electromagnetic compatibility is just one more of the engineering design and performance requirements in a given system and should be treated as exactly thus.

Recognition of electromagnetic compatibility problems is demonstrated by the program at the Army proving grounds at Ft. Hauchucha, Arizona, or the Navy program now underway at the Navy Electronics Laboratory. All of these agencies, that is ECAC, Ft. Hauchucha, and the Naval Electronics Laboratory are spending a considerable part of their time to define the existing conditions and I believe that this group collectively knows that the "status-quo" is not as good as it should be. Therefore, appreciable effort is going into defining the existing conditions.

If you'll pardon my bluntness. I do not believe the best state of the art from an engineering standpoint and manufacturing standpoint has been anywhere near the fully utilized state that it could be in the government procurement cycle for electronic equipment. I think we all recognize that at any given time it was virtually impossible to get a waiver from a given branch of the military service while the other two services were granting them freely. At another period of time the cycle was reversed and another agency would not grant waivers where other agencies did. This has led to a collapse in the communication between industry and government, who after all is the customer and I'm sure that industry conforms to the ultimate wishes of the customer. I am sure that I am not giving the impression that everything is as black as the ace of spades. For I do not mean to do this. I want to establish the fact, that we have made mistakes, if we can call it this, in the past and that we should learn from the past and proceed in the future.

### III. PRESENT DAY PROBLEMS

Today we find that we are in a whole new complex set of problems and these particular problems are arising from new industries and new contractors who are totally unprepared to cope with the various electromagnetic compatibility specifications. There are many companies

in today's complex areas that are doing an excellent job in meeting overall requirements of MIL-E-6051 or major weapons systems, however for each major contractor that's doing an excellent job we find numerous others who are not. These companies who are not have not been burnt from a management or financial standpoint on electromagnetic compatibility and they are vulnerable in their supply situation to existing military procurement agencies. I would like to give some examples of this and trust that the message will be carried to the management in these companies' industries or government agencies. I believe that it is a fairly well-known fact in our particular industry, that is, those in the electromagnetic compatibility consulting industry, that our laboratories are filled with engineering test work. What type of test work is this? The majority of it I am reluctant to report is the "fix it" work. Today I feel that those in the EMC industry are still spending more time on the measurement and fix it work than they are in the design and elimination of electromagnetic compatibility problems. In addition to our laboratories being busy with the measurement and fix it work we have made various visits to the military procurement design and operational agencies to discuss these various compatibility problems with them and we find it rare to find their personnel at their home base. In fact it is with very high recurrence rate that we find that they are out of town on firefighting EMI problems.

We continually find the contractor has come to us six months too late. What was a very simple problem to correct in the design and prototype stage is now a major operational problem and even a greater redesign problem when cost and time are considered. We in the electromagnetic compatibility industry are continually educating people along these lines and as long as we have the management recognition within a company which is generally obtained by a company being burnt on a given contract, we find that these companies come to us early at their bid stage or early in their contract stage. EMC is readily obtained at a low cost and in many, many cases leads to a reduction in cost versus their former experience as the electromagnetic compatibility control program is such that most of the problems are recognized and solved at the design stage and this leads to a very early and successful systems integration and provides an exceptionally high functional reliability. Electromagnetic compatibility engineering is no different from any other field where an ounce of prevention is worth a ton of cure.

How, then, are we to convince our respective managers, whether in industry or in government, that the best possible fire department is one that never goes to a fire or the best possible EMC program is one where management recognizes that this is part of the normal design and manufacturing of a given electronic system and/or its components. Due to the numerous years of experience and the qualified personnel in this industry as illustrated by the attendance at this and other conferences, I feel that we have to make our efforts made known to particular segments of the government and industry in the problem areas that I will mention. These problem areas are illustrated in a few cases to show that we have not solved the communication problem of those with whom we work and/or those who establish policies within our industry and our governmental agencies.

One of the major problem areas which we see today exists in the general ground support areas in the total aerospace industry. We will see excellent control plans, engineering services and capabilities on the airborne vehicle within NASA and our military weapons

systems but find a complete collapse of electromagnetic compatibility in silos, block houses and other major ground support equipment areas. We are finding some recognition in the block house area and those involved with the prelaunch or countdown because of the necessity to get true "go" or "no go" signals. However, it has taken quite a bit of pioneering and educational effort to convince the engineers, contracting officers et cetera of this ground support equipment that electromagnetic compatibility requirements do apply to their equipment. We have heard the statement so many times quoted, "this is not airborne and therefore radio interference and electromagnetic compatibility does not apply to us." In many cases these statements come from those closely allied to or within the computer industry and the same engineer who makes the statement is in the next minute complaining that somebody's "off-on" transient makes his computer inoperative!

Inasmuch as I mentioned "computer" and in particularly at this point, "digital computers," I think all of us will have a smile from the numerous problems which we have encountered on digital equipment because of the extreme high level broadband level of interference voltages which they generate and their extreme vulnerability to transients of all types. I feel that the "ground" computer industry in many instances is not abreast to the equivalent engineer in the airborne computer industry. Those working on airborne computers from their experience in the ICBM field and prior to that in the aircraft field have found the necessity for electromagnetic compatibility whether their equipment was a radio emitting or receiving equipment or not. In any event computers readily malfunction under all types of transients and their basic methods of operation do generate appreciable energy throughout the radio frequency spectrum. The computers used on the ground, whether for the processing of data related to flight test work or the payroll computer down at the headquarters, all fall into a vulnerability area that needs to be examined more closely.

Another major problem area is the "never-never land" between the power engineer and the electronics engineer. We find today that, due to computers as mentioned above and communications systems used below a hundred KC, that there is a lack of firm definition of systems responsibility as to the proper control of stray energy in these frequencies. We find in many cases the harmonics of 400 cycle or other higher frequency power supplies appearing as interference at orders as high as the hundredth harmonic or in some cases even greater. When we fall into this condition that the harmonics from a power supply are occupying the spectrum with very high signal levels from 10 kc on up to several megacycles that the power engineer does not recognize nor does he know how to control these harmonics. He is not a filter engineer and surely he is not a transmission engineer. The transmission engineer on the other hand is an expert in the megacycle and higher frequency bands and has very little experience with considering power lines as a transmission line. The electromagnetic compatibility engineer, on the other hand, is fairly experienced in this field and can solve these problems fairly easily if he can get a meeting of minds among the power and electronic engineers as to whose responsibility this is and where the correction should be made and at what design level problems of this type should be assigned to in the future. To date the historical factors are that the power engineer gives very little consideration to harmonics above the third, fifth or perhaps as high as seven and the harmonics appearing at higher frequencies are really not his problem and are really basically those of the communication engineers. It is the age old problem "It's not my problem but yours."



A similar situation exists on large complexes where electronic equipment is deployed over a wide area. This is true in industry as well as military, in industry we find it in large processing plants such as refineries, chemical plants, etc. and the military we find it in block houses, missile tracking stations, or in various military bases where the communication equipment, tracking equipment and launch sites by necessity are deployed over great distances. Again we run into the problem of jurisdiction between electrical and electronic people. The major problem areas that we continually run into in this area is the lack of definition of a ground, or what the electrical, electronic and instrumentation engineer means by the word "ground". We encounter numerous problems where the placement of various conductors whether in trays, racks, suspended on messengers, an other types of installation, is wholly left to the electrical contractor, and the electrical contractor experience is completely lacking, as to any regard to electromagnetic compatibility. In fact, his total experience is limited to the National Electrical Safety Code, and as long as the building site inspector, whether military or state, approves the installation he feels that he has performed a satisfactory job, and I believe he is correct as he was not given any plans or specifications to guide him in his bidding or construction.

The number of cases that we have run into where power lines have been interlaced with high impedance lines, where teletype lines have been interlaced with instrumentation lines, etc. are far too numerous to illustrate here. We need, a clear definition as to what is an electronic installation and what is an electric or power installation. The same situation which I mentioned in regard to these large missile complex is also true with respect to the various silos, which are being built at this time on the ICBM Programs. The military procurement cycle on these at this time is such that one agency breaks down the specifications in such a way that an A & E contractor, who is generally only power oriented, designs the silo from a facility stand point. After the A & E has finished his respective specifications, the specifications are broken down into as many denominators as possible to favor the most numerous competitive bids.

The procurement then becomes one of a component or sub-system approach, and when the silos are completed they are fully integrated from a power stand point, but there is no consideration given whatsoever of looking at the electromagnetic fields created by the individual sections that have been put together for the power, light, heating, air conditioner, and other facilities to make the silos inhabitable. In numerous cases the electronic tenant, that is a missile system, its countdown, launch check-out equipment, etc. cannot live in the facility do to the failure to recognize electromagnetic compatibility. There have been contract awarded by the United States Air Force to various companies in our industry, to clean up this situation and many of the large contractors, that is the missile companies such as the prime contractor on the Atlas, Minuteman and others, have corrected this with their own in house technical personnel.

Another major area of concern is that within the ship building industry, where the ship building company, which is basically the structural manufacturer, has been modifying ships for telemetry and tracking useage or radar pick up, and our other patrol, and numerous other communication duties. These companies have found that

they are more or less on the overnight basis in the electronic system bases, as all of this equipment is being supplied and/or procured by them to mount or install within these various ships. This has lead to numerous compatibility problems in that the project managers on these projects do not allow for any possibility of problems to integrate the various equipment on to the end item, in this case the ship. I think it is somewhat a reflection against the electromagnetic compatibility engineers in general, that the years of know-how that existed in supplying electronic equipment to aircraft could not be utilized within a ship.

There are numerous other problem areas that could be mentioned, and one that comes to my mind quite readily are the various communications, advance warning stations, such as the Dew Line stations, etc. on our various outer perimeter defense systems. The use of shielded rooms is very common. These shielded rooms present quite a problem in themselves, in that they are invariably put together by structural people. The filters and other RF provisioning to utilize the room are supplied by power people and when the room is in essence ready for operation it is generally found that the room is completely unoperatable. This has been touched on by many on various articles in the trade magazines. Mr. John O'Neil of the Signal Corp, approximately twelve to eighteen months ago, wrote an excellent article expressing his and/or perhaps the United States Army view point in the various difficulties along these lines.

We collectively must reach some way to inform those in new industries coming into the military scope and those utilizing or contaminating RF Spectrum, in order that they may be aware of any possible electromagnetic compatibility problems that they may encounter, and we must tell them, that there are services available to supply them, if they do not have the in-house capability.

On the positive side of the ledger, we see major recognition by the governmental agencies in areas such as project HERO and project RAD-HAZ. These are major government activities as I'm sure you all are aware, that are concerned with the effects of the electromagnetic environment around the system. For example, in project HERO the initials themselves, HERO are derived from "Hazards, Electromagnetic Radiation-Ordinance" and RAD-HAZ from a contraction of radiation hazards. Generally speaking, as the name HERO indicates, this is concerned with the electromagnetic environment of various ordinance devices, and Project RAD-HAZ has to do with radiation hazards to personnel. I'm sure that you are all aware that there are also radiation hazards to equipment. Not that it will effect the failure rates as far as the components itself, but it may cause the equipment to work to other than its design specifications, and we have excellent examples of the environmental effects of electromagnetics field in the electronic counter measures field. There is, at the present time, other high order governmental recognition, such as in the area of secure communications, and other EMC plans, which are beyond the scope of this paper, to improve and correct existing conditions, and to prevent future EMC problems. It has always been my major concern by the expressions and illustrations shown here, that, before these long term plans and programs become wholly effective, to see that the existing situation does not further deteriorate.

#### IV. FUTURE RECOMMENDATIONS

In order that we can assist the total defense effort, through the conservation of the RF Spectrum to control the electromagnetic environment and to have intra and inter system compatibility, we must look at the total meaning of "how do we obtain electromagnetic compatibility?" This can only be obtained by looking at the total concept. This total concept consist of four major phases:

##### Phase I:

The black box component, chassis, or console level: such as equipment or sub-systems that would be covered by Mil-I-26600, Mil-I-6181D, Mil-I-16910, Mil-I-11748 and others. At this time I feel that 50% of our total compatibility problems lie in this Phase I category.

##### Phase II:

Intra-Systems Level: Here specifications such as Mil-E-6051, covers the intra-system compatibility problem, and much effort is being done today particularly within the Air Force at ASD, BMS, and SSD and the others in complying with specifications such as Mil-E-6051 or its equivalent. It is my feeling that 30% of the major compatibility efforts lie into this problem area, and when Phase I and II are concerned we now have encountered approximately 70%-80% of the total compatibility problems that we are confronted with at this time. Most field an operational compatibility problems are encountered at the Phase II level. However, in a large majority of cases the Phase II level problems are due to negligence of Phase I requirements.

##### Phase III:

Inter-System Compatibility: At this time there is no existing specifications requiring inter-system compatibility requirements by the military, nor do I know of any contractual requirements requiring inter-system compatibility. This would be the case typically as compatibility between a Minuteman, between Atlas a B-52 and a B-58, a Army Ground to Air Missile versus an Air Force Air to Air Missile, versus a Ship Launched Sea to Air Missile. We have seen individual system requirements within the governmental services requiring this but in very nebulous terminology because it is very difficult from the present procurement systems and the state of the art to state in advance the total contribution to the end electromagnetic environment about a given weapons system, will be known in advance, therefore, it would be extremely difficult at this time to state in RFQ or in contract terms what would be the compatibility problems between any two of the major systems that I have mentioned.

I feel that the problems in the Phase III are some 10% of the total electromagnetic compatibility. The reason I have selected the 10% is that if Phases I & II have been complied with the probability of the inter-system compatibility is very high and further that the total inter-system complex contributes little to the total RF environment.

##### Phase IV:

System to Environment Compatibility and Environment to System Compatibility: Examples of this would be that a given weapon or space system as mentioned is emitting stray and spurious energies, as well as fundamental energy, and the stray effects of

this is therefore contributing to the total RF environment. This one system to an unknown degree is contributing to the electromagnetic environment in a given area and this environment may cause reactions to other systems that is susceptible to these environments, therefore, having an environmental to systems compatibility problem. I feel that this is perhaps some 10% of the total compatibility area. The work of project HERO, RAD-HAZ, ECAC, Ft. Huachuca, etc. is in Phase IV. Phase IV is obviously necessary at this time because there has been some deteriorations of Phases I, II, and III respectively. But I again would like to repeat that unless emphasis is placed in Phases I, II, and III, Phase IV will never be under control.

I think it is appropriate at this time that I state that the four levels or the four phases of electromagnetic compatibility are not new. In fact, I can make no claim whatsoever as to the originality of these statements, or the four level concept, in as much as this information was presented to the industry and military in 1950 or 1951, through the Rand Company, to all existing and future electronic and/or missile manufacturers who were interested enough to attend symposiums sponsored by the United States Air Force at the Rand Corporation in Santa Monica, California. I had the honor of attending this meeting, which many then considered was really in the "wild blue yonder" and was many, many years in advance of its time. The gentlemen who made these statements, I believe, are among us today, or their representatives, in as much as the originator of this, to the best of my knowledge was Mr. Paul Georgi, then of Headquarters, One Detachment, Air Research Development Command and another distinguished gentlemen in our field, Colonel Woolwine, along with other RFI noteables such as, N.D. Flynn, Major Al Blue, of the United States Air Force, and many others were present when this information was presented to major industry and government leaders.

The four levels of compatibility are just as valid today, if not more so, when they were made in the above referenced meetings.

## V. CONCLUSIONS AND RECOMMENDATIONS

Numerous recommendations could be made as to improve the situation, however, in bringing this to a conclusion I think a few major points should be briefly mentioned. And if these major points are recognized, the other recommendations would merely be details of the major items.

1. Recognition is essential for the long term compatibility program of military, industry, and space programs. The four levels of compatibility requirement must receive the full recognition. Today by the programs as stated by this paper in the RF environmental area is excellent. We have to immediately embark on the other three levels with somewhat of the philosophy of the weak link in the chain. Phase I. continues to be the weakest link in the chain with Phase II, III, and IV being other links, but greater strengths when compared to Phase I. When Phase I is fully under control, Phases II, III, and IV will become much less of a problem. When Phases I and II are under control Phases III and IV become less of a problem. When Phases I, II, and III are fully under control Phase IV will be a minor problem.

2. Control Plans or Specifications. It is essential in the weapons system under procurement, or future procurement, be procured in such a manner that electromagnetic compatibility receives full recognition as one of the design requirements and one of the functional objectives of this system. This can be reached by control plans and/or adequate specifications. I do not believe that specifications ever can be written which will fully acknowledge the problems of tomorrow's systems, however, existing specifications with control plans, just as new items are designed, will reflect the needs of the new systems. I feel that all of the services should give the same emphasis to control plans for electromagnetic compatibility as is given today by only part of the governmental agencies. The specification area always needs correction and much work is being done today particularly at ASD in the near issuance of Mil-Std-826. I feel that specifications within the other services and NASA need to be upgraded to reflect the requirement of Phases III and IV, or Phases I and II need to be tightened in such a way that phases III and IV will be more or less automatically met.

3. Instrumentation: There is much discussion today that the so called RFI meters and instrumentation are out of date. I do not wholly agree with this concept, we can obtain full systems compatibility without using RFI meters as such and can perform this compatibility in terms of the equipment's own receiving and/or emitter equipment. I feel that better instrumentation is necessary to meet all of the conditions of Phase I and Phase II. Phases III and IV as illustrated in this paper need to be thought of more in terms of the end system performance rather than RFI or Field strength instrumentation.

4. Central Control; The establishment of "central policy agency" within the government to coordinate the policies and requirements of Phases I, II, III and IV.

Perhaps this is under consideration today by agencies such as ECAC, if not ECAC or an equivalent agency should be established or expanded to coordinate the requirements on a Tri Service bases of Phases I, II, III and IV. Each of the individual services then should take this policy direction and come up with the necessary requirements for their particular systems in order that the systems itself will have full compatibility and that an Air Force, Army Navy or NASA system will not violate the environment that exist today or is planned for the future of other services systems. We have a somewhat similar example to this governmental agency in the industry today in regard to the FCC, however, the problems of the military and space agency are considerably different than the scope of the FCC. The basic policy concept, I believe is one of the same and that is to have a central agency determining policy for electromagnetic compatibility and spectrum conservation among all government services and NASA.

Each of us here today, can help in "bringing" bits and pieces" of this message or related messages in your terminology for your own individual cases to the management attention, not only in your company or individual industry, but to all industries on a

collective basis. I heard "Rupt" Haskens of NRL, at one time mention in the corridors here " that we spend too much time waltzing each other". This I believe hits the nail on the head. We will not in the immediate future, or in the long run, serve our nation in the electromagnetic compatibility area by "waltzing" each other or convincing each other of our respective needs. Doctors have never cured a patient by discussing them with each other. However, the discussion with each other does give us common outlooks and common objectives, so that we collectively speaking will have the same general view points to curing this patient. We can make immediate steps by offering our services as speakers to other engineering societies, to attend briefings wherever possible, etc. in order that we may reach higher levels within the governmental agencies who are in essence the ones that establish policy for electromagnetic compatibility. I would like to feel that the major part of our effort perhaps, today is at a third tier of operation. This third tier of operations in the governmental system would be more or less a kin to a system as follows:

Tier 1. would be the requirements, planning for governmental use of the electromagnetic spectrum some five to ten years in advance.

Tier 2. would be these same governmental agencies, who are at the present time developing specifications, design objectives, etc for next years weapons and space system.

Tier 3. is the existing weapons systems and/or space systems that are at today's operational level, and are "fire fighting" today EMC problems.

I think it is obvious that the majority of us are working to some 90% of our own capabilities in the Tier 3 level, as this is where the existing electromagnetic compatibility problems exist, and some 10% divided into Tier 2 and Tier 1. We are working Tier 2, but need more activity in Tier 1.

ECAC and the other agencies are working on today's problem, yet the work on today's problem has given us the foundation and know-how for tomorrow's problem. We need to be more active immediately into the Tier 2 level for next years systems, and with this background we will be invited into the Tier 1 level.

## THE BEHAVIOR OF NONLINEAR MIXING

R. D. Trammell, Jr., and E. W. Wood  
Engineering Experiment Station  
Georgia Institute of Technology  
Atlanta, Georgia

(Work Done Under Contract With the U. S. Army  
Electronics Research and Development Laboratory)

Abstract. - The purpose of this paper is to discuss the basis for the formation of spurious products and to show methods for prediction of troublesome spurious responses. Considerable research has been expended toward these goals for a period in excess of ten years. Many investigations in this field begin with the normal binomial expansion of two summed sine or cosine functions and eventually attempt to show that the mixer rigorously follows these equations in the formation of spurious products. Many devices and methods have been employed for demonstrating that mixers behave according to the assigned mathematical model, and more recently researchers have accurately predicted the amplitudes of the spurious products generated by certain mixer types up to about the fifth order of generation.

The majority of experimental evidence demonstrates that, for the conditions established during the experiment, the mixer will follow the mathematical model. Unfortunately, devices for reducing spurious products based upon the theories so established do not always function as intended. In fact, the data presented by any given investigator may not agree with the data extracted by another, even though the conditions for both experiments were believed to be established in the same manner.

This paper discusses the effects of injected local oscillator and input signal harmonics, emphasizes their relative importance in producing responses, and demonstrates their experimental effect on mixer measurements. Possible sources of such harmonics are outlined.

The absolute response level is shown to affect the relative spurious response rejection measurements for responses having large  $q$  values.

A reliable mixer response prediction method based on sample response measurements is presented. Its application to receiver spurious response prediction is discussed along with associated pitfalls and limitations. The basis for the method and the various relationships for its use are examined. Experimental results illustrate the accuracy of the prediction procedures to the tenth order of generation.

### I. INTRODUCTION

The process of combining two unrelated signals to obtain a third signal at the sum or difference frequency has been employed in electronic devices for many years. The circuits which accomplish the combining process generally produce unwanted products as well as the required signal. The unwanted products are generated by nonlinearities within or prior to the mixing circuit and are classified as products of nonlinear mixing.

Linear mixing may be defined as that form of mixing which produces only the sum and difference frequency of the two input fundamental frequencies. It produces no harmonics or other mixing products and is the desired, but thusfar unattained type of mixing. The analog multiplier more nearly approaches a truly linear mixer than any other known device, but only at very low frequencies of operation.

Nonlinear mixing is the form of mixing presently used for heterodyning two frequencies to obtain the sum or difference frequencies. The resultant by-products of such mixing are a never ending annoyance to the design engineer and to the receiver operator. Considerable effort has been directed toward the problems of nonlinear mixing for more than ten years. The results of many investigations are inconclusive and suppression devices based on other studies are not entirely effective. In many cases, the data obtained by one observer will not conform to that taken by another, even though the test conditions were believed to be identical.

## II. MIXER MEASUREMENT

The greatest problem in establishing a mixer's conformity to current theory appears to stem from the difficulty in obtaining accurate experimental data. Many factors contribute to measurement error when the data are to reflect the action of the mixer nonlinearity alone. Depending upon relative rejection, the injected harmonics of either the local oscillator or the input signal can have a highly detrimental effect on the mixer measurement accuracy. The harmonics of the smaller signal are particularly troublesome in this respect.<sup>1</sup> Tables I and II show the changes in measured rejection when the harmonics of the two input sources were introduced separately into a diode mixer system. It is noted that the harmonics of the local oscillator source are not significant response generators for the 1N82A diode mixer on which the data were taken. This is due to the fact that the mixer generates a much greater level of spurious responses than do the harmonics injected by the local oscillator. Such would not always be the case if the harmonic level of the local oscillator source were greater or the spurious response levels of the mixer were lower. A high degree of harmonic rejection must be obtained for accurate measurement of the mixer nonlinear characteristics.

Another possible source of harmonic injection is created by the use of filters to reduce the harmonic level injected by the signal generators. The stop-band impedance characteristic of the filters is such that nearly all incident power is reflected back along the input path. This condition is usually true at both the input and output terminals of the filter and causes any harmonics coming from the mixer to be reflected back into the mixer. Since the mixer generates substantial harmonic levels related to either input signal, the filters could cause simulated harmonic injection by reflection. The effects of these reflected harmonics can be reduced by the addition of attenuators between the filter and mixer. Other sources of mismatching can be similarly treated to prevent the reflection of mixer generated harmonics.

A similar error contribution can be introduced through intermodulation products created in either the signal generators or the instrument used as an IF detector. Care must be taken to properly isolate the two signal input sources and the detection instrument in order that intermodulation will not be a factor in the measurements.



Another source of measurement difficulty results from the various frequencies selected for the test. Under certain conditions, two spurious mixer products may fall simultaneously within the detector passband and the reading obtained will usually correspond to the larger of the two. To illustrate this phenomenon, assume that 10 Mc, 11 Mc, and 1 Mc are chosen as, respectively, the local oscillator, input signal, and intermediate frequencies. Further assume that the level of the (2, 7, +) response is to be obtained. The first numeral designates the local oscillator harmonic,  $p$ , the second numeral designates the signal harmonic,  $q$ , and the sign designates the sum or the difference frequency of the given product. The input signal frequency is set to 3 Mc and the reading is made. Under the above conditions, the investigator has probably obtained an erroneous measurement since the (2, 7, +) and the (1, 3, -) responses both occupy the 3 Mc frequency position. The (1, 3, -) response level is generally about 20 db greater than that of the (2, 7, +) response; thus the former response will predominate at the common frequency.

The fact that the level of a given ( $p, q, \pm$ ) response pair is independent of sign (for a simple nontuned mixer) enables one to measure the (2, 7, +) response by measuring the (2, 7, -) response. The only difference lies in their relative frequencies of occurrence. With a suitable choice of sign, a unique frequency is found at which the true level of the response may be measured. A considered choice of operating frequencies is also helpful in this respect.

### III. MIXER THEORY

The mixer is essentially a nonlinear element functionally connected into the electronic circuit. As a nonlinear element, the mixer may be described mathematically as a polynomial of degree  $n$ . Substitution of the representation for two summed cosine waveforms into the mixer polynomial yields the multiplicity of frequency terms normally associated with nonlinear mixing.<sup>2</sup> The amplitude coefficient of each frequency is a series of terms involving either odd or even orders of the mixer polynomial. The usual approach is to assume that only the lowest order of generation for a given frequency is significant, thus greatly simplifying the problem. If the mixer is operated at an appropriately low level and the bias is properly established, good conformity to this theory may be obtained from the experimental data. At high levels of operation, the assumption no longer holds and poor conformity is the result.

### IV. MIXER PREDICTION

The mixer prediction system discussed hereafter is almost entirely divorced from the representative mixer polynomial and the search for the polynomial constant coefficients usually associated with mixer prediction. This method utilizes a representative sample of measured mixer responses to predict the levels of all responses whose order is represented. The method is not as sensitive to bias or overdrive conditions as are former methods of prediction. Though based on the same simplified system of lowest order generating terms as former methods, this system actually arrives at an effective set of polynomial constants and an effective local oscillator to input signal power ratio. The effective polynomial constants are never actually derived because the system utilizes them in the form of a sample measured response

representative of the associated order. However, if the absolute power level of either input to the mixer were known, these effective constants could be calculated.

The procedure for response calculation is repetitive and can be learned very easily. Essential to the process, however, is a set of constant coefficients which are different for each order, but which are readily produced. These constant coefficients are associated with the primary or lowest order generating term producing a given response. They are computed by dividing each term of a Pascal's triangle of binomial coefficients by the factor  $2^{(n-1)}$ , where  $n$  is the polynomial term order or the value of  $(p + q)$ . These coefficients may be arranged in triangular form as shown in Table III. For use in the prediction method, the coefficients are expressed in decibels as shown in Table IV.

#### Triangle Relationships for Prediction

The mixer response prediction method is based on certain ratio relationships existing between responses of common order, i.e. those of the same row in the triangle of response factors shown in Table V. The ratio between the adjacent members of a row of responses whose fixed constants have been removed is the ratio of the input signal level to local oscillator level. This is extended to include the ratio between any two members of the same row if the ratio of the input signal level to local oscillator level is raised to a power determined by the spaces separating the two members of the row. These relationships are easily verified using the triangle arrangement of response factors shown in Table V. The fixed constants have been removed from the factors shown in this table and are those constants represented in decibels in Table IV. The relationships are seen to remain true only for constant input levels such that  $e_p$ , the local oscillator voltage, and  $e_q$ , the input signal voltage, have the same respective value in each response within the row.

A relationship between rows along the diagonals is also seen to exist when the input levels are the same respectively in all rows. Along diagonals of constant  $q$ , the ratio of adjacent responses is found to equal the ratio of the order coefficients,  $K_n$ , either multiplied or divided by  $e_p$ . Along diagonals of constant  $p$ , the ratio of adjacent responses is found to equal the same ratio of order coefficients,  $K_n$ , multiplied or divided by  $e_q$ . This relationship can be carried to nonadjacent responses in a diagonal simply by raising  $e_p$  or  $e_q$  to the power whose value equals the spaces separating the two responses.

It is obvious that the ratio established is identical for any two responses lying in the same two rows regardless of the  $p$  or  $q$  diagonal in which they both lie. The order constant,  $K_n$ , is the same for each response in a given row, and the spaces along any diagonal separating any two given rows is a constant. This fact provides a second method of determining the unknown responses since it allows calculation between rows rather than along rows. In essence, the relationships between rows provide a cross-check on the calculation made along rows and vice versa. If a measurement error is

made or errors are accumulating, a check calculation using the second method will generally indicate that such an error exists. The second relationship does not reduce the number of measurements required for prediction unless the relative values of the order coefficients are known prior to the experiment and either  $e_p$  or  $e_q$  is accurately known at the point of the mixer non-linearity.

An example of the relationships discussed above is presented that considers the fourth, fifth, and sixth orders of generation as shown in Table V. The responses and harmonics (4, 0), (3, 1), (2, 2), (1, 3) and (0, 4) belong to the fourth order of generation and consist, after removing the constant, of the respective factors presented in Table V. The responses and harmonics of the fifth and sixth orders of generation may be similarly designated and consist of their respective values shown in Table V.

Consider the ratios of the fourth order;

$$\begin{aligned} \frac{(4, 0)}{(3, 1)} &= \frac{e_p^4 K_4}{e_p^3 e_q K_4} ; & \frac{(3, 1)}{(2, 2)} &= \frac{e_p^3 e_q K_4}{e_p^2 e_q^2 K_4} ; \\ \frac{(2, 2)}{(1, 3)} &= \frac{e_p^2 e_q^2 K_4}{e_p e_q^3 K_4} ; & \frac{(1, 3)}{(0, 4)} &= \frac{e_p e_q^3 K_4}{e_q^4 K_4} ; \end{aligned} \quad (1)$$

all of which reduce to the ratio  $e_p/e_q$ . Consider the ratios separated by two positions in the triangle row;

$$\begin{aligned} \frac{(4, 0)}{(2, 2)} &= \frac{e_p^4 K_4}{e_p^2 e_q^2 K_4} ; & \frac{(3, 1)}{(1, 3)} &= \frac{e_p^3 e_q K_4}{e_p e_q^3 K_4} ; \\ \frac{(2, 2)}{(0, 4)} &= \frac{e_p^2 e_q^2 K_4}{e_q^4 K_4} ; \end{aligned} \quad (2)$$

all of which reduce to the squared ratio  $e_p^2/e_q^2$ . The example can be carried to other spacings and other rows with the result that the ratio of signal level to local oscillator level raised to the power designated by the spaces separating the responses is always obtained.

Consider now the ratios of responses along constant p diagonals;

$$\frac{(4, 0)}{(4, 1)} = \frac{e_p^4 K_4}{e_p^4 e_q K_5} ; \quad \frac{(3, 1)}{(3, 2)} = \frac{e_p^3 e_q K_4}{e_p^3 e_q^2 K_5} ;$$

$$\frac{(2, 2)}{(2, 3)} = \frac{e_p^2 e_q^2 K_4}{e_p^2 e_q^3 K_5}; \quad \frac{(1, 3)}{(1, 4)} = \frac{e_p e_q^3 K_4}{e_p e_q^4 K_5}; \quad (3)$$

all of which reduce to the ratio  $K_4/K_5 e_q$ . The ratios of responses along constant  $q$  diagonals;

$$\begin{aligned} \frac{(4, 0)}{(5, 0)} &= \frac{e_p^4 K_4}{e_p^5 K_5}; & \frac{(3, 1)}{(4, 1)} &= \frac{e_p^3 e_q K_4}{e_p^4 e_q K_5}; \\ \frac{(2, 2)}{(3, 2)} &= \frac{e_p^2 e_q^2 K_4}{e_p^3 e_q^2 K_5}; & \frac{(1, 3)}{(2, 3)} &= \frac{e_p e_q^3 K_4}{e_p^2 e_q^3 K_5}; \end{aligned} \quad (4)$$

all reduce to the ratio  $K_4/K_5 e_p$ . The ratios along constant  $p$  diagonals between the fourth and sixth orders of generation;

$$\begin{aligned} \frac{(4, 0)}{(4, 2)} &= \frac{e_p^4 K_4}{e_p^4 e_q^2 K_6}; & \frac{(3, 1)}{(3, 3)} &= \frac{e_p^3 e_q K_4}{e_p^3 e_q^3 K_6}; \\ \frac{(2, 2)}{(2, 4)} &= \frac{e_p^2 e_q^2 K_4}{e_p^2 e_q^4 K_6}; & \frac{(1, 3)}{(1, 5)} &= \frac{e_p e_q^3 K_4}{e_p e_q^5 K_6}; \end{aligned} \quad (5)$$

all reduce to the ratio  $K_4/K_6 e_q^2$ . Carrying the example to other rows and diagonals results in the findings discussed earlier.

#### Prediction Procedure

The entire response prediction procedure is computed using expressions in decibels. The resultant operations are simple algebraic additions, and multiplication or division by integers. Although there are other procedures than will be given here,<sup>3</sup> the best results thusfar have been obtained with the following method.

The measured data required to predict the spurious response levels are the levels of responses having  $q = 1$  for all orders which will be predicted and the  $(1, 2)$  response level. These data are obtained in the manner used to obtain spurious response levels for communications receivers, i.e. with a common response level at the intermediate frequency.

The triangle response relationships discussed previously depend on a constant input level rather than a constant output level, so that data must be converted to the constant input form prior to the calculations. This is most easily accomplished if the data are first established as rejections by subtracting each response level from the value of the  $(1, 1)$  response. The

resulting values are the changes in decibels required to lower the respective spurious response input levels to the input level of the (1, 1) response. The associated output level will be altered by a factor of  $q$  times the change in input level. The constant output rejection of a spurious response times the  $q$  value of the spurious response therefore yields the constant input response rejection which is required for calculation.

The first step in the calculation process is that of subtracting from the converted measured response levels the respective values in Table IV. This removes the constant coefficients, allowing the ratios of any two adjacent responses of the same generating order (row) to be equal. With the ratio of signal level to local oscillator level easily determined by subtracting the converted (2, 1) response rejection from the converted (1, 2) response rejection, all responses belonging to the generating orders represented are readily calculated in the constant input form. The common ratio is added successively to the value of the representative response of the given order to yield the value of the next adjacent response. The respective values of Table IV are added and the data are returned to the constant output form by reversing the procedure used to convert to the constant input form. Since the data are still in terms of rejection, the constant input value for a given spurious response indicates that number of decibels required to raise its level to that of the (1, 1) response. This value divided by the  $q$  of the response is the number of decibels that the input level must change to raise the response level by the desired amount. It is the required constant output rejection value for the response.

Figures 1 and 2 show plots of response density versus decibel error for the predicted response levels of a 1N82A diode mixer and a 1N21B diode mixer. Triangle arrangements of the predicted and measured response rejections are shown in Tables VI and VII respectively. These data are typical of the results possible with the above method of response prediction. Measurements were made on the diodes using the circuit shown in Figure 3. The local oscillator level at the diode anode was +2 dbm (50Ω) in each case and the diode conversion loss was nominally 6 db at the (1, 1) responses.

The entire prediction scheme can be expressed as a generalized equation representing the rejection value of any chosen response:

$$R_{p,q} = M_{1,1} + \frac{q-1}{q} M_{2,1} - 2 \frac{q-1}{q} M_{1,2} - \frac{1}{q} M_{(n-1),1} - K_{p,q} \quad (6)$$

$R_{p,q}$  = Rejection to the (p, q, ±) responses in db.

$M_{1,1}$  = Measured value of (1, 1, ±) responses in dbm.

$M_{2,1}$  = Measured value of (2, 1, ±) responses in dbm.

$M_{1,2}$  = Measured value of (1, 2, ±) responses in dbm.

$M_{(n-1),1}$  = Measured value of [(n-1), 1, ±] responses in dbm.

$n = p + q$

$K_{p,q} = (C_{p,q} - C_{(n-1),1})/q$

$C_{p,q}$  = Response constant from Table IV for (p, q, ±) responses.

$C_{(n-1),1}$  = Response constant from Table IV for [(n-1), 1, ±] responses.

The generalized equation can also be written to express the absolute response level for the system sensitivity:

$$A_{p,q} = 2 \frac{q-1}{q} M_{1,2} - \frac{q-1}{q} M_{2,1} + \frac{1}{q} M_{(n-1),1} + K_{p,q}. \quad (7)$$

$A_{p,q}$  = Absolute response value in dbm.

The generalized error function for the system,

$$E_{p,q} = M_{p,q} + \frac{q-1}{q} M_{2,1} - 2 \frac{q-1}{q} M_{1,2} - \frac{1}{q} M_{(n-1),1} - K_{p,q}, \quad (8)$$

can be written in terms of the measurement accuracy,  $\pm e$  db:

$$E_{p,q} = \pm e \pm \frac{q-1}{q} e \mp 2 \frac{q-1}{q} e \mp \frac{1}{q} e. \quad (9)$$

In the limit as  $q \rightarrow \infty$ , the maximum possible error is  $\pm 4e$  db. Lower values of  $q$  yield successively less possible error. Actually, the absolute maximum possible error is only  $\pm 3e$  db since the error in measuring the absolute response level is considered in equation (9). The limiting case for equation (9) indicates the maximum differences to be expected between measured and predicted values.

#### Applications

The prediction method is quite versatile and is useful in both the design and measurement of receiving equipments or other nonlinear devices. The method's application to design is significant in that the spurious response rejection can be obtained for different sensitivity levels than that at which the sample measurements are made. The ratio of signal level to local oscillator level is changed by that number of decibels required to change from the old to the new sensitivity level and the computation carried out with the new ratio. Table VIII shows the calculated relative spurious response rejections for the 1N82A diode mixer with a 10 db increase in detector sensitivity. A comparison of these values with those shown in Table VI indicates the dependence of spurious response rejection on relative receiver sensitivity. The relative variation of response rejection with changes in the detector sensitivity is dependent on the  $q$  of the response. Figure 4 shows the normalized envelope curve which relates this fractional change in response rejection to the value of the response  $q$ . A knowledge of this fact is essential to proper receiver design and measurement.

The mixer spurious response prediction method may be directly applied to receiver spurious response predictions provided that certain precautions are observed and certain conditions are met. It is obvious that the preselector of the receiver must be accurately measured for its relative attenuation at different frequencies in order that the effects of the preselector may be removed before the data are applied in the prediction method. The data are taken and the mixer response rejection values are calculated by the methods previously considered. The preselector rejection value at each response is then added to the respective mixer rejection value to give the overall receiver rejection to any response. No experimental data are available on receiver

response prediction, but several factors are known which will affect measurements and calculations for certain receiver types.

In double or triple conversion receivers, the IF amplifiers may produce harmonics which will interfere with second and third mixer measurements. Receivers having no RF amplification stages and only single conversion present no immediate problems other than those of measuring the preselector and mixer characteristics. The addition of RF amplification without low-pass filtering prior to the mixer may introduce sufficient harmonic content to influence the response measurements. Overloading the RF amplifier may also affect the results of the prediction procedure as well as the spurious response bandwidth (SRB).

The SRB for any given spurious response is equal to  $\frac{BW(IF)}{q}$  for the ideal IF passband described in Figure 5. For the IF passband represented in Figure 6, the SRB for any given spurious response is the same as the IF bandwidth at any response level. Since most IF selectivity curves are neither triangular nor rectangular shaped, the actual SRB lies somewhere between  $BW(IF)$  and  $\frac{BW(IF)}{q}$ . The prediction procedure for spurious response levels described in this paper supplements established frequency analysis methods<sup>4</sup> for determining the actual SRB, providing RF overload does not occur. If an RF overload condition exists, the measured SRB for most receiver spurious responses will tend to approach that of  $\frac{BW(IF)}{q}$  since more relative input power is needed to excite a spurious response to a prescribed response level.

## V. CONCLUSIONS

Harmonics of either input signal to a mixer can have considerable effect on spurious response generation and particularly on spurious response measurement accuracy. The input signal harmonics of the smaller signal are known to have a far greater influence on spurious response generation than those of the larger signal. The relative importance of harmonic response generation is dependent on the level of mixer spurious response generation.

Spurious response prediction using the method discussed in this paper is promising but still rather inaccurate in some cases. The relationships between triangle rows has not been fully explored and the application to actual receivers has not been attempted. Further investigation is necessary to determine the usefulness of the prediction method and to improve its accuracy. The procedure must be applied to systems of more than one nonlinear element and thereafter to communications receivers. These investigations should eventually culminate in methods for improved spurious response rejection.

## ACKNOWLEDGEMENTS

The contents of this paper are a result of Contract DA 36-039 AMC-02294(E) with the U. S. Army Electronics Research and Development Laboratory.

## REFERENCES

1. E. W. Wood, R. D. Trammell, Jr., C. W. Stuckey, H. W. Denny, E. E. Donaldson, Jr., and R. M. Cook, Georgia Institute of Technology, Engineering

Experiment Station, Electronic Equipment Interference Characteristics-Communication Type, "Quarterly Report No. 1, Project A-678," Contract No. DA 36-039 AMC-02294(E), p. 71, 15 February 1963 to 15 May 1963.

2. R. N. Bailey, E. W. Wood, R. D. Trammell, Jr., and J. R. Walsh, Jr., Georgia Institute of Technology, Engineering Experiment Station, Electronic Equipment Interference Characteristics-Communication Type, "Final Technical Report, Project A-543," Contract No. DA 36-039 sc-87183, p. 117, 1 September 1961 to 15 February 1963.
3. E. W. Wood, R. D. Trammell, Jr., C. W. Stuckey, H. W. Denny, E. E. Donaldson, Jr., and R. M. Cook, Georgia Institute of Technology, Engineering Experiment Station, Electronic Equipment Interference Characteristics-Communication Type, "Quarterly Report No. 1, Project A-678," Contract No. DA 36-039 AMC-02294(E), pp. 63-103, 15 February 1963 to 15 May 1963.
4. E. W. Wood and R. N. Bailey, "The Spectral Behavior of Spurious Responses," 1963 IEEE International Convention Record, Vol. 11, Part 8, pp. 123-135, 1963.



TABLE I  
ALTERATIONS TO SPURIOUS RESPONSE LEVELS BY INJECTION OF  
SIGNAL SOURCE HARMONICS

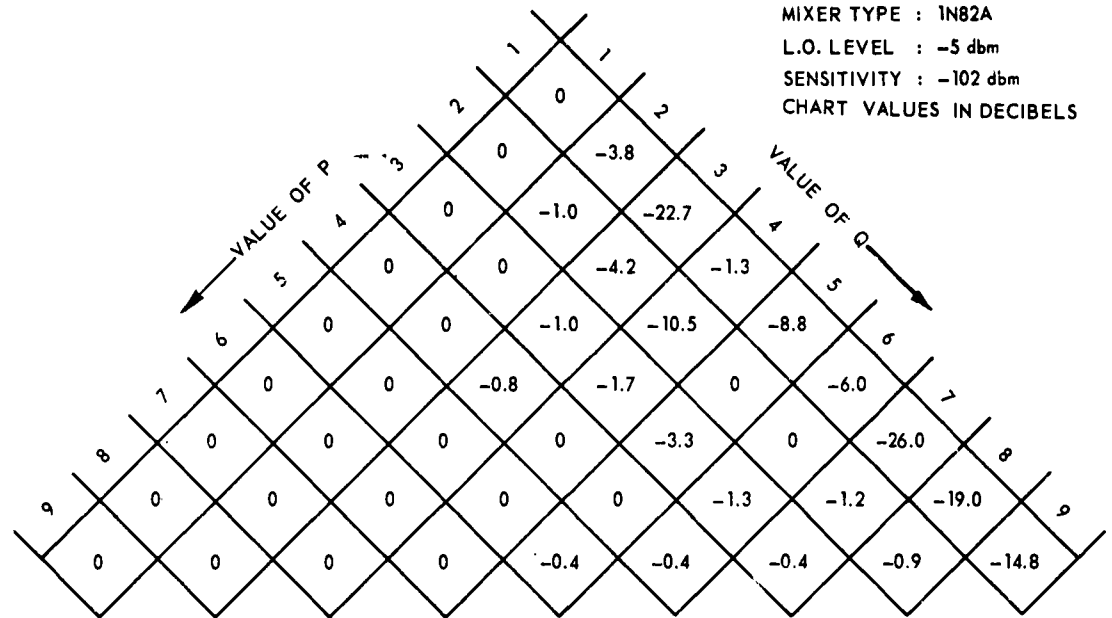


TABLE II  
ALTERATIONS TO SPURIOUS RESPONSE LEVELS BY INJECTION OF  
LOCAL OSCILLATOR SOURCE HARMONICS

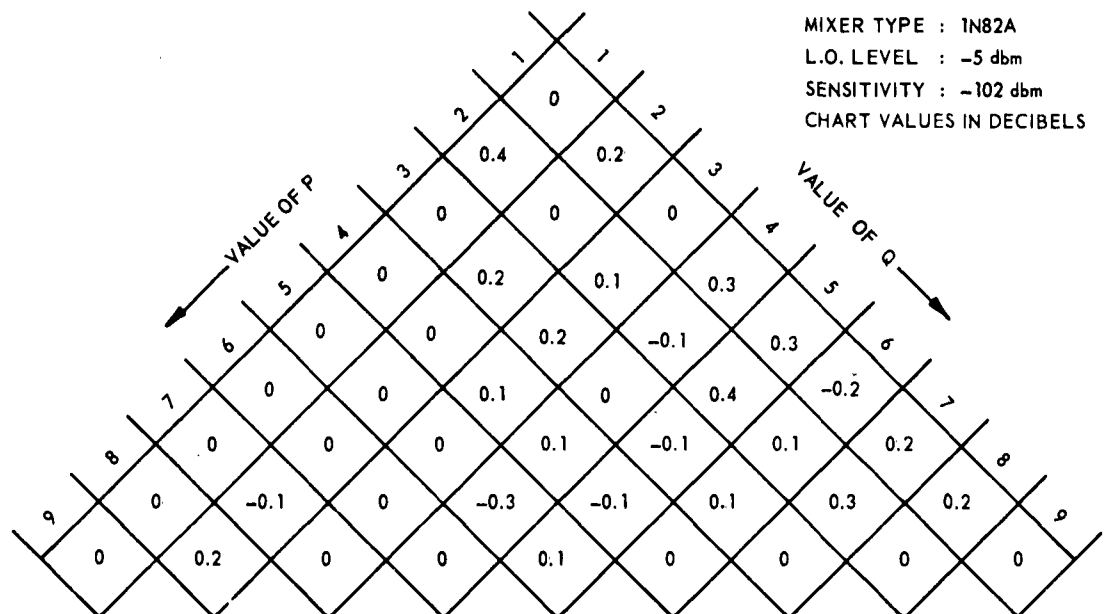


TABLE III  
PASCAL'S TRINAGLE OF BINOMIAL COEFFICIENTS DIVIDED BY  $2^{(n-1)}$  WHERE  $n$  IS  
THE POWER TO WHICH THE BINOMIAL IS TO BE RAISED

P - Q	10	9	8	7	6	5	4	3	2	1	0	1	2	3	4	5	6	7	8	9	10	Q - P
0												1										$K_0$
1										1		1										$K_1$
2									$\frac{1}{2}$		1	$\frac{1}{2}$										$K_2$
3							$\frac{1}{4}$		$\frac{3}{4}$		1	$\frac{3}{4}$										$K_3$
4					$\frac{1}{8}$		$\frac{1}{2}$		$\frac{1}{2}$		1	$\frac{1}{2}$		$\frac{1}{4}$								$K_4$
5				$\frac{1}{16}$		$\frac{5}{16}$		$\frac{3}{8}$		$\frac{5}{8}$		1	$\frac{5}{8}$		$\frac{5}{16}$		$\frac{1}{16}$					$K_5$
6			$\frac{1}{32}$		$\frac{7}{64}$		$\frac{7}{32}$		$\frac{21}{64}$		$\frac{15}{32}$		$\frac{35}{64}$		$\frac{3}{16}$		$\frac{1}{32}$					$K_6$
7			$\frac{1}{64}$		$\frac{1}{64}$		$\frac{1}{16}$		$\frac{7}{64}$		$\frac{7}{64}$		$\frac{35}{64}$		$\frac{21}{64}$		$\frac{7}{64}$		$\frac{1}{64}$			$K_7$
8			$\frac{1}{128}$		$\frac{1}{16}$		$\frac{1}{32}$		$\frac{7}{32}$		$\frac{35}{64}$		$\frac{63}{128}$		$\frac{7}{16}$		$\frac{1}{16}$		$\frac{1}{128}$			$K_8$
9		$\frac{1}{256}$		$\frac{9}{256}$		$\frac{9}{54}$		$\frac{21}{64}$		$\frac{63}{128}$		$\frac{63}{128}$		$\frac{105}{256}$		$\frac{9}{64}$		$\frac{9}{256}$		$\frac{1}{256}$		$K_9$
10	$\frac{1}{512}$		$\frac{5}{256}$		$\frac{45}{512}$		$\frac{15}{64}$		$\frac{105}{256}$		$\frac{63}{128}$		$\frac{105}{256}$		$\frac{15}{64}$		$\frac{45}{512}$		$\frac{5}{256}$		$\frac{1}{512}$	$K_{10}$

TABLE IV  
SPURIOUS RESPONSE TRIANGLE FOR A MIXER HAVING A POLYNOMIAL  
REPRESENTATION OF THE TENTH DEGREE

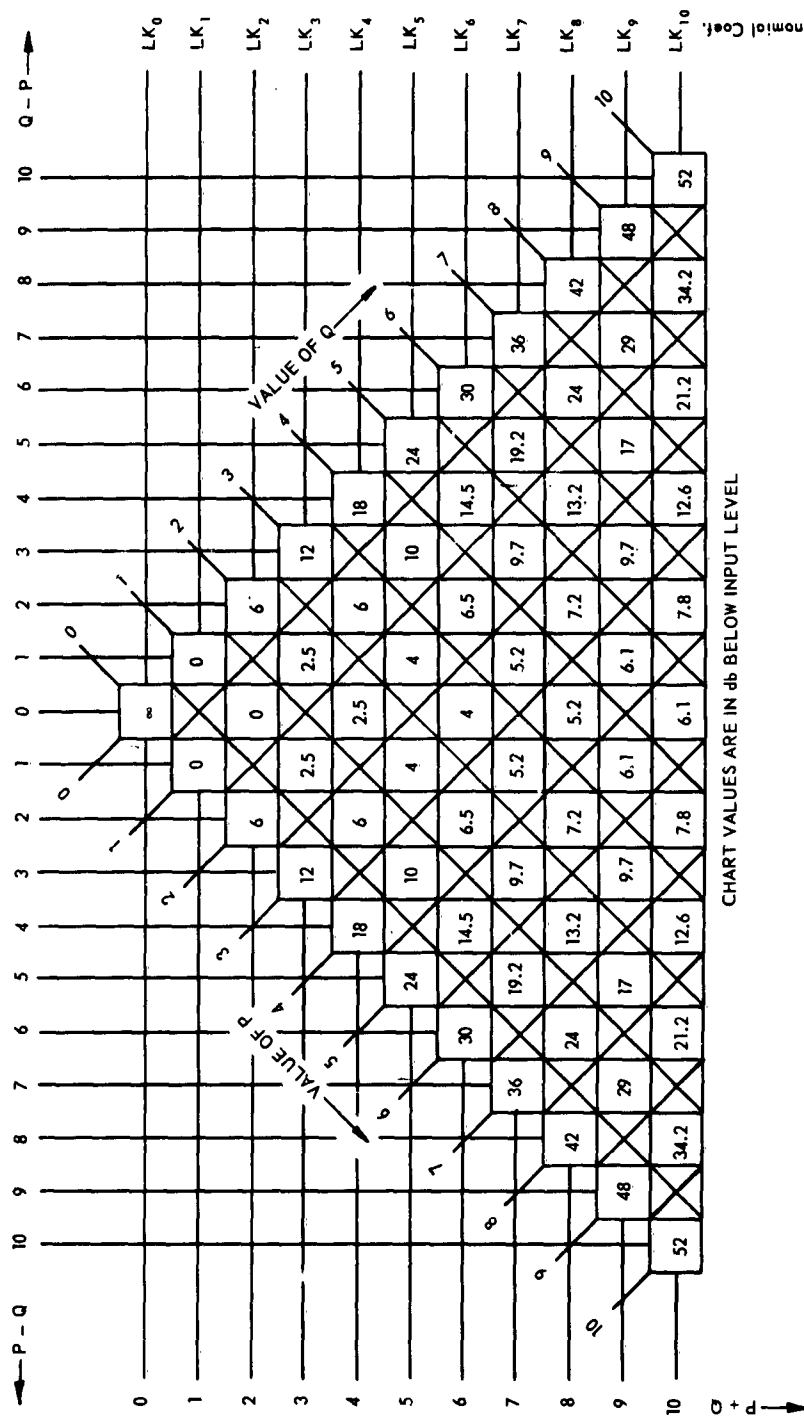


TABLE V  
RESPONSE FACTORS

$e_p$  = LOCAL OSCILLATOR VOLTAGE  
 $e_q$  = SIGNAL VOLTAGE  
 $k_n$  = ORDER CONSTANT

VALUE OF $p$	0	1	2	3	4	5	6	7	8	9	10
0	$k_0$	$e_p k_1$	$e_p^2 k_2$	$e_p^3 k_3$	$e_p^4 k_4$	$e_p^5 k_5$	$e_p^6 k_6$	$e_p^7 k_7$	$e_p^8 k_8$	$e_p^9 k_9$	$e_p^{10} k_{10}$
1	$e_q k_1$	$e_p e_q k_2$	$e_p^2 e_q k_3$	$e_p^3 e_q k_4$	$e_p^4 e_q k_5$	$e_p^5 e_q k_6$	$e_p^6 e_q k_7$	$e_p^7 e_q k_8$	$e_p^8 e_q k_9$	$e_p^9 e_q k_{10}$	
2	$e_p^2 k_2$	$e_p e_q^2 k_3$	$e_p^2 e_q^2 k_4$	$e_p^3 e_q^2 k_5$	$e_p^4 e_q^2 k_6$	$e_p^5 e_q^2 k_7$	$e_p^6 e_q^2 k_8$	$e_p^7 e_q^2 k_9$	$e_p^8 e_q^2 k_{10}$		
3	$e_p^3 k_3$	$e_p^2 e_q k_4$	$e_p^3 e_q^2 k_5$	$e_p^4 e_q^3 k_6$	$e_p^5 e_q^3 k_7$	$e_p^6 e_q^3 k_8$	$e_p^7 e_q^3 k_9$	$e_p^8 e_q^3 k_{10}$			
4	$e_p^4 k_4$	$e_p^3 e_q k_5$	$e_p^4 e_q^2 k_6$	$e_p^5 e_q^3 k_7$	$e_p^6 e_q^4 k_8$	$e_p^7 e_q^4 k_9$	$e_p^8 e_q^4 k_{10}$				
5	$e_p^5 k_5$	$e_p^4 e_q k_6$	$e_p^5 e_q^2 k_7$	$e_p^6 e_q^3 k_8$	$e_p^7 e_q^4 k_9$	$e_p^8 e_q^5 k_{10}$					
6	$e_p^6 k_6$	$e_p^5 e_q k_7$	$e_p^6 e_q^2 k_8$	$e_p^7 e_q^3 k_9$	$e_p^8 e_q^4 k_{10}$						
7	$e_p^7 k_7$	$e_p^6 e_q k_8$	$e_p^7 e_q^2 k_9$	$e_p^8 e_q^3 k_{10}$							
8	$e_p^8 k_8$	$e_p^7 e_q k_9$	$e_p^8 e_q^2 k_{10}$								
9	$e_p^9 k_9$	$e_p^8 e_q k_{10}$									
10	$e_p^{10} k_{10}$										

TABLE VI

L.O. LEVEL : +2 dbm  
SENSITIVITY : -95 dbm

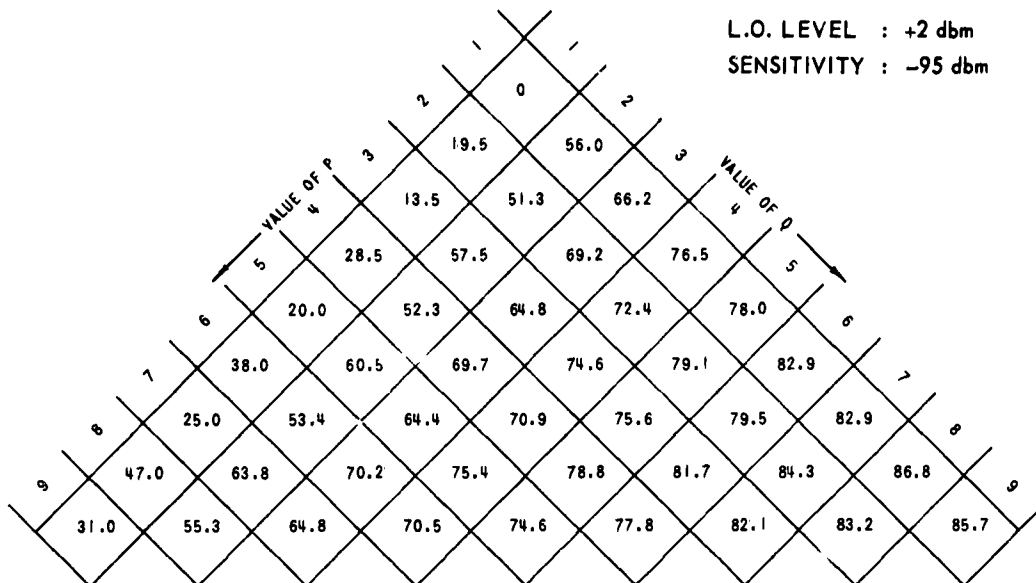


CHART VALUES ARE IN db

CALCULATED REJECTION VALUES FOR THE 1N82A DIODE MIXER USING CONSTANT  
OUTPUT DATA OF ONE RESPONSE IN EACH ROW

L.O. LEVEL +2 dbm  
SENSITIVITY : -95 dbm

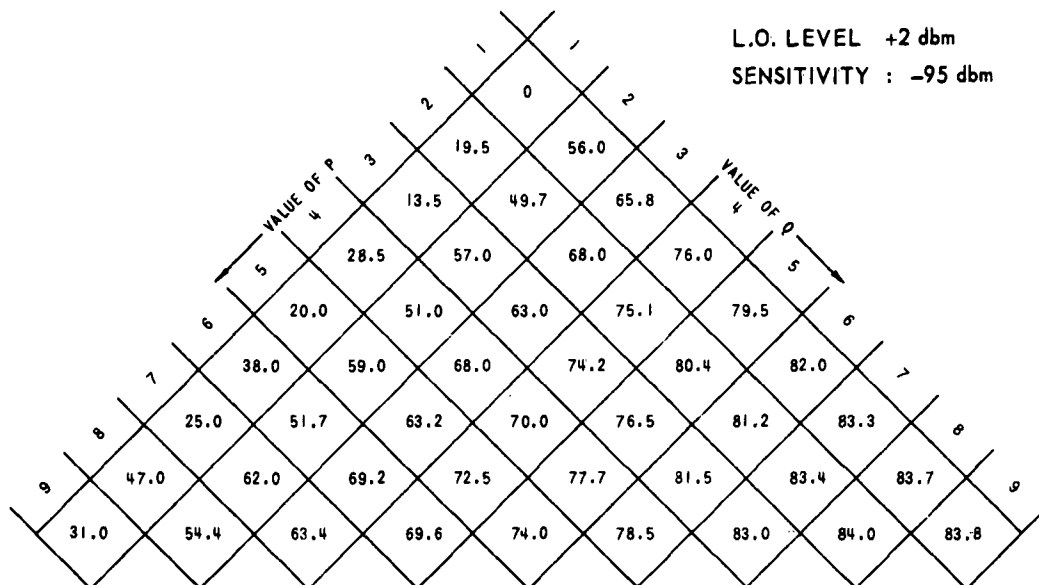


CHART VALUES ARE IN db

MEASURED VALUES FOR THE 1N82A DIODE MIXER

TABLE VII

L.O. LEVEL : +2 dbm  
SENSITIVITY : -95 dbm

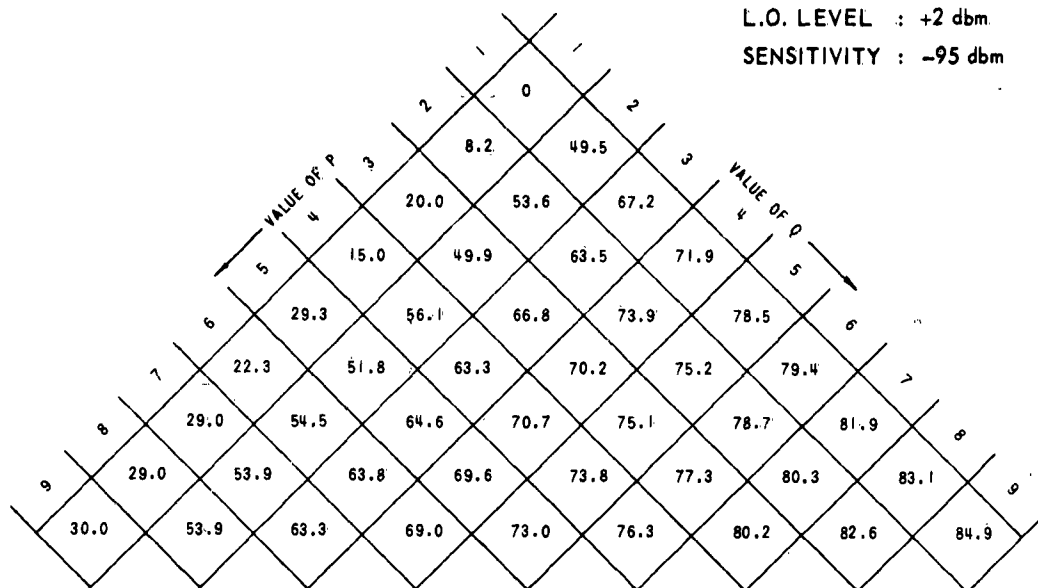


CHART VALUES ARE IN db

CALCULATED REJECTION VALUES FOR THE 1N21B DIODE MIXER USING CONSTANT  
OUTPUT DATA OF ONE RESPONSE IN EACH ROW

L.O. LEVEL : +2 dbm  
SENSITIVITY : -95 dbm

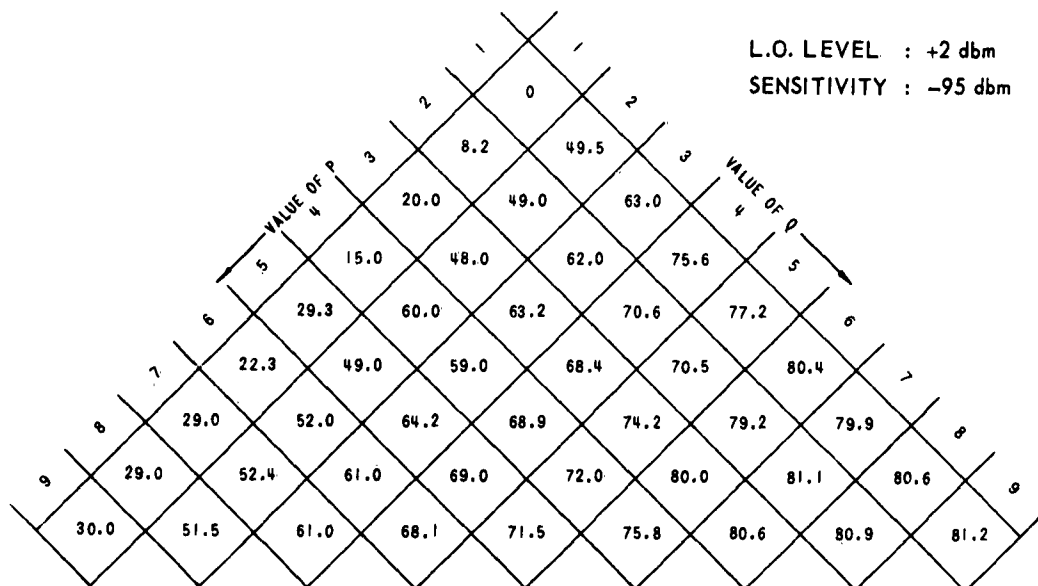


CHART VALUES ARE IN db

MEASURED REJECTION VALUES FOR THE 1N21B DIODE MIXER

TABLE VIII  
CALCULATED SPURIOUS RESPONSE REJECTIONS 1N82A DIODE MIXER

10 db INCREASE IN DETECTOR SENSITIVITY

L.O. LEVEL : +2 dbm  
SENSITIVITY : -105 dbm

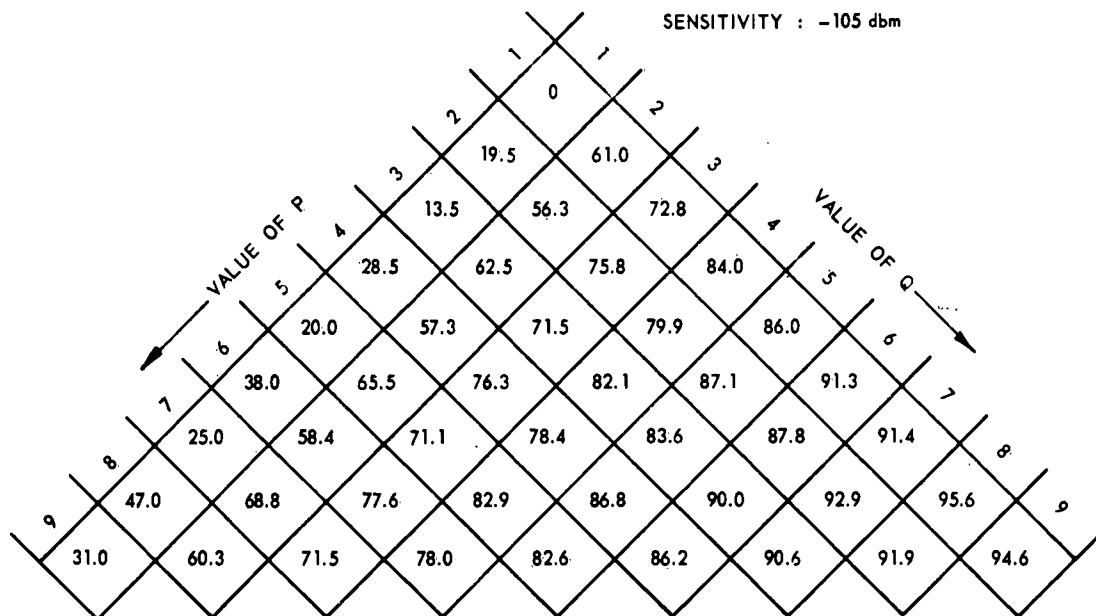


CHART VALUES IN DECIBELS

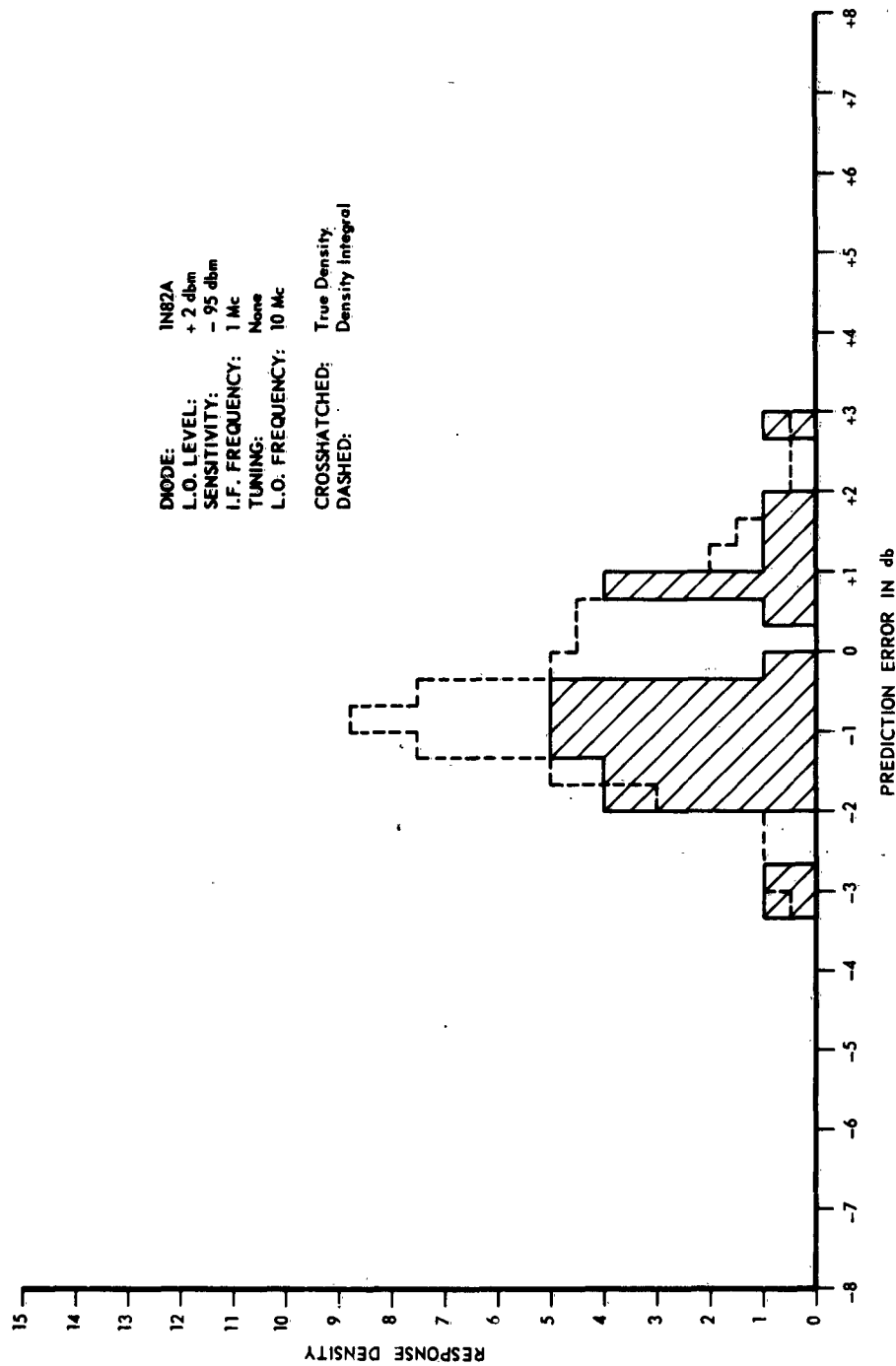


Figure 1. Response Density Versus Decibel Error for the 1N82A Diode Mixer Predicted Spurious Responses.



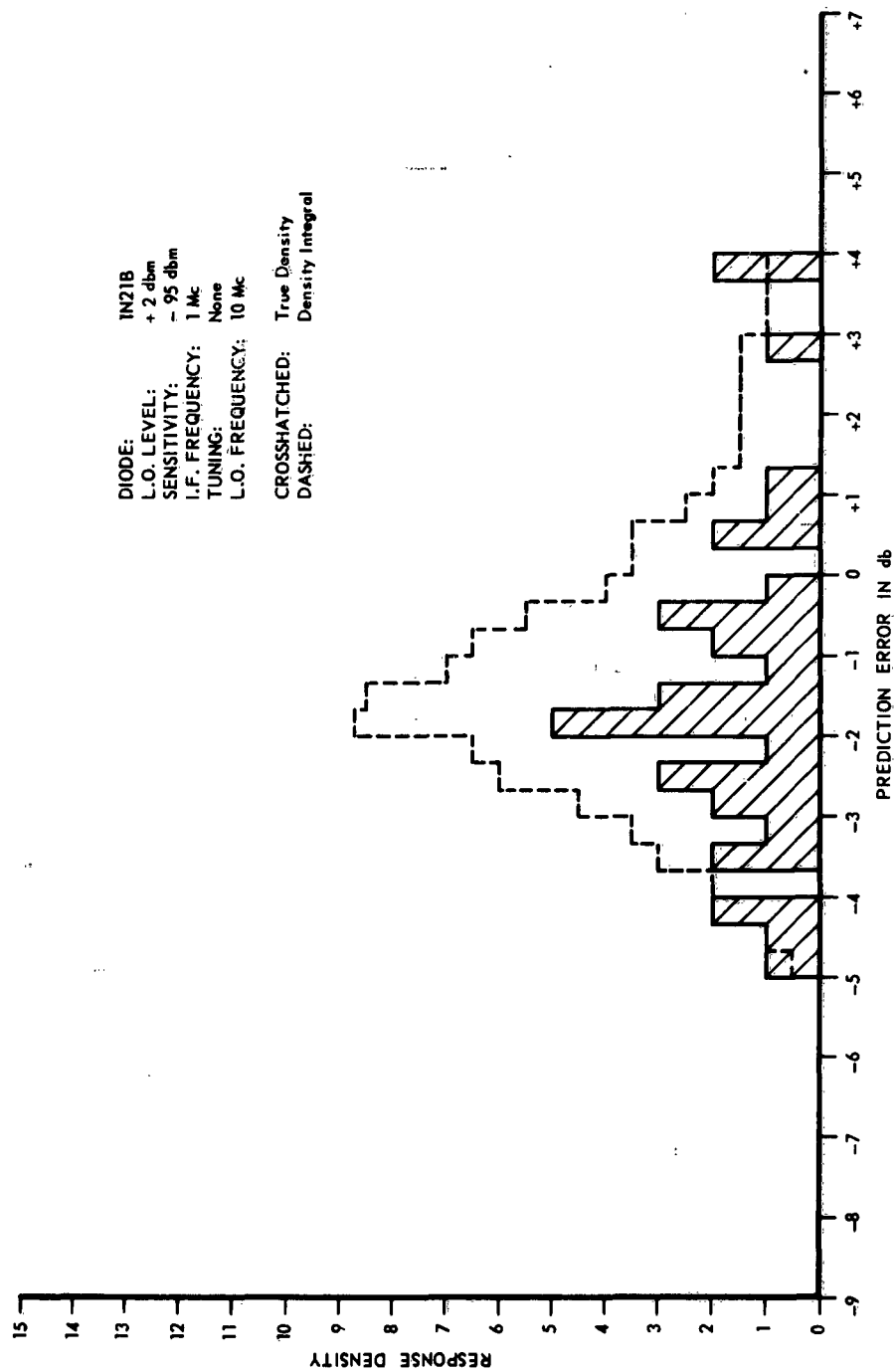


Figure 2. Response Density Versus Decibel Error for the 1N21B Diode Mixer  
 Predicted Spurious Responses.

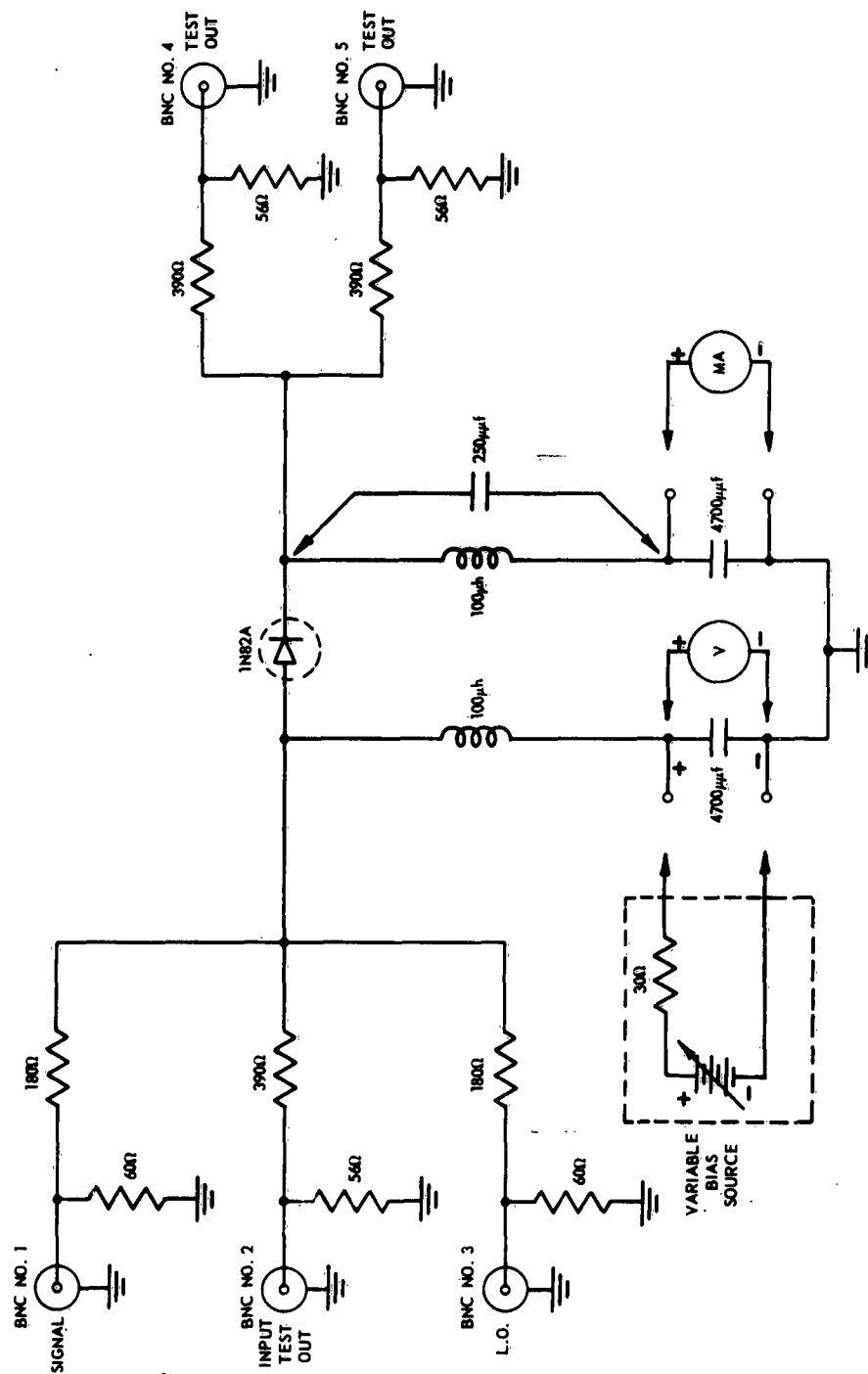


Figure 3. Schematic Diagram of 1N82A Test Mixer.

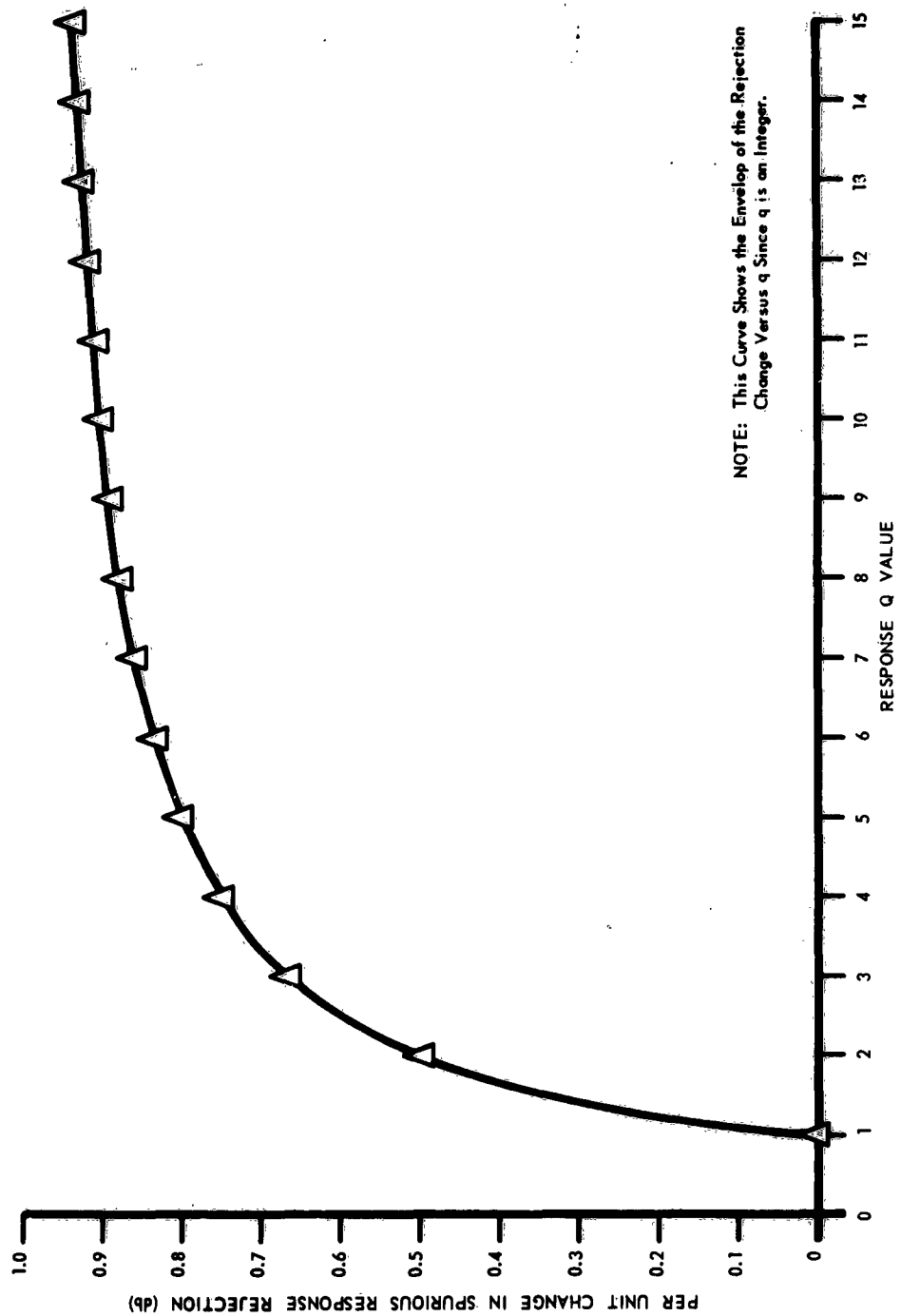


Figure 4. Change in Spurious Response Rejection with a Change in Detector Sensitivity.

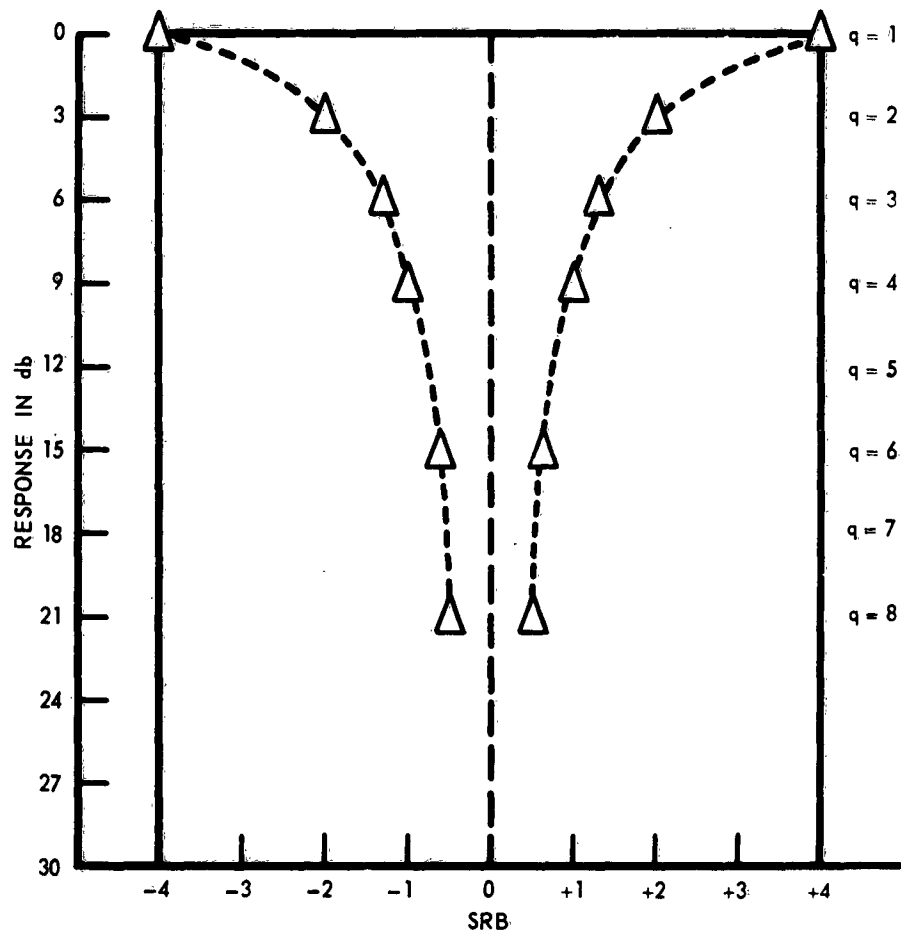


Figure 5. SRB Versus  $q$  for Rectangular IF Passband.

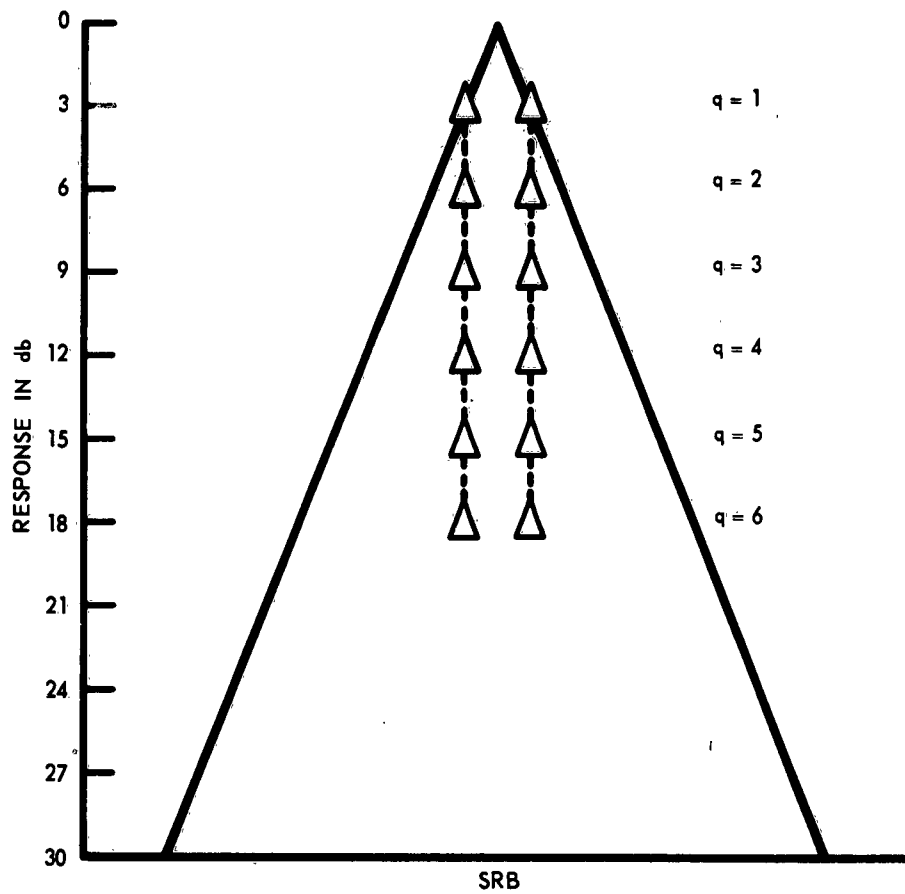


Figure 6. SRB Versus  $q$  for Triangular IF Passband.

## MIXER ANALYSIS AND DESIGN

R. W. Long  
Ground Systems Group,  
Hughes Aircraft Company  
Fullerton, California

**Abstract.** - An analysis and design technique is developed in this paper that allows the analysis or design of a mixer for a specified spurious level. The procedure assumes that a maximally flat filter is used and approximates a relationship between the order and level of spurious signals. The procedure involves determining the critical spurious and then spacing these spurious from the passband by a fractional bandwidth which will assure that the level of the spurious at the output of the filter will be less than or equal to the specified spurious signal level. The most straightforward application of this technique will optimize the percentage bandwidth for a given mixing ratio or "spot" in the mixer chart.

A method is presented which will allow the bandwidth to be adjusted to any value less than the allowable bandwidth in such a way as to increase the suppression of the spurious signals equally on both sides of the filter bandpass. Where additional bandwidth is required, several techniques are suggested for lowering the spurious signal level prior to filtering. The analysis and design technique is extended to cover the case where multiple output passbands are used. This technique allows large increases in the percentage bandwidth. Examples are given of single and double filter design.

### I. THE ANALYSIS OF A MIXER WITH A SINGLE OUTPUT FILTER

The simplest mixer combines two input frequencies,  $f_1$  and  $f_2$ , to provide a multiplicity of output frequencies,  $f_0$ :

$$f_0 = pf_2 \pm qf_1 \quad (1)$$

where  $f_2 > f_1$  and  $p$  and  $q$  are integers. In general, the desired output frequency will correspond to  $p = q = 1$ . The other values of  $p$  and  $q$  provide output frequencies referred to as spurious mixing products. A bandpass filter is used to select the desired mixing product and eliminate the unwanted spurious signals (Figure 1).

In order to analyze a mixer, it is necessary to know the amplitudes of the spurious mixing products with respect to the amplitude of the desired mixer output. The amplitudes of the spurious products are a function of the nonlinearity of the mixing element and the amplitudes of the input signals to the mixer. The introduction of these parameters as variables may be avoided by making a simple conservative approximation to the amplitude of the spurious signals as a function of the order of the spurious signal. Experience has indicated that if the mixing levels are such that the desired output signal

is approximately 6 db lower in level than the level of the smaller signal, the spurious signals will be successively 6 db lower for each order of spurious according to the relationship:

$$A_2(M) = -(M - 2) \text{ 6 db} \quad (2)$$

where

$A_2(M)$  = the level of the  $M^{\text{th}}$  order spurious referred to the level of the second order output,

$M$  = the order ( $p + q$ ) of the spurious signal.

The approximation of equation (2) provides a simple basis for the mixer analysis. Using the results of the analysis, it is possible to consider measured spurious levels in an existing mixer to provide a more exact design for a specific requirement.

The purpose of the bandpass filter is to provide an amount of suppression which will bring the level of each spurious signal at the output of the filter below a specified maximum level. The amount of attenuation that a Butterworth or maximally flat filter provides is a function of the normalized deviation from the center frequency,  $x$ , in the following manner.

$$e = (1 + x^{2n})^{-1/2} \quad (3)$$

where

$e$  = the normalized output voltage,

$n$  = the number of tuned circuits in the filter,

$B$  = the half-bandwidth of the filter,

$$x = \frac{f - f_c}{B},$$

$f_c$  = the center frequency of the filter.

As equation (3) indicates, the steepness of the skirts of the band-pass characteristic is determined by the number of tuned circuits in the filter. The shape of the filter bandpass is often specified and is defined:

$$S_f = \frac{\text{Bandwidth at -60 db}}{\text{Bandwidth at -3 db}} = \text{the filter shape factor.} \quad (4)$$

For the maximally flat filter response, the use of 10 tuned circuits will provide a shape factor of 2. If the filter response is changed to Tschebyscheff, the same shape factor may be achieved with fewer tuned circuits at the expense of amplitude variations within the passband. The maximally flat response has

been chosen here for its simplicity of analytical expression and does not preclude the use of a Tschebyscheff-type filter in a specific application.

If the maximum spurious level,  $L_s$ , is specified, one may determine the amount of suppression required for each order spurious signal by determining the difference between the prescribed spurious level and the actual level:

$$L_s - A_2(M) = L_s + (M - 2) \text{ db.} \quad (5)$$

The value of normalized deviation from the center frequency required to provide this amount of attenuation of the spurious signals may be determined as a function of the order of the spurious by equating the required attenuation, equation (5), and the filter response function, equation (3). Equation (3) must be expressed in db to provide the same units in each equation.

$$L_s + (M - 2)6 = -10 \log (1 + x^{2n}) \quad (6)$$

$$x(M) = x_M = \left\{ \log^{-1} \left[ \frac{L_s + (M - 2)6}{-10} \right] - 1 \right\}^{1/2n} \quad (7)$$

For values of  $x > x_M$ , the level of the  $M^{\text{th}}$  spurious signal out of the filter will be less than  $L_s$ .

Spurious combinations up to the tenth order are illustrated in the normalized mixer chart of Figure 2. Many other spurious combinations exist but are not included in the chart since they are generally of a very low level. The chart is used to determine "open areas" where a mixer can be designed to operate over a given percentage bandwidth with a specified spurious level. It should be noted that experience has indicated that the graphical size of an opening between spurious combinations on the mixer chart is not proportional to the percentage bandwidth that can be achieved. To illustrate the analysis and design procedure, a region that is bounded by the following spurious signals was chosen.

$$f_{o3} = f_2 + 2f_1,$$

$$f_{o1} = f_2,$$

$$f_{o10a} = 2f_2 - 8f_1,$$

$$f_{o10b} = 10f_1.$$

The mixers under discussion are often used in conjunction with frequency synthesizers in which the input frequencies to the mixer are changed in increments. In this type of system the input frequencies to the mixer are specified:

$$f_1 = (N_1 + n_1) \Delta f \quad (8)$$



where

$\Delta f$  = the frequency difference in  $f_1$  steps,

$N_1$  = a constant (may be an integer),

$n_1$  = an integer between 0 and  $c_1 - 1$ ,

$c_1$  = the number of steps in  $f_1$ ;

$$f_2 = (N_2 + n_2) c_1 \Delta f \quad (9)$$

where

$N_2$  = a constant (may be an integer),

$n_2$  = an integer between 0 and  $c_2 - 1$ ,

$c_2$  = the number of steps in  $f_2$ .

The procedure followed in performing a design analysis of the mixer is to determine that condition of input frequencies which brings each spurious signal to the closest proximity of the passband. This spacing may then be normalized by dividing by the half-bandwidth and set equal to the minimum value of  $x_M$  as a constraint which ensures the specified maximum spurious level,  $L_S$ . In general there will be at least four bounding spurious signals, two on each end of the passband. The four spurious signals result in four equations from which  $N_1$  and  $N_2$  are determined. Since there are four equations and two unknowns, it is necessary to determine which two of the equations impose the limiting condition in terms of spurious level. The spacing of the spurious signals from the passband is defined with reference to the center frequency,  $f_c$ , of the passband which for the sum mixer has the form:

$$f_c = (c_1 N_2 + N_1 + \beta) \Delta f, \quad (10)$$

where

$\beta \Delta f = B$  = the half bandwidth of the filter.

The third order spurious is above the center frequency.

$$f_{o3} = f_2 + 2f_1 = c_1(N_2 + n_2) \Delta f + 2(N_1 + n_1) \Delta f$$

$$f_{o3} - f_c = c_1(N_2 + n_2) \Delta f + 2(N_1 + n_1) \Delta f - (c_1 N_2 + N_1 + \beta) \Delta f$$

The difference in minimum for  $n_1 = 0$  and  $n_2 = 0$ .

$$f_{o3} = (c_1 N_2 + 2N_1) \Delta f. \quad (11)$$

The difference between  $f_{o3}$  and  $f_c$  may be normalized by dividing by B, the half bandwidth and set equal to  $x_3$ ,

$$\frac{f_{o3} - f_c}{B} = x_3 = \frac{(N_1 - \beta) \Delta f}{\beta \Delta f}. \quad (12)$$

Equation (12) may now be solved for  $N_{1a}$ :

$$N_{1a} = (x_3 + 1) \beta \quad (13)$$

where the subscript, a, has been added to  $N_1$  to indicate that it is associated with  $f_{o3}$ . The first order spurious is  $f_{o1} = f_2$ .

$$f_{o1} = f_2 = c_1 (N_2 + n_2) \Delta f$$

$$f_c - f_{o1} = (c_1 N_2 + N_1 + \beta) \Delta f - c_1 (N_2 + n_2) \Delta f.$$

The difference is a minimum for  $n_2 = c_1 - 1$

$$f_{o1} = c_1 (N_2 + c_2 - 1) \Delta f. \quad (14)$$

The difference between  $f_c$  and  $f_{o1}$  is normalized by dividing by the half bandwidth, B and set equal to  $x_1$ :

$$\frac{f_c - f_{o1}}{B} = x_1 = \frac{[N_1 + \beta - c_1(c_2 - 1)] \Delta f}{\beta \Delta f} \quad (15)$$

Solving equation (15) for  $N_{1b}$ :

$$N_{1b} = (x_1 - 1) \beta + c_1(c_2 - 1) \quad (16)$$

Equations (13) and (16) indicate that the first and third order spurious signals define  $N_1$  independently. Since the separation of both the first and third order spurious signals from the passband center frequency increases with  $N_1$ , the larger value of  $N_1$  is the correct one. The correct value may be determined when values are assigned to the parameters or by direct comparison of equations (13) and (16).

The first tenth order spurious signal is  $f_{o10a}$ .

$$f_{o10a} = 2f_2 - 8f_1 = 2c_1(N_2 + n_2)\Delta f - 8(N_1 + n_1)\Delta f$$

$$f_{o10a} - f_c = 2c_1(N_2 + n_2)\Delta f - 8(N_1 + n_1)\Delta f - (c_1N_2 + N_1 + \beta)\Delta f$$

The difference is minimum for  $n_2 = 0$  and  $n_1 = c_1 - 1$ .

$$f_{o10a} = [2c_1N_2 - 8(N_1 + c_1 - 1)]\Delta f. \quad (17)$$

The difference of  $f_{o10a}$  and  $f_c$  is then normalized and the ratio set equal to  $x_{10}$ :

$$\frac{f_{o10a} - f_c}{B} = x_{10} = \frac{[c_1N_2 - 9N_1 - 8(c_1 - 1) - \beta]\Delta f}{\beta\Delta f} \quad (18)$$

$$c_1N_{2a} = (x_{10} + 1)\beta + 9N_1 + 8(c_1 - 1). \quad (19)$$

The second tenth order spurious signal is  $f_{o10b}$ .

$$f_{o10b} = 10f_1 = 10(N_1 + n_1)\Delta f$$

$$f_c - f_{o10b} = (c_1N_2 + N_1 + \beta)\Delta f - 10(N_1 + n_1)\Delta f$$

The difference is minimum for  $n_1 = c_1 - 1$

$$f_{o10b} = 10(N_1 + c_1 - 1)\Delta f. \quad (20)$$

The difference of  $f_c$  and  $f_{o10b}$  is then normalized and the ratio set equal to  $x_{10}$ :

$$\frac{f_c - f_{o10b}}{B} = x_{10} = \frac{[c_1N_2 - 9N_1 + \beta - 10(c_1 - 1)]\Delta f}{\beta\Delta f} \quad (21)$$

$$c_1N_{2b} = (x_{10} - 1)\beta + 9N_1 + 10(c_1 - 1). \quad (22)$$

The limiting value of  $N_2$  may be found, as with  $N_1$ , by comparing equations (19) and (22) either directly or after assigning values. It has been noted that the  $N_1$  terms always have the same multiplier in equations (19) and (22).

It should be noted that an eleventh order spurious passes through the passband. It has been found in the past that this spurious signal may be kept adequately low by optimizing the mixing input levels.

A mixer design may be illustrated by assigning values to the design parameters and then determining  $N_1$  and  $N_2$ . The following values will be assumed for the purpose of illustration:

$$f_c = 25.000 \text{ mc/s},$$

$$c_1 = 8,$$

$$c_2 = 8,$$

$$L_s = -60 \text{ db},$$

$$n = 10 \text{ tuned circuits (filter response: maximally flat)}.$$

The values of  $x_M$  resulting from this set of parameters are tabulated in Table I.

Using the  $x_M$  values of Table I, the equations for  $N_1$  and  $N_2$  may be evaluated to determine the design values.

$$N_{1a} = (x_3 + 1)\beta = 90.153,$$

$$N_{1b} = (x_1 - 1)\beta + c_1(c_2 - 1) = 91.847.$$

Thus,  $N_1 = N_{1b} = 91.847$  as determined by the first order spurious signal.

$$c_1 N_{2a} = (x_{10} + 1)\beta + 9N_1 + 8(c_1 - 1) = 950.190,$$

$$c_1 N_{2b} = (x_{10} - 1)\beta + 9N_1 + 10(c_1 - 1) = 901.190.$$

$$\text{Thus, } N_2 = N_{2a} = \frac{950.190}{8} = 118.774 \text{ as determined by } f_{o10a}.$$

The design may now be detailed:

$$f_c = (c_1 N_2 + N_1 + \beta) \Delta f$$

$$\Delta f = \frac{f_c}{c_1 N_2 + N_1 + \beta} = \frac{25.000 \text{ mc/s}}{1073.537} = 0.0232875 \text{ mc/s},$$

$$f_1 = (c_1 N_2 + N_1) \Delta f = 1042.037 \Delta f = 24.266437 \text{ mc/s},$$

$$f_c = (c_1 N_2 + N_1 + \beta) \Delta f = 1073.537 \Delta f = 24.999993 \text{ mc/s},$$

$$f_h = (c_1 N_2 + N_1 + 2\beta) \Delta f = 1105.037 \Delta f = 25.733549 \text{ mc/s},$$

$$BW = 2\beta \Delta f = 63 \Delta f = 1.467112 \text{ mc/s},$$

$$\frac{BW}{f_c} = \frac{2\beta \Delta f}{(c_1 N_2 + N_1 + \beta) \Delta f} = 5.868\%.$$

The input frequencies,  $f_1$  and  $f_2$ , may now be resolved using the values of  $N_1$  and  $N_2$  determined. Table II lists the two input frequencies as a function of the frequency step number,  $n_1$  or  $n_2$ .

Computing the actual values of the normalized spacing of the spurious signals from equations (12), (15), (18), and (21) allows verification of the design. It was shown that  $f_{01}$  and  $f_{010a}$  imposed the limiting conditions in determining  $N_1$  and  $N_2$ ; therefore, equations (15) and (18) should equal  $x_1$  and  $x_{10}$ , respectively. The fact that  $f_{03}$  and  $f_{010b}$  were not the determining spurious indicates that equations (12) and (21) should be greater than  $x_3$  and  $x_{10b}$ , respectively. Thus  $f_{01}$  and  $f_{010a}$  will appear at the output of the band-pass filter at the specified maximum level,  $L_s$ , for the indicated frequency combinations. The other spurious signals will always be at a level less than  $L_s$ . The verification of the design is:

$$\frac{f_{03} - f_c}{B} = \frac{N_1 - \beta}{\beta} = 1.916 > x_3,$$

$$\frac{f_c - f_{01}}{B} = \frac{N_1 + \beta - c_1(c_2 - 1)}{\beta} = 2.138 = x_1,$$

$$\frac{f_{010a} - f_c}{B} = \frac{c_1 N_2 - 9N_1 - \beta - 8(c_1 - 1)}{\beta} = 1.145 = x_{10},$$

$$\frac{f_c - f_{010b}}{B} = \frac{c_1 N_2 - 9N_1 + \beta - 10(c_1 - 1)}{\beta} = 2.700 > x_{10}.$$

## II. ADJUSTING THE FREQUENCY INCREMENT

The design procedure that has been developed allows the bandwidth to be maximized for a specified spurious level. Thus, the frequency increment is a function of the number of steps and the allowable bandwidth. If it is required to specify the frequency increment, it may be accomplished by modifying the design as long as the prescribed increment is less than that indicated by the design:

$$\Delta f' = k \Delta f, \text{ where } k < 1. \quad (23)$$

When the frequency increment is reduced for a given number of steps in frequency, the total bandwidth is reduced. The design may be optimized for the new frequency increment by maintaining the same center frequency. This will provide additional rejection of the spurious signals on each side of the filter passband. The center frequency is defined by the following equation for a sum mixer:

$$f_c = (c_1 N_2 + N_1 + \beta) \Delta f. \quad (24)$$

To obtain the new frequency increment,  $k \Delta f$ ,  $N_1$  and  $N_2$  must be multiplied by a constant,  $k_1$ ,

$$f_c = (k_1 c_1 N_2 + k_1 N_1 + \beta) k \Delta f. \quad (25)$$

The factor,  $k_1$ , may be determined:

$$k_1 = \frac{\frac{f_c}{\Delta f} - \beta}{N_1 + c_1 N_2} \quad (26)$$

In the modified design,  $N_1$  and  $N_2$  have the values:

$$N_1' = k_1 N_1, \quad (27)$$

$$N_2' = k_1 N_2. \quad (28)$$

This technique may also be used for difference mixers, but the equations are somewhat different. The center frequency of a difference mixer is written

$$f_c = (c_1 N_2 - N_1 - (c_1 - 1) + \beta) \Delta f. \quad (29)$$

Again the frequency increment may be changed to  $k \Delta f$  by multiplying  $N_1$  and  $N_2$  by  $k_1$  to maintain the same center frequency.

$$f_c = [k_1 c_1 N_2 - k_1 N_1 - (c_1 - 1) + \beta] k \Delta f \quad (30)$$

$$k_1 = \frac{\frac{f_c}{\Delta f} - \beta + c_1 - 1}{c_1 N_2 - N_1} \quad (31)$$

The new values of  $N_1$  and  $N_2$  for the difference mixer are

$$N_1' = k_1 N_1, \quad (32)$$

$$N_2' = k_1 N_2. \quad (33)$$

When multiple output filters are used to obtain more bandwidth, this technique may still be used to obtain a prescribed frequency increment, but the equations must be modified slightly. If a larger frequency increment is required, it is probably because the mixer design has not provided sufficient bandwidth. If this is the case, a filter with a better shape factor, multiple filters, or a change in mixing ratio is indicated to achieve greater bandwidth.

### III. THE ANALYSIS OF A MIXER WITH TWO OUTPUT FILTERS

If several filters are used at the output of a mixer, the percentage bandwidth possible for a given filter shape factor and specified spurious level is increased. To illustrate the increase in percentage bandwidth, a second filter will be added to the previous mixer and the analysis modified to determine the effect of adding the second filter. The block diagram of the new circuit is shown in Figure 3.

The new mixer has the same normalized bandwidth,  $(c_1 c_2 - 1) \Delta f$ . Thus the half bandwidth of each filter is  $0.25 \times$  the full mixer bandwidth or  $0.25 (c_1 c_2 - 1) \Delta f = B = \beta \Delta f$ . From this the passbands of the two filters may be determined:

$$f_L = (c_1 N_2 + N_1) \Delta f = \text{the lower band-edge of the lower filter,} \quad (34)$$

$$f_{cL} = (c_1 N_2 + N_1 + \beta) \Delta f = \text{the center frequency of the lower filter,} \quad (35)$$

$$f_c = (c_1 N_2 + N_1 + 2\beta) \Delta f = \text{the upper band-edge of the lower filter and the lower band-edge of the upper filter,} \quad (36)$$

$$f_{cU} = (c_1 N_2 + N_1 + 3\beta) \Delta f = \text{the center frequency of the upper filter,} \quad (37)$$

$$f_U = (c_1 N_2 + N_1 + 4\beta) \Delta f = \text{the upper band-edge of the upper filter.} \quad (38)$$

The same procedure of determining the separation between the spurious signals and the bandpass centers will be followed. Each step must be duplicated for the lower and upper passbands to determine the critical spurious signals. As this work is simply an extension of the prior analysis, it is tabulated below with a minimum of additional description. In the equation numbering used, the difference between the spurious frequency and the center frequency is written in the (a) equation. At the end of the equation, the values of the parameters  $n_1$  and  $n_2$  used in the equation are stated. These values correspond to the smallest difference between the spurious frequency and the center frequency. The (b) equation is derived from the (a) equation

by normalizing the (a) equation by dividing by  $\beta \Delta f$  and setting the resulting equation equal to  $x_M$ . The (c) equation is the result of solving the (b) equation for  $N_1$  or  $N_2$ .

$$f_{03} - f_{cU} = \left[ 2N_1 + c_1 N_2 + c_1 \frac{c_2}{2} - (c_1 N_2 + N_1 + 3\beta) \right] \Delta f, \quad (39a)$$

$$n_1 = 0$$

$$n_2 = \frac{c_2}{2}$$

$$x_3 = \frac{N_1 + c_1 \frac{c_2}{2} - 3\beta}{\beta}, \quad (39b)$$

$$N_{1a} = (x_3 + 1)\beta - 1/2; \quad (39c)$$

$$f_{03} - f_{cL} = [2N_1 + c_1 N_2 - (c_1 N_2 + N_1 + \beta)] \Delta f, \quad (40a)$$

$$n_1 = 0$$

$$n_2 = 0$$

$$x_3 = \frac{N_1 - \beta}{\beta}, \quad (40b)$$

$$N_{1b} = (x_3 + 1)\beta; \quad (40c)$$

$$f_{cU} - f_{01} = [c_1 N_2 + N_1 + 3\beta - c_1(N_2 + c_2 - 1)] \Delta f$$

$$n_1 = --- \quad (41a)$$

$$n_2 = c_2 - 1$$

$$x_1 = \frac{N_1 + 3\beta - c_1(c_2 - 1)}{\beta}, \quad (41b)$$

$$N_{1c} = (x_1 + 1)\beta - (c_1 - 1); \quad (41c)$$



$$f_{cL} - f_{o1} = \left[ c_1 N_2 + N_1 + \beta - \left( c_1 N_2 + c_1 \frac{c_2}{2} - c_1 \right) \right] \Delta f, \quad n_1 = \text{---} \quad (42a)$$

$$n_2 = \frac{c_2}{2} - 1$$

$$x_1 = \frac{N_1 + \beta - c_1 \left( \frac{c_2}{2} - 1 \right)}{\beta}, \quad (42b)$$

$$N_{1d} = (x_1 - 1)\beta + c_1 \left( \frac{c_2}{2} - 1 \right) = (x_1 + 1)\beta - c_1 + 1/2; \quad (42c)$$

$$f_{c10a} - f_{cU} = \left[ 2c_1 \left( N_2 + \frac{c_2}{2} \right) - 8(N_1 + c_1 - 1) - (c_1 N_2 + N_1 + 3\beta) \right] \Delta f, \quad n_1 = c_1 - 1 \quad (43a)$$

$$n_2 = \frac{c_2}{2}$$

$$x_{10} = \frac{c_1 N_2 - 9N_1 + c_1 c_2 - 8(c_1 - 1) - 3\beta}{\beta}, \quad (43b)$$

$$c_1 N_{2a} = (x_{10} - 1)\beta + 9N_1 + 8(c_1 - 1) - 1; \quad (43c)$$

$$f_{o10a} - f_{cL} = [ 2c_1 N_2 - 8(N_1 + c_1 - 1) - (c_1 N_2 + N_1 + \beta) ] \Delta f, \quad n_1 = c_1 - 1 \quad (44a)$$

$$n_2 = 0$$

$$x_{10} = \frac{c_1 N_2 - 9N_1 - 8(c_1 - 1) - \beta}{\beta}, \quad (44b)$$

$$c_1 N_{2b} = (x_{10} + 1)\beta + 9N_1 + 8(c_1 - 1); \quad (44c)$$

$$f_{cU} - f_{o10b} = [c_1 N_2 + N_1 + 3\beta - 10(N_1 + c_1 - 1)] \Delta f.$$

$$n_1 = c_1 - 1 \quad (45a)$$

$$n_2 = \text{---}$$

$$x_{10} = \frac{c_1 N_2 - 9N_1 + 3\beta - 10(c_1 - 1)}{\beta}, \quad (45b)$$

$$c_1 N_{2c} = (x_{10} - 3)\beta + 9N_1 + 10(c_1 - 1); \quad (45c)$$

$$f_{cL} - f_{o10b} = [c_1 N_2 + N_1 + \beta - 10(N_1 + c_1 - 1)],$$

$$n_1 = c_1 - 1 \quad (46a)$$

$$n_2 = \text{---}$$

$$x_{10} = \frac{c_1 N_2 - 9N_1 + \beta - 10(c_1 - 1)}{\beta}, \quad (46b)$$

$$c_1 N_{2d} = (x_{10} - 1)\beta + 9N_1 + 10(c_1 - 1). \quad (46c)$$

A direct comparison of the single and dual filter mixers is possible if the same design parameters are used in the dual filter mixer. The parameters are:

$$f_c = 25.000000 \text{ mc/s},$$

$$c_1 = 8,$$

$$c_2 = 8,$$

$$L_s = -60 \text{ db},$$

$$n = 10 \text{ tuned circuits (filter response: maximally flat),}$$

$$x_M \text{ values as tabulated in Table I.}$$

Using these parameters,  $N_1$  is calculated to have the following values:

$$N_{1a} = 44.576,$$

$$N_{1b} = 45.076,$$

$$N_{1c} = 42.423,$$

$$N_{1d} = 41.923.$$

Thus, the largest value of  $N_1$  is chosen since it represents a limiting condition:  $N_1 = 45.076$ . This indicates that the third order spurious in the lower passband is one of the limiting spurious signals. Using this value of  $N_1$ , the values of  $N_2$  are determined:

$$c_1 N_{2a} = 462.967,$$

$$c_1 N_{2b} = 495.968,$$

$$c_1 N_{2c} = 446.468,$$

$$c_1 N_{2d} = 477.968.$$

The largest value of  $N_2$  is a limiting condition. Thus  $N_2 = \frac{495.968}{8} = 61.933$ .

The second limiting spurious signal is the spurious signal 10a in the upper passband.

Using the values

$$N_1 = 45.076 \text{ and}$$

$$N_2 = 61.933,$$

the design of the mixer may be detailed by determining the frequency increments and then the input frequencies.

$$f_c = (c_1 N_2 + N_1 + 2\beta) \Delta f = 25.000000 \text{ mc/s},$$

$$\Delta f = \frac{25.000000 \text{ mc/s}}{c_1 N_2 + N_1 + 2\beta} = 0.043703 \text{ mc/s},$$

$$f_L = (N_1 + c_1 N_2) \Delta f = 23.623351 \text{ mc/s},$$

$$f_{cL} = (N_1 + c_1 N_2 + \beta) \Delta f = 24.311673 \text{ mc/s},$$

$$f_c = (N_1 + c_1 N_2 + 2\beta) \Delta f = 24.999995 \text{ mc/s},$$

$$f_{cU} = (N_1 + c_1 N_2 + 3\beta) \Delta f = 25.688317 \text{ mc/s},$$

$$f_U = (N_1 + c_1 N_2 + 4\beta) \Delta f = 26.376639 \text{ mc/s},$$

$$\frac{BW}{f_c} = \frac{4\beta}{c_1 N_2 + N_1 + 2\beta} = 11.01 \text{ percent}.$$

The input frequencies,  $f_1$  and  $f_2$ , may now be determined using the values of  $N_1$  and  $N_2$  determined. Table III lists the two input frequencies as a function of the frequency step number,  $n_1$  or  $n_2$ .

#### IV. CONCLUSION

A technique of mixer analysis and design has been presented which alleviates the necessity of designing a mixer by trial and error. In deriving this technique, an assumption was made concerning the way in which the level of a spurious signal was related to its order. This assumption was conservative and did not take into account the control of spurious level by choice of nonlinear element, optimization of mixing input levels or cancellation of certain spurious by balanced mixer techniques. In a system that requires large percentage bandwidth and an extremely low spurious level, it would be worthwhile to combine several or all of these techniques to meet the specifications. The  $x_M$  values used in the mixer design could then be based on measured spurious levels at the input of the mixer.

The extension of this technique to provide a more extensive general analysis is a formidable task, but has been undertaken. Though the technique has been directed to frequency synthesis, it is also applicable to the receiver spurious problem.

In applying this technique of mixer analysis and design to other spots in the mixer chart, it will be found that it is not possible to solve directly for  $N_1$  as in this example. It is necessary to determine the two limiting equations and solve them simultaneously for  $N_1$  and  $N_2$ . The limiting equations may be determined by comparing the sum of the constants (the terms not involving  $N_1$  or  $N_2$ ) in the equations as normalized and set equal to the appropriate  $x_M$ . The equation in which the sum of  $x_M$  and all of the constants (brought over to the same side of the equation) is largest is a limiting equation. There will be a limiting equation at the maximum mixing ratio and one at the minimum ratio, so that the comparison will be made between the two equations defining the spurious at one extreme of the mixing ratio and then the other. In some cases there is only one spurious signal at one extreme of the mixing ratio; this will of course be a limiting condition.

Table I. Value of  $x_M$  as a Function of M

$$x_M = \frac{20}{\sqrt{\log^{-1} \left[ \frac{-L_s - (M - 2) 6}{10} \right] - 1}}$$

<u>M</u>	<u><math>x_M</math></u>
1	2.138
2	1.995
3	1.862
4	1.738
5	1.622
6	1.513
7	1.413
8	1.318
9	1.229
10	1.145

Table II.  $f_1$  and  $f_2$  as a Function of  $n_1$  and  $n_2$

<u><math>n_1</math> or <math>n_2</math></u>	<u><math>f_1</math> in mc/s</u>	<u><math>f_2</math> in mc/s</u>
0	2.138887	22.127550
1	2.162174	22.313850
2	2.185462	22.500150
3	2.208749	22.686450
4	2.232037	22.872750
5	2.255324	23.059050
6	2.278612	23.245350
7	2.301899	23.432650

Table III. $f_1$ and $f_2$ as a Function of $n_1$ and $n_2$		
$n_1$ or $n_2$	$f_1$ in mc/s	$f_2$ in mc/s
0	1.969956	21.653263
1	2.013659	22.002887
2	2.057362	22.352511
3	2.101065	22.702135
4	2.144768	23.051759
5	2.188471	23.401388
6	2.232174	23.751007
7	2.275877	24.100631

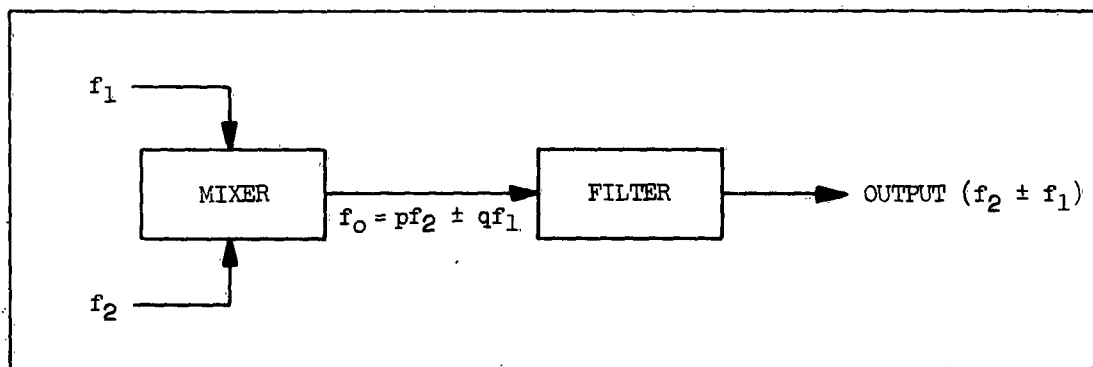


Figure 1 The Single Filter Mixer

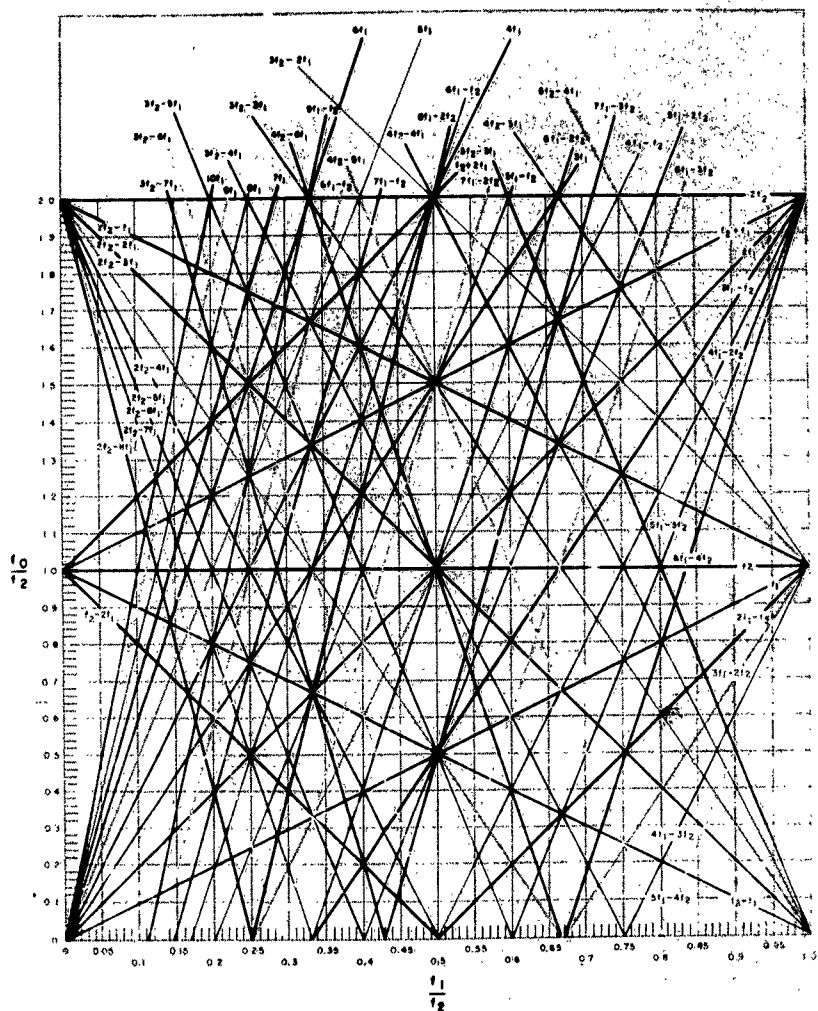


Figure 2 Mixer Chart, with  $f_1$  and  $f_2$  as mixer input frequencies ( $f_2 > f_1$ ) and  $f_0$  as desired output frequency. Lines intersected when tracing straight up from value of  $f_1/f_2$  represent combination frequencies, values of which can be found either from labels on lines or from scale ordinates. Only intersections near desired combination (sum or difference) need be considered. After T. T. Brown, Electronics, June 1954.

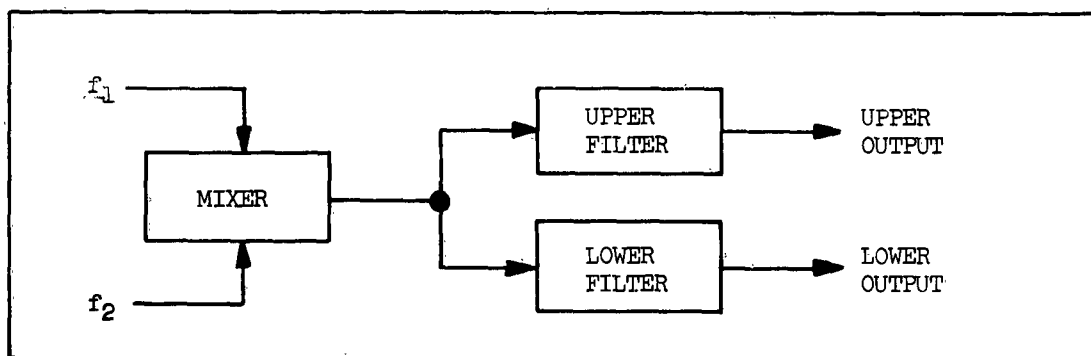


Figure 3 The Dual Filter Mixer



## OFF-TUNING EFFECTS PRODUCED BY INTERFERENCE

R. J. Mayher  
IIT Research Institute  
Electromagnetic Compatibility Analysis Center  
Annapolis, Maryland

Abstract. - This paper considers the analysis of off-tuned pulsed interference and continuously modulated off-tuned interference. For pulsed interference, the threshold probability of detecting the off-tuned pulses will be presented. For the case of a modulated interfering signal, the detected output signal as a function of the off-tuning is given. The modulated signal is considered for both an amplitude and a frequency modulated signal.

### I. INTRODUCTION

The analysis of interfering problems is generally characterized by non-design parameters. One of the most common of these parameters is that of a difference in frequency between the interfering carrier and the tuned frequency of the victim receiver. This difference in frequency, or off-tuning produces different effects depending upon the type of interfering signal and the type of receiver to be considered.

In many analysis problems a receiver can be approximated by the IF amplifier and detector combination shown in Figure 1. This is the case where there has been ideal mixing and the IF amplifier is the predominant filter. For problems consistent with these basic assumptions the off-tuned interference problem consists of three basic analysis sections. These are

1. Analysis of combinations of off-tuned signals
2. IF amplifier effects
3. Transformation of signals through nonlinear detectors

The predominant interference effect is then used to determine the type of desired output, and graphs of these functions can be obtained from the detector output. This paper considers off-tuned pulsed signals as well as off-tuned continuously modulated signals and presents separate types of answers for both. The next section considers the general treatment of both types of interfering signals.

### II. GENERAL DISCUSSION

The problem of signal combinations, IF amplifier effects and detector transformations will next be discussed for general analysis considerations.

The mathematical handling of signals and combinations of signals has been adequately treated in numerous reports.\* It is in many cases convenient to describe signals in the quadrature form

\*For a specific discussion of combinations of off-tuned interfering signals and the general topic of detection modeling the reader is referred to Reference 1. For a general discussion of signals and combinations of signals see Reference 2 and 3.

$$(1a) \quad v(t) = X(t) \cos \omega_0 t - Y(t) \sin \omega_0 t$$

where

$X(t)$  = the in-phase or even quadrature component

$Y(t)$  = the out-of-phase or odd quadrature component

This can also be written as (see Figure 2)

$$(1b) \quad v(t) = \sqrt{X^2(t) + Y^2(t)} \cos [\omega_0 t + \phi(t)]$$

$$(1c) \quad v(t) = V(t) \cos [\omega_0 t + \phi(t)]$$

where

$$(2) \quad \phi(t) = \tan^{-1} \frac{Y(t)}{X(t)}$$

Since any desired signal or interference can be written in this form their combination is also of the same form and is given by

$$(3a) \quad v(t) = s(t) + \sum_{j=1}^n I_j(t)$$

$$(3b) \quad = \left[ X_s(t) + \sum_{j=1}^n X_{I_j}(t) \right] \cos \omega_0 t + \left[ Y_s(t) + \sum_{j=1}^n Y_{I_j}(t) \right] \sin \omega_0 t$$

where

$s(t)$  = the desired signal

$I(t)$  = the undesired or interfering signal

Since the next analysis considers a linear amplifier the desired and undesired signal can be combined or treated separately. The principle of superposition can then be used to linearly combine the outputs.

Although the details of a specific problem have not been carried out the general signal analysis problem has been formulated and the subsequent problems will generally use the formulations of Eq. 3b.

The next step or operation is to analyse the effects or changes the IF amplifier produces upon Eq. 3b. For a linear bandpass amplifier this can be shown to be\*

$$(4) \quad v'(t) = \text{Re} \left\{ e^{j(\omega_0 t)} \int_{-\infty}^{\infty} h(\tau) v(t-\tau) e^{-j[\phi(t-\tau) + \theta(\tau)]} d\tau \right\}$$

where

$v'(t)$  = IF amplifier output  
 $\text{Re}$  means take the real part of  $\left\{ \right\}$

\*See reference 3 Eq. 2.66; note the slight change in nomenclature.

$h(t)$  = the low pass impulse response of the network  
 $\theta(\tau)$  = the low pass phase response of the network

It is apparent that since the output signal is a narrow band signal the output can again be written in the form of Eq. 1 as

$$(5) \quad v'(t) = X'(t) \cos \omega_0 t + Y'(t) \sin \omega_0 t$$

where the output is obtained from the combined input signal or the input signals operated on separately by Eq. 4.

Since the detector is nonlinear the IF amplifier output must be combined as in Eq. 5 and operated on by the appropriate detector function. The most common detectors that could be discussed consist of linear envelope, square law, phase modulation, frequency modulation and synchronous detection. Since the details become somewhat involved, the general cases will be briefly discussed and specific examples of only the square law and frequency detector will be given. The detected output of these detectors can be described by

#### 1. Half-wave square law envelope detector

$$(6) \quad v_o(t) = K_{SQ} [V^2(t) - \overline{V^2(t)}]$$

where,

$K_{SQ}$  = square law detector constant

#### 2. Frequency detector

$$(7) \quad v_o(t) = K_{FM} \left[ \frac{1}{2\pi} \frac{d\phi(t)}{dt} \right]$$

$K_{FM}$  = Frequency detector constant

The output signal is next subject to the effects of a low pass filter. The output signal of this filter is then examined for its predominant interfering effect from which interference degradation curves can be obtained. At this point it is convenient to divide the general problem into the area's of pulsed interference on pulse (or digital systems) and continuously modulated systems.

### III. PULSED SYSTEMS

#### A. General Discussion

For pulsed radar or digital communications systems it is desired to use threshold probability of detection as the output for interference prediction. In many pulsed problems the interfering pulses can also be considered independent of each other. For this particular case it is therefore desired to compute the individual probability of detecting an off-tuned interfering pulse given that the pulse has been received. It is therefore also not necessary to use the general form of Eq. 3b. The second analysis category or the effect of the IF amplifier on a non-design off-tuned pulse cannot however be neglected. The beginning point in the analysis is therefore Eq. 4 in which the effect of the IF amplifier is taken into account.

Generally, amplifiers are designed around video  $\tau\beta$  products of  $\frac{1}{2}$ . The pulse reproduction of amplifiers designed around this value is not approximately constant but rather approaches the impulse response discussed in the previous section. (This is only true because the integral of the gaussian function ( $\text{erf } x$ ) or the step function response of a gaussian shaped passband can also be closely approximated with the sine function)

Previously, it was determined that the step function response of a large number of IF amplifiers could be approximated by a  $\sin x$  impulse response, a steady state portion, and a second  $\sin x$  impulse response. A mistuned pulse with this characteristic was previously shown. It is desired to calculate the probability of this pulse plus noise exceeding a threshold  $B$ . This probability can be calculated by dividing the pulse into independent correlation intervals ( $\tau$  independent  $\sim 1/\beta$ ) and calculating the total probability of detection from

$$(8) \quad P_T = \left[ 1 - (1 - P_I)^2 (1 - P_{SS})^{\tau\beta - 2} \right]$$

where

$P_I$  = Probability of detection due to the leading or trailing edge impulse response

$P_{SS}$  = Probability of detection due to the steady state portion (for each independent interval)

$\tau\beta = 2 + K, K = 1, 2, 3, \dots$

The detection probability from the steady state portion can be calculated in the usual manner from the detection tables of Marcum or others.

In order to calculate the detection probability from the  $\sin x$  impulse responses an envelope density function of signal and noise was obtained for the  $\sin x$  pulse. The normalized detection probability obtained from this density function is

$$(9) \quad P_{SB}' = \int_{B/\sqrt{N}'}^{\infty} r' e^{-\left(\frac{r'^2}{2} + \frac{A'^2}{2N'}\right)} I_0 \left[ \frac{r'A'}{\sqrt{N'}} \right] dr'$$

where

$N' = N(1 + .05 A^2/N)$

$N$  = Mean noise power

$A$  = Peak  $\sin x$  amplitude

$A' = .64A$

$I_0[\ ]$  = Bessel function of first kind and zero order

The standard threshold probability of detection usually tabulated is

$$(10) \quad P_{SB} = \int_{B/\sqrt{N}}^{\infty} r e^{-(r^2/2 + A^2/2N)} I_0 \left[ \frac{rA}{\sqrt{N}} \right] dr$$

Two difficulties are now encountered. First, the specific parameters of the amplifier will probably not be known. Second, even if they are known it is not always possible to evaluate Eq. 4. The approach that must be adopted is therefore to study the effects that various limiting types of amplifiers have on the problem.

Since the details of inserting the function for a particular type of amplifier is more complicated than space permits only the results will be discussed. For the discussion of IF amplifier effects it is most convenient to think in terms of a Laplace transformation of the input signal. The output of Laplace transform analysis is mathematically divided into a steady state and a transient solution. The first transient for pulsed interference is caused by the leading edge of the pulse impinging on the system and acting similar to an impulse. This in turn produces a corresponding impulse response. The trailing edge of the pulse, of course, produces the same effect.

For normal on-tuned pulses the steady state solution adds to these impulse responses to produce the total output pulse. If the pulse is sufficiently off-tuned the IF amplifier attenuates the steady state response to a point where its contribution can be considered negligible. For the specific case of a far off-tuned pulse of a width ( $\tau$ ) much greater than the reciprocal of the IF bandwidth, the output will result in the response shown in Figure 3a. A second example as shown in Figure 3b where an intermediately off-tuned pulse produces an output with a nonnegligible steady state portion. Since it is desired to obtain the off-tuned pulse shape a portion of the problem still remains. A transient response is chosen and it must also be assumed that other transients in the system do not contribute significantly to the output. Kallman, et al,<sup>4</sup> have derived transient shapes due to cascades of ideal filters. An ideal filter is defined as one which gives flat time delay or linear phase shift. The step response of an ideal filter tends to change from an error function to the  $\int \sin x / x$  type response as the number of filters is increased from one to  $\infty$ . Therefore, the transient response varies between the gaussian response and  $\sin x / x$  response (fitted by the form  $\sin x$  for ease of analytical computation).

The peak-to-average ratios of these transients are within 20% of 2.0 whether the transients are similar to  $\sin^2 x$ ,  $\sin^2 x / x^2$ , or  $e^{-2x}$ . The transient is averaged over a time interval  $\tau = 1 / \text{bandwidth}$  where the reciprocal bandwidth relationship is approximately true. The  $\sin^2 x$  pulse shape was chosen for ease of computation. A comparison between this response, a square pulse and the gaussian response is shown in Figure 4. The probability of threshold detection of the off-tuned pulse will next be discussed.

#### B. Detection Analysis

The probability of detection tables derived by Marcum<sup>5</sup> and others apply strictly to constant amplitude signals. For design signals with video time bandwidth products ( $\tau\beta$ ) of approximately 1.5 or greater the output pulse amplitude is (approximately) constant and the peak amplitude can be used to calculate the detection probability. This  $\tau\beta$  product is, however, only used when little distortion can be tolerated in pulse reproduction.

The difference between the modified probability ( $P_{SB}'$ ) and the normal probability ( $P_{SB}$ ) can be taken into account by modifying the normal signal to noise ratio ( $A/\sqrt{N}$ ) and the threshold to noise ratio ( $B/\sqrt{N}$ ). The two conversion equations obtained from Eq. 9 and Eq. 10 are

$$(11) \quad A'^2/N = (A^2/N) \left( .64^2 / (1 + .05A^2/N) \right)$$

$$(12) \quad B'^2/N' = (B^2/N)(1 + .05 A^2/N)^{-1}$$

These conversion equations have been plotted and are shown in Figure 5 and 6. The correct probability of detecting sin x pulses can now be obtained by using the conversion curves of signal to noise ratio and threshold and the standard detection tables. This probability is correct for all responses of approximately sin x shape and is not a function of the off-tuning. Two modified probability of detection curves are shown in Figure 7. Two curves of 3 db peak power reduction are also plotted, and it can be seen that these intersect the true detection curves at the 50% probability point and have approximately symmetric and opposite errors about this point. The calculation of detection probability for a sufficiently large number of sine shaped pulses can therefore be approximated by a simple 3 db power reduction. For a mistuned pulse, the total probability of the impulses as well as the steady state can be obtained through the use of Eq. 8 providing the peak signal power is known.

In order to apply Eq. 8 to calculate the total probability of detecting the off-tuned pulse, it is now only necessary to obtain the peak value of the steady state portion of the overall pulse. Applying the conservation of energy axiom the steady state power amplitude is found to be

$$(13) \quad \text{INR} \cdot \tau\beta - 2 \text{ INR} \cdot F = \sum_{1}^n \widehat{\text{INR}}_{SS}$$

where

INR = the interference to noise ratio ( $\wedge$  means a peak value)

F = a factor derived from the previous discussion

$$(14) \quad \widehat{\text{INR}}_{SS} = \frac{1}{\tau\beta - 2} \sum_{1}^n \widehat{\text{INR}}_{SS}$$

therefore

$$(15) \quad \widehat{\text{INR}}_{SS} = \text{INR} \left( \frac{(\tau\beta - 2F)}{(\tau\beta - 2)} \right)$$

It is now only necessary to apply these results and Eq. 8 to obtain the complete probability of threshold detecting an off-tuned pulse.

#### IV. CONTINUOUSLY MODULATED SYSTEMS

##### A. General Discussion

The first problem to analyze in continuously modulated systems is again that of combination of undesired interfering signals with the desired signal. Since again it will be impossible to obtain the exact output of Eq. 4, it will be desirable to observe the trends that limiting forms of IF amplifiers produce. It will usually be sufficient to use tone modulated

information signals to indicate these trends. The beginning point in the analysis is again interfering signals of the form of Eq. 3b which describes general combinations of desired and undesired signals. The limiting forms of IF amplifiers can also again be considered as being between that of the square and the gaussian bandpass characteristic. The problem at this point can be divided further into AM and phase or frequency analysis problems.

#### B. AM System Analysis

For the AM desired and AM undesired signal case the off-tuned interfering signal components are attenuated in amplitude to a degree depending upon the amount of off-tuning and the attenuation of the particular amplifier to be analysed. If the square IF amplifier is considered the bandpass characteristic has the effect of eliminating all components outside the passband while linearly changing the phase of all components that have been passed. All other amplifiers (where the gaussian is a particular example) change the relative amplitude of the interfering signals as well as the relative signal phases. The result is that the interfering information components act completely changed and can be of comparable amplitude to the carrier signal. These two specific limiting cases should be clearly separated. In the first, ideally, only the phase of the signal components is changed. This in essence means, that in the case of voice, where phase has relatively little significance, the information bearing signal will be detected. If both the amplitude and phase of the signal are of importance, as in a video signal, the result will be a distorted signal.

In this second case the signal is changed in amplitude and frequency with the result that both audio and video type of signals are distorted. The exact degree of distortion is, of course, still dependent on the amplifier parameters. It is apparent, however, that the limiting result is a completely distorted signal.

In the case in which only the phase has been linearly changed by the off-tuning, the interfering signal can be expressed from Eq. 3b and Eq. 4 as

$$(16) \quad I'(t) = A_I \cos [(\omega_o + \Delta\omega)t + \phi_I + K\phi\Delta\omega] \\ + A_I m_I \cos [(\omega_o + \Delta\omega - \omega_I)t + \phi_I + K\phi(\Delta\omega - \omega_I)] \\ + A_I m_I \cos [(\omega_o + \Delta\omega + \omega_I)t + \phi_I + K\phi(\Delta\omega + \omega_I)]$$

where

$I$  = Interfering signal nomenclature

$\Delta\omega$  = The radian off-tuned frequency

$K\phi$  = The IF amplifier phase constant

This can in turn be approximately rewritten as

$$(17) \quad I'(t) \approx A_I \cos [(\omega_o + \Delta\omega)t + \phi_I + K\phi\Delta\omega] \\ + A_I m_I' \cos [(\omega_o + \Delta\omega - \omega_I)t + \phi_I + K\phi\Delta\omega] \\ + A_I m_I' \cos [(\omega_o + \Delta\omega + \omega_I)t + \phi_I + K\phi\Delta\omega]$$

where

$$m_I' = m_I \cos(K\phi\omega_I)$$

Although this approximation is certainly not general it does show the only slightly modified nature of the original signal and does allow us to write from Eq. 7 and Eq. 17 the square law detected output for an AM desired signal and the off-tuned interfering signal. This is found to be

$$(18) \quad V_o(t) \approx 2A_s^2 m_s^2 \cos^2 \omega_s t + A_I^2 m_I'^2 \cos^2 \omega_I t \\ + A_s^2 m_s^2 \cos^2 \omega_s t + A_I^2 m_I'^2 \cos^2 \omega_I t \\ + 2 A_s A_I \cos(\Delta\omega t + \phi_I + K\phi\Delta\omega) [1 + m_I \cos\omega_s t + m_I' \cos\omega_I t \\ + m_s m_I' \cos \omega_s t \cos \omega_I t]$$

The square law output is chosen because it offers a complete solution and still exemplifies the nature of the problem. The linear detector produces an infinite number of cross product terms and becomes difficult to handle. The fundamental terms are the same, however, in each case. The IF amplifier changed the magnitude of the interfering sideband but only changed the phase of the beat term (the predominant interfering term). The undesired components can also be seen to be reduced by a power of the undesired to desired carrier ratio's [for the case when  $s(t) > I(t)$ ].

For the general output in which both the amplitude and phase has been changed the answer can be shown to be

$$(19) \quad V(t)^2 = A_{11}^2 + A_{12}^2 + \dots A_{IN}^2 + A_s^2 + 2A_s^2 m_s \cos\omega_s t + A_s^2 m_s^2 \cos^2 \omega_s t \\ + 2A_s [A_{11} \cos(\Delta\omega_1 t + \theta_1) + \dots A_{IN} (\cos\Delta\omega_N t + \theta_N)] \\ + 2A_{11} A_{12} \cos [(\Delta\omega_1 + \Delta\omega_2)t + \theta_1 + \theta_2] \\ \vdots \\ + 2A_{1j} A_{IN} \cos [(\Delta\omega_j + \Delta\omega_N)t + \theta_j + \theta_N] \\ \vdots \\ + 2A_{IN-1} A_{IN} \cos [(\Delta\omega_{N-1} + \Delta\omega_N)t + \theta_{N-1} + \theta_N] \\ + 2A_s m_s \cos\omega_s t [A_{11} \cos(\Delta\omega_1 t + \theta_1) + \dots A_{IN} \cos(\Delta\omega_N t + \theta_N)]$$

where the DC terms have not been removed



The answer consists of DC terms, the desired and undesired terms, interference cross product terms, and the interference and the desired signal cross product terms. Due to the involved nature of the multiple interference terms no simplification will be made.

Another type of interfering problem of interest is a wideband FM off-tuned signal interfering with a narrow band AM system. For a tone modulate FM the interfering signal produces the IF impulse response shown in figure 8. This interfering signal can be written as

$$(20) \quad I(t) = \left\{ \frac{AT}{\pi T} + \sum_{k=1} \left[ \frac{2AT}{\pi} \left( \frac{\cos \pi K\tau/2T}{T^2 - K^2\tau^2} \right) \right] \right\} \cos \frac{2\pi Kt}{\tau} \cos[(\omega_0 + \Delta\omega)t + \phi_I]$$

where,

$T$  = pulse period  
 $\tau/2$  = pulse width  
 $A$  = pulse amplitude

For any particular set of parameters a finite number of terms can be used to approximate the desired pulse train. For the particular case of commercial FM

where

$$T = \frac{1}{75\text{KC}}$$

and,

$$T \gg \tau$$

Assume for convenience that

$$T = 10\tau$$

Substituting these values into Eq. 20 the following approximation was obtained

$$(21) \quad \begin{array}{l} I_{\text{cosine}} \\ \text{pulse} \end{array} (t) \approx \sum_{k=1} \left[ .998 \cos \frac{2\pi t}{t} + .996 \cos \frac{\pi t}{T} + .991 \cos \frac{2\pi t}{3T} \right. \\ \left. + .984 \cos \frac{\pi t}{2T} \right]$$

It is therefore only necessary to substitute the value of the constant coefficient into Eq. 19 to obtain the detected output signal.

A number of off-tuned AM interfering examples have now been given. The last type of problem to be discussed consists of FM systems subject to off-tuned signals.

#### C. FM System Analysis

For the FM signal case the limiter preceding the detector ideally peaks the combined signal amplitude constant. The result is a type of signal similar to the previous problem in which only the phase change was considered.

For an off-tuned AM interfering signal the IF output signal obtained from Eq. 18 can be used. Applying this to the ideal FM detector Eq. 7 the output can be shown to be (without the factor of  $2\pi$ )

$$(22) \quad \frac{d\phi(t)}{dt} = B_s \omega_s \cos \omega_s t +$$

$$\frac{R_I [1+m'_I \cos \omega_I t] [\Delta\omega - B_s \omega_s \cos \omega_s t] \left\{ \cos[\Delta\omega t + \phi_I - B_s \cos \omega_s t] + R_I [1+m'_I \cos \omega_I t] [\Delta\omega - B_s \omega_s \cos \omega_s t] \right\}}{1 + R_I^2 [1+m'_I \cos \omega_I t]^2 + 2R_I [1+m'_I \cos \omega_I t] \cos[\Delta\omega t + \phi_I - B_s \cos \omega_s t]}$$

$$\frac{R_I m'_I \omega_I \sin \omega_I t \sin [\Delta\omega t + \phi_I - B_s \cos \omega_s t]}{1 + R_I^2 [1+m'_I \cos \omega_I t]^2 + 2R_I [1+m'_I \cos \omega_I t] \cos[\Delta\omega t + \phi_I - B_s \cos \omega_s t]}$$

where

$B =$  the FM modulation factor

$R_I = A_I / A_s$

Although this answer still involves Bessel series expansions the form can be readily reduced for any desired formulation. The general case of an off-tuned FM interference signal can be handled in a similar fashion and the answer can be shown to be

$$(23) \quad \frac{d\phi(t)}{dt} = \omega_s B_s \cos \omega_s t +$$

$$\frac{R_I (\Delta\omega + B_I \omega_I \cos \omega_I t - \omega_s B_s \cos \omega_s t) \left\{ \cos[\Delta\omega t + \phi_I + B_I \cos \omega_I t - B_s \sin \omega_s t] + R_I \right\}}{1 + R_I^2 + 2R_I \cos [\Delta\omega t + \phi_I + B_I \cos \omega_I t - B_s \sin \omega_s t]}$$

## V. SUMMARY

The off-tuned signal cases that have been discussed introduce complications that are difficult to handle both from the standpoint of not knowing the exact equipment parameters and the mathematical complications of handling unsymmetrical signals. The philosophy adopted has been to study the trends introduced by limiting forms of amplifiers and from this to predict a desired output. The probability of threshold detecting an off-tuned pulse signal has been given. The off-tuning effects introduced by interfering signals to AM and FM desired signal receivers has been discussed and some specific results presented. The interfering signals are predominated by terms proportioned to powers of the undesired to desired carrier ratio's and the beat interfering term. The basic approach and philosophy that has been used for these problems can be extended to more complicated problems, however, increased mathematical complication can be expected.

#### ACKNOWLEDGEMENT

The work described above is sponsored by the three Military Departments, and is being conducted under Contract No. AF 19 (604)-8440 with the Electronic Systems Division, Air Force Systems Command.

#### REFERENCES

1. R. J. Mayher "Interference Detection Modeling" ECAC Technical Memorandum No. X003-18 June, 1963.
2. S. O. Rice "Mathematical Analysis of Random Noise" Dover Publications.
3. D. Middleton "Introduction to Statistical Communication Theory" McGraw Hill.
4. H. E. Kallman, "Transient Response" Proc. IRE Volume 33 #3 March 1945.
5. J. I. Marcum, "A Statistical Theory of Target Detection by Pulsed Radar" IRE IT-6 #2 April 1960.

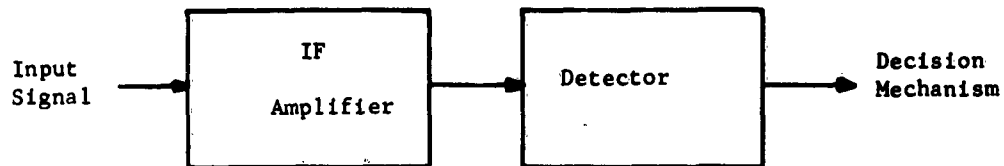
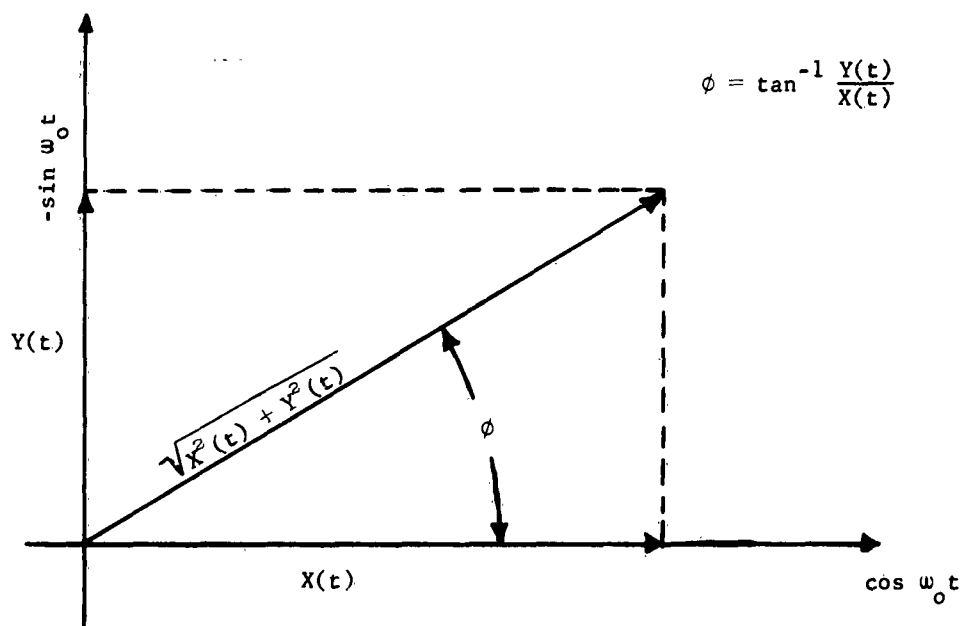


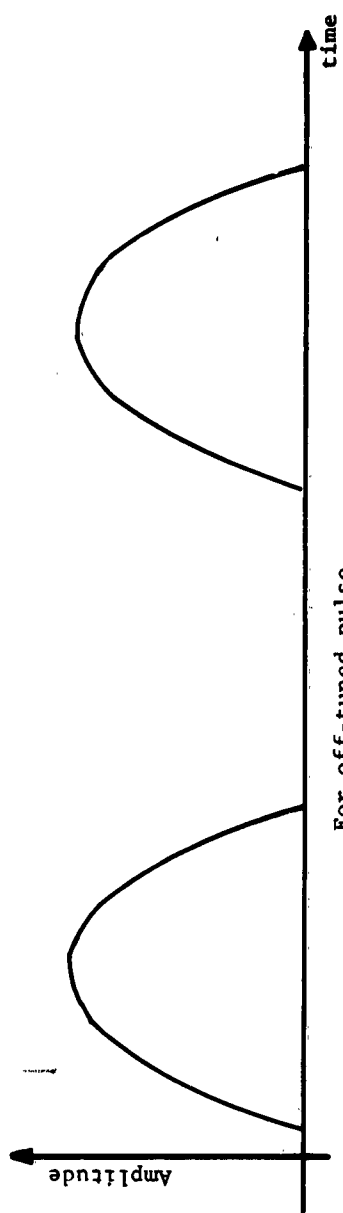
Figure 1

# TYPICAL RECEIVER

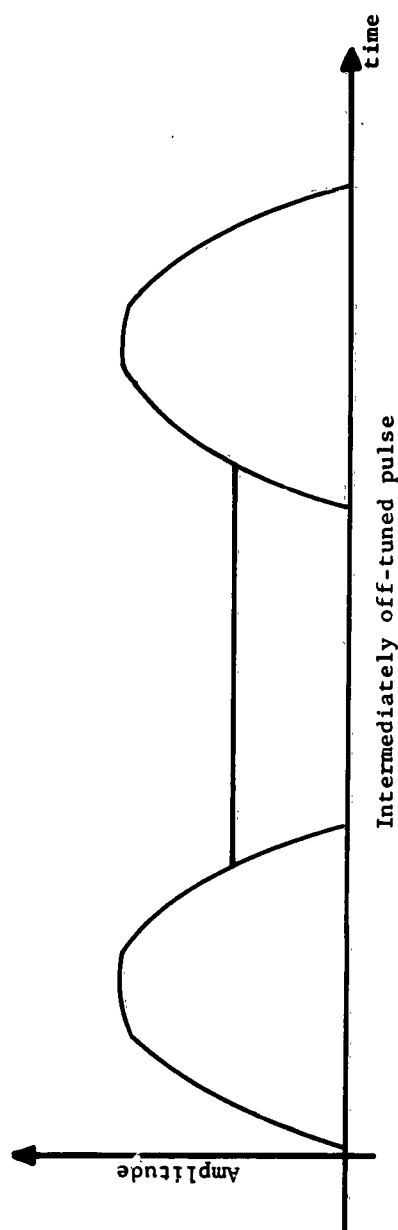


# VECTOR SIGNAL RELATIONSHIPS

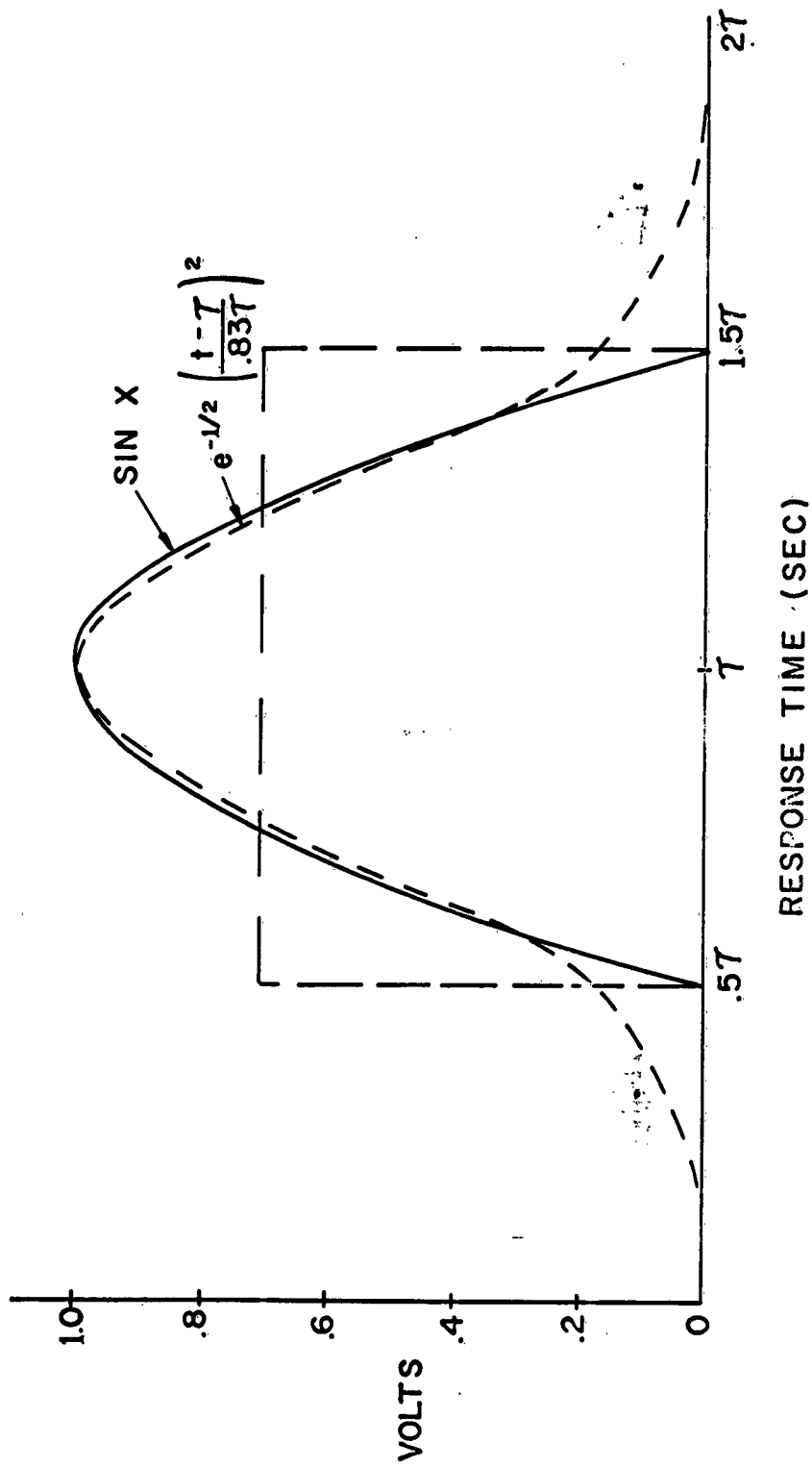
Figure 2



For off-tuned pulse  
Figure 3a



Intermediately off-tuned pulse  
Figure 3b



SIN X FITTED ON GAUSSIAN IMPULSE RESPONSE CURVES ARE  
FITTED AT THE POWER 3 DB POINTS

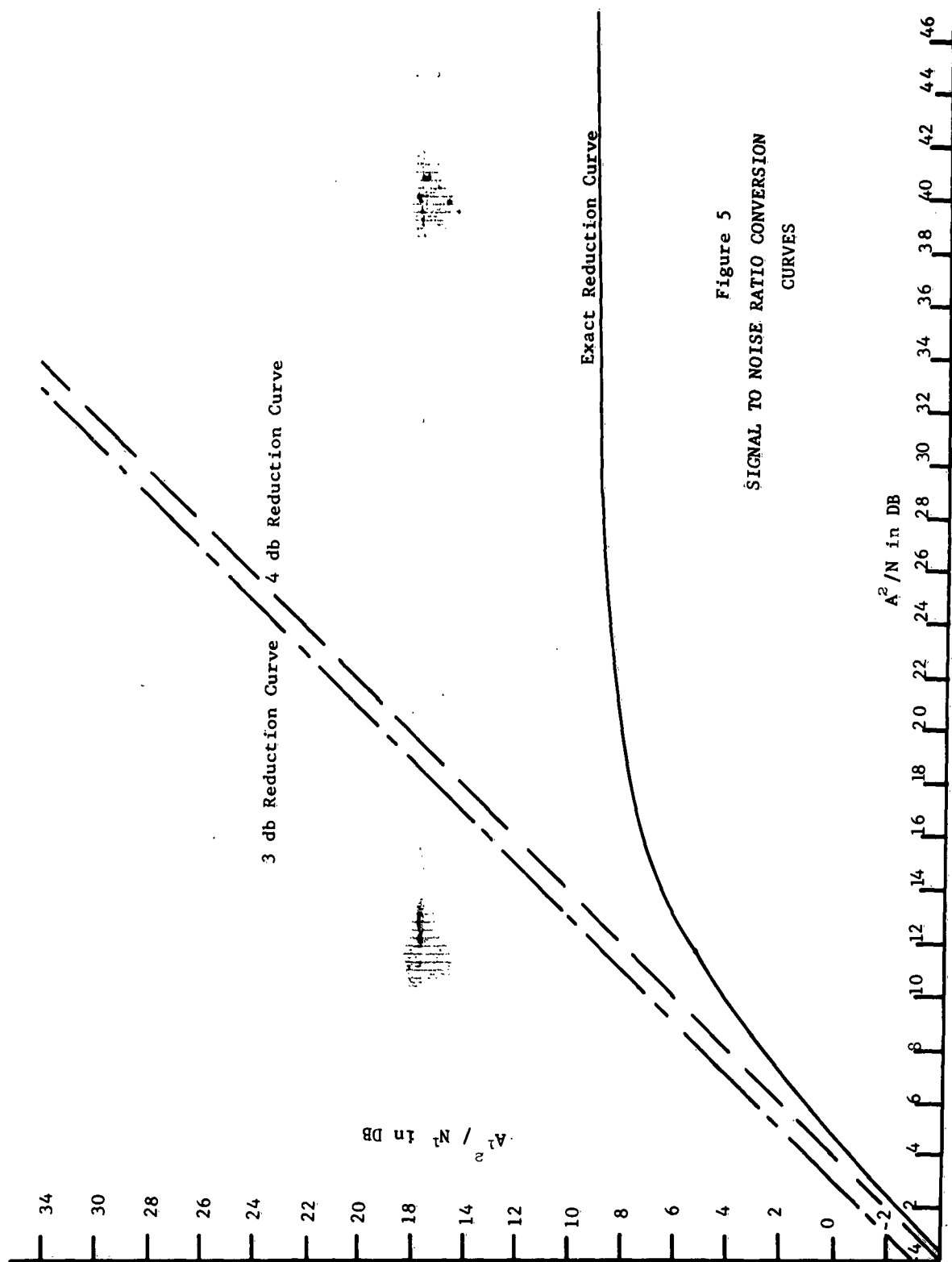


Figure 5  
SIGNAL TO NOISE RATIO CONVERSION  
CURVES

Figure 6  
THRESHOLD TO NOISE RATIO CONVERSION CURVE

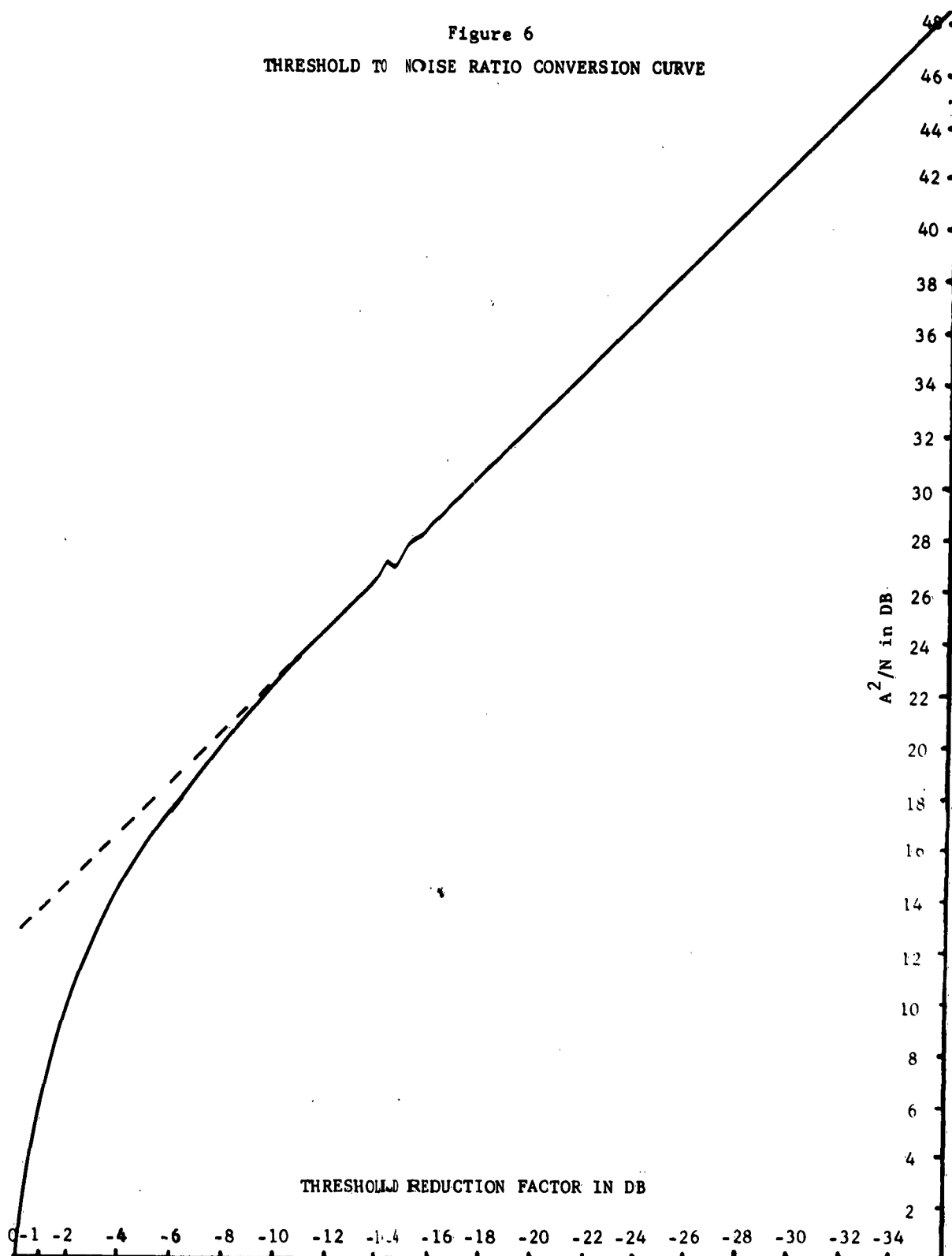


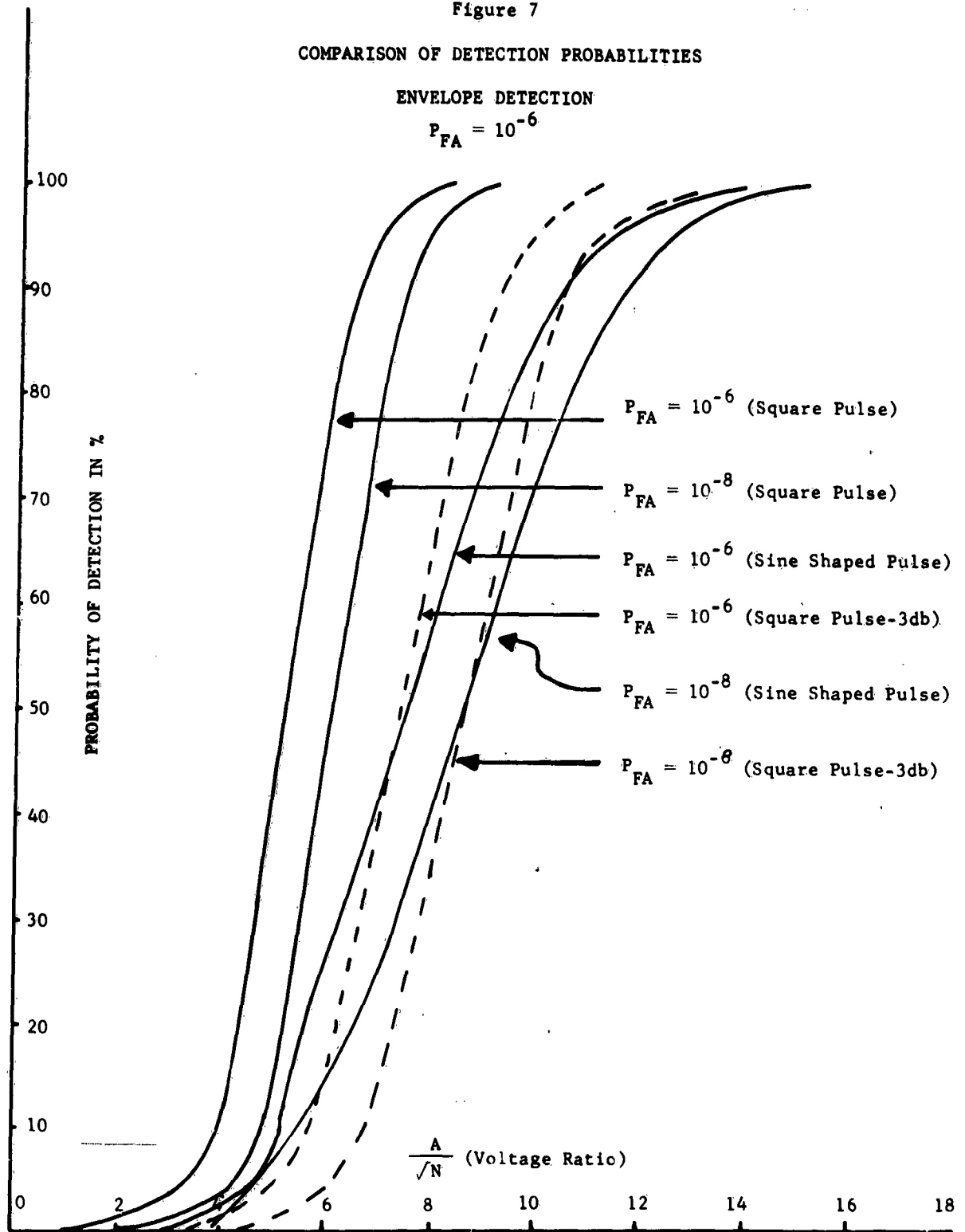


Figure 7

COMPARISON OF DETECTION PROBABILITIES

ENVELOPE DETECTION

$$P_{FA} = 10^{-6}$$



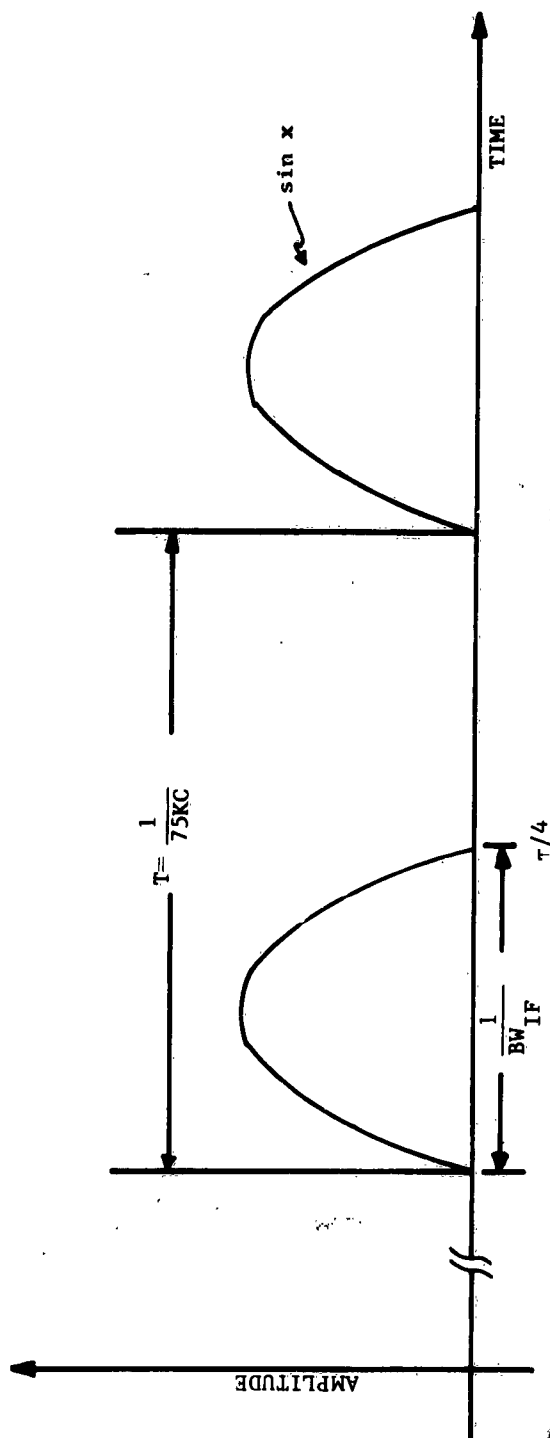
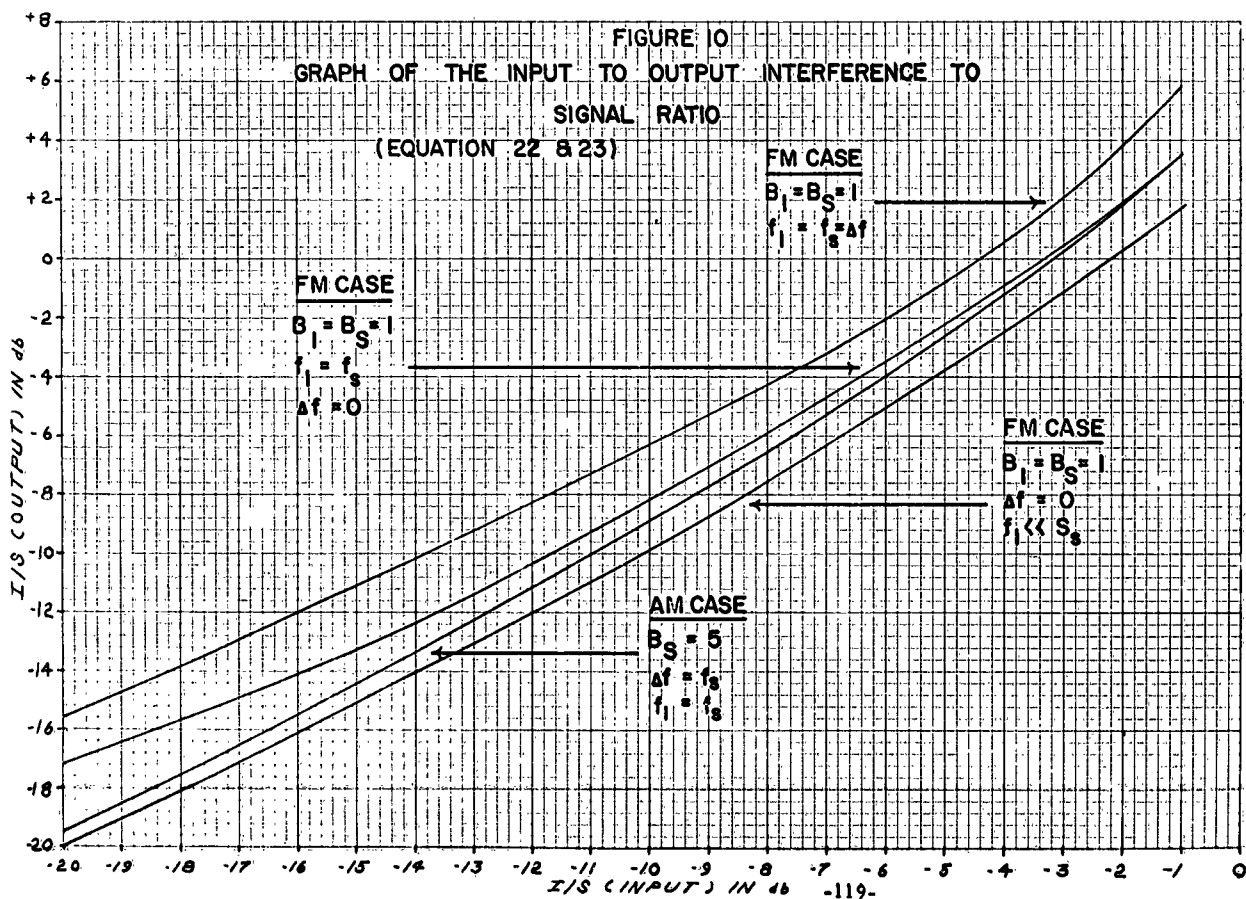
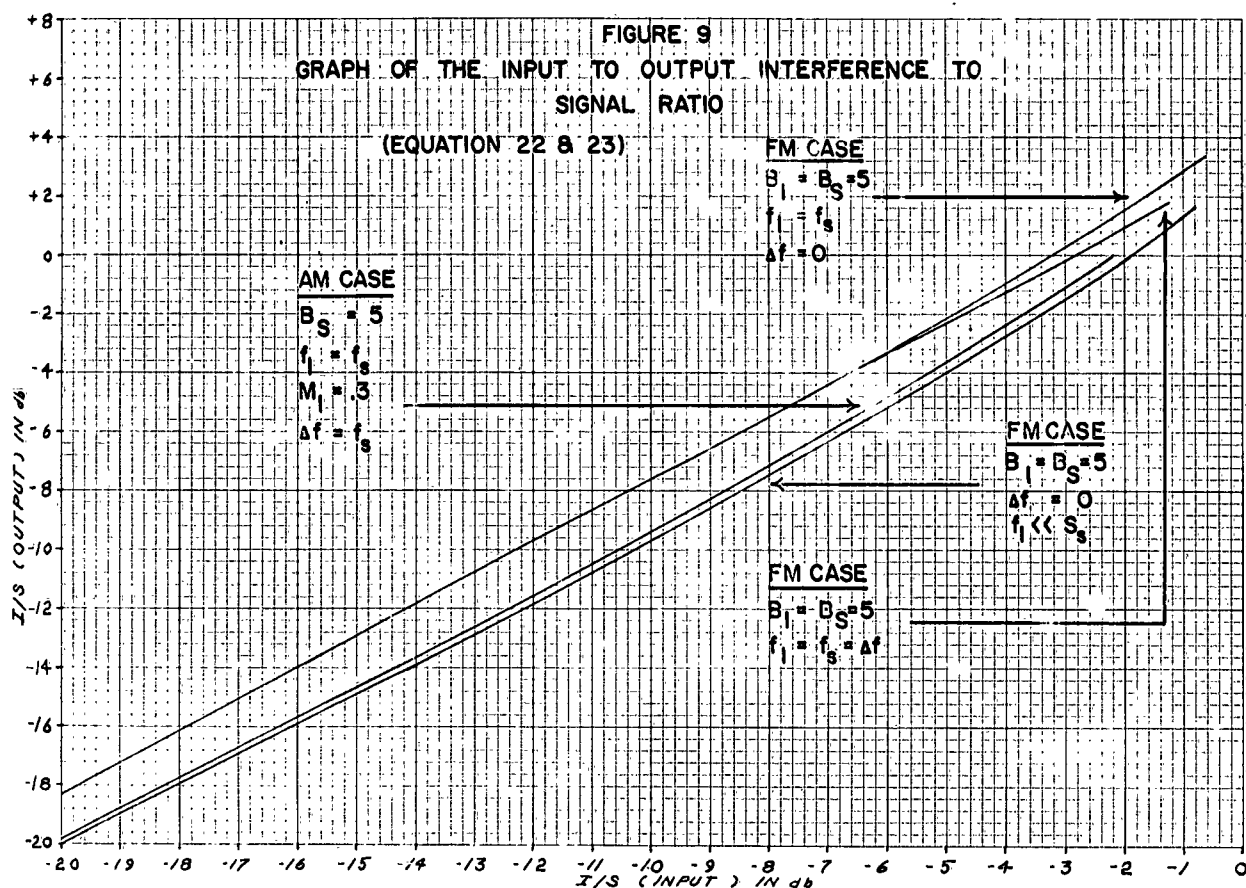


Figure 8 Cos X Pulse Approximation



# RADIO FREQUENCY INTERFERENCE IN DIGITAL TWO-PHASE COHERENT COMMUNICATION SYSTEMS

A. Krinitz  
ADCOM, Inc.  
Cambridge, Massachusetts

**Abstract.** - The evaluation of error rates due to (unintentional) radiofrequency interference in digital two-phase coherent communication systems requires detailed statistical data about the interference and presents a computational problem which may become prohibitive for any but the simplest forms of interference such as Gaussian, CW or impulse noise. Consequently, the least upper bound on the error rate or the probability of error which is derived in this paper and which can be easily evaluated from relatively simple interference data and which is applicable to any wide-sense stationary radio frequency interference, including non-Gaussian interference, becomes a very useful performance criterion.

The simplest form of interference data is the average interference power in the receiver passband from which the signal-to-interference ratio

$$\rho = \frac{\text{maximum signal amplitude at receiver filter output}}{(\text{average interference power at receiver filter output})^{1/2}}$$

may be evaluated. The least upper bound on the probability of error and on the average error rate for the class of wide-sense stationary interference (not necessarily Gaussian) with a uniformly distributed r-f phase and with a given  $\rho$  is shown to be

$$\frac{1}{\pi} \cos^{-1} \rho \quad \text{for } \rho \leq \gamma = 0.794$$

and

$$\frac{\gamma^2 \cos^{-1} \gamma}{\pi} - \frac{1}{\rho^2} \quad \text{for } \rho \geq \gamma = 0.794$$

Three important properties obtain:

1. The least upper bound gives the exact average error rate for CW interference if  $\rho \leq \gamma = 0.794$  and for intermittent CW interference, with a duty cycle =  $(\gamma/\rho)^2$  if  $\rho \geq \gamma = 0.794$ .

2. Relatively close agreement between the least upper bound and the error rate for Gaussian interference is achieved for  $\rho < 1$ .
3. The least upper bound coincides with the error rate due to pulse interference for  $\rho$  in the vicinity of  

$$0.794/(\text{number of interfering pulses per bit})^{1/2}.$$

## I. INTRODUCTION

The ultimate performance criterion for a binary communication system is the error rate or the probability of error. Extensive analyses of error rates for Gaussian, CW and impulse interference have been reported in the literature. It is the purpose of this paper to present a method for evaluating the performance in the presence of more general forms of (unintentional) radio frequency interference. In connection with this two types of problems are encountered:

- (1) the scarcity of data about the statistics of the interference or its waveform characteristics and,
- (2) the prohibitive computational problem of evaluating the error rates from the interference data for any but the simplest forms of interference such as Gaussian, CW and impulse noise.

The approach undertaken here was designed to overcome these particular problems. We have assumed at the outset that the r-f phase of the interference is uniformly distributed and that only the simplest interference data are available, namely the signal-to-interference ratio in the receiver passband. Such information does not uniquely determine the error rate or the probability of error. However, as is shown in Section IV, the signal-to-interference ratio does fix an upper bound on the average error rate. Furthermore, the particular upper bound is a least bound because interference waveforms exist with the given signal-to-interference ratio (and not necessarily matched to the signal waveform) which will produce an error rate equal to the upper bound.

The least upper bound is obtained as a simple function of the signal-to-interference ratio and is applicable to any wide-sense stationary interference including any non-Gaussian interference.

Graphs comparing the bound with the actual error rate for specific interference waveforms are given together with some general conclusions.

The pertinent communication receiver is shown in Figure 1. The information is carried by the RF phase of the signal waveform, with the zero

degree phase corresponding to a Mark, and the 180 degree phase corresponding to a Space. Aside from this phase difference, the waveforms representing Mark and Space are identical.

The IF stage is not explicitly indicated in the block diagram and the local oscillator frequency and phase are assumed to be locked to the RF carrier of the signal. The impulse response,  $h(t)$ , of the filter is such that (1) the magnitude of the signal component at the filter output will take on a maximum value,  $A$ , at equally spaced instants of time  $t_k = kT$ ; where  $k$  is an integer and  $T$  is the baud length; and (2) there is no intersymbol overlap at the filter output at the time instants  $t_k$ . Since the receiver is synchronized to the transmitter, the time instants  $t_k$  are known a priori. The filter output is therefore sampled at  $t_k$ ; if the sample is positive the decision is a Mark, and if the sample is negative the decision is a Space.

## II. DESCRIPTION OF INTERFERENCE

The interference is represented as a modulated RF waveform,

$$\text{Re} \left[ I(t) e^{j\omega_i t} e^{j\phi} \right],$$

where  $I(t)$  is a complex valued time function whose magnitude is the amplitude modulation and whose phase is the phase and frequency modulation;  $\omega_i$  is the RF carrier frequency; and  $\phi$  is a phase angle.

At the sampling instant the filter output due to the interfering waveform is given by

$$i_k = \text{Re} \left[ \int_{-\infty}^{\infty} h(u) I(t_k - u) e^{-j\omega u} e^{j(\omega_i t_k - \omega_c t_k + \phi)} du \right] \quad (1)$$

where  $\omega$  is the frequency separation

$$\omega = \omega_i - \omega_c \quad (2)$$

and where the contribution from frequencies in the neighborhood of  $\omega_i + \omega_c$  has been neglected.

It is convenient to define the amplitude of the interference component as

$$j_k = \left| \int_{-\infty}^{\infty} h(u) I(t_k - u) e^{-j\omega u} du \right| \quad (3)$$

so that Equation (1) may be rewritten as

$$i_k = j_k \cos(\omega_i t_k - \omega_c t_k + \phi) \quad (4)$$

It is assumed that the phase angle  $\phi$  is a random variable uniformly distributed between 0 and  $2\pi$ ; and that the waveform  $I(t)$  is a member of an ensemble of some wide-sense stationary process. Consequently, the average value of  $I(t) I^*(t+\tau)$  must be a function of  $\tau$  only.

### III. THE PROBABILITY OF ERROR AT A SAMPLING INSTANT

An error is made whenever the interference component,  $i_k$ , is of opposite sign and greater magnitude than the magnitude,  $A$ , of the signal component. Therefore, for a given  $j_k$ , the probability of error at the  $k^{\text{th}}$  sampling instant is

$$\Pr(\text{error}/j_k) = p_k \Pr(i_k > A) + (1-p_k) \Pr(i_k < -A) \quad (5)$$

where  $p_k$  is the probability of a Space at the  $k^{\text{th}}$  sampling instant and  $(1-p_k)$  is the probability of a Mark at the  $k^{\text{th}}$  sampling instant. It follows from Equation (4) that for a uniformly distributed phase angle  $\phi$

$$\Pr(i_k > A) = \Pr(i_k < -A) = \begin{cases} \frac{1}{\pi} \cos^{-1} \frac{A}{j_k} & \text{for } j_k \geq A \\ 0 & \text{for } j_k \leq A \end{cases} \quad (6)$$

Hence (5) becomes

$$\Pr(\text{error}/j_k) = \begin{cases} \frac{1}{\pi} \cos^{-1} \frac{A}{j_k} & \text{for } j_k \geq A \\ 0 & \text{for } j_k \leq A \end{cases} \quad (7)$$

Averaging Equation (7) over the random variable  $j_k$  we obtain the probability of error at the  $k^{\text{th}}$  sampling instant

$$\Pr(\text{error}) = \epsilon_k = \int_{j_k=A}^{\infty} w_k(j_k) \frac{1}{\pi} \cos^{-1} \frac{A}{j_k} dj_k \quad (8)$$

where  $w_k(j_k)$  is the probability density function of  $j_k$  and  $\epsilon_k$  is used to designate the probability of error at the  $k^{\text{th}}$  sampling instant. Note that for a wide-sense stationary process the functions  $w_k(x)$  need not be the same functions for all  $k$ .

#### IV. EVALUATION OF THE LEAST UPPER BOUND

In this section the least upper bound on  $\epsilon_k$  is obtained for the class of wide-sense stationary interference with a given interference power at the output of  $h(t)$  in Figure 1.

Consider the function  $\frac{1}{\pi} \cos^{-1} A/j_k$  which is represented in Figure 2 by the curve a-b-c. Inasmuch as  $d^2/dx^2 \cos^{-1}(A/x)$  is negative for  $x > A$ , the line a'-b', which is tangent to a-b-c at some point  $J_k > A$ , will always dominate the curve a-b-c. Thus

$$\frac{1}{\pi} \cos^{-1} \frac{A}{j_k} \leq \frac{1}{\pi} \left[ \cos^{-1} \frac{A}{J_k} + \frac{A/J_k^2}{\sqrt{1 - (A/J_k)^2}} (j_k - J_k) \right] \quad \text{for } j_k > A$$

where the equality holds at  $j_k = J_k$ . Substituting into Equation (8) and redefining the variable of integration we obtain

$$\epsilon_k \leq \frac{\mu_k}{\pi} \cos^{-1} \frac{A}{J_k} + \frac{1}{\pi} \frac{A/J_k^2}{\sqrt{1 - (A/J_k)^2}} \left[ \int_{x=A}^{\infty} x w_k(x) dx - \mu_k J_k \right] \quad (9)$$

where

$$\mu_k = \int_{x=A}^{\infty} w_k(x) dx \leq 1 \quad (10)$$

is the probability that  $j_k$  is equal to or is larger than  $A$ . The point  $J_k$  is chosen to be

$$J_k = \left[ \overline{j^2} / \mu_k \right]^{1/2} \quad (11)$$

where  $\overline{j^2}$  is the mean square value of  $j_k$ , that is,

$$\overline{j_k^2} = \overline{j^2} = \int_{-\infty}^{\infty} x^2 w_k(x) dx \quad (12)$$

Since  $I(t)$  is a wide-sense stationary process, the output of the time invariant linear filter in Figure 1 must also be wide-sense stationary. Consequently  $\overline{j_k^2}$ , as given by Equation (12), must be independent of  $k$ .

From Equations (10), (11), and (12), and the fact that  $w_k(x)$  is non-negative, we obtain



$$J_k = \left[ \frac{1}{\mu_k} \int_{-\infty}^{\infty} x^2 w_k(x) dx \right]^{1/2} \geq \left[ \frac{1}{\mu_k} \int_{x=A}^{\infty} x^2 w_k(x) dx \right]^{1/2} \\ \geq \left[ \frac{A^2}{\mu_k} \int_{x=A}^{\infty} w_k(x) dx \right]^{1/2} \geq A \quad (13)$$

Consequently, as long as  $\mu_k > 0$ ,  $J_k \geq A$ . If  $\mu_k = 0$  the error rate becomes zero, for the interference will always be of smaller magnitude than the signal.

Note that

$$\int_{x=A}^{\infty} \left[ x - \int_{x=A}^{\infty} x \frac{w_k(x)}{\mu_k} dx \right]^2 \frac{w_k(x)}{\mu_k} dx \geq 0$$

which, after some manipulation, may be rewritten as

$$\left[ \mu_k \int_{x=A}^{\infty} x^2 w_k(x) dx \right]^{1/2} \geq \int_{x=A}^{\infty} x w_k(x) dx$$

Hence

$$\left[ \mu_k \int_{-\infty}^{\infty} x^2 w_k(x) dx \right]^{1/2} \geq \int_{x=A}^{\infty} x w_k(x) dx$$

so that as a result of (11) and (12) we get

$$\mu_k J_k \geq \int_{x=A}^{\infty} x w_k(x) dx$$

Thus, the second term on the right-hand side of Equation (9) is non-positive and

$$\epsilon_k \leq \frac{\mu_k}{\pi} \cos^{-1} \frac{A}{J_k} \quad (14)$$

The signal-to-interference ratio at the output of the filter  $h(t)$  (see Figure 1) may be defined as

$$\rho = \frac{A}{\left[ \overline{j^2} \right]^{1/2}} = \frac{A}{\sqrt{\mu_k} J_k} \quad (15)$$

where we have made use of Equation (11). Note that for a wide-sense stationary process  $\rho$  is independent of  $k$ . Substitution of Equation (15) into Equation (14) yields

$$\epsilon_k \leq \frac{\mu_k}{\pi} \cos^{-1} \sqrt{\mu_k} \rho \quad (16)$$

Recall that according to Equation (10),  $\mu_k \leq 1$ . Hence only two cases need be considered, one corresponding to  $\mu_k = 1$  and one to  $\mu_k < 1$ .

Case 1:  $\mu_k = 1$

In this case Equation (16) yields

$$\epsilon_k \leq \frac{1}{\pi} \cos^{-1} \rho \quad (17)$$

Case 2:  $\mu_k < 1$

For any given  $\rho$  the maximum value of  $\mu_k \cos^{-1} \sqrt{\mu_k} \rho$  occurs at

$$\mu_k = \gamma^2 / \rho^2 \text{ for all } k \quad (18)$$

where  $\gamma$  is the solution of the transcendental equation

$$\gamma = \cos \frac{\gamma/2}{\sqrt{1-\gamma^2}} \quad (19)$$

By trial and error

$$\gamma = 0.794 \quad (20)$$

Consequently, for  $\mu_k < 1$ , Equations (16) and (18) give

$$\epsilon_k \leq \frac{\gamma^2 \cos^{-1} \gamma}{\pi} \frac{1}{\rho^2} \text{ for } \rho > \gamma \quad (21)$$

The two cases are depicted graphically in Figure 3 in view of which the range  $\rho < \gamma$  must correspond to Case 1. Equations (17) and (21) can therefore be combined as follows:

$$\epsilon_k \leq \begin{cases} \frac{1}{\pi} \cos^{-1} \rho & \text{for } \rho \leq \gamma = 0.794 \\ \frac{\gamma^2 \cos^{-1} \gamma}{\pi} \frac{1}{\rho^2} & \text{for } \rho > \gamma = 0.794 \end{cases} \quad (22)$$

a plot of which is given in Figure 4. Note that the bound is independent of the sampling instant  $t_k$ . It follows from Equation (8) that the upper bound given by the right-hand side of Equation (22) is actually approached by an interfering waveform whose  $w_k(j_k)$  is of the form shown in Figure 5a if  $\rho \leq \gamma$ , and Figure 5b if  $\rho > \gamma$ . Figure 5a shows a single impulse located at  $j_k = A/\rho$  while 5b shows two impulses, one of area  $(1-\gamma^2/\rho^2)$  located at  $j_k = 0$ , and one of area  $\gamma^2/\rho^2$  located at  $j_k = A/\gamma$ . Since the plots in Figure 5 are independent of  $k$ , the interference waveform corresponding to Figure 5a is a continuous wave and that corresponding to Figure 5b may be characterized as an intermittent CW.

The signal-to-interference ratio  $\rho$  may be readily calculated by first squaring and averaging Equation (3). Thus

$$\overline{j_k^2} = \overline{j^2} = \int_{-\infty}^{\infty} \int_{-\infty}^{\infty} h(\tau) K_{II}(\tau - \tau') e^{-j\omega(\tau - \tau')} h(\tau') d\tau d\tau' \quad (23)$$

where  $K_{II}(\tau)$  is the autocorrelation function of  $I(t)$ , that is

$$K_{II}(\tau) = \overline{I(t)I^*(t+\tau)} \quad (24)$$

The autocorrelation function is then expressed in terms of its spectral density  $L(\sigma)$ ,

$$K_{II}(\tau) = \int_{-\infty}^{\infty} L(\sigma) e^{j\sigma\tau} d\sigma \quad (25)$$

which upon substitution into Equation (23) yields

$$\overline{j^2} = \int_{-\infty}^{\infty} |H(\omega - \sigma)|^2 L(\sigma) d\sigma \quad (26)$$

where

$$H(\omega) = \int_{-\infty}^{\infty} h(\tau) e^{-j\omega\tau} d\tau \quad (27)$$

With the help of Equation (15), the signal-to-interference ratio becomes

$$\rho = \frac{A}{\left[ \int_{-\infty}^{\infty} |H(\omega - \sigma)|^2 L(\sigma) d\sigma \right]^{1/2}} \quad (28)$$

which is a function of the frequency separation  $\omega$ .

Thus we have shown that for the class of wide-sense stationary interference processes with a given spectral power density, or a given  $\rho$ , the right-hand side of Equation (22) yields the least upper bound on the probability of error.

#### V. THE ERROR RATE AND THE PROBABILITY OF ERROR

A random variable  $z_k$  corresponding to the  $k^{\text{th}}$  sampling instant is defined such that

$$z_k = \begin{cases} 1 & \text{if an error is made at the } k^{\text{th}} \text{ sampling instant} \\ 0 & \text{if no error is made at the } k^{\text{th}} \text{ sampling instant} \end{cases} \quad (29)$$

The total number of errors made in a sequence of  $N$  sampling instants is therefore given by

$$\sum_N z_k$$

where the summation extends over  $N$  values of  $k$ . The number of errors per bit or the error rate  $e$  is

$$e = \frac{1}{N} \sum_N z_k \quad (30)$$

so that the average error rate becomes

$$\bar{e} = \frac{1}{N} \sum_N \bar{z}_k \quad (31)$$

In view of Equation (29) we have

$$\bar{z}_k = \Pr(z_k = 1) = \Pr(\text{error})$$

which, with the help of Equation (8), becomes

$$\bar{z}_k = \epsilon_k \quad (32)$$

Substitution of Equation (32) into Equation (11) yields the average error rate

$$\bar{e} = \frac{1}{N} \sum_{k=1}^N \epsilon_k \quad (33)$$

Thus, in contrast to the case of strictly stationary interference, the average error rate is not, in general, given by the probability of error. However, since the right-hand side of Equation (22) is independent of  $k$ , the least upper bound on the average error rate  $\bar{e}$  is the same as the least upper bound on the probability of error  $\epsilon_k$ . Hence

$$\bar{e} \leq \begin{cases} \frac{1}{\pi} \cos^{-1} \rho & \text{for } \rho \leq \gamma \\ \frac{\gamma^2 \cos^{-1} \gamma}{\pi} \frac{1}{\rho^2} & \text{for } \rho > \gamma \end{cases} \quad (34)$$

## VI. COMPARISON OF LEAST UPPER BOUND WITH ACTUAL ERROR RATES

Actual error rates have been computed<sup>1</sup> for

1. Gaussian interference
2. CW interference
3. Pulse interference

The least upper bound is compared with the actual error rates for Gaussian interference in Figure 4 and for pulse interference in Figure 6.

Error rates from CW interference (which have not been plotted) are equal to the least upper bound for  $\rho \leq \gamma = 0.794$  and fall off sharply along the 0 db abscissa as the asymptote for  $\rho > \gamma = 0.794$ .

## VII. CONCLUSIONS

In view of the scarcity of detailed interference data and the computational difficulties encountered in the evaluation of error rates for any but the simplest forms of interference, the least upper bound becomes a useful measure of performance. The bound can be easily evaluated from only the knowledge of the signal-to-interference ratio and it is the least upper bound for the class of wide-sense stationary interference (including non-Gaussian interference) with a uniformly distributed r-f phase and a given signal-to-interference ratio in the receiver passband.

The least upper bound coincides with the actual error rate for classes of interference waveforms enumerated in the abstract.

## ACKNOWLEDGEMENTS

The work reported here was performed at Melpar's Applied Science Division (formerly at Watertown, Massachusetts) and was supported by the Air Research and Development Command at Rome Air Development Center under Contract AF 30 (602)-2528.

The presentation of this paper was made possible through the support received from ADCOM, Inc., Cambridge, Massachusetts.

## REFERENCES

1. A. Krinitz, "Long Range Communications Interference Study — Technical Note on Radio Frequency Interference in Digital Two-Phase Coherent Communication Systems," Melpar Technical Note, Applied Science Division (formerly at Watertown, Massachusetts). Prepared for Rome Air Development Center, Air Research and Development Command under Contract AF 30 (602)-2528.

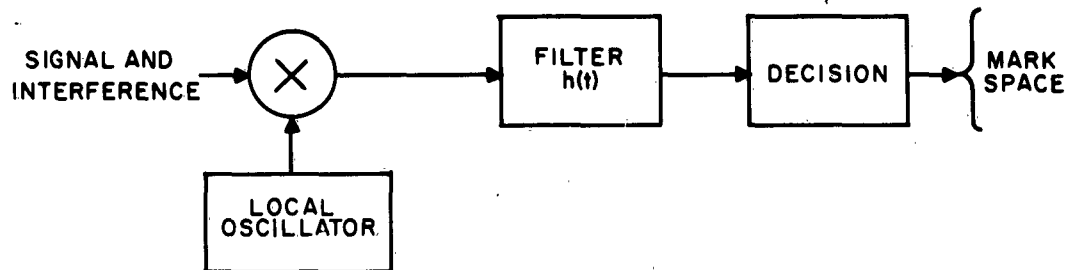


Figure 1 Receiver

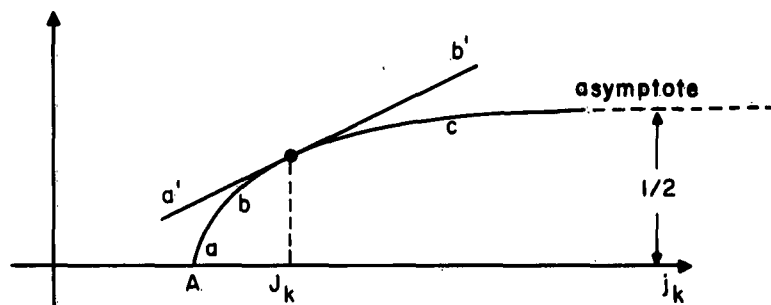


Figure 2 Upper bound for  $1/\pi \cos^{-1} A/j_k$

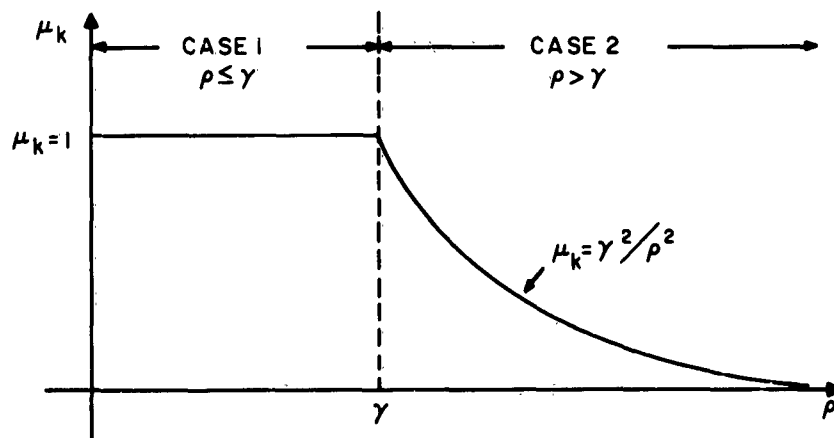


Figure 3 Graphical representation of Cases 1 and 2

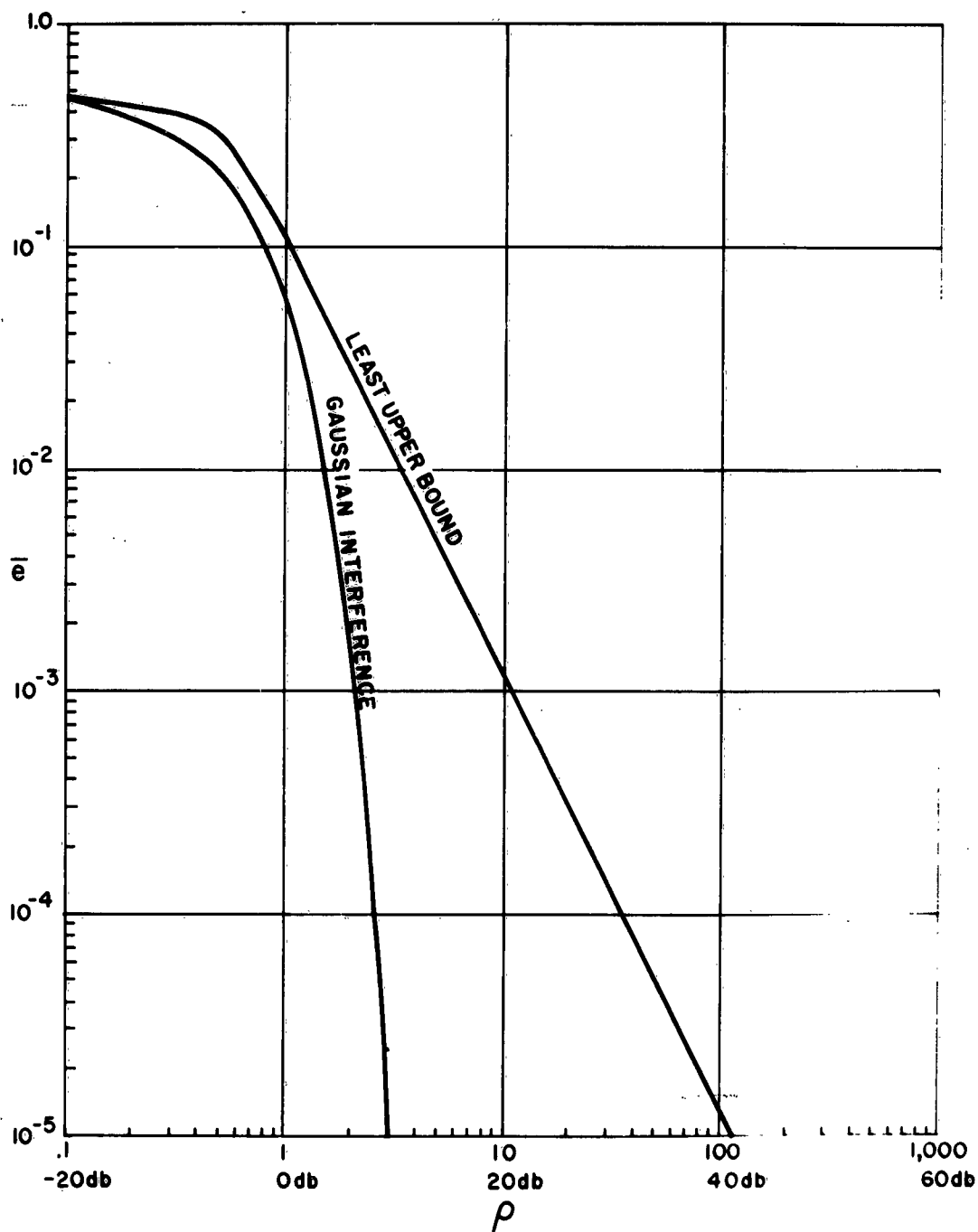


Figure 4 Average error rates corresponding to the least upper bound and Gaussian interference



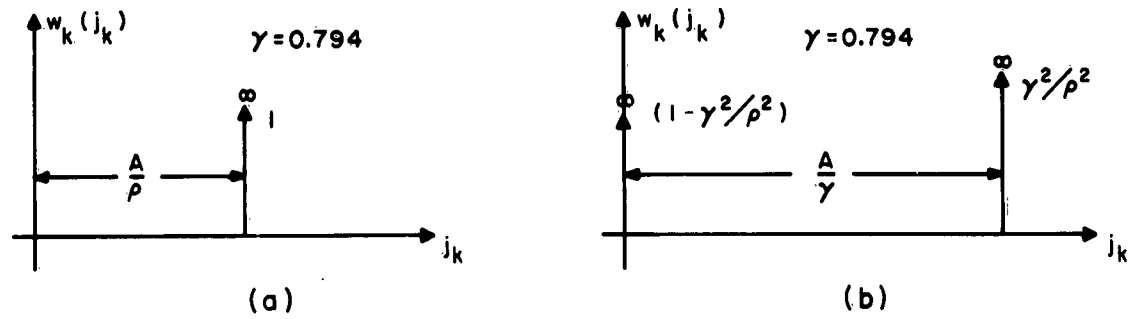
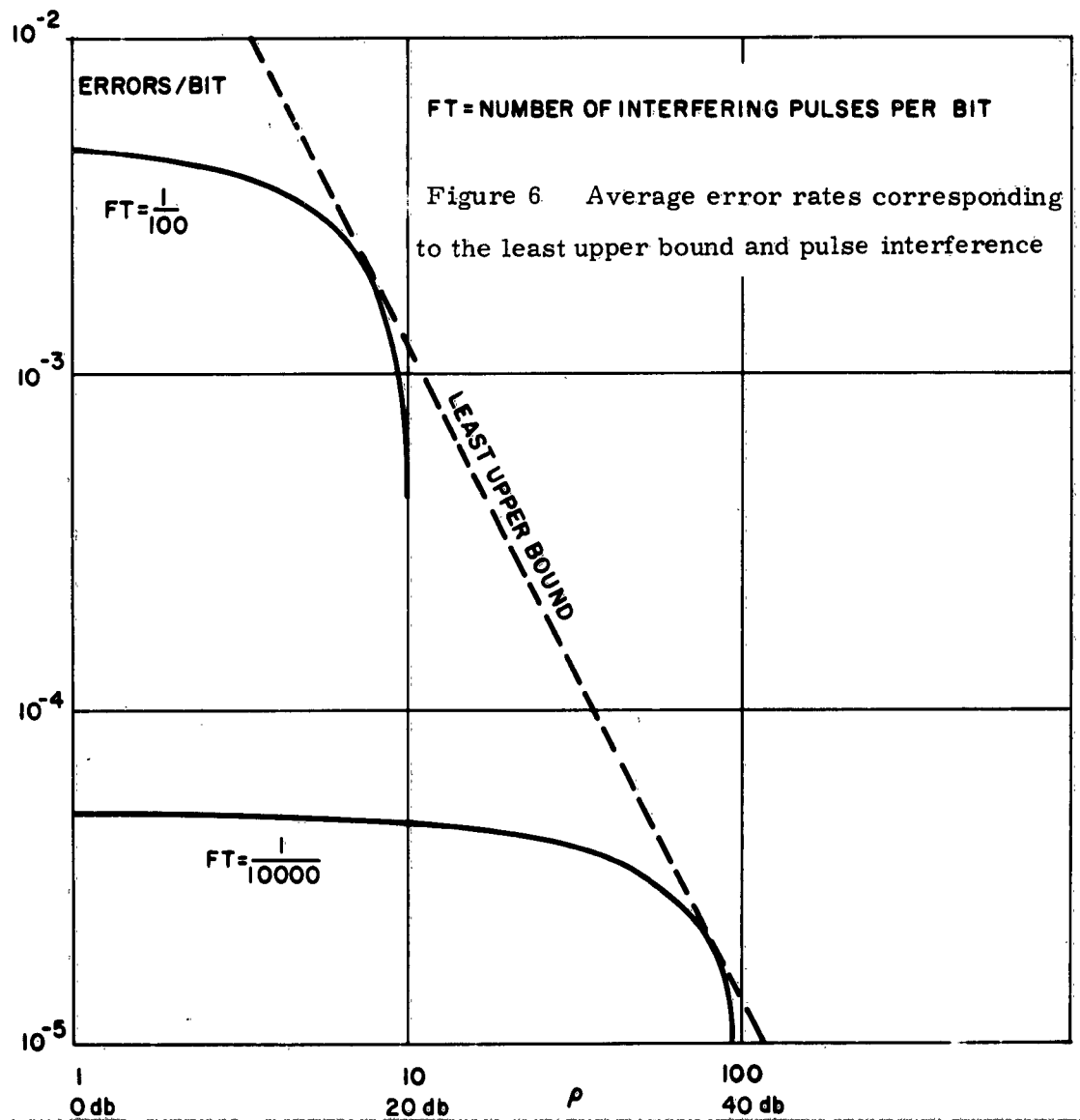


Figure 5  $w_k(j_k)$  corresponding to the upper bound



## LOW-PASS TRANSMISSION LINES FOR RFI PROTECTION

H. G. Tobin and L. J. Greenstein  
IIT Research Institute  
Chicago, Illinois

**Abstract** - This paper deals with the analysis, design and fabrication of transmission lines which may be used to protect electroexplosive devices from inadvertant firing. Analysis was performed in order to determine the attenuation characteristics of various transmission lines. Initial investigation was concerned with the dissipation of a conventional line. Such a line is defined as one which has no variation in geometry as a function of length, in material properties as a function of frequency, and which has a homogeneous material between its two conductors. A general technique is described for optimizing the attenuation characteristics of a distributed line in order to achieve the desired amount of rf protection. This technique is applied to the conventional line and the optimum line parameters derived. It is shown that the attenuation of such a line will vary at a rate no greater than the square root of frequency. A more rapid change in attenuation is possible if a line utilizing two layers of dielectric is used. Analysis is given which shows, under optimum conditions, that the attenuation may vary as the second power of the frequency. The general optimization technique is used to derive the required line parameters for such a line. Difficulties in obtaining materials with the proper electrical characteristics, and the fabrication of lines using these materials are discussed. The results of measurements performed upon fabricated lines is presented. The correlation between the analytical results and those obtainable with a practical line is discussed.

### I. INTRODUCTION

Situations commonly arise in which it becomes necessary to provide audio control or intelligence signals to certain equipments which must operate in a high-intensity, rf environment. If cables are necessary to transmit these signals from one location to another, rf energy may be coupled into the cable and transmitted to the equipment, causing undesirable responses. The gravity of this situation increases directly with the length of the cable runs and the sensitivity of the victim equipments to high frequency inputs. To reduce the danger of inadvertant responses, several techniques could be employed. The most important of these are as follows:

1. The cable being used to provide the low-frequency signal could be shielded so as to minimize the leakage of spurious electromagnetic energy into the sensitive circuits.
2. A lumped-element, low-pass filter could be provided at the electrical input to each sensitive device so that only energy in the pass-band of the control signal is transmitted.
3. The control cables could be designed so as to pass the desired signal satisfactorily while providing high attenuation to frequency above the bandwidth of the control signals, i. e. provide the low-pass filtering in the transmission line itself.

The most effective and economical technique for protection of the sensitive devices may well be some combination of these three approaches. To limit the necessity for external shielding and filtering, however, it appears desirable to first obtain the maximum benefit from the inherent filtering capabilities of the transmission lines. Such lines would have some specified value of attenuation in the pass-band, the value of this attenuation dependent upon the degradation of the control signal which is tolerable, while providing considerable attenuation at higher frequencies.

Several instances where such lines might be useful can be cited. The first of these is in the protection of ordnance devices from either inadvertant firing or from causing bake-off of the detonating powder. Another instance in which attenuating cable could be used is the case where rf energy is being carried on power leads thereby causing interference with the equipment being supplied. Digital transmission systems might also be upset by the introduction of rf energy on the information carrying leads.

This paper will discuss the design of cables to perform the desired low-pass filtering. Included will be a theoretial analysis of lines in order to determine the optimum characteristic available, a discussion of the practical problems, from both a material availability and a material fabrication limitations viewpoint, and the presentation of results obtained with fabricated lines.

## II THEORETICAL ANALYSIS

### Introduction

The design of transmission cable to provide desired low-pass characteristics necessitates a knowledge of the theoretical behavior of various line configurations. Depending on the criterion applied, any number of procedures could be used to optimize a given line. The particular technique used in the subsequent analysis is as follows: A maximum attenuation,  $\alpha_1$  is specified at the upper frequency limit of the pass-band,  $f_1$ . The minimum RF attenuation ( $\alpha_2$ ) desired above the pass-band is then selected. The optimization technique then consisted of minimizing the frequency ( $f_2$ ) at which this latter attenuation occurs.

Expressions of the attenuation as a function of frequency were derived for various line configurations. The optimum line design using the above techniques was then found. Only the results of these analyses will be presented here. Detailed derivations are given in the Final Report on "Two-Conductor Low-Pass Transmission Line Theory," Contract No. N178-7927, submitted to the U.S. Naval Weapons Laboratory, Dahlgren, Virginia. Copies of this report have been submitted to DDC and are available from that agency.

The optimum line design, as found from the procedure outlined above, will not always be a realistic one. The limitations of material properties and the fabrication techniques possible with these materials may require that compromises be made between the optimum design and one which may be achieved with relative ease. The analysis, together with considerations of the above practical limitations, will allow a judicious compromise to be made between the various requirements of protection, weight, etc.

### Conventional Distributed Transmission Line

A differential length of conventional transmission line may be represented as shown in Figure 1. The circuit behavior of this line may be characterized in terms of its characteristic impedance,  $Z_0$ , and its propagation constant,  $\gamma$ . For a line with a series impedance of  $Z$  ohms per meter and a shunt admittance of  $Y$  ohms per meter, the values of the transmission parameters are given by

$$Z_0 = \sqrt{Z/Y} \quad \text{ohms} \quad (1)$$

$$\gamma = \sqrt{ZY} \quad (2)$$

In order to determine the attenuating properties of any particular line, it is necessary to find the real part of the propagation constant. The real part is called  $\alpha$  and is the attenuation of the line in nepers/meter. For the line in Figure 1,  $\alpha$  may be shown to be

$$\alpha = \left\{ \frac{1}{Z} \left[ \sqrt{(R^2 + \omega^2 L^2)(G^2 + \omega^2 C^2)} + RG - \omega^2 LC \right] \right\}^{1/2} \quad \text{nepers/meter} \quad (3)$$

At low frequencies  $\alpha$  is given by

$$\alpha_0 = \sqrt{RG} \quad \text{nepers/meter} \quad (4)$$

while at high frequencies, the value of the parameter asymptotically approaches

$$\alpha_H = \frac{R}{Z} \sqrt{\frac{C}{L}} + \frac{G}{Z} \sqrt{\frac{L}{C}} \quad \text{nepers/meter} \quad (5)$$

A series of curves given the attenuation as a function of frequency for different values of the high frequency attenuation are shown in Figure 2. In plotting these curves it is assumed that the low frequency attenuation is very close to zero. A value of other than zero attenuation at low frequencies causes a toe in the attenuation curve at the low frequency end. The same curves are replotted in Figure 3 so that all curves have an attenuation of 3 db/meter at  $\omega/\omega_1 = 1$ . The optimization technique, as previously described, then consists of minimizing the frequency at which the attenuation rises to a prescribed value.

From Figure 3, it can be seen that all curves initially rise at the same rate as the curve indicated by  $\alpha_H = \infty$ . Along this line, the attenuation increases in proportion to the square root of frequency. This then is the optimum condition we are interested in. In order that the attenuation will increase as the square root of frequency, it is necessary that  $\alpha_0$  be very small and  $\alpha_H$  be very large. These limiting conditions can be obtained by requiring that either

$$R = C = 0 \quad (6)$$

or

$$L = G = 0 \quad (7)$$

If (6) holds, then

$$\alpha = \sqrt{\frac{\omega LG}{2}} \quad \text{nepers/meter} \quad (8)$$

while if (7) holds

$$\alpha = \sqrt{\frac{\omega RC}{2}} \quad \text{nepers/meter} \quad (9)$$

A line which satisfies (6) will be called an LG line while one which satisfies (7) will be called an RC.

#### Double - Layer Line -- Circuit Analysis

The preceding analysis has shown that the optimum conventional transmission line will give an attenuation which increases in proportion to the square root of frequency. In an attempt to determine whether this rate of change of attenuation could be increased, several other types of transmission lines were studied. The analysis of the response of any transmission line may be determined by analyzing a circuit model similar to that analyzed for the conventional distributed line. This circuit representation is valid if the propagating wave on the line is comprised solely of the TEM mode. If this is not the case, the circuit approach may be accurately used only in those ranges of the frequency spectrum where the longitudinal component of the electric field is small compared to the radial component.

One type of line which was investigated was the double-layer line, Figure 4. In this configuration the inter-conductor region is composed of two media, such that the boundary between them is equipotential with respect to the conductors. Assume now that one medium consists of a low-loss dielectric, while the other consists of a conducting, or partially conducting, material. If the material whose parameters are designated by the subscript 1 in Figure 4 is a semiconductor or conductor, and the second material is a dielectric, then the circuit element representation of the distributed line can be given by the configuration of Figure 5a. The lossiness of the dielectric material and the dielectric constant of the lossy material can be neglected to a first approximation, thus leading to the configuration of Figure 5b where  $G_2$  and  $C_1$  have been removed. The normalized attenuation of such a line is

$$g = y^{1/2} \left\{ \left[ \frac{1 + k^2 y^2}{1 + y^2} + \frac{1 + ky^2}{1 + y^2} \right]^{1/2} - \left[ \frac{1 + k^2 y^2}{1 + y^2} - \frac{1 + ky^2}{1 + y^2} \right]^{1/2} \right\} \quad (10)$$

where

$$g \equiv \frac{2a}{RC}$$

$$y \equiv \frac{\omega C}{G} \quad (10')$$

$$k \equiv \frac{LG}{RC}$$

Figure 6 shows curves of normalized attenuation  $g$  vs. normalized frequency  $y$ , with  $k$  as a parameter. For very large  $k$ , and very low  $y$  it can be shown the  $g(y)$  has a square-law variation, i. e.  $g \propto y^2$ . This represents the steepest variation of attenuation with frequency ( $a \propto \omega$ ) that can be theoretically attained with this line.

Let us now assume that the attenuation below some frequency  $f_1$  is not to exceed some specified value  $a_1$ , and that we wish to minimize the frequency  $f_2 > f_1$  above which the attenuation equals or exceeds some cut-off attenuation  $a_2 > a_1$ . To minimize  $f_2$  within the constraint that  $a \leq a_1$  for all  $f < f_1$ , we can employ the curves of Figure 6 and solve for  $f_2$  and the corresponding line parameters for various values of  $k$ . The simplicity of this approach attests to the utility of the normalized representation, and can be described as follows:

For a curve corresponding to a specific value of  $k$ , two points  $(y_1, g_1)$  and  $(y_2, g_2)$  are selected which have the following properties:

- (1)  $g_2/g_1 = a_2/a_1$
- (2)  $g < g_1$  for  $y < y_1$
- (3)  $g \geq g_2$  for  $y > y_2$
- (4) The average slope of  $g$  with respect to  $y$  between  $g_1$  and  $g_2$  is the maximum average slope attainable between any two points which satisfy the above three conditions.

The values of  $y_1, y_2, g_1$  and  $g_2$  obtained in this manner are the normalized values of  $\omega_1, \omega_2, a_1$ , and  $a_2$ , respectively, where the normalizations are given by (10'). If  $\omega_1 (\cong 2\pi f_1)$ ,  $a_1$  and  $a_2$  are specified, then  $\omega_2 (\cong 2\pi f_2)$  can be determined for each  $k$ , and represents the minimum cut-off frequency for that  $k$ .

As an example of how these curves may be used the above technique was applied to a coaxial line having an outer conductor of 1" diameter, an inner conductor of 0.25" diameter, and a dielectric film of thickness 1 mil as region 1. In addition, it is assumed that a non-magnetic conducting material is used. For such a line, the inductance is  $L = 0.3 \mu\text{h/m}$ . The specified values of  $f_1$ ,  $\alpha_1$ , and  $\alpha_2$  were 20 kc, 0.33 nepers/m., and 5.78 nepers/m., respectively. The values of  $f_2$  calculated using the above technique are tabulated for various  $k$  in Table 1. The corresponding optimum line parameters  $R$ ,  $G$ , and  $C$  are also given, as well as the relative dielectric constant of the film and the conductivity of the conducting medium required to achieve the calculated values of  $C$  and  $G$  for the assumed line dimensions.

The validity of the above result is dependent on the relative accuracy of the circuit model used. An analysis of the fields present in such a line was performed. It can be shown that a TEM mode will propagate on such a structure only when

$$\mu_1 \epsilon_1 = \mu_2 \epsilon_2 \quad (11)$$

and

$$\frac{\mu_1 \sigma_1}{\epsilon_1} = \frac{\mu_2 \sigma_2}{\epsilon_2} \quad (12)$$

Even in the lossless line, these conditions will not, in general, be satisfied. The TM mode can be shown to be capable of propagation within such a structure. However, for the lines under consideration, the component of electric field along the axis of the cable can be shown to be negligible in comparison to the radial component. For frequencies below 100 mc, the circuit model is of sufficient validity to allow the attenuation of the line to be determined by this means.

### III. LINE FABRICATION

The preceding analysis has indicated a technique for optimizing a given line configuration so as to obtain desired filtering properties. Several comments concerning the attainment of the theoretical optimum should be made. The two-layer line, although giving a response considerably better than the conventional line, requires materials with dielectric constants beyond the state-of-the-art. Materials which can be found with the required dielectric constant are usually not capable of easy fabrication into a conventional coaxial arrangement. In many cases, the thinness of the dielectric film would be difficult to produce while still maintaining the bulk material properties. Although some attempts were made to fabricate a line in the laboratory with the predicted two-layer response, no success was attained.

<sup>1</sup> Tobin, H. G., "Two-Conductor Low-Pass Transmission Line Theory," Quarterly Report No. 7, Armour Research Foundation, Chicago, Ill. pp. 3-22

It was felt that even if a laboratory model of this line could be constructed mass production of such a line would probably be difficult and expensive.

The greatest feasibility of attaining a commercial attenuating cable was felt to lie with the LG or the RC line. However, even for this latter line, excessive values of dielectric constant, or very thin layers of dielectric material may be required, in order to achieve a desired response characteristic. It was felt, therefore, that the design of LG lines will offer the best compromise between cost and production difficulty so as to allow attenuating cable to be widely used.

The following sections describe cables which have been fabricated both in the laboratory and commercially, to fulfill the low-pass attenuation requirement. Although primary attention was given to the LG line, some effort was made to fabricate both the two-layer line and the RC line. Both of these were prepared in the laboratory in the form of a strip line, since high dielectric constant plates are available which would allow one to attain the necessary capacity. For purposes of this study, a target goal of 3 db/meter of attenuation at 20 kc was specified with as rapid a rise in attenuation as possible beyond that frequency.

#### IV. ATTENUATION MEASUREMENTS

##### Measurement Techniques

The attenuation of a transmission line may be determined by a measurement of the input impedance of a line under open-circuit and short-circuit load conditions. If the open-circuit input impedance is denoted by  $Z_{oc}$  and the short-circuit input impedance by  $Z_{sc}$ , then the propagation constant of the line will satisfy the following relationship:

$$\tanh \gamma l = \sqrt{\frac{Z_{sc}}{Z_{oc}}} \quad (13)$$

This equation can be solved to determine  $\gamma$  and thus  $\alpha$ . As  $\alpha$  increases however, the input impedance under any load conditions approaches  $Z_o$ , the characteristic impedance of the line. It then becomes difficult to determine the line parameters by a measurement of the input impedance.

An alternate scheme has been devised to make these determinations. For an open-circuit load, the magnitude of the ratio of receiving end to sending end voltages can be shown to be

$$A \equiv \left| V_R / V_S \right| = \left| \frac{2e^{-\gamma l}}{1 + e^{-2\gamma l}} \right| \quad (14)$$



For  $\cos 2\beta l \approx 1$ , the attenuation may be approximated by

$$e^{-\alpha l} \approx \frac{1}{A} \left\{ 1 - \sqrt{1 - A^2} \right\} \quad (15)$$

For values of  $A < 0.4$ , this can be further simplified to

$$e^{-\alpha l} \approx \frac{A}{2} \quad (16)$$

with better than one percent accuracy. For any value of  $\beta$ , the attenuation as found from (15) will be less than, or equal to the actual attenuation of the line.

### Experimental Results

The experimental setup for both voltage and impedance measurements is shown in Figure 7. A ground plane of 1/32" copper sheeting was placed on a bench-top, with all of the instruments and the line under measurement being grounded to this plane. The following will give the results of measurements performed upon certain of the lines. The attenuation values given for these lines were in most cases derived through a measurement of the ratio of input and output voltages under open circuit load conditions. Impedance measurements were generally made to obtain a check of the attenuation at one or two frequencies at the low end of the frequency band.

The first line which was fabricated and measured was a strip RC line. The response of this line as a function of frequency is shown in Figure 8. Included is the theoretical response of a line with the measured values of R and C determined by input impedance measurements. The constancy of the attenuation at frequencies above one megacycle is due to the presence of inductance which is neglected in the theoretical derivation.

Attenuation measurements performed upon the two-layer lines which were fabricated indicated that little correlation existed between the theoretical and obtained values of attenuation. One of the main difficulties encountered with all models of the two-layer line was the prohibitively high value of series resistance which was present. In one strip line, the series resistance at dc was measured as 190 ohms. In addition, the conducting epoxy which was employed as the conducting medium was found not to meet the specifications of the manufacturer. One type was found to have a resistivity four orders of magnitude greater than the manufacturer's literature claimed. It is felt, therefore, that a good physical model of the two-layer line has not yet been constructed. In addition, it should be noted that the requirements on the material as indicated in Table 1 may preclude the construction of the type of two-layer line described here.

Several types of commercially fabricated LG cable were tested. Initial tests were performed upon coaxial lines which had an O. D. of approximately 0.5 inches and an inner conductor diameter of 0.05 inches. The center conductor in these initial samples was solid copper. Two different conducting dielectrics were used in these lines. In one case the

dielectric consisted of a conducting polyethylene while the other used a conducting silicon rubber compound. Commercial braid was also applied to these samples. When the initial attenuation measurements indicated that the theoretical response of these lines was not being obtained, the lack of sufficient contact between the conductors and the dielectric was determined to be at fault. For that reason, a portion of the conducting rubber line was treated by applying a conducting silver adhesive to the outer surface. The attenuation measurements performed upon these three types of lines are shown in Figure 9. Although the response of the cables varied approximately as the square root of frequency, the value of attenuation at low frequencies was much too small. Additional tests indicated that the full capabilities of these lines were not being realized due to the poor contact between the inner conductor and the dielectric.

One technique employed to eliminate this contact consisted of using a stranded center conductor rather than a single wire. For the same average diameter the stranded wire will offer more contact area to the conductor. At the same time, the overall diameter of the cable was reduced to that of RG-59/U. This was done in order that the finished cable would be more flexible than the original models. The results of the attenuation measurements upon this cable are shown in Figure 10. Also shown for comparison is the attenuation of a cable of the same size which uses a solid center conductor. The great difference in response of these two lines is evident. The dotted line in this figure indicates the design performance of this cable. The apparent constancy of the attenuation at high frequencies is due to two factors: The first of these is the presence of capacitance between the two conductors of the cable. This capacitance will cause a flattening of the high frequency response of an LG cable. A portion of the observed flattening is also due to inadequacies in the measurement procedure at the higher frequencies. The increased attenuation of the line requires that more signals be supplied at the input in order that the signal present at the output be within the sensitivity of the output measuring device. This is difficult to achieve without special equipment. However, measurements made with attenuation does continue to increase.

## V. CONCLUSIONS

The feasibility of using audio signal leads to provide attenuation to unwanted rf energy has been demonstrated. For a conventional cable, however, the attenuation above the desired pass-band will increase at a rate no greater than the square root of frequency. The use of a double-layer line will, in theory, allow a rate of increase of attenuation proportional to the second power of frequency. However, the difficulties involved in the practical fabrication of such a line may not allow full benefit to be derived from its use.

This paper has been concerned with lines which employ dissipative losses only to provide the filtering. Analysis has also been performed for lines which incorporate reflective losses to increase the sharpness of the cut-off characteristic. The use of lumped elements periodically spaced along the cable would be one technique for accomplishing this. Laboratory models to meet specific design criteria have not been constructed. If sufficient need for this type of cable is developed, little difficulty in its design should be encountered.

The rf attenuation of transmission lines designed to carry audio signals may not be sufficient to provide complete interference protection to sensitive devices. However, in order that the requirements on additional filtering and shielding might be reduced, the use of attenuating cable may be desirable. As with similar devices and techniques, however, the designer must balance restrictions on size, weight, cost, etc. against his particular technical requirements, and then attempt to reach an optimum compromise.

TABLE 1  
OPTIMIZED LINE PARAMETERS  
TWO-LAYER TRANSMISSION LINE

k	f <sub>2</sub> (kc)	R (ohms/m)	G (mhos/m)	C (μfd/m)	σ (mhos/m)	ε <sub>r</sub>
1	5,570	LG = RC			---	---
3	1,500	0.084	24	77	6	1,390
10	360	0.015	120	240	30	4,320
30	167	0.0069	500	720	125	13,000
100	118	0.0023	1330	1815	333	32,700
300	99	0.00088	3200	3630	800	65,400
1000	88	0.00037	9680	7730	2420	140,000
∞	82	0	∞	∞	---	---

$$f_1 = \omega_1 / 2\pi = 20 \text{ kc}$$

$$\alpha_1 = 0.35 \text{ nepers/m. (3 db/m.)}$$

$$\alpha_2 = 5.78 \text{ nepers/m. (50 db/m.)}$$

} Specified  
Conditions

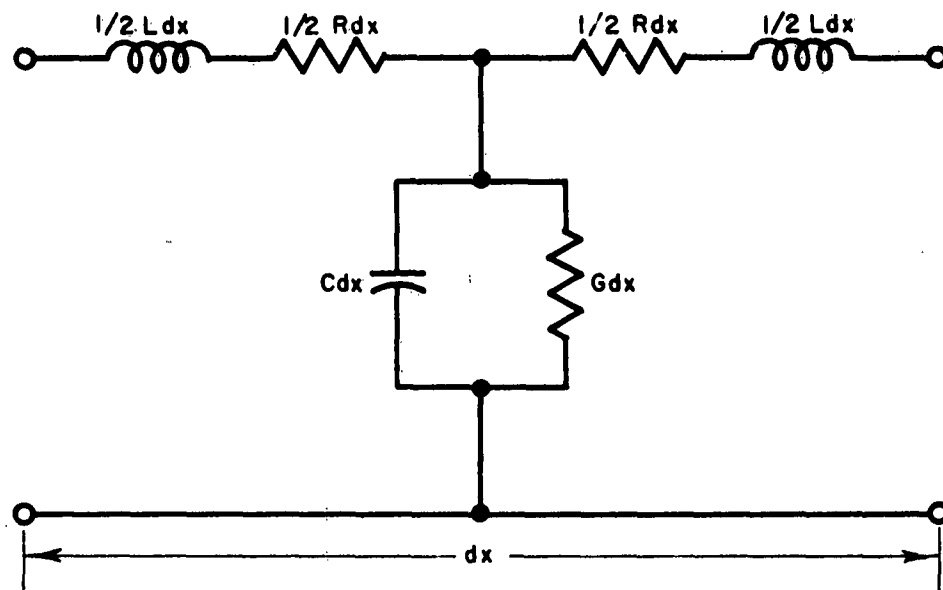


FIG. 1 CIRCUIT REPRESENTATION OF A CONVENTIONAL DISTRIBUTED TRANSMISSION LINE

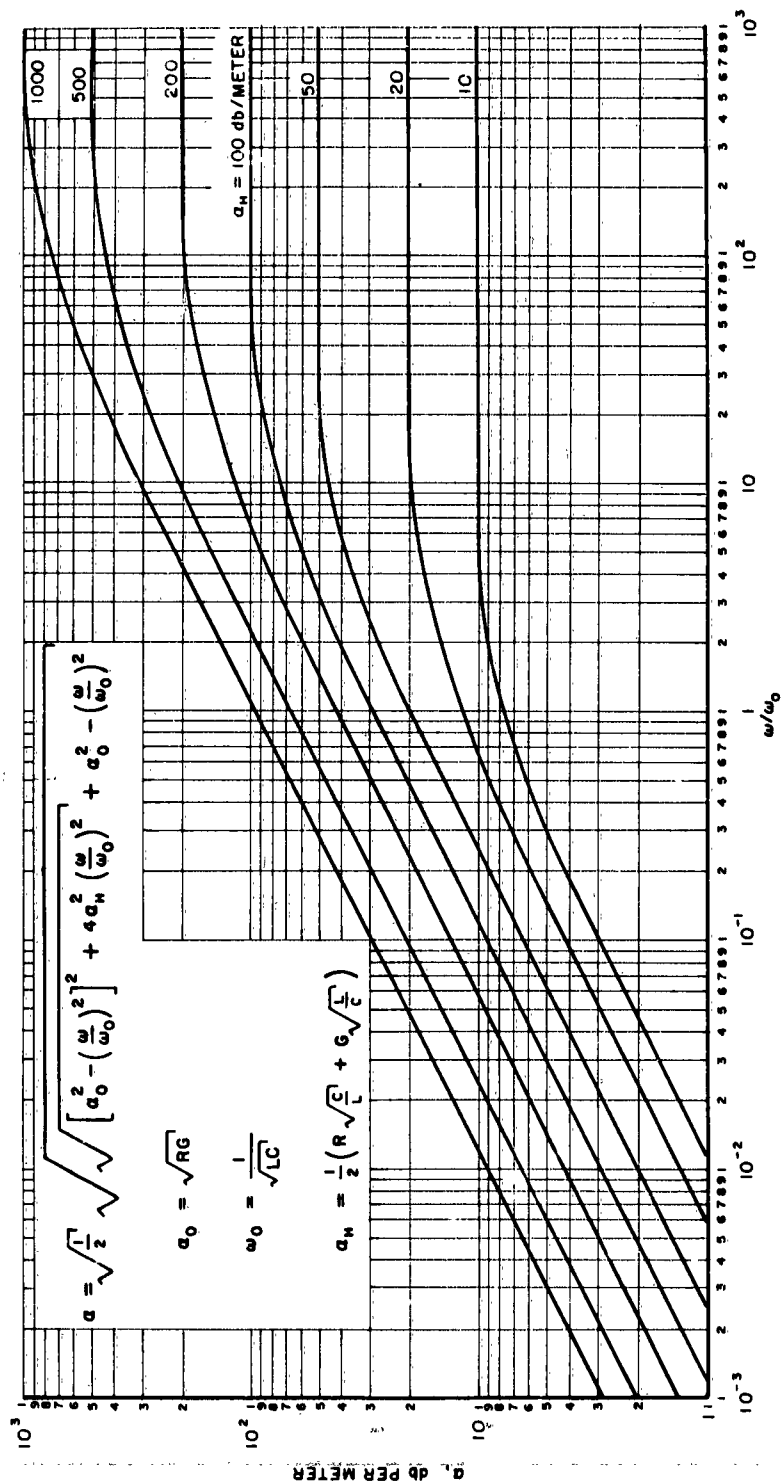


FIG. 2 NORMALIZED ATTENUATION CHARACTERISTICS OF CONVENTIONAL TRANSMISSION LINE,  $a_0 = 0$

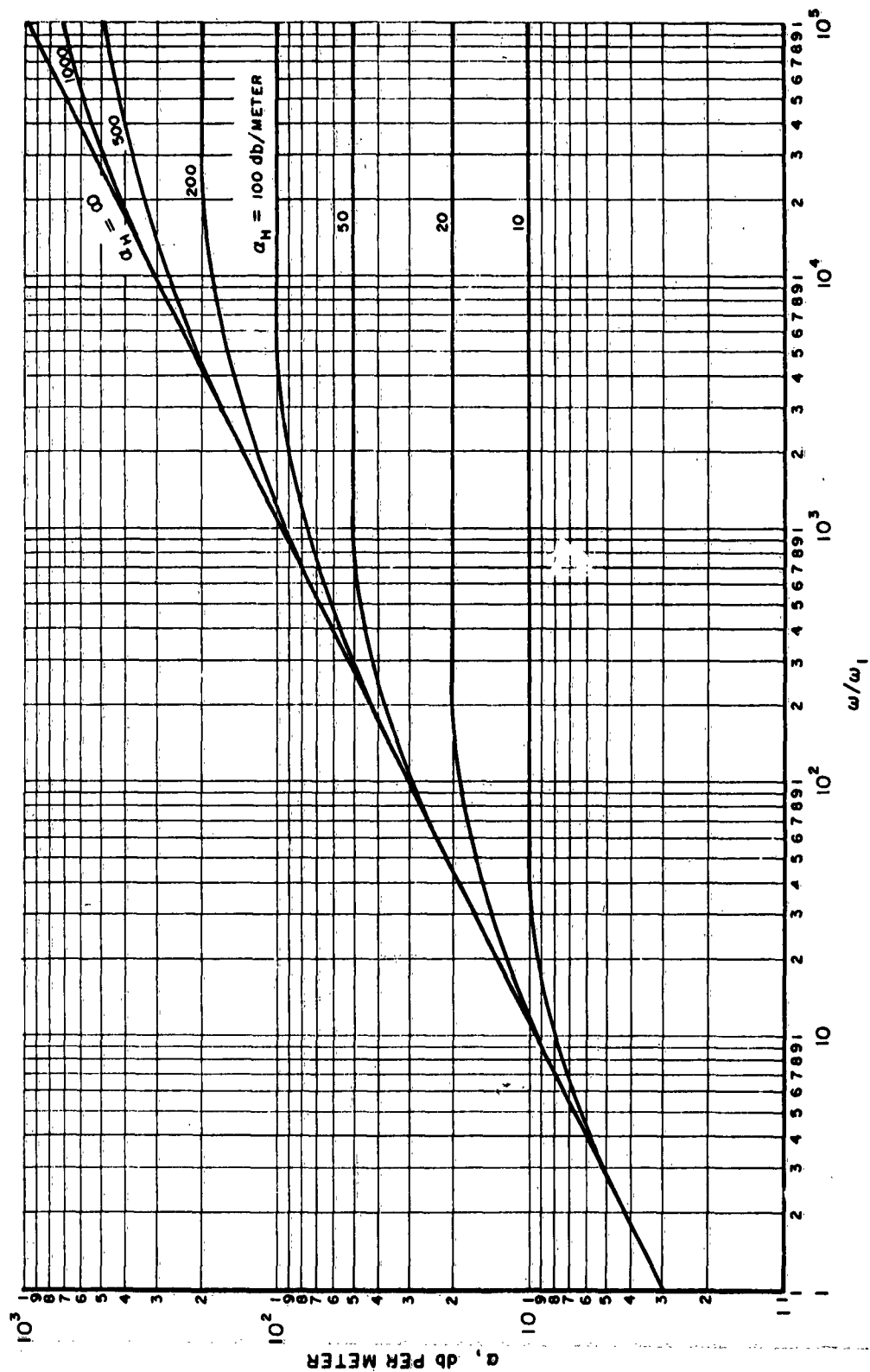
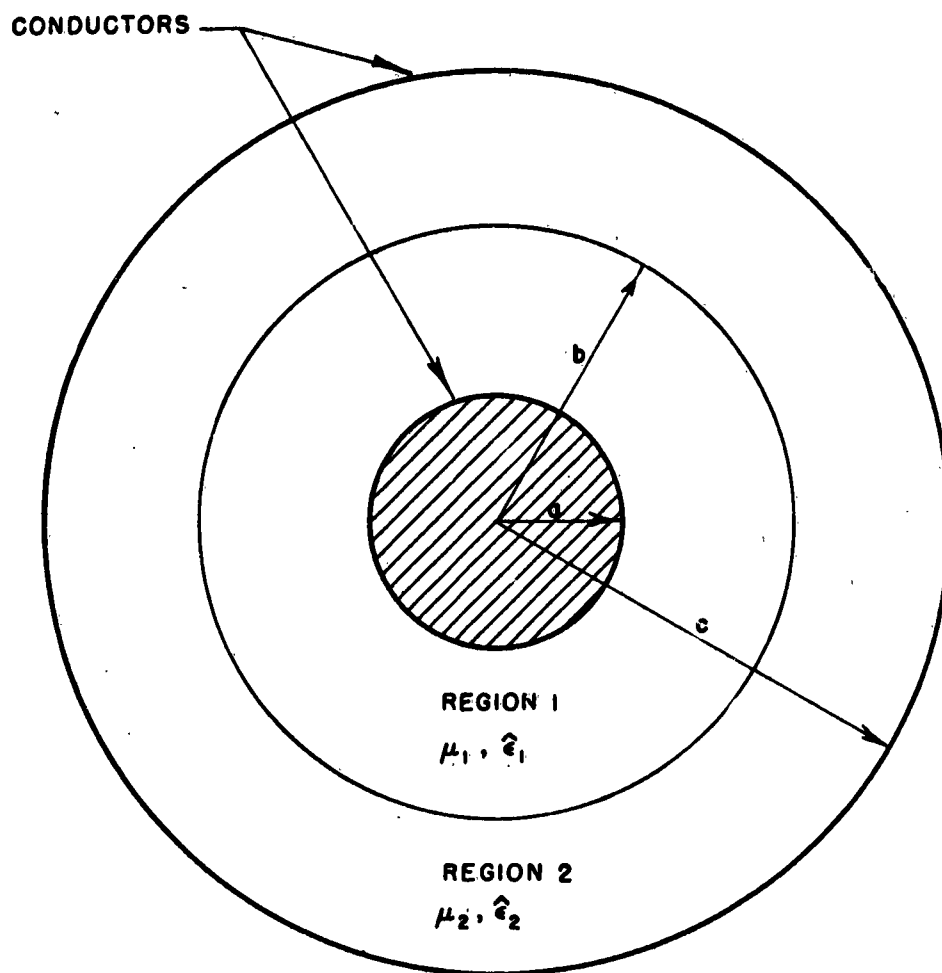
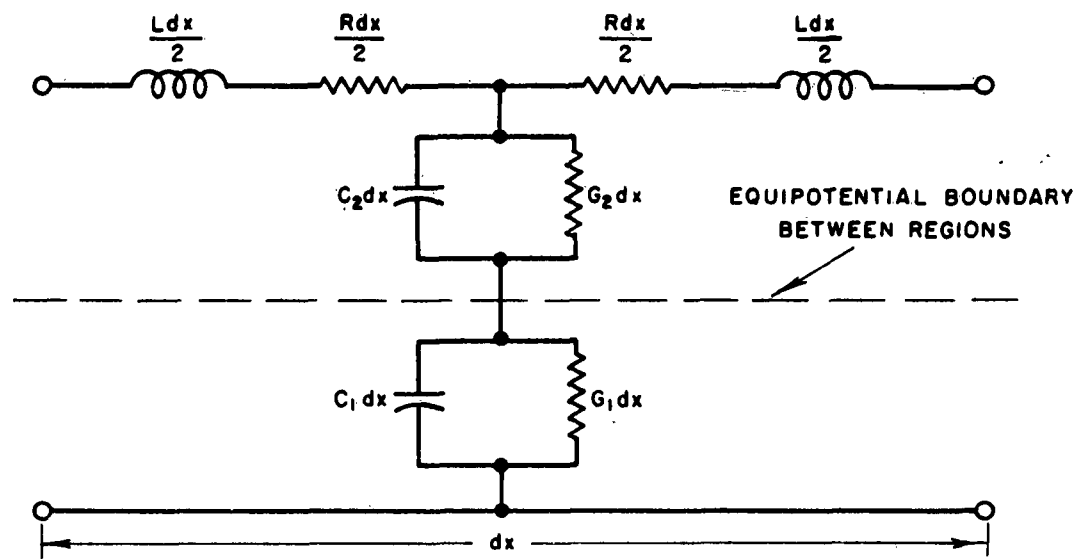


FIG. 3 NORMALIZED ATTENUATION CHARACTERISTICS OF CONVENTIONAL TRANSMISSION LINE,  $\alpha_0 = 0$

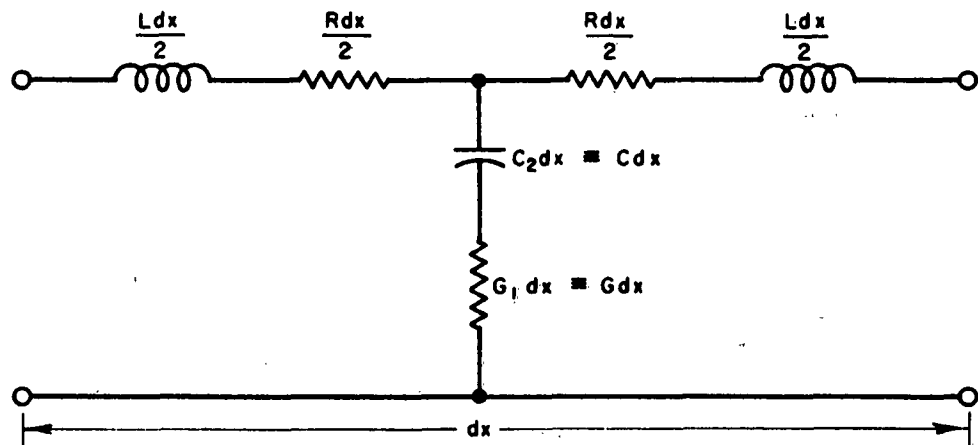


**FIG. 4 TWO-LAYER COAXIAL TRANSMISSION LINE,  
CROSS-SECTIONAL VIEW**





(a) GENERAL REPRESENTATION



(b) IDEAL REPRESENTATION

FIG. 5 CIRCUIT REPRESENTATION OF LINE

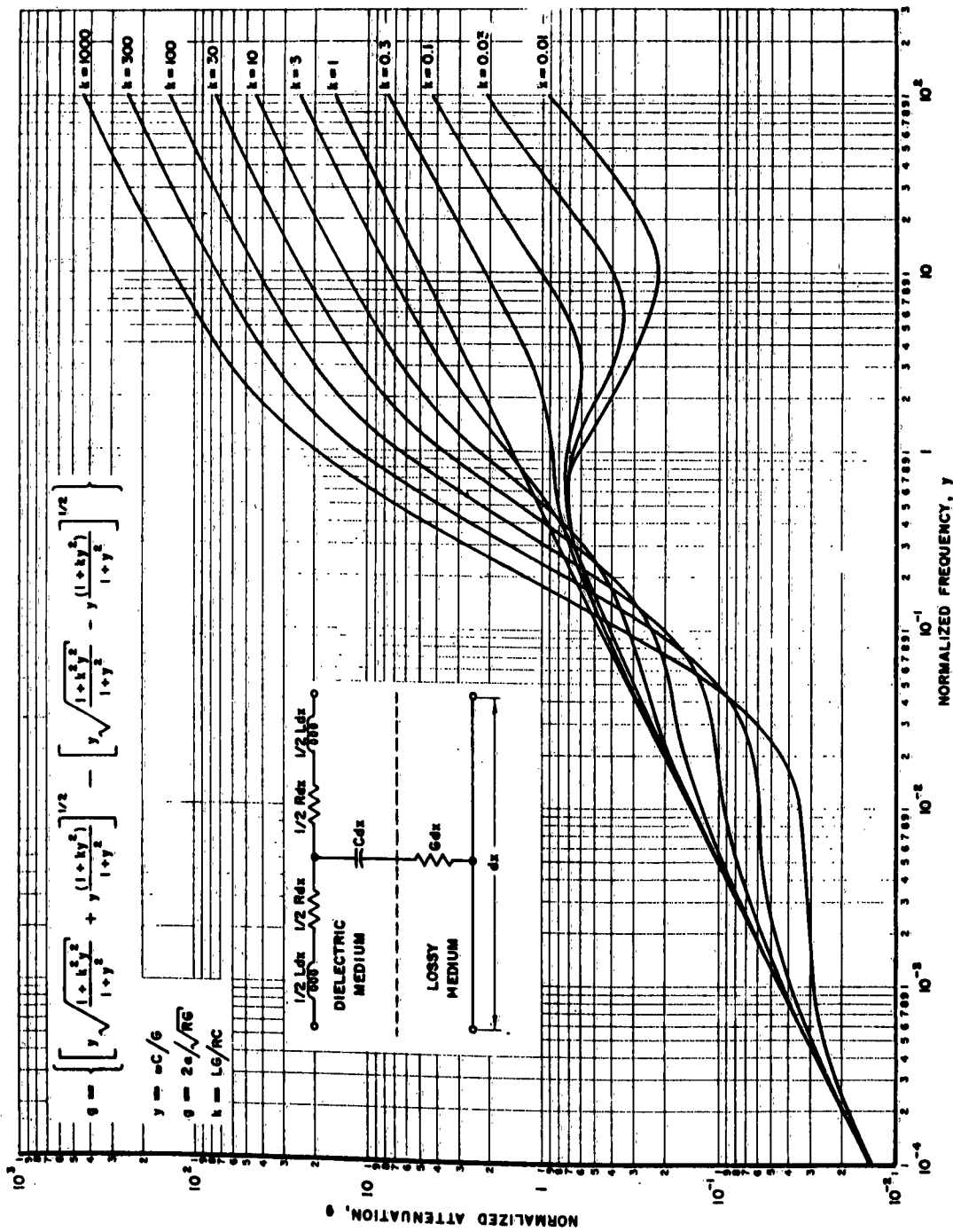


FIG. 6 NORMALIZED ATTENUATION — FREQUENCY CURVES TWO LAYER TRANSMISSION LINES

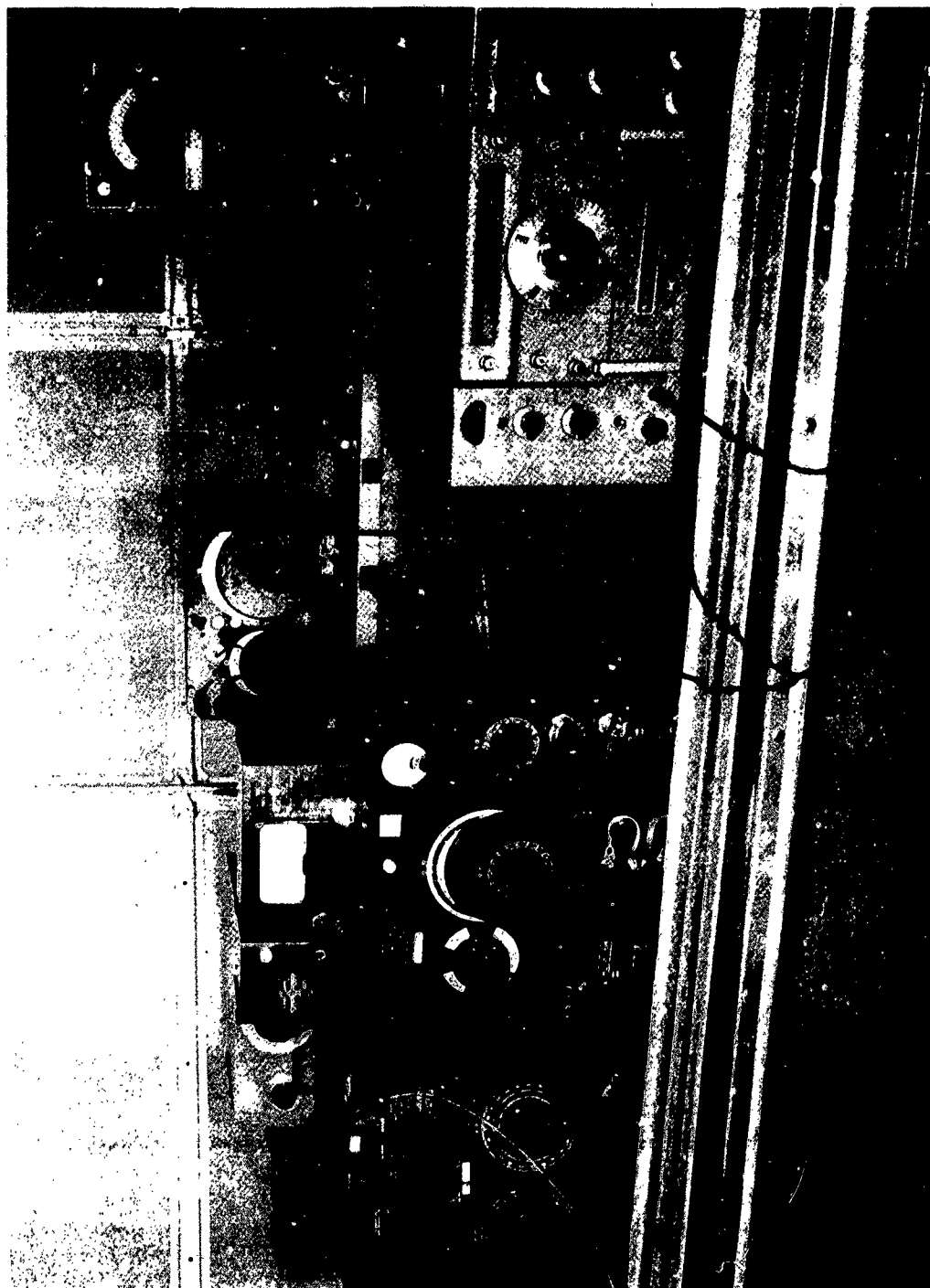


FIGURE 7 EXPERIMENTAL TEST SETUP

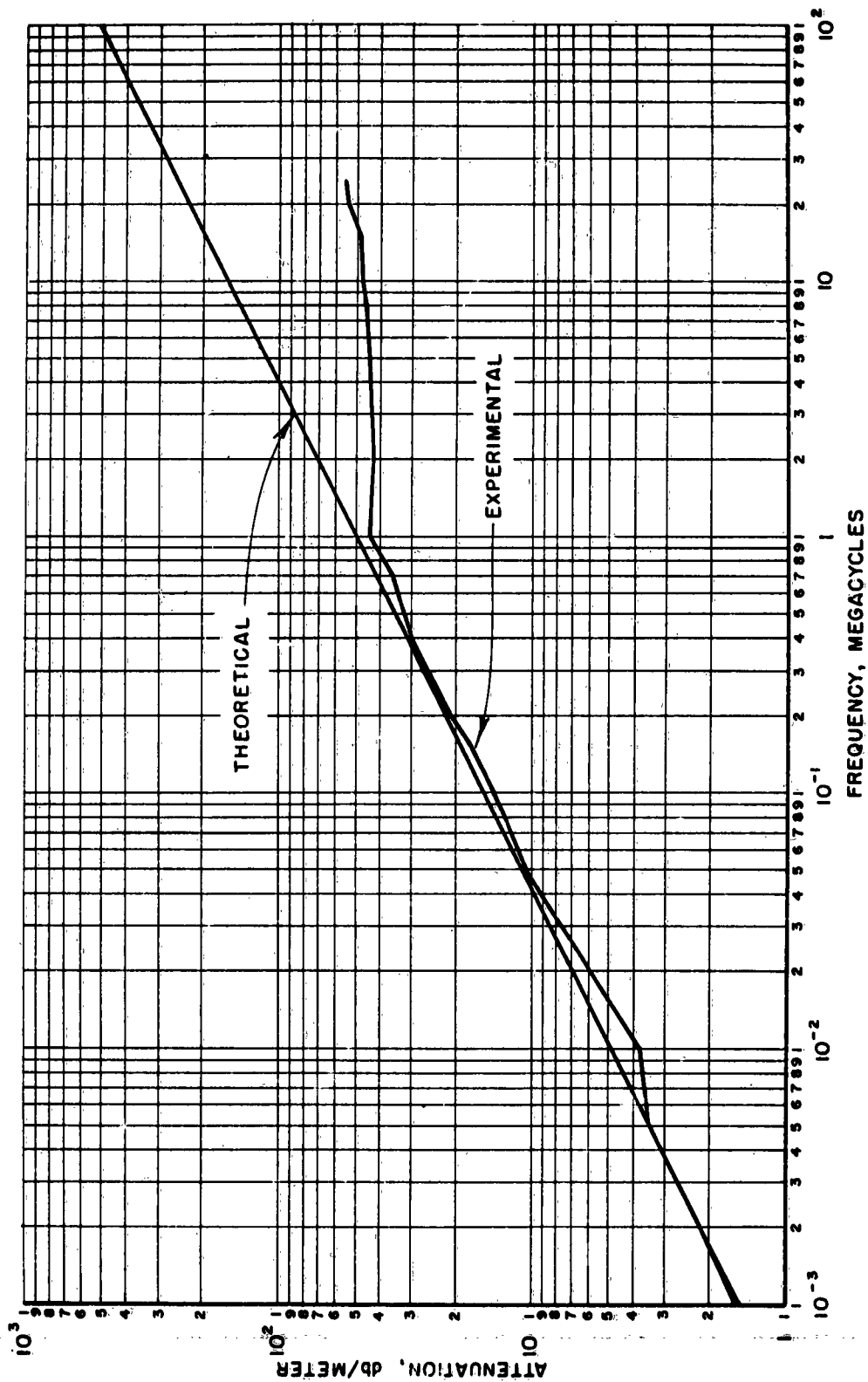


FIG. 8 ATTENUATION OF RC LINE

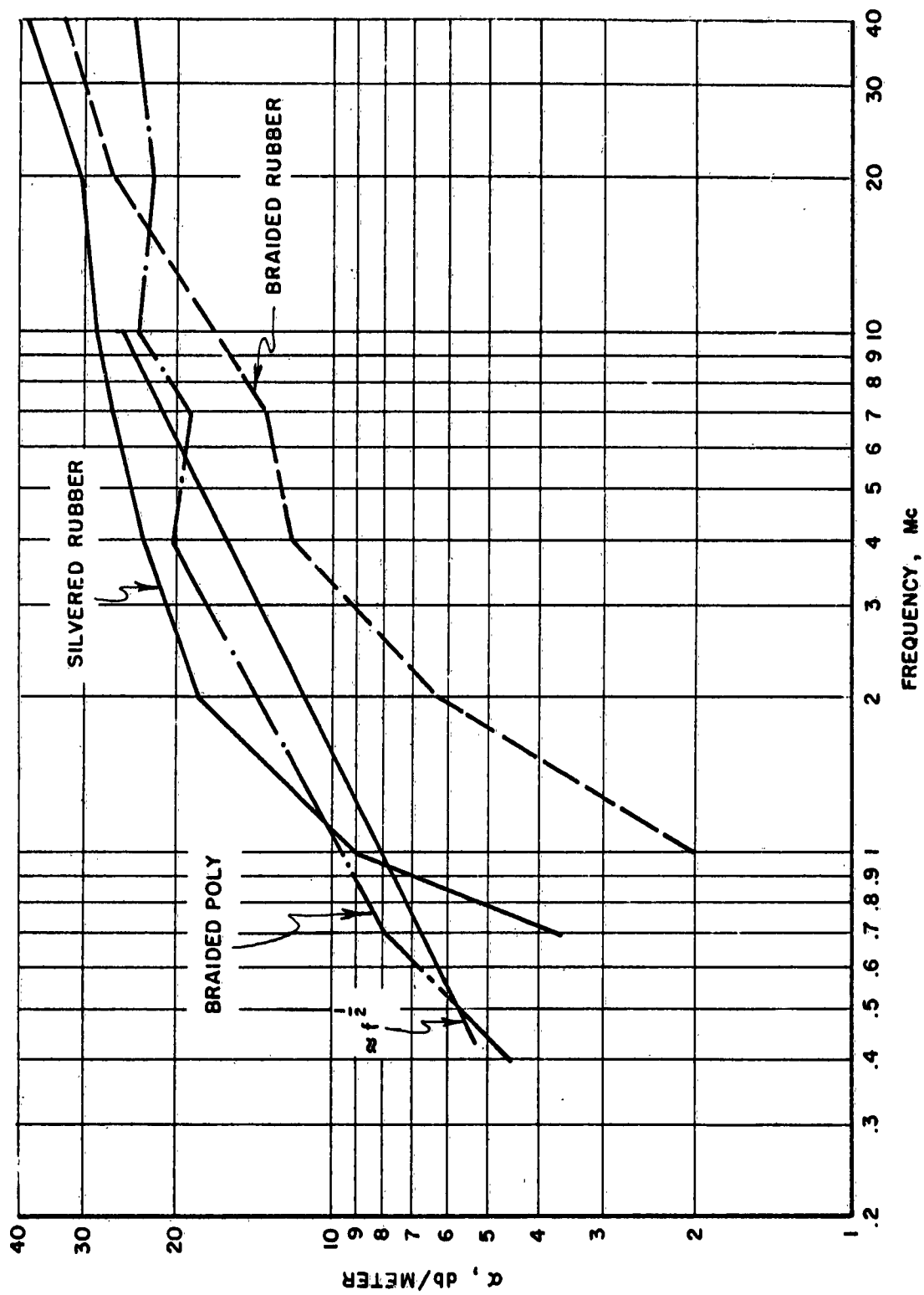


FIG. 9 RESPONSE OF FABRICATED LINES

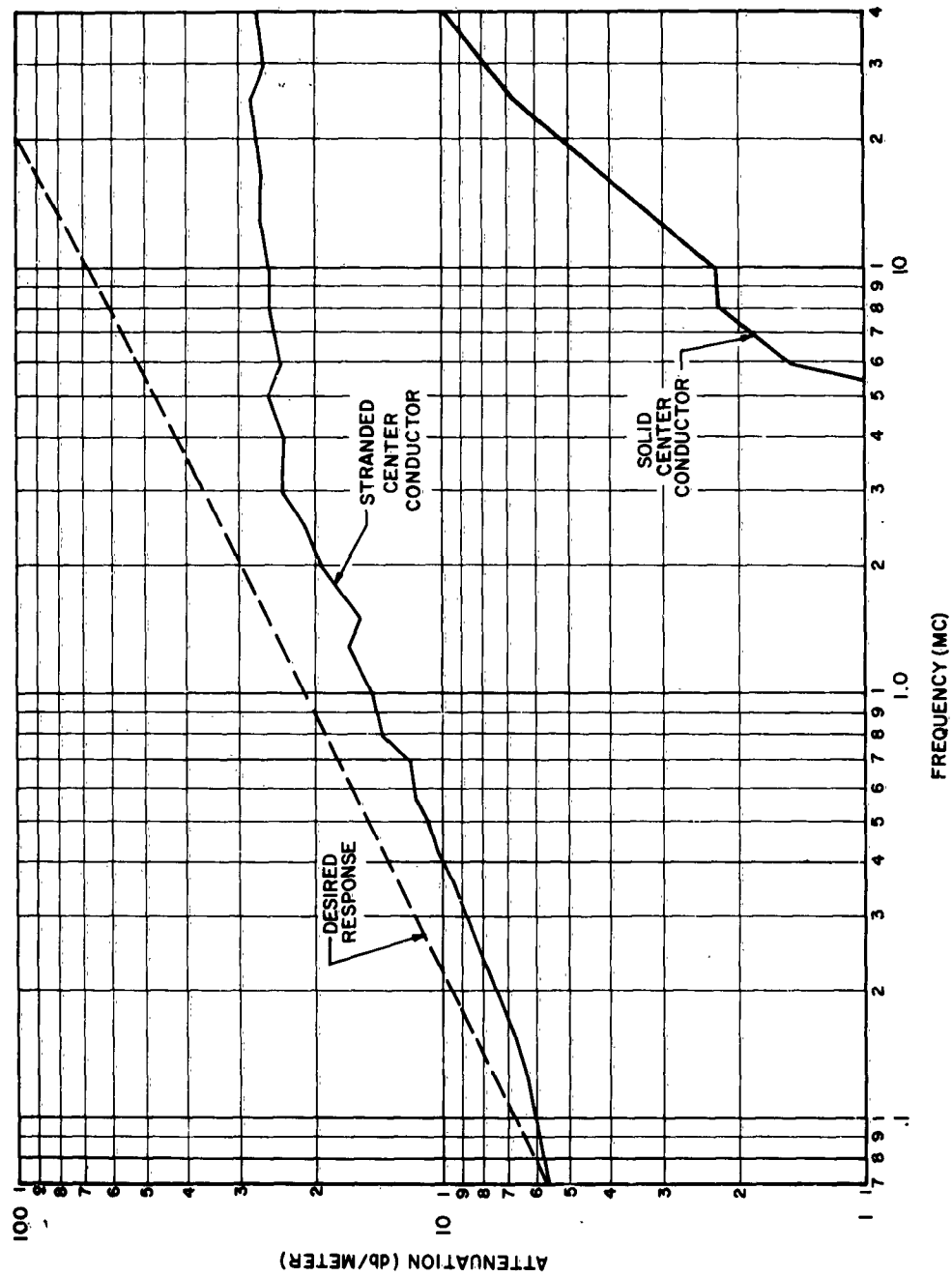


FIG. 10 ATTENUATION OF CONDUCTING POLYETHYLENE CABLE (0.17" O.D. OF DIELECTRIC)

# THE REALIZATION OF COMPATIBLE STRUCTURE GROUNDING SYSTEMS

H. W. Ervin and D. R. Lightner  
White Electromagnetics, Inc.  
4903 Auburn Avenue  
Bethesda 14, Maryland

and

Robert Powers  
Electromagnetic Vulnerability Laboratory  
Rome Air Development Center  
Griffiss Air Force Base, New York

Abstract. - This paper discusses the design and implementation of grounding systems which must be used in structures or complexes which house electronic equipment which are susceptible to or capable of generating electromagnetic energy. Grounding systems are analyzed as two separate entities: (1) earth grounding system, and (2) reference plane grounding system. Criteria is developed for the design and implementation of compatible grounding systems based upon theoretical and practical considerations.

## I. INTRODUCTION

Personnel responsible for the design and implementation of structural grounding systems to comply with the requirements of (1) power companies, (2) electronic and instrumentation users, and (3) electromagnetic interference personnel, are sorely aware of the need for reliable design criteria which is compatible with the requirements of all concerned. Grounding systems basically consist of two types: (1) earth grounding systems for the safeguard of persons and property from hazards associated with electricity, and (2) reference plane grounding systems for the establishment of a low impedance plane for usage in buildings housing electronic equipments susceptible to or capable of radiating electromagnetic energy. Electrical requirements of each grounding system are entirely divorced and the effective application of one system requirement can not be construed to indicate effective application of both system requirements.

Criteria is presented for the effective design and implementation of "earth" grounding systems based upon (1) a theoretical analysis, (2) evaluation of existing criteria, and (3) an investigation of the effectiveness of existing earth grounding techniques. Final results are graphically presented which illustrate approximate earth grounding resistance as a function of (1) number of ground rods used around the periphery of the structure foundation, (2) depth of ground rod penetration, and (3) structure foundation area. Due regard is given to terrain considerations which effect the magnitude of soil

resistivity. Such an analysis is also applied to earth ground grid meshes which must be resorted to when ground rods cannot be used due to high earth resistivity or impracticality of implementation due to terrain considerations.

Reference planes must reflect an extremely low impedance to all users in order to realize effective benefit from their usage. Formulas are derived which express the maximum resistance and self-inductance resulting from square and rectangular reference plane grid meshes. Final results are presented, for square and rectangular grids, in graphical form illustrating maximum resistance and self-inductance as a function of (1) number of grids, (2) structure foundation area, and (3) conductor types used in grid construction. Design criteria is established by utilizing wire size and number of grids to a point where further impedance reduction is not economically practical for the percentage impedance reduction obtained relative to expense incurred.

## II. Earth & Reference Plane Grounding Systems

Discussion of grounding philosophy. There have been numerous noteworthy articles written in the past relative to the design and implementation of grounding systems. Grounding problems have been approached by each author relative to his specific interests and concepts of a grounding system. Systems have been designed and implemented in time gone by that have proven quite effective in achieving the required results. Yet the grounding problem is still with us and poses one of the most confusing and perplexing problems encountered in the design of structures which must house a complex electronic equipment.

Why has the grounding problem been magnified in recent years and what is the basis of the existing confusion?

A compatible grounding system of the past was one which (1) offered a sufficiently low impedance to earth to preclude the inducement of potentials which might prove harmful to personnel or equipment as a result of power system fault currents, lightning, etc. and (2) provide a low DC resistance return path for power and electronic equipment users. Grounding systems were designed and implemented which were compatible with such grounding requirements. Electronic and electrical equipments functioned normally and design and test engineers accepted the grounding design and implementation criteria as valid, which it was under these circumstances.

The advent of the missile age and associated complex electronic systems has produced problem areas that were here-to-fore non-existent; (1) electromagnetic interference, both conducted and radiated, was found to deteriorate electronic systems and component performance to intolerable limits, (2) shielding was found to be ineffective in attenuating electromagnetic energy to degrees necessary to preclude interference with electronic equipments



which were susceptible to extremely low level signals, (3) design engineers could no longer depend upon existing grounding systems as a neutral return path due to potentials that were found to be present, etc.

Extensive testing and analysis has led to the conclusion that a great majority of such problem areas are directly attributable to existing outmoded grounding systems. Two avenues of recourse have been pursued to rectify the shortcomings of grounding systems and grounding system technology; (1) revamping of existing systems in an attempt to realize the necessary electrical and electronic grounding requirements, and (2) evolvement of new concepts in the design and implementation of grounding systems for use in the construction of new building and complexes.

Unfortunately, revamping procedures have produced less than desirable results in many circumstances. Resultant effectiveness of revamping techniques is definitely limited due to the physical and monetary impracticality associated with implementing necessary grounding requirements. Evolvement of new concepts and philosophies in the design and implementation of grounding systems are greatly reducing the interference problems associated with modern electronic complexes. Structures housing electronic equipments which are either susceptible to or capable of generating electromagnetic interference are being designed to fulfil two basic grounding requirements; (1) provide a safeguard for personnel and property from hazards associated with electricity, and (2) to provide a low impedance reference plane or instrumentation ground for electronic users within the confines of the structure.

Instrumentation ground has become referred to as an equipotential reference plane. This in turn infers a metallic conductive media which offers zero impedance to any current which may flow through it; such a reference plane could be schematically illustrated as a single-point. As in all other electronic design applications, the realization of exact electrical performance is impossible, but the attempt to achieve the most compatible performance within the realm of practical feasibility is an essential requirement.

Both types of grounding systems are divorced in application but cannot be divorced in implementation; both must be implemented during construction and compatible techniques must be implemented to electrically isolate the two systems while at the same time obtain and maintain the electrical and electronic requirements associated with each. Until requirements and implementation techniques of each system are understood and faithfully implemented, compatible grounding systems shall not be realized.

The theoretical design of electronic and electrical grounding systems is relatively simple, as compared to the problems involved in the effective implementation of such systems. However, it is the responsibility

of cognizant personnel entrusted with the design of electromagnetically compatible structures to insure that grounding systems are made available within instructures that fulfil the grounding requirements of all perspective users. Resultant performance of electronic equipments, subsystems, systems and complexes will revolve around the electromagnetic compatibility of the resultant grounding system.

Basic Criteria. There are certain basic concepts which must be fully realized and accepted in order to understand the detailed requirements associated with grounding systems.

1. Each grounding system (earth and instrumentation) must function as an electrically isolated entity. Large amounts of power and extraneous signal currents can be expected to flow upon all members of the earth grounding system: such currents must be electrically isolated from the instrumentation ground in order to preclude the inducement of intolerable potentials on this media.

2. The instrumentation ground must be one homogeneous mass constructed to offer a negligible amount of DC and rf impedance to current flow. Impedance in the reference plane will produce extraneous potentials that will be reflected to all equipments and wiring connected to the reference plane.

3. The instrumentation ground must be electrically connected to earth ground at one point and at one point only: The earth ground connection is necessary only to preclude electrical hazards to personnel and equipments, and will not effect the compatible performance of the instrumentation ground if removed entirely.

4. The entire earth grounding system must be one homogeneous mass which offers a minimum impedance to current flowing to earth ground. If excessive impedance is inserted between any member and earth ground, the member will be subjected to standing waves and may radiate or re-radiate electromagnetic energy within the confines of the structure.

Non-compliance with any one of the above criteria will be as disastrous as designing an electronic circuit using Ohm's Law and omitting any one of the basic parameters. Violation of the above basic grounding criteria are commonplace, with the inevitable results of entire electronic complexes that are plagued with problems associated with electromagnetic interference.

This paper shall deal only with those structures and complexes housing sensitive electronic systems, sub-systems or equipments which are susceptible to electromagnetic interference in its many forms. All such structures or complexes shall be assumed to require both earth and instrumentation grounding systems.

Earth Grounding Systems. An earth grounding system consists of (1) metallic conductors designed to provide a direct low impedance path for current flow to earth ground and all electrical connections thereon, and (2) all metallic media and connections which are electrically bonded to the earth grounding system. Low resistance paths to earth ground are normally realized by proper usage of copper grid meshes and rods or combinations thereof, which are buried beneath the surface of the earth. Underground metallic piping systems are also used in some cases to provide a low impedance earth ground. Metallic media and wiring such as structural steel, structural safety grounds on electrical power equipments, power line filters, lightning arrestors, etc. are bonded to the underground mesh, rod or piping systems and form an integral part of the earth grounding system.

All metallic media subjected to radiated or conducted electromagnetic energy outside the confines of the structure or complex in question should be bonded to the grounding system. All shielding media implemented as an integral part of the structure or complex, which serves the purpose of providing an interference free environment within the structure, should be bonded to the earth grounding system. All wiring or cable which enters the confines of the structure may radiate, re-radiate or conduct electromagnetic energy induced upon it by extraneous sources and should be filtered and the filter encasement should be bonded to the earth grounding system. All metallic members or equipments within the confines of the structure which make electrical contact, by any means whatsoever, with any other member serving as an integral part of the earth grounding system, must in turn be bonded, by means of a low impedance connection, to the earth grounding system.

Design of Earth Grounding Systems. An abundance of noteworthy material exists relative to approximating the earth grounding resistance obtainable from various ground rod and grid mesh configurations. Applicable formulas are used in this paper to calculate grounding resistance as a function of (1) number of ground rods used around the periphery of the structure foundation, (2) depth of ground rod penetration into the earth, and (3) structure foundation area. Formulas are also used to calculate ground resistance provided by grid meshes, below the surface of the earth, as a function of (1) area of coverage, and (2) number of grids per side. Calculated data is presented in graphical form which is readily adaptable to the determination of ground rod configurations which are compatible with specific structure requirements.

Ground resistance is commonly computed either by application of the strict concepts of field theory or by the average potential method. Although the latter method is not absolutely exact from the standpoint of theoretical physics, it furnishes fairly accurate results and is readily adaptable to problems at hand. In recent years it has been accepted almost universally as the only practical means of solving problems of a more involved nature.

The grounding resistance of many closely spaced parallel ground rods can be expressed by the following formula:<sup>1</sup>

$$R = \frac{\rho}{2\pi n L_1} \left[ \log_e \frac{4L_1}{b} - 1 + \frac{2k_1 L_1}{\sqrt{A}} (\sqrt{n-1})^2 \right] \quad (1)$$

where:

- R = grounding resistance (ohms)
- $\rho$  = soil resistivity, ohm-centimeters.
- $L_1$  = length of each rod, cm.
- $2b$  = diameter of rods, cm.
- $n$  = number of equally spaced rods in area A
- A = area of rod coverage
- $k_1$  = coefficient

The coefficient  $k_1$  in equation (1) is obtained from the expression for the resistance of a horizontal thin plate. With  $L_1$  increasing toward infinity, equation (1) approaches this value. The coefficients  $k_1$ , for square and rectangular plates at earth surface, are plotted as curve A in Figure 1<sup>2</sup>.

In most practical cases, grids or rod beds are buried to depths much less than  $\sqrt{A}$  so that the coefficient  $k_1$  for the surface level holds with sufficient accuracy. Further study and criteria shall be based upon values of  $k_1$  for the surface level.

The determination of soil resistivity as a function of the locality were measured and depth of ground rod penetration cannot be practically realized with a high degree of accuracy. This is due to the effects of various terrain considerations upon soil resistivity and the accuracy of various methods available to measure soil resistivity.

Equation 1 can be rearranged and partially simplified as follows:

$$R = \frac{0.52 \rho}{n L_1} \left[ \log_e \frac{4L_1}{b} - 1 + \frac{2k_1 L_1}{\sqrt{A}} (\sqrt{n-1})^2 \right] \quad (2)$$

Equation 2 has been used by the author to calculate ground resistance as a function of (1) number of evenly spaced rods, (2) area coverage, and (3) depth of earth penetration. Resultant data is presented graphically in Figure 3. Figure 3 can be simply used to predict ground rod configurations compatible with a specific situation. Calculations have been based on a value of soil resistivity equal to 50 ohms per meter. Earth resistance resulting from soil resistivities other than the assumed value can be calculated as follows:

$$R_1 = R \left( \frac{\rho_1}{\rho} \right) \quad (3)$$

where:

R = resistance obtained from Figure 3  
 $\rho$  = 50 ohms/meter  
 $\rho_1$  = measured value of soil resistivity

Ground grid meshes are often required to complement rod beds or to be used separately when deep driven rods are impractical due to terrain considerations. The following formula can be used to calculate the ground resistance of an earth ground grid mesh:<sup>3</sup>

$$R = \frac{\rho}{\pi L} \left( \log_e \frac{2L}{a^1} + k_1 \frac{L}{\sqrt{A}} - k_2 \right) \quad \text{ohms} \quad (4)$$

where:

L = total length of all connected conductors  
 2a = diameter of conductors (cm)  
 $a^1 = a$  for conductors on earth surface  
 $a^1 = a \times 2Z$  for conductors buried at a depth of Zcm  
 A = area covered by conductors (cm<sup>2</sup>)  
 $k_1, k_2$  = coefficients

The coefficient  $k_1$  is the same that was used in equations 1 and 2 in the previous discussion. Coefficient,  $k_2$  has been calculated for loops encircling areas of the same shape and depth as used for calculating  $k_1$ . Calculated results are shown in Figure 2.

Equation (4) has been slightly simplified for the purpose of data calculation as indicated by the following formula:

$$R = \frac{1.045\rho}{L} \left( \log_e \frac{2L}{a} + k_1 \frac{L}{\sqrt{A}} - k_2 \right) \quad (5)$$

where:

$A = \frac{1}{\sqrt{12}}$  conductor diameter (in) X depth (ft).  
 L = rod length (ft.).  
 $\rho$  = soil resistivity (ohm-meter)

Resistance has been calculated by the author as a function of foundation area, area of grid coverage and number of grids per side, using 4/0 copper cable. The resistivity of the earth was assumed as 50 ohms per meter for calculation purposes. Coefficients  $k_1$  and  $k_2$  vary only slightly with area and the error introduced by using calculated data for square and rectangular grids is negligible. Calculated data is presented graphically in Figure 4.

Grounding resistance offered by various grid meshes can be reduced most significantly by increasing the number of grids and by increasing the area of grid coverage. Data has been extrapolated from Figure 4 and re-plotted in Figure 5 to show ground resistance as a function of area of grid mesh coverage as well as single and optimum numbers of grids per side.

Various factors are illustrated by such graphical illustrations worthy of consideration in developing optimum design criteria for earth grid meshes; (1) a far greater reduction in ground resistance is realized by using increased areas of grid coverage up to approximately 90,000 sq. ft. Beyond 90,000 sq. ft. a maximum reduction in ground resistance is realized by optimum usage of number of grids and (3) the average optimum reduction of ground resistance resulting from the additional grids is approximately 0.2 ohms.

In many cases it may be necessary to use a combination of ground rods and a grid mesh below ground to obtain a sufficiently low ground resistance.

The mutual resistance between the two grounding systems can be approximated by the following equations:

$$R_{12} = R_{21} = \frac{\rho}{\pi L} \left( \log_e \frac{2L}{L_1} + k_1 \frac{L}{\sqrt{A}} - k_2 + 1 \right) \text{ (ohms)} \quad (6)$$

where:

$R_{12} = R_{21}$  = mutual resistance of both systems and remaining parameters are equivalent to those used in previous formulas.

The combined rod bed and grid resistance can be expressed as follows:

$$R = \frac{R_{11} R_{22} - R_{12}^2}{R_{11} + R_{22} - 2R_{12}} \quad (7)$$

where:

$R_{11}$  = resistance of grid alone  
 $R_{22}$  = resistance of rodbed alone  
 $R_{12}$  = mutual resistance between systems.

The reduction in ground resistance achieved by adding rods to a grid will hardly warrant the extra cost. Yet there are points in favor of such an arrangement:

(1) insure practically constant ground resistance for soil resistivity which may fluctuate near the earth's surface due to extreme climatic conditions, or (2) rods used to provide a reliable ground source and grid used as a safety measure to equalize fault potentials over the earth's surface.

Reference Plane Grounding System. A reference plane grounding system consists of (1) a metallic media (copper grid mesh) used as a common connecting point by all other members of the reference plane grounding system, (2) all metallic members that are bonded to the grid mesh, i. e. (a) shields of all configurations, (b) electronic equipment chassis, (c) electronic circuit neutrals, (d) cable trays which are common only to the interior of the structure, etc., and (3) all electrical connections and related parts used in conjunction with the grid mesh and the many members. All three constituents of a reference plane grounding system must be designed and implemented to yield and maintain the lowest possible dc and rf impedance to current flow.

Design of Reference Plane Grid Mesh. The initial problem is to determine the number of grids, associated dimensions and wire size to be used in constructing a reference plane grid mesh to obtain an optimum reduction in resultant impedance. Figure 6 illustrates a hypothetical application of such a grid mesh. The maximum impedance (resistance and self-inductance) offered to current flow by the grid mesh is encountered between points (A) and (B). The following paragraphs shall pertain to the development of expressions describing variations in impedance between points (A) and (B) as a function of various parameters.

For a prescribed length and width of a specific grid mesh the following two factors are working in opposing directions to change the resistance ( $R_{AB}$ ) between points (A) and (B) as a result of changes in the number of grids per side: (1) as the number of grids is increased,  $R_{AB}$  decreases due to the decreasing length of the grid elements and (2) as the number of grids is increased,  $R_{AB}$  increases due to the additional cables added to obtain the increased number of grids.

The following equation has been derived which expresses the maximum resistance offered by a square grid mesh:

$$R_{AB}]_n = \frac{R_e]_{n-1}}{2n} \left[ \frac{2k]_{n-1}[2(n-1)]}{1+2(n-1)} + 2 \right] \quad (8)$$

where

- $R_{AB}]_n$  = resistance between points A & B for n grids per side (ohms)
- n = number of grids per side
- $R_e]_{n-1}$  = resistance of one element of total length equal to the length of one entire side of the grid (ohms)
- k = multiplication factor to account for additional grids

The resistance of one element of total length equal to the length of one entire side of the grid ( $R_e]_{n-1}$ ) can be calculated by the following formula:

$$R_e]_{n-1} = \rho \frac{l}{A} \quad (9)$$

where

$$\begin{aligned} \rho &= \text{resistivity of conducting media} \quad \frac{\text{ohms}}{\text{circular mil foot}} \\ l &= \text{length of conductor (ft.)} \\ A &= \text{cross-sectional area of conductor (circular mils)} \end{aligned}$$

Equation 8 is a recursion type formula and can only be used by calculating  $R_{AB}$  progressively from  $n=1$  to  $n=n$ .  $R_{AB}$  has been calculated for values of  $n$  (grids per side) up to and including thirty (30). Such calculations have been performed for grid mesh areas of  $(100 \text{ ft.})^2$  to  $(1000 \text{ ft.})^2$  and for cable sizes of 1 inch, 3/4 inch, and 4/0. Resultant data is presented graphically in Figures 7, 8 and 9.

The distributed self-inductance of the grid mesh must also be considered for development of optimum design criteria. The high frequency self-inductance of copper calbe can be approximated by the following formula:

$$L = 0.609l \left( 2.303 \log_{10} \frac{4l}{d} - 1 \right) \quad (\mu\text{henries}) \quad (10)$$

where

$$\begin{aligned} L &= \text{low frequency self-inductance } (\mu\text{henries}) \\ l &= \text{length of conductor (ft.)} \\ d &= \text{diameter of conductor (ft.)} \end{aligned}$$

The high frequency self-inductance of a copper grid mesh consisting of "n" grids per side can be computed using Equations 8 and 10 as follows:

$$L_{AB}]_n = \frac{0.609l \left( 2.303 \log_{10} \frac{4l}{d} - 1 \right)]_n}{2} \left[ \frac{2k]_{n-1} [2(n-1)]}{1 + 2(n-1)} + 2 \right] \quad (11)$$

μhenries

$L_{AB}$  has been calculated for values of  $n$  (grids per side) up to and including thirty (30). Such calculations have been performed for grid mesh areas of  $(100 \text{ ft.})^2$  to  $(1000 \text{ ft.})^2$  and for cable sizes of 1 inch, 3/4 inch, and 4/0. Resultant data is graphically presented in Figures 7, 8 and 9 along with resistance data.

The maximum impedance offered by a rectangular grid mesh is different than the impedance offered by a square grid mesh with an equivalent number of mesh loops. The following expression has been derived which expresses the maximum resistance between points A and B of a rectangular grid mesh:



$$R_{AB} \Big]_{n_w} = \frac{R_{ew} \Big]_{n+1}}{n_w} \left[ k + k_n (n - n_w) \right] \quad (\text{ohms}) \quad (12)$$

where

- $R_{AB} \Big]_{n_w}$  = Resistance of rectangular grid mesh between points A and B (ohms)
- $R_{ew} \Big]_{n+1}$  = Resistance of a single conductor of length equal to the width of the grid mesh (ohms).
- $n_w$  = number of grids along the short side or width of the rectangular mesh.
- $k$  = coefficient computed for square grid meshes with various numbers of grids per side.
- $k_n$  = correction factor to account for lengths greater than widths using  $n_w$  grids.
- $n$  = number of grids along the long side or length of the grid mesh.

Equation 12 has been used to calculate the resistance of a rectangular grid mesh for length to width ratios of 2 and 3, and for 1 inch and 4/0 cable as a function of foundations or grid mesh area and number of grids on the short side of a rectangular grid mesh. Resultant data is graphically presented in Figures 10, 11 and 12, and 13.

Previous formulas and graphical representations can be used to design reference plane grid meshes with a minimum or designated dc or rf impedance to current flow, for any specific structure application. All formulas have been verified by use of other techniques of mathematical analysis and by actual construction and measurements of various grid configurations. All calculations are based upon the assumption that the contact impedance between mating members of the grid mesh is negligible as compared to the impedance of the conductors. Such an assumption will be valid if electric welding techniques are used to weld or fuse all metallic mating surfaces.

Reference Plane Members. All metallic members which serve as an integral part of the reference plane grounding system must present less dc and rf impedance to current flow than the maximum design impedance of the grid mesh. A good rule of thumb to follow in such circumstances is that the summation of the maximum grid mesh resistance and the total resistance of each member should be less than the maximum resistance specified or required for the reference plane grounding system.

$$R_{MAX} \Big]_{RP} + R_J < R_{Spec} \quad (13)$$

where

- $R_{MAX} \Big]_{RP}$  = maximum design resistance of the reference plane grid mesh.
- $*R_J$  = resistance of jumper or member from outermost point to connection at grid mesh.

---

\* Various text books, such as "Radio Engineers Handbook" by Frederick E. Terman, are available which present formulas for calculating the impedance, of various types of metallic conductors.

$R_{spec}$  = maximum specified resistance for the reference plane grounding system

Solid rectangular bond straps are often required to connect various metallic members to the grid mesh or others metallic members which serve as an integral part of the reference plane grounding system. Dimensions of such bonding straps should be selected so as to offer a minimum amount of impedance to current flow. The reactance associated with self-inductance is by far the greatest impedance of the bond strap. The self-inductance of a rectangular bond strap can be computed as follows:

$$\begin{aligned}
 & (l \geq d) \\
 L = 2 (\log_{10} & \frac{l + \sqrt{l^2 + [0.2235 (a+b)]^2}}{0.2235 (a+b)} - \sqrt{l^2 + [0.2235 (a+b)]^2}) \quad (14) \\
 & + 0.2235 (a+b) \times 10^{-9} \quad (\text{henries})
 \end{aligned}$$

where:

$l$  = length of bond strap (cm)  
 $a$  = width of bond strap (cm)  
 $b$  = thickness of band strap (cm)

This equation has been used to calculate the self-inductance of a solid rectangular strap for length-to-width ratio values of 0.1, 0.667, 0.5, 1.0, 5.0 and 10.0 while thickness (b) was held constant. Results of such calculations are presented graphically in Figure 14. Results indicate that the length-to-width ratio of a bond strap should be  $\leq 5/1$ , and preferably  $\leq 3/1$  when mechanically feasible.

Electrical Connections and Related Parts. The electrical connections of mating metallic surfaces is one of the most important ingredients of a reference plane grounding system and is, unfortunately, one of the most abused. If improperly implemented or if subjected to corrosive deterioration the RF impedance across two metallic mating surfaces may be far greater than the total impedance of the entire remainder of the grounding system.

All metallic mating surfaces and connecting hardware must be constructed of galvanically compatible metals. When a more noble metal is joined to a less noble metal, electro-chemical corrosion will occur. This simple battery cell action produces a high corrosion rate on the less noble metal, while the more noble metal remains unharmed. One of the attendant problems involves the coating of the noble metal with its less noble counterpart, resulting not only is mechanical weakness, but, electrically, a high impedance joint is formed. In fact, a rectifier of sorts is formed creating all of the problems relative to harmonic generation, etc.

Metallic mating surfaces which are susceptible to oxidation must be protected by application of a protective coating around the entire periphery of the mating surfaces. The electrical impedance offered by oxide films formed over an extended period of time can be quite significant relative to overall design impedance of the entire reference plane grounding system.

Electrical connection between metallic mating surfaces must be implemented in order to realize a rigid and low impedance contact. Some of the more important mechanical considerations are as follows:

(1) Mating surfaces of metallic members should be welded or brazed around the entire periphery of the contacting area in all cases where possible and practical.

(2) In lieu of welded or brazed connections, bolted sections may be used. Bolted sections must be implemented to insure (1) a consistent contact pressure over an extended period of time, (2) minimal crevice area around metallic mating surfaces, and (3) a high resistance to atmospheric corrosion over an extended period of time. It is recommended that palnuts be used to maintain a permanently tight joint.

(3) Rivets should not be used as an electrical connection on metallic members subjected to fluctuations in stress or strain or minute movements of the bond connections.

(4) Protective or non-conducting coatings must be removed from the contact area of all mating surfaces before the bond connection is made.

The above criteria and precautionary measures constitute only a few of the bonding requirements necessary in order to realize an electromagnetically compatible reference plane grounding system.

Criteria presented in the previous paragraphs constitutes only the basic building blocks of compatible grounding systems. Many problem areas and techniques for compatible implementation cannot be adequately covered in this paper; i. e. (1) variations in soil resistivity as a function of soil type, moisture content, temperature and salt content, (2) periodic spacing of bond straps on metallic members to minimize standing waves, (3) coatings and surface treatment to prevent corrosion, harmonic generation and corona, (4) test requirements to insure that compatible grounding systems are realized both during and after final implementation, (5) specific technique for implementing a single "ground-well" between the grounding systems, (6) techniques for implementing an equipotential grounding system in structures utilizing long cable runs, such as missile checkout complexes, etc. Solutions to such problems may be analyzed by referring to existing literature, compliance with good engineering practices and/or reliance upon recommendations acquired through knowledgeable consultant agencies.

### III. CONCLUSIONS

Structure grounding systems must be designed and implemented to comply with the electrical and safety requirements of all prospective users. Such systems must basically perform the following functions: (1) provide a safeguard for persons and property from hazards associated with electricity, and (2) provide a low impedance reference plane for structures or complexes housing electronic and instrumentation facilities which are susceptible to or capable of radiating electromagnetic energy.

There is an optimum number of ground rods for each foundation area, beyond which little reduction in grounding resistance is realized. Applicable formulas are used in this study to calculate grounding resistance as a function of (1) number of ground rods used around the periphery of a structure foundations, (2) depth of ground rod penetration into the earth, and (3) structure foundation area. Calculated data is presented in graphical form which is readily adaptable to the determination of ground rod configurations compatible with specific structure requirements.

Formulas are derived which express the maximum resistance and self-inductance of a reference plane grounding system as a function of (1) number of grids, (2) size of grids conductors and (3) foundation area of structures where grid meshes are to be implemented. Such formulas have been derived for both square and rectangular reference plane grid meshes as a function of the prestated parameters. Calculated data is presented in graphical form with variables that are readily adaptable to the design of reference planes which are compatible with specific structure requirements. Graphical illustrations can be effectively used to determine the number of grid meshes and size of mesh conductors necessary to achieve optimum impedance reduction at a minimal cost.

Complimentary construction techniques are described which are necessary for effective implementation of the recommended structure grounding system. Recommendations are presented relative to (1) preferred bonding techniques, and (2) techniques for corrosion proofing.

### ACKNOWLEDGEMENTS

The contents of this paper are a result of a contract for the Electromagnetic Vulnerability Laboratory, Contract No. AF30(602)-2691, placed with White Electromagnetics, Inc., by the U.S. Air Force, Rome Air Development Center.

### REFERENCES

1. Schwarz, S.S., "Analytical Expressions for the Grounding Resistance of grounding Rods, Transactions AIEE," August 1954.

2. Dwight, A.B. , "Calculations of Resistance to Ground," Transactions of AIEE, Electrical Engineering, Vol. 55, December 1936, PP 1-13.
3. Terman, Frederick E. , Radio Engineers Handbook, McGraw Hill, 1943.

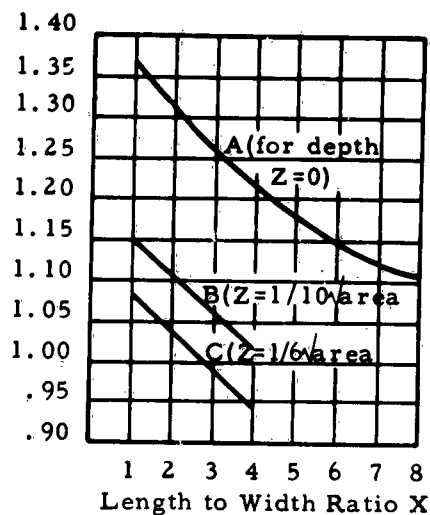


FIGURE 1. VALUES OF COEFFICIENT  $k_1$  AS FUNCTION OF LENGTH TO WIDTH RATIO  $X$  OF AREA.

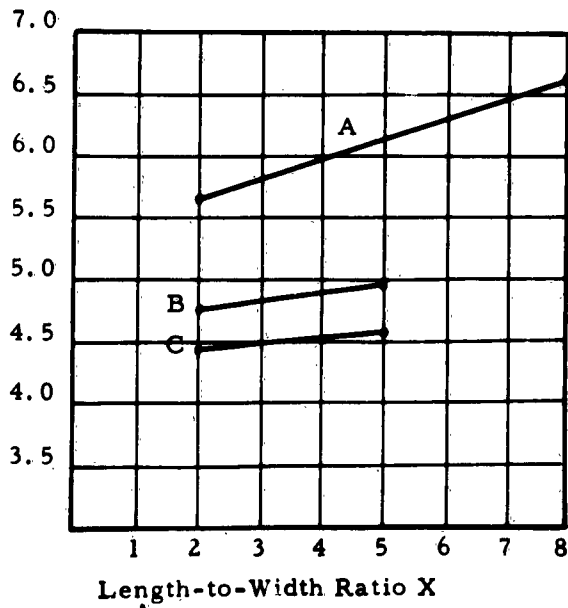
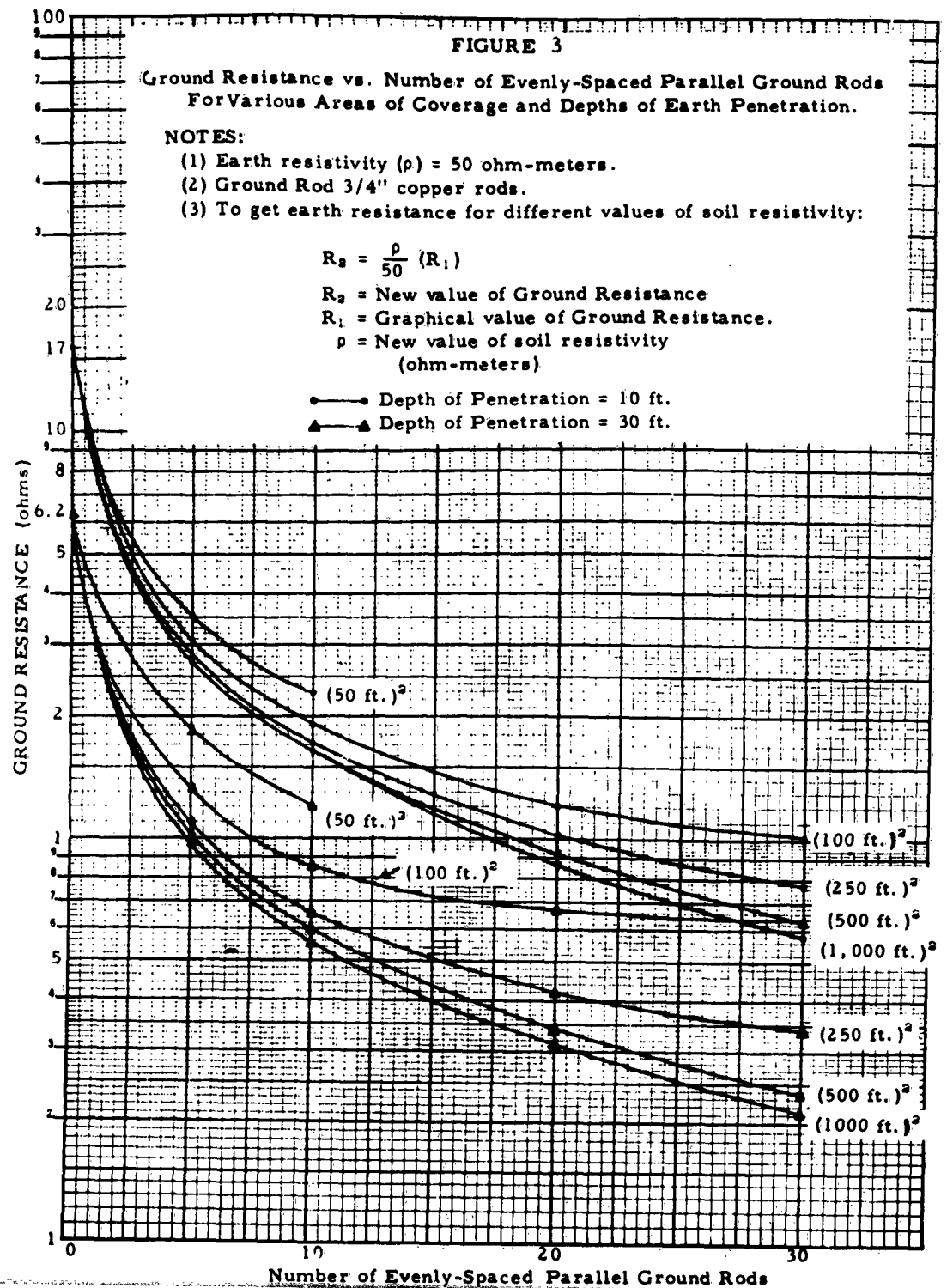
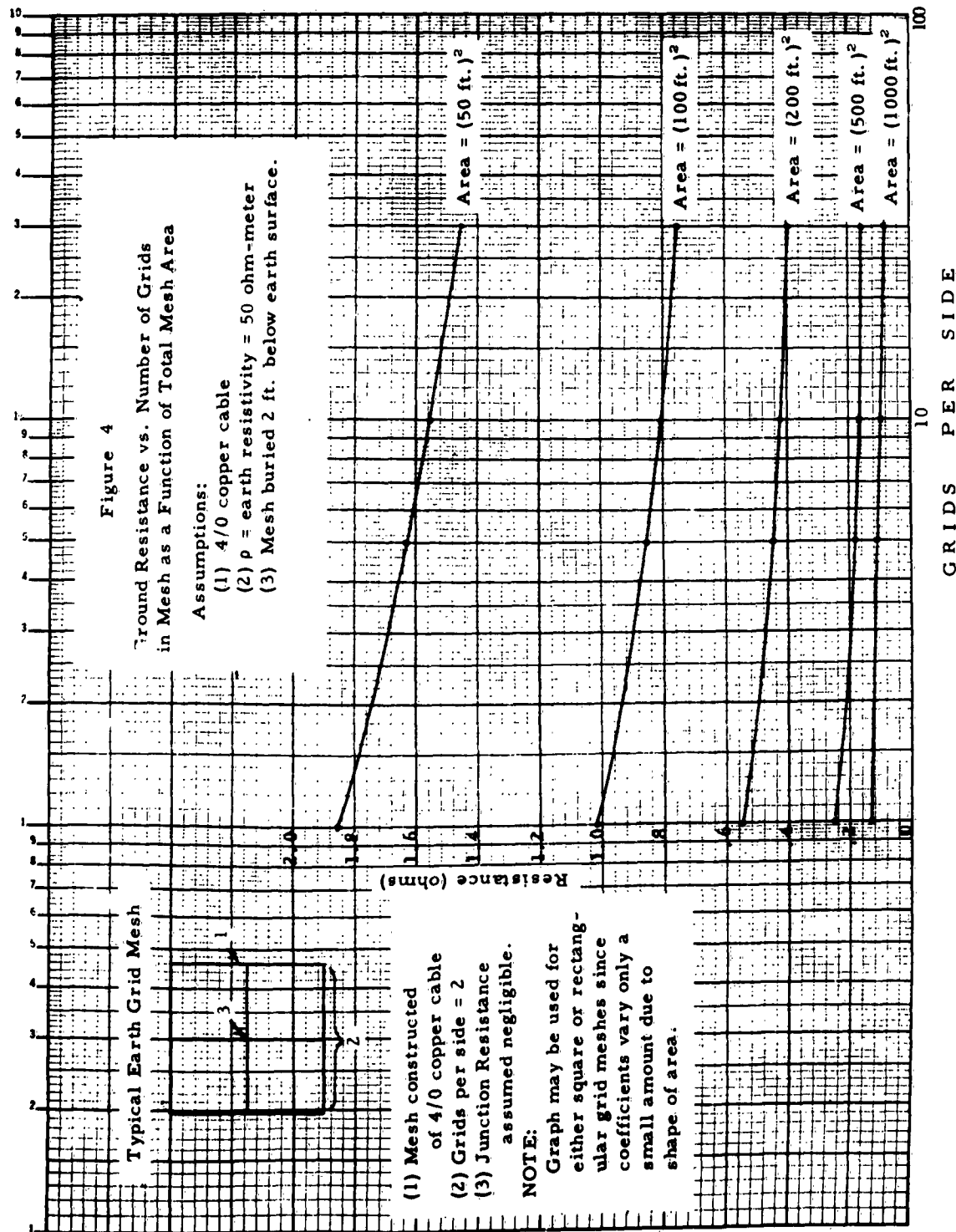


Figure 2. VALUES OF COEFFICIENT  $k_2$ , CORRESPONDING TO COEFFICIENT  $k_1$







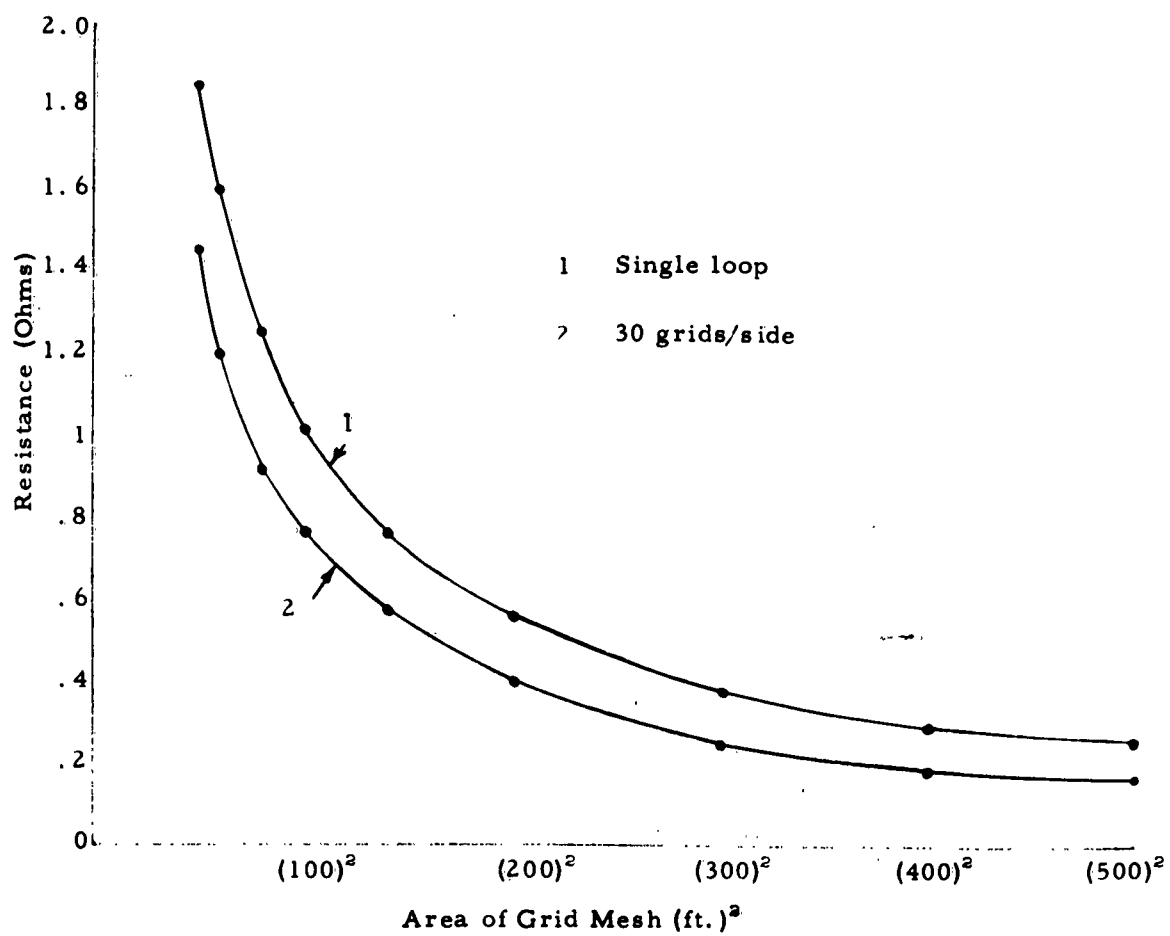


Figure 5 Ground Resistance vs. Grid Mesh Area

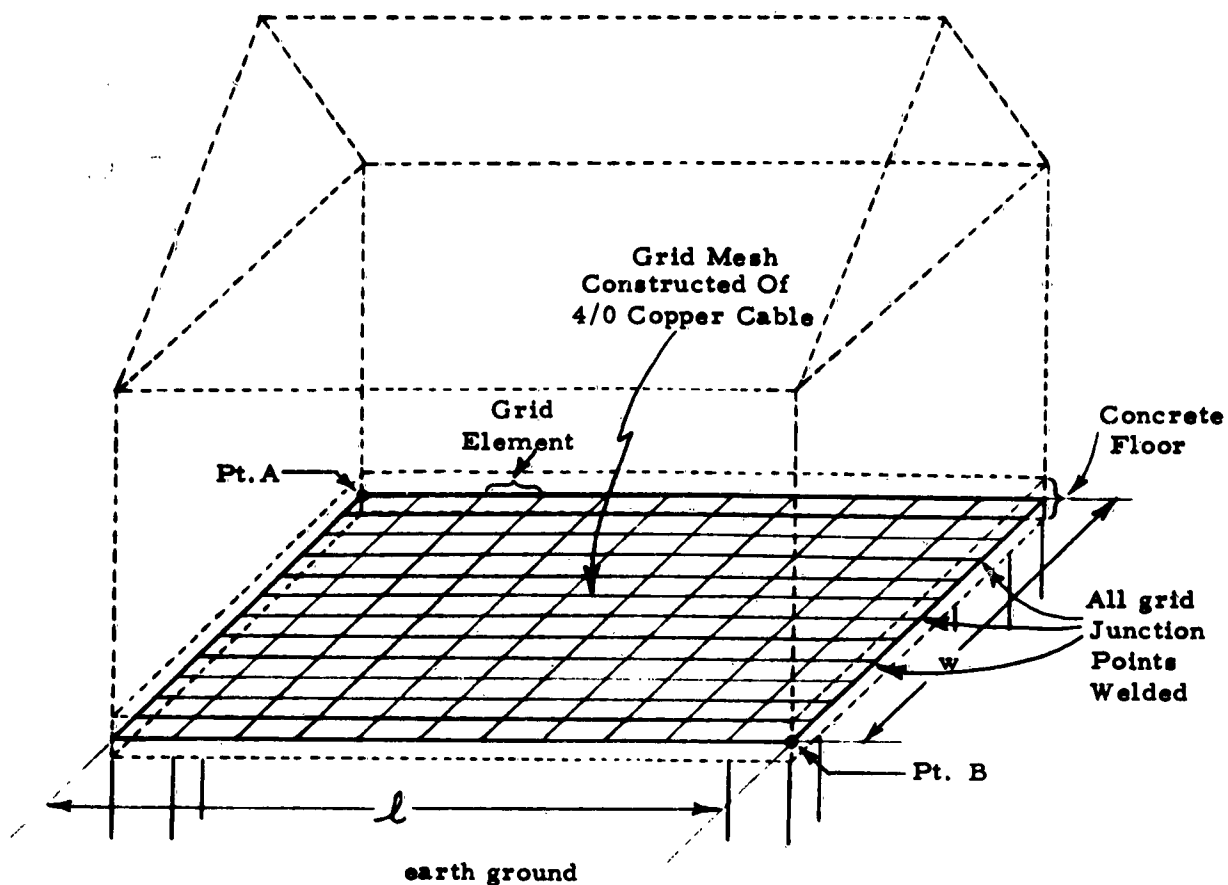
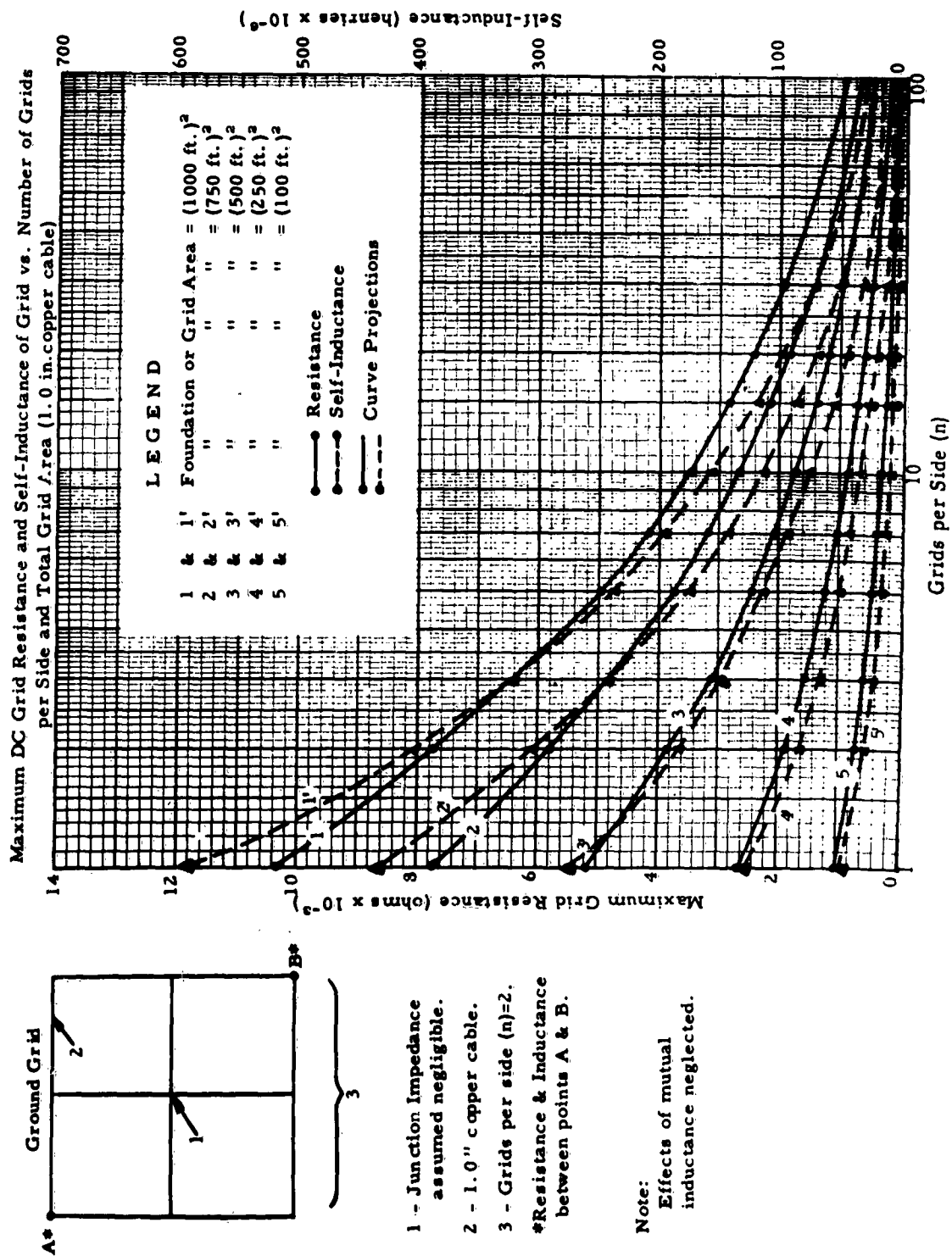


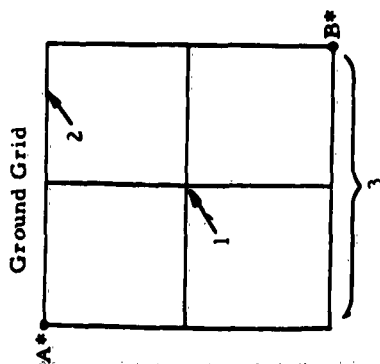
Figure 6 HYPOTHETICAL APPLICATION OF REFERENCE PLANE GRID MESH.

$l$  = length of grid mesh or foundation  
(11 grids per length)

$w$  = width of grid mesh or foundation  
(12 grids per width)

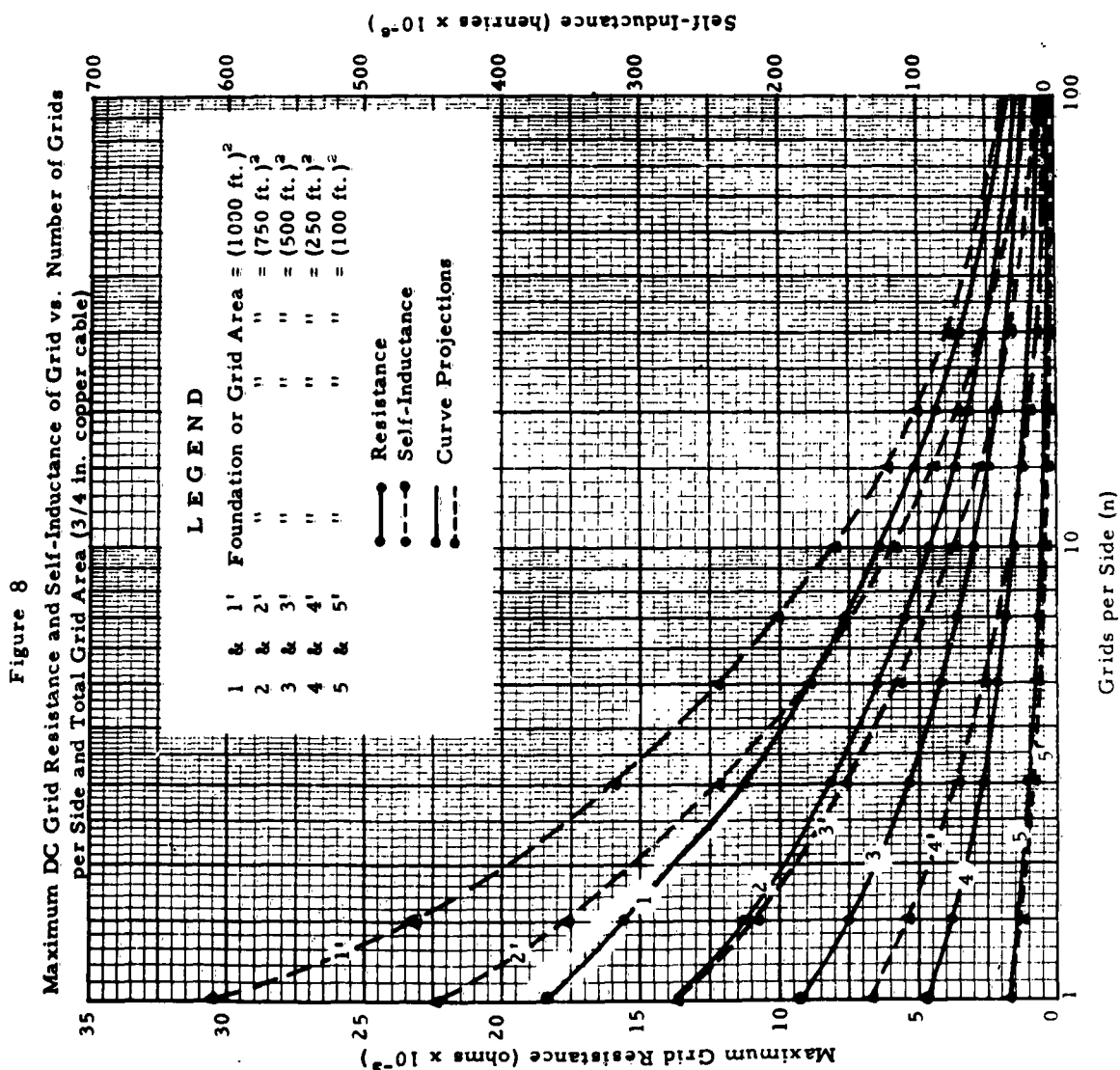
Figure 7

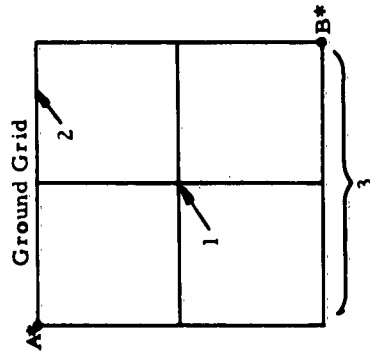




- 1 - Junction Impedance assumed negligible.
- 2 - 3/4" copper cable.
- 3 - Grids per side (n)=2
- \* Resistance & Inductance between points A & B.

Note:  
Effects of mutual inductance neglected.





- 1 - Junction Impedance assumed negligible.
- 2 - 4/0 Copper Cable.
- 3 - Grids per side (n)=2.
- \* Resistance & Inductance between points A & B.

Note:  
Effects of mutual inductance neglected.

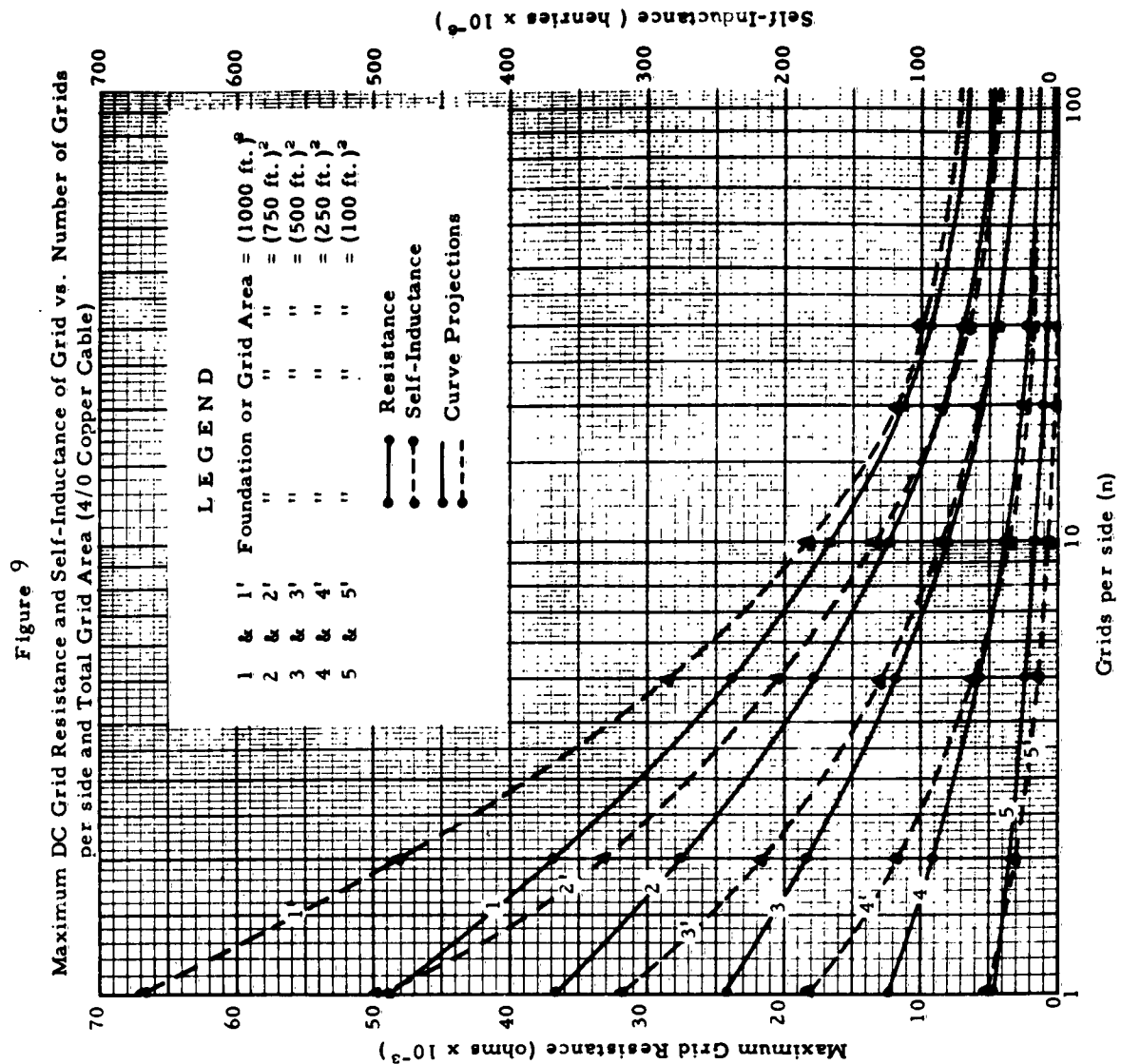
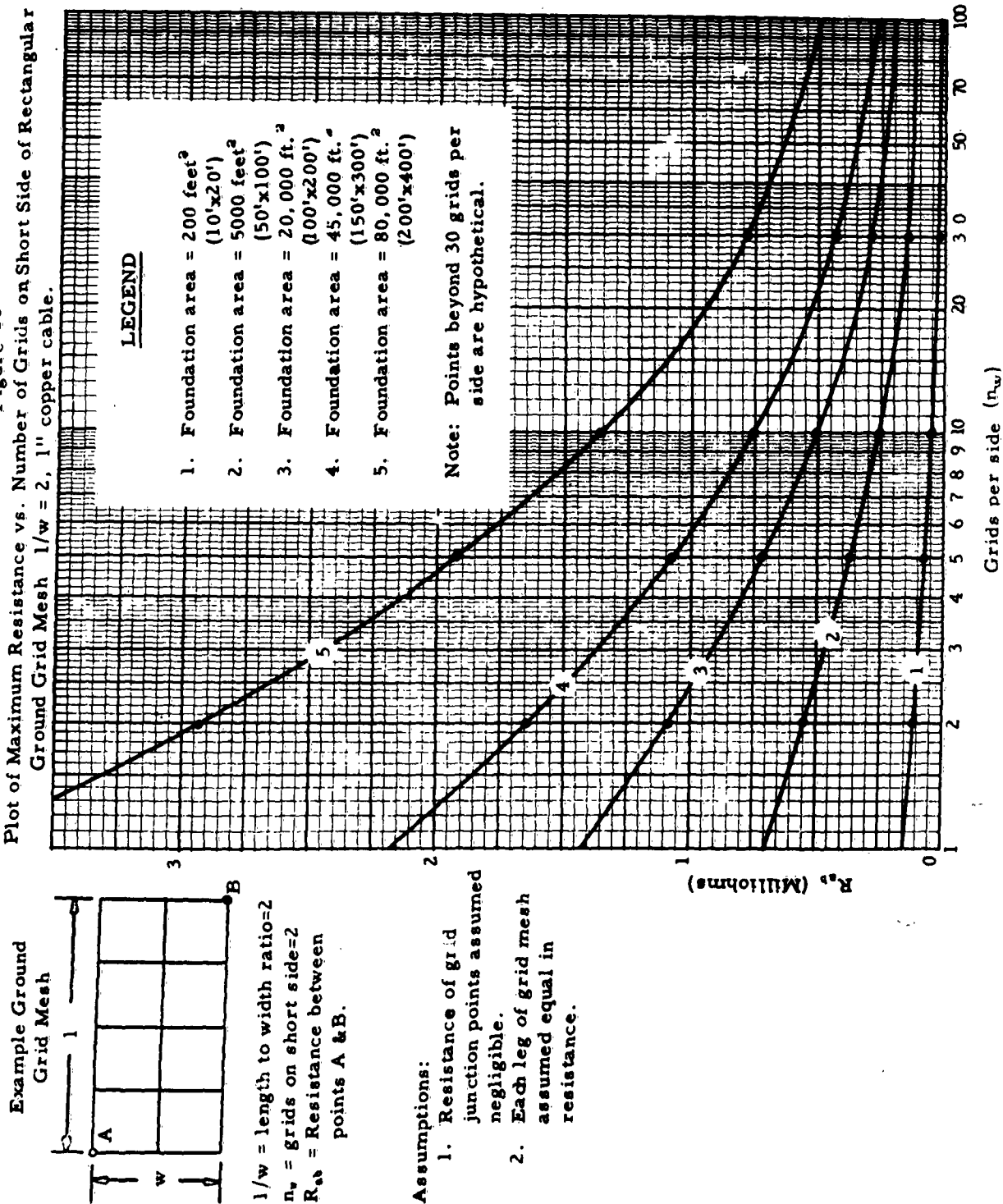
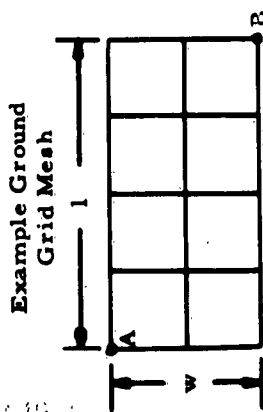


Figure 10  
Plot of Maximum Resistance vs. Number of Grids on Short Side of Rectangular  
Ground Grid Mesh  $l/w = 2, 1''$  copper cable.





$1/w$  = length to width ratio=2  
 $n_v$  = grids on short side=2  
 $R_{ab}$  = Resistance between points A-B.

#### Assumptions:

1. Resistance of grid junction points assumed negligible.
2. Each leg of grid mesh assumed equal in resistance.

Figure 11

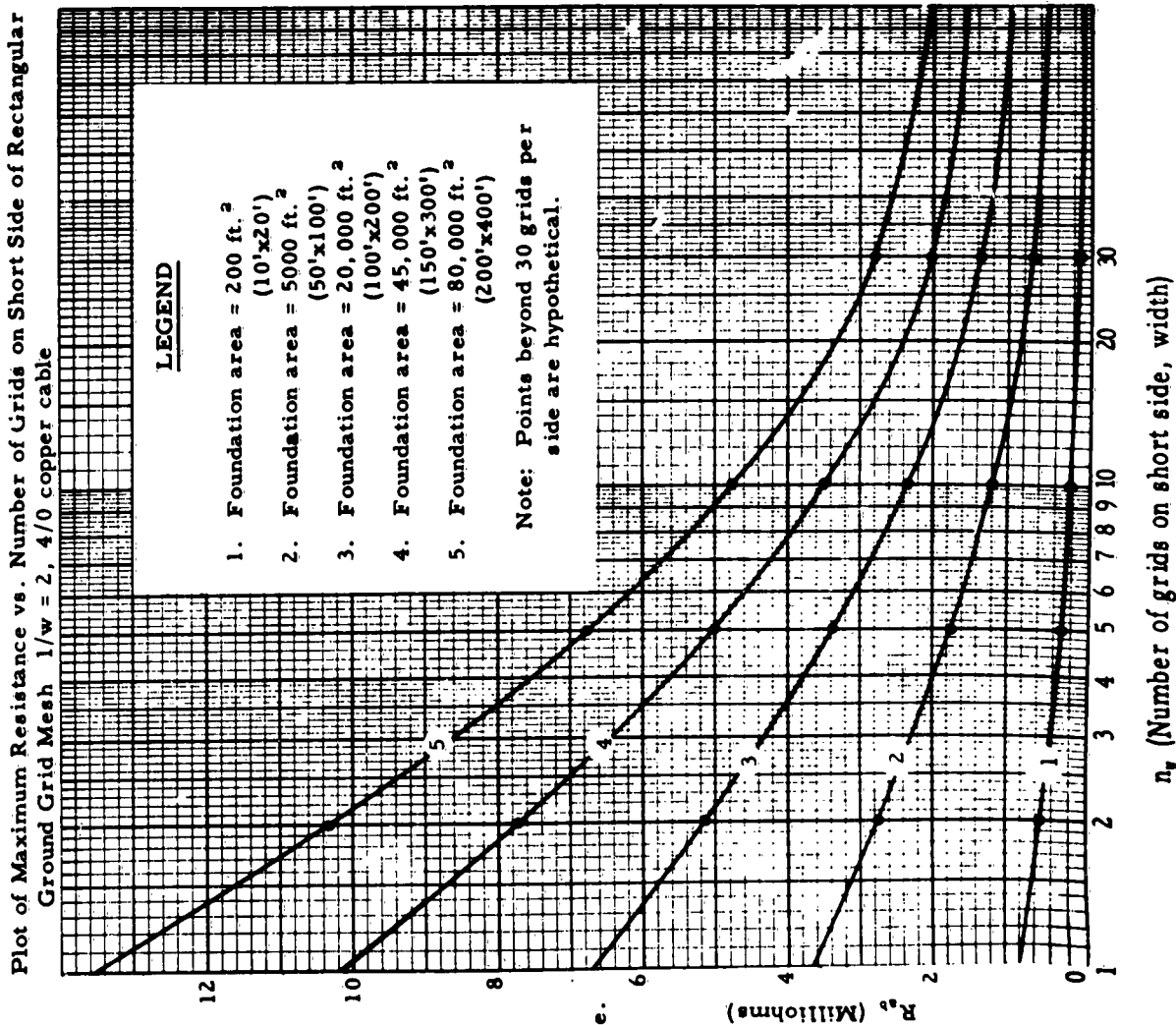
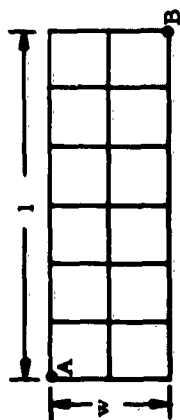
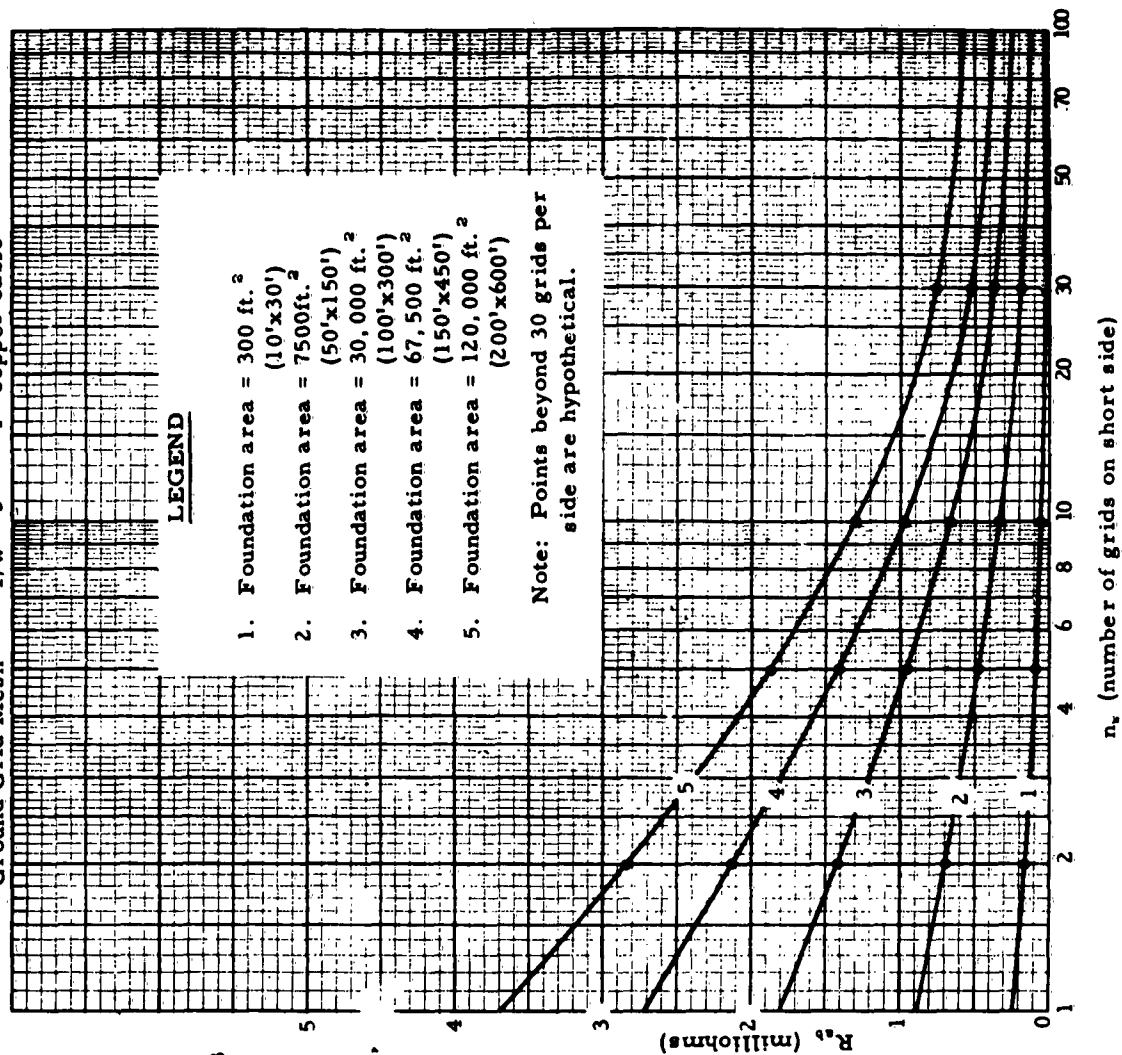


Figure 12

Plot of Maximum Resistance vs. Number of Grids on Short Side of Rectangular Ground Grid Mesh  $l/w = 3$  1" copper cable



$l/w =$  length to width ratio  
 $= 3$

$n_s =$  grids on short side  
 $= 2$

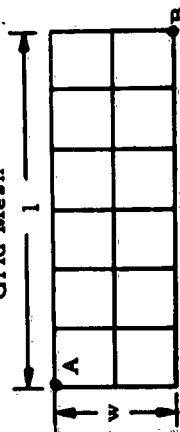
$R_{AB} =$  Resistance between points, A & B.

Assumptions:

1. Resistance of grid junction points negligible.
2. Each leg of grid mesh assumed equal in resistance.



Example Ground Grid Mesh



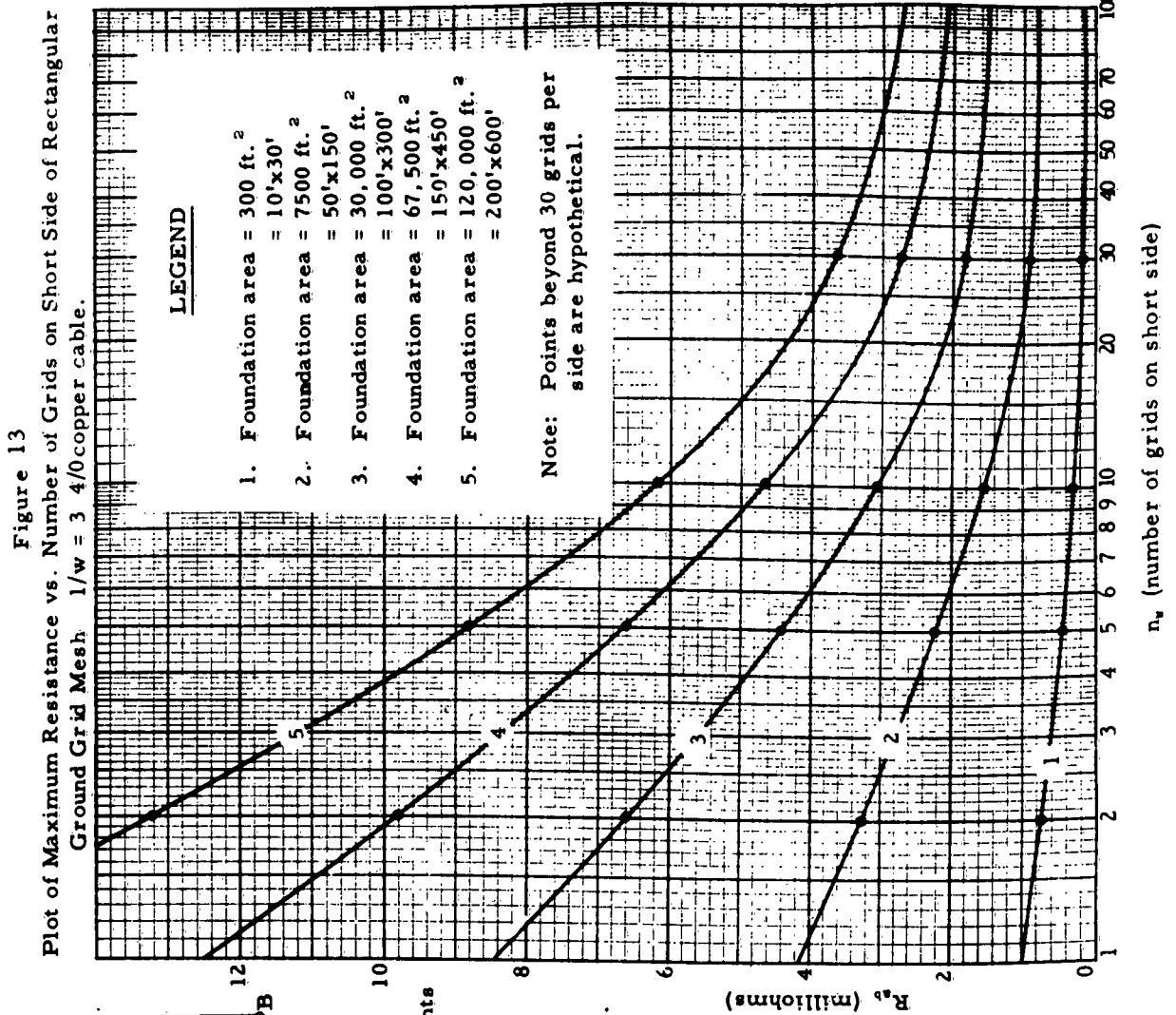
$1/w = \text{length to width ratio} = 3$

$n_s = \text{grids on short side} = 2$

$R_{AB} = \text{Resistance between points A \& B.}$

#### Assumptions:

1. Resistance of grid junction points negligible.
2. Each leg of grid mesh assumed equal in resistance.



L/W	L(henries)
10	$18.692 \times 10^{-9}$
5	$6.592 \times 10^{-9}$
1	$.264 \times 10^{-9}$
5	$.01 \times 10^{-9}$
2	$1.298 \times 10^{-9}$

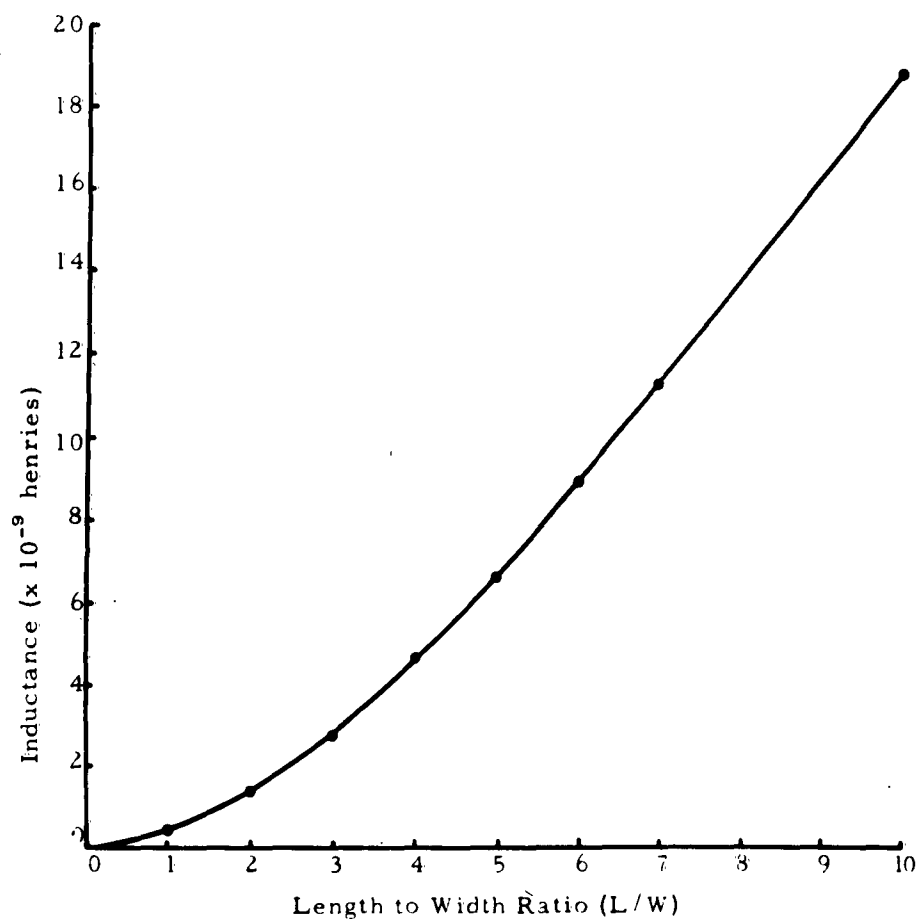


Figure 14-Self-Inductance vs. Length/Width Ratio of Rectangular Bar

# ELECTROMAGNETIC COUPLING BETWEEN COAXIAL, SINGLE-WIRE, TWO-WIRE, AND SHIELDED TWISTED PAIR CABLES

M. Kaplit  
The Moore School of Electrical Engineering  
University of Pennsylvania  
Philadelphia, Pennsylvania

Abstract. - This paper presents the results of an experimental investigation of electromagnetic coupling between coaxial, single-wire, two-wire, and shielded twisted pair cables over the frequency range of 100 cps to 50 kc. The coupling was measured for matched, short-circuit, and open-circuit loaded cables when different combinations of similarly loaded parallel cables are used, enabling electric and magnetic coupling to be determined. These results are given as transfer impedances for different cable spacings and frequencies, worst case conditions being measured for shielded twisted pair cables.

A brief summary of shielding effectiveness measurements is given. These are contrasted with the technique presented in this paper since many of them determine the shielding effectiveness of only a single cable.

## I. INTRODUCTION

In an analysis of the electromagnetic compatibility aspects of any given electronic system, one of the major considerations is the cabling used to interconnect the various components. A recent effort was made to predict the performance of systems installed on shipboard. In such installations it is quite common, because of limited space, to find heavy power cables and sensitive electronic equipment input cables running side by side with limited or no separation.

However, to make suitable predictions, one must have quantitative data on the coupling between the various commercial types of cable which may be used. We have had little success in finding such data in spite of the fact that there are a number of publications discussing the general principles involved. For this reason an experimental program was initiated whose preliminary results are reported here. Since immediate interest was in the lower frequencies, the actual range investigated was from 100 cps to 50 kc.

These measurements are similar to those made by the Material Laboratory of the New York Naval Shipyard,<sup>1</sup> by Newman and Albin,<sup>2</sup> and by Gooding and Slade,<sup>3</sup> in that the pickup between parallel cables was measured as a function of both frequency and cable spacing.

The Material Laboratory and Newman and Albin both measured voltage transfer ratios between cables with matched loads for frequencies above 85 kc. Gooding and Slade measured the transfer impedances and voltage transfer ratios between coaxial cables and 300 ohm two-wire lines, but for coaxial cable

measurements do not mention the actual cables employed. In addition, the Signal Equipment Co. has also measured coupling as a function of both cables' lengths.<sup>4</sup>

In this study the exciting cable passes through and is grounded at each end of a shielded (i.e. metallic) room which contains a second cable and a voltmeter to measure the signal coupled into it.

This procedure seems more satisfactory than that of trying to relate the "shielding effectiveness" of each cable to the expected transfer impedance because the relationship is not obvious. Of course, if the pickup for a specific combination of cables is known and the shielding effectiveness of these and other cables is also known from any of several useful comparison methods, the pickup for these other cables can probably be estimated.

Four types of shielding effectiveness tester have appeared in the literature. The first of these is the so-called triaxial tester. It is simply a shield placed over one end of a short-circuited piece of the cable whose shielding effectiveness is to be measured. This cable is then energized and the pickup is measured between the added shield and an extension of the cable's inner conductor. The shielding effectiveness of the cable is defined by Schatz and Taylor<sup>5</sup> as the ratio of voltage between the shield and the cable's outer conductor to the current in the cable, and by Allen<sup>6</sup> as the ratio of the energy fed into the cable to the energy leaked into the region between the cable and the shield.

Another procedure is to place a short-circuited length of coaxial cable through a ground plane, whose area is very large compared to the square of the wavelength, and measure the radiated field. The radiated field can be determined theoretically, and Robl and Schatz<sup>7</sup> define a shielding factor as the ratio of the field radiated by the cable to the field radiated by a rod carrying the same current and having the same over-all length.

The Material Laboratory<sup>8</sup> mentioned previously has also designed a radiation box which measures the power radiated into it by a cable passing through it. By comparison with other cables, a measure of relative shielding effectiveness can be obtained. The Signal Equipment Co.<sup>4</sup> also used a toroid surrounding the cable to measure the external field, and they regard the ratio of voltage coupled to the toroid to the current in the cable as a measure of shielding effectiveness.

Unfortunately, none of these procedures measures or even predicts the actual coupling between cables. This paper presents the results of an experimental investigation of electromagnetic pickup between various cables as a function of frequency and some possible cable terminations.

## II. EXPERIMENTAL CONFIGURATION

The actual experimental configuration is as shown in Fig. 1. The signal generator was placed outside the shielded room, approximately 8' long, 6' wide, and 8' high, and the exciting cable passes through but is grounded

at each end of the room, enabling the cable's shielded load to be placed outside the room also. The pickup cable, its load, and the voltmeter are inside the room in order to reduce external noise. A jig holds the two cables parallel over a length of 4' which is essentially all of their effective coupling length. The jig also enables the cable's center-to-center spacing to be varied. The voltmeter was a HP-302 wave analyzer which has a sensitivity of 1  $\mu$ v over the frequency range of 0 to 50 kc. When greater sensitivity was needed and could be employed, a Quan-Tech model 203 low noise amplifier with a gain of 100 from 0 to 500 kc was placed before the wave analyzer. To check the system operation, the principle of reciprocity was verified by interchanging the signal generator and the voltmeter.

### III. EXPERIMENTAL RESULTS

This section presents the most typical experimental results. The measurements are displayed as graphs of either transfer impedance between cables, i.e. the voltage induced in the 4 ft long pickup cable for 1 ampere of current in the exciting cable, or of the voltage transfer ratio when so-called "electrostatic" coupling was measured. The dimension shown on each curve is the center-to-center spacing between the parallel cables with the smallest being for adjacent ones. With the exception of the electrostatic coupling measurements, when both cables have open-circuit loads, the exciting cable has a short-circuit load and the pickup cable is terminated, as is indicated on each graph, in an open-circuit, a short-circuit, or a resistor approximately equal to its high frequency characteristic impedance. If a coaxial cable is employed as the pickup cable, the measured value is dependent on the grounding scheme. When a wire (ground) connects the outer conductor at both ends, there is appreciably more pickup than without. This condition is designated "loop" on the figures.

Figure 2 displays the coupling between RG-62/U and RG-59/U coaxial cables. The maximum transfer impedance is  $3 \times 10^{-3}$  ohms at 2 kc for a matched or short-circuit load on the pick-up cable in the "loop" condition. When the loop is not present, the maximum transfer impedance is  $6 \times 10^{-6}$  ohms and occurs at 4 kc. In both cases the inherent shielding of the coaxial cables becomes stronger above 5 kc. With an open-circuit load and "loop" condition, the curve for transfer impedance is similar to that for a short-circuit load, except that its maximum is about a third as great and occurs a few kc higher.

Figures 3 and 4, which display the coupling between an RG-22A/U shielded twisted pair cable and a RG-59/U coaxial cable and RG-22A/U respectively, are similar in that for matched or short-circuit loads the transfer impedances are maximum at about 40 kc. However, the maximum values of the transfer impedance are  $6 \times 10^{-5}$  ohms and  $3 \times 10^{-6}$  ohms respectively. For the RG-22A/U to RG-22A/U coupling there was no loop effect, but there was an order of magnitude increase in the coupling between a RG-22A/U and RG-59/U in a loop condition.

Figure 5 displays the coupling between a 300 ohm twin lead and another one with and without a shield. When there is no shielding, the

transfer impedance is proportional to the frequency. With a copper braid shield and a matched or short-circuit load, the transfer impedance is almost the same as for an unshielded cable, until about 7 kc when the shield begins to become effective in reducing the coupling. For an open-circuit load the transfer impedance is reduced at least an order of magnitude by the shield. For an open circuit load a single ground at the voltmeter end of the shield is most effective in reducing coupling, but the ground condition was not critical for matched and short-circuit loads.

The coupling between an RG-62/U and a 300 ohm twin lead is displayed in Fig. 6. The results indicate that below 5 kc the coupling is greater for a matched or short-circuit load than for an open-circuit one. The maximum transfer impedance is  $1.3 \times 10^{-3}$  ohms at 4 kc.

Figure 7 displays the coupling between a single wire and a RG-59/U or a RG-22A/U cable, and it is experimentally and theoretically a measure of the maximum voltage that cable can induce in another. For a coaxial cable with a "loop", about 30% of this voltage is obtained, while for the RG-22A/U only about 15% is obtained.

Finally, Fig. 8 displays several examples of "electrostatic" coupling. Once again, the "loop" ground condition increases the coupling between coaxial cables.

#### IV. CONCLUSIONS

Data has been obtained for coupling between various cables in the frequency range of 100 cps to 50 kc. This coupling is measured in terms of transfer impedance. The transfer impedance increases with frequency until the cable's shielding becomes an important factor. The effect of multiple grounds in decreasing the shielding effectiveness of coaxial cables has been clearly demonstrated.

This is only a preliminary report and future work will include extensions to higher frequencies and a more precise definition of shielding terminology.

#### ACKNOWLEDGEMENTS

The author would like to thank Dr. R. M. Showers of the Moore School of Electrical Engineering, University of Pennsylvania, for his constant encouragement and many valuable suggestions. Thanks are also due to Mr. H. Finkelstein for assisting in the experimental work. The work reported here was performed under Contract NObsr 85170, with the Bureau of Ships, Department of the Navy.

#### REFERENCES

1. Weinberger, E.F. and L. Auerbach, "Research to Determine the Crosstalk Between Representative Coaxial Cables and an Armored Power Cable," Lab. Project 4908-35A, Pt. 1, Progress Report 6, Material Lab., New York Naval Shipyard, Brooklyn, N. Y., June 11, 1958.

2. Newman, I. M. and A. L. Albin, "An Integrated Approach to Bonding, Grounding, and Cable Selection," Proceedings of the 7th Conference on Radio Interference Reduction and Electronic Compatibility, Nov. 1961.
3. Gooding, F. H. and H. B. Slade, "Shielding of Communication Cables," AIEE Trans., vol. 75, Pt. II, July 1955.
4. Final Report on Research and Development Contract No. NObsr 64507, Signal Equipment Co., Inc., Seattle, Wash., 1955.
5. Schatz, E. R. and M. E. Taylor, "The Measurement of RF Leakage from Coaxial Cables," Proc. of the Third Conference on Radio Interference Reduction, February 1957.
6. Allen, T. A., "A Proposed Standard for Testing the Shielding Effectiveness of Coaxial Cables and Shielding Material," Proceedings of Sixth Conference on Radio Interference Reduction and Electronic Compatibility, Oct. 1960.
7. Robl, R. F. and E. R. Schatz, "A Free-Space Method for Measuring Coaxial Cable Shielding Effectiveness," Proc. Fourth Conference on Radio Interference Reduction and Electronic Compatibility, October 1958.
8. Weinberger, E. F. and L. Auerbach, "Development of a Technique for Measuring Shielding Effectiveness," Lab Project 4908-35A, Pt. 2, Final Report, Material Laboratory, New York Naval Shipyard, Brooklyn, New York, June 14, 1956.

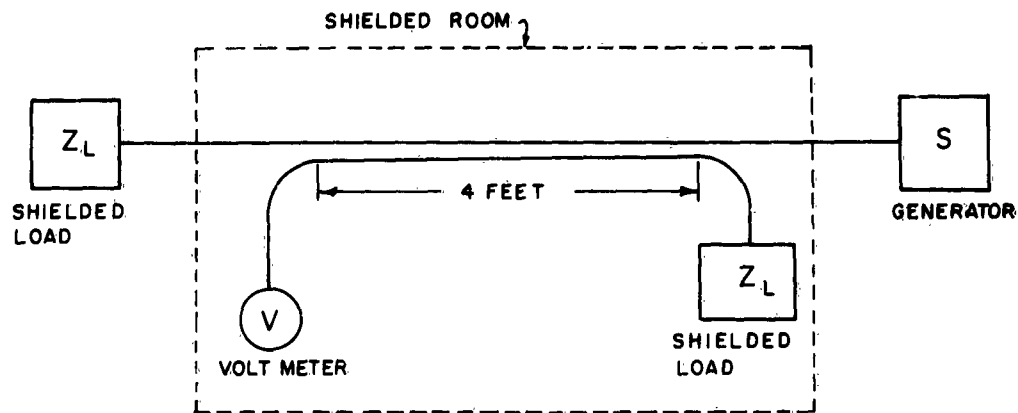


FIGURE 1 EXPERIMENTAL CONFIGURATION

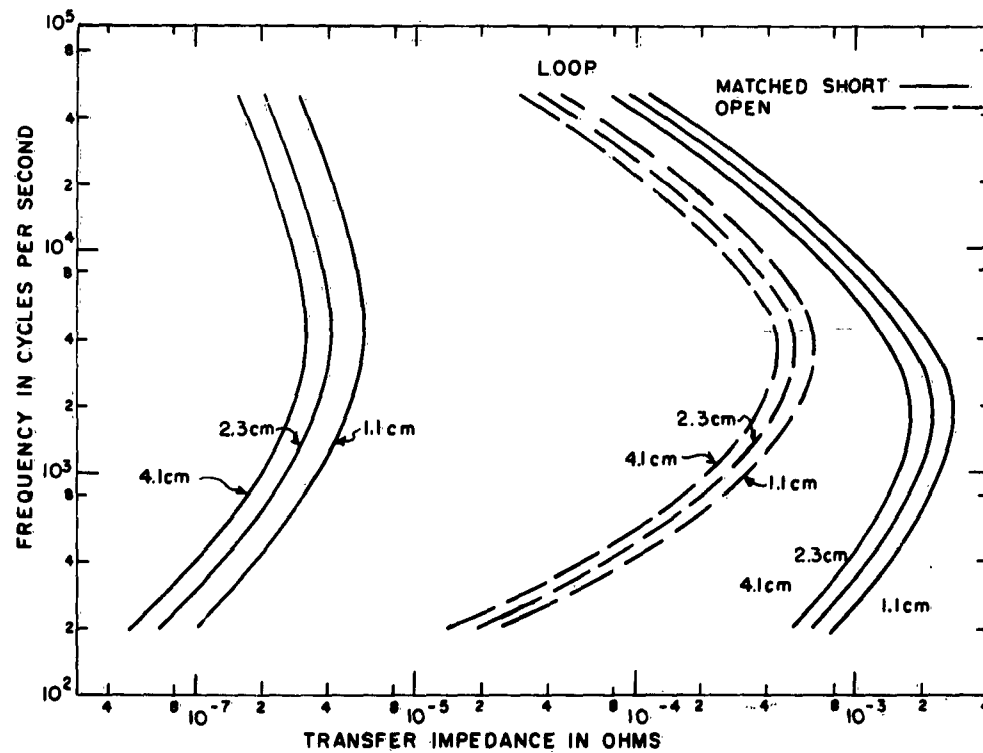


FIGURE 2 ELECTROMAGNETIC COUPLING BETWEEN RG-62/U AND RG-59/U COAXIAL CABLES



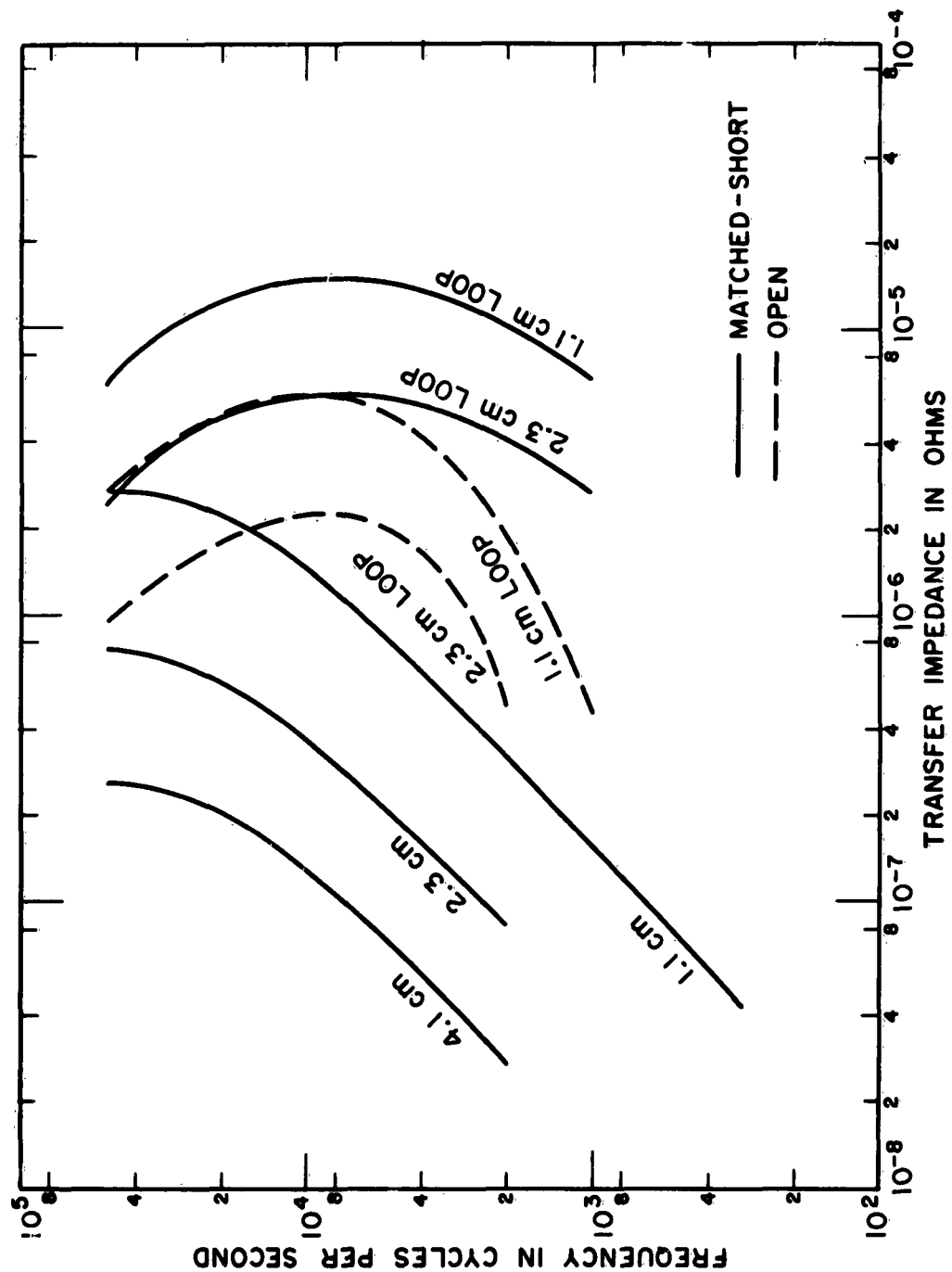


FIGURE 3. ELECTROMAGNETIC COUPLING BETWEEN AN RG-22A/U SHIELDED TWISTED PAIR CABLE AND AN RG-59/U COAXIAL CABLE

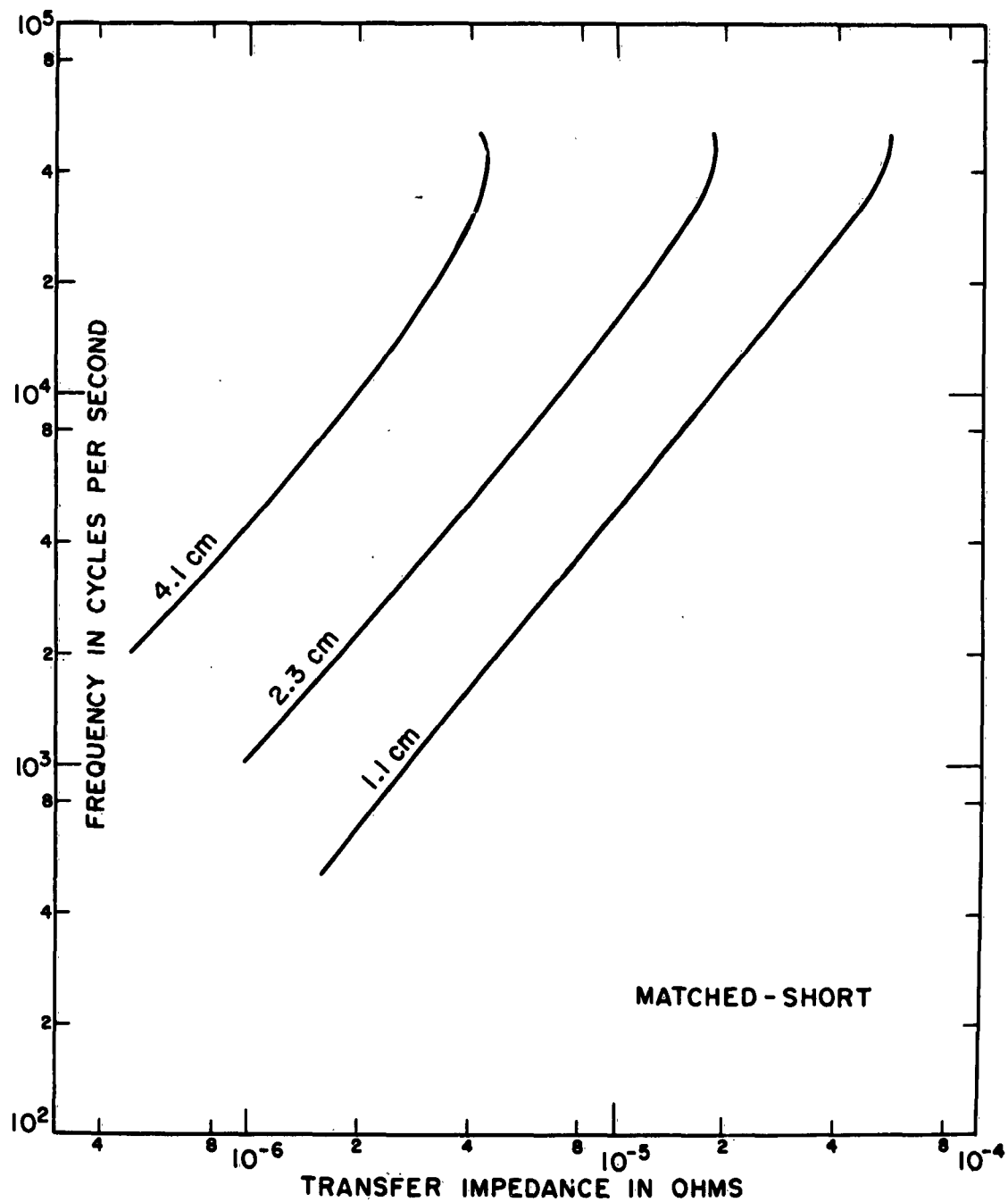


FIGURE 4 ELECTROMAGNETIC COUPLING BETWEEN RG-22A/U SHIELDED TWISTED PAIR CABLES

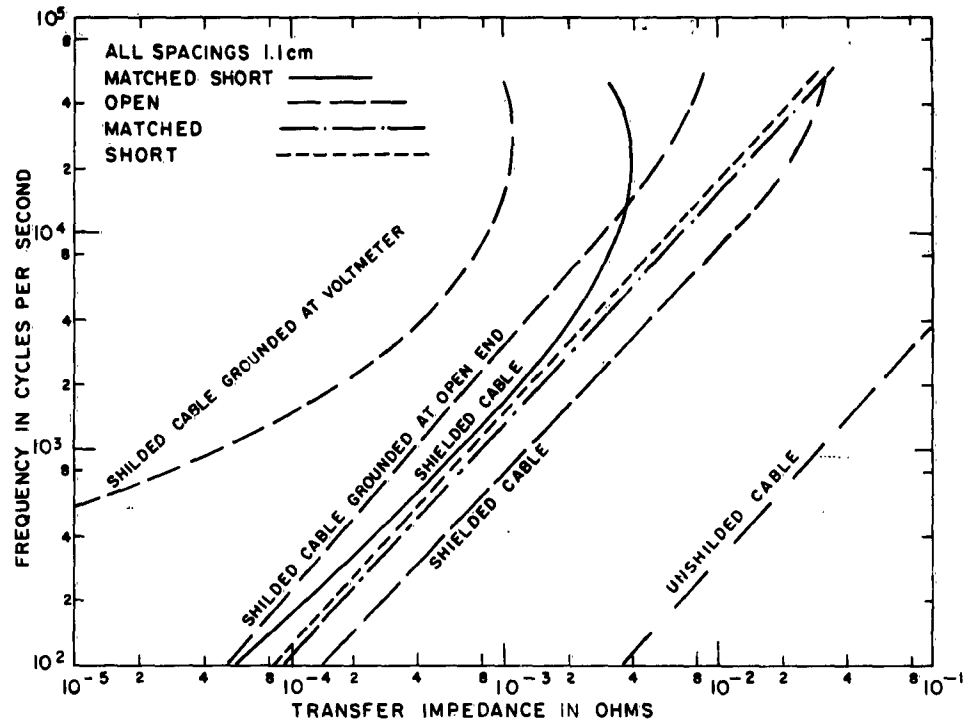


FIGURE 5 ELECTROMAGNETIC COUPLING BETWEEN A 300 OHM TWIN LEAD AND A 300 OHM TWIN LEAD WITH AND WITHOUT A COPPER BRAID SHIELD

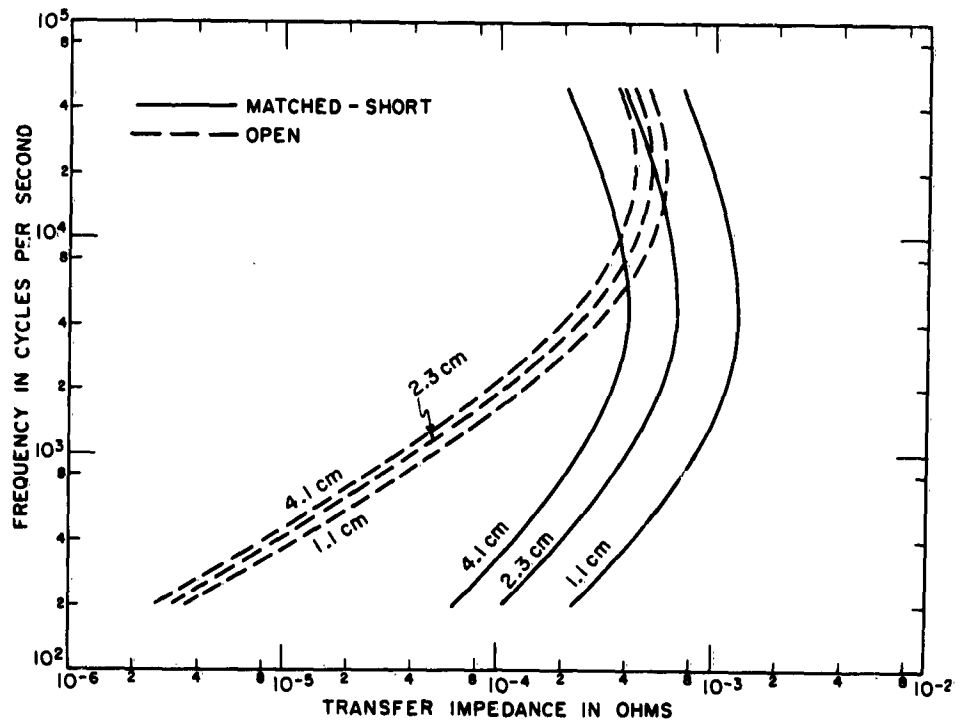


FIGURE 6 ELECTROMAGNETIC COUPLING BETWEEN AN RG-62/U COAXIAL CABLE AND A 300 OHM TWIN LEAD

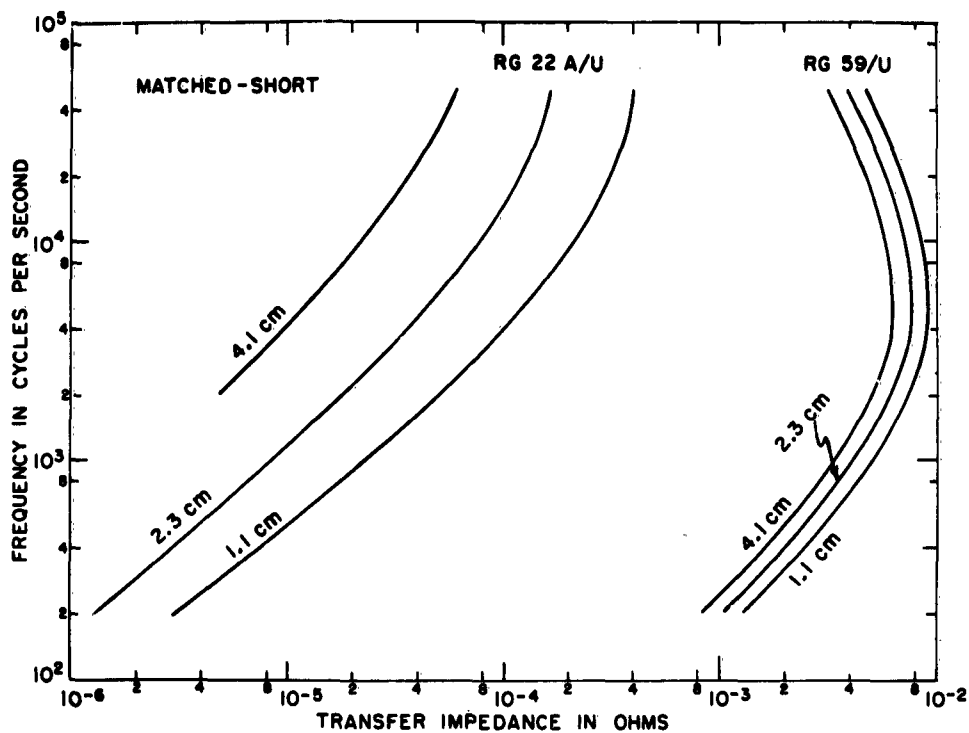


FIGURE 7 ELECTROMAGNETIC COUPLING BETWEEN EITHER AN RG-59/U COAXIAL CABLE OR AN RG-22A/U SHIELDED TWISTED PAIR CABLE AND SINGLE WIRE LINE

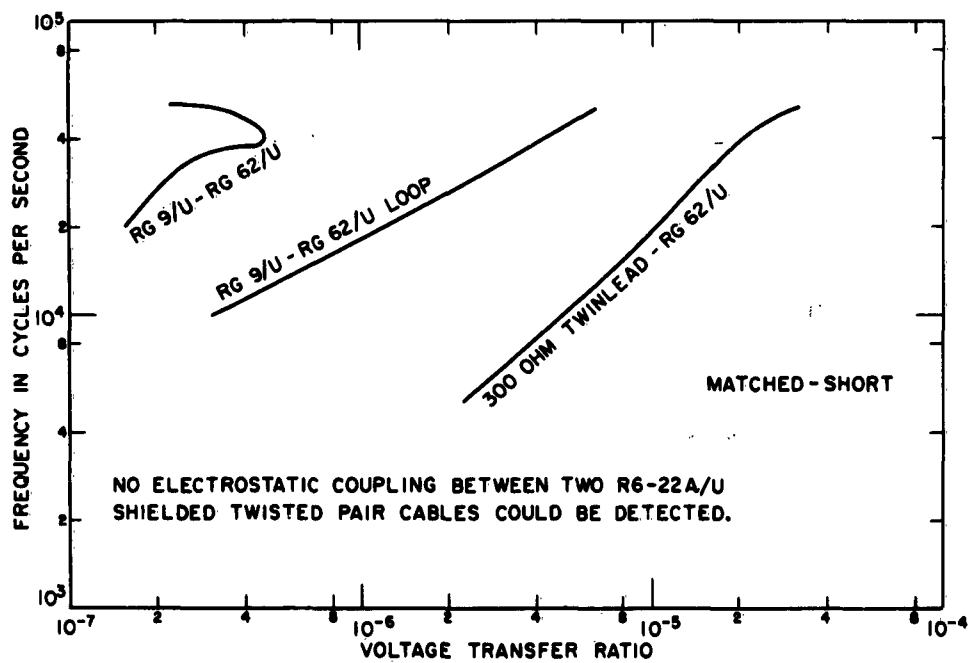


FIGURE 8. ELECTROSTATIC COUPLING

## ACHIEVING ELECTROMAGNETIC COMPATIBILITY BY CONTROL OF THE WIRING INSTALLATION

G. J. King  
AIRCRAFT DIVISION  
Douglas Aircraft Company, Inc.  
Long Beach, California

Abstract - Control of the wire routing and grouping of the many equipments and systems that are installed in modern aircraft is necessary to assure the electromagnetic compatibility of the ultimate system. Controlled classification of the wiring and the bundles reduces the interaction of equipments caused by the inadvertent coupling resulting from random installation. Wire routing control is mandatory to prevent the interaction of individual systems and may also be required with wiring associated with systems that are susceptible to self-interference. The minimum design concept for adequate wiring isolation is defined in this paper. Definitive grounding of systems and the attendant grounding methods, including the bonding of all equipment installations, is a significant part of the overall compatibility of the electrical/electronic environment. Emphasis is directed towards this area.

### I. INTRODUCTION

For many years aircraft have been increasingly burdened with electrical and electronic equipment. These equipments have been evolved from the simple dc systems, of not so many years ago, to the modern integrated complexes operating entirely on an ac power source. As a result, the modern environment is one that is dynamic in nature where the equipments are subjected to an ambient electromagnetic field of complex shape and frequency. It is not strange that some of this ambient energy will appear on the wiring.

Much has been done to reduce interference at the component, equipment and system levels. Little information is available concerning the installation of equipment inter-connecting wiring. Sporadic interest has occurred in wiring compatibility where the various schemes vary from the custom installation (the reference is to "build-it" and "fix-it" methods) to the over-designed brute-force technique. The airframe manufacturer is confronted with the installation problem in which the inter-connecting wire coupling effects upon any of the equipments can only be estimated. Few equipment manufacturers are prepared to indicate the necessary installation precautions required for compatibility. The precautions would include requirements for special wiring (other than single conductor), threshold susceptibility values over a specified frequency range, and the characteristics of the conducted and radiated energy over a broad frequency range. The fact remains that special installation requirements of wiring is necessary because most equipments radiate, and almost all equipments are susceptible somewhere in the electromagnetic spectrum.

The method of wiring control to be described classifies all of the interconnecting wiring in accordance with the energy carried by each wire and the probability of that wire becoming either a "transmitter" or a "receiver." A high degree of compatibility is achieved by physical separation of the categories of bundles and by grouping only the wires of similar characteristics and voltage levels.

For example: a wire carrying 28 volts to a lamp would not be susceptible to a wire carrying 115 volts to a motor. However, if the 28 volt wire is connected to a servo amplifier then a degree of susceptibility might exist. Therefore, the first problem is the inductive susceptibility of a wire. The induced voltage is dependent upon the separation distance of the wires and the coupling area or parallel distance. There are many other factors, but if the spacing between the wire is infinite and the parallel length is zero a coupling problem will not exist.

The other factors are modifiers useful to the design engineer to determine the minimum required separation versus the maximum parallel distance before the threshold susceptibility is exceeded.

The other problem of wire coupling is that experienced from electro-static fields (voltage) usually associated with the radio frequency spectrum. Physical isolation will reduce some of the voltage coupling but not as effectively as for magnetic field coupling. Generally, electrostatic coupling is associated with high impedance circuits. Many low impedance circuits can become carriers of electrostatic energy that is conducted directly to a susceptible circuit. Such circuitry is adversely affected by external coupling. Frequently, the reduction of external coupling does not alleviate the problem. Many of these were found to be caused by coupling between the internal wiring. The usual precautions are employed for electrostatic isolation such as shielded wiring and, equally important, the proper grounding of the shield. The grouping of susceptible wires away from "transmitter" wiring frequently reduces the requirements for shielding.

The wire classification methods, described in this paper, have evolved over a number of years. However, it was only a few years ago that the environment reached the degree of complexity where the extensive use of classified wiring was required.

An analysis was conducted on one model of aircraft to determine what could be done to control the interference caused by the interconnecting wiring. All of the empirical and theoretical data collected over the years was evaluated and a logical model of the proposed method was developed. The aircraft was completely remodeled with the new system. After testing the aircraft, it was found necessary to change one wire from a single braid coaxial to a double braid. Filters that had been installed on the original aircraft to reduce interference were found to be unnecessary after implementation of the classification technique. The aircraft was a complex military type that had a history of multiple interferences. Once the wire classification had been implemented, several of the more vexing problems were revealed as being self-induced.

A second model airplane had a similar history of severe and subtle interferences that were subdued by the usual costly rework and loss of time. The entire system was carefully categorized by detailed evaluation of each equipment. After test, one fix was required - the installation of a diode to quiet down the inductive kick of a relay. The subtle interferences were resolved to be self-induced within specific systems.

The latter aircraft has been in current production for one year without any interference problems. Wire classification will make the product like "peas in a pod" as compared to others without wire classification which may exhibit wide variance of interference from unit to unit.

## II. DESIGN FOR INTERWIRING COMPATIBILITY

Design Concept - The minimum design concept for adequate wiring isolation is based upon classification according to the energy and power that the wire carries. A second consideration is that of the impedance of the wire that may carry spurious energy. This will indicate whether the interference may be induced by either magnetic or electrostatic fields or both. The third consideration is the division according to the susceptibility of a given wire to either inductive or electrostatic coupling. For example: a wire to the input of an amplifier is more susceptible to spurious energy than a wire connected to a motor.

Category I - Power Wiring - Category I is comprised of the following examples:

1. Three Phase distribution wiring (115/200 volts ac)
2. Single phase distribution wiring (115 volts ac)
3. Other wiring carrying 115 volts ac

There are two sources of coupled energy that can cause interference into numerous systems: the magnetic field and the electrostatic field. Of the two, the magnetic field is the most difficult to handle since shielding is ineffective. The practical method for magnetic field isolation is physical separation where the current-carrying wires are isolated from other wiring that is susceptible to magnetic coupling. Power systems are insensitive to coupled magnetic fields from other power lines. Motors, relays, most power transformers, actuators, and other power devices are inherently insensitive to induced voltages, induced phase shift, transients, etc. Therefore, it is possible to group all distribution power lines into one category. Primary, or feeder wiring, is not grouped with distribution wiring to minimize damage in the case of fault currents.

All of the noted wires may be bundled into groups dependent upon the installed wiring configuration.

Category II - Secondary Power - Secondary power wiring is grouped into Category II. Secondary power wiring is generally classed as wiring carrying watts of power at voltages less than 115 volts (ac/dc). Secondary power wiring can be troublesome in restricted areas such as cockpits, radio racks, conduit runs, and other areas requiring dense wiring runs. Since the magnetic field is directly related to the current, and secondary power lines are found in sensitive equipment wire bundles, it has been necessary to create this category. Secondary power lines are usually associated with interior lighting circuits, synchro circuits, small motors, actuator circuits, etc. Therefore, Category II is comprised of the following examples:

1. Low-voltage power circuits
2. Low-voltage lighting circuits
3. Synchro and servo circuits not in Category III
4. Includes wiring from an equipment power supply to other equipments within the same system for dc voltages up to 5000 volts.

Category III - Control Wiring - Reference was made in Category I on the coupling effects of the magnetic and electrostatic fields. In Category III, the wiring is grouped according to the transient fields that exhibit both characteristics. Line

transients occasioned by operating characteristics of the equipment can produce transient magnetic fields associated with a fast rise time of the current. High voltage transients, caused by the familiar "inductive kick-back" can produce broad-band RF voltages. Therefore, Category III is similar to Category II except that it also carries transient energy. Category III is comprised of the following examples:

1. All wiring that involves the operation of relays (solenoid), stepper switches, automatic homing switches, intermittent pulsing energy, etc.
2. Any other wire that can produce pulse energy caused by operating characteristics of the system or equipment such as wiring to flashing incandescent or fluorescent exterior lights.

Note: Category III can be converted to a Category II by reducing or eliminating transient energy. Category III could be eliminated entirely by use of transient suppressors at each relay or inductive device. Other wiring could be placed in Category II by determining the frequency of occurrence of transient energy that could affect other equipment. If the transient does not affect a critical circuit or an equipment listed under safety of flight, then it may be changed to Category II. Eventually, by consideration of these elements in the design stage, the need for this category may not be required.

Category IV - Sensitive Wiring - Sensitive wiring is somewhat of a misnomer since sensitiveness is directly related to susceptibility in this case. There are many wires within a system or complex that would appear under this category. Most of the wiring in this category is susceptible to electrostatic types of energy because of high impedance circuits. Low impedance circuits are susceptible to magnetic fields. However, a low impedance circuit can act as a carrier of electrostatic energy that will conduct spurious energy directly into a sensitive circuit such as a microphone input to an amplifier. Dual protection is usually required for these circuits.

Category IV is comprised of the following examples:

1. All microphone circuits. These invariably require twisted/shielded leads to reduce coupled magnetic fields and prevent the conduction of electrostatic RF fields.
2. All audio output and video output circuits.
3. All sensitivity control circuits and volume/gain controls.
4. All cathode and grid circuits.
5. Signal wiring requiring a "shield out" shield.
6. All metering and bridge input circuits.
7. All circuits associated with signal inputs to a computer.
8. All signal circuits associated with a demodulator.

A high percentage of the above wires are required by the designer to be shielded. To avoid ground circuit problems it is necessary to emphasize that all shielded wire shall be insulated with an external non-conductive jacket.

Category V - Susceptible Wiring - Experience has shown that certain wiring is extremely susceptible to most all levels of electrical energy. Such wiring shall be routed free of all other wiring and must not be grouped into a bundle unless associated



with a single system. Antenna cables may be grouped provided that the shielding integrity of the entire system is good. High power antenna cables and pulse cables shall be run separately.

Category V is comprised of the following examples:

1. All radio antenna coaxial cables.
2. All wiring to electro-explosive devices.
3. Fire Warning shielded wires.
4. Fuel Quantity coaxial cables.
5. Liquid Oxygen indicator coaxial cables.
6. Other wiring pertaining to safety of flight items such as anti-skid systems, spoiler actuator circuits, etc.

Category VI - System Wiring - Category VI is a compromise designed for convenience of installation. To minimize extensive separation of system wiring bundles and to reduce the resulting wiring complexity, certain system bundles may contain wiring that otherwise would appear in Categories II, III, and IV. The category does not contain wiring that is classed as Category I or V. System groups may be installed only after careful analysis has indicated that the system is free of self-induced interference. An example would be the Automatic Flight Control System (AFCS) that is inherently susceptible. The AFCS usually has many interconnecting wires between multiple black boxes grouped in close proximity. These runs, and the long runs from the immediate area to the control center, are classed as Category VI. There may be more than one system within the complex that has been classified as a Category VI. It is suggested that each system bundle be identified and routed separately. It is not recommended that bundles of Category VI be grouped together.

Design Limits for Separation - Minimum coupling between wires of the various categories can only be controlled by specifying the minimum distances to be maintained throughout the cable run. Table I gives the minimum design data for physical isolation. Modifications to the rather rigid requirements are described in subsequent paragraphs. It must be emphasized that the design parameters noted in (Table I) are to be used as the minimum, and that the compromises suggested be used only where necessary. Compromises are the responsibility of the Electromagnetic Compatibility engineer and are useful only when the threshold susceptibility of a given wire is known.

Classifying the categories as "transmitters" and "receivers" will help in understanding why the groups are spaced and will assist in the selection of compromises where required. It will be noticed that Categories I, II, and III may be classed as transmitters and that Categories IV, and V as good broadband receivers. Category VI is in the position of proving that it will not interfere with itself since it contains potential transmitters and receivers. Another way of classification is to consider that Categories I and II carry relatively intense magnetic fields, Category III carries magnetic fields of similar intensity and transient RF fields of relatively high energy with a broadband distribution. Categories IV and V are then susceptible to these fields. The third consideration is that the groups carry similar types of energy: Category I, power line voltages (115/200 volts ac); Categories II and III carry low voltage power (28 volts ac-dc), and Categories IV and V carry signal voltages and frequencies. The method of classifying is based upon the minimum voltage gradients between wires within any given category.

Installation Consideration-The possibility of maintaining the minimum separation distance for all categories throughout the aircraft is remote. Structural areas and design prohibit such luxuries. Requirements for the three common areas of minimum isolation are noted in the following:

Lightening Holes-Wire bundles shall maintain the minimum spacing until they immediately enter the lightening hole and shall break away at the first opportunity. Lightening hole parallel runs are added to compute the overall parallel run. Normally, there is no restriction on the category of bundles. It is preferred, however, to route Categories IV, V, and VI through adjacent holes wherever possible. The category to be routed through adjacent holes depends upon the physical size of the bundle, see Figure 1.

Common Plugs-Common equipment plugs and bulkhead plugs are treated the same as for lightening holes. Common plug wiring should break into categories as soon as possible, see Figures 2 and 3.

Conduit-Grouping of bundles in conduit will be similar to the grouping used for marriage clamping. Non-metallic conduit is preferred. Metallic conduit may be used to increase the isolation when conduits are closely nested and to take advantage of the shielding effects. Aluminum conduit should be used for electrostatic shielding and special purpose steels for magnetic "shielding." Unrestricted use of metallic conduit should be discouraged since the reflected inner fields could increase coupling between wires within the conduit, see Figure 4.

Compromises-Practical considerations for the installation of bundles require some modification of the basic rules. It must be emphasized that modification of the basic rules must be held to an absolute minimum. There will be areas where the minimum spacing of the bundles cannot always be maintained. Other areas may require that the wires originating at an equipment plug must be bundled together for a specified distance. The installation designer must control the wiring to ensure that the compromised areas do not result in an unbalance towards the interference end of the scales. What is lost on one end of the scales must be regained on the other.

Category VI-Category VI is a compromise as noted under the categories.

Marriage Clamping-The minimum design spacing may be relaxed in close areas such as cockpits, control centers, and other dense areas. This is based upon achieving separation in the rest of the aircraft that results in coupling far below threshold sensitivity. The following categories may be marriage clamped:

Category

1. II with III
2. IV with V
3. VI with either II, III or IV

It is recommended that Category I not be marriage clamped with any other category or group. Maximum distance should be maintained between Category I and Categories IV and V.

Special Wiring-Special wiring includes all types of wiring configurations other than the single-conductor-insulated wire. Special wires are always used for the control of interference and, in the wire categorization plan, they are used for isola-

tion purposes where the minimum physical isolation distances must be reduced for practical reasons. Therefore, the special wiring would replace the single conductor wire under certain installation conditions.

There are two types of special wire: twisted wires (two or more) and shielded conductors (one or more). Twisted wires are used for control of radiated or induced magnetic fields, and the shielded wire is used for the containment or exclusion of electrostatic fields. Combinations of both are used where the circuitry may be susceptible to magnetic and electrostatic fields. Configurations recommended for use include the following: twisted pairs, shielded twisted pairs, shielded single conductor, and the various configurations of coaxial cable.

Special wiring is used only when and where necessary if not called out in the system design. Use of special wiring is an admission that the system is susceptible or radiates over some specified portion of the electromagnetic spectrum (just like a gasket is an admission that a perfect mechanical joint cannot be obtained). Requirements for extensive use of special wiring may be reduced by considering the environmental effects preliminary to the design of the electrical/electronics portion of the system. Wire categorization does not require, per se, additional requirements for the use of special wire. The necessity for the use of special wire can be reduced in many cases. Unrestricted use of shielded wire can produce more problems than it cures, and the unrestricted use of twisted wiring is frowned upon because of the increased cross sectional area. Special wiring installed for the prevention of coupling can be eliminated for the most part. Under the categorization rules, special wiring is used only in areas where the design separation distances cannot be achieved.

Special Wiring and Pigtails - Electronic and electrical equipment racks are frequently so highly congested that wire separation to the design limits is an impossibility. The problem can be resolved by considering all of the wires emanating from a single equipment plug as a pigtail to where the wires can break out into categories at a distribution center or a terminal board. Pigtail length can vary from two to ten feet. Lengths in excess of ten feet should be considered for classification into categories. Since space isolation is not possible in a pigtail, the only recourse is to specify the use of special wiring, refer to Figure 5. Power wiring should be twisted with the ground return for wires grouped under Categories I and II. Single conductor signal wiring should be shielded (Categories IV and V). Two conductor signal wirings (Categories IV and V), such as microphone circuits, should be twisted and shielded. Category II, other than power wiring, and Category III do not require special wiring. In general, the requirement for special wiring to achieve isolation in a pigtail grouping does not exist after the wiring has entered the proper categories. Figure 6 is a description of an equipment rack utilizing pigtails from the equipment plugs to the terminal junction and then to the categorized ship's wiring.

In referring to Figure 5, it will be noticed that the categorized wiring has been labeled in a definite order. When using parallel runs (where all of the categories are in the same plane) it is desirable to locate the bundles for minimum coupling. The suggested order would be: 1, 2, 3, 6, 4, and 5 where Category I is always the farthest distance from any terminal board wiring and/or Categories IV and V.

Ground Wires - Ground wires shall always take the category of the mating "hot" wire. Twisting of pairs of wires always refers to the hot wire and the (ground) return. Twisted pairs of wires may be used on circuits of either transmission (Categories

I, II, and III) or circuits of reception (Categories IV and V). The former reduces the magnetic field coincident with current flow and the latter inhibits induced magnetic fields. Twisted wires may also be used to reduce the loop aperture where a tight twist results in minimum loop area.

Ground Studs-All ground studs will take on the category of the attaching wire. This immediately states that only one category can be connected to a given ground stud.

### III. INSTALLATION CONTROL

Engineering Control-Engineering control of the wiring installation is a corollary to the wire classification plan. Previously, engineering furnished the wiring schematics and pertinent data. Actual installation of the aircraft wiring was accomplished without specific engineering requirements for a specific installation design. Wiring installations were then frequently modified by the electromagnetic compatibility group to reduce interwiring interference. If the wiring installations could not be modified for diverse reasons, efforts for interference reduction were then directed at the affected equipment. Occasionally, this resulted in equipment redesign to operate satisfactorily in an interference environment. More often, external filters were required. The desired engineering control is accomplished by carefully designing the installation on the development aircraft in accordance with the data contained in this paper. From this effort, engineering control of the actual wire runs and locations is established. Engineering documents define the classification of each bundle where each wire in the bundle is identified. Application of the engineering control made it mandatory that subsequent aircraft would be wired identical to the development aircraft.

### IV. CONCLUSIONS

Application of a classification plan to all of the wiring in the aircraft will result in a considerable reduction of system interferences caused by inadvertent wire coupling. Many of the knotty problems associated with the equipment or auxiliary hardware can then be defined as having been caused by wire coupling. The reverse may also be true. Interferences, mistakenly laid to wire coupling, may be resolved as system deficiencies. Wire classification is a distinct aid in the solution and tracking down of many electromagnetic compatibility problems. The classification plan does not conflict with circuit or interconnecting wiring design. It is merely a specific installation procedure. The preparation of drawings that apply a part number to the wiring are not affected by the classification requirements. Removals or additions of equipment to an existing aircraft present no major problems. Economically, the costs of engineering design are more than offset because of the minimum rework for a given production design. Rework of the final installation design for two military types of aircraft has been negligible. Wire classification eliminates the wide variance in compatibility found on aircraft that contain a random wiring installation.

### ACKNOWLEDGMENT

The material presented herein is based upon work conducted by the Aircraft Division of Douglas in the performance of contracts for the Bureau of Naval Weapons.

**TABLE I. MINIMUM SEPARATION DISTANCES (INCHES) BETWEEN CATEGORIES**

CATEGORY	DESCRIPTION	SEPARATION (INCHES)
I	PRIMARY FEEDERS	12
	DISTRIBUTION WIRING	6
II	SECONDARY POWER	3
III	CONTROL WIRING	3
IV	SENSITIVE WIRING	3
V	SUSCEPTIBLE WIRING	3
VI	SYSTEM WIRING	3 (INCLUDING OTHER VI's)

**FIGURE 1. EXAMPLE OF CATEGORIZED WIRES GROUPED AT A COMMON PLUG**

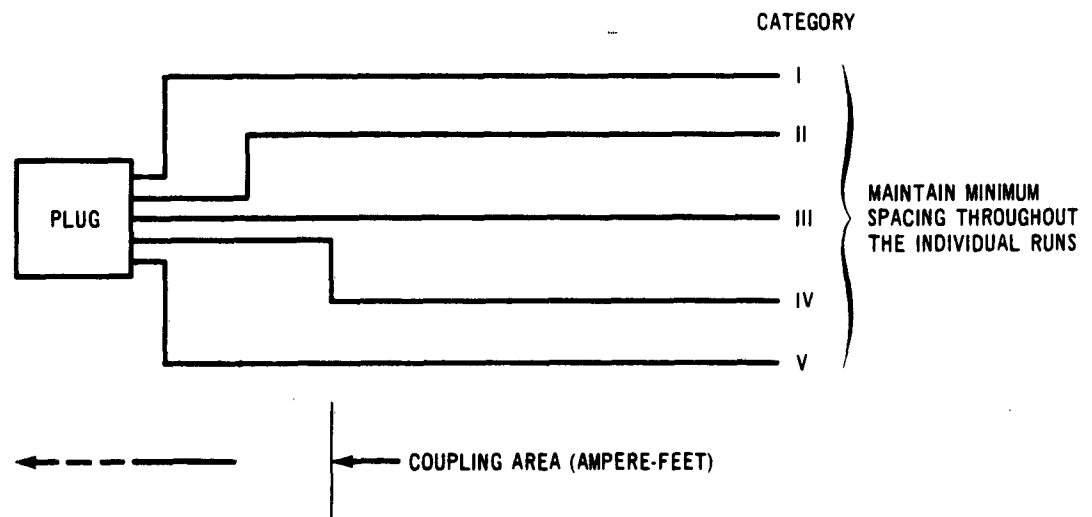


FIGURE 2. EXAMPLE OF CATEGORY VI WIRES GROUPED AT A COMMON PLUG

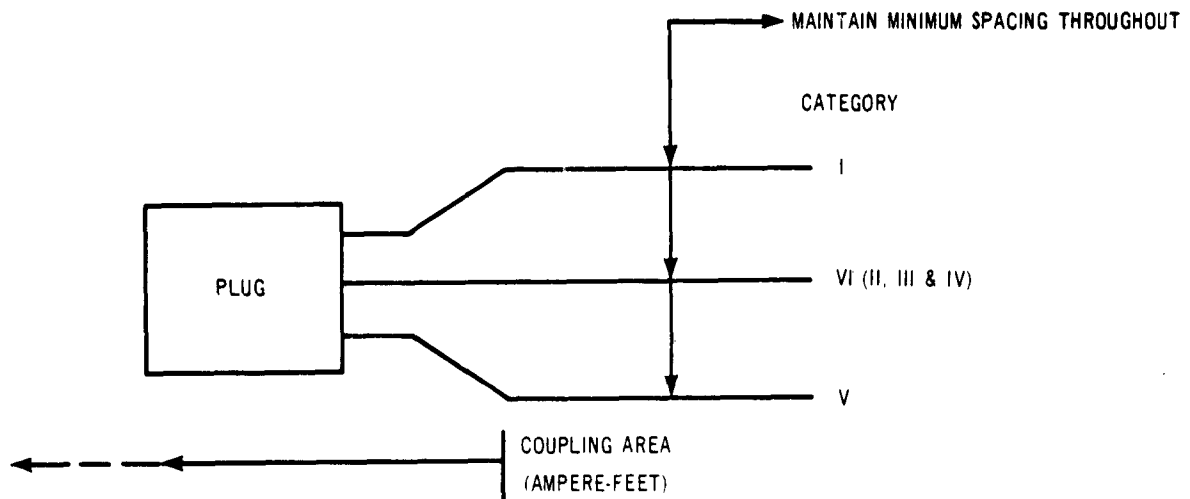
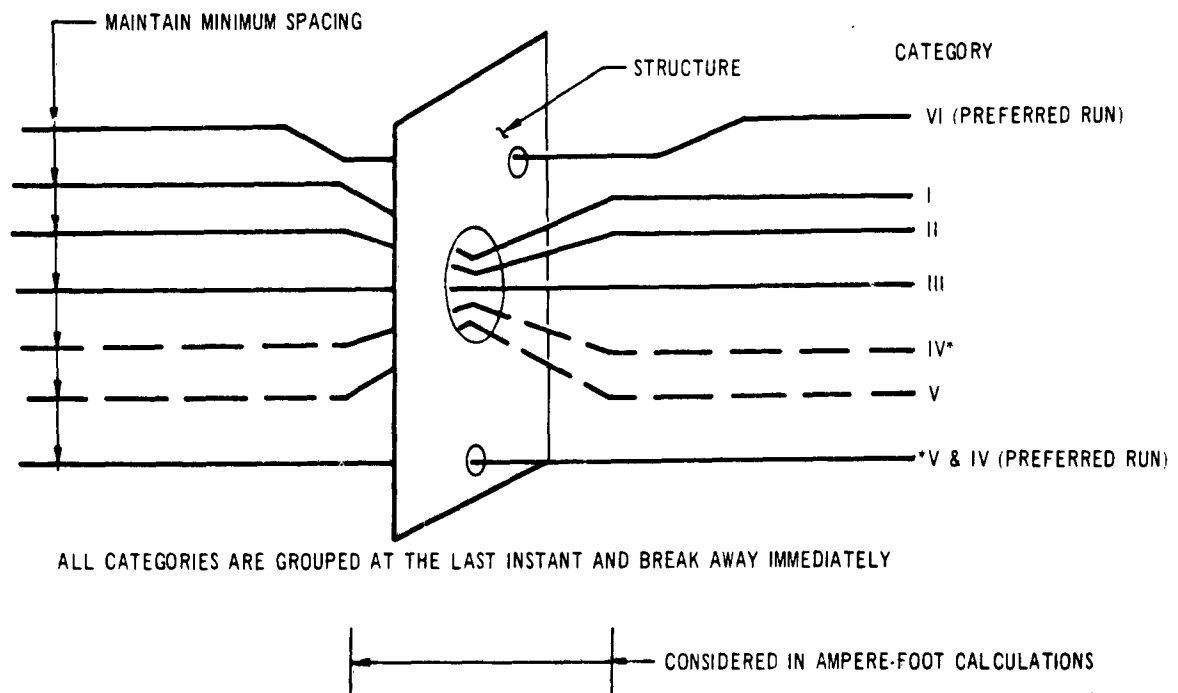
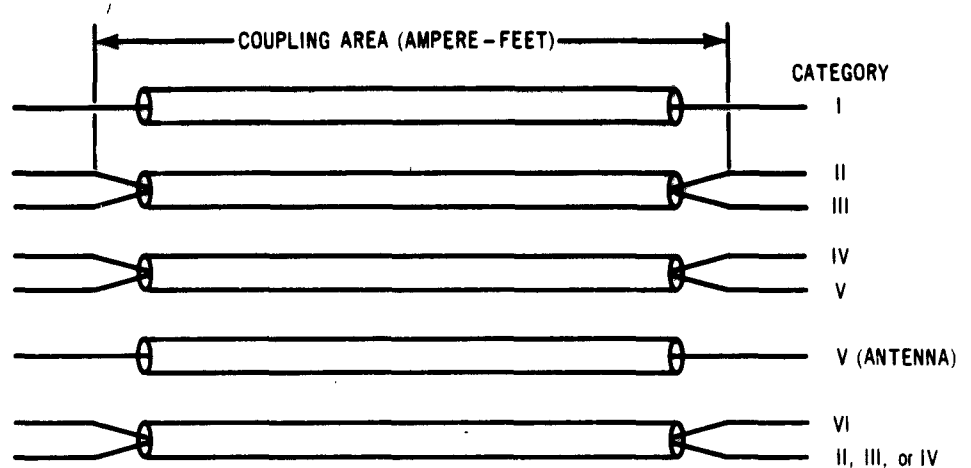


FIGURE 3. EXAMPLE OF CATEGORIZED WIRES GROUPED AT A LIGHTENING HOLE



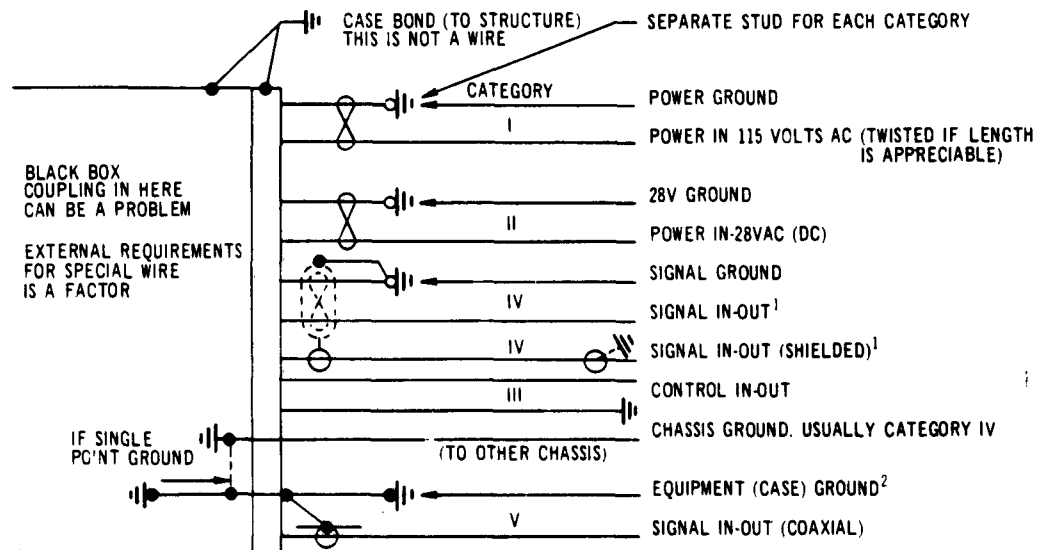
**FIGURE 4. GROUPING OF CATEGORIES THROUGH CONDUIT**



**NOTES:**

1. Metallic conduit may be used to achieve isolation effects when minimum spacing cannot be obtained.
2. Do not use long runs of metallic conduit for Categories IV, V, and VI. (This would cause closer coupling of the enclosed wires because of reflection effects.)
3. Steel (high  $\mu$ ) conduit may be used for increased isolation for Categories I, II, and III.

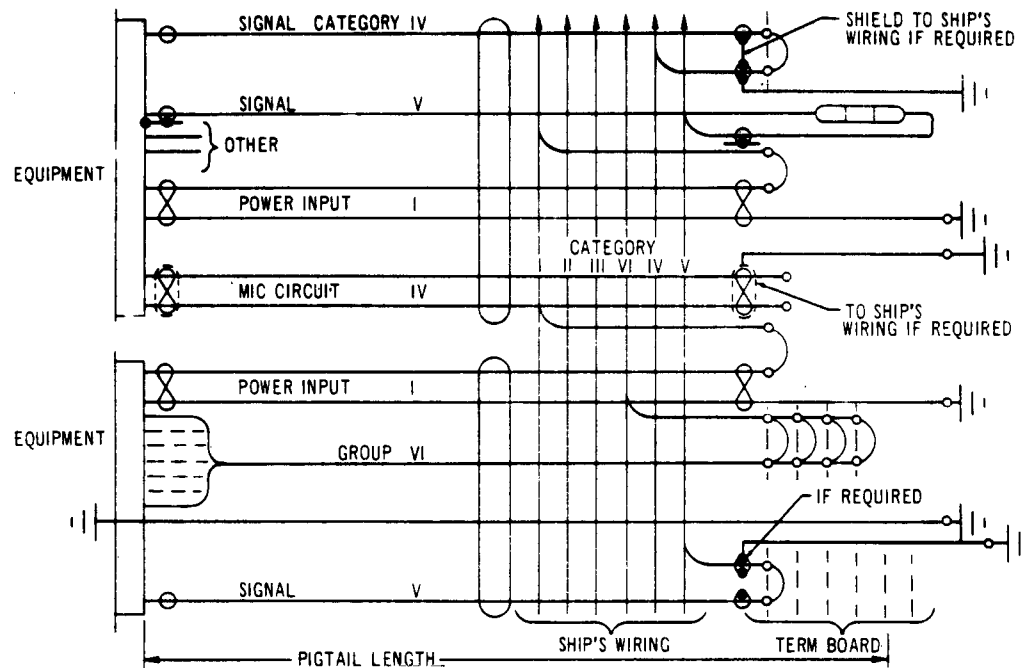
**FIGURE 5. GROUNDING TECHNIQUES FOR SPECIAL WIRE**



**NOTES:**

1. Shield ground point depends upon location of mating ground and whether SHIELD-IN or SHIELD-OUT techniques are being used.
2. Usually will take Category I designation.

FIGURE 8. SPECIAL WIRING REQUIREMENTS FOR EQUIPMENT PIGTAILS





## COMPATIBILITY ANALYSIS SENSITIVITY

H. M. Sachs and T. N. Truske  
IIT Research Institute  
Electromagnetic Compatibility Analysis Center  
Annapolis, Maryland

Abstract - The major requirements associated with an overall interference prediction analysis include (a) data, either measured or synthesized, describing the pertinent emission and susceptibility characteristics of those equipments involved in a problem, and the environmental and operational constraints (locations, frequencies, duty cycles, etc.) associated with the systems under consideration; (b) basic mathematical models, capable of processing signals through the receivers to be analyzed; and (c) supplementary models, capable of representing or describing overall system degradation due to such signals. These separate areas have been and are being investigated in considerable detail, but relatively minor effort has been expended to integrate the input data and prediction models so that the data requirements will be compatible with the modelling techniques and evaluation criteria employed.

This paper represents an initial step to close this gap. It will discuss the relationships between system performance parameters, the process of predicting performance, and the model input requirements to accomplish such predictions; and will, in particular, lay the groundwork for answering the question, "What changes in the spectrum signature requirements for interference predictions should be made?"

The paper will deal primarily with signal emission characteristics, and their relation to the requirements of search and tracking radar interference prediction models. Several prediction output criteria will be considered, with emphasis on (a) mean probability of pulse detection, or false alarm rate, (b) ppi scope degradation, and (c) increase in target acquisition time. The sensitivity of the prediction of these criteria to certain of the model input parameters will be analyzed, and evaluation will be made of input data requirements in terms of dynamic range of data, amplitude accuracy, frequency accuracy, etc.

### I. INTRODUCTION

This paper will discuss some of the factors of significance in defining basic modelling capabilities and needs for electromagnetic interference prediction, and in ultimately establishing the data base requirements for interference analysis.

The ensuing discussion will deal primarily with radar emission characteristics, and their relation to the requirements of interference prediction models. Basic prediction output capabilities will be considered, without detailed regard to the techniques employed in providing model input data. After a review of representative model outputs and the significance of emission parameters (and to a lesser degree receiver and antenna parameters)

on these outputs, the model emission characteristics requirements will be enumerated. Such requirements become the criteria for input data parameter specification, whether the parameters are defined by direct measurements, or by empirical or analytic rules.

## II. INTERFERENCE PREDICTION OUTPUTS

Several radar model output representations have been considered by ECAC, each based on a particular evaluation objective. Some of these are currently available by way of computer processing; others must be computed manually at this time. In either case, such outputs provide a framework for initial establishment of model data input needs.

For search or tracking type radars, the following principal output predictions apply:

- a. False alarm
- b. Plan-Position-Indicator (ppi) scope degradation
- c. Increase in target acquisition time
- d. Probability of target acquisition
- e. Range tracking accuracy
- f. Angle tracking accuracy

Items (a), (b) and (c) above relate to search systems, while items (a), (c), (d), (e) and (f) relate to tracking systems. The primary output from which the above outputs are generated is the mean probability of pulse detection, which is equivalent to the false alarm rate output listed above. For the purposes of this report, only items (a), (b) and (c) have been investigated.

## III. MEAN PROBABILITY OF PULSE DETECTION

Representative predictions were made in accordance with the processing rules of the Center's Search Radar Prediction Model. With respect to the model requirements analysis, the following relationship was employed:

$$M = K \int P_d P_o d(S_L)$$

M = mean probability of pulse detection

$P_d$  = probability of pulse detection<sup>1</sup>

$P_o$  = probability of pulse occurrence, based on long-time transmitter and receiver antenna gain distributions, and absolute power levels at the receiver input terminals

K = normalizing factor, such that the most likely value of antenna gain coincides with 50% probability of pulse detection

$S_L$  = parameter of integration = relative interference signal level

A typical probability of detection curve was used. This curve is shown in Figure 1.

Three classes of antenna coupling conditions were considered. One involved fixed orientation source and victim antennas. The second case involved one system antenna (source or victim) scanning in azimuth and the other system antenna fixed, such that the probability of occurrence was described by the statistical distribution of scanning antenna gain times the gain of the fixed antenna along the path joining the source and victim. The third case involved both the source and victim antennas scanning in azimuth, such that the probability of occurrence was described by the statistical distribution of the antenna gain product.

Figure 2a shows the gain statistics of a typical radar antenna used for this analysis, while Figure 2b illustrates the gain-product statistics curve employed.

The three curves of Figure 3, generated from the antenna relationships described above, give an indication of the mean pulse detection behavior to those parameters affecting interference signal level. Such parameters might include transmitter fundamental, harmonic, or spurious output levels; absolute antenna gains; propagation loss; receiver sensitivity, selectivity, or spurious response levels; detection function curve shape, and others.

Table I summarizes the graph in terms of the influence of such power level uncertainties on the prediction of mean probability of pulsed interference using the curves of Figure 3. For example, for the case of two non-scanning radars, a situation can exist where an uncertainty of 0.8 db in power at the receiver input terminals can result in a 0.2 change in mean probability of pulse detection. For this same case, a 4.4 db change in level could cause a 0.8 change in M. Similar data involving antenna scanning conditions are provided.

It should be noted that these values of change in M are based upon power changes about the curve 50% point. Figures 4 and 5\* describe the error in mean pulse detection (change in M) for various confidence levels and values of uniformly distributed input data errors.

It is worthwhile to compare the numbers in Table I and the data of Figures 4 and 5 with typical accuracies of some of the parameters that influence the relative signal level. Such accuracies are listed in Table II. It is recognized that an interference prediction process involves the acceptance of a number of such uncertainties; therefore, the prediction of mean probability of pulse detection in many cases can only be described statistically.

---

\*

The generation of these curves is described in Appendix I.

By referring to the curves of Figures 4 and 5, it can be seen that a 5 db error could result in a change of M ( $\Delta M$ ) no greater than .25 60% of the time or .60 90% of the time. The 5 db error could represent the cumulative error due to signal amplitude, antenna gain, and propagation path loss deviations.

#### IV. PPI SCOPE DEGRADATION

Predictions of ppi scope degradation are based upon rules established to classify interference on ppi displays in accordance with AFM 100-24, ADC Supplement No. 2<sup>2</sup>. The basis for such predictions is the receiver interference pulse output statistics, processed using the following relationship:

$$N = 10^{-4} \sum_{p_n = -S_r}^{p_n = 20 + S_r} n \frac{p_n}{S_r} + 20 N_{20}$$

where

N is related to scope interference class

n = number of interfering pulses whose amplitudes range from

$$\frac{p_k + p_{k-1}}{2} \text{ to } \frac{p_{k+1} + p_k}{2}$$

$\frac{p_n}{S_r}$  = power level of interfering pulses with respect to receiver threshold sensitivity, expressed in db.

$N_{20}$  = number of interfering pulses whose amplitudes exceed the receiver threshold sensitivity by 20 db.

The factor N represents false alarm count weighted by the power level of such pulses up to the level of receiver saturation. This number correlates with class of ppi scope degradation as follows:

Class 1	$N \leq 3.7$
Class 2	$3.7 < N \leq 8.6$
Class 3	$8.6 < N \leq 12.7$
Class 4	$12.7 < N \leq 22$
Class 5	$22 < N$

These ranges of N have resulted in approximately 55% confidence in correct ppi scope classification, and approximately 90% confidence that classification will be in error by no more than one scope class.

Figure 6 illustrates the sensitivity of the value N, and the ppi classification in terms of parameter uncertainty of the type described previously. This analysis was conducted using the antenna gain product distribution of Figure 2b, plus the inclusion of terrain-reflection effects as synthesized by ECAC's MSS-1 prediction model. Only a single interfering source was considered.

It can be concluded from Figure 6 that the prediction of ppi display interference class is significantly less sensitive to those parameters that establish the abscissa of this curve than the prediction of mean probability of interference. For example, the range of assignment of interference as Class 2 is 15 db for the situation considered, the Class 3 range is 18 db, and the Class 4 range is 10 db.

#### V. INCREASE IN TARGET ACQUISITION TIME

An analysis of the effect of interference on increased target acquisition time for tracking systems during automatic range lock-up was performed. The relationship used for this analysis (assuming a single interfering radar) was

$$t = t_0 (1 + MT\alpha)$$

where

$t$  = total range gate scan time

$t_0$  = time for one complete range search under "no-interference" conditions

$M$  = average number of detected interference pulses per second =  $(\text{prf}) p_{dm}$

$T$  = dwell time

$\alpha$  = ratio of range gate width to  $1/\text{prf}$

If  $t = nt_0$ , then

$$p_{dm} = \frac{n-1}{(\text{prf}) \alpha T}$$

By specifying the antenna scanning relationships to be considered during the target acquisition phase (whether or not the interference source can be considered scanning), use can be made of Figure 3 in converting the calculated values of  $p_{dm}$  to relative signal levels. The resultant plot of increase in acquisition time versus relative signal level (Figure 7) provides an indication of the sensitivity of the prediction process to these levels.

Figure 7 illustrates three examples of increase in acquisition time sensitivity. Two cases assume non-scanning antenna coupling effects, while one case considers the interference source antenna scanning. It can be seen that the non-scanning systems acquisition time is very sensitive to input signal level. Acquisition time increase for the one system scanning case shows a lesser increase rate, compared with the curves for non-scanning systems. For the curve shown, the function sensitivity to power errors increases with increasing relative signal strength.

#### VI. INTERPRETATION OF ANALYSIS

The previous partial analysis of ECAC model sensitivities enables certain basic conclusions to be drawn. They include the following:

Model sensitivity to relative signal level is variable, dependent not only on those factors that affect the signal level relationship, but on the criteria employed for system evaluation, and the model processing techniques.

In terms of mean probability of pulse detection, the sensitivity of the model is such that the parameter range to go from low to high values of that variable in many cases is exceeded by measurement uncertainties. The prediction sensitivity decreases when scanning antenna systems are considered.

The signal level variations which will give a specified ppi scope interference class with a confidence of approximately 55% range from 10 to 18 db for the example analyzed.

Increase in target acquisition time curves for non-scanning systems changes rapidly with a small (3 db) change in relative signal strength. The curve for one system scanning exhibits less sensitivity.

The qualitative implication of these analyses is that some sacrifice in input data amplitude accuracy can be accepted without a significant increase in uncertainty in prediction accuracy beyond that uncertainty which would exist based on "state of art" definitions of input parameters.

## VII. MODEL INPUT SPECIFICATIONS

With the above conclusions in mind, model input accuracies relative to transmitter emissions will be considered in terms of data dynamic range and amplitude and frequency accuracies. These and other data terms are defined on Figure 8.

Dynamic Range - In order to stipulate minimum required emitter emission levels of interest, consider a typical example. Assume a 400 mc receiver with a -120 dbm sensitivity and at a distance of one mile from the emitter. The frequency of this receiver was chosen to minimize the propagation loss, while the sensitivity and separation figures were selected as limiting values bracketing the majority of problems the Center would be called upon to analyze. Then,

$$P_t = S_r - G_t - G_r - L$$

where

$P_t$  = transmitter power output

$S_r$  = receiver sensitivity = -120 dbm

$G_t$  = mean transmitter antenna gain = -10 db

$G_r$  = mean receiver antenna gain = -10 db

$L$  = free space propagation loss = 90 db

$$P_t = -120 + 10 + 10 + 0 = -10 \text{ dbm}$$

To consider all interference cases of significance, a value of 0.1 mean probability of pulse detection was selected. Interference above this level would be considered by the model if approximately -15 db were added to

$P_t$  (see Figure 3, two scanning antennas case). Thus, the significant emission lower limit for the example selected is -25 dbm.

For this frequency range, wideband instrumentation sensitivity specified in MIL-STD-449A (paragraph 5.2.3.5.2) is -80 dbm/m<sup>2</sup>. The power level threshold capability of the standard corresponds to

$$P_t = P_d - G_M + 10 \log (4 \pi r^2)$$

where

$P_d$  = power density threshold = -80 dbm/m<sup>2</sup>

$G_M$  = transmitter antenna gain = 27 db

$r$  = measurement distance = 1600 meters (1 mile)

$$P_t = -80 - 27 + 10 \log (32 \times 10^6) = -32 \text{ dbm}$$

On the basis of this simple example, it can be seen that the amplitude threshold requirement of the model coincides closely with that corresponding to the capability currently stipulated in MIL-STD-449A.

Amplitude Accuracy - An implied result of the model output analysis previously discussed is that accuracy of the power level parameter is not severe, taking into account basic measurement uncertainties. Another example may also show this, as well as give an indication of the degree of acceptable uncertainty in this parameter.

Assume the basic model inputs have the following standard deviations relative to an assumed normal distribution of input data:

Transmitter Antenna Gain	2 db
Receiver Antenna Gain	2 db
Propagation Path Loss	3 db
Frequency Accuracy Effects on Amplitudes	2 db

and model processing techniques have the following standard deviations, again assuming normal distribution of the variable:

Integration Routine	2 db
Pulse Distortion Routine	1 db
Detection Function	2 db
Other Effects	1 db

The total standard deviation of the prediction can be determined based on the values given above and using assumed values for the input signal deviations. These overall deviations are tabulated below:

Standard Deviation of Input Signal	Standard Deviation of Prediction	Increase in Standard Deviation of Prediction
0 db	5.6 db	-
2 db	5.9 db	0.3 db
4 db	6.9 db	1.3 db
6 db	8.2 db	2.6 db

On the basis of the assumptions made, a 2 db standard deviation in the emission power or power density level would be reflected as an increase of only 0.3 db or about 5% in the standard deviation of the model prediction. It seems practical to accept input data uncertainty of this magnitude under circumstances which present difficulty in providing finer data. Therefore, a reasonable amplitude accuracy requirement at this time might be considered as  $\pm 6$  db (corresponding to the value of 2 db standard deviation) with somewhat better accuracy (perhaps  $\pm 3$  db) in the region around the emitter fundamental frequency.

Figures 9a and 9b show some of the data used to specify integration and data representation error. The data were obtained using one of the ECAC prediction models and random balance testing techniques<sup>3</sup> which considered the combined effects of antenna, transmitter, receiver and frequency separation data variations. The data again show that the number of points used to represent the emission spectrum or the number of spurious receiver responses does not critically affect model power output if other parameter data variations are also present.

An additional factor effecting the data accuracy requirements concerns the sensitivity of prediction model computed average power to variation in the emission spectrum input data. Frequently the bandwidth of a typical victim radar equipment is sufficiently wide so that a number of emission spectrum data points are contained in the main response region of the receiver. This condition reduces the effects of emission input data errors since the individual, random variations in the input data due to spectrum measurement or representation errors tend to average out. To show the significance of this effect, idealized emission spectrum data were degraded by introducing data point errors which were normally distributed with standard deviations of 5, 10 and 15 db (mean error of zero). The errors in integrated receiver power output for a receiver whose bandwidth is five times the data point frequency separation are shown in Table III.

The bandwidth averaging in the case treated reduces the magnitude of input data errors by about 40%. The example indicates that a larger tolerance on amplitude errors in emission data gathered for use in predicting the average power out of wideband receivers may be acceptable.

Frequency Accuracy - An indication of frequency accuracy can be obtained by observation of the prediction model output in performing the integration of the interfering transmitter spectrum times the receiver response, or

$$\overline{INR} = k \int p_t(f) \frac{|H(f)|^2}{N} df$$

where

$\overline{INR}$  = average output interference to noise ratio

$p_t(f)$  = transmitter power density spectrum

$|H(f)|^2$  = receiver power-gain response

$N$  = average output noise power

$k$  = normalizing factor



As  $\Delta f$ , the difference between the transmitter tuned frequency and receiver tuned frequency is varied, the above integrations will essentially describe the receiver pulse selectivity characteristic. The frequency accuracy of input data is dictated by the maximum slope of this characteristic.

An inspection of representative L-band computer-generated receiver pulse selectivity curves (see Figures 10 to 12) indicated at least one data-set which had a maximum skirt falloff of 14 db for a value of  $\Delta f$  of 1.0 mc. Assuming a linear-in-db relationship, a 2 db amplitude accuracy would require a frequency accuracy of 140 kc, or 1.5 parts in  $10^4$ .

This degree of accuracy, from a measurement standpoint, precludes the use of a wavemeter, but is well within the capabilities of other frequency-measuring techniques.

#### VIII. CONCLUSIONS

Table IV summarizes the prediction model requirements generated thus far, these requirements applying to emitter power and power density inputs. They have been developed on the basis of limited model analysis, and have not been related to the wide variety and quantity of problems to be processed at ECAC. Nevertheless, it is believed they provide a reasonable insight into the input needs for attacking radar compatibility analyses.

#### IX. ACKNOWLEDGEMENT

The work described above is sponsored by the three Military Departments and is being conducted under Contract No. AF 19 (604)/8440, with the Electronic Systems Division, Air Force Systems Command.

#### REFERENCES

1. Marcum and Swerling, Studies of Target Detection by Pulsed Radar, IRE Transactions, PGIT, Vol. IT-6, April 1960, No. 2.
2. L. Katz, The San Diego Problem, Summary of Phase II Operations, ECAC-TDR-63-4, August 1963.
3. F. J. Anscombe, Quick Analysis Methods for Random Balance Screening Experiments, Technometrics, Vol. 1, No. 2, p 195, May 1959.

#### APPENDIX I

##### MODEL ERROR ACCURACY RELATIONS

To describe the parameter sensitivity of any model, it is necessary to specify measures determining appropriate model accuracy error relationships. One such measure is shown in Figure I-1. Thus, for a given model, a given error,  $e_1$ , would induce an error effect,  $ee_1$ , which would not be exceeded with confidence,  $c_2$ , or some corresponding error effect,  $ee_1$ , will not be exceeded with confidence,  $c_3$ . The ECAC SR prediction model being used for current parameter sensitivity analyses suggests certain error and error effects measures which are most appropriate to describe parameter sensitivity error effects relationship. For example, in Figure I-2, data outputs from the model have been plotted to yield a curve of total pulses received over one scan time of a victim radar,  $N$ , as a function of victim interference or range separation,  $R$ . The curve labeled  $\epsilon = 0$  represents that obtained if no errors in the input data or

model representation of the SR were present. The curve labeled  $\epsilon = +\epsilon'$  is that obtained if a positive constant error equal to  $\epsilon'$  were present in the model, either due to inaccuracies in data input or data representation. The curve labeled  $\epsilon = -\epsilon'$  represents that obtained if a constant negative error were present in the model input data or data representation. The curves defined by  $\epsilon = \pm \epsilon'$  define a region containing all possible values of  $N$  as a function of  $R$  which might be obtained for errors ranging between  $\pm \epsilon'$ . As shown on Figure I-2 at a given range,  $R_1$ , values of  $N$  might be obtained ranging from  $N^-$  to  $N^+$  due to the input errors of  $\pm \epsilon'$ . The range of error in  $N$  at various equipment range separations as a function of  $\epsilon$  is the item of interest here.

To represent the information in Figure I-2 more generally, certain data on the curve are modified as shown on Figure I-3. On Figure I-3, an average per scan pulse detectability factor is defined where this factor,  $M$ , is equal to the number of pulses detected,  $N$ , divided by the total number of pulses possible in a given interference situation,  $N_c$ . The total number of pulses,  $N_c$ , is defined as the pulse repetition frequency of the interference radar times the scan time of the victim radar times the ratio of the victim radar displayed range to its maximum interpulse range. Defined in this way, the curve ordinate can be used to develop a more general error effects measure,  $\Delta M$ . At a given range,  $R_1$ , and for some specified range of error values,  $\Delta \epsilon'$ , the maximum range of the average detectability factor,  $\Delta M$ , can be determined.

In Figure I-4 a curve of  $\Delta M$  as a function of range and  $\Delta \epsilon'$  is shown. Similar curves could be constructed for other values of  $\Delta \epsilon$  ( $\Delta \epsilon''$ ,  $\Delta \epsilon'''$ , etc.). Using the data of Figure I-4 and assuming certain distributions of equipment range separation, curves such as that shown on Figure I-5 can be obtained. Figure I-5 shows the cumulative probability of  $\Delta M$  as a function of  $\Delta \epsilon$  and  $\Delta M$ . This curve is obtained by examining the distribution of  $\Delta M$  for a given  $\Delta \epsilon$  over the range,  $R$ , where  $\Delta M$  is non-zero. This, in one sense, represents a worse case representation of error effects since in many situations, equipments will be at ranges where  $\Delta M$  would be zero. In these cases, the cumulative distributions of  $\Delta M$  would be skewed toward zero. Using the data of Figure I-5, the error effects-error relationship originally desired can be defined as shown in Figure I-6. The functions of Figure I-6 are obtained by taking the locus of points in  $\Delta M$  with varying  $\Delta \epsilon$  for a given level of cumulative probability and plotting these to show  $\Delta M$  as a function of  $\Delta \epsilon$  for a constant level of cumulative probability on  $\Delta M$ . Thus the curve given in Figure I-6 shows for a given maximum error variation, say  $\Delta \epsilon$ , that a specific error effect,  $\Delta M_1$ , will not be exceeded with confidence level  $c_1$ . Figure I-7\* shows several curves of  $\Delta M$  as a function of  $\Delta \epsilon$  for various confidence levels obtained for different equipment situations. Figure I-7a is obtained for a situation where the interference source is not rotating and the victim equipment is scanning. Figure I-7b is obtained for a situation where both antennas are scanning. Several qualifications are appropriate at this point. i) The effects on the error relationship of scanning compared to non-scanning transmitting antenna systems is generally to reduce the  $\Delta M$  for a given  $\Delta \epsilon$  and  $c$ . This is due to the larger signal distribution variance obtained when both antennas are scanning. Thus additional distribution changes due to  $\Delta \epsilon$  error are relatively less significant than in the case where the transmitter antenna is not rotating. ii) The assumptions regarding equipment range distributions are not rigid, e.g., the curves shown were obtained assuming a uniform distribution of equipments over the range where  $\Delta M$  was non-zero. Other distributions could be applied; for example, equipment likelihood presence decreasing with decreasing equipment range separation.

\* Figures referred to (i.e. I-7a and I-7b) are given with text as Figures 4 and 5.

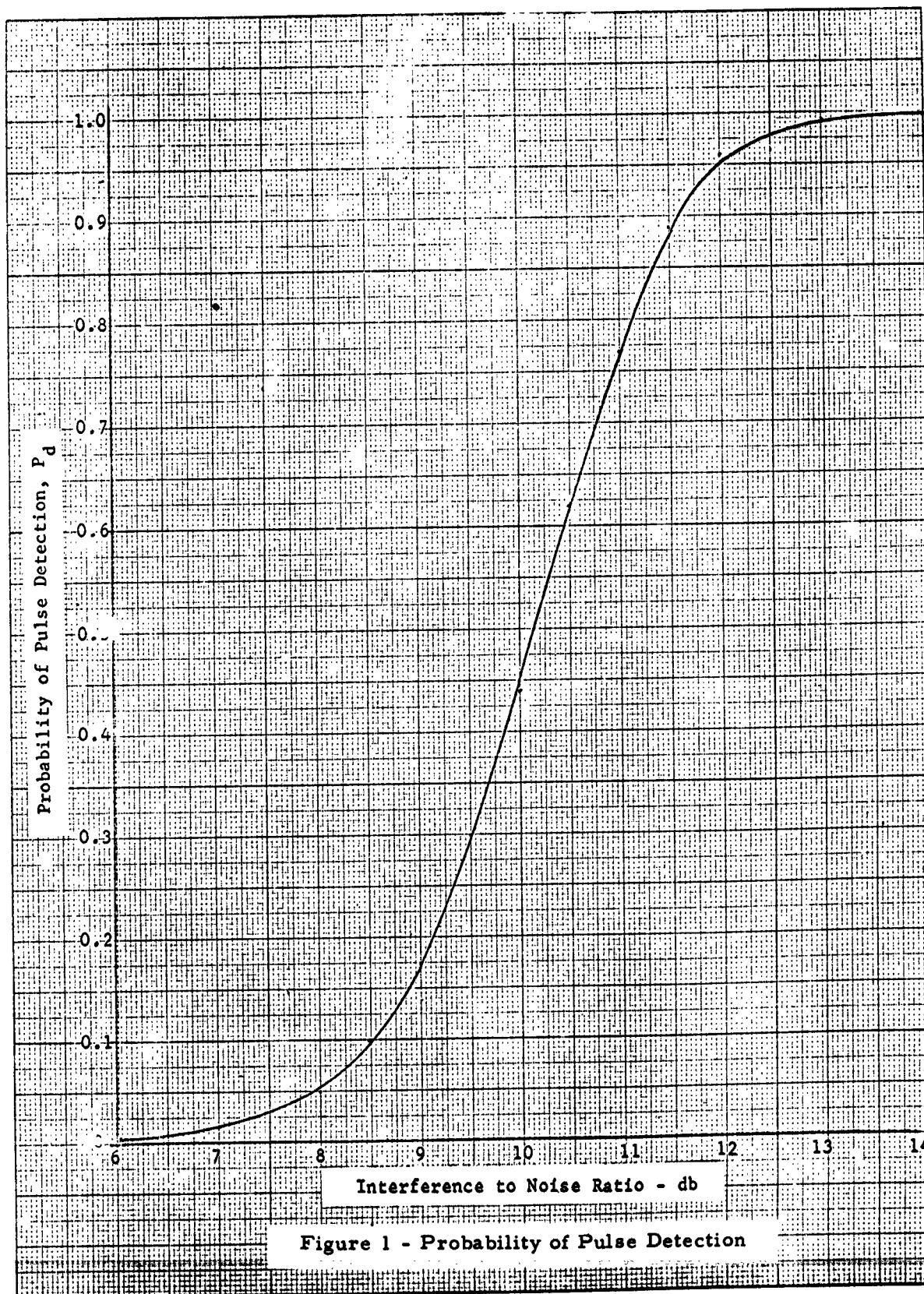
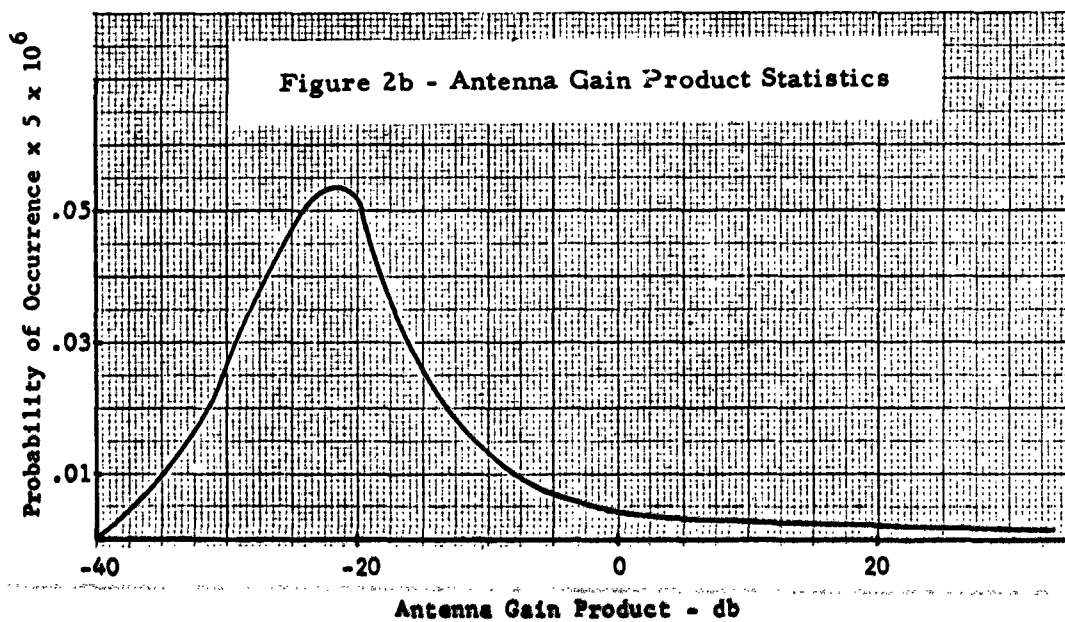
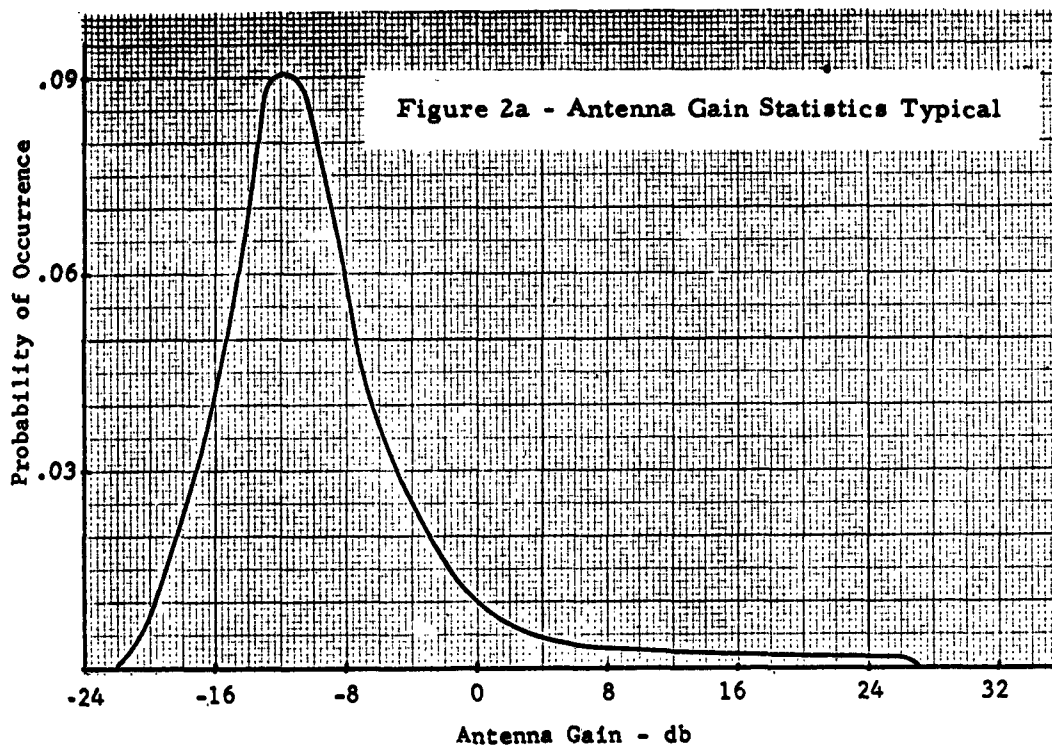


Figure 1 - Probability of Pulse Detection



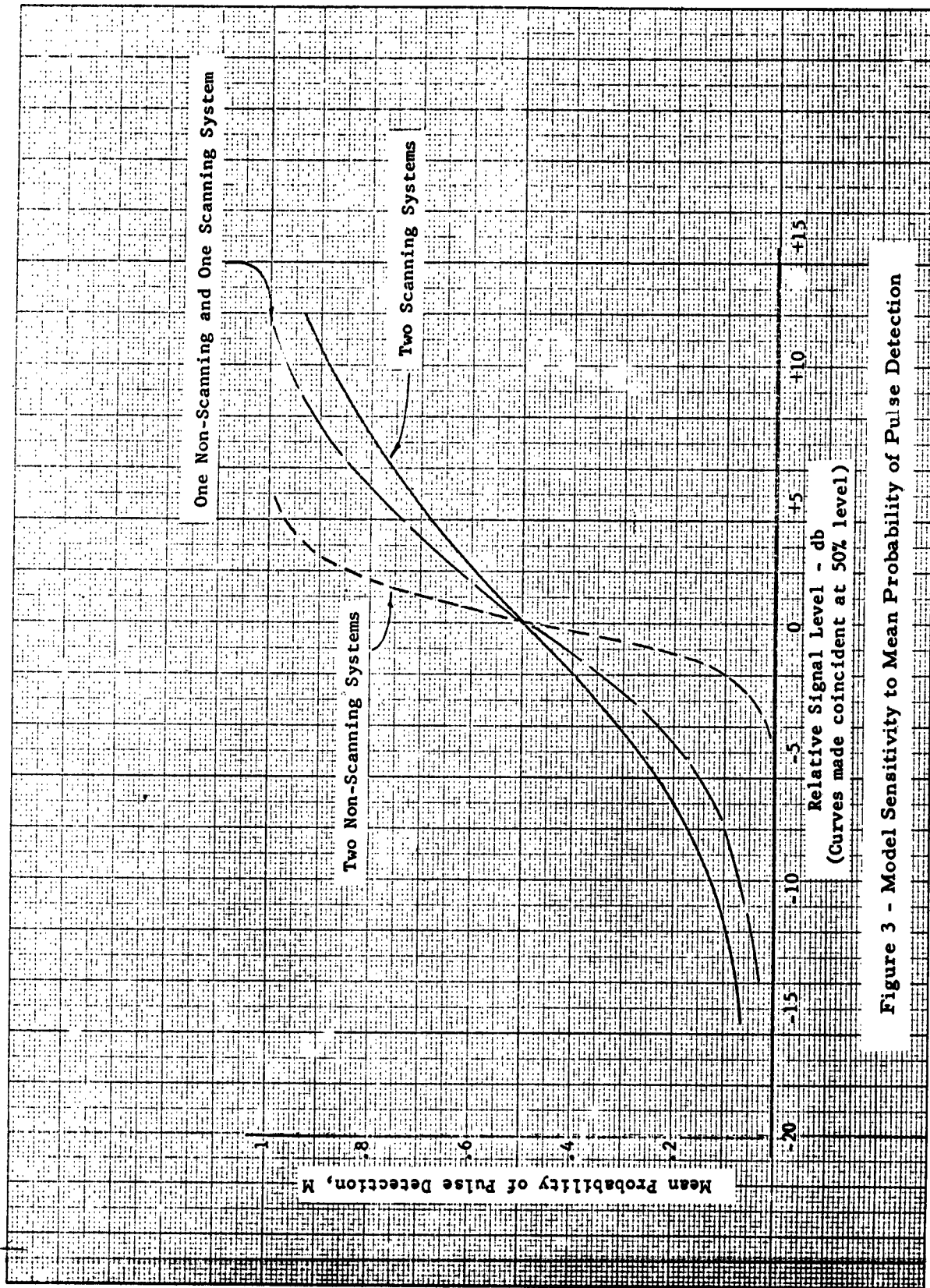


Figure 3 - Model Sensitivity to Mean Probability of Pulse Detection

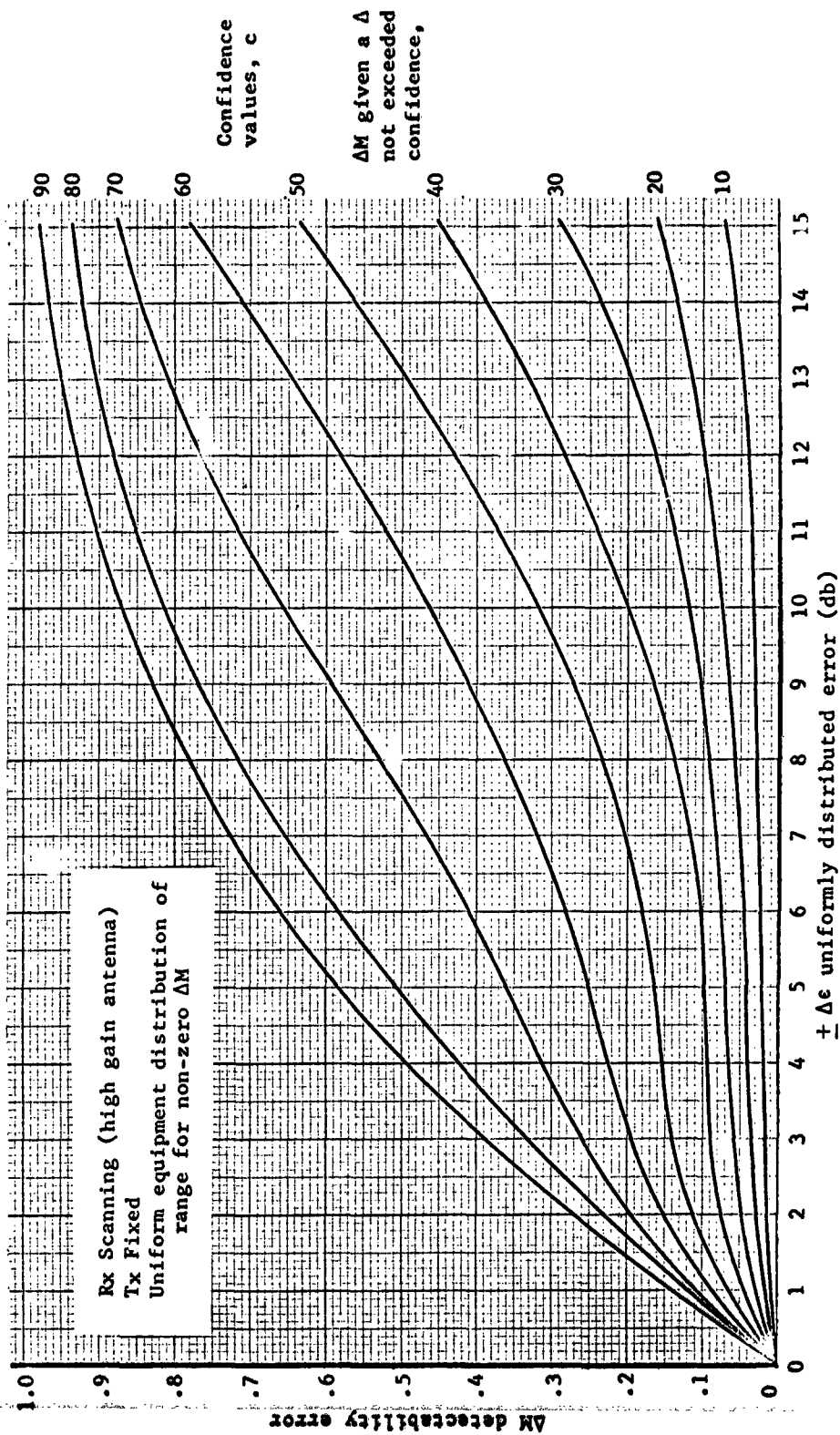


Figure 4 - Detectability Error with Input Error and Confidence Levels

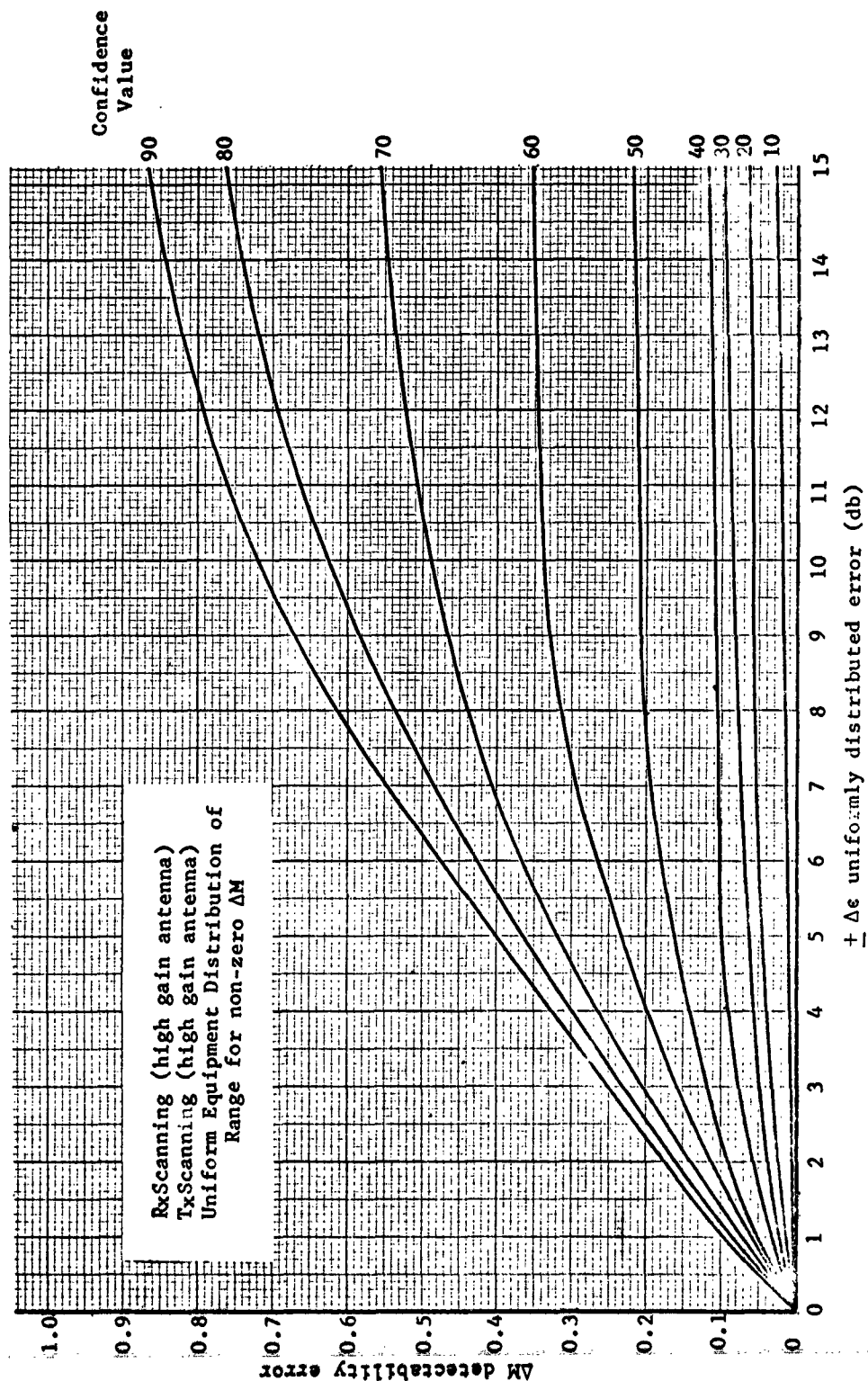


Figure 5 - Detectability Error with Input Error and Confidence Levels



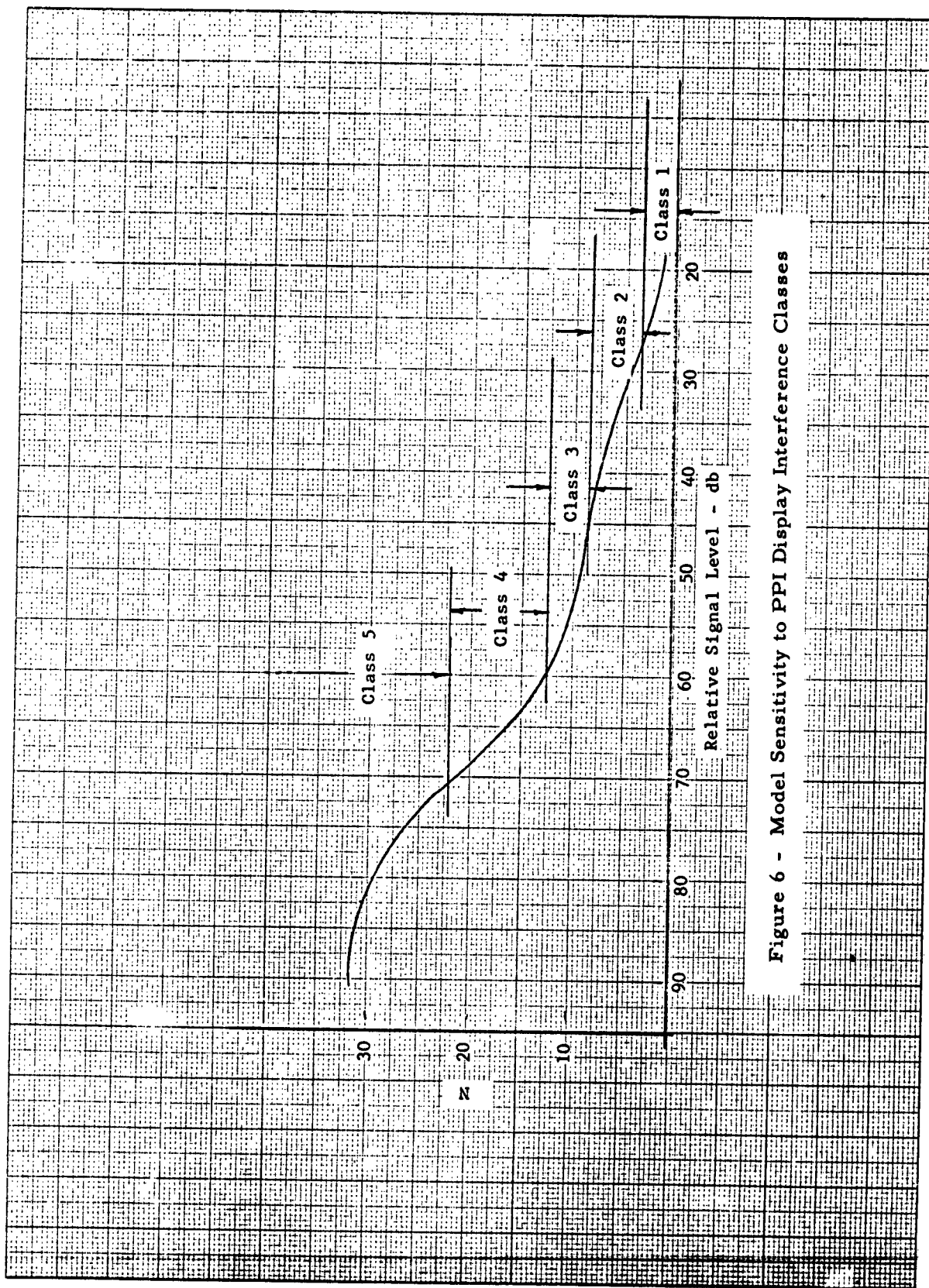


Figure 6 - Model Sensitivity to PPI Display Interference Classes



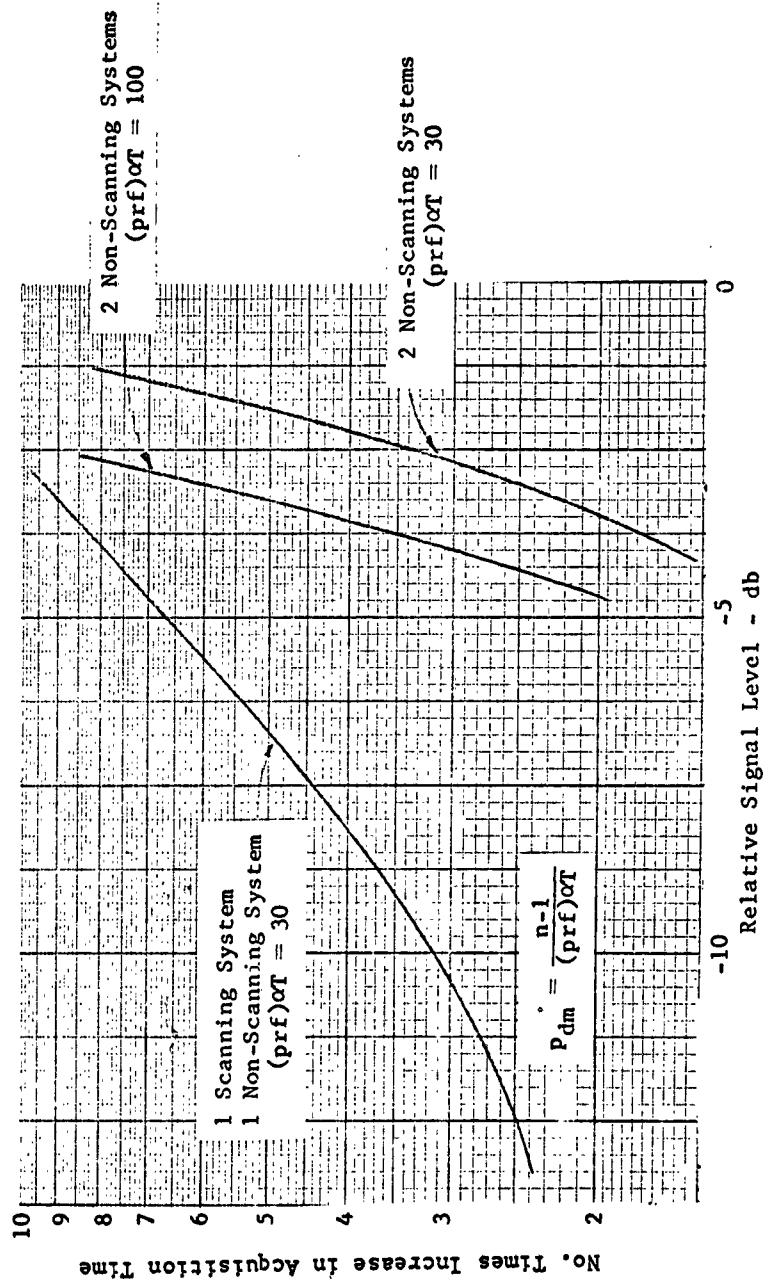


Fig. 7 - Increase in Acquisition Time with Relative Signal Level

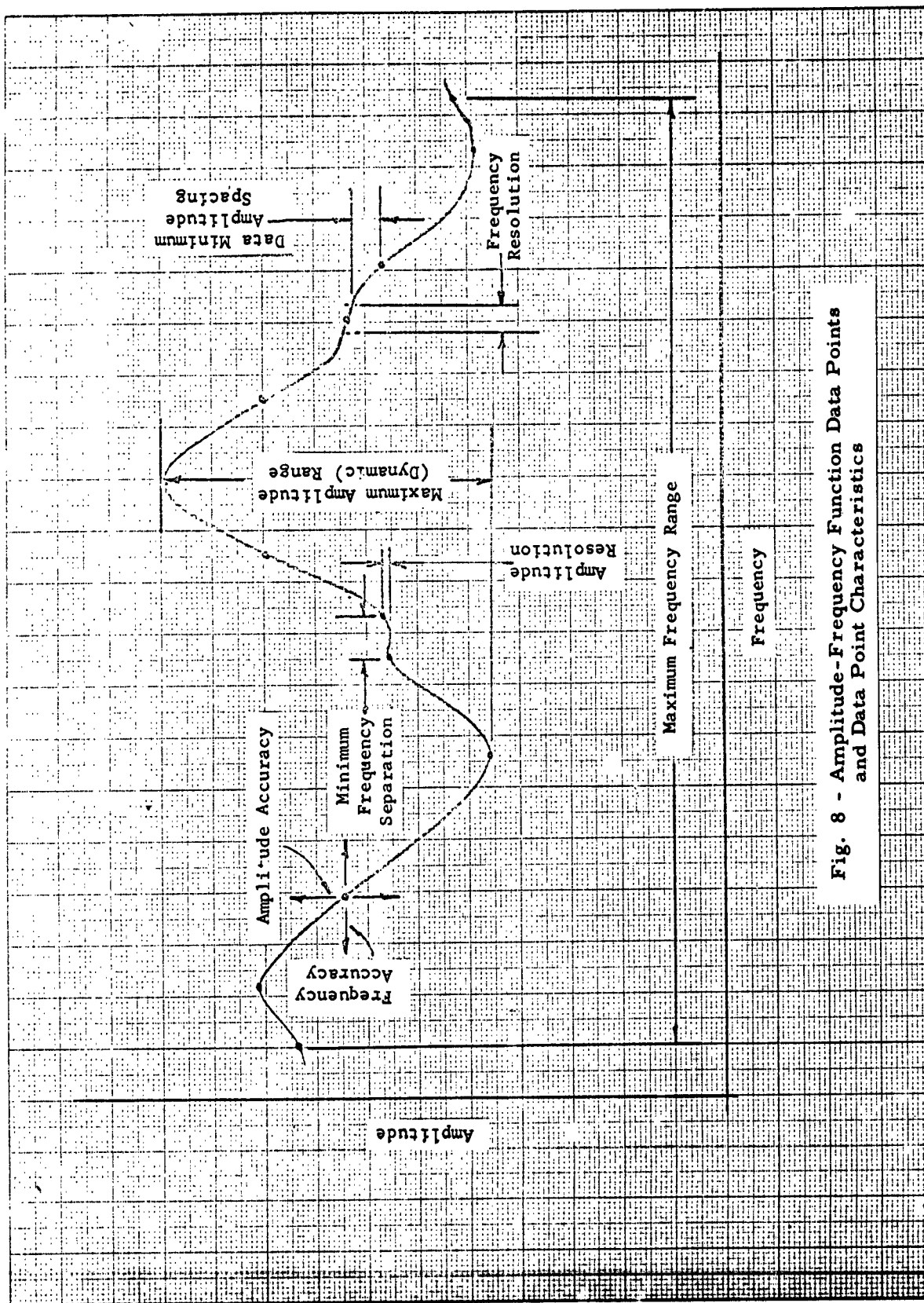
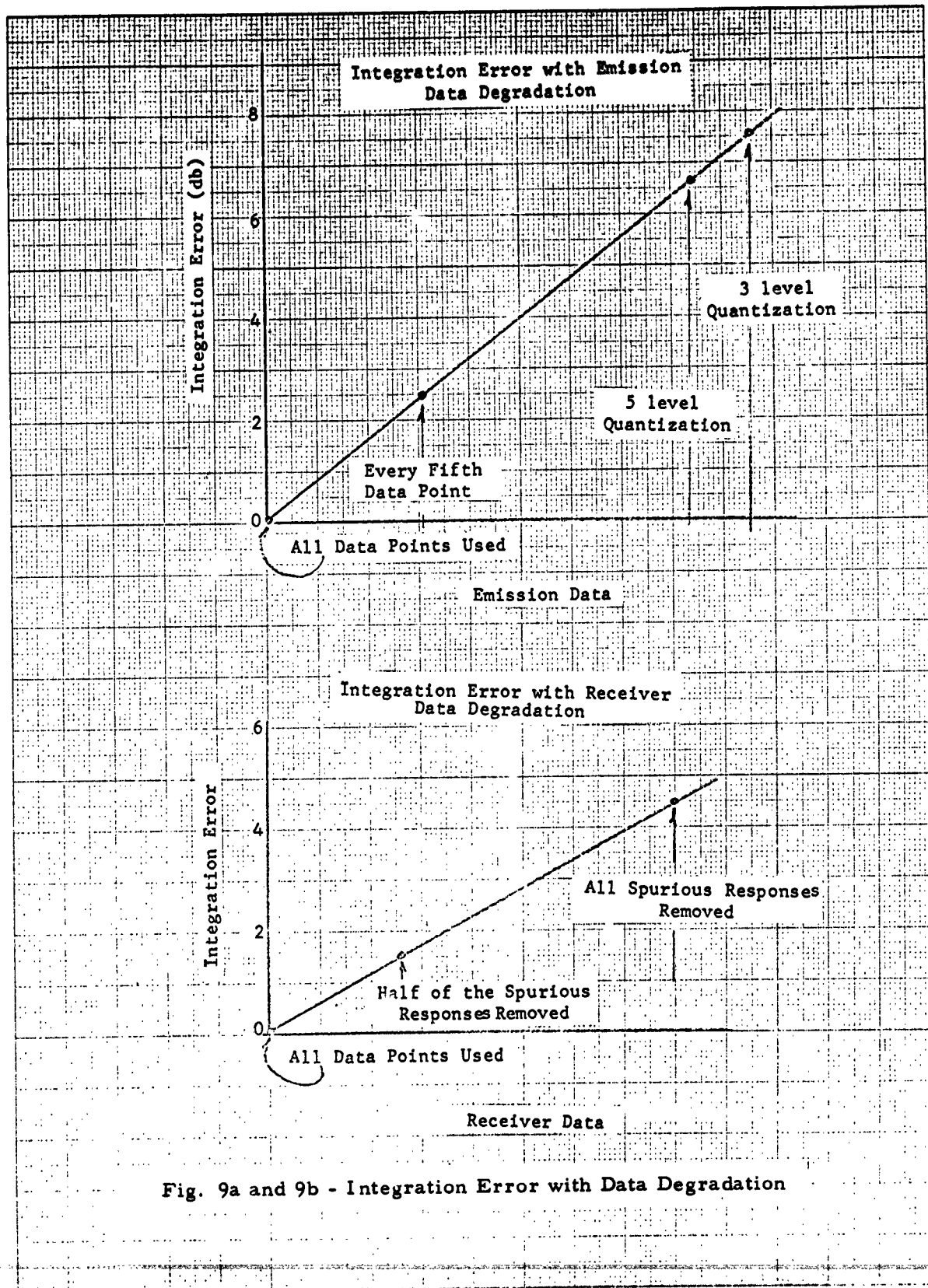


Fig. 8 - Amplitude-Frequency Function Data Points and Data Point Characteristics



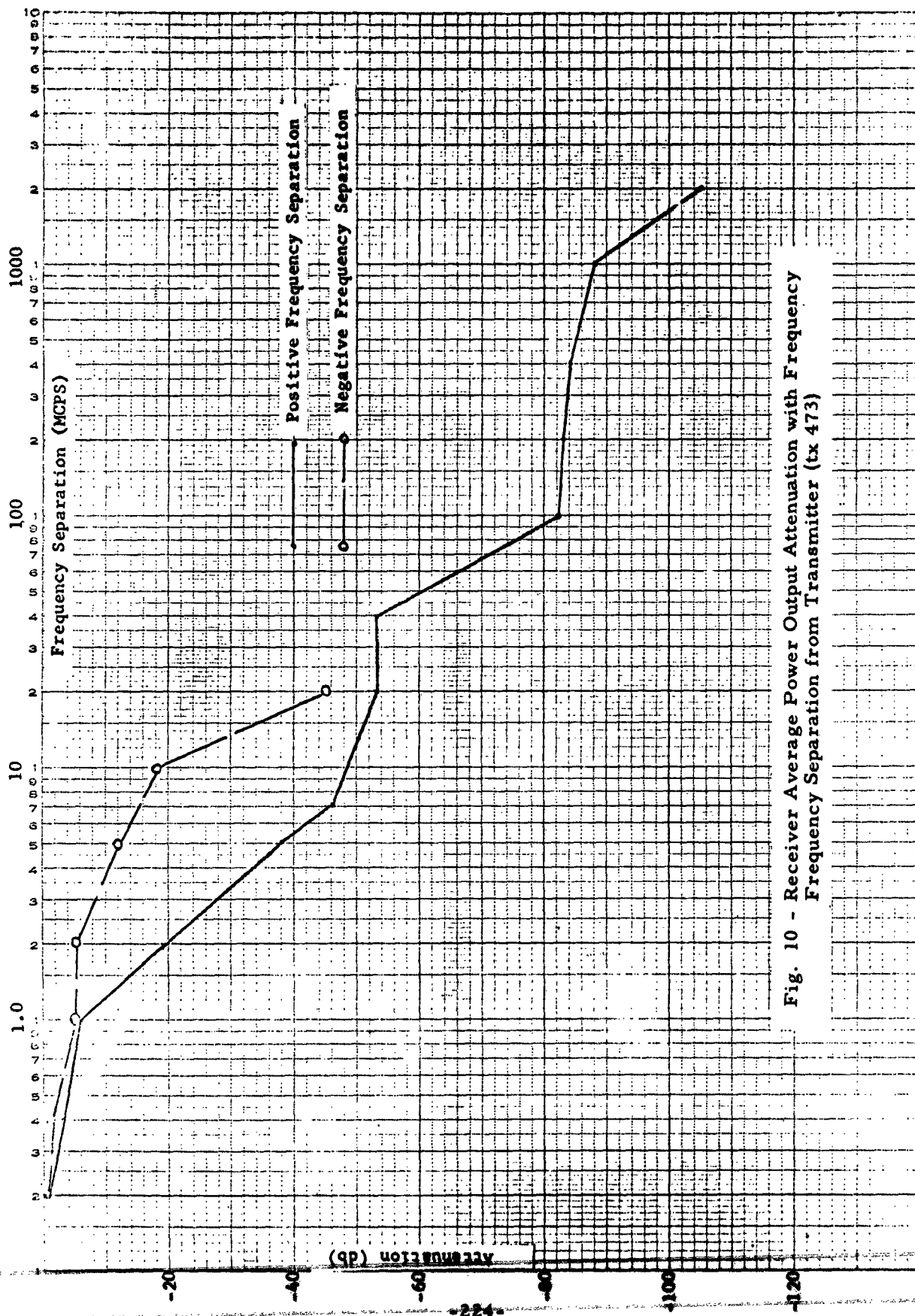


Fig. 10 - Receiver Average Power Output Attenuation with Frequency Separation from Transmitter (tx 473)

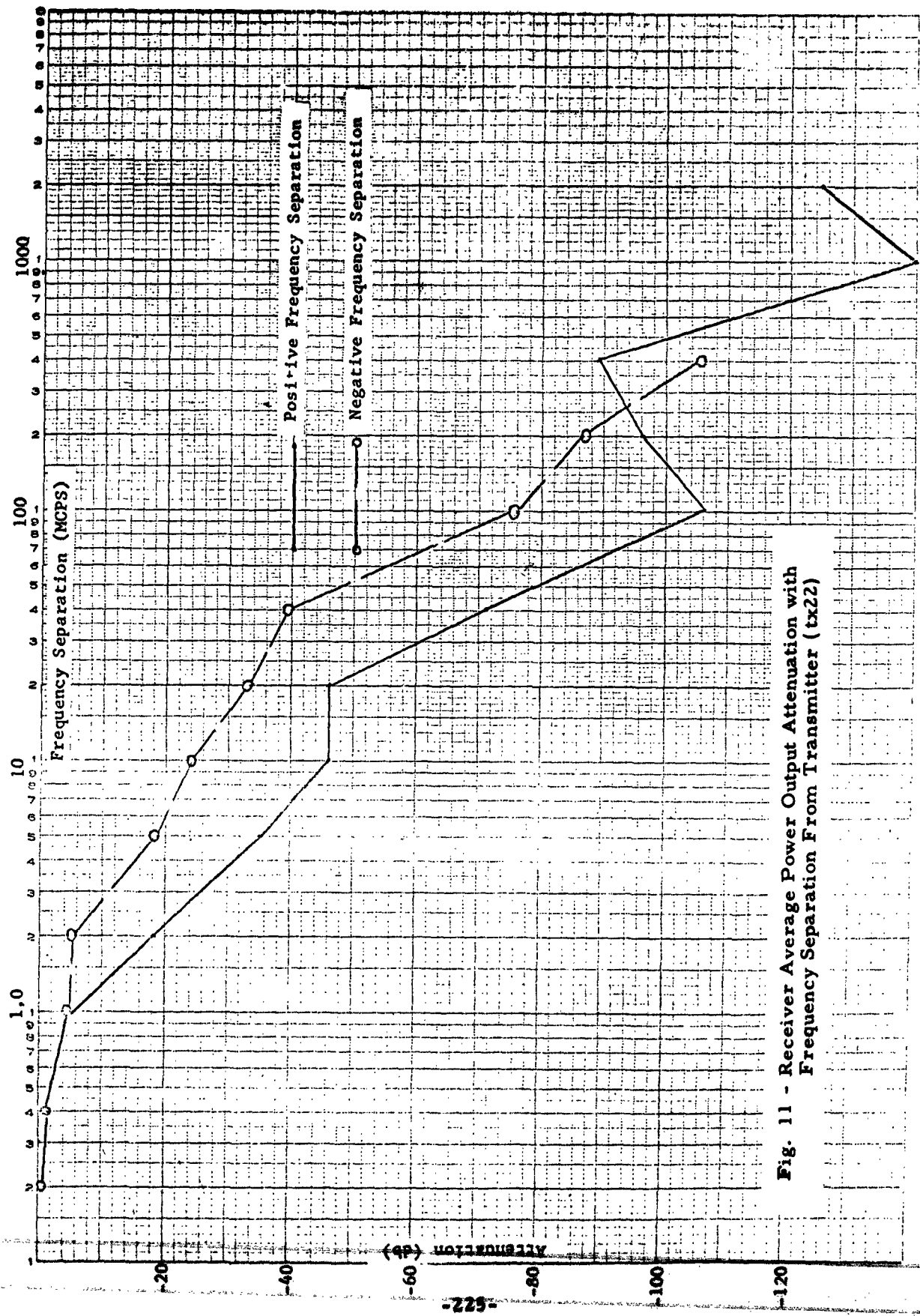


Fig. 11 - Receiver Average Power Output Attenuation with Frequency Separation From Transmitter (tx22)

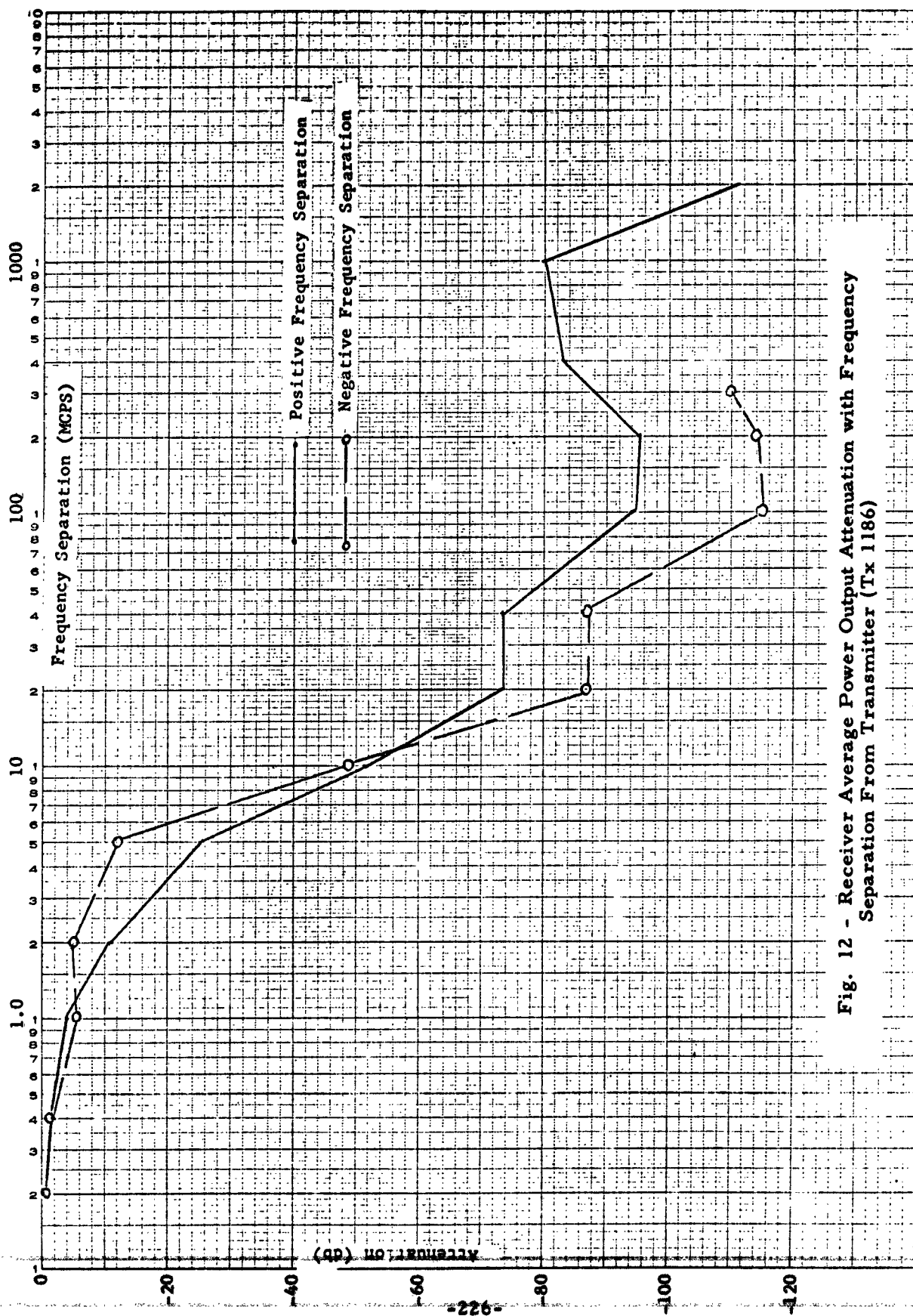


Fig. 12 - Receiver Average Power Output Attenuation with Frequency Separation From Transmitter (Tx 1186)



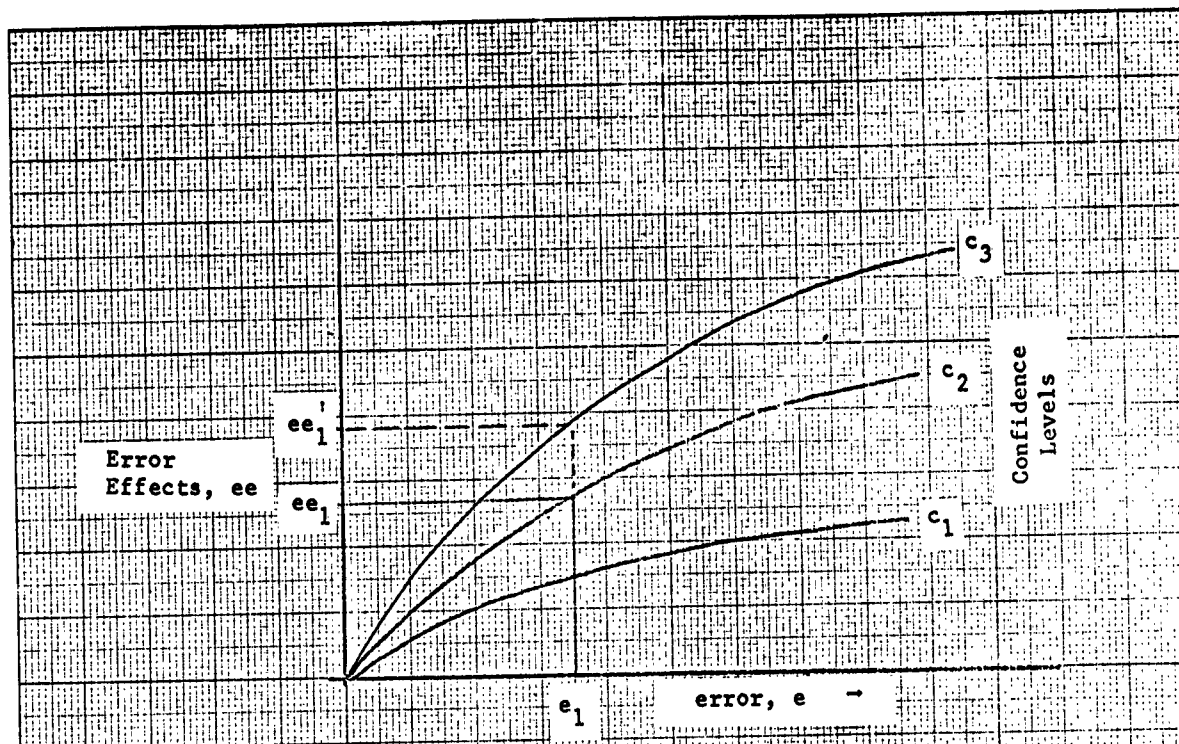


Fig. I-1 - Error Effects with Error and Effects Confidence

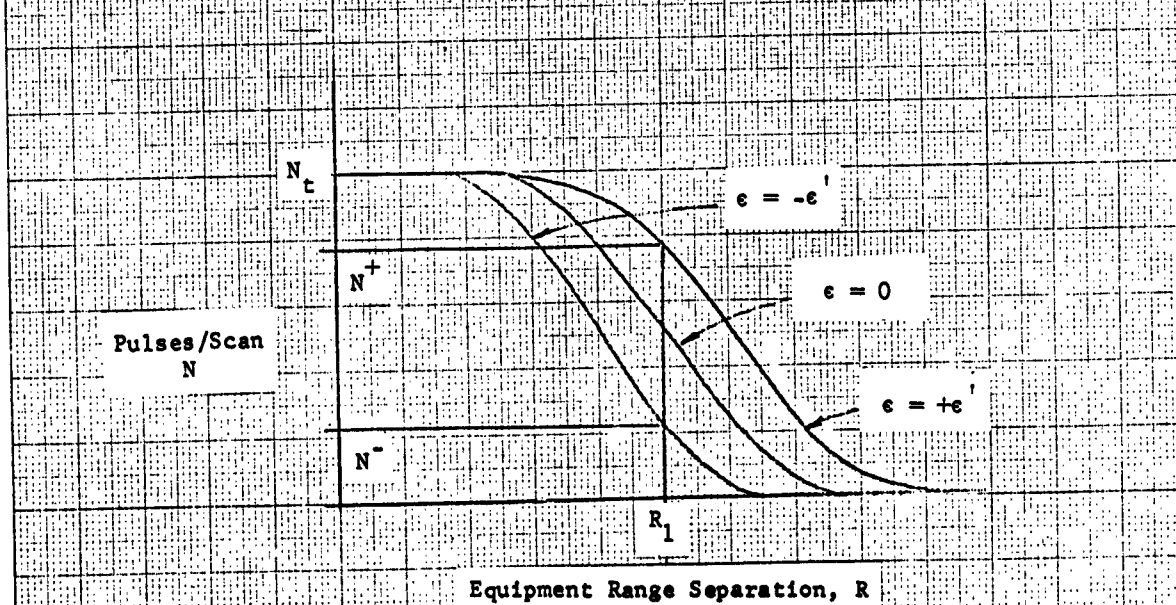


Fig. I-2 - Pulses/Scan,  $N$ , with Range Separation,  $R$ , and Error,  $\epsilon$

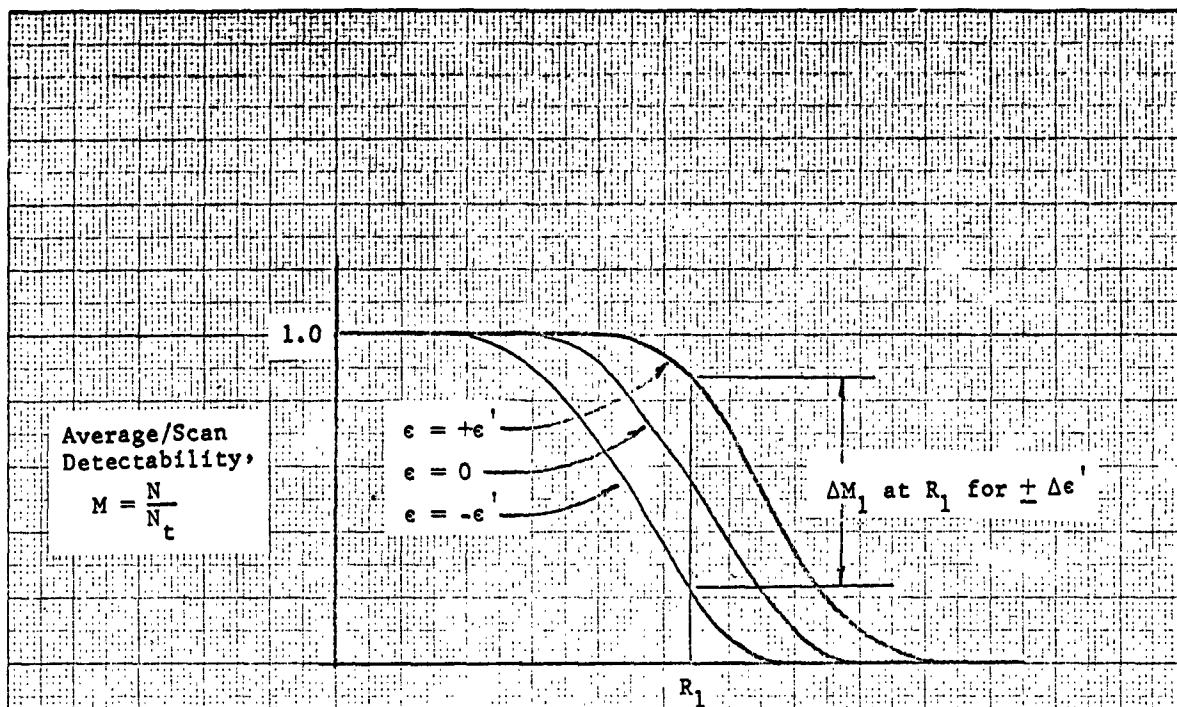


Fig. I-3 - Average Scan Detectability with Range, R, and Error,  $\epsilon$

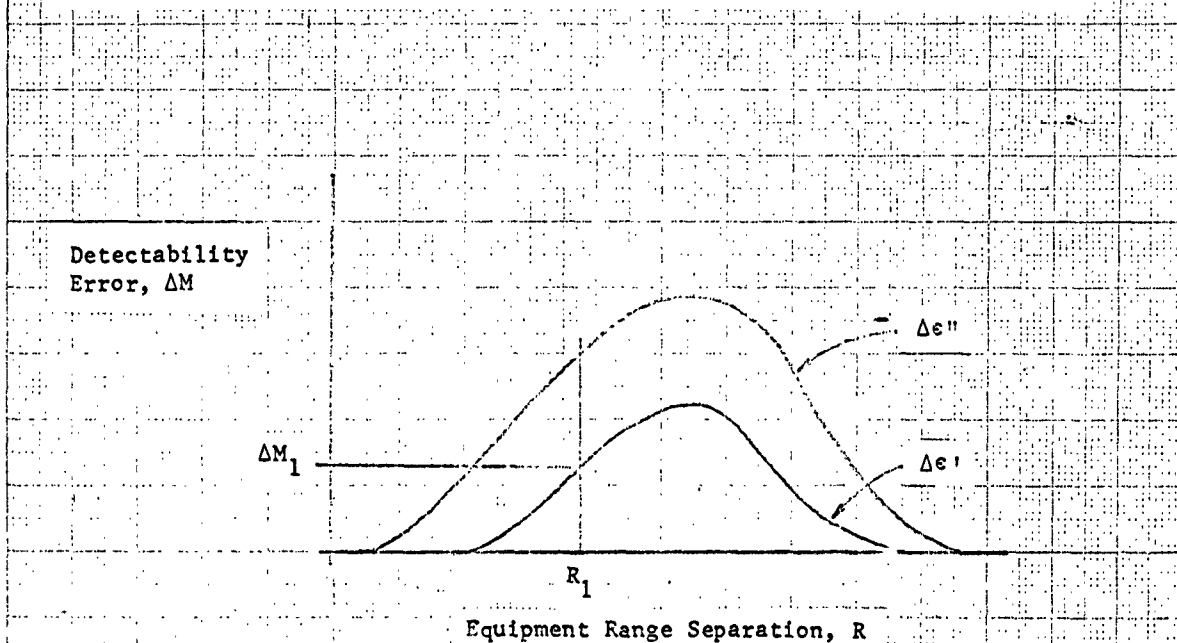


Fig. I-4 - Detectability Error,  $\Delta M$ , with Range R, and Error,  $\epsilon$



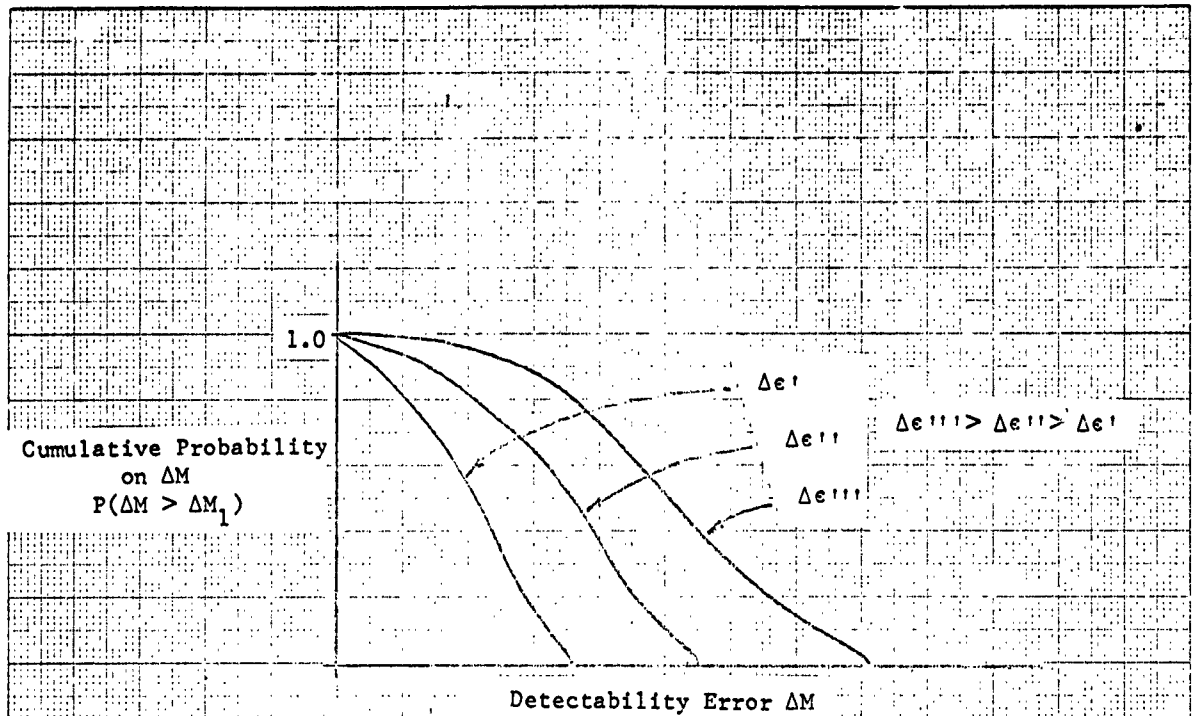


Fig. I-5 - Cumulative Probability on  $\Delta M$  with Detectability Error

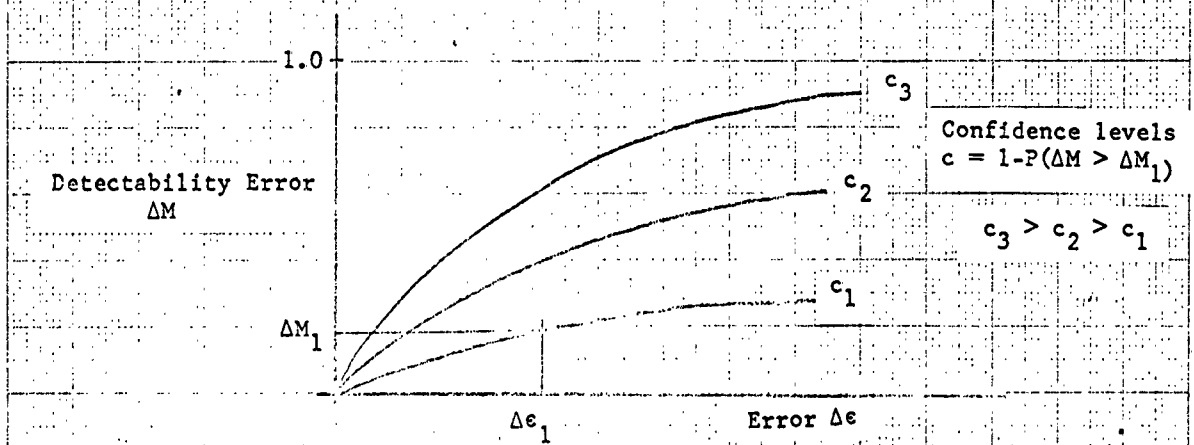


Fig. I-6 - Detectability Error  $\Delta M$  with Error,  $\Delta \epsilon$ , and Confidence,  $c$

Table I - The Effect of Uncertainty in Power Level on Mean Probability of Pulse Detection

	Maximum Rate of Change of Mean Probability of Pulse Detection	db Change for 0.2 Change of Mean Probability of Pulse Detection	db Change for 0.8 Change of Mean Probability of Pulse Detection
2 Non-Scanning Systems	.2/db	0.8 db	4.4 db
1 Scanning, 1 Non-Scanning	.08/db	3.0 db	15.5 db
2 Scanning Systems	.05/db	4.0 db	23 db

Table II - Typical Parameter Measurement Accuracies

Signal Amplitude Measurement

Wide-Band . . . . .	2 db
Narrow-Band . . . . .	3 db

Antenna Gain Measurement . . . . . 2 db

Propagation Standard Deviations

Tropo-Scatter Region . .	2.5 db
Intermediate Region . . .	9 db

Table III - Emission Spectrum Error Reduction Due to Receiver Bandwidth Averaging (Bandwidth 5 times Data Point Frequency)

Input Data $\sigma$	Mean Absolute Error		Integration Error Reduction
	Without Bandwidth Averaging	With Bandwidth Averaging	
5.0 db	4.0	2.6	35%
10.0 db	8.0	3.6	55%
15.0 db	12.0	7.4	38%

Table IV - Interference Prediction Model Requirements Relative to Emission Characteristic Inputs

Amplitude Dynamic Range	All values > -25 dbm
Amplitude Accuracy	$\pm 3$ db or better near emitter fundamental, $\pm 6$ db or better elsewhere
Frequency Accuracy	1.5 parts in $10^4$ or better

## THE ANALYSIS AND SYNTHESIS OF RADAR EMISSION SPECTRUMS BY DIGITAL COMPUTER METHODS

Robert B. Marcus

HRB-Singer, Inc.

**Abstract.** - The Electromagnetic Compatibility Branch of the U. S. Army Electronics Research and Development Laboratory, Fort Monmouth, New Jersey, is studying the radio frequency interference problem in the future field army. The subject matter presented in this paper was developed while the author was a resident contract engineer at E. C. Branch at Fort Monmouth.

The E. C. Branch is employing a large scale computer study to simulate the battlefield R. F. environment in the future field army. In the absence of measured equipment characteristics, especially for equipment not yet built, it became necessary to synthesize the emission spectra. A knowledge of the characteristics of previously measured spectrums and the physical laws governing the characteristics are used as a guide in the synthesis procedure.

A model based on the lobe structure of the radar rather than the line structure was generated in the computer. A rather slow computer, the Burrows 220, was available and the lobe structure greatly reduced the computation time compared to that of the line structure. If a victim receiver's bandwidth is less than that of a single lobe, a modified line structure can be used. The paper elaborates further on this point.

Spectrums based on rectangular and trapezoidal pulses with various rise times were generated. These were compared with measured emission spectra of existing radars. It was found that the synthesized spectrum based on a trapezoidal pulse was a better fit than that based on a rectangular pulse.

In comparing the synthesized spectrums with existing measured spectrums an analysis of existing spectrums was made. However, as is usually the case some aspects of the measured spectrums are not fully explained and need further investigation.

### I. INTRODUCTION

The Electromagnetic Compatibility Branch of the U. S. Army Electronics Research and Development Laboratory, Fort Monmouth, New Jersey, is studying the interference problem in the future field army. A large scale computer study will be used to simulate the battlefield environment. In the absence of measured equipment characteristics especially for equipment not yet built, the characteristics will be synthesized. A knowledge of the characteristics of previously measured equipment and a knowledge of the physical laws governing the characteristics are used as a guide in the synthesis procedure.

The problem of modelling radar emission spectrum characteristics arose. To date several radar emission spectrums have been measured under the DOD electromagnetic compatibility program. Two of these spectrum signatures were used as a guide in the synthesis procedure. The two measured spectrums were compared with two synthesized spectrums and were thereby analyzed. The procedure can be used to analyze existing spectrum signatures and to synthesize or model nonexistent ones.

A little background material on pulsed signals will be considered. Although the principles are quite simple they will help form a clear picture of the problem.

Let us consider the envelope of a carrier modulated with a rectangular pulse as shown in Figure 1.

The amplitude of the envelope will be normalized to one for convenience. The pulse width is  $\tau$  and  $f_r$  is the pulse repetition frequency.

From the Fourier analysis the spectrum components of the envelope are defined as follows:

$$C_n = \frac{\sin n \pi f_r \tau}{n \pi} \quad (1)$$

when  $C_n$  is the amplitude of the  $n^{\text{th}}$  sideband pair.

The carrier is defined when  $n = 0$ . By using L'Hospital's rule  $C_n$  can be defined when  $n$  equals zero.

$$C_{(0)} = \frac{d(\sin n \pi f_r \tau) / dn}{d(n \pi) / dn}$$

$$C_{(0)} = \frac{\pi f_r \tau \cos n \pi f_r \tau}{\pi}$$

$$C_{(0)} = f_r \tau$$

The amplitude of the carrier is  $f_r \tau$  which incidentally is the duty cycle. The amplitude of the sidebands are defined by setting  $n$  equal to the sideband number. It can be seen that when  $n f_r \tau$  equals an integer the sine function goes to zero. If  $\frac{1}{f_r \tau}$  is an integer the function periodically goes to zero. If  $\frac{1}{f_r \tau}$  does not equal an integer the function will go through minima periodically. There will be a pair of sidebands corresponding to each  $n$  number located on each side of the carrier. The line structure is the familiar  $\sin X/X$  structure as shown in Figure 2.

If  $\frac{1}{f_r \tau}$  is an integer, the amplitude of the spectrum lines goes to zero at frequencies equal to integral multiples of  $\frac{1}{\tau}$ . The lines are separated by a frequency equal to the pulse repetition frequency. Hence from the carrier to the

first zero there or  $\frac{1}{f_r \tau}$  intervals spaced by a frequency separation of  $f_r$ . Since the spectrum line occurring at the last interval is zero there are  $\frac{1}{f_r \tau}$  lines including the carrier from the carrier to the first null. If  $\frac{1}{f_r \tau}$  is not an integer there will not be an integral number of lines in the interval from the carrier to the carrier plus and minus a frequency of  $\frac{1}{\tau}$ .

The envelope of the spectrum is a lobe structure. The first lobe is symmetrical about the carrier and extends to a frequency of  $\frac{1}{\tau}$  above and below the carrier. The width of the succeeding lobes are half that of the first lobe and have a width of  $\frac{1}{\tau}$ .

A simple example will illustrate how the number of lines in each lobe is determined and what the frequency of the nulls is relative to the carrier. For example:

$$\text{Amplitude} = 1$$

$$f_r = 100 \text{ cps}$$

$$\tau = 0.001 \text{ sec}$$

$$\frac{1}{\tau} = 1000 \text{ cps}$$

$$\frac{1}{f_r \tau} = 10$$

The first null occurs at 1000 cps above and below the carrier. Every successive null will be separated an additional 1000 cps from the carrier. There are ten intervals between the carrier and the first null and between successive nulls. Excluding the carrier every tenth line will have zero amplitude. If the pulse envelope has an amplitude of one, the carrier will have an amplitude of  $f_r \tau$  or 0.1. To determine the amplitude of each spectral line in the above example the equation for the spectral line amplitude can be used thusly:

$$\text{Carrier} \quad C_{(0)} = f_r \tau = 100 \times 0.001 = 0.1$$

$$C_{(1)} = \frac{\sin(\pi \times 0.1)}{\pi} = \frac{0.309}{3.14} = 0.0983$$

$$C_{(2)} = \frac{\sin(2\pi \times 0.1)}{2\pi} = \frac{0.588}{6.29} = 0.0935$$

$$C_{(3)} = \frac{\sin(3\pi \times 0.1)}{3\pi} = \frac{0.809}{9.42} = 0.0859$$

$$C_{(4)} = \frac{\sin(4\pi \times 0.1)}{4\pi} = \frac{0.951}{12.57} = 0.0757$$

$$C_{(5)} = \frac{\sin(5\pi \times 0.1)}{5\pi} = \frac{1.00}{15.71} = 0.0636$$

$$C_{(6)} = \frac{\sin(6\pi \times 0.1)}{6\pi} = \frac{0.951}{18.85} = 0.0505$$

$$C_{(7)} = \frac{\sin(7\pi \times 0.1)}{7\pi} = \frac{0.809}{21.99} = 0.0368$$

$$C_{(8)} = \frac{\sin(8\pi \times 0.1)}{8\pi} = \frac{0.588}{25.13} = 0.0234$$

$$C_{(9)} = \frac{\sin(9\pi \times 0.1)}{9\pi} = \frac{0.309}{28.27} = 0.0123$$

$$C_{(10)} = \frac{\sin(10\pi \times 0.1)}{10\pi} = 0$$

These spectral lines occur on both sides of the carrier spaced at intervals of 100 cps. It might be noted that  $C_{(11)}$  will be negative because the sine function will be between  $\pi$  and  $2\pi$  radians. Rather than showing a negative spectral line, which indicates phase reversal, most diagrams just consider the amplitude of the line.

The amplitude of the spectral lines corresponds to their voltage. In order to determine the power in each line the unit voltage pulse will be considered to be a unit power pulse also. The power in each spectral line will therefore be the square of its voltage; the equation for the power in each spectral line is therefore:

$$P_n = \left( \frac{\sin n \pi f_r \tau}{n \pi} \right)^2 \quad (2)$$

The power is average power as the spectral lines are continuous in time. However, if a receiver has a bandwidth greater than one spectral line it will receive a pulse made up from the combination of the lines it receives. The pulse will have a peak value associated with it which will be equal to the average power in the lines divided by the duty cycle. The shape of the pulse will depend upon the number of lines and their location in the spectrum. In order to find the fractional power in each line it will be necessary to divide the average power in each line by the duty cycle because the normalized power is peak power.

To find the fractional power in the first lobe of the previous example the fractional power in each line in the first lobe will have to be added together. The lobe, in this example, consists of the carrier and twenty lines on each side. However, two of these lines,  $C_{(10)}$ , have zero amplitude. The normalized average power in each line is equal to the amplitude squared. The fractional normalized power in each line is the normalized average power in each line divided by the total normalized average power. The total normalized average power is equal to the duty cycle  $f_r \tau$ .

The fractional normalized power in each line in the example is as follows

$$P_{(0)} = (f_r \tau)^2 \times \frac{1}{f_r \tau} = f_r \tau = 0.1$$

$$P_{(1)} = \left( \frac{\sin \pi \times 0.1}{\pi} \right)^2 \times \frac{1}{f_r \tau} = (0.0983)^2 \times \frac{1}{0.1} = 0.0966$$

$$P_{(2)} = \left( \frac{\sin 2\pi \times 0.1}{2\pi} \right)^2 \times \frac{1}{f_r \tau} = (0.0935)^2 \times \frac{1}{0.1} = 0.0874$$

$$P_{(3)} = \left( \frac{\sin 3\pi \times 0.1}{3\pi} \right)^2 \times \frac{1}{f_r \tau} = (0.059)^2 \times \frac{1}{0.1} = 0.0348$$

$$P_{(4)} = \left( \frac{\sin 4\pi \times 0.1}{4\pi} \right)^2 \times \frac{1}{f_r \tau} = (0.0457)^2 \times \frac{1}{0.1} = 0.0209$$

$$P_{(5)} = \left( \frac{\sin 5\pi \times 0.1}{5\pi} \right)^2 \times \frac{1}{f_r \tau} = (0.0364)^2 \times \frac{1}{0.1} = 0.0133$$

$$P_{(6)} = \left( \frac{\sin 6\pi \times 0.1}{6\pi} \right)^2 \times \frac{1}{f_r \tau} = (0.0255)^2 \times \frac{1}{0.1} = 0.0065$$

$$P_{(7)} = \left( \frac{\sin 7\pi \times 0.1}{7\pi} \right)^2 \times \frac{1}{f_r \tau} = (0.0168)^2 \times \frac{1}{0.1} = 0.0028$$

$$P_{(8)} = \left( \frac{\sin 8\pi \times 0.1}{8\pi} \right)^2 \times \frac{1}{f_r \tau} = (0.0104)^2 \times \frac{1}{0.1} = 0.0011$$

$$P_{(9)} = \left( \frac{\sin 9\pi \times 0.1}{9\pi} \right)^2 \times \frac{1}{f_r \tau} = (0.0064)^2 \times \frac{1}{0.1} = 0.0004$$

$$P_{(10)} = \left( \frac{\sin 10\pi \times 0.1}{10\pi} \right)^2 \times \frac{1}{f_r \tau} = 0$$



The fractional power in the first lobe is the sum of the fractional power in the carrier plus that in the ten sideband pairs of the following sum:

$$P_{T1} = 0.1 + 2(0.0966) + 2(0.0874) + 2(0.0738) + 2(0.0573) \\ + 2(0.0404) + 2(0.0255) + 2(0.0135) + 2(0.00548) \\ + 2(0.00151)$$

$$P_{T1} = 0.903$$

The first lobe contains 0.903 or 90.3% of the power. That is the average power in the first lobe is 90.3% of the total average power or if the pulse made up of all the lines in the first lobe is considered, it will have a peak power of 90.3% of the total peak power.

The above example shows the nature of the calculations necessary to determine the power in part of a spectrum generated by a carrier modulated by a rectangular wave.

In order to determine how much power, either peak or average, a receiver will be subject to from a radar it will be necessary to calculate the spectral power to which the receiver will be subjected. Propagation and antenna gain also enter the picture but will not be covered here as they encompass complete fields of study by themselves. The bandwidth and center frequency of the receiver must be known. One would then have to determine the order of  $n$  in equation (2) for all the lines that fall in the receiver bandwidth. The total fractional power would be obtained by adding the fractional power in all the lines within the receiver bandpass. The peak power in the receiver could then be determined and receiver degradation would be determined from measured or synthesized interference parameters of the receiver.

If a typical high power search radar is considered we can get an idea of what is involved. A typical search radar (the AN/FPS-8) has the following characteristics:

Peak power = 2 megawatts

PRR = 360 pps

Pulse width = 3 microseconds

If the pulse width is taken as 3.003 microseconds,  $\frac{1}{f_r \tau}$  will be an integer.

The difference in results in taking the pulse width as 3.003 instead of 3.000 microseconds is insignificant.

With these parameters we get:

$$\frac{1}{f_r \tau} = \frac{1}{360 \times 3.003 \times 10^{-6}} = 925$$

$$\frac{1}{\tau} = \frac{1}{3.003 \times 10^{-6}} = 333 \times 10^3 = 333 \text{ kc}$$

The first lobe has  $2 \times 925$  spectral lines plus the carrier. Two of these lines have zero amplitude. Each succeeding lobe contains 924 lines plus two nulls. Not counting the first lobe there are 3 lobes per megacycle of spectrum. The radar in question is very high powered and has significant output out to 3075 Mc above its center frequency and 325 Mc below its center frequency. A computer program was written which would generate the fractional power line by line in each lobe and print out the fractional power in each lobe. However, with  $2 \times 925$  lines in the first lobe and 925 lines in each succeeding lobe and a total of 9225 lobes in a 3075 Mc wide spectrum the total number of lines calculated would be 8,533,125. The computer available at the time was the Burrows 220 whose operations took in the order of a few milliseconds. If it took about 100 logical operations to generate a line, the computation time to generate the radar's spectrum would be in the order of several days. If a faster computer would be used, the time would still be long if the generated spectrum were used in a more encompassing computer study of Battlefield radio frequency interference.

Further consideration was made to see if the problem could be simplified and if a universal normalized spectrum could be synthesized that would be more conservative of computer time and which with some modification would apply to more than one radar.

It has been determined that the number of lines in half the first lobe and all the succeeding lobes is determined by  $\frac{1}{f_r \tau}$ ;  $f_r$  and  $\tau$  can vary, it is their product that determines the number of lines. The frequency of the nulls is determined by  $\frac{1}{\tau}$ . The percentage power in a lobe is not determined by  $\frac{1}{\tau}$ . It seemed as if the percentage of fractional power in a lobe does not vary significantly with the number of lines in the lobe. To prove this contention a program was written for the Burrows 220. The program is shown in Figure 3.

Starting with  $\frac{1}{f_r \tau} = 2$  and continuing until  $\frac{1}{f_r \tau} = 99$  the fractional power in the first nine lobes was calculated. The computer language is ALGOL 58. The print out lists the value of  $\frac{1}{f_r \tau}$  in the left hand column followed by the fractional power in the first nine lobes. The fractional values are in floating point 50 form. That is the first two digits are the characteristics followed by the value. The program including compiling took 35 minutes.

For  $\frac{1}{f_r \tau} = 2$ , the power in the first lobe is 0.9052847 times the total power and for  $\frac{1}{f_r \tau} = 99$  the power in the first lobe is 0.9028225 times the total power. After  $\frac{1}{f_r \tau} = 4$  the change is very small. The difference in the succeeding lobes is even smaller as  $\frac{1}{f_r \tau}$  is changed. The power in the first lobe for  $\frac{1}{f_r \tau} = 925$  was calculated using another program: it is 0.9028153 which differs by 0.007 db from a first lobe based on  $\frac{1}{f_r \tau} = 4$ . Therefore, if the fractional or percentage power in each lobe is calculated based on  $f_r \tau = 0.25$  or  $\frac{1}{f_r \tau} = 4$  the values obtained are very close to those based on any number of lines per lobe.

At this point it will be pointed out that while the percentage power in a given lobe is practically constant as  $f_r$  and  $\tau$  vary, the power density in a lobe varies inversely with  $\tau$  because the frequency coverage of a lobe varies inversely with  $\tau$ . Thus, if  $\tau = 1 \mu s$  the first lobe is 2 Mc wide and all succeeding lobes are 1 Mc wide.

The ALGOL 58 program shown in Figure 4 was written which generates the fractional power in each lobe based on  $\frac{1}{f_r \tau} = 4$ .

There is no limit to the number of lobes which can be generated. The program shown in Figure 4 stopped at 5000 lobes but it can be used for any number of lobes. The third instruction from the last (IF M GTR 5000 \$ GO TO L2\$) put the upper limit at 5000. The instruction can be changed to any number desired. If the number exceeds four integers the format will have to be changed to accommodate the extra integers. When  $\frac{1}{f_r \tau} = 4$  there are four intervals in each lobe. The fractional power in the carrier is  $f_r \tau$  or 0.25. The next three lines are based on the squares of the sines of  $45^\circ$ ,  $90^\circ$  and  $135^\circ$ . In each succeeding lobe the sine function are the identical numbers. The sine square of  $45^\circ$ ,  $90^\circ$  and  $135^\circ$  are 0.5, 1.0 and 0.5 respectively. These numbers were used directly in the program without generating the sine functions.

The program generates the fractional power in 5000 lobes or any desired number of lobes. These figures can be applied to any spectrum generated by an RF carrier being modulated with a rectangular pulse. The frequency limits of the lobes are determined by the emitter center frequency and  $\tau$ .

The spectrum as generated by the preceding program can be used as a basis of synthesizing a radar spectrum for the study of battlefield radio frequency interference or interference in other situations. The entire spectrum would not have to be generated but only that portion which falls in the victim receiver's bandwidth.

The measured spectrum of two radars, the AN/FPS-8 and the AN/FPS-6, were compared with the synthesized spectrum based on a rectangular modulating pulse. The spectrums were measured using a receiver with a 5 Mc bandwidth. The spectrums are plotted in power density spectral level versus frequency.

The power density was obtained by measuring the field strength in volts per meter, squaring the result and dividing by the impedance of free space ( $120\pi$ ). The power density in watts per square meter was thus obtained. The power density in watts per square meter was converted to dbm/m<sup>2</sup>. Since most pulsed signals are related to broadband type signals a spectral level of radar signals is usually desired. The power density was divided by the receiver bandwidth of 5 Mc and then converted to dbm/m<sup>2</sup>/Mc. If the power density is desired, 7 db is added to the levels in Figures 6 and 7.

Figure 6 shows the measured spectrum of the AN/FPS-8 compared with a synthesized spectrum based on rectangular and trapezoidal pulses. The program shown in Figure 5 compares the power in a receiver with 5 Mc bandwidth tuned to the radar center frequency to the power in the same receiver as it is tuned in successive 5 Mc increments from the center frequency.

The AN/FPS-8 has a pulse width of 3 microseconds making  $\frac{1}{T}$  equal to  $\frac{1}{3}$  Mc. The first lobe is  $\frac{2}{3}$  Mc wide and each successive lobe is  $\frac{1}{3}$  Mc wide. If a 5 Mc bandwidth receiver were centered on the radar center frequency, it would receive the first lobe and the next six and one half lobes on both sides. Since the computer program is set up for an integral number of lobes, the half lobe on both sides was omitted. The per cent power is affected very little because the eighth lobe contains 0.09 per cent of the power and the first lobe 90.3 per cent of the power. The power in a 5 Mc bandwidth from the 7th through the 21st lobe was then calculated and the number of db down from the power in the receiver centered on the first lobe calculated.

The next interval is centered an additional 5 Mc away and so on. The print out was used to plot the points on Figure 6 which show the synthesized rectangular pulse spectrum. The spectrum based on a trapezoidal pulse is also shown on Figure 6. On the low frequency side of the fundamental frequency the measured spectrum drops into the noise rather quickly. The cause of the drop-off is the attenuation in the waveguide below its cut-off frequency.

The AN/FPS-6 has a pulse length of 2 microseconds which results in  $\frac{1}{T} = 0.5$  Mc. The first lobe is 1 Mc wide and each successive lobe  $\frac{1}{2}$  Mc wide. There are 10 lobes in a 5 Mc receiver bandwidth except when the receiver is centered on the first lobe, in which case it receives the first lobe plus four side lobes on both sides. The computer program summed up ten lobes in each increment and compared the power to that of the first lobe plus the two groups of four side lobes. Figure 7 shows the AN/FPS-6 measured spectrum compared to that based on rectangular and trapezoidal pulses.

Both the AN/FPS-8 and AN/FPS-6 show the drop off on the low side of the fundamental caused by the waveguide cut-off. For the AN/FPS-8 the measured spectrum agrees reasonably close to the theoretical rectangular pulse spectrum near the center frequency. From about 1.44 to 1.88 Gc the measured spectrum jumps below and above the theoretical rectangular pulse spectrum. From 2 Gc to

about 2.5 Gc the spectrum is about an average of 12 db below the theoretical rectangular spectrum which is not bad when little is known about the effect of antenna gain at these frequencies. In the region of the second harmonic from about 2.51 to 3.12 Gc the measured spectrum drops into the noise while the theoretical rectangular pulse spectrum is from 30 to 23 db above the noise. From 3.05 Gc to 4.1 Gc the measured spectrum again appears and is from 7 db above to about 20 db below the theoretical rectangular pulse spectrum. However, some points are very close to the theoretical spectrum. Past 4.10 Gc except for a prominence at 4.3 to 4.4 Gc the measured spectrum drops below the noise except for the harmonics.

The measured spectrum of the AN/FPS-6 is fairly close to that of the theoretical rectangular pulse spectrum out to 3.45 Gc at which place it begins dropping below it and it stays about an average of 10 to 20 below the theoretical rectangular pulse spectrum out to 5.33 Gc where it disappears except for peaks occasionally poking up out of the noise.

The range of measurements covered up to the 7th harmonic of the AN/FPS-8 and 3rd harmonic of the AN/FPS-6. The 3rd and 6th harmonics of the AN/FPS-8 did not show up. In order to synthesize a spectrum some provision for the harmonics should be made. The harmonics show up as peaks because the side energy was well below the noise level of the measuring receiver. A fair estimate of harmonic levels would be 60 db down for the 2nd and 3rd harmonics and 90 db down for the 4th, 5th, 6th and 7th.

The actual radar pulse envelopes have rise and fall times associated with them. An exponential rise and fall pulse leads to a very complicated Fourier analysis and would take up a large amount of computer time to calculate. It was decided to see if a trapezoidal pulse, whose spectrum would be closer to an actual spectrum would be a better fit to the measured spectrum.

The Fourier terms for the power in each line for a carrier modulated with a trapezoidal pulse is as follows:

$$B_n = \left\{ \frac{1}{2 a n^2 \pi^2 f_r \tau} \left[ \cos n \pi f_r \tau - \cos n \pi f_r \tau (1 + 2a) \right] \right\}^2$$

The power in the carrier is:

$$B_0 = f_r \tau (1 + a)^2$$

where  $f_r$  is the pulse repetition frequency and  $\tau$  the pulse length and  $a$  is the fraction of the pulse width comprising the rise and fall time. Figure 8 illustrates the trapezoidal pulse.  $n$  is the line number starting with zero for the carrier.

These formulas give the average power in each line based on a normalized peak power of one. The normalized fractional power is obtained by dividing these values by the duty cycle of  $f_r \tau (1 + a)$ .

The fractional powers are obtained from the following formulas:

$$B_n' = \frac{1}{f_r \tau (1+a)} \left\{ \frac{1}{2 a n^2 \pi^2 f_r \tau} [\cos n \pi f_r \tau - \cos n \pi f_r \tau (1+2a)] \right\}^2$$

$$P_o' = \frac{[f_r \tau (1+a)]^2}{f_r \tau (1+a)} = f_r \tau (1+a)$$

It was determined in the same manner as that for the rectangular pulse that the power in each lobe for a trapezoidally modulated wave was almost constant with the number of lines per lobe. The change after  $\frac{1}{f_r \tau} = 4$  was very small. Again  $\frac{1}{f_r \tau}$  was chosen to be 4.

Unfortunately, a photograph of the pulse envelope of the two radars was not taken. The question as to how long the rise time should be had to be resolved. In the formula "a" is the fraction of the flat portion of the pulse constituting the rise and fall time. Various values were tried when "a" is large the trapezoidal spectrum falls below that of a rectangular pulse spectrum rather rapidly as the frequency departs from the carrier as "a" decreases, the spectrum approaches that of a rectangular pulse spectrum. It was found that after "a" reaches 0.001, a further decrease results in a small change in the level of the spectrum. Therefore, an "a" of 0.001 was chosen.

Programs were written to generate the spectrum based on the trapezoidally modulated carrier with an "a" of 0.001 for a receiver bandwidth of 5 Mc and for 3 lobes and 5 lobes per Mc. The spectrums for the rectangular and trapezoidal pulses coincide close to the center frequency. It is interesting to note that the spectrum based on the trapezoidal pulse falls and rises and falls several times before going below the bottom of the scale. The spectrum of the AN/FPS-6 follows the trapezoidal pulse spectrum closer than it follows the rectangular pulse spectrum. The AN/FPS-6 follows the trapezoidal pulse spectrum more closely to about 3 Gc but from 3 to 4.12 Gc it follows the rectangular pulse spectrum more closely. Above 4.12 Gc the trapezoidal spectrum is below the bottom of the scale and the measured spectrum is below the noise level except for the 4th, 5th and 7th harmonic and few peaks protruding above the noise level. It seems as if the trapezoidal pulse spectrum is a better fit above 4.12 Gc. The reasons for those differences are unknown and it would be interesting to compare more spectrum signatures with theoretical spectrums.

## II. CONCLUSIONS

For modeling purposes a synthesized spectrum can be used as a first approximation to a radar spectrum. However, the differences between measured and theoretical values will have to be resolved by comparing more measured spectrums with theoretical spectrums.

Since there was a fair agreement between measured and theoretical values, it seems as if the spectrum measurements have produced valid data. The effect of antenna gain and ground reflection on the measured spectrums will have to be resolved by further measurements.

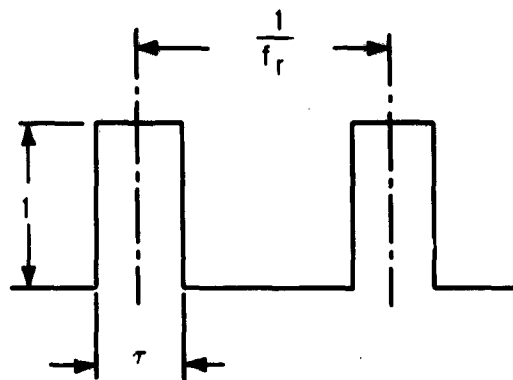


FIG. 1 - RECTANGULAR MODULATION ENVELOPE

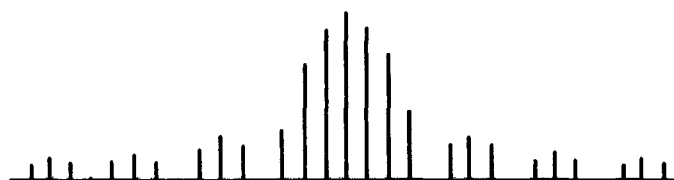


FIG. 2 - ABSOLUTE AMPLITUDE OF SPECTRAL LINES

```

0200      BAC-220 ON LINE H&P VERSION      2/1/62
0200      DUMPS
0400      INTEGER N,M,F$
0400      ARRAY Y(8)$
0400      F=2$
0402      PI=3.1415927$
0404      L1.. BEGIN X=0$ FOR N=(1,1,F=1)$
0421      X=X+(SIN(N.PI/F)/N.PI)*2 ENDS
0450      A=(2F.X)+(1.0/F)$
0465      FOR M=(1,1,8)$ BEGIN Y(M)=0$
0479      FOR N=((M,F)+1,1,(M,F)+F=1)$
0499      Y(M)=Y(M)+(F)(SIN(N.PI/F)/N.PI)*2 ENDS
0535      WRITE (SSODS,FORM)$
0543      OUTPUT ODS (F,A,(FOR M=(1,1,8)$ Y(M)))$
0570      FORMAT FORM (I2,B1,I11,R2,B(I11,R2),W)$
0580      F=F+1$
0583      IF F GT 99$ GO TO L2$
0589      GO TO L1$
0590      L2.. FINISH$
COMPILED PROGRAM ENDS AT 0597
PROGRAM VARIABLES BEGIN AT 4463

```

FIG. 3 - COMPUTER PROGRAM AND PRINT OUT SHOWING FRACTIONAL POWER IN FIRST NINE LOBES AS A FUNCTION OF  $1/f, T$





63	5000282247	492557087	482355445	4841490051	4825139441	4816801784	4812014545	4790220543	4770213747
64	5000282248	492557088	482355447	4841490054	4825139442	4816801786	4812014546	4790220544	4770213748
65	5000282249	492557089	482355448	4841490057	4825139443	4816801787	4812014547	4790220545	4770213749
66	5000282250	492557090	482355449	4841490060	4825139444	4816801788	4812014548	4790220546	4770213750
67	5000282251	492557091	482355450	4841490063	4825139445	4816801789	4812014549	4790220547	4770213751
68	5000282252	492557092	482355451	4841490066	4825139446	4816801790	4812014550	4790220548	4770213752
69	5000282253	492557093	482355452	4841490069	4825139447	4816801791	4812014551	4790220549	4770213753
70	5000282254	492557094	482355453	4841490072	4825139448	4816801792	4812014552	4790220550	4770213754
71	5000282255	492557095	482355454	4841490075	4825139449	4816801793	4812014553	4790220551	4770213755
72	5000282256	492557096	482355455	4841490078	4825139450	4816801794	4812014554	4790220552	4770213756
73	5000282257	492557097	482355456	4841490081	4825139451	4816801795	4812014555	4790220553	4770213757
74	5000282258	492557098	482355457	4841490084	4825139452	4816801796	4812014556	4790220554	4770213758
75	5000282259	492557099	482355458	4841490087	4825139453	4816801797	4812014557	4790220555	4770213759
76	5000282260	492557100	482355459	4841490090	4825139454	4816801798	4812014558	4790220556	4770213760
77	5000282261	492557101	482355460	4841490093	4825139455	4816801799	4812014559	4790220557	4770213761
78	5000282262	492557102	482355461	4841490096	4825139456	4816801800	4812014560	4790220558	4770213762
79	5000282263	492557103	482355462	4841490099	4825139457	4816801801	4812014561	4790220559	4770213763
80	5000282264	492557104	482355463	4841490102	4825139458	4816801802	4812014562	4790220560	4770213764
81	5000282265	492557105	482355464	4841490105	4825139459	4816801803	4812014563	4790220561	4770213765
82	5000282266	492557106	482355465	4841490108	4825139460	4816801804	4812014564	4790220562	4770213766
83	5000282267	492557107	482355466	4841490111	4825139461	4816801805	4812014565	4790220563	4770213767
84	5000282268	492557108	482355467	4841490114	4825139462	4816801806	4812014566	4790220564	4770213768
85	5000282269	492557109	482355468	4841490117	4825139463	4816801807	4812014567	4790220565	4770213769
86	5000282270	492557110	482355469	4841490120	4825139464	4816801808	4812014568	4790220566	4770213770
87	5000282271	492557111	482355470	4841490123	4825139465	4816801809	4812014569	4790220567	4770213771
88	5000282272	492557112	482355471	4841490126	4825139466	4816801810	4812014570	4790220568	4770213772
89	5000282273	492557113	482355472	4841490129	4825139467	4816801811	4812014571	4790220569	4770213773
90	5000282274	492557114	482355473	4841490132	4825139468	4816801812	4812014572	4790220570	4770213774
91	5000282275	492557115	482355474	4841490135	4825139469	4816801813	4812014573	4790220571	4770213775
92	5000282276	492557116	482355475	4841490138	4825139470	4816801814	4812014574	4790220572	4770213776
93	5000282277	492557117	482355476	4841490141	4825139471	4816801815	4812014575	4790220573	4770213777
94	5000282278	492557118	482355477	4841490144	4825139472	4816801816	4812014576	4790220574	4770213778
95	5000282279	492557119	482355478	4841490147	4825139473	4816801817	4812014577	4790220575	4770213779
96	5000282280	492557120	482355479	4841490150	4825139474	4816801818	4812014578	4790220576	4770213780
97	5000282281	492557121	482355480	4841490153	4825139475	4816801819	4812014579	4790220577	4770213781
98	5000282282	492557122	482355481	4841490156	4825139476	4816801820	4812014580	4790220578	4770213782
99	5000282283	492557123	482355482	4841490159	4825139477	4816801821	4812014581	4790220579	4770213783

THE PROGRAM IS AS FOLLOWS:

INTEGER N,M,A\$

M=2\$

PI=3.1415927\$

A=1\$

ONE=0.5000000\$

TWO=1.0000000\$

THREE=0.5000000\$

$X = 0.25 + (8.0) \left( \frac{ONE}{(PI)^2} \right) + \left( \frac{TWO}{(2PI)^2} \right) + \left( \frac{THREE}{(3PI)^2} \right)$ \$

WRITE (\$\$ODS1,FORM1)\$

OUTPUT ODS1 (A,X)\$

FORMAT FORM1 (14,B2,111,W)\$

L1..FOR N=(4M)-3\$ BEGIN Y=0\$

$Y = 4 \left( \frac{ONE}{(N \cdot PI)^2} \right) + \left( \frac{TWO}{(N+1)PI^2} \right) + \left( \frac{THREE}{(N+2)PI^2} \right)$  ENDS\$

WRITE (\$\$ODS2,FORM2)\$

OUTPUT ODS2 (M,Y)\$

FORMAT FORM2 (14,B2,111,W)\$

M=M+1\$

IF M GTR 5000\$ GO TO L2\$

GO TO L1\$

L2..FINISH\$

FIG. 4 - COMPUTER PROGRAM

```

0200 SAC-220 ON LINE MAP VERSION 2/1/62
0201 DUMP 5
0202 INTEGER M,N,A,P,SS
0203 ARRAY Y(7),Z(16)S
0204 P1=3.1415927S
0205 ONE=0.5000000S
0206 TWO=1.0000000S
0207 THREE=0.5000000S
0208 A=9S
0209 S=2S
0210 X=0.29*(0.1*(ONE/(P1+2))*(TWO/(SP1+2))*(THREE/(3P1+2)))S
0211 FOR M=(2,1,7)S DO IN N=(4N)-3S
0212 Y(M)=Y(M+1)+4*(ONE/(N:P1+2))*(TWO/((N+1)P1+2))*(THREE/((N+2)P1+2))ENDS
0213 Q=2.Y(7).X8
0214 WRITE (SS,M)S
0215 FORMAT MHD (INTERVAL NUMBER,02,FRACTIONAL POWER,02,RELATIVE DBS,M)
0216 S
0217 L1=FOR P=(2,1,16)S BEGIN N=((4A)-3+4(P-2))S
0218 Z(P)=Z(P+1)+4*(ONE/(N:P1+2))*(TWO/((N+1)P1+2))*(THREE/((N+2)P1+2))ENDS
0219 V=LOG10(Z(16))S
0220 T=4.3429160VS
0221 WRITE (SS,DBS,FORM)S
0222 OUTPUT DBS(9,Z(16),T)S
0223 FORMAT FORM (M9.16,M7:11,09,M9:2,M)S
0224 S=0+1S
0225 FOR P=(1,1,16)S Z(P)=0S
0226 A=A+1S
0227 IF A GT 21000S GO TO L2S
0228 GO TO L1S
0229 L2=FINISH
0230 COMPILED PROGRAM ENDS AT 0230
0231 PROGRAM VARIABLES BEGIN AT 4000

```

FIG. 5 - PROGRAM FOR COMPUTING RELATIVE POWER IN RECEIVER OF 5 MC BANDWIDTH IN STEPS OF 5 MC BASED ON 3 LOSES PER MC

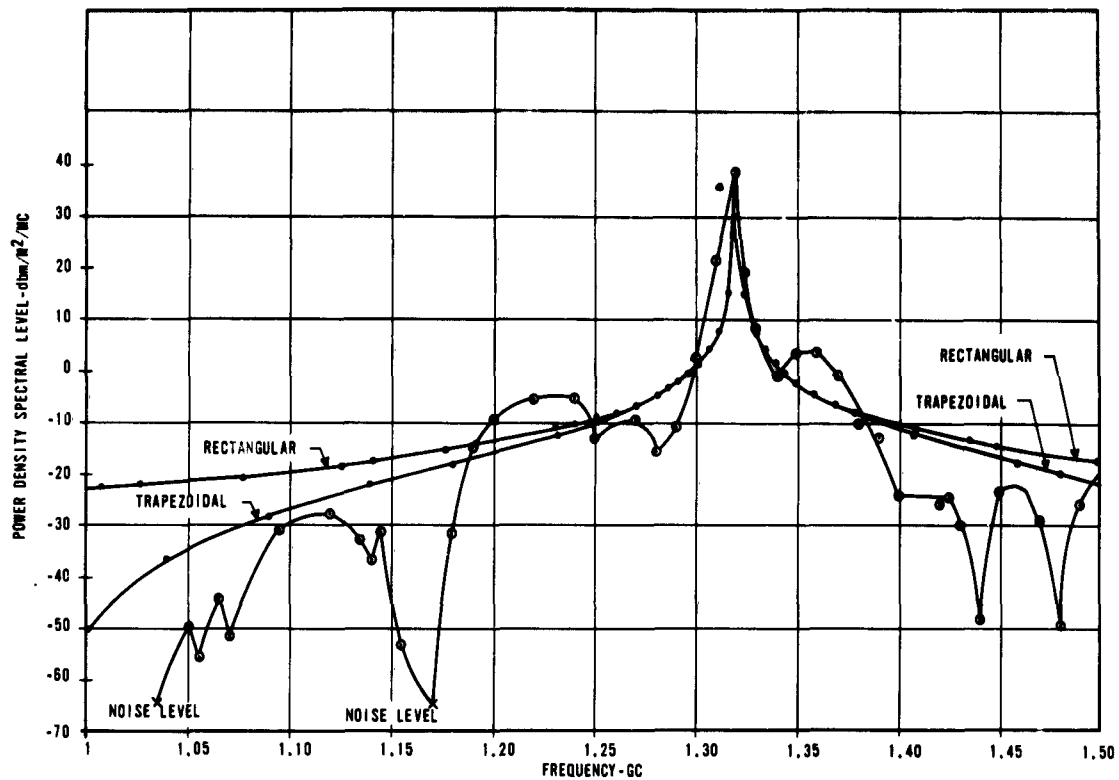


FIG. 8 - OUTPUT SPECTRUM OF AN/FPS-8 MEASURED AT 5340 FEET WITH RECEIVING ANTENNA HORIZONTALLY POLARIZED

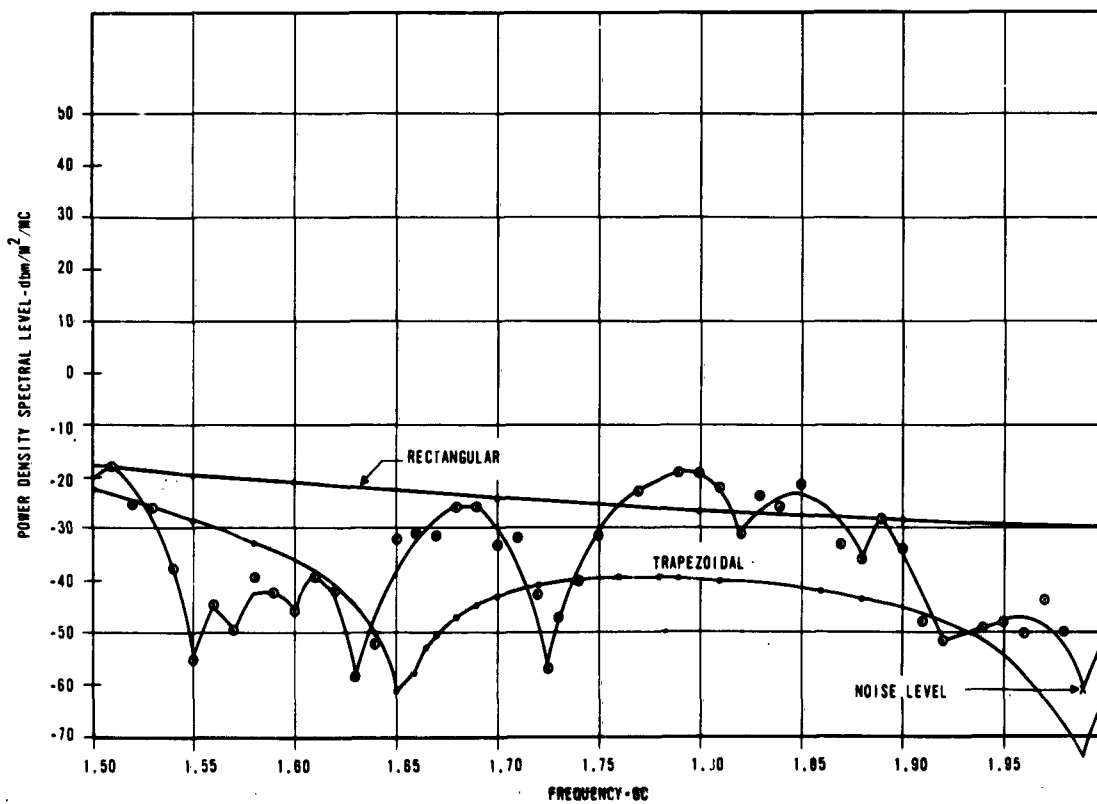
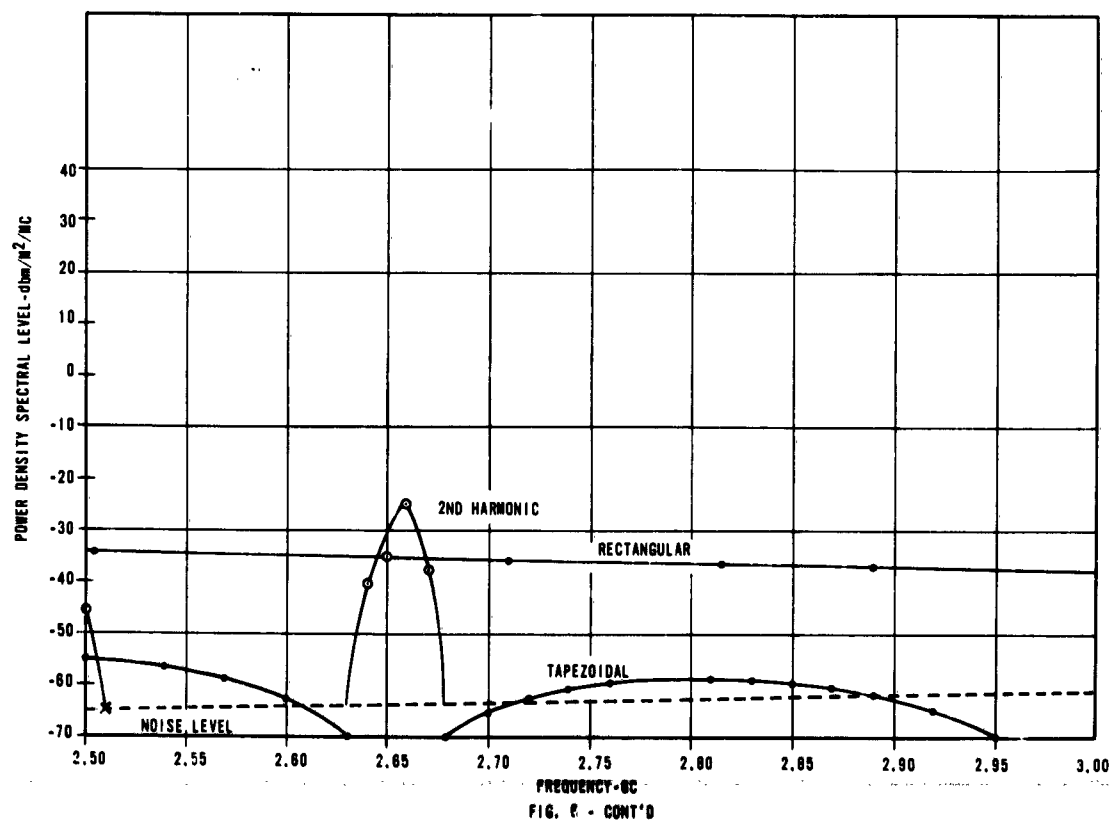
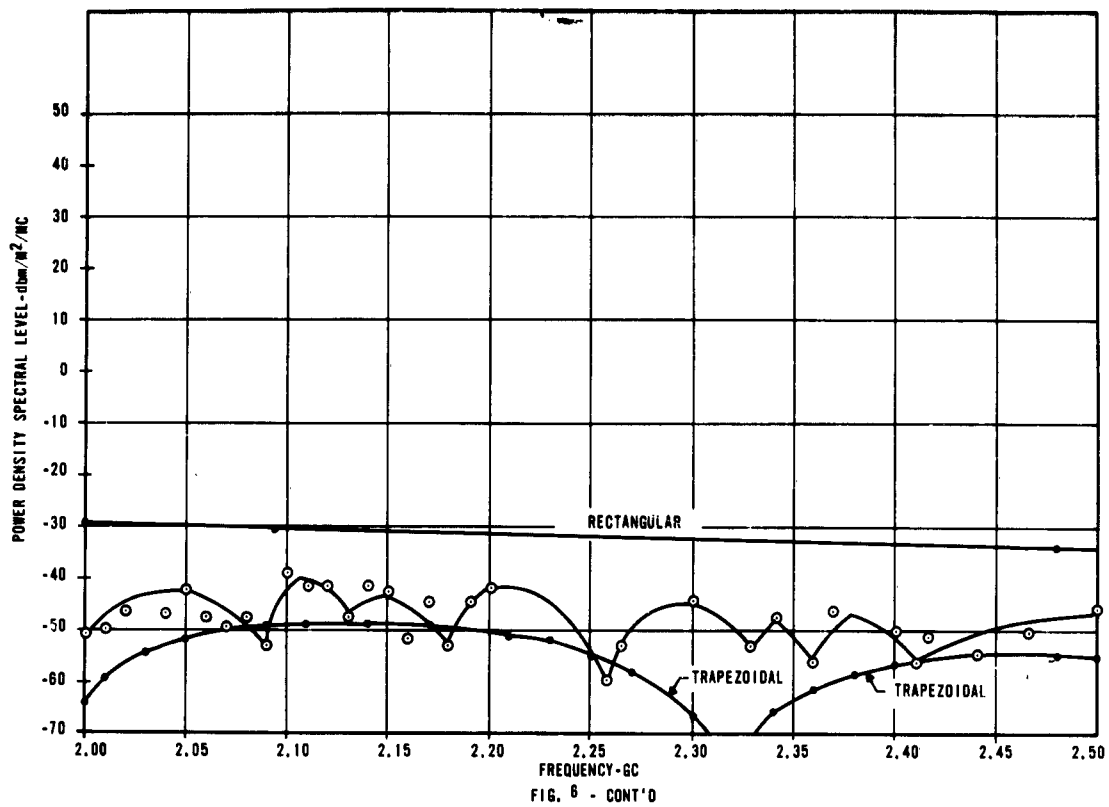
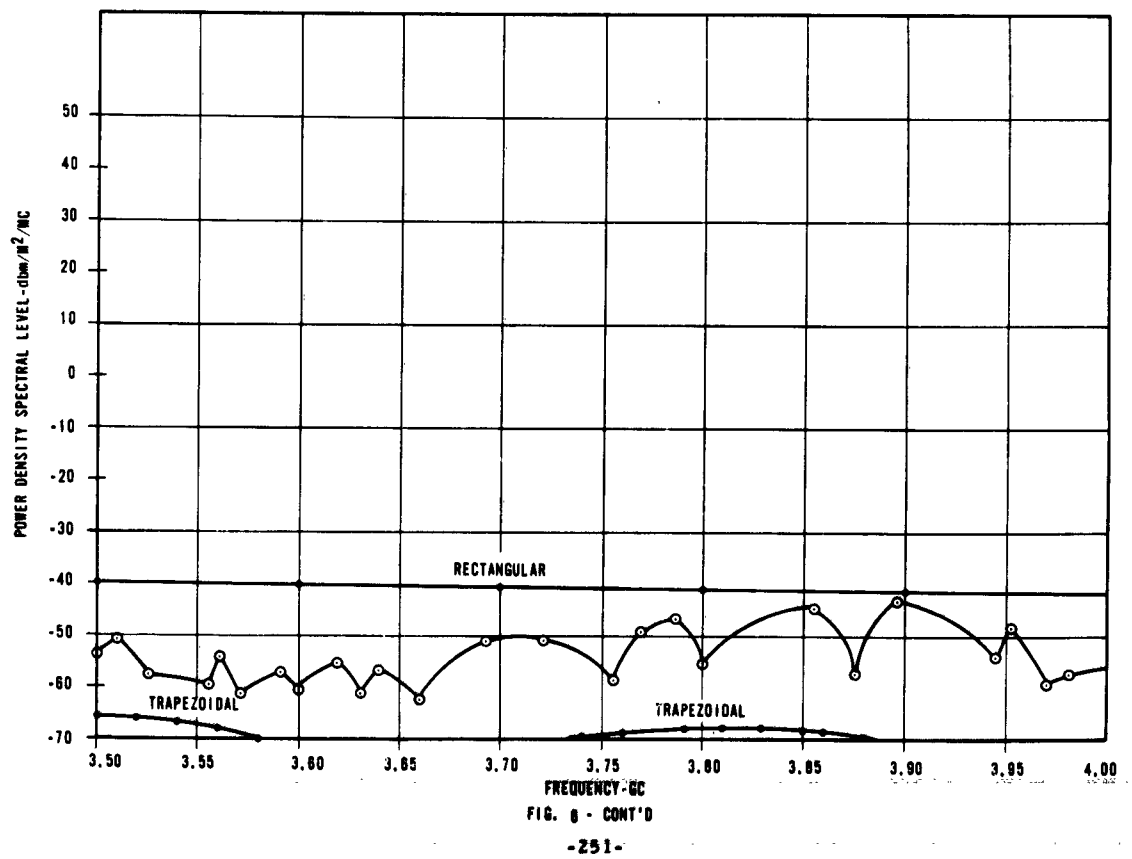
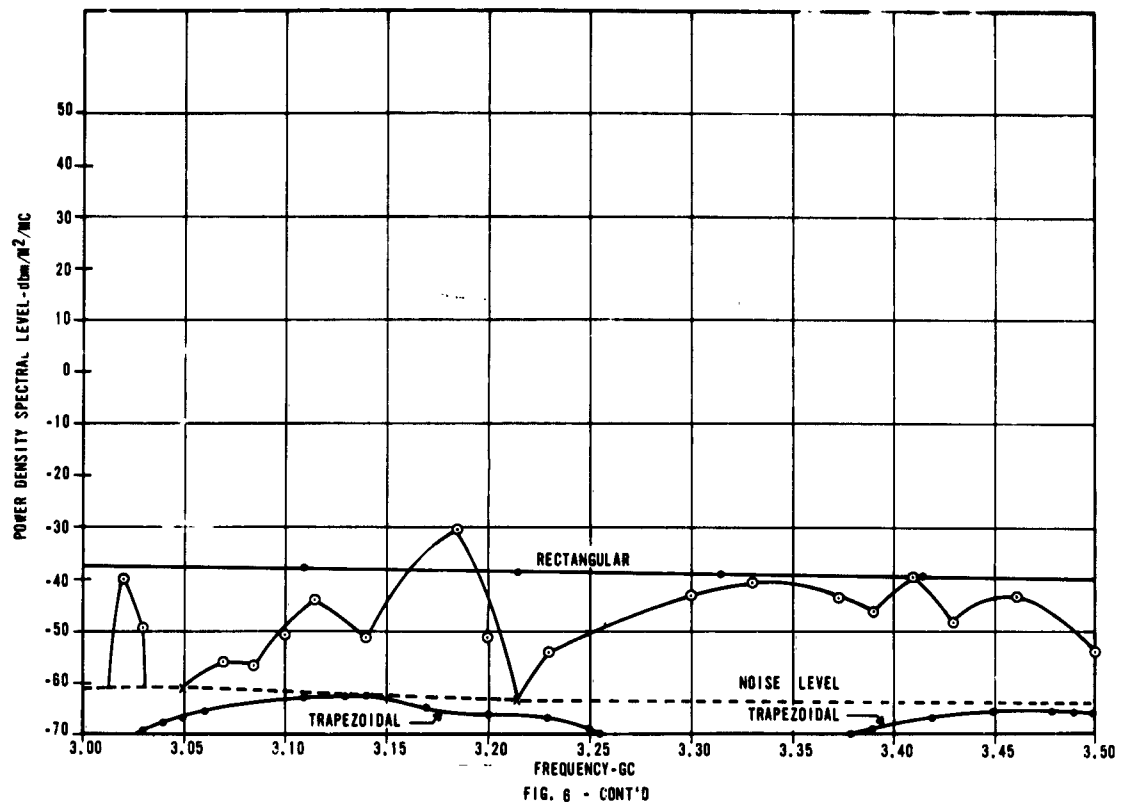


FIG. 8 - CONT'D





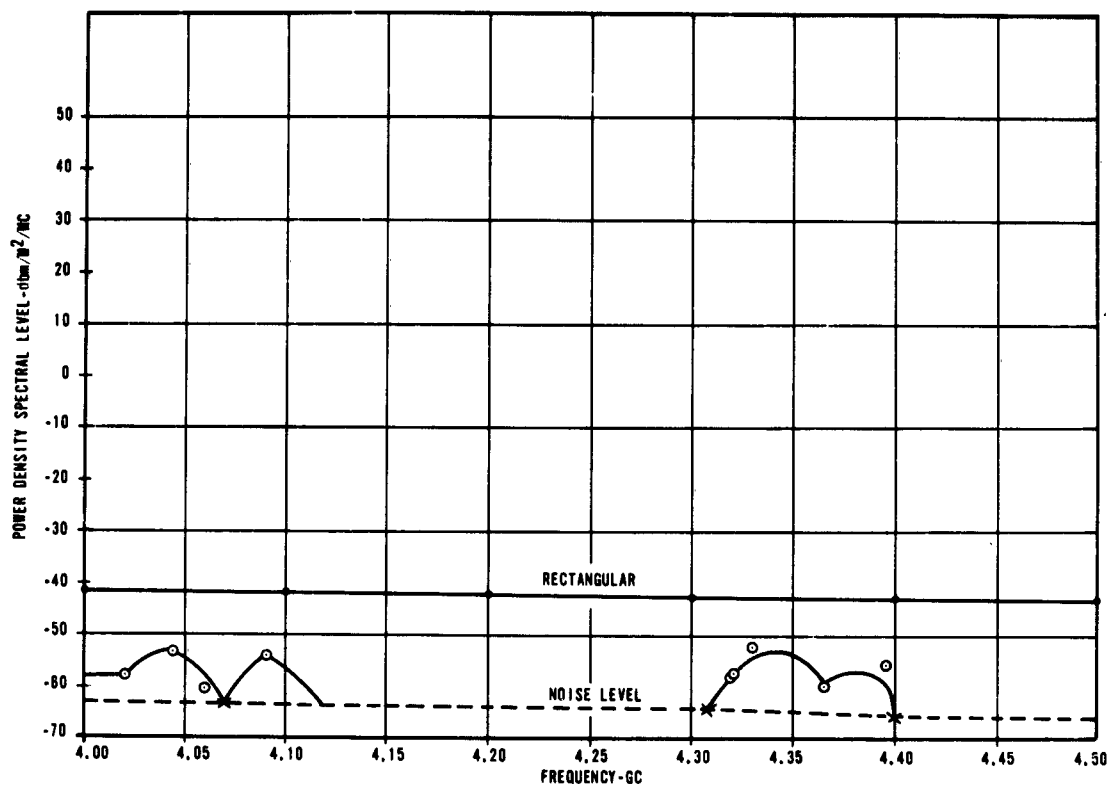


FIG. 8 - CONT'D

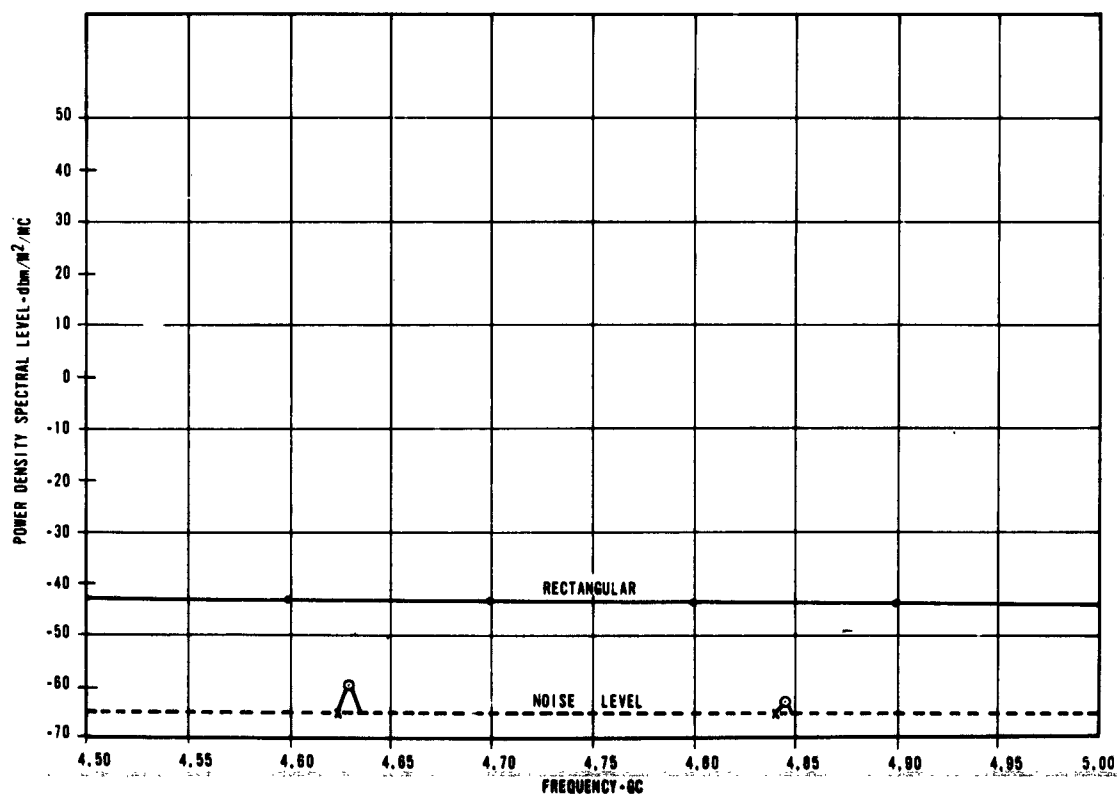
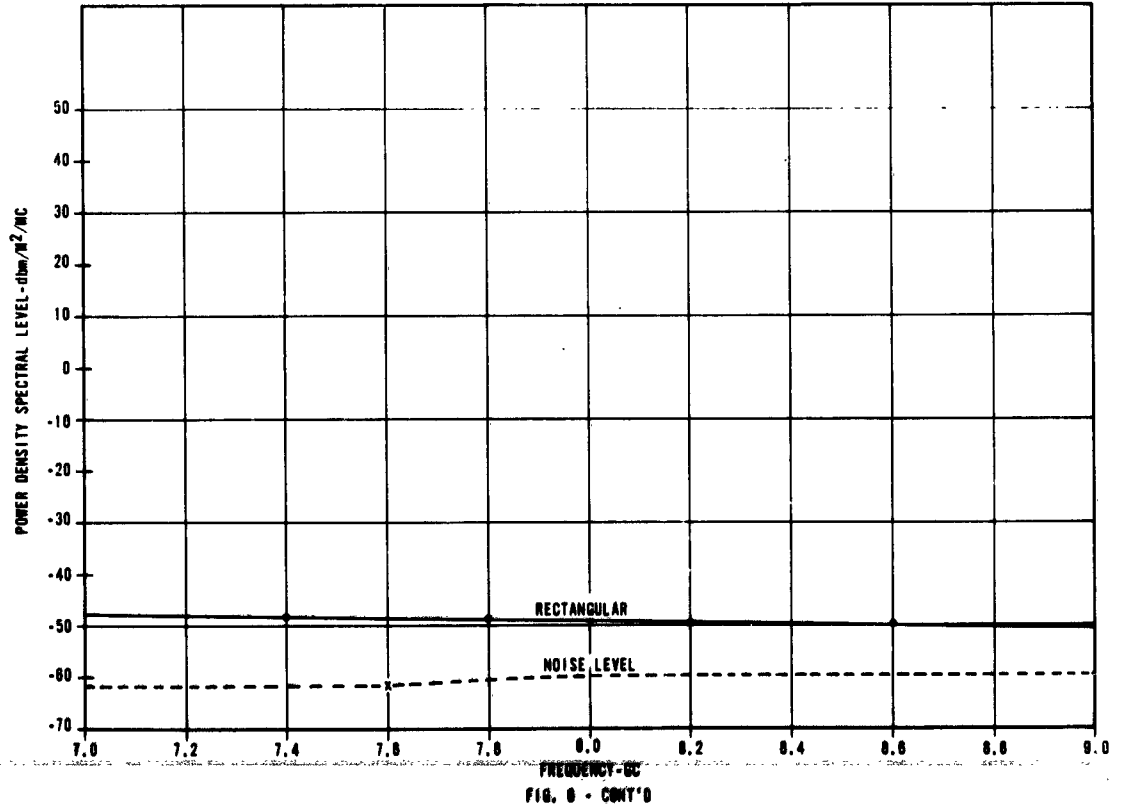
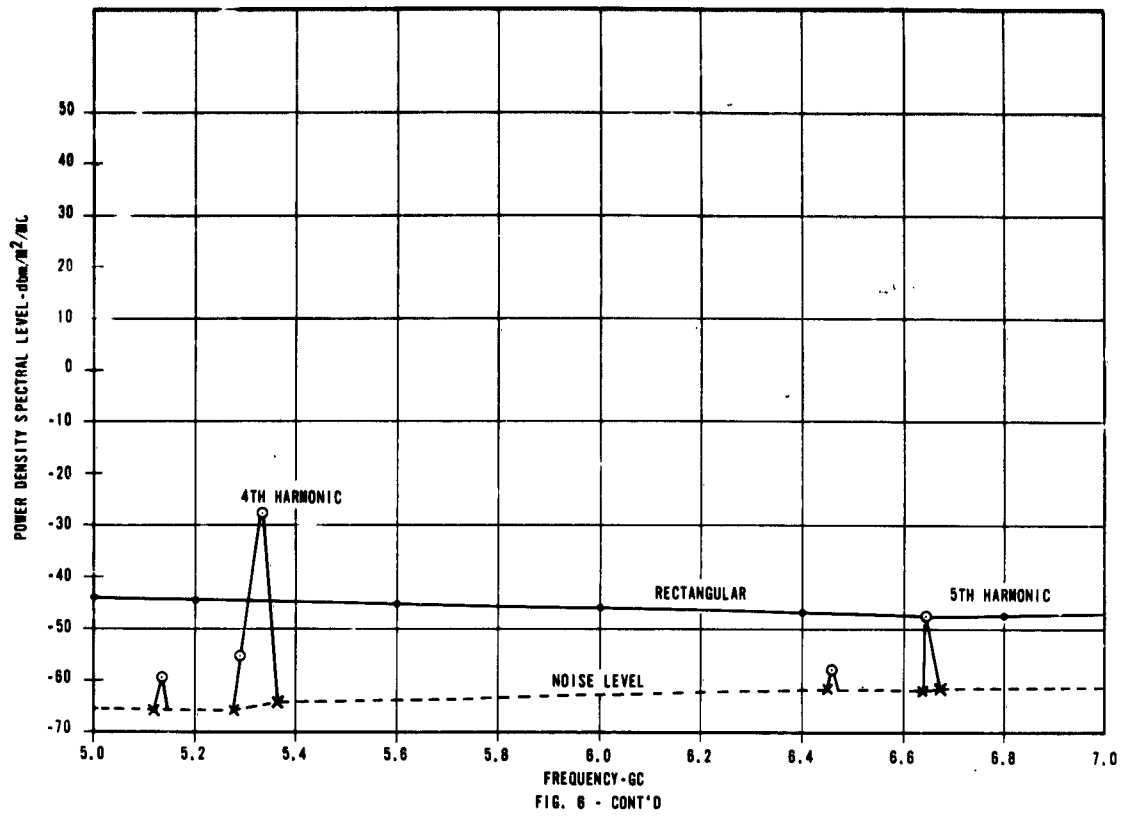


FIG. 8 - CONT'D





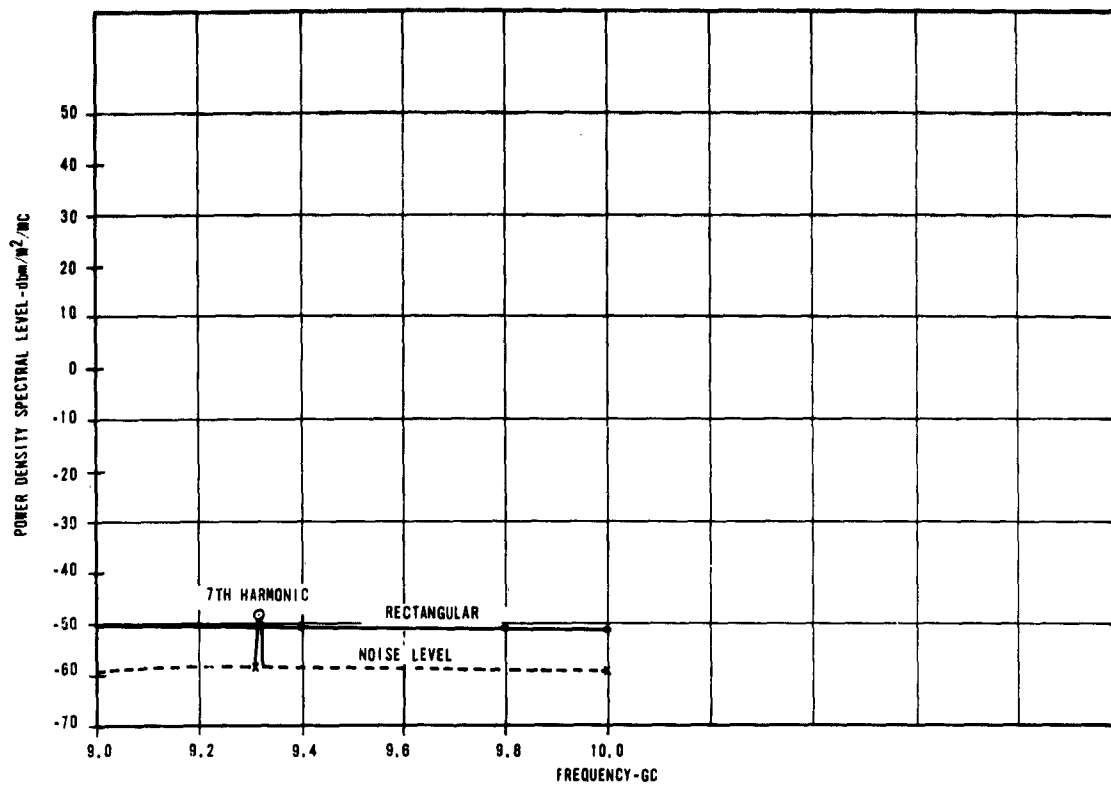


FIG. 8 - CONT'D

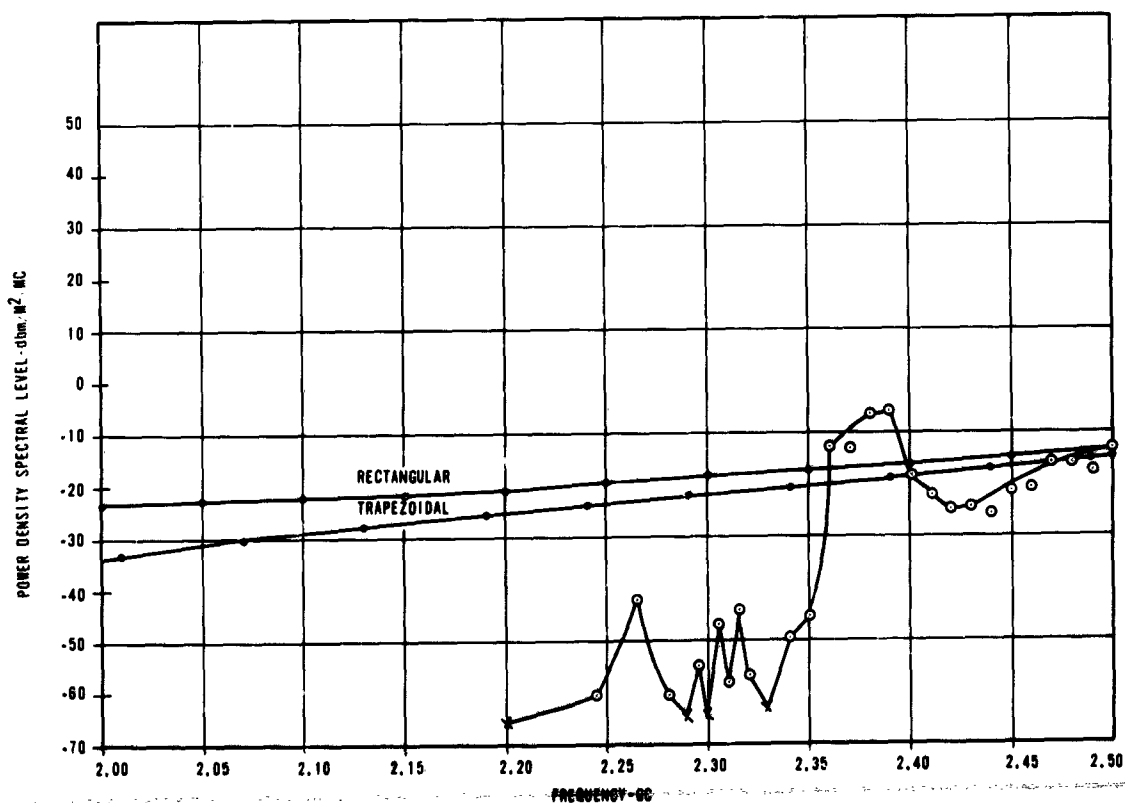
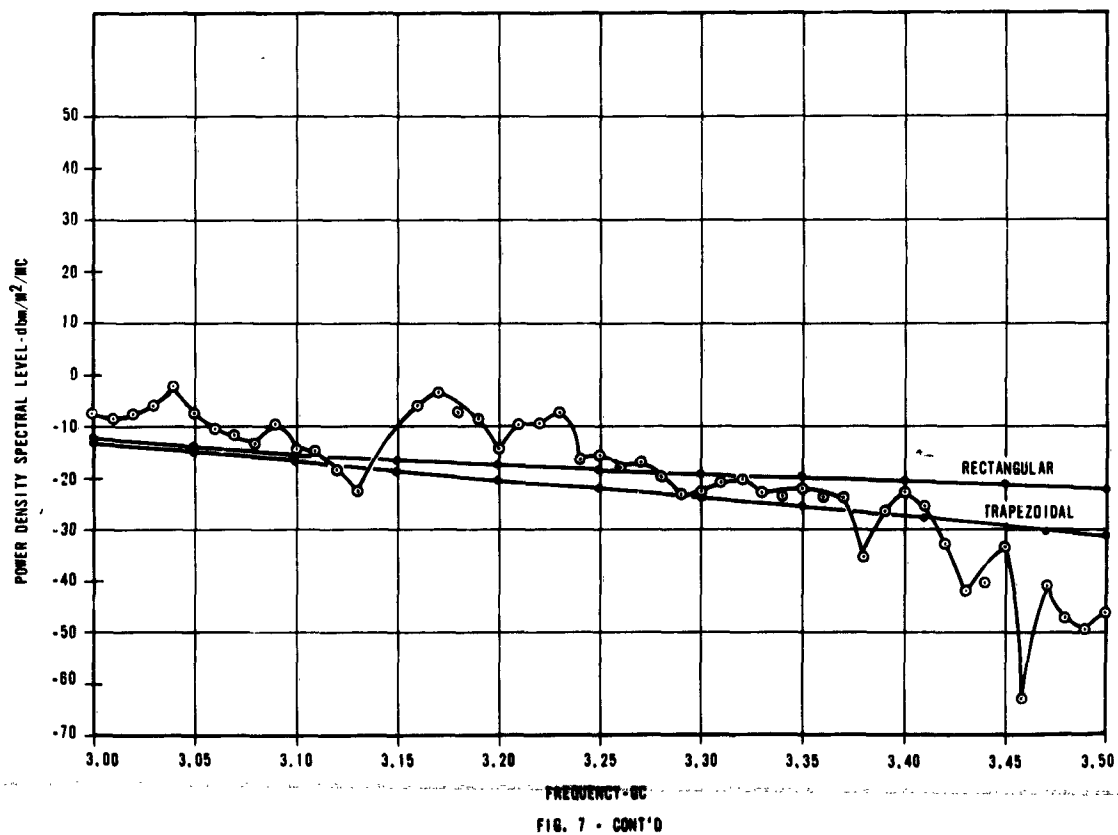
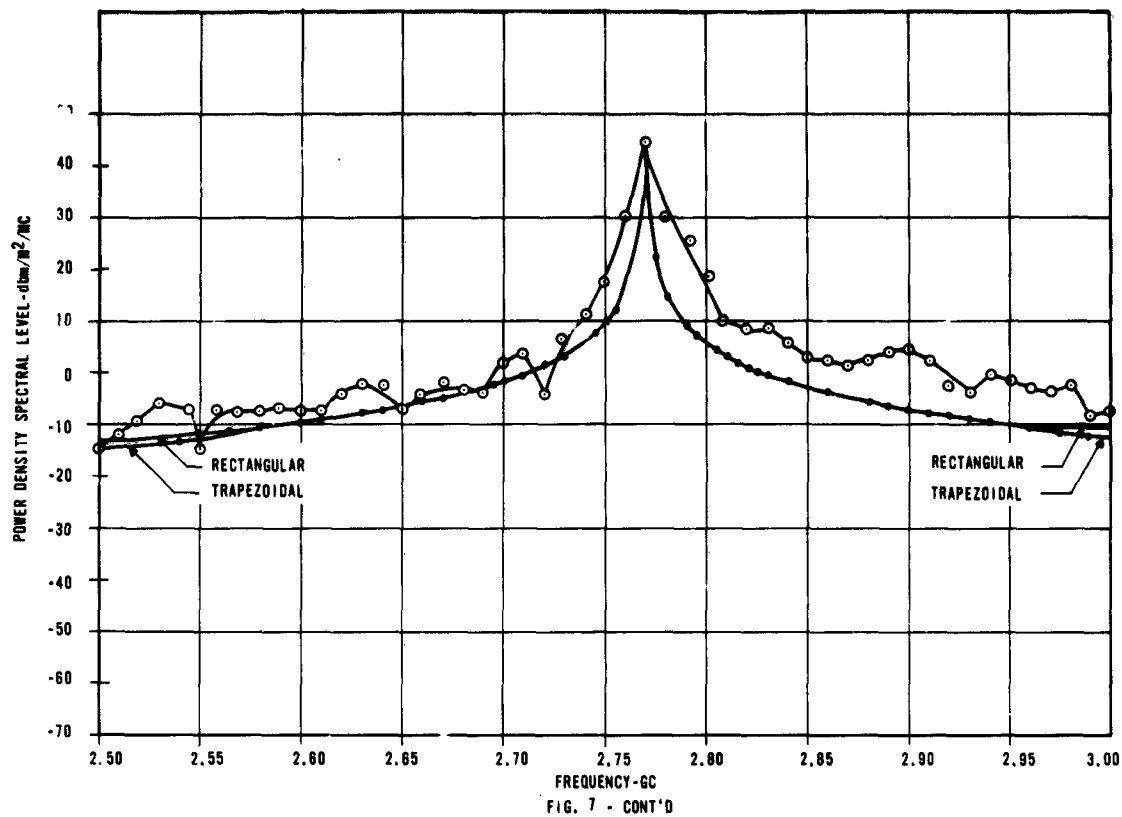
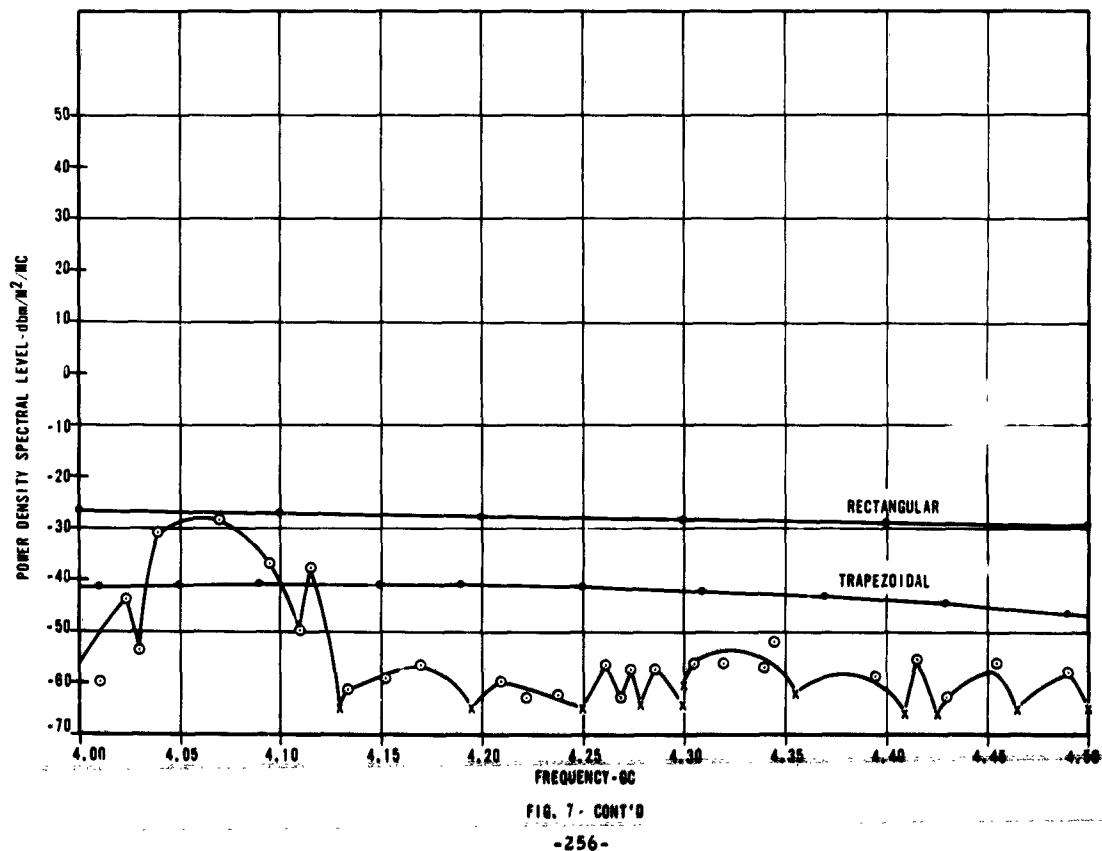
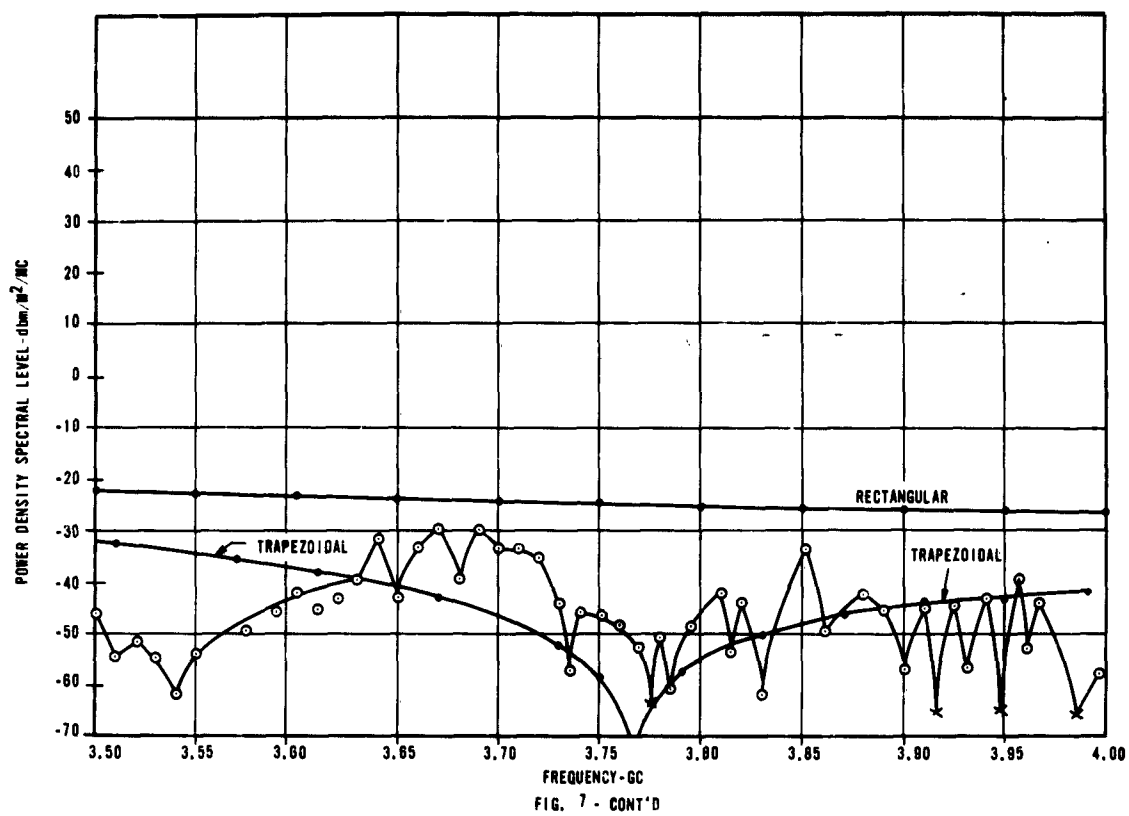


FIG. 7 - OUTPUT SPECTRUM OF AN/FPS-6 MEASURED AT 5105 FEET RECEIVING ANTENNA VERTICALLY POLARIZED





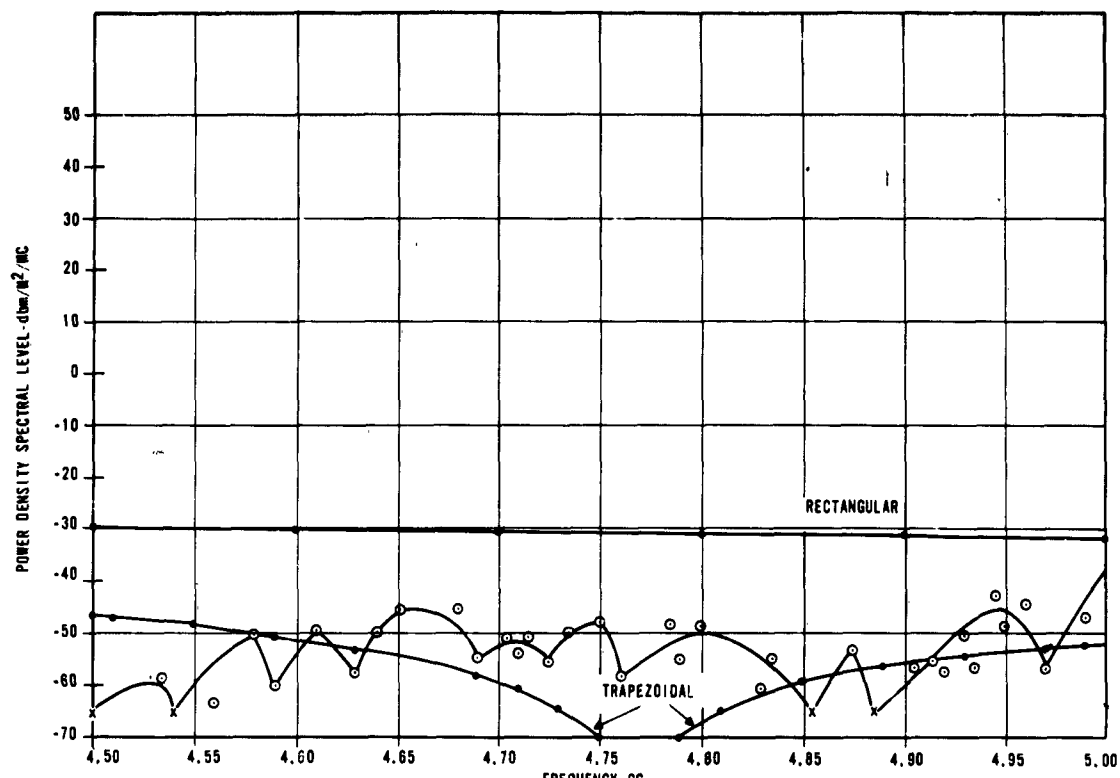


FIG. 7 - CONT'D

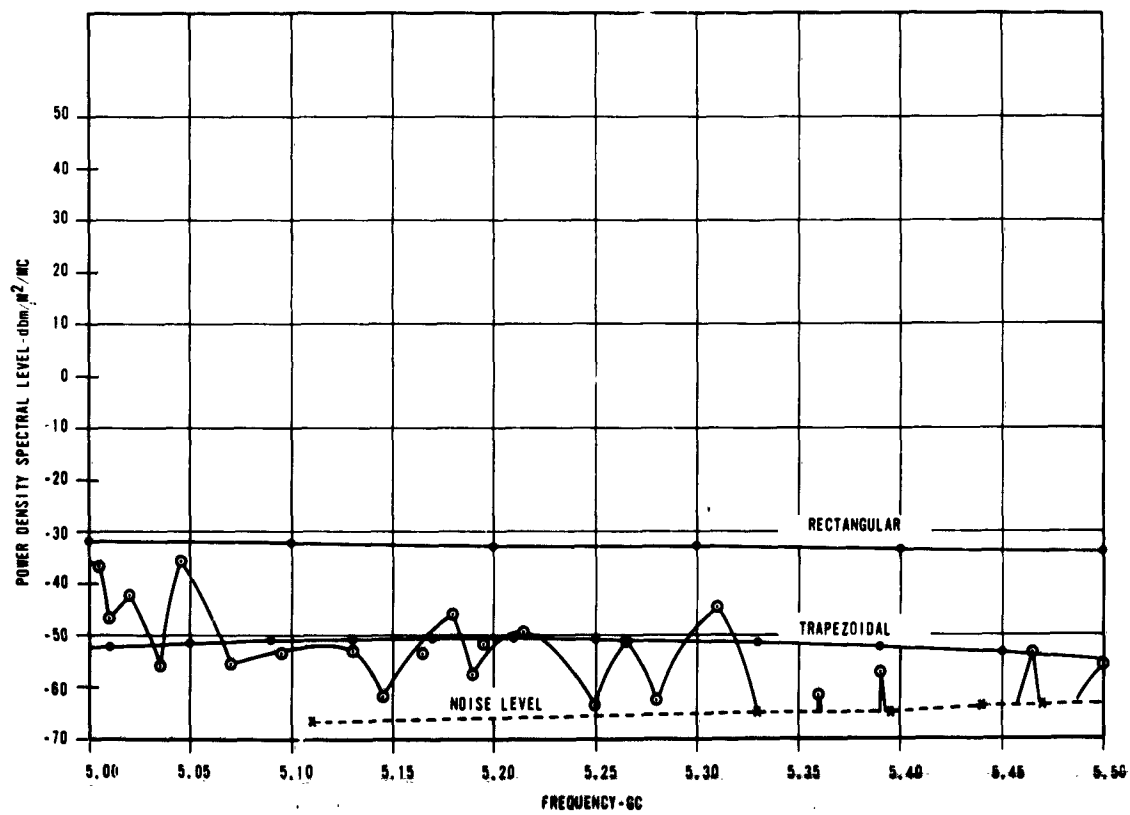
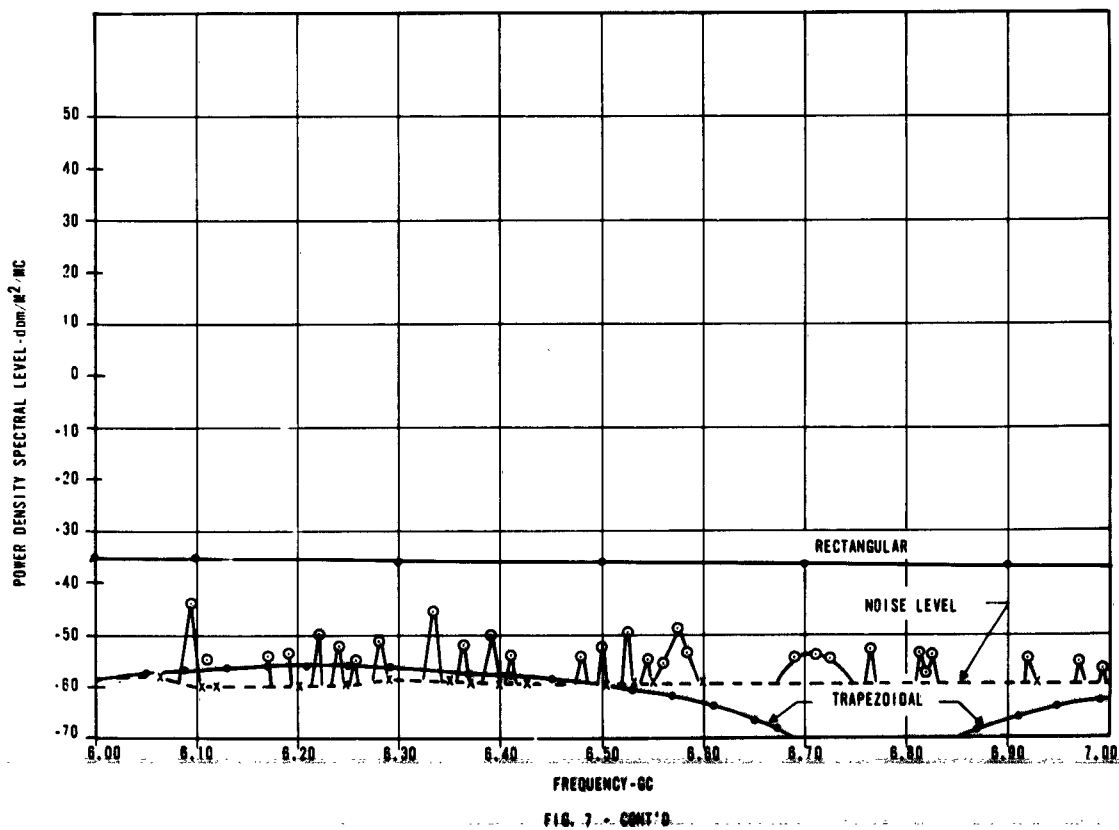
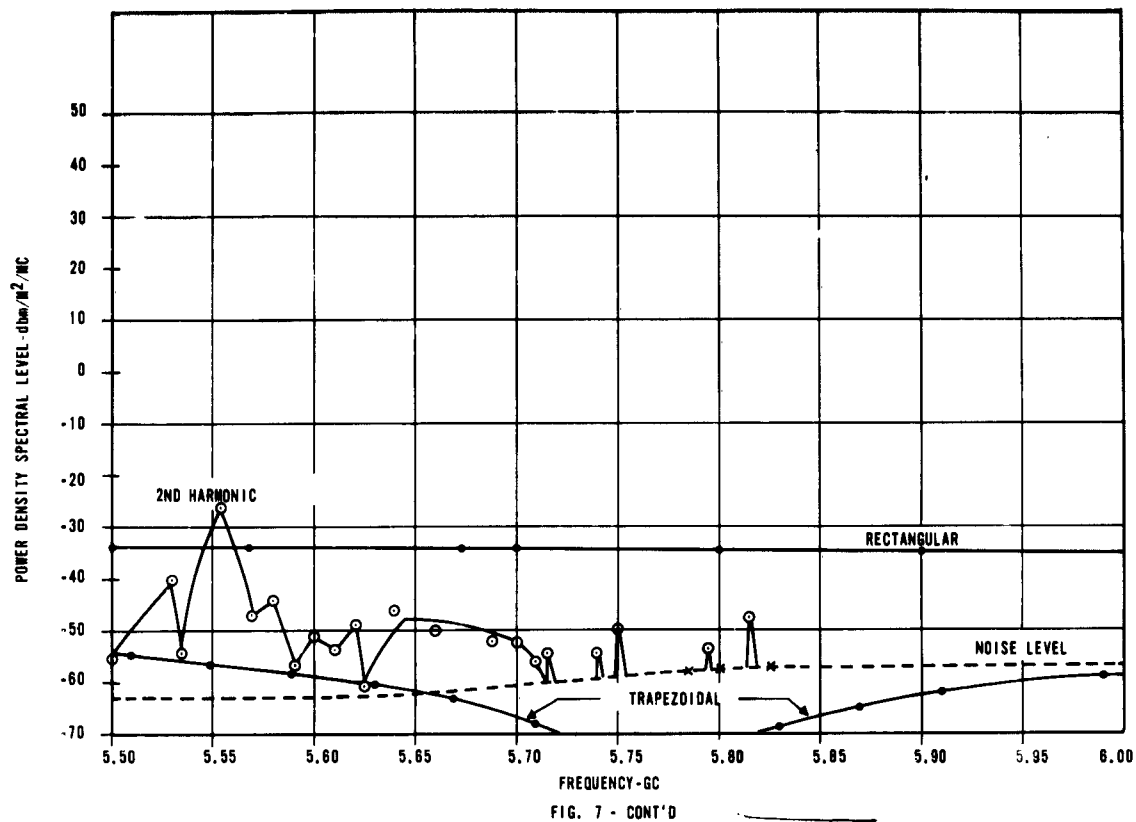
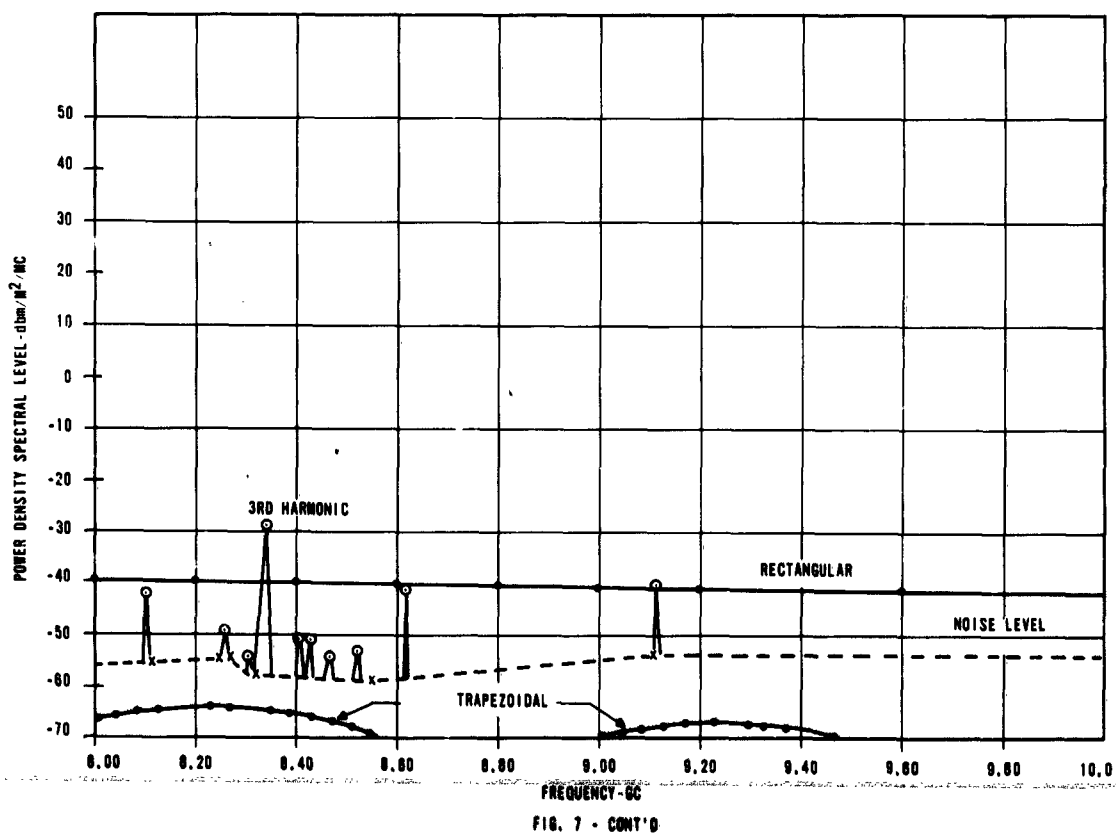
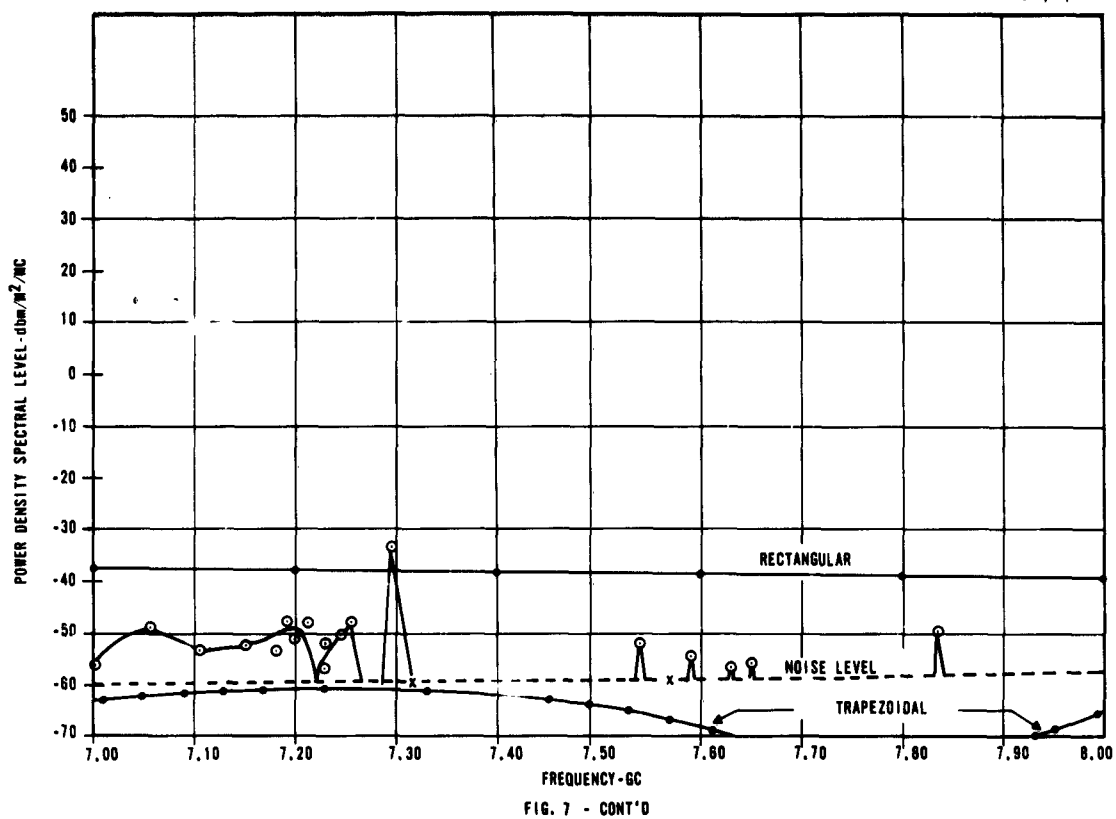


FIG. 7 - CONT'D





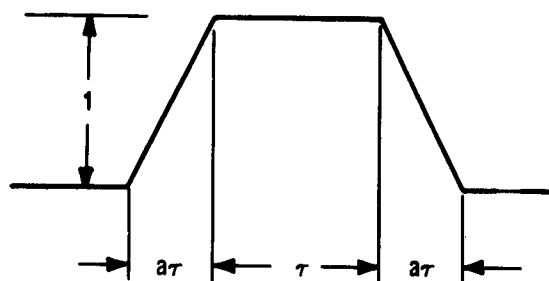


FIG. 8 - TRAPEZOIDAL PULSE



## ADVANCED RECEIVER MODEL SYSTEM "ARMS"

D. H. Cook, J. L. Pierzga, and F. N. Leahy  
IIT Research Institute  
Electromagnetic Compatibility Analysis Center  
Annapolis, Maryland

Abstract. - An advanced receiver model system (ARMS) has been developed to provide the Analysis Center with the capability of handling complex interference problems with a fast reaction time. This capability has been initially planned as a manual technique using the computer as a tool for providing input data to the system. The means of obtaining receiver selectivity curves, spurious response levels and shapes of the spurious responses will be discussed.

Details of the method for handling any special circuits included in the receiver (over a normal matched filter receiver) will be described. The methods used for treating a pulse compression receiver will be presented as an example.

The type of outputs which can be provided by the ARMS will be discussed. The plans for systems and output degradation criteria will be presented.

### I. INTRODUCTION

The development of the "ARMS" technique for interference prediction results from a need for the rapid solution of interference problems that may vary in some significant detail from those presently programmed for computer solution. This variation may be anything from a requirement for data not in the normal input files to the requirement for a special receiver configuration that has not yet been programmed. Another and pressing need is for the solution of interference problems involving small numbers of transmitters and single to small numbers of receivers. These problems need not involve the use of high speed computer time. In fact their solution can often be accomplished manually in less time than is required for pre-processing and computer scheduling.

### II. ADVANCED RECEIVER MODEL SYSTEM "ARMS"

Figure 1 shows a simplified logic diagram of the system. The key to the flexibility of the ARMS lies in the manual control for handling each of the assigned problems. The procedure for handling each problem is determined by analyzing the prediction requirements and then, from a knowledge of the victim receivers, the development of a flow diagram for both information requirements and step by step mathematical computations. The program control schedules inputs, outputs, and sequential operations. To a large extent the operations are determined by the equipment models. This function is shown as Block 1 of Figure 1. It is a manual operation in the same sense that a computing program is developed manually.

The data file shown as Block 2 includes all sources such as equipment catalogues, EFES files, engineering reports, technical manuals, design specifications, nominal characteristics file, equipment model catalogues, pseudo data, and any other sources and synthesis techniques necessary to obtain the inputs required for the computations that follow. The pre-processing operation of Block 3 covers the arrangement of the input data and the coding, if required for computer operations.

The form of the interference power computations as shown in Block 4 is determined by the prediction computation. It may be either a power level or an interference to noise ratio with associated pulse rates. This computation may be a computer program such as Search Radar Prediction Program, giving an INR and pulse rate, the Master Simulation System Program 1, the Master Simulation System Program 2 or it may be a manual operation as explained in Section 5.

The output of the power computation block is shown as Block 5, a switching or branch point. This indicates the capability of using any of the mathematical models that have been developed or will be developed to represent special receiver configuration or functions.

A few examples (see Block 6) are F.T.C., S.T.C., M.T.I., Video Integrator, Correlator, Log Receiver, Pulse Compression, and DFX. Since several of these models may be used together it is necessary that their computation be scheduled and this is done as a program control function after analyzing the prediction requirements and the equipment model.

The output of Block 6 is in the same form as the output of Block 4 either a power level or an INR associated with a pulse rate. This output will have been modified by the mathematical representation of any special circuitry and be in the correct form for input to the prediction model of Block 7.

The specific prediction output from ARMS will depend upon the problem presented for solution. It will represent the results of the problem analysis and may take any of several different forms such as frequency assignments, system degradation, distance separation from interfering sources, and optimum power assignments among others.

There is however a general approach to the ARMS prediction that will better illustrate this phase of the program. This is shown in Figure 2. This can be used to define the degradation of any radar or communication system as a result of interference. For most cases this plot can also represent parameter degradation.

The ordinate expresses the percent of operating efficiency of the system under consideration. The abscissa is divided into units of power level that represents the interference input to the system. There are three power bands illustrated. The first labeled G0 represents the infinite number of power levels below which the system is not effected by interference. In this area the operation is good in fact very nearly 100%. The next power band is labeled D0. In this region the operation is doubtful due to interference.

This is the region in which the operation is degraded from nearly 100% efficiency to nearly zero efficiency. The third band labeled NO includes the infinite number of power levels where the system operating efficiency is degraded from nearly zero to zero efficiency as a result of interference.

Obviously if any attempt had been made to scale the abscissa then the center or DO region would appear as a fine hairline separating the region of no interference or good operation from that of total interference or no operation. Even for the case of practical values of interference ranging from minus 150 dbm to zero dbm the DO region would appear very small since it normally covers in the neighborhood of 15 db or less. Since this region is so small it is found that for most cases the curve may be approximated by a straight line within normal prediction accuracy. Where greater accuracy is needed, a statistical approach may be used such as the Marcum<sup>1</sup> Detection curves for pulsed systems.

Once the operating zones are defined and the prediction curves developed then the prediction must be related to the specific system. The form this will take may be a tracking-error vs interference for the case of track radar, an articulation score for a communication system, or a predicted interference clutter on a PPI scope for the case of a search radar.

The output shown as Block 8 Figure 1 will then be a report indicating the technique followed with a numerical result together with a variance or probable accuracy figure.

### III. PULSE COMPRESSION RECEIVER MATHEMATICAL MODEL

The application of ARMS to a pulse compression radar is shown in the flow diagram of Figure 3. The top part of figure 3 shows the block diagram of the system while on the bottom is shown the functional operation of the pulse compression filter. The received pulse with linear frequency shift is filtered and each frequency is delayed an amount to compress the wide pulse and increase its amplitude.

The initial block of the flow computes the power level or INR which is in the pass band of the matched filter receiver. This computation can be either done on the computer for a complex environment or manually for a small number of interfering sources. Block 2 is a tabulation of the result of the first calculation. Blocks 3 and 3a are logic blocks to determine the type of modulation of the interfering pulse. If the interference is a CW pulse, the detuning effects and the peak values are computed in blocks 4a and 5a. Blocks 6a and 7a are the element models which reflect the action of the pulse compression filter on the interfering pulse. For pulses which are the compressed pulse width and smaller the INR or power level are decreased by a factor D, and the pulse width is increased by a factor D. D is the compression ratio for the system and is equal to T (stretched pulse width) times  $\Delta$  (the frequency deviation). For pulses equal to or wider than 5 times the compressed pulse width, the power level, pulse width, or INR is not changed. There is a linear change in INR for pulse widths between the compressed pulse width and five times the compressed pulse width.

For design FM pulses with the proper deviation the power level or INR is increased by D and the pulse width is decreased by D. For FM pulses with opposite frequency deviation the power level or INR is decreased by 2D and the width is increased by 2D.

The effects of the pulse compression filter on other types of interfering signals is being studied and will be included when the study is completed.

#### IV. APPLICATION

A recent problem involving a search radar receiver site as a victim together with seven different interference environments consisting of from 4 to 21 interfering transmitters was processed using the ARMS technique.

The problem was to determine the degradation of the PPI display as a function of the interference under the different environments. Categories<sup>2</sup> established by the Air Force were used to grade the interference densities on the PPI scope. Figure 4 shows the possible configurations of the victim receiver. The terms of the problem limited these combinations to the following, Log-receiver, DFX Receiver, Raw Receiver, Lin Log Receiver, Lin Log Receiver with F.T.C. and Lin Log Receiver with M.T.I. The equipment model was established from data obtained from a military agency having cognizance of the victim equipment. Data on the transmitters was obtained during an area problem in which a victim receiver was monitored. The results of the prediction could therefore be validated by checking against data acquired by the monitor.

After preprocessing, the required data for each of the transmitters and one receiver was fed into the Master Simulation System Program -1.

The output from this computer program was a summary of the pulse rates associated with each of 15 discrete power levels. This process was continued until each receiver model was subjected to each of the seven environments.

The output for each of the seven receiver-environments was then evaluated by comparing the calculated power levels to the known M.D.S. for the receiver. In addition a plot of input power levels vs pulses per second for each situation was obtained.

For the case of the Lin-Log receiver with F.T.C. the effect of applying the F.T.C. mathematical model was to change the power levels associated with each of the pulse rates.

A more sophisticated case was the Lin Log Receiver with M.T.I. In this case the following model was used.

$$M = 2 \sum_{i=1}^I M_i \quad (1)$$

$$\left. \begin{aligned} M_i &= P_i \left( 1 - \sqrt{\frac{S_t}{S_i}} \right) & S_t < S_i \\ M_i &= 0 & S_t \geq S_i \end{aligned} \right\} \quad (2)$$

where

$M$  = Total detected pulse rate.

$M_i$  = Detected pulse rate at each quantized antenna gain level.

$P_i$  = Percent of occurrence of  $S_i$ .

$S_i$  = Signal to noise output of M.T.I. circuit.

$S_t$  = Signal to noise ratio that will give 50% probability of detection from Marcum curves.

$I$  = Total number of lobe to lobe antenna look angles.

In order to apply this model it was necessary to have a computer read out of power level vs PPS for each antenna lobe to lobe antenna look angle. This eliminated the calculation of  $P_i$  leaving equation 2 in the form

$$M_i = \left( 1 - \sqrt{\frac{S_t}{S_i}} \right) \quad (3)$$

Since this equation equals by definition zero when  $S_i \leq S_t$  a graphic solution was developed and shown in Figure 5. By entering the abscissa with  $S_i$  a value for  $M_i$  is obtained from the ordinate opposite the appropriate curve. There is a different curve for each transmitted pulse width from 2  $\mu$ -sec to 6  $\mu$ -sec.

This operation has the effect of changing the pulse distribution or pulse ratio associated with each calculated power level. This in turn will change the shape of the PPI vs Power Level curve and the number of detected pulses that will be displayed on the PPI scope.

#### V. MATRIX SOLUTION TO ONE TO ONE INTERFERENCE PROBLEM

In the preceding section the application of the ARMS technique was described. For the power computation a computer program, the Master Simulation System -1, programmed for the 1105 computer was used. This computation

involved the solution of a single transmitter receiver interference situation. Each environment having several transmitters necessitated the solution of the problem one time for each transmitter-receiver combination. The solutions were then summed for the results of all the transmitters effecting a single receiver.

As a result of experience gained in solving this and other problems it was apparent that a need existed for a quick solution of problems containing small numbers of interfering transmitters. A procedure for manual computation of interference power has therefore been developed. Upon development it became apparent that problems unrelated to the straight interference power computation were clarified and in some cases solved by the approach taken. Work is therefore continuing on this phase of the ARMS program.

Briefly the manual power calculation is based upon the solution of the power equation below.

$$P_{rx} = \sum_{j=1}^J G_{tj} P_L G_{rj} \int_0^{\infty} P_{tx}(f) |H(f)|^2 df \quad (4)$$

where

$P_{rx}$  = Peak power at receiver in milliwatts

$G_{tj}$  = Transmitter antenna gain

$J$  = Final  $j$  or number of antenna quantized parts

$P_L$  = Propagation path gain

$G_{rj}$  = Receiver antenna gain

$P_{tx}$  = Peak power of transmitter pulse in mw/mc

For manual computation equation 4 will take the form of equation 5

$$[P_{rx}(f_i)] = [P_{tx}(f_i)] [G_{tj}] [P_L] [G_{rj}] [H(f_i)^2] \quad (5)$$

The numbers in the development of these matrices come from a real transmitter-receiver interference environment and can therefore be considered typical. A basic column matrix  $[P_{tx}(f_i)]$  can be developed by quantizing a spectrum envelope representing the transmitted pulse from a given interference source.

At present the synthesis technique (based upon measured data) uses the spectrum envelope<sup>3</sup> of a trapezoidal pulse with a slope of 40 db per decade see Figure 6. A perfect rectangular pulse would have a spectrum envelope of 20 db per decade.

By using the transmitter tuned frequency and the peak pulse power this basic matrix can be converted see Figure 7 into a column matrix that completely describes the transmitted pulse in terms of its power spectrum.

In Figure 7 the left hand or Basic Matrix is a profile of the quantized spectrum envelope. Each frequency band, normalized in units of  $1/\tau$  has an associated db level. These levels represent ratios of pulse power relative to the power contained in the band about the transmitter tuned frequency. This is an approximation which can be justified by the fact that the quantization includes sufficient side lobes to cover about 98% of the total power under the curve.

To convert the basic matrix to one representing a specific transmitter requires the application of the transmitter pulse power to the quantized levels and then the evaluation of  $1/\tau$ . This, together with the tuned frequency, converts the generalized frequency bands into specific bands relative to the tuned frequency as shown in figure 7.

A similar row matrix see Figure 8 can be developed to completely describe the receiver by means of a quantized receiver selectivity curve. In this case the selectivity curve is approximated by a 5.5 db per octave drop from the 3 db to the 20 db points and then a 40 db per octave drop from the 20 db point to some given threshold. This technique was developed for the MSS-2 cull program. (see Figure 9).

The curve is then quantized into 11 levels each representing a frequency band normalized to  $BW/2$ . This is then converted into a receiver matrix. The deviation units  $BW/2$  are converted into frequencies above and below  $f_0$  or the receiver tuned frequency.

The two row matrices can immediately be combined into a single row matrix by adding the db in the receiver matrix to the dbm in the transmitter matrix for corresponding bands. If no frequency bands coincide this constitutes a visual cull.

There remains the antenna gain matrices and the propagation loss matrix.

If the transmitter and receiver antenna-waveguide gains are to be quantized in a four level manner as in the MSS-1 the table of Figure 10 may be used.

Using the data shown, the transmitter antenna matrix will be as illustrated in Figure 11.

Again using the data shown plus Figure 10 the receiver antenna gain matrix will appear as Figure 12.

There are a number of different methods for developing the propagation loss between specified points. Sixteen of these are developed in Reference 4. For the case being illustrated a smooth earth diffraction model was used and resulted in a fixed or constant gain figure of -139.5 db. This number was used in Figure 13 to develop the row matrix representing the product

$$[G_{tj}] [P_L] [G_{rj}]$$

The final product of this row matrix and the column matrix previously developed which are shown together in Figure 14 will be the output or power matrix  $[P_{rx}]$  as shown in Figure 15.

This output matrix is of interest from a prediction standpoint since each column represents the spectrum of an associated pulse train as seen by the receiver. In addition, the peak power associated with each of these pulse trains or pulse rates is used in the prediction model as a threshold cull. It is also possible to develop a statistical picture of the detected pulse rates and from this predict interference to a PPI or an A scope.

#### VI. FUTURE DEVELOPMENT (ARMS)

As more problems are processed with the ARMS program, a library of problems will be available. The experience gained in using ARMS will be used as a feedback to recommend possible improvements or simplifications of the techniques used in the prediction such as: Receiver Synthesis, Transmitter Synthesis, Antenna Synthesis, Propagation Loss and the Treatment of the Mathematical or Element Models.

The ARMS prediction program will use the results of improved interference prediction studies as they become available. As an example, the transmitters in a complex environment could be processed through ARMS up to the receiver section. This environment could then be represented statistically (Probability of pulse overlap, probability of pulse spacing, etc.) and then processed statistically in the interference power block of ARMS. This will provide a realistic prediction program for systems such as: IFF, (which is sensitive to pulse spacing) and Sequential Detection Schemes, (which require a certain sequence of hits to declare a target.)

Also in multiple transmitter environment situation, the probability of single, double and triple pulse overlap would be included in the prediction program. This assumes increasing importance as the number of interfering sources increases.

Use of the manual ARMS program for a period of time indicates certain areas which have become a routine type calculation and can be automated and programmed for running on the computer. Certain of the more commonly used mathematical models such as FTC, MTI and STC have already been programmed and others will be added.

#### VII. CONCLUSIONS

The ARMS technique appears to supplement the best feature of an automated prediction program with the manual or hand calculations required by the variations in equipment models and prediction requirements.

Future development of the automated program can be guided by experience gained in the use of the ARMS techniques in solving current problems



as they occur. This eliminates delays in the handling of brush-fire type of interference problems.

An insight into the accuracy requirements and effects of parameter variations can be derived by numerical analytic methods using the ARMS procedures.

The development of numerical methods for use in different types of problems provides an expanding capability for interference predictions.

The interference power and INR ratio calculations are well developed and several alternate methods of computation are available.

The mathematical element models for different receiver configurations are well advanced and continuous work is being done in this area.

There is a great deal of work to be done on the prediction models. Also system degradation studies are still in the elementary stages. It is expected that this area will receive the greatest attention in the immediate future.

#### ACKNOWLEDGEMENT

The work described above is sponsored by the three Military Departments, and is being conducted under Contract No. AF 19 (604)-8440 with the Electronic Systems Division, Air Force Systems Command.

#### REFERENCES

- (1) J. I. Marcum, "Statistical Theory of Target Detection by Pulsed Radar", RAND Corp. RM 753-4.
- (2) ADC Supl 2 to ARM 100-24, HQ ADC Emt. AF Base Colorado, 15 May 1961.
- (3) W. A. Hurd, J. L. Cundiff, C. E. Blakely, "An Analog and Digital Computer Investigation of the Spectrum Characteristics of Pulsed Signals", TM X003-4 ECAC, 15 December 1961.
- (4) W. Frazier, P. D. Newhouse, P. Oyer, T. Truske, "A Search Radar Model", ECAC TDR - April 1963.

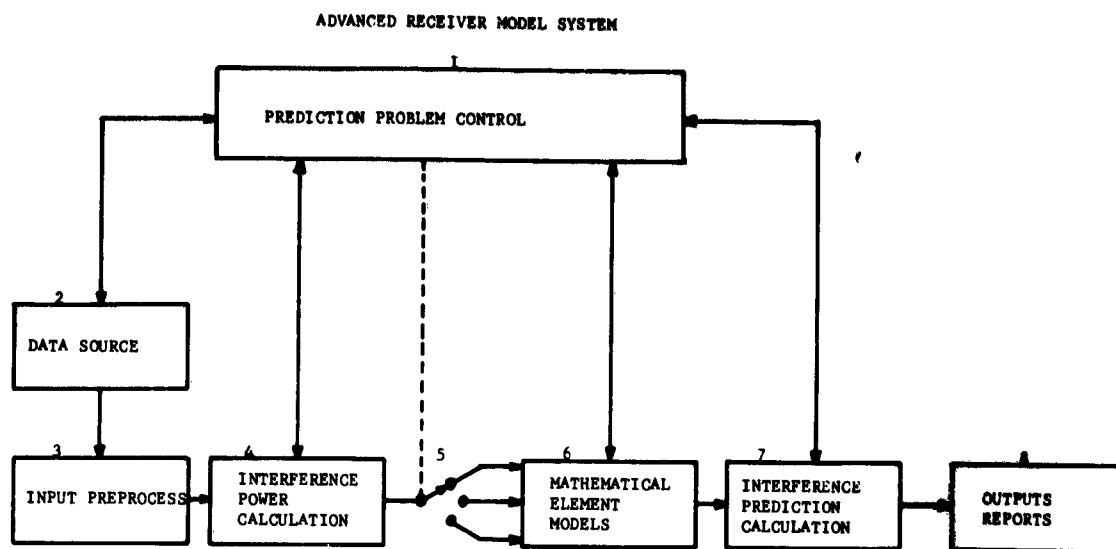


FIGURE 1.

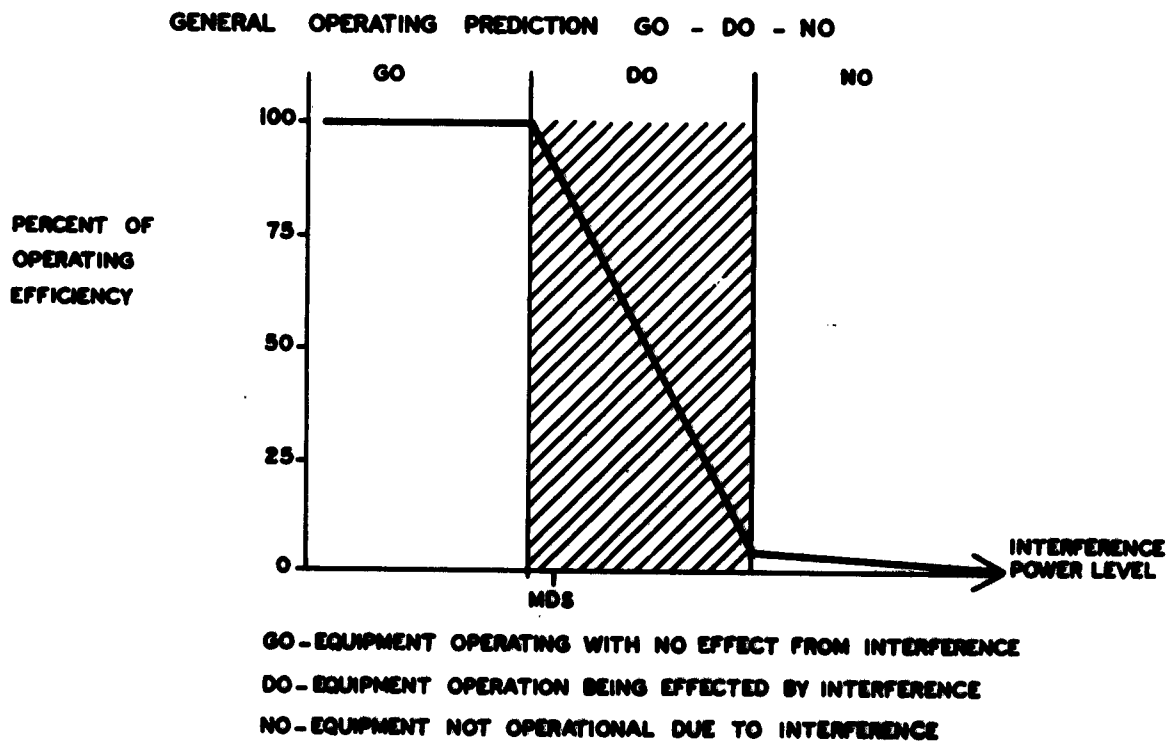
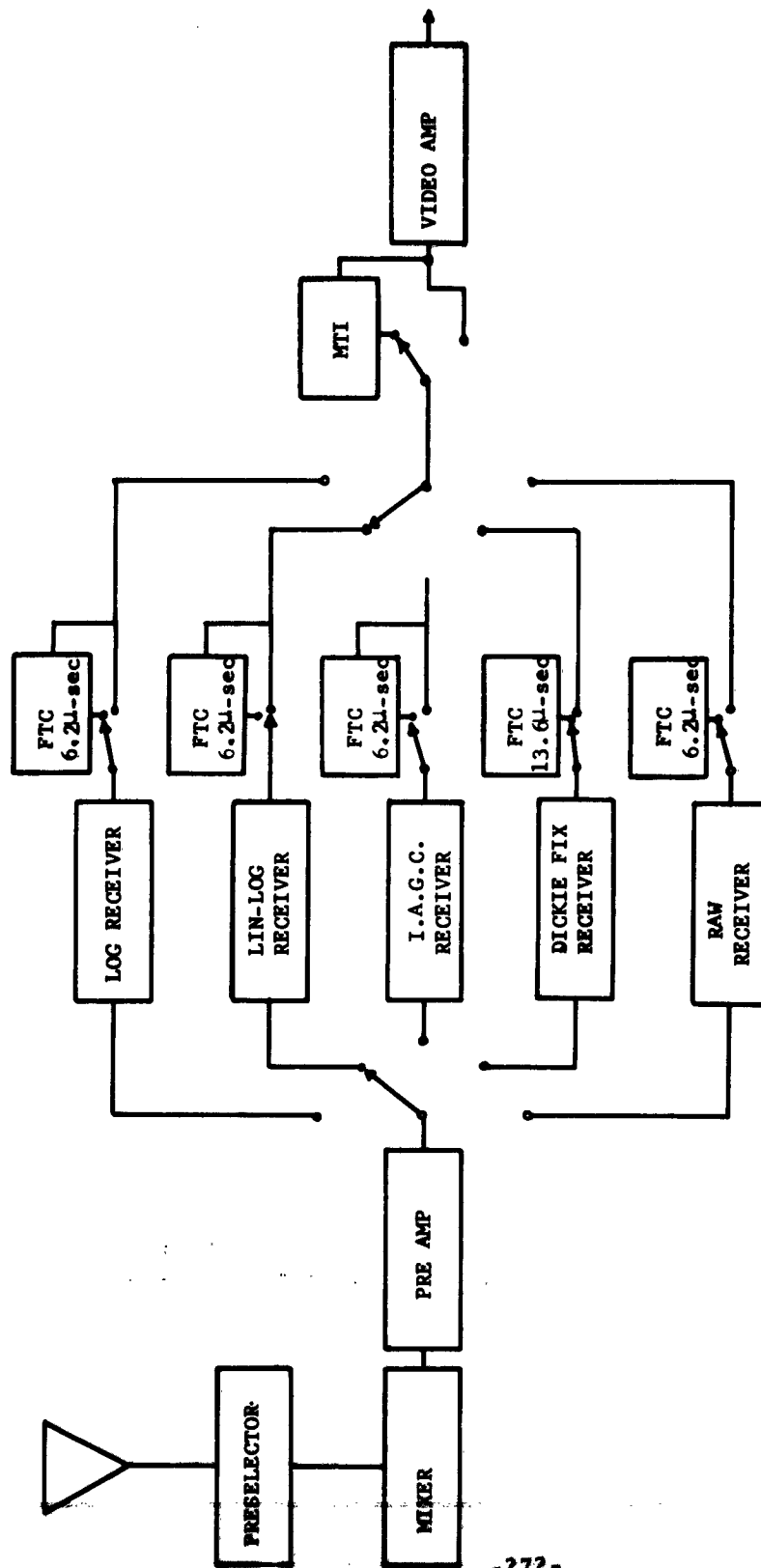


FIGURE 2

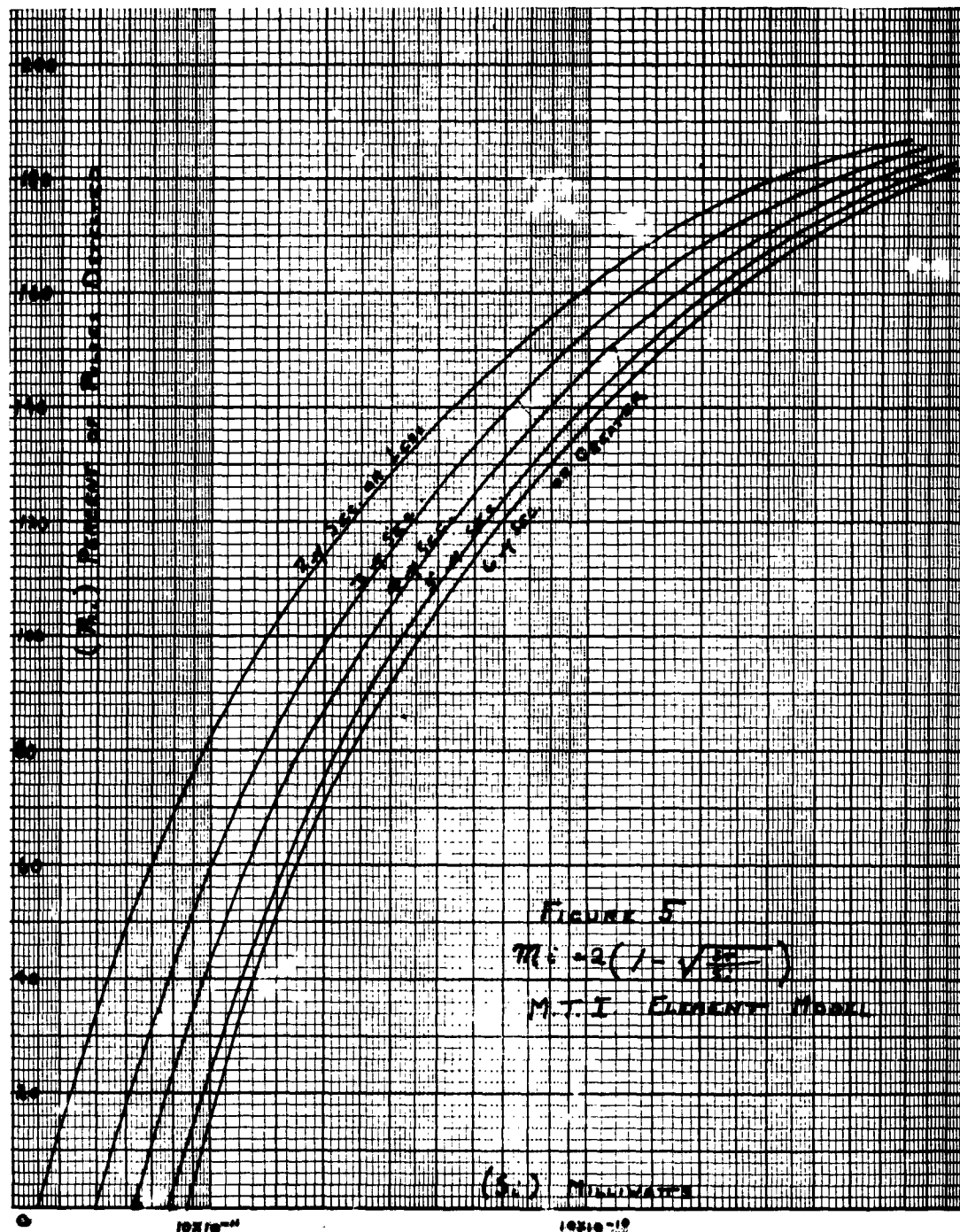


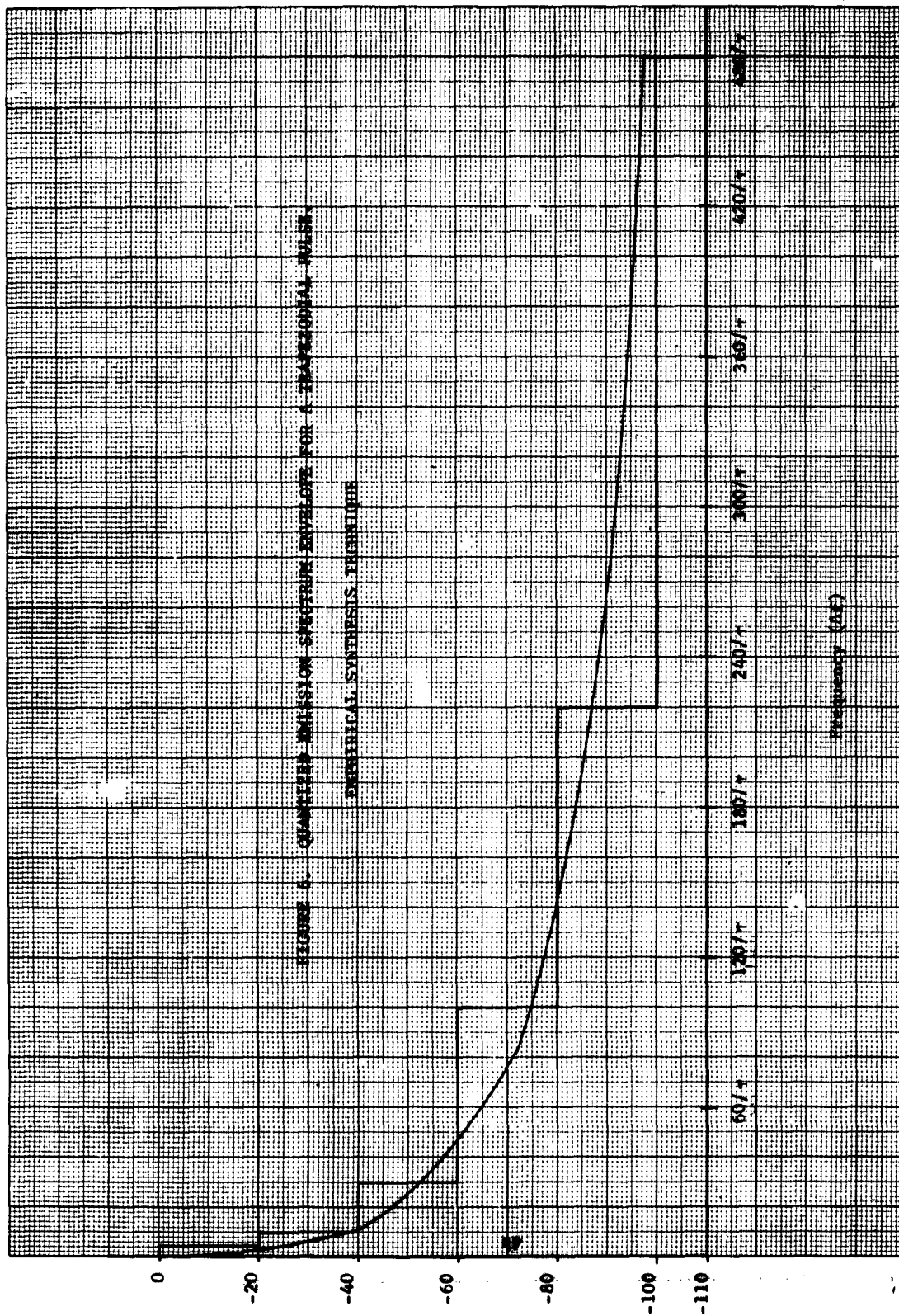
# RECEIVER EQUIPMENT MODEL



NOTE: RAW RECEIVER NOT NORMALLY USED REQUIRES  
SPECIAL HOOKUP

FIGURE 4.





# TRANSMITTER MATRIX

$$\tau = 2 \mu\text{-sec} \quad 1/\tau = .5 \text{ mc}$$

$\Lambda$

$$P_t = 500 \text{ KW} \quad \text{or } 87 \text{ dbm}$$

## INPUT DATA

$$f_o = 1302 \text{ Mc}$$

$$\text{PRF} = 380 \text{ PPS}$$

## BASIC MATRIX

Frequency ( $\Delta f$ )	db
$-320/\tau$ to $-180/\tau$	-100
$-180/\tau$ to $-80/\tau$	-80
$-100/\tau$ to $-30/\tau$	-60
$-30/\tau$ to $-10/\tau$	-40
$-10/\tau$ to $-4/\tau$	-20
$-4/\tau$ to $+4/\tau$	0
$+4/\tau$ to $+10/\tau$	-20
$+10/\tau$ to $+30/\tau$	-40
$+30/\tau$ to $+100/\tau$	-60
$+100/\tau$ to $+200/\tau$	-80
$+220/\tau$ to $+480/\tau$	-100
Spurious	-60
Spurious	-60
Spurious	-60

## TRANSMITTER MATRIX $\Lambda$ $P(f_1)$

Frequency (mc)	db
1142 1212	-13
1212 1252	07
1252 1287	27
1287 1297	47
1297 1300	67
1300 1304	87
1304 1307	67
1307 1317	47
1317 1352	27
1352 1412	07
1412 1542	-13
	27
	27
	27

FIGURE 7.

RECEIVER MATRIX  $|H(f_1)|^2$

$$\delta = 900 \text{ Kc}$$

$$f_o = 1302 \text{ Mc}$$

$$|H(f_1)|^2$$

BASIC MATRIX

Frequency ( $\Delta f$ )

-100 $\delta$ to -40 $\delta$	-100
- 40 $\delta$ to -25 $\delta$	- 80
- 25 $\delta$ to -15 $\delta$	- 60
- 15 $\delta$ to -7.5 $\delta$	- 40
-7.5 $\delta$ to -2.2 $\delta$	- 20
-2.2 $\delta$ to +2.2 $\delta$	0
+2.2 $\delta$ to 7.5 $\delta$	- 20
7.5 $\delta$ to 15 $\delta$	- 40
15 $\delta$ to 25 $\delta$	- 60
25 $\delta$ to 40 $\delta$	- 80
40 $\delta$ to 100 $\delta$	-100

RECEIVER MATRIX

Frequency

1212 1266	-100
1266 1280	- 80
1280 1288	- 60
1288 1295	- 40
1295 1300	- 20
1300 1304	0
1304 1309	- 20
1309 1316	- 40
1316 1324	- 60
1324 1338	- 80
1338 1392	-100

FIGURE 8.



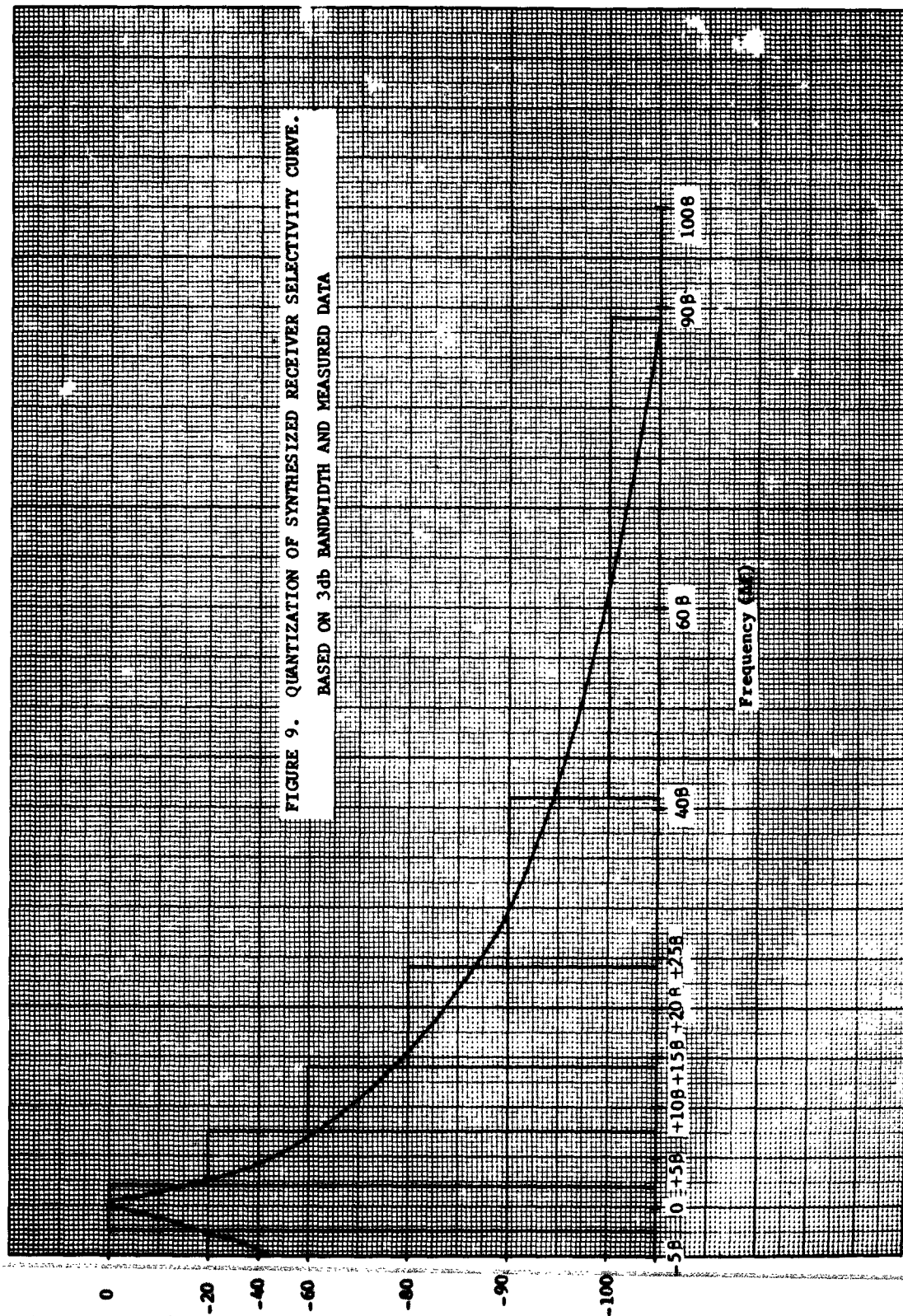


FIGURE 9. QUANTIZATION OF SYNTHESIZED RECEIVER SELECTIVITY CURVE.  
BASED ON 3db BANDWIDTH AND MEASURED DATA

# TYPICAL ANTENNA GAIN TABULATION

## ANTENNA GAIN PATTERNS

### GAIN WITH RESPECT TO NOMINAL

NOMINAL ANTENNA AND WAVEGUIDE GAIN db	MAIN BEAM	MAJOR SIDE LOBES	MINOR SIDE LOBES	BACK LOBE
< 5	0	0	0	0
5 - 10	0	-5	-10	-15
11 - 20	0	-10	-20	-30
21 - 30	0	-18	-32	-40
> 30	0	-16	-40	-50
BEAM WIDTH	3.6°	14.4°	162°	180°
PERCENT = $\frac{\text{BEAM WIDTH}}{360}$	1	4	45	50

FIGURE 10.

FIGURE 11.

TRANSMITTER ANTENNA GAIN PROFILE

INPUT DATA Nominal antenna waveguide gain = 27.5 db

FROM FIGURE 10 MB = 0 db SL = -18 db TL = -32 db BL = -40 db

% PPS 1.0 4.0 45.0 50.0

PRF = 380 PPS

$G_{tj}$  MATRIX

	MB	SL	TL	BL
	27.5	9.5	-4.5	-12.5
PPS	4	14	171	190

FIGURE 12.

RECEIVER ANTENNA GAIN PROFILE

INPUT DATA Nominal beyond line-of-sight antenna waveguide gain = 34 db

FROM FIGURE 10 MB = 0 SL = -16 TL = -40 BL = -50

% PPS 1.0 4.0 45.0 50.0

$G_{rj}$

	MB	SL	TL	BL
	34	18	-6	-16 db
% PPS	0	5	45	50

# $T_x \times P_x$ ANTENNA GAIN PROPAGATION PRODUCT

$$\begin{array}{c}
 G_t \\
 \text{TRANSMITTER ANTENNA} \\
 \text{MATRIX} \\
 (\text{gain} = 27.5 \text{ db})
 \end{array}
 \times
 \begin{array}{c}
 G_r \\
 \text{RECEIVER ANTENNA} \\
 \text{MATRIX} \\
 (\text{gain} = 34 \text{ db})
 \end{array}
 =
 \begin{array}{c}
 P_L \\
 \text{PROPAGATION} \\
 \text{PATH GAIN}
 \end{array}$$

$$\begin{array}{c}
 \text{MB -0} \quad \text{SL -18} \quad \text{TL -32} \quad \text{BL -40} \\
 \begin{bmatrix} 27.5 & 9.5 & -4.5 & -12.5 \end{bmatrix}
 \end{array}
 \times
 \begin{array}{c}
 \text{MB -0} \quad \text{SL -16} \quad \text{TL -40} \quad \text{BL -50} \\
 \begin{bmatrix} 34 & 18 & -6 & -16 \end{bmatrix}
 \end{array}
 =
 \begin{array}{c}
 \begin{bmatrix} -139.5 \end{bmatrix}
 \end{array}$$

$$G_t \times G_r \times P_L$$

$$\begin{array}{c}
 \text{DB} \quad \text{MB-MB} \quad \text{MB-SL} \quad \text{MB-TL} \quad \text{MB-BL} \quad \text{SL-MB} \quad \text{SL-SL} \quad \text{SL-TL} \quad \text{SL-BL} \quad \text{TL-MB} \quad \text{TL-SL} \quad \text{TL-TL} \quad \text{TL-BL} \quad \text{BL-MB} \quad \text{BL-SL} \quad \text{BL-TL} \quad \text{BL-BL} \\
 \begin{bmatrix} -78 & -94 & -118 & -128 & -96 & -112 & -136 & -146 & -110 & -126 & -150 & -160 & -118 & -134 & -158 & -168 \end{bmatrix}
 \end{array}$$

$$\begin{array}{c}
 \text{PPS} \quad 4 \quad 19 \quad 171 \quad 190 \quad 2 \quad \text{PPS} \quad 1.0 \quad 4.0 \quad 45.0 \quad 50.0 \\
 0 \quad 0 \quad 2 \quad 2 \quad 0 \quad 0 \quad 7 \quad 7 \quad 0 \quad 3 \quad 82 \quad 86 \quad 0 \quad 4 \quad 91 \quad 95
 \end{array}$$

FIGURE 13.

APR 1964

**Frequency Mc dbm**

1212 - 1266	-93
1266 - 1280	-53
1280 - 1288	-33
1288 - 1295	07
1295 - 1300	47
1300 - 1304	87
1304 - 1309	47
1309 - 1316	07
1316 - 1324	-33
1324 - 1338	-53
1338 - 1392	-93

$$\begin{bmatrix} G_r \times G_r \times P_L \end{bmatrix}$$

MB/	SL	TL	BL	SL/MB	SL	TL	BL	TL/MB	SL	TL	BL	MB/MD	SL	TL	BL
-78	-94	-118	-128	-96	-112	-136	-146	-110	-126	-150	-160	-118	-134	-158	-168
0	0	2	2	0	0	7	7	0	3	82	86	0	4	91	95
PPS															

**FIGURE 14.**

# OUTPUT MATRIX

POWER LEVEL IN dbm

Frequency Mc

1288 - 1295	-71	-87	-111	0	89	-105	0	0	-103	0	0	0	-101	0	0	0
1295 - 1300	-31	-47	-71	-81	-49	-65	-89	-99	-63	-79	-103	-113	-71	-87	-111	0
1300 - 1304	+9	-7	-31	-41	-9	-25	-49	-59	-23	-39	-63	-73	-31	-47	-71	-81
1304 - 1309	-31	-47	-71	-81	-49	-65	-89	-99	-63	-79	-103	-113	-71	-87	-111	0
1309 - 1316	-71	-87	-111	0	-89	-105	0	0	-103	0	0	0	-101	0	0	0

282

PPS 0 0 2 2 0 0 7 7 0 3 82 86 0 4 91 95

h

P<sub>ij</sub>

+9 -7 -31 -41 -9 -25 -49 -59 -23 -39 -63 -73 -31 -47 -71 -81

Sum of

Power

Levels

FIGURE 15.

## COMPUTER PROCESSING OF ANTENNA PATTERNS

H.N. Kritikos and M.R. Dresp  
The Moore School of Electrical Engineering  
University of Pennsylvania  
Philadelphia, Pennsylvania

Abstract. - This paper demonstrates the usefulness of electronic digital computers in reducing antenna pattern data. Three methods of simplifying the data and the error involved in the simplification are examined. The three methods are: first, reduction of the pattern to constant gain sections; second, simplification by band limiting the spherical harmonic spectrum; third, the determination of the probability distribution function of the gain.

### I. INTRODUCTION

In the past few years the general trend in the field of communications has been an integrated or a systems approach to the various engineering problems. It seems that this type of approach is now reaching the domain of antennas which are an important part of many complex systems.<sup>1,2</sup> To be more precise a systems approach or view-point is the evaluation of a component part, in this case the antenna, in terms of the performance of the entire system. In the light of these arguments to simply provide the gain, the beam-width, the average amplitude of the sidelobes of an antenna, is perhaps too little or not enough depending on the particular application and the environmental conditions. The underlying difficulty is that the true pattern is a complicated function which is experimentally time consuming to determine, and then difficult to analyze.

In this paper an attempt is made to develop methods of processing the antenna field pattern data in such a way that the results are meaningful for particular applications. This antenna data processing is carried out with the aid of an electronic computer which simplifies the computations and greatly increases the flexibility of the operation.

Three different methods of reducing the antenna data have been considered here. The three methods are: first, the simplification of the pattern by reducing the data into constant gain sections; second, the analysis of the pattern into a spherical harmonic spectrum; third, the determination of the statistical distribution of the pattern.

The novelty of the antenna data reducing methods which are presented in this paper lies not only in the use of the electronic digital computer but also in the introduction of an error criterion for the simplification of the antenna pattern. The criterion used here is the root mean square (RMS) error.

### II. THE APPROXIMATION OF THE GAIN FUNCTION INTO CONSTANT GAIN SECTIONS

It has been common practice in many applications to divide the antenna pattern into constant gain sections. The division is done arbitrarily

and is entirely based on an intuitive appraisal of the situation. The division of the pattern into sections is as follows:

The pattern is considered to be

$$\begin{aligned} G(\theta, \vartheta) &= G_1 \text{ for } \Delta\Omega_1 \\ &= G_2 \text{ for } \Delta\Omega_2 \text{ where } G_1 \dots G_n \text{ are constants} \\ &\vdots \\ &= G_n \text{ for } \Delta\Omega_n \end{aligned} \quad (1)$$

$$\sum \Delta\Omega_n = 4\pi$$

$$\text{and also } \int G(\theta, \vartheta) d\Omega = \sum_n G_n \Delta\Omega_n = 4\pi \quad (2)$$

In order to remove the arbitrary nature of this partition, the standard deviation of the fluctuations of the gain within one section is calculated. If one places an upper limit on the standard deviation, then a more meaningful partition of the gain into constant gain sections can be made. The partition certainly is not unique but one has a measure of the error which is being made.

The antenna pattern then can be represented as follows:

$$\begin{aligned} G(\theta, \vartheta) &= G_1 \text{ for } \Delta\Omega_1 \text{ with } S_1^2 \\ &= G_2 \text{ for } \Delta\Omega_2 \text{ with } S_2^2 \\ &\vdots \\ &= G_n \text{ for } \Delta\Omega_n \text{ with } S_n^2 \end{aligned} \quad (3)$$

where the partition has been taken such that  $S_n^2 \leq S_{\max}^2$ ,  $S_{\max}^2$  being the maximum permissible standard deviation.

The quantity  $S$  is the common RMS error and is

$$S_n^2 = \frac{1}{\Delta\Omega_n} \int (G(\theta, \vartheta) - \bar{G}_n)^2 d\Omega \quad (4)$$

where  $\bar{G}_n$  is the average gain corresponding to section  $\Delta\Omega_n$ . The setting of a maximum allowable RMS error per section allows the mechanization of such a simplification procedure. A digital computer can be easily programmed to make automatically the partitions and give the mean gain.



In order to convert the data into a digital form, the pattern is sampled at regular intervals. For example, for the cases examined below 180 samples were taken. The data then becomes a series  $G_k$  of numbers which is ready to be fed into the computer. The maximum acceptable error per section is specified, and then a starting point is chosen. The starting point is determined arbitrarily from the utilitarian aspects of the antenna. This process is done in "pint" language on an electronic digital computer.\*

Figure I shows the gain of an experimentally obtained pattern which has a  $\theta$  symmetry. The starting point was taken to be at  $\theta = 0$ . Two approximations have been made; one with a .436 RMS error and the other with a .138 RMS error. Notice that the number of sections for the approximation is worse, and it only gives a rough picture of the pattern. Figures 2, 3, 4, 5 also show progressive approximations of an experimentally obtained high gain pattern. The gain for this case is in DB. For these cases only a slice of the total pattern was examined. This slice of stereo angle was  $\Delta\Omega = 2\pi\Delta\theta = \sum \Delta\Omega_k = \sum \sin\theta_k \Delta\theta_k \Delta\phi$  ( $\theta$  constant,  $0 < \theta < \pi$ ).

### III. APPROXIMATION BY BAND LIMITING THE SPHERICAL HARMONIC SPECTRUM

The approach in this section is analogous to the smoothing of stationary time series by the omission of the higher order Fourier components. The antenna gain, since it is a function described on the surface of a sphere, can in general be represented as a series of spherical harmonics. A simplification of the pattern can take place by omitting higher order terms. From a spectral analysis, as it will be shown below, the root mean square error of this smoothing by the omission of higher order terms can be determined. Therefore, in this case as before, one has an RMS criterion of simplification of the pattern.

Following this approach one has

$$G_t = G_o + G_r \quad (5)$$

where

$G_t$  is the total gain

$G_o$  is the simplified gain

$G_r$  is the part of the gain which represents the undesirable fluctuations.

Function  $G_t$  can be expanded into spherical harmonics

$$G_t = \sum_{\mu=0}^{\infty} \sum_{m=0}^{\infty} \left[ A_{\mu}^m \cos m\theta + B_{\mu}^m \sin m\theta \right] P_{\mu}^m(\cos\theta) \quad (6)$$

---

\* RPC 4000 Royal Precision Company

Each one of the terms  $A_\mu^m$  is considered as a part of a two dimensional spectrum.

Similarly,

$$G_o = \sum_{\mu=0}^1 \sum_{m=0}^1 \left[ A_\mu^m \cos m\theta + B_\mu^m \sin m\theta \right] P_\mu^m(\cos\theta) \quad (7)$$

and

$$G_r = \sum_{\mu=2}^{\infty} \sum_{m=0}^{\infty} \left[ A_\mu^m \cos m\theta + B_\mu^m \sin m\theta \right] P_\mu^m(\cos\theta) \quad (8)$$

Notice that

$$\sum \sum = \sum_1 \sum_1 + \sum_2 \sum_2 \quad (9)$$

Effectively then, the harmonic spectrum has been partitioned into two parts; part one shown in the summation  $\sum_1 \sum_1$  and part two shown in the summation  $\sum_2 \sum_2$ .

Obviously one has the additional relation

$$\int G(\theta, \theta) d\Omega = 4\pi$$

Because of the orthogonality relations, this reduces to  $A_o^0 = 2\pi$  (10)

The RMS error introduced by the omission of a number of terms is easily computable below

$$\bar{e}^2 = \frac{1}{4\pi} \int \left[ G_t - G_o \right]^2 d\Omega = \frac{1}{4\pi} \int (G_r)^2 d\Omega \quad (11)$$

$$= \frac{1}{4\pi} \sum_{\mu}^2 \sum_{m}^2 \left[ (A_\mu^m)^2 + (B_\mu^m)^2 \right] \frac{2}{2\mu+1} \frac{(m-\mu)!}{(m+\mu)!} \quad (12)$$

Because of the two dimensional distribution, the partition of the higher order terms for the same RMS error is not unique (see Figure 6).

The spherical harmonic spectrum of the pattern is determined by numerical methods. With the aid of a computer, the expansion coefficients of the spherical harmonic spectrum were determined in the following manner.

The gain data in this analysis was taken in the range from 0-180° at one degree intervals. The pattern as in the case before had a 0 symmetry. Using the above analysis and equations, a program for the harmonic spectrum was compiled. This was done in the "pint" language on a digital computer.

#### IV. STATISTICAL DISTRIBUTION OF THE GAIN

The probability density function of the gain in the conventional sense is defined as follows:

If  $P(G \leq G_1)$  is the probability that the gain  $G$  is smaller or equal than a prescribed value  $G_1$  then

$$P(G \leq G_1) = \frac{\sum_i \Delta\Omega_i}{4\pi} \quad (13)$$

where  $\Delta\Omega_i$  are the sections of stereo angle which correspond to gains  $G$  of smaller or equal than the prescribed value  $G_1$ , ( $G \leq G_1$ ).

The probability density function can be calculated from the data by simple enumeration techniques. The procedure which was used is as follows:

The data are converted to a discrete form by sampling the gain function. In this way the gain function reduces to a set of values  $G_k$  which correspond to a set of equal elements of stereo angle  $\Delta\Omega_k$ . The size of the element of the stereo angle is dictated by practical considerations such as the complexity of the gain functions, etc.

The probability density function then is obtained from the relation

$$P(G \leq G_1) = \frac{f_k}{K} \quad (14)$$

where  $f_k$  is the number of sections  $\Delta\Omega_k$  in which the gain  $G$  is smaller or equal than  $G_1$  ( $G \leq G_1$ ).  $K$  is the total number of equal sections  $\Delta\Omega_k$ .

The probability density function was found with the aid of a digital computer. The program was designed to satisfy the condition

$$P(G \leq G_1) = \frac{f_k}{K} \quad (15)$$

for specified values of gain  $G_1$ . The results are shown in figures (9) and (10).

## V. CONCLUSIONS

In this paper it was demonstrated that the processing of data can be done easily and with great flexibility with an electronic digital computer.

The data are processed in such a way that a series of simplified patterns are obtained. This series of curves range from very simple approximations of the antenna pattern to better approximations and finally to the exact pattern. The RMS error for all of these cases is calculated. These series of approximations will then be available to the field engineer who will choose the one which best suits his particular application.

Two methods of simplifying the pattern were investigated: The first method "reduction to constant gain sections" is appropriate for high gain antenna patterns. The second method "band limiting the spherical harmonic spectrum" is appropriate for low gain or omnidirectional patterns. The computer also easily provides the probability distribution function of the gain.

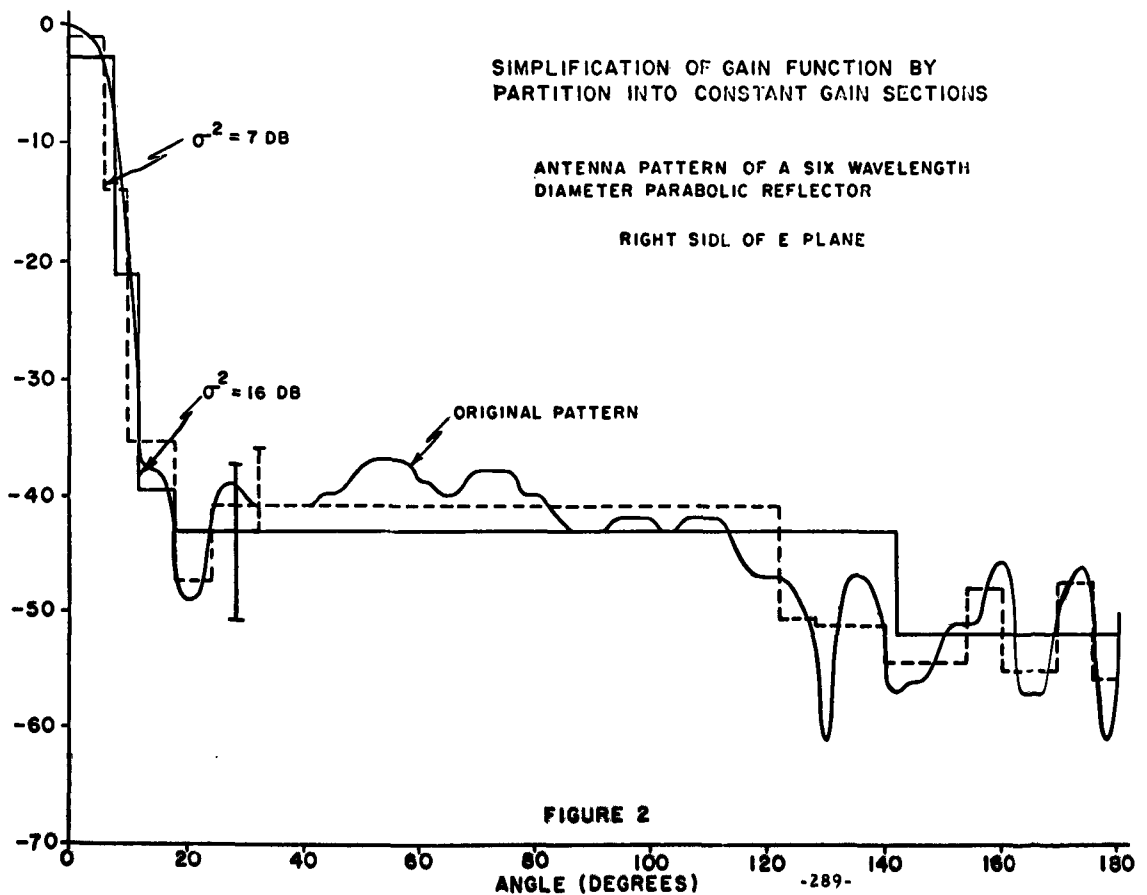
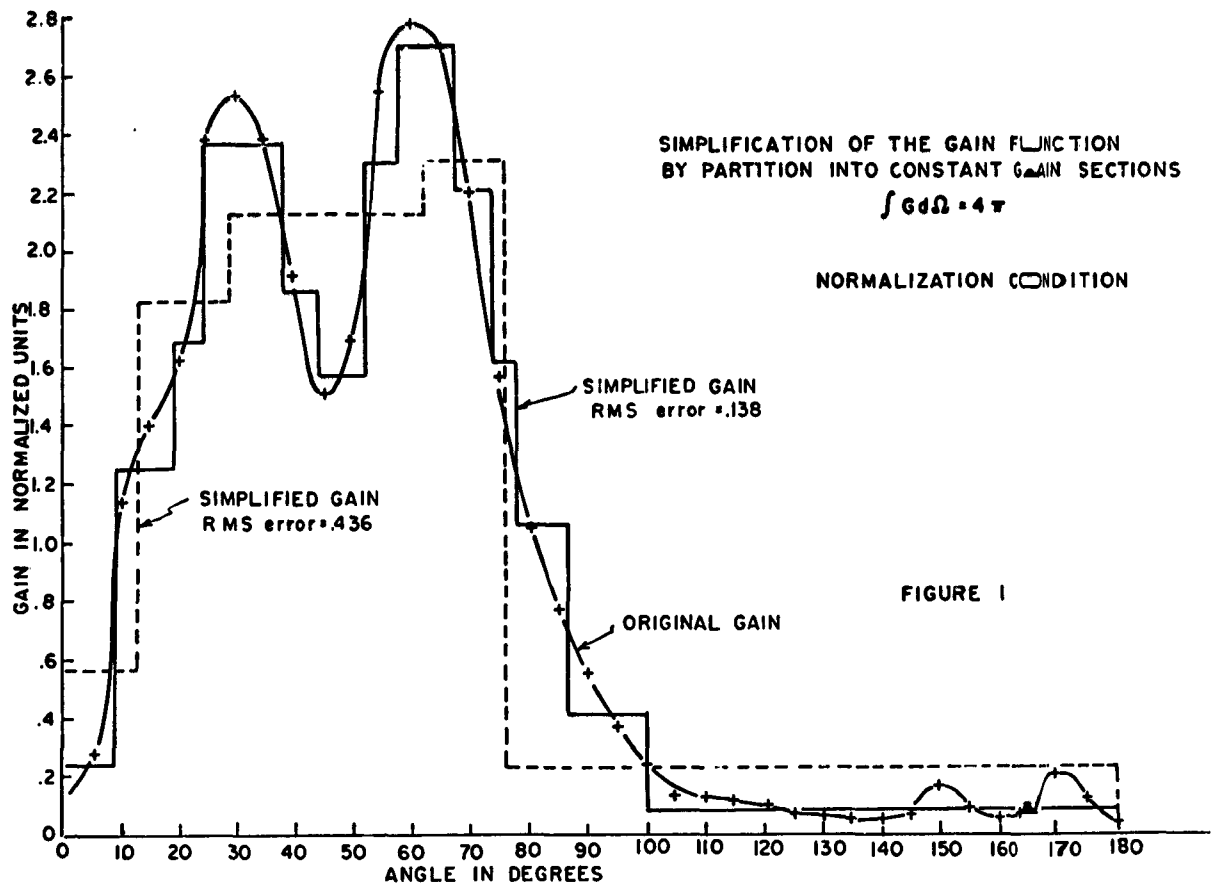
In conclusion, it can be said that the work presented in this paper presents evidence to indicate that the inclusion of a small digital computer as an integral part of an antenna testing site alone can be of considerable value to present day testing procedures.

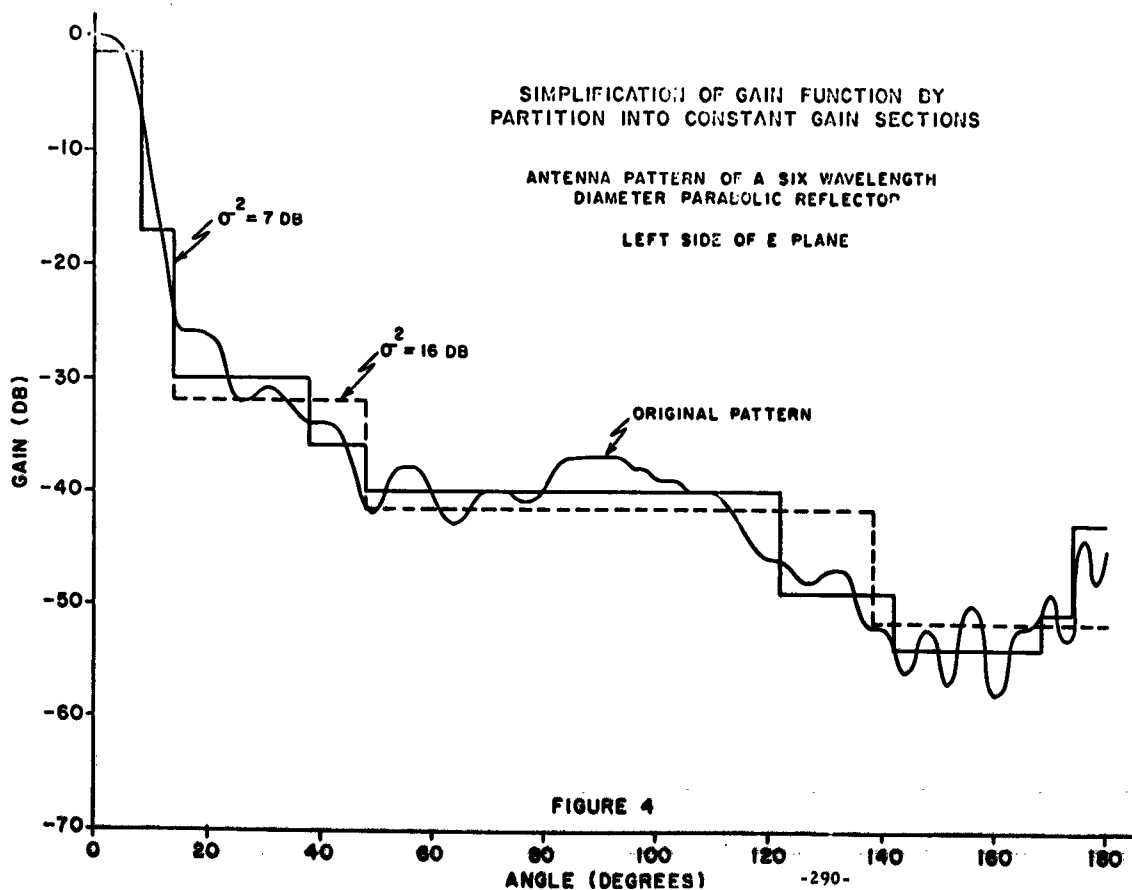
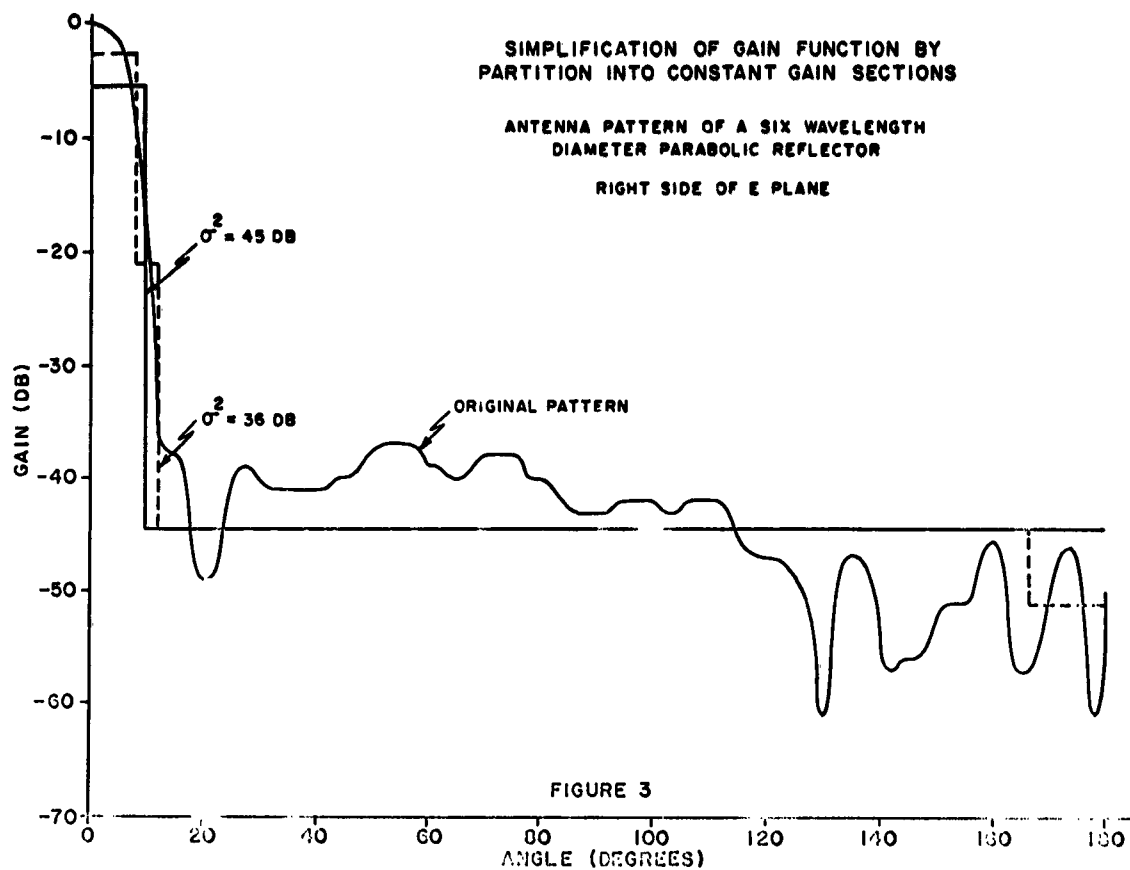
## ACKNOWLEDGEMENTS

This paper was prepared in part under the support of the U.S. Air Force, Rome Air Development Center, Contract No. AF30(602)-2888. The authors also wish to thank Mr. T.C. Lowe for his assistance in the writing of the computer programs. We are indebted to the Moore School of Electrical Engineering for making their digital computer available to us.

## REFERENCES

1. Prepared for Rome Air Force Development Center, Technical Report RADC-TDR-61-312, Interference Analysis Study, Jansky and Bailey, Jan. 1962, Contract No. AF30(602)1934.
2. Armour Research Foundation, Chicago, Wide Angle Radiation Measurements, W.W. Long, October 1960, Proc. of 6th RFI Conference.





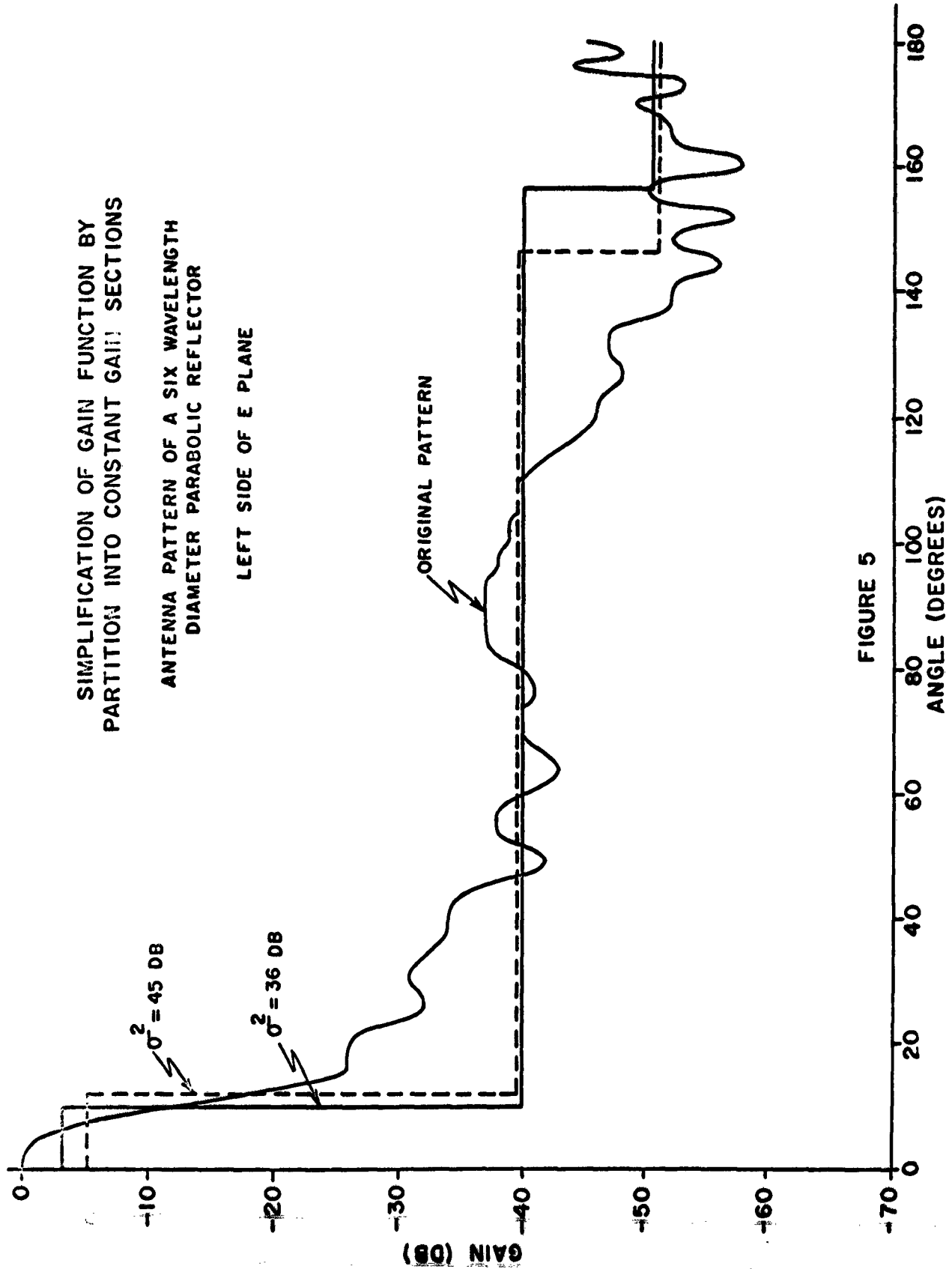


FIGURE 5

$n \backslash m$							
0	$A_0$						
1	$A_1$	$A_1^1$					
2	$A_2$	$A_2^1$	$A_2^2$				
3	$A_3$	$A_3^1$	$A_3^2$	$A_3^3$			
4	$A_4$	$A_4^1$	$A_4^2$	$A_4^3$	$A_4^4$		
5	$A_5$	$A_5^1$	$A_5^2$	$A_5^3$	$A_5^4$	$A_5^5$	
6	$A_6$	$A_6^1$	$A_6^2$	$A_6^3$	$A_6^4$	$A_6^5$	$A_6^6$

Omitted Terms

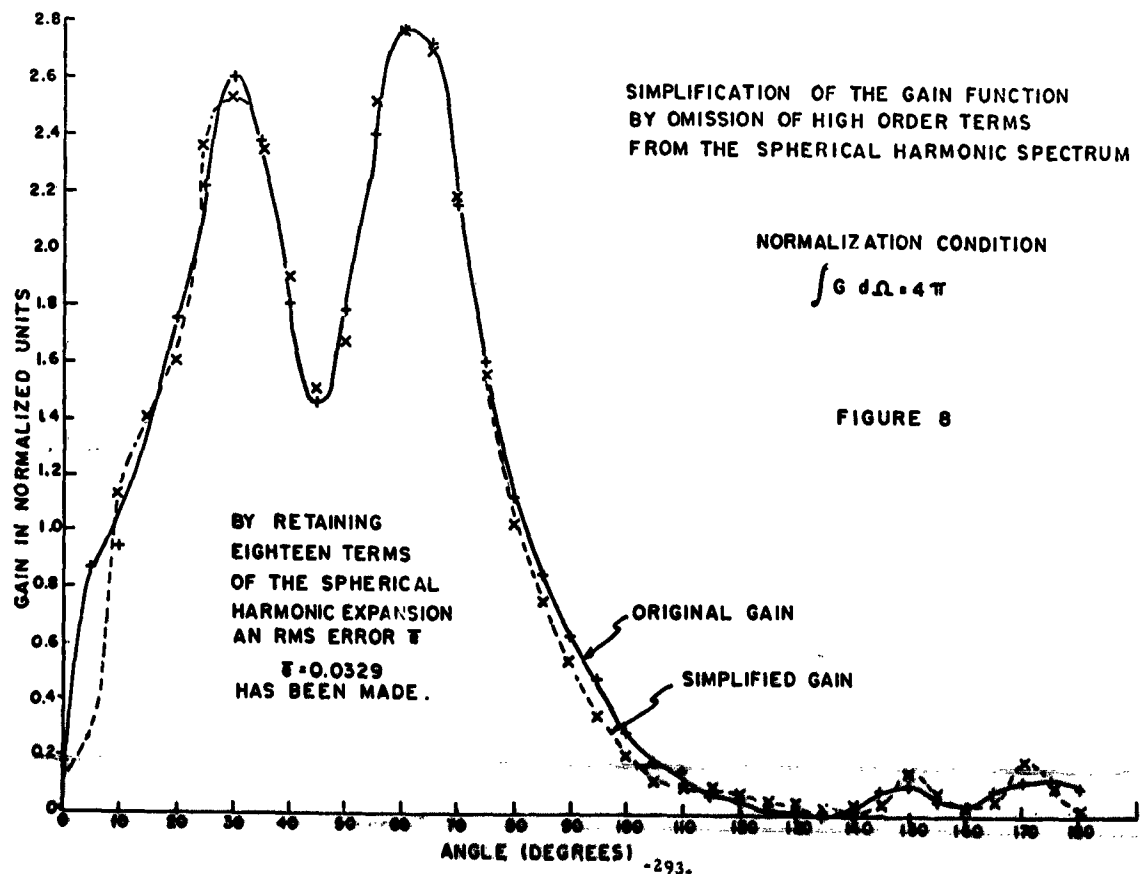
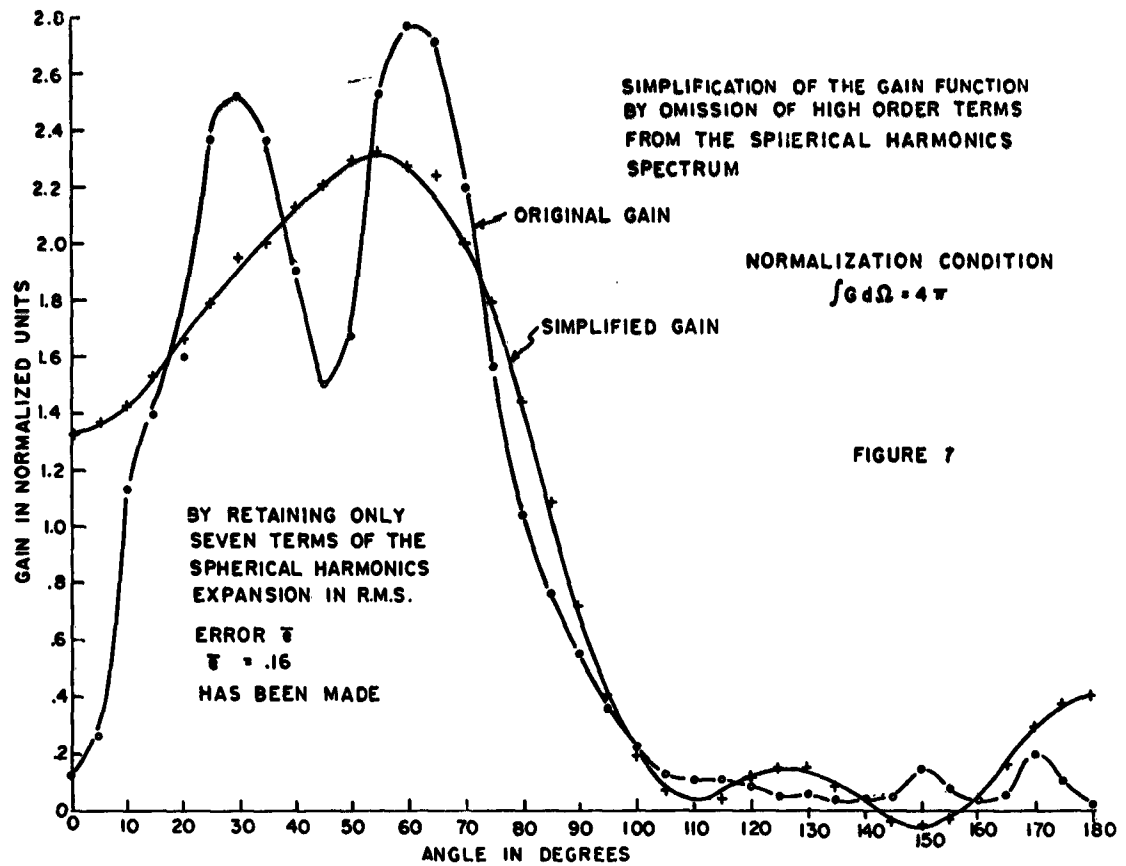
$n \backslash m$							
0	$B_0$						
1	$B_1$	$B_1^1$					
2	$B_2$	$B_2^1$	$B_2^2$				
3	$B_3$	$B_3^1$	$B_3^2$	$B_3^3$			
4	$B_4$	$B_4^1$	$B_4^2$	$B_4^3$	$B_4^4$		
5	$B_5$	$B_5^1$	$B_5^2$	$B_5^3$	$B_5^4$	$B_5^5$	
6	$B_6$	$B_6^1$	$B_6^2$	$B_6^3$	$B_6^4$	$B_6^5$	$B_6^6$

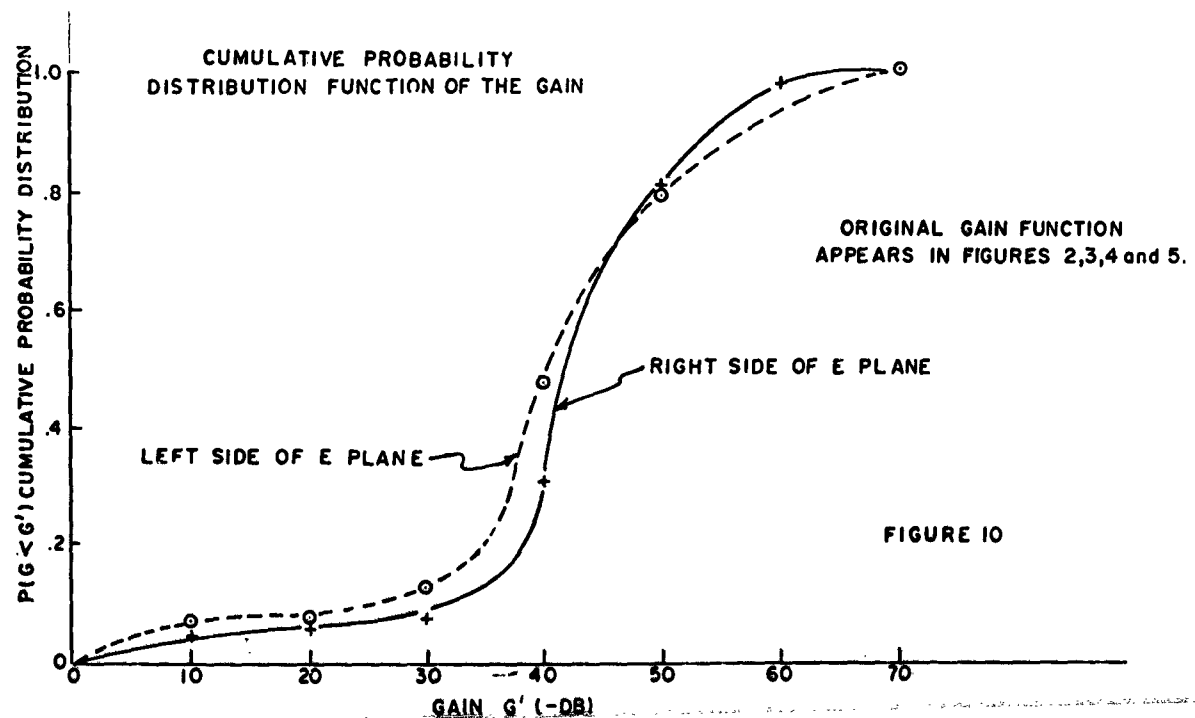
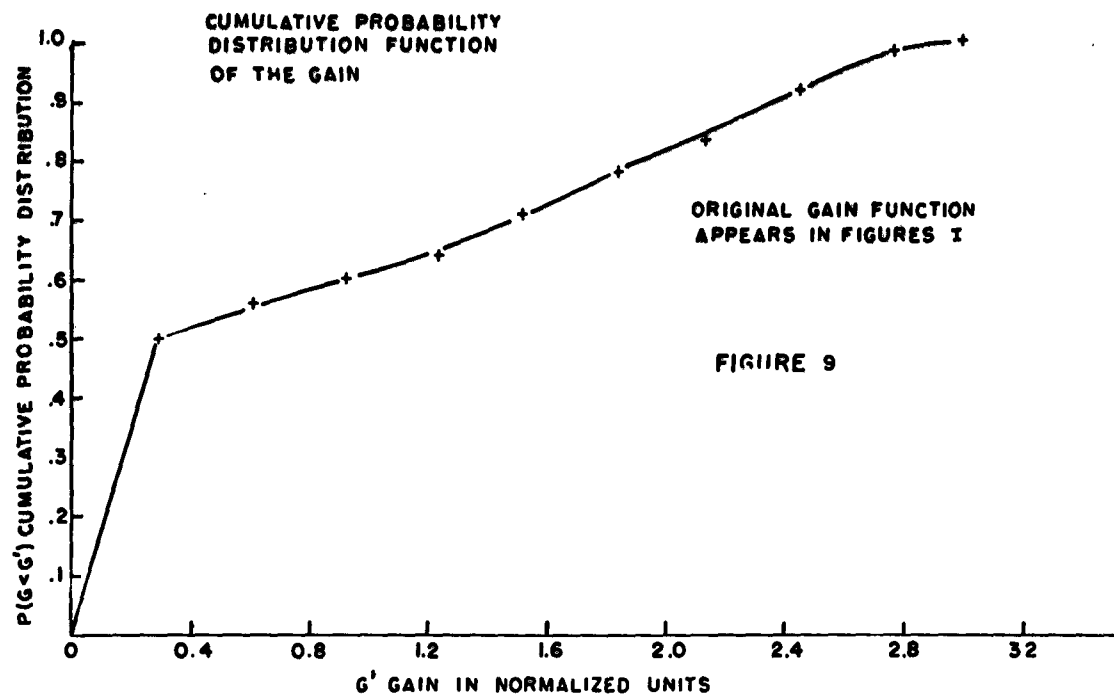
Omitted Terms

The Legendre Spectrum

Figure 6







## THE USE OF DIRECTIONAL COUPLERS AS HARMONIC PADS

L. Young  
Stanford Research Institute  
Menlo Park, California

**Abstract.** - Interference caused by the radiation of harmonic frequencies from high-power transmitters can be reduced or eliminated by using filters external to the high-power tube. The most compact filters are usually rejection filters, which operate by reflecting, rather than absorbing, all or most of the unwanted frequencies. To protect the tube from the reflected harmonic power and to avoid harmonic resonances in the line, it is then advisable to use a harmonic pad between the transmitter and the rejection filter. It is possible to adapt 3-db and 0-db directional couplers for use as harmonic pads, as will be described in this report.

### I. INTRODUCTION

High-power tubes generate a substantial amount of harmonic power, when they are used to full efficiency. If this harmonic power is allowed to reach the antenna, and is radiated, it may cause interference to other radio equipment in the vicinity or in line-of-sight. A harmonic-frequency-suppression filter may be inserted in the transmission line to prevent the unwanted frequencies from reaching the antennas. Such a filter should preferably meet all the following requirements:

1. It should attenuate sufficiently all the major frequency components of the unwanted spectrum; for instance, 60-db of attenuation is often specified.
2. It should attenuate all possible modes in which the unwanted frequencies can propagate in the transmission line.
3. It should attenuate as many harmonics as possible; generally the second and third harmonics are the strongest, but appreciable power may, for instance, also be carried up to the tenth harmonic.
4. It should preferably attenuate by absorbing, rather than reflecting, the spurious frequencies.

In addition, the filter should be compact, inexpensive, easily available, etc. Leaky-waveguide filters<sup>1-4</sup> typically have high attenuation up to about the fourth harmonic, and have a VSWR in the stop band which is generally better than about 1.5:1. Their attenuation eventually falls off as the frequency is increased. Waffle-Iron Filters<sup>5-7</sup> have been used to attenuate strongly up to the tenth harmonic, but they are rejection filters, reflecting the spurious frequencies back to the transmitter. Combinations of leaky-wave filter with waffle-iron filter have also been constructed to combine the advantages of ab-

sorption (and therefore low VSWR in the stop-band) with strong attenuation. A VSWR of 3:1 is probably adequate in the stop band.<sup>8,9</sup> Thus, a short, well-matched pad having absorptive attenuation of 3-db or more should be sufficient in most instances, when used with a rejection filter of high attenuation. A circuit using two harmonic pads is shown schematically in Fig. 1.

Another approach to harmonic padding is to use a 0-db directional coupler with an in-line geometry between the input and one of the decoupled ports, as shown schematically in Fig. 2. The input power at the fundamental frequency then crosses over in virtue of the 0-db coupling, whereas at higher frequencies the 0-db coupling no longer holds, and the power tends to go straight on, past the coupling aperture; the harmonics can then be absorbed in a dummy load.

A similar circuit can be devised for 3-db directional couplers, except that this requires a pair of high-pass filters (Fig. 3a) or reduced-width waveguides (Fig. 3b).

The following brief comparison between leaky-waveguide harmonic pads and directional-coupler harmonic pads is intended to help the system designer make his choice: Leaky-wave filters are more compact, and require no additional dummy load (since the loads are built into the side waveguides). Directional couplers, on the other hand, are more readily available in a wide range of waveguide sizes. Leaky-waveguide filters operate better at the low harmonic frequencies, but are of little use at harmonic frequencies above their design specification for the very reason that directional couplers function as harmonic pads, namely, because the higher frequencies tend to go straight on past any coupling apertures placed flush with the waveguide walls. Thus an optimum combination may well be a leaky-waveguide filter followed by a 0-db directional coupler (Fig. 2) or a 3-db directional coupler (Fig. 3); or an integral combination of a leaky-wave filter with a directional coupler (Section IV).

## II. EXPERIMENTAL TECHNIQUES

The basic experimental set-up is shown in Fig. 4. A swept-frequency generator is synchronized with a pen-and-chart recorder, and the reflected power is recorded continuously. Several signal generators have to be used to cover the whole spectrum of interest. For the couplers tested, most of the measurements were made from the second through fifth harmonic bands. The performance tends to improve with frequency, and the couplers may in general be expected to improve in their performance as harmonic pads at frequencies beyond the fifth harmonic.

Three modes were launched in turn, the  $TE_{10}$ ,  $TE_{01}$ , and  $TE_{20}$  modes, using suitable launchers and long tapers.<sup>10</sup> The incident and reflected powers were sampled by means of 20-db cross-guide directional couplers placed in the single-mode waveguide before the taper started. The incident power was used for a reference output to the automatic leveller circuit in the recorder unit; however, since this did not remove all the variation, both the incident power and the reflected power were recorded on the chart, and the difference was reduced by hand to obtain the figures reproduced later in this report. There were quite

rapid variations with frequency, probably mostly due to imperfect directivity in the cross-guide couplers. Only the peak reflections were plotted, and joined by straight lines; the actual performance is probably somewhat better since no allowance was made for the directivity of the cross-guide couplers, which is in the order of 20 db. (For instance, if the reflected power is 6 db below the incident power, the reflection coefficient recorded with a directional coupler of 20 db directivity could lie anywhere between about -4 and -8 db. Such variations were indeed observed and moved in frequency as expected when the spacing between the harmonic pad and the cross-guide coupler was changed by inserting an extra length of waveguide.)

### III. DIRECTIONAL COUPLERS AS HARMONIC PADS

To the best of my knowledge, the first use of a 0-db directional coupler to separate the harmonic frequencies from the fundamental band was made by V. G. Price,<sup>11</sup> who used a 0-db branch-guide directional coupler. The same idea, using a 0-db transvar directional coupler, was used by E. M. T. Jones at SRI<sup>12</sup>. In the early work, it was hoped to introduce substantial attenuation (say, more than 30 db) at the harmonic frequencies, between the input and the fundamental-frequency output (Fig. 2). These hopes were largely disappointed, since the attenuation was sometimes less than 10 db, and the reflection at certain frequencies was also high. The author used a 0-db branch-guide directional coupler with waffle-iron filters in the branches and realized about 30-db of attenuation from the 2nd to the 5th harmonic.<sup>13</sup> It then became apparent that the most practical application of directional couplers (0-db or 3-db) was as harmonic pads (not filters), where high attenuation was not the primary object, but where it was desired to combine low, steady attenuation over a wide frequency band (many octaves, to include perhaps ten or more harmonics) by absorption, rather than reflection, leaving the high attenuation to a more compact rejection filter (e.g., multi-cavity band-pass filter, or waffle-iron low-pass filter).

An experimental program was then undertaken, testing other types of directional couplers. In particular, short-slot couplers have been tested, both sidewall<sup>14</sup> and topwall, both in 3-db and 0-db configurations. Most of the results of these measurements are published in Ref. 13, and the ensuing remarks are a summary of the principal results, plus the results on one new 3-db coupler circuit, which has only recently been tested.

Branch-guide couplers<sup>15,16</sup> have been built both with plain waveguide branches, and with additional chokes in their branches,<sup>17</sup> and used in both the 0-db and 3-db configurations. Finally a branch-guide coupler with waffle-iron filters in the branches was also built,<sup>13</sup> and used as a 0-db coupler harmonic pad. The branch guide coupler has the advantage that the coupling between the parallel waveguides is not just through coupling apertures,<sup>17</sup> but is through waveguides of definite length, into which chokes<sup>17</sup> or filters<sup>13</sup> may be built. It is a very interesting and potentially useful device, but would be considerably more expensive and is less readily available than the short-slot couplers which will now be described.

Two sidewall short-slot couplers, Model 284 HS 22, and two topwall short-slot couplers, Model 284 HT-1332, were purchased from Microwave Development Laboratories. Each coupler is a 3-db hybrid, and the phase of their two outputs is such that two like couplers can be cascaded to form a 0-db coupler. The two 3-db sidewall couplers cascaded into a single 0-db coupler are sketched in Fig. 5, and the two topwall couplers are similarly shown in Fig. 6. The best results were obtained with the sidewall couplers, i.e., the lowest overall reflections were recorded when they were tested as indicated in Fig. 4. The spacing between the two separate 3-db couplers (Fig. 5) does not appear to be critical, but when in one experiment the slots were completely merged, the performance deteriorated distinctly; it therefore seems advisable to retain some center-wall between the two slots, though the length of that center-wall should not be critical.

The highest recorded reflection for the 0-db sidewall coupler (Fig. 5) from the second to the fifth harmonic, inclusive, was -5 db for the  $TE_{10}$  mode, and -8 db for the  $TE_{01}$  mode;<sup>13</sup> however, it was higher for the  $TE_{20}$  mode, in which it reached -0.5 db at 6.4 Gc. The average reflection was much better in all cases, being generally between -10 and -20 db, but could not be measured accurately because of the limited directivity of the cross-guide couplers (Fig. 4), which was only about 20 db.

The 3-db couplers performed even better than the 0-db couplers, in all cases, which qualitatively may be attributed to the momentum of the incident harmonic power, which probably prefers to keep going in the same direction; thus there is less chance of it being reflected into the (reverse) output of a 3-db coupler (Fig. 3) than crossing over into the (forward) output of a 0-db coupler (Fig. 2). The problem with the 3-db coupler harmonic pad is the necessity for a high-pass filter to turn the incident fundamental power round. It is difficult to build a high-power, high-pass filter insensitive to mode configuration in a multi-mode waveguide. The circuit of Fig. 3b is probably a good compromise between effectiveness and simplicity. A perspective view is sketched in Fig. 7. Its action may be explained as follows.

The two vertical septums to the right in Fig. 3b or Fig. 7 are each 1/4-inch thick and create three parallel waveguides, each of width 1.780 inches. This is sufficiently beyond cut-off in the fundamental pass band (2.7 - 2.9 Gc). The front edges of the two septums are placed approximately in the same plane where the single common wall had begun before it was machined out. They are then adjusted for optimum match in the pass band. (The pass-band VSWR was quickly adjusted to be better than 1.2, but no attempt was made to improve it further.)

The reduced-width waveguides may be expected to pass on most power in the  $TE_{10}$  mode from the second harmonic on up. Modes can propagate in the WR-284 input waveguide and be close enough to cut-off there, that they would be cut off in the three waveguides of reduced width; however, when such modes enter the large central region of the coupler, the mode patterns will change, and some power may be expected to couple into the three waveguides on the right in the  $TE_{10}$  or some other propagating mode. It is hoped that this power is always sufficient to preserve the effectiveness of the harmonic pad under all conditions.

The experimental performance of the 3-db coupler is shown in Figs. 8 and 9 up to 15.5 Gc. Figure 8 shows the highest reflection coefficient peaks (compare Ref. 13) in the  $TE_{10}$  and  $TE_{01}$  modes for the 3-db coupler of Fig. 3b and Fig. 7. Figure 9 shows the same for the  $TE_{20}$  mode. Here the solid line is for the 3-db coupler of Fig. 3b and Fig. 7, while the broken line is for the 0-db coupler of Fig. 2 and 5. (The performance of this same 0-db coupler in the  $TE_{10}$  and  $TE_{01}$  modes is plotted in Fig. 16 of Ref. 13.) It is seen from Figs. 8 and 9 that the 3-db coupler (Fig. 7) performs much the same as the 0-db coupler (Fig. 5) in the  $TE_{10}$  and  $TE_{01}$  modes,<sup>13</sup> but is somewhat better in the  $TE_{20}$  mode, since the greatest reflection coefficient (which is still at the same frequency, 6.4 Gc), is only about -3 db, as compared with about -0.5 db for the 0-db coupler.<sup>13</sup>

#### IV. A SUGGESTED DIRECTIONAL-COUPLER, LEAKY-WAVE FILTER COMBINATION

So far, directional couplers have been discussed only in connection with using them as harmonic pads, where the required attenuation is not too high. However, the attenuation of directional-coupler harmonic pads increases with frequency, precisely as the attenuation of conventional leaky wave filters falls off. One can think of many suitable combinations, as already hinted at the end of Section I. One such possible combination is sketched in Fig. 10, where two leaky-wave filters are connected by a 3-db sidewall coupler, which itself sprouts side-waveguides in all available directions. The whole filter is constructed as an integral unit, and could be designed to attenuate well beyond the fourth or fifth harmonic.

#### V. CONCLUSIONS

The experiments indicate that 3-db and 0-db directional couplers can be used as harmonic pads. Of the various types of couplers investigated so far, the short-slot sidewall coupler gave the best overall results, with the 3-db coupler (Fig. 7) perhaps having the edge over the 0-db coupler (Fig. 5). However, other types of coupler may be equally good or better, and further tests on more couplers and in more modes should be made.

In general, directional couplers improve in performing as harmonic pads as the frequency is increased. This is in contrast with leaky-waveguide filters which perform better at the lower harmonic frequencies (for which the side waveguides have a higher impedance). Sidewall couplers, in particular, offer a simple means of harmonic padding, and of extending the absorptive attenuation well beyond the first few harmonics.

#### ACKNOWLEDGMENTS

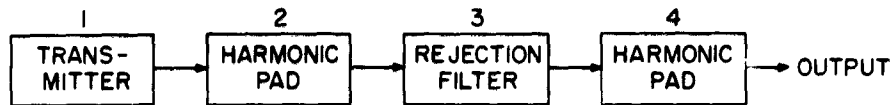
The measurements were ably performed by Mr. R. Larrick, Mr. P. Reznick, and Mr. E. Fernandes. This work was supported by Contract AF 30(602)-2734 and AF 30(602)-3174 for the Rome Air Development Center. The work is under the guidance of Capt. Owen Allen at RADC.

#### REFERENCES

1. V. G. Price, R. H. Stone and V. Met, "Harmonic Suppression by Leaky-Wall Waveguide Filters," WESCON Convention Record, Part 1, Vol. 3, pp. 112-118 (1959).
2. V. Met, "Absorptive Filters for Microwave Harmonic Power," Proc. IRE 47, pp. 1762-1769 (October 1959).
3. Edward G. Cristal, "Analytical Solution to a Waveguide Leaky-Wave Filter Structure," IEEE Trans. PTGMITT-11, pp. 182-190 (May 1963).
4. Edward G. Cristal, "A 1-5/8-Inch Coaxial Leaky-Wave Filter for the Suppression of Spurious Energy," The Microwave Journal, Vol. 6, No. 9, pp. 72-76 (September 1963).
5. E. Sharp, "A High-Power Wide-Band Waffle-Iron Filter," IEEE Trans. PTGMITT-11, pp. 111-116 (March 1963).
6. L. Young and B. M. Schiffman, "New and Improved Types of Waffle-Iron Filters," Proc. IEE, Vol. 110, No. 7, pp. 1191-1198 (July 1963).
7. L. Young, B. M. Schiffman, and O. W. Allen, Jr., "The Waffle-Iron Filter--A Microwave Filter to Suppress Spurious Frequencies at the Source," presented at the Fifth National Symposium on Radio Frequency Interference in Philadelphia, Pennsylvania (June 5, 1963).
8. L. A. Robinson, E. G. Cristal, B. M. Schiffman, and L. Young, "Suppression of Spurious Frequencies," Quarterly Progress Report 2, SRI Project 4096, Contract AF 30(602)-2734, Stanford Research Institute, Menlo Park, California (October 1962).
9. E. G. Cristal, L. Young, and B. M. Schiffman, "Suppression of Spurious Frequencies," Quarterly Progress Report 3, SRI Project 4096, Contract AF 30(602)-2734, Stanford Research Institute, Menlo Park, California (January 1963).
10. L. Young, B. M. Schiffman, E. G. Cristal, and L. A. Robinson, "Suppression of Spurious Frequencies," Quarterly Progress Report 4, SRI Project 4096, Contract AF 30(602)-2734, Stanford Research Institute, Menlo Park, California (June 1963).
11. V. G. Price, "Measurement and Control of Harmonic Microwave Energy," Final Report, Change B, Report TIS R60ELM112-5, Contract AF 30(602)-1670, General Electric Microwave Laboratory, Palo Alto, California (20 May 1960), RADC TR-60.



12. E. M. T. Jones, E. D. Sharp, H. Guthart and S. B. Cohn, "Investigation of High Power Filter Techniques," Final Report, pp. 9, 10, and 11, SRI Project 2797, Contract AF 30(602)-1998, Stanford Research Institute, Menlo Park, California (March 1961), RADC-TR-61-152.
13. L. Young, "Waveguide 0-db and 3-db Directional Couplers as Harmonic Pads," The Microwave Journal, to be published.
14. H. J. Riblet, "The Short-Slot Hybrid Junction," Proc. IRE, 40, pp. 180-184 (February 1952).
15. J. Reed, "The Multiple Branch Waveguide Coupler," IRE Trans. PGMTT-6, pp. 398-403 (October 1958).
16. L. Young, "Synchronous Branch Guide Directional Couplers for Low and High Power Applications," IRE Trans. PGMTT-10, pp. 459-475 (November 1962).
17. L. Young, "The Application of Branch-Guide Couplers to the Suppression of Spurious Frequencies," Fourth IRE-PGRFI Symposium, San Francisco, California (June 1962).



1. THE HIGH-POWER TRANSMITTER GENERATES SPURIOUS FREQUENCIES CAUSING RADIO FREQUENCY INTERFERENCE.
2. THIS HARMONIC PAD PREVENTS DAMAGE TO THE TUBE BY ABSORBING HARMONICS REFLECTED BY THE REJECTION FILTER.
3. THE REJECTION FILTER (E.G. A LOW-PASS WAFFLE-IRON FILTER) IS CAPABLE OF HIGH ATTENUATION AT THE SPURIOUS (E.G. HARMONIC) FREQUENCIES BY REFLECTING THEM.
4. A SECOND HARMONIC PAD MAY BE ADDED IF IT IS DESIRED TO MATCH THE OUTPUT OF THE FILTER AT HARMONIC FREQUENCIES.

FIG. 1 SHOWING THE USE OF HARMONIC PADS

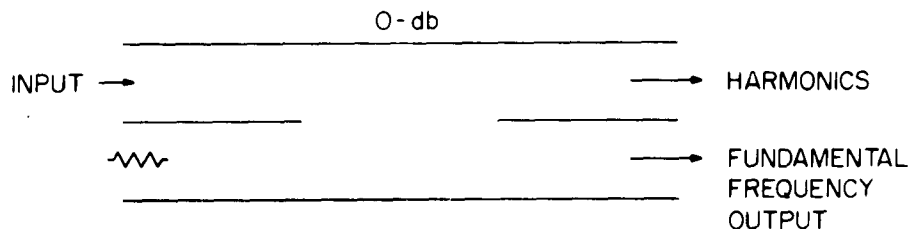
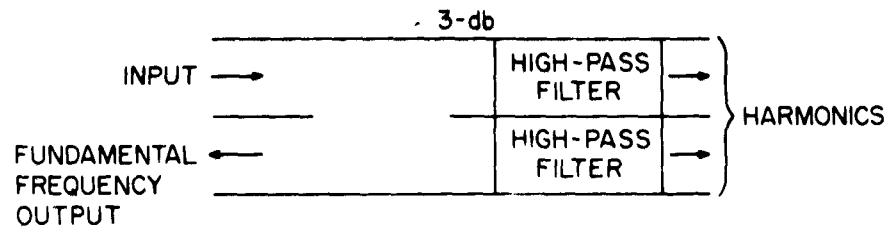
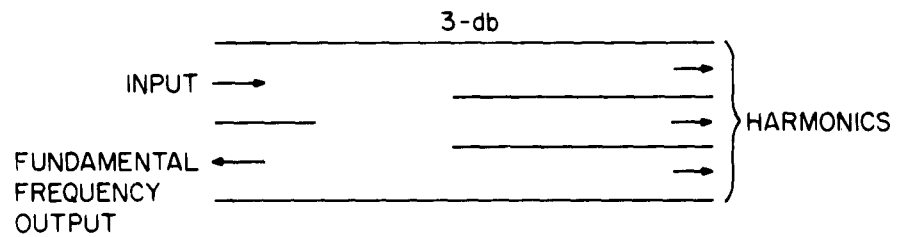


FIG. 2  
SCHEMATIC OF 0-db SHORT-SLOT  
COUPLER USED AS HARMONIC PAD



(a)



(b)

FIG. 3  
SCHEMATIC OF TWO 3-dB SHORT-SLOT-  
COUPLER CIRCUITS USED AS HARMONIC PADS

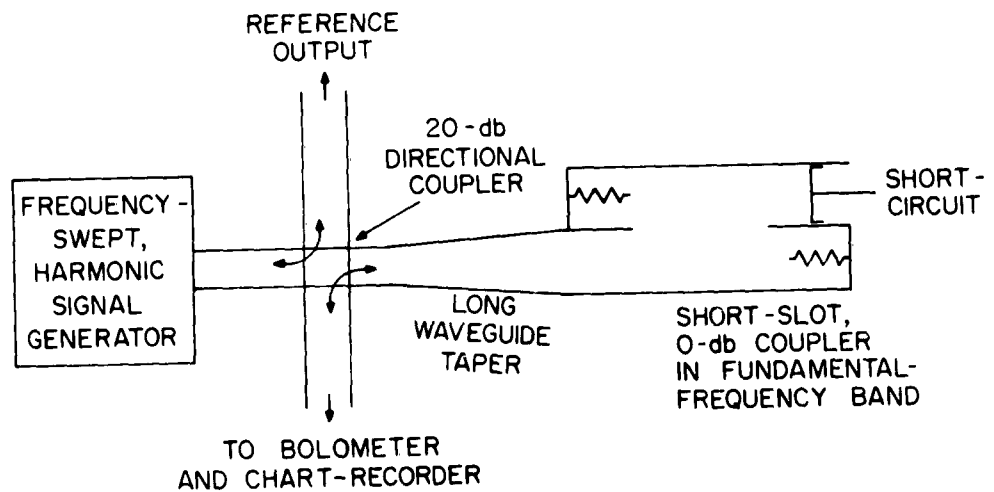


FIG. 4  
SET-UP FOR CONTINUOUSLY RECORDING  
REFLECTED POWER FROM A HARMONIC PAD

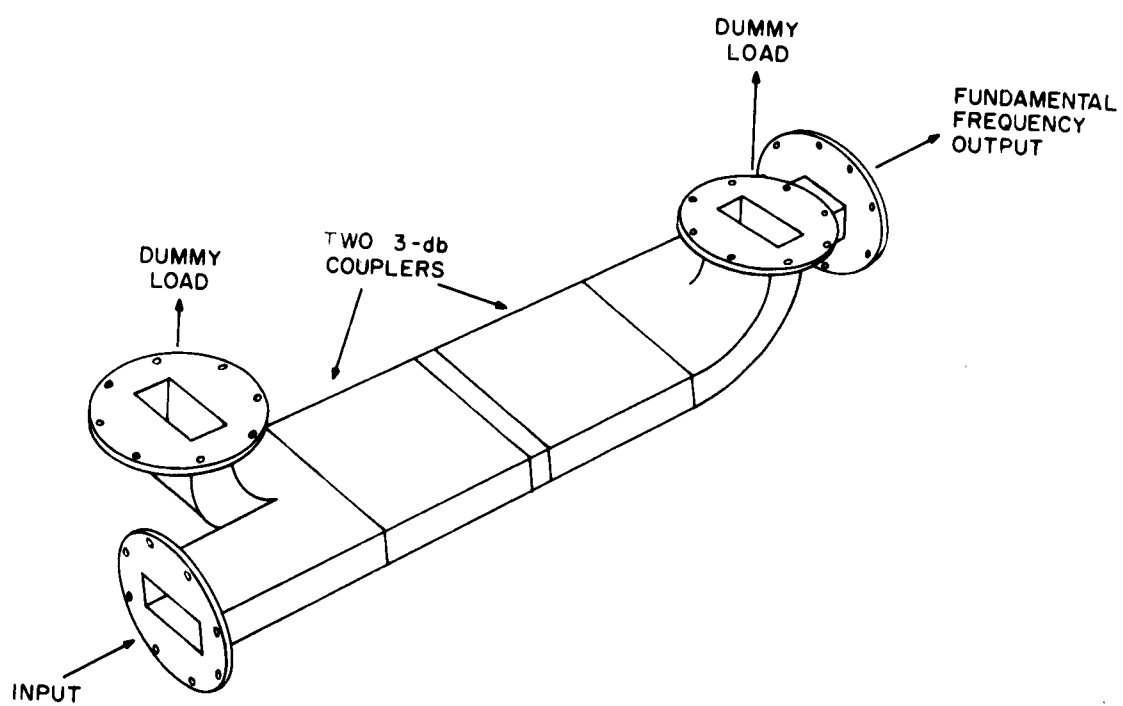


FIG. 5  
SKETCH OF 0-db SHORT-SLOT  
SIDE-WALL COUPLER

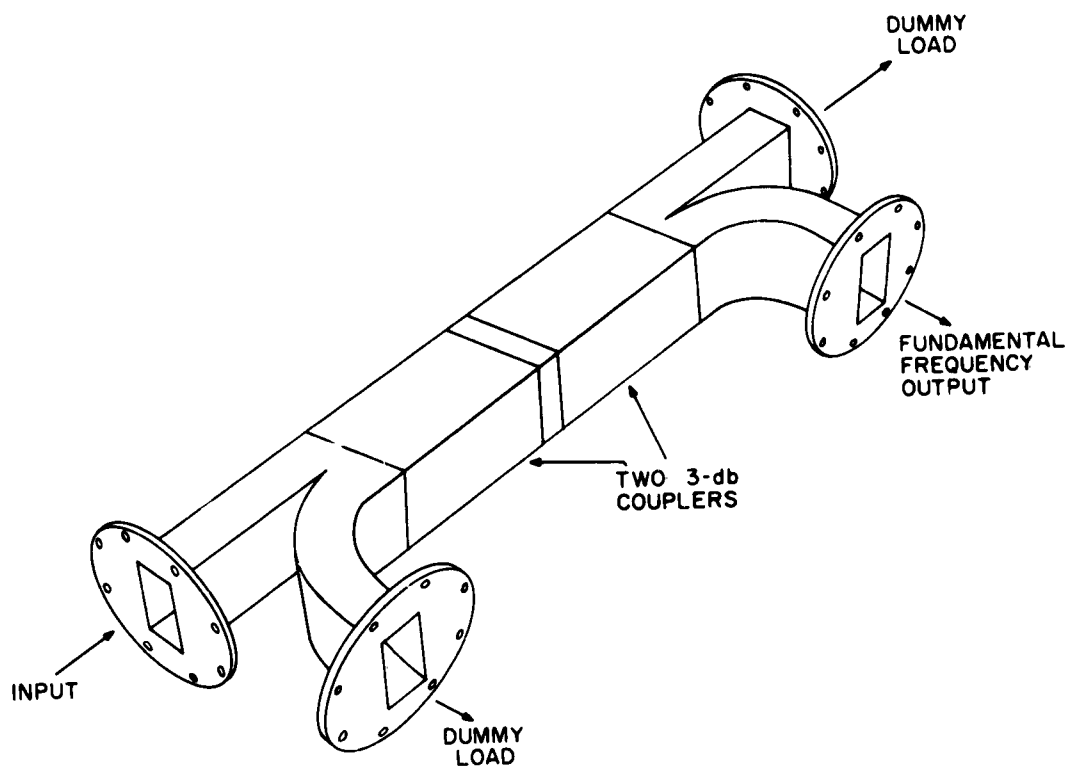


FIG. 6  
SKETCH OF 0-db SHORT-SLOT  
TOP-WALL COUPLER

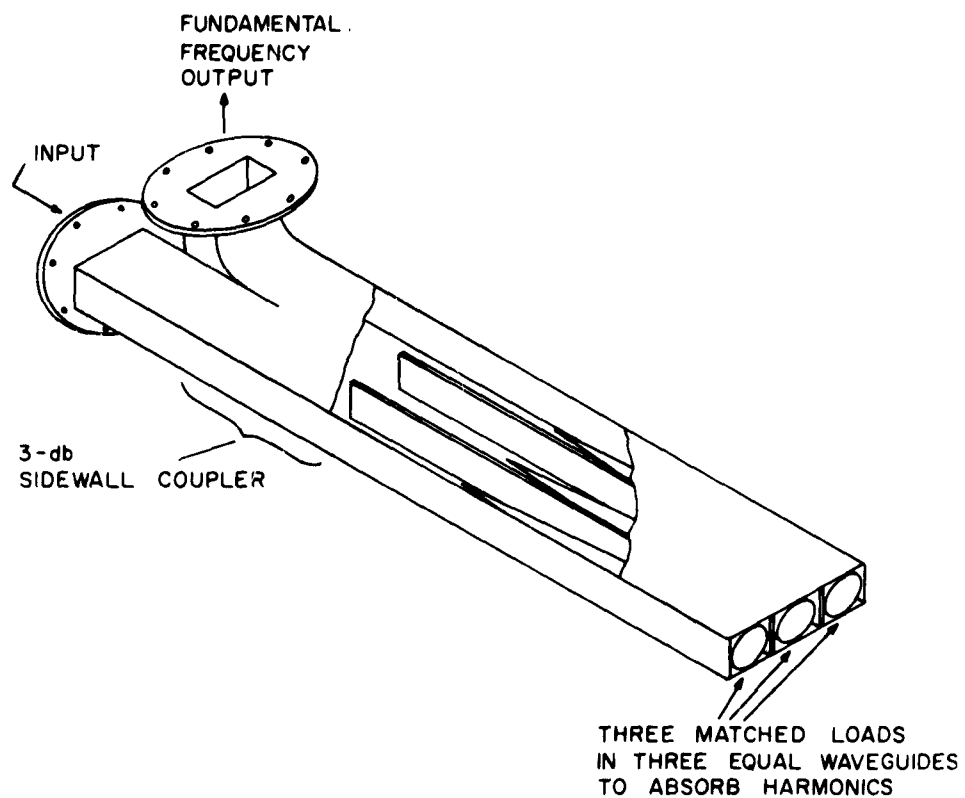


FIG. 7  
 SKETCH OF 3-dB SIDE-WALL  
 COUPLER WITH THREE CUT-OFF  
 WAVEGUIDES TO ABSORB HARMONICS

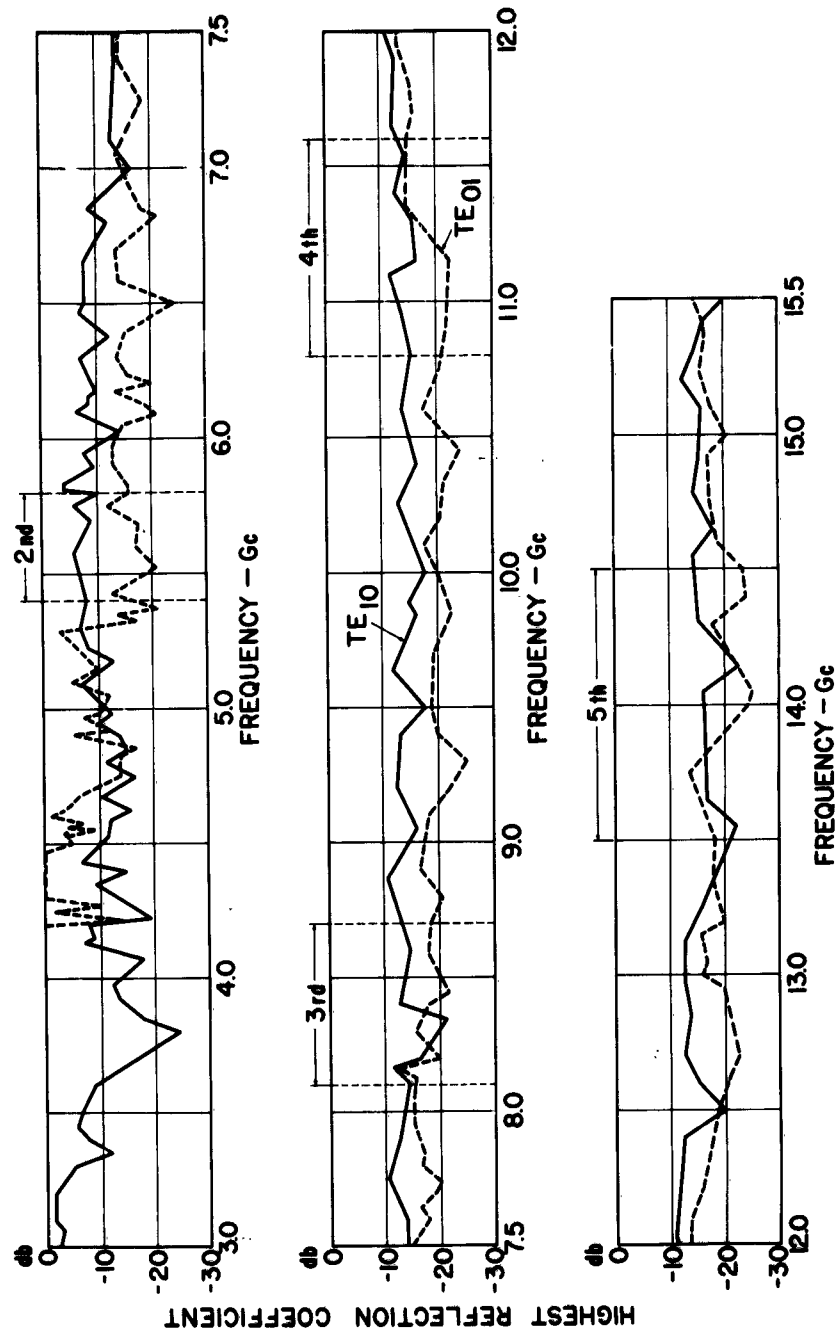


Fig. 8 Reflection Coefficients in the Stop-Band of the 3-dB Sidewall Coupler (Fig. 7) in the TE<sub>10</sub> and TE<sub>01</sub> Modes

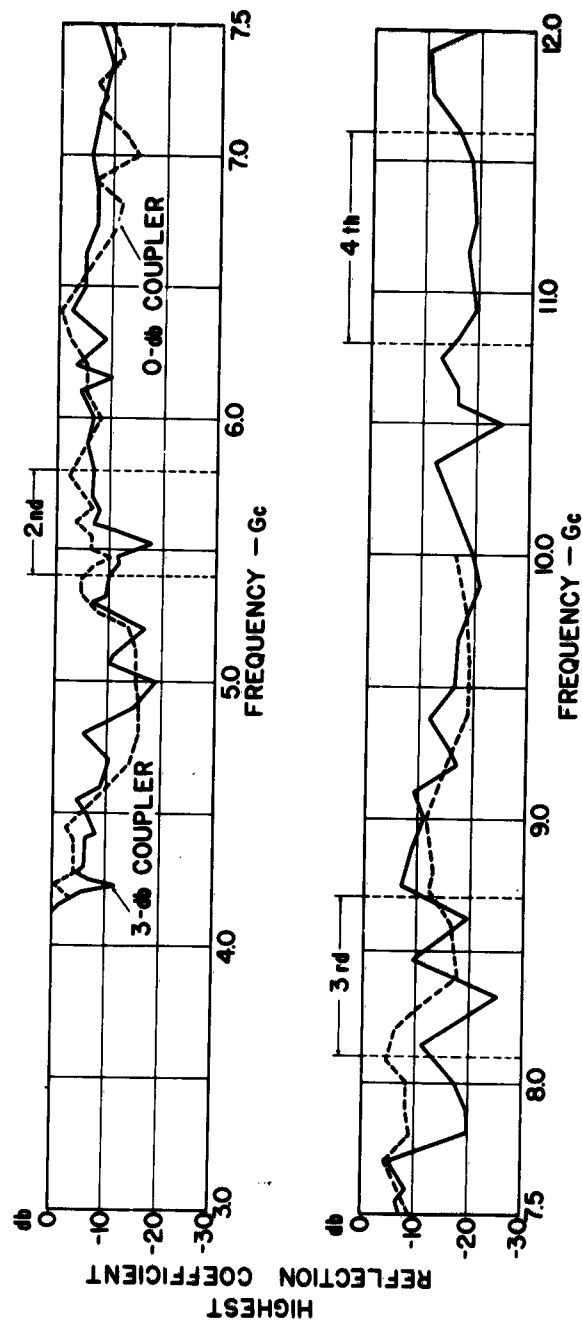


Fig. 9 Reflection Coefficients in the Stop-Band of the 3-dB (Solid Line) and 0-dB (Broken Line) Sidewall Couplers (Figs. 7 and 5, Respectively) in the  $TE_{20}$  Mode



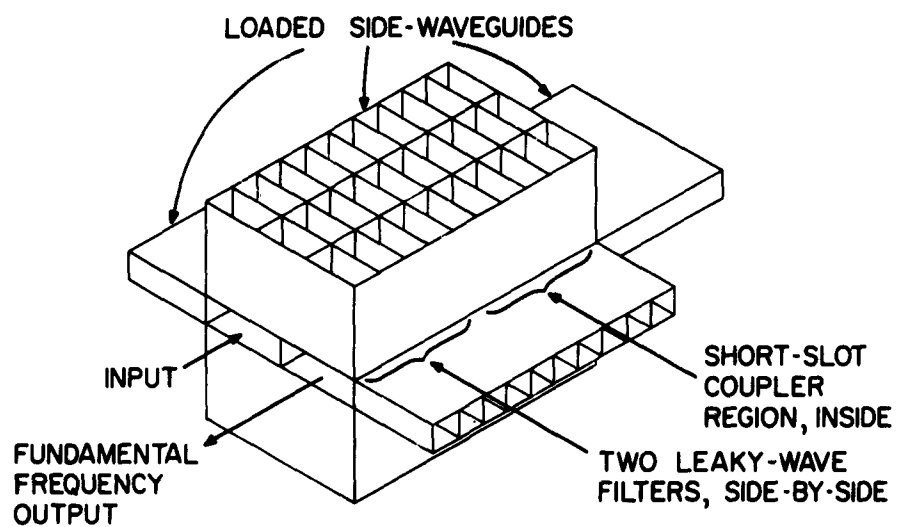


FIG. 10

SUGGESTED COMBINATION OF LEAKY-WAVE  
PRINCIPLE WITH 3-db DIRECTIONAL COUPLER  
AS HARMONIC FILTER ABSORBING UP TO HIGH  
HARMONIC FREQUENCIES

## A STANDARD RESPONSE INDICATOR FOR PULSED SYSTEMS

W. R. Free and L. A. Hill  
Sperry Microwave Electronics Company  
Division of Sperry Rand Corporation  
Clearwater, Florida

**Abstract.** - This paper describes a new instrument for use with pulsed systems which indicates electronically and visually the signal-plus-noise to noise ratio of a system receiver video output. The portable self-contained unit is fully transistorized, and was designed under Air Force contract as part of the AN/MSM-63 (XW-1) spectrum signature measurement equipment. The electronic indication consists of a d-c step whenever the signal-plus-noise to noise ratio  $(S+N)/N$  is above a preselected limit (or within upper and lower limits), while the visual indication consists of a meter calibrated in db which registers the detected ratio.

By utilizing this instrument it is possible to eliminate human operator judgment in determining the actual level of a desired receiver response. Thus, the reliability and repeatability of such measurements are greatly enhanced when this standard response indicator is incorporated into a measurement technique.

The operation of the indicator and its application in other measurement functions, as well as that associated with obtaining spectrum signatures of the type delineated in MIL-STD-449A, is described.

### I. INTRODUCTION

During the development of the AN/SM-63 (XW-1) Mobile Spectrum Signature Measurement System, it became apparent that a device for determining the presence and/or absence of a given signal-to-noise ratio at the output of a remote receiver would be necessary in order to perform receiver spectrum signature measurements on a radiated basis.

Although MIL-STD-449A indicates the requirement for a standard response indicator for closed-system tests as well as radiated tests, the equipment to be used is not defined or described. From experience, it was known that distortion analyzers are used to perform this function during spectrum signature measurements on communications receivers. However, these equipments are not compatible with pulsed systems since they operate by means of a frequency division multiplex technique, while pulsed systems require a time division multiplex technique with synchronization to the received PRF. After a comprehensive search failed to locate any equipment capable of performing the standard response indicator function, a decision to develop a suitable instrument was made.

### II. DESCRIPTION OF OPERATION

A block diagram of the standard response indicator developed is shown in Figure 1. There are two inputs required for the unit - the video output from the receiver under test and a PRF synchronization waveform from the simulated radiator. The video and noise from the receiver under test is amplified in a video amplifier (block 1). The gain of this amplifier is controlled by an AGC loop consisting of blocks 2, 3 and 4. The output from the video amplifier is split into two channels, a noise channel and a pulse channel. The noise immediately preceding each pulse is sampled by means of a 15 usec noise gate, starting 25 usec before the pulse, in the noise channel (block 2). This noise sample

is amplified in a threshold amplifier (block 3). This amplifier has an adjustable threshold which determines the noise level at the output of the video amplifier. The amplified noise samples are integrated and converted into a d-c AGC voltage in the AGC driver stage (block 4). This AGC voltage controls the gain of the video amplifier to maintain the noise level at the output of the video amplifier constant, independent of the input noise level. This level is established by the threshold setting in block 3.

It is apparent from the above discussion that the combination of the input video amplifier and the AGC loop results in a known, constant noise level at the input of the pulse channel, independent of the input noise level, and since the pulse amplitude has been changed proportionally to the noise amplitude in the common video amplifier, it is only necessary to measure the pulse amplitude to establish the  $(S+N)/N$  ratio of the input video signal.

The desired pulse is gated into the pulse channel by means of a pulse gate (block 8). The gated pulse is applied to a transistorized peak voltmeter (block 9) which provides a continuous, direct reading of  $(S+N)/N$  ratio in db on a front panel meter. The gated pulse is also routed to a pulse amplitude evaluation circuit (block 10). This circuit contains two limits which may be adjusted independently in the range from 0 to 20 db. The lower limit is set by means of a front panel control labeled " $(S+N)/N$  Ratio" and the upper limit is set by means of a front panel control labeled " $(S+N)/N$  Range". An output pulse is obtained from this circuit only when the gated pulse amplitude falls between these two limits. The upper limit may be eliminated, if desired, by setting the " $(S+N)/N$  Range" control in the maximum position. An output pulse from the pulse amplitude evaluator circuit changes the state of a bistable multivibrator which is the Go/No-Go output generator (block 11) which controls the standard response indicator light (block 12) and derives the Go/No-Go output signal. In addition, the output pulses from the pulse amplitude evaluator are routed to the front panel "Pulse Count" output jack which provides a count of the number of pulses whose amplitudes fall within the two selected limits.

A mode switch (block 15) is provided to reverse the operation of the standard response indicator and the Go/No-Go output signal. When the mode switch is in the "mode 1" position, the standard response indicator light is on and a +12 VDC "Go" signal is present at the Go/No-Go output jack when the input video falls within the preset limits. When the mode switch is in the "mode 2" position, the standard response indicator light is on and a +12 VDC "Go" signal is present when the input video falls outside the preset limits. These two modes are desirable since some tests require that a standard response be established and other tests require that a standard response be degraded.

The timing of the various gating waveforms is determined by the PRF synchronization waveform from the simulated radiator, which is applied at the front panel "Reference PRF Input" jack, and the PRF trigger delay circuit (block 7). The PRF trigger delay circuit generates a trigger delayed from the previous PRF pulse to initiate the gates 25 usec before the next pulse. The delay range of the PRF trigger delay circuit is 25 usec to 10 msec, which allows the unit to operate over a PRF range from 100 to 20,000 pps. The extremely large delay range of this circuit generated a serious calibration problem. For proper operation, it is necessary that the delay be positioned to an accuracy of approximately  $\pm 5$  usec. To circumvent the calibration and dial resolution problems resulting from this accuracy requirement, a gate position indicator (block 13) and gate position indicator light (block 14) were provided. The pulse position generator consists of a 25 usec gate generator, a coincidence

circuit, and a bistable multivibrator. The 25 usec pulse generator is triggered by the delayed trigger from the output of the PRF trigger delay circuit. The 25 usec gate waveform is compared with the reference PRF waveform in the coincidence circuit. The delay is increased until the trailing edge of the 25 usec gate is coincident with the leading edge of the following PRF pulse. This condition is shown graphically in Figure 2. The coincidence of the trailing edge of the 25 usec gate and the leading edge of the PRF pulse changes the state of the bistable multivibrator, causing the gate position indicator to light. Thus, accurate positioning of the delayed trigger is assured without precision calibration of the delay dial. The accurately positioned delayed trigger triggers the noise gate generator (block 5) and the pulse gate generator (block 6). The noise gate generator provides a 15 usec gate waveform for the noise gate and the pulse gate generator produces a 50 usec gate waveform for the pulse gate. The relative positions and widths of the various gating waveforms with respect to each other, as well as the input video reference PRF waveforms are shown in Figure 2.

### III. EQUIPMENT SPECIFICATIONS

The completed standard response indicator is shown in Figure 3. This is a portable, fully transistorized unit packaged in a 18" x 11" x 13" transport case and weighs approximately 40 lbs. The input power requirement is 105-125 volts, 1 amp., 50-400 cps.

#### Specifications:

Input Pulse Width Range:	0.25 usec - 10 msec
Pulse Repetition Rate Range:	100 - 20,000 pps
Input Noise Range:	0.1 - 0.5 volts rms
Input Pulse Range:	0.05 - 5.0 Volts peak
Accuracy at 25°C:	± 1 db
Video Input Impedance:	150K ohms
Go/No-Go Output Impedance:	100 ohms
(S+N)/N Ratio Range:	0 - 20 db
Counter Output:	15 volt pulse, 15 usec wide
Mode Switch:	Reverses Go/No-Go Output Signal and Indicator
Indicator Lights:	(1) Standard Response "Go" (2) Gate Position "Go" (3) Power "ON"

The required function of the standard response indicator when used with the MSM-63 system is to determine the presence or absence of a selectable (S+N)/N ratio at the output of a remote receiver under test, and to provide an output signal indicative of which of these two conditions exists. Since the unit is normally located remote from the equipment van, the output and synchronization signals are transmitted by means of a data link. To further clarify

the standard response indicator's function within the system, two typical receiver test procedures are described in the following section.

#### IV. UTILIZATION OF THE INSTRUMENT

A block diagram of the test set-up for a receiver spurious response test utilizing the MSM-63 system is shown in Figure 4. At the system-under-test site, the video output from the receiver under test is connected to the standard response indicator video input jack. The Go/No-Go signal output from the standard response indicator is connected to the appropriate input jack of the data link transceiver for transmission to the MSM-63 van, and the reference PRF output from the data link is connected to the reference PRF input jack of the standard response indicator. The standard response indicator mode switch is placed in the "mode 1" position and the "(S+N)/N Ratio" and "(S+N)/N Range" controls are adjusted to obtain the desired standard response limits.

At the MSM-63 system site, the Go/No-Go signal output from the data link is connected to the automatic tuning circuit of the radiating signal source. The reference PRF waveform from the radiating signal source is connected to the appropriate input jack of the data link for transmission to the standard response indicator. The radiating signal source is tuned to its lowest frequency (250 Mc) and adjusted for maximum output power. If this is not a spurious response frequency of the receiver under test, a standard response will not be established at the receiver under test output, the indicator light on the front panel of the standard response indicator will not light, and the d-c voltage level at the Go/No-Go output jack will remain at zero. The frequency of the radiating signal source is automatically increased by means of the automatic tuning circuit until a spurious response frequency is encountered. At this point a standard response is established at the output of the receiver under test, the indicator light on the front panel of the standard response indicator comes on, and the d-c voltage level at the Go/No-Go output jack changes from zero to +12 Volts. This d-c level change is transmitted by means of the data link to the automatic tuning circuit, and lights a standard response indicator light on the operator's console, notifying the operator that a spurious response frequency has been encountered. The operator is required to optimize the tuning of the signal source and establish the spurious response threshold level.

A block diagram of the test set-up for a receiver adjacent signal interference test is shown in Figure 5. The equipment interconnections are the same as the spurious response test set-up with the following exceptions:

1. A second radiating signal source has been added. This source is tuned to the tuned frequency of the receiver under test and simulates the desired signal. The power output is adjusted to establish a standard response at the output of the receiver under test with no interference present.
2. The reference PRF synchronization waveform is obtained from the desired emitter rather than the interfering emitter.
3. The standard response indicator is operated with the mode switch in the "mode 2" position. The standard response is normally established at the output of the receiver under test, and in this mode the indicator light and the auto-tune inhibit signal are off.

The interfering signal source is automatically increased from below or decreased from above the tuned frequency of the receiver by means of the automatic tuning circuit until the standard response at the output of the receiver is degraded. At this point the indicator light on the front panel of the standard response indicator comes on, and the d-c voltage level at the Go/No-Go output jack changes from zero to +12V. This d-c level change is transmitted by means of the data link to the automatic tuning circuit of the interfering signal source. This level change inhibits the automatic tuning circuit and lights a standard response indicator light on the operator's console, notifying the operator that the standard response has been degraded. The operator is required to increase the desired signal level until the standard response is reestablished.

#### V. CONCLUSIONS

Since the standard response indicator is a portable, self-contained instrument, it is felt that this unit is adaptable to other instrumentation techniques. Some of the more apparent applications are:

- . Closed-System Spectrum Signature Measurements
- . RFI Specification Testing
- . Radar Receiver Development
- . ECM Studies
- . ECCM Studies

One of the more important advantages of this instrument is the significant improvement in the repeatability of standard response measurements. Due to the fact that the entire detection and indication process is accomplished electronically, the human judgment factor in determining what constitutes a standard response is completely eliminated.

In conclusion, it is felt that the development of this standard response indicator for pulsed systems has provided a timely, economical, and reliable solution to an existing problem in the performance of response level measurements and the determination of signal-plus-noise to noise ratios.

#### ACKNOWLEDGEMENTS

This work was sponsored by the U. S. Air Force, Rome Air Development Center, as part of the AN/ISI-63 (XW-1) Spectrum Signature Measurement Set, under contract AF30(602)-2539.

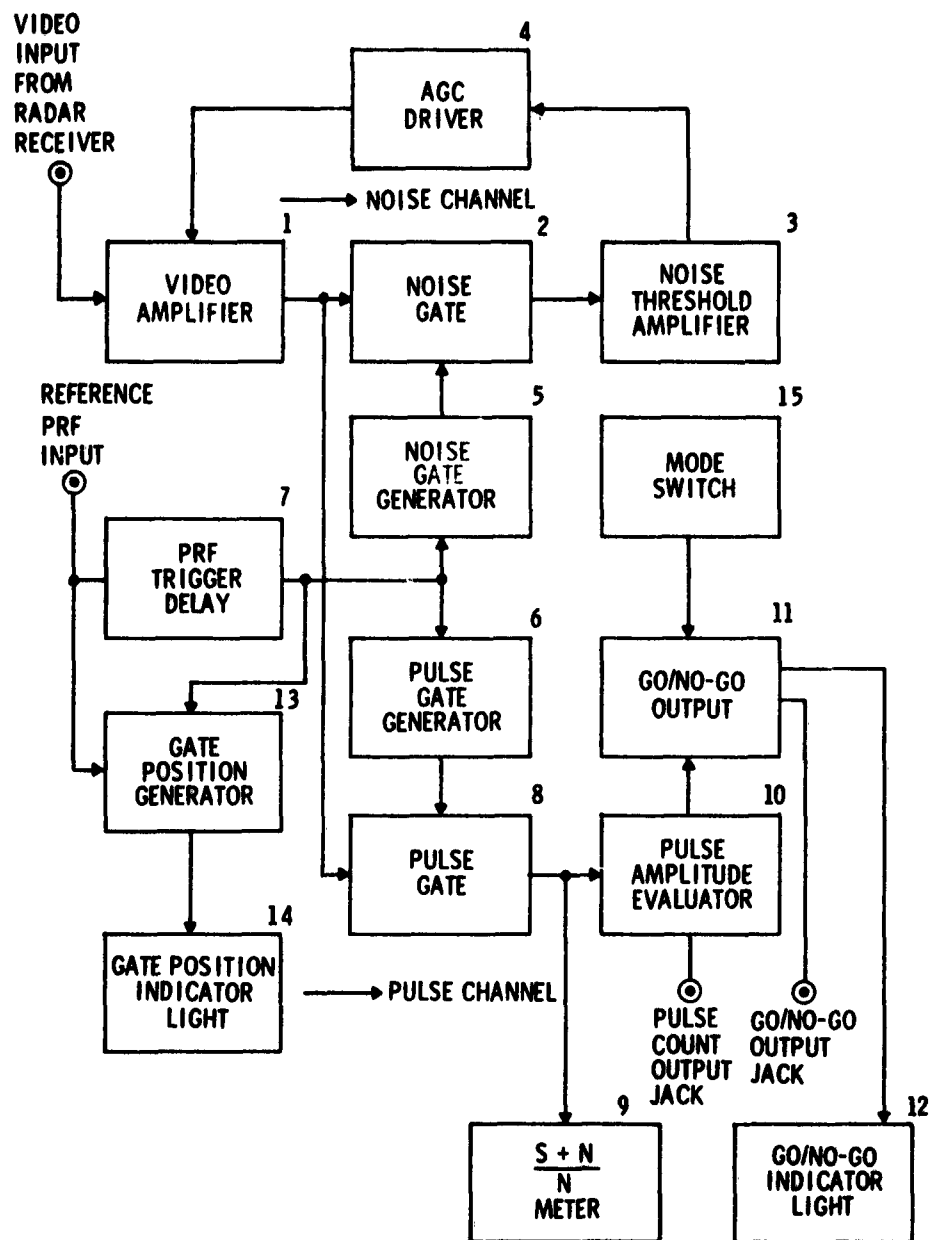


Figure 1. Block Diagram of the Standard Response Indicator

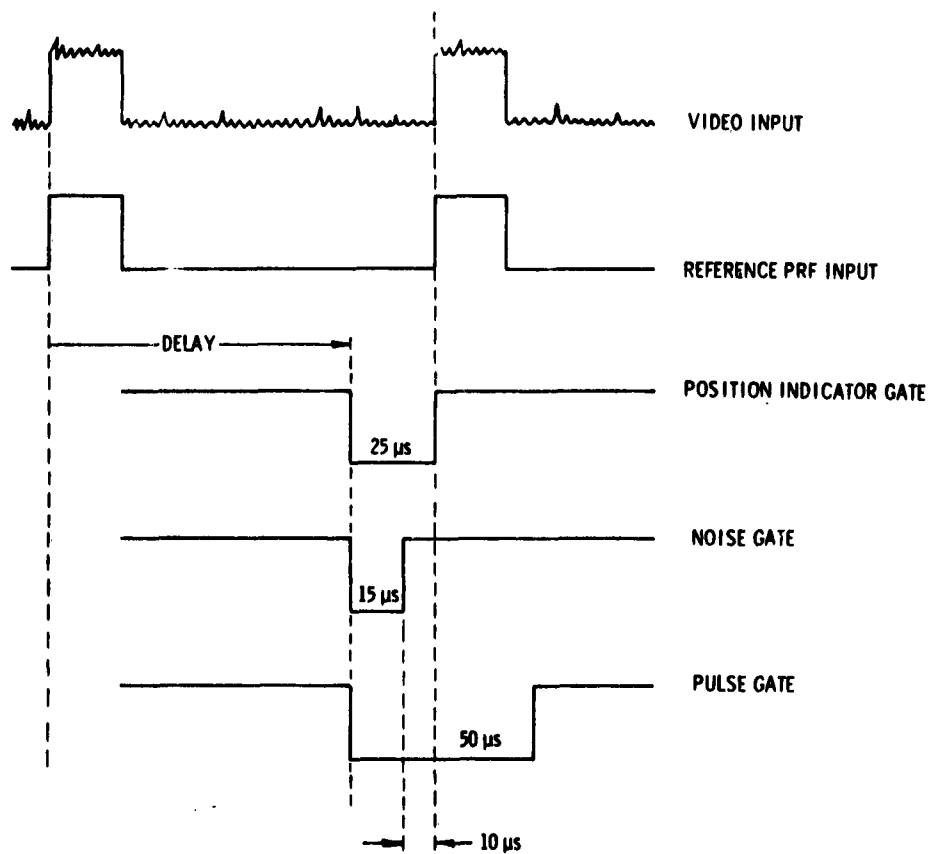


Figure 2. Timing Waveforms for Standard Response Indicator Gates



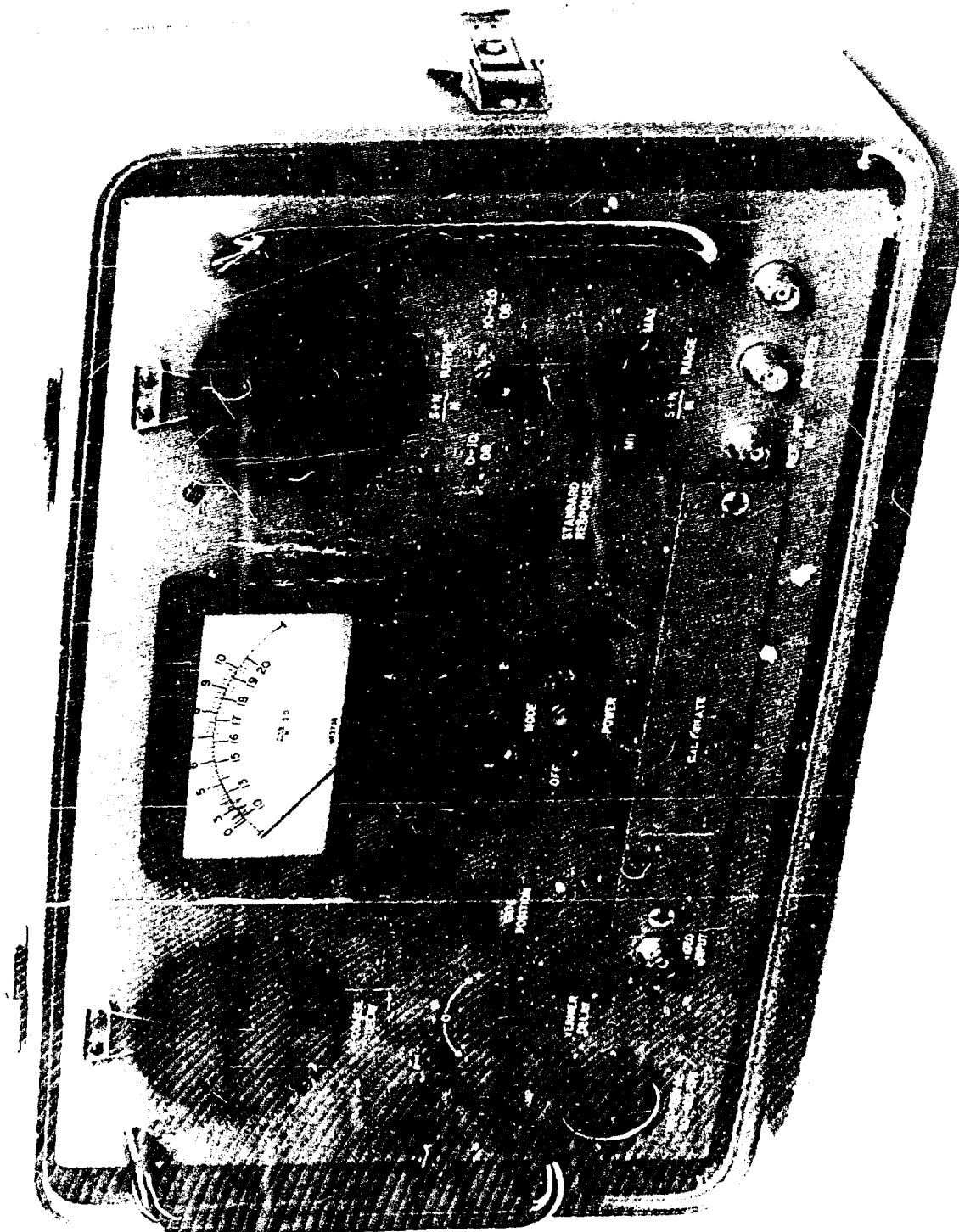


Figure 3. Standard Response Indicator

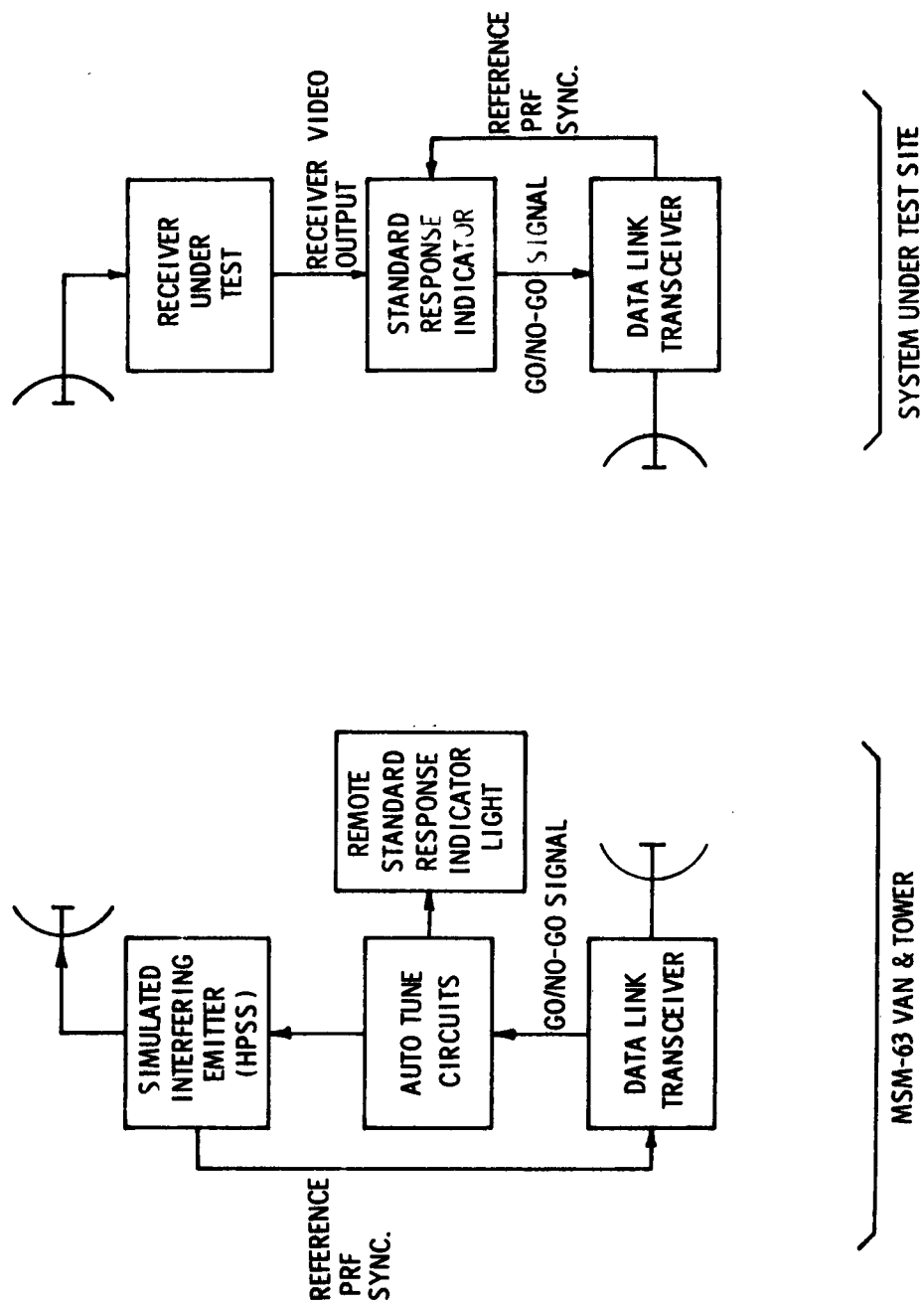


Figure 4. Receiver Spurious Response Test Set-Up

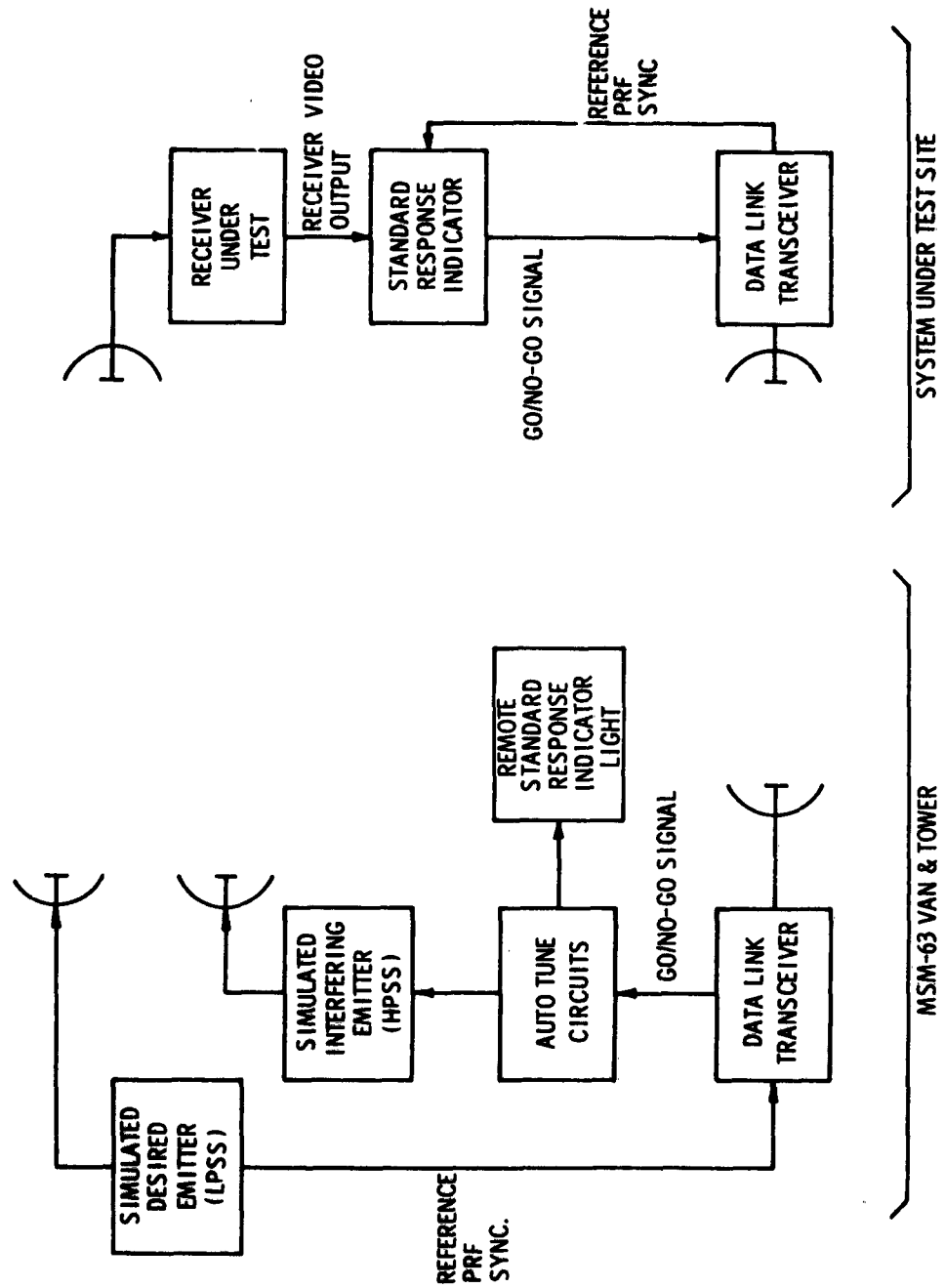


Figure 5. Receiver Adjacent Signal Interference Test Set-Up

## RI/FI INSTRUMENTATION TO 21 GC.

S. Abrams and B. Leibowitz  
Polarad Electronic Instruments  
Long Island City, New York

**Abstract.** - This paper discusses the development of instrumentation to increase the frequency range of the Company's standard 1 to 10 gc. Model FIM Field Intensity Meter to 21 gc. The calibrated receiver consisted of a basic unit and four plug-in heads to cover the 1 to 10 gc. range. The selected head received the R. F. input signal and converted it to a 260 mc. I. F. signal which was then passed on to the basic unit. This discussion will be limited primarily to the development of two additional heads required to give the increased frequency coverage from 10 to 21 gc.

### I. INTRODUCTION

The common basic unit used in conjunction with the plug-in heads contains the power supplies, metering circuits, and all the complementary electronics below the R. F. frequencies. In addition it contains the R. F. input, coaxial attenuators, and switches for the 1 to 10 gc. heads, which are coupled to the heads through external coaxial line jumpers. The basic unit was adaptable for use with the additional heads except for the R. F. coaxial section which caused too great a loss at the 10 to 21 gc. frequencies. To eliminate these losses it was necessary to design the new heads with solely waveguide components, and, therefore, they have complete self-contained microwave sections from R. F. input to I. F. output.

### II. DESCRIPTION OF BLOCK DIAGRAM

The block diagram represents the component sections of the new heads. The two waveguide heads are identical except for the use of WR 75 size waveguide for the lower band head and WR 51 for the higher frequency head. In the "USE" position the waveguide switch couples the R. F. waveguide input to the rotary attenuator. The rotary attenuator is calibrated in -dbm only whereas the four previous heads indicate both -dbm and microvolts. Microvolts could not be included because of the difficulty in defining the waveguide input impedance and relating power to voltage. The attenuator is calibrated from 0 to -100 dbm.

The signal then passes through the preselector to the mixer where it is mixed with the second harmonic of the klystron local oscillator. The 260 mc. I. F. is then transferred to the basic unit. In the "CALIBRATE" position the output of the doubler is coupled through the waveguide switch in place of the R. F. input signal. The output of the doubler is 0 dbm (1 milliwatt). By setting the attenuator scale to the desired level the system can be calibrated through the full 0 to -100 dbm range of the attenuator.

### III. COMPONENT DESIGN

Because of the change from the coaxial to a waveguide type system, a majority of the component parts had to be redesigned. The change from a Type N input connector to WR 75 or WR 51 waveguide input created the problem of input impedance. Where the coaxial input was a nominal 50 ohms throughout the frequency range, the waveguide input impedance is determined by the following formula for the dominant TE 1, 0 mode of propagation:

$$Z_{in} = \frac{600}{\sqrt{K}} \left( \frac{b}{a} \right) \sqrt{\frac{1}{1 - \left( \frac{f_c}{f} \right)^2}}$$

Where K = dielectric constant (equal to 1 for air)  
a = width of waveguide  
b = height of waveguide  
f<sub>c</sub> = cut-off frequency of waveguide  
f = operating frequency

It can be seen that the impedance is a function of operating frequency. For WR 75 waveguide it varies from 840 ohms at 10 gc to 351 ohms at 15.5 gc. For WR 51 waveguide it varies from 480 ohms at 15.5 gc to 358 ohms at 21 gc. This variations results in a different input voltage for a given power level where the input signal is varied in frequency. The system in the 10 gc to 21 gc operating range is calibrated solely in power as previously indicated.

The waveguide switch is manually operated by a front panel control. In the "USE" position the input is coupled to the rotary attenuator through the rotary waveguide section of the switch. At the same time the ganged "OFF-ON" switch removes the power from the calibrating klystron oscillator. This prevents any interference between the calibrating signal and the input signal. In the "CALIBRATE" position, the waveguide section of the switch rotates so that the output of the calibrating frequency doubler is fed to the rotary attenuator input. The R. F. input at the same time is terminated with polyiron. The "OFF-ON" switch is also energized, so as to apply the calibrating oscillator voltages. The switch has an insertion loss of less than .1 db, crosstalk suppression greater than 85 db, leakage less than 70 db, and a VSWR of 1.06.

The rotary type attenuator was chosen because of its excellent frequency response vs attenuation characteristics. This is achieved by attenuating the signal in a circular waveguide where the electric and magnetic field mode propagation is symmetrical about the center axis. Rectangular to circular transitions were developed to transpose the rectangular waveguide input and output to a circular waveguide propagation. To achieve a 0 to -100 dbm range a two section

attenuator had to be used. The rate of attenuation with variation in attenuator position varies as the cosine square law, and the accuracy of the dial reading can be set to  $\pm 2\%$  or 0.2 db, whichever is greater. The insertion loss is less than .5 db.

The FIM -2 specification for image rejection requires a minimum rejection of 60 db. This was achieved in the lower frequency heads with a double tuned preselector. In the upper frequency heads this proved inadequate. The attenuation of the preselector selectivity curve varies as a function of  $f/f_0$  where  $f_0$  is the dial frequency and  $f$  is the input signal. Since the first I. F. is a fixed 260 mc, as the dial frequency is increased the image frequency,  $\frac{f + 520 \text{ mc}}{f_0}$ , shifts relatively closer to  $f_0$ . In the upper frequency heads it appears close enough so that the image rejection falls below the required minimum of 60 db. It was, therefore, necessary to redesign the preselector into a triple tuned device. The addition of the third tuned section at the same time increased the insertion loss. It was possible, however, to limit it to 6 db and at the same time increase our image rejection to a minimum of over 60 db. These specifications proved satisfactory from a systems standpoint. The addition of the third tuned section necessitated a change in the mechanical tracking system. The system for the double-tuned preselector included a cam driving head containing two rows of screw adjustments for the fine tuning of the of the preselector choke position. The head had to be enlarged to accept a third row of tuning screws with an additional coupling system for the third choke.

The local oscillator used for mixing purposes is a klystron, external cavity type. The KS band head is the same type as used in the FIM-M band head and the KU band head contains the one used in the FIM-X band head. In the new heads, however, the second harmonic is used to mix with the input signal. The Polarad Velocitron ZV1011 is used as the klystron tube. The ceramic type construction enables it to operate at much higher temperatures than the glass type tube, making it possible to remove the klystron cooling blower which is desirable from a cost and packaging standpoint.

The calibrating section consists of a klystron oscillator, a frequency doubler, and a power monitoring system. The oscillator is the same as that which is used as the local oscillator except that it has fine tuning adjustments which may vary the cavity choke position and reflector voltage sufficiently to fine tune its frequency to that of the receiver section. The Polarad Velocitron ZV1011 is again used here not only to eliminate the cooling blower but also for the high power it is capable of delivering to the doubler. The additional power is required because of the relatively high conversion loss in the broadband doubler. Frequency doubling is used because the klystrons operating in the 10 to 21 gc range are relatively costly and not as reliable. The oscillator output is fed through a coaxial low pass filter in the doubler.

The frequencies of the fundamental for the KS band are 5 to 7.5 gc. and for the KU band 7.5 to 10.5 gc. The impedance of the filter is 62 ohms to match that of the 1N286A conversion diode. The non-linear characteristics of the diode causes generation of the second harmonic which is fed through a coax to waveguide transition to the output waveguide. The low pass filter cut-off frequency is between the primary and secondary harmonic frequencies and thus prevents the doubled frequency power from returning to the oscillator. The primary power is attenuated in the waveguide high pass filter. To set the system for one milliwatt output into the waveguide switch, the d. c. current through the crystal is set for a predetermined current through a monitoring meter. The d. c. of the diode is routed through the meter and parallel potentiometer to ground. It has been determined empirically that for a selected current the output of the doubler will be  $\pm 1.5$  dbm as a function of frequency. A center value of current operation is selected, and the power set position is centered on the meter by adjusting its parallel potentiometer. Since the conversion loss of the doubler varies from 13 to 18 db as a function of frequency, the oscillator coupling probe position must be varied for each frequency to set the doubler output level for 1 milliwatt as indicated on the power set meter. This section is also adaptable for use as a signal generator. By removing a front panel waveguide jumper, the calibrating signal is available at the panel waveguide output. Its output level is controlled by the rotary attenuator and is available from 0 to -100 dbm.

#### IV. CONCLUSION

In the first of each of the two new heads constructed, the performance of the prototypes exceeds that of the design specifications. Some of the most significant results are listed below:

	<u>Spec.</u>	<u>KS Head</u>	<u>KU Head</u>
1. Minimum sensitivity	-70 dbm	-79 dbm	-74 dbm
2. Minimum image rejection	60 db	70 db	65 db
3. Frequency accuracy	$\pm 1\%$	.3%	.3%
4. Frequency doubler calibration output accuracy	$\pm 2$ db	$\pm 1.5$ db	$\pm 1.5$ db

The increase in frequency range necessitated the design of four additional antennas to cover the KS and KU band ranges. Each band required a new directional and a new omnidirectional antenna with waveguide outputs. Flexiguide is used to couple the antenna output to the receiver input, and, with its maximum insertion loss of .5 db throughout the band, it may be ignored in field intensity calculations. The directional antennas have a beam width of 5 degrees and the following are their gain characteristics:

<u>ANTENNA</u>		<u>GAIN</u>	<u>FREQUENCY</u>
Directional	CA-KS	30.20	12.5
	CA-KU	32.25	18
Omnidirectional	CA-KSO	5.44	12.5
	CA-KUO	8.00	18

With the addition of these new antennas and heads Polarad has extended the range of their FIM to an upper level never before covered in this type of equipment.

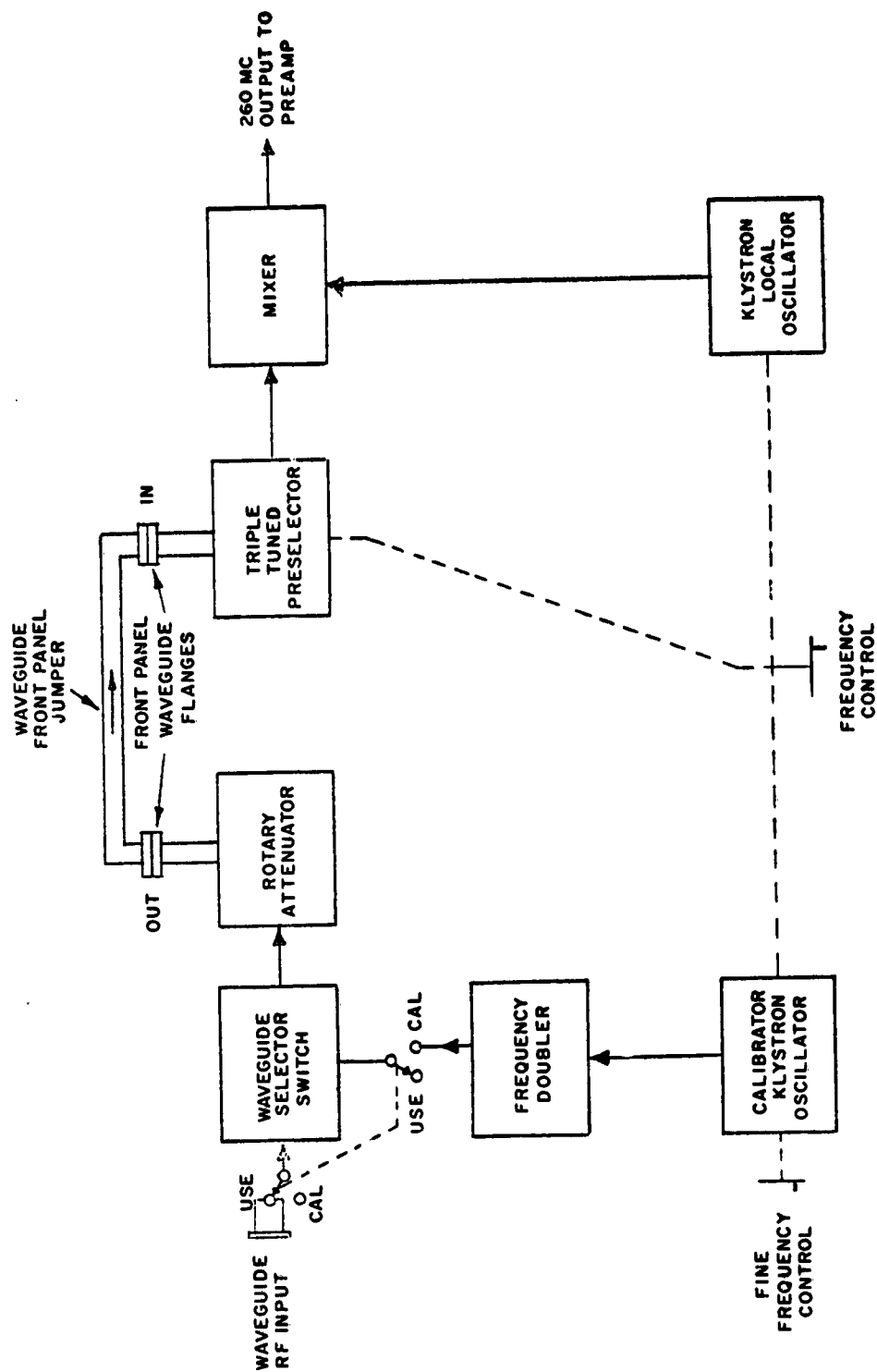
#### ACKNOWLEDGEMENTS

The experimental work for this investigation was performed by the Receiver Group of Polarad Electronic Instruments working on the AN/TRM-6 (XA-3) (AF 33(600)-41420). Messrs. K. Tomlinson and H. Carter of the Wright-Patterson Air Development Center contributed invaluable assistance in this project.

#### REFERENCES

1. Radio Research Laboratory Staff, Very High Frequency Techniques, Volume II, McGraw-Hill.
2. Montgomery, Massachusetts Institute of Technology, Radiation Laboratory Series, Technique of Microwave Measurements, Volume II, McGraw-Hill.





BLOCK DIAGRAM

KS BAND AND KU BAND TUNING UNITS

## TRACKING NOTCH FILTER FOR THE REJECTION OF CW INTERFERENCE

W. B. Warren, Jr.  
Georgia Institute of Technology  
Atlanta, Georgia

Abstract. - A tunable, single frequency rejection filter is described which uses a phase locked oscillator to obtain a narrow rejection notch in the region of 455 kc. The notch response is obtained by cancelling the signal to be rejected with a locally generated signal of equal amplitude and opposite phase. Automatic phase and amplitude control of the cancellation signal permits the rejection notch to automatically track frequency and amplitude changes of the signal being rejected. A notch width of less than 100 cycles is maintained over a 10% bandwidth centered at 455 kc. The cancellation of single frequency signals exceeds 50 db.

### I. INTRODUCTION

The presence of undesired CW signals can greatly complicate the task of making accurate measurements or of maintaining adequate communications. In the case of small amplitude CW interference, measurement errors occur or annoying heterodynes reduce the readability of a desired signal. When the interfering signal is large, saturation and blocking of the measurement or communication equipment may occur, and the equipment is rendered inoperative. The remedial measures necessary to overcome this CW interference vary with the frequency location of the interfering signal with respect to the desired signal. If the frequencies of these two signals are sufficiently spread apart, a band-pass filter centered on the desired signal or a notch filter centered on the interfering signal can be used to provide the necessary interference rejection. Such suppression techniques are typified by the conventional "Q" multiplier which can provide pass band tuning or a variable frequency rejection notch.

In some cases, the interfering signal may be spaced very close in frequency to components of the desired signal, and the conventional notch filter may not be an adequate means of suppression of the undesired signal. The width of the notch may be so wide as to greatly attenuate components of the desired signal as well as the interfering signal. Or, if the notch is sufficiently narrow to avoid undue attenuation of desired signal components, slow shifts in the frequency of the interfering signal may cause the interference to "slip out" of the rejection notch. Such frequency shifts can result from frequency instability of the interference source, or from frequency instability of the local oscillator of the measurements or communication receiver being used.

### II. ACTIVE NOTCH FILTERS

These disadvantages of the conventional notch filter can be overcome, to large extent, by the use of an active notch filter to provide the required interference rejection. An active filter can provide an extremely narrow rejection notch which can be easily tuned and provide the facility for tracking slow drifts in the frequency of the interference. One such active filter is illustrated in Figure 1.

In this filter, the notch action is obtained by generating a local signal whose amplitude and phase are identical to that of the interfering signal. Subtracting this local signal from the input signal results in cancellation of the interference, with the desired signal remaining unchanged. To obtain effective interference cancellation, it is necessary that the frequency of the local signal be controlled only by the interference, since any variation in the frequency of the source of cancellation signal due to the desired signal can cause portions of the desired signal to be cancelled along with the interference. One convenient method of accomplishing the necessary frequency control is to make use of a phase locked oscillator as the source of the cancellation signal. Figure 2 shows a block diagram of a typical locked oscillator system.

### III. LOCKED OSCILLATOR

In this system the necessary control voltage for tuning the oscillator is derived from a comparison of the phase of the input signal with the phase of the output of the oscillator. Since the phase detector output is averaged by the low pass filter, only those components of the input signal whose frequencies lie within the low pass filter bandwidth of the frequency of the local signal can effect any control over the frequency of the local signal. The locking loop is a frequency servo and as such, it seeks a stable condition where the error voltage is nulled, i.e., the tuning voltage at the oscillator is zero. This null condition occurs when the local signal is in quadrature with interfering CW signal. Consequently, an additional  $90^\circ$  phase shift of the oscillator signal appearing at the phase detector will produce a signal whose phase is either  $0^\circ$  or  $180^\circ$  with respect to the interfering signal.

Figure 3 shows a simplified schematic of the local signal source together with the necessary frequency control loop to permit this oscillator to track the frequency of the interfering signal. The oscillator used has a short term stability in the order of 1 part in  $10^7$ . This high degree of short term stability is necessary to prevent noise sidebands generated by the local oscillator from obscuring components of the desired signal lying very close to the frequency of the interfering signal. The positive feedback from collector to emitter is through the resonant transformer whose turns ratio permits the current gain to be set to desired value (about 2:1) while maintaining very small loading of the resonant winding by the transistor portion of the circuit. The frequency of oscillation is then insensitive to variations in the transistor parameters. This is evidenced by the fact that replacement of the oscillator transistor causes a frequency change of less than 10 cps at an operating frequency of 455 kc. The level of oscillation is maintained at a low value by the limiting action of the diodes  $D_1$  and  $D_2$ . This permits the operation of the transistor in its linear region and reduces the effect of distortion products in lowering the frequency of oscillation. The oscillator output is taken from a small resistor in the emitter circuit to reduce the effects of external circuit loading on the oscillator frequency. The frequency of oscillation is controlled by the inductance of the transformer secondary resonating with the capacitance of the voltage controlled capacitors. The dual capacitor arrangement is used to overcome the tendency of the capacitors to conduct on peaks of the oscillator signal with consequent changes in the DC

voltage level on the control line. In addition, the dual arrangement provides a convenient, isolated point for connection of the control voltage. The phase of the local signal oscillator and the interfering signal are compared in the balanced phase detector consisting of the split load phase inverter and the diodes,  $D_3$  and  $D_4$ . The capacitors,  $C_1$  and  $C_2$ , are charged to equal and opposite voltages through  $D_3$  and  $D_4$  whenever the two signals being compared are in quadrature. Consequently, the voltage appearing at the junction of  $R_1$  and  $R_2$  is zero. A change in the phase relation of the two signals from quadrature causes unequal charging of the two capacitors, resulting in a change in the voltage level at the junction of  $R_1$  and  $R_2$ . This voltage changes on either side of zero depending on whether the phase angle between the local and interfering signals increases or decreases. This voltage at the junction of  $R_1$  and  $R_2$  is fed to the low pass network as indicated in Figure 3.

Stability considerations for the locked oscillator require that the loop phase shift must not equal  $180^\circ$  at any frequency at which the loop gain equals or exceeds unity. Unfortunately, this particular loop has a "built-in"  $90^\circ$  phase shift in the form of the phase error being used to control the frequency of the oscillator. The phase error is the integral of the frequency error and it is this integral relationship which introduces a  $90^\circ$  phase lag. As a result of this "built-in"  $90^\circ$  lag, the low pass loop filter must add less than  $90^\circ$  additional lag at any frequency at which the loop gain exceeds one. This requirement greatly restricts the types of low pass networks that can be used as the loop filter. For example, a "constant K" LC section may introduce as much as  $180^\circ$  phase shift. While a simple RC low pass section can add almost  $90^\circ$ . Although the simple RC section alone could not produce an unstable condition, its use would require that the phase shift in the remainder of the loop circuitry be very small. In actual practice this elimination of small phase shifts in the portion of the loop outside the filter is difficult to accomplish with the result that the use of the simple RC low pass often results in an unstable condition. Figure 3 shows two sections of a commonly used low pass structure which permits control of the maximum value of transmission phase shift. An important feature of this structure is the fact that only a fixed amount of attenuation can be obtained on high frequency components no matter how high in frequency these components may be. The amount of the fixed attenuation is directly related to the maximum phase shift and is the price that must be paid to obtain the necessary control of the phase shift. This fixed attenuation is the maximum attenuation that can be obtained on undesired signals which may appear in the control loop and produce undesired phase modulation of the oscillator. In order to obtain the necessary maximum attenuation, a two section network is used in which the values are proportioned in such a manner that when the phase shift through one of the networks is large, the shift through the other network is small and vice-versa. The eventual attenuation of the combination of the two networks is the product of the individual attenuations, provided the networks are adequately isolated from each other.

#### IV. AUTOMATIC PHASE CONTROL

Unfortunately, the desired quadrature relationship between the local and the interfering signals is established only when the natural frequency of the oscillator is the same as the frequency of the interfering signal. If the

interfering signal frequency changes, an error voltage must be developed in the loop in order to tune the oscillator to this new frequency. Under this condition, the quadrature relationship can no longer be maintained.

The addition of an automatic phase control circuit operating on the oscillator output signal permits the phase of the cancellation signal to be held constant even though the frequency of the interfering signal changes. Figure 4 illustrates the method of obtaining automatic phase correction of the local signal from the locked oscillator.

In this circuit, the phase of the output of the voltage controlled phase shifter is compared in the phase detector with the phase of the interfering signal. Any difference of the phase of these two signals from a quadrature relationship will cause an error voltage to appear at the phase detector output. This error voltage is applied to the voltage controlled phase shifter in the proper polarity to return the phase of the signals at the phase detector to quadrature. If a large loop gain is provided, the error voltage will be small and the resultant phase tracking quite accurate. The low pass filter serves to reject those frequency components of the error signal which do not arise from heterodynes between the output of the voltage controlled phase shifter and the interfering CW signal.

The voltage controlled phase shift is obtained by means of a six stage RC phase shift network in which the normal fixed capacitors have been replaced by voltage variable capacitors. A typical stage of this phase shifter is shown in the schematic of Figure 5. The amplitude response of this network is constant with respect to both frequency and the values of R and C, while, the phase shift is a function of these variables. Referring now to Figure 5, the necessary push-pull drive signal to the phase shift network is supplied by the split-loaded phase inverter,  $Q_1$ . The resistance of the phase shift network is furnished by a fixed resistor, while the capacitance is supplied by the series combination of the coupling capacitors and the capacitance of the reversed biased diode,  $D_1$ . The coupling capacitors provide the necessary DC isolation of the bias voltage and the control voltage. These capacitor values are selected to be large enough that the total capacitance in the phase shifter is determined almost entirely by the capacitance of the diode, and at the same time having a sufficiently low value that no appreciable low frequency phase shift is introduced in the control voltage. This last condition is necessary to prevent instability from occurring in the phase correction servo loop. The emitter follower presents a high impedance load to the phase shift network, and also provides a low impedance output to drive the next stage.

A balanced phase detector of the shunt switch type is used to derive the phase error signal. This switch is composed of an NPN-PNP transistor pair connected in parallel with the signal path. The switching voltage is derived from the local signal oscillator which is fed through a phase splitter to provide the necessary push-pull switching signal to the bases of the transistors. Subsequent averaging of the phase detector output by the low pass filter provides an error voltage proportional to the cosine of the phase difference between the interfering and local signals.

The averaged phase error is passed through a DC amplifier to increase the loop gain and provide the required drive signal for the voltage controlled phase shifter. A differential input stage minimizes DC drift problems and also provides a convenient point for applying negative feedback to the amplifier. Gain control is obtained by varying the amount of negative feedback applied to the amplifier.

#### V. AUTOMATIC AMPLITUDE CONTROL

Slow amplitude variations of the interfering signal will cause imperfect cancellation as long as a fixed amplitude cancellation signal is used. Automatic amplitude control can be applied to the cancellation signal to cause it to follow the amplitude variations of the interference. The amplitude control action is obtained by comparing the amplitudes of two dc voltages which are derived from the interfering signal and the local signal. Figure 6 illustrates the technique involved. Any difference in the levels of these two voltages is amplified and applied to the variable gain amplifier in such a manner as to reduce this difference voltage to zero. The dc voltage proportional to the local cancellation signal is easily derived by using a rectifier and low pass filter. This method is effective since the cancellation signal is a clean CW signal with no other signals superimposed upon it. However, the interfering CW signal may be embedded in a large number of other signal components so that a product type detector followed by a low pass filter is necessary to provide the dc voltage proportional to the amplitude of the interference alone. The local reference signal for this product detector should be of constant amplitude and have the same frequency and phase as the interfering signal. The proper reference signal is obtained by phase shifting the output of the voltage controlled phase shifter by  $90^\circ$ . The addition of the  $90^\circ$  phase shift is necessary to provide an in-phase reference since the automatic phase correction loop has already forced the phase corrected signal to a  $90^\circ$  phase angle with respect to the interfering signal. Since the output of the variable gain amplifier is used as the cancellation signal, it is important to insure that no phase shifts are associated with changes in gain of the amplifier. Otherwise, the degree of interference cancellation obtained will vary with changes in the amplitude of the interference.

#### VI. RESULTS

A complete cancellation filter with provisions for automatic compensation for changes in both the amplitude and frequency of the interfering signal is shown in the photograph of Figure 7. The filter operates at a nominal frequency of 455 kc, but the automatic frequency control permits signals to be tracked over a 10 kc bandwidth around this center frequency. The rejection of single frequency signals exceeds 50 db. This cancellation action is illustrated by the photographs of Figure 8. Figure 8(a) is the normal spectrum analyzer presentation of the output of an HP 650A oscillator at 455 kc. The large carrier component obscures the 60 cycle sidebands and shows small 120 cycle and 180 cycle sidebands. The amplitude of the carrier component was then reduced by about 50 db using the cancellation filter, and the gain of the spectrum analyzer was increased. The result is shown in the photograph of Figure 8(b).

The residual carrier component is the middle one of the group of five large components, the slight shift in the frequency scale being caused by a small drift in the oscillator frequency. The 60 cycle and 120 cycle sidebands are now clearly seen. In addition, the lack of a symmetrical distribution of the sidebands about the carrier indicates that phase as well as amplitude modulation is taking place. Figure 9(a) illustrates the spectrum observed at the output of an HP 606A oscillator at 455 kc. No distinct sidebands are visible. Figure 9(b) shows the 120 cycle sidebands actually present and which are now visible when the carrier is suppressed by about 60 db and the gain of the spectrum analyzer is increased.

## VII. CONCLUSIONS

An active cancellation filter can provide a rejection notch of very narrow bandwidth which can be used to good advantage in situations where the signal to be rejected is changing in frequency.

## ACKNOWLEDGEMENTS

The assistance of Mr. C.S. Wilson in the construction of the equipment is gratefully acknowledged.

This work was sponsored by the Rome Air Development Center under Air Force Contract Number AF 30(603)-2904.

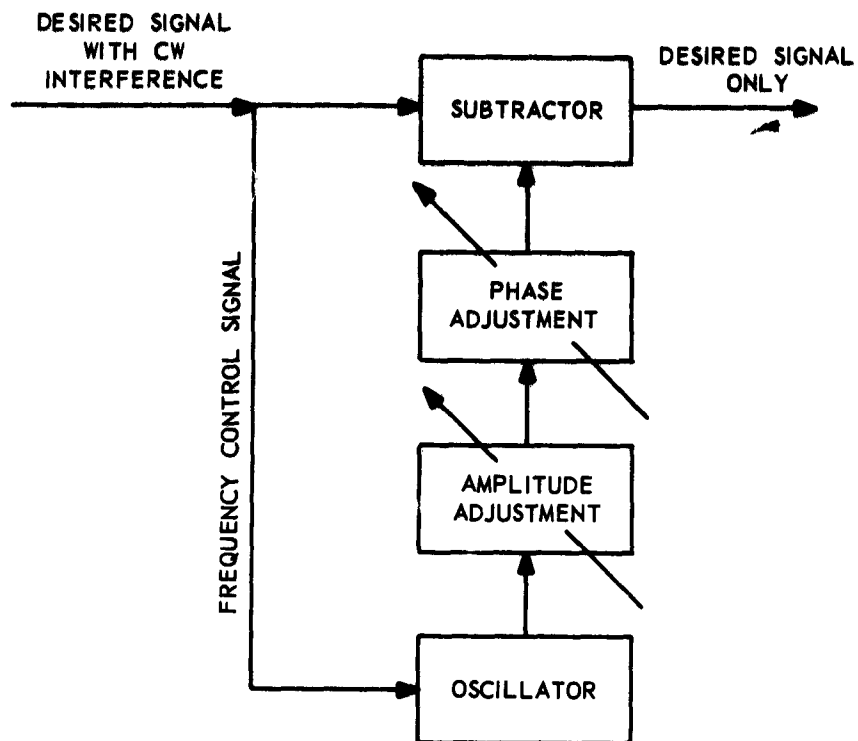


Fig. 1 CANCELLATION FILTER

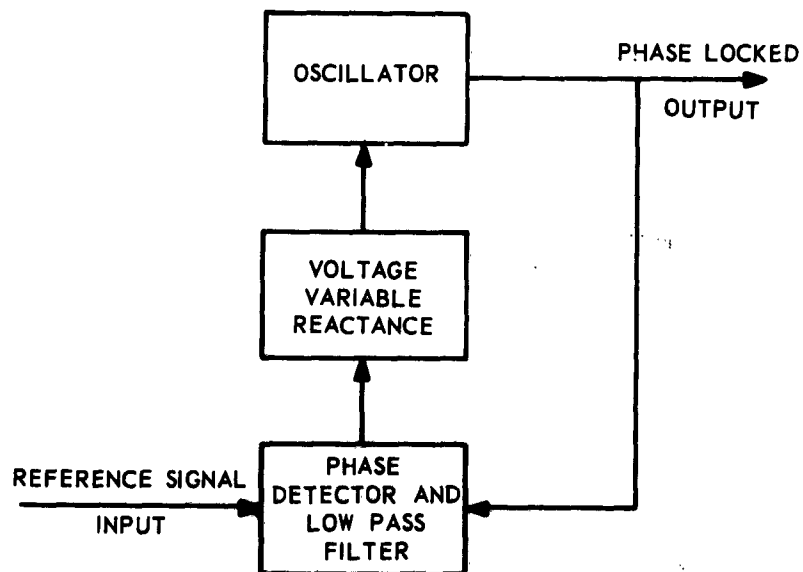


Fig. 2 PHASE LOCKED OSCILLATOR



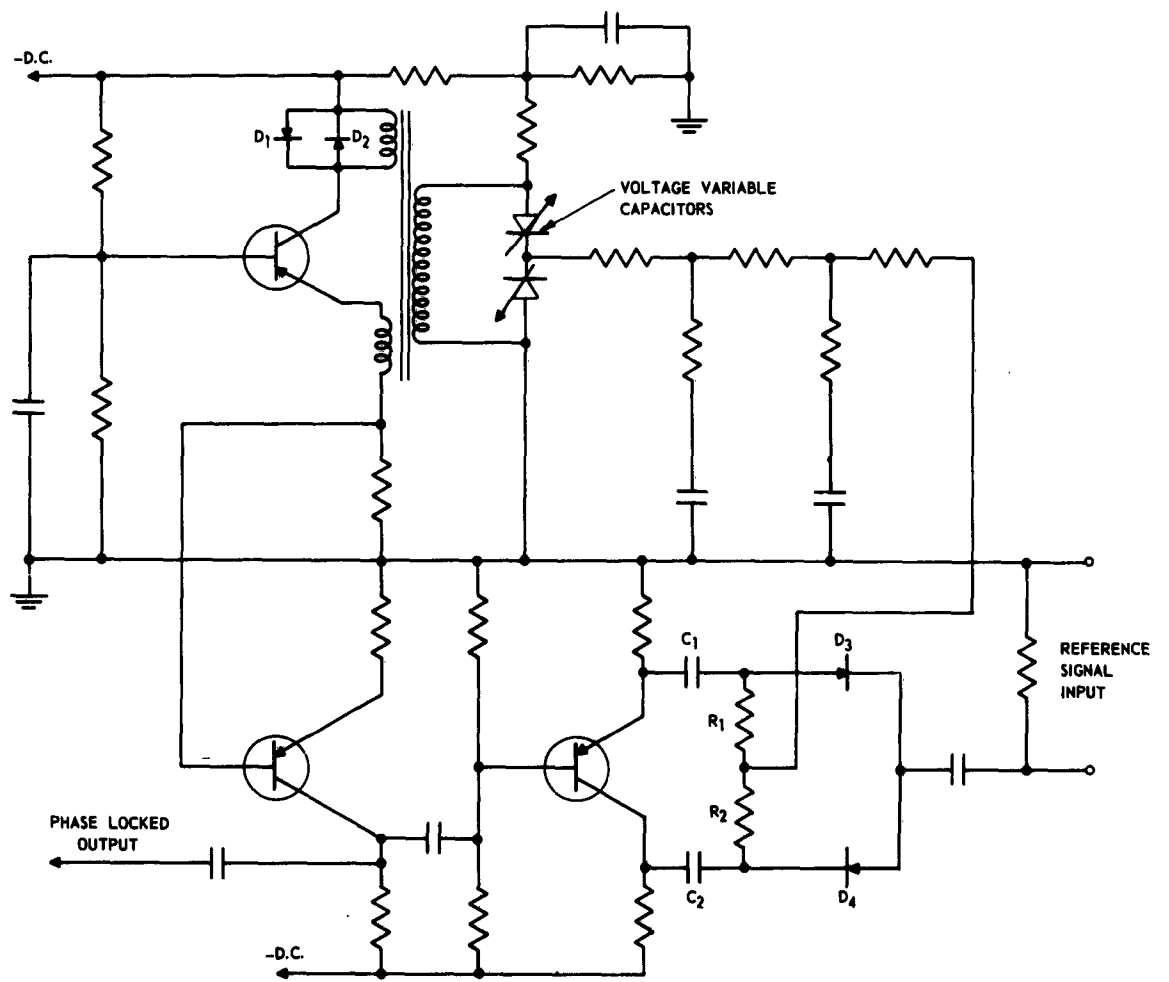


Fig. 3 PHASE LOCKED OSCILLATOR

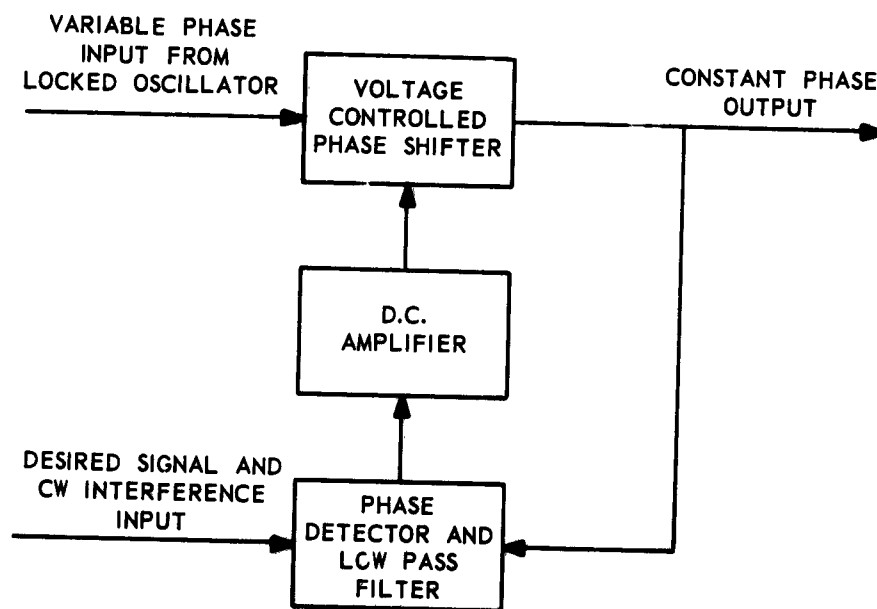


Fig. 4 PHASE CORRECTION CIRCUIT

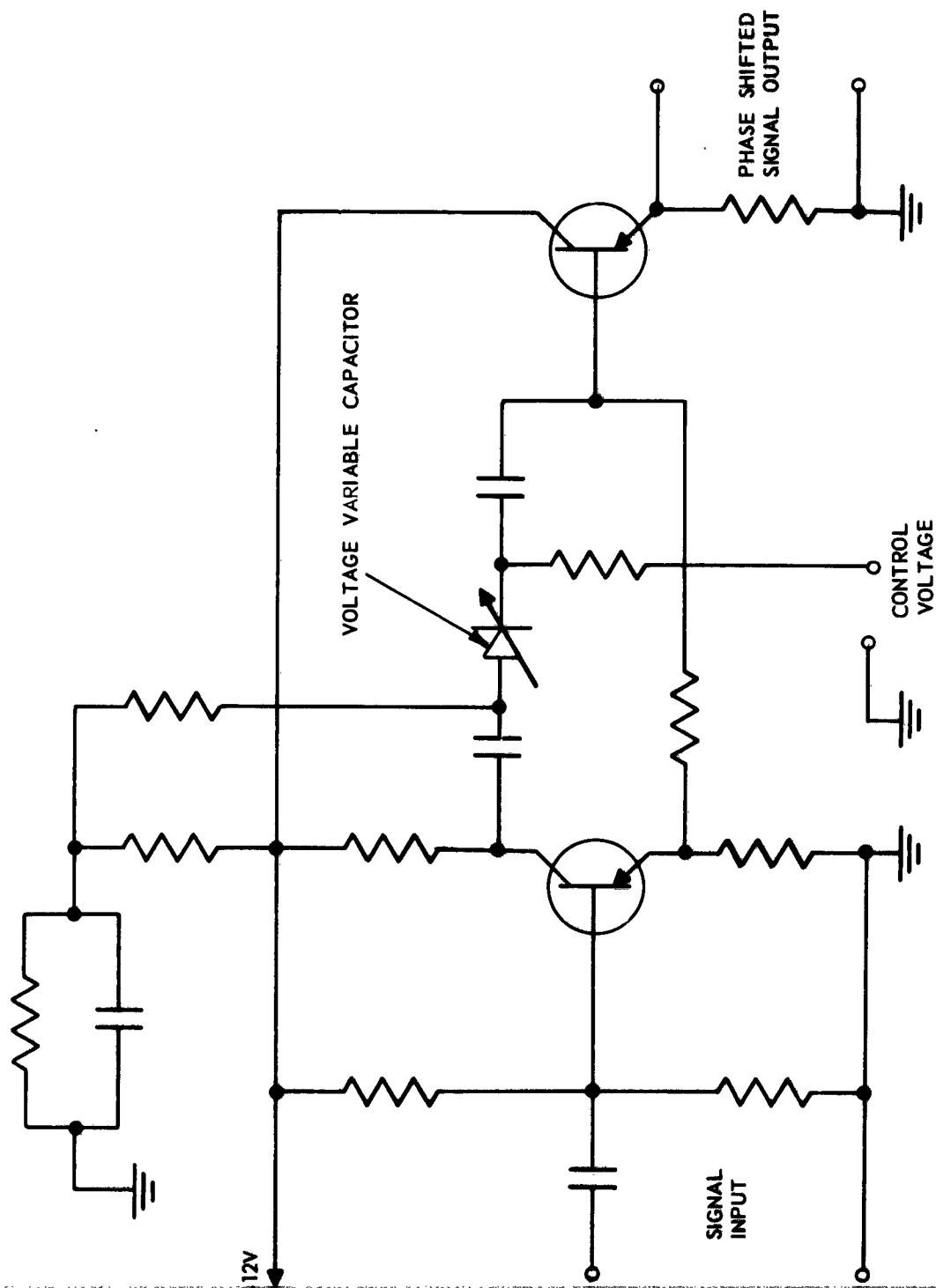


Fig. 5 VOLTAGE CONTROLLED PHASE SHIFTER

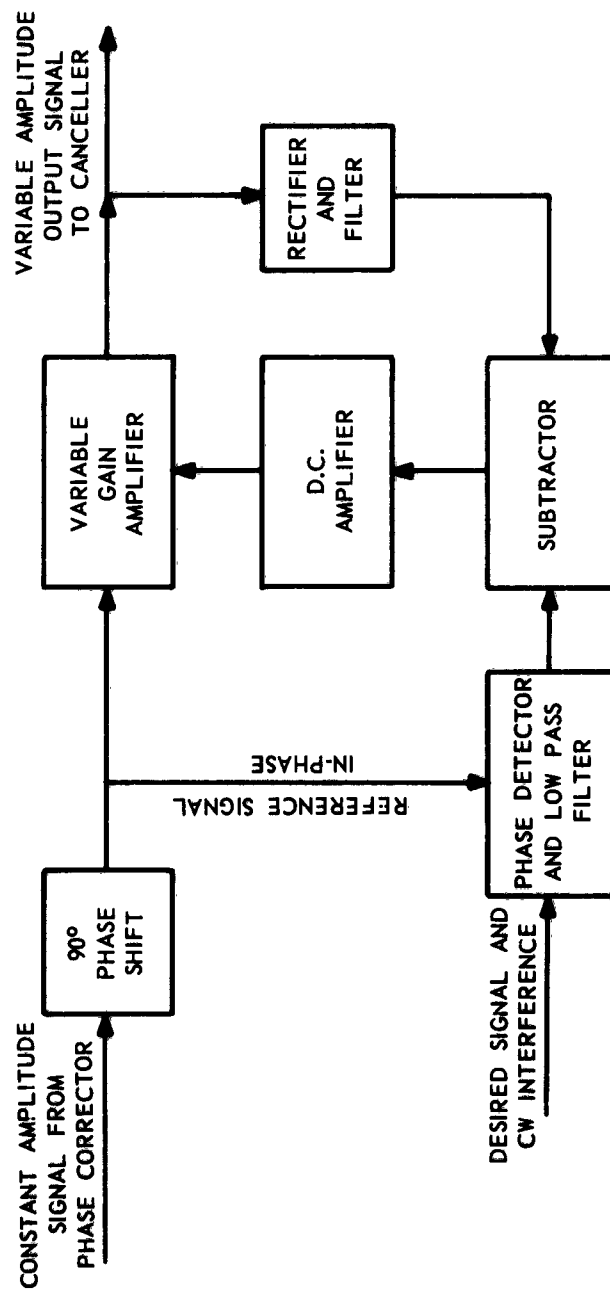


Fig. 6 AMPLITUDE CORRECTION CIRCUIT

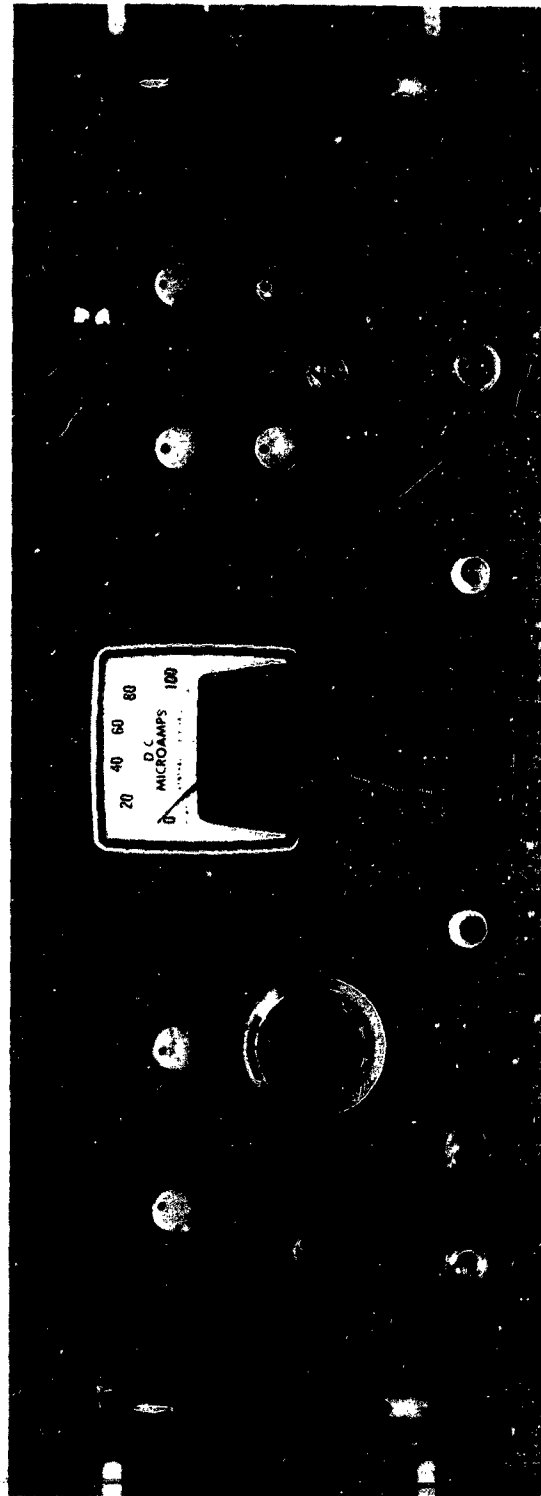


Figure 7 - Front Panel View of Filter



Figure 8(a) Oscillator Spectrum With Full Carrier

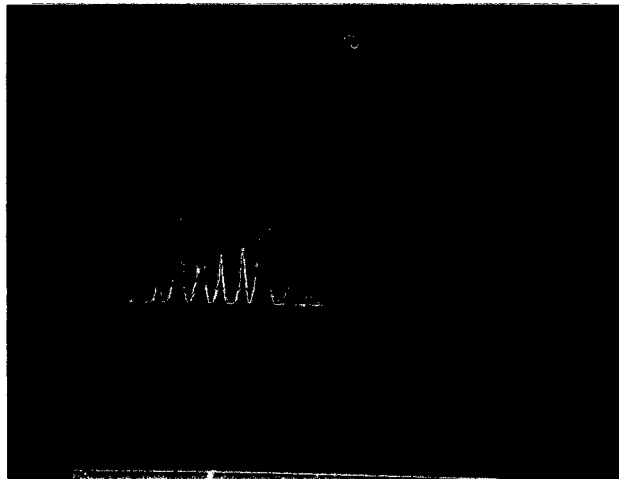


Figure 8(b) Oscillator Spectrum - Carrier Reduced 50 db

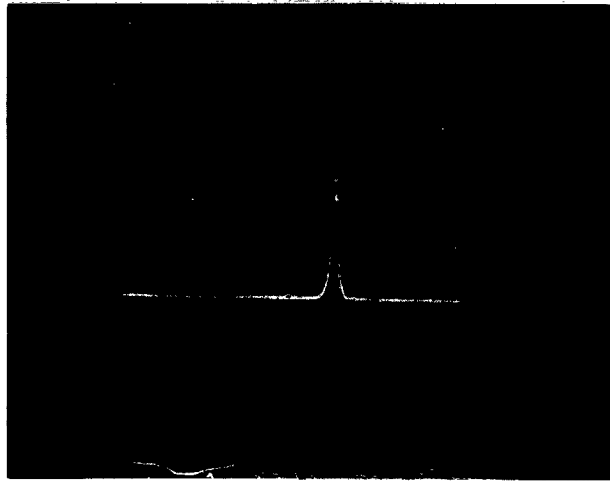


Figure 9(a) Oscillator Spectrum With Full Carrier

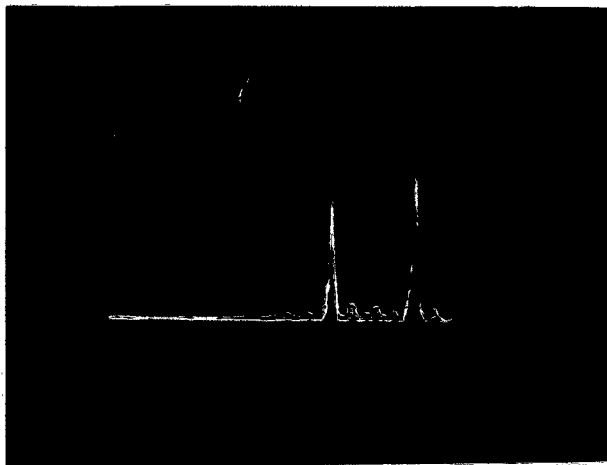


Figure 9(b) Oscillator Spectrum - Carrier reduced 60 db

## COMPARISON OF TRANSMITTER SPECTRUM SIGNATURE DATA AND RADIATED FIELD STRENGTH DATA FOR TRANSMITTER EMISSIONS

P. F. Chen and C. E. Blakely  
Bell Aerosystems Company  
Tucson, Arizona

Abstract - Harmonic emissions from transmitters are one of the common sources of RF interference encountered in communications systems. Transmitter spectrum signature data available to date were obtained under laboratory condition with the transmitter terminated in a resistive load. These data are presently being used as inputs to the Interference Prediction Model of the Electromagnetic Environmental Test Facility being developed by Bell Aerosystems Company under contract to the U.S. Army Electronic Proving Ground in Fort Huachuca.

This paper discusses the development and present status of the work being done to compare the transmitter spectrum signature data using a resistive load and the transmitter radiated emission level data using an electrically short whip antenna mounted on a tactical military vehicle. A review of previous work in the area of analyzing these data by others is also presented.

A description of the transmitter emission level data collection procedure as well as the test transmitter-vehicle will be given. The transmitter spectrum signature data obtained with a resistive load was converted to field strength and fitted with a linear regression line on log-log coordinates. This regression line is compared with the regression line obtained from the radiated field strength data of the vehicle mounted transmitters.

Several conclusions are drawn regarding the two regression lines. First, the linear regression on log-log coordinates is a very good fit to the data in both the radiated and dummy load tests for the first 10 harmonics. Second, in general only the first 10 harmonics are detectable for low power Military HF and VHF equipments. Third, there are large differences between the measured field strength data and the dummy load data converted to field strength.

The results are illustrated by several curves.

### I. INTRODUCTION

One facet of the complex problem of calculating and predicting interference is the determination of the radiated power from a transmitter antenna combination at its fundamental and each spurious and harmonic frequency. The data available for such purposes will always be approximations to the true output for a particular device or transmitter. These approximations must be estimated from a knowledge of the parameters of the system together with measured data from as many equipments as time and economic considerations will permit. It is the purpose of this paper to compare one statistically proven functional relationship between the amplitude of the harmonics and the harmonic order of the transmitter and the fundamental frequency for two types of measurements as described below. This paper is limited to a study of this particular problem.



The Spectrum Signature Program attempts to evaluate the interference potential of transmitters by two different methods. They are the open field or radiated power method and the closed system or resistive load method. The first method is reserved for those transmitters that normally employ a single antenna or, at most, two antennas. The second method is reserved for those transmitters employing more than two antennas. The above discussion refers to the possibility of using various antennas for different applications and not to the simultaneous use of more than one antenna. Excluding the possibility that a new antenna may be developed for a system which invalidates method number one, several problems still exist in the evaluation of transmitter radiated power.

Since little is known about the combined characteristics of a transmitter and antenna system at other than the fundamental frequency, it is desirable to compare the radiated power obtained by method number one with that obtained by method number two. The power levels measured into the resistive load must be converted from watts to watts/meter<sup>2</sup> at the appropriate distance for this comparison. This was accomplished in the present study by means of the computer propagation program developed as part of the EMETF effort. The results were then compared with the measured field strength results and a result obtained previously by one of the authors.

A second area of interest in the study presented here is the effect of the vehicle on antenna patterns. Due to mobility and simplicity requirements most military vehicles employ whip antenna structures. These antennas are usually mounted at some convenient point on the vehicle which is generally quite low in elevation. Thus the antenna couples strongly into the vehicle structure, which distorts the pattern severely. A typical pattern is shown in Figure I.

## II. REVIEW OF PREVIOUS WORK

In general, the harmonic amplitudes decrease in magnitude as the harmonic order increases. This being the case, it seems reasonable to expect the amplitudes to decrease in some orderly manner. It has been shown by Blakely<sup>1</sup>, Heisler<sup>2</sup> and Hurd, et al<sup>3</sup> that the harmonics actually behave in a linear fashion. Plots of harmonic power versus harmonic order on log-log coordinates have shown that the trend is linear on these coordinates. Assuming this relationship, Hurd and Huntoon fitted a straight line

$$Y = a + b(x - \bar{x})$$

to a set of measured data using the least-squares method where their Y was in db below the carrier, and x was the logarithm of the harmonic order. Appropriate statistical tests were performed which proved that the assumptions of linearity and constant group variance were indeed justified. The hypothesis of constant group variance was tested using Bartlett's test and the hypothesis of linearity using the V<sup>2</sup> (or F) distribution test.

For the particular set of data used, the regression line obtained was

$$Y = 29.7 + 45.8 \log n \quad (1)$$

and the over-all estimate of  $\sigma$  was

$$S = 15.8$$

For the observed data the following tolerance limits were obtained:

90% confident that 95% of the data lie between  $Y_1 \pm 32.5$ .  
 95% confident that 95% of the data lie between  $Y_1 \pm 32.8$ .

The above results were for a group of data obtained from a group of 21 communications type transmitters. The method was also applied to individual equipment types with very good correlation in most cases.

Other more elegant methods have been used to fit a curve to transmitter harmonic radiations. The method of orthogonal polynomials was used by Blakely and Bailey<sup>4</sup> to examine the effect of complex transmitter loads on the level of harmonic emissions. The results of their study indicated an equation of the form

$$Y = 42.7 + 2.66x$$

was a good fit for these data. In this case  $Y$  is the level in db below the carrier and  $x$  is the harmonic order. Table XI of their paper presents a comparison of some results of measurements made into a dummy load and in an open field. These results show good agreement on the lower frequency, and poor agreement on the higher frequency.

This paper also contains some results taken from a paper by S. Kurokawa and T. Takahashi<sup>5</sup> which shows very good agreement between transmission line and radiated field strength measurements.

### III. MEASUREMENT METHOD AND EQUIPMENT

Typical combinations of military equipments and vehicles were selected and employed in the measurement program to generate the radiated spurious and harmonic emissions.

The selected military type radio sets were two of each of the AN/VRC-8, AN/VRC-9, AN/VRC-10, AN/GRC-9, and AN/GRC-19. Each was mounted in turn on three different vehicles of the same type. The vehicle types were the M-38 (jeep), M-37 (3/4-ton truck), and M-315 (2½-ton truck), thus producing six samples of data for each vehicle-equipment combination.

The test transmitter-vehicle combination was placed in the center of a circle and tuned to the assigned frequency. An M-37 3/4-ton truck was modified with a large copper ground plane mounted on top to act as a field intensity receiving vehicle. A quarter-wave whip antenna was used as the receiving antenna. Under the ground plane a bench was provided for the NF-105 field intensity meter and other test equipments. (See Figures II and III.)

An integral part of this test equipment was a series of Hewlett-Packard signal generators to calibrate the NF-105 by the substitution technique.

Primary power for the test equipment was provided by a PU-286B mounted on a trailer towed by the modified M-37.

This field intensity measuring vehicle was driven in a circular path approximately one wavelength in radius at the lowest transmitter fundamental frequency. A continuous strip tape recorder provided a permanent record for each harmonic of the transmitter frequency to which the field intensity meter was tuned. A calibrated receiving system was used to obtain an absolute power level calibration.

At frequencies below 30 Mc, a loop antenna of one-meter diameter was used to obtain the field intensity measurement. The meter reading in db above one microvolt is corrected to field strength by adding the standard antenna correction factor.

$$E_{\text{db}\mu\text{v}/\text{m}} = V_{\text{db}\mu\text{v}} + \text{CF} \quad (2)$$

where

and  $V_{\text{db}\mu\text{v}}$  = meter reading in volts.  
CF = standard antenna correction factor.

Since the field strength in db above one microvolt per meter is related to field strength in volts per meter by

$$E_{\text{db}\mu\text{v}/\text{m}} = 120 + 20 \log E \quad (3)$$

and E (volts per meter) is related to the power density by

$$P_d = \frac{E^2}{Z_0} \quad (4)$$

where

$Z_0 = 120\pi$ , characteristic impedance of free space.

Therefore,

$$P_d(\text{dbm}/\text{m}^2) = 10 \log \frac{E^2}{120\pi \times 10^{-3}} \quad (5)$$

$$P_d(\text{dbm}/\text{m}^2) = 4.26 + 20 \log E \quad (6)$$

Combining equations (2), (3), and (6) the field intensity in dbm/m<sup>2</sup> becomes

$$P_d(\text{dbm/m}^2) = 4.26 + V_{\text{db}\mu\text{V}} + \text{CF} - 120$$

$$P_d(\text{dbm/m}^2) = V_{\text{db}\mu\text{V}} + \text{CF} - 115.74$$

At frequencies above 30 Mc, a quarter-wave antenna mounted on top of the field intensity measuring vehicle with the copper ground plane was calibrated against a standard dipole by subjecting both antennas to the same electromagnetic field and noting the difference.

The additional correction factors that must be considered in this frequency range are cable loss and impedance mismatch between the antenna and the FI meter. Including these factors the corrected voltage is

$$V(\frac{\lambda}{2}) = V_r(\frac{\lambda}{4}) + \text{CF}_2 + \text{CF}_1 + 1.7$$

where

$V_r(\frac{\lambda}{4})$  = meter reading with quarter-wave antenna

$\text{CF}_2$  = quarter wave to dipole correction factor

$\text{CF}_1$  = cable loss

1.7 db = mismatch loss

$V(\frac{\lambda}{2})$  = meter reading with a standard dipole antenna.

To transform the meter reading in db $\mu$ V to power density in dbm/m<sup>2</sup> consider the following:

$$P_d(\text{dbm/m}^2) = \frac{P_a}{A_{\text{eff}}} = P_a(\text{dbm}) - A(\text{db}) \quad (7)$$

where

$$P_a = \frac{V^2}{50} \quad (8)$$

and

$$A_{\text{eff}} = \frac{G_A \lambda^2}{4\pi} \quad (9)$$

where

$V$  = meter reading in volts  
 $50 \text{ ohms}$  = reference impedance  
 $G_A$  = gain of the antenna  
 $\lambda$  = wavelength in meters

$$P_a(\text{dbm}) = 10 \log \frac{P_a}{10^{-3}} \quad (10)$$

Combining equations (8) and (10)

$$P_a(\text{dbm}) = V_{\text{db}\mu\text{v}} - 107 \quad (11)$$

where

$V_{\text{db}\mu\text{v}}$  = meter reading corrected for a standard  
 half-wave dipole in db above one microvolt.

The effective area  $A_{\text{eff}}$  of the standard half-wave dipole antenna is

$$A_{\text{eff}} = \frac{G_A \lambda^2}{4\pi}$$

The gain  $G_A$  of the dipole is given as 1.64. Hence,

$$A_{\text{eff}} = \frac{1.64}{4\pi} \left(\frac{c}{f}\right)^2 \quad (12)$$

and

$$A_{\text{db}} = 10 \log \frac{1.175 \times 10^4}{f^2}$$

$$A_{\text{db}} = 40.7 - 20 \log f \quad (13)$$

From equations (7), (11), and (13)

$$P_d(\text{dbm/m}^2) = V_{\text{db}\mu\text{v}} - 107 - (40.7 - 20 \log f)$$

It was necessary to convert the spectrum signature data to  $\text{watts/m}^2$  at the correct distance and height before comparing with the radiated field measurement. The propagation path loss, as determined by the computer program, used for the Interference Prediction Model was used for this conversion.<sup>6</sup>

Essentially

$$P_{\text{dbm}/m^2} = \frac{P_{\text{dbm}}}{A_{\text{eff}}} - L_p(\text{db}) \quad (14)$$

where

$L_p(\text{db})$  = propagation path loss

$P(\text{dbm})$  = transmitter power

$A_{\text{eff}}$  = effective area of an isotropic antenna.

The effective area of an isotropic antenna is

$$A_{\text{eff}} = \frac{\lambda^2}{4\pi}$$

$$A_{\text{db}} = 10 \log_{10} \frac{\lambda^2}{4\pi}$$

Therefore, equation (14) becomes

$$P_{\text{dbm}/m^2} = P_{\text{dbm}} - 10 \log_{10} \frac{\lambda^2}{4\pi} - L_p(\text{db})$$

#### IV. RESULTS

The recordings for each of the runs were averaged in azimuth to obtain the equivalent omnidirectional radiated power level. The six samples were then combined to obtain the levels versus harmonic number for the particular vehicle-equipment combination. Some of the results are shown in Table I and plotted in Figures IV through VIII. On the figures the range of values is indicated by the vertical line for each harmonic, and the average at each harmonic by the circle. A straight line of the form

$$Y = a + b \log n$$

was calculated for each of the data sets. Actually, the last term is negative. However  $b$  is also negative as the curves are drawn. The resulting lines are also shown on the figures. In general, the results are much the same as those obtained by previous workers for the resistive loads.

For comparison purposes, the spectrum signature data for each of these equipments were obtained and averaged at each of the harmonics. The results were then converted to power density at the same distance and height

above ground from the radiating vehicle as the measured data. These results are also plotted on the respective figures as a dashed line.

The regression line that was fitted to the two sets of data follows that outlined by Hald<sup>7</sup>. It is of the form

$$Y_i = a' + b(x_i - \bar{x})$$

$$= a + bx_i$$

where

$$a' = \frac{\sum_{i=1}^k n_i \bar{y}_i}{\sum_{i=1}^k n_i} = \bar{y}$$

$$\bar{x} = \frac{\sum_{i=1}^k n_i x_i}{\sum_{i=1}^k n_i}$$

$$b = \frac{\sum_{i=1}^k n_i (x_i - \bar{x}) \bar{y}_i}{\sum_{i=1}^k n_i (x_i - \bar{x})^2}$$

and  $x_i = \log n$

The results of reference 3, obtained by combining a variety of transmitters, are also plotted on the curves. These results are identified as the empirical curve on the figures. It was not possible to apply any propagation loss to these data since a large number of different frequencies were combined to generate the curve. Therefore, this curve is plotted in the same units as the original data which is simply db below the carrier.

Several interesting observations may be made with respect to these curves. First, the empirical curve is generally pessimistic with respect to actual measured levels. Second, the radiated levels tend to remain at a

higher level than the spectrum signature data corrected for propagation for the higher order harmonics. This is probably due to either the transmitter antenna combination being more efficient at the higher harmonics or the fact that the method employed to obtain the spectrum signature data is introducing some errors. The latter is probably more correct, since the dummy load method actually mismatches the transmitter at the higher frequencies.

Another observation with respect to these curves is the small number of harmonics detected in the radiated test. A comparison with spectrum signature data will reveal that harmonics very much higher than the 10th are quite often found. In the radiated tests, harmonics above the 10th were seldom detected. The sensitivity of the measurement setup was approximately -80 dbm at the threshold of the linear portion of the range.

Spurious emissions of a nonharmonic nature were not detected in the radiated field strength measurements leading to the conclusion that this component of the transmitter spectrum is of little or no significance in the prediction of interference.

#### REFERENCES

1. Blakely, C. E., "Receiver and Transmitter Spectrum Signatures," presented at Second PGRFI Symposium, Washington, D.C., June 1960.
2. Heisler, K. G., Jr., "Preparation of Statistical Input Functions for Interference Prediction," 7th ARF Conference on RFI Reduction and Electronic Compatibility," November 1961.
3. Hurd, W. A., et al, "An Analysis of the Correlation Between Transmitter Harmonic Levels and Harmonic Order," Tech Memorandum MES-1 USNESS, Annapolis, Md., 1962.
4. Blakely, C. E., Bailey, R. N., "The Distribution and Correlation of Transmitter Interference," Proceedings of the 7th ARF RFI Conference, November 1961.
5. Kurokawa, S. and Takahashi, T., "A Method for the Direct Measurement of Spurious Emissions," J. Radio Res. Lab., Japan; July 1955.
6. "The Interference Prediction Model Theory and Computer Programs," Bell Report No. 60009-435.
7. Hald, A., "Statistical Theory With Engineering Applications," John Wiley and Sons, Inc.



TABLE I. POWER DENSITY DBM/M<sup>2</sup>

	$f_o$	$2f_o$	$3f_o$	$4f_o$	$5f_o$	$6f_o$	$7f_o$	$8f_o$	$9f_o$	$10f_o$
AN/VRC-8 WITH 3/4-TON VEHICLE $f_o = 20.4$ MC	+1.5	-49.9	-68.9	-68.2	-78.5	-67.7	-85.5	-79.4	-76.6	-64.8
	-0.7	-52.7	-78.6	-71.6	-78.4	-71.8	*	*	-72.6	-69.5
	+2.5	-50.5	-66.3	-79.2	-77.6	-73.1	*	*	**	**
	+2.6	-53.1	-59.9	-70.1	-72.7	-52.3	-83.7	-81.9	-71.9	-67.6
	+2.6	-56.2	-59.3	-66.1	-75.2	-58.4	*	*	-74.9	-71.5
	+4.4	-57.0	-64.6	*	-71.3	-43.3	*	*	-76.3	-73.0
AN/VRC-9 WITH 3/4-TON VEHICLE $f_o = 32.8$ MC	+7.6	-46.0	-55.4	-57.5	-57.4	-54.0	-57.9	*	**	*
	+6.1	-42.5	-52.2	-60.0	-63.4	-55.9	-56.3	*	-63.8	*
	+7.2	-47.5	-43.0	-56.7	-58.9	-59.8	-55.1	*	-67.7	*
	+7.6	-49.9	-59.5	-65.8	-56.7	-62.2	-53.9	*	**	*
	+5.4	-43.9	-58.7	-65.7	-55.5	-66.6	-65.8	*	-62.7	*
	+6.5	-46.7	-57.4	-69.2	-57.9	-60.2	-62.1	*	-67.3	*
AN/VRC-10 WITH 1/4-TON VEHICLE $f_o = 46.6$ MC	-2.7	-67.8	**	**	-66.8	-64.4	**	*	-72.8	*
	+4.1	-69.4	-63.6	-72.3	-62.6	-72.1	**	*	**	*
	+5.8	-71.1	-65.3	-67.9	-63.0	-70.7	**	*	-68.1	*
	+2.9	-49.6	-53.4	-54.1	-45.1	-58.7	-50.0	-74.0	**	*
	+5.7	-42.8	-69.2	-55.8	-55.4	-52.8	-59.5	-70.6	-63.9	*
	+4.8	-40.1	-59.5	-55.7	-51.7	-60.0	-64.5	-72.4	-65.9	*
AN/CRC-9 WITH 1/4-TON VEHICLE $f_o = 11.63$ MC	+4.2	-43.4	-42.2	-59.8	-73.6	-78.0	-85.8	-71.9	-79.2	-70.9
	+3.9	-47.7	-74.5	-59.2	-74.0	-76.7	*	-76.9	-67.7	-66.1
	+4.2	-47.5	-54.7	-63.8	-65.5	-87.2	*	*	-76.8	-76.4
	+4.9	-46.1	-64.2	-58.8	-72.5	-82.1	*	-77.7	-82.7	-73.6
	+5.3	-52.3	-63.2	-72.3	-76.8	-81.0	*	-78.4	-77.3	-67.2
	+6.4	-47.5	-55.7	-58.1	-68.5	-84.4	*	-78.3	-79.1	-74.0
AN/CRC-19 WITH 1/4-TON VEHICLE $f_o = 11.63$ MC	+12.5	-37.4	-55.7	-69.3	-78.5	*	*	*	*	*
	+12.3	-37.1	-51.7	-67.6	*	*	*	*	*	*
	+13.3	-36.5	-60.7	-70.8	*	*	*	*	*	*
	+13.5	-32.1	-54.1	-65.0	-74.5	*	*	*	*	*
	+14.1	-31.6	-54.7	-64.9	*	*	*	*	*	*
	+13.4	-29.9	-49.7	-65.0	*	*	*	*	*	*

\*Signal too low in the nonlinear region of field intensity meter.

\*\*Interference encountered.

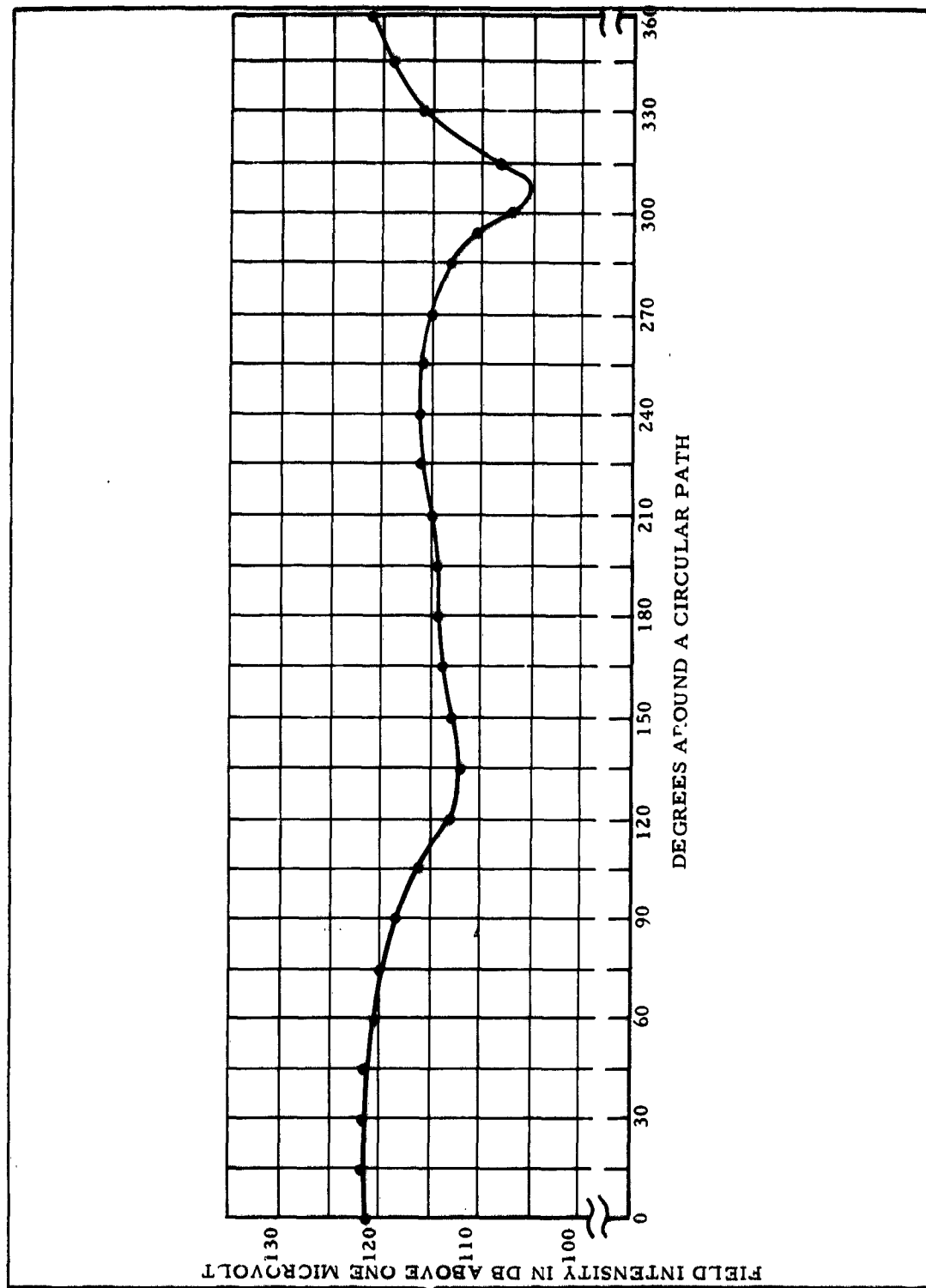


Figure 1. A Typical Azimuthal Pattern for Transmitter -  
Antenna - Vehicle Combination

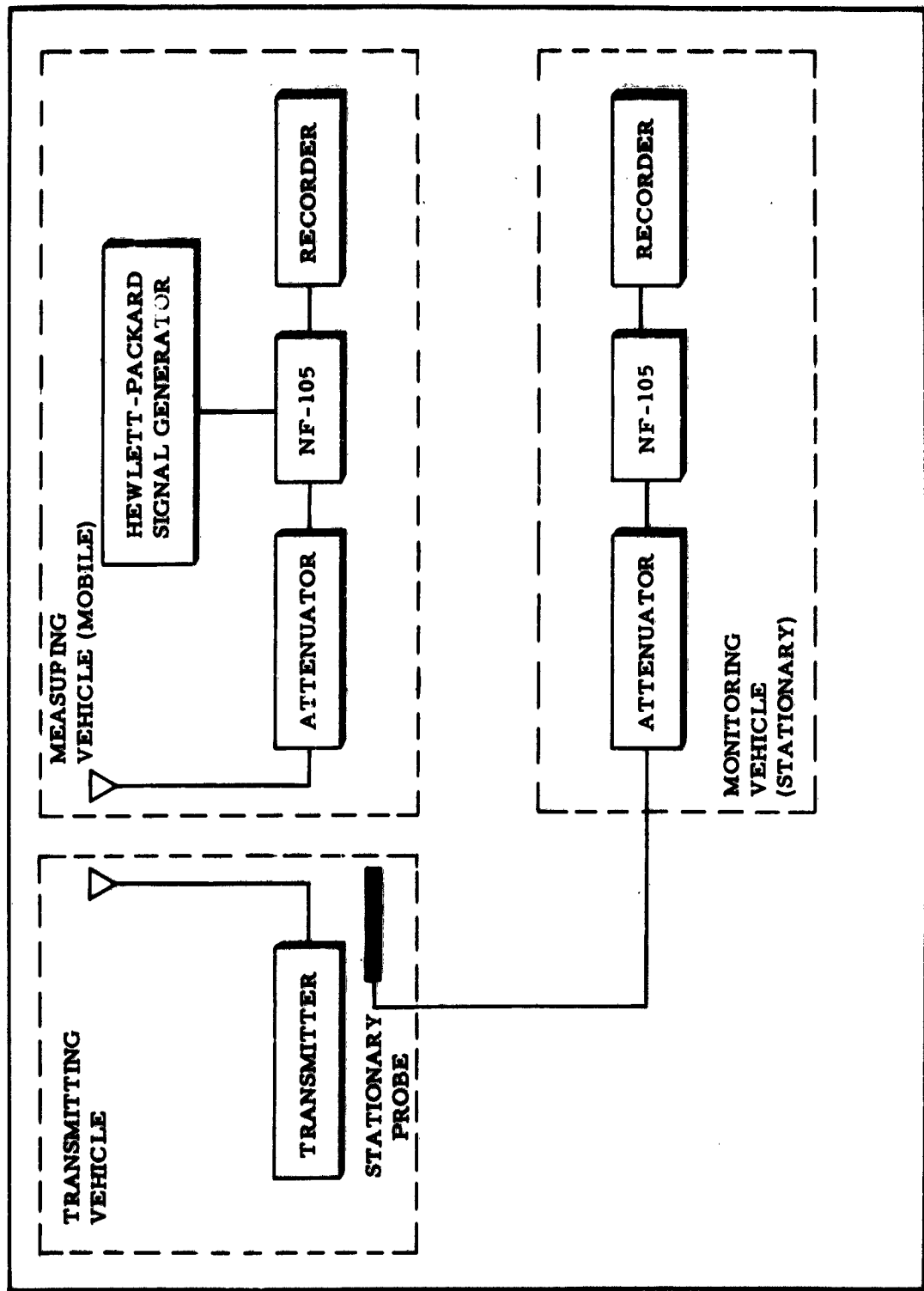


Figure II. Block Diagram of Test Setup

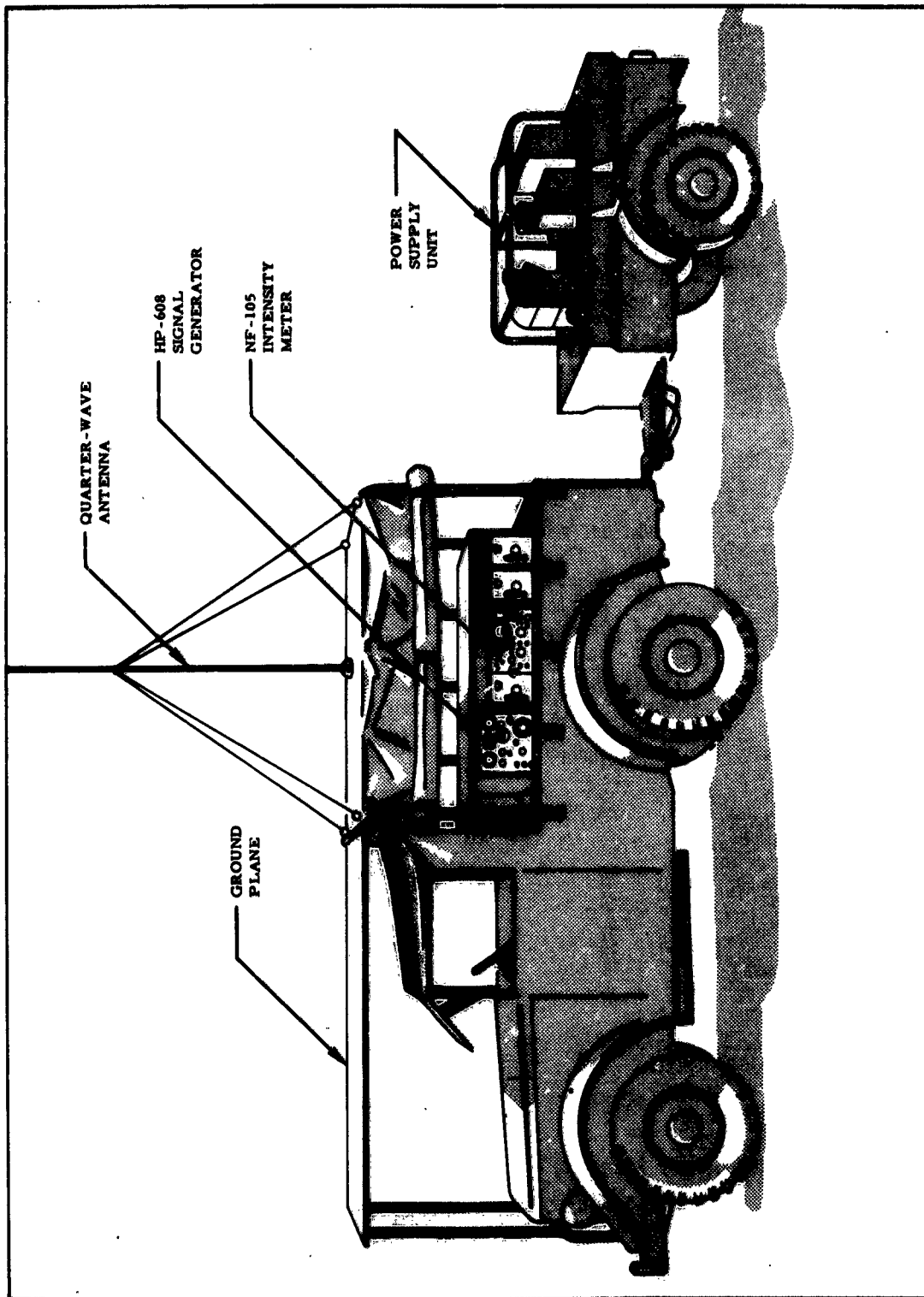


Figure III. Exterior View of FI Shelter

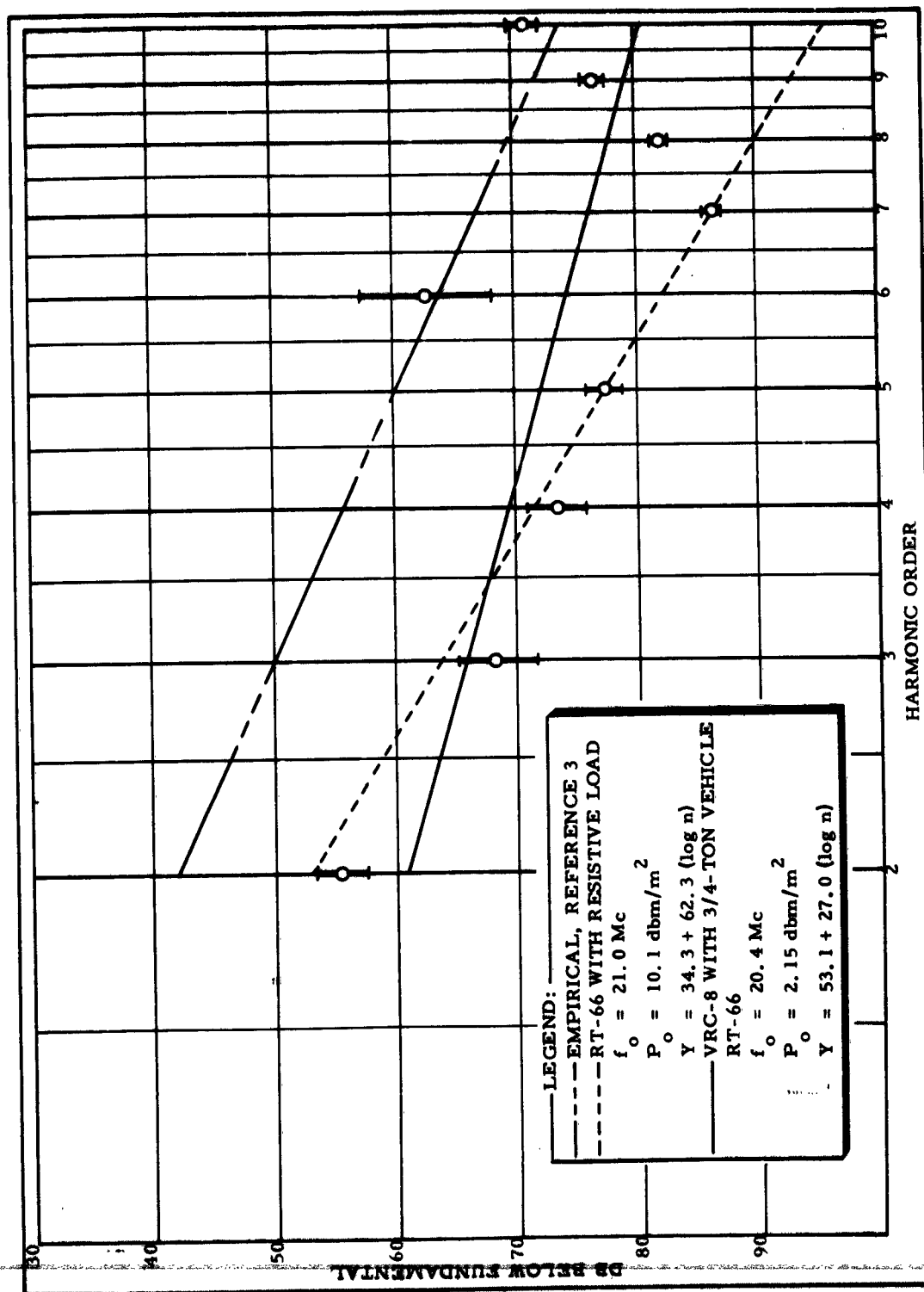


Figure IV. A Comparison of the Regression Line Obtained From Spectrum Signature and Radiated Field Data For the Transmitter RT-66.

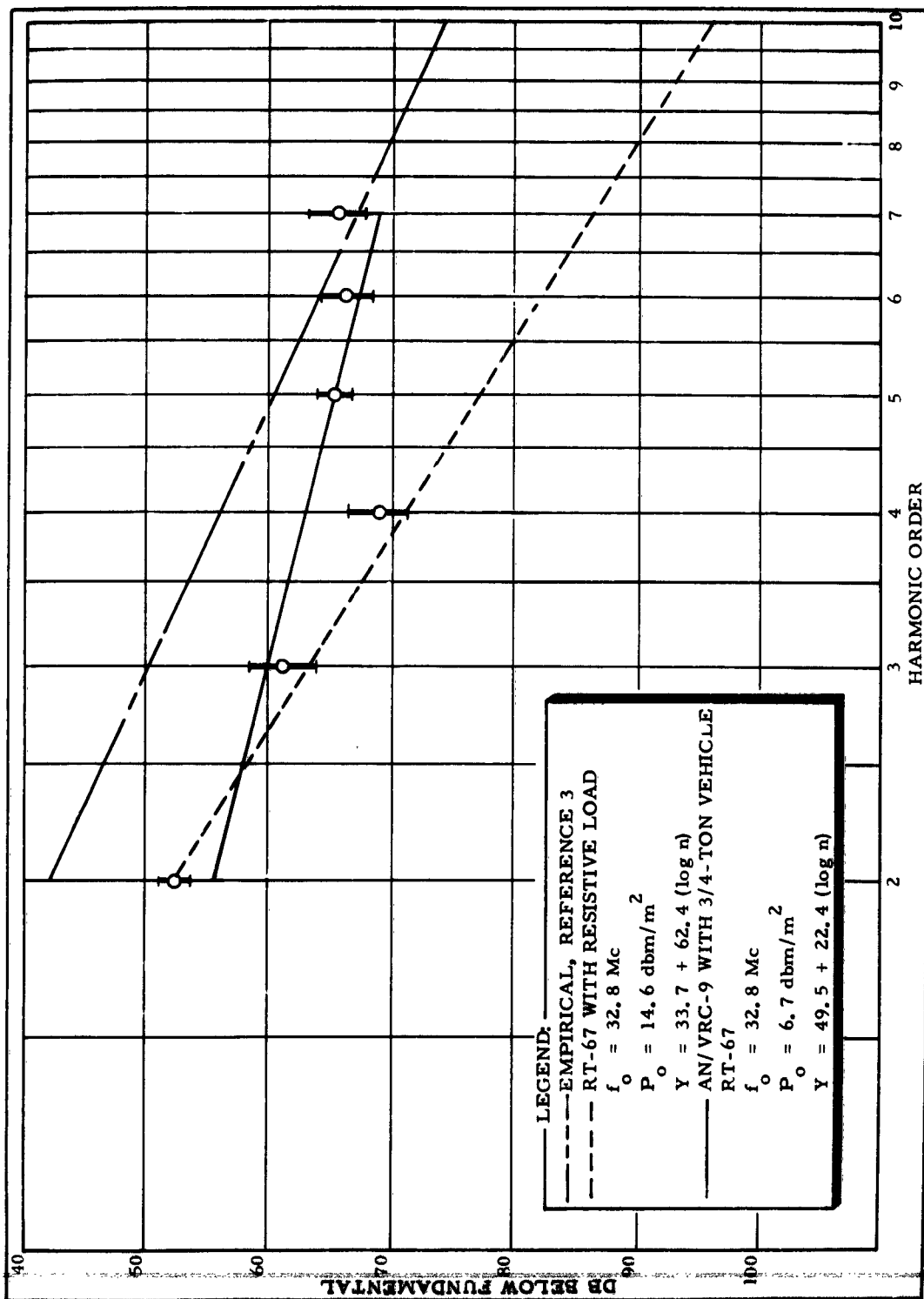


Figure V. A Comparison of the Regression Line Obtained From Spectrum Signature and Radiated Field Data For the Transmitter RT-67.

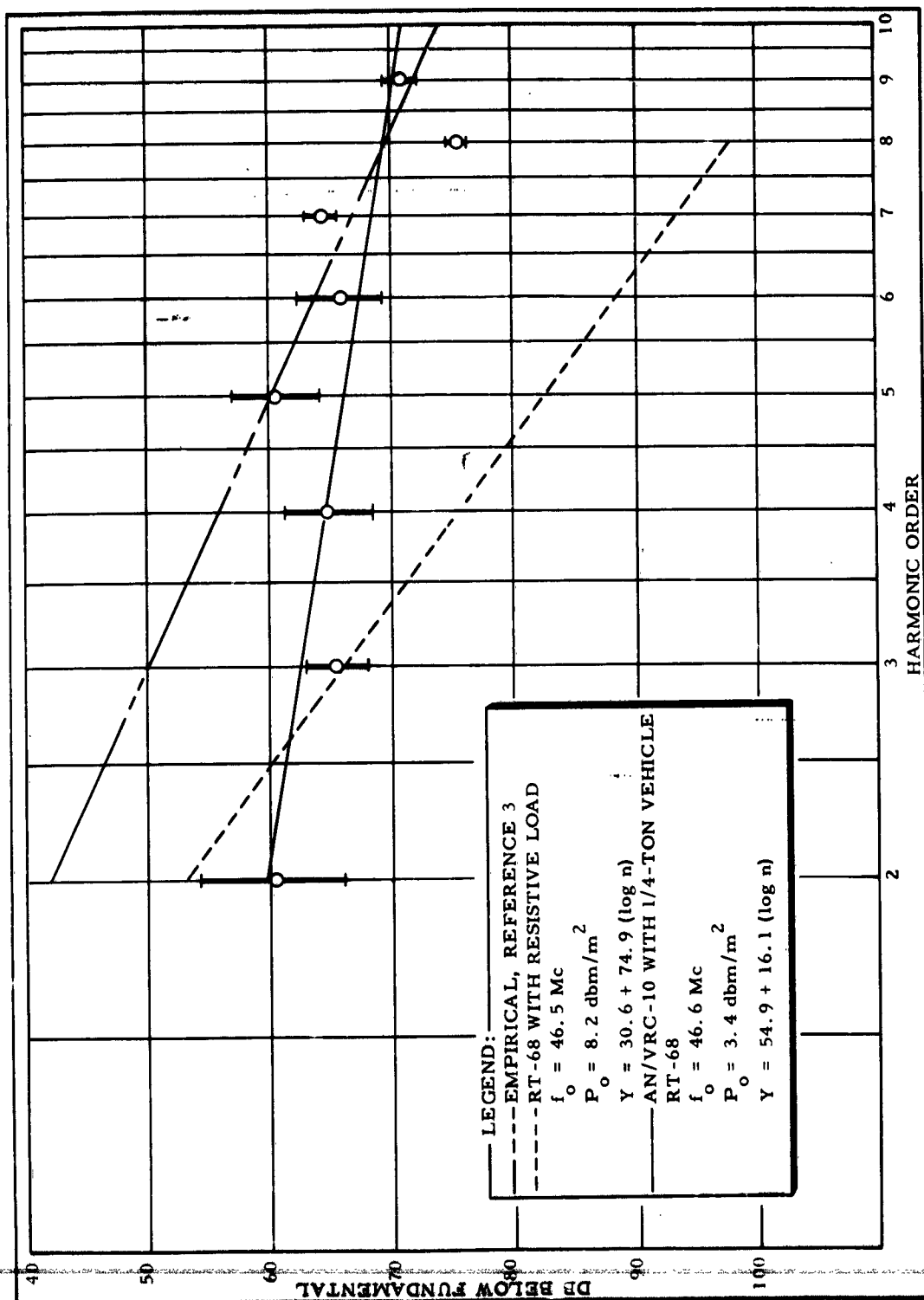


Figure VI. A Comparison of the Regression Line Obtained From Spectrum Signature and Radiated Field Data For the Transmitter RT-68.

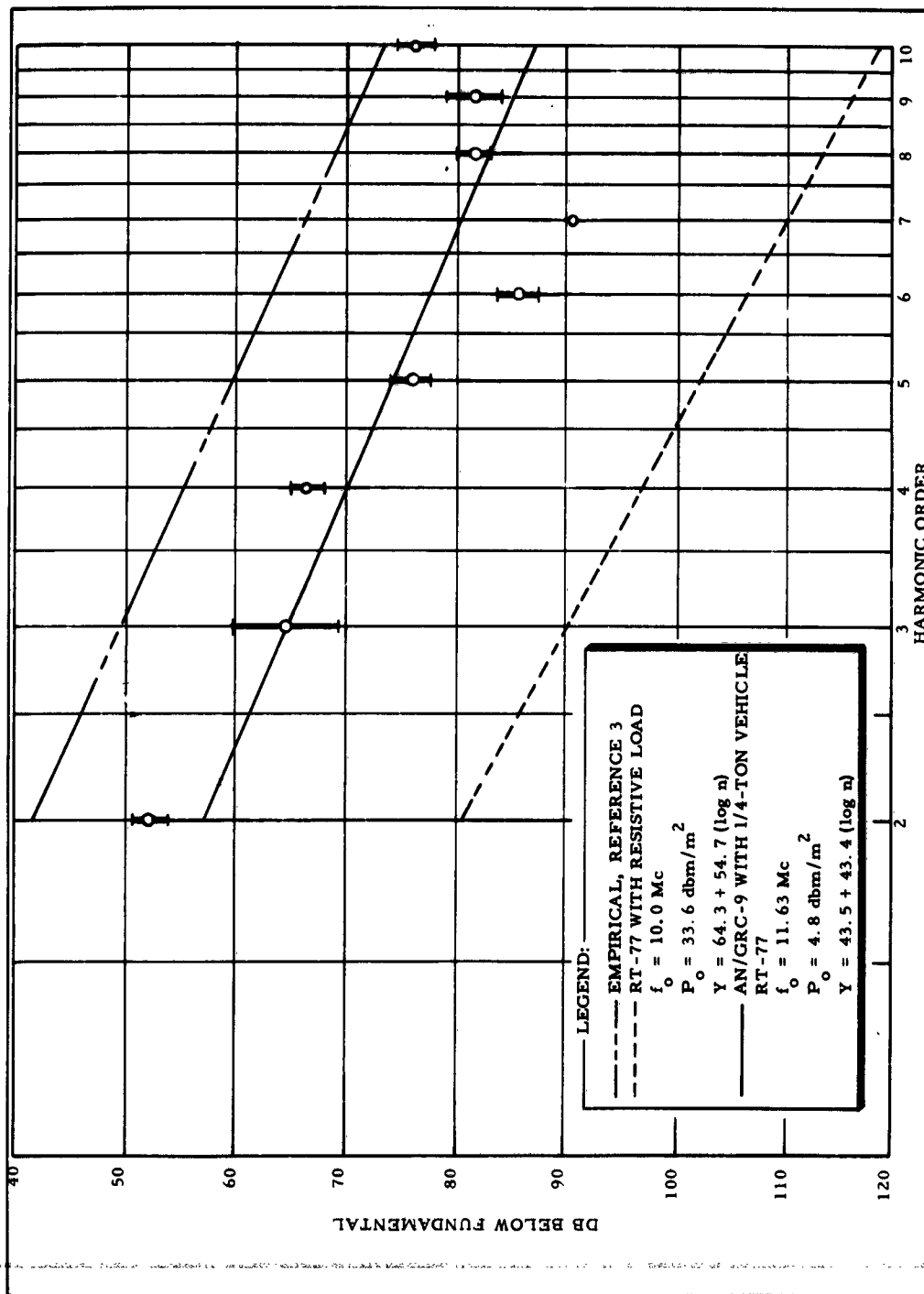


Figure VII. A Comparison of the Regression Line Obtained From Spectrum Signature and Radiated Field Data For the Transmitter RT-77.



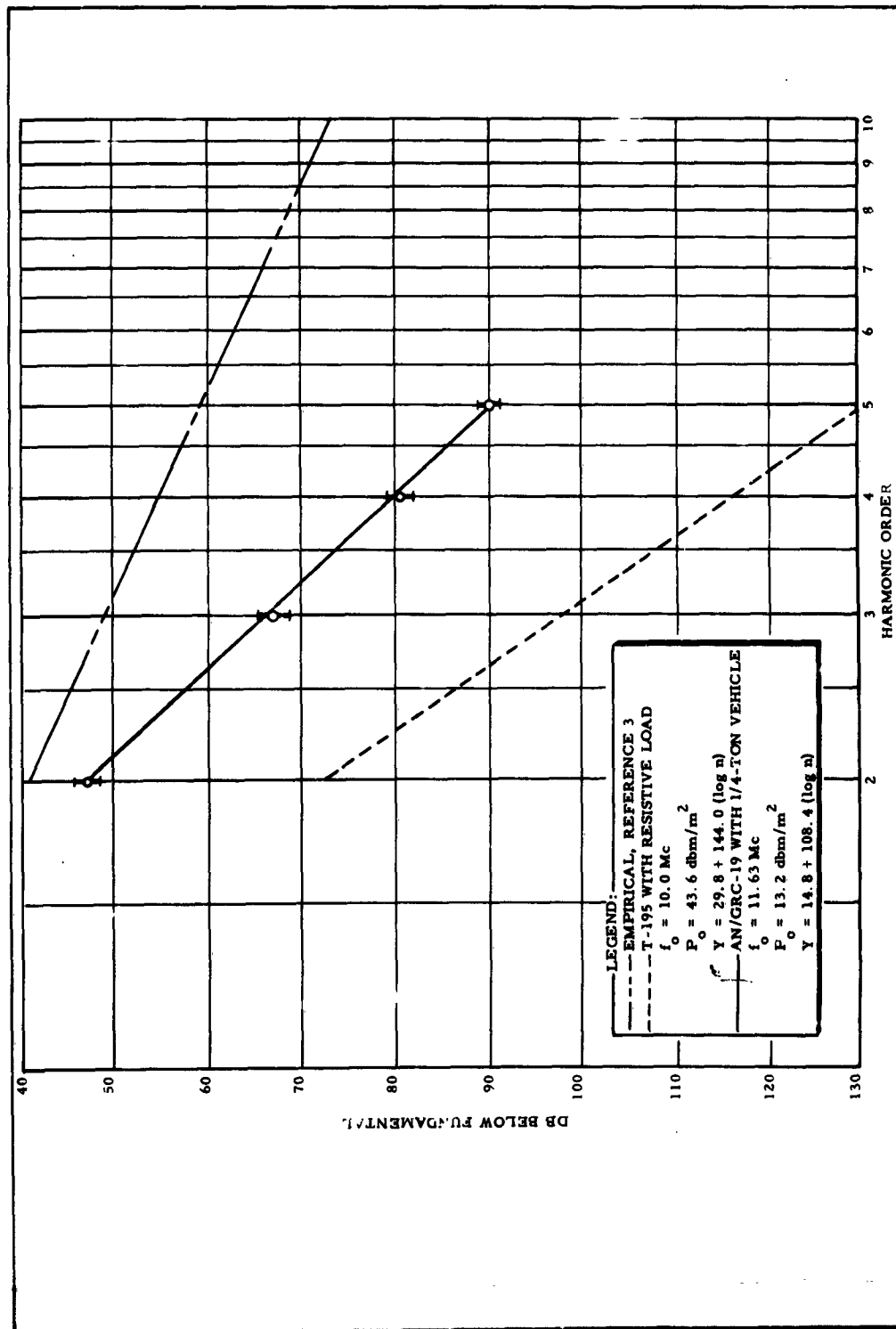


Figure VIII. A Comparison of the Regression Line Obtained From Spectrum Signature and Radiated Field Data For the Transmitter T-195.

**ANALYSES OF AIRBORNE RADIO FREQUENCY INTERFERENCE  
(RFI) PROBLEMS**

R. E. Haydon  
Federal Aviation Agency  
Washington, D. C.

T. F. Barone, L. J. Grady, T. E. Selby  
HRB-Singer, Inc.  
State College, Pennsylvania

**Abstract.** - An analysis of radio-frequency interference (RFI) in the nation's air navigational system has been conducted for the Federal Aviation Agency. Three frequency bands have been carefully studied: 108 Mc to 140 Mc, 328 Mc to 336 Mc, and 960 Mc to 1215 Mc. They are used for VOR, Localizer, Communications, Glide Slope, TACAN, DME, and Beacon, respectively. Investigation of actual interference reports and laboratory tests of interference susceptibility of on-board navigation equipment were used to supplement the study.

A system to detect, measure, identify and locate interference sources has been recommended for use in the existing FAA flight inspection program. The nature of the FAA program and the desired operational requirements for the system indicated consideration of five major problem areas: (1) Interference recognition, (2) Transmitter location finding, (3) Hand-off between operations, (4) Aircraft operational problems, and (5) Determination of operator responsibility for the RFI system.

At present, work is proceeding on a contract to implement the recommended system for basic (low) altitude flight inspection.

**I. INTRODUCTION**

The procedures used for air navigation and traffic control in the United States are based, to a large degree, on the performance of the air traffic control and navigation facilities operated by the Federal Aviation Agency. The maintenance of a satisfactory level of performance of these facilities is of extreme importance. In-flight inspection is one of the means employed by the Agency to assure the performance of these facilities. Like all systems which employ radio frequencies, air traffic control and navigation radio signals, transmitted from FAA operated facilities, are vulnerable to interference. These interfering sources must be identified, located, and eliminated to ensure the effectiveness and reliability of the navigational system. The identification and location of radio-frequency interference (RFI) sources is an important function which FAA flight inspection aircraft must perform in co-operation with the Federal Communications Commission and other agencies of the Federal Government.

## II. SYSTEM REQUIREMENTS

The objective of the RFI system is to detect, identify, and locate the sources of interference. It was necessary to determine the type of interference signals to be located so that the major effort of the system could be expended on interference signals which could be reduced. Some of the most common causes of RFI were found to be:

- (a) Industrial plastic welders
- (b) Co-channel interference by other navigational facilities
- (c) Broadcast and FM radio stations
- (d) Misc: Garage doors, remotely controlled; FM tuners; etc.

The requirements of the RFI locating system and the problems it is designed to solve can be categorized into five major areas. These are entitled interference recognition, transmitter location finding, hand-off between operations, aircraft operational problems, and determination of operator responsibility for the RFI system. The system recommended and the problems they solve are discussed under these categories in the sections that follow.

### 1. Interference Recognition

The system must be able to identify co-channel interference caused by other facilities and identify the interfering facility from either its identification transmission or its geographical location.

#### a. Aircraft Location

The problem here is two-fold. First, many so-called interference signals are the result of an attempt to use the facilities from outside their frequency protected areas. Second, this constitutes a considerable portion of the interference reported to the FAA. If a receiver is far enough from the source of a signal, other signals will begin to interfere with the signal desired.

#### b. Interference Display

The RFI system should provide a clear channel to the radio-frequency input signals at the antenna to allow the display of the adjacent channels surrounding the desired signal. It should receive the signals present and display them in such a manner that normal reception with no interference is easily recognized. Unusual receptions and modulations must be displayed in such a manner that they can be recognized, categorized into types of possible interfering sources, and recorded for playback and comparison at a later time at another location.

Current nav-aid receivers are not designed to recognize interference signals and to distinguish between malfunctions caused by interfering signals and those caused by other means. TACAN receivers, for example, provide only those outputs which first pass through a pulse delay coincidence. Also, the audio channels in VOR receivers amplify only the frequencies between 350 and 3,500 cps for communication reception. A much broader signal bandwidth is desired for interference recognition.

### c. RFI Signal Identification

The system should provide a means for identifying the characteristics of an interference signal by the type of transmitter that is emitting the interference signal. Pilots and panel operators appear to have a good grasp of the interference types that produce heterodynes and broadcast station modulation in their VOR audio channels. It is believed that sufficiently discriminating displays can be developed so that catalogs of the appearance of interference types can be compiled to enable the pilots and operators to become familiar with and quickly identify types of interference. For this purpose, a means of simulating interference situations should be provided to train the pilots and operators to recognize these situations.

## 2. Location Finding Requirements

The system must be able to determine the direction of arrival of the interference signal in the presence of the desired signal without requiring that the aircraft change its attitude sufficiently to fly it off course. This pertains only to the High Altitude KC-135 and Intermediate Altitude SAFI flights. Within these restrictions, it is believed that a nonmaneuverable flight cannot perform the final location search for the address of the interfering transmitter. However, the capability of picking up the signal the second time is greatly enhanced if its general location is indicated.

The problems contributing to this requirement include the undesirability of removing or "turning off" the facility signal at the instant the interfering signal is detected for the purpose of performing simple direction finding. Also, the adjacent channel rejection characteristics of nav-aid receivers are believed to be of such quality that any interfering signal will occupy the same frequency bandwidth as the desired signal. On this basis, the desired signal cannot be tuned out by virtue of its frequency.

The basis for this belief was confirmed with tests performed on typical nav-aid receivers.

The intermediate and high altitude flights are planned to the point that if one deviates from its course, the value of the flight check operation is lost. Thus the use of an

array to provide a fixed-beam antenna that could be scanned by changing the aircraft attitude is not desirable.

The final requirement for direction finding is that the antennas not be large enough to affect the performance of the aircraft, taking it out of the common carrier class (Ref. Part 04, Civil Air Regulations). This essentially eliminates the possibility of using a rotating high-gain antenna which would be quite large at 100 Mc or even at 1,000 Mc.

The recommended system provides a solution to this problem. It takes advantage of the fact that the interfering signals (in order to be interfering) will be strong signals. A narrow-beam, high-gain antenna pattern is usually used to obtain bearings on weak signals. For these strong signals, however, an antenna pattern which contains a very sharp null is recommended. The null is used to suppress the interfering signal. Direction is determined at the moment the null is swept past the direction of arrival of the undesired signal.

This, however, solves only part of the problem and additional requirements are placed on the final location technique. During final location operations, the strength of the undesired signal will increase as the interfering transmitter is approached. Provision must be made to reduce the saturation sensitivity of the receivers used for final search. A special antenna must be available with capabilities of suppressing signals not originating from directly below the aircraft. It must provide a means of determining, within one-tenth of a mile, the exact location of the aircraft when maximum signal strength indicates that the aircraft is directly over the source of interference.

These rather stringent requirements on the system for final location are necessary for use in the metropolitan areas where a score of industrial manufacturing processes can be housed in the same city block.

### 3. The Hand-Off Problem

The gap to be filled between the detection of an interference situation and the final location operation adds technical and recording requirements to the system. The system must preserve a record of the characteristics of the interference signal to provide an adequate description of this signal for the operator performing the final location tasks. The object of this record is to allow the final search personnel to assure themselves that the signal whose location they are tracking is the same signal that caused the interference detected by the earlier flight.

The system must record the direction of the antenna pattern null, its effect upon the signal strength of the undesired signal, the attitude of the aircraft, and an indication of the

aircraft location (such as the event, operation, or photo number). In the intermediate and high altitude flight check operations, the exact position of the aircraft is not known until after the flight has terminated. A computer determines the exact position of the aircraft at various times along its flight path from recorded data. The direction of arrival of the signal is of little value in locating the source of the signal unless the position at which it arrived is also known to a comparable accuracy.

The recorded interference signal characteristics made in the aircraft should be reproducible to provide a comparable display to assist ground crews or pilots and technicians of basic altitude aircraft in the final search operation.

The system operation should include an analysis function performed after the flight to combine signals and indications recorded during the flight. The antenna sweep, the aircraft attitude, and the video signal are combined to produce the direction of arrival of the interfering signal with respect to magnetic North. This can then be combined with the aircraft location to provide a direct bearing to the transmitter location.

#### 4. Flight Check Operations

The system to be installed in the basic altitude aircraft must include some method of determining the location of the aircraft when certain relative bearings are obtained. The system should be as simple as possible and take advantage of the fact that the DC-3 Basic Flight Inspection aircraft can be maneuvered at low altitudes and can interrupt its flight check operations.

The system to be installed in the intermediate altitude aircraft must be compatible with 22 different TACAN and VOR receivers. However, its controls and indicators must be simple in order to conserve the small amount of panel and workspace available to the operator. It must record automatically both the bearing information and the interference signal characteristics.

In addition to the other characteristics required, the system must provide automatic tuning in order to minimize the additional tasks placed upon the panel operator in the high altitude aircraft (Jet Operations). A transfer switch must be designed to shift the tuning control head from the navigation receiver to the interference detection system. This will automatically tune the interference receiver and should enable the panel operator to determine if he has a case of interference without seriously interrupting his data collection operations.

The system must be able to accurately locate the interfering emitter when the aircraft passes directly over the offending emitter. The geographical position of the aircraft must be precisely determined when the received signal strength reaches

its maximum. The system must, therefore, have this capability of measuring relative signal strength.

#### 5. Determination of Operator Responsibility for the RFI System

In assigning operator responsibility for the RFI system, there are two conditions which must be met:

- (a) The size of the flight check crews should not be increased.
- (b) Operating the RFI system should not interfere with performance of the operator's normal duties.

The degree to which each of these requirements can be fulfilled depends on several factors, such as crew size and crew duties, which vary between the three types of aircraft (KC-135, C-131E, DC-3) which currently perform the majority of the facilities flight checking. The fact that these factors are not the same in each type of aircraft means that there can be no universal "best" solution to the operating responsibility problem. Instead, it is necessary to develop separate solutions, each one tailored to fit the environment in a specific aircraft.

The flight check procedure used at basic altitudes is completely different from those used at high and intermediate altitudes. Each basic altitude flight check collects detailed data on a single navigational facility. In contrast, each high and intermediate altitude flight check collects less comprehensive data on a large number of navigational facilities. Because high and intermediate altitude flight checks involve elaborate pre-planned flight paths, it is desirable not to deviate from these paths to chase an interfering signal. The DC-3, however, has no such restrictions and is extremely flexible in its operations.

### III. RECOMMENDATIONS

The DC-3 Basic Flight Inspection system is a manual system and it is therefore necessary for the panel operator to pay close attention to the panel during all periods of data collection. During a normal flight check, this operator will not have sufficient time to operate the RFI system in addition to collecting other flight check data.

The solution is to cease normal flight check operations upon detection of RFI and to then maneuver the aircraft so as to obtain the maximum information on the interfering signal. When data collection on the interfering signal has been completed, the aircraft would then return to its normal flight check operations.

While this stopping and starting of routine flight check operations might prove extremely impractical in the KC-135 and the C-131E, the greater flexibility of the DC-3 flights should permit its occurrence without any loss of normal flight check data.

Three separate interference systems were recommended for installation in the three different flight check aircraft. They all follow the same system operating philosophy which was formulated to perform the detection, identification, and location function as an addition to existing operations. Several electronic equipment functions and operating methods were brought together to form an integrated system. Figure 1 illustrates this integrated system.

A two-lobe antenna pattern with a deep null is electronically rotated in azimuth by sweeping the phase combinations of a three-antenna array. The rate of rotation is controlled by the beam-sweep function generator. The signals received by the antennas are converted to an intermediate frequency, amplified and processed through a sweeping receiver and a demodulating receiver.

In the sweeping receiver, a sweeping local oscillator (SLO) and a mixer scan a narrow band intermediate frequency amplifier (NIF) through the frequencies adjacent to the desired signal. A video detector measures the strength of the signals at each frequency. This distribution of signal strengths is displayed on a panoramic indicator.

Interference signals will have their frequency components distributed differently than will signals from nav-aid transmitters, and each will be recognizable on this type of display.

When the null in the antenna pattern is pointing toward the interference transmitter, the amplitude of the received signal will be decreased and it will disappear from the indicator display. By correlating the direction of the antenna pattern null with the disappearance of the interference signal, the direction to the interference transmitter may be established.

The demodulating receiver extracts the modulation characteristics from the received signals and provides a selection of either AM or FM receiver output for identification purposes.

The video signals from the sweeping receiver, the audio signals from the demodulating receiver, the frequency sweep, and the antenna position indications are combined and recorded on magnetic tape to provide an automatic data collection capability. The displays can then be reproduced, analyzed, and used as a basis for locating the interfering transmitter after the inspection flight is completed. The recording capability eliminates the need for additional panel operators to continually monitor and analyze the interfering signal information at the location where it is received.



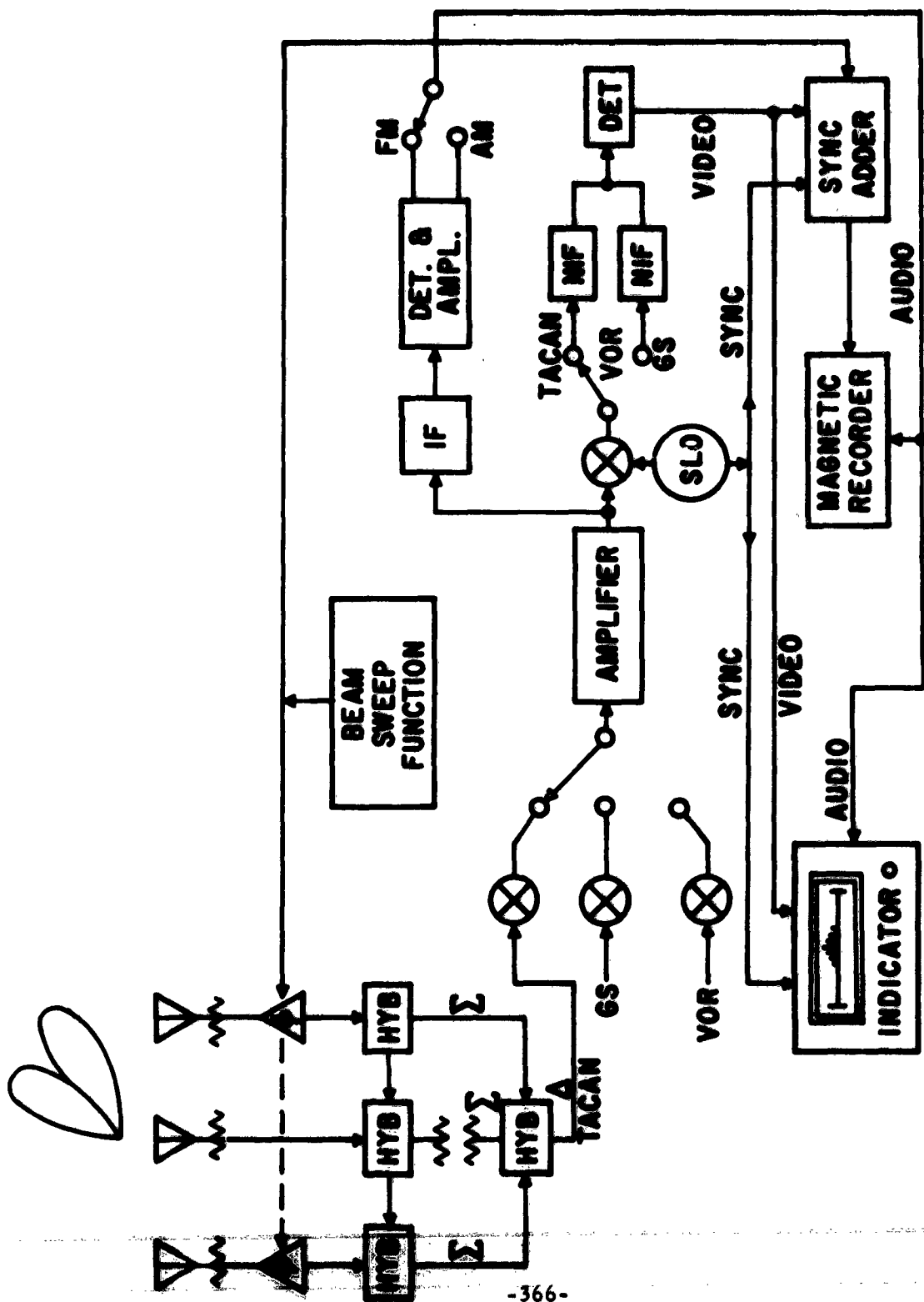
All of the functions mentioned are not necessary in each of the flight check aircraft. However, the description serves to show how these functions will be used where they occur in the recommended installations.

A hardware development program has been initiated in order that the recommended system be tested and put into operation with a minimum of delay. The development contract awarded may be summarized by the following recommendations which, in part, are included in the conclusions and recommendations of the parametric study and analysis project.

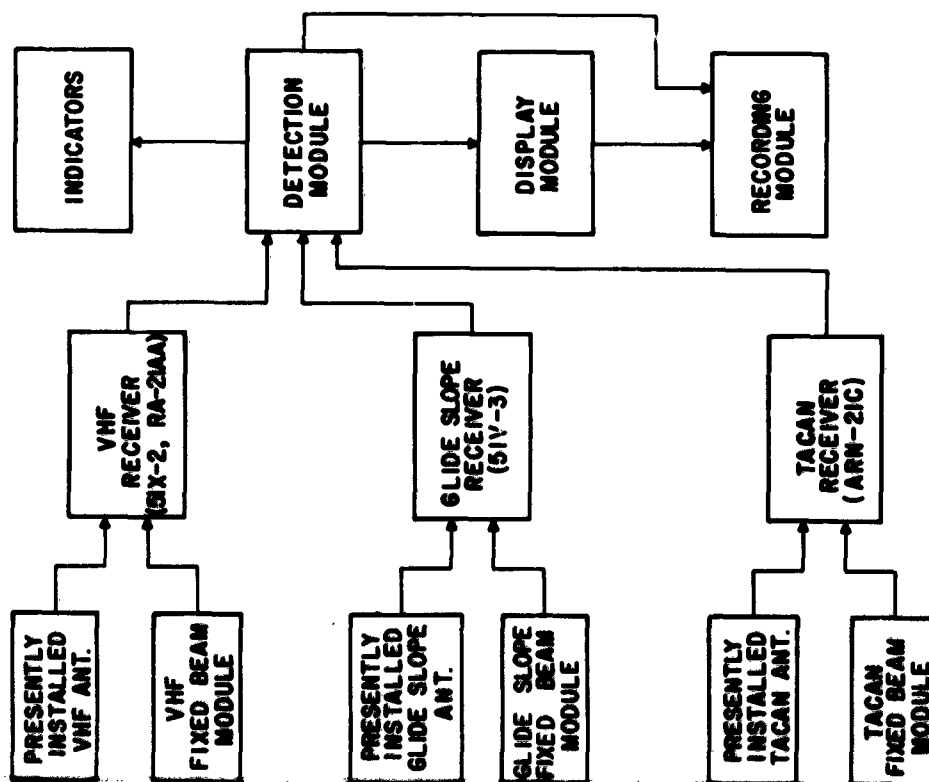
- (1) A modularized system
- (2) "New" antennas, as described previously
- (3) The DC-3 must interrupt its normal mission to "track down" an interference source.
- (4) The DC-3's and the FAA mobile RFI vans are recommended for use in pinpointing an RFI source, through a hand-off of pertinent information.

#### IV. ACKNOWLEDGMENTS

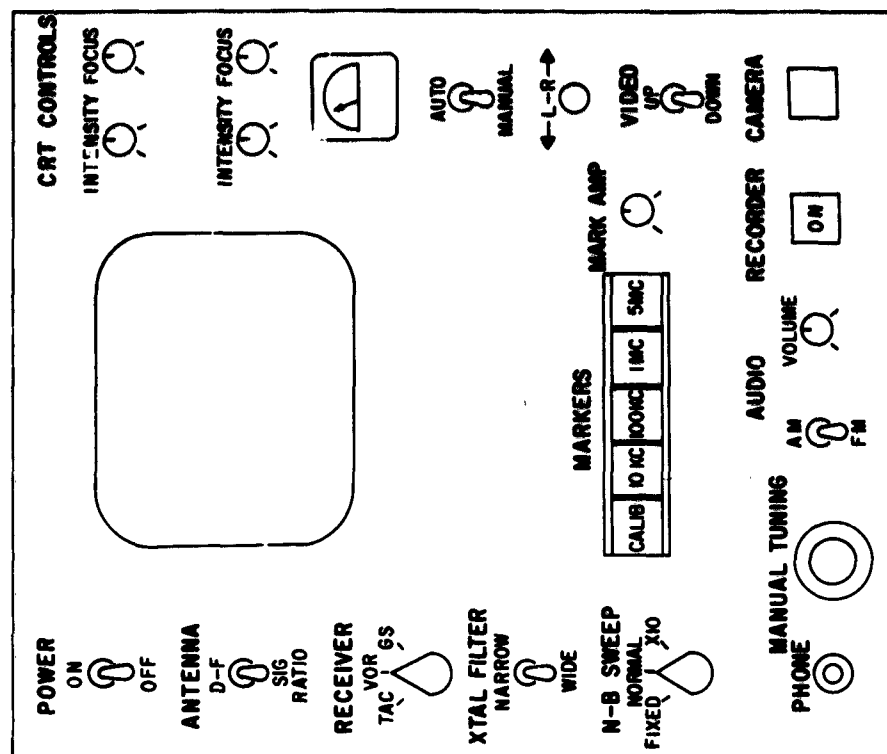
The authors are indebted to V. A. Rathfelder and W. R. Chubb for their work on the initial study. Tests of receiver susceptibility were conducted by V. Ritter.



Typical RFI System Operating Diagram



Functional Diagram of the  
Basic Flight Inspection RFI System



## MUTUAL GAIN OF RADAR SEARCH ANTENNAS\*

R. C. Johnson

Engineering Experiment Station  
Georgia Institute of Technology  
Atlanta, Georgia

**Abstract.** - Experimental data indicate that the gain characteristics of radar search antennas can be described by Gaussian curves; further, mutual gain measurements with pairs of antennas indicate that the mutual gain characteristics can be described by a Gaussian curve having a median gain equal to the sum of the median gains of the individual antennas and a standard deviation equal to the square root of the sum of the squares of the individual standard deviations.

Modifications of an AN/SPS-10 antenna resulted in significant improvements in the radiation characteristics. The median gain was reduced 10 db with no degradation of the main lobe. A brief evaluation of two modified antennas aboard two destroyers at sea indicated that about a 20 db increase in isolation between the two SPS-10 radars was achieved, as predicted.

### I. INTRODUCTION

The susceptibility of radar search antennas to radio-frequency interference (RFI) is determined to a great extent by the minor-lobe structure. The use of detailed, three-dimensional patterns of radar search antennas to predict RFI is not practical because the minor-lobe structure changes with frequency and site modifications. In addition, some of the most troublesome interference problems are caused by Fresnel-zone radiation between closely spaced equipments, and the lobe structure of a Fresnel-zone pattern depends on the distance to the observation point. The problem is further complicated when one considers orthogonally polarized signals and out-of-band frequencies.

Radar search antennas are characterized by a high-gain lobe which continuously scans 360 degrees in azimuth; therefore, the main lobe contributes to the interference problem only a small part of the time. As the search antenna rotates, the gain in the direction of the interfering source varies continually. One does not need a detailed description of the gain variation: a statistical description is sufficient, and it offers a more useful approach for predicting RFI.

Compare, for example, the detailed pattern of Figure 1 and the statistical gain distribution of Figure 2. Since the gain of the antenna is above isotropic for only about 5.3 degrees, the probability that the gain is less than isotropic is 0.98 as illustrated on the gain distribution curve. Similarly, one can see from the detailed pattern that the gain is less than -10 db more than half the time, and this is illustrated on the gain distri-

\*Supported by the Bureau of Ships under Contract N0bsr-85387.

bution curve where the probability that the gain is less than -10 db is shown to be 0.74. Although the peak gain of the antenna is almost 30 db, the median gain (the gain for which the ordinate of the cumulative gain distribution curve is equal to 0.5) is only -13 db. Note the strong distinction between median gain and average gain (which is unity for a lossless antenna).

The statistical gain distributions of two large radar antennas were first investigated by the Statistical Analysis Group of the Georgia Tech Engineering Experiment Station.<sup>1</sup> The statistical distributions of far-zone antenna patterns have also been investigated by personnel of the IIT Research Institute.<sup>2</sup> A preview of the present program was given by Long,<sup>3</sup> and initial results were reported by Johnson.<sup>4</sup> The results contained in the present paper were reported in more detail elsewhere.<sup>5-7</sup>

## II. GAIN CHARACTERISTICS OF RADAR SEARCH ANTENNAS

Statistical gain studies with the AN/SPS-10 and AN/SPS-6 antennas have shown that the gain characteristics of both antennas can be described by a Gaussian curve having a median gain of -13 db and a standard deviation of 6 db. In Figures 3 and 4, the dashed lines indicate the limits of the measured cumulative gain distribution curves. In other words, the gain distributions for in-band frequencies which were measured in the Fresnel zone or far zone all lie within the dashed lines. Note how well the measured characteristics are described by the Gaussian curves. The measurement program under this contract also included other studies,<sup>5-7</sup> but the results are not reported here.

Note that the present investigation concerns a statistical analysis of the measured gain characteristics in a complete 360° antenna pattern. The main lobe and the first few side lobes are determined chiefly by the amplitude and phase distributions in the aperture (for both the far zone and the Fresnel zone); however, the rest of the minor lobes in a 360° pattern are influenced by many other factors such as spill-over and back-radiation from the primary feed horn, edge currents on the reflector, scattering off of the primary feed and supporting structures, and leakage through mesh-type reflectors. Other investigators have devoted considerable effort to the study of detailed Fresnel-zone patterns; however, since it is impossible to theoretically consider all of the factors contributing to a 360° pattern, their work (although valuable for many purposes) is not directly related to the present statistical study.

## III. MUTUAL GAIN OF TWO RADAR SEARCH ANTENNAS

### A. Theoretical predictions

Consider two isolated antennas—one transmitting and the other receiving energy. The received power can be calculated from the well-known power transmission equation,

$$P_r = \frac{g_t g_r \lambda^2}{16 \pi^2 R^2} P_t, \quad (1)$$

where  $P_t$  is the transmitted power,  $P_r$  is the received power,  $\lambda$  is the wavelength,  $R$  is the distance between antennas,  $g_t$  is the gain of the transmitting antenna, and  $g_r$  is the gain of the receiving antenna. This equation can be written in the logarithmic form,

$$L_r = G_t + G_r + L_t - N, \quad (2)$$

where  $L_t$  is the transmitted power in dbm,  $L_r$  is the received power in dbm,  $G_t$  is the gain of the transmitting antenna in db,  $G_r$  is the gain of the receiving antenna in db, and  $N = 20 \log (4\pi R/\lambda)$  is a space attenuation factor in db.

In the case of two interfering search radars, the values of  $G_t$  and  $G_r$  are continually changing because the antennas are rotating. Previous discussion has dealt with the statistical gain distributions of a single antenna; but to make use of Equation 2, it is necessary to know the statistical distribution for the mutual gain,  $G_m = G_t + G_r$ . The statistical distribution for the mutual gain can be determined mathematically by taking the convolution of the distributions of the transmitting and receiving antennas (when the gains are expressed in decibels); this operation is inconvenient but not too difficult. If, however, the distributions of the individual antennas are Gaussian, then the convolution (or the statistical distribution for the mutual gain) is also Gaussian with a mean equal to the sum of the individual means and a standard deviation equal to the square root of the sum of the squares of the individual standard deviations. This can be expressed mathematically as

$$m_m = m_t + m_r \quad (3)$$

and

$$\sigma_m = \sqrt{\sigma_t^2 + \sigma_r^2}, \quad (4)$$

where  $m_m$ ,  $m_t$ , and  $m_r$  are the means and  $\sigma_m$ ,  $\sigma_t$ , and  $\sigma_r$  are the standard deviations for the mutual gain, gain of the transmitting antenna, and the gain of the receiving antenna, respectively.

Measured characteristics of the SPS-10 and the SPS-6 antennas have shown that the statistical gain distributions are Gaussian. Therefore, the mutual gain distributions will also be Gaussian with means and standard deviations calculated according to Equations 3 and 4.

#### B. Mutual gain measurements

Two experiments were conducted to measure the mutual gain of two radar antennas. The first experiment measured the statistical distribution of mutual gain for the SPS-10 and SPS-6 antennas, and the second experiment measured the statistical distribution of the mutual gain for two SPS-10 antennas. Both experiments were conducted on the 50-foot range, which is well within the Fresnel zone, and at a frequency of 5500 Mc.

The arrangement of the antennas for the first experiment is illustrated in Figure 5. The SPS-10 antenna is on the pad in the foreground

and the SPS-6 antenna is on the receiving tower in the background. Since 5500 Mc is more than four times the design frequency for the SPS-6 antenna, the insertion loss of the rotary joint is a function of both angular orientation and small frequency shifts. To avoid this uncertain loss, the rotary joint of the SPS-6 antenna was by-passed. Figure 5 shows a long taper from L-band to C-band waveguide installed behind the reflector feed-horn.

The experiment was conducted in the following manner. The SPS-6 antenna, which was used as a receiving antenna, was rotated continuously. The SPS-10 antenna, which was used as a transmitting antenna, had a special drive mechanism to rotate the antenna two degrees for each revolution of the SPS-6 antenna. During 180 revolutions of the SPS-6 antenna, the SPS-10 antenna made one revolution. This was considered to be a good sample of all possible relative orientations of the antennas. The range was calibrated by comparing the received power with the power that would be received using isotropic antennas with the same separation.

The gain characteristics of the reflector and feed of the SPS-6 antenna at 5500 Mc can be described by a Gaussian curve having a median gain of -5 db and a standard deviation of 7 db.<sup>5</sup> Likewise, the gain characteristics of the SPS-10 antenna at this frequency can be described by a Gaussian curve having a median gain of -13 db and a standard deviation of 6 db. Thus, mutual gain should also be Gaussian with a median gain of -18 db and a standard deviation of 9.2 db. Figure 6 illustrates the predicted Gaussian curve and the measured points; the agreement is very good.

The second experiment involving two SPS-10 antennas was performed in the same manner, except the rotary joint of the receiving antenna was not by-passed. The arrangement of the antennas is illustrated in Figure 7. Based on the measured characteristics of a single SPS-10 antenna, the mutual gain of two SPS-10 antennas should be Gaussian with a median gain of -26 db and a standard deviation of 8.5 db. Figure 8 illustrates the predicted Gaussian curve and the measured points; again the agreement is very good.

### C. Discussion of mutual gain

The experimental results demonstrate that the statistical distribution of mutual gain for two radar search antennas can be predicted from the gain distributions of the individual antennas according to Equations 3 and 4. With the additional knowledge of transmitted power, operating wavelength, and distance between the antennas, the distribution of received power can be calculated with Equation 2.

For example, suppose two destroyers are equipped with SPS-10 radar sets and are located 2000 yards apart. Suppose one of the radar sets is operating at 5500 Mc and is transmitting pulses with a peak power level of 285 kilowatts. The statistical distribution of mutual gain for the antennas is Gaussian with a median gain of -26 db and a standard deviation of 8.5 db. Therefore, the power level of the pulses received by the antenna of the other radar set will have a Gaussian distribution with a median of -54 dbm and a standard deviation of 8.5 db as illustrated in Figure 9. Note that 74 percent of the received pulses are within  $\pm 10$  db of the median value, -54 dbm. Figure 9 also illustrates cases where the separations are 500 and 10,000 yards.

For a second example, suppose the receiving antenna belongs to an SPS-6 radar set and other conditions remain the same. It was shown that the

statistical distribution for the median gain of an SPS-10 antenna and the reflector and feed of an SPS-6 antenna has a median gain of -18 db and a standard deviation of 9.2 db. In an operating situation, however, the rotary joint of the SPS-6 antenna will not be by-passed. A median insertion loss of  $1\frac{1}{4}$  db was the lowest value observed for the rotary joint at C-band frequencies;<sup>5</sup> thus, it is reasonable to assume a median of -32 db for the mutual gain. The power level of the pulses received through the SPS-6 antenna will have a Gaussian distribution as illustrated in Figure 10.

#### IV. IMPROVED RADIATION CHARACTERISTICS FOR THE AN/SPS-10 ANTENNA

The SPS-10 antenna has a parabolic-cylinder reflector with a hoghorn feed, and it is usually installed aboard ships for the function of surface search. The horizontal pattern, illustrated in Figure 1, shows an aperture diffraction pattern out to about 60° on each side of the main lobe. The broad lobes at 90° on each side of the main lobe are caused by spill-over at the sides of the reflector, and most of the back radiation is due to spill-over under the reflector. Note that the spill-over regions are more significant in determining the median gain than the aperture diffraction region around the main lobe. Also, the high spill-over lobes at 90° sometimes cause the appearance of false targets on the radar display.

Techniques for reducing spill-over in the SPS-10 antenna were studied and evaluated.<sup>7</sup> The most practical antenna modifications consist of an extension under the existing reflector and a pair of "blinders" for the hoghorn feed. The reflector extension reduces spill-over under the reflector, and the blinders reduce spill-over at the sides of the reflector. The reflector extension adds about 10 per cent in area to the original reflector, but it does not change the silhouette of the antenna.

Note by comparing the patterns in Figures 1 and 11, that radiation in all spill-over regions was greatly reduced. Measurements showed that the modifications reduced the median gain from -13 db to -23 db without degrading the gain and shape of the main lobe (see Figure 12).

A brief evaluation of two modified SPS-10 antennas was conducted aboard the USS Eaton (DD 510) and the USS Bache (DD 470) operating out of Norfolk, Virginia. Both minor-lobe interference and main-lobe interference were of interest during these tests. Minor-lobe interference is characterized by a "spiral" appearance on a PPI display. While main-lobe interference is characterized by a "swirl" on the display when either of the two interfering antennas is directed toward the other.

During tests with the original antennas, the two ships started with a separation of about 1000 yards and opened to a separation of 15,000 yards. Continual (100 per cent) minor-lobe interference was observed until the separation was almost 4000 yards. The interference then decreased rapidly until the separation was about 6000 to 7000 yards; after that, only main-lobe interference was observed. The main-lobe interference was still observed with a separation of 15,000 yards.

During tests with the modified antennas, no minor-lobe interference was observed with the ships separated 1000 yards; however, main-lobe interference was present, as expected. The ships closed to a separation of 500 yards, and partial (about 50 per cent) minor-lobe interference was observed.



To summarize, these data indicate that the minor-lobe interference was reduced by about 20 db or a factor of 10 in range. For example, about 50 per cent minor-lobe interference was observed at a range of 5000 yards with the original antennas but was not observed with the modified antennas until the range was closed to 500 yards. This improvement was predicted by the statistical analysis of the gain characteristics of the original and the modified SPS-10 antennas.

#### V. CONCLUSIONS

The statistical distribution of the radiation characteristics of a search radar can be a useful tool for approaching the radio-interference problem. Statistical gain studies of some radar search antennas (only the SPS-10 and SPS-6 antennas are reported here) have shown that the gain characteristics can be described by Gaussian curves. A single Gaussian curve is a valid description of the gain characteristics of an antenna, for horizontal cuts, for all in-band frequencies and all ranges (including the Fresnel zone).

Mutual gain measurements with pairs of radar search antennas have shown that the statistical distribution for mutual gain is also Gaussian with a median gain equal to the sum of the median gains of the individual antennas and a standard deviation equal to the square root of the sum of the squares of the individual standard deviations. With the additional knowledge of transmitted power, operating wavelength, and distance between antennas, a power probability distribution of received radar energy may be determined for two interfering radars.

It was found that modifications of the SPS-10 antenna can result in significant improvements of the radiation characteristics. A modified SPS-10 antenna has three advantages over the original version. They are (1) a 20 db increase in isolation between two SPS-10 radars, (2) a removal of the side spill-over lobes which sometimes cause the appearance of false targets on the radar display, and (3) a 10 db increase in isolation from other equipments including jammers. In the case of minor-lobe jamming, the interfering transmitter power would have to be increased by a factor of 10 in order to cause the same interference.

Field change kits for the SPS-10 were fabricated and installed aboard two destroyers. A brief evaluation at sea indicated that about a 20 db increase in isolation between the two SPS-10 radars was achieved, as predicted.

#### ACKNOWLEDGMENTS

The work reported in this paper was accomplished through the efforts of several persons. Specific reference should be made to Dr. M. W. Long and Mr. R. G. Shackelford.

#### REFERENCES

1. R. D. Wetherington, H. R. Brewer, and J. H. MacKay, Analysis of Some Near Zone Microwave Antenna Patterns Recorded by the Naval Ordnance Test Station, Interim Technical Report No. 2, Contract No. NOrd-16189, Georgia Institute of Technology, 1 February 1958.
2. H. M. Sachs and J. J. Krstansky, "Radar Transmitter and Receiver Spectral Signatures," Second National Symposium on Radio Frequency Interference, Washington, D. C., June 1960.
3. M. W. Long, "Wide Angle Radiation Measurements," Proceedings of the 6th Conference on Radio Interference Reduction and Electronic Compatibility, IIT Research Institute (formerly the Armour Research Foundation), Chicago, Illinois, October 1960.
4. R. C. Johnson, "Susceptibility of Radar Search Antennas to RFI," Fourth National Symposium on Radio Frequency Interference, San Francisco, California, June 1962.
5. R. C. Johnson, Statistical Characteristics of Gain and Mutual Gain of Radar Antennas, Final Report, Volume I, Contract No. NObsr-85387, Georgia Institute of Technology, 15 September 1963.
6. R. C. Johnson and R. G. Shackelford, Statistical Gain Characteristics of the AN/SPS-29 Antenna, Final Report, Volume II, Contract No. NObsr-85387, Georgia Institute of Technology, 15 September 1963.
7. R. C. Johnson, Modifications to Improve the Radiation Characteristics of the AN/SPS-10 Antenna, Final Report, Volume III, Contract No. NObsr-85387, Georgia Institute of Technology, 15 September 1963.

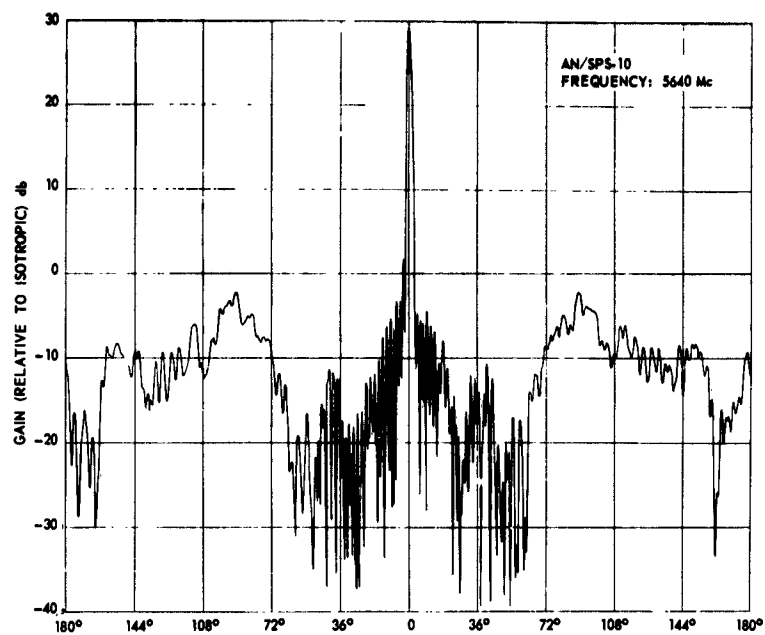


Fig. 1. Horizontal pattern of the AN/SPS-10 antenna

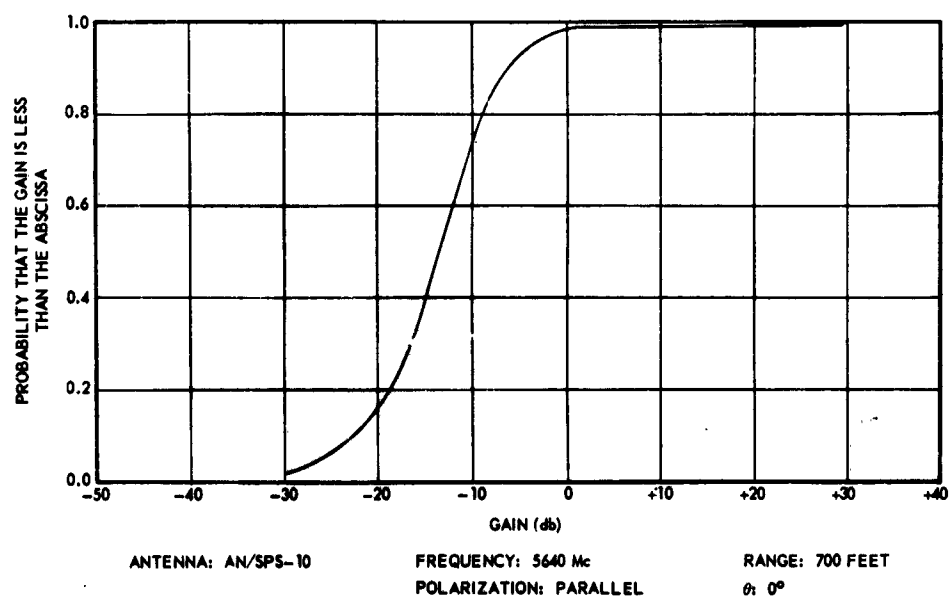


Fig. 2. Cumulative gain distribution for the AN/SPS-10 antenna

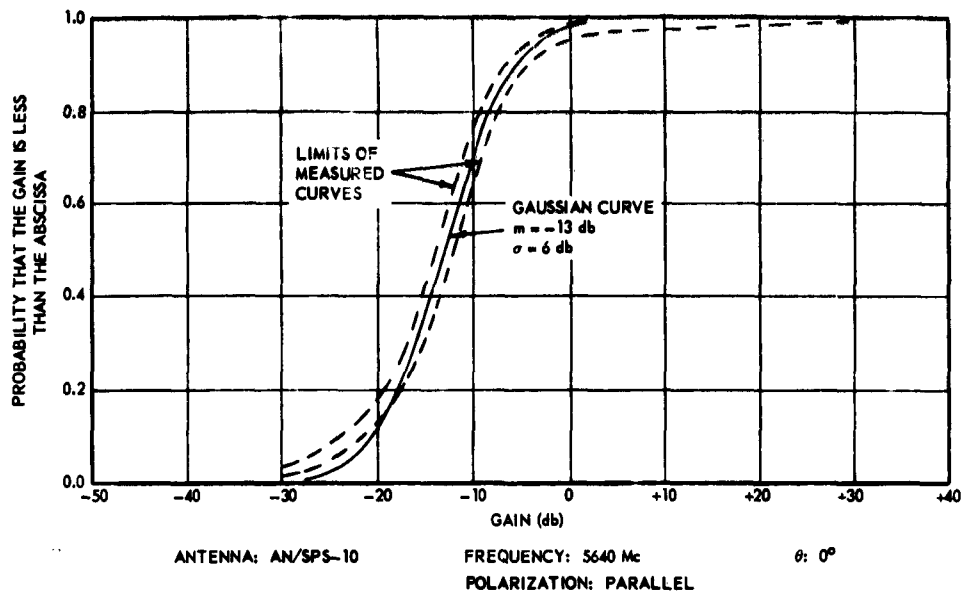


Fig. 3. Comparison of a Gaussian curve with the limits of the measured cumulative gain distributions for the AN/SPS-10 antenna

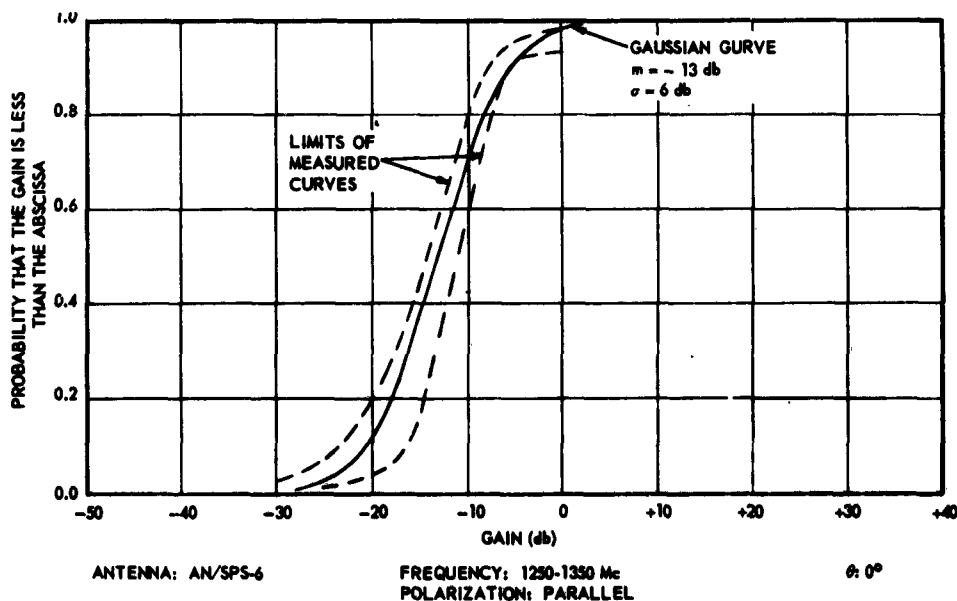


Fig. 4. Comparison of a Gaussian curve with the limits of the measured cumulative gain distributions for the AN/SPS-6 antenna



Fig. 5. Mutual gain experiment involving an AN/SPS-10 antenna (foreground) and an AN/SPS-6 antenna (background)

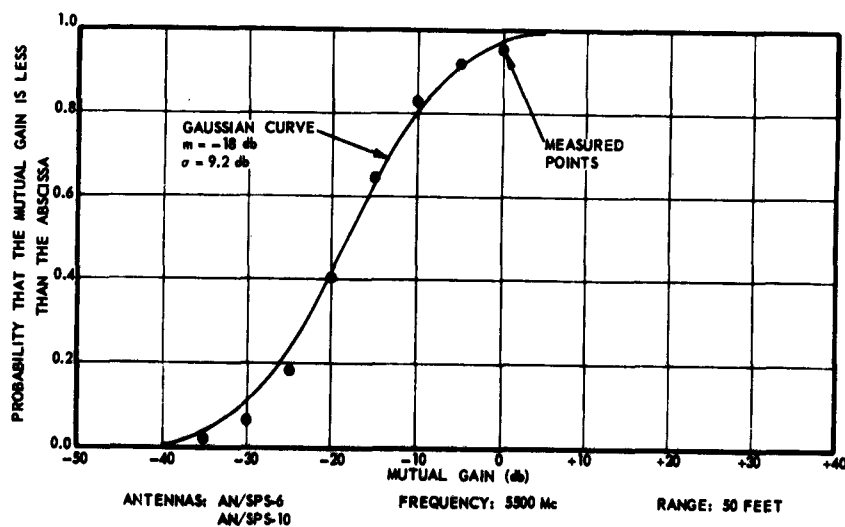


Fig. 6. Cumulative distribution of the mutual gain of the AN/SPS-6 (reflector and feed) and AN/SPS-10 antennas

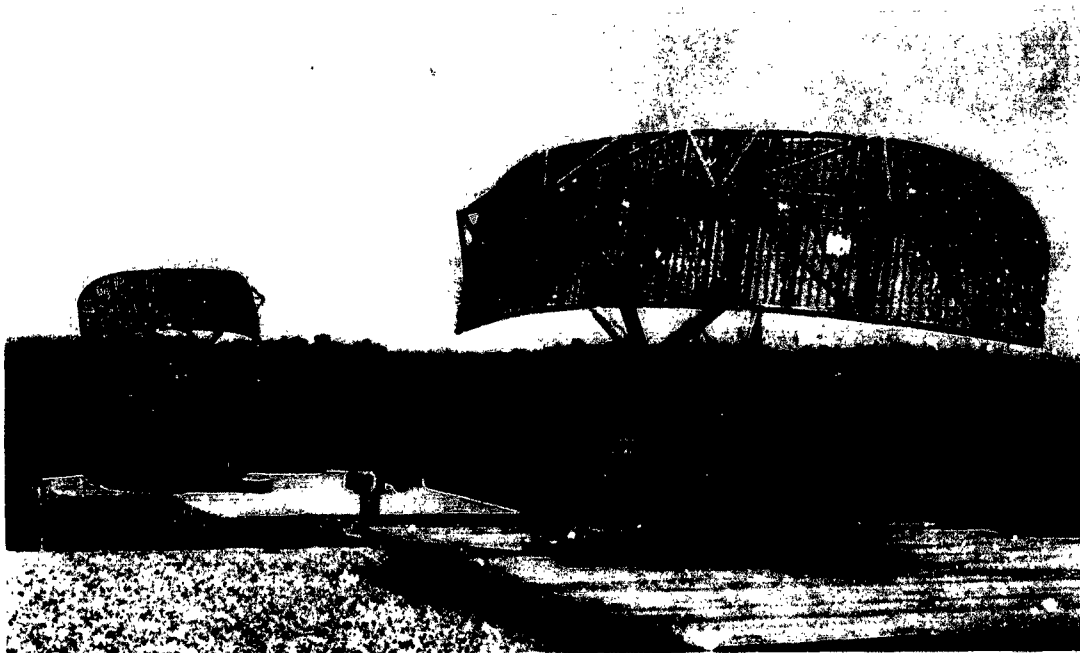


Fig. 7. Mutual gain experiment involving two AN/SPS-10 antennas

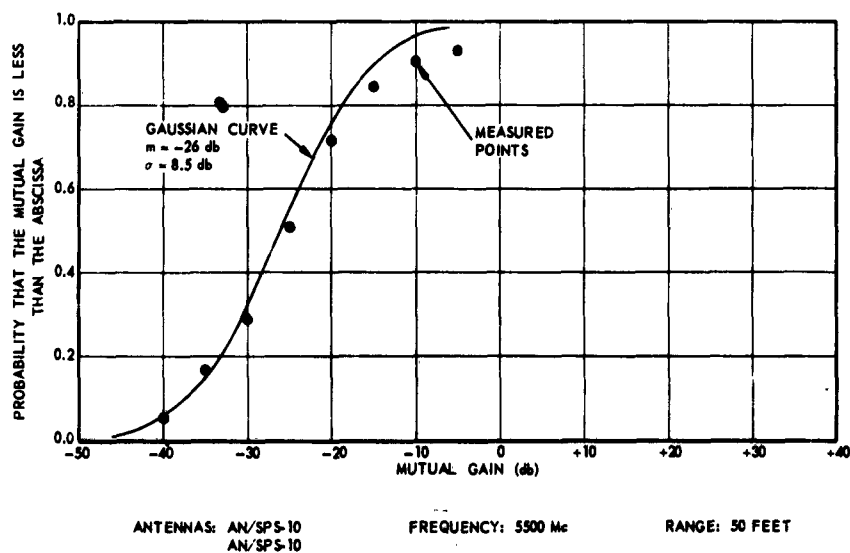


Fig. 8. Cumulative distribution of the mutual gain of two AN/SPS-10 antennas

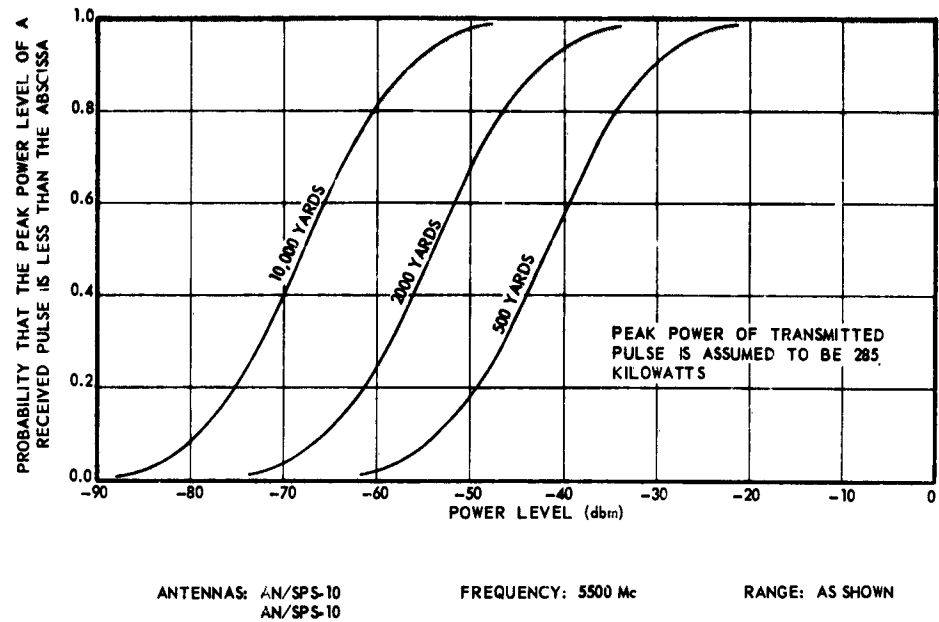


Fig. 9. Cumulative distributions of the power level of the pulses received through the antenna of one AN/SPS-10 radar set due to transmissions from another distant AN/SPS-10 radar set

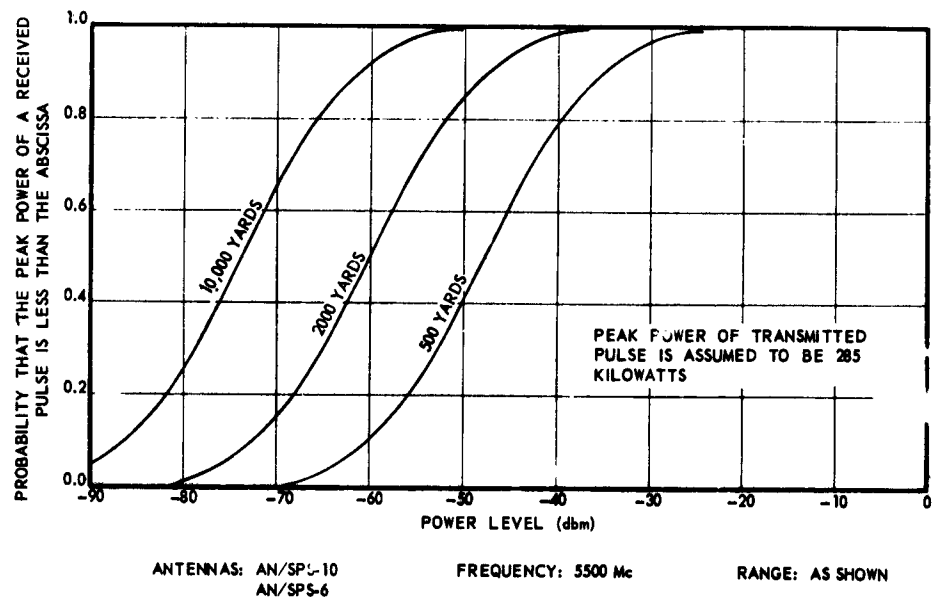


Fig. 10. Cumulative distributions of the power level of the pulses received through the antenna of an AN/SPS-6 radar set due to transmissions from a distant AN/SPS-10 radar set

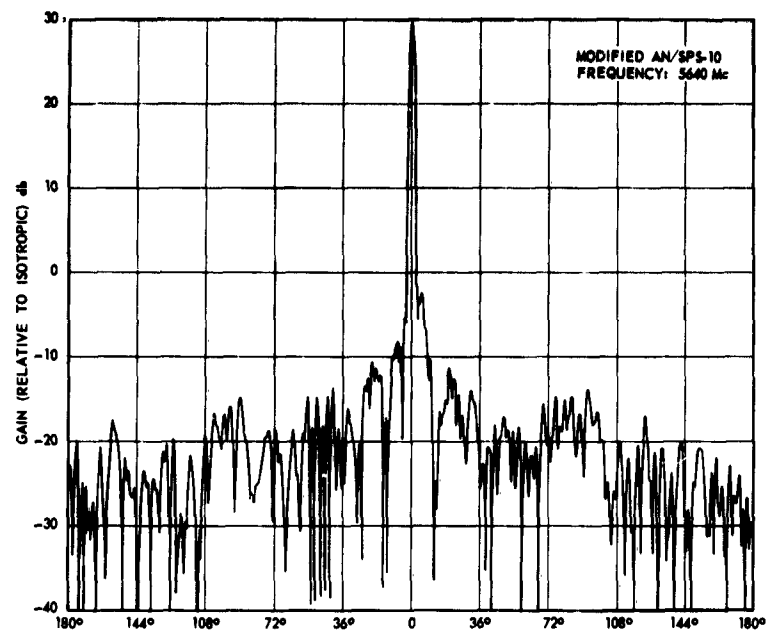


Fig. 11. Horizontal pattern of the modified AN/SPS-10 antenna

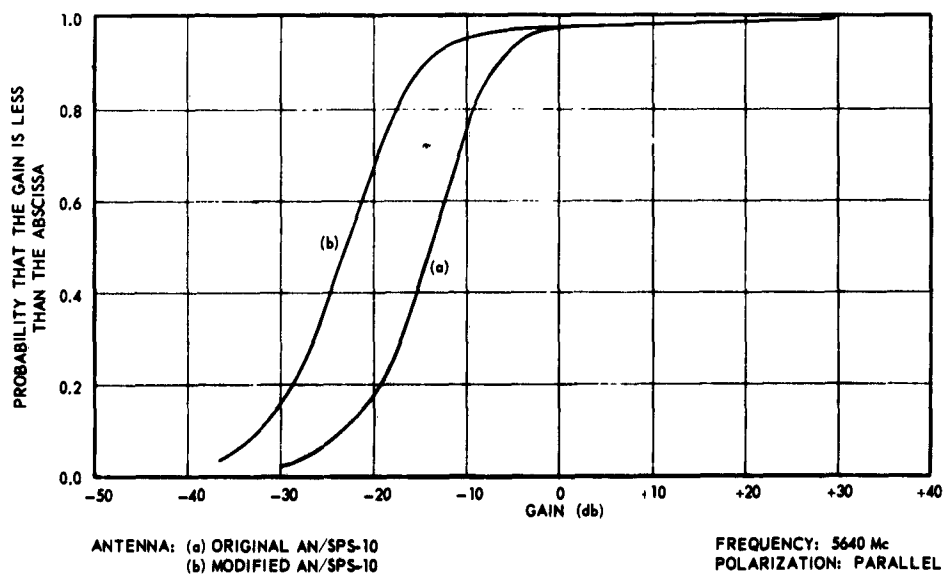


Fig. 12. Cumulative gain distributions for the original and modified AN/SPS-10 AN/SPS-10 antennas



## PROBABILITY OF INTERFERENCE FROM RANDOMLY DISPERSED SOURCES

P. F. Christopher  
IIT Research Institute  
Electromagnetic Compatibility Analysis Center  
Annapolis, Maryland

**Abstract.** - An approximate (but general) two dimensional probability density function is illustrated for randomly located interference sources. The cumulative distribution is derived for interference strength greater than that required for receiver failure. Original portions of the analysis include:

1. A general propagation loss power law.
2. A general standard deviation of interference strength due to fixed sources.

The results represent probability of receiver failure for a fixed desired signal source and interferers dispersed with uniform probability density. They are useful when the variance of interference power is much greater than the variance of desired signal. The maximum density of interference sources per square mile is then found as a function of allowable probability of failure.

### I. INTRODUCTION

When mobile communication or radar equipments are to be dispersed randomly throughout an area, the probability of interference at a given receiver is difficult to anticipate.

For interference problems concerning VHF and UHF equipments we are often given:

1. A description of the terrain.
2. The spectrum signature for each transmitter, and the transfer function for a victim receiver.
3. The antenna gain statistics of interference sources and victim receivers.
4. The interference power level  $S_f$ , which abruptly causes receiver failure, expressed in dbm.

From these four, we would like to derive the relationship between the probability of receiver failure,  $P_f$ , and the density of randomly dispersed interference sources,  $d$ .

For some time it has been possible to predict interference from fixed sources. In particular, the works of Bullington<sup>1</sup> and Egli<sup>2</sup> are important.

Some other work has been performed, but all previous work has lacked either the random variable of distance to source or lacked general terrain features.

We develop a two-dimensional probability density function for the randomly dispersed sources and derive a cumulative distribution for the interference strength greater than that required for receiver failure. From the cumulative distribution of  $S_r$  we express the maximum density of interference sources per square mile as a function of allowable probability of receiver failure.

## II. BASIC THEORY

Signal strength from fixed sources has been analyzed by Bullington<sup>1</sup> and Egli<sup>2</sup>. Their results indicate that the uncertainty in received signal strength at a fixed distance can be represented by a log-normal distribution. Further, the variance of this log-normal distribution can be considered as independent of distance to the source, if terrain is the major cause of variance.

Therefore, if a certain level of interference causes receiver failure, the probability of receiver failure is found from the cumulative Gaussian distribution.

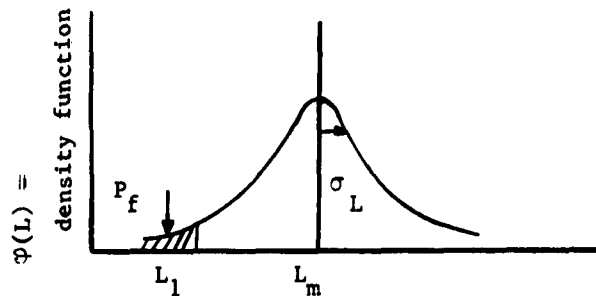


Figure 1. Propagation Loss Density Function

If  $L_1$  represents a low propagation loss which can cause receiver failure, the area below  $L_1$  represents a-priori probability of receiver failure,  $P_r$ , due to a fixed interference source.

Notice that interference power:

$$S_{\text{undesired}} = S_u = P_t + G_t + G_r - L \quad (1)$$

where,

$P_t$  = transmitter power available at receiver tuned frequency.

$G_t$  = transmitter antenna gain for appropriate direction.

$G_r$  = receiver antenna gain.

Figure 1 assumes  $P_t$ ,  $G_t$ , and  $G_r$  are fixed. One might also consider the quasi-normal variation  $G_t$  and  $G_r$  to achieve a log-normal interference density function (See Figure 2)

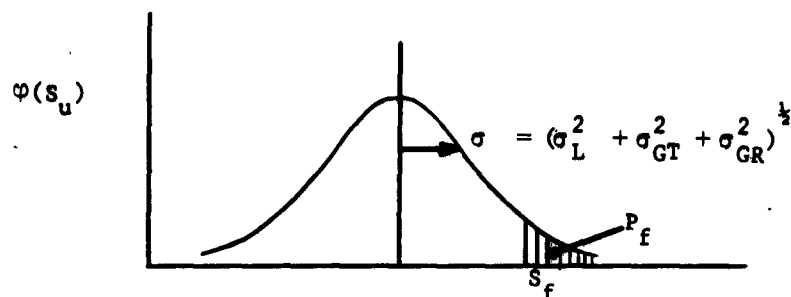


Figure 2.  $S_u$  Undesired Signal Power from a Source at Fixed Distance,

for fixed transmitter power  $P_t$ . In either case, one evaluates the cumulative normal statistics to find the probability of receiver failure  $P_f$ . Unfortunately this method is valid only for specific interference source locations.

Next we seek a probability density function for distance to randomly located interference sources. For simplicity, we consider a case which corresponds to an operational situation where interference sources can be scattered uniformly over the entire area. When the interference sources are spread uniformly over the area, the distance density function is simply as shown in Figure 3. (See Appendix I)

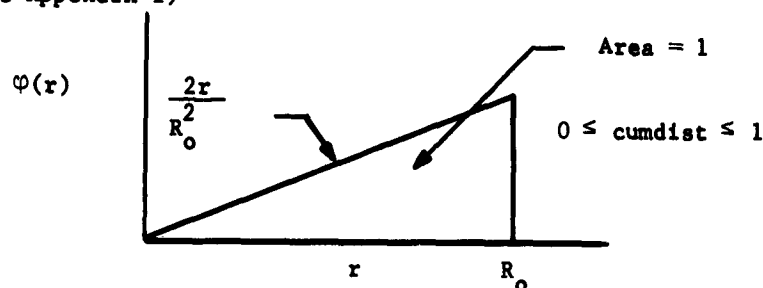


Figure 3. Distance Probability Density Function.

$R_0$  is arbitrarily large.

It will be convenient later to work with  $\varphi(\log_e r)$  because there are simple relations between propagation loss (in db) and  $\log r$ . Figure 4 shows the density function of the transformed variable.

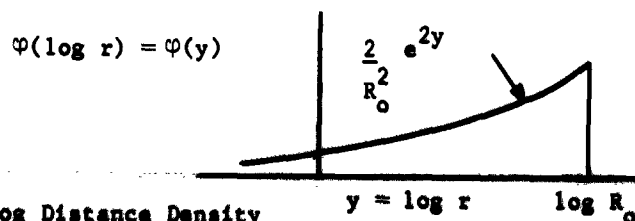


Figure 4. Log Distance Density Function

A general distance probability density function is treated in APPENDIX IV.

Also, we know that mean propagation loss often has the following form, if a given propagation mode is involved:

$$L_m = L_1 + b \log_e r \quad (2)$$

where,  $b = 10n (1/\log_e 10)$

and  $n = \text{power law}$

## II. MATHEMATICAL CONSIDERATIONS

At this point in the discussion, we realize that a given interference level can occur as a function of terrain, distance, or antenna angle.\* A convenient means for evaluating the possibility of high level interference is to construct the two dimensional probability density function. The two dimensional density function is pictured in Figure 5 and the density function is mathematically described as:

$$\varphi(S,y) = \frac{2}{R_o^2} e^{2y} \left[ \left( \frac{1}{\sqrt{2\pi}\sigma} \right) e^{-\frac{[S - (S_1 + by)]^2}{2\sigma^2}} \right] \quad (3)$$

NOTE: In Equation (3) the units of S are negative dbm. This is done in order that S might have the same sign as propagation loss. Also, antenna gain statistics and terrain effects are lumped into one Gaussian variable with,

$$\sigma = (\sigma_{\text{terrain}}^2 + \sigma_{\text{antenna}}^2)^{\frac{1}{2}}$$

S = random variable signal strength, either desired or undesired. However, within all subsequent expressions we consider S to signify only the random undesired signals.

$S_1$  = interference strength from a mean 1-mile source, i.e. interference strength which passes through the receiver.

Let  $S_f$  = interference level which causes receiver failure. The probability that an interference source delivers power equal to or greater than an interference level  $S_f$  is found by taking a cut through the two dimensional density function  $f$  at  $S_f$ .  $VOL_1 + VOL_2$  in Figure 5 represents the

\*Random tuned frequency can also be considered, although tediously.

probability of receiver failure due to a randomly located interference source. Fortunately, this volume can be closely approximated.

A convenient means for approximation<sup>4</sup> is to introduce a cosine approximation to the Gaussian density function. As long as we avoid the Gaussian tails beyond  $2.76 \sigma$ , we have expression (4).

$$\text{normal } [u, \sigma] \doteq \frac{1.14}{2 \pi \sigma} \left[ 1 + \cos \frac{1.14}{\sigma} \left\{ s - u \right\} \right] \quad (4)$$

The approximation given in expression (4) allows us to derive a useful result. Equation (3) becomes:

$$\varphi(S, y) = \frac{2}{R_o^2} e^{2y} \left[ \frac{1.14}{2 \pi \sigma} \left\{ 1 + \cos \frac{1.14}{\sigma} \left( s - \left\{ s_1 + by \right\} \right) \right\} \right] \quad (5)$$

The problem will be broken into two parts to derive the cumulative distribution. The cumulative distribution:

$$P(S > S_f) = \text{VOL}_1 + \text{VOL}_2 \quad (6)$$

$$\text{VOL}_1 = \int_{-\infty}^{y_1} \int_{\text{lim}_1}^{\text{lim}_2} \frac{2}{R_o^2} e^{2y} \left[ \frac{1.14}{2 \pi \sigma} \left\{ 1 + \cos \frac{1.14}{\sigma} (s - \{s_1 + by\}) \right\} \right] ds dy \quad (7)$$

where,

$$\text{lim}_1 = \frac{\sigma}{1.14} \left[ -\pi + \frac{1.14}{\sigma} (s_1 + by) \right]$$

and

$$\text{lim}_2 = \frac{\sigma}{1.14} \left[ +\pi + \frac{1.14}{\sigma} (s_1 + by) \right]$$

With or without the cosine approximation the following simplification occurs:

$$\text{VOL}_1 = \int_{-\infty}^{y_1} \frac{2}{R_o^2} e^{2y} dy = \frac{e^{2y_1}}{R_o^2} \quad (8)$$

$$\text{VOL}_2 = \int_{y_1}^{y_1 + \frac{2 \pi \sigma}{1.14b}} \int_{\text{lim}_1}^{S_f} \varphi(S, y) ds dy \quad (9)$$

And if we let

$$C_1 = \frac{1.14}{2 \pi \sigma}$$

and

$$C_2 = \frac{1.14}{\sigma}$$

then,

$$\text{VOL}_2 = \frac{2}{R_o^2} \int_{y_1}^{y_1 + \frac{2\pi}{C_2 b}} e^{2y} \left[ C_1 \left[ S_f + \frac{1}{C_2} \sin C_2 \left\{ S_f - (S_1 + by) \right\} - \frac{1}{C_2} \left( -\pi + C_2 S_1 + C_2 by \right) \right] \right] dy \quad (10)$$

Except for the cosine approximation, this could not have been written in closed form. But

$$y_1 = \frac{S_f - S_1 - \pi/C_2}{b}$$

and

$$y_1 + \frac{2\pi}{C_2 b} = \frac{S_f - S_1 + \pi/C_2}{b}$$

The result is found to be\*

$$\begin{aligned} \text{VOL}_2 = C_1 \frac{2}{R_o^2} & \left[ \frac{S_f + \pi/C_2 - S_1}{2} \left( e^{\frac{2(S_f - S_1 + \pi/C_2)}{b}} - e^{\frac{2(S_f - S_1 - \pi/C_2)}{b}} \right) \right. \\ & - \frac{b}{4} \left( 2e^{\frac{2(S_f - S_1 + \pi/C_2)}{b}} \left\{ \frac{S_f - S_1 + \pi/C_2}{b} - 1 \right\} \right. \\ & - 2e^{\frac{2(S_f - S_1 - \pi/C_2)}{b}} \left\{ \frac{S_f - S_1 - \pi/C_2}{b} - 1 \right\} \left. \right) \\ & - \frac{e^{2/b(S_f - S_1)}}{C_2^2 b^2 \left( \left( \frac{2}{C_2 b} \right)^2 + 1 \right)} \left( e^{2\pi/C_2 b} - e^{-2\pi/C_2 b} \right) \left. \right] \quad (11) \end{aligned}$$

Collecting terms,

\*See Appendix II.

$VOL_1 + VOL_2$  = the probability that one interference source which lies within  $R_0$  will give a signal strength greater than  $S_f$ . This probability:

$$P(S > S_f) = C_1 \frac{e}{R_0^2} \frac{2(S_f - S_1)}{b} \left[ \left\{ \frac{b}{2} - \frac{2}{C_2^2 b [(2/C_2 b)^2 + 1]} \right\} e^{\frac{2\pi}{C_2 b}} + \left\{ -\frac{b}{2} + \frac{2}{C_2^2 b [(2/C_2 b)^2 + 1]} \right\} e^{-\frac{2\pi}{C_2 b}} \right] \quad (12a)$$

$$= \frac{2C_1}{R_0^2} \left\{ \frac{b}{2} - \frac{2}{C_2^2 b [(2/C_2 b)^2 + 1]} \right\} \sinh \left( \frac{2\pi}{C_2 b} \right) e^{\frac{2(S_f - S_1)}{b}} \quad (12b)$$

Equation (12) is the basic result of this paper. Notice, however, that  $R_0$  must be chosen large enough that it does not intersect the cut at  $S_f$ . The integration assumed no intersection. Further, it can be shown that for probability of receiver failure from many sources  $P_f$  less than (.1).\*\*

$$P_f \doteq P(S > S_f) \pi R_0^2 d$$

or

$$P_f \doteq [VOL_1 + VOL_2] \pi R_0^2 d \quad (13a)$$

where,

$d$  = density of interference sources per square mile. (When  $d$  is variable, use APPENDIX IV.)

Equation (12) can be solved for  $(VOL_1 + VOL_2)$  and  $d$  can be found as a function of  $P_f$ . We may wish to solve for  $d$  because one usually anticipates an allowable probability of failure.

$$d \doteq \frac{P_f}{(VOL_1 + VOL_2) \pi R_0^2} \quad (13b)$$

For specific propagation loss power laws and each discrete value of  $(P_f < .1)$ , we can plot  $d$  vs  $(S_f - S_1)$ . Examples of such plots are shown in Figures 6 through 11, included at the end of this paper.  $S_f$  can be determined from  $\frac{S_{\text{desired}}}{S_{\text{undesired}}}$  and we recognize that receiver failure is often considered to

occur at some low  $\frac{S_{\text{desired}}}{S_{\text{undesired}}}$  level. In the previous analysis it was assumed that the desired signal level was constant. This analysis is useful in many cases where the standard deviation of the undesired signals is more than twice the standard deviation of the desired signals.

Consider the one-dimensional example of desired and undesired sources at an equal distance. The desired source will lie on an engineered path and the undesired source will be on a random path. Assume the standard deviations associated with the desired and undesired propagation losses to be 7 db and 17 db respectively. Further, the undesired source's antenna might have random orientation to raise the standard deviation of the undesired signal even greater than 17 db. Here, the convolution of the two Gaussian processes results in a new Gaussian process, of standard deviation  $(17^2 + 7^2)^{1/2} = 18.4$  db. But the standard deviations which furnished the basis of the calculation were so approximate that it is not worth our while to work with an 18.4-db process instead of a 17-db process. This illustrates the general point: When the standard deviation of the undesired signals is more than twice the standard deviation of the desired signals, we may treat the desired signal as a constant. The undesired signal statistics can then dominate our interest.

However, the desired signal level may very well have an unique distribution of its own. In that case, we should generate the density function (in db) formed of:

$$S_d - S_u$$

We will not treat such a case here, although it may sometimes be considered.

#### IV. EXAMPLES

The derivation and the curves in Figures 6 through 11 become more valuable when one realizes the types of problems to which the curves can be applied. These two simple examples are chosen for interest rather than for realistic numbers and, for the sake of simplicity, they have been restricted to co-channel interference situations.

##### EXAMPLE I

In an FM communication system, suppose receiver failure occurs when

$$\frac{S_{\text{desired}}}{S_{\text{undesired}}} = 1$$

Further, assume omnidirectional antennas on the sources and receiver. Let the propagation loss from the interference sources have a standard deviation of 8 db due to terrain and have mean loss displaced 6 db above free space loss. (These figures must be supplied for each different problem.) Let propagation loss from the desired source have a much smaller standard deviation about



a mean free space value. Also, let transmitted power from the sources be identical.

Then, for a desired signal source at 5 miles distance, we may calculate  $S_f - S_1$  to find the maximum allowable density of interference sources per square mile.

$S_f$  = interference signal strength at which failure occurs  
 = desired signal strength  
 = undesired signal from a mean 2.5 mile interference source.

$S_1$  = undesired signal from a mean 1 mile source.

$$S_f - S_1 = 10 \log_{10} \left( \frac{2.5}{1} \right) \doteq 8 \text{ db}$$

The 8 db has the same sign as propagation loss because the units of S were chosen in negative dbm.

If we are interested in probability of receiver failure

$$P_f = 10^{-3}$$

we enter Figure 7A at  $S_f - S_1 = +8$  db and interpolate between the top two curves to get

$$d \doteq 1 \times 10^{-5} \text{ interference sources/mi}^2$$

Figure 10 allows a higher density, having been drawn for fourth power propagation loss. A low density can often be raised in proportion to the number of channels. It can also be raised by time sharing or by introducing directional antennas. The next example will show a sharp improvement by use of highly directional antennas.

## EXAMPLE 2

The value of the analysis becomes more apparent when directional antennas are introduced. For calculation purposes, let the main beam gain of the desired source be 30 db; let an interferer's antenna gain be normally\* distributed with the mean approximately -13 db and the standard deviation 6 db. Interference signals of Example (1) would now be attenuated by 43 db relative to desired signals on the average. Also, the interference signals of Example (1) now have the new standard deviation:

$$\sigma = (\sigma_{\text{terrain}}^2 + \sigma_{\text{antenna}}^2)^{\frac{1}{2}} = (8^2 + 6^2)^{\frac{1}{2}} = 10$$

For square law propagation loss enter Figure 7B at

$$8 \text{ db} - 43 \text{ db} = -35 \text{ db}$$

and find

$$d = .11 \text{ interference sources/mi}^2.$$

In these examples, four orders of magnitude were gained by placing high gain antennas on the sources. Even more density could have been achieved by placing a directional antenna on the receiver.

#### V CONCLUSIONS

The approximate allowable average density of interference sources per square mile has been derived. The derivation is useful when both the allowable probability of receiver failure is less than (.1) and the receiver failure occurs abruptly at a known interference level.

#### ACKNOWLEDGMENT

The work described above is sponsored by the three Military Departments, and is being conducted under Contract No. AF 19 (604)-8440 with the Electronic Systems Division, Air Force Systems Command.

R. Campbell has performed a great number of density calculations from which Figures 6 through 11 were constructed.

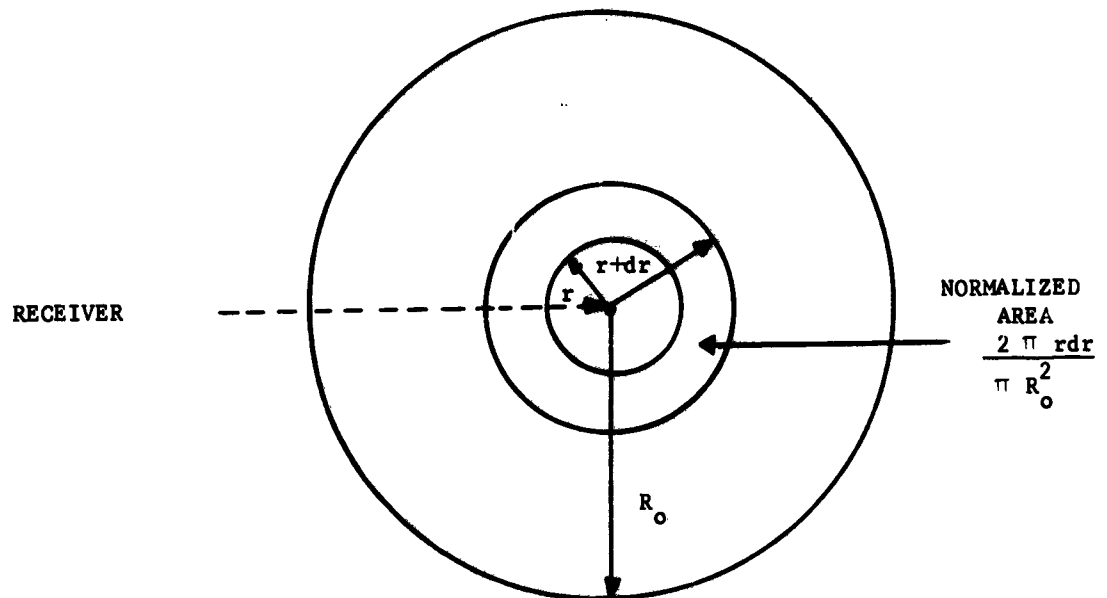
#### REFERENCES

1. K. Bullington, "Characteristics of Beyond-the-Horizon Radio Transmission," Proc. IRE, Vol. 43, pp 1175 - 1180, Oct. 1955.
2. Egli, "Radio Propagation Above 40 MC Over Irregular Terrain, Proc. IRE, Oct. 1957.
3. R. C. Johnson, "Statistical Gain Characteristics of the AN/SPS-10 Antenna," No. bar 85387, G. I. T. EES, March 1962.
4. D. H. Raab, et al, "A Cosine Approximation to the Normal Distribution," Psychometrika, Vol. 26, Dec. 1961.

# APPENDIX I.

## DERIVATION OF DISTANCE PROBABILITY DENSITY FUNCTION

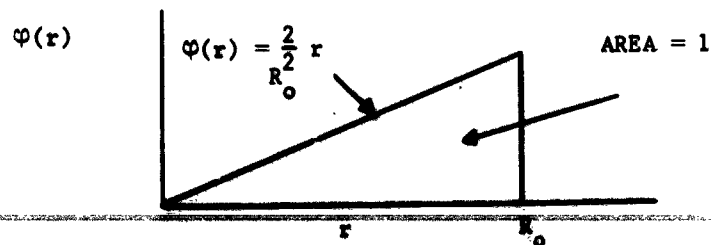
Suppose an interference source is placed at random inside a circle of radius  $R_0$  and there is equal probability of the source lying in any unit area.



The probability that the source lies between the distance ( $r$ ) and ( $r + dr$ ) is equal to the normalized annular area

$$\frac{2\pi r dr}{\pi R_0^2}$$

Therefore, the distance probability density function is simply a linear function of  $r$ .



**APPENDIX II**  
**AN INTEGRAL CONTAINED IN VOL<sub>2</sub>**

The form

$$\int_{y_1}^{y_1 + 2\pi/C_2 b} e^{2y} \sin(C_2 S_f - C_2 S_1 - C_2 b y) dy$$

is evaluated by changing variables:

$$Y = C_2 S_f - C_2 S_1 - C_2 b y$$

and

$$dY = -C_2 b dy$$

The new lower limit is:

$$Y_1 = C_2 S_f - C_2 S_1 - C_2 b \left( \frac{S_f - S_1 - \pi/C_2}{b} \right) = +\pi.$$

The new upper limit is:

$$Y_2 = -\pi$$

The integral is now of standard form and is found to be:

$$-(1/C_2 b) e^{\frac{2(S_f - S_1)}{b}} \left[ e^{2\pi/C_2 b} - e^{-2\pi/C_2 b} \right] \left[ \frac{1}{(2/C_2 b)^2 + 1} \right]$$

# APPENDIX III

## APPROXIMATION FOR $P_f$

When  $n$  sources are placed with uniform probability inside a circle of radius  $R_0$ , the expected number of sources which cause failure is:

$$\begin{aligned} [\text{VOL}_1 + \text{VOL}_2] \pi R_0^2 d &= E = p_1 + 2p_1^2 + 3p_1^3 + \dots + np_1^n \\ &= p_1 [1 + 2p_1 + 3p_1^2 + \dots + np_1^{n-1}] \\ &= p_1 \left[ \frac{1}{(1-p_1)^2} \right] \end{aligned} \quad (\text{III-1})$$

when,

$n$  is large

and

$p_1$  is the probability of failure due to a single source.

But

$$\begin{aligned} P_f &= p_1 + p_1^2 + p_1^3 + \dots + p_1^n \\ &= p_1 (1 + p_1 + p_1^2 + \dots + p_1^{n-1}) \\ &= p_1 (1/(1 - p_1)) \end{aligned} \quad (\text{III-2})$$

Solve (III-1) for  $p_1(E)$  and substitute in (III-2) to obtain:

$$P_f = \frac{2E + 1 - \sqrt{4E + 1}}{2E} \left[ 1 + \left( \frac{2E + 1 - \sqrt{4E + 1}}{2E} \right) + \dots \right] \quad (\text{III-3})$$

or

$$P_f \doteq E$$

if

$$P_f \leq .1$$

Less than 10% error results when  $P_f = .1$ .

#### APPENDIX IV

##### PROBABILITY OF INTERFERENCE FROM ARBITRARILY DISPERSED SOURCES

It is easily conceivable that the distance probability density function is far different than the linear function assumed in Equation (3). The distance density function could, for instance, be Rayleigh distributed. It is desired that some means be found for describing the probability of interference for a general distance probability density function.

We first assume that an arbitrary distance density function can be expanded in a Taylor series about the point  $r = 0$  such that

$$\varphi(r) = \sum_{n=0}^{\infty} \varphi^{(n)}(0) \frac{(r)^n}{n!} \quad (\text{IV-1})$$

and if

$$y = \log_e r,$$

$$\varphi(y) = \varphi(r) \left| \frac{dr}{dy} \right| = \sum_{n=0}^{\infty} \varphi^{(n)}(0) \frac{e^{ny}}{n!} |e^y|$$

or

$$\varphi(y) = \sum_{n=0}^{\infty} \varphi^{(n)}(0) \frac{e^{(n+1)y}}{n!} \quad (\text{IV-2})$$

An integration similar to that required to derive Equation (12b) yields:

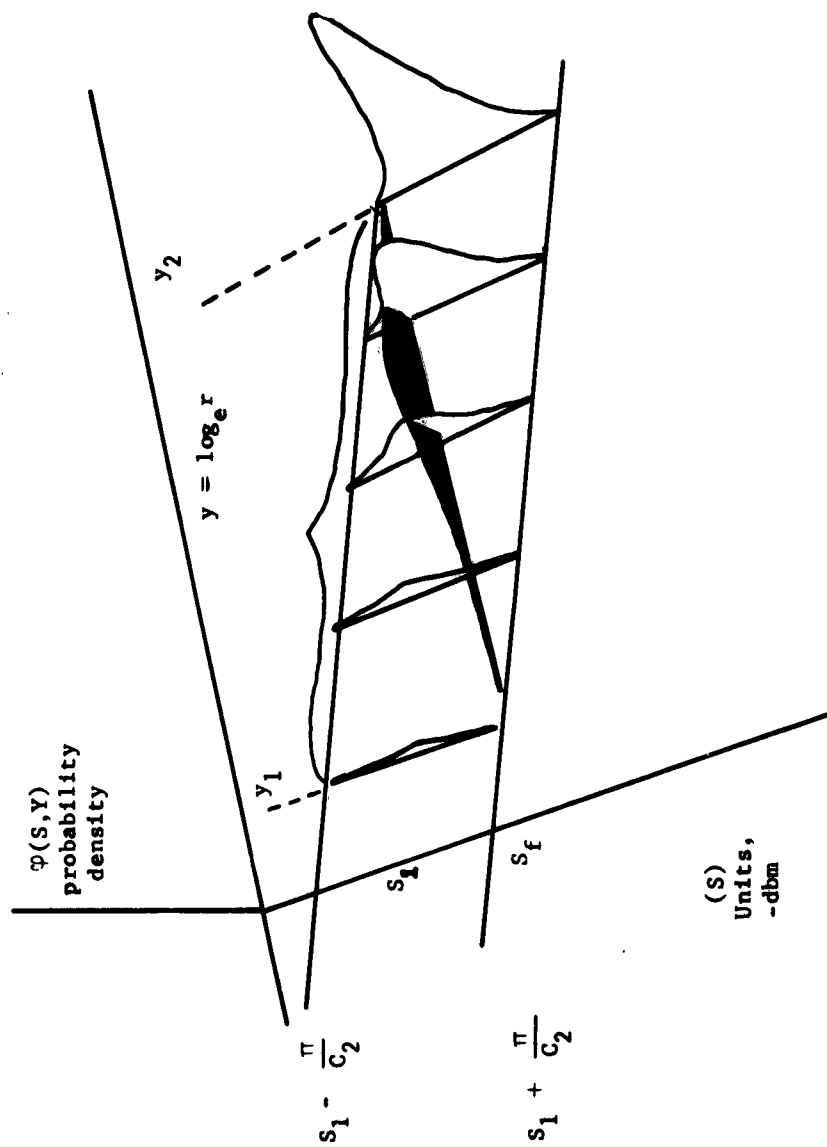
$$P(S > S_f) = 2 C_1 \sum_{n=0}^{\infty} \frac{\varphi^{(n)}(0)}{n!} e^{\frac{(n+1)\Delta}{b}} \left\{ \frac{\Delta}{2} + \frac{\pi}{2C_2} - \frac{\Delta}{(n+1)} - \frac{\pi}{(n+1)C_2} + \frac{b}{(n+1)^2} - \frac{1}{C_2^2 b [((n+1)/C_2)^2 + 1]} \right\} \sinh \left[ \frac{(n+1)\pi}{C_2 b} \right] \quad (\text{IV-3})$$

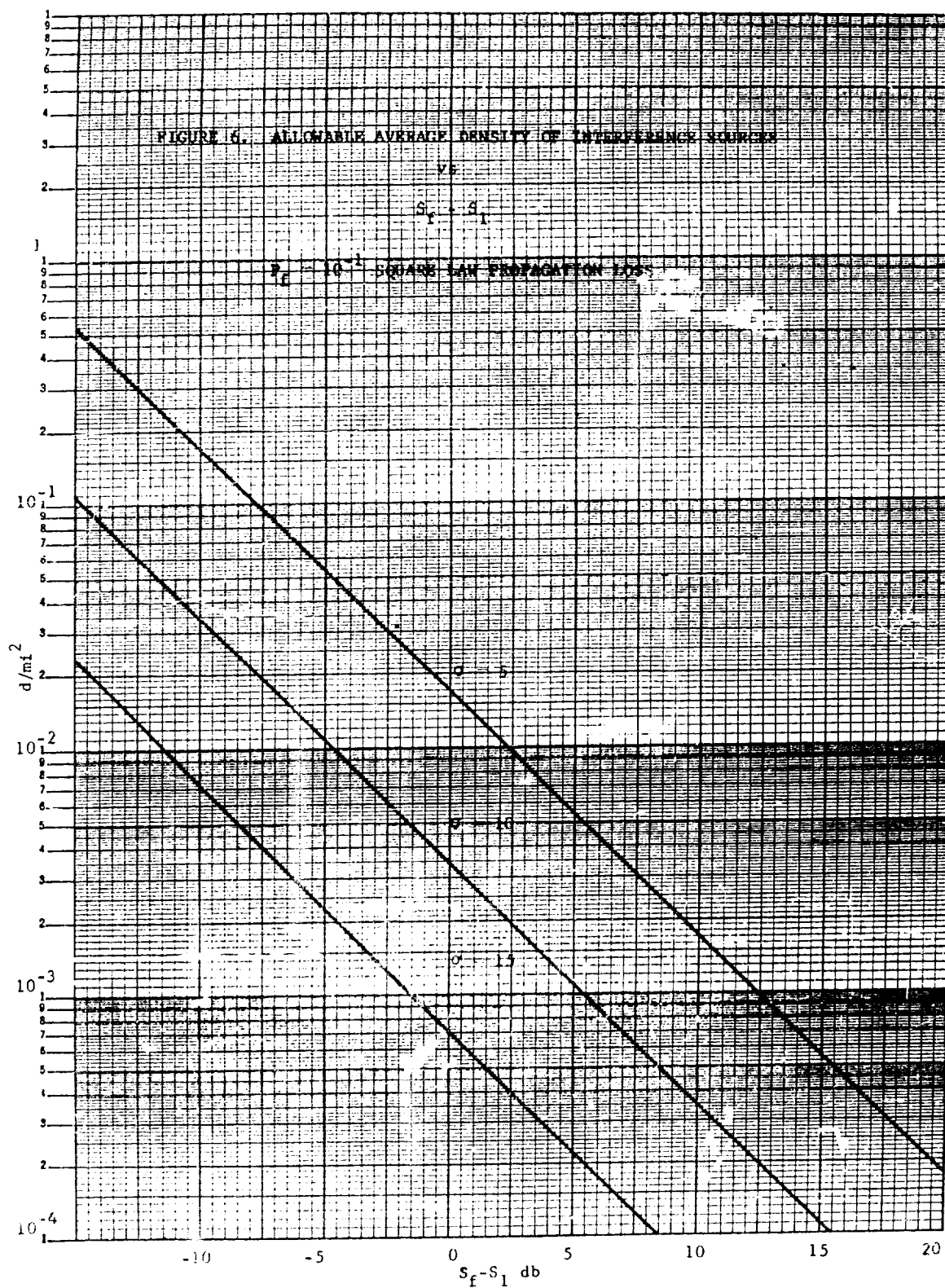
where,

$$\Delta = S_f - S_1$$

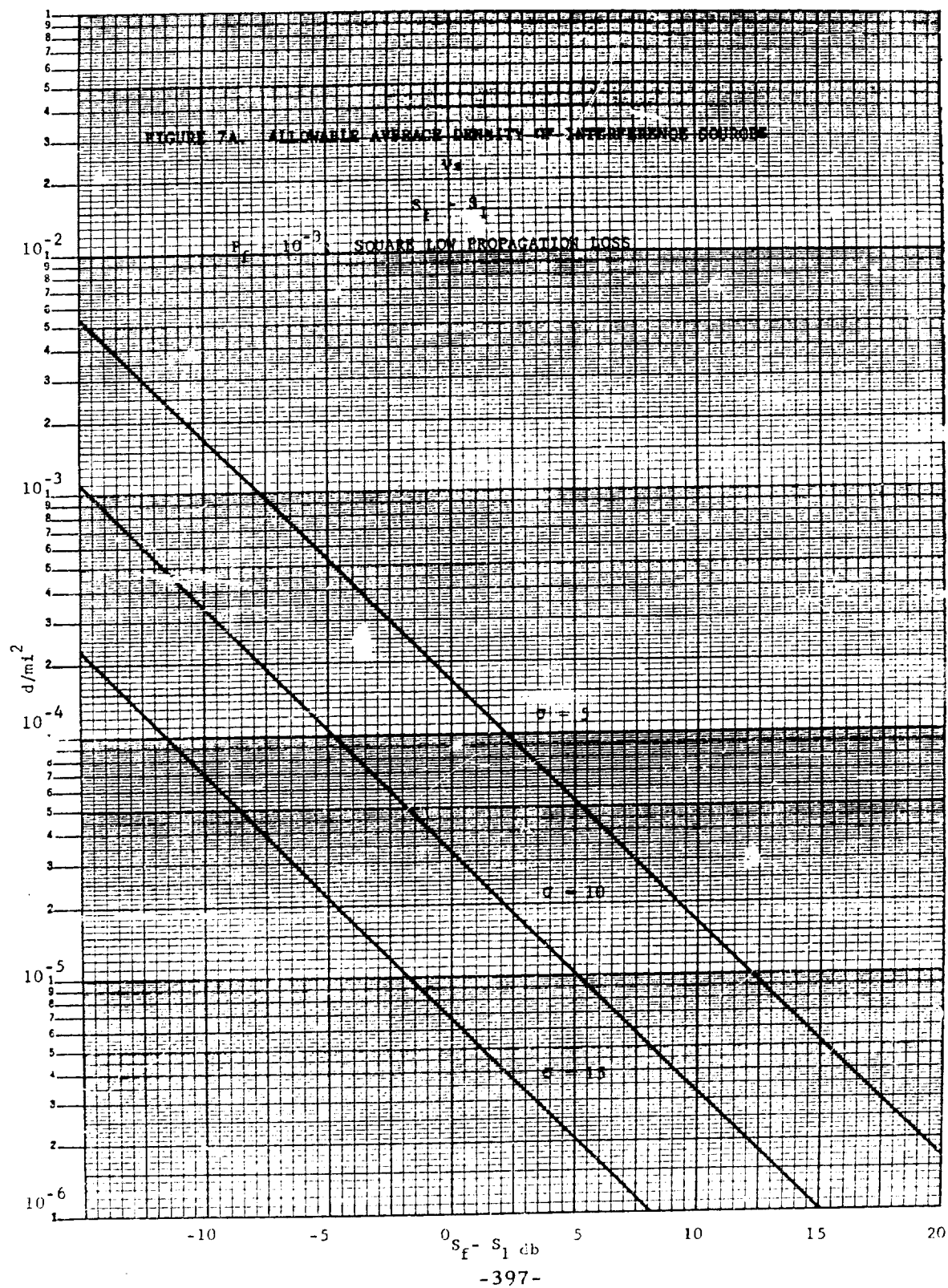
Equation IV-3 may be useful for hand calculations when the series can be terminated quickly.

FIGURE 5. JOINT PROBABILITY DENSITY FUNCTION FOR S AND Y.

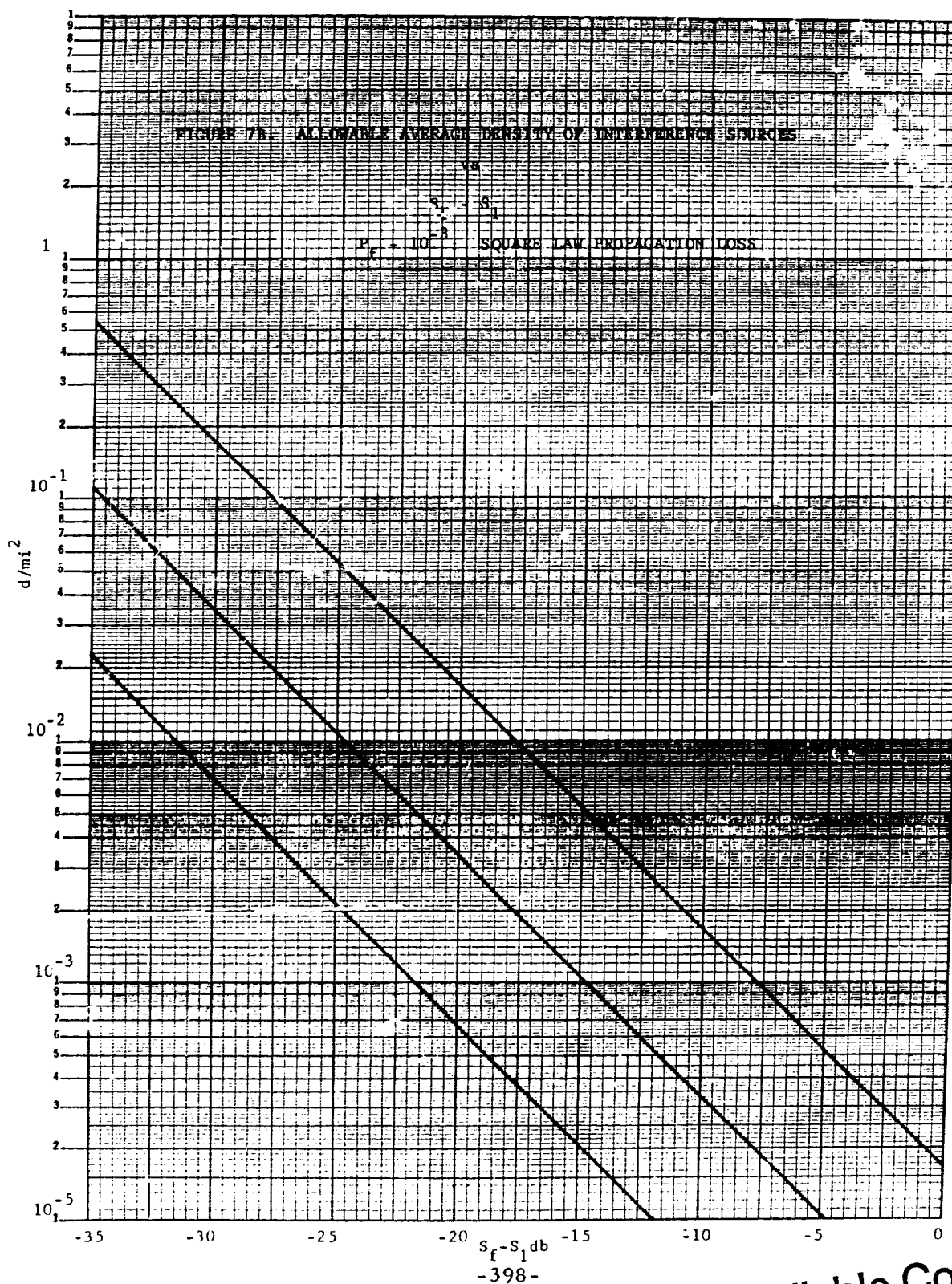




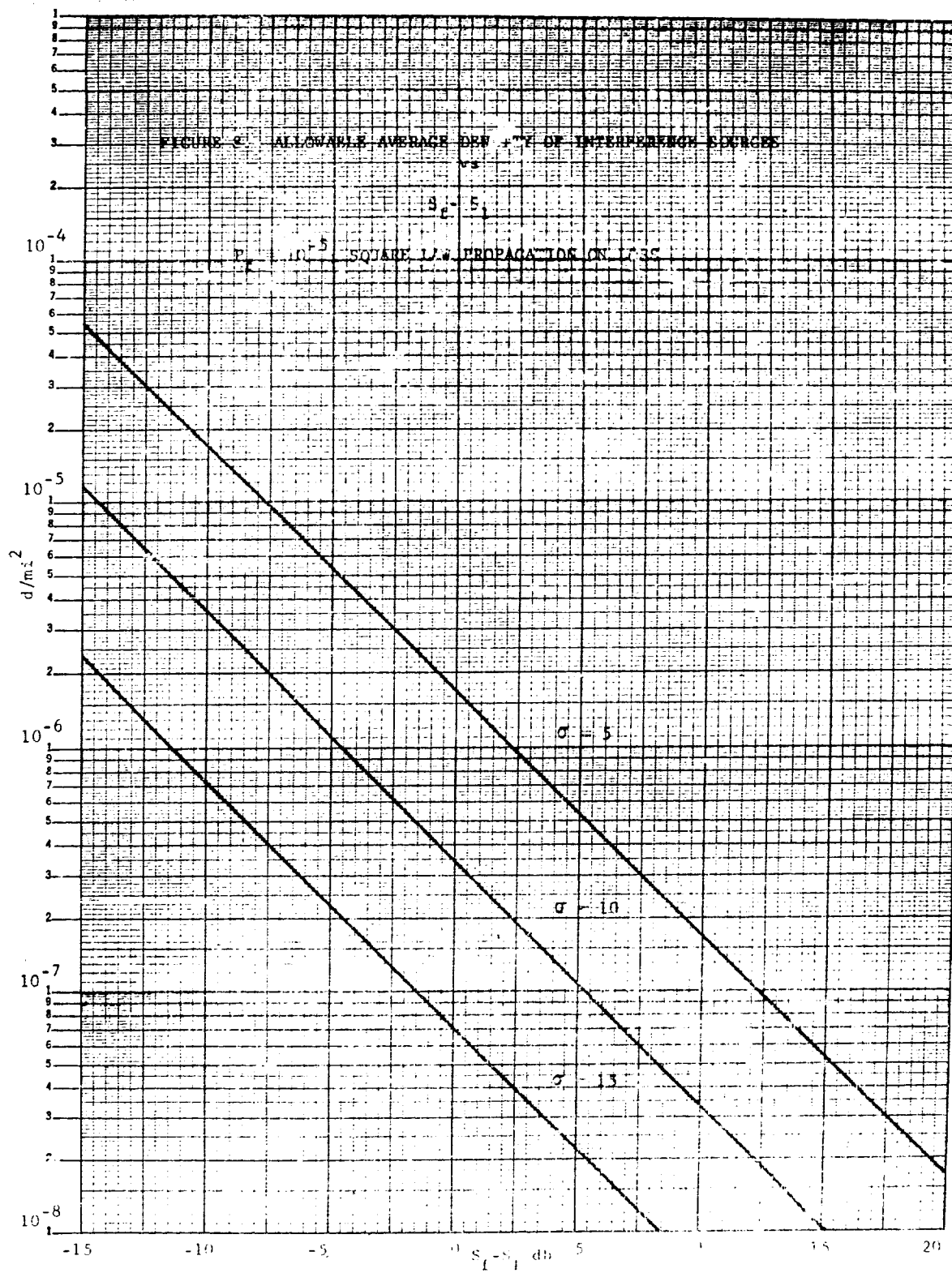


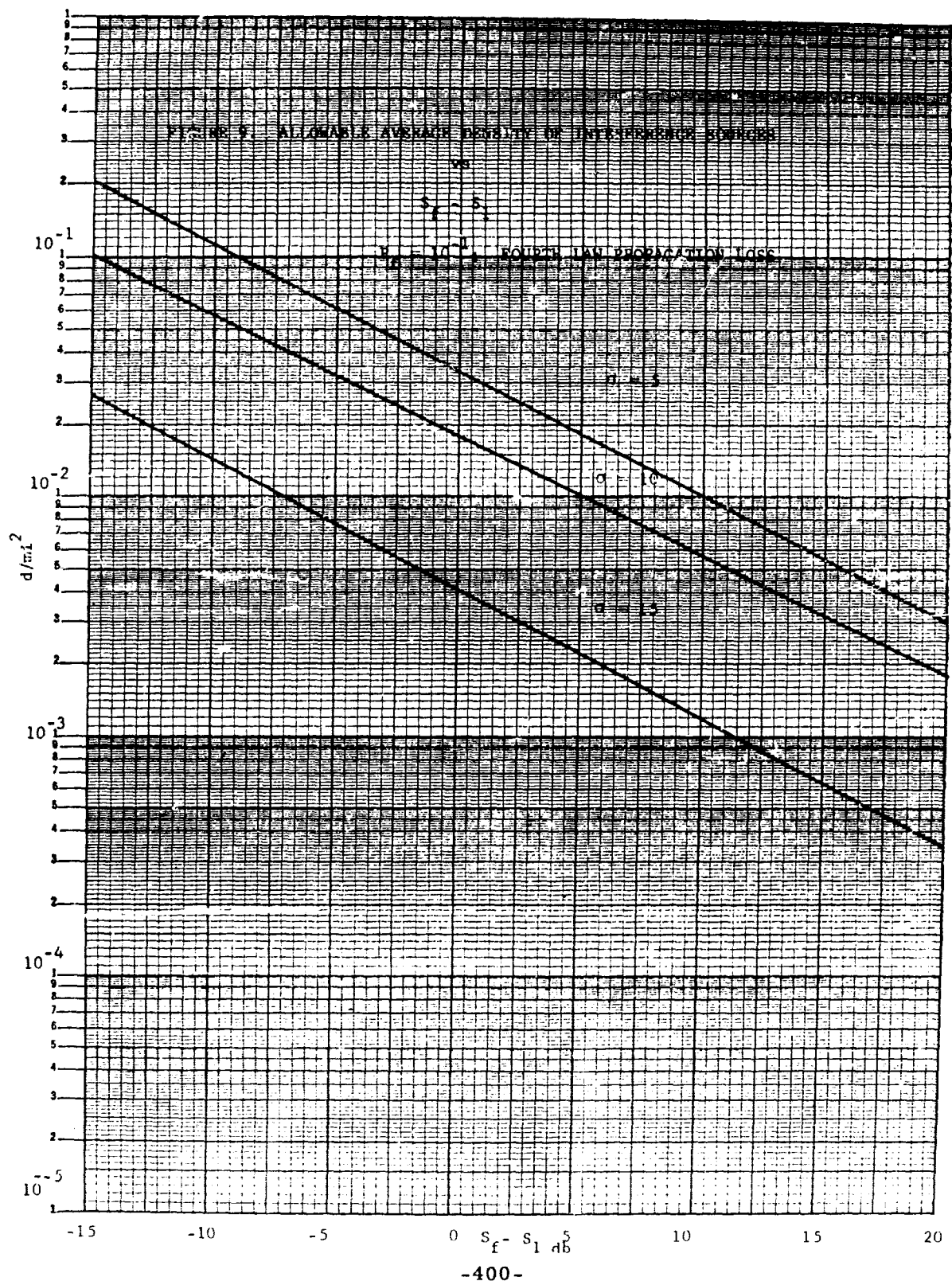


Best Available Copy

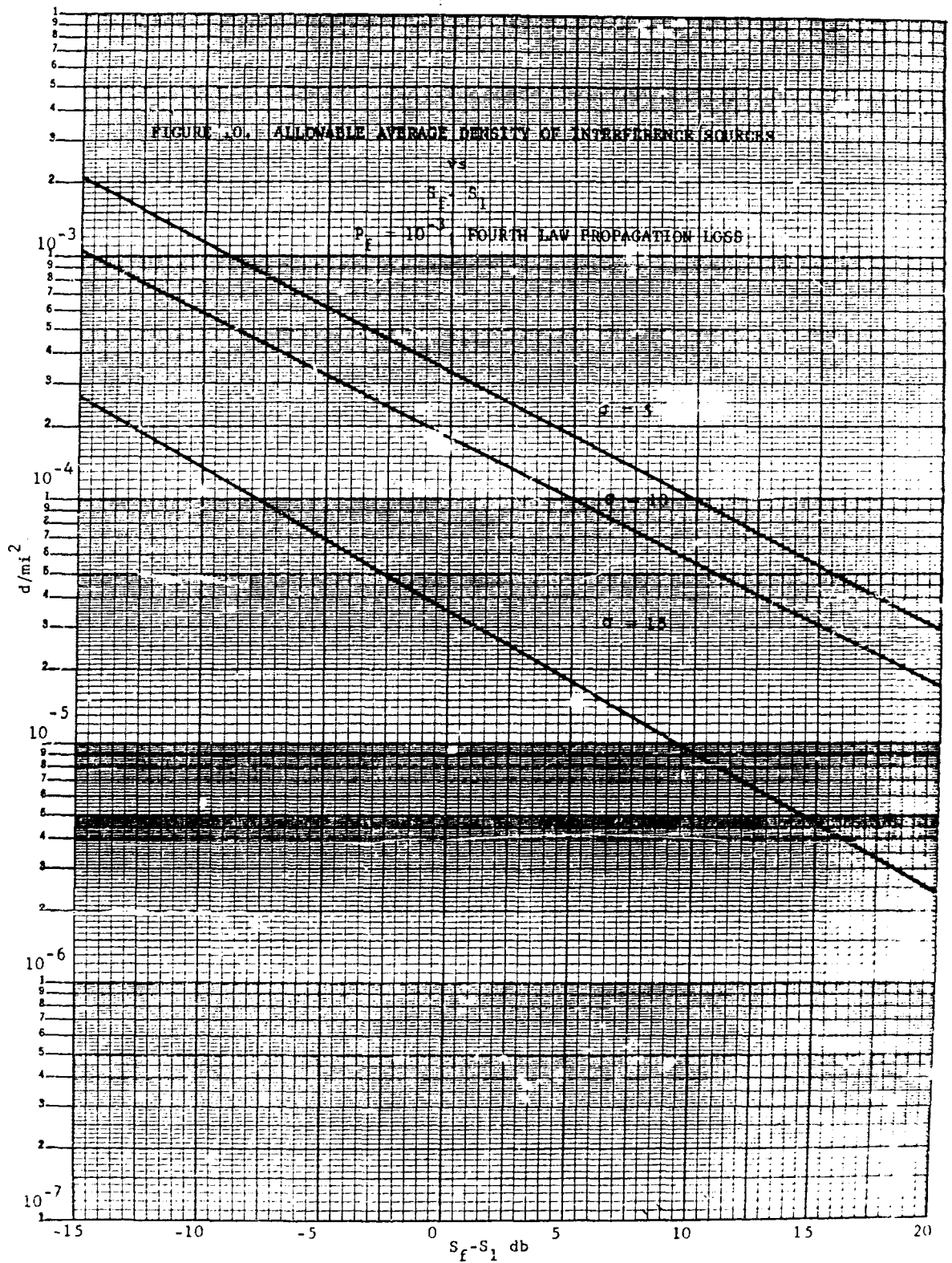


Best Available Copy

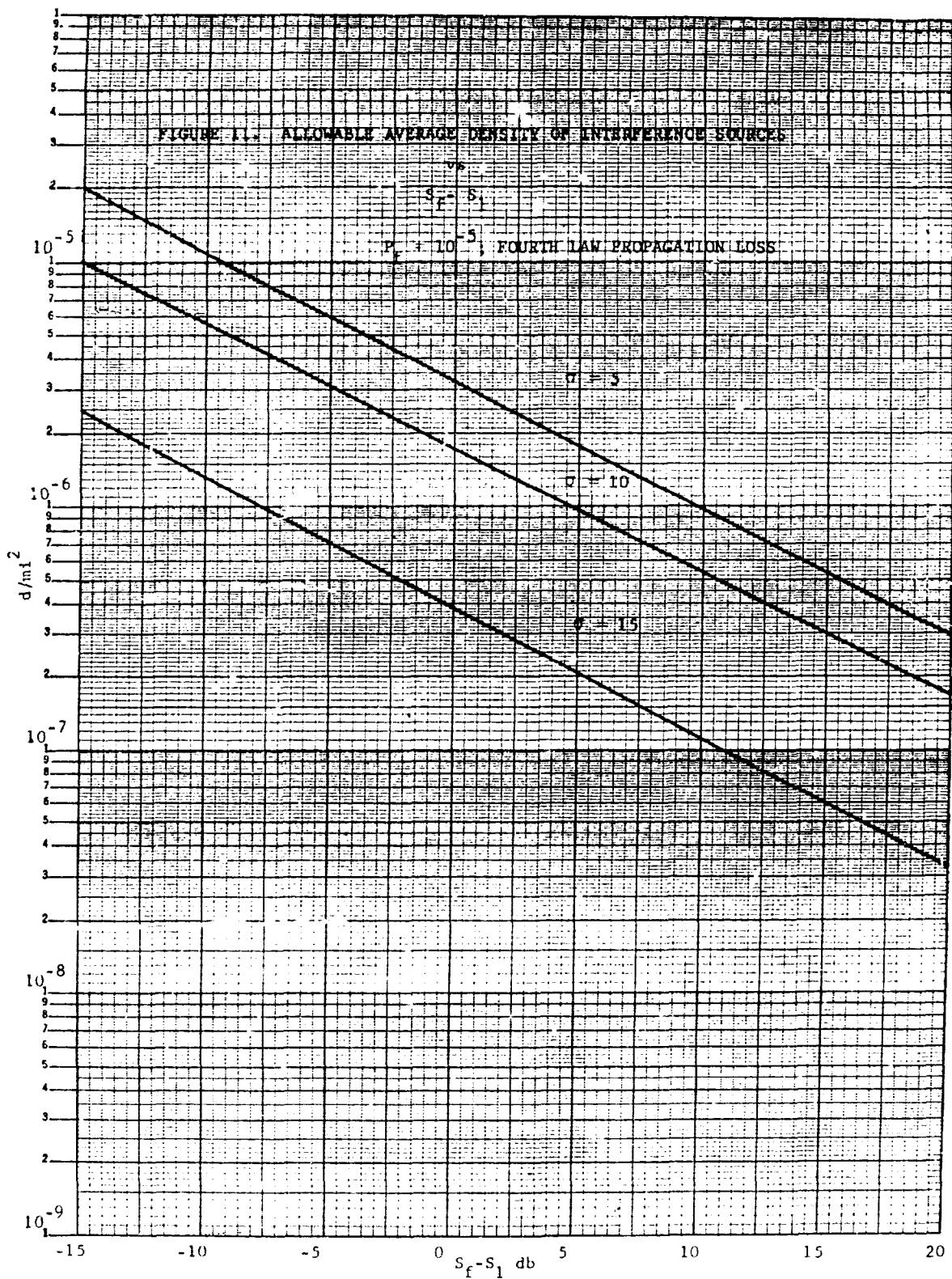




Best Available Copy







## ANALYSIS AND EVALUATION OF ELECTROMAGNETIC COMPATIBILITY TESTS

Dr. William B. McIntosh and Capt George D. Brosious  
U. S. Army Electronic Proving Ground  
Fort Huachuca, Arizona

**Abstract** - The term electromagnetic compatibility test is first defined and then used in development of the subject. A brief description of the test facility is given, including a description of its two complementary subdivisions: a computer-based Interference Prediction Model and a field facility.

The present concept of testing requires that the model be validated against the field facility for each problem and then be used to solve problems under conditions of deployment, terrain, vegetation, and the like, which cannot be duplicated in the field facility.

Validation is accomplished by comparing results obtained by the model and the field facility from a set of test links and an environment which are identical, insofar as possible in both model and field.

The status of model validation is discussed, with emphasis on the statistical methods used in the analysis. Application of a validation analysis to a model use problem is considered with reference to the qualifications which must be placed on conclusions drawn from model results. Contemplated improvements in validation techniques, based on analysis of path coefficients, are reviewed.

### I. INTRODUCTION

During this conference, the term Electromagnetic Compatibility has been used many times. It is appropriate to define what we mean by an Electromagnetic Compatibility Test. The definition presently used at the Army Electronic Proving Ground is: A test, or series of tests, designed to determine the compatibility of Army communications-electronic equipment, systems, and concepts, to perform assigned tasks without unacceptable degradation under the conditions imposed by physical and electromagnetic environments of the type normally encountered in tactical operations. To accomplish this type of testing, a test facility must have the capability of assessing the interference problem regarding: equipments (whether presently in the hands of troops or developmental prototype, or merely drawing board design); systems (such as fire control systems made up of both radar and communication equipment, random access discrete address communications systems, and data transmission systems); and concepts (such as the signal plan to support operations of the newly conceived Air Assault Division).

## II. THE TEST FACILITY

The facility which is used by the Army Electronic Proving Ground to provide these capabilities is the Electromagnetic Environmental Test Facility, or more commonly, the EMETF. The EMETF is further subdivided into two functionally independent, but interrelated, components - an Electromagnetic Environmental Field Facility, and a computer-based Interference Prediction Model. The field facility represents an outdoor electromagnetic laboratory, in that approximately 400 Army communications transmitters are deployed over a 2400 square mile area, automatically controlled to facilitate the development of a new electromagnetic environment every 30 seconds, and provided with the capability to objectively measure degradation to communications links by the use of Voice Interference Analysis Sets (VIAS). The Interference Prediction Model is basically a tool which can be used to evaluate the performance of a communications receiver in a specified environment. Receivers are processed sequentially, one at a time. Thus, any number of desired links can be evaluated by specifying the environment and the location of each test link transmitter and receiver. The model is presently capable of studying the effects of any number of CW, AM, FM, and SSB communications transmitters on CW, AM, FM or SSB receivers. The effects of changing equipment types or of variations in the environment can be studied by processing the problem once for each set of conditions.

The two EMETF components are interrelated in that both are required to accomplish the entire task of investigating the radio frequency interference problem that can exist among the communications-electronic equipment of army units in combat. Without the model, the investigation of compatibility problems is limited to the physical environment of Arizona and the parameters of the field facility. Without the field facility, the model cannot be validated within a reasonable and desired degree of confidence, and its predictions would be of only limited use.

The use of the EMETF in the conduct of compatibility testing is also further subdivided into two parts: (1) validation testing, to insure that the model is technically capable of representing the communications-electronic equipment involved in the test and to provide data for the establishment of confidence limits on computer outputs; and (2) evaluation testing, which actually considers a specific interference problem involving Army communications-electronic equipment, deployed in accordance with established signal plans in support of an Army tactical operation. Since validation testing is the basis for the determination of the method of analysis to be used in the evaluation of computer outputs, validation will be discussed in detail, later. Evaluation testing, as presently accomplished, provides the basic data from which desired conclusions can be reached, following necessary analysis. This testing phase can be conducted in the field facility, or the model, or in a combination of both. Since the more complex case, from the standpoint of analysis, is presented by conduct of this phase in the prediction model, this is the phase that will be discussed next. The first step in Model Testing is to establish a realistic environment. In present testing, the environments utilized are



those of: (1) A division in Germany (5,077 transmitters); (2) An airborne brigade in Germany (911 transmitters); (3) An amphibious brigade in Cambodia (1,495 transmitters); and (4) A corps in Arizona (18,069 transmitters). These deployments are described by an elevation matrix, in conjunction with the 3 dimensional coordinates of each transmitter and receiver. Spectrum Signature data (measured or synthesized) provide the necessary equipment description. Selection of the receivers to be tested is based on the requirement to achieve an adequate sample of the equipments and/or systems under test. Frequency assignments are made based on applicable Army practices - a minimum of three replications of frequency assignments are used under present test philosophy. After the physical constants necessary for the propagation equations have been specified, the program is ready to be run. Although the model has the capability of many types of outputs, the final output presently utilized is the Articulation Index (AI) - the same output which is obtained from the VIAS in the field facility. These indexes describe the performance of a specific receiver, both under conditions of no interference, and under the conditions created by the electromagnetic environment selected for the particular test. In addition, in those cases where interference exists, the transmitter or transmitters causing the interference are identified.

### III. VALIDATION

We will assume that given a suitable field facility including whatever is necessary to solve a particular problem, the experimental design, analysis and interpretation would pose no problems. Our concern is directed principally toward the question of just how does one go about accomplishing the same goals when in fact the desired field conditions cannot be provided, but when a model-field complex such as the EMTF is available; a facility in which the field capabilities are severely circumscribed, but in which the model capability is limited only by the ingenuity of man. The fundamental problem, then, is this: What qualifications must be placed on the analysis when it is performed on the model output? The solution of these problems lies in the proper use of the validation techniques.

System Validation Considerations - In essence, system validation is accomplished by a comparison of results obtained by the model and the field facility from a set of test links and an environment which exhibit, insofar as possible, identical conditions within the set.

Since the outputs of the model and the field facility are in the same units, the articulation indexes or AI scores, the first thought might be to compare these AI scores directly, and, indeed, this can be done. However, there is a peculiarity of the AI scale which makes a simple comparison either difficult or impossible to interpret, depending upon how the links were chosen for test. The AI scale is bounded at either end. The input to the VIAS is the signal plus interference and noise in the audio range. For all instances in which the signal plus noise to noise ratio lies above a certain value, the AI score is 100;

for all ratios below another value, the AI score is zero. The resulting AI scores have been shown to be monotonically related to intelligibility, where the latter is in essence defined as the proportion of a message which is received correctly. The relationship between AI and intelligibility, however, is not linear, nor, in fact, is there a unique relation at all. Different curves result, as the kind of noise is varied. Further, the extraneous accoustical background of the listener, and even his own psychological state, is likewise important. To belabor the comparison with one example: a well-rested soldier listening with earphones on a field trial to a message with random noise interference can tolerate a relatively low signal-to-noise ratio, and still receive an entire message. On the contrary, a tired and hungry soldier in battle, edgy and fearful because of the shells exploding nearby, listening to a loudspeaker in the noise of a command post, and receiving the identical message but with interference which consists of other voice messages with meaningful content, may completely miss the intended transmission. It is factors such as these which complicate evaluation of or comparisons among tests in which human listeners directly produce intelligibility data. However, the use of the AI scoring, in conjunction with records of the nature of the interference and other features of the test, renders subsequent evaluation of, or comparisons among, equipment performance possible.

In describing system validation, we shall first consider the simple case in which only the desired signal is being received. Under these conditions, the information fed from the receiver to the VIAS equipment is proportional to the RF power at the input terminals of the receiver. This, in turn, is inversely related in a loose way to the magnitude of the intervening distance between transmitter and receiver. Accordingly, if for a series of tests the resulting AI referred to as the upper performance limit (UPL), is plotted against distance, a curve of the sort shown in figure 1 would result. Now, suppose that in the validation test the links were chosen so that the majority were at distances which corresponded to those located between the upper and lower knees of the curve, as shown in figure 2. Clearly we would expect a considerable scatter of points when field and model AI scores are compared. In fact, it might be difficult for anyone but a statistician to recognize any relation whatever between the two sets of measurements. This results from the fact that both field and model are in effect being used to evaluate the audio signal and noise over a rather narrow range of signal to noise, the particular range which is critical for the VIAS. On the other hand, suppose the test links were chosen in two groups, one at very short distances and the other at abnormally long ranges for the equipment under test, we would expect results similar to those of figure 3. Obviously, we would have to admit that agreement between field and model results is excellent here, however meaningless this agreement may be. And we may note that the variability in signal to noise ratios between field and model on a given link would vary in absolute terms as much as in the previous case. It just happens that this variation lies outside the range in which it exerts any effect on the AI scores. Clearly, the examples illustrated are extremes, and any intermediate condition could exist. Agreement between model and field, i.e., validation, could then range anywhere from perfect to non-

existent, essentially independent of model accuracy. To put it another way, the validation which can result is at the control of the test designer, and under these circumstances the burden of intellectual honesty lies heavily on his shoulders.

We must also distinguish between two aspects of validation: (1) The kind of validation which is optimal for purposes of developing the model and (2) The kind, similar but by no means identical, which is required when the model is to be used as a predicting tool for real problems. An additional and related consideration is the question to what extent the results from a specific validation with respect to an item of test equipment can be applied to the use of the model. We shall next discuss these points briefly:

Validation for Development - We can further subdivide a validation for development test into separate tests on specific model modules, or components, as opposed to a full systems test. Suppose, for example, we are testing an equipment which belongs to a class that has been tested before, and for which the model has been proven accurate. In this instance we would be primarily concerned with the correctness of the several types of input data. This is to say, we would be concerned whether we were representing correctly in the model the essential characteristics of, say, the receiver, such as selectivity, sensitivity, and important spurious responses. Similar testing can be done on transmitters. The results of these module validations can be carried over into evaluation testing with confidence. There is one area, however, which is subject to uncertainty, the realm of propagation. First we must recognize that of the many factors which affect signal power between transmitter and receiver there are a number which can neither be controlled for experimental purposes nor in some cases even be measured satisfactorily. Further, their variation with respect to time is often rapid. The final result is that there will always be some residual variation between field and model results in any validation test. Even though the model may have been developed to the point that it can stochastically duplicate the field results, it is clear that it can never predict with complete accuracy the results of a specific transmission. There is an additional source of discrepancy between field and model in evaluation testing. Even though the propagation module has been validated over a considerable variety of terrain, vegetation, and the like, the assumption must be made that under other physiographic conditions, the validation may not be applicable.

To summarize this section, we should in theory be capable of performing, under UPL conditions, a developmental validation of the model in terms of modules or groups of modules, as illustrated in figure 4. We shall at this time ignore the bottom scale in the figure. As can be seen, we feel that the accuracy of representation of the modulation generating devices and the VIAS scoring machines is relatively high. Representation of the transmitter-antenna modules is good. We see that the receiver, being somewhat more complex in terms of the way it processes a RF signal, is probably not quite so well represented. The least satisfactory portion of the system by far is the propagation module.

Validation for Utilization - No interference case. Consider the aspect of validation for utilization. As a point of departure, assume that we have in fact a perfect model from the equipment stand-point; that is, we somehow can eliminate propagation vagaries from the picture. Our perfect model, by definition, should produce the identical AI score given by the field for each communication link under test. A comparison between AI scores would then appear as shown in figure 5. Now, when we begin to use this perfect model, we come up with a number of reasons why we can no longer expect precise agreement. An important source of variation and its effect is illustrated in figure 6. In validation for the development, which resulted in the hypothetical perfect model, each individual item of equipment was played in the model using its unique measurements. This is totally impractical in the actual use of the model. Not only do we not know the probability density distribution for each equipment parameter, but even given this, the method of allocating these among all equipments to correspond to a specific situation is not known. The result is that we must at present be content to program the means of each distribution into the model input. These means, further, are the means derived from the spectrum signatures program, and typically are based upon measurements of only three sets. In many instances, this can hardly be considered to be an adequate sample. The result of all this is that, even ignoring propagation, we expect an increased variability between model and field results. Now if we should also include the uncontrolled aspects of propagation in the picture, it becomes even worse, as depicted in figure 7. In an actual case, in which the model is not perfect, using data taken under the conditions of intermediate distance as shown in figure 2, we obtained the results shown in figure 8.

We have now briefly discussed model validation from the developmental and use aspects, next a word about the transfer from use validation to use itself. The point has been made that validation of equipment is transferable from the actual validation test to prediction usage, whereas the transfer of propagation validation is subject to uncertainties. This is pertinent in that it governs our existing procedures.

Still considering only the UPL case, recall that distance was earlier related to the AI scores in figure 1 and that the relative accuracy of groups of model modules was indicated in figure 4 to be essentially the same except for the propagation group.

Accordingly, if for convenience and practicality, we decide to consider our validation in two parts, we have the option of making the division along the total signal path, from start to finish, on one side or the other of the propagation group. The choice is obvious, since signal power is measured at the receiver terminals with relative ease. We can then make a comparison of AI score against received signal power, and we would expect a relationship similar to that shown in figure 9. This curve should be similar to or identical with the one shown earlier in which AI was related to distance, (figure 1) but, and this is of considerable

practical utility, the scatter of data points around the curve is considerably reduced. This scatter should, in fact, result almost entirely from the fact that in validation for utilization the model is using means rather than individual measurements. Or to put the matter differently, if the model was fed the individual receiver characteristics, no point scatter beyond that inherent in measurement accuracy should result.

The previous discussion has taken care of the events between the receiver terminals and the final result. The prior events can be handled by the expedient of comparing received signal strength as measured in the field and as computed by the model. This can be done by conventional statistics techniques of linear regression, in which the line of best fit is found by the method of least squares, and, further, the data can be used to set confidence bounds to the ability of the model to predict received signal strength.

Figure 10 illustrates this approach. The straight line shown is the least squares line representing the regression of signal strength received in the field against signal strength predicted by the model. The pair of curved lines represent the 95 per cent confidence bounds for the line. These bounds were computed using a factor  $\sqrt{(2F)}$ , rather than the usual Student's  $t$ , so that the regression line may be used for repeated prediction. (Reference 1, sec. 5.4).

The graph of figure 10 is used in the following manner. From a given predicted received signal strength, say  $x(m)$ , enter the graph along the X-axis at  $x(m)$ , read vertically to the regression line, thence horizontally to the Y-axis obtaining  $y(m)$ . Then  $y(m)$  is the point estimate of the mean received signal strength produced by all field test links for which the model predicted the value  $x(m)$ . To obtain a confidence interval estimate, repeat the process using the curved lines instead of the regression line. In this manner, two additional readings for the ordinate are obtained, a lower  $y(l)$  and an upper  $y(u)$ . These two points, symmetrically distributed about  $y(m)$ , represent the 95 per cent confidence bounds for the mean field received signal strength corresponding to a single model prediction. The process is repeated for every different value predicted by the model and collectively represents the validation of all modules from and including the signal source to the receiver input terminals. Presumably, the greatest single contributor to the observed variability is the propagation module.

The information just obtained is used in the following fashion. From the validation test will obtain not only a curve which relates UPL AI to received signal strength for the model, but also a comparable curve for the field. The two curves may or may not be identical. Suppose the model and field curves relating AI to signal strength are as shown in figure 11. The model computes the AI that can be found by entering the X-axis at the value of the predicted received signal strength,  $x(m)$ , reading up to the model curve, and across to obtain the ordinate. Let this resulting articulation index be  $AI(m)$ . In order to provide an estimate

of the comparable AI for a field measurement,  $AI(f)$ , the process is repeated using the field curve of figure 11. From the figure, it should be clear that if the model and field curves happened to coincide,  $AI(f)$  and  $AI(m)$  would be identical. If the curves differ, as in figure 11, then  $AI(f)$  and  $AI(m)$  would likewise differ.

To obtain interval estimates for the field AI scores, figure 11 is entered on the X-axis with the two numbers,  $y(l)$  and  $y(u)$ , obtained previously from figure 10. For the  $y(u)$  point (the numerically smaller of the two, since the signal strength scales are in minus dbm) the process of transferring through the field curve gives an upper limit for the field, say  $AI(fu)$ . From the number corresponding to  $y(l)$  we obtain the lower field limit,  $AI(fl)$ . Assuming that the variability of the data points used to obtain the field curve was small (compare figure 9), we have obtained the two AI scores between which we are 95 per cent confident that the mean field UPL AI for all links with the predicted model signal strength would lie.

In reality, the variability for the field curve is too high to be ignored. A modified approach, which uses the joint variability of the relations depicted in figures 10 and 11, is being investigated. It appears likely, however, that the variation contributed by propagation is sufficiently larger than that contributed by the curve of figure 11 so that as a first approximation, the method described can be used.

The procedures described above clearly require a separate AI curve for each equipment type. It is anticipated, however, that a single curve of the kind shown in figure 10 can be used for all AM, FM and CW equipment.

With some reflection, it should become clear that the confidence bounds for predicted field AI scores can vary considerably. If the predicted signal strength is sufficiently high, then the field signal strength bounds,  $y(u)$  and  $y(l)$ , will likewise be high enough so that either when applied to figure 11 would yield an AI score of 100. Conversely, if the predicted signal strength is sufficiently low, the two comparable AI scores can both be zero. All types of intermediate conditions are possible. For example, the AI pairs could be 98 and 100, or 83 and 100, or 27 and 63, or 0 and 17.

Let us summarize what has been accomplished to this point. By indicating those uncertainties which can be eliminated through the use of validation techniques by dividing validation into two groups, and by utilizing the mean characteristics of equipment, we have been able to assess the effect of these sources of variability in terms of interpreting the model AI outputs. We have been able in this sense to obviate the problems involved in interpretation of boundary values of AI scores. We have been able to transfer the predictable features of equipment from the validation for utilization test into the real utilization. We have, in fact, been able to make our entire evaluation hinge essentially upon the accuracy with which the model is able to handle propagation phenomena.

And we can even extend this one step further. Since from the model we obtain the distribution of received signal strength, we are able to ascertain how any postulated bias in the model predicted signal strength would affect the predicted AI scores. For example, in a particular use or situation we may be able to append to our results a statement like the following: These results (AI scores from the model) will still be valid even though the model overestimates received signal strength by an average of k dbm.

Validation for Utilization - Interference case. Up to now we have been considering only the so-called upper performance case. It is obviously the simpler one, but it is also obvious that we must likewise consider the problem of model AI accuracy under the conditions of interference. In the time remaining, we shall discuss this and other problems briefly, quite briefly in part because we shall relate it to the procedures already discussed, and partly because we do not feel that our solutions are at this time quite as satisfactory as they are for the UPL case.

Consider figure 12, which is actually figure 4 to which interfering generators have been added. Most of the problems of representation and of actual measurement are the same here as they are for the UPL case. All representation problems are identical except for the receiver, wherein the problems of handling two or more discrete signals through the detector stage become complex. The measurement problems which existed in the UPL case are also identical, but at least one additional measurement is desirable, the level of each signal as it reaches the detector. This results from the obvious fact that the several signal powers measured at the receiver input reach the detector with different degrees of amplification or attenuation, provided they are not of the same frequency as the desired signal. Thus we are in effect validating separately the RF and IF sections of the receiver on the one hand and the detector and audio stages on the other.

Analysis of Model Output - Space limitations preclude discussion in any detail of the relationships between the AI scores and actual intelligibility. Suffice it to say that a combination of previous research and current efforts are expected to provide the required information on this matter. Assuming, then, the ability to provide the translation from one scale to the other, we next present an approach for utilization of the kind of information gained from our compatibility testing.

There exists a variety of uses for communication in the Army. The types of nets, the priority of the transmitted messages, the number of allowable repetitions, the type of message traffic, and the conditions under which the recipient receives the message, all result in different intelligibility requirements for different nets. Clearly an infantry commander requesting that artillery fire be directed against a machine gun that has immobilized his company needs a net with considerably higher intelligibility than a special services officer in the rear echelon requesting that more volley ball nets be sent to a rest area.

In conjunction with our current testing, and with the cooperation of the cognizant army agency, we have developed a minimum acceptable intelligibility criterion for each of the various communication nets for a field army. Once these intelligibility criteria are available, they may be used in the following manner, as shown in figure 13. The AI scores for all nets of a given classification are plotted on this chart, with the Lower Performance Limit (LPL), which describes the interference condition, as the ordinate and the UPL, which describes the no-interference condition, as the abscissa. Clearly, if there happened to be no interference on any net, all such points would fall along the diagonal, where the UPL and LPL are the same. The triangle is further subdivided into three areas based on the predetermined minimum intelligibility which is acceptable for that net type. The interpretation from here on is relatively simple. These may be some nets which for one reason or another do not meet the intelligibility requirement even in the absence of interference. These are those which would fall along the diagonal of the C triangle. If any such net should suffer further degradation of performance because of interference, the plotted point would fall somewhere inside the C triangle. There is no real concern for these cases, since interference has only made an unacceptable situation even more so.

Other nets, and normally the majority, would, in the absence of interference, fall along the diagonal of triangle A. Any such net, under the influence of interference, would be dropped vertically. Under slight or moderate interference, depending upon the UPL for that net, the plotted point would fall somewhere inside triangle A, and the net would be usable in terms of the required intelligibility. If stronger interference is manifested, the point would be expected to drop into rectangle B. The set of such points represents the nets which would be usable in the absence of the specific interference predicted, but which would be effectively eliminated from the usable communication complex when the predicted interference did exist.

This A and B classification is then used in the determination of a Compatibility Index, as well as in the final validation process to determine what qualifications, if any, must be placed on these indexes. The compatibility index is basically a ratio of test links not experiencing interference to the total number of test links considered. Links not experiencing interference have been classified A, based on the criterion given above, which is in turn based on the use of a minimum acceptable intelligibility for each type of link. Links which have experienced interference are classified as B, and the desired ratio, or compatibility index is expressed simply as  $A/(A+B)$ . Thus, perfect compatibility, or the condition of no interference, would have an index value of 1. The application of these indexes to the actual problem can be used to give an overall comparison (at this point in time, an absolute value has not been determined to establish the break point between compatible and non compatible), as well as an insight into the causal relationship of the various factors which affect the compatibility rating (such as frequency assignment method, transmitter characteristics, and receiver characteristics). This index differs from many other kinds of indexes, in that confidence limits can



be placed upon it, utilizing the binomial distribution, and that tests of significance can be made between indexes.

The use of the A-B classification in the final validation of compatibility indexes is based on the requirement to determine whether the model is capable of producing accurate results, under the conditions imposed by the specific test. This, in turn, requires that these accuracies be established for the values of minimum acceptable intelligibility and for the majority of UPL values used in the test. The method used for this type of validation is based on a comparison of model A-B classification with classifications made on field facility data, taken under the same conditions. A contingency test is used to determine whether there are any significant differences between the performance of the model and the field facility. If the results of the comparison indicate that no significant differences exist, the compatibility indexes derived from the model outputs can be used without qualification, when the model is predicting in a geographical area similar to that of the field facility. The qualifications which must be applied for any extrapolation to other areas of the world are based on the capability of the model to represent the propagation phenomena in that particular locale. The main factors affecting ability to predict propagation losses are terrain features, ground constants, vegetation effects, and refractivity. Since the effect of terrain features is accounted for in the model by a terrain matrix peculiar to each problem, it is necessary to consider only the remaining three factors. The determination to be made must consider the accuracy of the available data, as well as the capability of the model to represent it. Unfortunately, sufficient information is not available in either of these areas, and the determination of necessary qualifications is essentially subjective. Propagation experiments are presently being conducted by Army agencies in northern Arizona, Colorado, and Thailand to provide information on which an objective determination of model capability in various geophysical areas can be based; however, the immediate future shows no promise for an improvement of basic data accuracy in areas other than those mentioned above. Before unnecessary attention is devoted to the improvement of these accuracies, it is important that consideration be given to the variability which inaccuracies would produce. A proposed method (analysis of path coefficients) for this determination is presented in the annex.

Fortunately, the one compatibility test which has been completed in the EMTF using the validation methods described above has not required qualification of results, due to a satisfactory comparison between field facility and model, and favorable results of a qualitative study which investigated the problems of extrapolation.

Up to this point, we have been considering methods and procedures actually used in the validation and subsequent analysis of EMTF results. Let us now consider the extension of these procedures into the future.

We have previously used two figures on which were indicated a scale of proportion of total variability contributed by each module group to the

total. The estimates provided on these slides are at the moment guesses. Given accurate measures, however this kind of information is particularly useful. In model development, we are able to focus primary attention on the module or the group which contributes the largest amount to the total variability. It obviously is not reasonable to work toward improving a module which contributes, say, one per cent of the total variability while another module might be contributing over half of the total. Similarly, in terms of evaluating the model results in any condition of use, it is very helpful to be able to pin down the sources of variation. Propagation is undoubtedly the major source of variation, but who can give an answer which tells how much propagation contributes? Is it 30 per cent? Is it 57 per cent? Or is it 83 per cent?

In our future development work we have proposed studies which will enable us to answer these questions. The experiments and the analysis are not too complex, and are described in the annex. The analysis is a powerful but little known technique known as analysis of path coefficients or analysis of correlation, from its similarity in concept with analysis of variance or analysis of chi-square. Application of the method requires that several factors which affect a variate can be specified, can be measured simultaneously in the field, and can be related to the variate under study by a linear causal diagram. The particularly attractive feature of this approach is that the collective effect of all factors not specified, and hence not observed and measured, can be considered as a single variate, stochastically independent of the specified ones. The mean and variance of this hypothetical unobserved variate can then be estimated, and its contribution to the total variability adduced. Clearly, if this last mentioned contribution is small, say on the order of a very few per cent, we know that we have come well along the road toward theoretical perfection, whereas if the contribution of the unknown variate to the total is large, further theoretical and developmental work is clearly indicated.

In summary, we have defined the concept of an electromagnetic compatibility test and have briefly described a facility which is being used to perform such tests. Particular emphasis has been given to the problem of validation of the computerized interference prediction model against the field facility. An example of the use which can be made of the model in evaluation of the Army's radio frequency compatibility problem has been explained. Further plans for further improvements were outlined.

#### REFERENCES

1. Natrella, Mary G. Experimental Statistics; Section 1. Ordnance Corps Design Handbook, ORDP 20-110. 1962
2. Li, C. C. Population Genetics. Univ. Chicago Press. 1955.

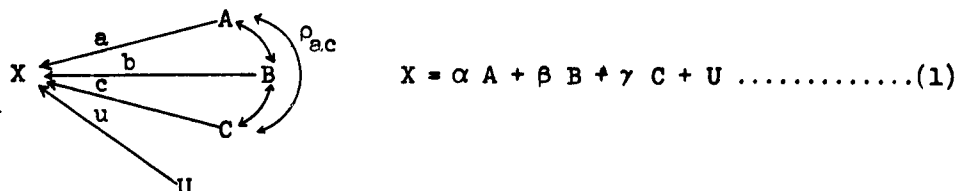
## Annex

In this annex we describe a method of ascertaining the extent to which each of a set of causal variates contributes to the total variability of another variate which is functionally dependent upon the causal set. The method is based upon the analysis of correlation, or analysis of path coefficients, as it is sometimes called.

The method presupposes that:

- (a) There may be any number of known causes.
- (b) All unknown causes can be lumped and treated as a single cause.
- (c) All causes and the resultant are variates.
- (d) A diagram relating the causes and the resultant can be drawn.
- (e) The causative relations can be expressed by a linear equation.
- (f) The unknown cause is statistically independent of each known cause.
- (g) A non-zero correlation may exist between any or all pairs of known causes.

Suppose, for example, the resultant is the variate X, the known causes are the variates A, B, and C, and the unknown cause is the variate U. Suppose the causal diagram and the equation of relation (linear regression equation) are



where  $\alpha$ ,  $\beta$ , and  $\gamma$  are the regression coefficients, and  $a$ ,  $b$ ,  $c$ , and  $u$  are standardized partial regression coefficients, or path coefficients. Doubleheaded arrows designate correlation between pairs of causes; for example,  $\rho_{ac}$  establishes that causes A and C are not independent. Non-zero correlations of necessity also exist between any two variates connected by a singleheaded arrow.

In order that this system can be studied, it is a necessary condition that an experiment can be performed such that simultaneous readings can be taken on the variates A, B, C, and X, thus giving rise to a set of multivariate data. From this set, the means, standard deviations, covariances, and correlation coefficients shown on the next page can be computed.

$\mu_a$	$\sigma_a$	$\sigma_{ab}$	$\sigma_{ax}$	$\rho_{ab}$	$\rho_{ax}$
$\mu_b$	$\sigma_b$	$\sigma_{ac}$	$\sigma_{bx}$	$\rho_{ac}$	$\rho_{bx}$
$\mu_c$	$\sigma_c$	$\sigma_{bc}$	$\sigma_{cx}$	$\rho_{bc}$	$\rho_{cx}$
$\mu_x$	$\sigma_x$				

Since the variate U is unknown and hence unmeasurable, direct computation of any quantities involving U is not possible.

In the theory of path coefficients it is shown that the following equations can be written for the causal diagram of (1):

$$\begin{cases} a + b\rho_{ab} + c\rho_{ac} = \rho_{ax} \\ a\rho_{ab} + b + c\rho_{bc} = \rho_{bx} \dots\dots\dots(2) \\ a\rho_{ac} + b\rho_{bc} + c = \rho_{cx} \\ u = \rho_{ux} \end{cases}$$

These equations follow from the general result that the correlation,  $\rho$ , between two variates is the sum of all paths, simple and compound, connecting the variates. Thus, between X and A there is the direct path, given the value of its path coefficient,  $a$ , and two compound paths,  $b\rho_{ab}$  and  $c\rho_{ac}$ . Only one doubleheaded arrow may be used in a compound path. Thus the apparent compound path  $c\rho_{bc}\rho_{ac}$  is not valid.

The first three equations of set (2) involve three unknowns,  $a$ ,  $b$ , and  $c$ ; hence the subset can be solved. It is also shown in theory that

$$a^2 + b^2 + c^2 + 2ab\rho_{ab} + 2ac\rho_{ac} + 2bc\rho_{bc} + u^2 = 1 \dots\dots\dots(3)$$

Since all terms in (3) but  $u^2$  are known,  $u$  may be found. Further, the regression coefficients may be found from the following relationships:

$$\alpha = \frac{a\sigma_x}{\sigma_a} \quad \beta = \frac{b\sigma_x}{\sigma_b} \quad \gamma = \frac{c\sigma_x}{\sigma_c}$$

The mean and variance of the unknown variate may be found from

$$\begin{aligned} \mu_x &= \alpha\mu_a + \beta\mu_b + \gamma\mu_c + \mu_u \\ \sigma_x^2 &= \alpha^2\sigma_a^2 + \beta^2\sigma_b^2 + \gamma^2\sigma_c^2 + 2\alpha\beta\sigma_{ab} + 2\alpha\gamma\sigma_{ac} + 2\beta\gamma\sigma_{bc} + \sigma_u^2 \dots(4) \end{aligned}$$

Equation (3) can be given a simple percentage interpretation,  $100 u^2$  is

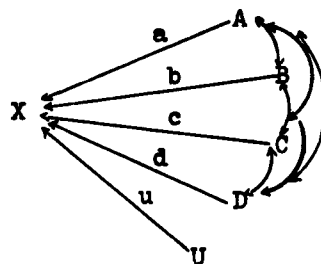
the percentage of the total variation in X which results from the unknown cause, U. This fact may be used to ascertain the state-of-the-art during a study. If  $100 u^2$  is small, say on the order of one or two per cent, then it is clear that the known causes have been satisfactorily accounted for. If, however,  $100 u^2$  is large, this is an indication that further causes must be sought if an adequate understanding of the system is to be attained.

A numerical example, somewhat exaggerated, follows. Consider a true situation in which there are four known causes, A, B, C, and D, plus a statistically independent unknown cause, U. This model is merely an extension by one cause of the general example described previously. The data for the example are given in table I, for which the causal diagram

Table I  
Data for example

A	B	C	D	U	X
12	10	18	5	4	106
2	22	9	3	7	89
2	6	6	6	2	41
12	14	15	1	1	103
5	10	15	1	10	81
18	4	9	8	8	98

and linear regression equation are



$$X = \alpha A + \beta B + \gamma C + \delta D + U \dots (5)$$

where  $\alpha = 3$ ,  $\beta = 2.5$ ,  $\gamma = 2$ ,  $\delta = 1$ .

The necessary computations of means, variances, covariances, and correlation coefficients are set forth in table II. The example will be analyzed assuming different levels of knowledge about the true condition.

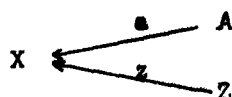
Case I. Assume an investigator has postulated an incorrect causal scheme in which the only known cause was A. The remaining causes, assumed (erroneously) to be independent of A, will be collectively identified in this case as Z, to distinguish them from the U of table I. The data thus available to the investigator are those shown in the first two columns of table III; the causal scheme and regression equation assumed are diagrammed to the left below table III. The proper causal scheme - although the investigator has no way of knowing this - is shown to the right beneath table III. The assumed regression equation is correct for the proper causal scheme.

Table II  
Summary of Computations from Table I

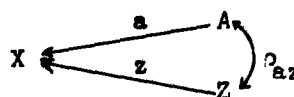
$\sigma_a = 5.93717$	$\sigma_b = 5.85947$	$\sigma_c = 4.24264$	$\sigma_d = 2.58199$
$\sigma_u = 3.24893$		$\sigma_x = 21.95197$	
$\sigma_{ab} = -15.83333$	$\rho_{ab} = -0.45513$	$\sigma_{ac} = 8.50000$	$\rho_{ac} = 0.33745$
$\sigma_{ad} = 5.83333$	$\rho_{ad} = 0.38052$	$\sigma_{bc} = 3.00000$	$\rho_{bc} = 0.12068$
$\sigma_{bd} = -9.33333$	$\rho_{bd} = -0.69691$	$\sigma_{cd} = -5.50000$	$\rho_{cd} = -0.50715$
$\sigma_{ax} = 89.00000$	$\rho_{ax} = 0.68287$	$\sigma_{bx} = 35.00000$	$\rho_{bx} = 0.27210$
$\sigma_{cx} = 63.50000$	$\rho_{cx} = 0.68181$	$\sigma_{dx} = -10.16667$	$\rho_{dx} = -0.17937$
$\sigma_{ux} = 10.50000$	$\rho_{ux} = 0.14800$		
$\sigma_{au} = \sigma_{bu} = \sigma_{cu} = \sigma_{du} = \sigma_{au} = \sigma_{bu} = \sigma_{cu} = \sigma_{du} = 0$			

Table III  
Data for Case I

A	X	Z	Y
12	106	75.7024	70
2	89	83.9504	83
2	41	35.9504	35
12	103	72.7024	67
5	81	68.3760	66
18	98	52.5536	44



$$X = \alpha A + Z$$



From the causal diagram, and using the method of equation (2), we write

$$\begin{aligned} a &= \rho_{ax} \\ z &= \rho_{zx} \end{aligned}$$

and since  $\rho_{ax}$  is 0.68287 (from table II) the solution  $a = 0.68287$  is obtained immediately. Then  $a^2 = 0.46631$  and  $z^2 = 1 - a^2 = 0.53369$ . Hence under the erroneous causal scheme it is found that the cause A contributes approximately 47 per cent to the total variation of X, leaving 53 per cent to be accounted for by the supposed unknown cause.

The mean and variance of the unknown cause are found to be

$$\begin{aligned} \mu_z &= \mu_x - \alpha \mu_a = 64.8725 ; \\ \sigma_z^2 &= \sigma_x^2 - \alpha^2 \sigma_a^2 = 257.1858 . \end{aligned} \quad \dots\dots\dots(6)$$

The regression coefficient,  $\alpha$ , is

$$\alpha = \frac{a \sigma_x}{\sigma_a} = 2.5248.$$

The individual Z entries may now be computed from the relation

$$Z = X - \alpha A.$$

Thus, for the first row of table III,

$$Z = 106 - 2.5248(12) = 75.7024,$$

and similarly for the remaining entries in the Z column.

From the proper scheme the effective values of the residual variate may be found. Denoting the residual variates collectively by Y, from (5) we have

$$Y = \beta B + \gamma C + \delta D + U$$

and numerically for the first row of table III we compute, after obtaining the numbers B, C, D, and U from table I,

$$Y = 2.5(10) + 2(18) + 1(5) + 4 = 70.$$

A comparison of the Z (erroneous) and Y (correct) entries in Table III shows that there is considerable agreement. Now, once the individual Z entries have been computed, the mean and variance of Z may be calculated directly, giving  $\mu_z = 64.8725$  and  $\sigma_z^2 = 257.1797$ . These agree with the computations in (6) within the limits imposed by the rounded Z entries of table III

The incorrect causal scheme assumes the Z and A sets to be linearly independent. This may be verified by computing the correlation coefficient,  $\rho_{ax}$ , which amounts to 0.00001. The miniscule difference from zero is attributable to rounding errors in Z. On the other hand, there is no necessary reason why the Y entries should be uncorrelated with the A. Computation of  $\rho_{ay} = 0.17326$  shows that a positive correlation does exist. It is this fact which accounts for the difference between the Z and Y columns in table III. It is the relatively small correlation which results in the considerable agreement.

This example illustrates one fundamentally important point. The validity of the analysis depends upon the accuracy of the causal scheme. Further, the causal scheme cannot be inferred from the data. Nor can an investigator make any headway by assuming that A and Z are correlated, for he must then solve the equations

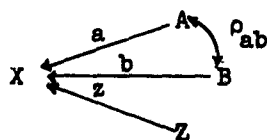
$$\begin{cases} a + z\rho_{az} = \rho_{ax} \\ a\rho_{az} + z = \rho_{zx} \end{cases}$$

which contain four unknowns, a, z,  $\rho_{az}$ , and  $\rho_{zx}$ , since no correlation coefficients involving Z can be computed from the observed data.

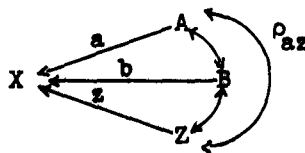
Case II. The analysis will follow the pattern and symbolism of Case I, with the exception that we assume cause B to be included in the known causes. The data thus available to an investigator are presented in the first three columns of table IV. The causal schemes and the assumed regression equation are given below the table, as before.

Table IV  
Data for Case II

A	B	X	Z	Y
12	10	106	33.3140	45
2	22	89	20.8836	28
2	6	41	16.9508	20
12	14	103	19.2972	32
5	10	81	34.6480	41
18	4	98	19.2672	34



$$X = \alpha A + \beta B + Z$$





From the assumed causal diagram, we write

$$\begin{cases} a + b\rho_{ab} = \rho_{ax} \\ a\rho_{ab} + b = \rho_{bx} \\ z = \rho_{zx} \end{cases}$$

and inserting numerical values where possible in the first two equations,

$$\begin{cases} a - 0.45513 b = 0.68287 \\ -0.45513 a + b = 0.27210 \end{cases}$$

Solution of the equations gives  $a = 1.01747$ ;  $b = 0.73517$ . Then

$$\begin{aligned} a^2 &= 1.03525 \\ b^2 &= 0.54047 & \alpha &= 3.7620 \\ 2ab\rho_{ab} &= -0.68089 & \beta &= 2.7542 \\ z^2 &= \frac{0.10517}{1.00000} \text{ (by subtraction)} \end{aligned}$$

The correlations,  $\rho_{az} = 0.00006$  and  $\rho_{bz} = 0.00010$ , as expected, are zero within the limits imposed by rounded values of  $Z$ . The correlation coefficients  $\rho_{ay} = 0.46900$  and  $\rho_{by} = 0.06869$  again, as in Case I, demonstrate that the true unknown variate need not be independent of the known causes when an erroneous causal scheme is used.

Two interesting facts can be gleaned from a comparison of Case II with Case I. First, we find the apparent anomaly that A accounts for over 100 per cent of the variation in X ( $a^2 = 1.03525$ ) and that B accounts for about 54 per cent ( $b^2 = 0.54047$ ), a combined total of 158 per cent. This is explained, however, by considering the effect due to the correlation between A and B ( $2ab\rho_{ab} = -0.68089$ ). The  $a^2$  and  $b^2$  effects cannot be considered separately. The effects of A and B acting jointly must be considered, and this is  $1.03525 + 0.54047 - 0.68089 = 0.89483$ .

Second, we observe that the agreement between the Z and Y columns for Case II is not as good as was true for Case I. For Case I, the average difference ( $Z - Y$ ) is 3.8292; for Case II the average difference is -9.2732. This results in large part from the rather high correlation between A and Y.

One additional fact is worth noting. Although it is clear that the estimates we obtain under erroneous assumptions concerning the unknown variate are not accurate, it is nevertheless instructive to compare the estimated variance of the unknown cause. In Case I this was estimated to be 257.2. For Case II, the comparable estimate is 50.68, a considerable reduction. Thus not only does the percentage of variation in X due to Z show a reduction from Case I to Case II, but also the variability of the unknown variate decreased sharply. As each additional cause is extracted from the unknown category, the variability of the remaining combined unknown causes must decrease, unless high negative correlations exist between the cause removed and at least one cause which remains in the unknown category.

Case III. This case will be discussed in outline only. The cause C is included under the known categories, leaving only D and U to be treated as the unknown Z.

$$\begin{array}{ll}
 \text{We obtain} & a = 0.86123 \\
 & b = 0.62599 \\
 & c = 0.31562 \\
 \text{and} & \\
 & a^2 = 0.74172 \qquad \alpha = 3.1843 \\
 & b^2 = 0.39186 \qquad \beta = 2.3452 \\
 2ab\rho_{ab} & = -0.49074 \qquad \gamma = 1.6331 \\
 c^2 & = 0.09962 \\
 2ac\rho_{ac} & = 0.18345 \\
 2bc\rho_{bc} & = 0.04769 \\
 z^2 & = \frac{0.02640}{1.00000} \text{ (by subtraction)}
 \end{array}$$

The mean difference between Z and Y is 4.3724, and the variance of Z is 12.7204. Each of these numbers represents an improvement over the comparable estimates from Case II. Similarly, the regression coefficients are closer on a percentage basis to the true values than they are in Case II

Case IV. This case represents the final analysis on the example, in which all known causes are accounted for. It is presented only in summary form.

$$\begin{array}{ll}
 \text{We obtain} & a = 0.81139 \\
 & b = 0.66731 \\
 & c = 0.38654 \\
 & d = 0.11762 \\
 \text{and} &
 \end{array}$$

$$\begin{aligned}
a^2 &= 0.65835 \\
b^2 &= 0.44530 \\
2ab\rho_{ab} &= -0.49286 & \alpha &= 3.00002 = 3 \\
c^2 &= 0.14941 & \beta &= 2.50002 = 2.5 \\
2ac\rho_{ac} &= 0.21167 & \gamma &= 1.99996 = 2 \\
2bc\rho_{bc} &= 0.06226 & \delta &= 1.00000 \\
d^2 &= 0.01383 \\
2ad\rho_{ad} &= 0.07263 \\
2bd\rho_{bd} &= -0.09684 \\
2cd\rho_{cd} &= -0.04565 \\
u^2 &= \frac{0.02190}{1.00000} \text{ (by subtraction)}
\end{aligned}$$

Since the example was set up with the U variates independent of each known variate, the U variates, if constructed in this case as the Z were computed in previous cases, work out to be identical with the U of table I.

These methods will be employed in two general areas. First, they will be used to study the contribution of the several module groups to the variation in AI scores, as indicated by the bottom portions of figures 4 and 12. It has been pointed out that the proportions used in those figures were merely guesses. For this use, it is anticipated that the application will be relatively straightforward, although there are various problems attendant upon obtaining the necessary measurements from the field for each module group. However, the model treatment should be simple, since the model operates by taking the power output from the transmitter and subtracting (or adding) the loss (or gain) in dbm encountered in each module. The effect of this is to make the regression coefficients unity for the model analysis. Presumably the regression coefficients are also near unity for the field. Further, it is likely that correlations between the effects of the several modules are low, which makes the analysis easier to interpret than the numerical example used here.

Second, the method will be applied to a study of subunits of the propagation module. The principal subunits are terrain, foliage, ground constants, and refractivity. There is no assurance that the regression coefficients will be approximately unity, nor is there any reason to believe that all correlations between the subunit measurements will be near zero.

An exposition of the method of path coefficients may be found in Reference 2, chapter 12.

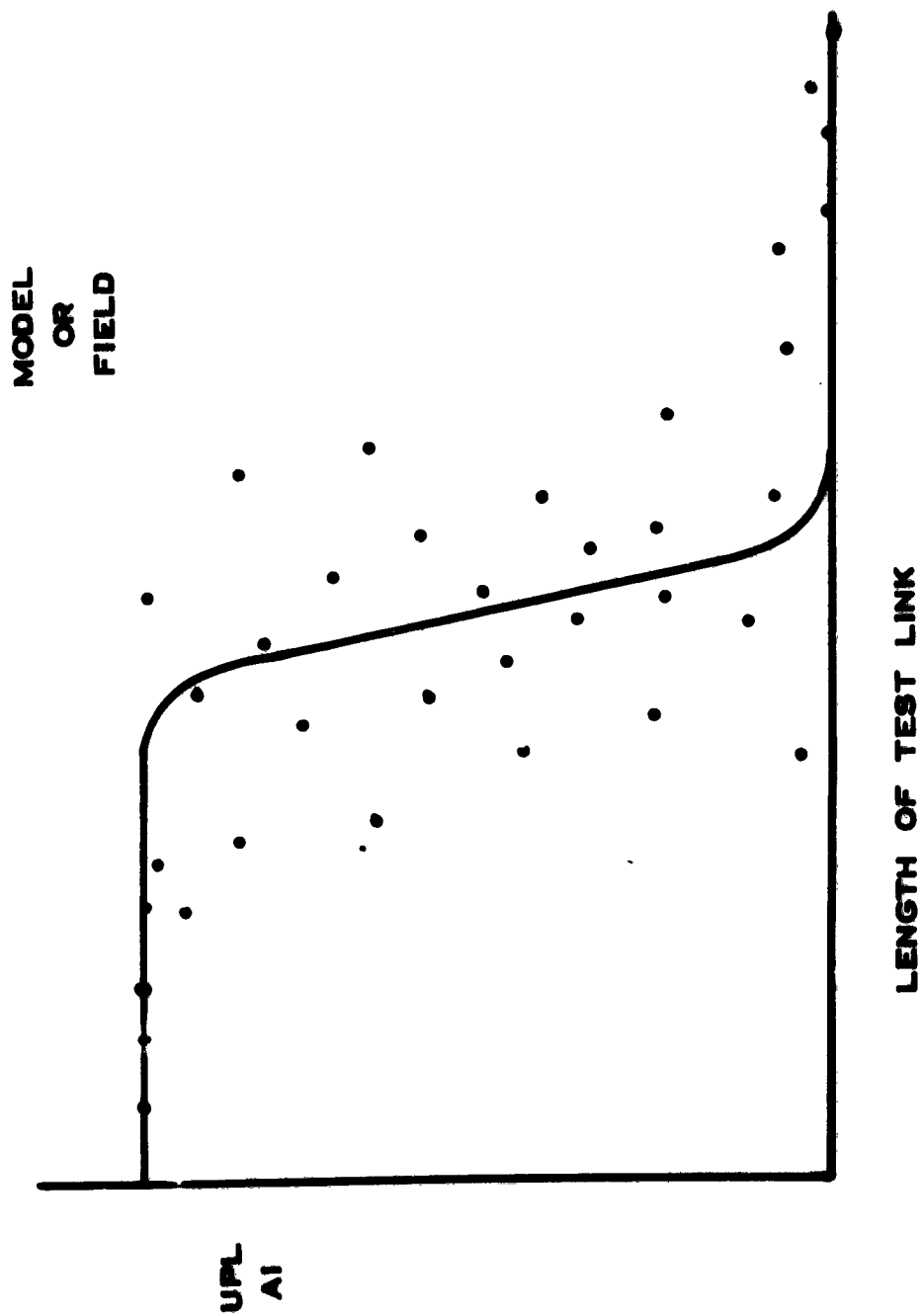


Figure 1. Upper Performance Limit Articulation Index versus Distance

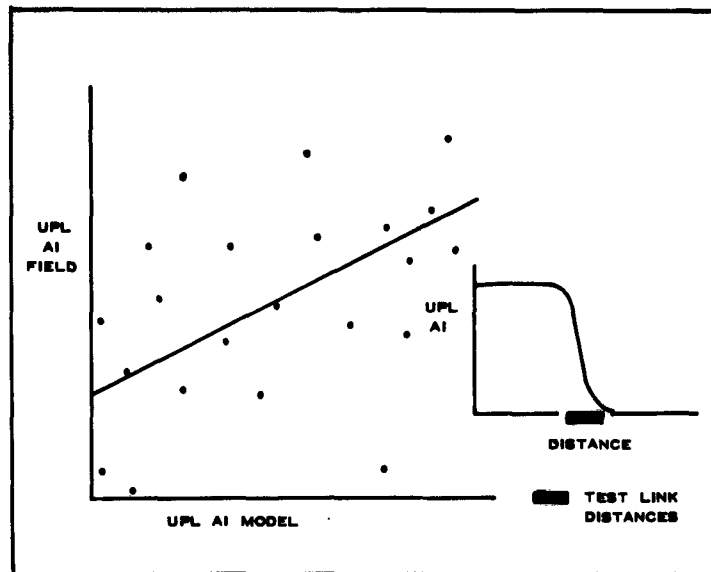


Figure 2. Upper Performance Limit versus Distance (Critical)

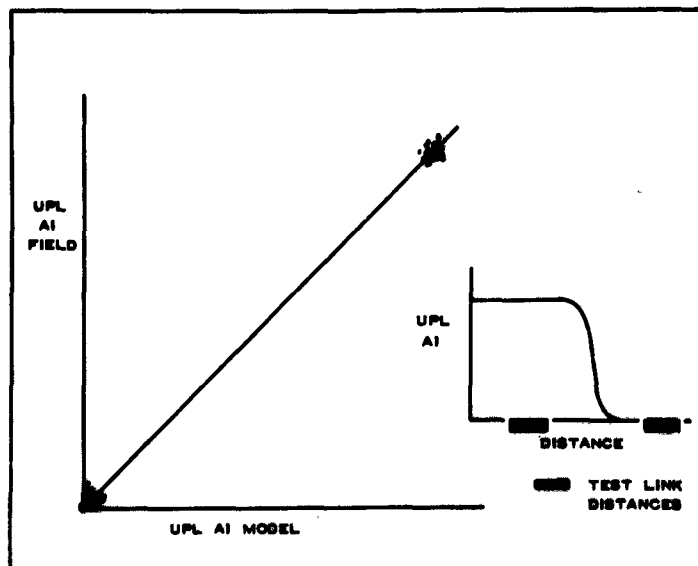
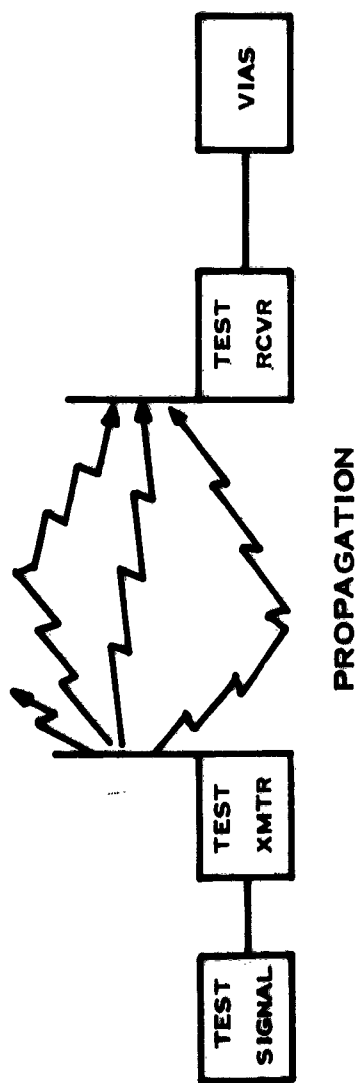


Figure 3. Upper Performance Limit versus Distance (Non-critical)



PROPAGATION

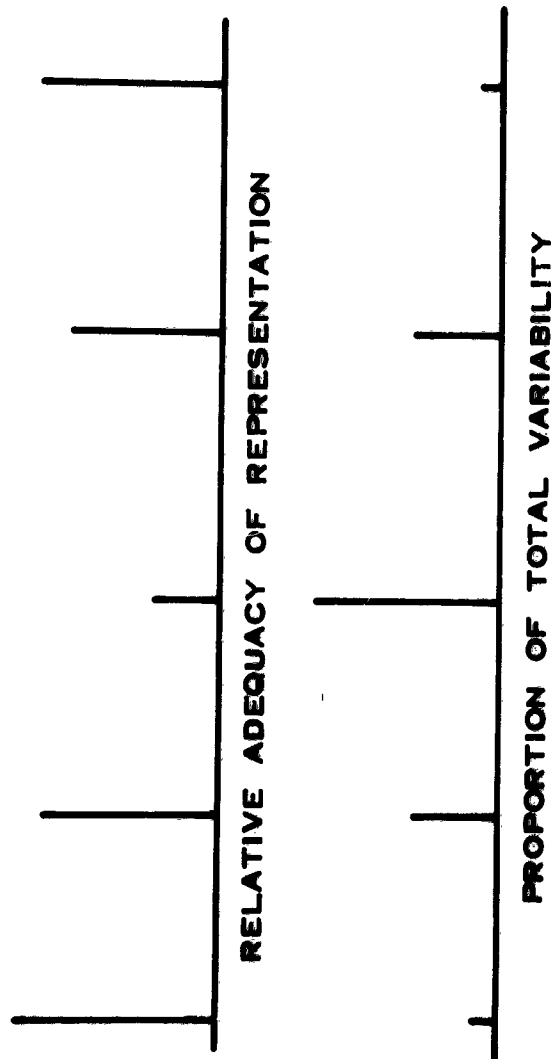


Figure 4. Developmental Model Validation by Modules (UPL)

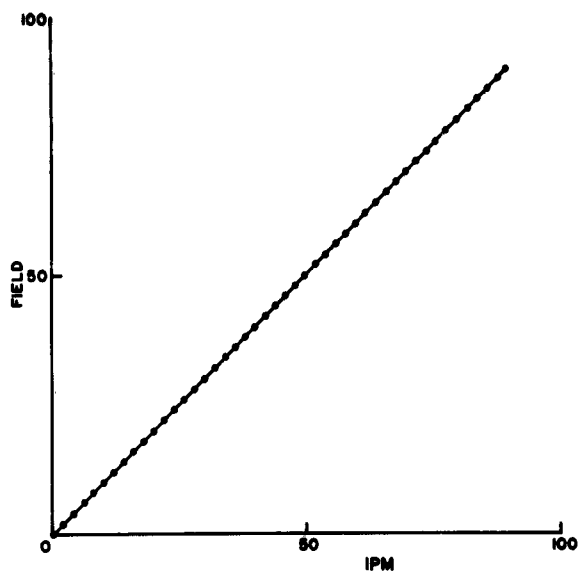


Figure 5. Field versus Model Comparisons, Theoretical Considerations  
Perfect Model

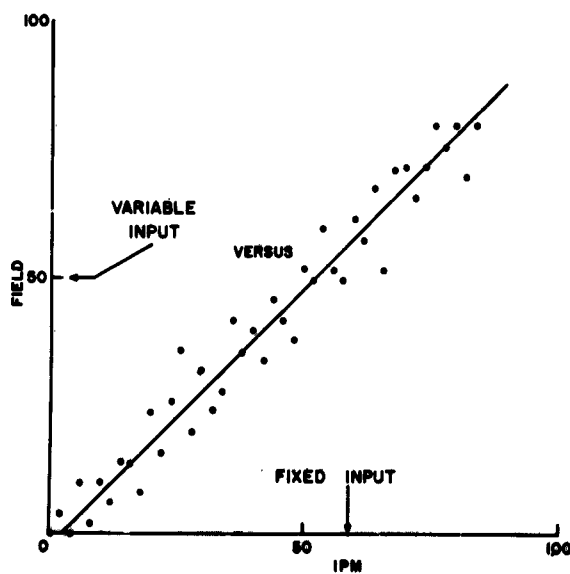


Figure 6. Field versus Model Comparisons, Theoretical Considerations  
Effect of Fixed Model Inputs

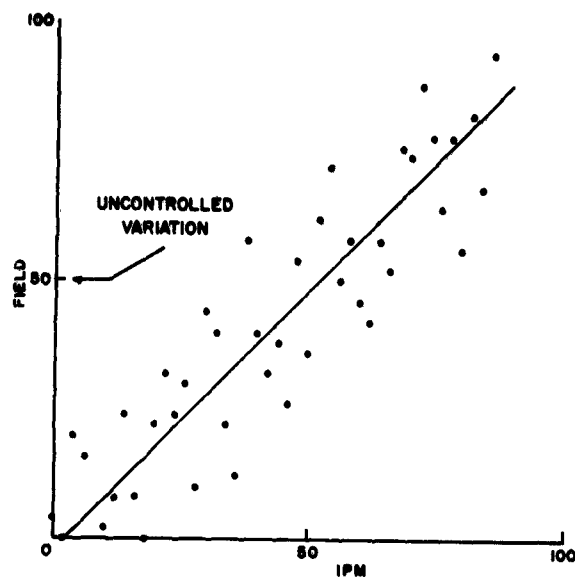


Figure 7. Field versus Model Comparisons, Theoretical Considerations  
Uncontrolled Field Variation

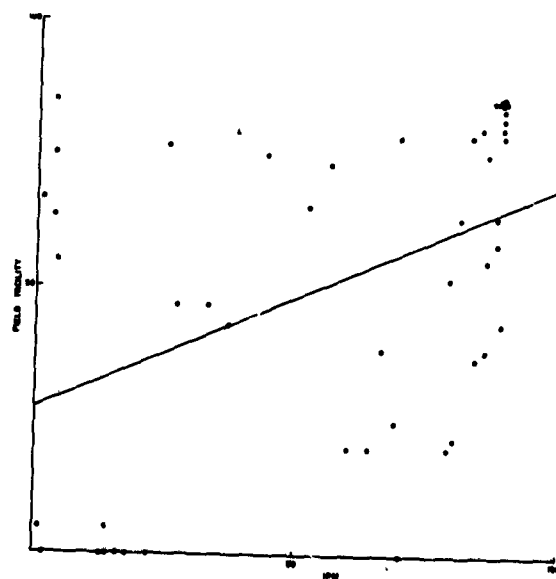


Figure 8. Field versus Model Comparisons - Actual Results  
Based on Critical Distances



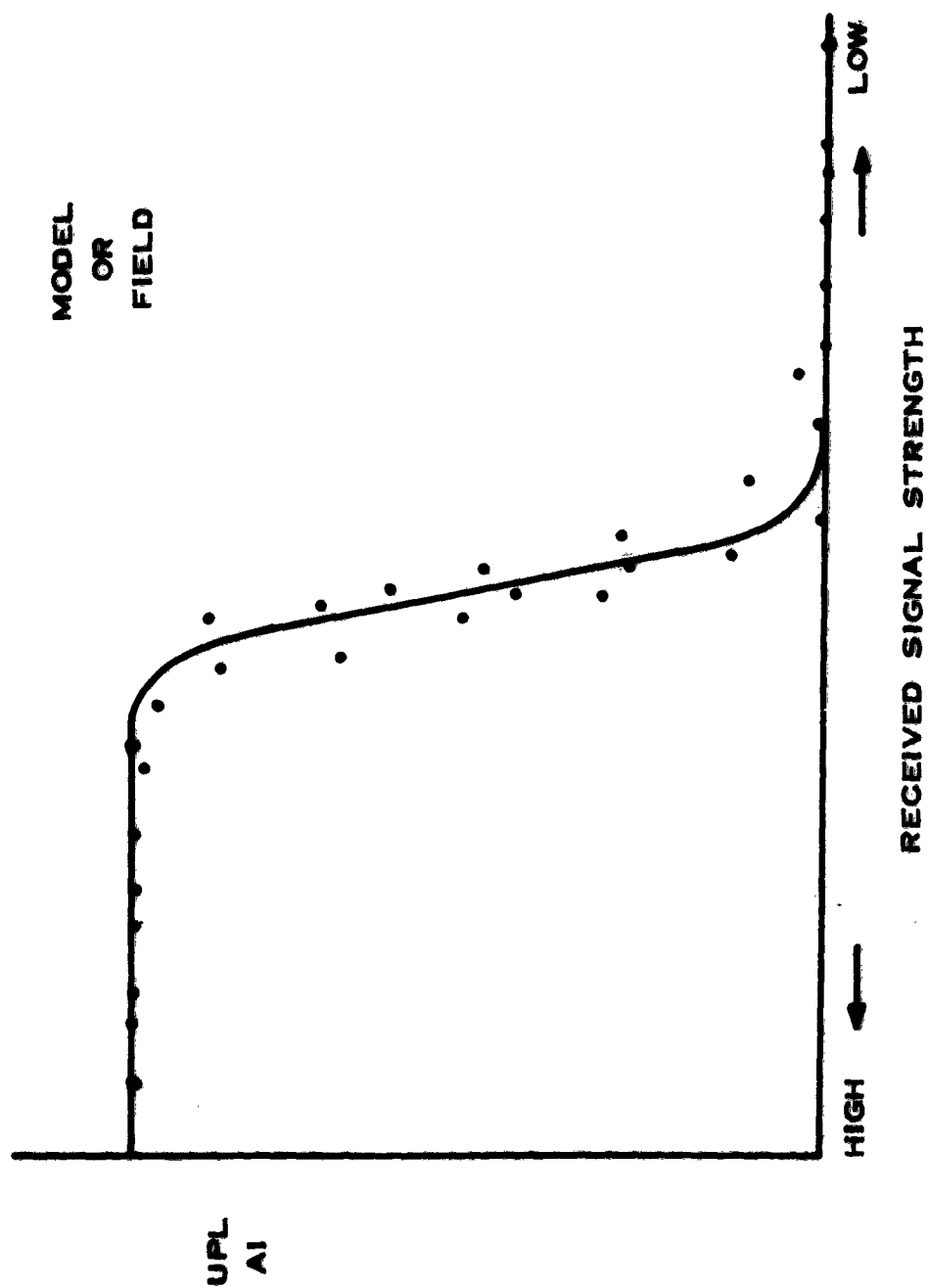


Figure 9. Upper Performance Limit Articulation Index versus Received Signal Strength

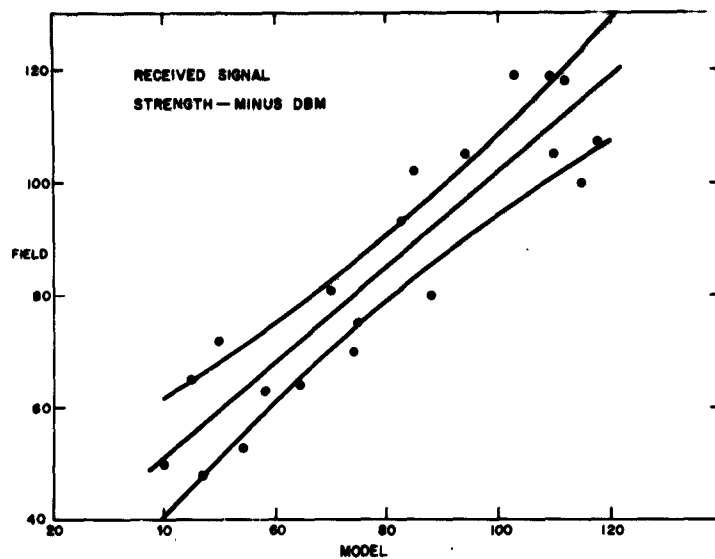


Figure 10. Received Signal Strength, Regression of Field Readings against Model Readings

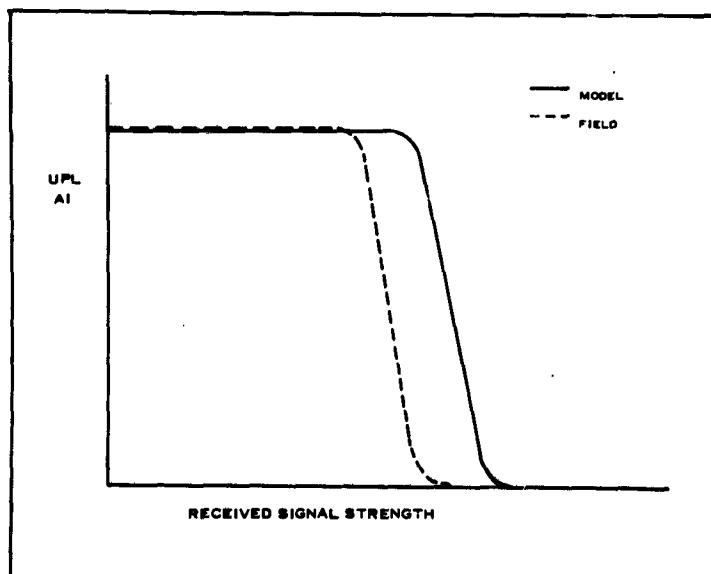


Figure 11. Upper Performance Limit Articulation Index versus Received Signal Strength for Model and Field

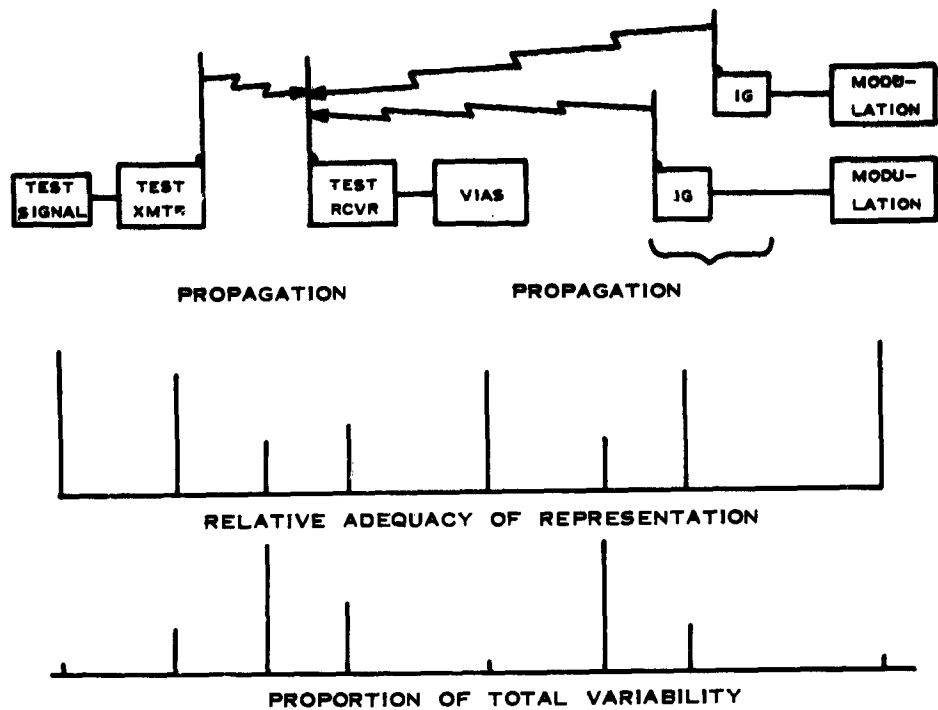


Figure 12. Developmental Model Validation by Modules (LPL)

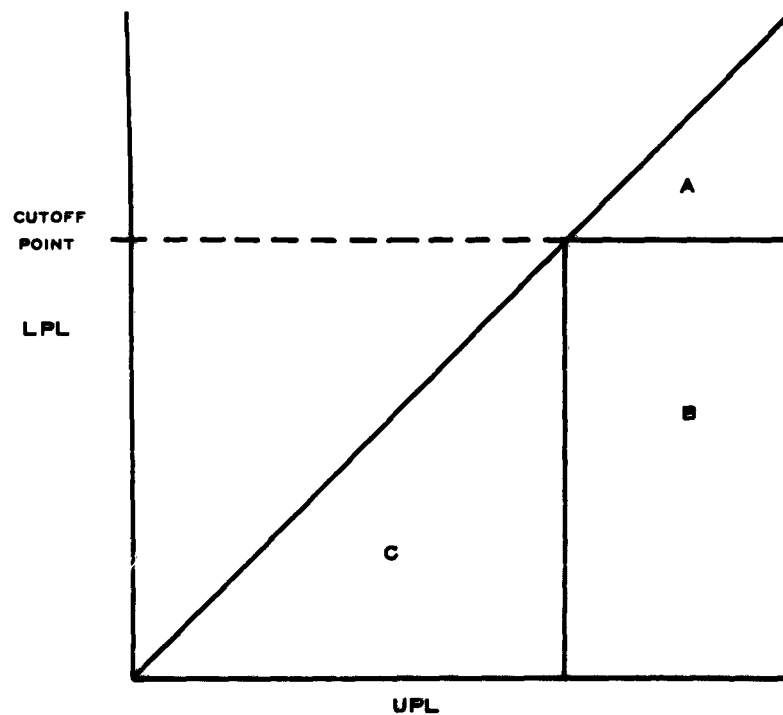


Figure 13. Graphical Application of Minimum Intelligibility to Validation

## **A WIDE STOP-BAND FILTER FOR A HIGH POWER S-BAND RADAR**

**J. P. Rooney**  
General Electric Company  
Palo Alto, California

**F. P. Ventolieri**  
Rome Air Material Area  
Rome, New York

**Abstract.** - The AN/FPS-6 is a high power S-band radar which emits high levels of spurious power at microwave frequencies. These emissions have, on occasion, hindered its application in areas of high radar and communication link density. The spurious outputs occur at harmonic frequencies and at frequencies just above and below the operating band. As a result, interference with several systems at the same time is possible.

The solution to this problem is a filter system capable of suppressing all of these outputs. Heretofore, high-power radar filters have been developed which attenuate a particular troublesome spurious output, such as a single harmonic frequency. The filter system described is the first to suppress all of the significant spurious microwave power.

It consists of five filter components of three different types. The choice of filter types to provide sufficient stop-band attenuation is described. The influence of environment, peak power requirements, and available space on the filter system design is shown.

The filter passed acceptance tests, which included low-power laboratory measurements of stop-band attenuation and far-field measurements after installation in an operating radar. In the laboratory measurements, attenuation in two modes was greater than 80 db over most of the stop band. In the far-field tests the filter system reduced much of the spurious signals to an undetectable level which was as much as 60 db below the levels observed without the filter system. In conclusion, it is believed that the filter system will permit interference-free operation of the FPS-6 radar in almost any radio frequency environment.

### **I. INTRODUCTION**

The AN/FPS-6 height-finding radar (Figure 1. - Outside view of temperate tower installation of FPS-6) is a very widely used set. The transmitting tube is a magnetron. Magnetrons have been shown to have many spurious outputs.<sup>1</sup> Measurements of the third harmonic output have shown levels about 30 db below the fundamental power, while the second harmonic can be 35 to 50 db below the fundamental. In addition, significant nonharmonic outputs have been observed close to the fundamental operating band. Under the various conditions of FPS-6 operation, it is conceivable that other spurious outputs can occur which could be detected by a sensitive receiver.

Since the AN/FPS-6 is a high-power radar and is usually operated in conjunction with other radars and with microwave communication systems, these spurious outputs represent a source of interference which can seriously degrade the performance of a radar complex. The method chosen by Rome Air Material Area to overcome this problem was to specify a filter to reduce all of the spurious outputs to a low level at the source of interference. Two filters were to be constructed for use at an operational installation.

The electrical design goals that were specified for the filter are shown in Figure 2.

#### Stop Band

Frequency ranges:	DC to 2700 Mc 2900 to 14,000 Mc
Attenuation	60 db minimum (as observed in the far-field)

#### Pass Band

Frequency range	2700 - 2900 Mc
VSWR (max.)	1.15
Insertion loss (max.)	0.15 db
Peak power (min.)	5 mw
Average power (min.)	5 kw

Figure 2. Electrical design goals

The 5 mw peak power is perhaps the highest operating power level of all radars utilizing WR-284 waveguide. It was a most important consideration in the design of the filter, since the filter had to permit breakdown-free operation of the radar with load VSWRs that could be as high as 1.5. Designing "splatter" filters that would provide high attenuation close to the operating band was expected to be difficult at this power level.

The mechanical design goals were simply that the filter should be suitable for the temperate tower AN/FPS-6 installations without hindering the operation or maintenance of the radar, capable of withstanding the operating and environment conditions, and also capable of withstanding the system waveguide pressure of 45 psi (absolute). Ease of installation, not involving rearrangement of the radar components, was an implied design goal.

## II. OVER-ALL DESIGN

### A. GENERAL CONSIDERATIONS

The design goals just discussed posed several basic problems which required an integrated solution. These problems are tabulated in Figure 3.

1. Achieving high attenuation over a wide stop band, including frequencies adjacent to the pass band.
2. Meeting the high peak power requirements.
3. Achieving the desired low VSWR in the pass band.
4. Overcoming space limitations in the radar installation.
5. Achieving the desired low attenuation in the pass band.

Figure 3. Basic design problems

In almost every type of filter, the total attenuation at a given stop band frequency is a direct function of filter length. When there are several frequencies to be attenuated, that is, when the stop band is wide, the over-all filter length increases further. The use of several component filters of different types appeared necessary to provide the wide stop band.

The high peak power level of 5 Mw precluded consideration of several filtering techniques which provide high stop-band attenuation per unit length but also have relatively low power handling capacity. From the beginning it appeared that waffle-iron filters would not be suitable for attenuating harmonic outputs because of this shortcoming.

Achieving a low VSWR over a fairly wide pass band in a long transmission line requires that discontinuities and junctions be matched at or near their effective terminal planes. The high peak power of the AN/FPS-6 requires further that the discontinuities, and also the obstacles required to match them, have small reflection coefficients in order to avoid high electric fields due to resonances. This implies that the discontinuities inherent in the design of filter components be kept as small as possible and that transmission line filters of unequal impedances be joined by means of gradual transitions. Solution of the first three basic problems requires that the filter be quite long.

Opposed to this requirement is the space limitation in the radar shelter. The waveguide run to be replaced by the filter is only about nine feet long. From the outset it was doubtful that the desired attenuation characteristics could be achieved in that length. It was anticipated, therefore, that the filter system would be convoluted, further increasing the total length because of the waveguide bends. In designing the filter components, length limitations would have to be considered and a judgment be made as to location and space allocation of each component.

The need for a long filter system to attain the desired stop-band attenuation characteristic obviously makes it difficult to achieve the desired low attenuation in the pass band. The nine feet of waveguide to be replaced by the filter system has an approximate theoretical attenuation of 0.1 db. The attenuation of the filter components would be about twice that of waveguide. If the filter system were to be 30 feet long, of which 20 feet would be taken up by filter components, the total attenuation of the system would be about 0.5 db, which is an increase of 0.4 db over the unmodified radar system.

Consideration of the basic problems dictated, therefore, that the filter system would have the following features: It would consist of several filter sections connected by bends; the various filter sections would have lengths appropriate to the stop-band attenuation required of each and compatible with the length and space limitations of the radar shelter; each section would have a low VSWR; and each section would be designed to transmit the full peak power of the radar without breakdown and with lowest attainable attenuation.

## B. MECHANICAL DESIGN

The temperate tower installation of the AN/FPS-6 allowed very little room for a filter. A clear volume approximately 4 feet high and 3 feet wide and deep was available above the r-f unit, which contains the duplexer and is a point of electrical attachment for the filter. It was also observed that the tower shook when the antenna changed position abruptly.

Electrical considerations dictated that four or five filter components would be required. The simplest configuration permitting the probable required lengths of filter components consisted of four bends and five straight sections. (Figure 4. --Filter configuration.) This figure shows the outlines of the filters actually developed for this configuration. The lengths of the

filter components were determined by the radii of the bends required for safe power handling capacity and low VSWR, and by appropriate clearances. These factors resulted in lengths of 36 inches or 55 inches for the first five sections. Section VI, which goes through an opening in the shelter roof, was made 55 inches long. Flexible waveguides were planned both for alignment and to permit some relative movement between the r-f unit and the filter. This configuration required no rearrangement of radar components other than waveguide.

The mounting of the filter posed some problems because of the limited floor area near the r-f unit. The implicit requirement of unimpaired access to the radar system components precluded a floor mounting of sufficiently wide base to withstand the apparent horizontal accelerations. The ceiling I-beams, however, offered convenient attachment points for clamps which would not require any drilling or alteration of the tower structure. The locations of cables, switches, lamps, fans, and other easily overlooked items were taken into account in the design of the filter and its supporting structures.

### C. ELECTRICAL REQUIREMENTS

There are two distinct frequency regions to consider when choosing and designing waveguide filter components:

- (a) The region where only the dominant ( $TE_{10}$ ) mode propagates
- (b) The region where propagation can occur in two or more modes.

These regions are shown in Figure 5, together with the design attenuation curves. In the dominant mode region, filters can be designed that are based primarily on transmission line or lumped-constant filter theory. In the multimode region leaky-wall filters based primarily on electromagnetic propagation principles are appropriate. Since waveguide is in itself a high pass filter, the design goal of high attenuation from dc to the dominant mode cut-off at 2078 Mc is already achieved by the system waveguide. The dominant mode region extends from 2078 Mc to 4156 Mc, the cut-off frequency of the  $TE_{20}$  mode. The spurious outputs of the FPS-6 magnetron within this range are frequently described as "splatter." This term is used as a broad classification adjective for filters designed to provide attenuation in this region.

Figure 5 shows how it was planned to achieve the desired stop-band attenuation by adding the attenuation characteristics of the various filter sections. The attenuation curves are expected characteristics of the filters when measured at low power and are based on preliminary models of the splatter filters and typical characteristics. In the multimode range these measurements are customarily performed in the  $TE_{10}$  and  $TE_{01}$  modes. There have been instances where the filter attenuation in this region, as measured in the far-field of an antenna, has been considerably less than the value obtained in low-power tests. For this reason it was endeavored to design the filter system so that the curve representing the summation of the low-power characteristics of the individual filter sections would have as great a value as possible, even exceeding the 60-db requirement. Two methods of achieving high attenuation near the pass band were considered:

- (a) An evacuated bandpass filter of the direct-coupled cavity type
- (b) Separate high-pass and low-pass filters whose cut-off frequencies bracket the pass band.

Approach (a), the evacuated bandpass filter, was carried as far as construction of a prototype, but considerations of maintaining the vacuum and difficulty in achieving the desired low VSWR led to its abandonment. Designs for high-pass and low-pass filters that could provide high attenuation close to the pass band while carrying the fundamental power without the use of pressure barriers or branching were carried to completion as usable filters.

The various sections developed for the filter system are described below, referring to Figures 4 and 5.

Section I. A low-pass reactive filter to provide high attenuation from 3100 Mc to approximately 3800 Mc. Its design is an extension of work by Rizzi.<sup>2</sup> The cavities are made of waveguides which are cut-off to pass band frequencies. They are a quarter-wavelength long at closely spaced frequencies in the stop band, so they present high series impedances at these frequencies, thereby reflecting the stop-band energy. The cavities are quarter-wavelength apart at mid-pass band frequencies so as to achieve a good match. This type of filter has inherently good power handling capacity.

Section II. A low-pass leaky-wall filter to provide high attenuation from 3700 Mc to approximately 6500 Mc. Leaky-wall filters<sup>3</sup> consist of a multiplicity of small secondary terminated waveguides connected to the primary waveguide by individual coupling slots. The secondary waveguides are cut-off to the pass band, but permit the higher frequencies to enter and be absorbed. Leaky-wall filters are usually designed to attenuate harmonic frequencies; Section II, however, represents an extension of this technique downward into the dominant mode region. Care had to be exercised to prevent absorption or reflection of passband energy. The section, and the other leaky-wall sections, used full height waveguide as the primary waveguide. The high peak power prevented consideration of reducing the primary waveguide height to achieve higher attenuation.

Section III. A low-pass leaky-wall filter to provide high attenuation in the third harmonic range and significant attenuation at higher frequencies. The filter had a low intrinsic VSWR and insertion loss in the passband and demonstrated satisfactory power handling capability.

Section IV. A second harmonic leaky-wall filter of standard design (General Electric Type MPF-2501) to provide high attenuation at the second harmonic and to contribute to the attenuation of higher frequencies.

Section V. A 36-inch-long waveguide spacer.

Section VI. A reduced-width-waveguide high-pass filter to provide high attenuation below 2600 Mc. The center section of this filter is a length of waveguide whose cut-off is only a few percent below the pass band. The proximity of cut-off to the pass band is limited by the increased insertion loss and reduced power handling capacity. The high impedance of the center section is matched to the system waveguide impedance by the long tapered waveguides at each end.



### III. EVALUATION

#### A. GENERAL

Acceptance testing of the filter consisted of low-power laboratory measurements of pass-band VSWR and insertion loss and stop-band attenuation, and of performance tests in an operating AN/FPS-6 radar. The test methods were described by Stone and Ventolieri at last year's Electromagnetic Capability Conference.<sup>4</sup> The operational tests were performed first because late arrival of waveguide components did not permit laboratory assembly of the filter system prior to the rather rigidly scheduled operational test date.

#### B. PERFORMANCE TESTING IN OPERATIONAL AN/FPS-6 RADAR

Briefly, these tests consisted of measuring the spurious outputs of the transmitter at a point in the far-field, installing the filter, and remeasuring the spurious outputs at the same point in the far-field. The results of these tests are shown in Figure 6. It can be seen that the third harmonic output of the transmitter was decreased by at least 36 db. Higher attenuation could not be demonstrated because the emitted signal level was not sufficiently higher than the minimum detectable level. The filter demonstrated high attenuation at two "splatter" frequencies: 51 db at 3215 Mc and at least 70 db at 2505 Mc.

No breakdowns were noted in the course of the testing, nor was there any indication of excessive filter VSWR.

#### C. LOW-POWER LABORATORY TESTS

Both filter systems built for delivery were fully tested in the laboratory. The pass band VSWR of serial number 1 varied between 1.38 and 1.04. At the low end of the band this could be attributed in part to the 1.22 VSWR of the reduced-width-waveguide high-pass filter. However, at other frequencies in the pass band, the high VSWRs which were encountered were due to the algebraic summation of the small reflections from several components. It was undertaken to match each of the other filter components to a maximum VSWR of 1.08. When this was achieved, the filter was reassembled and found to have a maximum VSWR of 1.29, as shown in Figure 7. The second filter assembly had a maximum VSWR of 1.34 after matching of individual components. The pass band insertion loss of both filters varied between 0.51 db and 0.71 db. This is somewhat higher than the 0.5 db that was originally estimated, but it must be kept in mind that there are 13 choke joints in the assembled filter and that the bends and flexible waveguides probably contribute slightly more loss than equivalent lengths of straight waveguide. The stop-band attenuation of the first filter assembly, shown in Figure 8, is typical of both assemblies. The attenuation in the dominant mode region was later shown to be as high as 100 db, as shown by the dotted curve.

### IV. CONCLUSIONS

This work resulted in the delivery of two filter systems which demonstrated high attenuation of most of the spurious outputs of the AN/FPS-6. This attenuation was more than 60 db from dc to 2550 Mc and from 3150 to 10,000 Mc, as measured in the laboratory. Field tests tended to confirm these measurements. Satisfactory high power operation was demonstrated without the use of pressure barriers or parallel branching circuits.

AN nomenclature was assigned to these filters and their components. Two systems installed at a critical site have been operating for almost five months. Figure 9 shows the filter components as they appeared when disassembled prior to packing and shipping.

Applications of these filters permits operation of the modified radars with a high degree of assurance that they will not be a source of microwave interference to the systems with which they are normally operated, or to other systems that could be affected by high level spurious outputs.

#### ACKNOWLEDGMENTS

This work was carried out on ROAMA Contract AF30(635)-28622-62-5. R. Z. Gerlack and R. H. Stone of the General Electric Company participated in the design and testing of the filters. The operational tests were performed by personnel of the Western Region Headquarters of the Ground Electronics Engineering-Installation Agency.

#### REFERENCES

1. K. Tomiyasu, "On Spurious Outputs from Pulsed Microwave Tubes and Their Control," IRE Transactions on Microwave Theory and Techniques, Vol. MTT-9 No. 6, Nov. 1961, pp. 480-484.
2. P. A. Rizzi, "Microwave Filters Utilizing the Cutoff Effect," IRE Transactions on Microwave Theory and Techniques, Vol. MTT-4 No. 1, Jan. 1956, pp. 36-40.
3. V. G. Price, R. H. Stone, V. Met, "Leaky-Wall Filters for Harmonic Suppression," WESCON Convention Record, Aug. 1959.
4. R. H. Stone, F. P. Ventolieri, "Operational System Performance of a High Power Harmonic Filter," Proceedings of the Eighth Tri-Service Conference on Electromagnetic Compatibility, Oct. 1962.



Fig. 1. Outside view of temperate tower installation of FPS-6 radar.

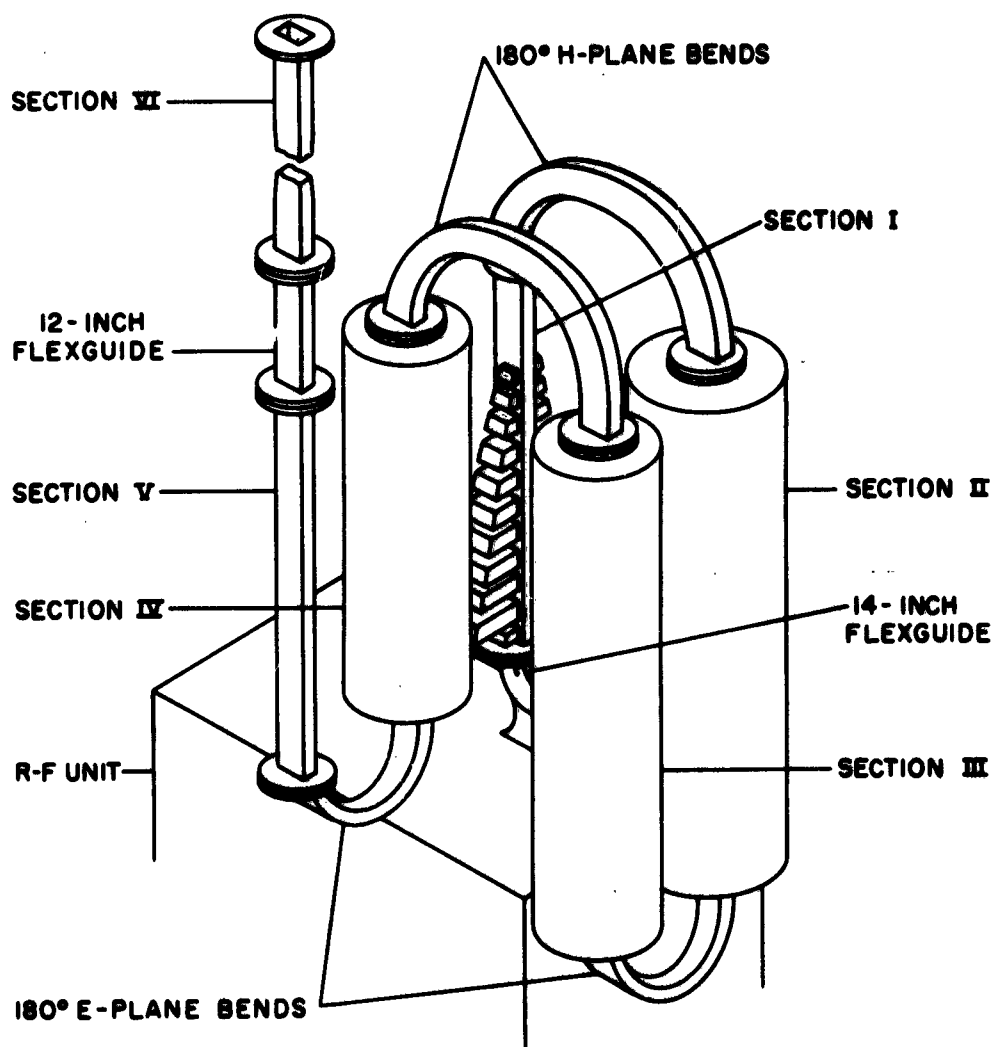


Fig. 4. Filter configuration.

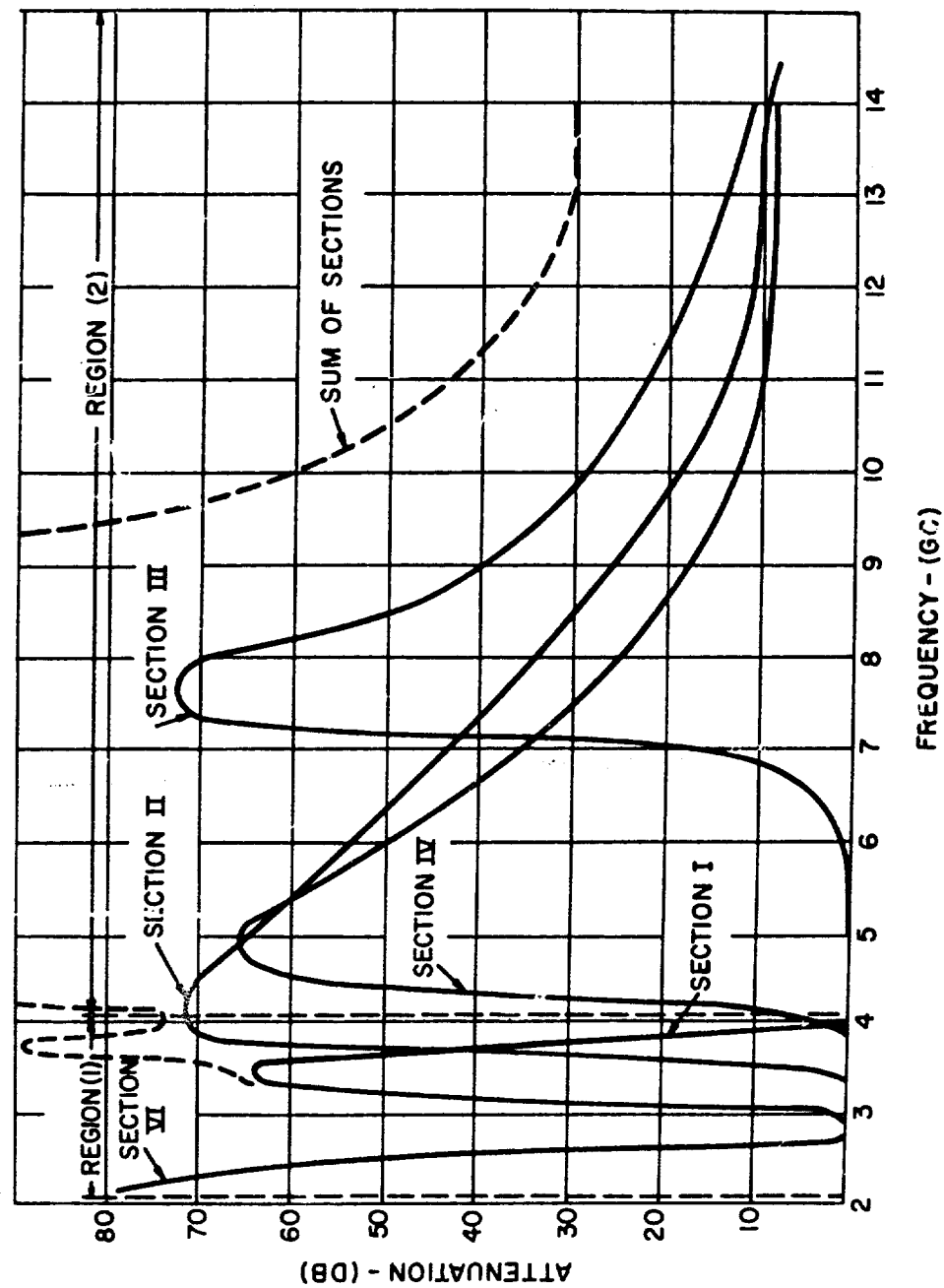


Fig. 5. Design attenuation of filter system.

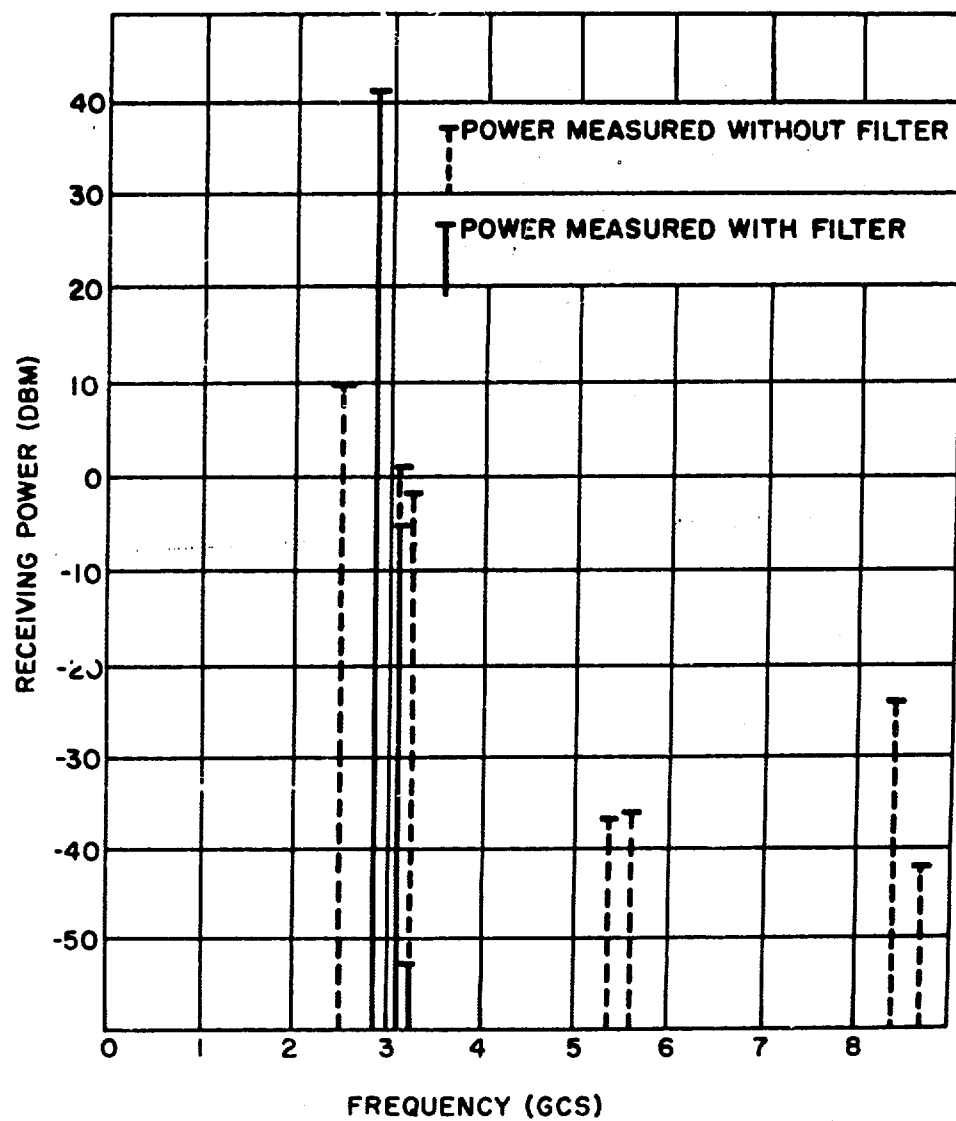


Fig. 6. Power level of fundamental and spurious frequencies radiated by AN/FPS-6 radar set, with and without filter assembly.

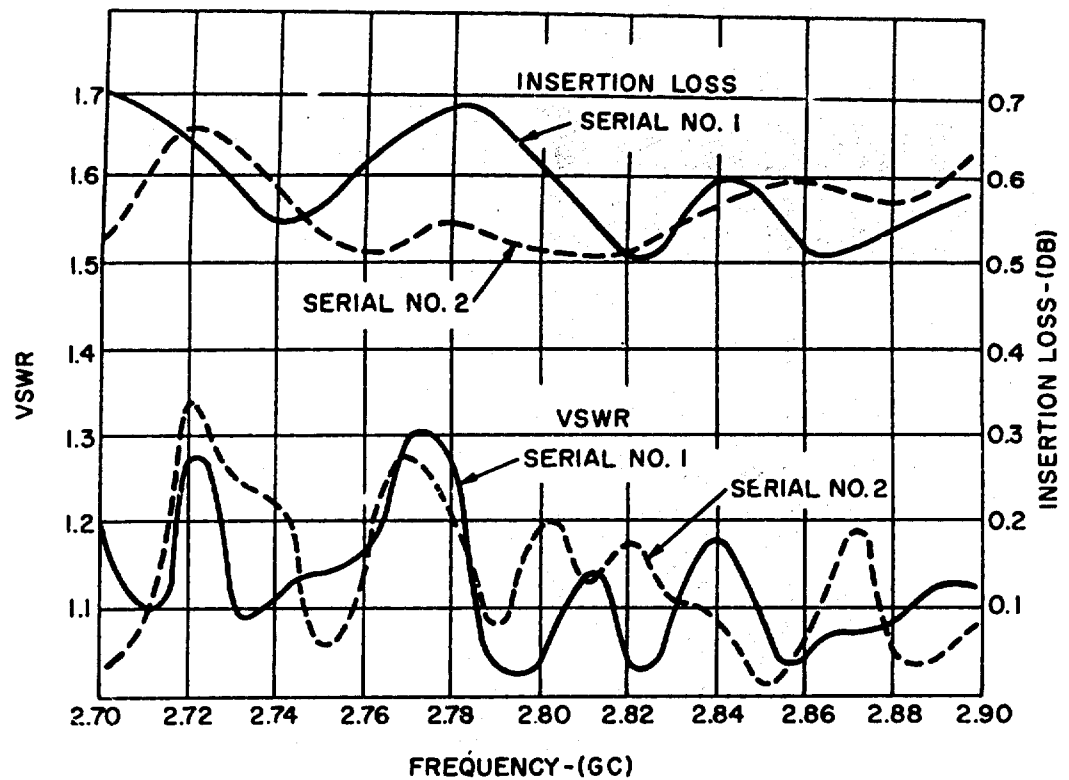


Fig. 7. Pass-band characteristics of FPS-6 filters -- (MPF-2509, serial nos. 1 and 2).

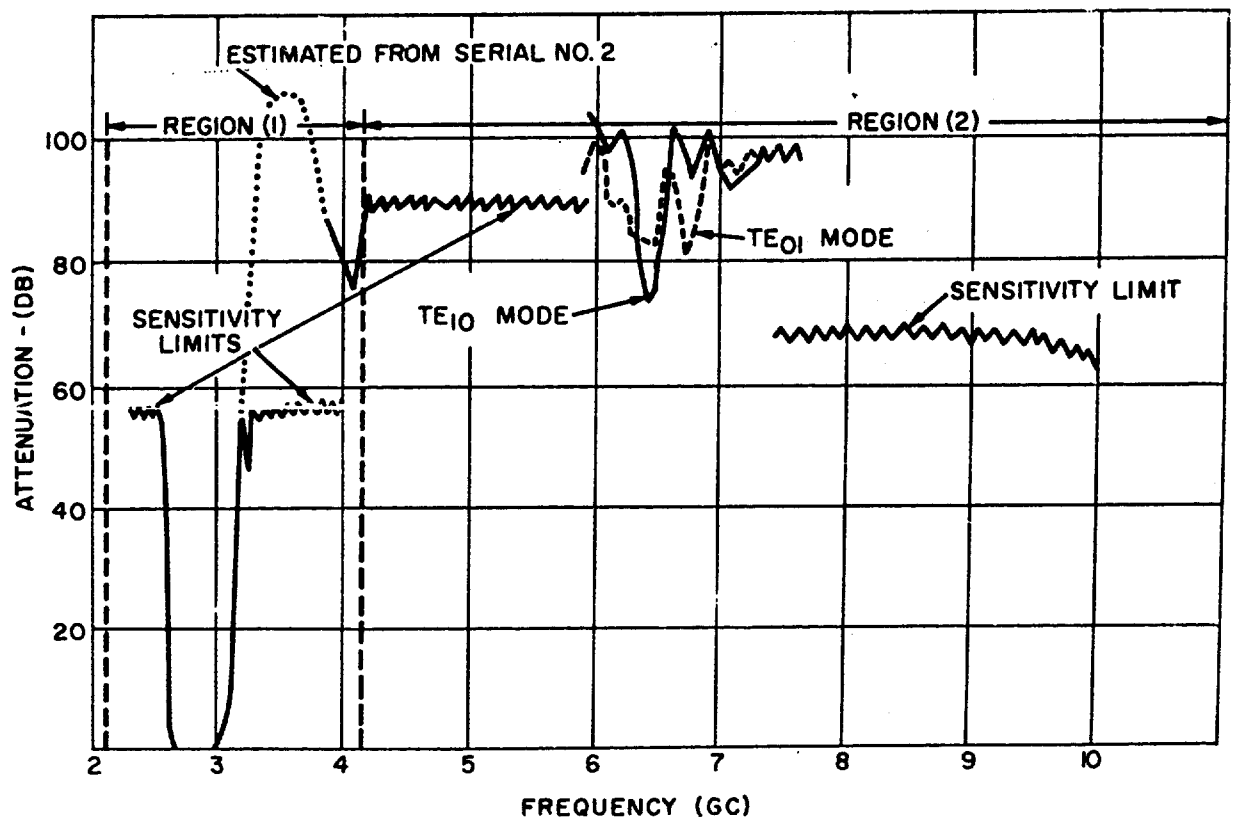


Fig. 8. Stop-band attenuation of first filter kit (for AN/FPS-6 radar), measured at low power in  $TE_{01}$  modes.

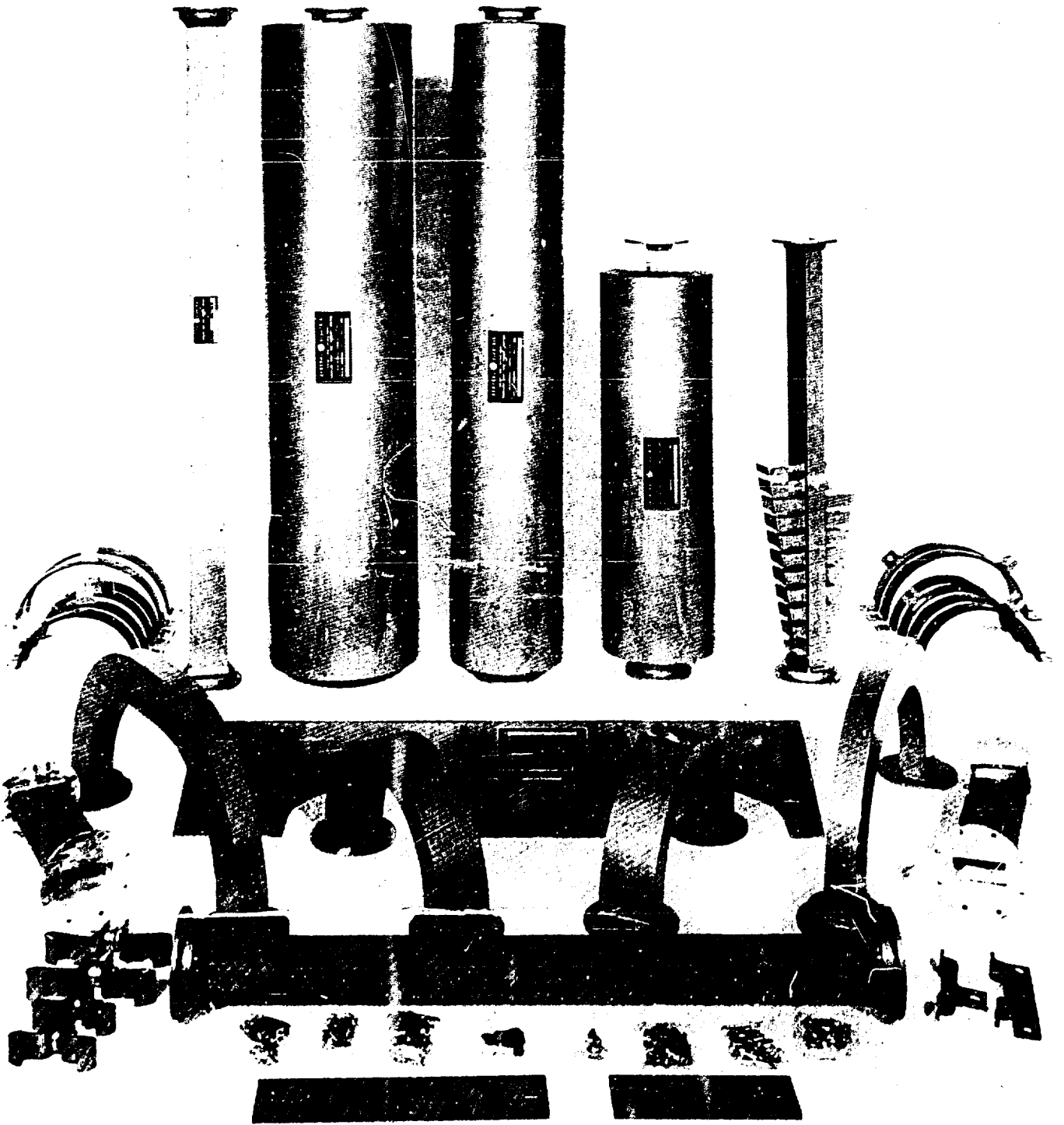


Fig. 9. MPF-2509 filter kit (Filter Assembly, electrical F-813/FPS-6).



A TECHNIQUE FOR DETERMINATION OF FILTER INSERTION LOSS  
AS A FUNCTION OF ARBITRARY GENERATOR AND LOAD IMPEDANCE

S. M. Vakil \*  
The Boeing Company  
Seattle, Washington

Abstract - Insertion loss is derived in terms of generator impedance, load impedance and filter open-circuit and short-circuit impedances. This expression contains a difference term which places great weight on the accuracy with which the filter's impedances are measured. It is shown that the use of this difference term can be avoided by introducing the filter's insertion loss in a circuit with known generator and load impedances. The resulting exact expression contains terms which are easily measurable with sufficient accuracy to provide reliable insertion loss values for the filter for any combination of generator and load impedances. Also shown is a simplified approximate expression for insertion loss which is applicable in a filter's attenuation band. A discussion of experimental verification of the expressions is followed by curves showing application of the approximate insertion loss expression to a particular filter.

I. INTRODUCTION

The insertion loss of a filter depends on the generator and load impedances associated with the filter as well as the characteristics of the filter. Simple relations which can be used to calculate a filter's insertion loss can be expressed in terms of generator and load impedances and directly-measurable filter characteristics. It will be found that such expressions contain an unavoidable difference factor involving two quantities which tend toward becoming equal in a filter's attenuation band. This places great emphasis on the accuracy with which the measurements are made. It is possible to substitute a filter insertion loss measurement for the critical difference measurement to secure an expression for insertion loss which relies only on filter parameters which can easily be measured with sufficient accuracy to provide reliable results. The following discussion shows how measured filter impedance data and insertion loss data measured in accordance with MIL-STD-220A can be used to calculate a filter's insertion loss for operation between arbitrary generator and load impedances.

II. INSERTION LOSS FORMULATION

Insertion loss of a filter operating between two impedances  $Z_G$  (source) and  $Z_L$  (load) is defined as: \*\*

$$P = \text{Insertion loss} = 20 \log \frac{E'_2}{E_2} = 20 \log \frac{I'_2}{I_2} \quad (1)$$

Where  $E_2$  and  $I_2$  are the voltage and current on the load side and  $E'_2$  and  $I'_2$  are the corresponding voltage and current that would be obtained if the filter were replaced by a direct connection (Figure 1).

\* Now with Lockheed Missiles & Space Co., Div. of Lockheed Aircraft Corp.

\*\* See References 1 and 2.

Appendix I expands equation (1) in terms of filter parameters,  $Z_G$ , and  $Z_L$ . The filter parameters are obtained by measuring the open-circuit and short-circuit impedances at the input and output terminals of the filter. The following form of insertion loss equation which is in terms of open-circuit and short-circuit impedances is of particular interest.

$$P = 20 \log AB = 20 \log \frac{Z_{o2}}{\sqrt{Z_{o1} (Z_{o2} - Z_{s2})}} \cdot \frac{Z_G + \frac{Z_G Z_L}{Z_{o2}} + Z_{s1} + \frac{Z_L Z_{o1}}{Z_{o2}}}{Z_G + Z_L} \quad (2)$$

The form of equation (2) indicates that the insertion loss relation is composed of two separable factors A and B, where

$$A = \frac{Z_{o2}}{\sqrt{Z_{o1} (Z_{o2} - Z_{s2})}} \quad (3)$$

$$B = \frac{Z_G + \frac{Z_G Z_L}{Z_{o2}} + Z_{s1} + \frac{Z_L Z_{o1}}{Z_{o2}}}{Z_G + Z_L} \quad (4)$$

Both are functions of filter parameters; A is a function of filter parameters only, while B is a function of  $Z_G$  and  $Z_L$ , in addition to the filter parameters. B is not, however, a function of the difference term  $(Z_{o2} - Z_{s2})$ . The open-circuit and short-circuit impedances  $Z_{o1}$ ,  $Z_{o2}$ ,  $Z_{s1}$ , and  $Z_{s2}$ , can be measured easily by conventional bridge or slotted line techniques. The measurement allows for computation of B for a particular value of  $Z_G$ , and  $Z_L$ . The factor A can also be calculated if the measurement accuracy is high enough so that the difference  $(Z_{o2} - Z_{s2})$  is greater than the errors inherent in bridge or slotted line measurements. In cases where the measurement of insertion loss in the attenuation band is desired, the short and open circuit impedances at either terminals become nearly the same and no distinction is possible between the values of  $Z_{o2}$  and  $Z_{s2}$  by slotted line or bridge techniques. In order to avoid reliance on the difference between impedance measurements in the attenuation band, the MIL-STD-220A measurements may be used to omit the direct calculation of the factor A in the insertion loss equation.

### III. EXACT EXPRESSION FOR INSERTION LOSS IN TERMS OF MEASURABLE QUANTITIES

Let  $P'$  be the measured insertion loss for a filter in a 50 ohm system and let  $B'$  be the value of B with  $Z_G = Z_L = 50$  ohms. The following relations are evident:

$$P - P' = 20 \log AB - 20 \log AB' = 20 \log \frac{B}{B'} \quad (5)$$

and

$$P = P' + 20 \log \frac{B}{B'} \quad (6)$$

Expanding (6) by the use of equation (4) to evaluate B and B', we have

$$P = P' + 20 \log \frac{\left| \frac{Z_G + \frac{Z_G Z_L}{Z_{o2}} + Z_{s1} + \frac{Z_L Z_{o1}}{Z_{o2}}}{50 + \frac{2500}{Z_{o2}} + Z_{s1} + \frac{(50) Z_{o1}}{Z_{o2}}} \right|}{\left| \frac{Z_G + Z_L}{100} \right|} \quad (7)$$

Thus, the critical difference measurements necessary for evaluating A are avoided and the insertion loss P can be calculated from  $Z_G$ ,  $Z_L$ ,  $P'$ ,  $Z_{o1}$ ,  $Z_{o2}$ , and  $Z_{s1}$  which must be supplied as functions of frequency. Equation (7) is exact in that no approximations have been used in its derivation. It should be noted that although equation (7) contains more independent variables than equation (2), it is not necessarily more difficult to evaluate, even in the filter's passband.

#### IV. APPROXIMATION FOR INSERTION LOSS IN TERMS OF MEASURABLE QUANTITIES

For the measurements made in the filter's attenuation band, it is possible to use an approximation for the factor B which is more convenient than the expression given in equation (4). This is done by noting that in the filter's attenuation band,  $Z_{o1}$  is approximately equal to  $Z_{s1}$  and  $Z_{o2}$  is approximately equal to  $Z_{s2}$ .

If the short circuit impedance  $Z_{s1}$  is replaced by  $Z_{o1}$ , in equation (4), we have an approximate form for factor B which we will call C; thus

$$C = \frac{Z_G + \frac{Z_G Z_L}{Z_{o2}} + Z_{o1} + \frac{Z_L Z_{o1}}{Z_{o2}}}{Z_G + Z_L} = \frac{(Z_G + Z_{o1})(Z_L + Z_{o2})}{Z_{o2}(Z_G + Z_L)} \quad (8)$$

Therefore, for calculation in the filter's attenuation band, the insertion loss equation becomes:

$$Q = P' + 20 \log \frac{C}{C'} = P' + 20 \log \frac{\left| \frac{Z_G + Z_{o1}}{50 + Z_{o1}} \right| \left| \frac{Z_L + Z_{o2}}{50 + Z_{o2}} \right|}{\left| \frac{Z_G + Z_L}{100} \right|} \quad (9)$$

Equation (9) shows that for approximate insertion loss measurement in the attenuation band of a conventional filter operating between impedances  $Z_G$  and  $Z_L$ , only  $P'$  and the open circuit impedances are needed. Q is used as the symbol for the approximate loss to indicate possible difference from P, which is an exact expression. The difference in P and Q for particular filters is a function of the difference between  $Z_{o1}$  and  $Z_{s1}$ ; it is also a function of frequency. It is not possible to state a percentage error resulting from the use of Q instead of P for evaluating the insertion loss of a filter; thus, if the best possible accuracy is required in the attenuation band of a filter, or if evaluation is desired

in a filter's passband, there is no alternative to measuring  $Z_{s1}$  along with  $Z_{o1}$  and  $Z_{o2}$  and then using equation (7) to evaluate P.

#### V. CONSIDERATIONS FOR EVALUATION OF THE INSERTION LOSS EXPRESSIONS

The impedances  $Z_G$ ,  $Z_L$ ,  $Z_{o1}$ ,  $Z_{s1}$ ,  $Z_{o2}$  and  $Z_{s2}$  used to evaluate the previous expressions for P and Q are those impedances seen looking outward from the filter terminals and those seen looking into the filter terminals when the opposite terminal pair is appropriately terminated. In particular,  $Z_G$  and  $Z_L$  are not necessarily the actual generator or load impedances but are those impedances seen at the filter terminals looking toward the generator and load. Elementary transmission-line theory shows that unless the generator and load impedances equal the surge impedances of the lines connecting them to the filter, the impedances seen looking from the filter terminals will vary with frequency and line length. In general, the impedances seen looking directly into the generator and load terminals will also vary with frequency.

The values of the open-circuit and short-circuit filter impedances are computed from bridge or slotted-line measurements. Such measurements are sensitive to transformation due to the phase constant of the line connecting the measurement instrument to the filter; thus the impedances computed should be those seen at the terminals of the filter.

The factor P' is the measured insertion loss of the filter in a 50 ohm system. The restatement of this definition is redundant and is included as a precaution to insure against erroneous results which can arise if MIL-STD-220A equipment is used improperly. Isolation attenuators used in certain MIL-STD-220A systems contain dc isolation capacitors which, used with the system's buffer networks, permit insertion loss measurements while the filter is operating at rated load current. These dc isolation capacitors cause the impedance of the attenuators to vary from the rated value of 50 ohms when operating below the rated frequency range. Thus, if such a system is used at frequencies below the specified lower-limit, the resulting insertion loss measurements will not be referenced to 50 ohms and will not yield accurate results if used as P' to evaluate equations (7) or (9). It is obvious from the derivation that 50 ohm generator and load impedances were used simply as a matter of convenience. The derivation can be carried out for any convenient pair of generator and load impedances where the insertion loss and the generator and load impedances can be measured.

As an item of interest, it will be noted that insertion loss is defined in MIL-STD-220A (reference 3) in terms of generator output voltage whereas traditionally it is defined in terms of load voltage or current (see reference 1). An expansion of equation (1) in terms of generator output voltage will yield an expression which is independent of generator impedance whereas expansion of equation (1) in terms of load voltage will yield equation (2). The requirement for isolation attenuators at the generator output and the load input makes the definition for insertion loss given in MIL-STD-220A approximately equal to the traditional definition given in reference 1.

## VI. EXPERIMENTAL VERIFICATION

A series of tests were conducted on two filters to verify the validity of the expression for  $Q$  for various generator and load impedance pairs. The impedances were limited to real values and the frequency coverage was limited to the range between 60 kilocycles and 150 kilocycles due to the difficulty in maintaining constant impedance at higher frequencies. The generator and load impedance pairs tested were (in ohms) 5.2 K, 50; 600, 50; 25, 50; 50, 25; 50, 600; and 50, 5.2 K. Five frequencies between 60 kilocycles and 150 kilocycles were measured for each pair. To evaluate  $Q$ , insertion loss was measured in a 50 ohm system and open-circuit impedance measurements were made at each frequency. The insertion loss measurements made between the various generator-load pairs differed from the calculated values for  $Q$  by less than 1.5 decibels in every case; in many cases, the agreement was within 0.5 decibel. One filter was tested in the frequency range between 2 megacycles and 10 megacycles using a 600 ohm signal generator and a 50 ohm receiver as the load. The differences between the measured values of insertion loss and the calculated values of  $Q$  were less than 2.0 decibels in the entire frequency range.

The magnitudes of the impedances tested cover a range in excess of 100 to 1 and the calculated results are in close agreement with the measured results. The results of these tests can be found in Boeing Document D2-11833 which has been released for ASTIA distribution.

## VII. AN EXAMPLE OF INSERTION LOSS MEASUREMENT AND CALCULATION RESULTS

Following is an example of the results of measurement and calculations performed on a particular filter (Boeing Part Number F26E7). Figure 2 is a graph of the real part of the filter's terminal impedances, and Figure 3 is a graph of the corresponding reactive components. The filter's input short-circuit impedance components are given along with both the input and output open-circuit impedance components. This is to allow evaluation of the function  $P$  as well as  $Q$ .

Figure 4 gives the measured values of  $P'$  for the filter along with the Boeing specification limit for the filter in a 50 ohm system (designated  $P_m$ ). The calculated values for  $Q$  for  $Z_G$  set equal to 5 ohms and  $Z_L$  set equal to 1000 ohms appear on this same graph. Figure 5 repeats the values for  $P'$  and  $P_m$  for the filter and gives the function  $Q$  for  $Z_G$  set equal to  $5 + j230$  ohms and  $Z_L$  set equal to  $5 + j210$  ohms. These values were selected by trial and error in an effort to minimize the value of  $Q$  in the vicinity of 15 megacycles where  $P'$  goes through a minimum. It is noteworthy that for this generator-load impedance pair, the insertion loss,  $Q$ , is more than 30 decibels less than  $P'$  at many of the frequencies where  $Q$  was calculated.

## VIII. PRACTICAL NEED FOR WORST-CASE ANALYSIS

Anyone attempting to use equations (7) or (9) for evaluating the insertion loss of a filter will have little difficulty in determining complex open-circuit and short-circuit filter impedances over the frequency range up to 400 megacycles; however, determining generator and load impedances is quite another matter. Generally, it is difficult to secure design information about generator and load impedances in a filter's passband; securing similar

information in the filter's attenuation band is usually impossible since equipment designers are not concerned with impedance behavior outside the operating frequencies of their equipment. Moreover, the impedances of interference sources are difficult to analyze since their coupling paths to the sensitive circuits are frequently devious. This points toward the need for facilities for conveniently measuring the complex impedance of devices under dynamic conditions.

It has been suggested that a family of curves for a particular filter depicting P or Q for various  $Z_G$ ,  $Z_L$  pairs would be useful in the absence of specific values for  $Z_G$  and  $Z_L$ ; such a family of curves is not difficult to prepare if computer services are utilized, but it must be remembered that all the impedances in P and Q are complex and both P and Q are sensitive to variations in the phase angles of their constituents as well as variations in their magnitudes. Thus, a useful family of such curves would necessarily include a large population.

As one alternative to the use of measured values for the generator-load impedance pairs or the preparation of a family of curves for selected generator-load impedance pairs, one turns toward looking for a possible "worst-case" analysis. The question to be answered in such a worst-case analysis here is; "What values of  $Z_G$  and  $Z_L$  will give the lowest possible insertion loss when evaluating P or Q?"

Cursory inspection of the function Q shows that Q becomes infinitely negative for  $Z_G = -Z_{O1}$  or  $Z_L = -Z_{O2}$ . This represents a condition of infinite insertion gain. The same values inserted into P cause the ratio of B/B' to appear to go through a minimum but whether this causes P to take on positive or negative values is not apparent. Investigations carried out to date indicate that significant minimum values do not exist. These investigations have followed the traditional point of view that solutions which result when the derivatives of P or Q are equated to zero may reveal extreme values for the functions. Further investigation reveals whether the solutions describe minimum or maximum values or whether they describe saddle points. It is believed that useful worst-case analyses will result only under the condition that certain restrictions are imposed on the complex variables in the expressions for P and Q. Such restrictions could be based on physical realizability; for instance, restricting  $Z_{O1}$ ,  $Z_{s1}$ ,  $Z_{O2}$ , and  $Z_{s2}$  to positive-real complex functions is reasonable since the filters under consideration are linear, passive devices.

In order to be useful, a worst-case analysis would have to show that the filter's insertion loss has a minimum value which is positive. The existence of a negative minimum value would do little more than serve to remind the user that under certain conditions, filters can be used as matching devices. Thus, in the event it is ultimately proved that minimum values, if they exist, need not be positive, we will be permanently faced with the task of evaluating insertion loss on the basis of specified (or measured) values of  $Z_G$  and  $Z_L$ .

#### IX. ACKNOWLEDGEMENT

The work reported here was performed under Air Force Contract AF 04(647)-289.

## X. REFERENCES

1. Johnson, Walter C., Transmission Lines and Networks  
McGraw-Hill Book Co., New York, New York, 1950
2. Harvard Univ. Radio Lab. Series, Very High Frequency Techniques  
McGraw-Hill Book Co., New York, New York, 1947
3. MIL-STD-220A, "Filter Insertion Loss Measurements"
4. Shea, Richard F., Principles of Transistor Circuits  
John Wiley & Sons, Inc., New York, New York, 1953
5. Van Valkenburg, M. E., Introduction to Modern Network Synthesis  
John Wiley & Sons, Inc., New York, New York, 1960
6. Vakil, Sadegh M., "A Technique for Calculating the Insertion Loss  
Caused by a Filter Operating Between Arbitrary Impedances", D2-11833,  
The Boeing Company, Seattle, Washington, 1963

## APPENDIX I

### DERIVATION OF INSERTION LOSS EQUATION IN TERMS OF FILTER OPEN-CIRCUIT AND SHORT-CIRCUIT IMPEDANCES

The definition for insertion loss is traditionally stated in terms of load voltage or load current for a circuit in two different conditions. (Reference 1) The circuit consists of a generator, a filter, and a load, with insertion loss defined as follows:

$$\text{Insertion Loss} = P = 20 \log E_2'/E_2 = 20 \log I_2'/I_2 \quad (A)$$

where  $E_2$ ,  $E_2'$ ,  $I_2$  and  $I_2'$  are defined above in Figures (1a) and (1a'). The generator driving electromotive force  $E_G$  is held constant for both circuits.

There are several methods for expanding equation (A) in terms of filter parameters,  $Z_G$ , and  $Z_L$ . In particular, we are concerned here with expanding the ratio  $E_2'/E_2$  or  $I_2'/I_2$  in terms of the filter's parameters which are measurable at the filter's terminals. To do this, we will first express  $E_2'$  as a function of  $E_G$ ,  $Z_G$ , and  $Z_L$  and then express  $E_2$  as a function of  $E_G$ , filter parameters,  $Z_G$ , and  $Z_L$ . Next the ratio of the quantities will be formed and transformed into the desired final form in terms of  $Z_G$ ,  $Z_L$  and the filter's open-circuit and short-circuit impedances.

It is convenient to carry out this derivation in terms of the networks' generalized A parameters (reference 4). The circuit conventions used are shown in Figure B. The A parameters are defined by the relations:

$$V_1 = A_{11} V_2 - A_{12} I_2 \quad (B)$$

$$I_1 = A_{21} V_2 - A_{22} I_2 \quad (B')$$

If a load  $Z_L$  is connected between the terminals 2 and 2',  $I_2$  is the current through  $Z_L$  and  $V_2$  voltage across  $Z_L$ ; Therefore

$$V_1 = A_{11} V_2 + \frac{A_{12} V_2}{Z_L} \quad (C)$$

and, solving equation (C) for  $V_2$

$$V_2 = \frac{V_1 Z_L}{A_{11} Z_L + A_{12}} \quad (D)$$

We are interested in expressing  $E_2$  and  $E_2'$  in Figures 1A and 1A' in terms of  $E_G$  and the impedances in the circuits. To do this, we will consider  $Z_G$  to be the sole element in a four-terminal network interconnecting emf generator  $E_G$  to the load  $Z_L$ .

Writing network equations equivalent to equations (B) and (B') for the network in Figure C will show the A parameters for this network to be:

$$\begin{bmatrix} a_{11}' & a_{12}' \\ a_{21}' & a_{22}' \end{bmatrix} = \begin{bmatrix} 1 & Z_G \\ 0 & 1 \end{bmatrix} \quad (E)$$

Thus, from equations (D) and (E) we see that

$$E_2' = \frac{E_G Z_L}{Z_L + Z_G} \quad (F)$$

The relation above obviously could have been written at sight without resorting to A parameters; however, the technique's value will be demonstrated as networks become more complicated. Let us assume a filter with A parameters  $a_{11}$ ,  $a_{12}$ ,  $a_{21}$ , and  $a_{22}$  is connected as shown in Figure D

A network with parameters  $a_{11}''$ ,  $a_{12}''$ ,  $a_{21}''$ , and  $a_{22}''$  equivalent to the two given cascaded networks can be found simply by multiplying the A matrices of the cascaded networks in the proper order; thus,

$$\begin{bmatrix} a_{11}'' & a_{12}'' \\ a_{21}'' & a_{22}'' \end{bmatrix} = \begin{bmatrix} 1 & Z_G \\ 0 & 1 \end{bmatrix} \begin{bmatrix} a_{11} & a_{12} \\ a_{21} & a_{22} \end{bmatrix} \quad (G)$$

and

$$\begin{bmatrix} a_{11}'' & a_{12}'' \\ a_{21}'' & a_{22}'' \end{bmatrix} = \begin{bmatrix} a_{11} + Z_G a_{21} & a_{12} + Z_G a_{22} \\ a_{21} & a_{22} \end{bmatrix} \quad (H)$$



Equations (D) and (H) immediately yield the result

$$E_2 = \frac{E_G Z_L}{Z_L (a_{11} + Z_G a_{21}) + a_{12} + Z_G a_{22}} \quad (I)$$

The ratio of  $E_2'$  to  $E_2$  from equations (F) and (I) is

$$\frac{E_2'}{E_2} = \frac{Z_L a_{11} + a_{21} Z_G Z_L + a_{12} + Z_G a_{22}}{Z_G + Z_L} \quad (J)$$

Equation (J) gives the ratio in terms of  $Z_G$ ,  $Z_L$ , and the filter's A parameters. The filter parameters which are of greatest practical interest are its open-circuit and short-circuit impedances. Combining relations given in references (1), (4), and (5), the following relations can be formulated:

$$A_{12} = A_{22} Z_{s1} \quad (K) \qquad A_{11} = \frac{A_{22} Z_{o1}}{Z_{o2}} \quad (M)$$

$$A_{21} = \frac{A_{22}}{Z_{o2}} \quad (L) \qquad A_{22} = \frac{Z_{o2}}{\sqrt{Z_{o1} (Z_{o2} - Z_{s2})}} \quad (N)$$

where  $A_{xx}$  are the A parameters as defined above while  $Z_{o1}$  is the impedance seen at the filter's input terminal-pair with the output terminal-pair open.  $Z_{s1}$  is the impedance seen at the input terminal-pair with the output terminal-pair shorted.  $Z_{o2}$  and  $Z_{s2}$  are the impedances seen at the output terminal-pair when the input is first open and then shorted. (K), (L) and (M) combine with (J) to yield

$$\frac{E_2'}{E_2} = \frac{\frac{a_{22} Z_L Z_{o1}}{Z_{o2}} + \frac{a_{22} Z_G Z_L}{Z_{o2}} + \frac{a_{22} Z_{s1}}{1} + \frac{a_{22} Z_G}{1}}{Z_G + Z_L} \quad (O)$$

Factoring  $a_{22}$  from equation (O) and using the relation given in equation (N) we have the expression in terms of  $Z_G$ ,  $Z_L$ , and the filter's open-circuit and short-circuit impedances.

$$\frac{E_2'}{E_2} = \frac{Z_{o2}}{\sqrt{Z_{o1} (Z_{o2} - Z_{s2})}} \cdot \frac{Z_G + \frac{Z_G Z_L}{Z_{o2}} + Z_{s1} + \frac{Z_L Z_{o1}}{Z_{o2}}}{Z_G + Z_L} \quad (P)$$

Thus, the insertion loss expression in terms of  $Z_G$ ,  $Z_L$ , and filter open-circuit and short-circuit parameters is

$$P = 20 \log \frac{Z_{o2}}{\sqrt{Z_{o1} (Z_{o2} - Z_{s2})}} \cdot \frac{Z_G + \frac{Z_G Z_L}{Z_{o2}} + Z_{s1} + \frac{Z_L Z_{o1}}{Z_{o2}}}{Z_G + Z_L} \quad (Q)$$

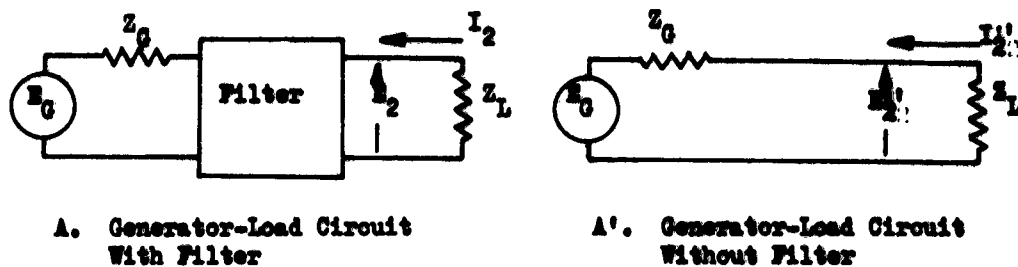


Figure 1 Conditions and Notation Used for Defining Insertion Loss

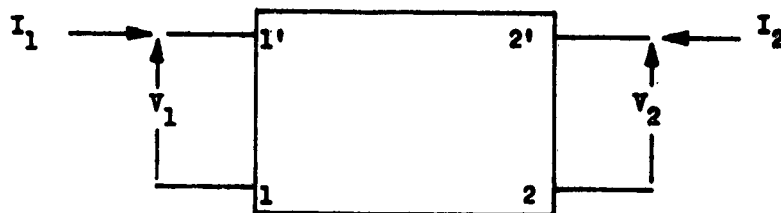


Figure B. Notation and Conventions for Four-Terminal Network Equations

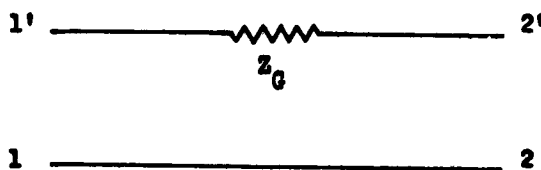


Figure C.  $Z_G$  as the Single Element in a Four-Terminal Network

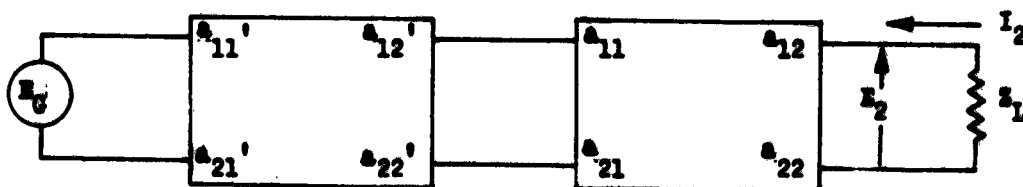


Figure D. Two Networks Cascaded Between Generator  $E_G$  and Load  $Z_L$

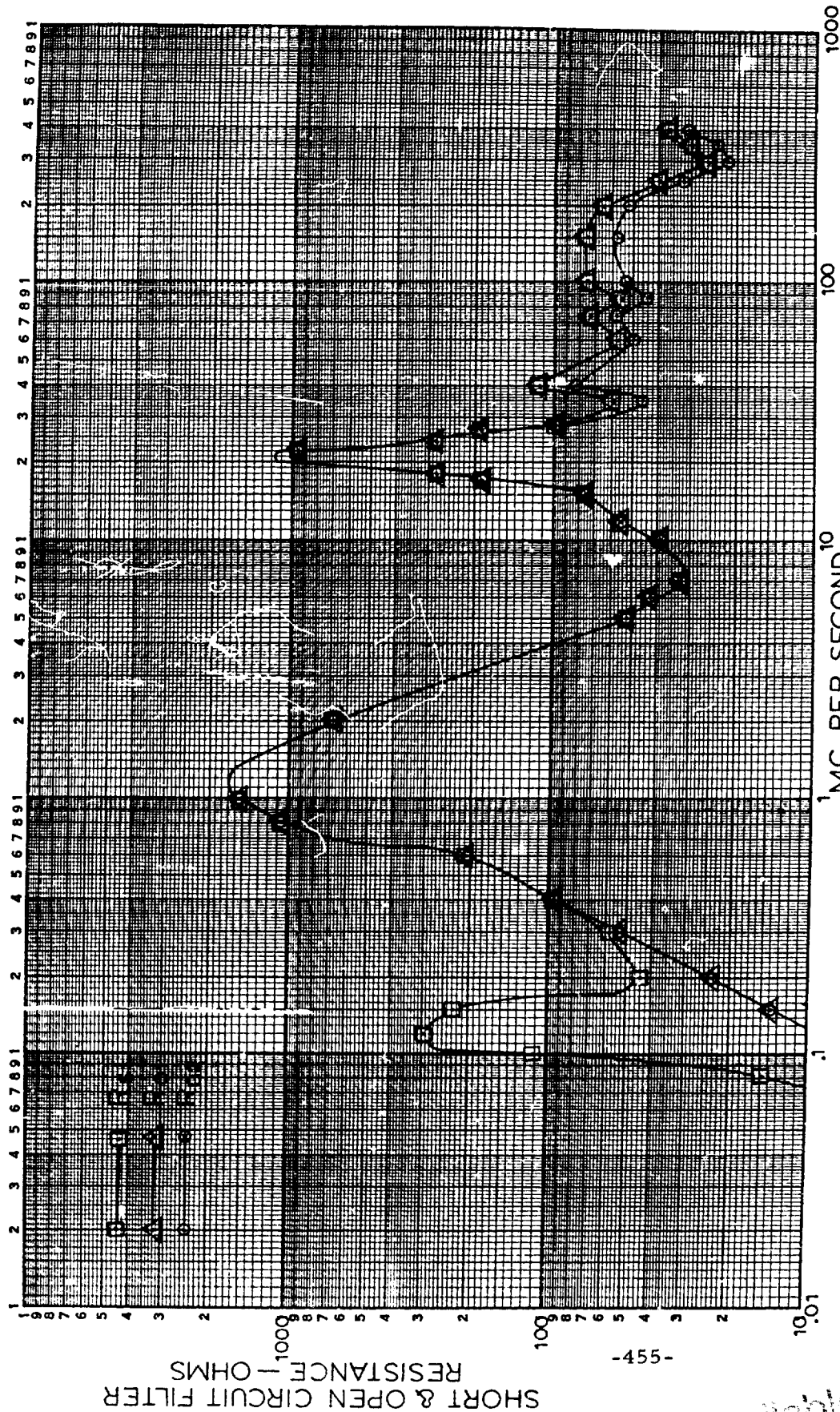


FIGURE 2: SHORT & OPEN CIRCUIT CHARACTERISTICS  
FOR FILTER:  
PART NO. JV 100/JN 17-1342A  
BOEING PART NO. F 26 E 7

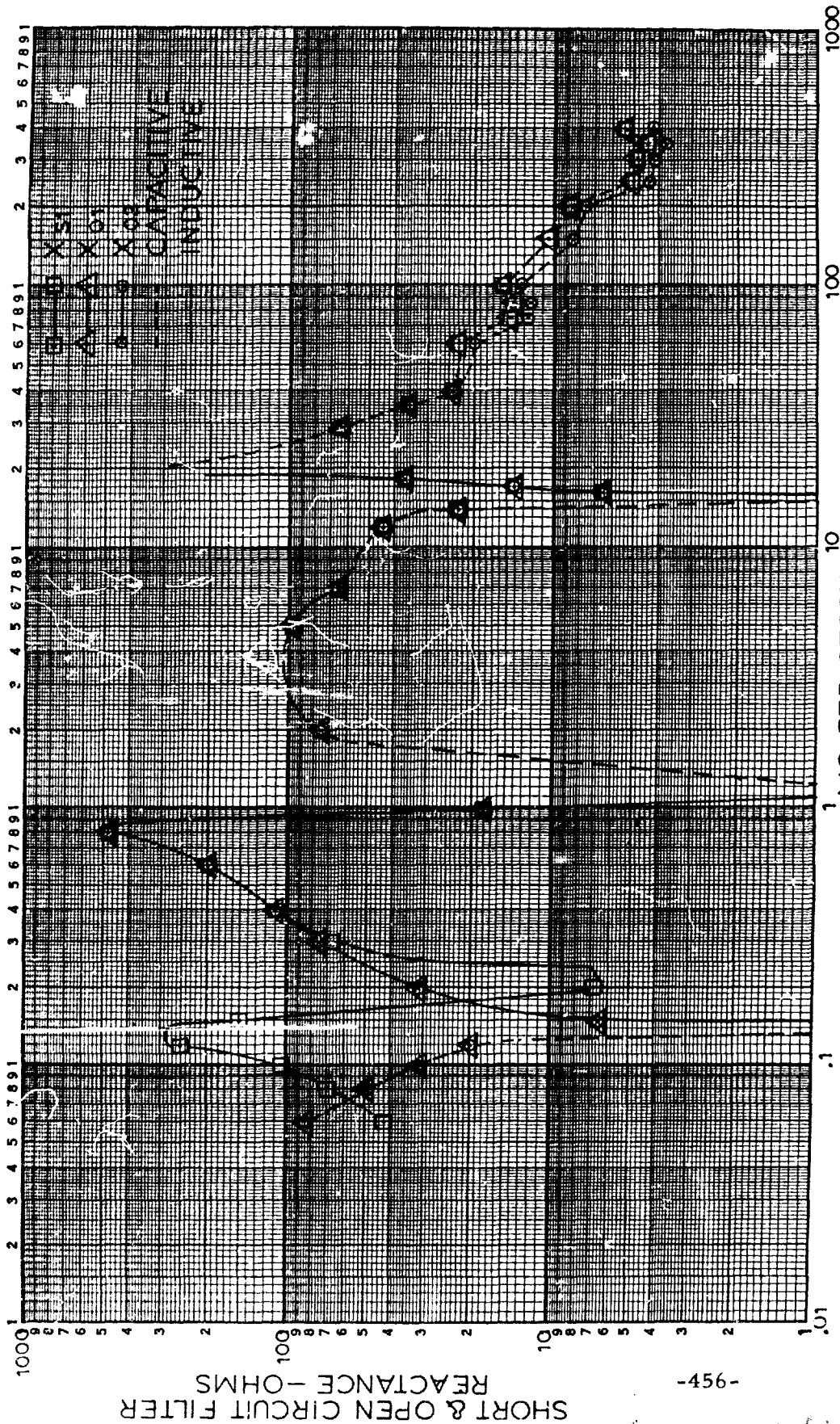
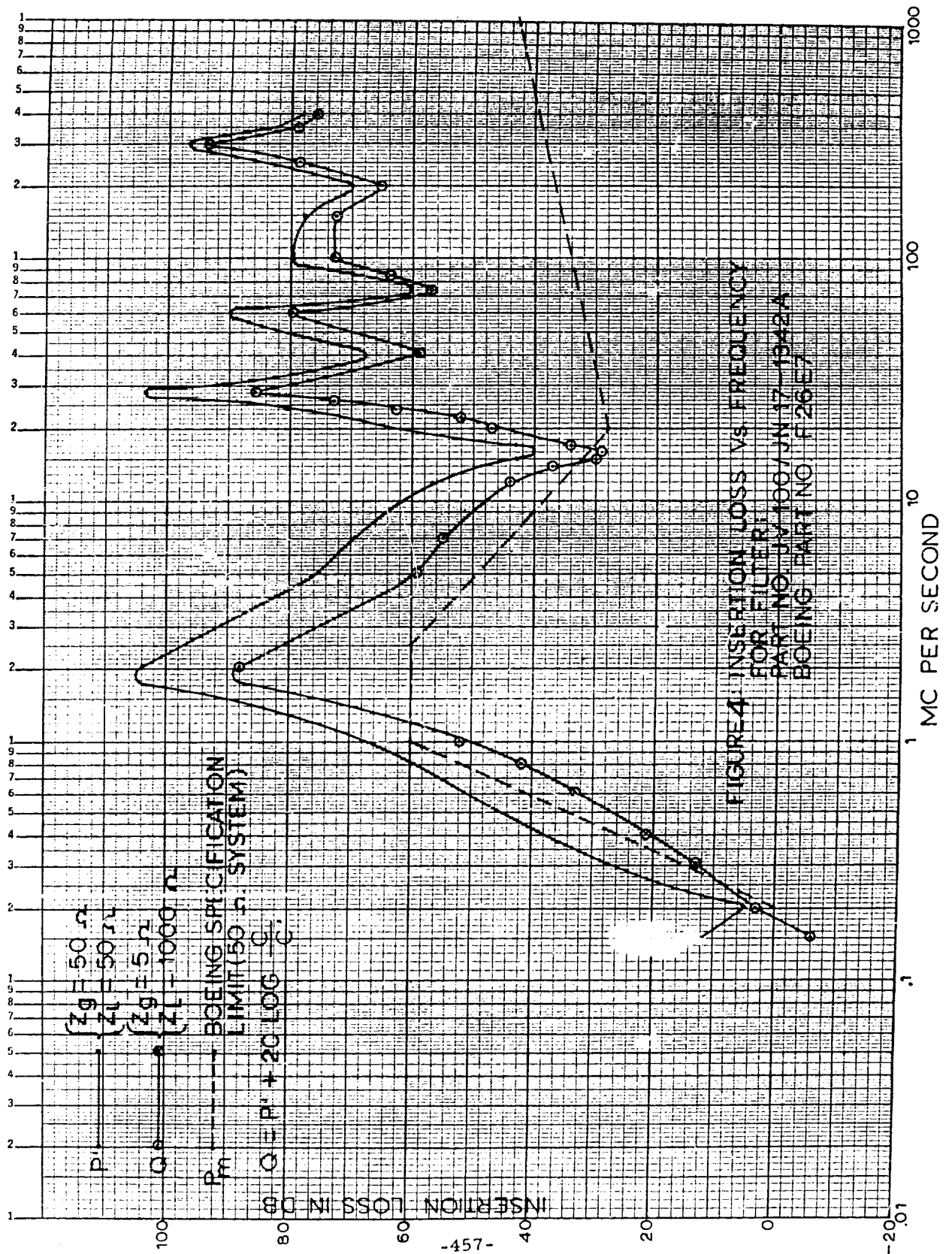


FIGURE 3: SHRT & OPEN CIRCUIT CHARACTERISTICS  
FOR FILTER:  
PART NO. JV 100/JN 17-1342A  
BOEING PART NO. F26E7



Best Available Copy

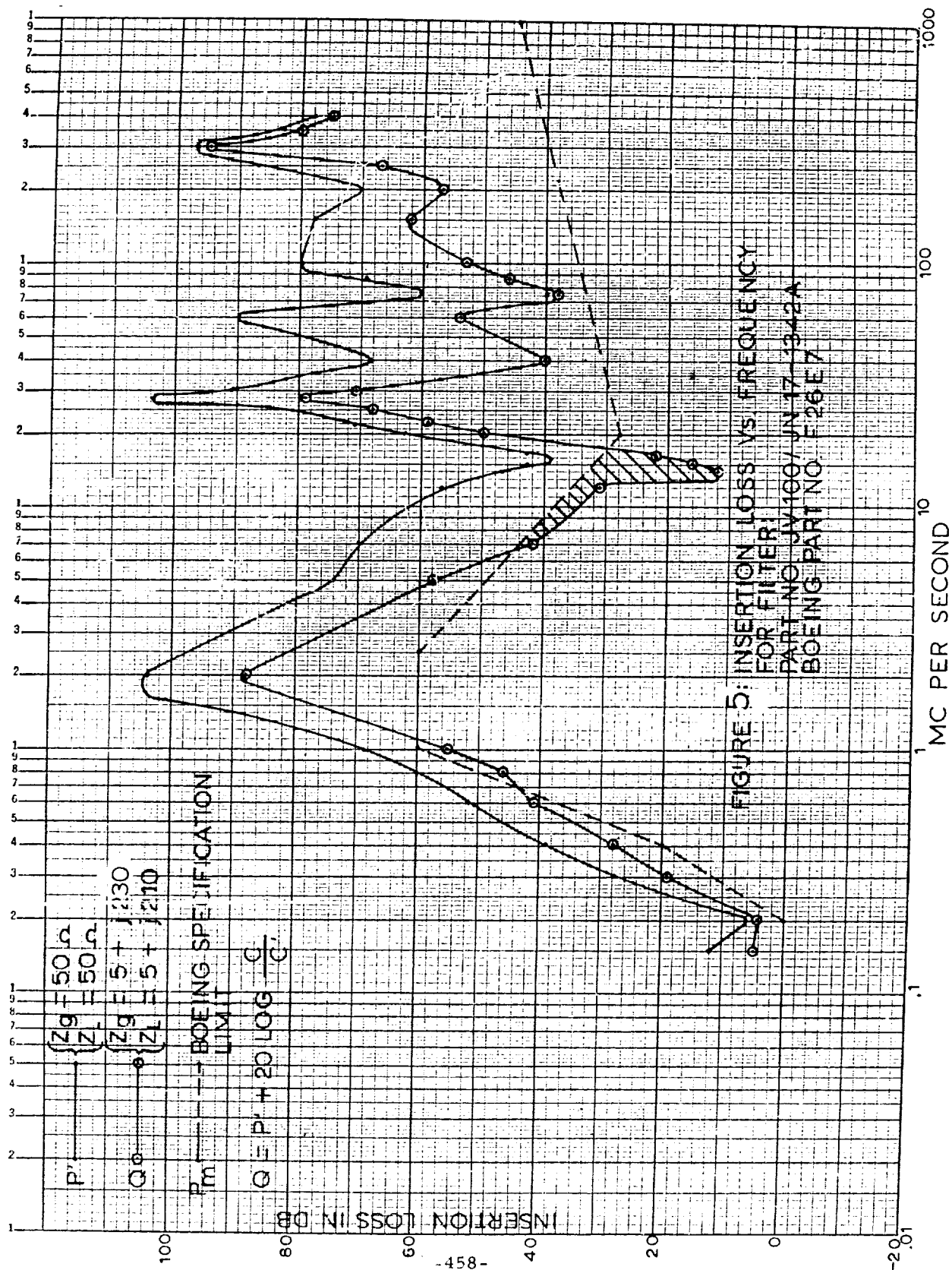


FIGURE 5: INSERTION LOSS VS. FREQUENCY  
FOR FILTER:  
PART NO. JV100/JN 17-342A  
BOEING PART NO. F 26 E 7



## ECAC MSS-2 INTERFERENCE PREDICTION PROGRAM - GENERAL

J. A. Zoellner  
IIT Research Institute  
Electromagnetic Compatibility Analysis Center  
Annapolis, Maryland

**Abstract.** - MSS-2 is a computer automated interference prediction data processing system designed for the UNIVAC 1107 computer at the ECAC. This computerized prediction system replaces an earlier one known as the MSS-1 which was implemented on the UNIVAC 1105 as an interim system for use by the ECAC. MSS-1 was limited to the simulation of a search radar environment, whereas MSS-2 will be able to accommodate, eventually, the prediction of the interference effects of all types of transmitters on all types of receivers in the frequency range designated by the D.O.D.

The MSS-2 system has been designed to take as direct input selected portions of the ECAC environment file and spectrum signature files now being accumulated under the auspices of the Department of Defense. The objective in the design of this scientific data processing system is to automatically enable the complete reconstitution of any specified environmental area (defined by geographic bounds, frequency range, organizational unit designation, etc.), in a large scale general purpose computer. Following this the system injects into the computer the spectrum signature data required, in order that an expandable computer library of mathematical models which simulate emission, response, antenna and propagation effects, can be brought to bear to yield interference predictions. The immediate level of planned computer automation design is, given the specification of a problem environment, to obtain a complete interference prediction in 1 - 3 days depending upon complexity. The structure of this data processing system and its use in the compatibility analysis work for the D.O.D. is discussed in this paper.

### I. INTRODUCTION

MSS-2 is an acronym standing for "Master Simulation System 2". It is a computer automated interference environment prediction system and is an essential part of the integrated ECAC Compatibility Analysis System. With it, the potential interference interactions in a large transmitter-receiver environment can be calculated quickly. The numeral 2 in the code name "MSS-2" differentiates it from an earlier computer prediction model called MSS-1, which was based upon work started at the RAND Corporation and which was used\* at the ECAC as a temporary expedient until such time as the UNIVAC 1107 could be installed and programmed. MSS-1 was implemented on the UNIVAC 1105, the only large scale computer readily available at that time.

MSS-2 is an expandable computer prediction system. In structure it is more than a computer program. Rather, it is a program library containing ~~compatible interference prediction program elements in subroutine form.~~ A

\*Cf. reference 1, for example.

number of new interference prediction programs (called Versions at ECAC) can be readily assembled at any time and with minimum effort.

The first version of MSS-2 to be programmed and assembled at the ECAC is a result of a very large effort which began in February 1963 and which resulted in the generation of the first interference prediction program to become operational on the Center's UNIVAC 1107. It is known as Version 1<sup>2,3,4</sup> and became operational in July 1963. Many engineers, mathematicians and programmers took part in this effort. In this paper, the relationship of MSS-2 to the ECAC Compatibility Analysis System is described and a general outline of the elements of MSS-2 is given.

## II. ECAC COMPATIBILITY ANALYSIS SYSTEM

The end purpose of ECAC is to provide the D.O.D. with the quickest possible problem solving reaction time in questions of electromagnetic compatibility. The keys to this desired performance are (1) a modern high-speed large-scale digital computer, (2) an electromagnetic equipment environment and equipment characteristics data base and (3) a collection of readily usable and validated interference prediction analysis programs which can be assembled or strung together in any desired fashion depending entirely on the requirements of each problem. ECAC has obtained the first key to putting this capability together by acquiring a UNIVAC 1107 having 32K core, 12 tape units on two channels and two magnetic drums having a capacity of about three quarters of a million words each. Average drum access time is 17 msec and the transfer rate is approximately 60 kc\*. Such a large and fast random access storage medium is required because of the need to store the large amounts of spectrum signature data required in analyzing multi-equipment environments.

The second and third keys to the achievement of the desired capability is to be found in the ECAC Compatibility Analysis System. A brief outline of the present status of this system is shown in Figure 1. The Analysis System breaks down into six subsystems. These are:

- 1) Environment Data Base Subsystem
- 2) Environment Simulator Subsystem
- 3) Nominal Characteristics Subsystem
- 4) 1-1 Subsystem
- 5) Terrain Information Subsystem
- 6) MSS-2 Subsystem

### Environment Data Base System

The Environment Data Base Subsystem is illustrated in the upper left hand portion of Figure 1 terminating in the magnetic symbol labeled "INPUT ENV.". Through this subsystem the electronic equipment environment is being assimilated by the Center and put into computer readable form. The first objective of the Center is the assimilation of the continental United States environment operating above 100 mc/sec, dubbed the "CONUS environment". This environment is defined by the locations of all electromagnetic equipment operating above 100 mc/sec,

\*60,000 36 bit words per second. -460-



the nomenclatures of the equipments employed and operating use information such as tuned frequency or frequencies employed, hours of operation and other pertinent data.

Environment data consists of two types normally called background and tactical. Tactical data is generally problem oriented. It is that which is added to the environment already there, defined as the background. Equipment installations in the background can also be singled out as belonging to a tactical deployment. A large portion of the CONUS environment comes to the Center via the survey form DD 1374 and is processed through use of the Census Bureau's FOSDIC system, an optical readout device which interprets optically coded patterns to produce a translation of the data to numeric form on magnetic tape. Environment information concerning much of the non-military government equipment installations also arrive at the Center in this way from such organizations as NASA, FAA, Weather Bureau and Coast Guard.

Other background environment data come to the Center through its so-called "extracted data" procedure. This is used, for example, to assimilate the FCC information and the IRAC list. The collection of information on the background environment mentioned thus far will be completed for CONUS in mid-1964, giving ECAC and D.O.D. a large part of the second key to achieving the quickest possible problem solving reaction time.

The last portion of the background environment to be discussed is called the "very mobile background". This consists of that portion of the background environment which is contributed by the existence of air traffic, ship traffic and other wide ranging vehicles. Reliable sources of this type of information are being sought at this time. Information about the very mobile background will be referenced by vehicle. ECAC will eventually have the capability to break out the electronic equipment environment caused by this vehicularly stated environment through the use of a 4-file employment-deployment information system. This 4-file system relates vehicle type to electronic equipment complement and relates operating use information to the type of job being performed by the vehicle. This manner of bringing environment information into the Center's computer system will also be employed to ingest tactical deployments through the statement of vehicle deployments.

Finally, environmental data can be assimilated into the Center's files through the use of the X-3 survey form. This input data system which is presently operational has been employed to bring both tactical and background data into the Center's magnetic tape files to cover specific problem areas outside of CONUS.

The manner in which this environment data base is used in solving problems is also illustrated in Figure 1. An environment selection program is used to extract environment data pertinent to the problem at hand. This selected background environment is then merged with any tactical environment added and with pertinent very-mobile background data. Following the merging of this data the environment records are sorted in order by equipment nomenclature code. This data labeled "INPUT ENV." is listed through the use of

summary listing programs and used as input to the Environment Simulator Subsystem.

#### Environment Simulator Subsystem

This subsystem is used to make changes in the input problem environment that are dictated by the problem requirements. The Environment Simulator Subsystem is represented in Figure 1 between the tape symbol marked "INPUT ENV." and the tape symbol marked "RUN ENV.". This subsystem is used, for example, to simulate the step tuning of a transmitter through a given frequency band by the introduction of new environment records identical in all respects but in tuned frequency or to change or assign tuned frequency, PRF, PW and even location parameters in any input environment record through the use of the Environment Modifier programs. At this juncture equipment installations can also be added to an environment.

The Center plans to implement several frequency assignment schemes. One of these is the so-called A-B-M plan for assigning frequencies to elements of a radio relay net. Another scheme which will be implemented is the FAM-15. This frequency assignment algorithm uses a priority scheme in making assignments. The output of the Environment Simulator Subsystem provides the input to the MSS-2 Subsystem.

#### Nominal Characteristics Subsystem

The purpose of this system is to provide nominal characteristics information on equipment systems pertaining to spectrum signature characteristics for use with the MSS-2 Subsystem. Such information is found in technical manuals, published manufacturer's specifications and other readily obtainable sources. The type of data to be found in the Nominal Characteristics File (NCF) consists, for example, of the 3, 20 and 60 db 1% frequency deviations, whether or not the local oscillator tracks above or below the tuned frequency, the image rejection factor, noise figure or minimum detectable signal level and so forth.

The employment of nominal characteristics data implies the need to synthesize spectrum signatures in making interference predictions. The requirement to take such steps in MSS-2 when, in fact, actual detailed spectrum measurements are being made in accordance with MIL-STD-449A arises partly from the need to consider large equipment environments immediately and partly because of a desire to use conservative representations of responses and emissions in making interference predictions. The rate at which actual spectrum signature measurements can be made is much too slow to ever provide ECAC with a complete file. In addition such field measurements are very costly. The posture which economics and time force ECAC to take is to use available spectrum signature measurements to uncover trends and relationships between nominal characteristics (such as output tube type) and spectrum signature characteristics to develop spectrum signature synthesis techniques. It is predicted that over 900 equipment systems will be documented by their

nominal characteristics in the NCF file by the end of the year. For more information concerning the NCF file and the synthesis techniques employed, see references 2, 3, and 4.

The use of actual spectrum signature data collected in accordance with MIL-STD-449A is not neglected in the ECAC Compatibility Analysis System. The actual use of spectrum signature data is in conjunction with the 1-1 Subsystem. Even when actual measurements are available it is necessary to employ synthesis techniques as tuned frequencies under which predictions are desired are never equal to the tuned frequencies at which measurements are made.

#### 1-1 Subsystem

The result of an interference prediction calculation using MSS-2 is a list of "likely" interference interactions referred to as the "reduced environment". Since MSS-2 predictions are made on a conservative basis, it is appropriate at times to also obtain estimates of interference-to-noise ratios whenever actual spectrum measurements are available. This is the purpose of the 1-1 Subsystem which is illustrated in the lower right hand portion of Figure 1 between the tape symbol "REDUCED ENV. 1" and "INTERFERENCE PREDICTIONS". Spectrum signature measurements are tabulated, punched on cards and, through appropriate computer programs called preprocessors, are placed upon magnetic tape files for use by the 1-1 SRP program itself. The 1-1 SRP presently uses a smooth earth propagation model known as the SCSE<sup>3</sup>. Also, through the use of the 1-1 SRP it is possible to determine the effects of certain receiver features upon the reception of pulse signals. These features are known as Element Models. Among the special receiver features represented by Element Models are FTC, STC and MTI.

#### Terrain Information Subsystem

Other than the alternative of further processing the "likely" interference cases constituting the reduced environment through the 1-1 Subsystem, it will also be possible to reprocess the reduced environment once again using MSS-2 but this time using a rough earth propagation model employing data derived from terrain elevation profiles. This use of MSS-2 is illustrated in the lower left hand portion of Figure 1. The requirement for this profile data is satisfied by the Terrain Information Subsystem<sup>6</sup> depicted in the lower center portion of that Figure. With this system it is possible to assimilate and retrieve terrain elevation data in a latitude-longitude grid pattern at interval spacings of from about 100 feet to  $\frac{1}{2}$  mile. The speed at which profiles can be "drawn" in the computer is approximately 1 mile/millisecond on terrain elevation data represented on a grid with 30 second intervals (approximately  $\frac{1}{2}$  mile).

### III. GENERAL OUTLINE OF MSS-2

The basic configuration of MSS-2 consists of various input data files, working data files, computer programs and output data files. The

general structure of MSS-2 using these ingredients is illustrated in Figure 2. The labels given to the elements depicted in the figure are entirely generic and each can stand for an entire collection of files and programs. For example, "PATH LOSS" could be a program based upon a CRPL method of predicting path loss, or a program based upon "free space" theory, or a program based upon smooth earth theory. It can also stand for a program based on rough earth theory having its own terrain elevation profiling capability. Likewise, for example, "ANT SYN" stands for any of a whole possible set of programs which use spectrum signature data to predict antenna pattern characteristics. The "S.S. DATA INPUT" file may be a file of nominal characteristics alone or a file containing actual measured data or some desirable mixture of the two types. Such is the nature of the definition of MSS-2 given by Figure 2. The elements in that figure are discussed in the material following under the headings of INPUT DATA FILES, WORKING DATA FILES, OUTPUT and COMPUTER ROUTINES.

#### INPUT DATA FILES

1. "ENV. DATA INPUT" - contains both background and tactical environment information in the DD 1374 format prepared via the ECAC summary listing capability. Input may be multireel. Environment data for approximately 20,000 equipments can be stored on one reel of magnetic tape.
2. "S.S. DATA INPUT" - contains a complete copy of one or more equipment characteristics libraries stored on magnetic tape. Several equipment characteristics libraries are envisioned. The first one to be implemented is the Nominal Characteristics File, (NCF), containing basic information on equipment characteristics obtainable from technical manuals, manufacturer's specifications and published test results. A second library will contain portions of actual spectrum signature data obtained through the spectrum signature measurement program being conducted in cooperation with the ECAC.

#### WORKING DATA FILES

1. "RCVR ENV. I" - contains only the receiver part of the "ENV. DATA INPUT" file.
2. "XMTR ENV. I" - same as "RCVR ENV. I" except for transmitters in the environment.

#### OUTPUT

1. "BINARY OUTPUT" - contains the results in binary form, i.e., numeric results are in fixed point or floating point internal 36 bit word format. This output, often called the "reduced environment", can be used as input to other programs such as those found in the ECAC terrain data processing system.
2. "HSP OUTPUT" - contains the same computer run results as the "BINARY OUTPUT" in a form printable by the high speed printer.

#### COMPUTER ROUTINES

1. "MAIN CONTROL PROGRAM" - performs the executive function of starting and properly sequencing the subprograms.
2. "ENV. DATA PROCESSOR" - splits out the receivers and transmitters in the environment and prepares the "RCVR ENV." and "XMTR ENV." data files and unique receiver and transmitter equipment lists for later use by the "S.S. DATA PREPROCESSOR".
3. "S.S. DATA PREPROCESSOR" - extracts the spectrum signature data required for the problem run using receiver and transmitter equipment lists prepared by the "ENV. DATA PREPROCESSOR" and places the required data on the magnetic drum, leaving a drum storage location index in core.
4. "S.S. DATA RECALL" - transfers the specific spectrum signature data required from storage on the magnetic drum to a working storage location in core where it can be operated upon.
5. "ENV. DATA INTERPRETER" - calculates the tuned frequency, modulation type and, where applicable, calculates the pulse repetition rate and pulse width from usage information given in the environment record. Calculation of these quantities can be made in several modes. One mode, for example, is to select frequencies at random on a uniform distribution basis if a frequency range of operation is indicated while another mode would be to make this selection on a most probable basis.
6. "OUTPUT CONVERTER" - converts the binary data in the "BINARY OUTPUT" to the format necessary for the "HSP OUTPUT".
7. "INR CALCULATION SUBPROGRAM" - performs the executive function in terms of sequencing and executing the computer programs directly which are shown beneath it in Figure 2.
8. "XMTR SYN" - determines the emission spectrum as a function of spectrum signature data and tuned frequency.
9. "RCVR SYN" - determines the response function given the spectrum signature data and the tuned frequency.
10. "ANT SYN" - determines the antenna gain characteristics given spectrum signature data.
11. "PATH LOSS" - computes the propagation path loss between the receiver and transmitter.
12. "INTEGRATOR" - performs the integration of the transmitter emission, receiver response, propagation and antenna gain functions to obtain the interference-to-noise ratio (INR).

The full details of the first version of MSS-2 to become operational at ECAC are described in subsequent papers being presented at this Conference.

#### ACKNOWLEDGEMENT

The work described above is sponsored by the three Military Departments and is being conducted under Contract Number AF18(604)-8440 with the Electronic Systems Division, Air Force Systems Command.

#### REFERENCES

1. Zoellner, J. A., Litzky, M. S. and Lustgarten, M. N., "The Computer Simulation of the Time Amplitude Interference in a Multiple Search Radar Environment and Its Uses", Proceedings of the Eighth Conference on Radio-Interference Reduction and Electronic Compatibility, November 1962.
2. Scott, J. B., "ECAC MSS-2 Interference Prediction Program - Cull Model", Ninth Conference on Radio Interference Reduction and Electronic Compatibility, October 1963.
3. Anderson, D. and Frazier, W., "A Propagation Model for Electromagnetic Compatibility Analysis", Ninth Conference on Radio Interference Reduction and Electronic Compatibility, October 1963.
4. Pethel, F., Fleck, R. and Marini, J., "Synthesis of Equipment Characteristics for Compatibility Analysis", Ninth Conference on Radio Interference Reduction and Electronic Compatibility, October 1963.
5. Payne, A., "The Use of an Automatic Parameter Assignment Algorithm in Interference Control", Proceedings of the Sixth Conference on Radio Interference Reduction and Electronic Compatibility, October 1960.
6. Iseli, J., "Automatic Terrain Information Processing System", Ninth Conference on Radio Interference Reduction and Electronic Compatibility, October 1963.



**Figure 1**

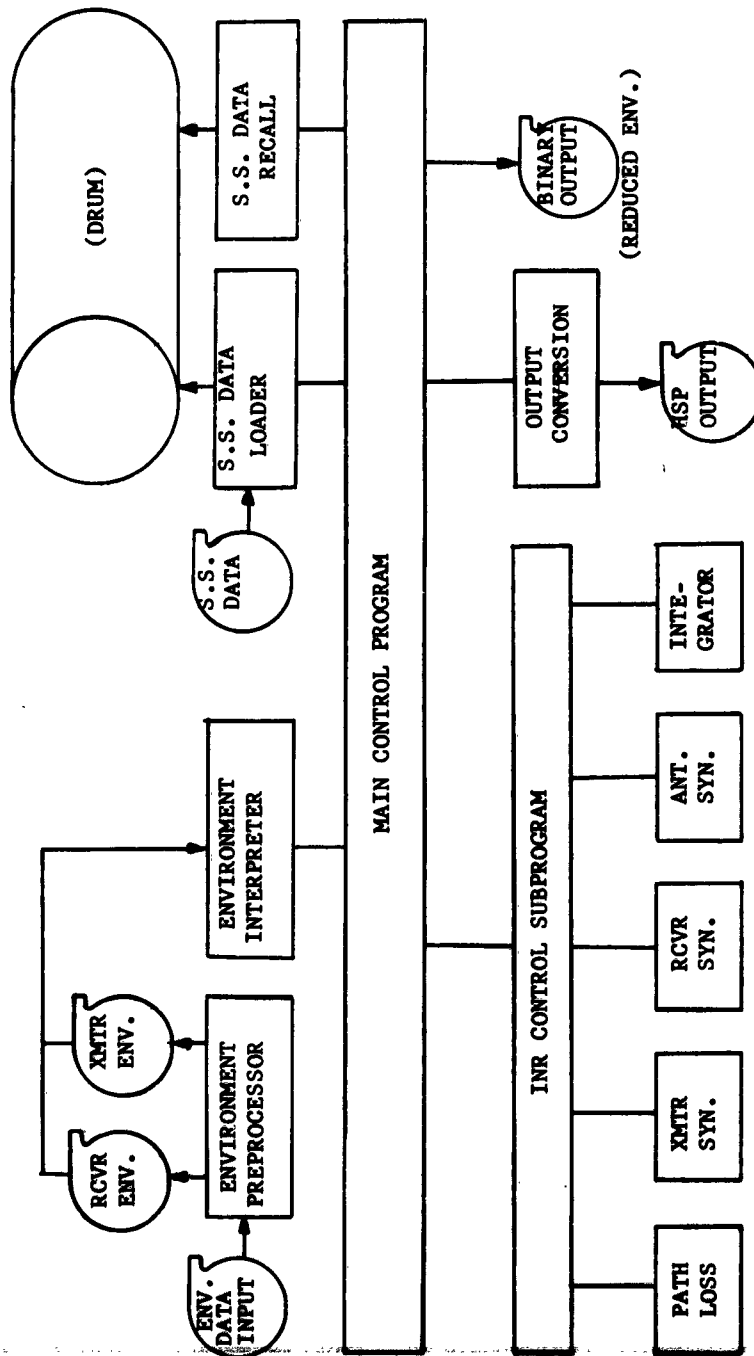


Figure 2. Basic Outline of MSS-2



## ECAC MSS-2 INTERFERENCE PREDICTION PROGRAM - CULL MODEL

J. B. Scott  
IIT Research Institute  
Electromagnetic Compatibility Analysis Center  
Annapolis, Maryland

**Abstract.** - The ECAC MSS-2 system is a collection of computer automated mathematical models designed to provide quick reaction time solutions to electromagnetic compatibility problems. The designed structure of the MSS-2 system is such that as knowledge is gained in the area of compatibility analysis, the additional knowledge can be reflected readily in additions to the automatic system.

The initial capability of MSS-2, often referred to as the "Cull Model", became operational during the summer of 1963. Implicit in the design of this system are several features which are unique in the realm of compatibility analysis. One of these features is the ability to directly use the broad data base that is being established at the ECAC.

Contained in this paper is a generic picture of the first operational version of the MSS-2 Interference Prediction System. Special emphasis in the discussion is placed on the unique features of the system. Use of the model is illustrated.

### I. BACKGROUND

The MSS-2 Subsystem is a collection of programs for a UNIVAC 1107 digital computer. The purpose of the programs is to provide the Electromagnetic Compatibility Analysis Center (ECAC) with a quick reaction time capability in the solutions of problems caused by radio frequency interference (RFI). Basically, the MSS-2 Subsystem is designed to examine an environment composed of equipments which emit electromagnetic energy (transmitters) and equipments which respond to electromagnetic energy (receivers) and to provide an indication of the degradation suffered by each receiver in the presence of undesired signals.

The existence of such a collection of programs is not all that is required to guarantee quick reaction time solutions to electromagnetic compatibility problems. Another important factor is the availability of accurate data to be used in the analysis process. This requirement has been met at the ECAC by establishing a broad data base consisting of equipment environmental information and equipment electrical characteristics information. The collection of equipment environmental data is referred to as the Environmental File and the collection of equipment electrical characteristics is referred to as the Nominal Characteristics File (NCF) and the Measured Data File. The data base is stored on magnetic tape in a format compatible with the MSS-2 Subsystem input requirements and serves as the primary source of input data for the MSS-2 Subsystem.

Equipment electrical characteristics contained in the NCF are those characteristics that are usually found in technical equipment manuals. Such information as receiver sensitivity, transmitter power output, and antenna main beam gain is contained in the NCF file. The employment of NCF data implies the need to synthesize spectrum signatures in making interference predictions. The need for the ability to synthesize spectrum signatures, even though detailed spectrum measurements are being made in accordance with MIL-STD-449A, is created because of the time and cost that would be involved in collecting measured data on such large equipment environments that are often involved in compatibility analysis problems. Synthesis rules based on measured spectrum signature data have been developed<sup>1</sup> and are being refined for predicting the behavior of electronic systems from NCF type data. Such rules are used in the MSS-2 Subsystem.

The ability to accurately calculate propagation path loss is a necessary requirement for a compatibility analysis system. The MSS-2 Subsystem now uses prediction curves based on empirical data. Development work is under way to provide more refined techniques for calculating propagation path loss<sup>2</sup>. For many problems, terrain has a profound influence on propagation path loss. Also under development at ECAC is an automatic terrain retrieval and profiling system<sup>3</sup> which will be used in conjunction with the MSS-2 Subsystem for providing more accurate interference calculations.

The present version of the MSS-2 Subsystem, often called the Cull Model, reflects a certain level in the development of analytical tools for the analysis of RFI. As these analytical tools are improved, additional versions of the MSS-2 Subsystem will be developed reflecting the increased capability. Knowledge of the need for continual change led to the organization of the MSS-2 Subsystem computer program into a collection of programs, called subroutines, tied together by a main control program. The main control program serves to call each subroutine in its sequential order and to provide to each subroutine the data required for it to operate. Thus, a change in the program can be made with relative ease by simply replacing the subroutine that is affected. Figure 1 provides a generic diagram of the MSS-2 Subsystem with its major subroutines. Section II of this paper describes the role that each subroutine plays in the compatibility analysis process.

## II. THE MODEL

Environmental data input to the MSS-2 Subsystem consists of magnetic tape records. For any given problem these records are a sub-set of the Environmental File portion of the ECAC data base. Derivation of such a sub-set is explained in the section titled Off-Line Environment Preprocessing.

An environmental file magnetic tape record consists of 50 computer words. The 50 computer words contain approximately 44 items of environmental data concerning one electronic system. A system may be a transmitter, a receiver, or a transceiver depending on the type of equipment contained in the system. Information contained in each record includes location of equipment, nomenclature, type of antenna, operating frequencies, modulation type, elevation of equipment, antenna height, PW-RPR, antenna motion, etc. Figure 2 is the tape format of an environmental file record.

Data contained in the environmental file is collected from many sources. Some of these sources are as follows:

1. The DOD collection plan implemented under AFR 100-3, AR 105-67, and OPNAVINST 2410.22
2. FCC listings
3. IRAC listings
4. Special inputs that may be dictated by a special problem.

The importance of this file cannot be over-emphasized. If all environmental data had to be collected for each problem to be analyzed, reaction time in many cases would make the solutions useless. Another advantage of this file is that all environmental data ultimately becomes standardized into one computer format thus eliminating the need for complicated format conversion routines as part of the analysis computer programs.

Use of environmental file data in the MSS-2 Subsystem will be discussed in appropriate sections throughout this paper.

Electrical characteristics of equipments contained in the environmental file are recorded and stored on magnetic tape. Sufficient information is contained in the Nominal Characteristics File (NCF) so that when used in conjunction with the environmental file, an adequate representation of a transmitter emission spectrum as well as a receiver response spectrum can be obtained through synthesis procedures.

The NCF actually consists of a collection of eight sub-files. They are as follows:

1. General Radar
2. General Communications
3. Radar Transmitters
4. Communications Transmitters
5. Radar Receivers
6. Communications Receivers
7. Radar Antennas
8. Communications Antennas

Each type of sub-file record consists of 300 computer words. The differences between radar and communications equipment, however, make it necessary to

construct separate files for each different category of equipment. Hence, the need for sub-files 3 through 8 above.

A further complication arises when attempting to develop an automatic filing system for equipment electrical characteristics. Many systems contain components identical with other systems. For example, an AN/VRC 19 system consists of a type T-278/U transmitter and a type R-394/U receiver. An AN/TRC-29 system consists of a type T-416/GR transmitter and the same type, R-394/U, receiver as the AN/VRC 19. To avoid such redundancies, the electrical characteristics of each type transmitter, receiver, and antenna are entered only once in sub-files 3 through 8, and sub-files 1 and 2 are used primarily to reference components to the systems to which they belong. Sub-files 1 and 2 allow up to six different transmitters, six different receivers, and six different antennas to be referenced for each system.

The importance of an existing, computer automated, NCF is comparable to the importance of the environmental file. Both files are necessary to ensure quick reaction time solutions to electromagnetic compatibility problems. Use of NCF data in the MSS-2 Subsystem will be discussed in appropriate sections throughout this paper.

The following paragraphs describe in detail the various subroutines which comprise the MSS-2 Subsystem computer program. Figure 1 shows the organization of these subroutines within the system.

#### A. Off-Line Environment Preprocessing

One of the first steps in preparing to use the MSS-2 Subsystem is to extract from the Environmental File portion of the ECAC data base the records of those equipments which are of interest to the problem. The reason for this step becomes clear when the number of equipments stored in the environmental file is considered. By the end of 1963, it is anticipated that the Environmental File will contain approximately 30,000 records resulting from the DOD collection plan for equipments operating above 100 mc within the continental limits of the U. S. Ultimately, records of an additional 300,000 equipments will be introduced into the file from FCC sources alone.

The Off-Line Environment Preprocessing step is accomplished by a search and retrieval computer program which is designed to select records from the file and write them on a problem tape. Selection can be made on such parameters as longitude, latitude, frequency, and equipment type. Another function of the Off-Line Environment Preprocessing program is to add to the environmental input tape records that have been prepared especially for the problem under consideration and which are not a normal part of the ECAC data base.

The final step in preparing the problem input tape is to sort the environmental records by systems nomenclature code so that all equipments of a particular type occur together on the tape. This step is desirable since computer time is greatly reduced in the analysis stages of the problem if the NCF of a particular type equipment is retrieved only once.

## **B. On-Line Environment Preprocessor**

The processing philosophy of the MSS-2 Subsystem is to assess the effect of all transmitters in the problem area against each receiver. This is accomplished by first choosing a receiver, then assessing the effect of each transmitter, in turn, on the chosen receiver. The next receiver is then selected and the transmitter processing is repeated. Since the environmental problem input tape consists of records representing transmitters, receivers, or systems such as the AN/TRC-28 which contains both a transmitter and a receiver; the environmental problem tape that results from the Off-Line Environment Preprocessing program is not suitable for this purpose.

One of the purposes of the On-Line Environment Preprocessor, therefore, is to separate the transmitter environmental records from the receiver environmental records and to store the resulting two files onto magnetic drum for later retrieval during the processing of the problem. Systems which contain other components are split out and an environmental record is written in separate files on magnetic drum for each transmitter and receiver component contained in the system.

During the process, each environmental record is expanded from a 50 word record to an 80 word record. Expansion of the record results from unpacking, scaling, and converting to floating point certain parameters used in later calculations. Also, as the environmental records are passed from tape to drum through core, a unique list of systems containing transmitters and a list containing receivers are compiled and retained in core. These lists are used by the NCF Loader to select only those NCF records that are applicable to the particular problem under consideration.

## **C. NCF Loader**

The Nominal Characteristics File Loader is a subroutine which passes the NCF tape and extracts from it for storage on magnetic drum those records containing equipment electrical characteristics which are pertinent to the problem under consideration. Use is made of the organization of the eight NCF Sub-files as well as the two lists of unique systems nomenclatures which are prepared by the On-Line Preprocessor and retained in core for use by this routine.

Organization of the NCF tape is such that all General NCF records, types 1 and 2, which contain references to the individual transmitter, receiver, and antenna component nomenclatures contained in the system are stored first on the NCF tape. As the type 1 and 2 records are being passed through the computer, several functions occur almost simultaneously. The systems nomenclature code contained in the NCF record is compared with the entries in the two unique lists of systems nomenclature codes stored in core. If a match does not occur, the system does not appear in the problem and the record is rejected. If a match does occur, the nomenclature codes of the transmitter, receiver, and antenna components contained in the system are extracted from the type 1 or 2 record and stored on magnetic drum. As they are being stored on the drum a list of unique transmitter components, a list of unique receiver components, and a list of unique antenna components are being compiled and retained in core.

When the tape passes beyond the type 1 and 2 records, record types 3 through 8 are read and, again, several functions occur almost simultaneously. The nomenclature code of each component record is compared against the entries in the proper lists of component nomenclature codes which were compiled from the type 1 and 2 NCF records. If a match does not occur, the record is rejected, and the component does not appear in the problem. However, if a match occurs, the record is written on magnetic drum for later retrieval by the NCF Recall subroutine when it is desired to simulate that particular type of equipment.

At this point in the execution of the MSS-2 Subsystem, the stage has been set so that analysis can actually begin. The problem environmental records have been stored on magnetic drum. NCF records containing component references for each type of environmental file record have been stored on drum, and the position of each record on drum is relative to the position of its systems nomenclature code in the list retained in core. Similarly, records containing electrical characteristics of each component in the problem are stored on drum, and they are positioned relative to the position of their nomenclature code in the component nomenclature code lists retained in core.

#### D. Environmental Interpreter

An environmental record contains space for recording up to three values of frequency, modulation type, and PW-PRF combinations. In addition, if the equipment normally operates over a range of frequencies or PW-PRF combinations, this fact may also be recorded. However, for a given problem run, specific values of these parameters must be chosen. Having been given an environmental record, the purpose of this subroutine, then, is to choose specific values of frequency, modulation type, and PW-PRF combination.

The Environment Interpreter subroutine operates on one of two possible modes under control of a run parameter. One mode selects values of the three parameters on a "most probable" basis, the other mode makes the selection on a "random basis". If the parameters are reported as discrete values, the most probable mode selects the values of the parameters for which the highest percentage of usage has been reported. If the parameters are reported as a range of values, the midpoint of the range is chosen. When operating in the random selection mode, if the parameters are recorded as ranges of values a random selection is made of one of the values from within the range. If the parameters are reported as discrete values with percentages of use  $\alpha$ ,  $\beta$ , and  $\gamma$ ; a random number,  $X$ , is generated and normalized to the interval  $(0, \alpha + \beta + \gamma)$ . If  $0 < X \leq \alpha$ , the value of the parameter corresponding to  $\alpha$  is chosen. If  $\alpha < X \leq \alpha + \beta$ , the values of the parameter corresponding to  $\beta$  is chosen; and if  $\alpha + \beta < X \leq \alpha + \beta + \gamma$ , the value of the parameter corresponding to  $\gamma$  is chosen.

#### E. NCF Recall

When an environmental record has been selected from magnetic drum to be processed it is necessary to locate the electrical characteristics of the equipment referenced in the environmental record. This is accomplished by examining the appropriate systems nomenclature code list in core to determine the position in the list of the systems nomenclature code of the equipment referenced by the environmental file record. Using the position of the code in the list, the general NCF record pertaining to the system is retrieved from magnetic drum. Contained in this general NCF record are references for up to six transmitters or receivers of which the system may be comprised and references for up to six antennas. These references, along with the lists of unique components stored in core, are used to retrieve from magnetic drum the electrical characteristics of each of the components that could be associated with the system under consideration.

#### F. NCF Component Selector

For cases where systems referenced by an environmental file record consist of only one transmitter and its antenna or only one receiver and its antenna the electrical characteristics of the equipment have been stored in core by the NCF Recall subroutine and further processing of the problem can continue. However, for systems consisting of more than one transmitter or more than one receiver it is necessary to determine which one of the possible components is operating during a specific problem.

This determination is made using the frequency, modulation type, and PW-PRF combination that was chosen by the Environmental Interpreter subroutine. The component selected is the one that compares favorably with the three pre-selected parameters. In the event that more than one transmitter or receiver component satisfies this criterion, one of the components that satisfies the criterion is arbitrarily selected.

If there is more than one antenna that can be used with the system the antenna reported in the environmental file record is the one chosen for use.

#### G. Receiver Spectrum Reader

A problem frequently encountered when considering the compatibility of equipments that emit and respond to electromagnetic energy is that of assessing the effect of a particular electromagnetic environment on a given receiver. In such a case, the electrical characteristics of the receiver may be known in greater detail than that recorded in the NCF file. For instance, the receiver response spectrum may have been actually measured, or it may be available resulting from design specifications of the receiver. Furthermore, it is often desirable to assess the impact of the environment on the receiver at all tuning positions throughout the tuning range of the receiver.

The Receiver Spectrum Reader subroutine provides the capability for introducing into the system sufficient environmental and electrical characteristics

data pertaining to a given receiver to handle this problem. Included in this data input are a sequence of points which describe in detail the actual receiver response spectrum and the information necessary to step-tune the receiver at successive fixed increments throughout its spectrum of operation.

This mode of operation of the MSS-2 Subsystem is controlled by an input parameter which causes the Receiver Spectrum Reader subroutine to be activated in its proper sequence. This input parameter also causes the receiver NCF Recall and Receiver Spectrum Synthesis routines to be bypassed, and it activates the logic in the control program required to loop back and step-tune the receiver after each analysis pass.

#### H. Power Calculation Control

The analysis portion of the MSS-2 Subsystem is largely contained in the Power Calculation Control program with its associated subroutines. Input to the Power Calculation Control program is the environmental and electrical characteristics of a transmitter and a receiver and their associated antennas. Output is the calculated value of the interference-to-noise ratio (INR).

Primary functions performed by the Power Calculation Control program are as follows:

1. Simulate the transmitter by synthesizing its emission spectrum using data from its environmental file and NCF record.
2. Calculate the propagation path loss between the transmitter antenna and the receiver antenna.
3. Attenuate the power at each point in the emission spectrum by the appropriate propagation path loss.
4. Simulate antenna patterns for both the transmitter and the receiver antenna by synthesizing the pattern data from the environmental file and NCF records.
5. Attenuate or increase the power at each point in the emission spectrum as they would be modified by the antenna patterns.
6. Simulate a receiver response spectrum by synthesizing the spectrum using data from its environmental file and its NCF record.
7. Calculate the INR using the modified transmitter emission spectrum and the receiver response spectrum.

#### I. Transmitter Synthesis and Transmitter Shaper

The Transmitter Synthesis and Transmitter Shaper subroutines synthesize the transmitter emission spectrum using data from the environmental file and NCF record. Synthesis procedures were developed for simulating the transmitter emission spectrum as well as the receiver response spectrum and the antenna patterns by relating measured spectrum signature data to certain environmental and electrical characteristics of the equipment.



For the transmitter, the envelope about the tuned frequency is defined as well as the envelopes about the second through the sixth harmonics. Figure 3 describes pictorially the results of the synthesis procedure. Steps followed by the subroutine are as follows:

1. Using the tuned frequency,  $f_0$ , extracted from the environmental record, the center frequencies of the second through the sixth harmonic are calculated.
2. Shaping parameters (see Figure 3) A, B, C, D, E,  $P_{dbm}$ , and  $H_p$  are calculated.
3. Using the center frequencies and the shaping parameters, the emission spectrum is defined by calculating a sequence of points of power (dbm) vs. frequency (mc) along the curves shown in Figure 3.

The shaping parameters provide the functional relationships between the equipment characteristics and the emission spectrum. The relationships are as follows:

$$A = (MMB)10^{T/K} \quad mc$$

where MMB is the emission bandwidth, T is a function of the output tube type, and K is a function of the modulation type. The emission bandwidth and the tube type are available from the NCF record and the modulation type is available from the environmental file record.

$$B = 8A \quad mc$$

$$C = 1.5B \quad mc$$

$$D = -10T \quad db$$

$$E = 45 \quad db$$

$$H_p = 60 \quad db$$

$$P_{dbm} = 10 \log_{10} P_I \quad dbm/mc$$

where

$$P_I = (PRF)(PW)^2(\text{Peak Power}) \quad \text{for radar}$$

$$P_I = \frac{\text{Average Power (kw)}}{\text{Emission Bandwidth(mc)}} 10^6 \quad \text{for CW}$$

The PW-PRF combination is available from the environmental file record while peak power for radar and average power for CW equipments is available from the NCF file.

## J. CRPL Path Loss

Propagation path loss between transmitter and receiver is estimated using empirical data collected under the auspices of the International Radio Consultative Committee (CCIR) and reported in CCIR document V/23-E. A sample of this data appears in Figure 4. The median value of the data has been estimated by fitting segmented straight lines to various regions of interest. It should be noted when examining Figure 4 that the ordinate is attenuation below free space, the abscissa is distance, and frequency is a parameter. The segmented straight lines roughly correspond to the so-called line-of-sight, intermediate, and diffraction regions of propagation. Within the line-of-sight region attenuation below free space is zero.

In calculating propagation path loss using these curves, the CRPL Path Loss subroutine performs the following functions:

1. Ensures that the transmitting and receiving antennas lie in each others far field by insuring that  $d_{MIN} < r$  where

$$d_{MIN} = \frac{\left[ \text{MAX}(L_{XMTR}^2, L_{RCVR}^2) f \right]}{3 \times 10^5}$$

and

$$r = \left[ d^2 + \frac{(h_{Xmtr} + \bar{h}_{Xmtr} - h_{Rcvr} - \bar{h}_{Rcvr})^2}{1000} \right]^{\frac{1}{2}}$$

$d_{MIN}$  describes the radius of the largest far field circle and  $r$  is the geometrical distance between the transmitting and receiving antenna.  $h_{Xmtr}$  and  $h_{Rcvr}$  denote the height above sea level of the transmitter and receiver sites in meters.  $\bar{h}_{Xmtr}$  and  $\bar{h}_{Rcvr}$  denote the height of the transmitter and receiver antennas above their respective sites, in meters.  $f$  is the frequency at which the path loss is to be evaluated, and  $d$  is the great circle distance, in kilometers, separating the transmitter and receiver site locations.  $d$  is calculated from the longitude and latitude of the transmitter and receiver sites. This information is provided in the environmental file records.  $f$ ,  $h_{Xmtr}$ ,  $h_{Rcvr}$ ,  $\bar{h}_{Xmtr}$ , and  $\bar{h}_{Rcvr}$  also are available from the environmental file records.  $L_{Xmtr}$  and  $L_{Rcvr}$ , the maximum linear dimensions of the transmitter antenna and receiver antenna, respectively, are available from the NCF records.

2. Free space path loss,  $L_{fs}$ , is computed.

$$L_{fs} = 32.45 + 20 \log_{10} f + 20 \log_{10} r.$$

3. Using  $f$  and  $d$ , attenuation below free space is estimated from curves similar to those shown in Figure 4 that have been previously stored in the computer.

4.  $L_{fs}$  is added to the estimated attenuation below free space to provide the total path loss between the transmitter and the receiver.

It should be noted at this point that normal execution of the MSS-2 Subsystem will result in propagation path loss being estimated as a median value loss. In other words, 50 per cent of the empirical data from which the curves were derived lies above the curve and 50 per cent lies below the curve. Additional analysis has been performed on the empirical data resulting in a series of curves that may be used instead of the median value curve. The additional curves allow a confidence level of other than 50 per cent to be placed on the path loss predictions. The confidence level for a particular problem run is specified by a run parameter.

Propagation path loss is calculated at the transmitter tuned frequency and at the center frequencies of each of the second through the sixth harmonics. To provide for the effects of propagation path loss on the transmitter emission spectrum, the value of each point used in defining the envelope about the fundamental response is decreased by an amount corresponding to the path loss calculated at the tuned frequency. Similarly, the value of each point in the envelope about each harmonic is decreased by an amount corresponding to the path loss calculated at the center frequency of that harmonic. After the emission spectrum has been attenuated by the path loss, the resulting spectrum, as it is seen by the receiver, might appear as shown in Figure 5. The effects of the antenna, however, have not yet been introduced.

#### K. Receiver Synthesis and Receiver Shaper

Generally, data on receiver selectivity characteristics are measured by recording the power into the receiver required to give a standard response at the output. Mathematically, the measurement procedure can be expressed as

$$\frac{N + p(f) |H(f)|^2}{N} = K$$

where

$N$  is the receiver noise,

$p(f)$  is the power into the receiver,

$|H(f)|^2$  is the receiver transfer function, and

$K$  is the standard response.

The above expression can be solved for  $\frac{|H(f)|^2}{N}$  in terms of the known quantities K and p(f),  $\frac{|H(f)|^2}{N} = \frac{K-1}{p(f)}$ , thus providing a measure of the transfer characteristics of a receiver if f, the frequency of the input signal, is varied throughout the possible response spectrum of the receiver. Synthesis of the receiver response spectrum, then, means to estimate the signal power required as input to the receiver to provide a standard output response as a function of frequency.

Estimation of the input signal power is accomplished in the following steps:

1. Center frequencies of spurious responses are calculated by evaluating

$$f_{sp} = \frac{p f_{LO} \pm f_{IF}}{q}$$

where

$f_{LO}$  is the frequency of the local oscillator,

$f_{IF}$  is the first IF frequency,

p is the harmonic order of the local oscillator,

q is the harmonic order of the spurious response,

and  $f_{sp}$  is the center frequency of the spurious response.

$f_{LO}$  is calculated by  $f_{LO} = f_o \mp f_{IF}$  where  $f_o$  is the receiver tuned frequency.  $f_o$  is available from the receiver environmental file record and  $f_{IF}$  is available from the receiver NCF record. The above expression is evaluated using  $q = 1, 2$  for  $2 \leq p \leq 7$  for positions of the local oscillator both above and below the receiver tuned frequency. Thus, 24 spurious response center frequencies are calculated. In addition, the center frequency of the image response is calculated.

2. Once the spurious response center frequencies have been calculated, the receiver response spectrum is defined by shaping a response envelope about the receiver tuned frequency, the image frequency, and each of the spurious response center frequencies. Data for the shaping procedure is available from the NCF record and includes the receiver sensitivity, receiver image rejection, and several known points on the receiver selectivity curve. Results of the shaping procedure are a sequence of points stored in the computer which express p(f), power required as input to the receiver to acquire a standard output response, as a function of frequency. Figure 7 illustrates a portion of a synthesized receiver response spectrum.

#### L. Integrator

The end product of the Power Calculation Control Program is the interference-to-noise ratio (INR) calculated from the following expression:

$$\text{INR} = G_T G_R \int_0^{\infty} \frac{P(f) |H(f)|^2}{N} df$$

where  $G_T$  is the gain of the transmitter antenna,

$G_R$  is the gain of the receiver antenna,

$P(f)$  is the transmitter emission spectrum after modification by propagation path loss,

and  $|H(f)|^2$  and  $N$  are as previously defined.

As shown in the previous section,  $\frac{|H(f)|^2}{N}$  can be replaced by  $\frac{K-1}{p(f)}$  where

$K$  is as previously defined and  $p(f)$  now represents the synthesized receiver response spectrum.

The Integrator subroutine, using numerical integration techniques, evaluates the expression

$$\int_0^{\infty} P(f) \frac{K-1}{p(f)} df.$$

$P(f)$  and  $p(f)$  are illustrated in Figure 6.

#### M. Antenna Synthesis

Synthesis of the transmitter and receiver antenna patterns is accomplished using data available from the environmental file records and NCF records. The pattern that is synthesized is a two-dimensional two-level pattern as shown in Figure 8. The main beam gain, labeled  $G_{MB}$  in Figure 8 is available from the NCF record. The side lobe gain,  $G_{SL}$ , is calculated using

$$G_{SL} = X + Y G_{MB}$$

where  $X = X_1$ ,  $Y = Y_1$  if  $G_{MB} \leq G_1$ ,

$X = X_2$ ,  $Y = Y_2$  if  $G_2 \geq G_{MB} > G_1$ ,

and  $X = X_3$ ,  $Y = Y_3$  if  $G_2 < G_{MB}$ .

$X_1$ ,  $X_2$ ,  $X_3$ ,  $Y_1$ ,  $Y_2$ ,  $Y_3$ ,  $G_1$ , and  $G_2$  have been determined using regression techniques on measured antenna pattern data.

Orientation of the two antennas with respect to each other are determined by the following operations simulation rules.

1. If the antenna is fixed, set  $G = G_{MB}$  if the other antenna lies in the main beam of the antenna under consideration. Otherwise, set  $G = G_{SL}$ .
2. If the antenna is rotating, nodding, or tracking, set  $G = G_{MB}$ .
3. If the antenna is sector scanning, set  $G = G_{MB}$  if the other antenna lies in the sector scanned. Otherwise, set  $G = G_{SL}$ .

When both antenna gains have been established the INR calculation is completed by forming the product of the gains with the previously calculated integral.

$$INR = G_T G_R \int_0^{\infty} P(f) \frac{K-1}{p(f)} df$$

Since one of the purposes of the MSS-2 Subsystem is to eliminate from consideration those transmitters which cannot interfere with the receiver under consideration, the calculated value of INR is compared with a threshold value which is low enough to permit the elimination of cases where the calculated INR value falls below the threshold value. This threshold value is introduced as a run parameter and can be varied from run to run.

#### N. Output Converter

A typical output from the MSS-2 Subsystem is shown in Figure 9. A line of information for each receiver in the problem is printed. If there are any transmitters in the problem that pass the INR threshold cull at the receiver under consideration, then the lines of print immediately following the receiver identify those transmitters. Referring to Figure 9, the columns of information proceeding from left to right across the page are as follows:

<u>Column</u>	<u>Contents</u>
1	Indicates whether the line pertains to a transmitter or a receiver. If a transmitter, indication is given as to whether it is desired or undesired.
2	The environment code number is a number which uniquely identifies each equipment in the problem run.
3	Nomenclature number is a code which identifies equipment type.

Modulation type is identified using the standard FCC codes for modulation type.

<u>Column</u>	<u>Contents</u>
5	Latitude of the equipment is given in degrees, minutes, and seconds.
6	Longitude of the equipment is given in degrees, minutes, and seconds.
7	Structural height of the antenna is given in feet above the site elevation.
8	A code is reported indicating whether the antenna is fixed, scanning, rotating, etc.
9	Site elevation in feet above sea level is given.
10	Tuned frequency in megacycles per second is given.
11	Pulse repetition frequency is reported in pulses per second.
12	Pulse width is reported in microseconds.
13	Great circle path distance between transmitter and receiver is reported in miles.
14	Peak power present at the receiver input terminals is reported in dbm.
15	The calculated value of INR is reported in db.
16	The frequency is reported at which maximum interference occurred.
17	A code is printed which indicates mutual antenna orientation.
18	The column entitled "Alarm No." may contain a code which indicates why the analysis pertaining to a particular equipment was aborted. Such things as missing data could cause this result.

In addition to the information contained in the columns, the INR threshold value, the propagation confidence level, and the environment interpreter mode for each run are printed in the upper right hand corner of the page.

### III. USAGE

~~The NSS-2 Subsystem and the required data base files became operational~~  
**1 July 1963. Several weeks of systems testing followed the operational date.**

During this time several minor programming bugs were eliminated, and some improvements were incorporated into the system. Timing runs were made using a sample deployment involving 45 transmitters and 45 receivers. Approximately six minutes of computer time was required to examine all receivers as effected by all transmitters.

#### ACKNOWLEDGEMENT

The work described above is sponsored by the three Military Departments and is being conducted under Contract Number AF19(604)-8440 with the Electronic Systems Division, Air Force Systems Command.

#### REFERENCES

<sup>1</sup>Fleck, R., Pethel, F., and Marini, J., "Synthesis of Equipment Characteristics for Compatibility Analysis", Proceedings of the Ninth Tri-Service Conference on Electromagnetic Compatibility, IIT Research Institute, Chicago, Illinois, October, 1963.

<sup>2</sup>Anderson, D. and Frazier, W., "A Propagation Model for Electromagnetic Compatibility Analysis", Proceedings of the Ninth Tri-Service Conference on Electromagnetic Compatibility, IIT Research Institute, Chicago, Illinois, October, 1963.

<sup>3</sup>Iseli, J., "Automatic Terrain Information Processing System", Proceedings of the Ninth Tri-Service Conference on Electromagnetic Compatibility, IIT Research Institute, Chicago, Illinois, October, 1963.



Figure 1  
MSS-2 SUBSYSTEM

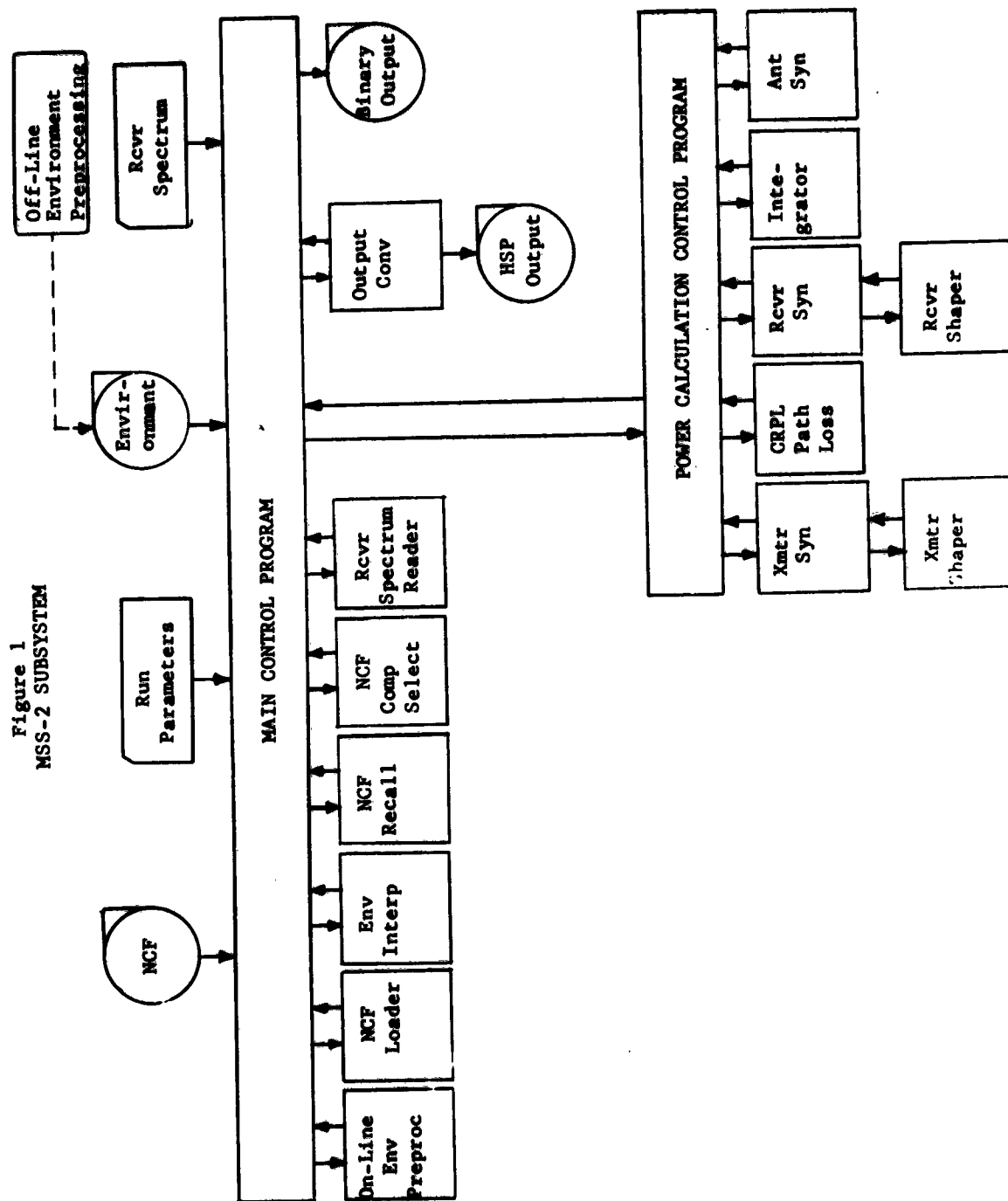


Figure 2. Tape Format of Environmental File Record 1/3

WORD	FORMAT						S <sub>1</sub>	S <sub>2</sub>	S <sub>3</sub>	S <sub>4</sub>	S <sub>5</sub>	S <sub>6</sub>	ITEM-FIELD NO.						V O B										
	S <sub>1</sub>	S <sub>2</sub>	S <sub>3</sub>	S <sub>4</sub>	S <sub>5</sub>	S <sub>6</sub>							S <sub>1</sub>	S <sub>2</sub>	S <sub>3</sub>	S <sub>4</sub>	S <sub>5</sub>	S <sub>6</sub>											
1	FLD						ASSIGNED EQUIPMENT NUMBER							-						1									
2	FLD						ASSIGNED EQUIPMENT NUMBER							-						2									
3	FLD	SP					CLASSIFICATION	PEACETIME CLEAR WEATHER (SUNDAY)							1	16B					3								
4	FLD	SP					DATE	PEACETIME CLEAR WEATHER (MONDAY)							2	16B					4								
5	FLD	SP					STATE	PEACETIME CLEAR WEATHER (TUESDAY)							6	16B					5								
6	SP	SP					TERRAIN	PEACETIME CLEAR WEATHER (WEDNESDAY)							9D	16B					6								
7	FLD	FLD	SP				SOURCE	Other Identifying Information	PEACETIME CLEAR WEATHER (THURSDAY)							9E	11	16B			7								
8	SP	SP	SP				CLEAR	SCREENED	PEACETIME CLEAR WEATHER (FRIDAY)							9F-14	9F-15	16B			8								
9	INT	SP					HEIGHT OF ANTENNA	Measured with respect to	PEACETIME CLEAR WEATHER (SATURDAY)							13A	16B				9								
10	FLD	INT	SP				Fixed vs. Scanning	PEACETIME INCLEMENT WEATHER (SUNDAY)							13B	21	16C			10									
11	INT	SP					ANTENNA ELEVATION	Type of Scanner	PEACETIME INCLEMENT WEATHER (MONDAY)							14A	16C				11								
12	INT	FLD	SP				Fixed Azimuth Direction	PEACETIME INCLEMENT WEATHER (TUESDAY)							14B-22	14B-25	16C			12									
13	INT	SP					FIXED AZIMUTH DEGREES	PEACETIME INCLEMENT WEATHER (WEDNESDAY)							14B-23	16C				13									
14	INT	SP					SCANNING DEGREES-FROM	PEACETIME INCLEMENT WEATHER (THURSDAY)							14B-26	16C				14									
15	INT	SP					SCANNING DEGREES-TO	PEACETIME INCLEMENT WEATHER (FRIDAY)							14B-26	16C				15									
16	INT	SP	SP				On Vs. Off	Alert or Combat Conditions	PEACETIME INCLEMENT WEATHER (SATURDAY)							16-37	16A	16C			16								
17	INT	FLD					Fixed Vs. Mobile	ORGANIZATIONAL UNIT DESIGNATION							7	4					17								
18	FLD	FLD	FLD				Primary Equipment Designation	Number of Transmitters	CITY OR BASE							20	21	5			18								
19	INT	FLD					SPARE	FOR FREQUENTLY MOVED EQUIPMENT ONLY							16D	8					19								
20	INT						ELEVATION							9A						20									
	FORMAT						S <sub>1</sub>	S <sub>2</sub>	S <sub>3</sub>	S <sub>4</sub>	S <sub>5</sub>	S <sub>6</sub>	ITEM-FIELD NO.																
	S <sub>1</sub>	S <sub>2</sub>	S <sub>3</sub>	S <sub>4</sub>	S <sub>5</sub>	S <sub>6</sub>							S <sub>1</sub>	S <sub>2</sub>	S <sub>3</sub>	S <sub>4</sub>	S <sub>5</sub>	S <sub>6</sub>											

Figure 2. Tape Format of Environmental File Record 2/3

W O R D	FORMAT						S <sub>1</sub>	S <sub>2</sub>	S <sub>3</sub>	S <sub>4</sub>	S <sub>5</sub>	S <sub>6</sub>	ITEM-FIELD NO.						W O R D
	S <sub>1</sub>	S <sub>2</sub>	S <sub>3</sub>	S <sub>4</sub>	S <sub>5</sub>	S <sub>6</sub>							S <sub>1</sub>	S <sub>2</sub>	S <sub>3</sub>	S <sub>4</sub>	S <sub>5</sub>	S <sub>6</sub>	
21	INT																		21
22	INT																		22
23	OCT																		23
24	OCT																		24
25	OCT																		25
26	OCT																		26
27	OCT																		27
28	OCT																		28
29	FLD																		29
30	FLD																		30
31	INT	INT	INT	INT	INT	INT	Antenna Horizontal Motion Rate 1	Antenna Horizontal Motion Rate 2	Antenna Horizontal Motion Rate 3				15	15	15	15	15	15	31
32	INT	INT	INT	INT	INT	INT	Motion Rate 1 Percent	Motion Rate 2 Percent	Motion Rate 3 Percent				15	15	15	15	15	15	32
33	FLD	FLD	FLD	FLD	FLD	FLD	Primary Mod. Type	Secondary Mod. Type	Tertiary Mod. Type				17	17	17	17	17	17	33
34	INT	INT	INT	INT	INT	INT	Midpoint of Interval Primary Mod. Type	Midpoint of Interval Secondary Mod. Type	Midpoint of Interval Tertiary Mod. Type				17-42	17-42	17-42	17-42	17-42	17-42	34
35	FPF	FPF	FPF	FPF	FPF	FPF	PRIMARY PW	TERTIARY PW					18	18	18	18	18	18	35
36	FPF	FLD	FLD	FLD	FLD	FLD	SECONDARY PW	EQUIPMENT OPERATED BY	SHEET NUMBER				18	3					36
37	INT	INT	INT	INT	INT	INT	Midpoint of Interval Primary PW-PRF	Midpoint of Interval Secondary PW-PRF	Midpoint of Interval Tertiary PW-PRF				18-43	18-43	18-43	18-43	18-43	18-43	37
38	INT	SP	SP	SP	SP	SP	Primary Frequency	Primary Frequency	Primary Frequency				19-44	19-44	19-44	19-44	19-44	19-44	38
39	INT	SP	SP	SP	SP	SP	Secondary Frequency	Secondary Frequency	Secondary Frequency				19-44	19-44	19-44	19-44	19-44	19-44	39
40	INT	SP	SP	SP	SP	SP	Tertiary Frequency	Tertiary Frequency	Tertiary Frequency				19-44	19-44	19-44	19-44	19-44	19-44	40
	S <sub>1</sub>	S <sub>2</sub>	S <sub>3</sub>	S <sub>4</sub>	S <sub>5</sub>	S <sub>6</sub>							S <sub>1</sub>	S <sub>2</sub>	S <sub>3</sub>	S <sub>4</sub>	S <sub>5</sub>	S <sub>6</sub>	
	FORMAT												ITEM-FIELD NO.						

Figure 2. Tape Format of Environmental File Record 3/3

WORD	FORMAT						S <sub>1</sub>	S <sub>2</sub>	S <sub>3</sub>	S <sub>4</sub>	S <sub>5</sub>	S <sub>6</sub>	ITEM-FIELD NO.						WORD
	S <sub>1</sub>	S <sub>2</sub>	S <sub>3</sub>	S <sub>4</sub>	S <sub>5</sub>	S <sub>6</sub>							S <sub>1</sub>	S <sub>2</sub>	S <sub>3</sub>	S <sub>4</sub>	S <sub>5</sub>	S <sub>6</sub>	
41	FLD	FLD	FLD			DATA SOURCE(O)						GEOGRAPHICAL AREA		WORK UNIT NUMBER				41	
42	FLD						BOOKLET NUMBER						-						42
43	INT	INT	INT			WEEKDAY DAY OPERATION		WEEKDAY NIGHT OPERATION		WEEKEND OPERATION		16-47 16-47 16-47				43			
44	PFP	PFP		PFP			PRIMARY PRF		TERTIARY PRF				18 18		44				
45	PFP	PFP		PFP			SECONDARY PRF		18				45						
46																	46		
47																	47		
48																	48		
49																	49		
50	INT						BINARY CHECK SUM						-		50				
													</						

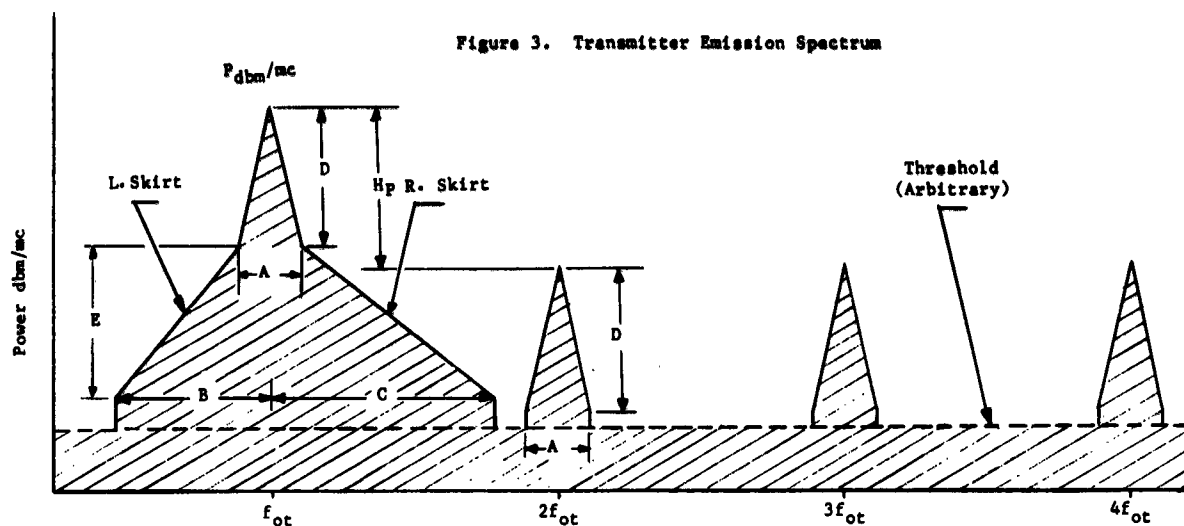


Figure 4. CCIR Empirical Curves

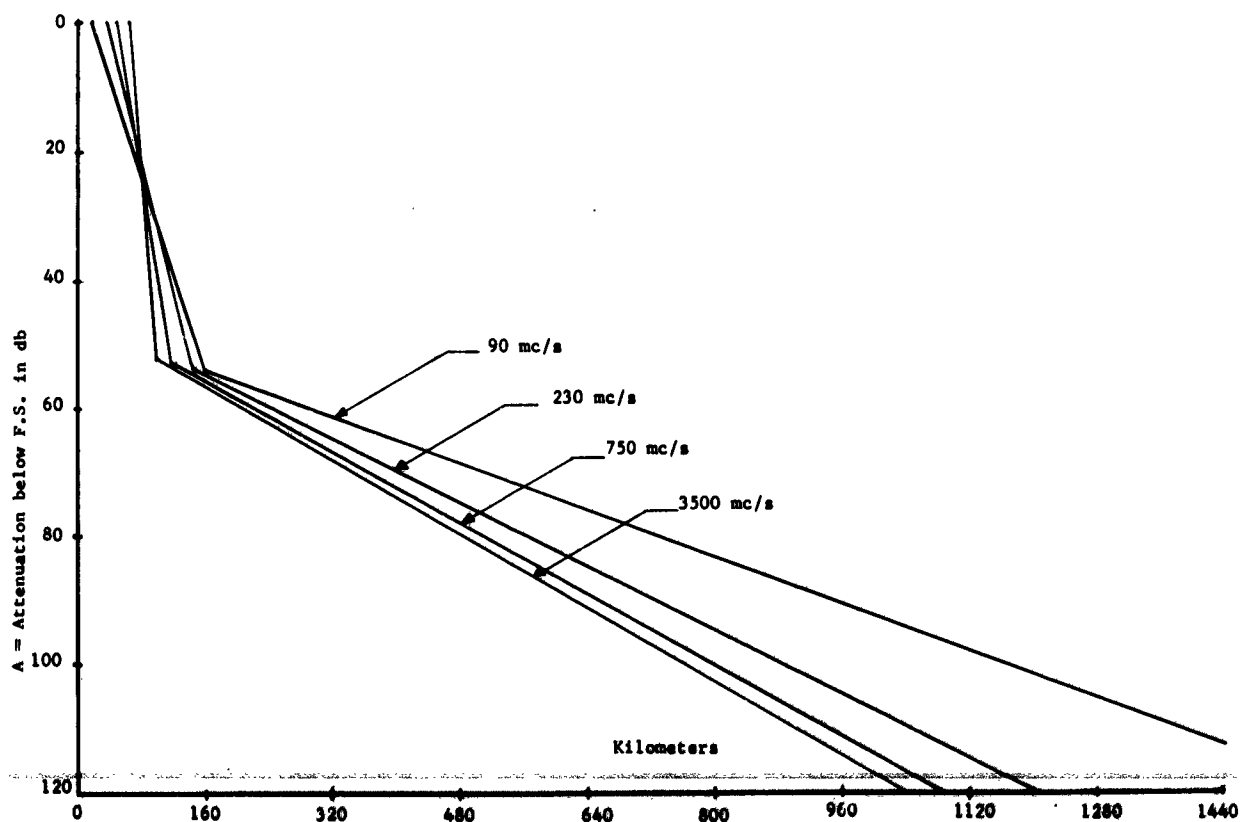


Figure 5. Emission Spectrum at Receiver Input Terminals

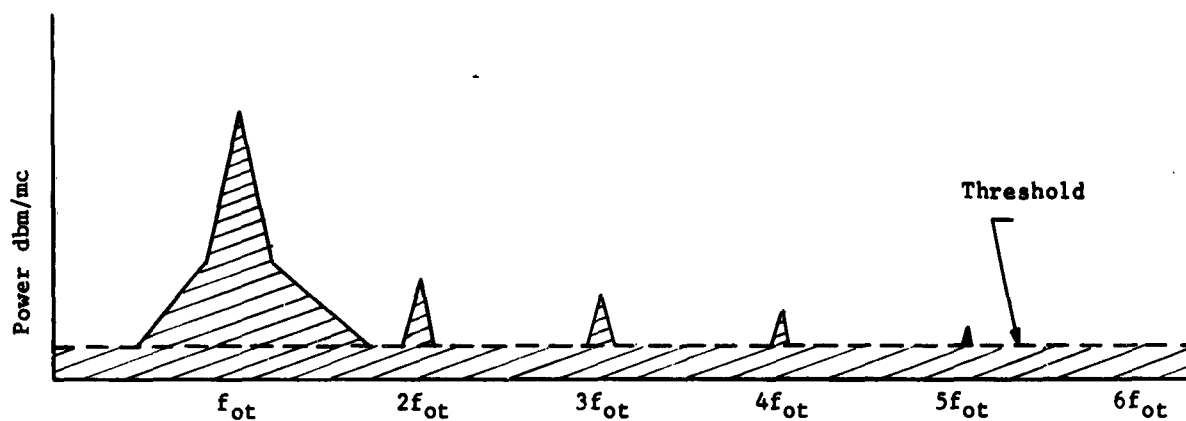


Figure 6. Spectrums to be Integrated

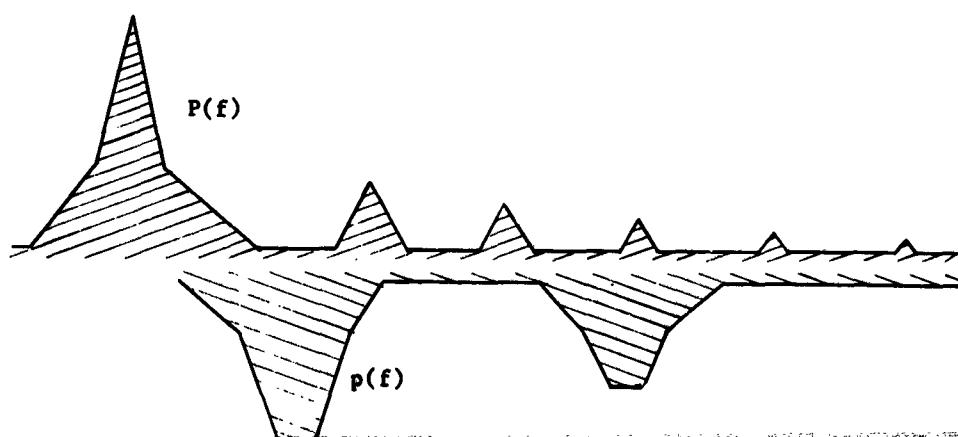


Figure 7. Receiver Response Spectrum

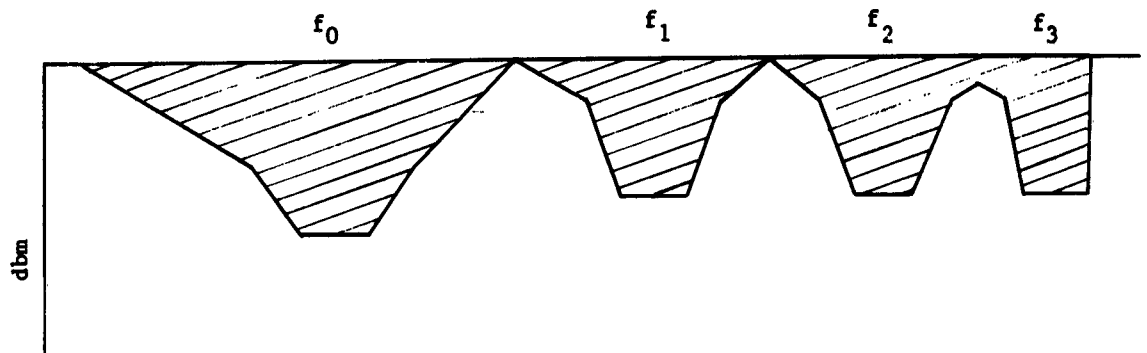
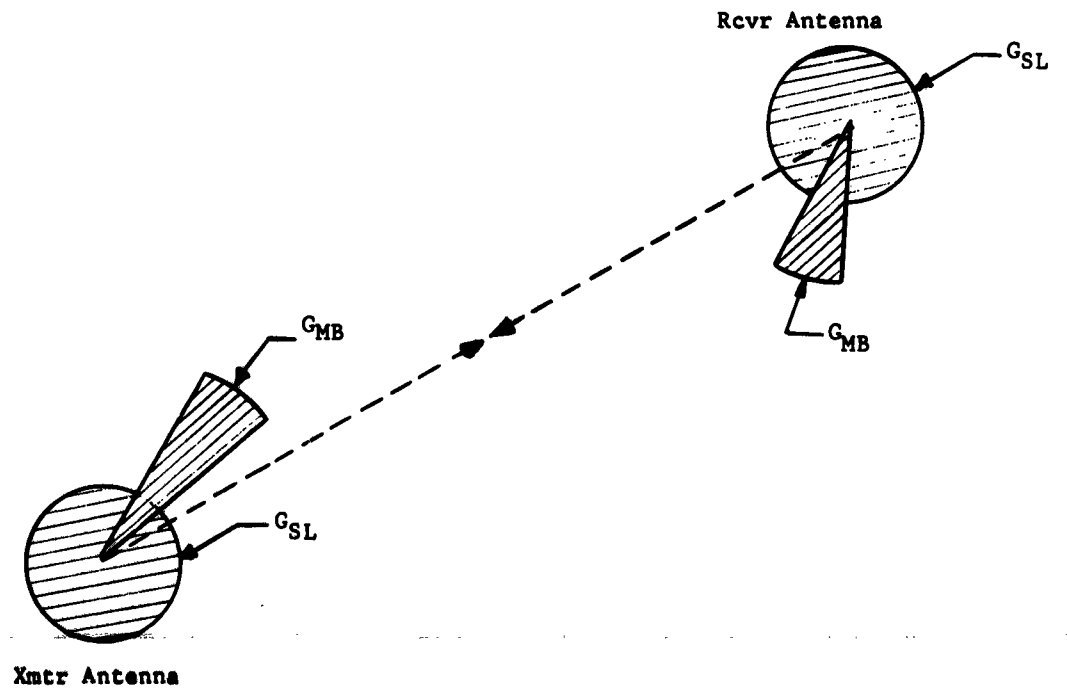


Figure 8. Antenna Representation







## **AUTOMATIC TERRAIN INFORMATION PROCESSING SYSTEM**

**J. Iseli  
IIT Research Institute  
Electromagnetic Compatibility Analysis Center  
Annapolis, Maryland**

**Abstract.** - As an integral part of its operational problem solving capability, the Electromagnetic Compatibility Analysis Center (ECAC) has created a data processing system for the UNIVAC 1107 which will provide the following automated Terrain Information processing capabilities.

- 1) The ability to create, maintain, compress, and retrieve from a multi-reel, random access, variable spaced, terrain elevation information file.
- 2) The ability to automatically generate terrain profiles between pairs of specified points, where elevation data points occur at discrete distances ranging from approximately every 100 feet to every 3000 feet.
- 3) The ability to automatically calculate terrain profile characteristics parameters required in propagation analysis.
- 4) The ability to generate visual terrain profile displays.

This paper discusses the above capabilities and their use in RFI analysis.

### **I. INTRODUCTION**

For the accurate estimation and simulation of electromagnetic interference, knowledge of the terrain between pairs of equipment locations is essential. Moreover, this knowledge must be gained in some sort of automatic way in any efficient large scale electromagnetic compatibility analysis system, since reaction time (time lapse between posing and solution of a problem) becomes prohibitively large if manual profiling is used in the analysis of environments consisting of large numbers of equipment pairs. Also, manual profiling significantly restricts the simulation capability of such an analysis system.

For these reasons, the ECAC has, in the past eighteen months, expended effort in the creation of an automatic computer profile generation capability. The acquisition of such a capability necessitates the solution of the following three problems:

- 1) To find an automatic or semi-automatic source of digitized terrain elevation information.
- 2) To generate a computer capability to store, compress, update and retrieve this information.

- 3) To design and implement, on a large scale digital computer, a data processing system to automatically generate terrain profiles and extract from them information required in RFI analysis, or, in particular, propagation analysis.

The ECAC is presently involved in the solution to the first problem and has satisfactorily resolved the last two. It is the purpose of this paper to present to the RFI community two data processing systems developed and implemented on a large scale digital computer by the ECAC to solve problems two and three above. The systems to be described are an integral part of the ECAC Electromagnetic Compatibility Analysis System.

## II. TERRAIN FILE

The basic unit of digitized terrain elevation information consists of a 121 by 121 matrix all of whose entries are elevation representations. This terrain matrix consists of elevations extracted from a suitable map by overlaying a mesh consisting of 121 vertical and 121 horizontal lines on a specified portion of the map and extracting elevations at each lattice point. The mesh spacing, that is, the distance separating adjacent vertical or horizontal elevation sites ranges from approximately every 100 feet to every 3000 feet at discrete intervals. (See Figure 1 for an enumeration of possible spacings.) Thus, there are eight possible collections of elevation matrices; one for each allowable spacing.

The ECAC terrain file consists of eight multi-reel, random access subfiles; one for each collection of elevation matrices of the same spacing. Each reel or magnetic tape belonging to a given subfile consists of a label block, index block, and an elevation matrix for each index entry and terminates with either an end of file or an end of reel sentinel block. For one magnetic tape in a file, the terrain file index consists of one computer word specifying the number of entries in the index, an entry for each elevation matrix contained on the tape, and a checksum for the block of information. Each entry in the index block consists of two computer words of the following form:

IDENT	BLANK	Word 1
a	b	Word 2

The first twelve binary bits of the first word contain a serially assigned integer used in retrieving the elevation matrix referenced by the entry. The remaining twenty four binary bits of the first word are left blank when the index occurs on magnetic tape. However, in applications, the index exists in core storage whereas the elevation matrices exist in bulk storage such as magnetic drum. In this case, the twenty four bits are used to specify the location in bulk storage of the first word of the elevation matrix referenced by the entry. The second word of an entry consists of two eighteen binary bit half words containing respectively the longitude and latitude, expressed in an

integral number of minutes, of the lower left hand location of the elevation mesh characterized by the elevation matrix referenced by the index entry. For computer implementation, elevations are coded in multiples of twenty feet and expressible in eleven binary bits. (See Figure 2.) Elevations are recorded in a matrix block by entering three per word where each required eleven bits is preceded by one bit whose function will be explained later. The elevations are recorded serially beginning at the lower left hand entry, up the first column, then up the second, the third, etc., until the whole matrix is recorded. These elevations are preceded by a computer word whose first, left-most, twelve binary bits contain the same serially assigned integer as the one in the index entry referencing this matrix block. The last word in the block is a checksum used in data processing.

Each terrain elevation information subfile can exist in two states: uncompressed and compressed. That just explained is the uncompressed state. In the compressed state, everything remains the same save that the terrain matrix blocks are compressed to minimize storage requirements. Compression is accomplished by coding the occurrence of serially repeating elevations, indicating this by entering a binary 1 in the left-most bit of the 12 bit word containing an elevation if the elevation is repeated, and a binary 0 if it is not. In case the elevation is repeated, the next third word, 12 binary bits, contains, right-justified, the number of times the elevation repeats.

Figure 3) represents an illustration of four computer programs and their inter-relationships, which presently comprise the ECAC Terrain Maintenance and Retrieval System. These are:

- 1) The terrain file preprocessor which takes terrain elevation information accrued manually, and formats it into a form suitable for inclusion into the ECAC terrain file by the terrain file updating and maintenance program.
- 2) The terrain file updating and maintenance program which provides the capability to create, update, and incorporate new terrain elevation information into the multi-reel, random access, uncompressed ECAC terrain elevation information file.
- 3) The terrain file compression program which transforms uncompressed reels of the uncompressed terrain file into compressed reels by coding redundant elevations, thereby minimizing storage requirements.
- 4) The terrain file retrieval and listing program which has two distinct functions which can be performed separately or jointly with the uncompressed terrain file. The retrieval function will retrieve specified elevation matrices from either the compressed or uncompressed terrain files and create an output tape containing these elevation matrices with their index. The listing function will retrieve specified elevation matrices from the uncompressed terrain file and format the information for a high speed printer listing.

This system provides the ECAC the ability to create, maintain, compress, and retrieve from a multi-reel, random access, terrain elevation information file.

### III. TERRAIN PROFILING AND EXTRACTION

Computer generation of Terrain Profiles is accomplished in the following manner: An approximation of the great circle path defined by two specified site locations is constructed by determining all points of intersection of the great circle path with the boundaries of the elevation meshes represented by elevation matrices. This is done assuming a fixed spacing for the elevation meshes. Beginning at the left-most site location, straight lines are drawn between the above determined intersection points. (See Figure 4.) The resultant line segment curve constitutes an approximation to the great circle path consistent with the accuracy of the terrain elevation information at the coarsest spacing. Each straight line segment lies wholly within the area represented by an elevation matrix. Thus, for each elevation matrix containing a segment of the great circle path approximation, a profile segment is generated by extracting elevations along the straight line. Extraction is accomplished by determining the inclination of the straight line segment lying within the elevation matrix. If the inclination is greater than  $45^\circ$ , elevations are extracted by linearly interpolating between given horizontal mesh elevations for each point of intersection of the straight line with a horizontal mesh line, and if less than  $45^\circ$ , interpolation is done with respect to vertical mesh lines. It is worth noting that extracted elevations are no more than the square root of two times the mesh spacing apart. The terrain profile between two given site locations is thus the collection of segment profiles determined by the great circle path approximation.

Once a profile is generated, it is necessary for propagation analysis to extract certain terrain dependent geometric parameters characterizing the intervening terrain between two equipment locations. (See Figure 5) These parameters, which are enumerated in Figure 5, are extracted from a terrain profile in a manner similar to that described in: "The Use of Angular Distance in Estimating Transmission Loss and Fading Range for Propagation Through a Turbulent Atmosphere Over Irregular Terrain" by K. A. Norton, P. L. Rice, and L. E. Vogler, which appeared in the October 1955 issue of the Proceedings of the IRE. Figure 6 illustrates the computer system which generates terrain profiles and extracts from them, terrain characteristics parameters. The computer programs involved are:

- 1) The Terrain Drum Load routine which loads a retrieved ECAC Terrain Elevation Information File onto magnetic drum; updates its index for retrieval purposes and completes its function by loading onto drum the updated index.
- 2) The Index Calculation routine which determines, in the required order, those elevations matrices required to generate the ~~terrain profile between two specified site locations.~~

- 3) The Path Calculation routine which determines the longitude and latitude of each point of intersection of the great circle path between two given site locations with the terrain matrices through which the path traverses.
- 4) The Terrain File Decompression routine which decompresses terrain matrices by decoding coded elevation redundancies. It should be noted that the system always uses either compressed or uncompressed terrain information, but no mixture of the two.
- 5) The Terrain Profile Generator which computes the segment profile along the straight line path connecting any two points within the area described by a given elevation matrix.
- 6) The Profile Generation Control program which coordinates the execution of the above four routines in generation of the terrain profile between two given site locations.
- 7) The Profile Normalizer which constructs a complete profile from segment profiles. For a specific terrain profile, it could happen that a required terrain matrix is not available when needed, either because it does not exist in the file or because it does exist but is in error. In either case, a profile is generated with segments missing due to lack of information. This routine has the additional function of statistically characterizing the terrain for those segments for which terrain information was lacking, thus enabling the system to utilize incomplete profile information.
- 8) The Profile Extractor which computes the terrain dependent parameters indicated in Figure 5, for each profile processed.
- 9) The Display Generator which formats a normalized terrain profile for plotting on a High Speed Printer.
- 10) The Profile Extraction Control program which coordinates the execution of the above three routines in performing any of the following functions, either individually or in any logical combination:
  - i) Generating a High Speed Printer (HSP) listing of a normalized profile.
  - ii) Generating an HSP profile plot.
  - iii) Extracting terrain characteristics parameters and recording them either on magnetic tape or as an HSP listing.
- 11) The Terrain Profiling and Extraction Control program which coordinates the above ten programs in providing the ECAC the

ability to automatically generate terrain profiles with elevations spaced at discrete intervals ranging from approximately every 100 feet to every 3000 feet, and extract from them terrain dependent parameters required in propagation analysis and output the option information specified in 10) above.

It is worth mentioning that this system, for any particular problem run, can process terrain information from any subfile (at any of the eight possible elevation spacings) and in either compressed or uncompressed form. Moreover, the system can utilize incomplete terrain information for any particular problem environment; that is, if for any problem area, terrain coverage is not available, that which is available can be utilized by the system in generating incomplete profiles which are statistically completed during profile extraction.

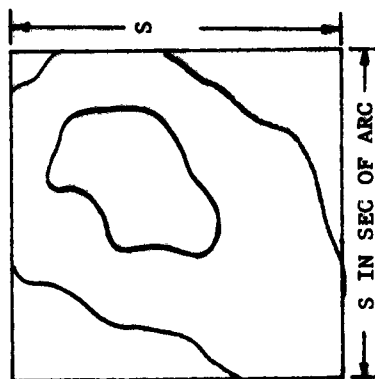
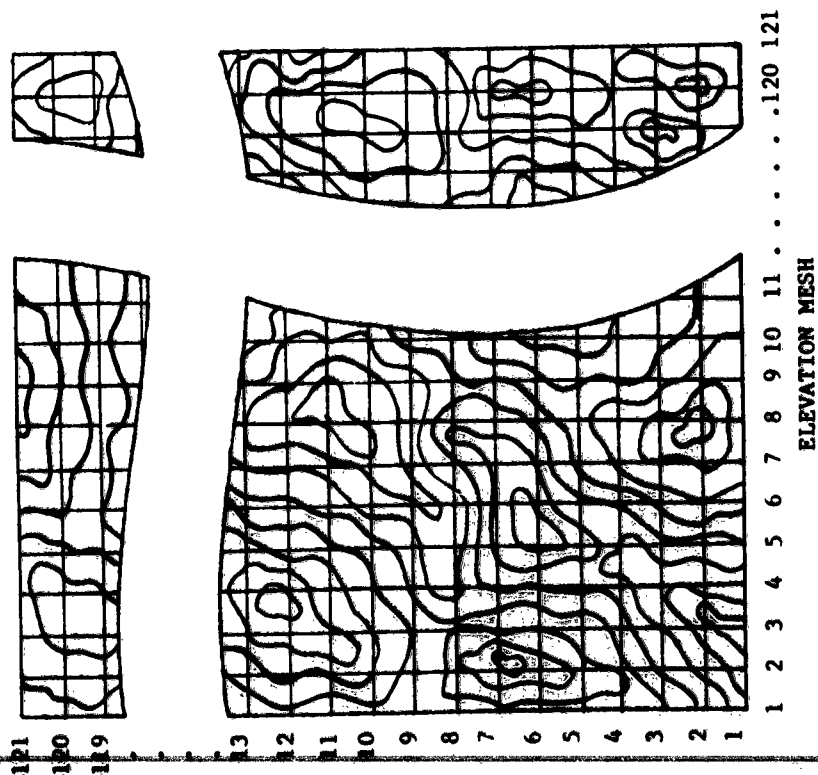
As an indication of the efficiency of this system, timing estimates of the profile generator used in conjunction with the 30 second spaced subfile come to approximately one mile per millisecond.

#### ACKNOWLEDGEMENTS

Credit is given to the following ECAC persons for significant design and programming contributions to the reported Data Processing Systems: Miss B. Black and Messrs. D. Anderson, R. Albert, F. Giordano, R. Gordon, M. Litzky, and W. Wiard. Gratitude is expressed for the developmental guidance given by Messrs. J. B. Scott and J. A. Zoellner.

The work described above is sponsored by the three Military Departments and is being conducted under Contract Number AF19(604)-8440 with the Electronic Systems Division, Air Force Systems Command.

# ECAC TERRAIN FILE



S VALUES	APPROX. DIST. IN FEET
1 SEC	100 FEET
2 SEC	200 FEET
3 SEC	300 FEET
5 SEC	500 FEET
6 SEC	600 FEET
10 SEC	1000 FEET
15 SEC	1500 FEET
30 SEC	3000 FEET

DESIGN MESH SPACINGS

Figure 1

# ECAC TERRAIN FILE FORMATS

## COMPRESSED ELEVATION MATRIX

IDENT	0	0	0	0
0	200	1	250	4
1	300		2	1 350
	3	0	400	0 350
1	300		3	0 250
1	275		2	1 300
	4	0	350	0 375
1	400		5	1 425
	3	1	450	5
0	425	0	400	0 375
0	350	0	325	1 300
	2	1	400	2
0	450	1	1	
CHECKSUM				

## UNCOMPRESSED ELEVATION MATRIX

IDENT	ERROR CODE	0	0
200	250	250	0
250	250	250	0
300	300	300	0
350	350	350	0
350	400	350	0
300	300	300	0
300	250	275	0
275	275	300	0
300	300	300	0
300	350	375	0
400	400	400	0
400	400	400	0
425	425	425	0
425	450	450	0
450	450	450	0
450	425	400	0
375	350	325	0
300	300	300	0
400	400	400	0
450	1	1	0
CHECKSUM			

## TERRAIN FILE INDEX

NO. OF ENTRIES		
IDENT	BLANK	
a	b	
IDENT	BLANK	
a	b	
IDENT	BLANK	
a	b	

## TERRAIN FILE TAPE

ECAC LABEL BLOCK
TERRAIN INDEX
FIRST ELEVATION MATRIX
SECOND ELEVATION MATRIX
LAST ELEVATION MATRIX
END OF FILE OR END OF REEL SENTINEL

Figure 2



# ECAC TERRAIN MAINTENANCE AND RETRIEVAL SYSTEM

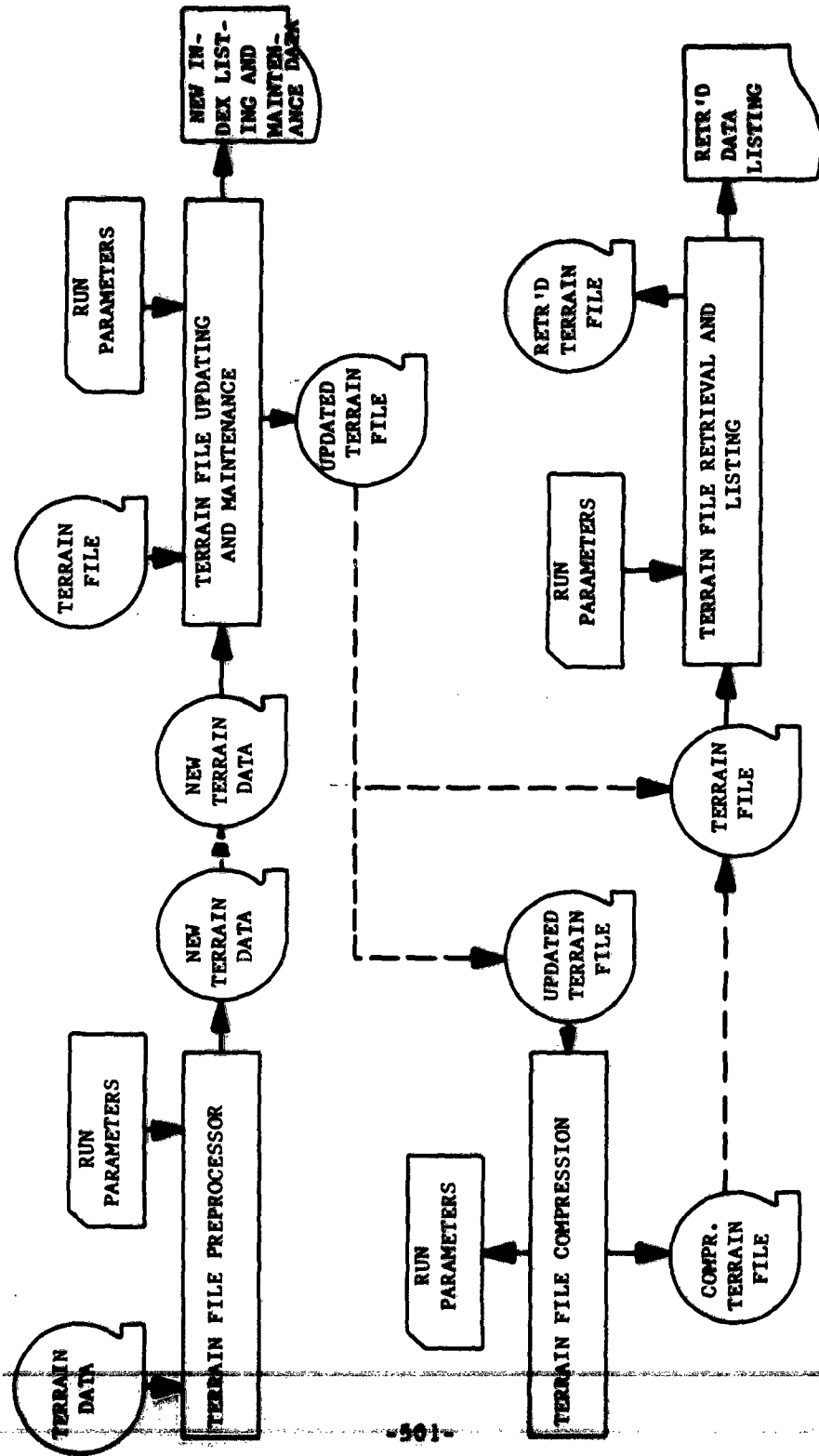


Figure 3

# ECAC TERRAIN PROFILE EXTRACTION

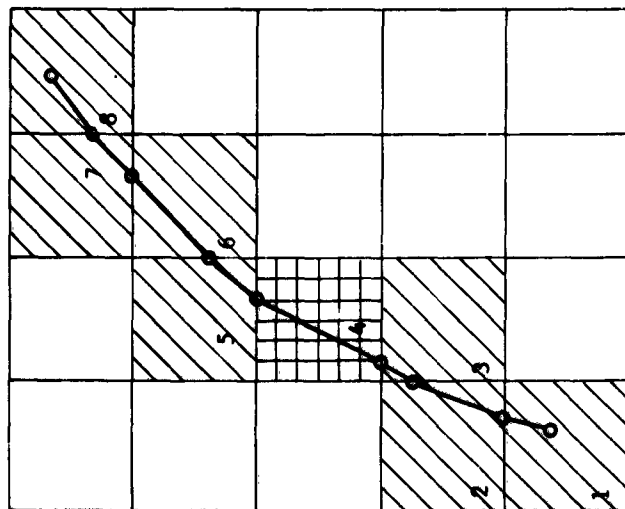


Figure A  
An Array of 20 Terrain Blocks

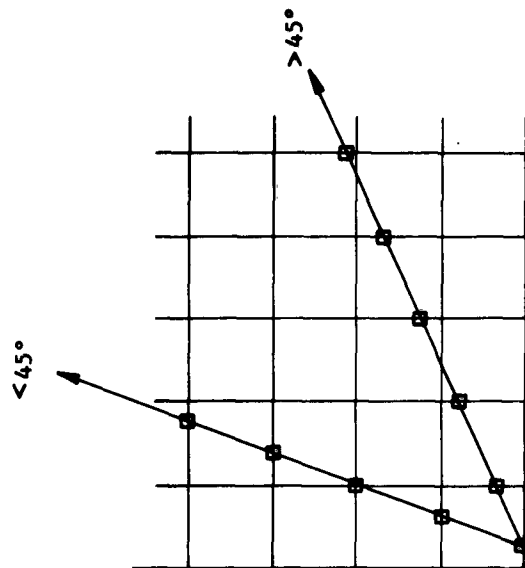


Figure B  
Interior of a Terrain Block

Figure 4

# ECAC PROFILE PARAMETER EXTRACTION

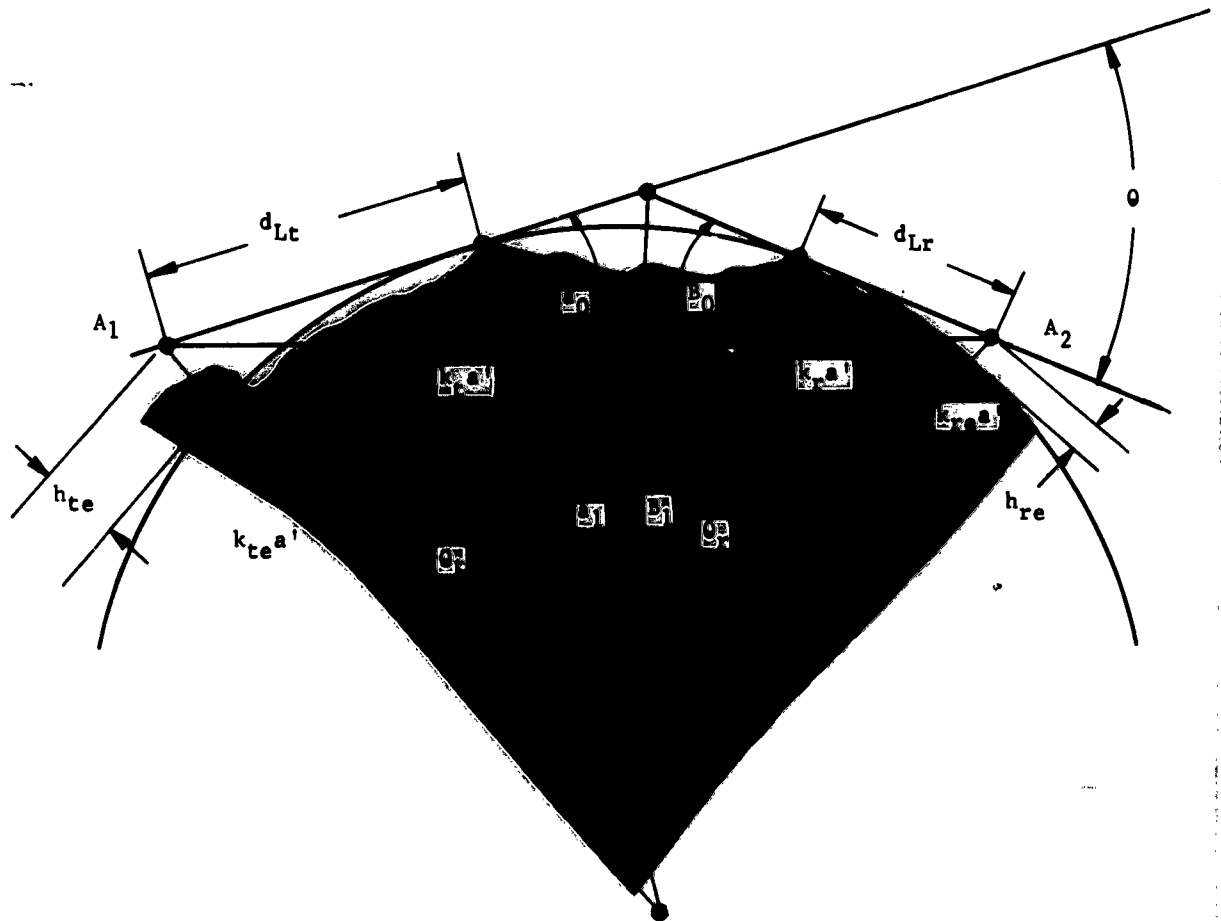


Figure 5

# ECAC TERRAIN PROFILING AND EXTRACTION SYSTEM

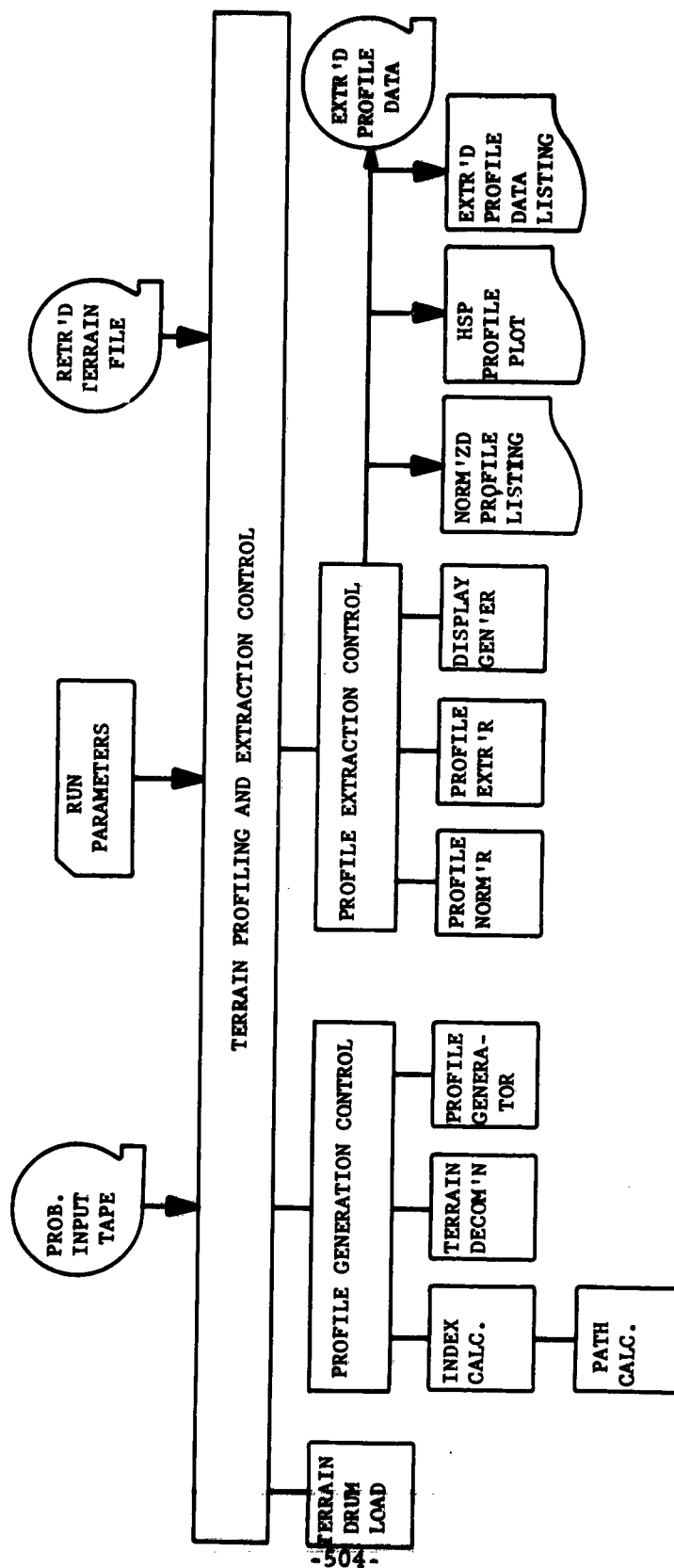


Figure 6

## A PROPAGATION MODEL FOR ELECTROMAGNETIC COMPATIBILITY ANALYSIS

W. E. Frazier and D. S. Anderson  
IIT Research Institute

Electromagnetic Compatibility Analysis Center  
Annapolis, Maryland

**Abstract.**- The computerized simulation of an electromagnetic interference environment requires an automatic representation of radio frequency propagation. Such a routine must have the capability to select the applicable mode of propagation and process the problem according to the appropriate theory. The Electromagnetic Compatibility Analysis Center (ECAC) is developing propagation models to fulfill these requirements.

This paper discusses an automatic propagation computation routine or model for both horizontally and vertically polarized tropospheric wave transmission. Input parameters for the model include effective antenna heights, path surface parameters, and atmospheric refractivity. The various modes of propagation included in the model are discussed. The techniques employed in the mode selection which are based on frequency and path geometry are also explained. Some computer results and an engineering flow diagram are presented.

### 1. INTRODUCTION

Radio propagation is one of the most important functions to be considered in a mathematical model formulated to simulate an electromagnetic environment. A computer automated propagation model for this purpose must be capable of operating in various modes of propagation. In a problem containing many emitters, the inputs necessary for an interference prediction at a given receiver would involve the parameters describing propagation paths of various lengths. Path loss calculations for some radiators would fall into the radio-line-of-sight category and others would be beyond radio-line-of-sight. Depending upon such parameters as frequency, polarization, path lengths, and effective antenna heights, energy may propagate from a radiating transmitter to a victim receiver via a number of ways or modes. This is true for both the within and beyond radio-line-of-sight categories. Furthermore, significant changes in received fields may be attributed to characteristics of the transmission path such as surface roughness, surface electrical properties, and atmospheric and ionospheric conditions.

Considering the above, two questions must be answered before an automatic propagation model may be constructed. The first is: "What prediction accuracy must the model provide?" It was decided that the prediction model discussed here should provide more than a gross estimate of the propagation phenomena. This dictates that the analysis should be based on valid theoretical methods. The second question is: "Over what frequency range should the model be applicable?" This model was designed to analyze problems involving frequencies from 50 Mc to 20 kMc.

Thus, it was determined that the initial problem areas would require the need for a tropospheric propagation model to predict basic median transmission loss over a smooth earth. The model should consider only paths involving far field propagation.

The propagation model given here is currently being used to predict basic median transmission loss over line-of-sight and beyond line-of-sight

paths when the transmitter and receiver are located in the troposphere. The theoretical equations used in the model are based on mathematical, physical methods by H. Bremner<sup>1</sup>, K. A. Norton<sup>2</sup>, and A. Fresnel<sup>3</sup>. A detailed collection of these and other methods is given in Propagation Data for Interference Analysis, RADC-TRD-61-313 by Dr. H. R. Reed. Tropo-scatter loss is computed using the empirical method by L. P. Yeh<sup>4</sup>. Loss predictions may be obtained for both horizontally and vertically polarized frequencies from 50 Mc to 20 kMc.

The character of the troposphere is assumed to be such that a standard earth atmosphere prevails which defines an effective earth radius of  $4/3$  the true average radius.

The programmed version of this model is referred to as the smooth-curve-smooth-earth propagation model<sup>5,6</sup> (SCSE). This name denotes the curve smoothing operations applied with the model in the computer program. These operations consist of limiting the value of the reflection loss, and providing for a smooth transition between B. L. O. S. intermediate or diffraction and tropo-scatter loss predictions.

## II. DESCRIPTION OF COMPUTER MODEL

As indicated on Figure 1, which is included to orient the reader for later discussions, the propagation regions represented within this model are:

1. Reflection Region
2. Intermediate Region
3. Diffraction Region
4. Tropospheric Scatter Region

Figure 1-A shows a  $4/3$  earth chart depicting a transmission path profile containing a transmitting antenna,  $h_t$ , and receiving antenna,  $h_r$ , on a smooth earth. Figure 1-B shows a propagation loss graph relative to the path profile in Figure 1-A. The propagation loss graph is positioned directly above and coordinated with the path profile and relates the general point-for-point correspondence between propagation loss, propagation regions, and the transmission path geometry.

Figure 1, shows that the reflection region theoretically begins near the transmitting antenna and ends at  $d_D$  miles. The intermediate region theoretically begins at  $d_D$  and continues to a distance  $d_G$  and includes the transmitter smooth earth radio horizon. The smooth earth diffraction field begins at  $d_G$  and continues on indefinitely (shown as the dotted curve beyond  $d_G$  in Figure 1-B). However, the predominant mode of propagation in the far diffraction region is tropospheric scatter. The theoretical distance where the scatter and diffraction fields become equal is designated as  $P_{DTS}$  miles. Beyond this distance, tropospheric scatter fields predominate.

Figure 2, is a functional block diagram of the smooth earth propagation model which is programmed for the UNIVAC 1107 computer at ECAC.

The diagram shows the basic sequence followed in making the various computations within the model.

First, the model must be supplied values for fifteen input parameters. Briefly, these parameters are: frequency,  $f_{mc}$ ; distance,  $d_{sr}$ ; antenna aperture dimension,  $L$ ; transmitter and receiver effective antenna heights,  $h_t$ ,  $h_r$ ; path surface electrical parameters at four locations, dielectric constants  $\epsilon_{r1}$ ,  $\epsilon_{r2}$ ,  $\epsilon_{r3}$ ,  $\epsilon_{r4}$  and conductivities  $\sigma_1$ ,  $\sigma_2$ ,  $\sigma_3$ ,  $\sigma_4$ ; modulus of the atmospheric refraction index,  $N_0$ ; and a polarization decision parameter,  $A_p$ . A more detailed explanation of these parameters will be given later along with the engineering flow diagram.

First, the limit of the near field is checked against the input value of path length,  $d_{sr}$ . If the path length is greater than the near field limit, the model will then determine in which of the included far field regions the receiver lies.

The path length is checked against the radio-line-of-sight distance,  $d(L.O.S.)$ , over a smooth  $4/3$  earth. If the receiver is within radio-line-of-sight of the transmitter, it will be in either the reflection region or in the L.O.S. intermediate region. The distance between the reflection and diffraction regions is referred to here as the intermediate region. For some path lengths, the receiver will be beyond radio-line-of-sight of the transmitter. In this model, the receiver will then be in either the B.L.O.S. intermediate region or in the diffraction region. In addition, the tropospheric scatter region is considered to coincide with the L.O.S. intermediate and diffraction regions.

The HV notation shown on the L.O.S. or B.L.O.S. intermediate and the diffraction blocks specifies that vertical polarization loss predictions require the use of horizontal-to-vertical loss conversion functions, HV functions, which are included in this model.

When the receiver is beyond radio-line-of-sight, the intermediate,  $L(I)$ , or diffraction,  $L(DF)$ , loss prediction is compared with the tropospheric scatter,  $L(TS)$ , loss prediction and the least value is used as the path loss prediction. In any region, the output path loss prediction is given in decibels, db.

A more detailed explanation of the SCSE model may now be given with the aid of an engineering flow diagram showing the mathematical equations used for computing the path loss. For convenience, the flow diagram is given first in sections showing the equations for the individual propagation regions and then a multi-mode propagation model.

The control section of the model, Figure 3, starts with the input parameters. These inputs are defined as follows:

- $d_{sr}$  = Great circle path length in statute miles between the transmitter and the receiver.
- $h_t = h_{te}$  = Effective height in feet to the center of radiation of transmitting antenna above a smooth earth.
- $h_r = h_{re}$  = Effective height in feet to the center of radiation of the receiving antenna above a smooth earth.
- $L$  = Largest linear dimension in feet of the transmitting or receiving antenna, whichever is the greater.
- $f_{mc}$  = Transmitted carrier frequency in megacycles per second.
- $\epsilon_{r1,2,3,4}$  = Permittivity of the earth relative to free space, a numeric. The subscript notation is to provide for an extension to the current work without necessitating changes in the input format.

It is intended that the subscripts for  $\epsilon_r$  and  $\sigma$  would denote the transmitter site, Fresnel reflection point, transmitter horizon, and receiver site, respectively. At the present time, the same values must be used for subscripts 1, 3 and 4, and must characterize the majority of the path surface. The Fresnel reflection zone is characterized separately with subscript 2. In the text to follow, the values for  $\epsilon_r$  and  $\sigma$  will be considered in terms of their intended use rather than the present representation.

- $N_s$  = Modulus of surface atmospheric refractive index, a numeric.  
 $A_p$  = Parameter which specifies horizontal ( $A_p = 0$ ) or vertical ( $A_p = 1$ ) polarization.

Using the wave length in meters for the input frequency,

$$\lambda_m = \frac{300}{f_m c} \text{ meters,} \quad (1)$$

the far field limit (Test I) is compared with the path length,  $d_{sR}$ .

$$(\text{Test I}) \quad d_{sR} > \frac{L^2}{\lambda_m} \quad (0.5773 \times 10^{-4}) \text{ miles,} \quad (2)$$

If the receiver is in the near field (Test I-NO), the program stops; and if in the far field (Test I-YES), the path length is compared with the radio-line-of-sight,

$$(\text{Test II}) \quad d_{sR} < \sqrt{2h_t} + \sqrt{2h_r} = d(L. O. S.) \quad (3)$$

When the receiver is within radio-line-of-sight (Test II-YES), then Test III is made to determine whether the receiver lies in the reflection region (Test III-YES) or in the L. O. S. intermediate region (Test III-NO).

$$(\text{Test III}) \quad \frac{0.01777}{f_m^{1/3} c} < \frac{h_t}{5280 d_t} = \tan \psi \quad (4)$$

When the receiver is beyond radio-line-of-sight (Test II-NO), it will be in either the B.L.O.S. intermediate region (Test IV-NO) or in the diffraction region (Test IV-YES). The B.L.O.S. propagation loss prediction from either the intermediate region or the diffraction region is compared with the tropo-scatter loss prediction (Tests V and VI). The lowest prediction is used as the path loss. Thus, the three possible B.L.O.S. outputs are intermediate loss (Test VI-NO), diffraction loss (Test V-NO), or tropo-scatter (Tests V or VI-YES).

It should be noted that any loss prediction may be given for horizontal or vertical polarization except for tropo-scatter which is considered here to be polarization independent.

The reflection region loss prediction method, Figure 4, assumes that two propagation paths exist between the transmitter and receiver antennas,



a direct or free space path and an indirect or reflected path. The indirect path is reflected from the earth in the Fresnel reflection zone between the two antennas. The free space loss is given by

$$L(\text{FS}) = 36.6 + 20 \log d_{s_n} + 20 \log f_{s_c} \quad \text{decibels.} \quad (5)$$

The variation of the reflection field relative to that of the free space field is considered due to three effects. The first is divergence of the reflected wave front due to spherical surface reflection. The divergence factor is given by

$$D = \left[ 1 + \frac{2d_t^2 d_r^2}{dh^2} \right]^{-\frac{1}{2}} \quad \text{numeric.} \quad (6)$$

Second, variation is caused by phase shift between the direct and indirect waves due to path length differences. This phase shift,  $\theta_1$ , is computed in degrees of the transmitted wavelength.

$$\theta_1 = \frac{1.385 \times 10^{-4} h_t^2 h_r^2 f_{s_c}}{d_{s_n}} \quad \text{degrees.} \quad (7)$$

Attenuation and phase shift of the indirect wave occurs during reflection. At this point the polarization parameter  $A_p$  is checked (Test X). If  $A_p = 1.0$ , the problem involves vertical polarization (Test X-NO); if  $A_p = 0$ , the problem involves horizontal polarization (Test X-YES). These variations are computed using the Fresnel reflection coefficient given by

$$R e^{i\phi} \quad (8)$$

Details of the equation for  $|R|$  and  $\phi$  are given on Figure 4.

These factors  $D$ ,  $\theta_1$ ,  $|R|$ , and  $\phi$  are combined in a propagation factor  $g(\theta)$ , which is used to compute the reflection loss,  $L(\text{rf})$ , and then the reflection region loss,  $L(\text{RF})$ .

$$g(\theta_1) = \left[ 1 + (DR)^2 + 2DR \cos(\theta_1 - \phi) \right]^{\frac{1}{2}} \quad (9)$$

$$L(\text{rf}) = -20 \log g(\theta_1) \quad \text{decibels} \quad (10)$$

$$L(\text{RF}) = L(\text{FS}) + L(\text{rf}) \quad \text{decibels} \quad (11)$$

In this model, beyond radio-line-of-sight paths (Test II-NO) will be in either the B. L. O. S. intermediate region (Test IV-NO) or in the diffraction region (Test IV-YES).

$$(\text{Test IV}) \quad d_{s_n} > \sqrt{2h_t} + \sqrt{2h_r} + \frac{162}{f_{s_c}^{1/3}} \quad \text{miles} \quad (12)$$

Equation (12) is derived using the angular distance in radians given by

$$\theta_2(\text{minimum}) = \frac{162}{5280 f_m^{1/3}} \quad \text{radians,} \quad (13)$$

where equation (13) is the expression for the minimum 4/3 earth angular distance for application of the diffraction region model. The angular distance for a general path is given by

$$\theta_2 = \frac{d_{sa} - \sqrt{2h_t} - \sqrt{2h_r}}{5280} \quad \text{radians.} \quad (14)$$

At this time the approach used to compute diffraction region loss will be discussed. Initially, it is assumed that the transmitted waves are horizontally polarized and the corresponding path loss computed. However, if the problem requirement was to predict diffraction loss for vertically polarized waves, the theoretical difference in loss between horizontally and vertically polarized diffraction fields is computed. This difference or conversion loss is added to the horizontal polarization computation to obtain a vertical polarization diffraction prediction. The conversion functions will be discussed later.

First, the techniques used to compute the horizontally polarized diffraction path loss will be explained. The basis for this method, Figure 5, was developed by K. A. Norton using H. Bremmer's diffraction equations.

The approach used to compute diffraction loss for tropospheric propagation from 50 Mc to 20 kMc proves to be much less complicated than the more general methods while not seriously affecting the prediction accuracy. Computations are simplified in the horizontal polarization case since many of the problem functions may be approximated by their limiting values. In particular, the calculation of the residual height gain,  $G[\tilde{h}(k')]$ , may be approximated for a wide range of antenna heights and surface conductivities if the transmission frequency is confined to the given range and a 4/3 earth atmosphere is assumed. For these conditions, the controlling variable  $K(k')$  lies in the range

$$K(k') \leq 0.001 \quad \text{numeric,} \quad (15)$$

with

$$b^\circ = 0^\circ \text{ to } 180^\circ \quad \text{degrees.} \quad (16)$$

In this range, the function  $\theta_o[K(k'), b^\circ]$  may be approximated by its asymptotic value.

$$\theta_o[K(k'), b^\circ] = 1.607 \quad \text{numeric.} \quad (17)$$

The height gain may now be simplified using the asymptotic value of  $\theta_o[K(k'), b^\circ]$  and the earth radius correction factor,  $k' = 4/3$ .

$$\tilde{h}(4/3) = 8.59 \times 10^{-5} \times h_{\text{feet}} \times f_m^{2/3} \quad (18)$$

This also results in the simple expressions<sup>6</sup> for horizontally polarized residual height gain,  $G [\bar{h}(4/3)]$ .

When

$$\bar{h}(4/3) \geq 2.0 \quad (\text{Test VII-YES})$$

$$G [\bar{h}(4/3)] = 0.89142 \log^2 \bar{h}(4/3) + 0.42177 \log \bar{h}(4/3) - 7.31675 \quad \text{decibels.} \quad (19)$$

When

$$\bar{h}(4/3) < 2.0 \quad (\text{Test VII-NO})$$

$$G [\bar{h}(4/3)] = 4.12806 \log^2 \bar{h}(4/3) - 2.54869 \log \bar{h}(4/3) + 8.06034 \quad \text{decibels.} \quad (20)$$

The smooth earth diffraction equation used to predict horizontal polarization loss,  $L(DF)_H$ , follows directly.

$$L(DF)_H = 61.7 + 10 \log d_{s1} + 16.667 \log f_{sc} + G [\bar{h}_t(4/3)] + G [\bar{h}_r(4/3)] + 488.69 \theta_0^{1/3} \theta_2 \quad \text{decibels.} \quad (21)$$

It should be noted that, although this model uses the limiting conditions as given above, the equations are programmed in the more general forms such that other values may be used at a later time to increase the capability of the model.

The intermediate region, Figure 6, begins within radio-line-of-sight, transcends the radio horizon of the transmitting antenna, and extends into the shadow region beyond radio-line-of-sight. In this model, the end of reflection region (Test III-NO) and the beginning of the diffraction region (Test IV-NO) are used as the L.O.S. and B. L.O.S. boundaries of the intermediate region respectively. In this region, non-uniform wave divergence in addition to trans-horizon ground waves produce electromagnetic fields which are extremely difficult and lengthy to compute. A very complex but precise method for calculating intermediate region field strength is given by H. Bremmer.

Propagation loss for receivers in the intermediate region is approximated here by linearly interpolating the loss at  $d_{s1}$  between the losses at the boundary distances. In order to check the validity of an interpolation method, loss predictions obtained by interpolation were compared to those computed using Bremmer's rigorous equations. Comparison of similar values obtained using the two methods showed an average error of approximately 1.8 db.

The boundary distance called  $d_D$  in miles, between the reflection and intermediate regions, is developed using the limiting value of the reflection angle  $\psi$ .

$$\psi^\circ(\text{limit}) = \tan^{-1} \frac{0.01777}{f_{mc}^{1/3}} = \tan^{-1} \frac{h'_t}{5280 d_{tD}} \quad (22)$$

From the above, the maximum Fresnel reflection distance,  $d_{tD}$ , may be computed as

$$d_{tD} = -H + \sqrt{H^2 + 2h_t} \quad \text{miles,} \quad (23)$$

and the boundary distance,  $d_D$ , is given as

$$d_D = -\frac{M}{2} \pm \sqrt{\left(\frac{M}{2}\right)^2 - N} \quad \text{miles} \quad (24)$$

where  $H = \frac{93.83}{f_{mc}^{1/3}} \quad (25)$

$$M = \frac{2h_t - 3d_{tD}^2}{d_{tD}} \quad (26)$$

$$N = 2(d_{tD}^2 - h_t - h_r) \quad (27)$$

The boundary between the intermediate and diffraction regions is given directly by Test IV, equation (12) or (28)

$$d_G = \sqrt{2h_t} + \sqrt{2h_r} + \frac{162}{f_{mc}^{1/3}} \quad \text{miles} \quad (28)$$

The intermediate region loss,  $L(I)_{H,V}$ , at  $d_{sm}$  is computed using the following expression for linear interpolation between the reflection loss,  $L(RF)_{H,V}$ , at  $d_D$  and the diffraction loss,  $L(DF)_{H,V}$ , at  $d_G$ .

$$L(I)_{H,V} = L(DF)_{H,V} - \left[ \frac{d_G - d_{sm}}{d_G - d_D} \right] [L(DF)_{H,V} - L(RF)_{H,V}] \quad \text{decibels} \quad (29)$$

This section details the method used here to convert a loss prediction for horizontal polarization to that for vertical polarization, Figure 7, when a receiver is in the diffraction region of a transmitter. This theoretical difference in path loss between horizontally and vertically polarized waves may be attributed to three factors which heavily depend on the electrical properties of path surface. One, the difference between horizontally and vertically polarized surface waves propagating between zero height antennas on a smooth plane earth. Two, the difference between plane earth and spherical earth propagation theory. Three, the difference in height gain when raised antennas are used. These three factors are used to compute a difference or conversion loss.

The theoretical prediction for vertical polarization diffraction loss is then given here as the algebraic sum of the conversion loss and the horizontal polarization loss values.

The conversion loss functions, HV functions, are obtained by taking the ratio of the vertical to horizontal theoretical equations as given in the literature<sup>2</sup>.

Reference to the flow diagram shows that after the diffraction loss for horizontal polarization,  $L(DF)_H$ , is computed, a polarization check is made (Test X). If the polarization is vertical (Test X-NO), the conversion loss due to spherical versus flat earth theories, HV-M, is computed using the surface parameters,  $\epsilon_{r3}$  and  $\sigma_3$ , at the transmitter radio horizon distance on the great circle path.

$$HV-M = 20 \log \frac{M_V}{M_H} = 0.0924809 f_{nc}^{1/3} d_{ra} \left[ \beta_{oH} - \beta_{oV} \right] + 10 \log \left[ \frac{\beta_{oH}}{\beta_{oV}} \right] \quad \text{decibels. (30)}$$

Using the surface parameters,  $\epsilon_{r1}$  and  $\sigma_1$ , at the transmitter site and the effective height of the transmitting antenna,  $h_{te}$ , the conversion loss due to the transmitting antenna height gain difference, HV-H<sub>t</sub>, is computed using the expressions

$$C_o = \frac{h_{te} f_{nc}}{156.8} \quad (31)$$

$$HV-H = 20 \log F \quad \text{decibels} \quad (32)$$

$$F = \left\{ \frac{1 + C_o^2 \left( \frac{\alpha_2}{\alpha_1} \right) - C_o \left( \frac{\alpha_2}{\alpha_1} \right)^{1/2} \frac{1}{\sqrt{\alpha_1}} \left[ (\alpha - \alpha_o) \left( 1 + \frac{\alpha}{\alpha_2} \right)^{1/2} + (\alpha + \alpha_o) \left( 1 - \frac{\alpha}{\alpha_2} \right)^{1/2} \right]}{1 + C_o^2 \alpha_2 - C_o (\alpha_2)^{1/2} \left[ \left( 1 - \frac{\alpha}{\alpha_2} \right)^{1/2} - \left( 1 + \frac{\alpha}{\alpha_2} \right)^{1/2} \right]} \right\}^{1/2} \quad (33)$$

HV-H<sub>r</sub> is computed for the receiving antenna by replacing the transmitter parameters with the effective height of the receiving antenna,  $h_{re}$ , and the surface parameters at the receiver site,  $\epsilon_{r4}$  and  $\sigma_4$ , in equations (31), (32) and (33).

The conversion loss due to cross polarized surface wave fields is given by

$$HV-A' = 20 \log (\alpha^2 + \epsilon_{r1}) \quad \text{decibels,} \quad (34)$$

$$\text{and} \quad \text{HV-A} = \text{HV-A}' + \text{HV-M} \quad \text{decibels} \quad (35)$$

where  $\epsilon_{r1}$  and  $\sigma_1$  for the transmitter site are used.

The diffraction loss |vertical polarization| is given as

$$L(\text{DF})_V = L(\text{DF})_H - |\text{HV-A}| + |\text{HV-H}_t| + |\text{HV-H}_r| \quad \text{decibels.} \quad (36)$$

Appendix II contains three graphs showing sample curves of HV-A', HV-M, and HV-H based on the surface parameters for sea water  $\epsilon_r = 81$  and  $\sigma = 4.64$  mho-m/m.

Figure 8 is an engineering flow diagram of the composite SCSE propagation model. The diagram shows how the control section refers the problem to either the reflection, intermediate, or diffraction mode sections. The conversion loss functions are applied following the diffraction mode computations. Finally, the tropo-scatter loss computation and tests are made to determine the predominate beyond line-of-sight electromagnetic field.

### III. COMPARISON OF SCSE PREDICTED AND CCIR MEASURED LOSS CURVES

In order to obtain a preliminary and gross validation of the SCSE model prediction capabilities, use was made of CCIR\* measured path loss data. These data are shown on Figure 9, and are extracted from DOC.V/23-E, CCIR Study Groups, Question No. 185(V), study program No. 138(V), National Bureau of Standards, 1 March 1962, Section 3- Empirical Predictions of All-Day, All - Year Median Values. These curves were developed using measurements from approximately 750 paths having a variety of antenna heights and other parameters. However, the following estimated values were given in DOC.V/23-E:  $h_t \doteq 32.8$  feet,  $h_r \doteq 984$  feet, and  $k \doteq 4/3$ . Based on the loss ranges of the tropo-scatter measured data, the average modulus of surface refractive index,  $N_s \doteq 294$ , was estimated at ECAC.

Using identical values for these parameters and horizontal polarization, a computer program of the SCSE model was used to generate a corresponding set of prediction curves. Both the CCIR measured and SCSE predicted curves were plotted on Figure 10 in order to observe their correlation.

---

\* International Consultative Committee of Radio Communications.

## APPENDIX 1

### COMPUTER RESULTS USING SCSE MODEL

Figure 11 is a sample output of the SCSE computer program. All the data of this output are in floating point notation. As shown on the output sheet, the input parameters for this problem were,

$f_{mc}$	= 5,000 Mc
$d_{1,1}$	= 20 miles
$h_t$	= 66.5 feet
$h_r$	= 25.0 feet
$L$	= 10.0 feet
$\epsilon_{r,1,2,3,4}$	= 81.0 numeric
$\sigma_{1,2,3,4}$	= 4.64 mho-m/m <sup>2</sup>
$N_s$	= 310 numeric
$A_p$	= 1.0 (vertical polarization)

These input parameters define an intermediate region problem which is computed by interpolating between the reflection loss at  $d_D$  (BIG LRF) and the diffraction loss at  $d_G$  (LDFV). The desired path loss, 157.292 db, at distance  $d_{1,1}$  is output as LOSS SM. This value is also found under intermediate output as LISM. Also listed as output is the corresponding free space loss (LFS SM) and the amount of path loss in excess of free space (LOSS-LFS SM).

In addition to the input and output data, forty-one intermediate results are available, as shown on Figure 11. The numbers above each of the printout labels correspond to those on the block diagram, Figure 8.

A further example of computer results using this model is shown in Figure 12. These curves are the result of a series of computer computations for horizontal polarization where certain input parameters ( $h_t$ ,  $h_r$ ,  $L$ ,  $\epsilon_{r,1,2,3,4}$ ,  $\sigma_{1,2,3,4}$ , and  $N_s$ ) were held constant and frequency and path length varied. These curves clearly show the characteristic lobe structure in the reflection region and the curve smoothing in the intermediate, diffraction, and tropo-scatter regions.

The data of Figure 12 is often presented in the form of Figure 13. Here the path loss in excess of free space is plotted as a function of distance for several frequencies. It is obvious that these curves have been simplified by neglecting the reflection region lobing and assigning free space loss to distance out to  $d_D$ .

## APPENDIX II

### WORKING CURVES OF THE HV FUNCTIONS BASED ON SEA WATER PARAMETERS

This appendix provides working curves of the HV functions along with an example problem illustrating their application. The data were computed using a UNIVAC 1107 computer program of the SCSE model shown in Figure 8.

Figures 14, 15, and 16 give conversion loss values for sea water conditions ( $\epsilon_r = 81$  and  $\sigma = 4.64 \text{ mho-m/m}^2$ ). Figure 14 also includes values for fresh water conditions ( $\epsilon_r = 81$  and  $\sigma = .005 \text{ mho-m/m}^2$ ). HV-A' values are shown on Figure 14 for frequencies between 1 Mc and 100 kMc. HV-M values are shown on Figure 15 for frequencies between 10 Mc and 100 kMc as well as distances from 0 miles to 500 miles on a  $4/3$  earth. HV-H values are shown on Figure 16 for effective heights from 1 foot to 100,000 feet and frequencies between 1 Mc and 100 kMc.

An application of the HV functions may be shown with the aid of the output data sheet, Figure 11, and the conversion loss graphs, Figure 14, 15, and 16. On the output sheet, Figure 11, the diffraction loss for horizontal polarization is given as LDFH = 178.331 db (output 25) corresponding to the path length DSUBG = 28.0639 miles (output 14). These values may also be read on Figure 12. Since the requirement was for vertical polarization,  $A_p = 1.0$  (input 15), the conversion loss must be computed and the loss prediction adjusted.

The following values are read on the output sheet and conversion loss curves when using the input values on Figure 11.

Function	Computed Value	Output No. (Figure 11)	Curve on Figure No.
HVM	0.440043 db	35	15
HVA PRIME	76.7012 db	36	14
HVHT	-38.3443 db	37	16
HVHR	-38.3601 db	38	16
HV	- 0.426760 db	39	NOT INCLUDED
LDFV	177.904 db	40	NOT INCLUDED

The value given as output 40 is the required prediction for vertically polarized diffraction propagation.

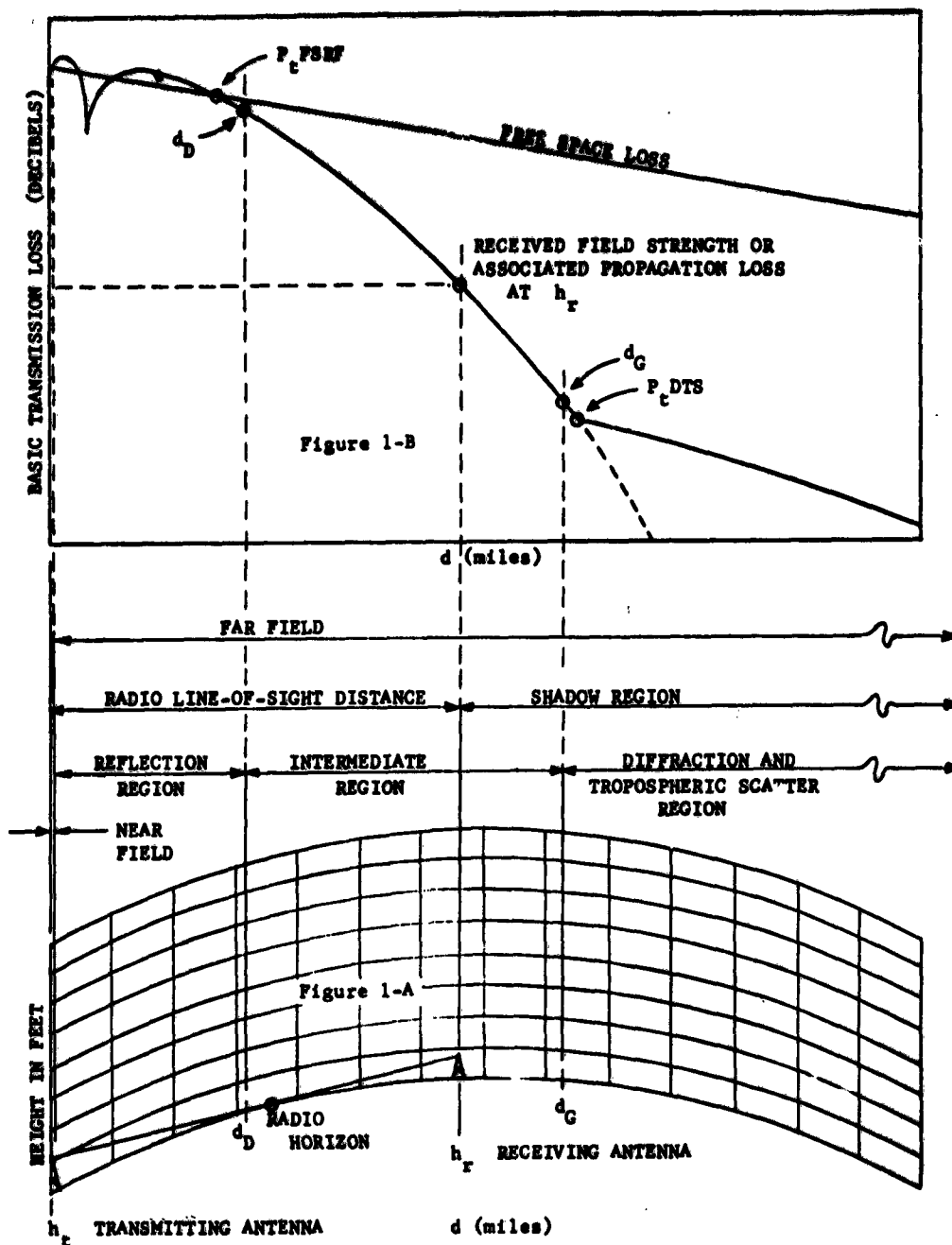


#### REFERENCES

1. H. Bremmer, Terrestrial Radio Waves, American Elsevier Publishing Company, Inc., New York, 1949.
2. K. A. Norton, P. L. Rice and L. E. Vogler, The Use of Angular Distance in Estimating Transmission Loss and Fading Range for Propagation through a Turbulent Atmosphere over Irregular Terrain, Proceedings of the Institute of Radio Engineers, Vol. 43; pp 1488-1526; October 1955.
3. H. R. Reed and C. M. Russell, Ultra High Frequency Propagation, John Wiley & Sons, Inc., New York, pp 396-400, 1953.
4. L. P. Yeh, Simple Methods for Designing Troposcatter Circuits, Institute of Radio Engineers National Conventions Records, 1960.
5. W. E. Frazier, A Smooth Earth Propagation Model for Radar Interference Prediction, DDC No. AD 297005L, 1961.
6. W. E. Frazier, Horizontal to Vertical (HV) Polarization Conversion Functions and a Comprehensive Flow Chart of the Revised SCSE Propagation Model, ECAC TM-X004-7, 1963.
7. W. E. Frazier, A Simple Model for Predicting Microwave Propagation Loss in the Intermediate Region, DDC AD 297003L, 1962

#### ACKNOWLEDGMENT

The work described above is sponsored by the three Military Departments, and is being conducted under Contract No. AF 19(60)4-8440 with the Electronic Systems Division, Air Force Systems Command.



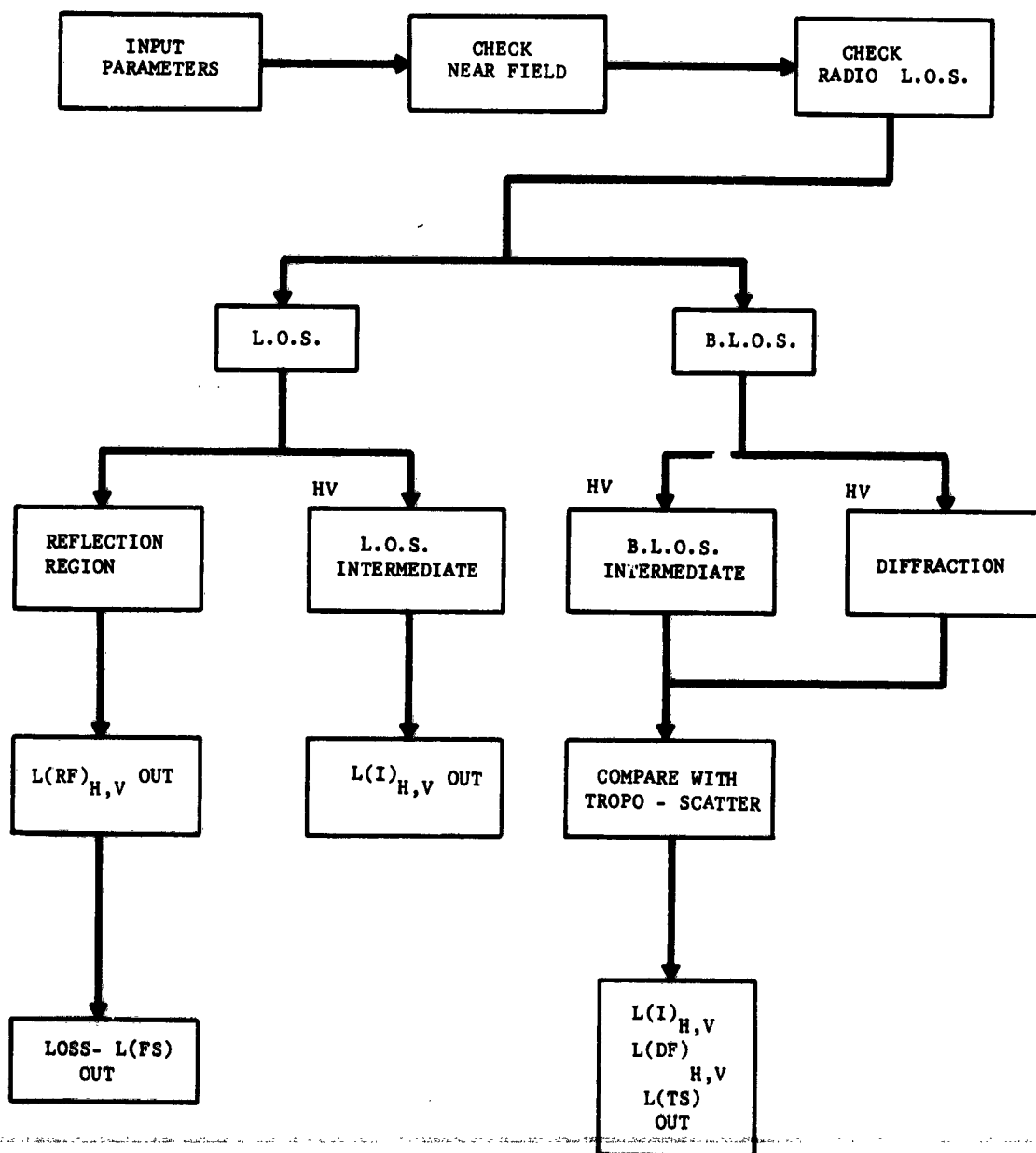
NOTE: - These curves are only intended to show trends and are not necessarily drawn to scale.

#### 4/3 EARTH CHART OF SMOOTH EARTH TRANSMISSION PATH AND CORRESPONDING PROPAGATION LOSS CURVE

Figure 1

# FUNCTIONAL BLOCK DIAGRAM OF SMOOTH EARTH PROPAGATION MODEL

FIGURE 2



### INPUT PARAMETERS AND CONTROL SECTION

Flowchart for calculating tropo-scatter loss (L(TS)) and diffraction loss (L(DIF)).

**INPUT PARAMETERS** (1 thru 15):

1. AT TRANSMITTER SITE
2. AT FRESNEL REFLECTION POINT
3. AT RADIO HORIZON OF TRANSMITTER
4. AT RECEIVER SITE

**Check Parameters:**

- CHECK RADIO FIELD L.O.S. (Note 13)
- CHECK RADIO FIELD (Note 14)

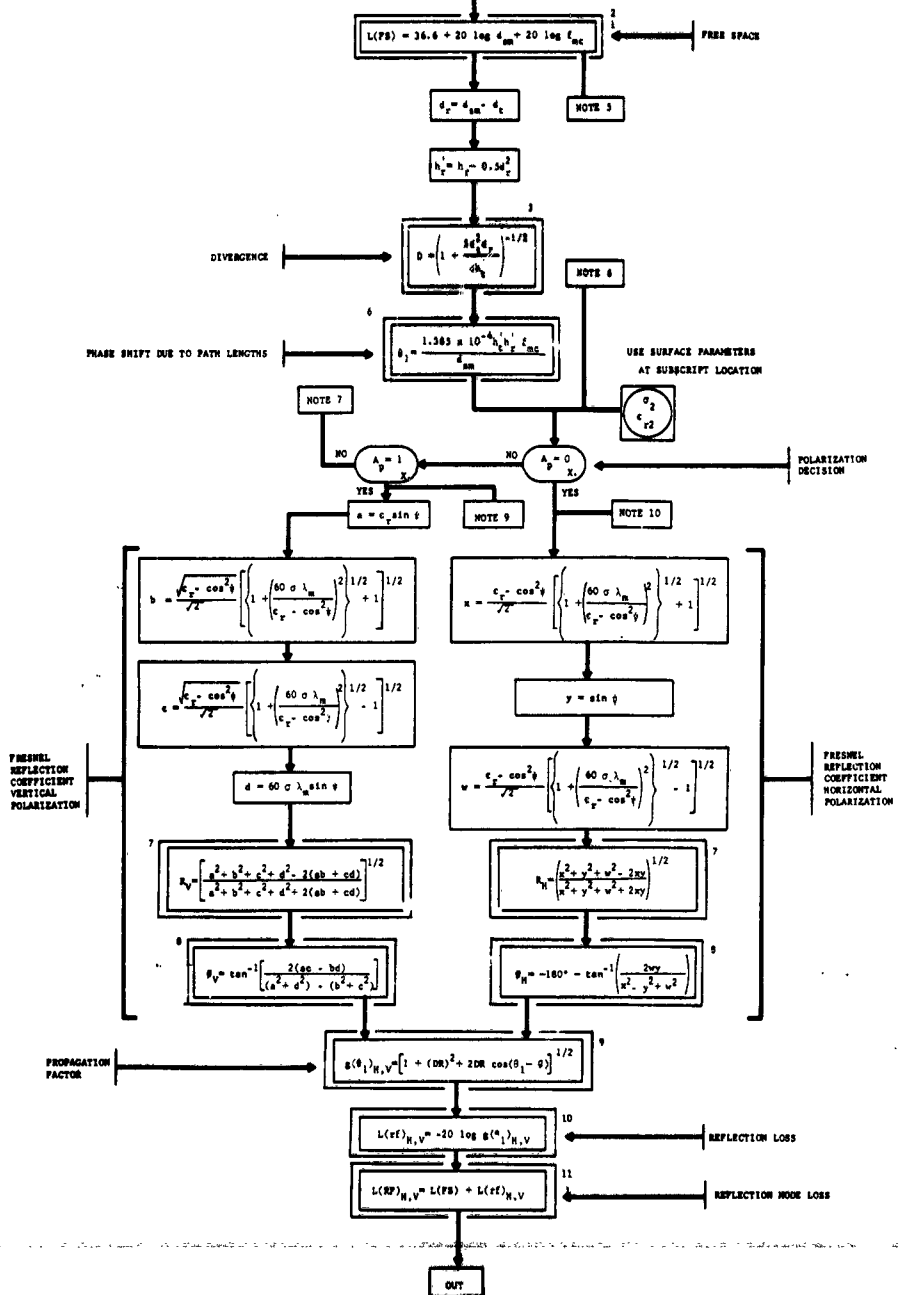
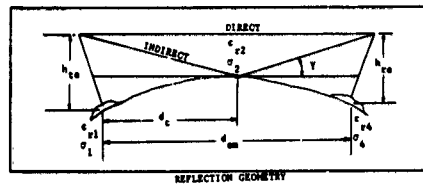
**Flowchart Steps:**

1.  $d > \frac{1}{m}$  (Note 1)
2.  $\lambda_m = \frac{300}{f_{mc}}$
3.  $d < \sqrt{\frac{2}{f_{mc}}}$  (Note 2)
4.  $d > \sqrt{\frac{2}{f_{mc}}}$  (Note 3)
5.  $d < \sqrt{\frac{2}{f_{mc}}}$  (Note 4)
6.  $d > \sqrt{\frac{2}{f_{mc}}}$  (Note 5)
7.  $d < \sqrt{\frac{2}{f_{mc}}}$  (Note 6)
8.  $d > \sqrt{\frac{2}{f_{mc}}}$  (Note 7)
9.  $d < \sqrt{\frac{2}{f_{mc}}}$  (Note 8)
10.  $d > \sqrt{\frac{2}{f_{mc}}}$  (Note 9)
11.  $d < \sqrt{\frac{2}{f_{mc}}}$  (Note 10)
12.  $d > \sqrt{\frac{2}{f_{mc}}}$  (Note 11)
13.  $d < \sqrt{\frac{2}{f_{mc}}}$  (Note 12)
14.  $d > \sqrt{\frac{2}{f_{mc}}}$  (Note 13)
15.  $d < \sqrt{\frac{2}{f_{mc}}}$  (Note 14)
16.  $d > \sqrt{\frac{2}{f_{mc}}}$  (Note 15)
17.  $d < \sqrt{\frac{2}{f_{mc}}}$  (Note 16)
18.  $d > \sqrt{\frac{2}{f_{mc}}}$  (Note 17)
19.  $d < \sqrt{\frac{2}{f_{mc}}}$  (Note 18)
20.  $d > \sqrt{\frac{2}{f_{mc}}}$  (Note 19)
21.  $d < \sqrt{\frac{2}{f_{mc}}}$  (Note 20)
22.  $d > \sqrt{\frac{2}{f_{mc}}}$  (Note 21)
23.  $d < \sqrt{\frac{2}{f_{mc}}}$  (Note 22)
24.  $d > \sqrt{\frac{2}{f_{mc}}}$  (Note 23)
25.  $d < \sqrt{\frac{2}{f_{mc}}}$  (Note 24)
26.  $d > \sqrt{\frac{2}{f_{mc}}}$  (Note 25)
27.  $d < \sqrt{\frac{2}{f_{mc}}}$  (Note 26)
28.  $d > \sqrt{\frac{2}{f_{mc}}}$  (Note 27)
29.  $d < \sqrt{\frac{2}{f_{mc}}}$  (Note 28)
30.  $d > \sqrt{\frac{2}{f_{mc}}}$  (Note 29)
31.  $d < \sqrt{\frac{2}{f_{mc}}}$  (Note 30)
32.  $d > \sqrt{\frac{2}{f_{mc}}}$  (Note 31)
33.  $d < \sqrt{\frac{2}{f_{mc}}}$  (Note 32)
34.  $d > \sqrt{\frac{2}{f_{mc}}}$  (Note 33)
35.  $d < \sqrt{\frac{2}{f_{mc}}}$  (Note 34)
36.  $d > \sqrt{\frac{2}{f_{mc}}}$  (Note 35)
37.  $d < \sqrt{\frac{2}{f_{mc}}}$  (Note 36)
38.  $d > \sqrt{\frac{2}{f_{mc}}}$  (Note 37)
39.  $d < \sqrt{\frac{2}{f_{mc}}}$  (Note 38)
40.  $d > \sqrt{\frac{2}{f_{mc}}}$  (Note 39)
41.  $d < \sqrt{\frac{2}{f_{mc}}}$  (Note 40)
42.  $d > \sqrt{\frac{2}{f_{mc}}}$  (Note 41)
43.  $d < \sqrt{\frac{2}{f_{mc}}}$  (Note 42)
44.  $d > \sqrt{\frac{2}{f_{mc}}}$  (Note 43)
45.  $d < \sqrt{\frac{2}{f_{mc}}}$  (Note 44)
46.  $d > \sqrt{\frac{2}{f_{mc}}}$  (Note 45)
47.  $d < \sqrt{\frac{2}{f_{mc}}}$  (Note 46)
48.  $d > \sqrt{\frac{2}{f_{mc}}}$  (Note 47)
49.  $d < \sqrt{\frac{2}{f_{mc}}}$  (Note 48)
50.  $d > \sqrt{\frac{2}{f_{mc}}}$  (Note 49)
51.  $d < \sqrt{\frac{2}{f_{mc}}}$  (Note 50)
52.  $d > \sqrt{\frac{2}{f_{mc}}}$  (Note 51)
53.  $d < \sqrt{\frac{2}{f_{mc}}}$  (Note 52)
54.  $d > \sqrt{\frac{2}{f_{mc}}}$  (Note 53)
55.  $d < \sqrt{\frac{2}{f_{mc}}}$  (Note 54)
56.  $d > \sqrt{\frac{2}{f_{mc}}}$  (Note 55)
57.  $d < \sqrt{\frac{2}{f_{mc}}}$  (Note 56)
58.  $d > \sqrt{\frac{2}{f_{mc}}}$  (Note 57)
59.  $d < \sqrt{\frac{2}{f_{mc}}}$  (Note 58)
60.  $d > \sqrt{\frac{2}{f_{mc}}}$  (Note 59)
61.  $d < \sqrt{\frac{2}{f_{mc}}}$  (Note 60)
62.  $d > \sqrt{\frac{2}{f_{mc}}}$  (Note 61)
63.  $d < \sqrt{\frac{2}{f_{mc}}}$  (Note 62)
64.  $d > \sqrt{\frac{2}{f_{mc}}}$  (Note 63)
65.  $d < \sqrt{\frac{2}{f_{mc}}}$  (Note 64)
66.  $d > \sqrt{\frac{2}{f_{mc}}}$  (Note 65)
67.  $d < \sqrt{\frac{2}{f_{mc}}}$  (Note 66)
68.  $d > \sqrt{\frac{2}{f_{mc}}}$  (Note 67)
69.  $d < \sqrt{\frac{2}{f_{mc}}}$  (Note 68)
70.  $d > \sqrt{\frac{2}{f_{mc}}}$  (Note 69)
71.  $d < \sqrt{\frac{2}{f_{mc}}}$  (Note 70)
72.  $d > \sqrt{\frac{2}{f_{mc}}}$  (Note 71)
73.  $d < \sqrt{\frac{2}{f_{mc}}}$  (Note 72)
74.  $d > \sqrt{\frac{2}{f_{mc}}}$  (Note 73)
75.  $d < \sqrt{\frac{2}{f_{mc}}}$  (Note 74)
76.  $d > \sqrt{\frac{2}{f_{mc}}}$  (Note 75)
77.  $d < \sqrt{\frac{2}{f_{mc}}}$  (Note 76)
78.  $d > \sqrt{\frac{2}{f_{mc}}}$  (Note 77)
79.  $d < \sqrt{\frac{2}{f_{mc}}}$  (Note 78)
80.  $d > \sqrt{\frac{2}{f_{mc}}}$  (Note 79)
81.  $d < \sqrt{\frac{2}{f_{mc}}}$  (Note 80)
82.  $d > \sqrt{\frac{2}{f_{mc}}}$  (Note 81)
83.  $d < \sqrt{\frac{2}{f_{mc}}}$  (Note 82)
84.  $d > \sqrt{\frac{2}{f_{mc}}}$  (Note 83)
85.  $d < \sqrt{\frac{2}{f_{mc}}}$  (Note 84)
86.  $d > \sqrt{\frac{2}{f_{mc}}}$  (Note 85)
87.  $d < \sqrt{\frac{2}{f_{mc}}}$  (Note 86)
88.  $d > \sqrt{\frac{2}{f_{mc}}}$  (Note 87)
89.  $d < \sqrt{\frac{2}{f_{mc}}}$  (Note 88)
90.  $d > \sqrt{\frac{2}{f_{mc}}}$  (Note 89)
91.  $d < \sqrt{\frac{2}{f_{mc}}}$  (Note 90)
92.  $d > \sqrt{\frac{2}{f_{mc}}}$  (Note 91)
93.  $d < \sqrt{\frac{2}{f_{mc}}}$  (Note 92)
94.  $d > \sqrt{\frac{2}{f_{mc}}}$  (Note 93)
95.  $d < \sqrt{\frac{2}{f_{mc}}}$  (Note 94)
96.  $d > \sqrt{\frac{2}{f_{mc}}}$  (Note 95)
97.  $d < \sqrt{\frac{2}{f_{mc}}}$  (Note 96)
98.  $d > \sqrt{\frac{2}{f_{mc}}}$  (Note 97)
99.  $d < \sqrt{\frac{2}{f_{mc}}}$  (Note 98)
100.  $d > \sqrt{\frac{2}{f_{mc}}}$  (Note 99)
101.  $d < \sqrt{\frac{2}{f_{mc}}}$  (Note 100)
102.  $d > \sqrt{\frac{2}{f_{mc}}}$  (Note 101)
103.  $d < \sqrt{\frac{2}{f_{mc}}}$  (Note 102)
104.  $d > \sqrt{\frac{2}{f_{mc}}}$  (Note 103)
105.  $d < \sqrt{\frac{2}{f_{mc}}}$  (Note 104)
106.  $d > \sqrt{\frac{2}{f_{mc}}}$  (Note 105)
107.  $d < \sqrt{\frac{2}{f_{mc}}}$  (Note 106)
108.  $d > \sqrt{\frac{2}{f_{mc}}}$  (Note 107)
109.  $d < \sqrt{\frac{2}{f_{mc}}}$  (Note 108)
110.  $d > \sqrt{\frac{2}{f_{mc}}}$  (Note 109)
111.  $d < \sqrt{\frac{2}{f_{mc}}}</$

ENGINEERING FLOW DIAGRAM OF SCSE PROPAGATION MODEL

REFLECTION REGION SECTION

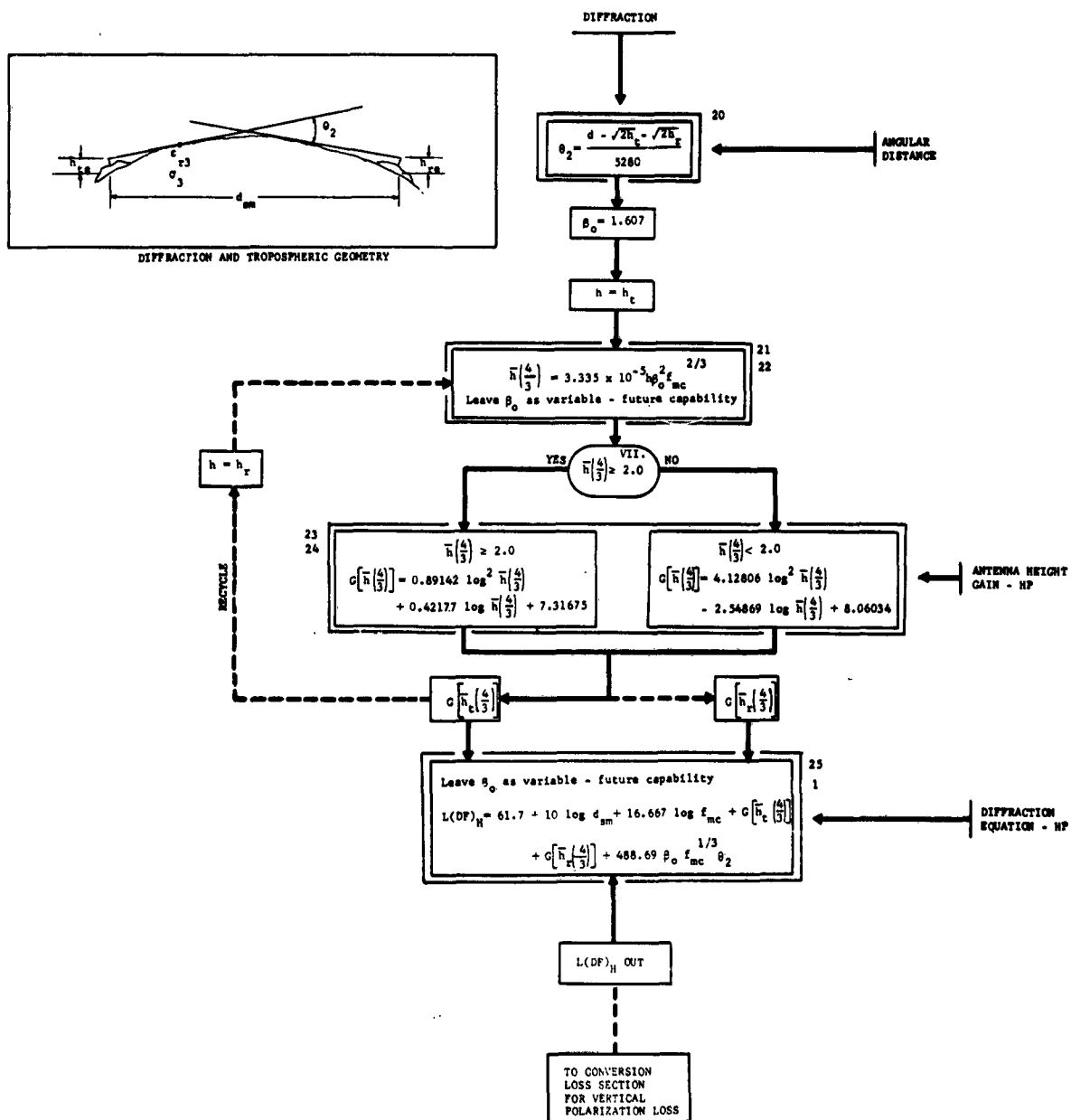
FIGURE 4



# ENGINEERING FLOW DIAGRAM OF SUSE PROPAGATION MODEL

## SMOOTH EARTH DIFFRACTION SECTION

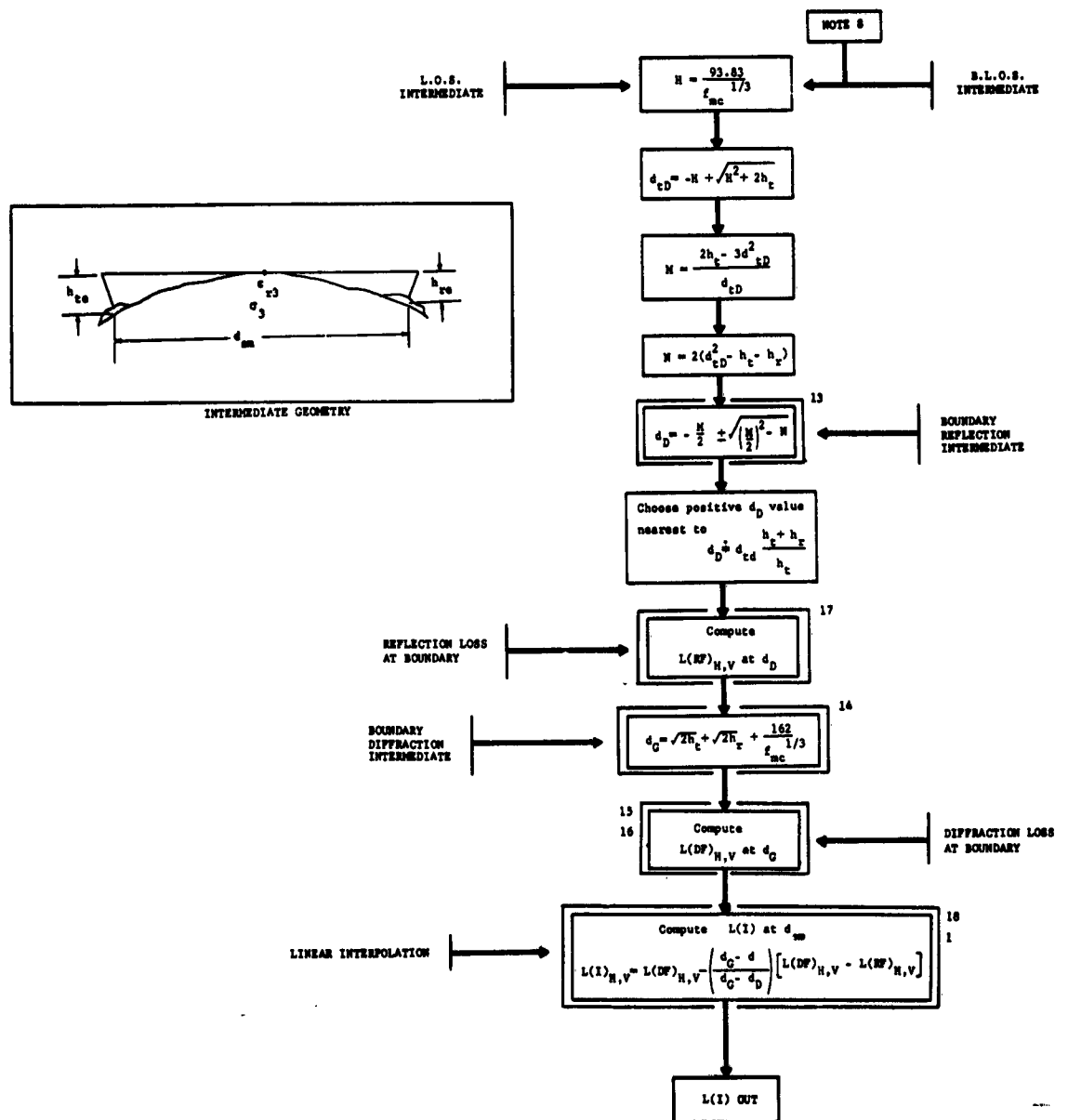
FIGURE 5



# ENGINEERING FLOW DIAGRAM OF BCSE PROPAGATION MODEL

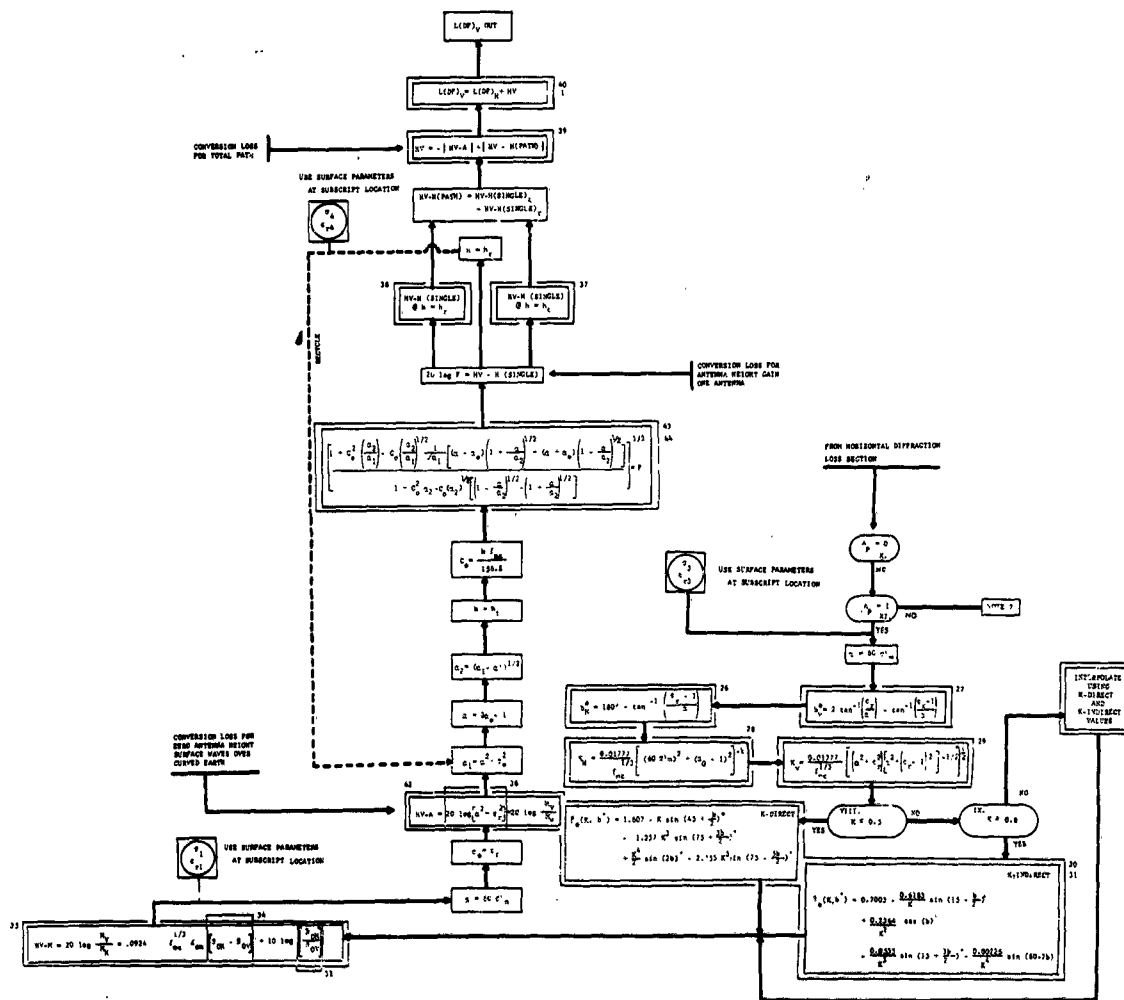
## INTERMEDIATE REGION SECTION

FIGURE 6



ENGINEERING FLOW CHART OF RICE PROPAGATION MODEL  
HORIZONTAL-TO-VERTICAL (HV) POLARIZATION CONVERSION LOSS SECTION

FIGURE 2







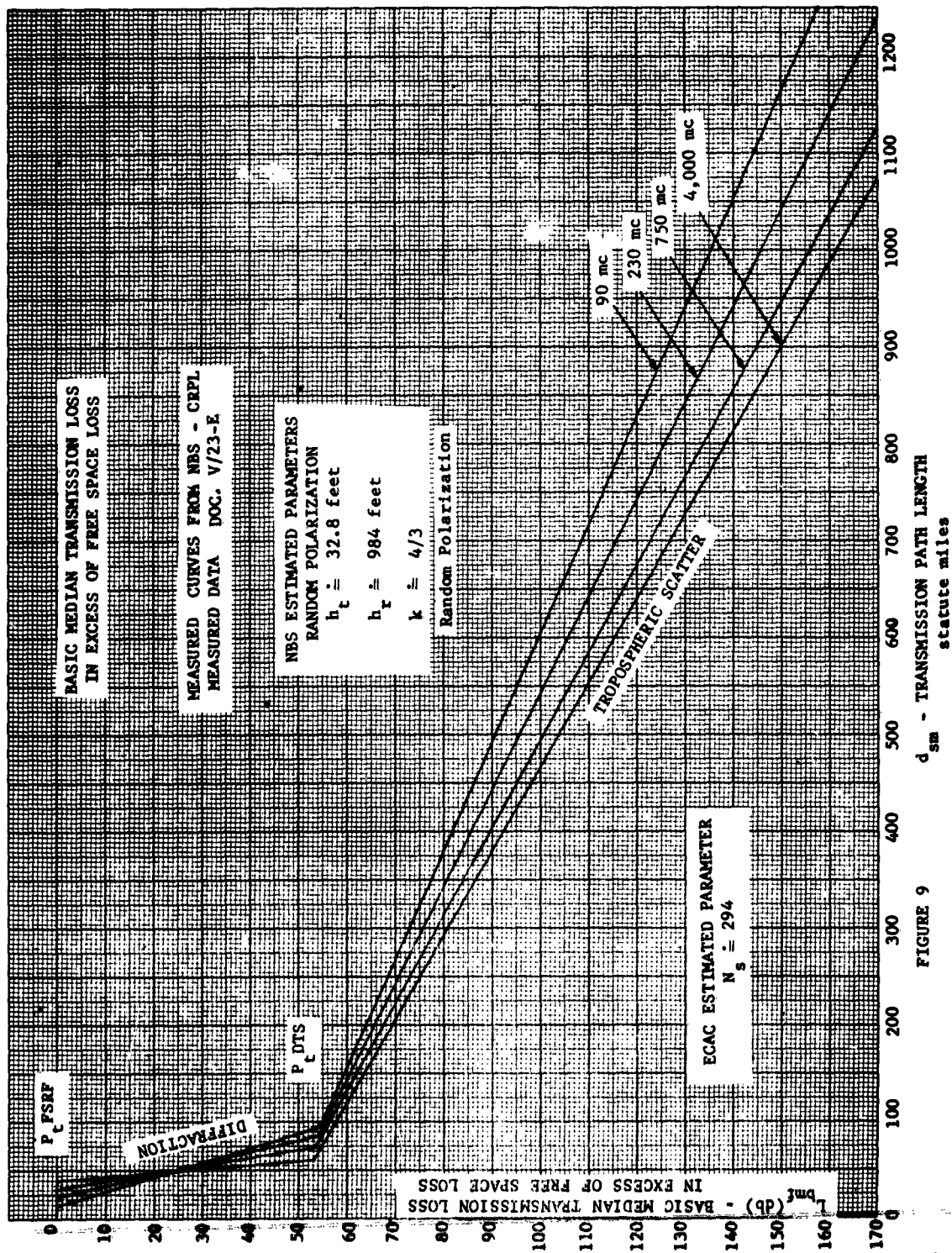


FIGURE 9

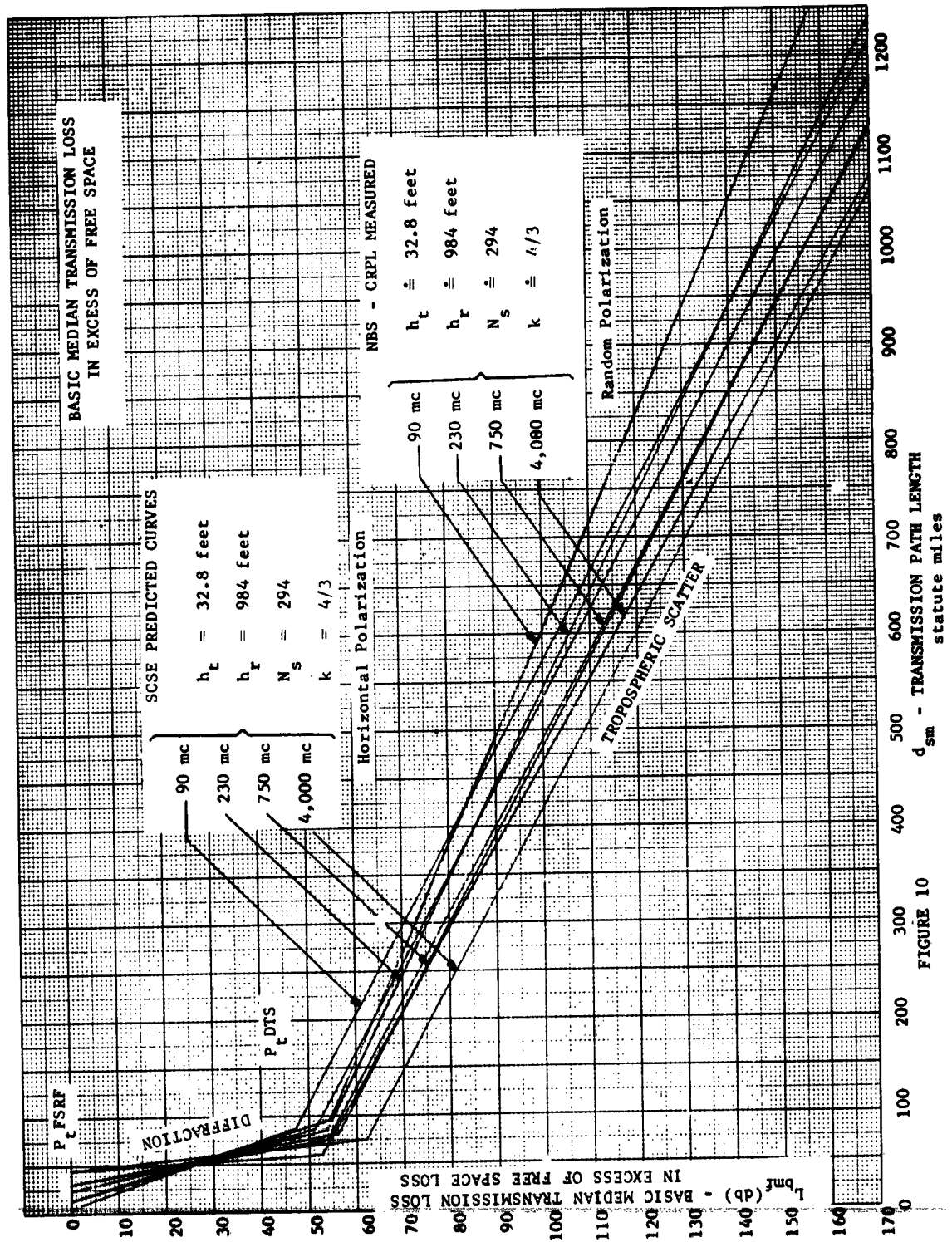
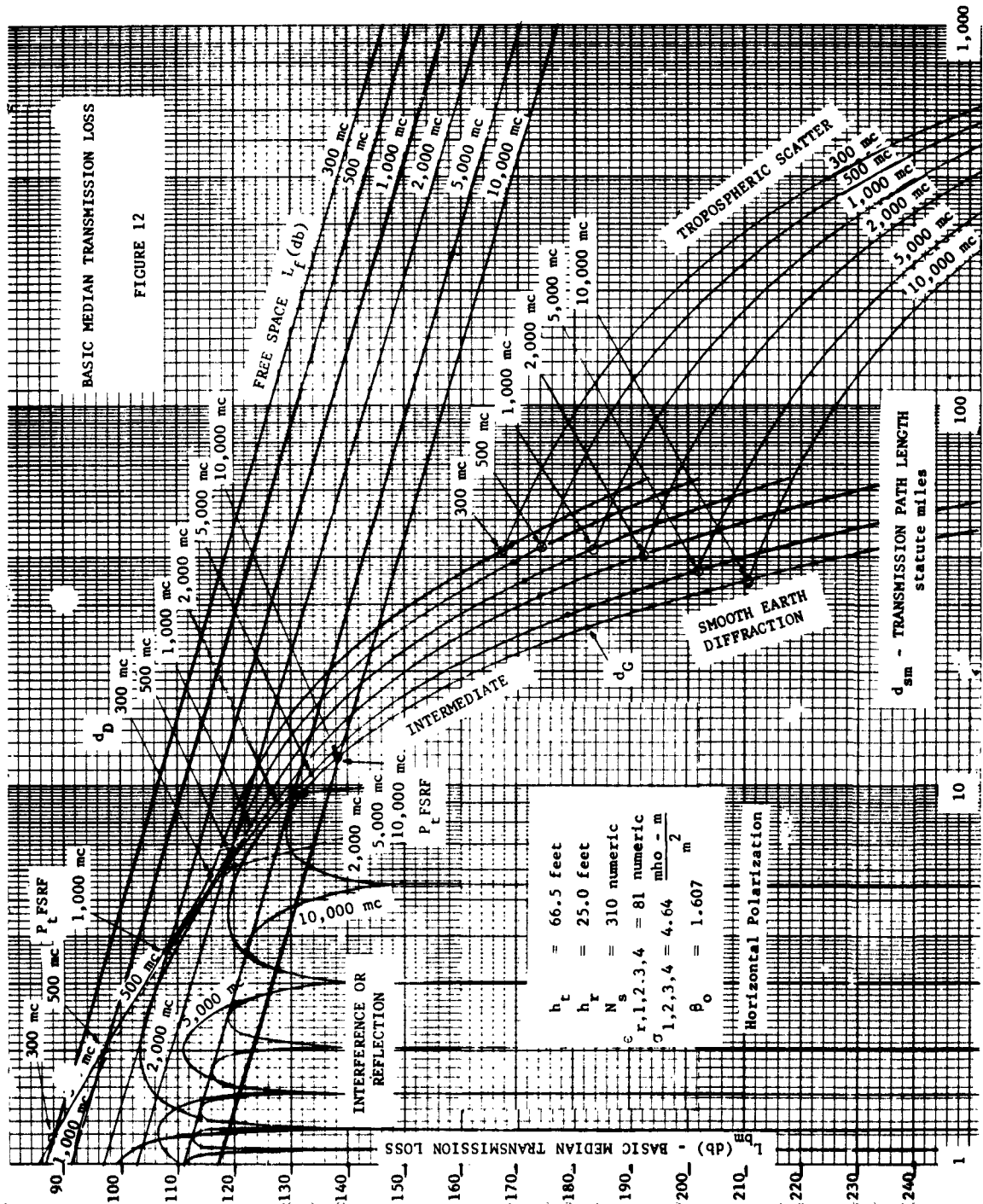
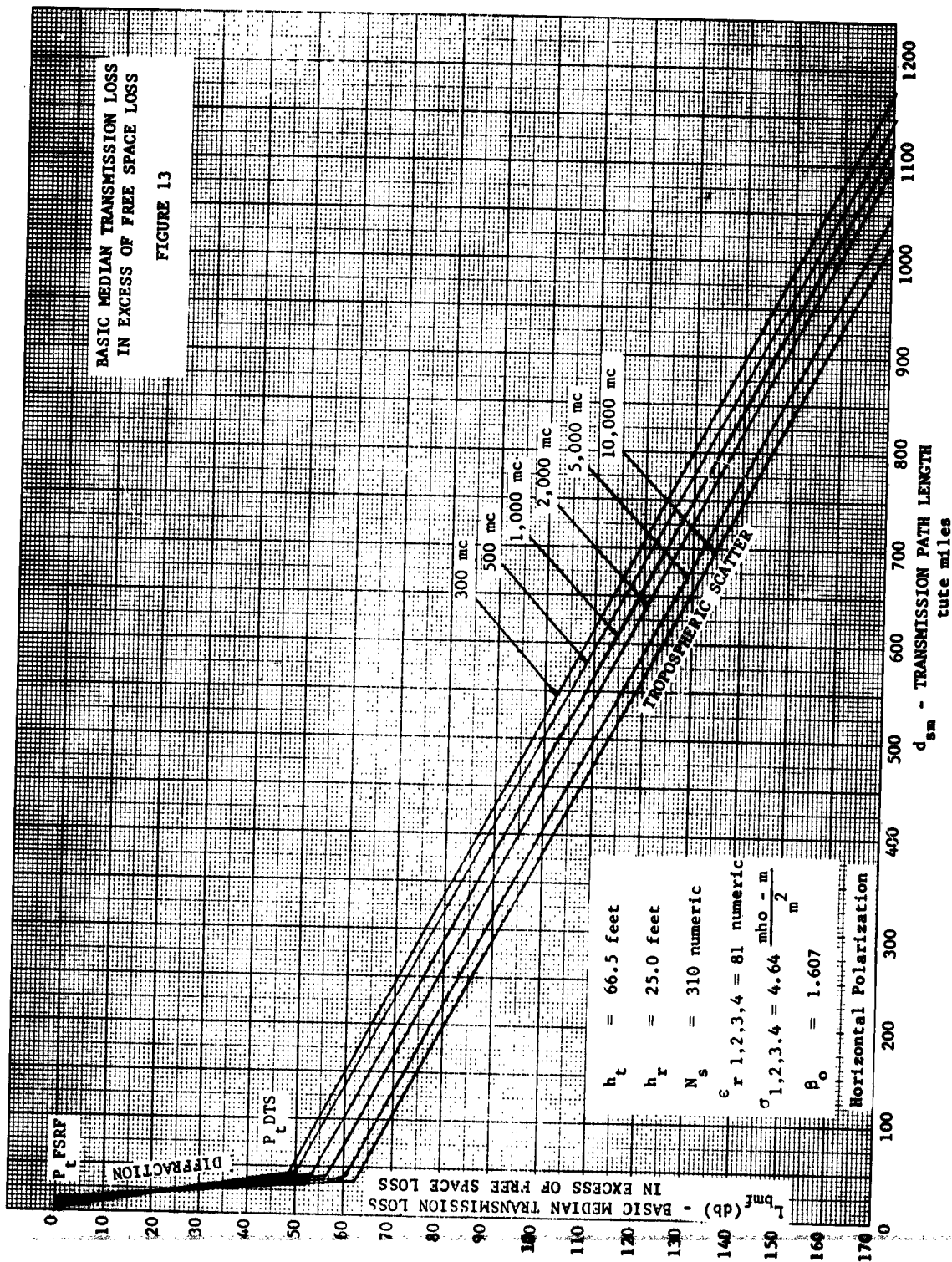


FIGURE 10







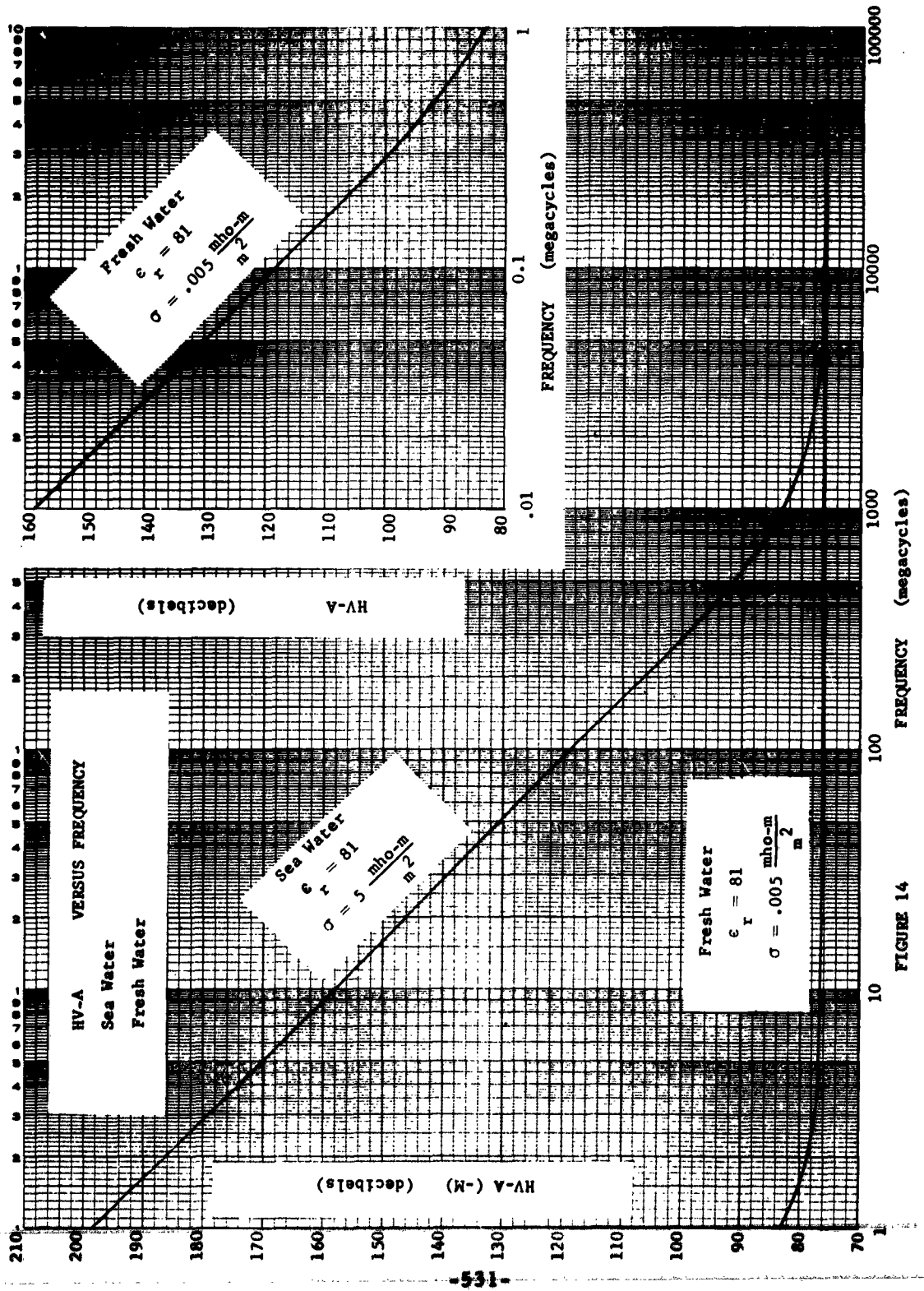


FIGURE 14



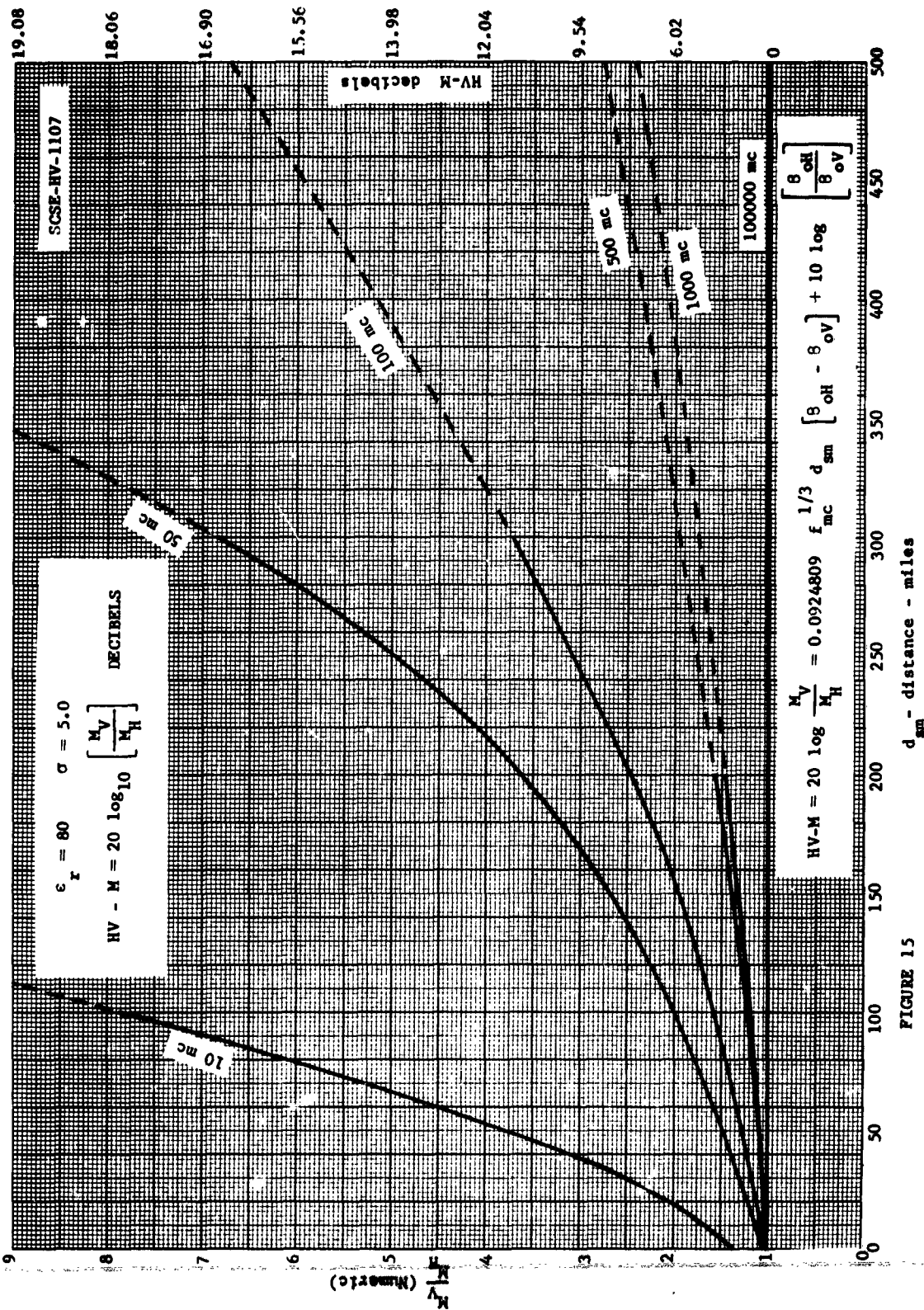


FIGURE 15



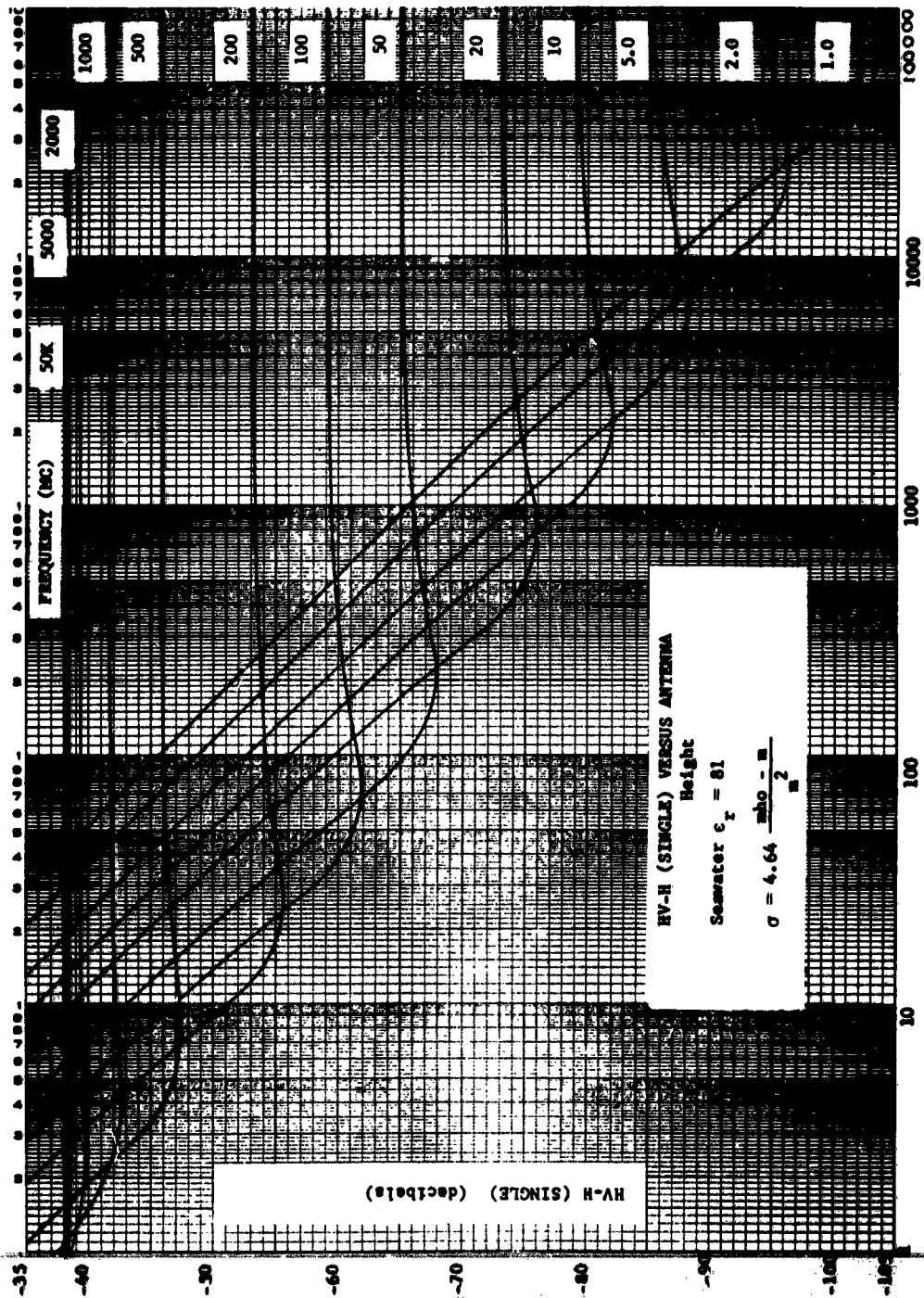


FIGURE 16 ANTENNA HEIGHT  $h$  (ft)

## SPECTRUM SIGNATURE SYNTHESIS FOR COMPATIBILITY ANALYSIS

R. W. Fleck, F. C. Pethel, J. W. Marini  
IIT Research Institute  
Electromagnetic Compatibility Analysis Center  
Annapolis, Maryland

**Abstract.**- This paper will discuss the basic procedures for obtaining spectrum signatures, the advantages and disadvantages of each method, and the particular features of the method selected by ECAC. The method for determining spurious responses in single and double conversion receivers will be discussed. Plots of synthesized receiver responses will be compared to measured response data and the problem areas discussed.

The synthesis of the gain characteristics of antennas is discussed with the special emphasis on high-gain reflector-type antennas. The pattern of the antenna is divided into a number of sectors, and the gain statistics of each sector are predicted theoretically or by means of regression techniques using empirical data.

### I. INTRODUCTION

The use of spectrum signatures in the analysis of interference problems is well known and has been widely discussed. Spectrum signatures are fundamental models of equipments. That is, the emission spectrum is a frequency domain characterization of a transmitting or radiating device. Factors which affect or alter the spectrum between the output tubes and the radiated spectrum may or may not be included in the signature. The effects of waveguide cutoff, transmission line losses, frequency selective characteristics of the antenna etc., are generally included in the measured spectrum signature. The receiver signature is a representation of the RF or preselector selectivity, the mixer, and the IF selectivity. In multiple conversion units a composite response results. The nonlinear characteristics are represented by the spurious responses. Other nonlinear effects such as cross modulation and intermodulation can generally be derived. Line losses and mismatching are not included in the measured receiver response and must be externally treated.

In the application of spectrum signature data to analysis, identification must be attached to the various emissions and responses for a more meaningful result. Spurious responses are generally described in terms of harmonics of the input signal, harmonics of the local oscillator, or both. The application of an approach to multiple conversion systems will be discussed later. In the case of transmitters, harmonic and spurious emissions are described as multiples of the tuned frequency and local oscillator. It is therefore possible to identify interference as to specific type, namely, adjacent channel, co-channel, spurious response, harmonic, spurious emission, intermodulation, etc.

Such fundamental inputs to compatibility analysis programs are generally extremely difficult to obtain. Only recently, under DOD's 449A collection program, was there any organized effort being made to collect and catalog this data. The problems encountered in measurement techniques, instrumentation, and the tremendous expense of the program have already pointed out that wholesale production of spectrum signature data by this means is not feasible. The philosophy of synthesizing spectrum signatures

from nominal data using measurements for regression trends and as a validation base was therefore made into a development task. The extended usefulness of such an approach is obvious in the areas of proposed or design stage equipments for which no measured data can be available. Experience gained, however, in the measurement or study of similar equipments is available through the synthesis processes.

There are problems in the field of electromagnetic compatibility in which a large number of potentially interfering sources of radiation must be considered. Such problems are best handled by an automatic computer. If numerical calculations are to be made, mathematical models on which the calculations are based must be formulated, and a large volume of data about each source must be stored. Even if the largest of modern computers is available, care must be exercised to avoid unnecessary complexity both in models used and in the form of the data stored.

An important and readily available body of data is the nominal characteristics of the various potential sources of radiation. A file of the nominal characteristics of both military and civilian equipments is being maintained at the Electromagnetic Compatibility Analysis Center. This file represents one source of data from which inputs to the mathematical models used in compatibility calculations can be generated or synthesized. The approach to synthesis at ECAC has been to develop a technique which is compatible with both our Data Base (source of nominal characteristics) and our analytical programs. Compromises have been necessary because of either restricted available data or operational computer problems but the result of our first phase has been a very useful synthesis technique. This technique is an ECAC operational capability presently being used as a part of our Master Simulation System.

This paper will discuss the basic procedures for obtaining spectrum signatures, the advantages and disadvantages of each method, and the particular features of the method selected by ECAC. The method for determining spurious responses in single and double conversion receivers will be discussed. Plots of synthesized receiver responses will be compared to measured response data and the problem areas discussed.

## II. APPROACH

There are three basic procedures for obtaining the necessary spectrum signatures:

1. pure mathematical method which requires a great deal of nominal data;
2. mathematical and empirical method in which shaping procedures and spurious levels are based on empirical data and such factors as sensitivity and bandwidth are determined from nominal data;
3. pure measurement method which requires spectrum signature data on every nomenclatured equipment.

The first method frequently requires more nominal data than is available and the third method is limited due to the large number of equipments and the time required to measure the spectrum signatures. ECAC has therefore developed synthesis techniques which generate spectrums by Method 2. A simplified

block diagram of the procedure for receivers is shown in Figure 1. Nominal data files supply the bandwidths and sensitivity. Skirt fall offs and spurious levels are based on empirical data.

### III. ANALYTICAL RECEIVER SPECTRUM SYNTHESIS

#### Amplifier Analysis

A thorough analysis of an RF or IF amplifier stage can be performed if the tube characteristics and all circuit parameters are known. However, due to unknown stray impedances, tube variations, etc., this method still has inherent uncertainties. Therefore simpler methods requiring less data can be used with sufficient accuracy for most prediction problems. A method of non-linear analysis for intermodulation prediction is mentioned in the section on mixers. A sufficiently accurate method to predict amplifier selectivity is given by the formulas:

$$A_i = 10 \log \left[ 1 + \left( \frac{F_i}{B_i} \right)^2 \left( \frac{F}{F_i} - \frac{F_i}{F} \right)^2 \right] \quad (1)$$

$$A_T = \sum_{i=1}^N (A_i - \bar{A}_i) \quad (2)$$

where:

$A_i$  = Attenuation of  $i$ th stage to  $F$  relative to  $F_i$ .

$F_i$  = Tuned frequency of the  $i$ th stage

$B_i$  = 3db bandwidth of the  $i$ th stage.

$F$  = The frequency of interest.

$A_T$  = Total attenuation to  $F$  relative to  $F_0$ .

$\bar{A}_i$  = Attenuation of the  $i$ th stage to  $F_0$  relative to  $F_i$ .

$F_0$  = Overall center frequency of the  $N$  stages.

$N$  = Number of stages.

The  $\bar{A}_i$  are normalizing factors required for stagger-tuned stages and are computed by substituting  $F_0$  for  $F$  in Equation 1.

For receiver synthesis, these equations are applied to each RF and IF strip individually and the results are combined to form the composite selectivity. As seen from the equations, the only data necessary for this analysis are the tuned frequency and bandwidth of each stage and the overall center frequency of the amplifier strip. This information is generally easier to obtain than are the various circuit parameters. Figure 2 shows three sets of calculated selectivity curves and the corresponding measured curves. Sufficient agreement exists to indicate the method's usefulness.

## Non linear Mixer Analysis

### General Approach

In order to determine the mixer function, the power series method of non linear analysis was selected. This procedure equates the output to:

$$i_p(t) = a_0 + \sum_{n=1}^N a_n e_i^n(t) \quad (3)$$

where:

$i_p(t)$  = Output current

$e_i(t)$  = Input voltage

$a_0$  &  $a_n$  = Constants

$N$  = Highest term of the expansion

If the local oscillator and incoming signal are free of harmonics and if the origin is shifted to the bias point, the mixer input is:

$$e_i(t) = E_{LO} \cos(\omega_{LO} t) + E_{RF} \cos(\omega_{RF} t) \quad (4)$$

where:

$E_{LO}$  = Peak L O voltage

$E_{RF}$  = Peak R F voltage

$\omega_{LO}$  = Angular L O frequency

$\omega_{RF}$  = Angular signal frequency

The expanded output will then be

$$i_p(t) = \sum_{p=0}^{N-q} \sum_{q=0}^N K_{pq} E_{LO}^p E_{RF}^q \cos(p\omega_{LO} \pm q\omega_{RF})t \quad (5)$$

The  $K_{pq}$  factor is a function of the  $a_n$  and expansion coefficients, and  $p$  and  $q$  are integers. If the mixer transfer characteristic is known or can be assumed, the values of  $a_n$  can be found by substituting  $N$  sets of  $E_i$  and  $E_o$  into Equation 3 (with  $a_0 = 0$ ) and solving these equations simultaneously. When the  $a_n$  are known, the  $K_{pq}$  can be found by expansion of Equation 3. For any given response, the only  $K_{pq}$  term of Equation 5 which will produce an input to the IF is the one for which:

$$\left| p w_{LO} \pm q w_{RF} \right| = w_{IF} \quad (6)$$

Therefore, the peak mixer output for a given response is:

$$I_{pq} = K_{pq} E_{LO}^p E_{RF}^q \quad (7)$$

The output for a desired signal is:

$$I_{11} = K_{11} E_{LO} E_D \quad (8)$$

where:

$I_{11}$  = Mixer output

$K_{11}$  = Coefficient for  $p = 1, q = 1$

$E_D$  = Peak level of RF input to the mixer

If  $I_{11}$  is selected to be the value of mixer output required to produce a minimum detectable signal, then  $E_D$  is the receiver sensitivity at mixer input. Since all the responses, by definition, produce an output at the intermediate frequency, the same output level is required for an MDS in each case. Therefore:

$$K_{11} E_{LO} E_D = K_{pq} E_{LO}^p E_{RF}^q \quad (9)$$

Solving for  $E_{RF}$  gives:

$$E_{RF} = \left( \frac{K_{11}}{K_{pq}} \right)^{\frac{1}{q}} \left( \frac{1}{E_{LO}} \right)^{\frac{p-1}{q}} (E_D)^{\frac{1}{q}} \quad (10)$$

Since it is the signal level at the antenna terminal which is of interest, Equation 10 can be changed to:

$$E_{RF}' G_{RF} = \left( \frac{K_{11}}{K_{pq}} \right)^{\frac{1}{q}} \left( \frac{1}{E_{LO}} \right)^{\frac{p-1}{q}} \left( E_D' \bar{G}_{RF} \right)^{\frac{1}{q}}$$

which becomes

$$E_{RF}' = A_{RF} \left( \frac{K_{11}}{K_{pq}} \right)^{\frac{1}{q}} \left( \frac{1}{E_{LO}} \right)^{\frac{p-1}{q}} (E_D')^{\frac{1}{q}} \left( \frac{1}{\bar{G}_{RF}} \right)^{\frac{q-1}{q}} \quad (11)$$

where:

$E_{RF}'$  = Peak level of spurious response at antenna for an MDS.

$A_{RF}$  = Inverse rejection of preselector to the spurious signal

relative to a tuned response  $\left( \frac{\bar{G}_{RF}}{G_{RF}} \right)$ .

$E_D'$  = Peak level of tuned response at antenna for MDS (sensitivity)

$\bar{G}_{RF}$  = Gain of preselector at tuned frequency

$G_{RF}$  = Gain of preselector at spurious frequency

This equation is used to calculate the MDS level of any spurious response. The shaping about a particular response is performed by first assuming that  $G_{RF}$  is approximately constant across the response bandpass. The selectivity is then determined by the overall IF curve. The rejection about a response relative to the peak response level is determined by considering that:

$$\left| q (F_{RF} + \Delta F_{RF}) - p F_{LO} \right| = F_{IF} + \Delta F_{IF} \quad (12)$$

or  $q \Delta F_{RF} = \Delta F_{IF}$

and similarly in db units:

$$q \Delta E_{RF}' = \Delta E_{IF} \quad (13)$$

In other words, to transfer the IF selectivity to the spurious response, it is necessary to divide the coordinates (db and  $\Delta F$ ) of the IF curve by  $q$  (see Figure 3). It should be remembered in using the resulting curves that an increase in spurious input level may not produce the same effect as the same increase in tuned response input.

#### Specific Analysis Studies

In order to study the effects on spurious responses of mixer parameter variations, and also in an effort to generate a capability to predict spurious responses in the absence of mixer data, ECAC is mathematically analyzing several theoretical mixer types. For perfectly linear and perfectly square law mixers, the LO voltage and conduction angle are varied. At each set of conditions, the resulting power series coefficients ( $a_n$ ) are computed. Unfortunately, the results are not complete at this time. However, it has been shown that for a linear mixer:

$$a_n = \frac{\bar{a}_n}{E_{LO}^{n-1}} \quad (14)$$

and for a square law mixer:

$$a_n = \frac{\bar{a}_n}{E_{LO}^{n-2}} \quad (15)$$

where:

$\bar{a}_n$  = Value of  $a_n$  for the mixer type with  $E_{LO} = 1$  volt

$a_n$  = Value for  $E_{LO} \neq 1$  volt

The plots of  $\bar{a}_n$  versus conduction angle are not complete but should be in the near future. If the results are meaningful, other power laws may be studied. It is hoped that this analysis will provide a means for non linear mixer analysis when only the mixer law is known.

By setting the  $e_i(t)$  in Equation 3 equal to the sum of three or more signals and expanding the series, intermodulation and cross modulation at the mixer can be studied. Contributions to intermodulation, cross modulation, and spurious responses by the RF amplifiers can be considered by a non linear analysis of the circuitry. However, due to lack of available data, this will be very difficult in most cases. Therefore, an analysis of theoretical amplifier tube characteristics, of the type being performed on mixers, will be attempted.

#### Model for Dual Conversion Receivers

If dual conversion systems are considered, the potential spurious response frequencies are:

$$F_{RF} = \frac{q_2 p_1 F_{LO_1} \pm (p_2 F_{LO_2} \pm F_{IF_2})}{q_1 q_2} \quad (16)$$

where:

$F_{RF}$  = The spurious frequency.

$p_1$  &  $q_1$  = Harmonics associated with first mixer.

$p_2$  &  $q_2$  = Harmonics associated with second mixer.

$F_{LO_1}$  = First LO frequency.

$F_{LO_2}$  = Second LO frequency.

$F_{IF_2}$  = Second IF frequency.

By the methods of the preceeding sections, it can be shown that:

$$E_{RF}' = \left[ \begin{array}{ccccccc} K_{11_2} & & & & & & \\ \frac{1}{K_{pq_2}} & \left( \frac{1}{E_{LO_2}} \right)^{p_2-1} & \left( \frac{K_{11_1}}{K_{pq_1} q_2} \right) & \left( \frac{1}{E_{LO_1}} \right)^{p_1 q_2-1} & \left( \frac{1}{G_{IF_1}} \right)^{q_2-1} & & \\ & q_2 & q_1 q_2 & q_1 q_2-1 & & & \\ & \left( A_{IF_1} \right) & \left( A_{RF} \right) & \left( \frac{1}{G_{RF}} \right) & E_D' & & \frac{1}{q_1 q_2} \end{array} \right] \quad (17)$$



where:

$K_{pq_1}$  = Coefficient for first mixer .

$K_{pq_2}$  = Coefficient for second mixer .

$E_{LO_1}$  = First LO voltage .

$E_{LO_2}$  = Second LO voltage .

$\bar{G}_{IF_1}$  = Peak gain of first IF .

$A_{IF_1}$  = Inverse rejection of first IF to the response .

The other terms are as previously defined.

Equations 16 and 17 predict the frequency and level of the responses. In order to shape the response, it is necessary to transfer the second IF curve to the second mixer input using  $q_2$  as the operator. The  $A_{IF_1}$  function is then applied to this curve and the composite is transferred to  $IF_1$  the input using the operator  $q_1$ .

For a simplified block diagram of a program using this procedure, refer to Figure 4. The amplifiers are analyzed as described earlier. The receiver sensitivity is either given in the characteristics file or is calculated from the noise figure. Then if there is only one mixer, or if insufficient data is available for the dual conversion analysis, the response frequencies, levels, and shapes are determined as described in the preceding sections. If data is available, the complex analysis discussed in this Section is applied.

#### IV. TRANSMITTER SPECTRUM SYNTHESIS

##### Harmonic Emission

Non linear analysis of transmitter circuitry is required if harmonic emissions are to be calculated analytically. The procedure is basically the same as was described for mixers. If the tube characteristics and biasing of the final are known, the harmonic content can be calculated by power series or Fourier analysis of the plate current. These results can then be operated on by the tuned circuit impedance to determine the output powers. Work is being performed at ECAC to establish a capability to approximate harmonic emission levels based on tube type. However, this work is also incomplete at the present time.

Since the necessary data for this method is frequently not available, ECAC's present models base harmonic output levels on the results of statistical analysis of measurements. One procedure is to analyze measurements on the individual equipments. Although this is the better approach, such data is not

always available. When this is the case, it is necessary to analyze the data on similar equipment types and determine the trends.

#### Emission Spectrum

The emission spectrum of a transmitted signal may be calculated if the modulation characteristics are known. The appropriate spectrum can be determined by calculating the Fourier integral of the modulating pulse for radar systems, by evaluating a series of Bessel functions for FM transmitters, or by applying mixer techniques to an AM transmitter. This can be quite time consuming and tedious if the problem contains very many transmitters. Therefore, the tendency at ECAC has again been to use measured data. When available, the measurements on the specific equipment should be used. If this is unavailable or if its use is not compatible with the particular computer prediction program in use, the spectrum can be approximated by statistical analysis of measurements on equipments with similar modulation characteristics.

### V. ANTENNA PATTERN SYNTHESIS

#### Discussion of Antenna Gain Characteristics

First, it is necessary to define more precisely the antenna characteristics under consideration. In usual engineering practice, the gain function of an antenna at a given frequency is considered to be a fixed function of the polar and azimuthal angles of a coordinate system whose origin is located at the antenna. For the purpose of compatibility predictions, however, it is not feasible to predict or even to use such a detailed description of the gain function. The fine structure of antenna patterns depends on changes in frequency, local environment, manufacturing tolerances and other factors that may not be known exactly. Consequently, it becomes necessary to treat the antenna gain function as a random surface, at least over regions where the characteristics are not controlled by design specifications. It is this random surface that must be modeled for compatibility purposes. Even here a complete statistical description of the surface is not necessary. Information sufficient for most purposes is provided by the cumulative density function associated with the various angular regions surrounding the antenna.

#### Synthesis of the Model of a Rotating Antenna

##### The Model

It should be pointed out here that the final form of the antenna model depends on the conditions of the problem and the mode of operation of the equipment and the corresponding antenna. This is best illustrated by considering a few concrete examples.

Consider, first, a radar antenna scanning continuously through 360°. At a fixed point at another site, the effective gain function of the antenna along the azimuthal cut observed would be represented by an azimuthal pattern as shown in Figure 5. If the antenna rotates at a uniform rate, the pattern shown is scanned uniformly. If one is interested, not in the exact order in which pulses of a given amplitude are received, but rather only in the number of pulses exceeding a given amplitude, then the pattern shown

in Figure 5 is more detailed than is necessary. In Figure 6, the percentage of the time that the gain is less than a given value is plotted versus the given value of gain. Figure 6 is obtained from Figure 5 by determining the number of degrees for which the given gain exceeds the antenna gain, and dividing this number of degrees by 360 to obtain the percentage time that this condition holds. Figure 6 contains all of the information of interest to be found in Figure 5. It may be regarded as a model of the parallel-polarization component of an azimuthal cut of the antenna at the fundamental frequency. Even here the representation is more detailed than necessary. The data required to store this model may be reduced by quantizing the cumulative curve<sup>1</sup> given in Figure 6.

It is also possible to approximate the curve with a known function. Except for the main beam, the cumulative gain curves of high-gain reflector-type antennas can be approximated by the cumulative probability density of a normally distributed variable.<sup>2</sup> This is illustrated in Figure 7 where the data of Figure 5, with the main beam deleted, is plotted on probability paper. The straight line is the cumulative density function of a normal distribution with a mean  $\mu = -6\text{db}$  and a standard deviation  $\sigma \approx 5\text{db}$ . These values of the mean and standard deviation together with a description of the shape of the gain function in the main beam constitute a satisfactory model, since the curve of Figure 6 may be reconstructed from this information.

#### The Synthesis

To synthesize the model of a rotating antenna at the operating frequency and for the parallel-polarization (i.e., to predict the curve in Figure 6), it is necessary to predict the shape of the pattern in the vicinity of the main beam, and to predict the values at the parameters  $\mu$  and  $\sigma$  that describe the remainder of the distribution. The shape of the pattern in the vicinity of the main beam is less of a problem, as it can be predicted with sufficient accuracy theoretically from design considerations. The remainder of the pattern is more difficult to treat theoretically, although this subject has been studied.<sup>4</sup> A purely empirical approach, nevertheless, has certain advantages. If the parameters  $\mu$  and  $\sigma$  are measured for a sufficient number of antennas of the same general type, then a prediction can be made of these parameters on a given antenna from its nominal characteristics using the technique of multiple regression.<sup>3</sup>

As an example, the mean for a number of measured patterns of four different high-gain reflector-type radar antennas is plotted versus the nominal gain of the antennas in Figure 8. The data used to calculate the means was obtained from the azimuthal cut by deleting the main-beam gain within  $\pm 1.5$  nominal main-beam widths. The least-squares line shown in the figure would be used to predict the parameter  $\mu$  of a high-gain reflector-type antenna with a given nominal gain  $G$ . There is a significant difference between the means estimated at 27db and at 35db, but the quantity of data is not sufficient to verify the linear relationship used. If sufficient data becomes available through the spectrum signature collection plan or from other sources, it should be possible to perform a large-scale regression analyses to predict the parameters in question using not only the nominal gain but also the dish dimensions and other quantities of possible significance available from the nominal characteristics file.

The standard deviation of the gain of the antennas is plotted

versus nominal gain in Figure 9. Again, the straight line can be used for prediction, although in this case the slope of the line has doubtful significance, and on the basis of the data presented, one might just as well use the estimate  $\sigma = 5\text{db}$  obtained by combining the data.

#### Synthesis of a More General Model

The model discussed above for the case of a rotating antenna is not suitable, however, if the antenna is stationary or being used in a sector scan mode. The reason is apparent from Figure 5. Consider that the antenna whose pattern appears in Figure 5 is scanning over a sector twenty degrees in width, and is being observed from such a direction that the sector lying between seventy and ninety degrees on the pattern is observed. If this sector is scanned at an uniform rate, then the model that should be used is the cumulative curve for the gain over the observed sector only. It is obvious from Figure 5, however, that the statistics of this sector are not the same as those of the entire 360 degree pattern. The statistical properties of the gain pattern vary from sector to sector.

An examination of the pattern in Figure 5 does disclose, nevertheless, the possibility of breaking the pattern into a number of sectors, as indicated by the dotted lines in that figure. The pattern in Figure 5 was plotted from Spectrum Signature measurements taken every  $2.5^\circ$ . Figure 10 shows for the sake of comparison a pattern measured by Johnson<sup>2</sup>, which exhibits much finer detail. Here the different character of the sectors is quite pronounced.

The divisions of the pattern were made arbitrarily at plus and minus 9 main beam widths, at  $+60^\circ$ , and at  $+140^\circ$ . The pattern in the first sector (the main beam sector) can be estimated theoretically from the nominal characteristics of a given antenna. Although the statistics of the remaining sectors are not homogeneous within each sector, they are more nearly so than over the entire 360 degrees of the pattern, and a suitable model of a sector scan or a rotating antenna can be formed as needed by combining the statistics of the sectors involved in proper proportion.

The statistics of the gain in the three remaining sectors are estimated empirically in the same fashion as for the model of a rotating antenna. Although the distributions in these sectors are not approximated as well by the normal distribution as was the case for the entire pattern, the fit is close enough for most purposes. The cumulative statistics for the various sectors of the pattern of Figure 5 are shown in Figure 11-13. Only the third sector, Figure 12, shows a definite systematic departure from normality.

The prediction of the statistics of a given sector is made empirically as was done in the case of the rotating antenna. Figure 14 shows the least-squares line obtained for each sector. The least-squares line of Figure 8 is also included in the figure. The standard deviations in each sector again seem to be independent of the gain. They equal 4.2, 4.4, and 4.9 for sectors 2, 3, and 4 respectively.

## VI. CONCLUSIONS

Spectrum signatures can be synthesized by analytical expressions if the required information is available and by empirical data if necessary. The analytical expressions for single and double conversion receivers were presented. Techniques for the synthesis of high-gain reflector-type antennae from nominal characteristics have been discussed. Although only two-dimensional examples have been discussed, the same considerations apply directly to three-dimensional antenna models, the principal difference being that the sphere surrounding the antenna would be divided into areas and the ordinate of the curves of the cumulative statistics would represent percentage of solid angle.

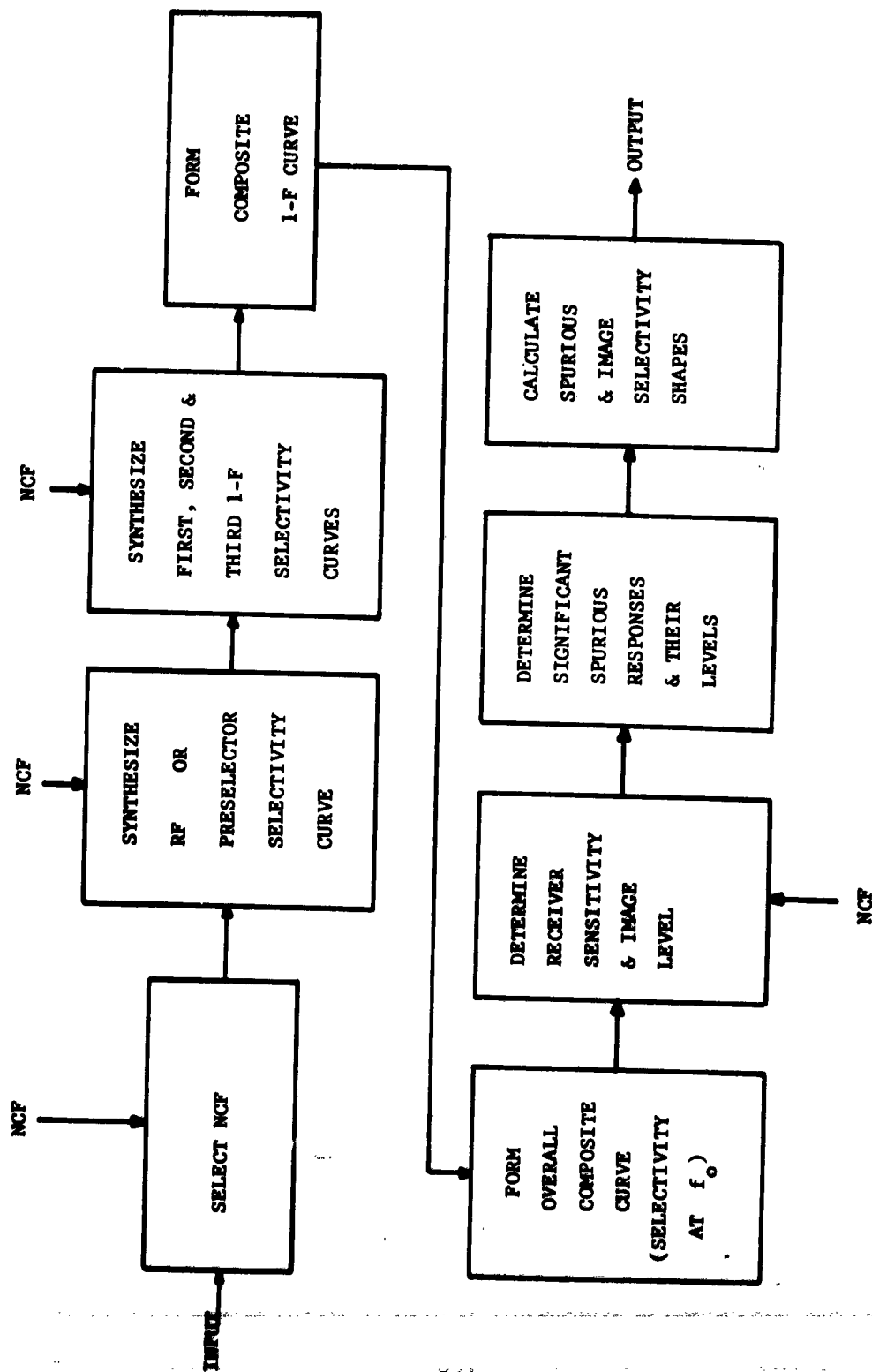
## ACKNOWLEDGEMENT

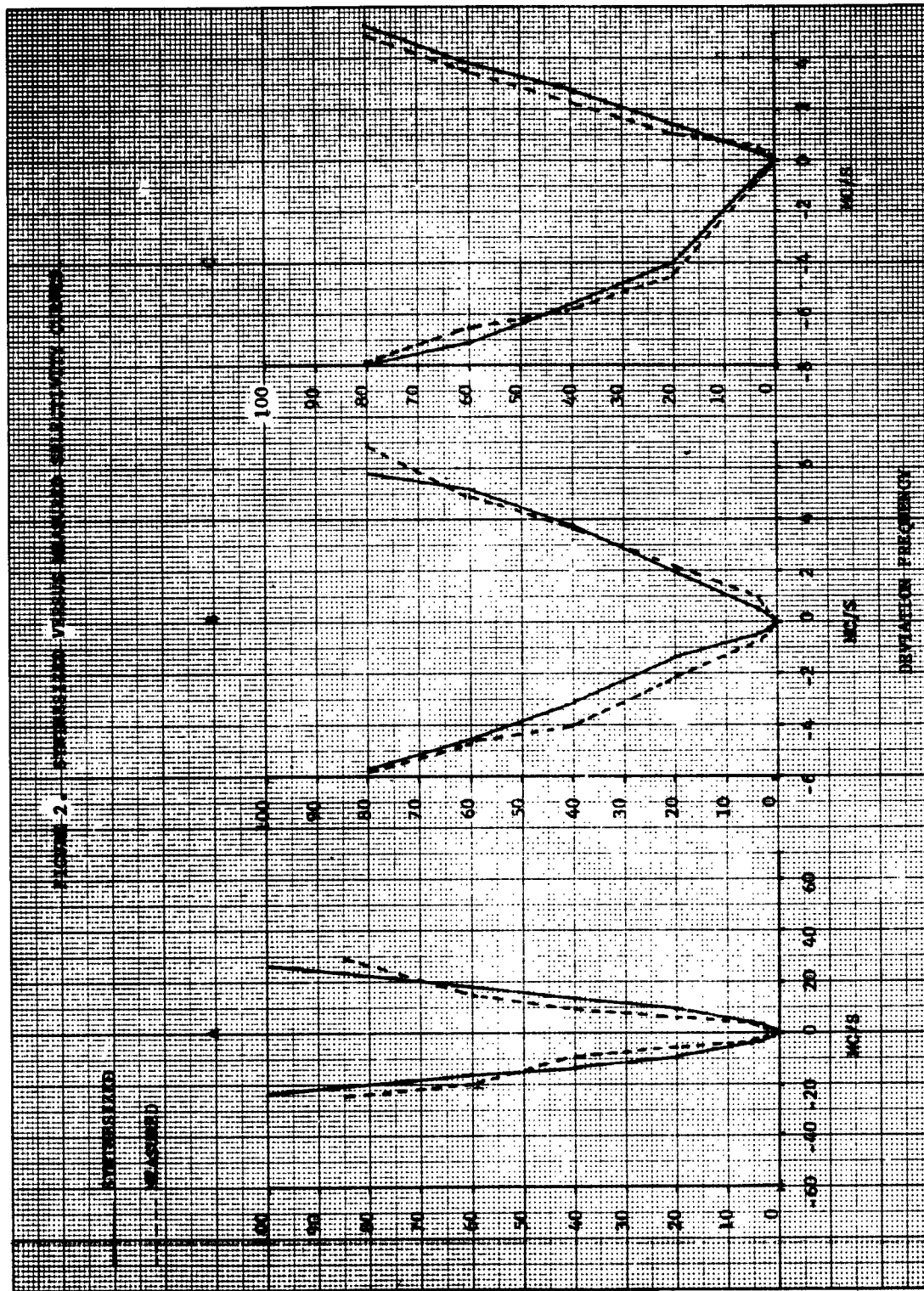
The work described above is sponsored by the three Military Departments and is being conducted under Contract No. AF 19 (604)-8440 with the Electronic Systems Division, Air Force Systems Command.

## REFERENCES

1. L. E. Silverman, J. J. Krstansky and H. M. Sachs, Three Dimensional Quantized Antenna Pattern Model, Proc. Seventh Conf. on Radio Interference Reduction and Electronic Compatibility, Chicago, Illinois, Nov. 7-9, 1961.
2. R. C. Johnson, Statistical Gain Characteristics of the AN/SPS-10 Antenna, Monograph from the Engineering Experiment Station, GIT, Buships Contract No. bsr-85387, March, 1962.
3. A. Hald, Statistical Theory with Engineering Applications, John Wiley and Sons, Inc., New York, Sections 6.6 and 6.7, 1952.
4. H. Kritikos, The Extended Aperture Method for the Determination of the Shadow Region Radiation of Parabolic Reflectors, IEEE Trans. on Antennas and Propagation, Vol. AP-11, pp 400-404, July, 1963.

FIGURE 1. FLOW DIAGRAM OF BASIC SYNTHESIS PROCESS





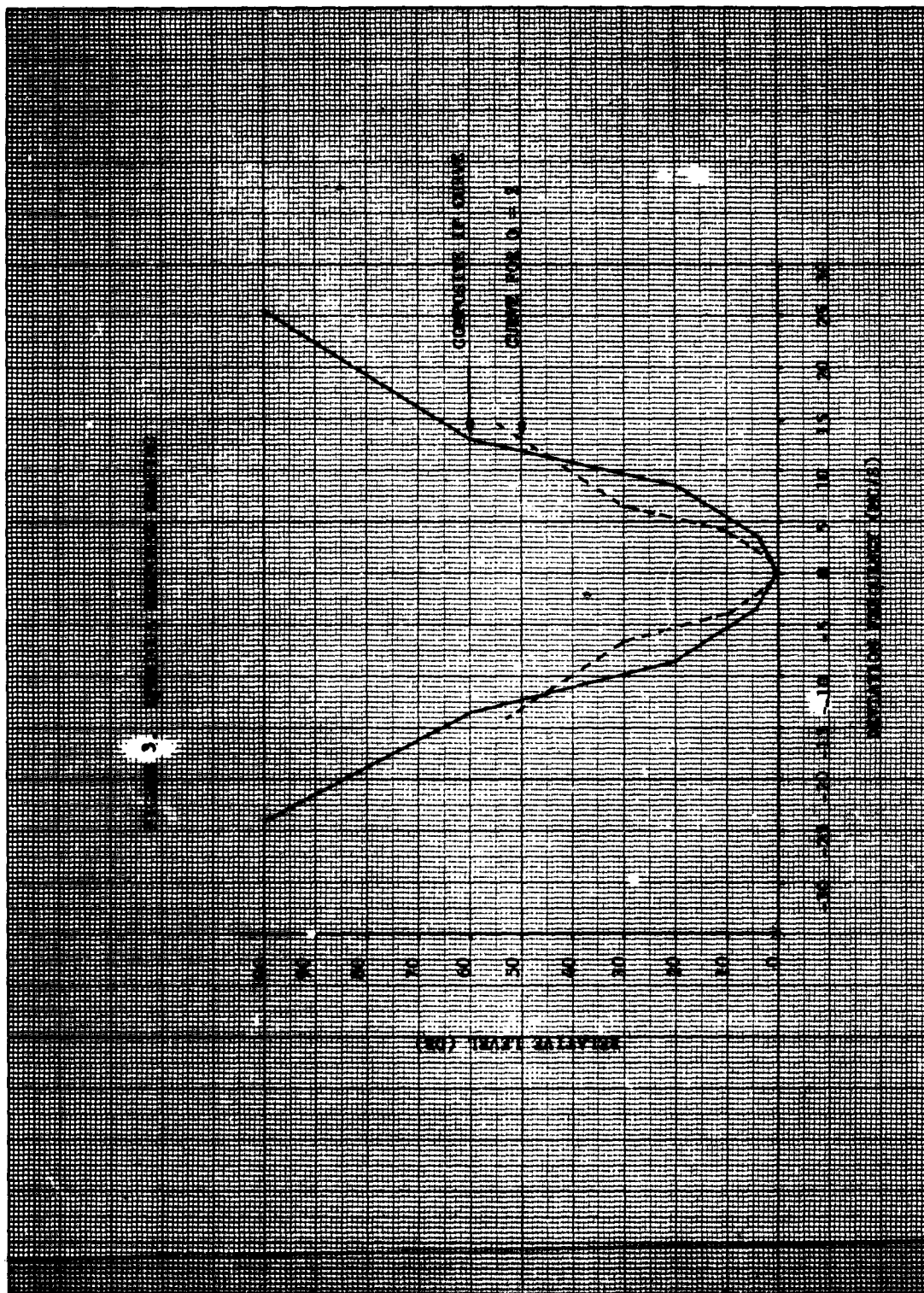
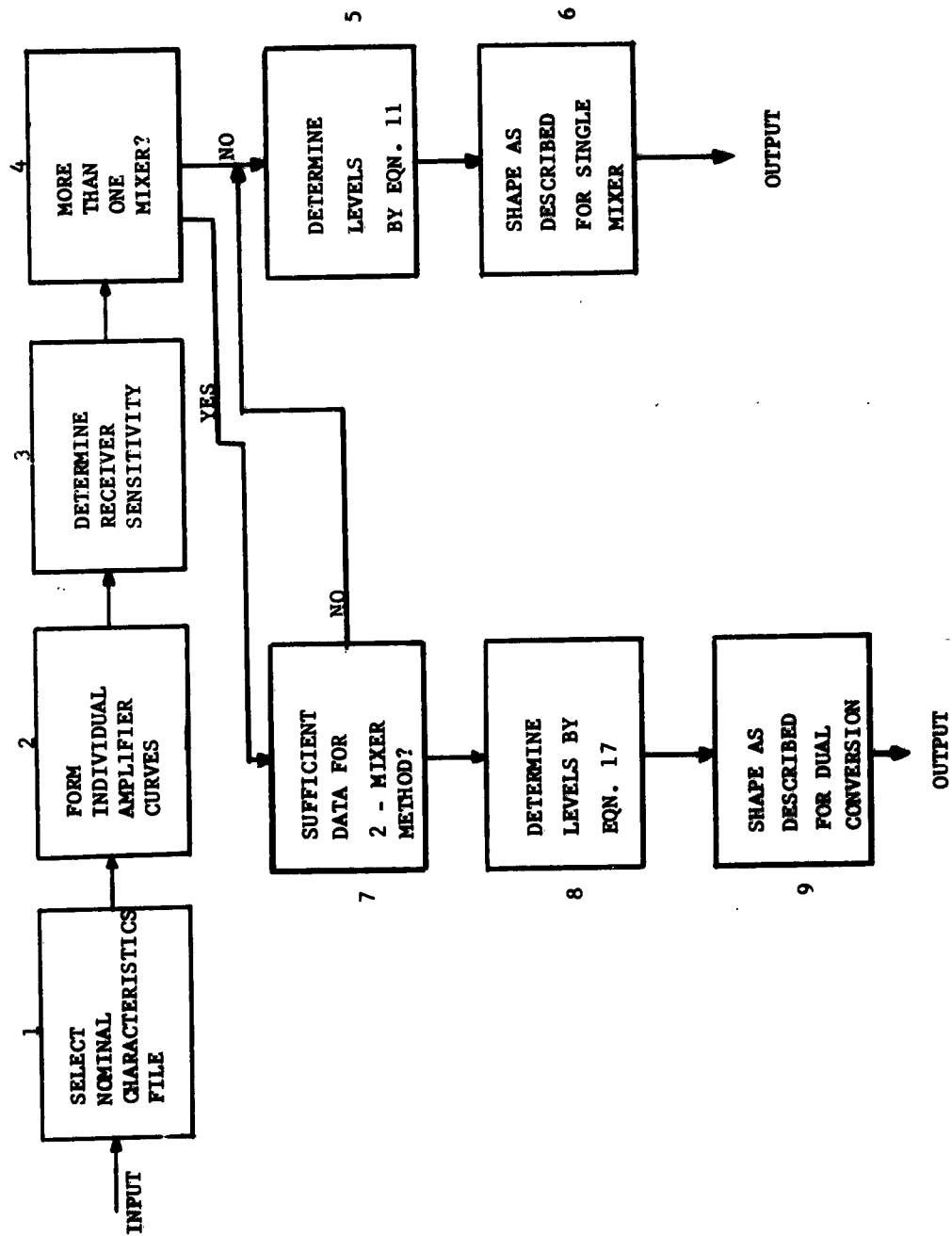




FIGURE 4. RECEIVER SYNTHESIS FOR DUAL CONVERSION RECEIVERS.



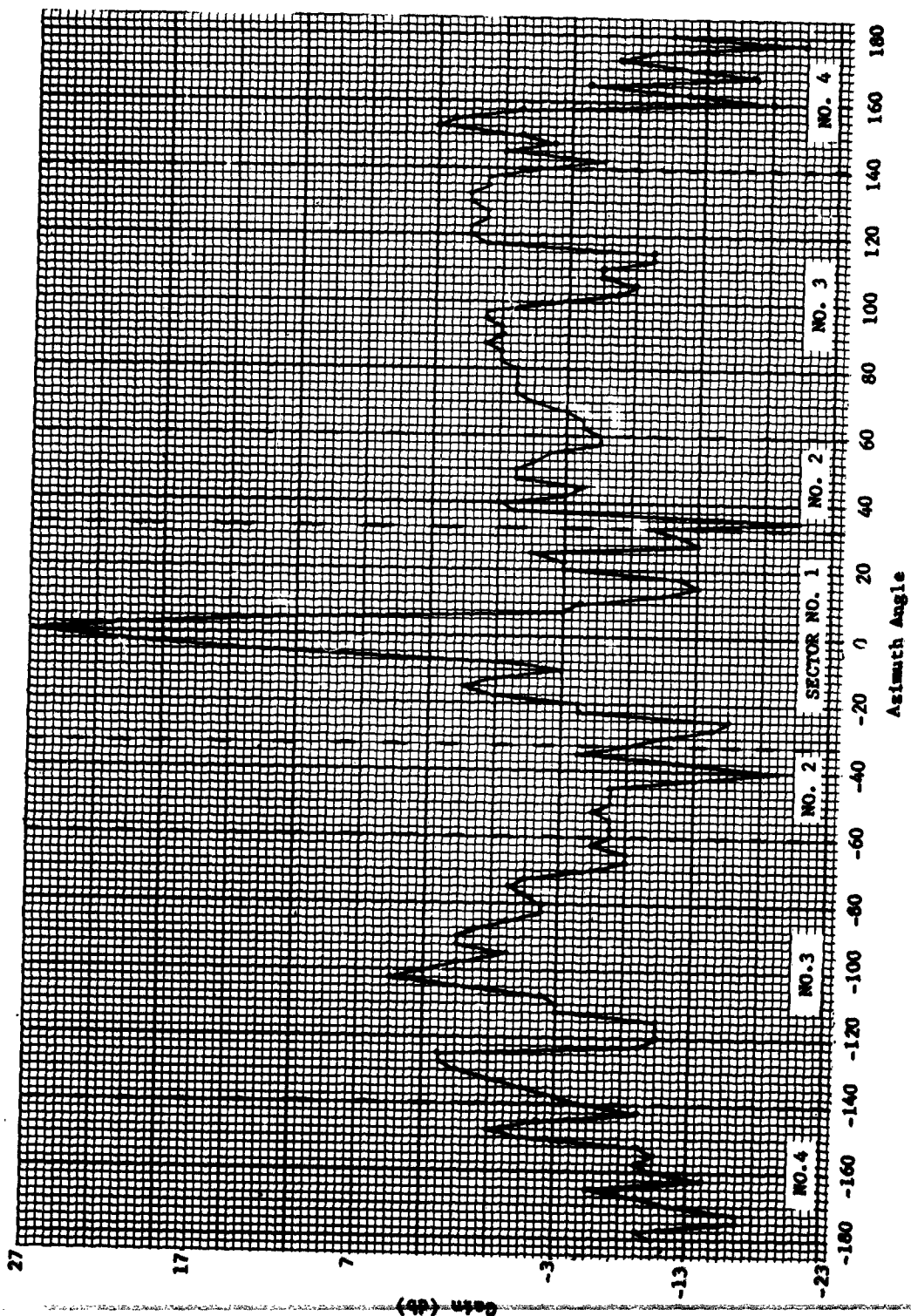


FIGURE 5. TPS-1D ANTENNA PATTERN

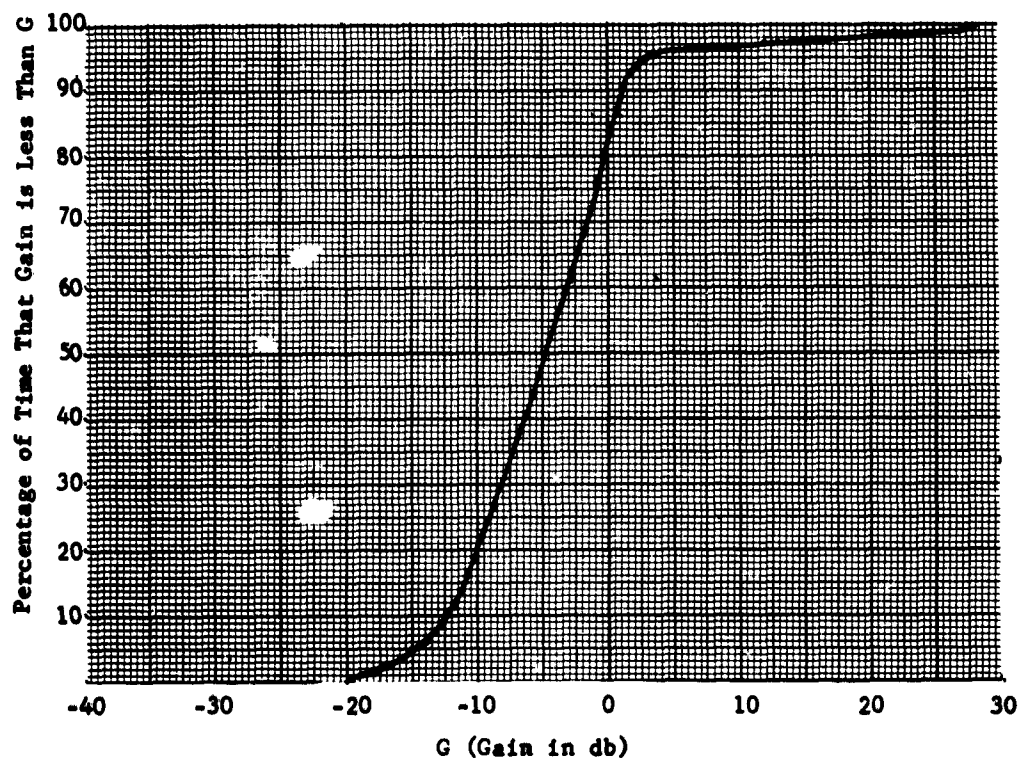


FIGURE 6. CUMULATIVE GAIN CURVE OF TPS-1D ANTENNA

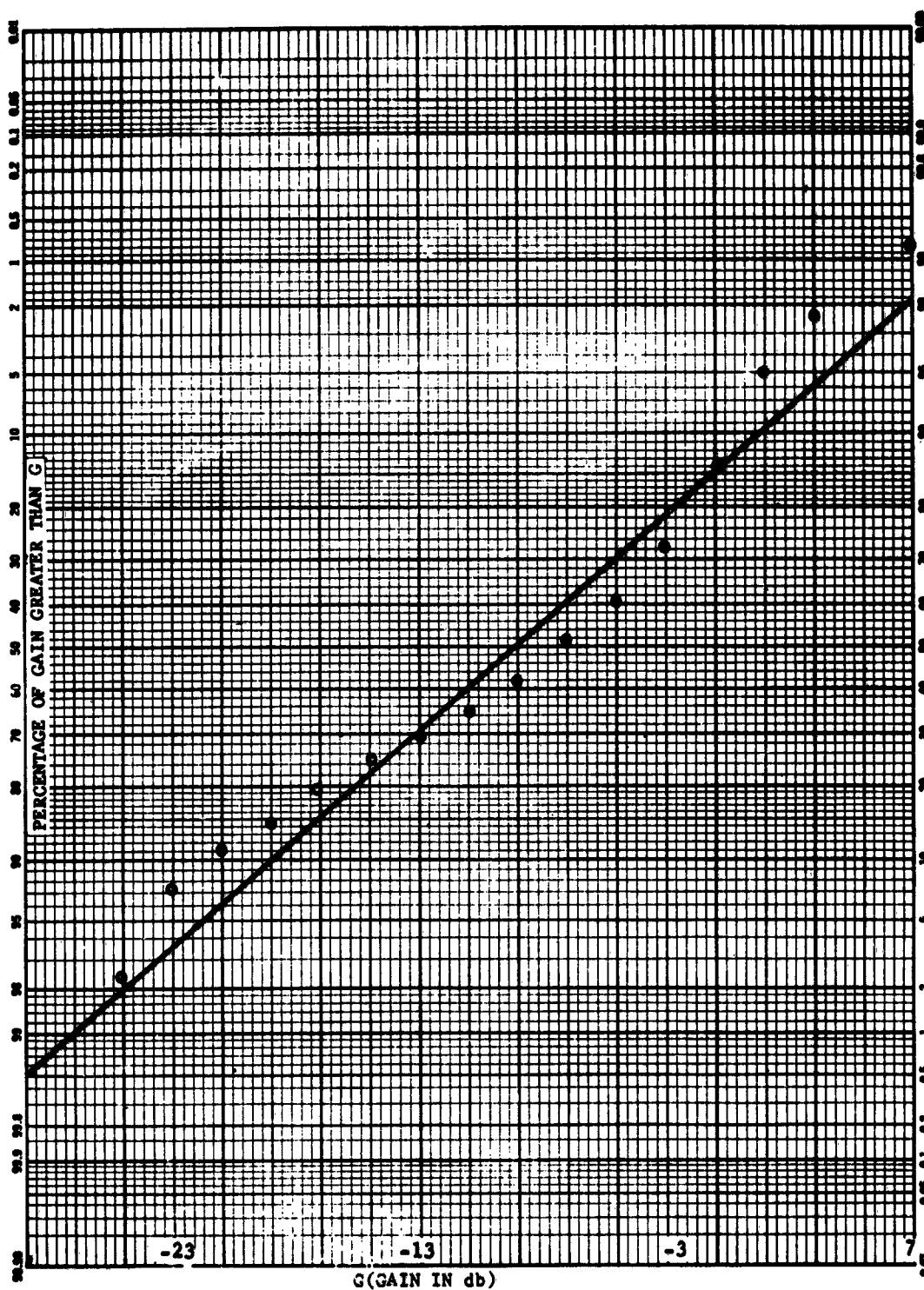


FIGURE 7. TPS-1D CUMULATIVE GAIN CURVE, MAIN BEAM DELETED.

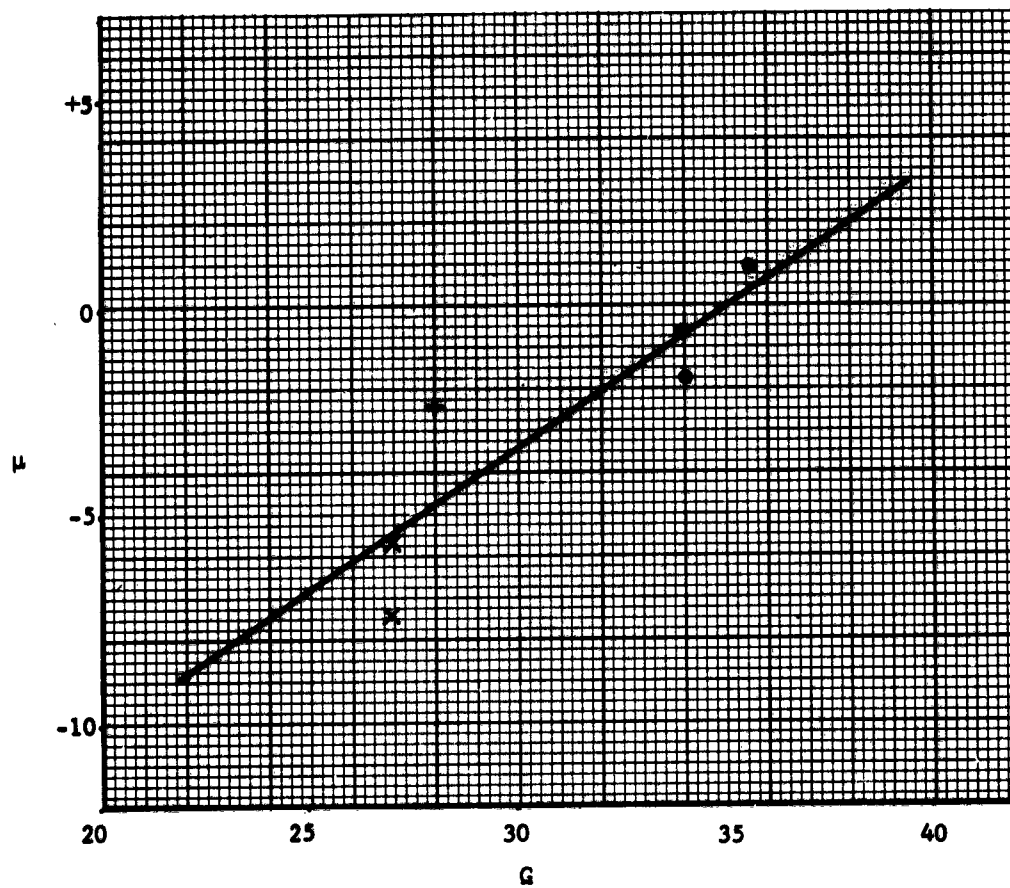


FIGURE 8. MEAN GAIN VERSUS NOMINAL GAIN

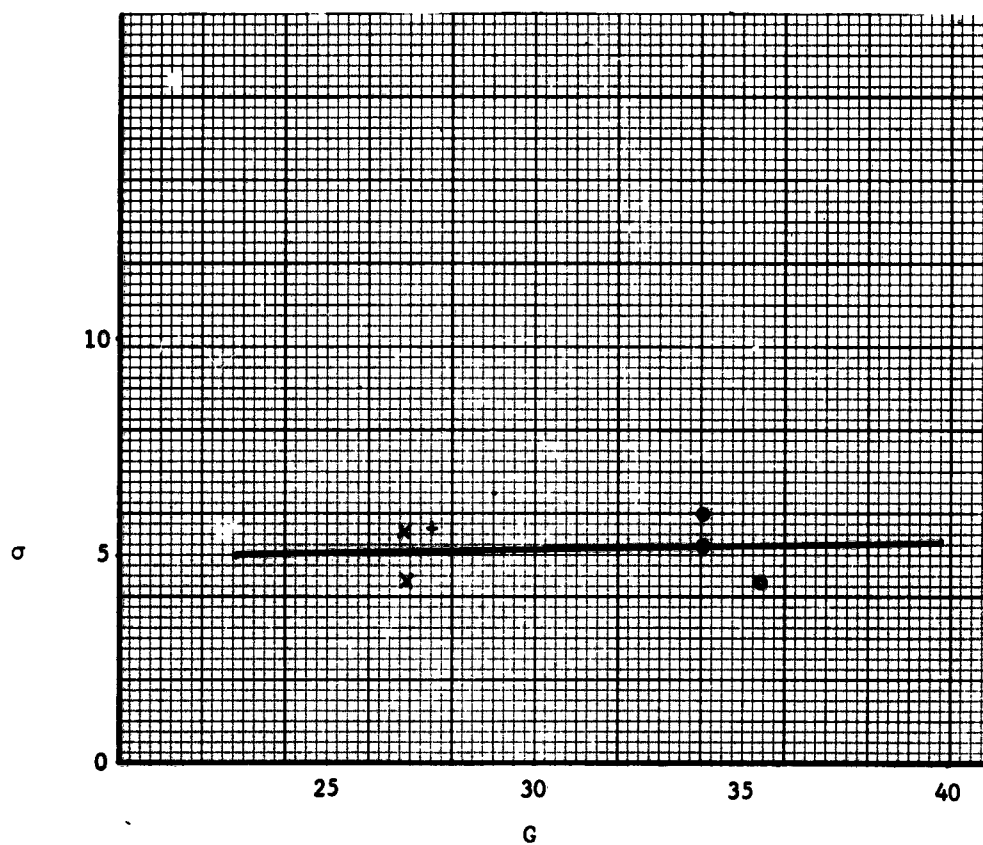


FIGURE 9. STANDARD DEVIATION VERSUS NOMINAL GAIN

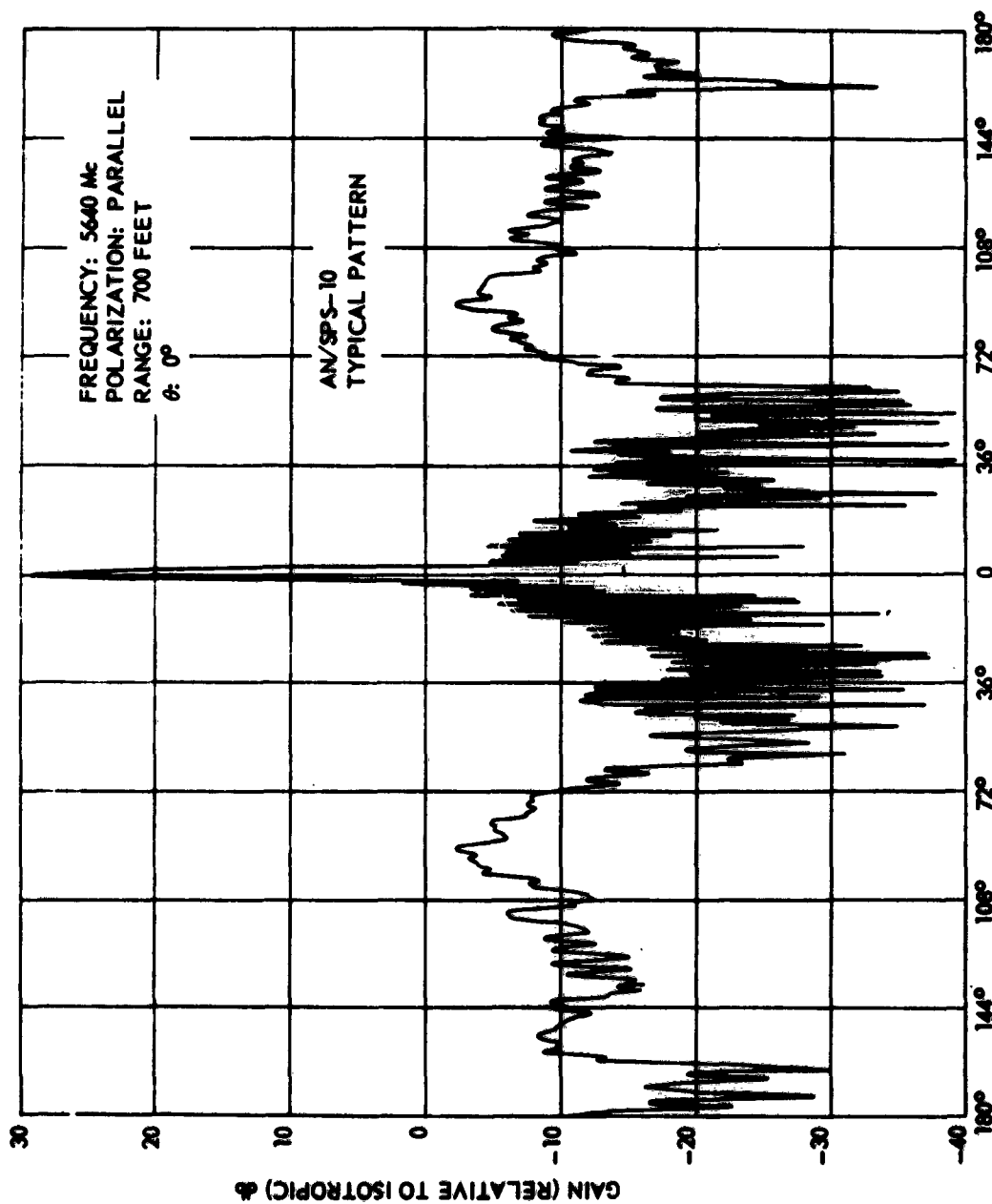


FIGURE 10. TYPICAL PATTERN OF THE AN/SPS-10 ANTENNA

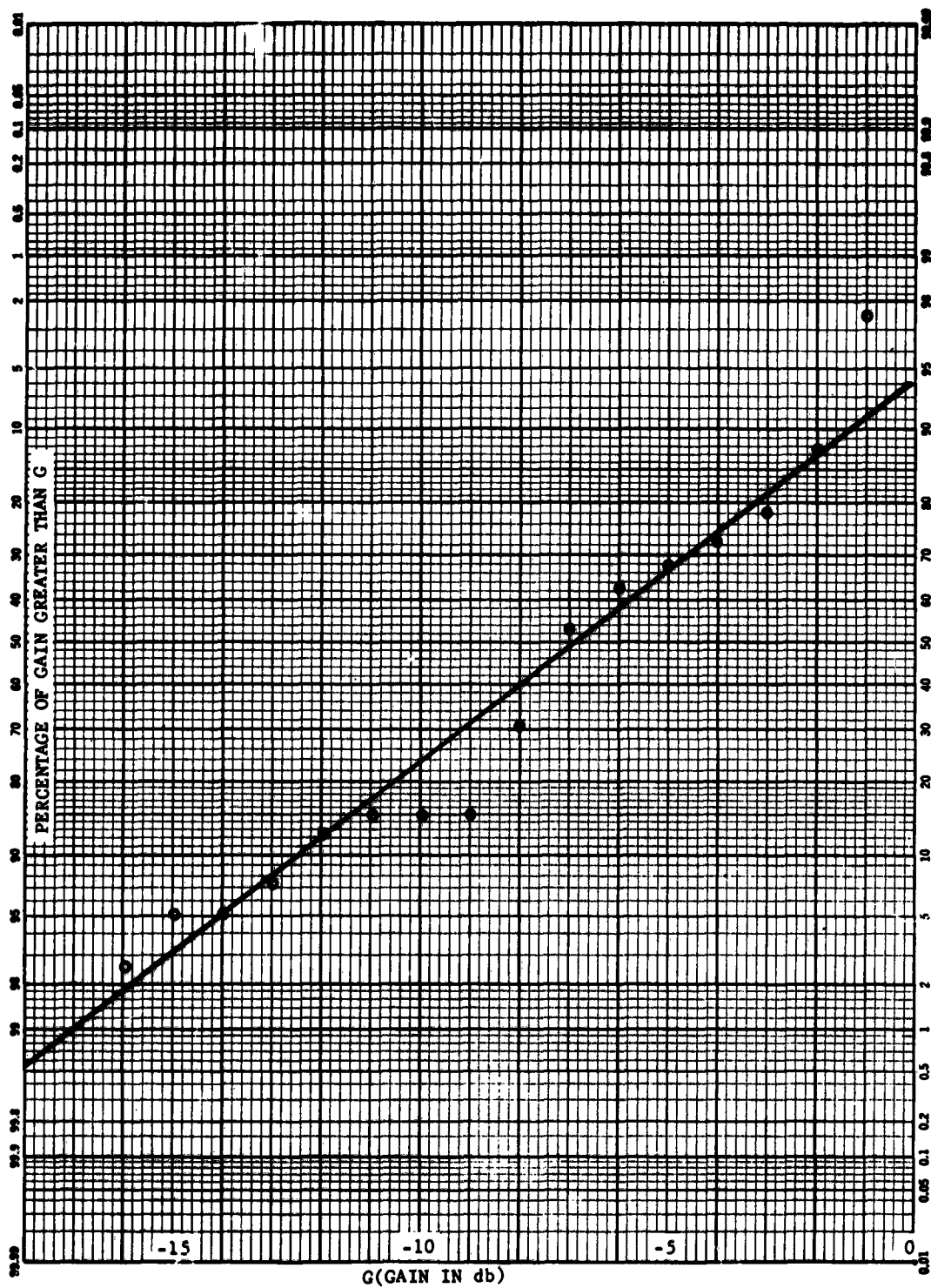


FIGURE 11. TFS-1D CUMULATIVE GAIN CURVE, SECTOR NO. 2



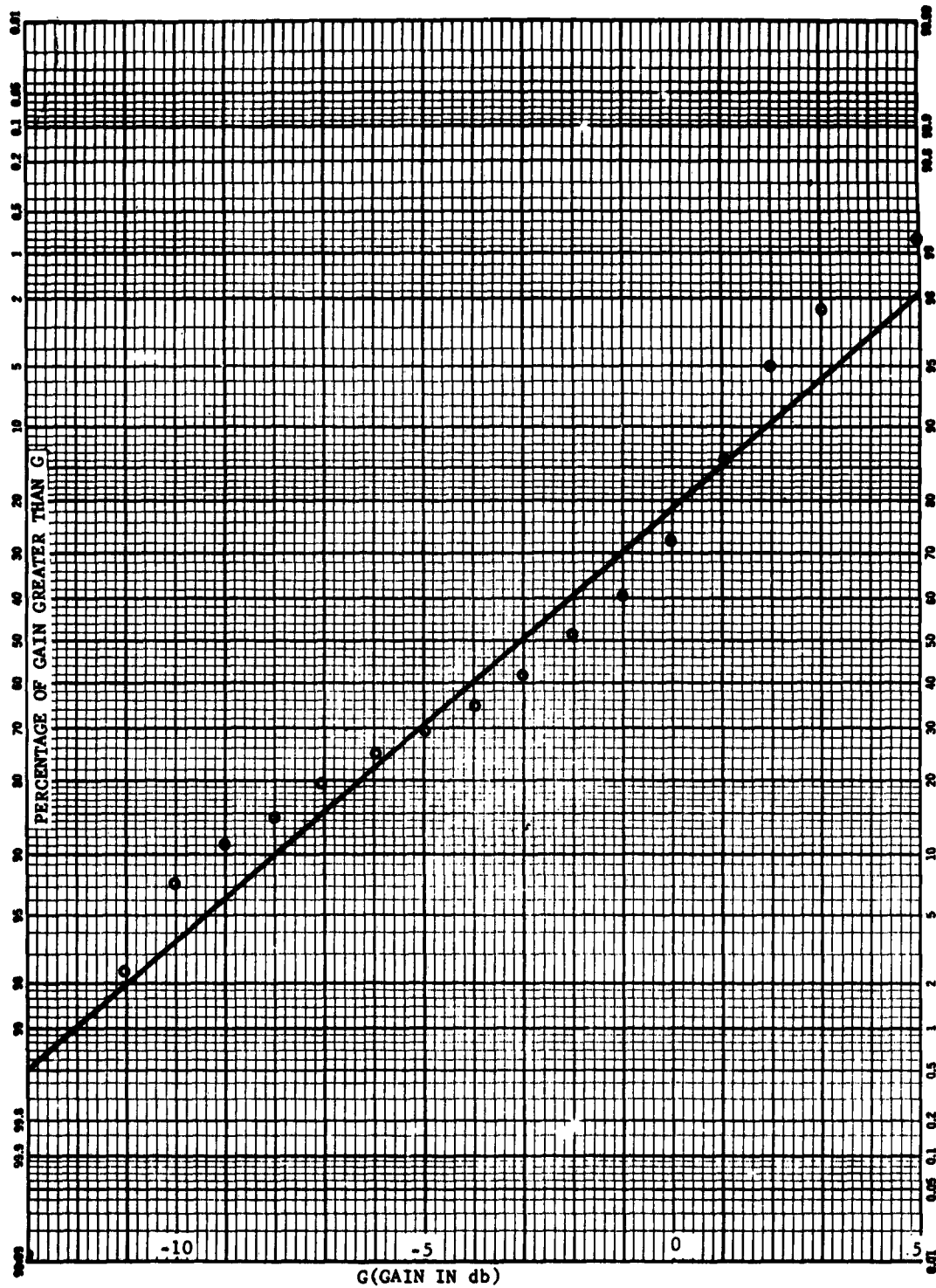


FIGURE 12. TFS-1D CUMULATIVE GAIN CURVE, SECTOR NO. 3  
-557-

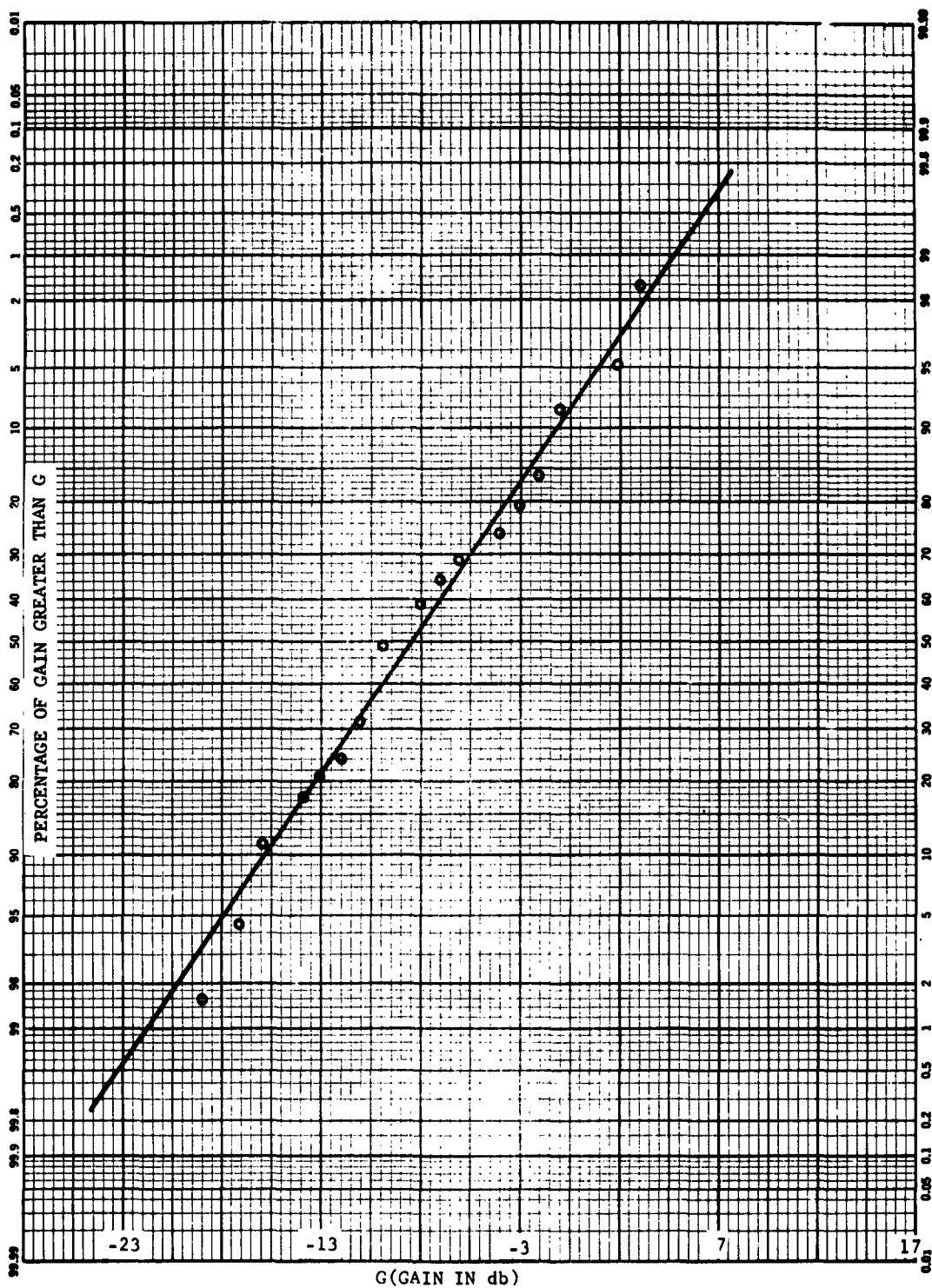


FIGURE 13. TPS-1D CUMULATIVE GAIN CURVE, SECTOR NO. 4

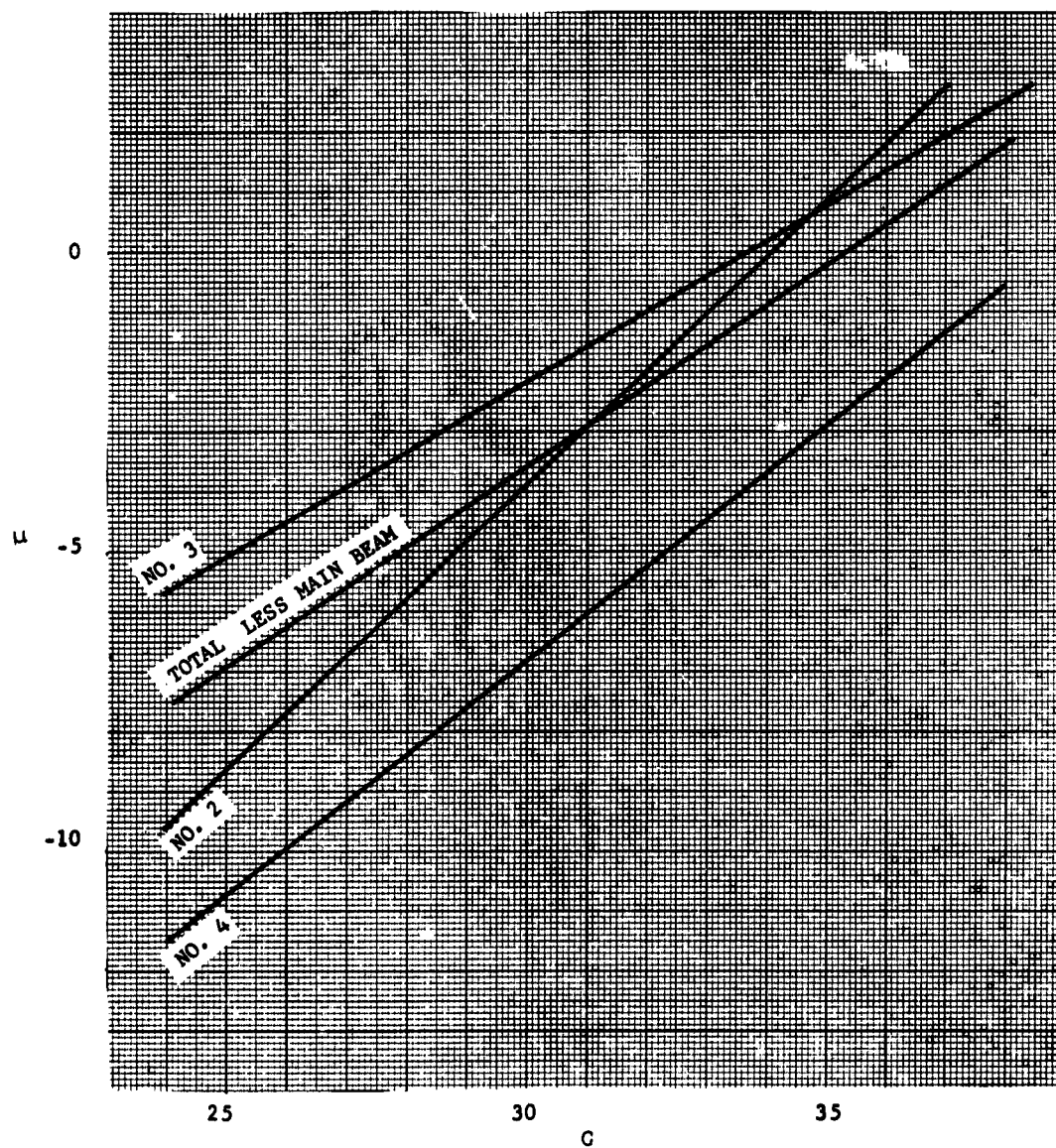


FIGURE 14. MEAN GAIN VERSUS NOMINAL GAIN FOR SECTORS 2, 3, and 4

THE APPLICATION OF ABSORPTION AND SCATTERING COEFFICIENTS FOR  
CONCENTRIC SPHERES TO THE PROBLEM OF EMI-FREE ENCLOSURES

R. A. Eldred, H. A. Lasitter, and J. Roberts  
U. S. Naval Civil Engineering Laboratory  
Port Hueneme, California

Abstract. - With the purpose of increasing the information about the lower frequency shielding effectiveness of closed structures composed of various arbitrary materials, an idealized problem is considered of the scattering and absorption of a plane electromagnetic wave impinging on a spherical shell. The region between the outer and inner radius of the sphere contains an arbitrary material; the other two regions are free space. The absorption and scattering coefficients for the incident plane wave are expressed as an infinite sum of spherical waves, using spherical Bessel functions. The coefficients are calculated numerically and shown for a large range of complex material parameters and frequencies from 100 kc to 1000 mc. Equations were programmed in FORTRAN, and numerical calculations accomplished on the IBM 1620 computer. Combinations of complex material properties of permeability, permittivity and conductivity were sought which gave large, broadband absorption coefficients. Several promising compositions have resulted, and are presented. The effects of varying the individual parameters are also discussed.

I. INTRODUCTION

In order to utilize a mathematically complete and general solution to the boundary value problem, the symmetrical configuration of a spherical shell has been used to approximate the closed walls of the normally cubical or rectangular shielded enclosure. The behavior of the impinging plane wave electromagnetic field external to the spherical structure is considered. In order to completely describe the perturbing effect of the spherical shell, knowledge of the field outside, inside, and within the shell material is necessary. This investigation has been primarily directed toward a systematic exploratory search for wall (or shell, in this case) materials that will give uniform absorption of plane EM waves in the broad spectrum between 0.1 and 1000 mc.

The assumptions made in this investigation are:

1. The spherical structure is isolated in space,
2. The wave incident on the surface of the outer sphere is a plane wave,
3. The shell material is homogeneous and isotropic,
4. The shell is composed of an arbitrary material with complex properties of  $\mu^*$ ,  $\epsilon^*$ , and  $\sigma$ . The inner sphere and the exterior region is free space.

The geometry of the spherical configuration is shown in Figure 1. For this case, the equations describing the absorption ( $C_a$ ) and scattering ( $C_s$ ) coefficients have been derived (Appendix A). The Mie<sup>a</sup> scattering equations as given by Stratton<sup>1</sup> and expanded to two concentric spheres by O. M. Salati<sup>2</sup> are essentially those used in this study. We have found that it is possible to extend the equations to cover three concentric spheres but only the two sphere solution is presented here.

The shell material parameters have been systematically varied over a wide range of values. Ranges of values of parameters were selected generally on the basis of known conductors or non-conductors. The good dielectrics and some magnetic materials are in the classification of non-conductors. The case of high conductors yields considerable simplification of the  $C_a$  and  $C_s$  equations and has been treated separately. The dimensional properties of the spherical shell structure have, in most cases, been selected to approximate the dimensions of actual shielded enclosures. The majority of data was computed on the basis of  $a_2$  (outer radius) = 5 meters (16.4 feet) and a shell thickness ( $a_2 - a_1$ ) = 0.15 meters (5.9 inches). In many cases data were taken at different radii to show the variation in  $C_a$  and  $C_s$ . The effect of shell thickness variation was also considered.

A total of 106 separate combinations of material parameters or dimensional variations were computed. Only a summary of the materials that gave large absolute values of absorption coefficients and broadband absorption is given here.

An IBM 1620 digital computer was used to facilitate numerical solution of the coefficients  $C_a$  and  $C_s$ . The computer program for the arbitrary material case as well as the special high conductivity case ( $\sigma > 10^4$  mhos/meter) is included in Appendix B.

## II. ABSORPTION AND SCATTERING COEFFICIENTS FOR THE CASE OF ARBITRARY MATERIALS

The relative scattering cross-section,  $C_s$ , is defined as the ratio of the absolute scattering cross-section to the geometrical cross-section of the outer sphere. In terms of energy,  $C_s$  is the ratio of the total scattered energy to the energy of the unperturbed incident wave crossing an area equal to the geometrical cross-section. Identical definitions hold for the relative absorption cross-section,  $C_a$ .

Expressing the relative cross-sections in terms of Stratton's external field coefficients,  $a_n^r$  and  $b_n^r$ ,

$$C_s = \frac{2}{\xi_2^2} \sum_{n=1}^{\infty} (2n+1) (|a_n^r|^2 + |b_n^r|^2)$$

$$C_a = - \frac{2}{\xi_2^2} \sum_{n=1}^{\infty} (2n+1) (R_e a_n^r + R_e b_n^r + |a_n^r|^2 + |b_n^r|^2)$$

where

$$\xi_2 = k_0 a_2 = \frac{\omega a_2}{c}; \quad a_2 = \text{radius of outer sphere.}$$

In Appendix A, expressions for the above field coefficients are derived for the case in which the inner sphere is free space, the region between the spheres contains an arbitrary dielectric or magnetic material, and the region outside the spheres is free space. The two coefficients are shown to have identical form except that the admittance of the material is replaced by impedance:

$$a_n^r = - \frac{j_n(\xi_2)}{h_n^{(2)}(\xi_2)} \frac{\{ h_n^{(1)}(\rho_1) [g \alpha_n^{(1)}(\rho_1) - \delta_n(\xi_1)] h_n^{(2)}(\rho_2) [g \alpha_n^{(2)}(\rho_2) - \delta_n(\xi_2)] - h_n^{(2)}(\rho_1) [g \alpha_n^{(2)}(\rho_1) - \delta_n(\xi_1)] h_n^{(1)}(\rho_2) [g \alpha_n^{(1)}(\rho_2) - \delta_n(\xi_2)] \}}{h_n^{(2)}(\xi_2) \{ h_n^{(1)}(\rho_1) [g \alpha_n^{(1)}(\rho_1) - \delta_n(\xi_1)] h_n^{(2)}(\rho_2) [g \alpha_n^{(2)}(\rho_2) - \delta_n(\xi_2)] - h_n^{(2)}(\rho_1) [g \alpha_n^{(2)}(\rho_1) - \delta_n(\xi_1)] h_n^{(1)}(\rho_2) [g \alpha_n^{(1)}(\rho_2) - \delta_n(\xi_2)] \}}$$

where  $h_n^{(1)}$  and  $h_n^{(2)}$  are the first and second spherical Hankel functions and  $j_n$  is the spherical Bessel function;

$g$ , the relative admittance of the material  $\sqrt{K_e/K_m}$ , is used in  $a_n^r$  and the relative impedance  $\sqrt{K_m/K_e}$  is used in  $b_n^r$ ;

$\xi_1 = k_0 a_1$ ,  $\xi_2 = k_0 a_2$  ( $k_0$  is propagation constant for free space,  $a_1$  and  $a_2$  are radii of spheres)

$\rho_1 = k a_1$ ,  $\rho_2 = k a_2$  ( $k$  is the propagation constant for the material);

and

$$\alpha_n^{(1)}(x) = \frac{h_{n-1}^{(1)}(x)}{h_n^{(1)}(x)} - \frac{n}{x} ;$$

$$\gamma_n(x) = \frac{j_{n-1}(x)}{j_n(x)} - \frac{n}{x} ;$$

$$\delta_n(x) = \frac{h_{n-1}^{(2)}(x)}{h_n^{(2)}(x)} - \frac{n}{x} .$$

Characterizing the material by complex permeabilities and permittivities we have,

$$\epsilon^* = \epsilon_0 (K_e' - i K_e'') = \epsilon_0 K_e ;$$

$$\mu^* = \mu_0 (K_m' - i K_m'') = \mu_0 K_m ;$$

where

$$K_e'' = K_e' \cdot \text{loss tangent} \quad \text{for dielectrics,}$$

and

$$K_e'' = \frac{\mu_0 c^2 \sigma}{\omega} \quad \text{for conductive materials.}$$

The propagation constant is given by  $k = k_0 \sqrt{K_e K_m}$ .

### III. DIELECTRIC MATERIAL

In general, high dielectric materials will give absorption curves with values that are much less than unity and have severe fluctuations in magnitude over the frequency range. For high dielectric materials small changes in thickness or in the radius of the shell structure will cause drastic changes in the shape of the absorption curves. This effect is illustrated for a change in radius in Figures 2 and 3, where a dielectric constant of 100 has been used. The radius of the spheres has been changed by a factor of two. The scattering coefficient for the same material is shown in Figure 4. The numbers shown in parenthesis are  $(K'_e, K''_e)$   $(K'_m, K''_m)$ , respectively.

### IV. MAGNETIC MATERIAL

The magnetic properties have been investigated on the basis of variation of the permeability ( $K'_m$ ) between 1 and 100 (see Figure 5) and a magnetic loss factor ( $K''_m$ ) between 0.1 and 100 (see Figure 6). The above data is based on a dielectric loss factor ( $K''_e$ ) of 100 and dielectric constant ( $K'_e$ ) of one. Small changes in the general shape of the curves indicate that wide variations in  $K'_m$  and  $K''_m$  have little effect on the uniformity of  $C_a$ . Figures 7 and 8 show the effect on  $C_a$  for variations of conductivity between  $10^{-4}$  and  $10^4$  mhos/meter and a permeability of 100, using a loss tangent of one. The most uniform curve for  $C_a$  occurs at (1,1) (100,100), indicating that a low conductivity ( $\sigma = 1$  mho/meter) is desirable in this combination.

### V. HIGH CONDUCTIVITY MATERIALS

The expressions for the  $a_n^r$  and  $b_n^r$  field coefficients can be simplified considerably for the high conductivity case ( $\sigma > 10^4$  mhos/meter).

For non-dielectric materials,

$$K_e'' = \frac{\mu_0 C^2 \sigma}{\omega} = \frac{1.8 \times 10^4 \sigma}{F}$$

where  $\sigma > 10^4$ , and  $F < 10^3$  mc, then  $K_e'' > 10^5$ .

The complex propagation constant  $k^* = k' - ik''$ , is



$$k' = k_0 \left[ \frac{9 \times 10^3 \sigma}{F} (\sqrt{K_m'^2 + K_m''^2} - K_m'') \right]^{1/2}$$

$$= \left[ \frac{4\pi^2 F \sigma}{10} (\sqrt{K_m'^2 + K_m''^2} - K_m'') \right]^{1/2}$$

and

$$k'' = \left[ \frac{4\pi^2 F \sigma}{10} (\sqrt{K_m'^2 + K_m''^2} + K_m'') \right]^{1/2}$$

$k'' > 70$  for  $F > 0.1$  mc, and  $\sigma > 10^4$  mhos/meter, where the approximation was made that  $K_e'' > K_e'$ .

The Hankel functions vary exponentially with their arguments, as

$$h_n^{(1)}(x) = e^{ix} p_n^{(1)}(x), \quad h_n^{(2)}(x) = e^{-ix} p_n^{(2)}(x)$$

where the  $p_n$  are polynomials in  $1/x$ , then it can be shown that for large arguments (See reference 1, page 359)

$$\left| \frac{h_n^{(1)}(p_2) h_n^{(2)}(p_1)}{h_n^{(2)}(p_2) h_n^{(1)}(p_1)} \right| \approx e^{2k''(a_2 - a_1)}$$

For a shell thickness  $(a_2 - a_1)$  greater than 10 inches  $e^{2k''(a_2 - a_1)} \gg 1$ . This approximation is also valid for a smaller shell thickness where the conductivity is high, the permeability is greater than that of free space, and for frequencies greater than 0.1 mc. The approximation is equivalent to the statement that the shell thickness must be larger than the skin depth, so that the fields are considerably damped before reaching the inner sphere.

Using this approximation, the field coefficients are greatly simplified, resulting in

$$a_n^r = - \frac{j_n(\xi_2)}{h_n^{(2)}(\xi_2)} \frac{g\alpha_n''(p_2) - \delta_n(p_2)}{g\alpha_n''(p_2) - \delta_n(p_2)}$$

with an equivalent expression for the  $b_n^r$  obtained by replacing  $g$  with  $1/g$ .

Using these expressions, the scattering and absorption coefficients were computed for various values of the material parameters. The resulting data had the following form:

1. The scattering coefficient for this case is independent of the material parameters, and is a function of the product of the outer radius  $a_2$  and the frequency  $F$ . For  $Fa_2$  less than 20 mc-meters, the scattering varies as the fourth power of the product  $Fa_2$ . This is the Rayleigh scattering, and corresponds to a wavelength greater than 10 times the radius. For  $Fa_2$  greater than 50 mc-meters, the scattering coefficient reaches a value of two (see Figure 9). The expression for the Rayleigh scattering is

$$C_s = 6.5 \times 10^{-7} (Fa_2)^4$$

2. The absorption coefficient varies as

$$C_a = \left[ \frac{\sqrt{K_m'^2 + K_m''^2} + K_m''}{\sigma} \right]^{1/2} f_a(F, a_2)$$

where  $f_a(F, a_2)$  is shown in Figure 10 for radii of 1, 5, 10, and 20 meters. From this graph it is seen that the factor  $f_a$  can be approximated by

$$f_a(F, a_2) \approx \sqrt{F \times 10^{-3}}$$

Then

$$C_a \approx \left[ \frac{F}{\sigma \times 10^3} (\sqrt{K_m'^2 + K_m''^2} + K_m'') \right]^{1/2}$$

Since  $F/(\sigma \times 10^3) = 18/K_e''$ , then

$$C_a = 6 \left( \frac{\sqrt{K_m'^2 + K_m''^2} + K_m''}{2 K_e''} \right)^{1/2}$$

Thus, for radii in the range of 1 to 20 meters, the absorption cross-section is almost independent of the radius.

#### VI. CONDUCTORS

The approximations made in the high conductivity case are no longer valid for materials less than 10,000 mhos/meter. For calculation of  $C_a$  where  $\sigma < 10^4$  mhos/meter it has been necessary to use the general equations describing any material. The results of low conductivities (1.0 to  $10^{-4}$  mhos/meter) are indicated in Figure 12. The most uniform curve of any material examined is given by a material conductivity of 0.01 mhos/meter.

Variation of the absorption curve for a change in the radius of the sphere has been investigated. The effect is to shift the maxima downward in frequency as the radius is increased. Figure 13 shows the effect of a radius change from 5 to 20 meters for material  $\sigma$  of 0.1 mhos/meter. This effect is true for most low to medium conductivity materials.

#### VII. VARIATION OF MATERIAL PARAMETERS WITH FREQUENCY

Generally, the variation in  $K_e'$ ,  $K_e''$ ,  $K_m'$ ,  $K_m''$  for most materials is not great over the frequency range of interest in this study. However, the list of materials given by Von Hippel<sup>3</sup> indicates there is a group of materials whose parameters vary rapidly in the range from 0.1 to 1000 mc. The listed parameter values for a ferramic were used to determine  $C_a$  as shown in Figure 14. Even with the large changes in  $K_e$  and  $K_m$  the curve appears uniform. However, only the data points shown were available and there may be variations due to a lack of data in the intermediate ranges.

### VIII. CONCLUSIONS

The uniform absorption curves occur for material whose conductivity is in the region 0.1 to 0.01 mhos/meter. Some magnetic materials also give near-uniform absorption curves. Dielectric materials with high dielectric constants and low loss factors are definitely not suitable. Low dielectric constant and high loss factor materials exhibit the characteristics of uniform absorption, however, the low conductivity materials make more suitable building materials.

The absorption coefficient should be as independent as possible of variations in the dimensional properties of the structure. The choice of a material will depend not only on the uniformity of the absorption vs. frequency curve, but also the behavior of the absorption coefficient with changes in radius and shell thickness.

### IX. FUTURE PLANS

1. An experimental program is underway to compare experimental measurements of synthesized materials with results predicted by the theory presented here.
2. Experimental verification of the approximation of the spherical shell for the cubical or rectangular configurations will be made.
3. Theoretical investigation of the triple sphere problem may be undertaken to extend the application of theory to multiple layer structures. There is a possibility that the theory can be extended to  $n$  concentric spheres, so that 2, 3, ...  $n-1$  layers can be considered.

## REFERENCES

1. Stratton, J. A., Electromagnetic Theory, McGraw-Hill, New York, 1941, p. 565.
2. Salati, O. M., University of Pennsylvania, private communication.
3. Von Hippel, A., Dielectric Materials and Applications, John Wiley & Sons, Inc., New York, p. 308.

## DEFINITION OF TERMS

$a_1$	inner radius
$a_2$	outer radius
$a_n^r, b_n^r$	coefficients of the external field
$C_a$	absorption coefficient
$C_s$	scattering coefficient
$E_o$	magnitude of incident wave
$F$	frequency in megacycles
$g$	relative admittance of material = $\sqrt{K_e/K_m}$
$h_n^{(1)}, h_n^{(2)}$	first and second spherical Hankel functions
$j_n$	spherical Bessel function of the first kind
$k$	propagation constant of material
$k_o$	propagation constant of free space
$K_e$	relative permittivity of material
$K_m$	relative permeability of material
$N$	index of refraction of material = $\sqrt{K_e K_m}$
$Q_a$	absorption cross-section
$Q_s$	scattering cross-section
$W_a$	power absorbed (watts)
$W_i$	power density of incident wave (watts/m <sup>2</sup> )
$W_s$	power scattered (watts)
$W_t$	power lost by incident wave (watts)
$z$	generalized Bessel function
$Z$	relative impedance of material = $\sqrt{K_m/K_e}$

$\alpha_n, \gamma_n, \delta_n$	dimensionless functions (see equations A4, A5, A6)
$\epsilon_0$	permittivity of free space = $1/c^2 \mu_0$
$\epsilon^*$	complex permittivity
$\mu^*$	complex permeability
$\mu_0$	permeability of free space = $4\pi \times 10^{-7}$ henries/meter
$\xi_s$	dimensionless variable for free space = $k_0 a_s$
$\rho_s$	dimensionless variable for material = $ka_s$
$\sigma$	conductivity of material (mhos/meter)
$\hat{i}_p$	unit vectors, $p = 1, 2, 3$

## APPENDIX A

### DERIVATION OF THE MATHEMATICAL EXPRESSIONS

1 Field coefficients. The following derivation is an application of the method used by Stratton<sup>1</sup> (section 9.25) to discuss the diffraction of a plane wave by a single sphere.

The total power scattered,  $W_s$ , and the total power lost by the incident wave,  $W_t$ , (measured at a distance large compared to the outer radius of the sphere) may be expressed in terms of the coefficients of the reflected part of the external field,  $a_n^r$  and  $b_n^r$ , for a single or double sphere by:

$$W_s = \frac{\pi E_o^2}{k_o^2} \sqrt{\frac{\epsilon_o}{\mu_o}} \sum_{n=1}^{\infty} (2n+1) (|a_n^r|^2 + |b_n^r|^2) \quad \text{watts}$$

$$W_t = -\frac{\pi E_o^2}{k_o^2} \sqrt{\frac{\epsilon_o}{\mu_o}} \sum_{n=1}^{\infty} (2n+1) (\text{Re } a_n^r + \text{Re } b_n^r) \quad \text{watts}$$

The total power absorbed by the sphere,  $W_a$ , is equal to the total power lost by the incident wave less the total power scattered. The power density of the incident wave is

$$W_i = \frac{1}{2} E_o^2 \sqrt{\frac{\epsilon_o}{\mu_o}} \quad \text{watts/m}^2$$

Defining the scattering (or absorption) coefficient as the ratio of the power scattered (or absorbed) to the power density of the incident wave times the geometrical cross-section,

$$C_s = \frac{W_s}{\pi a_2^2 W_i} \quad \text{and} \quad C_a = \frac{W_a}{\pi a_2^2 W_i} = \frac{W_t - W_s}{\pi a_2^2 W_i},$$

where  $a_2$  = outer radius.

The dimensionless scattering and absorption coefficients are then

$$C_s = \frac{2}{\sum_{n=1}^{\infty} (2n+1) (|a_n^r|^2 + |b_n^r|^2)}$$

and

$$C_a = -\frac{2}{\sum_{n=1}^{\infty} (2n+1) (R_e a_n^r + R_e b_n^r + |a_n^r|^2 + |b_n^r|^2)}$$

where  $\bar{k}_2 = k_0 a_2$ .

The field coefficients are obtained by expressing the fields in the three regions in terms of the spherical vector wave functions and solving at the boundaries. Letting  $z_n(x)$  be any Bessel function where  $x = kr$ , the four vector wave functions are:

$$\begin{aligned} \vec{m}_{e1n} = & \pm \frac{1}{\sin \theta} z_n(x) P_n'(\theta) \frac{\cos \theta}{\sin \theta} \hat{i}_2 \\ & - z_n(x) \frac{dP_n'}{d\theta} \frac{\sin \theta}{\cos \theta} \hat{i}_3 \end{aligned}$$



$$\begin{aligned}
\vec{n}_{e1n} = & \frac{n(n+1)}{x} y_n(x) P'_n(\theta) \frac{\sin \theta}{\cos \theta} \hat{1}_1 \\
& + \frac{1}{x} \frac{d}{dx} [x y_n(x)] \frac{dP'_n}{d\theta} \frac{\sin \phi}{\cos \phi} \hat{1}_2 \\
& \pm \frac{1}{x \sin \theta} \frac{d}{dx} [x y_n(x)] P'_n(\theta) \frac{\cos \phi}{\sin \phi} \hat{1}_3.
\end{aligned}$$

In terms of these vector wave functions and the field coefficients, the fields in the three regions are:

a. inner region (free space)

$$\vec{E} = E_0 e^{i\omega t} \sum_{n=1}^{\infty} x^n \frac{2n+1}{n(n+1)} \left[ a_n^t \vec{m}_{01n}^{(1)} - i b_n^t \vec{n}_{e1n}^{(1)} \right]$$

$$\vec{H} = \sqrt{\frac{\epsilon_0}{\mu_0}} E_0 e^{i\omega t} \sum_{n=1}^{\infty} x^n \frac{2n+1}{n(n+1)} \left[ b_n^t \vec{m}_{e1n}^{(1)} + i a_n^t \vec{n}_{o1n}^{(1)} \right],$$

where  $z_n^{(1)} = j_n$   $k = k_0$  ;

b. middle region (arbitrary material)

$$\begin{aligned}
\vec{E} = E_0 e^{i\omega t} \sum_{n=1}^{\infty} x^n \frac{2n+1}{n(n+1)} & \left[ a_n^{(2)} \vec{m}_{o1n}^{(2)} + a_n^{(3)} \vec{m}_{o1n}^{(3)} \right. \\
& \left. - i (b_n^{(2)} \vec{n}_{e1n}^{(2)} + b_n^{(3)} \vec{n}_{e1n}^{(3)}) \right]
\end{aligned}$$

$$\vec{H} = \sqrt{\frac{\epsilon_0}{\mu_0}} E_0 e^{i\omega t} \sqrt{\frac{K_e}{K_m}} \sum_{n=1}^{\infty} e^{-n} \frac{2n+1}{n(n+1)} \left[ b_n^{(2)} \vec{m}_{ein}^{(2)} + b_n^{(3)} \vec{m}_{ein}^{(3)} + i(a_n^{(2)} \vec{n}_{oin}^{(2)} + a_n^{(3)} \vec{n}_{oin}^{(3)}) \right],$$

$$z_n^{(2)} = h_n^{(1)}, \quad z_n^{(3)} = h_n^{(2)}, \quad k = k_0 \sqrt{K_e K_m};$$

c. outer region (free space)

$$\vec{E} = E_0 e^{i\omega t} \sum_{n=1}^{\infty} e^{-n} \frac{2n+1}{n(n+1)} \left[ \vec{m}_n^{(1)} + a_n^r \vec{m}_{oin}^{(4)} - i(\vec{n}_{ein}^{(1)} + b_n^r \vec{n}_{ein}^{(4)}) \right] \quad (A1)$$

$$\vec{H} = \sqrt{\frac{\epsilon_0}{\mu_0}} E_0 e^{i\omega t} \sum_{n=1}^{\infty} e^{-n} \frac{2n+1}{n(n+1)} \left[ \vec{m}_{ein}^{(1)} + b_n^r \vec{m}_{ein}^{(4)} + i(\vec{n}_{oin}^{(1)} + a_n^r \vec{n}_{oin}^{(4)}) \right] \quad (A2)$$

$$z_n^{(1)} = j_n, \quad z_n^{(4)} = h_n^{(2)}, \quad k = k_0.$$

The boundary conditions are

$$\hat{L}_1 \times (\vec{E}' - \vec{E}'') = 0 \quad \hat{L}_2 \times (\vec{H}' - \vec{H}'') = 0 \quad (A3)$$

where primes and double primes refer to two different regions.

Denoting  $\xi_m = k_0 a_m$  and  $\rho_m = k a_m = \xi_m \sqrt{K_e K_m} = N \xi_m$ , we have the following relations:

$$\frac{d}{df_m} [f_m h_n^{(l)}(f_m)] = f_m h_n^{(l)}(f_m) \alpha_n^{(l)}(f_m) ;$$

$$\alpha_n^{(l)}(f) = \frac{h_{n-1}^{(l)}(f_m)}{h_n^{(l)}(f_m)} - \frac{n}{f_m} \quad (A4)$$

where  $l = 1$  or  $2$

$$\frac{d}{d\xi_m} [\xi_m j_n(\xi_m)] = \xi_m j_n(\xi_m) \delta_n(\xi_m) ;$$

$$\delta_n(\xi_m) = \frac{j_{n-1}(\xi_m)}{j_n(\xi_m)} - \frac{n}{\xi_m} \quad (A5)$$

$$\frac{d}{d\xi_m} [\xi_m h_n^{(2)}(\xi_m)] = \xi_m h_n^{(2)}(\xi_m) \delta_n(\xi_m) ;$$

$$\delta_n(\xi_m) = \frac{h_{n-1}^{(2)}(\xi_m)}{h_n^{(2)}(\xi_m)} - \frac{n}{\xi_m} \quad (A6)$$

The field coefficients, determined by substituting the fields into the boundary equations, may be written in matrix form as:

$$\begin{bmatrix} j_n(\xi_1) & -h_n^{(1)}(\rho_1) & -h_n^{(2)}(\rho_1) & 0 \\ j_n(\xi_1)\delta_n(\xi_1) & -h_n^{(1)}(\rho_1)g_n^{(1)}(\rho_1) & -h_n^{(2)}(\rho_1)g_n^{(2)}(\rho_1) & 0 \\ 0 & h_n^{(1)}(\rho_2) & h_n^{(2)}(\rho_2) & -h_n^{(2)}(\xi_2) \\ 0 & h_n^{(1)}(\rho_2)g_n^{(1)}(\rho_2) & h_n^{(2)}(\rho_2)g_n^{(2)}(\rho_2) & -h_n^{(2)}(\xi_2)\delta_n(\xi_2) \end{bmatrix} \begin{bmatrix} a_n^t \\ a_n^{(2)} \\ a_n^{(3)} \\ a_n^r \end{bmatrix} =$$

$$\begin{bmatrix} 0 \\ 0 \\ -j_n(\xi_2) \\ -j_n(\xi_2)\delta_n(\xi_2) \end{bmatrix}$$

(A7)

The equations involving the  $b_n$ 's are identical to those above except the relative admittance  $g = \sqrt{K_e/K_m}$  is replaced by the relative impedance  $Z = \sqrt{K/K_e}$ . Therefore, (1) it is necessary to solve only for the  $a_n$ 's, (2) the scattering and absorption coefficients are not changed when  $g$  and  $Z$  are interchanged in later equations.

Since the relative permittivity and permeability enter the equations only in the sum of interchangeable quotients  $\sqrt{K_e/K_m}$  and  $\sqrt{K_m/K_e}$  and in a product,  $k = k_0 \sqrt{K_e K_m}$ , it follows that the scattering and absorption coefficients are unchanged when  $K_e$  and  $K_m$  are interchanged. This fact decreases the number of data points required. For example, the results for  $K_e = a - ib$  and  $K_m = c - id$  are identical to those with  $K_e = c - id$  and  $K_m = a - ib$ . This is especially helpful when non-conductors are considered.

For calculational purposes the following substitutions are made:

$$h_n^{(1)}(\rho) = \frac{e^{i\rho}}{i\rho} f_n^{(1)}(\rho) ; \quad h_n^{(2)}(\rho) = \frac{e^{-i\rho}}{-i\rho} f_n^{(2)}(\rho); \quad (A8)$$

$$\begin{aligned} \Phi_n^{(l)}(\rho_m) &= f_n^{(l)}(\rho_m) [\alpha_n^{(l)}(\rho_m) - Z \delta_n(\xi_m)] \\ &= f_{n-1}^{(l)}(\rho_m) - f_n^{(l)}(\rho_m) [Z \delta_n(\xi_m) - \frac{\eta}{\rho_m}] ; \end{aligned} \quad (A9)$$

$$\Lambda_n^{(l)}(\rho_2) = f_n^{(l)}(\rho_2) [Z \delta_n(\xi_2) - Z \delta_n(\xi_2)] ; \quad (A10)$$

$$\begin{aligned} R &= e^{i(\rho_2 - \rho_1)} \Phi_n^{(2)}(\rho_1) \Phi_n^{(1)}(\rho_2) \\ &\quad - e^{-i(\rho_2 - \rho_1)} \Phi_n^{(1)}(\rho_1) \Phi_n^{(2)}(\rho_2) ; \end{aligned} \quad (A11)$$

$$\begin{aligned} T &= e^{i(\rho_2 - \rho_1)} \Phi_n^{(2)}(\rho_1) \Lambda_n^{(1)}(\rho_2) \\ &\quad - e^{-i(\rho_2 - \rho_1)} \Phi_n^{(1)}(\rho_1) \Lambda_n^{(2)}(\rho_2) . \end{aligned} \quad (A12)$$

Then the reflected field coefficient is given by

$$a_n^r = - \frac{j_n(\xi_2)}{h_n^{(2)}(\xi_2)} \frac{R}{T + R} \quad (A13)$$

For good conductors ( $\sigma > 10^4$  mhos/meter or better) the magnitude of the exponentials is large, so that the first terms in T and R are much larger than the second terms. In this case, referred to as the high conductivity case, the field coefficient is given by

$$a_n^r = - \frac{j_n(\xi_2)}{h_n^{(2)}(\xi_2)} \frac{\alpha_n^{(1)}(f_2) - Z \delta_n(\xi_2)}{\alpha_n^{(1)}(f_2) - Z \delta_n(\xi_2)}$$

2. Mathematical Functions. The recursion relation for all spherical Bessel functions, including  $f_n^{(k)}$ , is:

$$y_n(x) = \frac{2n-1}{x} y_{n-1}(x) - y_{n-2}(x).$$

The initial values ( $n = 1$ ) for the functions are

$$h_{-1}^{(2)}(\xi) = \frac{\cos \xi}{\xi} - i \frac{\sin \xi}{\xi},$$

$$h_0^{(2)}(\xi) = \frac{\sin \xi}{\xi} + i \frac{\cos \xi}{\xi},$$

$$f_{-1}^{(1)}(\rho) = i, \quad f_0^{(1)}(\rho) = 1, \quad f_{-1}^{(2)}(\rho) = -i, \quad f_0^{(2)}(\rho) = 1.$$

The spherical Bessel function of real argument,  $j_n(\xi)$ , is equal to the real part of either spherical Hankel function.

A recursion relation for  $y_n$  is:

$$y_n(\xi) = \frac{1}{\xi - y_{n-1}(\xi)} - \frac{n}{\xi}$$

with

$$y_0(\xi) = \cot \xi$$

### 3. Parameters.

a. Relative Permittivity:  $K_e = K'_e - iK''_e$

The dielectric loss factor,  $K''_e$ , may be produced both by migrating charge carriers (ohmic losses) and by the formation or orientation of electric dipoles (electric polarization losses). For materials in which the ohmic losses predominate, denoted "conductors", the conductivity is the parameter which is approximately independent of frequency. For materials in which the polarization predominates, denoted "non-conductors", the loss factor is the parameter which is approximately independent of frequency.

b. Relative Permeability:  $K_m = K'_m - iK''_m$

The magnetic loss factor,  $K''_m$ , is produced by the formation or orientation of magnetic dipoles.

c. Index of Refraction:  $N = N' - iN'' = \sqrt{K_e K_m}$

$$U = K_m' K_e' - K_m'' K_e''$$

$$V = K_m'' K_e' + K_m' K_e''$$

$$W^2 = U^2 + V^2$$

$$N = \sqrt{\frac{W+U}{2}} \quad , \quad N'' = \sqrt{\frac{W-U}{2}} \quad .$$

d. Relative Impedance:

$$Z = Z' + iZ'' = \sqrt{\frac{K_m}{K_e}} = \frac{K_m}{N}$$

$$Z' = \frac{K_m' N' + K_m'' N''}{N'^2 + N''^2} \quad .$$

$$Z'' = \frac{K_m' N'' - K_m'' N'}{N'^2 + N''^2} \quad .$$



## APPENDIX B

### FORTRAN COMPUTER PROGRAM

A FORTRAN program for an IBM 1620 is given here. The input and output are arranged to simplify graphing the coefficients as a function of frequency. The frequency is entered via the typewriter, all other parameters via cards. The program may be used for a conductor (conductivity held constant) or a non-conductor (loss factor held constant).

The program may be divided into four basic sections:

(1) Enter data, rearrange data to suitable form, initialize Bessel functions.

(2) Begin DO loop for each term in sum, calculate Bessel functions.

(3) Calculate  $\frac{2n+1}{F_2^2} |a_n^r|^2$  and

$$- \frac{2n+1}{F_2^2} (Re a_n^r + |a_n^r|^2) \quad \text{using relative}$$

impedance, then calculate  $\frac{2n+1}{F_2^2} |b_n^r|^2$  and

$$- \frac{2n+1}{F_2^2} (Re b_n^r + |b_n^r|^2) \quad \text{using relative}$$

admittance, and add the two to give  $Q_a$  and  $Q_s$ .

(4) Test ratios  $Q/C$  and  $Q_s/C_s$  to determine whether to continue or end the sum. (The sum will end if both ratios are less than .1%.) Both type and punch  $C_a$  and  $C_s$  and prepare program to enter new data as per second instruction at beginning of program.

The rate of convergence depends on the magnitude of the product of the outer radius and the frequency. For this reason it is recommended that results for the higher frequencies be attempted only when absolutely necessary. For a radius of 5 meters, 2-4 terms must be calculated at 1 mc, 5-10 at 10 mc, 15-30 at 100 mc, 100-150 at 1000 mc. Each term requires about 10 seconds.

**Input/Output:** A 10-position field is reserved for each of the 8 input variables entered via cards. These are  $K_e'$ ,  $K_e''$ ,  $K_m'$ ,  $K_m''$ ,  $a_2$ ,  $\delta$ ,  $n$ , 2 for a non-conductor and  $K_e'$ ,  $\sigma$ ,  $K_m'$ ,  $K_m''$ ,  $a_2$ ,  $\delta$ ,  $n$ , 1 for a conductor, where  $\delta$  is the shell thickness and  $n$  is an integer to label each set of input variables and identify the set with a graph. Note that the last variable is 1 for a conductor and 2 for a non-conductor.

After the eight parameters are entered, they are printed with the same format by the typewriter. The operator then enters the first frequency via the typewriter. When the calculation is completed,  $F$ ,  $C_a$ , and  $C_s$  are both typed and punched. If a graph of the coefficients as a function of the frequency is desired, it is suggested that the operator immediately plot the results, then select and enter another frequency value. In this way a frequency plot may be made quickly and completely.

The punched output, when printed out by an IBM 407, is of the form:

Figure 1

1.00	1.00E+01	1.00	.00	5.00	.1500	1
1.0	1.129E-02	3.985E-04				
10.0	5.286E-02	2.149E-00				
4.0	2.020E-02	1.062E-01				
30.0	6.436E-02	2.150E-00				
7.0	3.826E-02	9.413E-01				
.1	8.311E-03	3.837E-08				

The first line of the output data is a replica of the input data. The last number of the line is a 1, therefore, a conductor is represented. The first term is  $K_e'$ , the second  $\sigma$ , the third  $K_m''$ , etc.

The frequencies under consideration are typed in the first column. The corresponding values of  $C_a$  and  $C_s$  are given in the second and third columns.

#### Comments on the program:

1. Switch 1 may be used to (a) stop calculation when an overflow occurs, or (b) inspect convergence of the infinite sums.
2. To consider the cases where the exponentials are too large to be handled by the computer either a separate program of equation A14 may be written, or the value of the exponent may be limited to some large, but usable, number. The latter is used in this program.

To facilitate the use of the absorption and scattering coefficients, the general program for the computation is included as a part of this report. The program for the special case where the material is a conductor is also included.

```

C   SCATTERING AND ABSORPTION COEFFICIENTS FOR DOUBLE CONCENTRIC
C   SPHERES WHEN REGION BETWEEN SPHERES CONTAINS ARBITRARY MATERIAL
C   AND ALL OTHER REGIONS CONTAIN AIR.
C   FREQUENCY SPECTRUM PROGRAM.
C   SWITCH 1 ON TO STOP CALCULATION. THE MESSAGE XXX X.XXXX X.XXXX
C   WILL BE TYPED, INDICATING NTH TERM IN SUM AND RATIOS OF NTH TERM
C   TO SUM, AND THERE WILL BE A PAUSE. TO RESUME CALCULATION TURN 1
C   OFF AND PUSH START. TO ENTER NEW DATA LEAVE 1 ON AND PUSH START.
C   AFTER CALCULATION COMPLETED THERE WILL BE A PAUSE. TO ENTER NEW
C   FREQUENCY TURN 2 ON AND PUSH START. TO ENTER NEW DATA SET TURN 2
C   OFF AND PUSH START.
C   FOR CONDUCTOR SET K = 1. FOR NON-CONDUCTOR SET K = 2.
    DIMENSION XA(8),YA(8),XAA(4),YAA(4)
    1 READ 101,XEP,YEP,XMU,YMU,RAD,E,N,K
      PRINT 101,XEP,YEP,XMU,YMU,RAD,E,N,K
101  FORMAT (T10.2,E10.2,F10.2,F10.2,F10.2,F10.4,I10,I10)
      PUNCH 104,N,XEP,YEP,XMU,YMU,RAD,E,K
104  FORMAT (///15X6HFIGURE14//F8.2,2XE9.2,F9.2,F9.2,F8.2,F8.4,I9)
      T = 1.-E/RAD
    2 ACCEPT 107,F
107  FORMAT (F7.1)
      GO TO (10,11),K
    10 A = 1.8E4*YEP/F
      GO TO 12
    11 A = YEP
    12 U = XEP*XMU-A*YMU
      W = SQRT (U*U+(XEP*YMU+A*XMU)**2)
      XN = SQRT((W+U)/2.)
      YN = SQRT((W-U)/2.)
      XZ = (XMU*XN+YMU*YN)/W
      YZ = (XMU*YN-YMU*XN)/W
      DEN = XZ*XZ+YZ*YZ
      XI = .02096*F*RAD
      XOHR = XN/XI/W
      YOHR = YN/XI/W
      CA = 0.
      CS = 0.
      XG = COS(XI*T)/SIN(XI*T)
      XBB = COS(XI)
      XB = SIN(XI)
      YBB = -XB
      YB = XBB
      B = XN*XI*(1.-T)
      C = YN*XI*(1.-T)
      IF (C-50.) 4,4,3
    3 C = 50.
      B = 50.
    4 E = EXP(C)
      XQ = COS(B)
      YQ = SIN(B)
      A = -1.

```

DO 6 N = 1,4  
 A = -A  
 XAA(N) = O.  
 YAA(N) = A  
 XA(N) = 1.  
 6 YA(N) = O.  
 DO 100 NSUM = 1,500  
 S = NSUM  
 Q = 2.\*S-1.  
 P = (4.\*S+2.)/XI/XI  
 XG = 1./(S/XI/T-XG)-S/XI/T  
 A = XBB  
 B = YBB  
 XBB = XB  
 YBB = YB  
 XB = Q\*XBB/XI-A  
 YB = Q\*YBB/XI-B  
 W = YB/XB  
 WW = 1.+W\*W  
 XH = XBB/XB-S/XI  
 YJ = (W\*XBB-YBB)/XB/WW  
 A = XOHR\*Q  
 B = YOHR\*Q  
 N = O  
 40 N = N+1  
 C = XA(N)  
 D = YA(N)  
 XA(N) = A\*C-B\*D-XAA(N)  
 YA(N) = A\*D-B\*C-YAA(N)  
 XAA(N) = C  
 YAA(N) = D  
 GO TO (40,41,40,42),N  
 41 A = A/T  
 B = B/T  
 GO TO 40  
 42 QA = O.  
 QS = O.  
 X = XZ  
 Y = YZ  
 DO 200 I = 1,2  
 N = O  
 XR = O.  
 YR = O.  
 XT = O.  
 YT = O.  
 A = S\*XOHR+X\*XH  
 B = S\*YOHR+Y\*XH  
 50 N = N+1  
 C = XA(N)

D = YA(N)  
 XA(N+4) = XAA(N)-A\*C+B\*D  
 YA(N+4) = YAA(N)-A\*D-B\*C  
 GO TO (50,51,50,52),N  
 51 A = S\*XOHR/T+X\*XG  
 B = S\*YOHR/T+Y\*XG  
 GO TO 50  
 52 C = XQ\*E  
 D = YQ\*E  
 YC = (W\*Y+X)\*YJ  
 XC = (W\*X-Y)\*YJ  
 DO 53 N = 1,2  
 L = 9-N  
 A = XA(L)  
 B = YA(L)  
 U = A\*C-B\*D  
 V = A\*D-B\*C  
 A = XA(N+4)  
 B = YA(N+4)  
 XR = A\*U-B\*V-XR  
 YR = A\*V-B\*U-YR  
 A = XA(N)  
 B = YA(N)  
 C = A\*XC-B\*YC  
 D = A\*YD-B\*XC  
 XT = C\*U-D\*V-XT  
 YT = C\*V-D\*U-YT  
 C = XQ/E  
 53 D = -YQ/E  
 XS = XR+XT  
 YS = YR+YT  
 A = YS/XS  
 B = XS+YS\*A  
 U = (XR+YR\*A)/B  
 V = (YR-XR\*A)/B  
 XS = (U+V\*W)/WW  
 YS = (V-U\*W)/WW  
 QA = P\*(XS-XS\*XS-YS\*YS)+QA  
 QS = P\*(XS\*XS+YS\*YS)+QS  
 X = XZ/DEN  
 200 Y = -YZ/DEN  
 CA = CA+QA  
 CS = CS+QS  
 RA = QA/CA  
 RS = QS/CS  
 IF (SENSE SWITCH 1) 175,170  
 175 PRINT 105,NSUM,RA,RS  
 105 FORMAT (I4,F8.4,F8.4)  
 PAUSE  
 IF (SENSE SWITCH 1) 176,170  
 170 IF (1-E-6-RA\*RA-RS\*RS) 100,180,180  
 100 CONTINUE  
 180 PUNCH 108,F,CA,CS

```

176 PRINT 108,F,CA,CS
108 FORMAT (5X F7.1,5X E10.3,5X E10.3)
PAUSE
IF (SENSE SWITCH 2) 2,1
END

```

RELATIVE SCATTERING AND ABSORPTION CROSS-SECTIONS FOR HIGH CONDUCTIVITY  
DOUBLE SPHERE

\* \* \* \* \*

ERR DENOTES MAXIMUM ALLOWED RATIO OF NTH TERM TO SUM, BMAX DENOTES THE  
CUTOFF TERM FOR THE INFINITE SUM.

PROGRAM SWITCHES

TURN 1 ON WHEN AN OVERFLOW (ERROR E3) OCCURS IN PROGRAM. WHEN SET OF DATA  
IS ENTERED TURN 1 OFF.  
2 IS OFF IF DATA IS TO BE ENTERED VIA CARDS. IT IS ON IF DATA IS TO BE  
ENTERED VIA TYPEWRITER.  
TURN 3 ON TO BRANCH TO ACCEPT ERR BMAX STATEMENT.

18 JUNE 1963

PROGRAM B

```

1 ACCEPT, ERR,BMAX
2 IF (SENSE SWITCH 2) 3,4
3 ACCEPT,RAD,SIGMA,XMU,YMU,F
GO TO 5
4 READ,RAD,SIGMA,XMU,YMU,F
5 PUNCH,RAD,SIGMA,XMU,YMU,F
W = SQR(XMU*XMU+YMU*YMU)
RAT = SQR((W+YMU)/(W-YMU))
CS = 0.
CA = 0.
XI = .02096*RAD*F
YK = SQR(3.948*SIGMA*F*(W+YMU))
AL = .02096*F/YK/(1.+RAT*RAT)*RAT
XG = AL*(XMU+RAT*YMU)
YG = AL*(XMU*RAT-YMU)
DEN = XG*XG+YG*YG
XBB = COS(XI)
XB = SIN(XI)
YBB = -XB
YB = XBB
XAL = 0.
YAL = 1.
B = 0.
100 B = B+1.
P = XBB
Q = YBB
XBB = XB

```

```

YBB = YB
XB = (2.*B-1.)/XI*XBB-P
YB = (2.*E-1.)/XI*YBB-Q
U = YB/XB
XZETA = 1./(1.+U*U)
XGAM = XBB/XB-B/XI
XQ = B*AL/XI
C = XAL-XQ
D = YAL-XQ*RAT
XAL = -C/(C*C+D*D)-XQ
YAL = D/(C*C+D*D)-XQ*RAT
I = 0
QS = 0.
QA = 0.
XBETA = XGAM-XZETA*(XBB+U*YBB)/XB-B/XI
YBETA = XZETA*(XBB*U-YBB)/XB
X = XG
Y = YG
150 XNUM = X*XAL-Y*YAL-XGAM
YNUM = X*YAL+Y*XAL
XDEN = XNUM+XBETA
YDEN = YNUM+YBETA
A = 2./XI/XI*(2.*B+1.)*XZETA/(XDEN*XDEN+YDEN*YDEN)
QS = A*(XNUM*XNUM+YNUM*YNUM)+QS
QA = A*(XNUM*(XBETA-U*YDEN)+YNUM*(YBETA+U*XDEN))+QA
IF (I) 160,160,170
160 X = XG/DEN
Y = -YG/DEN
I = 1
GO TO 150
170 CS = QS+CS
CA = QA+CA
IF (SENSE SWITCH 1) 190,174
174 IF (E-RMAX) 175,175,176
175 IF (ERR-QS/CS-QA/CA) 100,180,180
176 PRINT, QA,QS
180 PUNCH,CA,CS,YK
190 IF (SENSE SWITCH 3) 1,2
END

```

The variables used in the program are:

a. Dummy variables: A,B,C,D,U,V,X,Y,K,L,N,P,Q,S.

b. Real variables:

CA absorption coefficient,  $C_a$

CS      scattering coefficient,  $C_s$   
 DEN     $|Z|^2$   
 E      shell thickness  $(a_2 - a_1)$ ;  $\exp(\text{Im}(\rho_2 - \rho_1))$   
 F      frequency in megacycles  
 NSUM   counting integer for terms in sum, n  
 QA     nth term of  $C_a$   
 QS     nth term of  $C_s$   
 RA      $Q_a/C_a$  ratio of nth term of  $C_a$  to the sum of the  
          first n terms  
 RS      $Q_a/C_a$  ratio of nth term of  $C_s$  to the sum of the  
          first n terms  
 RAD    outer radius,  $a_2$   
 T      ratio of radii,  $a_1/a_2$   
 XI      $\xi_2 = k_0 a_2$   
 W      ratio of imaginary part to real part of Bessel  
          function  $h_n^{(2)}(\xi_2)$

c. Complex variables: The prefixes X and Y denote the real and imaginary parts of the complex variables.

XA(1)    $f_n^{(1)}(\rho_2)$   
 XA(2)    $f_n^{(2)}(\rho_2)$   
 XA(3)    $f_n^{(1)}(\rho_1)$   
 XA(4)    $f_n^{(2)}(\rho_1)$   
 XA(5)    $\phi_n^{(1)}(\rho_2)$   
 XA(6)    $\phi_n^{(2)}(\rho_2)$   
 XA(7)    $\phi_n^{(1)}(\rho_1)$

XA(8)  $\phi_n^{(2)}(\rho_1)$   
 XAA(N)  $f_{n-1}^{(2)}(\rho_m)$  corresponding to XA(N)  
 XB  $\xi_2 h_n^{(2)}(\xi_2)$   
 XBB  $\xi_2 h_{n-1}^{(2)}(\xi_2)$   
 XC  $Z[\gamma_n(\xi_2) - \delta_n(\xi_2)]$   
 XEP  $K'_e$   
 YEP  $K''_e$  for non-conductor;  $\sigma$  for conductor  
 XG  $\gamma_n(\xi_1)$   
 XH  $\gamma_n(\xi_2)$   
 XJ  $\gamma_n(\xi_2) - \delta_n(\xi_2)$   
 XMJ  $K_m$   
 XN N (index of refraction)  
 XOHR  $1/\rho_2$   
 XQ  $\exp(i \operatorname{Re}(\rho_2 - \rho_1))$   
 XR numerator of  $a_n^r$ , R in equation A13  
 XS denominator of  $a_n^r$ ;  $a_n^r$   
 XT T in equation A13  
 XZ Z (relative impedance)



$$\epsilon^* = \epsilon_0 (K_e' - iK_e'')$$

$$\mu^* = \mu_0 (K_m' - iK_m'')$$

$$\tan \delta_e = \frac{K_e''}{K_e'}$$

$$\tan \delta_m = \frac{K_m''}{K_m'}$$

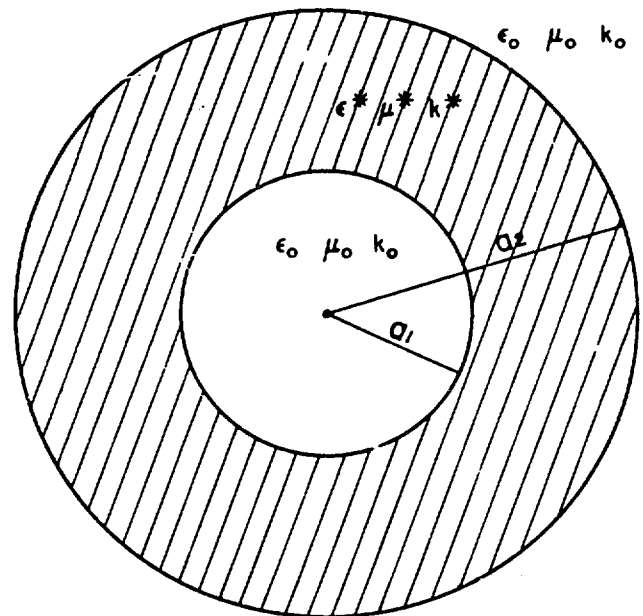


FIG.1 DIAGRAM OF SPHERICAL CONFIGURATION.  
INNER AND OUTER REGIONS ARE FREE SPACE

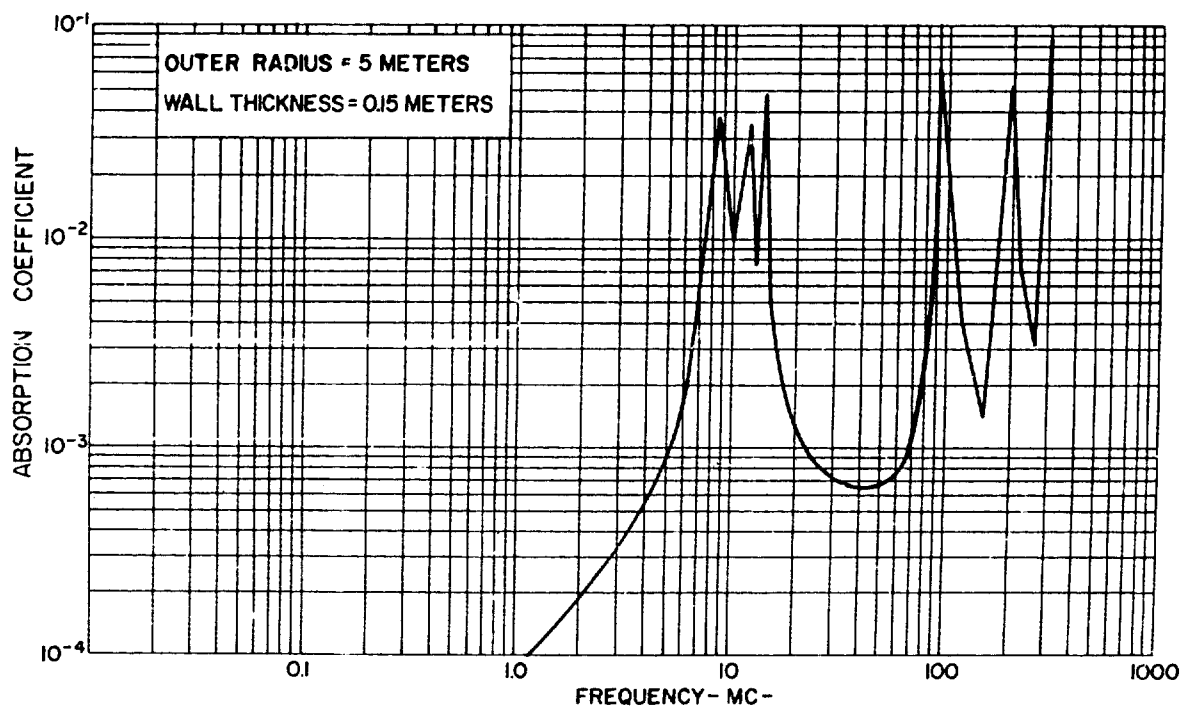


FIG.2 ABSORPTION COEFFICIENT VS FREQUENCY IN MC  
FOR MATERIAL WITH HIGH DIELECTRIC CONSTANT (100,0.1)(1,0)

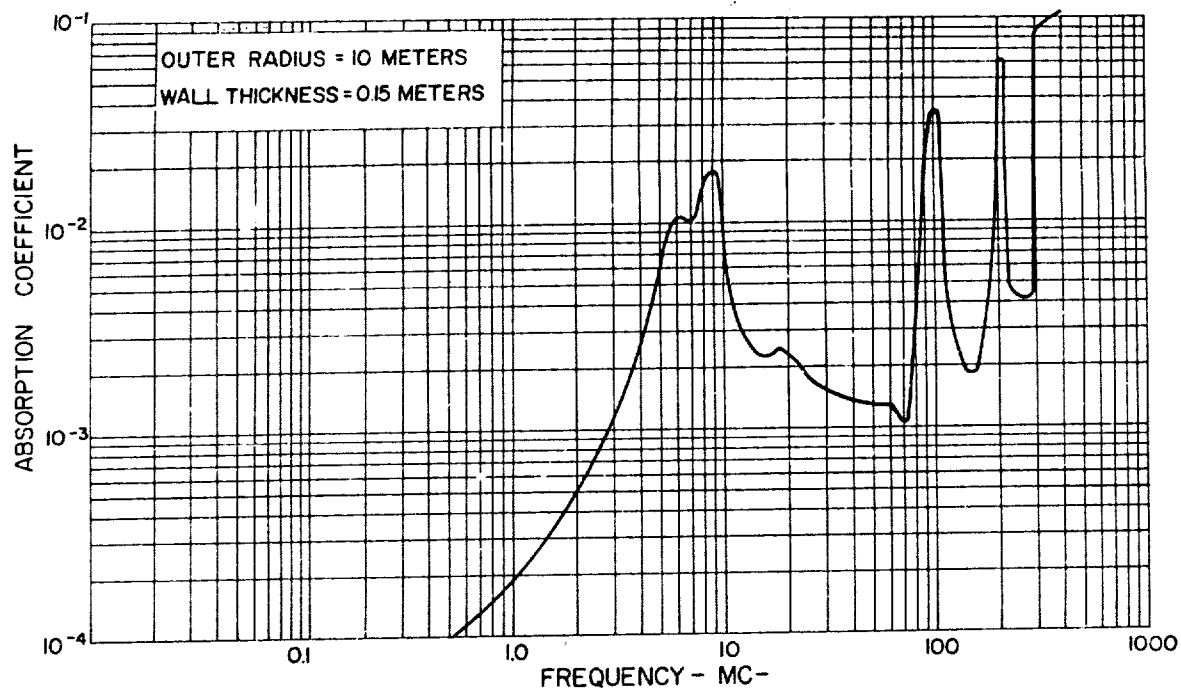


FIG. 3 ABSORPTION COEFFICIENT VS FREQUENCY IN MC  
FOR MATERIAL WITH HIGH DIELECTRIC CONSTANT (100,0.1)(1,0)

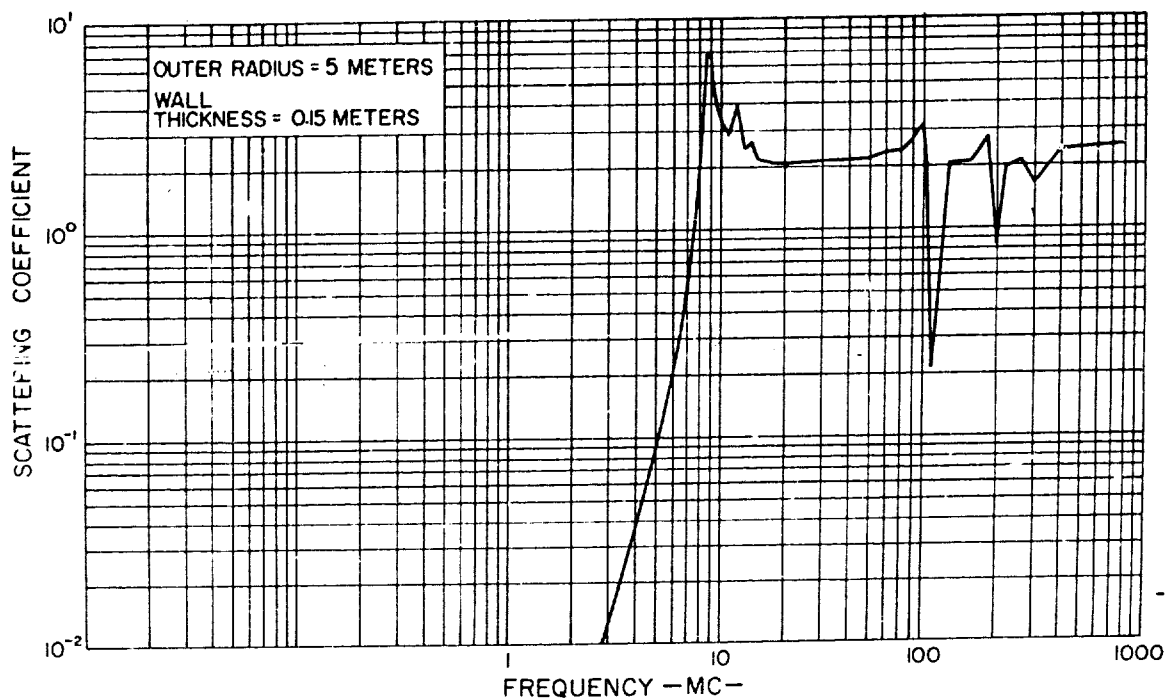


FIG. 4 SCATTERING COEFFICIENT VS FREQUENCY IN MC  
FOR MATERIAL WITH HIGH DIELECTRIC CONSTANT (100,0.1)(1,0)

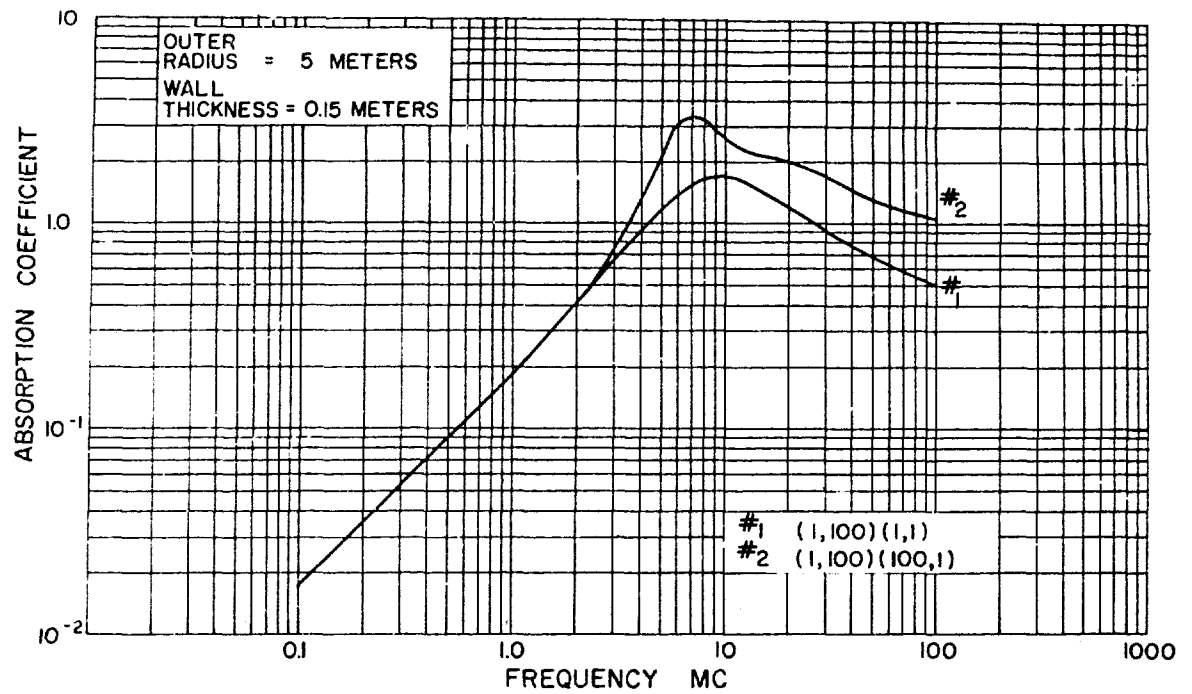


FIG. 5 ABSORPTION COEFFICIENT VS FREQUENCY IN MC FOR VARIATIONS IN PERMEABILITY BETWEEN 1 and 100

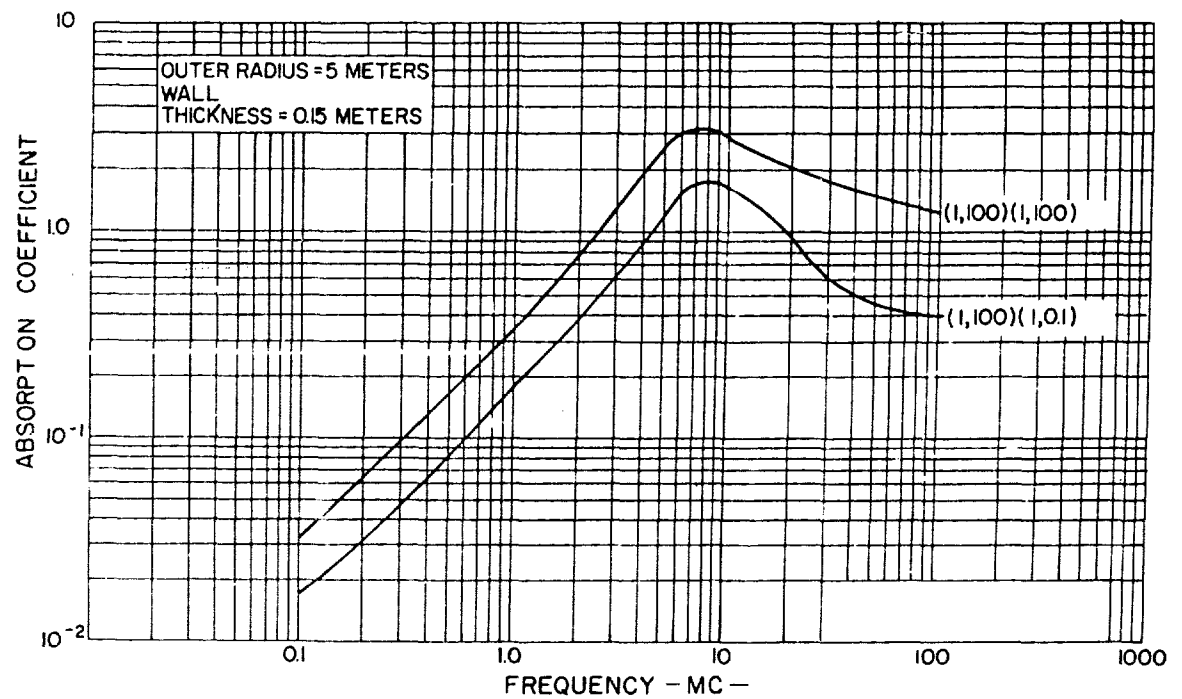


FIG. 6 ABSORPTION COEFFICIENT VS FREQUENCY IN MC FOR VARIATIONS BETWEEN 0.1 AND 100 IN THE MAGNETIC LOSS FACTOR

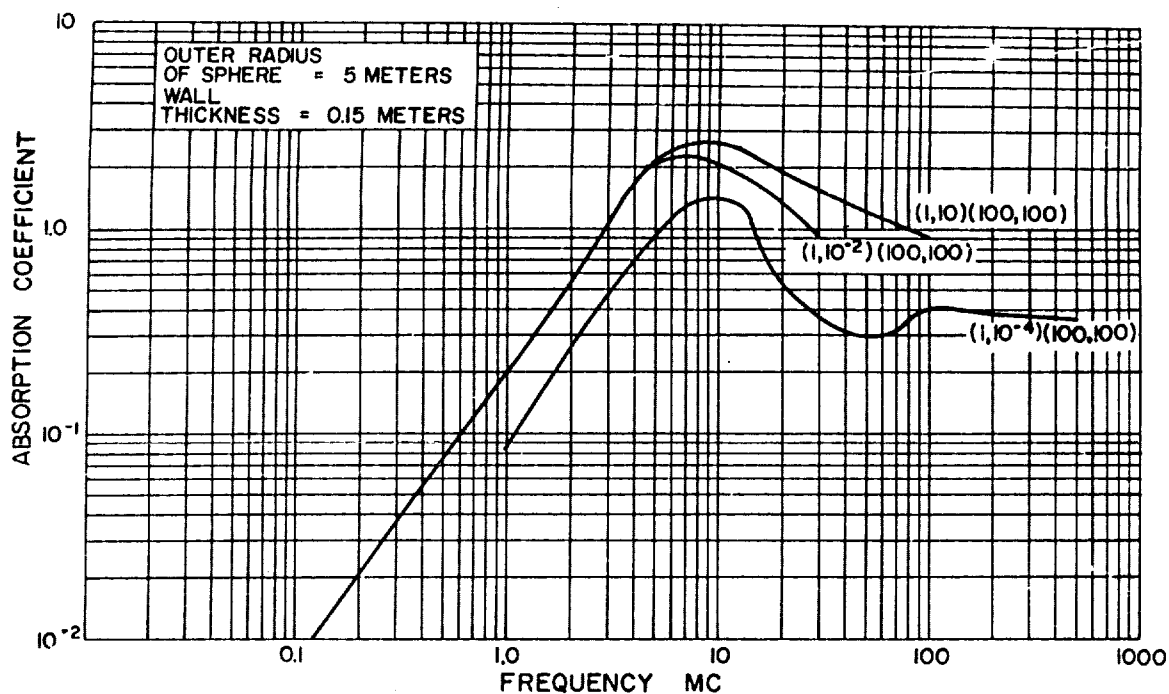


FIG.7 ABSORPTION COEFFICIENT VS FREQUENCY IN MC  
VARIATION OF CONDUCTIVITY FROM  $10^{-1}$  TO  $10^{-4}$  mho/METER  
FOR HIGH PERMEABILITY MATERIAL  $\mu = 100$

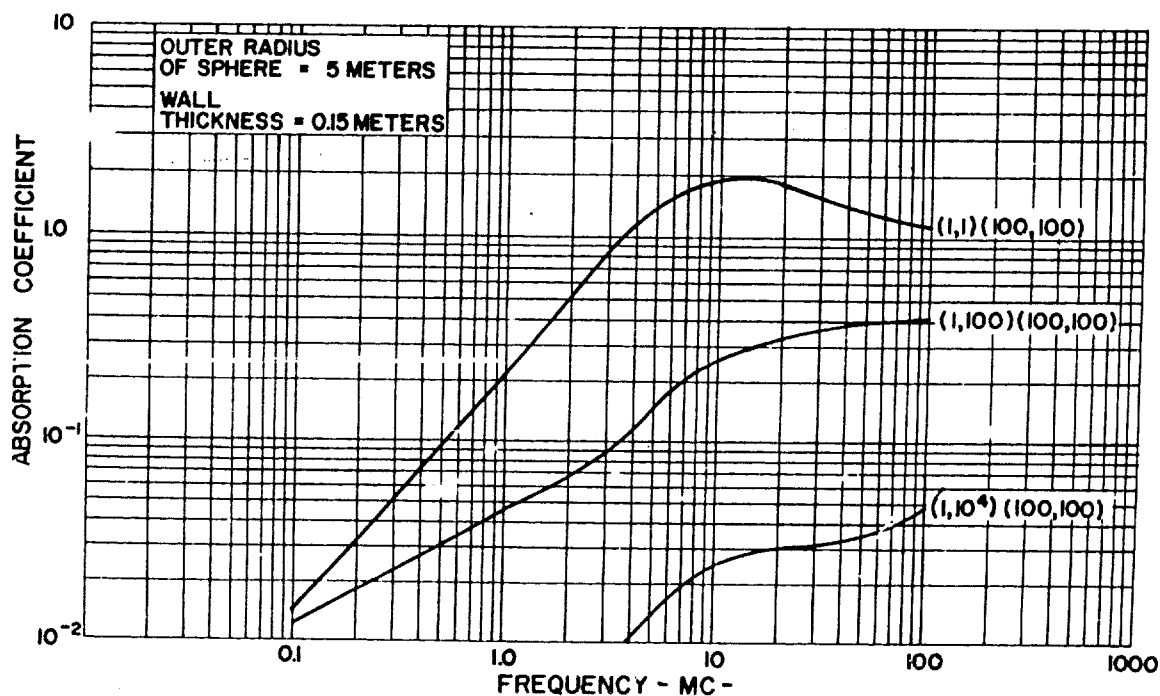
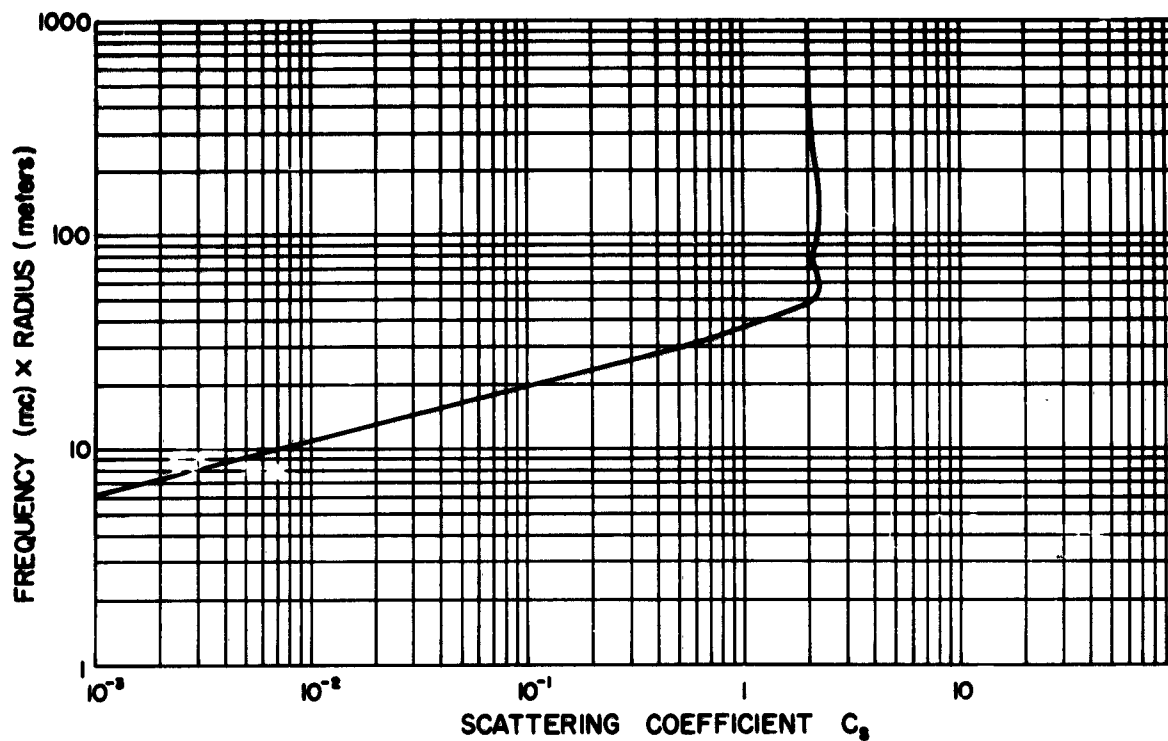
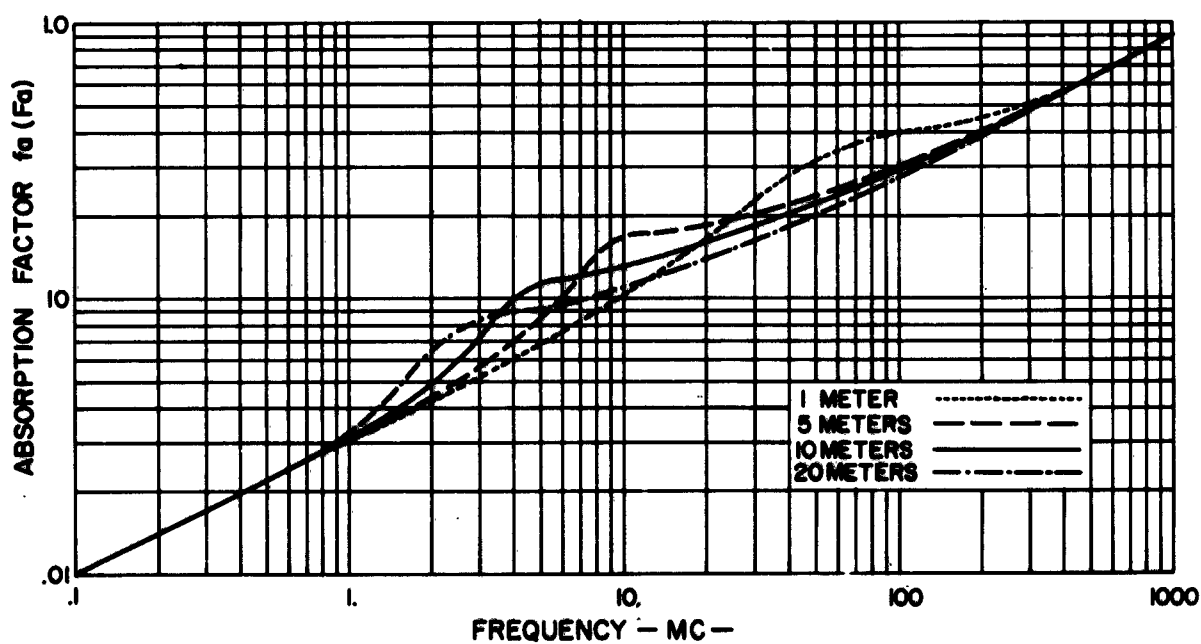


FIG.8 ABSORPTION COEFFICIENT VS FREQUENCY IN MC  
VARIATION OF CONDUCTIVITY FROM  $1$  TO  $10^4$  mho/METER  
FOR HIGH PERMEABILITY MATERIAL  $\mu = 100$



**FIG.9 SCATTERING COEFFICIENT FOR CONDUCTIVE MATERIALS VERSUS MEGACYCLE — METER PRODUCT**



**FIG.10 ABSORPTION FACTOR VS FREQUENCY IN MC FOR CONDUCTIVE MATERIALS**

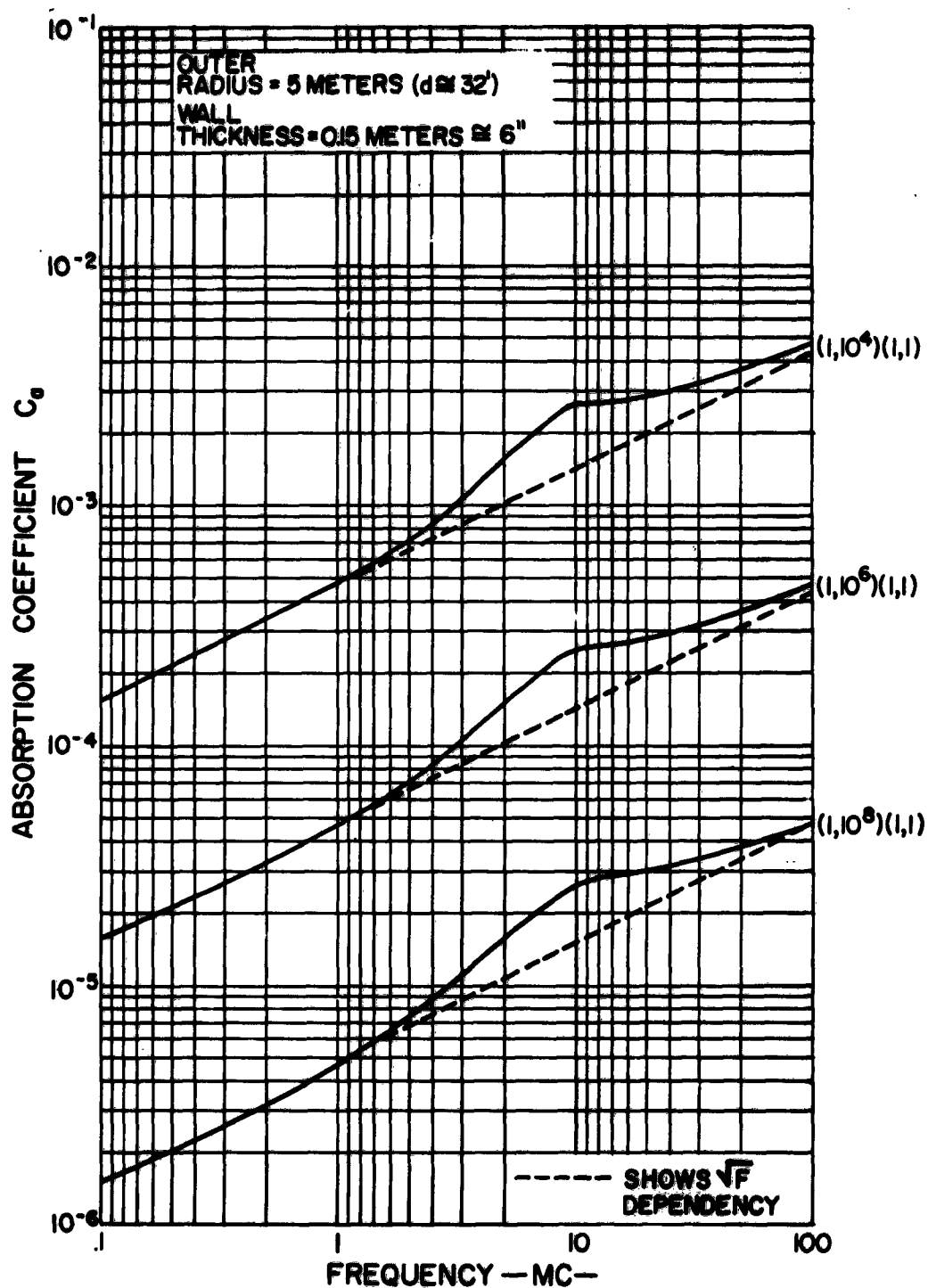


FIG. II ABSORPTION COEFFICIENT VS FREQUENCY  
 FOR MATERIAL CONDUCTIVITY VARIATIONS  
 BETWEEN  $10^4$  and  $10^8$  MHO/METER

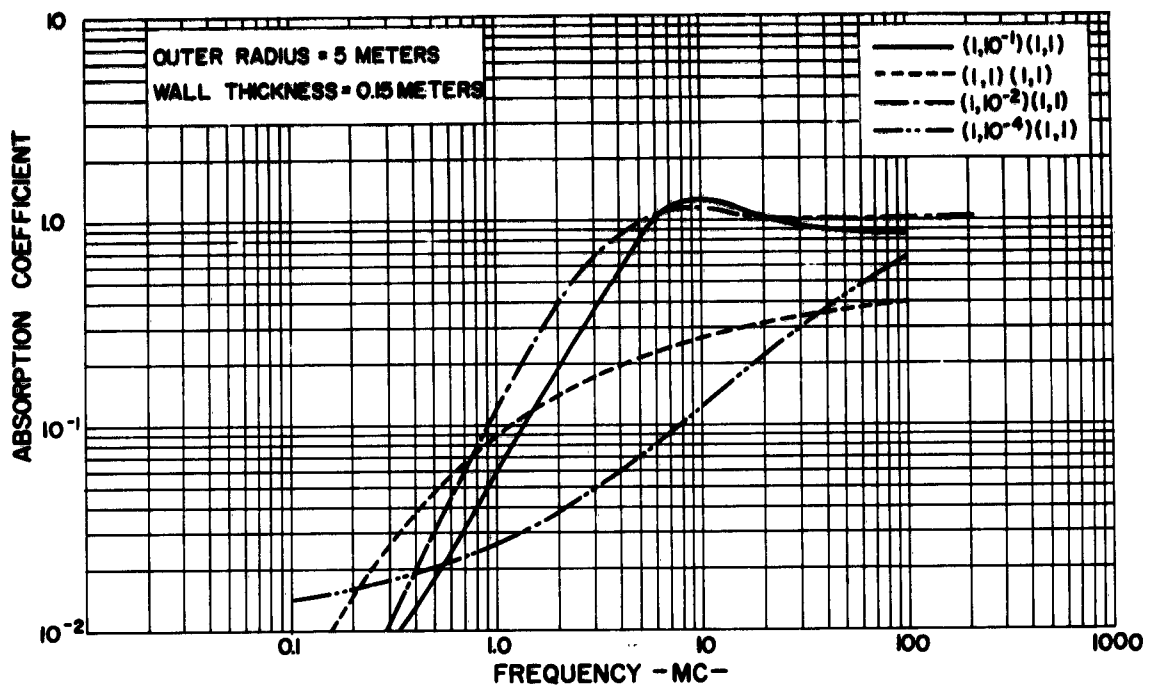


FIG. 12 ABSORPTION COEFFICIENT VS FREQUENCY IN MC  
FOR MATERIAL CONDUCTIVITY VARIATIONS  
BETWEEN 1 and  $10^{-4}$  mho/METER

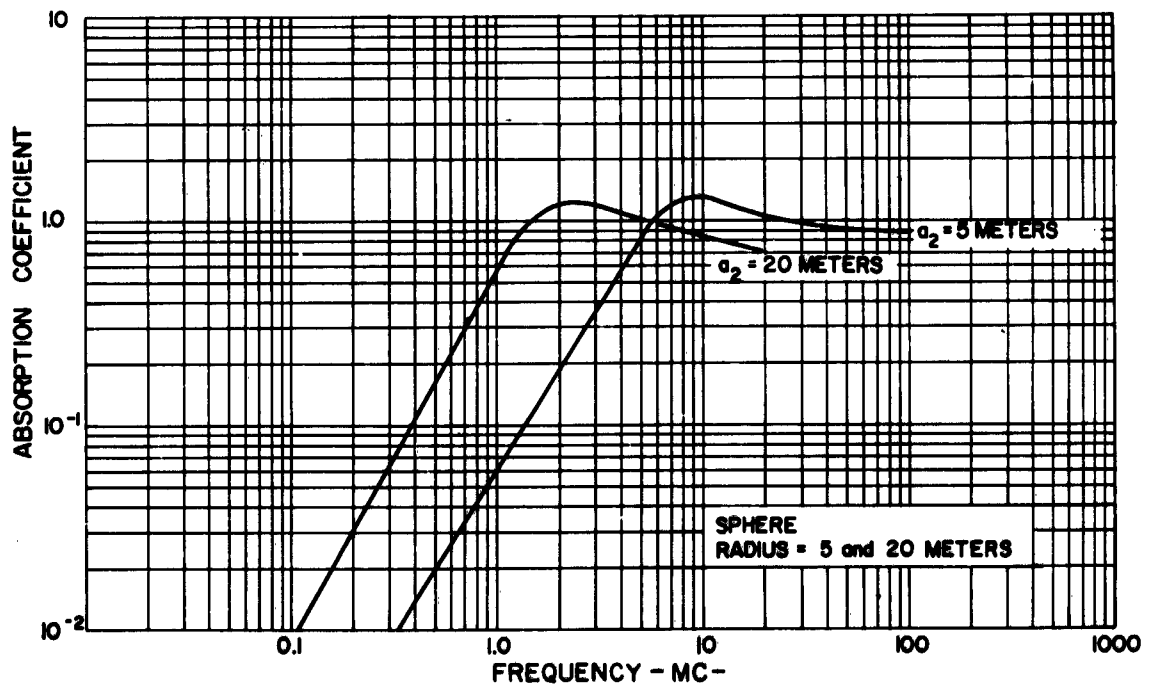


FIG. 13 ABSORPTION COEFFICIENT VS FREQUENCY IN MC  
FOR MATERIAL OF 0.1 mho/METER CONDUCTIVITY

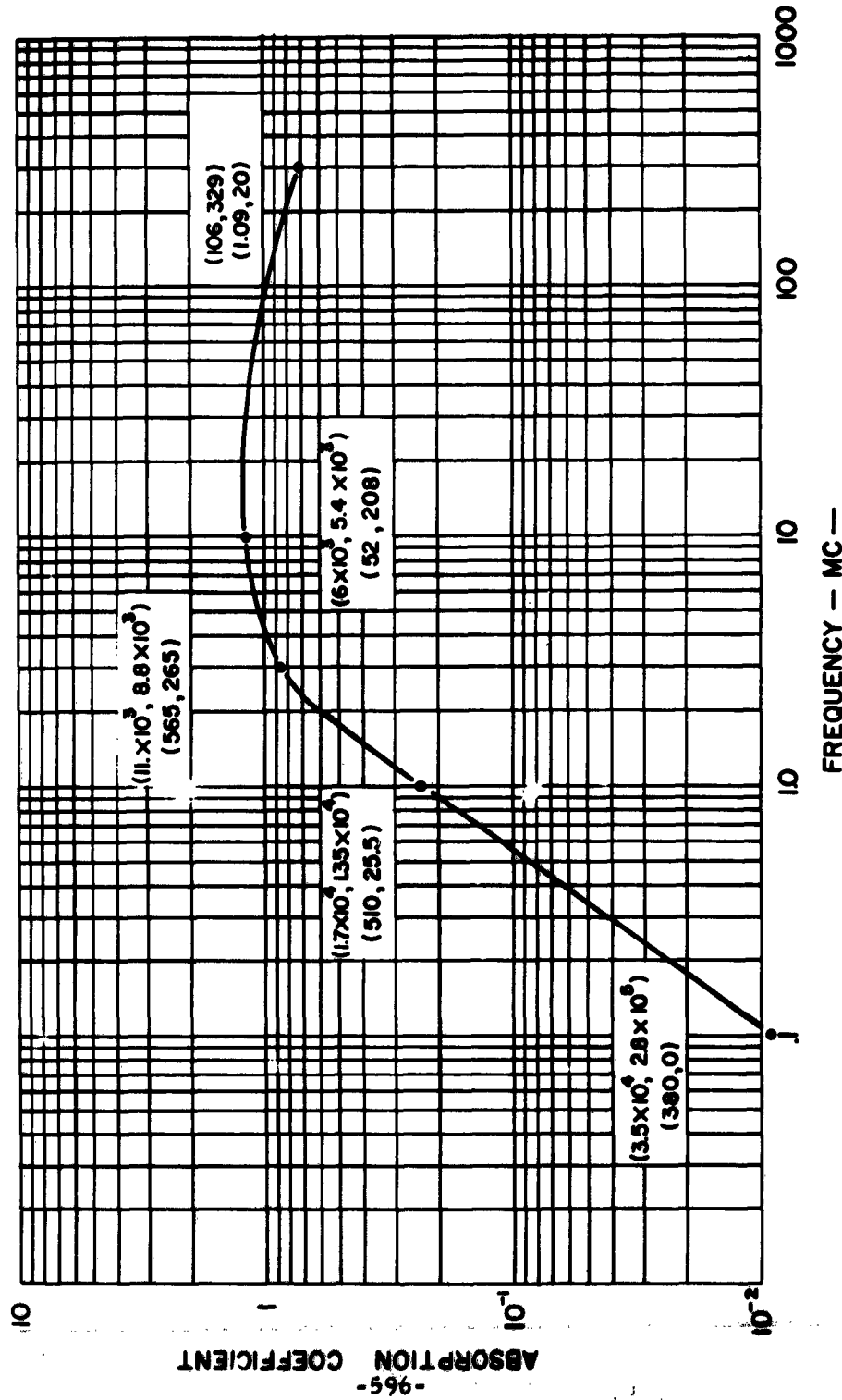


FIG.14 ABSORPTION COEFFICIENT FOR FERRAMIC



## SHIELDING THEORY AND PRACTICE

R. B. Schulz, V. C. Plantz, and D. R. Brush  
The Boeing Company  
Seattle, Washington

**Abstract.** - Plane-wave shielding theory is developed and discussed for a number of important cases such as single, double, and laminated shields. For application to design, the basic expressions are modified and plotted with universal parameters for convenient use in performance calculations of both solid and perforated sheets. Performance of solid copper and iron shields have been calculated and are presented in both tabular and graphical form. For these and other materials, measurement results of various experimenters are tabulated for a number of different material forms and for various incident-wave impedances. Some consideration is given to shielding discontinuities and trends in modern shielding enclosures.

### INTRODUCTION

Shielding prevents coupling of undesired radiated electromagnetic energy into equipment otherwise susceptible to it.

Some of the most difficult shielding problems occur in mobile systems in which many transmitters, receivers, and other sensitive equipment must be mounted closely together, and weight is minimized. Increased electronic requirements of future vehicles for integration of more electronic functions within one compact enclosure accentuate these problems. In aircraft, for example, structural shielding effects can range from 20 to 100 db. This generally is not sufficient to protect receiving antennas from undesired signals generated within the aircraft. Signal-generating equipment must also be shielded to protect other equipment. Transmitter equipment cases must provide a shielding effectiveness of at least 100 db to reduce harmonic and spurious leakage via this path.

Other difficult shielding situations involve equipment of extremely high sensitivity. Among these are radio astronomy, missile guidance, and tracking systems for satellites and space vehicles.

To assist in understanding the mechanism of shielding behavior, Part I of this paper presents the development of plane-wave shielding theory, largely in accordance with the method of Schelkunoff.<sup>1</sup> In order to apply this theory to shielding design, Part II presents this information in the form of modified formula and design curves in the manner of Air Force Manual 100-85.<sup>2</sup> Part II also provides design data for aperture shielding derived from the work of Jarva.<sup>3</sup> Tables of typical calculations have been extracted from the invaluable work of Vasaka<sup>4</sup> and measured values of performance have been obtained from a large variety of sources including the personal experience of the authors.

## PART I - THEORETICAL DERIVATIONS

### 1.0 Basic Plane-Wave Shielding Theory

The manner in which an electromagnetic shield transmits plane electromagnetic waves has been shown to be analogous to the manner in which a conventional two-wire transmission line transmits electrical current and voltage. With reference to Figure 1, corresponding diagrams and transmission equations in MKS units are given. In Figure 1a, the distributed series impedance  $Z$  and shunt admittance  $Y$  per unit length are complex constants; in Figure 1b,  $\mu$ ,  $g$ , and  $\epsilon$  are the electrical constants of initial magnetic permeability, electrical conductivity, and dielectric constant, respectively, all in MKS units.

#### 1.1 Penetration Loss

For the transmission-line characteristic impedance,

$$K = \sqrt{\frac{Z}{Y}} ; \quad (3)$$

the corresponding intrinsic impedance of sheet material is

$$\eta = \sqrt{\frac{j\omega\mu}{g}} = (1 + j) \sqrt{\frac{\pi\mu f}{g}} \quad (4)$$

For air,  $g \rightarrow 0$ , and

$$\eta_0 = \sqrt{\frac{\mu}{\epsilon}} . \quad (5)$$

The transmission-line propagation constant is

$$\Gamma = \sqrt{ZY} ; \quad (6)$$

in the planar sheet the propagation constant is

$$\sigma = \sqrt{j\omega\mu(g + j\omega\epsilon)} . \quad (7)$$

For a metallic sheet,

$$\sigma = \sqrt{j\omega\mu g} = (1 + j) \sqrt{\pi\mu fg} \quad (8)$$

and, in air,

$$\sigma = \sqrt{-\omega^2\mu\epsilon} = j\omega\sqrt{\mu\epsilon} . \quad (9)$$

Since, in general,

$$\sigma = \alpha + j\beta, \quad (10)$$

where

$\alpha$  = attenuation constant

$\beta$  = phase constant

of the medium, it is readily apparent that  $\alpha = 0$  in air and, in metals,

$$\alpha = \beta = \sqrt{\pi \mu f g} . \quad (11)$$

The penetration loss of a wave passing through the shield of thickness  $\ell$  once is

$$A = \alpha \ell \text{ nepers} = 8.686 \alpha \ell \text{ decibels} . \quad (12)$$

## 1.2 Wavelength

If the phase velocity of the wave is represented by  $v$  and the wavelength by  $\lambda$ ,

$$\beta = \frac{\omega}{v} = \frac{2\pi}{\lambda} . \quad (13)$$

In air,  $v = 1/\sqrt{\mu \epsilon} = c$ , the velocity of light, and

$$\lambda = \frac{c}{f} . \quad (14)$$

In metals, the phase velocity

$$v = \sqrt{\frac{\omega}{\mu g}} = c \sqrt{\frac{\omega \epsilon}{g}} \quad (15)$$

is radically slower. For example, characteristic values for copper are

$$\epsilon_0 = 8.854 \times 10^{-12} \doteq \frac{1}{36\pi} \times 10^{-9} \text{ farad/meter} \quad (16)$$

$$g = 5.8005 \times 10^7 \text{ mhos/meter}$$

and

$$v_{\text{Cu}} \doteq c \times 10^{-9} \sqrt{f} . \quad (17)$$

Associated with this small phase velocity is a wavelength drastically shorter than in air.

$$\lambda = \frac{v}{f} = \lambda_0 \sqrt{\frac{\omega \epsilon}{g}} \quad (18)$$

For copper,

$$\lambda_{\text{Cu}} \doteq \lambda_0 \times 10^{-9} \sqrt{f} . \quad (19)$$

### 1.3 Transmission-Line Equations

The input impedance and output current and voltage of a transmission line of length  $\ell$  terminated in an impedance  $Z(\ell)$  are given by the expressions

$$Z = K \frac{Z(\ell) \cosh \Gamma \ell + K \sinh \Gamma \ell}{K \cosh \Gamma \ell + Z(\ell) \sinh \Gamma \ell},$$

$$I(\ell) = \frac{K}{K \cosh \Gamma \ell + Z(\ell) \sinh \Gamma \ell} I(0), \quad (20)$$

$$V(\ell) = \frac{Z(\ell)}{Z(\ell) \cosh \Gamma \ell + K \sinh \Gamma \ell} V(0).$$

Similarly, the impedance normal to, and output fields of, an infinite planar sheet of thickness  $\ell$  are

$$Z = \eta \frac{Z(\ell) \cosh \sigma \ell + \eta \sinh \sigma \ell}{\eta \cosh \sigma \ell + Z(\ell) \sinh \sigma \ell},$$

$$H(\ell) = \frac{\eta}{\eta \cosh \sigma \ell + Z(\ell) \sinh \sigma \ell} H(0), \quad (21)$$

$$E(\ell) = \frac{Z(\ell)}{Z(\ell) \cosh \sigma \ell + \eta \sinh \sigma \ell} E(0),$$

where  $Z(\ell)$  is the impedance looking to the right of the plane  $x = \ell$ .

### 1.4 Reflection Loss

If  $Z(\ell) \neq \eta$ , reflection occurs at the boundary  $x = \ell$ . At this plane, let  $E_t^i$ ,  $H_t^i$  be the incident electric and magnetic fields;  $E^r$ ,  $H^r$  the reflected fields; and  $E^t$ ,  $H^t$  the transmitted fields. Since the fields are continuous across the plane,

$$E^i + E^r = E^t, \quad H^i + H^r = H^t. \quad (22)$$

The reflected wave travels back to the source impedance for a sheet with a matched impedance at the plane  $x = 0$ . Thus

$$E^i = \eta H^i, \quad E^r = -\eta H^r, \quad E^t = Z(\ell) H^t. \quad (23)$$

When equations (23) are substituted in equations (22), the following expressions are obtained for reflection coefficients

$$q_E = \frac{E^r}{E^i} = \frac{Z(\ell) - \eta}{Z(\ell) + \eta} = \frac{k - 1}{k + 1}, \quad k = \frac{Z(\ell)}{\eta} \quad (24)$$

$$q_H = \frac{H^r}{H^i} = \frac{\eta - Z(\ell)}{\eta + Z(\ell)} = \frac{1 - k}{1 + k}, \quad q_E = -q_H$$

and for the corresponding transmission coefficients

$$p_E = \frac{E^t}{E^i} = \frac{2Z(\ell)}{\eta + Z(\ell)} = \frac{2k}{1 + k} = 1 + q_E \quad (25)$$

$$p_H = \frac{H^t}{H^i} = \frac{2\eta}{\eta + Z(\ell)} = \frac{2}{1 + k} = 1 + q_H$$

When two mismatched interfaces must be considered as in a planar sheet, the net transmission coefficient is the product of the transmission coefficients across the two boundaries.

$$p = p_E = p_H = p_E(0) \cdot p_E(\ell) = p_H(0) \cdot p_H(\ell) = \frac{4k}{(1 + k)^2} \quad (26)$$

By definition, the reflection loss is

$$R = -20 \log_{10} |p| = 20 \log_{10} \frac{|1 + k|^2}{4 |k|} \quad (27)$$

When  $k$  is either small or large,

$$R \doteq 20 \log_{10} \frac{1}{4 |k|}, \quad |k| \ll 1; \quad (28)$$

$$R \doteq 20 \log_{10} \frac{|k|}{4}, \quad |k| \gg 1.$$

### 1.5 Shielding Effectiveness

The reflection-loss expression (27) is given on the basis that the reflected wave either travels back to infinity or suffers sufficiently high penetration loss that successive re-reflections may be neglected as in Figure 2a. Figure 2b illustrates the more general case whereby they may not be neglected. For this case, the transmission coefficients across the sheet are

$$T_H = \frac{H(\ell)}{H^i} = \frac{H(\ell)}{H(0)} \frac{H(0)}{H^i}, \quad (29)$$

$$T_E = \frac{E(\ell)}{E^i} = \frac{Z(\ell)}{Z_w} \frac{H(\ell)}{H^i} = \frac{Z(\ell)}{Z_w} T_H$$

where  $E(0)$ ,  $H(0)$  and  $E(\ell)$ ,  $H(\ell)$  are the actual values at interfaces 0 and  $\ell$ , respectively, with reflection taken in account;  $Z_w$  is the impedance of the incident wave. With the use of equations (21) for sheets of thickness 0 and  $\ell$ , the following

ratios are obtained:

$$\begin{aligned}\frac{H(\ell)}{H(0)} &= \frac{\eta}{\eta \cosh \sigma \ell + Z(\ell) \sinh \sigma \ell}, \\ \frac{E(\ell)}{E(0)} &= \frac{Z(\ell)}{Z(\ell) \cosh \sigma \ell + \eta \sinh \sigma \ell}.\end{aligned}\quad (30)$$

From expressions (23),

$$\begin{aligned}\frac{H(0)}{H^i} &= \frac{2Z_w}{Z_w + Z(0)}, \\ \frac{E(0)}{E^i} &= \frac{2Z(0)}{Z_w + Z(0)},\end{aligned}\quad (31)$$

where  $Z(0)$  is the impedance at interface 0 looking into the sheet. By substituting these equations into expressions (29) and performing some algebraic manipulation, the following formula is obtained:

$$T_H = p_H \left(1 - q_H e^{-2\sigma \ell}\right)^{-1} e^{-\sigma \ell}, \quad (32)$$

where

$$p_H = \frac{4 Z_w \eta}{(Z_w + \eta) [Z(\ell) + \eta]}, \quad q_H = \frac{(Z_w - \eta) [Z(\ell) - \eta]}{(Z_w + \eta) [Z(\ell) + \eta]}. \quad (33)$$

When  $Z(\ell) = Z_w$ ,

$$p = \frac{4k}{(k+1)^2}, \quad q = \frac{(k-1)^2}{(k+1)^2}, \quad (34)$$

where  $k$  is the ratio of characteristic impedances,  $Z_w/\eta$ .

Then,  $T_E = T_H$ , or

$$T = p \left(1 - q e^{-2\sigma \ell}\right)^{-1} e^{-\sigma \ell}. \quad (35)$$

By definition, the total shielding effectiveness is

$$\begin{aligned}S &= -20 \log_{10} |T| \\ &= 20 \log_{10} \left| \frac{(1 - q e^{-2\sigma \ell}) e^{\sigma \ell}}{p} \right| \\ &= 20 \log_{10} |e^{\sigma \ell}| - 20 \log_{10} |p| + 20 \log_{10} |1 - q e^{-2\sigma \ell}| \\ &= A + R + B,\end{aligned}\quad (36)$$

where the correction term due to successive re-reflections is defined as

$$B = 20 \log_{10} \left| 1 - \frac{(k-1)^2}{(k+1)^2} e^{-2\sigma \ell} \right|. \quad (37)$$

Expression (36) is the complete formula for shielding effectiveness of a single shield and is the basic starting point for the material presented in Part II, Design Data.

## 1.6 Discussion

The theory of shielding thus far developed may be called the transmission theory of shielding since attention has been focused on waves passing through the shield. A different physical picture of shielding is possible. The fields are produced by electric currents, the original field by currents in a source antenna and a secondary field by currents induced in the shield. The latter group of currents flow in directions such that their fields oppose and tend to cancel the original field on the side of the shield opposite from the source.

The principal weakness in application of this theory from the engineering viewpoint is that it is difficult to compute the induced currents without first solving the shielding problem itself. In order to find the induced currents, the tangential magnetic field strength must be calculated at both surfaces of the shield; but the shielding effectiveness is then determined. On the other hand, this theory presents a physical picture from which it can be readily concluded that a greater impairment in shielding will occur if the shield is cut so as to interfere with the induced current flow than if it is cut along lines of flow. For example, if a plane wave is incident upon a perfectly conducting shield with an infinitely long slit, more power will be transmitted when the E vector is perpendicular to the slit than when it is parallel to it. The two physical pictures of shielding are complementary.

## 2.0 Crossed-Field Shielding Effectiveness

In the previous theoretical development, shielding effectiveness has been derived on the basis of incident-to-transmitted ratios of the E field or of the H field, the resulting expression (36) being the same for either case. (This result must be expected since the impedance of the transmitted wave is identical to the impedance of the incident wave.) The question arises whether a ratio of  $E(\mathcal{L})$  to  $H^i$  or  $H(\mathcal{L})$  to  $E^i$  might be a more sensitive indicator of shielding performance. To determine the answer, let the corresponding transmission coefficients be

$$T_{HE} = \frac{E(\mathcal{L})}{H^i}, \quad T_{EH} = \frac{H(\mathcal{L})}{E^i} \quad (38)$$

As in expressions (29),

$$\begin{aligned} T_{HE} &= \frac{E(\mathcal{L})}{E(0)} \frac{E(0)}{E^i} \frac{E^i}{H^i} = TZ_w \\ T_{EH} &= \frac{H(\mathcal{L})}{H(0)} \frac{H(0)}{H^i} \frac{H^i}{E^i} = T \frac{1}{Z_w} \end{aligned} \quad (39)$$

The measure of shielding effectiveness would then be

$$\begin{aligned} S_{HE} &= -20 \log_{10} |T_{HE}| = -20 \log_{10} |T| - 20 \log_{10} |Z_w|, \\ S_{EH} &= -20 \log_{10} |T_{EH}| = -20 \log_{10} |T| + 20 \log_{10} |Z_w|. \end{aligned} \quad (40)$$

Since the wave impedance  $Z_w$  is not dependent upon shielding properties, any sensitivity of indication resides in the  $T$  term and is identical to the complete expression for shielding effectiveness already derived. There is no theoretical advantage in the crossed-field measurement of shielding performance. From the experimental viewpoint, there may be serious disadvantage since poorer signal-to-noise ratios should be expected in the E-field measurement of a low-impedance wave or the H-field measurement of a high-impedance wave.

### 3.0 Multi-Media Shielding Theory

To develop the theory for any number of multiple sheets or laminations of a single sheet, illustrated by Figure 3, the approach beginning with equations (29) may be extended. Consider first only two sheets separated by air gap, e.g., a double shield. Then the transmission coefficient is

$$T = \frac{E(\mathcal{L}_3)}{E^I} = \frac{E(\mathcal{L}_3)}{E(\mathcal{L}_2)} \frac{E(\mathcal{L}_2)}{E(\mathcal{L}_1)} \frac{E(\mathcal{L}_1)}{E(0)} \frac{E(0)}{E^I}, \quad (41)$$

where the subscripts 1, 2, and 3 refer successively to the first sheet, the air gap, and the second sheet. If note is taken how equations (32) and (33) were formed from equations (29) through (31), it is easy to write a general formula for any number  $n$  of sheets (both metals and air gaps). Let the constants of a typical sheet be  $\eta_m$ ,  $\sigma_m$ ,  $\mathcal{L}_m$ ; let the impedance looking to the right of each section be  $Z(\mathcal{L}_m)$ ; let  $Z_w$  be the characteristic impedance of the incident wave. Then the transmission coefficient for the H-field is

$$T = p \left[ (1 - q_1 e^{-2\sigma_1 \mathcal{L}_1})(1 - q_2 e^{-2\sigma_2 \mathcal{L}_2}) \dots (1 - q_n e^{-2\sigma_n \mathcal{L}_n}) \right]^{-1} \times e^{-\sigma_1 \mathcal{L}_1 - \sigma_2 \mathcal{L}_2 - \dots - \sigma_n \mathcal{L}_n}, \quad (42)$$

where

$$p = \frac{2\eta_0 \cdot 2\eta_1 \cdot 2\eta_2 \cdot \dots \cdot 2\eta_n}{(Z_w + \eta_1)(\eta_1 + \eta_2)(\eta_2 + \eta_3) \dots (\eta_n + Z_w)}, \quad (43)$$

$$q_m = \frac{(\eta_m - \eta_{m-1})[\eta_m - Z(\mathcal{L}_m)]}{(\eta_m + \eta_{m-1})[\eta_m + Z(\mathcal{L}_m)]}$$



#### 4.0 Laminated Shielding

For a laminated sheet of two different materials, as in Figure 4,  $n = 2$ , and

$$T = p \left[ (1 - q_1 e^{-2\sigma_1 \ell_1}) (1 - q_2 e^{-2\sigma_2 \ell_2}) \right]^{-1} e^{-\sigma_1 \ell_1 - \sigma_2 \ell_2}, \quad (44)$$

where

$$\begin{aligned} p &= \frac{8 \eta_0 \eta_1 \eta_2}{(Z_w + \eta_1)(\eta_1 + \eta_2)(\eta_2 + Z_w)}, \quad (45) \\ q_1 &= \frac{(\eta_1 - \eta_0)[\eta_1 - Z(\ell_1)]}{(\eta_1 + \eta_0)[\eta_1 + Z(\ell_1)]}, \quad Z(\ell_1) = \eta_2 \frac{Z_w \cosh \sigma_2 \ell_2 + \eta_2 \sinh \sigma_2 \ell_2}{\eta_2 \cosh \sigma_2 \ell_2 + Z_w \sinh \sigma_2 \ell_2}, \\ q_2 &= \frac{(\eta_2 - \eta_1)(\eta_2 - Z_w)}{(\eta_2 + \eta_1)(\eta_2 + Z_w)}. \end{aligned}$$

The penetration loss of the laminated sheet is simply the sum of those for the two lamina,

$$A = 20 \log_{10} \left| e^{\sigma_1 \ell_1 + \sigma_2 \ell_2} \right| = 8.686 (\alpha_1 \ell_1 + \alpha_2 \ell_2). \quad (46)$$

The corresponding reflection loss is

$$\begin{aligned} R &= -20 \log_{10} |p| = 20 \log_{10} \left[ \frac{1}{8} \left( 1 + \frac{\eta_1}{Z_w} \right) \left( 1 + \frac{\eta_2}{\eta_1} \right) \left( 1 + \frac{Z_w}{\eta_2} \right) \right] \\ &= 20 \log_{10} \frac{1 + \frac{\eta_1}{Z_w}}{2} + 20 \log_{10} \frac{1 + \frac{\eta_2}{\eta_1}}{2} + 20 \log_{10} \frac{1 + \frac{Z_w}{\eta_2}}{2}, \quad (47) \end{aligned}$$

or the sum of the reflection losses at each interface. It should be noted that  $\eta_1$  and  $\eta_2$  both vary as  $\sqrt{f}$ ; hence, reflection loss at the metal-to-metal interface is independent of frequency, whereas it is a function of frequency for metal-air interfaces. This property is particularly important in low-frequency shielding.

The correction term due to successive re-reflections is

$$\begin{aligned} B &= 20 \log_{10} \left| (1 - q_1 e^{-2\sigma_1 \ell_1}) (1 - q_2 e^{-2\sigma_2 \ell_2}) \right| \\ &= 20 \log_{10} \left| 1 - q_1 e^{-2\sigma_1 \ell_1} \right| + 20 \log_{10} \left| 1 - q_2 e^{-2\sigma_2 \ell_2} \right|, \quad (48) \end{aligned}$$

which is not simply the sum of correction factors for the individual lamina since  $q_1$  involves the impedance looking into the second sheet.

## 5.0 Double Shielding

Of considerable importance is the case of two shielding sheets separated by an air space (Figure 5);  $n = 3$ ,  $\eta_2 = Z_w$ ,  $\alpha_2 = 0$  and  $\sigma_2 = j\beta_0 = j2\pi/\lambda_0$ . Then,

$$\begin{aligned}
 p &= \frac{16 Z_w^2 \eta_1 \eta_3}{(Z_w + \eta_1)^2 (Z_w + \eta_3)^2}, \quad (49) \\
 q_1 &= \frac{(\eta_1 - Z_w) [\eta_1 - Z(\ell_1)]}{(\eta_1 - Z_w) [\eta_1 + Z(\ell_1)]}, \quad Z(\ell_1) = Z_w \frac{Z(\ell_2) \cos \beta_0 \ell_2 + j Z_w \sin \beta_0 \ell_2}{Z_w \cos \beta_0 \ell_2 + j Z(\ell_2) \sin \beta_0 \ell_2}, \\
 q_2 &= \frac{(Z_w - \eta_1) [Z_w - Z(\ell_2)]}{(Z_w + \eta_1) [Z_w + Z(\ell_2)]}, \quad Z(\ell_2) = \eta_3 \frac{Z_w \cosh \sigma_3 \ell_3 + \eta_3 \sinh \sigma_3 \ell_3}{\eta_3 \cosh \sigma_3 \ell_3 + Z_w \sinh \sigma_3 \ell_3}, \\
 q_3 &= \frac{(\eta_3 - Z_w)^2}{(\eta_3 + Z_w)^2}.
 \end{aligned}$$

The transmission coefficient for this case is

$$T = p \left[ (1 - q_1 e^{-2\sigma_1 \ell_1}) (1 - q_2 e^{-j2\beta_0 \ell_2}) (1 - q_3 e^{-2\sigma_3 \ell_3}) \right]^{-1} \quad (50)$$

$$\cdot e^{-\sigma_1 \ell_1 - j\beta_0 \ell_2 - \sigma_3 \ell_3}.$$

Components of the shielding expression become

$$\begin{aligned}
 A &= 8.686(\alpha_1 \ell_1 + \alpha_3 \ell_3), \\
 R &= 20 \log_{10} \left| \frac{1 + \frac{\eta_1}{Z_w}}{2} \right| + 20 \log_{10} \left| \frac{1 + \frac{Z_w}{\eta_1}}{2} \right| + 20 \log_{10} \left| \frac{1 + \frac{\eta_3}{Z_w}}{2} \right| \\
 &\quad + 20 \log_{10} \left| \frac{1 + \frac{Z_w}{\eta_3}}{2} \right|, \quad (51) \\
 B &= 20 \log_{10} \left| 1 - q_1 e^{-2\sigma_1 \ell_1} \right| + 20 \log_{10} \left| 1 - q_2 e^{-j2\beta_0 \ell_2} \right| \\
 &\quad + 20 \log_{10} \left| 1 - q_3 e^{-2\sigma_3 \ell_3} \right|.
 \end{aligned}$$

It should be noted that  $\beta \ll |\sigma_1|, |\sigma_3|$ ; hence, the middle term of B may be significant when the other two are negligible.

For the special case where both metallic sheets are of the same material and thickness,  $\sigma_1 \ell_1 = \sigma_3 \ell_3 = \sigma \ell$  and

$$\begin{aligned}
 A &= 2 \times 8.686 \alpha \ell \\
 R &= 2 \times \left[ 20 \log_{10} \left| \frac{1 + \frac{\eta}{Z_w}}{2} \right| + 20 \log_{10} \left| \frac{1 + \frac{Z_w}{\eta}}{2} \right| \right] = 2 \times \left[ 20 \log_{10} \left| \frac{1 + \frac{\eta}{Z_w}}{4 \left| \frac{\eta}{Z_w} \right|} \right|^2 \right] \\
 B &= 20 \log_{10} \left| 1 - q_1 e^{-2\sigma \ell} \right| + 20 \log_{10} \left| 1 - q_2 e^{-j2\beta_0 \ell_2} \right| \\
 &\quad + 20 \log_{10} \left| 1 - q_3 e^{-2\sigma \ell} \right|.
 \end{aligned} \tag{52}$$

The penetration and reflection losses are both double those of a single sheet. However, the correction term differs from double the value of a single sheet in  $q_1$  and by the middle term of B. This term may be rewritten as

$$B_2 = 20 \log_{10} \left| 1 - q_2 \left( \cos 4\pi \frac{\ell_2}{\lambda_0} - j \sin 4\pi \frac{\ell_2}{\lambda_0} \right) \right|. \tag{53}$$

### 5.1 Electrically-Thick Materials

For the common case of metals sufficiently thick that re-reflections within the metal may be neglected due their high penetration loss,  $Z(\ell_2) \doteq \eta$  and

$$q_2 = \frac{(Z_w - \eta)^2}{(Z_w + \eta)^2} = \frac{\left(1 - \frac{\eta}{Z_w}\right)^2}{\left(1 + \frac{\eta}{Z_w}\right)^2}. \tag{54}$$

Normally,  $\eta \ll Z_w$ ,  $R \doteq 2 \left[ -20 \log_{10} 4 \frac{\eta}{Z_w} \right]$ , and

$$q_2 \doteq \frac{1 - 2 \frac{\eta}{Z_w}}{1 + 2 \frac{\eta}{Z_w}} \doteq 1 - 4 \frac{\eta}{Z_w}. \tag{55}$$

The middle term of B becomes

$$B_2 = 20 \log_{10} \left| 1 - \left(1 - 4 \frac{\eta}{Z_w}\right) \left( \cos 4\pi \frac{\ell_2}{\lambda_0} - j \sin 4\pi \frac{\ell_2}{\lambda_0} \right) \right|. \tag{56}$$

For much of the frequency range where  $\frac{\ell_2}{\lambda_0} \ll \frac{1}{8}$ , and

$$B_2 \doteq 20 \log_{10} \left| 4 \frac{\eta}{Z_w} + j 4 \pi \frac{\ell_2}{\lambda_0} \right|. \quad (57)$$

Since  $\left| 4 \eta / Z_w + j 4 \pi \ell_2 / \lambda_0 \right|$  is much less than one,  $B_2$  is negative and the double shield is considerably less effective than the sum of two single shields over a considerable portion of the frequency spectrum.

For example, consider a double copper shield with an air spacing of 1 inch = 2.54 cm and an incident free-space wave with an impedance of 377 ohms at a frequency of 1 mc,

$$\begin{aligned} 4 \frac{\eta}{Z_w} &= 4 \frac{(1+j) 2.61 \times 10^{-7} \sqrt{10^6}}{377} = (1+j) 2.77 \times 10^{-6}, \\ 4 \frac{\ell_2}{\lambda_0} &= 4 \pi \frac{2.54 \times 10^{-2}}{300} = 1.06 \times 10^{-3}, \end{aligned} \quad (58)$$

$$\begin{aligned} B_2 &\doteq 20 \log_{10} \left| 2.77 \times 10^{-6} + j (2.77 \times 10^{-6} + 1.06 \times 10^{-3}) \right| \\ &\doteq 20 \log_{10} \left| 1.06 \times 10^{-3} \right| \doteq -60 \text{ db.} \end{aligned}$$

This result need not always be the case. For instance, at frequencies high enough such that

$$\ell_2 = (2k-1) \frac{\lambda_0}{4}, \quad k = 1, 2, 3, \dots,$$

$$B_2 = 20 \log_{10} \left| 1 + a_2 \right| \doteq 20 \log_{10} 2 = 6 \text{ db.} \quad (59)$$

At shielding resonances, performance of the double shield can be as much as 6 db better than the sum of two separate single shields having the same total metal thickness.

## 5.2 Comparison of Double and Single Shields

Let us compare the double shield with a single shield of the same total metal thickness.  $A$  is the same, but  $R$  is half its former value and the middle term of  $B$  disappears. The difference is thus

$$\Delta = S_{\text{double}} - S_{\text{single}} = 20 \log_{10} \left| \frac{1 + \frac{\eta}{Z_w}}{4 \frac{\eta}{Z_w}} \right|^2 + 20 \log_{10} \left| \frac{1 - a_2 e^{-j2\beta_0 \ell_2}}{1 - a_2} \right| \quad (60)$$

Again for  $\eta/Z_w \ll 1$  and  $\ell_2/\lambda_0 \ll 1/8$ ,

$$\begin{aligned} \Delta &\doteq -20 \log_{10} 4 \left| \frac{\eta}{Z_w} \right| + 20 \log_{10} \left| 4 \frac{\eta}{Z_w} + j 4 \pi \frac{\ell_2}{\lambda_0} \right| \\ &\doteq 20 \log_{10} \left| 1 + j \frac{\pi \frac{\ell_2}{\lambda_0}}{\frac{\eta}{Z_w}} \right|. \end{aligned} \quad (61)$$

It is immediately apparent that, for very low frequencies such that  $\pi \ell_2/\lambda_0 \ll |\eta/Z_w|$ ,  $\Delta = 0$  and the double shield offers no gain in performance over a single shield of the same total metal thickness.

At higher frequencies for which  $\pi \ell_2/\lambda_0 \gg |\eta/Z_w|$ ,

$$\Delta = 20 \log_{10} \frac{\pi \frac{\ell_2}{\lambda_0}}{\left| \frac{\eta}{Z_w} \right|} \quad (62)$$

Since this expression is valid for

$$\frac{1}{\lambda_0} = \frac{f}{3 \times 10^8} \gg \frac{1}{\pi \ell_2} \left| \frac{\eta}{Z_w} \right|, \quad (63)$$

its frequency of validity for a free-space wave incident upon a double copper shield with an air spacing of 1 inch = 2.54 cm is

$$f \gg \frac{3 \times 10^8}{\pi 2.54 \times 10^{-2}} \cdot \frac{3.68 \times 10^{-7} \sqrt{f}}{377} \quad (64)$$

$$f \gg .135 \text{ cps.}$$

Thus, for this particular but common case, expression (62) may be used for frequencies in excess of 2 cps, or throughout practically the entire frequency spectrum. A basic assumption here is that the penetration loss is high enough to avoid re-reflections:  $A \geq 15$  db.

For thinner shields, the lower-frequency limit for validity of expression (62) will be set by

$$A = 8.686 \alpha \ell = 15. \quad (65)$$

For copper,  $\alpha = 15.1 \sqrt{f}$ ; hence,

$$\sqrt{f} = \frac{15}{8.686 \times 15.1 \ell} = \frac{1}{8.69 \ell} \quad (66)$$

With  $\ell = 2.54 \times 10^{-2}$  inch =  $6.34 \times 10^{-4}$  meter, a commonly encountered thickness,

$$f = \frac{1}{(8.69 \times 6.34 \times 10^{-4})^2} = 3.3 \times 10^4 \text{ cps.} \quad (67)$$

or equation (62) is valid for  $f \geq 33 \text{ kc}$ , still most of the RF spectrum.

At  $f = 10^6$ ,

$$\Delta = 20 \log_{10} \frac{4\pi \frac{l_2}{\lambda_0}}{4 \left| \frac{\eta}{Z_w} \right|} = 20 \log_{10} \frac{1.06 \times 10^{-3}}{\sqrt{2} 2.77 \times 10^{-6}} = 49 \text{ db.} \quad (68)$$

A double shield of copper with 1-inch spacing is 49 db superior at 1 mc to a single shield of the same total metal thickness.

## PART II - DESIGN DATA

### 1.0 Relation of Theory to Design Information

It is obvious to any person experienced in shielding that a wide difference exists between shielding theory and practice. Actual shielding performance depends upon many details wherein physical shielding configurations unavoidably differ from the ideal.

Some design data based upon single-shield theory are presently available and are reproduced here as Part II. The purpose of this paragraph is to clarify their relation to Part I. The theoretical development already given is in terms of MKS units whereas the design data here are given in hybrid units of more convenience to a designer. The following tabulations supply multiplying factors to make this transition.

### TRANSITION FROM THEORY TO DESIGN DATA

Symbol	Theory Unit	Multiply Theory Unit by	Design Unit
A	db	1	db
B	db	1	db
R	db	1	db
S	db	1	db
f	cps	1	cps
g	mho/meter	$(5.80 \times 10^7)^{-1}$ ohm meter	dimensionless
$\mu$	henry/meter	$(4\pi \times 10^{-7})^{-1}$ meter/henry	dimensionless
c	farad/meter	$36\pi \times 10^9$ meters/farad	dimensionless
L, r, d	meters	39.37 inches/meter	inches

## 2.0 Calculation of Shielding Effectiveness of Sheet Materials

Shielding behavior for transverse electromagnetic waves can be analyzed using transmission-line equations. The signal source is considered a plane wave front incident upon an infinite planar sheet, a point source encased in a spherical shield, or two parallel current filaments encased in a cylindrical shield. This analysis has been rearranged and the results are condensed here so as to be applicable, with good approximation, to the choice of materials in the design of shielding enclosures.

### 2.1 Terms

Shielding terms are defined as follows:

S = Shielding effectiveness or insertion loss, representing the reduction (expressed in db) of the level of an electromagnetic wave at a point in space after a metallic barrier is inserted between that point and the source. Measurements are made in real powers, reactive powers, voltages, or currents.

$$S = A + R + B, \quad (69)$$

where:

A = Penetration or absorption loss in db inside the barrier,

R = Total reflection loss in db from both surfaces of the shield, neglecting the effect of multiple reflections inside the barrier,

B = A positive or negative correction term which need not be taken into account when A is more than 15 db. It is caused by the reflecting waves inside the shielding barrier, and is calculated in db. When a metallic barrier has an A of less than 15 db, it is designated as "electrically thin."

### 2.2 Shielding Expressions

All terms in the previous shielding-effectiveness equation (69) may be expressed as functions of the material conductivity,  $g$ , and permeability,  $\mu$ , relative to copper, and the frequency,  $f$ , in cps, as well as the physical relationships that exist.

Reflection Loss-The reflection loss,  $R$ , depends upon the electrical nature of the source and upon the distance,  $r$ , in inches of the shield from the source as shown in Figure 6. Equations (70), (71), and (72) are utilized in finding the reflection loss. They are stated in Figure 6.

**Penetration Loss** - The penetration loss, A, depends not only upon  $\mu$ , f, and g, but also upon the thickness, d, in inches of the shielding material.

$$A(\text{db}) = 3.34 \sqrt{\mu f g d} \quad (73)$$

**Correction Term for Internal Reflections** - If A is equal to 15 or more, the correction term, B, may be neglected; however, if A is less than 15, the correction for multiple reflections within the shielding material must be made. This correction term B is complicated, since it depends on all material, dimensional, and frequency parameters. In the general case,

$$B(\text{db}) = 20 \log_{10} \left[ 1 - X 10^{-\frac{A}{10}} (\cos 0.230 A - j \sin 0.230 A) \right], \quad (74)$$

where the factor, X, is a real and imaginary function of  $\mu$ , f, g, and r. Expressions for X are given in Figure 7. In almost all practical cases,  $X = 1$ ; the only notable exception is the special case of extremely low-frequency shielding against low-impedance (chiefly magnetic) fields. Values of X for this case are given in Figure 12.

### 2.3 Universal Curves of Shielding Performance

Universal curves for R and A are given in Figures 8 through 11. Furthermore, the sum of A + B may also be obtained from Figure 11 for the common case of  $X = 1$  ( $m < .01$  or  $> 100$ ). If X is not equal to one, it may be determined from Figure 12 and B must then be calculated from equation (74).

### 2.4 Calculated Data

Material properties such as those given in Figure 13 may be used to calculate the shielding effectiveness of various materials. Effectiveness of copper and iron from 60 cps to 10 Gc is given in Figures 14 through 18 and graphically presented in Figure 18. The effective wavelengths of various frequencies of electromagnetic energy in copper and iron are given in Figure 19.

For distances between signal source and shielding material other than those shown in the above data, corrections must be made using the established formulas previously given. If the distance is much less than 12 inches, the reflection loss to magnetic fields will be smaller and the reflection loss to electric fields greater.

In practically all cases, the total shielding effectiveness is greater than absorption, or penetration loss alone. Despite this fact, many designers ignore reflection losses, and thus design a shielded enclosure much thicker than necessary. The available reflection loss should be included in the calculations to prevent over-designing the enclosure. In mobile applications, this consideration can result in important weight savings.



At frequencies as low as 60 cps, both penetration loss and reflection loss become small for magnetic fields, indicating that, for lower frequencies approximating dc, very thick metallic barriers would be necessary to shield against magnetic fields. For example, the tables indicate that, to obtain a shielding effectiveness of 100 db at 60 cps for magnetic fields, it will be necessary to provide an iron barrier with a permeability of 1000 and a thickness of about 300 mils.

### 3.0 Shielding Calculations for Perforated Sheets, Screening, and Waveguide Arrays

The basic procedure modifies that presented in Section 2.0. Penetration loss reflections, open area, skin-depth effects, and coupling between closely spaced openings must be accounted for. Where the subscript a refers to the aperture, the shielding effectiveness,  $S_a$ , becomes

$$S_a = A_a + R_a + B_a + K_1 + K_2 + K_3 \quad (78)$$

and the terms are given in Figure 20. For ease of use, the various terms are plotted in Figure 21.

### 4.0 Measured Performance of Shielding Materials

Actual measurements of shielding effectiveness against low-impedance, plane, and high-impedance waves have been obtained by various experimenters and are tabulated in Figures 22 through 24.

### 5.0 Shield Discontinuities

A shielded equipment case cannot be constructed with one continuous metallic sheet. Some discontinuities are necessary to accommodate input and output lines, power lines, antennas, front-panel seams, control shafts, ventilating holes, etc., as shown in Figure 25. The design and construction of these discontinuities become very critical when it is necessary to incorporate them without appreciably reducing the shielding effectiveness of the overall shielded enclosure. Some design and construction considerations are given below.

#### 5.1 Seams - No Gasket

Clean metal-to-metal mating surfaces, together with good pressure contact obtained by use of set screws or rivets, are necessary to prevent electromagnetic leakage. Corrosion or anodizing cannot be tolerated.

#### 5.2 Seams - Metallic Gasket

Shielding can be considerably improved by using various types of metallic gaskets, which are flexible, resilient, conductive materials placed between shielding surfaces to be jointed. They are frequently made of knitted wire-mesh. Clean metal-to-metal mating surfaces and a good pressure contact are required. Experi-

mental evidence indicates that an optimum pressure on various conducting gasket materials is approximately 20 psi. A typical variation of shielding insertion-loss with pressure is shown in Figure 26. Instead of knitted wire mesh, another type RF gasket is sometimes employed. Essentially, it is a 10-mil strip of beryllium copper, perforated to have jagged points on both surfaces. It can be imbedded in rubber and requires very little pressure to give a good metal-to-metal contact of low RF impedance. It does not require clean metal-to-metal mating surfaces. A commercial variation utilizes wire stubs oriented perpendicular to the mating surfaces.

### 5.3 Holes and Screening

Any holes in the equipment used for ventilation or for any other purpose will materially decrease the shielding effectiveness of the case. The larger the diameter of the hole and the higher the applied frequency, the greater will be the leakage. Holes must be kept as small as possible - not larger than those in 22-mesh, 15-mil copper screening, if more than a nominal 50-db shielding effectiveness is required up to 1000 mc.

### 5.4 Waveguides

Waveguides are hollow conducting tubes capable of propagating electromagnetic energy with little attenuation above some cutoff frequency and severely attenuating such energy below the cutoff frequency. The latter property is often used in the construction of shielded enclosures to permit airflow without negating electromagnetic-shielding effectiveness. Constructions which appear somewhat like automobile radiator cores are frequently used as a parallel assembly of waveguides permitting adequate airflow at a high cutoff frequency. For 100-db of attenuation, the length of the waveguide must be at least three times the diameter of the hole. The maximum permissible diameter ( $d_{\max}$ ) can be obtained by dividing the wavelength ( $\lambda_{\min}$ ) for the highest frequency under consideration by 3.4, where both diameter and wavelength are expressed in the same units.

$$d_{\max} = \frac{\lambda_{\min}}{3.4} \quad (\text{single waveguide only}) \quad (79)$$

### 5.5 Control Shaft-Grounded

Metallic control shafts protruding through the equipment case must be grounded to the case by use of a gasket or serrated metallic fingers.

### 5.6 Control Shaft - Not Grounded

A control shaft made of insulating material can protrude through the case by insertion inside a waveguide attenuator.

### 5.7 Fuse Receptacle

The fuse receptacle requires a large hole, and should be provided with a metallic cap.

#### **5.8 Phone and Meter Jacks**

These jacks should be provided with metallic caps.

#### **5.9 Panel Meter**

The panel meter requires a large hole in the case, modified as shown in Figure 25 to provide a continuous shield. All meter leads should be filtered.

#### **5.10 Pilot Lamp**

The pilot lamp should be properly filtered or covered with screening material or perforated metal.

#### **5.11 Filtered Lines**

All unshielded lines should be properly filtered with pi-section filters, shielded transformers, or feed-through capacitors. The degree of attenuation required of the filter depends on the level of undesired signals present in the lines themselves. Additional filter considerations are properly the subject of another paper.

#### **5.12 Unfiltered Lines**

Open wiring is normally a point of excessive leakage when not filtered. Such lines can be tolerated only if they do not carry high levels of undesired signals, or if they do not provide an easy RF entry into the equipment. It may be necessary to provide shielded conduit or shielded transmission lines with an outer wall having a shielding effectiveness as high as that of the shielding enclosure itself. At connectors, the braid shielding of all conductors should be carried well into the connector wall and grounded to it.

#### **5.13 Antenna Lead-Ins**

Unshielded antenna lead-ins are undesirable and are not permitted under the design requirements of Specifications MIL-I-26600 and MIL-I-6181D. Shielded antenna lead-ins are satisfactory, provided the shielding effectiveness of the transmission line is as effective as that of the shielded case itself.

### **6.0 Multiple Shields**

Multiple shielding layers provide a greater shielding effectiveness than a single shield. Because of successive reflections in the interspace between two shields, the total decibel value of shielding effectiveness is less than the sum for the separate shields. In the highly effective portion of the frequency spectrum, practical experience indicates two 70-db shields result in approximately 120-db shielding effectiveness.

Doubly-shielded enclosures are commonly manufactured in two basic configurations. One, termed an isolated double shield, has complete insulation between the two shields except for one common point of electrical connection, usually grounded externally. The purpose of this construction is to prevent circulating conductive currents from coupling energy from one shield to the other. In practice, this purpose is often violated because of the practical necessity for entering the enclosure at other points with water pipes, conduit for telephone lines, etc.

Another configuration is the cell-type enclosure in which panel sections of the enclosure surface form completely shielded cells. In this construction, inner and outer shields are effectively connected at many points and the addition of extra connections for utilities has little effect.

Performance-wise, there is little difference between the configurations per se. The reliability of joint construction, door construction, and air inlets (if any), as well as filter performance are far more important.

#### 7.0 Trends in Modern Shielding Enclosures

Significant trends in shielding enclosures include extension of the frequency range at both ends, reduction of internal standing waves, and a combination with acoustically anechoic properties.

The RF frequency range is being extended at the low end by increased use of high-permeability materials in substantial thicknesses, at the high end by eliminating troublesome trihedral and dihedral joints through the use of preformed corners, and by using lossy filters with improved high-frequency performance.

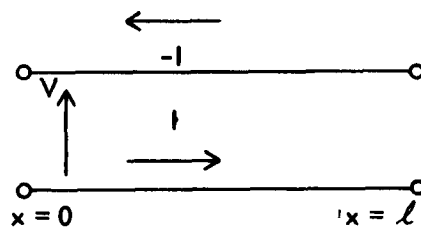
Internal standing waves are reduced by use of electromagnetically lossy material in a manner similar to acoustical material for anechoic chambers.

#### ACKNOWLEDGEMENT

A portion of this material was assembled under Contract DA 36-039 AMC-02308 (E) for the U. S. Army Electronics Research and Development Laboratory, Fort Monmouth, N. J.

#### REFERENCES

1. S. A. Schelkunoff, "Electromagnetic Waves," D. Van Nostrand Company, 1943.
2. Air Force Manual 100-85, "Mutual Electromagnetic Interference," September 1960.
3. W. Jarva, "Shielding Efficiency Calculation Methods for Screening, Waveguide Ventilation Panels, and Other Perforated Electromagnetic Shields," Proceedings of the Seventh Conference on Radio Interference Reduction and Electronic Compatibility, Armour Research Foundation, November 1961.
4. C. S. Vasaka, "Theory, Design and Engineering Evaluation of Radio-Frequency Shielded Rooms," Report No. NADC-EL-54129 of USNADC, 13 August 1956.

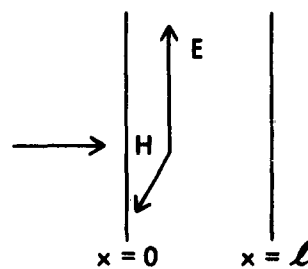


Along the line:

$$\frac{dV}{dx} = -ZI \quad (1)$$

$$\frac{dI}{dx} = -YV$$

a. Conventional Transmission Line



Within the sheet:

$$\frac{dE}{dx} = -j\omega\mu H \quad (2)$$

$$\frac{dH}{dx} = -(g + j\omega\epsilon) E$$

b. Plane Wave Normally Incident Upon an Infinite Planar Sheet

Figure 1 Plane Wave Analogy

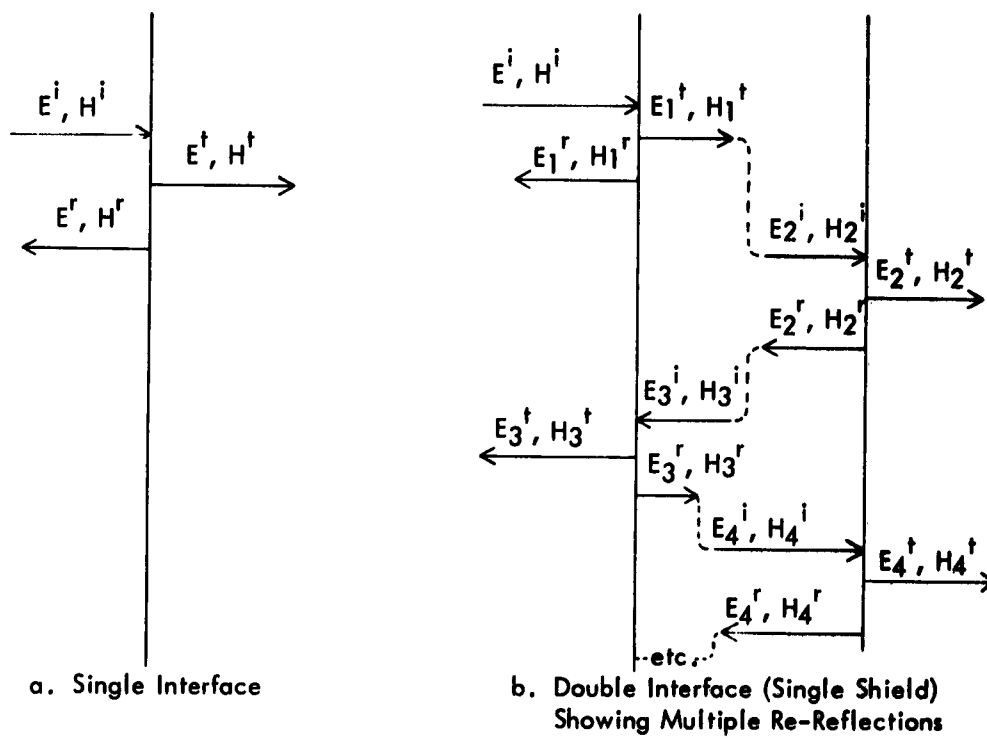


**Figure 2 Reflection of Waves at Interfaces**

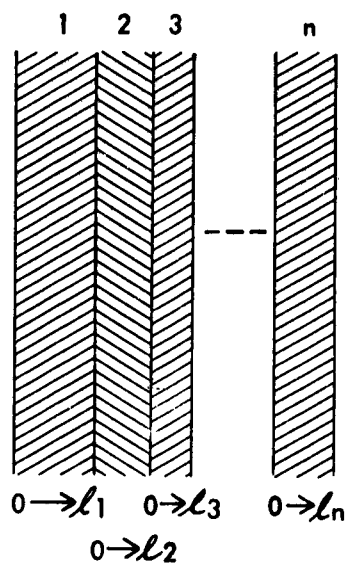


Figure 3 Multi-Lamina Shielding

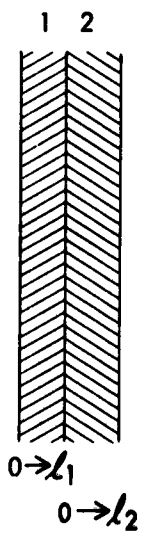


Figure 4 Laminated Shield

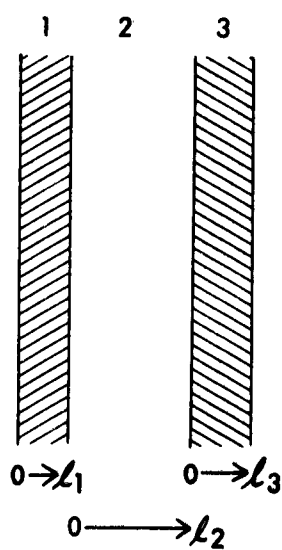


Figure 5 Double Shield

NATURE OF SOURCE	REFLECTION LOSS, R	CONDITION
LOW IMPEDANCE (SUCH AS LOOP AT DISTANCE $\ll \lambda/2\pi$ )	$20 \log_{10} \left[ \frac{0.462}{\sqrt{\frac{f_0}{\mu}}} + 0.136 \sqrt{\frac{f_0}{\mu}} + 0.354 \right]$ (70)	$f_p \ll 2 \times 10^9$
HIGH IMPEDANCE (SUCH AS ROD AT DISTANCE $\ll \lambda/2\pi$ )	$354 - 20 \log_{10} \left( \sqrt{\frac{\mu^3}{g}} + \frac{1}{g} \right)$ (71)	$f_p \ll 2 \times 10^9$
PLANE WAVE (SUCH AS ROD OR LOOP AT DISTANCE $\gg \lambda/2\pi$ )	$168 - 20 \log_{10} \left( \sqrt{\frac{\mu}{g}} \right)$ (72)	$f_p > 2 \times 10^9$

**Figure 6 Expressions for Reflection Loss**



NATURE OF SOURCE	CORRECTION FACTOR, $\chi$
LOW IMPEDANCE	$4 \frac{(1-m^2)^2 - 2m^2 - 12\sqrt{2}m(1-m^2)}{[1+(1+\sqrt{2}m)^2]^2}, \text{ WHERE } m = 0.766 \sqrt{\frac{\mu}{\epsilon}} \quad (75)$ <p> <math>= 1</math> FOR <math>m \ll 1</math>,  <math>= 1</math> FOR <math>m \gg 1</math>. </p> <p>IN PRACTICAL APPLICATION, <math>m \gg 1</math> AND <math>\chi = 1</math>, EXCEPT FOR VERY LOW FREQUENCIES. FOR <math>m</math> BETWEEN 0.05 AND 20, CONSULT FIGURE 12.</p>
HIGH IMPEDANCE	$4 \frac{(1-a^2)^2 - 2a^2 - j 2 \sqrt{2}n(1-a^2)}{[1+(1-\sqrt{2}n)^2]^2}, \text{ WHERE } n = 0.520 \times 10^{-18} \sqrt{\frac{\mu^3}{\epsilon}} \quad (76)$ <p> <math>= 1</math> FOR <math>n \ll 1</math>. </p> <p>FOR ALL PRESENTLY KNOWN SHIELDING MATERIALS USED THROUGHOUT THE RADIO SPECTRUM, <math>n \ll 1</math> AND <math>\chi = 1</math>.</p>
PLANE WAVE	1

Figure 7 Correction Factor in Correction Term for Reflections

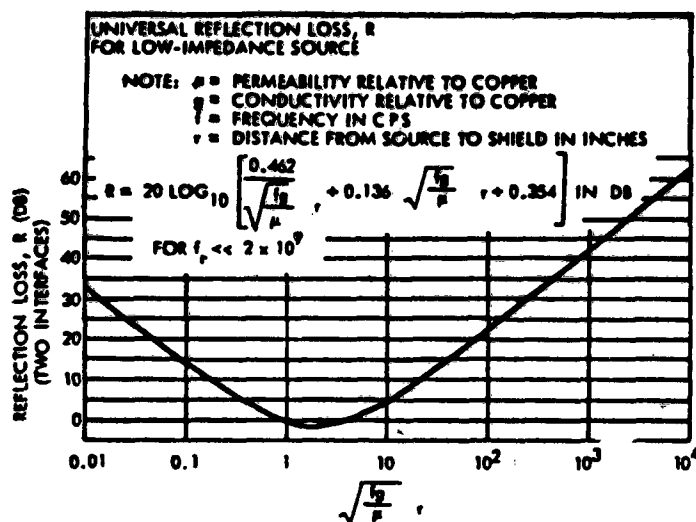


Figure 8 Universal Reflection Loss for Low-Impedance Source

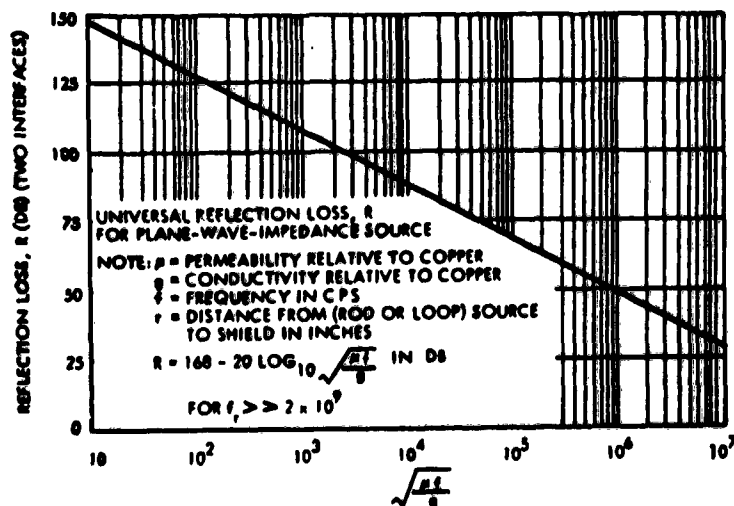


Figure 9 Universal Reflection Loss for Plane-Wave Impedance Source

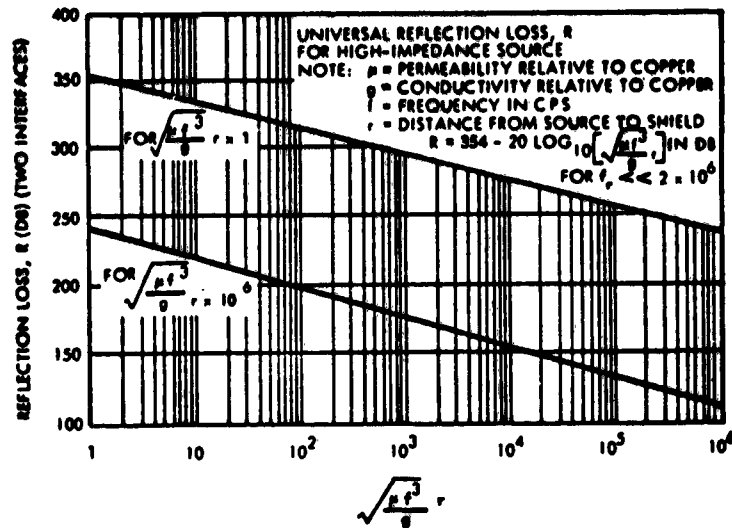


Figure 10 Universal Reflection Loss for High-Impedance Source

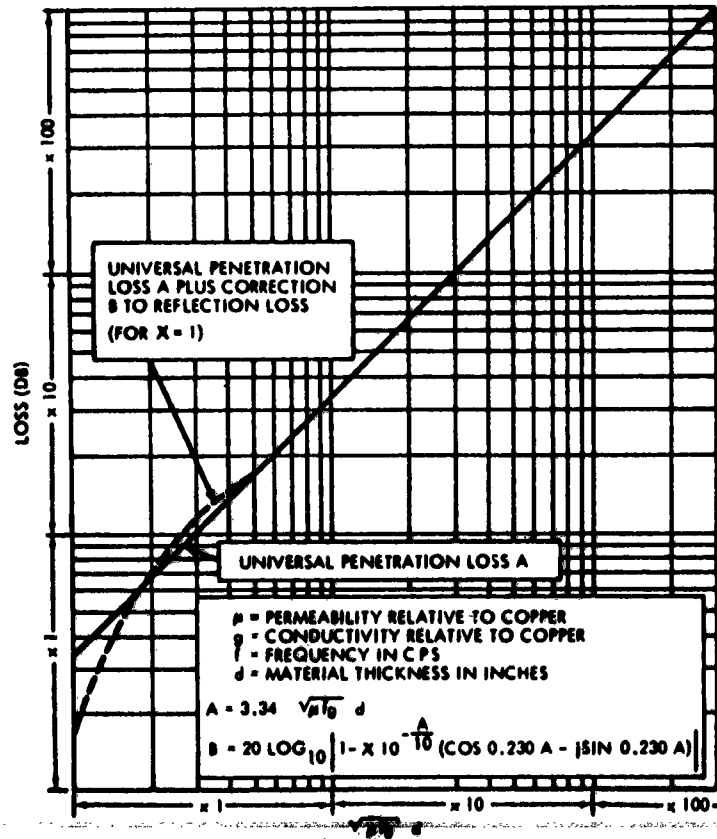


Figure 11 Universal Penetration-Loss Curve

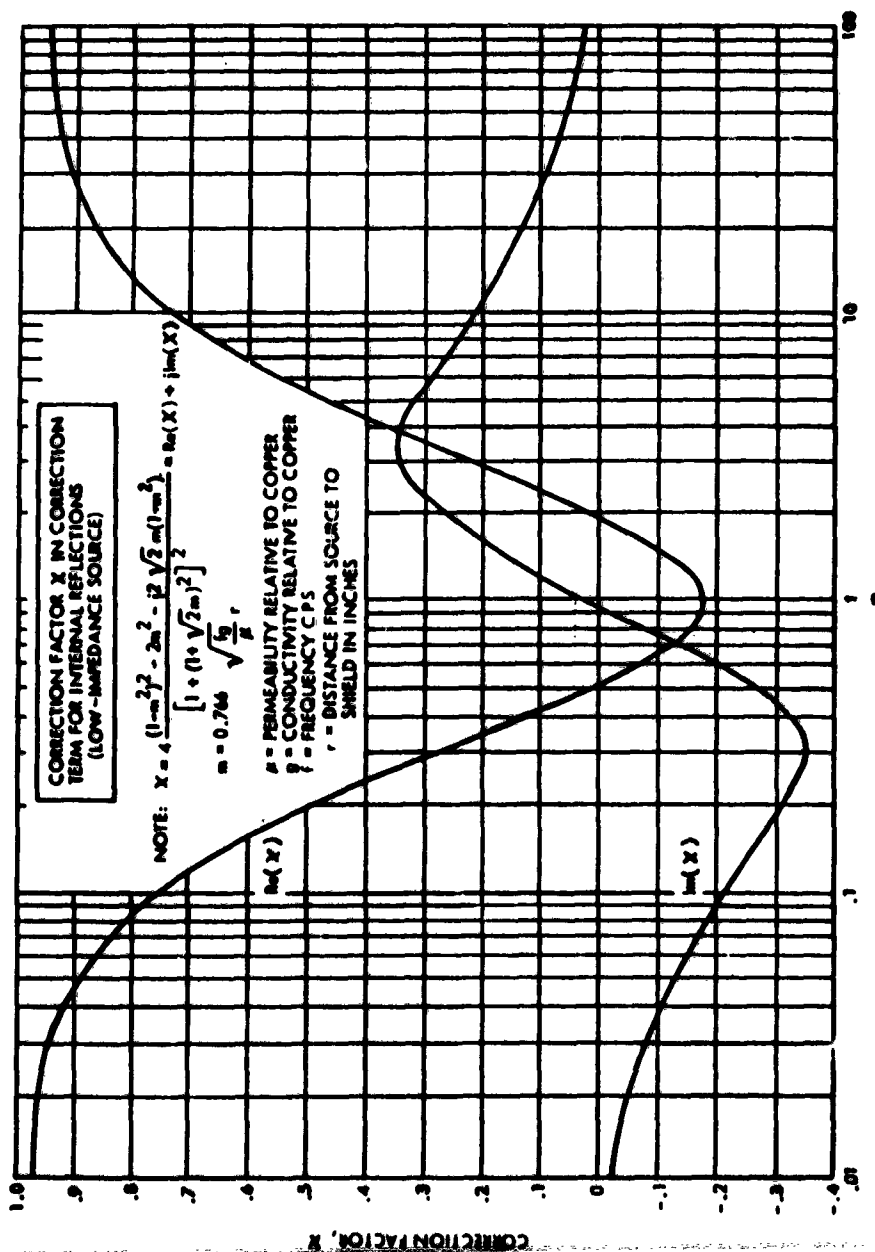


Figure 12 Correction Factor in Correction Term for Internal Reflections

METAL	RELATIVE CONDUCTIVITY	RELATIVE PERMEABILITY	PENETRATION LOSS/MIL AT 150 kc (db)
SILVER	1.05	1	1.32
COPPER, ANNEALED	1.00	1	1.29
COPPER, HARD- DRAWN	0.97	1	1.26
GOLD	0.70	1	1.08
ALUMINUM	0.61	1	1.01
MAGNESIUM	0.38	1	0.79
ZINC	0.29	1	0.70
BRASS	0.26	1	0.66
CADMIUM	0.23	1	0.62
NICKEL	0.20	1	0.58
PHOSPHOR- BRONZE	0.18	1	0.55
IRON	0.17	1000	16.9
TIN	0.15	1	0.50
STEEL, SAE 1045	0.10	1000	12.9
BERYLLIUM	0.10	1	0.41
LEAD	0.08	1	0.36
HYPERNICK	0.06	80,000	88.5
MONEL	0.04	1	0.26
MU-METAL	0.03	80,000	63.2
PERMALLOY	0.03	80,000	63.2
STEEL, STAINLESS	0.02	1000	5.7
NOTE: USE EQUATION (73) FOR PENETRATION LOSS AT OTHER FREQUENCIES.			

**Figure 13 Electrical Properties of Various Shielding Materials**

FREQUENCY	IRON $\mu$	PENETRATION LOSS/MIL THICKNESS (db)	
		COPPER $\mu = 1, g = 1$	IRON $g = 0.17$
60 cps	1000	0.026	0.334
1000 cps	1000	0.106	1.37
10 kc	1000	0.334	4.35
150 kc	1000	1.29	16.9
1 mc	700	3.34	36.3
15 mc	400	12.9	106.0
100 mc	100	33.4	137.0
1500 mc	10	129.0	168.0
10,000 mc	1	334.0	137.0

NOTE: OTHER VALUES OF  $\mu$  FOR IRON ARE 600 AT 3 mc, 500 AT 10 mc AND 50 AT 1000 MC.

Figure 14 Calculated Penetration Loss of Metal Sheet

FREQUENCY	IRON $\mu$	REFLECTION LOSS <sup>1</sup> (db) FOR GIVEN SOURCE IMPEDANCE					
		<< 377 $\sim$		377 $\sim$		>> 377 $\sim$	
		COPPER <sup>2</sup> $\mu = 1$ $g = 1$	IRON <sup>2,3</sup> $g = 0.17$	COPPER $\mu = 1$ $g = 1$	IRON $g = 0.17$	COPPER <sup>2</sup> $\mu = 1$ $g = 1$	IRON <sup>2</sup> $g = 0.17$
60 cps	1000	22.4	-0.9	150.0	112.7	278.7	241.0
1000 cps	1000	34.2	0.9	138.0	110.5	242.0	204.4
10 kc	1000	44.2	8.0	128.0	90.5	212.0	174.0
150 kc	1000	56.0	18.7	117.0	78.8	176.8	139.0
1 mc	700	64.2	28.1	106.2	72.1	152.0	116.0
15 mc	400	76.0	42.2	96.4	62.7	116.9	83.1
100 mc	100	84.2	56.5	88.2	60.5	92.0	64.4
1500 mc	10	*	*	76.4	58.8	*	*
10,000 mc	1	*	*	68.2	60.5	*	*

\*AT THESE FREQUENCIES THE FIELDS APPROACH 377 OHMS IN IMPEDANCE AND BECOME PLANE WAVES.

- NOTES:
1. SHIELDING MATERIAL MUST BE OF SUFFICIENT THICKNESS TO PROVIDE 15 db PENETRATION LOSS OR BETTER. OTHERWISE, THE TOTAL REFLECTION LOSS HAS TO BE CORRECTED BY THE B FACTOR AS INDICATED IN EQUATION 87 AND FIGURE 16.
  2. THE SIGNAL SOURCE DISTANCE IS 12 INCHES. FOR OTHER DISTANCES, THE REFLECTION LOSS MUST BE RECALCULATED USING FIGURE 6.
  3. THE REFLECTION LOSS FOR IRON IS ZERO AT 630 cps AND AT 60 cps IS A NEGATIVE QUANTITY. IT IS AGAIN ZERO AT 31.5 cps AND THEN BECOMES A POSITIVE QUANTITY FOR STILL LOWER FREQUENCIES.
  4. STRONG PLANE WAVES BELOW 1.6 mc (WITH THE EXCEPTION OF 550- TO 1600-KC RADIO BROADCAST SIGNALS) SELDOM EXIST IN THE VICINITY OF A SHIELDED ROOM.

Figure 15 Calculated Reflection Loss of Metal Sheet (Both Interfaces)

SHIELD THICKNESS (mils)	B-TERM (db)					
	60 cps	100 cps	1 kc	10 kc	100 kc	1 mc
COPPER, $\mu = 1$ , $g = 1$ , MAGNETIC FIELDS						
1	-22.22	-24.31	-28.23	-19.61	-10.34	-2.61
5	-21.30	-22.07	-15.83	-6.98	-0.55	+0.14
10	-19.23	-18.59	-10.37	-2.62	+0.57	0
20	-15.35	-13.77	-5.41	+0.13	+0.10	
30	-12.55	-10.76	-2.94	+0.58	0	
50	-8.88	-7.07	-0.58	0		
100	-4.24	-2.74	+0.50			
200	-0.76	+0.50	0			
300	+0.32	+0.53				
COPPER, $\mu = 1$ , $g = 1$ , ELECTRIC FIELDS AND PLANE WAVES						
1	-41.52	-39.31	-29.38	-19.61	-10.33	-2.61
5	-27.64	-25.46	-15.82	-6.96	-0.55	+0.14
10	-21.75	-19.61	-10.33	-2.61	+0.57	0
20	-15.99	-13.92	-5.37	+0.14	+0.10	
30	-12.73	-10.73	-2.90	+0.58	0	
50	-8.81	-6.96	-0.55	+0.14		
100	-4.08	-2.61	+0.51	0		
200	-0.62	+0.14	0			
300	+0.14	+0.58				
IRON, $\mu = 1000$ , $g = 0.17$ , MAGNETIC FIELDS						
1	+0.95	+1.23	-1.60	-1.83		
5	+0.93	+0.89	-0.59	0		
10	+0.78	+0.48	+0.06			
20	+0.35	+0.08	0			
30	+0.06	+0.06				
50	0	0				
IRON, $\mu = 1000$ , $g = 0.17$ , ELECTRIC FIELDS AND PLANE WAVES						
1	-19.53	-17.41	-8.35	-1.31		
5	-6.90	-5.17	+0.20	0		
10	-2.56	-1.31	+0.36			
20	+0.16	+0.54	0			
30	+0.58	+0.42				
50	+0.13	0				
NOTE: THIS B-TERM CORRECTION HAS TO BE APPLIED TO THE REFLECTION LOSS VALUES SHOWN IN FIGURE 13 WHEN THE TOTAL PENETRATION LOSS OBTAINED FROM FIGURE 14 IS < 15 db.						

Figure 16 B-Term Correction for Single Metal Sheet

THICKNESS (mils)	FREQUENCY	TYPE OF FIELD	R REFLECTION LOSS (db)	A PENETRATION LOSS (db)	B CORRECTION TERMS (db)	TOTAL SHIELDING EFFECTIVENESS S = R + A + B (db)
<b>COPPER</b>						
1	60 cps	MAGNETIC	22.4	0.026	-22.2	0.23
10	60 cps	MAGNETIC	22.4	0.26	-19.2	3.46
300	60 cps	MAGNETIC	22.4	7.80	+0.32	30.52
10	1 kc	MAGNETIC	34.2	1.06	-10.37	24.89
10	10 kc	MAGNETIC	44.20	3.34	2.62	44.92
10	10 kc	ELECTRIC	212.0	3.34	-2.61	212.73
10	10 kc	PLANE WAVES	128.0	3.34	-2.61	128.73
30	10 kc	MAGNETIC	44.20	10.02	+0.58	54.80
10	150 kc	MAGNETIC	56.0	12.9	+0.5	69.4
10	150 kc	ELECTRIC	176.8	12.9	+0.5	190.2
10	150 kc	PLANE WAVES	117.0	12.9	+0.5	130.4
10	1 mc	MAGNETIC	64.2	33.4	0	97.6
10	1 mc	ELECTRIC	52.0	33.4	0	185.4
10	1 mc	PLANE WAVES	108.2	33.4	0	141.6
<b>IRON</b>						
1	60 cps	MAGNETIC	-0.9	0.334	+0.95	0.38
10	60 cps	MAGNETIC	-0.9	3.34	+0.78	3.22
300	60 cps	MAGNETIC	-0.9	100.0	0	99.1
10	1 kc	MAGNETIC	0.9	13.70	+0.06	14.66
10	10 kc	MAGNETIC	8.0	43.5	0	51.5
10	10 kc	ELECTRIC	174.0	43.5	0	217.5
10	10 kc	PLANE WAVES	90.5	43.5	0	134.0
30	10 kc	MAGNETIC	8.0	130.5	0	138.5

Figure 17 Typical Calculated Values of Shielding Effectiveness



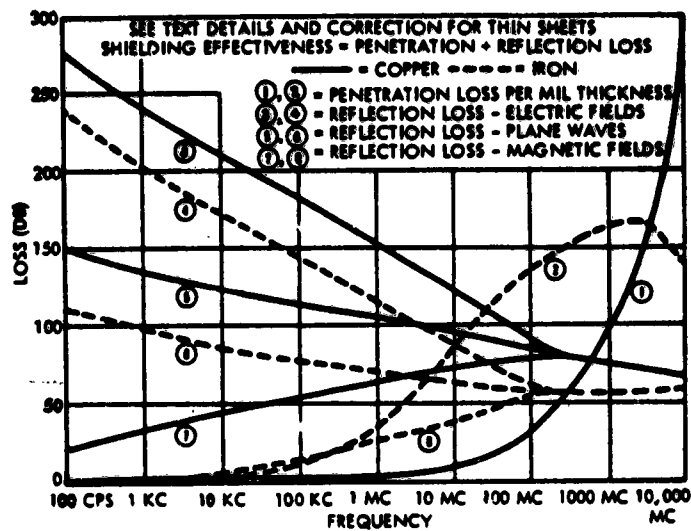


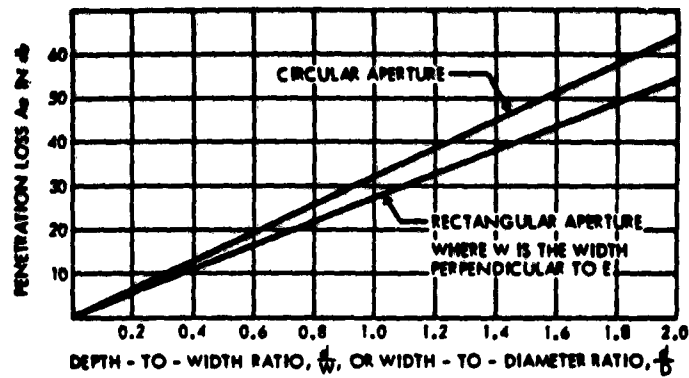
Figure 18 Calculated Shielding Effectiveness of Metal Barriers

FREQUENCY	WAVELENGTH (MILS)	
	COPPER	IRON
100 mc	1.64	0.399
10 mc	5.20	0.561
1 mc	16.4	1.51
100 kc	52.0	39.9
10 kc	164	126
1 kc	520	399
100 cps	1640	1260
10 cps	5200	3990

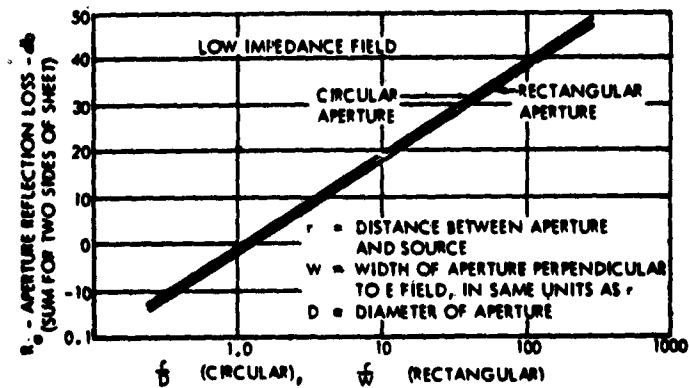
Figure 19 Wavelengths of Electromagnetic Waves in Copper and Iron

SYMBOL	ITEM	APERTURE		COMMENTS
		RECTANGULAR	CIRCULAR	
$A_0$	PENETRATION LOSS	$27.3 \frac{d}{w}$	$32 \frac{d}{D}$	$d$ = DEPTH OF APERTURE, INCHES $w$ = WIDTH OF RECTANGULAR APERTURE, INCHES 1 TO E FIELD $D$ = DIAMETER OF CIRCULAR APERTURE, INCHES
$R_a$	APERTURE REFLECTION LOSS (SUM FOR 2 SIDES OF SHEET)	$20 \log_{10} 0.785 \frac{r}{w}$	$20 \log_{10} 0.92 \frac{r}{D}$	$\ll 377 \Omega$
		$20 \log_{10} \frac{1 + (1.7 \times 10^{-4} f_w)^2}{4 (1.7 \times 10^{-4} f_w)}$	$20 \log_{10} \frac{1 + (1.47 \times 10^{-4} f_w)^2}{4 (1.47 \times 10^{-4} f_w)}$	$377 \Omega$
		-----	-----	$\gg 377 \Omega$
$R_0$	CORRECTION TERM DUE TO SUCCESSIVE REFLECTIONS WHEN $A_0 \leq 15$ db	$20 \log_{10} (1 - 10^{-\frac{A_0}{10}})$		$\frac{D}{87.5} \frac{D}{3.68} \ll 1$
$K_1$	LOSS TERM DUE TO NUMBER OF OPENINGS PER UNIT SQUARE	$-10 \log_{10} \sigma$ , $r \gg w, D$ ZERO, $r \ll w, D$		$\sigma$ = AREA OF SINGLE APERTURE, INCHES <sup>2</sup> $n$ = NUMBER OF HOLES PER SQUARE INCH
$K_2$	CORRECTION TERM FOR PENETRATION OF CONDUCTOR AT LOW FREQUENCIES	$-20 \log_{10} (1 + 35p^{-2.3})$		$P = \left\{ \begin{array}{l} \text{WIRE DIAMETER, SCREENING} \\ \text{SKIN DEPTH} \end{array} \right.$ $P = \left\{ \begin{array}{l} \text{CONDUCTOR WIDTH BETWEEN} \\ \text{HOLES/SKIN DEPTH} \end{array} \right.$ PERFORATED SHEETS,
$K_3$	CORRECTION FOR CLOSELY SPACED SHALLOW HOLES	$20 \log_{10} (\coth \frac{A_0}{8.586})$		

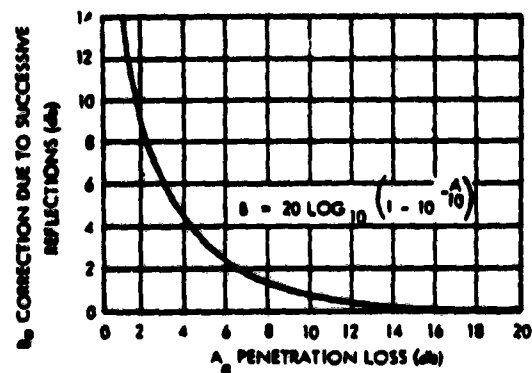
Figure 20 Terms for Aperture Shielding



a - Penetration Loss

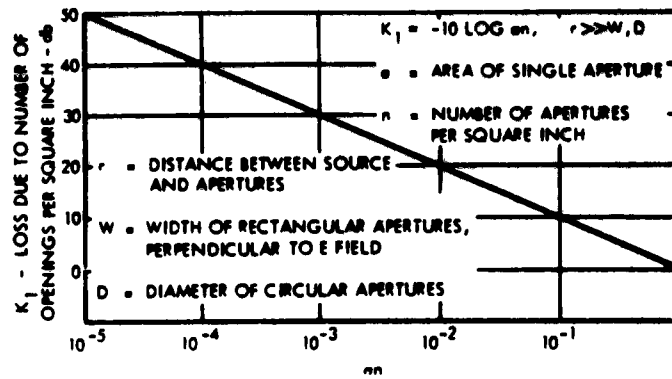


b - Reflection Loss

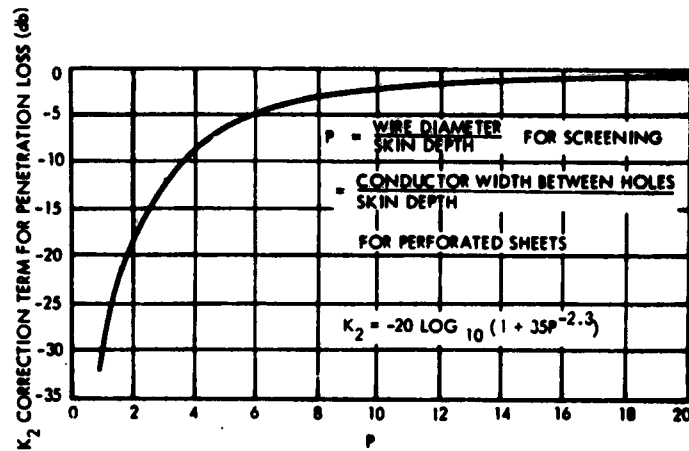


c - Correction Due to Re-reflection

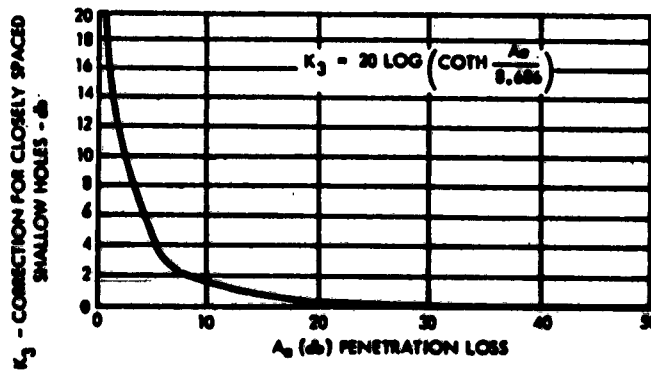
Figure 21 Aperture Shielding



d - Loss Due to Density of Openings



e - Correction for Skin Effect



f - Correction for Closely Spaced Shallow Holes

Figure 21 Aperture Shielding (continued)

FORM		MATERIAL	THICKNESS (MILS)	NOMINAL EFFECTIVENESS (dB)					
GEN- ERAL	DETAIL			0.1 kc	1kc	10kc	80kc	1mc	10mc
SOLID SHEET		Cu	125 63 31 4.5	8 4	22 11	58 29	97 59 34	120 55	
		Al	125 63 31	5 1 1	18 16 10	50 35 24	78		
		STEEL ( $\mu = 242$ )	63 31	25 4	40 28	80 59	94	92	120
		BRASS	31				42		
	CLAD 2 SIDES	Cu-CLAD STEEL	31				107		
	1 SIDE ONLY		94				103		
	2 LAYERS 1 INCH APART	Cu (OXIDIZED)		2	6	18			
MESH (SCREENING)	NO. 22	Cu					31	43	43
	NO. 16	BRONZE					18		
	NO. 4	GALVANIZED STEEL					10	17	21

Figure 22 Measured Effectiveness of Shielding Materials Against Low-Impedance Waves

FORM		MATERIAL	THICKNESS (mils)	NOMINAL EFFECTIVENESS (dB)		
GENERAL	DETAILED			200 kc	1 mc	5 mc
SOLID SHEET		Cu	2.5	109	106	114
		Al	5	107	109	118
		STAINLESS STEEL	18	97	95	99
		STEEL ( $\mu_r = 250$ )	4.5	105	99	101
		AA- CONETIC FOL ( $\mu_r = 10,000$ )	3.5	97	130	
PERFOR- ATED SHEET	45 MIL DIA, 225/50, INCH	Al	20	3040 mc		9380 mc
				40		62
MESH (SCREEN- ING)	NO. 16	Al	DIA = 13	34		36
	NO. 22	Cu	DIA = 15	200 kc	1 mc	5 mc
				118	106	100
						80

Figure 23 Measured Effectiveness of Shielding Materials against Plane Waves

FORM		MATERIAL	THICKNESS (MILS)	NOMINAL EFFECTIVENESS (dB)	OPEN AREA (%)	AIR-FLOW STATIC PRESSURE (inches of water)	
GENERAL	DETAILED					-200 cu ft / min	400 cu ft / min
MICROCELL	1/4-INCH CELL, 1 INCH THICK	AL	3	> 90		0.06	.26
	9-MIL HOLES, 20-MIL CENTERS	95% CU 5% NI	7	> 90	12	> 2	
		100% NI	3	> 90	50	0.2	0.4
			7	> 90	50	0.2	0.5
ELECTRONESH	40 COUNT	CU-NI	5	> 90	36	0.4	1.7
	25 COUNT		5	78	49	0.2	0.5
	40 COUNT	CU	3	78	57	0.2	0.5
	25 COUNT		3	78	54	0.2	0.4
PERFORATED SHEET	1/8-INCH DIA., 3/16-INCH CENTERS	STEEL	40	58	32	0.27	> 0.6
	1/4-INCH DIA., 5/16-INCH CENTERS		40	48	46		
	7/16-INCH DIA., 5/8-INCH CENTERS	AL	37	35	45		
				55	36		
MESH (SCREENING)	NO. 16 16 x 16/ SQ. IN.	AL	20 (dia)	55			
	NO. 22			45 (1.4 in to 40 mil)			
	NO. 12	CU	20 (dia)	50	50		
	NO. 16	BRONZE		45 (1.4 in to 40 mil)			
	NO. 10	MONEL	18 (dia)	40			
	NO. 4	GALVANIZED STEEL	30 (dia)	28 <sup>2</sup> (1.4 in to 40 mil)	74		
COATINGS	NO. 2			24	88		
		SILVER PAINT		85 in 1 ms 2 1/2			
		GRAPHITE		84	67	50	
		CONDUCTING GLASS		73	53	39	

<sup>1</sup> THESE DATA HAVE BEEN OBTAINED BY VARIOUS EXPERIMENTERS.

<sup>2</sup> DIFFERENT VALUES OBTAINED BY DIFFERENT EXPERIMENTERS.

Figure 24 Measured Effectiveness of Shielding Materials Against High-Impedance Waves

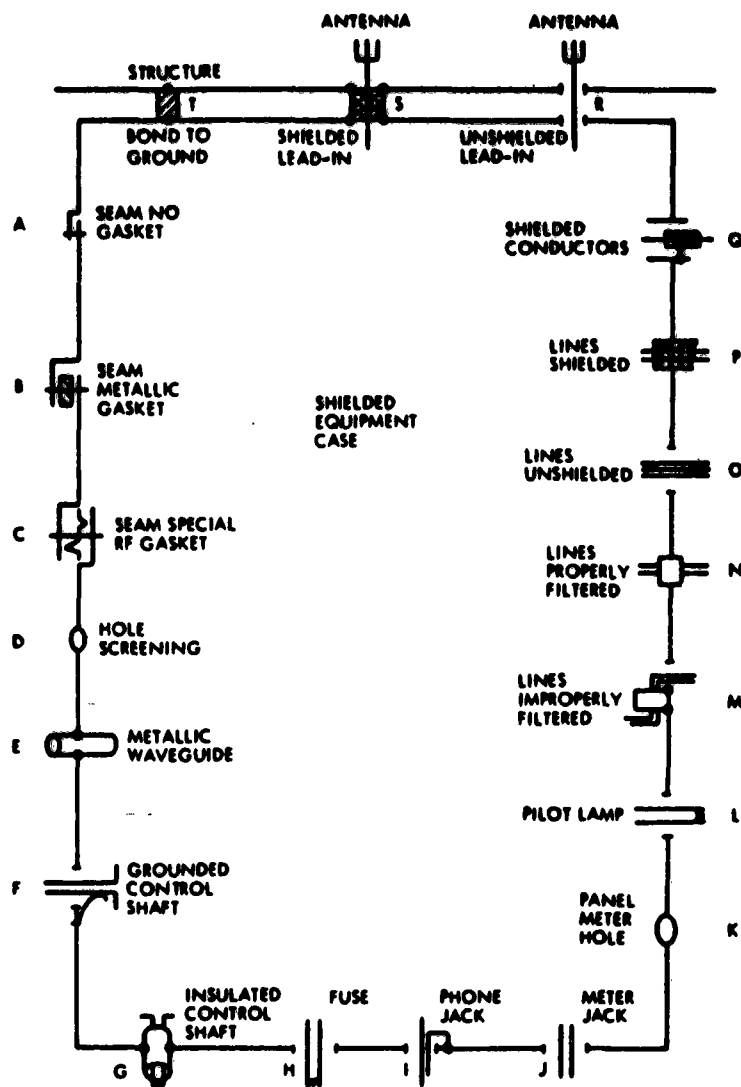


Figure 25 Typical Shielding Enclosure Discontinuities

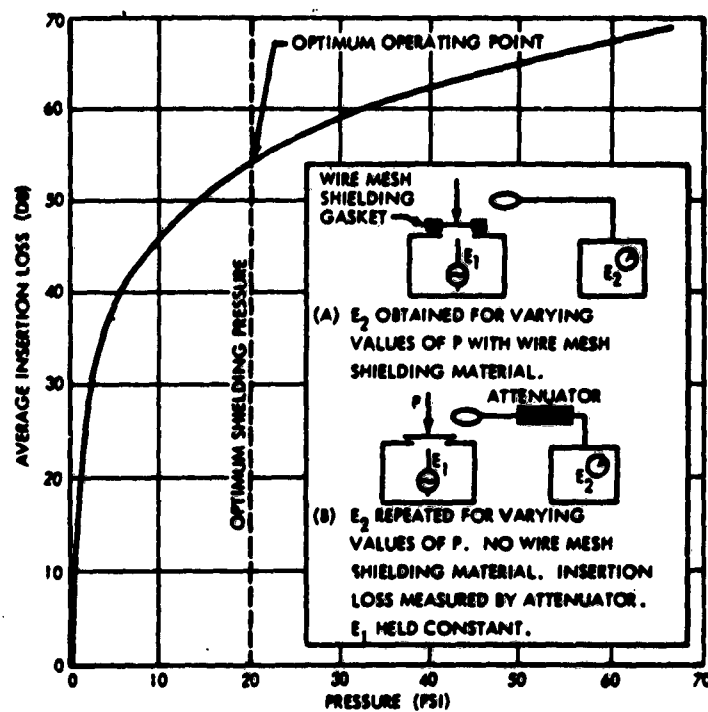


Figure 26 Typical Insertion Loss as a Function of Gasket Pressure



## SHIELDING A FLIGHT VEHICLE AGAINST ELECTROMAGNETIC INTERFERENCE DURING TEST

R. O. Lange  
General Dynamics Corporation, Astronautics Division  
San Diego, California

**Abstract.** - This paper discusses the construction of a 40' x 40' x 20' high shielded anechoic facility, its evaluation, the method of physically supporting the vehicle during test, and use of the test chamber in a program of electromagnetic interference elimination on the Centaur space vehicle. The frequency range of interest is 200 MC through 6 Gc. The discussion of construction covers principally the design of the facility and the solution of problems involved in maintaining the integrity of the metal shielding subsequent to providing the required apertures. Evaluation includes the results of tests made during various stages of construction and upon completion of alterations. Use of the chamber includes the purposes for which the facility was built and its present and anticipated usefulness.

### I. INTRODUCTION

Centaur is a high-energy, liquid-hydrogen-fueled, upper stage space vehicle. Its immediate mission is to launch the Surveyor spacecraft on lunar missions. The test chamber was designed for general use in evaluation of space vehicles. Its specific use for Centaur testing required installation of signal line conduits and an increase in power and air conditioning capacity. Centaur electrical systems were required to be tested under simulated free space radiation conditions. The requirement included the elimination of all spurious radiation in the frequency bands being used, whether originated by the vehicle or by sources outside the test chamber. The systems being tested included power generation and distribution, vehicle orientation, autopilot, guidance, telemetry, tracking, and destruct. In addition certain mechanical systems were required to be operated where an electrical signal was generated, as, for example, equipment containing thermostat controls, solenoid-operated valves, or boost pumps powered by electric motors.

Radiation originating outside a test chamber can theoretically be reduced to the point of elimination by lining the test chamber with an integral metal shield of appropriate thickness, permeability, and conductivity. In practice, however, this principle is incapable of being carried out to perfection. The curve of performance versus cost approaches perfection asymptotically, so that a point is reached where increased performance is prohibitively expensive. Also, as a practical matter, a point is reached where a flaw in workmanship will lose more performance than additional money can buy. The elimination of spurious radiation originating within the chamber is a matter of absorbing the radiation with suitable surrounding material, rather than allowing it to reach the metal shielding of the chamber and be reflected back into the vicinity of the vehicle. In this area the details of construction are not as critical as in the case of the metal shielding, and the important factor is the quality of the absorbent material used.

Installation of the best metal shielding and anechoic panels will be ineffective unless a way is found to provide the required apertures through the shielding without compromising its integrity. In this area the design engineer and the installation technician have equally critical functions.

## II. DESIGN AND CONSTRUCTION OF THE TEST FACILITY

### Enclosure Shell.

A 40' x 40' x 20' high enclosure shell was constructed. A 5" reinforced concrete slab floor was poured, with rods protruding for anchoring of the walls. The walls were constructed of 8" x 8" x 16" lightweight cement block, reinforced vertically with rods and pilasters, and horizontally with strips of steel mesh. The roof was constructed of standard steel decking over 1" insulation material, supported by steel bridge sections and joists. Wall apertures were left for a vehicle access door (20' x 17' high), personnel door (6' x 7' high), and air conditioning ducts. The construction of the enclosure shell did not incorporate any design features uniquely qualifying it for use as an electromagnetic interference control facility, except for the large access door and the absence of windows.

### Shielding.

The entire enclosure shell, except for access and air conditioning apertures, was lined with electromagnetic shielding. In the 200 MC to 6 Gc range the insertion loss theoretically obtainable using sheet steel shielding is, by absorption alone, more than 150 db per mil thickness, using the standard formula: 1,2,3,4,5,6.

$$A = 3.338 \times 10^{-3} t(fGu)^{\frac{1}{2}} \quad (1.1)$$

where

A = absorption loss in db  
t = thickness of shielding in mils  
f = frequency in cps  
G = conductivity relative to copper  
u = permeability relative to a vacuum.

Since even 150 db of insertion loss would be more than acceptable, it was apparent that the thickness of shielding to be used was not to be determined by the db's of insertion loss required. The thickness chosen was that thickness considered to be the minimum required for structural soundness and good solderability. 4,5,7,8,9,10,11,12,13,14,15.

The walls were lined vertically with 36" wide sheets of 24 gauge galvanized steel. Sheets were joined by a standard sheet metal joint consisting of interlocking flanges, as shown in Figure 1. With the flange assembled, the sheet containing the male flange was secured to the cement block wall with 5/8" stub nails on 8" centers. Nail lengths were kept at a minimum in order to avoid any antenna effect as a result of these protuberances. The antenna effect of such a protuberance is much discussed in the literature, not demonstrated or quantitatively evaluated, and sometimes disputed. However, the possibility of setting up such a radiating source is generally considered to be avoidable by keeping protuberances small and bonding them to the metal shield. In this instance it was not considered necessary to bond the nail head to the shield since the seam was flattened to cover the nail head (Figure 1) and soldered along its entire length. 2,6,16,17.

The ceiling shield was constructed of 4' x 8' x 3/4" Douglas fir plywood panels laminated on the exposed side with 24 gauge galvanized sheet steel (Figure 1). Panels were suspended from the joists by insulators and "Unistrut" channels. Ceiling panels were joined with metal strips adhered by continuous solder joints. The ceiling shield was joined to the wall shield with 1 1/2" x 1 1/2" x 1/8" galvanized steel L sections, fastened to the concrete block walls with "Ramset" gun nails on 18" centers and to the laminated ceiling panels with flat head wood screws on 12" centers (Figure 1). The L sections were continuously soldered with "Eccoshield VX" conductive caulking compound to the wall and ceiling shields. All screw and nail heads were peripherally soldered with the same material, in order to insure total seal and electrical continuity of the shielded area. 15

The floor shield was formed of 18 gauge galvanized sheet steel with joints butt welded and ground smooth (Figure 1). Since the more complicated sheet metal joint used for the walls was not structurally required at the floor, the heavier gauge steel was used in order to permit use of a butt weld. No kraft paper or other material was used between the floor shield and the cement slab, in spite of an awareness of literature mentioning galvanic action 5,17 at the interface of these materials. The use of paper would have prevented the application of heat required to form the butt welds. In any event the walls were constructed of cement in direct contact with steel. In the absence of moisture, at least, it was believed that no galvanic action problem would result. The floor shield was joined to the wall shield with 1 1/2" x 1 1/2" x 1/8" galvanized steel L sections, fastened to the walls and floor slab with "Ramset" gun nails on 18" centers. The L sections were continuously soldered to the wall and floor shields, and all nail heads were peripherally soldered.

At the apertures, the metal shielding was continuously soldered to metal door frames and air conditioning duct flanges.

#### Shielding Ground.

Preliminary design called for the installation of ground wells 12 feet apart in a grid pattern beneath the chamber floor as frequently advocated 3,4,18,19 in the literature. Soil analysis, a history of electrical testing at the locality, and a dearth of convincing theoretical evidence of the utility of an elaborate grounding system in southern California, reduced the ground design to one well. The soil at the site is highly resistive, consisting of hardpan, sand, and rock. There is no moisture and no significant temperature change. Under these conditions no charge distribution gradient develops in the vicinity of the earth contact, so that the metal structure itself acts as the only significant ground. A single earth contact was established by installing a ground well 3 inches in diameter, 16 feet deep, adjacent to the floor slab. The well was provided with a copper electrode 3/4 inch in diameter and 16 feet long, clamped to a copper grounding strap. The grounding strap was brought through the wall and brazed to a copper bus bar. The bus bar has now been extended to encompass most of the periphery of the test chamber, and is bonded every few feet to the wall shield. The space in the ground well surrounding the electrode was filled with magnesium sulfate to afford some conductivity and to retard corrosion of the electrode. The well requires periodic cleaning and maintenance.

#### Illumination.

Incandescent lighting was provided by attaching fixtures and wire

conduits to the ceiling shield, without puncturing the shield. The box enclosing each socket was fastened by short lengths of bolt soldered to the shield. Conduits were soldered to the shield at convenient intervals. At the point of entry into the chamber all wires were brought in through the shield in a single conduit, with a small junction box soldered to the inside of the wall shield at the point of entry. The conduit was designed as a waveguide with a cutoff frequency above 6 Gc. The conduit was made an integral part of the metal shield by peripheral soldering. The lighting fixtures used were long enough to permit subsequent installation of the anechoic panels (see Figure 1). Twenty-five lighting fixtures were used. For each light the absorptive effect of a cylindrical plug of anechoic material 6 inches in diameter was sacrificed. The alternative would have been a portable lighting installation, to be removed during tests.

#### Convenience Outlets.

Power outlets at various frequencies, voltages, and amperages were soldered to the wall shield along one side of the chamber. Lines were brought in through the junction box used for the lighting conduit. A plywood enclosure was built around the junction box and around all outlets, with hinged access doors dimensioned to accommodate the 2' x 2' anechoic panels to be installed subsequently. With this arrangement, an outlet in use required that one hinged anechoic panel remain slightly ajar; panels would remain in place over outlets not in use. In any event, during full-scale tests these outlets would not be exposed since at that time all lines would be brought in from outside checkout trailers, as discussed under Signal Line Conduits, below. The principal function of the convenience outlets was to provide power to operate roll-in test equipment for component or subsystem checks.

#### Filters.

A filter bank was provided externally to the test chamber, to accommodate power lines terminating at the checkout trailers and at the convenience outlets in the test chamber. The power and signal lines running from the checkout trailers to the space vehicle could not be filtered, due to their large number and impedance match considerations.

#### Air Conditioning Ducts.

Two air conditioning systems were required, one for area cooling and the other for component cooling aboard the space vehicle. Both units were located outside the chamber, with ducts brought in through the ceiling shield. The area cooling air was supplied through ceiling diffusers, with air return ducts installed at wall registers. The component cooling system was designed to connect to the vehicleborne duct system. Since the component cooling duct was required to remain in place during roll of the vehicle about its longitudinal axis (discussed under PHYSICAL SUPPORT OF THE VEHICLE, below), it was given a flexible "elephant trunk" design. Metal was kept at a minimum within the chamber, in the air conditioning duct design. A helical wire reinforcement was required in the "elephant trunk", however the duct was designed to attach to a plastic flange at the ceiling, so that no conducting path from the outside was provided. All air conditioning apertures were provided with honeycomb sections made up of cells having a length of at least four times their greatest cross sectional dimension and having a cutoff frequency above 7 Gc (based on their dimensions as

individual waveguides). While there is evidence in the literature that correction factors must be provided to determine the anticipated insertion loss where many waveguides are used in juxtaposition, as in the case of honeycomb sections, there does not appear to be any alternative method of bringing in thousands of cubic feet per minute of cooling air. The location of 10-inch honeycomb duct sections in the 40' x 40' ceiling did not, in this case, produce any noticeable degradation of shielding efficiency. All air conditioning apertures were provided with extensions inside the chamber, representing the thickness of the anechoic panels to be added. With the exception of a flange, no metal was used on the chamber side of the honeycomb sections.

#### Doors.

The 6' x 7' personnel door was made of 2½" plywood clad with 18 gauge galvanized sheet steel on all surfaces, with seams soldered. The door was fitted with 7" wide brass hinges and panic hardware with paddle operated three-point latching device. A continuous "technit" gasket was used to seal the periphery of the door against the frame. This design has proven satisfactory for a door of this size. Under conditions of constant use the door requires frequent attention to maintain the latches and gasket in a tight fitting condition.

The 20' x 17' vehicle access door was made of 2" x 6" tongue and groove Douglas fir, laminated on the inside with 24 gauge galvanized sheet steel. It was made in two sections, hung from a rail on the outside of the building. A continuous "technit" gasket was used between the two halves of the door and between the peripheral edge of the door and the metal door frame. A pressure fit is obtained incrementally through a series of latching levers and 64 peripheral bolts, all located inside the shielded enclosure. This design would not be considered acceptable in areas of severe corrosion or under requirements of frequent accessibility. Opening and closing the door is a process requiring several manhours to shift the anechoic panels, operate the latches and bolts, and clean the mating surfaces after exposure to the atmosphere. This expenditure of time is justified however, where the door must be operated only infrequently. Estimates received from vendors indicate that the installation of an instant access door with protective vestibule would cost nearly as much as was spent on the entire facility.

The door is presently being reworked to include a pneumatic seal and additional clamping devices on the outside of the building. The basic principle of an economical, infrequent-use access door will, however, be retained. Serious consideration is being given to the possibility of installing a metal frame inside the chamber to permit the soldering in place of a sheet metal diaphragm to completely close the aperture between infrequent openings. Such a diaphragm would weigh 500 pounds, and would thus entail handling difficulties.

#### Flooring.

No material was found which would support the weight of the vehicle and handling tool (12 tons) and offer any significant power absorption capability. It was decided to utilize a wood floor with asphalt tile covering, then to provide absorbency by covering the floor with anechoic material similar to that used for the walls. The material will sustain reasonable foot traffic if covered in walk areas with 1/4" plywood sheets. The flooring was constructed of 1" marine plywood

panels over 2" x 3" Douglas fir cribbing on 16-inch centers (see Figure 1). Removable panels were used in the vicinity of the vehicle access door to permit access to the tightening bolts installed at the bottom edge of the door.

#### Anechoic Material.

All wall and ceiling areas and the inside surface of the vehicle access door were covered with 2' x 2' x 9" thick anechoic panels. The material is rated by the manufacturer as having 5% power reflectivity at the lowest frequency of interest (200 MC) and less than 1% power reflectivity above 400 MC. In order to avoid puncturing or unnecessarily soldering to the metal shielding, the material was installed with adhesive. Wall panel installation was relatively easy since the panels were of rigid, free standing design. The weight of the 2' x 2' panels (6 pounds) resulted in a problem in adhering the material to the ceiling. Adhesives either dried and failed within a short time or remained wet and dripped until failure. Cascading material became a hazard. A general purpose contact cement was eventually found to be satisfactory. The anechoic material was shaped as required to fit tightly around light fixtures and air conditioning ducts. The 6' x 7' personnel door aperture was covered by a movable panel constructed by bonding the anechoic material to a plywood frame. The frame was provided with legs for support in an upright position, and with casters and handles to enable personnel to pull it into place upon exiting. The anechoic panels for the 20' x 17' vehicle access door were shaped, where required, and stacked in the door aperture. They were numbered when in position. They were then taken down and their positions were marked on the metal inner surface of the door. Strips of "Velcro touch and close" tape were fixed to the door, with mating strips fixed to the anechoic panels. In this arrangement the anechoic panels may be readily removed and stacked within the chamber when the door is to be opened.

The material used proved to be satisfactory from the standpoint of power absorptivity. It did not however offer sufficient longterm structural rigidity to withstand the handling operations involved in opening and closing the door, or the slight vibration proceeding from an air conditioning installation on the roof. Plans are now in work to install a crosshatch of tape on the ceiling in order to halt structural failure of the material. The basic design of the material, providing a facing section and a base section made up of cones, with the two sections joined at the cone tips with adhesive, does not afford great structural strength to this soft material. For future applications a one-piece panel design will be sought. A one-piece panel of homogeneous material would have the further advantage of being able to be cut into small plugs to cover utility and other outlets when not in use.

#### Signal Line Conduits.

In order to remove all reflective surfaces from the vicinity of the vehicle, the checkout equipment was required to be located in checkout trailers outside the test chamber. This arrangement required that the test cables be brought in through the metal wall shield (see Figures 2 and 3). Approximately 1,000 lines, contained in 30 prefabricated cables ranging to 3 inches in diameter, were involved. Filtering of the lines was not feasible, due to the large number of lines involved and the requirement of maintaining impedance matches. Literature on aperture design was of no assistance, generally merely containing the admonition: Bring in no unfiltered lines. Discussions of conventional waveguide theory were similarly inapplicable since they were inevitably

predicated on achieving efficiency of waveguide transmission. The problem here was to build as bad a waveguide as possible, in order to maintain the integrity of the electromagnetic shielding against the transmission of radiated interference. By the standard formula: 21,22,23

$$f_c = \frac{30}{\lambda_c} \quad (1.2)$$

where

$f_c$  = cutoff frequency in Gc  
 $\lambda_c$  = cutoff wavelength in centimeters,

the cutoff wavelength for a cutoff frequency of 6 Gc is 5 centimeters. Using the formula for circular waveguides: 21,24

$$\lambda_c = \frac{2\pi r}{Z_n}, \quad \frac{2\pi r}{\lambda_0} \geq Z_n \quad (1.3)$$

where

$\lambda_c$  = cutoff wavelength in centimeters  
 $r$  = radius of waveguide in centimeters  
 $Z_n$  = Bessel function zero ( = 1.841 for dominant  $TE_{1,1}$  mode)  
 $\lambda_0$  = wavelength of propagation in free space,

the required diameter of a conduit with a cutoff frequency of 6 Gc is 2.9 centimeters, or 1.15 inches. Clearly a conduit of this dimension would not accommodate the test cables involved. In addition to the dimension problem, the presence of conducting signal lines in the conduit introduced a further complicating factor.

Significant attenuation occurs only when a waveguide is operated at a wavelength greater than its cutoff wavelength, as is shown by the formula: 23

$$A = 54.5 \frac{d}{\lambda_c} \left[ 1 - \left( \frac{\lambda_c}{\lambda_g} \right)^2 \right]^{\frac{1}{2}} \quad (1.4)$$

where

$A$  = attenuation per unit length in db  
 $d$  = length  
 $\lambda_c$  = cutoff wavelength  
 $\lambda_g$  = operating wavelength.

Design objectives were (1) to construct a conduit which would act as a wave trap, barring the transmission of energy by absorption and reflection, and (2) to use as small a conduit as possible in order to achieve the highest possible cutoff frequency, thus increasing the value of  $A$  in attenuation formula (1.4).

The conduit design finally arrived at is shown in Figure 3. It consists of a 5" diameter iron pipe containing two 90-degree bends. The conduit is dismountable at the bends, to permit introduction of bulky connectors and rigid cable sections. The conduit sections are joined by bolted flanges and by a

threaded collar which is soldered to the metal wall shielding. The collar permits unneeded conduits to be removed and their apertures to be sealed by a threaded plug. The 90-degree bends furnish reflective surfaces both inside and outside the conduit. Each conduit was required to accommodate various cables. Cables had to be capable of being switched from one to another conduit to minimize interference. Also cables were required to be added or deleted as the R & D program progressed. For these reasons flexibility of design was a requirement, and conduits could not be tailored to fit individual cables. A method was sought of effectively shrinking the conduit to the size of the cables it carried, by packing various materials around the cables. The results of these efforts are described under Evaluation of Signal Line Conduits, below. Present configuration requires the use of eight conduits. Their location in the wall was determined by considerations of convenience and the avoidance of metal reinforcement rods. Within the selected area, individual locations were calculated so that no distance was equal to or a multiple of any other distance. This precaution was intended to avoid a spatial grating effect resulting from a periodicity of structure.<sup>24</sup> When the optimum cable arrangement is determined by experience, the ends of the conduit will be sealed with potting compound to retard corrosion of the packing material in the conduit.

### III. PHYSICAL SUPPORT OF THE VEHICLE

It was desirable to support the vehicle with a mobile frame permitting easy access to all components, and with a minimum of exposed metal in a position to cause reflection of radiation emanating from the vehicle. The supporting frame must also allow the vehicle to be rotated about its longitudinal axis. This rotation would provide access to all components and connectors, and would also permit a radiating antenna to be orientated away from the handling tool, floor, or other installation which might interfere with anechoic operation. These requirements were met by the construction of a tricycle handling tool on casters, with cantilevered I-beam (see Figure 2). The vehicle tank section fits over the I-beam and rotates on bearings which support internal structural members. A motorized rotating mechanism is used. Test cables are long enough to permit 180 degrees of rotation before connections must be broken. The space vehicle so adapted will remain as a test vehicle. If flight vehicles are required to be rotated, a nylon sling handling tool is envisioned. Since the floor was not designed to support the weight of the space vehicle and its handling tool during movement, metal plates were used to bring the vehicle into the chamber. Plates were left in place under the casters of the handling tool.

### IV. EVALUATION OF THE FACILITY

#### Evaluation of the Enclosure.

Prior to selection of the building site environmental tests were conducted in various areas. The results of these tests were a factor in site selection, although other practical considerations were involved. During construction of the facility, evaluations were made (1) upon completion of the cement block shell, (2) upon installation of the galvanized sheet steel shielding, and (3) upon installation of the anechoic panels. The building is located in an expanding industrial area, within range of numerous television stations and military installations. Under these conditions the ambient radiation signals were significantly strong and dependable to be used as sources without the generation of any signals for evaluation purposes. The ambient



signals (Figure 4) exceeded the levels specified by MIL-I-26600 at virtually all frequencies in the 0.2 MC to 400 MC range. These readings, taken upon completion of the cement block shell, were equal to those taken at the site prior to commencement of construction. After installation of the metal shielding, as shown in Figure 4, ambient signals were attenuated below the noise level of the measuring equipment, except in the 50-100 and 200 MC ranges. Installation of the anechoic panels, as shown in Figure 4, resulted in the further attenuation of the remaining signals. The results indicated a major source of leakage at 50-100 MC. It appeared to be more than coincidental that the wavelength at 100 MC, being 9.83 feet, was exactly the width of each section of the large vehicle access door. Rework of the door has resulted in considerable improvement. Redesign of the door seal and the installation of clamps is expected to afford the 100 db of insertion loss at the door area, already obtained at the other areas of the chamber.

#### Evaluation of Signal Line Conduits.

In order to determine the optimum conduit configuration, three conduits were designed and tested. All were four feet in length and capable of being bolted firmly to the metal shield of the test chamber. One was a straight conduit, 5 inches in diameter. The second was 5 inches in diameter, with two 90-degree bends. The third was of 5-inch square cross section, with two 90-degree bends. The conduits containing the bends were made in two sections, with mounting flanges, which permitted one end to be rotated in relation to the other. The results of the tests on these conduits may be summarized as follows (see Figure 5):

(1) In the range of 200 MC to 1 Gc (below cutoff), the conduits with bends afforded an insertion loss of 10-20 db greater than that of the straight conduit, the difference increasing with frequency. Interpretation: In the region far below cutoff, the reflection losses afforded by the bends are not significant, since the attenuation losses are great regardless of the shape of the conduit.

(2) In the range of 1 Gc to 6 Gc (above cutoff) the conduits with bends afforded an insertion loss of 5-10 db greater than that of the straight conduit, the difference decreasing with frequency. Interpretation: As cutoff is reached and passed the reflection losses within the conduit due to the bends are significant. At the highest frequencies the tendency of the conduit to force the generation of other than the fundamental mode of propagation increases the total energy penetration of the shield.<sup>22</sup>

(3) Of the conduits with bends, the square conduit afforded slightly more insertion loss at P-band frequencies, while the round conduit afforded slightly more at S-band frequencies. The cutoff frequency for the square conduit was 1.18 Gc, while that for the round conduit was 1.38 Gc, using the formulas:<sup>4,5</sup>

$$f_c = \frac{5900}{b} \quad (1.5)$$

$$f_c = \frac{6920}{d} \quad (1.6)$$

where

$f_c$  = cutoff frequency in MC

$b$  = inside dimension of square waveguide in inches

$d$  = inside diameter of circular waveguide in inches.

The slightly higher cutoff frequency of the round conduit with bends could be expected to result in superior insertion loss performance at the lower frequencies, however this fact was not evident from the test results. The difference in performance between the two conduits with bends was not considered to be significant. At the conclusion of these tests it was decided to use the round conduit with bends in view of its easier manufacture and installation.

Tests were then run on the round conduit with bends to determine the effects of (1) running a single test cable through the conduit and terminating it at both ends, (2) incrementally filling the conduit with cables, (3) enclosing the cable bundle in a metal sheath and grounding the sheath to the conduit,<sup>25</sup> (4) supplying power through the cables, and (5) turning one bend of the conduit 90 degrees from the plane of the other bend. The effect of running test cables through the conduit was as follows: At frequencies below cutoff, the cables degraded performance of the conduit, due apparently to the conductive copper path provided by the cables to the low frequency interference. At frequencies above cutoff, the cables improved performance, due apparently to the smaller cross sectional area remaining in the conduit for the transmission of radiated energy.<sup>21,26</sup> These effects were accentuated with each increase in the cable bundle. The placement of several cables in one conduit was undesirable as it degraded the performance of the conduit at the telemetry frequencies. Degradation at this area of the spectrum was serious because it was the area in which interference was being generated by sources not subject to control. Equally undesirable was the alternative of providing an aperture in the shielding for each cable with its individual conduit. As a compromise it was decided to install eight conduits with not more than the equivalent of two 1 $\frac{1}{4}$ " cables, or one larger cable, in each conduit. In order to reduce the number of cables, it was decided to introduce coax cables by means of through fittings. Enclosing the cable bundle with a sheath and grounding it resulted in an increased insertion loss of 10 db at all frequencies. Supplying power on the cables produced no noticeable effect. Turning one bend of the conduit 90 degrees produced no noticeable effect at X-band frequencies. There was evidence of a slight increase in insertion loss at P-band frequencies, however the required reorientation of dipole antennas left the results subject to conjecture. At any rate no assumptions could be made regarding the orientation of the random interference sources expected to be radiating at these frequencies, so that it was decided to install the conduit bends in any plane dictated by convenience of access and good binding of threads.

A final series of tests were run on the round conduit with bends, to effectively reduce the diameter of the conduit by surrounding the cable bundle with various conductive packing materials. The cable bundle was sheathed for a distance extending through the conduit and several feet on each end. For each test a reference level was established using antennas 4 feet apart in air. The antennas were then placed the same distance apart at the ends of the conduit, to assure a worst condition reading. The reference level was rechecked after each reading through the conduit. Tests were narrowband, CW, radiated, conducted in the range of 200 MC to 6 Gc.<sup>27,28</sup> Insertion loss was measured in db. Tests included (1) open conduit, (2) conduit and cables with grounded sheath, and (3) conduit and cables with grounded sheath surrounded, in turn, with steel wool, aluminum wool, monel fibers, salt water, mercury, and a combination of steel wool and aluminum wool. The results are shown in Figure 6. The best material at all frequencies was the combination of steel wool and aluminum wool, one material being used on each side of the conduit, with no mixing. Results improved with tighter packing of the materials and with the use of finer grades. This combination was chosen

because of its superior performance as well as the ease of handling of the material. While there is undoubtedly a possibility of corrosion and degradation of performance of the fibers with time, sealing of the conduits and periodic replacement of the material is expected to maintain the conduits in a satisfactory operating condition.

#### V. USE OF THE FACILITY

The shielded anechoic test facility was designed for use in conducting electromagnetic compatibility checks on components, systems, and the entire spacecraft with all electrical systems in operation. It provides the ideal environment for conducting radiation and susceptibility checks. It is particularly useful in the isolation and measurement of spurious signals suspected of causing equipment malfunctions. The environment due to each radiator can be measured at all points on the vehicle without the interference of outside radiation. This information is vital in the location of antennas as well as of components which exhibit susceptibility to the radiation of the antennas. In addition the test chamber offers the only opportunity before flight to operate all electrical systems simultaneously in a simulated outer space radiation environment.

#### VI. CONCLUSIONS

The design of a large shielded anechoic test facility for use in an R & D program requires at each stage the observance of flexibility and an appreciation of possible future design trends. The chamber must assume a simple geometric shape. As a practical matter the vehicle must be accommodated horizontally, since the length of space vehicles changes drastically with payload and fairing configurations, and planning for great heights involves prohibitive building and door costs. Obtaining an integral metal shield is principally a matter of workmanship and maintainability rather than of the thickness or type of metal used. The choice of anechoic material involves a compromise between accepting a poorer absorptivity at the lower frequencies or providing a building large enough to accommodate thick and expensive panels. At the present state of the art, achieving 1% power reflectivity at the telemetry frequencies requires wall and ceiling panels 19 inches thick costing \$6.00 or more for each square foot of wall and ceiling, and floor as well unless another solution is found.

Where test equipment is designed for a specific test chamber, signal lines can be filtered, thus eliminating the problem of bringing prefabricated cables through the metal shield. Where test equipment costing millions of dollars is already designed and is used at different locations, the test facility itself must be flexible enough to accommodate the equipment without tampering with the signal lines. The use of through conduits provides a practical solution of the entry problem, particularly at gigacycle frequencies.

While a fortune can be spent on large doors, it is possible to obtain a satisfactory door seal at low cost provided frequent access is not required and all mating surfaces are cleaned before each closing. The facility described in this paper was built at a total cost, excluding air conditioning units, of \$56,000. A shielded anechoic test chamber need not, therefore, become the major cost item in a test program.

Expansion of the test chamber to 40' x 60' is planned. The only

anticipated modifications to current design are the use of more rugged anechoic panels and some refinements to the door seal. The latter task may include the installation of an inner metal diaphragm as discussed under Doors, above. The decision will depend on the success of current rework efforts and the anticipated frequency of required access.

#### REFERENCES

1. S. Vogel, "RFI Causes, Effects, Cures", Electronics, June 21, 1963.
2. O. P. Schreiber, "Designing and Applying RFI Shields and Gaskets", Electronic Design, September 27, 1962.
3. C. S. Vasaka, "Shortcuts to R-F Shield Design", Electronic Industries, March, 1957.
4. C. B. Pearlston, "Case and Cable Shielding, Bonding, and Grounding Considerations in Electromagnetic Interference", IRE Transactions on RFI, October, 1962.
5. Handbook on Radio Frequency Interference, Volume 3, Frederick Research Corporation, 1962.
6. "Electromagnetic Compatibility - A Lecture Series", Volume II, Chapter I, Presented by Armour Research Foundation, 1961, Contract AF33(616)-8507, ARF Project EL65.
7. N. H. Cale, "A Comparison of R-F Shielding Materials", Electronic Industries, December, 1962.
8. C. M. Jorgenson, "Shielding in Modern Computer Design", Data Control, December, 1958.
9. B. Butterfield, "Polyform - A New Approach to Electromagnetic Shielding Enclosures", Electrical Design News, August, 1962.
10. "Metal Foil Wallpaper for RF Shielding", Electrical Design News, June, 1963.
11. A. M. Intrator, "Using Sheet Steel in the Construction of Shielded Rooms", Electrical Engineering, September, 1953.
12. R. G. Klouda, "Requirements of Measurements of Shielded Installations", Proceedings of the 7th Conference on Electromagnetic Compatibility, IIT, November, 1961.
13. W. T. Cronenwelt, "The Shielding Effectiveness of a Conducting Plane", IRE Transactions on RFI, October, 1962.
14. W. Jarva, "Shielding Efficiency Calculation Methods for Screening, Waveguide Ventilation Panels, and Other Perforated Electromagnetic Shields", Proceedings of the 7th Conference on Electromagnetic Compatibility, IIT, November, 1961.
15. E. E. Buckley, "Metal-Foil Shielding and Conductive Mastics for Inexpensive Shielded Enclosures", Proceedings of the 5th National Symposium on RFI, IEEE, June, 1963.

16. "Designing and Applying RFI Shields", Electrical Design, September 27, 1962.
17. H. W. Kenny and B. L. Conard, "A Practical Approach to R-F Shielded Enclosure Design", Ace Engineering and Machine Co., Inc., 1962. (Also appears as "RFI Shielded Enclosures" in Electrical Design News, September, 1962.)
18. R. Rudenberg, "Grounding Principles and Practice - I", Electrical Engineering, January, 1945; -II, C. Jones, February, 1945; -III, A. A. Johnson, March, 1945; -IV, W. R. Bullard, April, 1945.
19. H. W. Ervin, et al, "RFI Design Criteria for Acceptance Test and Checkout Complexes", Proceedings of the 5th National Symposium on RFI, IEEE, June, 1963.
20. "Selection of Waveguide Filters for Shielded Compartments", Radio Engineering, July, 1961 (translation from Russian).
21. P. F. Mariner, Introduction to Microwave Practice, Academic Press, 1961
22. I. L. Kosow, Microwave Theory and Measurements, Prentice-Hall, 1963.
23. Reference Data for Radio Engineers, International Telephone and Telegraph Corp., 1962.
24. N. Marcuvitz, Waveguide Handbook, M.I.T. Radiation Laboratory Series, Volume 10, McGraw-Hill Book Co., 1951.
25. F. H. Gooding and H. B. Slade, "Shielding of Communications Cables", Electrical Engineering, June, 1955.
26. H. A. Wheeler, "Universal Skin-Effect Chart for Conducting Materials", Electronics, November, 1952.
27. A. R. Kall, "Military Specifications for RFI - Their Requirements and Test Procedures", Electronic Design, September 27, 1962.
28. C. E. Blakely, "Spectrum Signature Measurements: Communications Systems", Electronic Design, July 19, 1963.

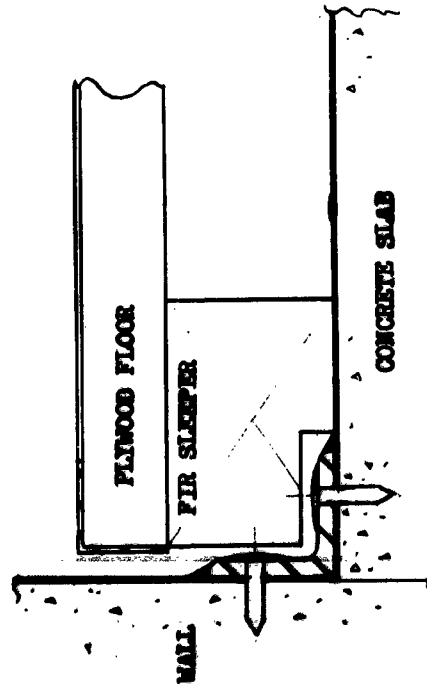
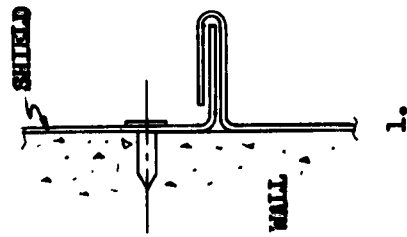
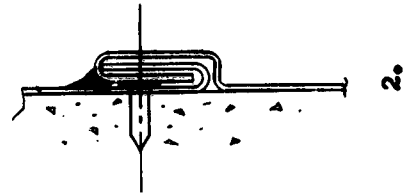
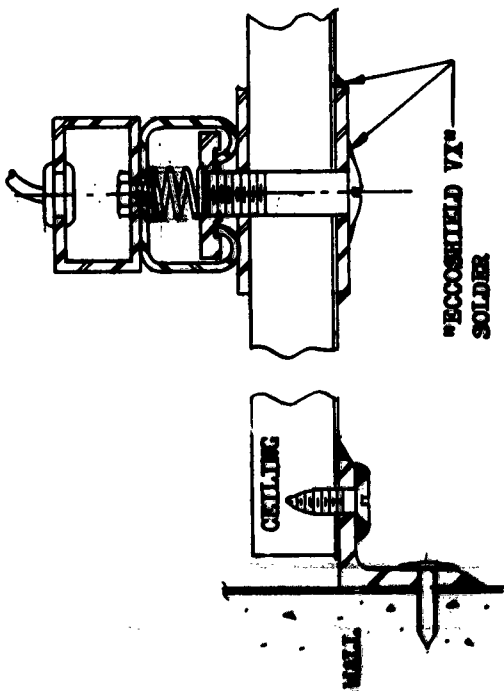
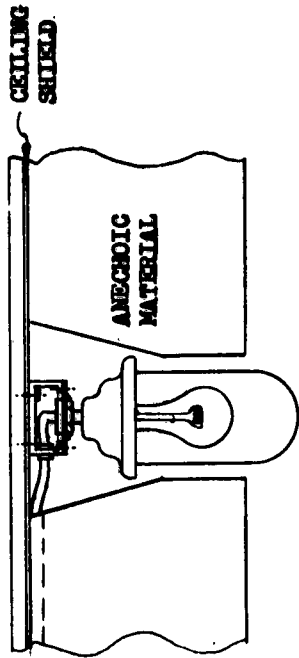


Figure 1. CONSTRUCTION DETAILS

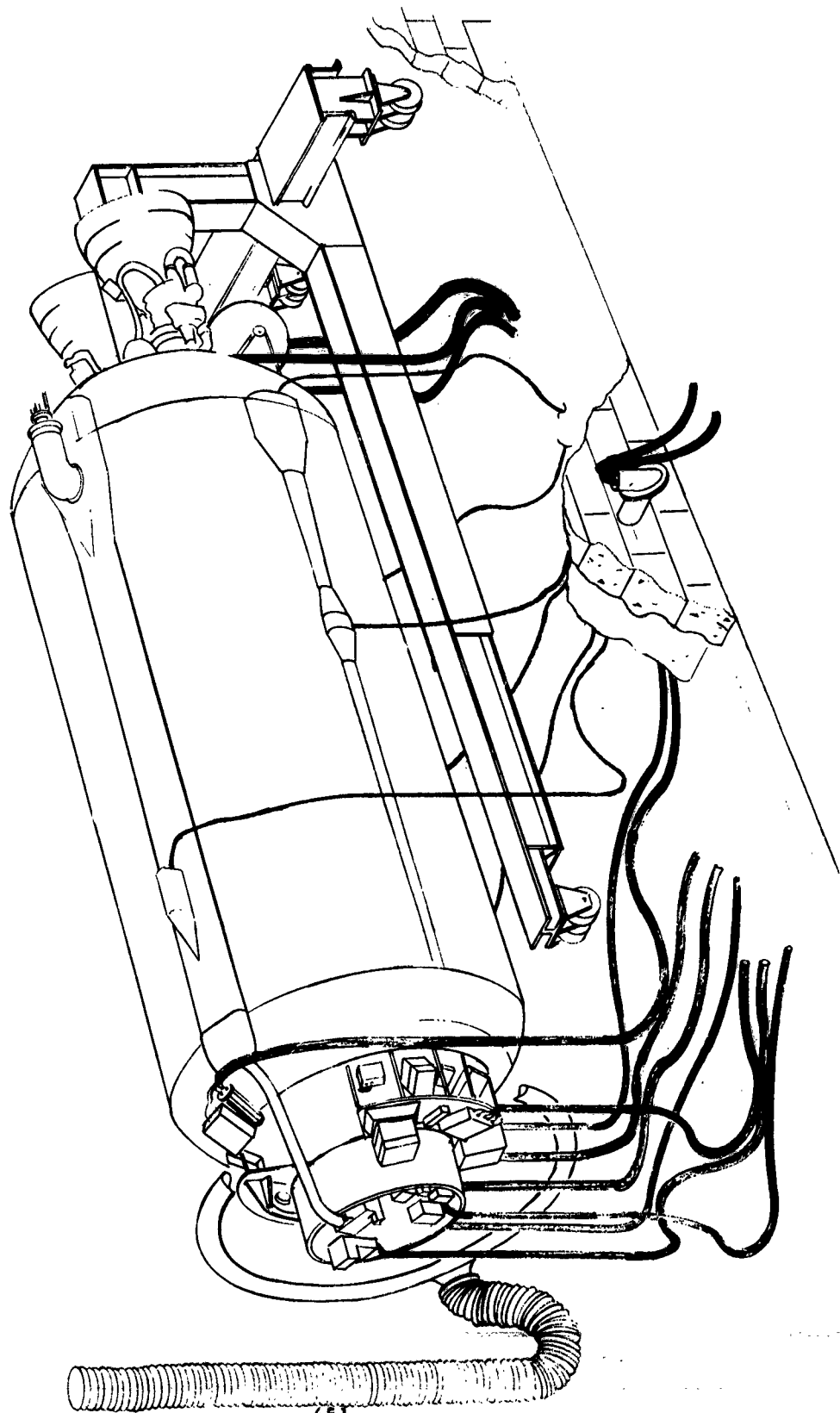
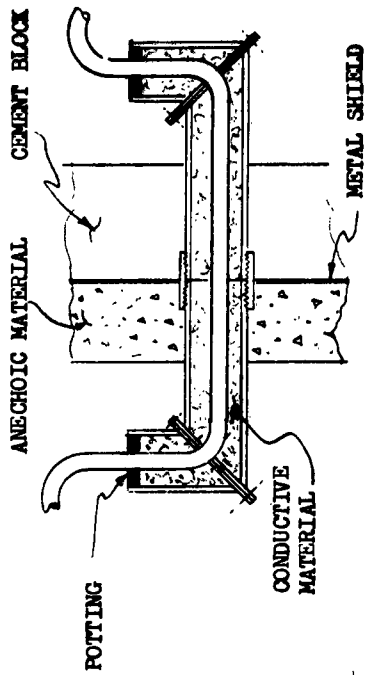


Figure 2. VEHICLE UNDER TEST



-652-

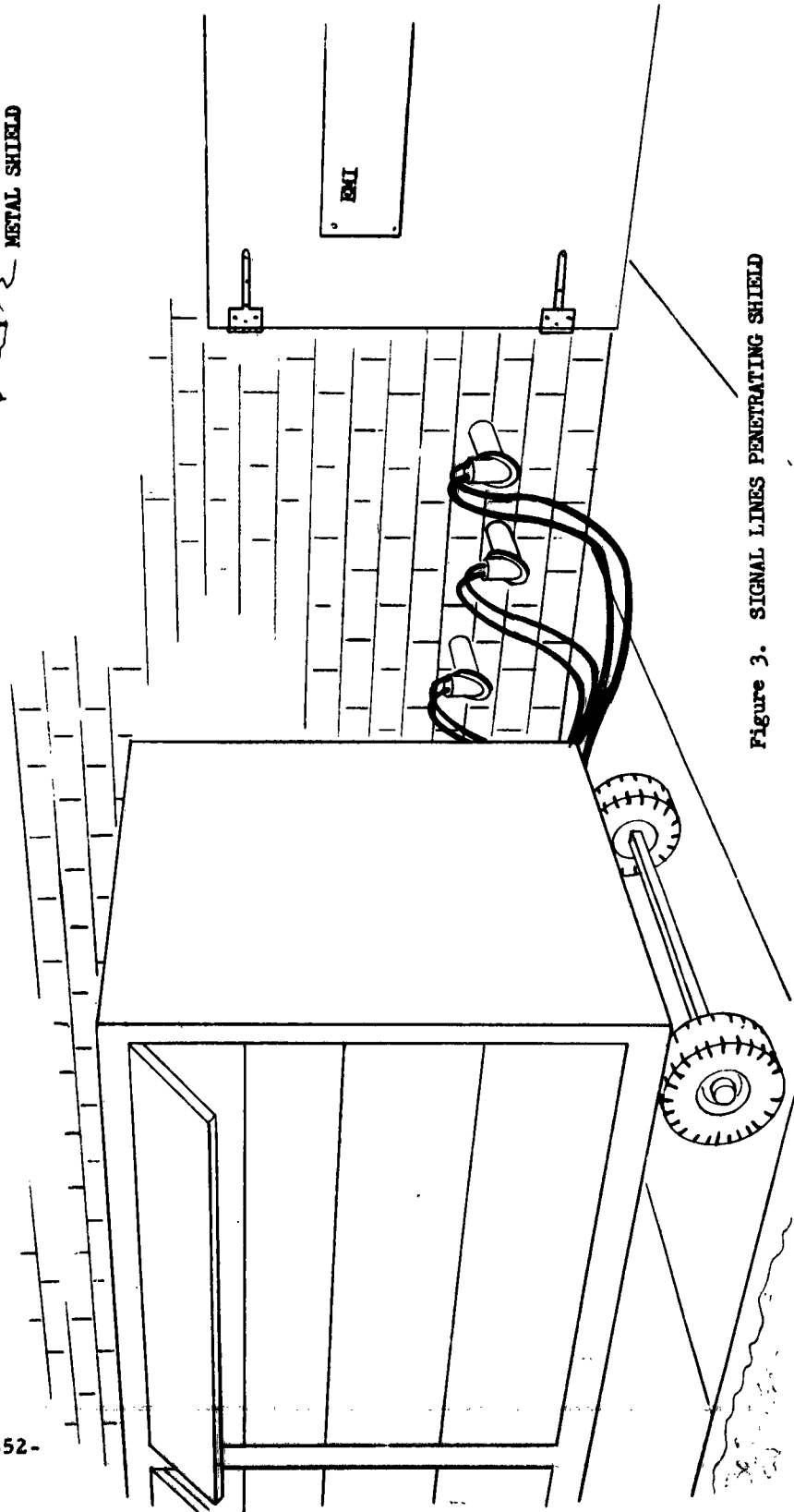


Figure 3. SIGNAL LINES PENETRATING SHIELD



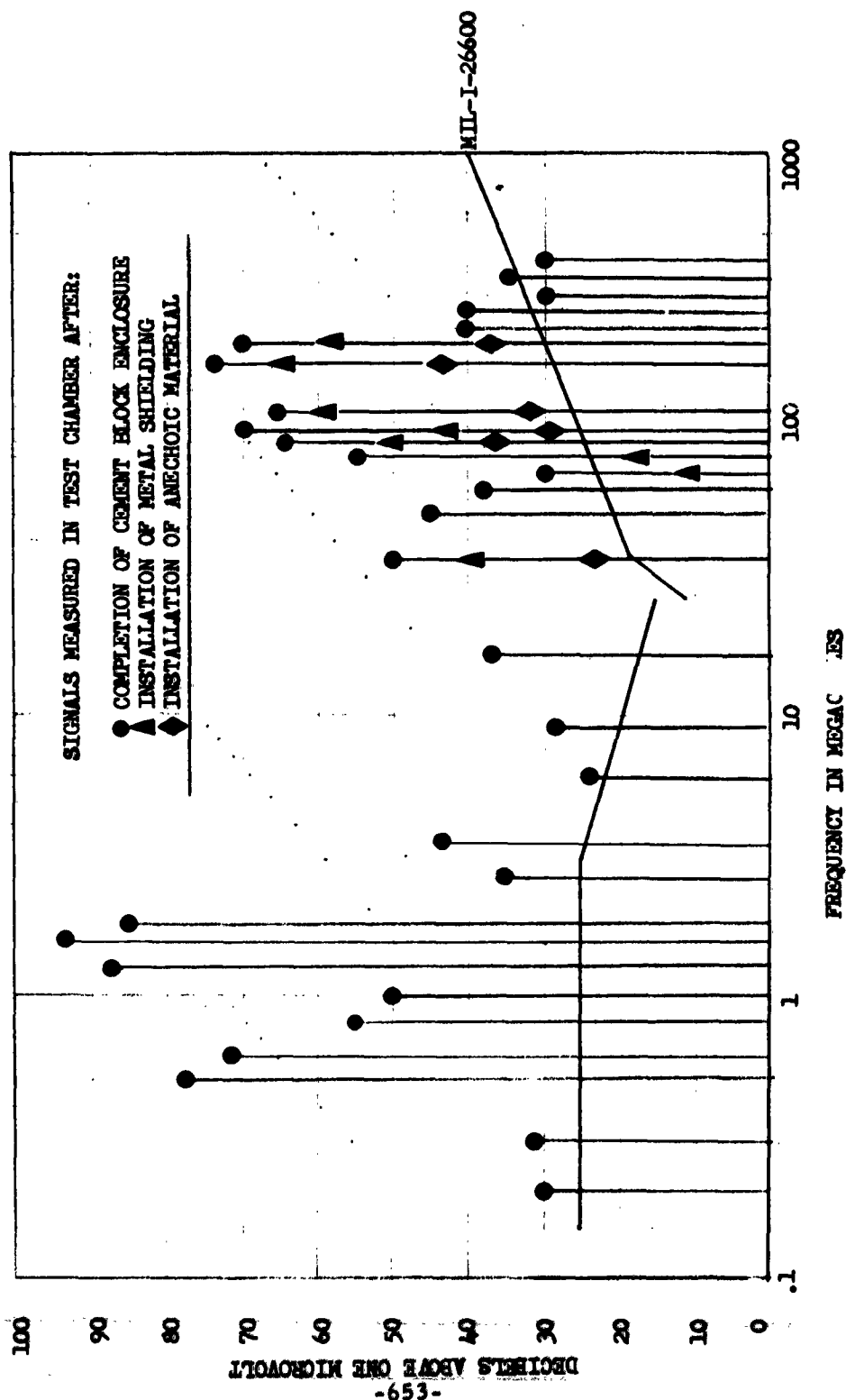


Figure 4. EVALUATION OF FACILITY DURING CONSTRUCTION

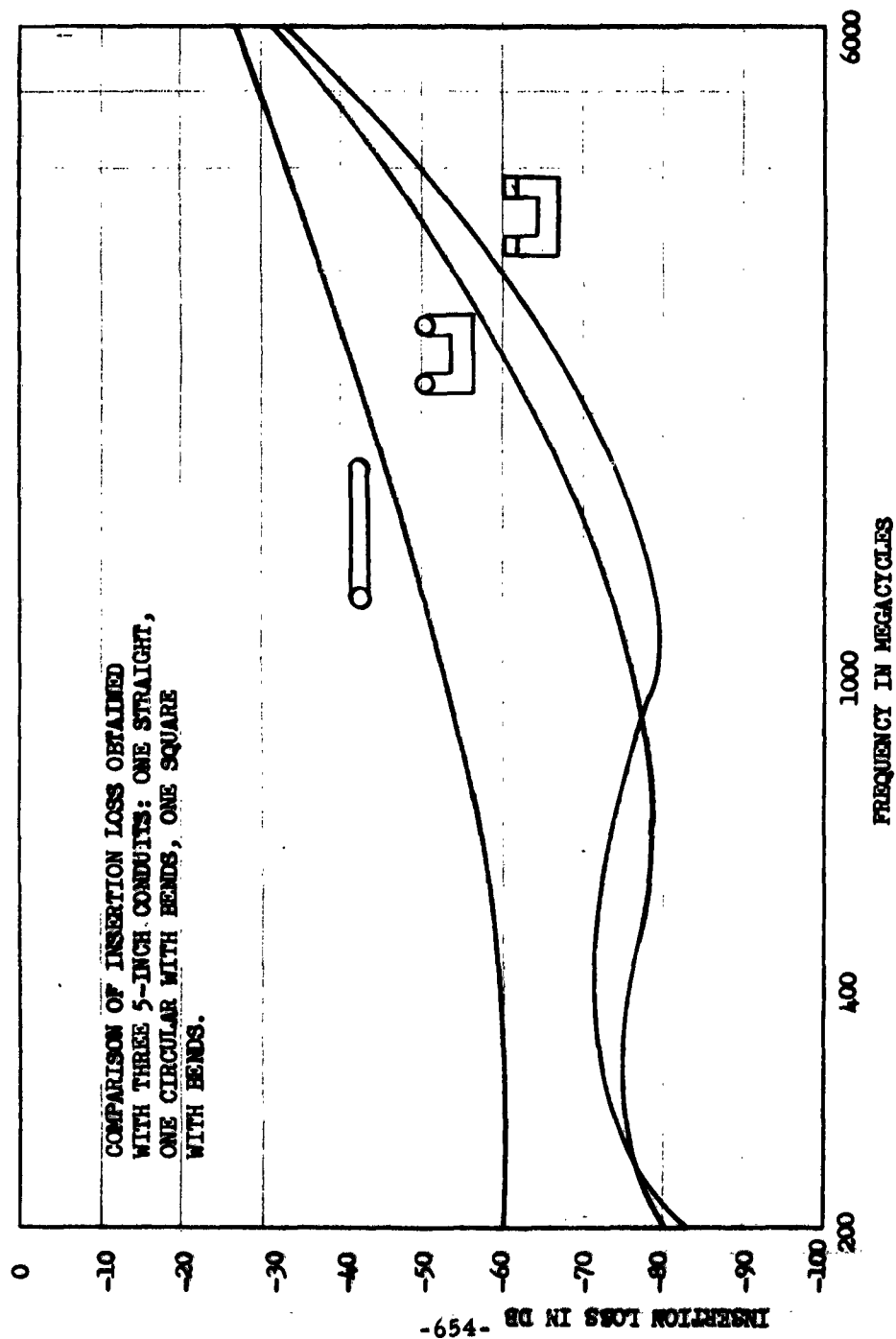


Figure 5. INSERTION LOSS OF OPEN CONDUITS

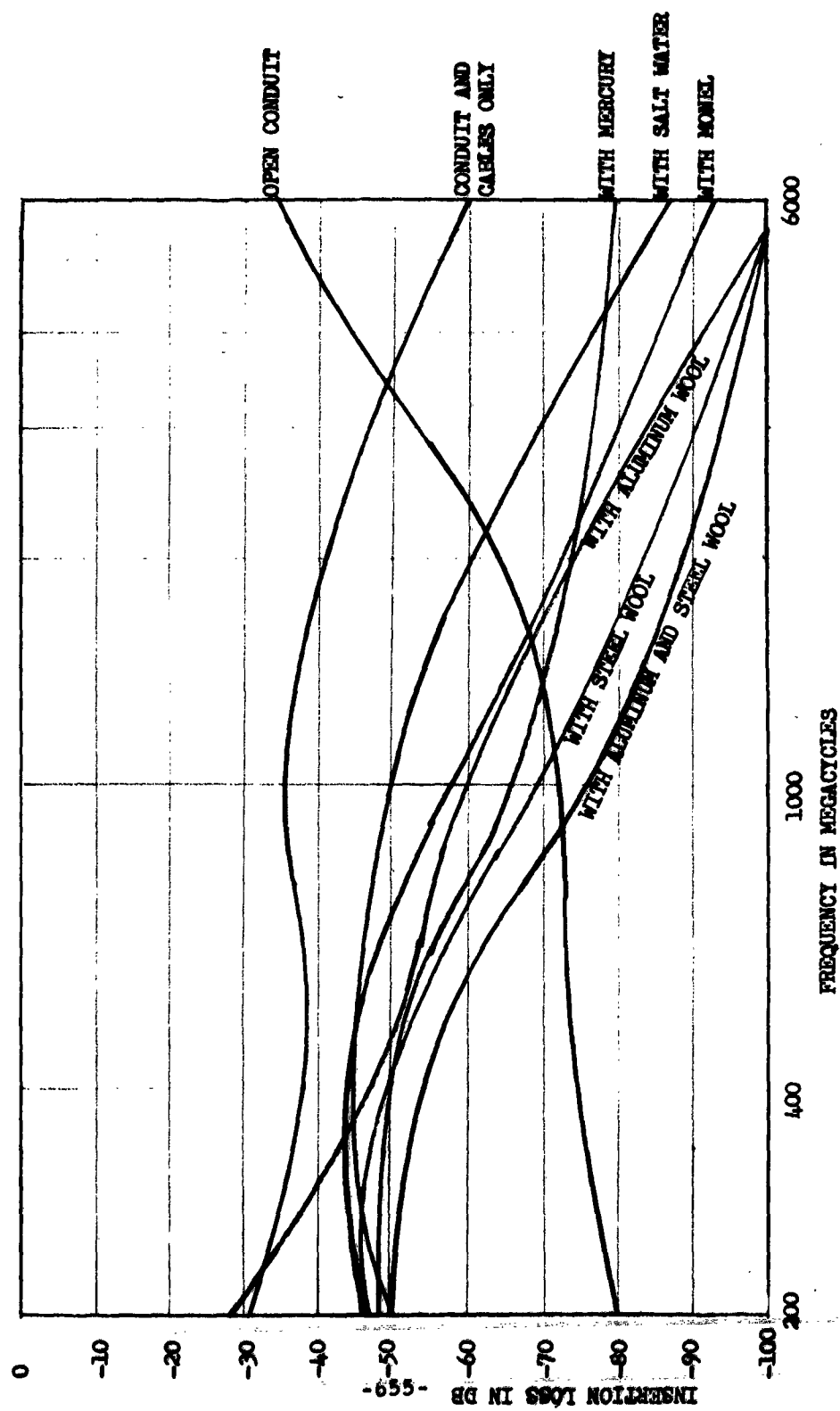


Figure 6. INSERTION LOSS OF ROUND CONDUIT WITH CONDUCTIVE MATERIALS

## PROPAGATION IN ABSORBENT-MATERIAL-LINED CAVITIES

J. W. Wright and W. E. White  
U. S. Naval Research Laboratory  
Washington, D. C.

Abstract. - Attempts to analyze microwave darkrooms in terms of "free space" transmission concepts are often unsuccessful. Experimental results are given for several darkroom models with various types of absorbent material, which illustrate the nature of the problem. Hence, we are studying modes of propagation which are more or less unique to absorbent-material-lined cavities. It is found, both theoretically and experimentally; e. g., in tunnel-like darkrooms, that a waveguide type mode can propagate with little attenuation. In fact, the "better" the absorbent material lining the tunnel, the lower the attenuation. Phase and amplitude measurements on such modes and information on how they are excited are presented in detail. The effect of these and other modes of propagation on the performance and evaluation of microwave darkrooms is discussed.

### I. INTRODUCTION

An intelligent use of the microwave anechoic chamber or darkroom certainly requires a rather detailed knowledge of the way in which electromagnetic energy propagates within such a darkroom. This is all the more true as, in recent years, materials have become commercially available for which claims of 40 - 50 db reduction of reflected energy are made. That these claims are in some sense justified can be seen in Figure 1. Since these data are taken from near-field measurements, it cannot be inferred that the total scattering cross section is 40 - 50 db below the absorption cross section for 2-ft. squares of the material. It is worth noting, however, that, at least for angles of incidence near normal, there is no gross "non-specular" reflection at bistatic angles away from normal, and that the behavior of the pyramidal material in this respect is, if anything, more regular than that of the other material.

It is just such results as these which make it tempting to analyze the behavior of darkrooms on the basis of geometrical or physical optics assuming specular reflection. Such attempts meet with considerable success in many practical situations, but sooner or later their inadequacy becomes apparent. There are, no doubt, as many demonstrations of the failure of the specular reflection approximation as there are investigators of the problem. We find the following example particularly convincing.

Figure 2 shows a radar cross section measurement of an object which has a forward scattering cross section large compared to its backscattering cross section. The darkroom is a figure of revolution generated by an exponential spiral, and the absorbent material is the foam pyramid type. The exponential spiral has the property that any ray emanating from the center (where the target in Figure 2 is placed) impinges on the walls of the darkroom at the same angle of incidence, which is  $15^\circ$  in this case. At a second bounce, the angle of incidence nowhere exceeds  $40^\circ$  and no ray returns to the vicinity of the horn without at least two encounters with the darkroom walls.

As the target is moved along the axis of the darkroom in the vicinity of the center, the interference between the backscattered energy and the "splash" (energy which, having been scattered by the target, has encountered a darkroom wall at least once) is measured. Analysis of this interference pattern yields the backscatter and the splash separately. If  $R$  is the range, the former varies as  $\frac{1}{R^4}$  as in free space and the latter roughly as  $\frac{1}{R^2}$ . For a target with a ratio of back- to forward-scattering cross section of -40 db, the two become equal at a range,  $R_0$ , of 20 - 25 cm from the horn. Since this distance is still small compared to the dimensions of the darkroom, it is perfectly clear that the reflection cannot be "specular." If it were considered that the splash could come from one or more images, and since the measured specular reflectivity is less than  $10^{-4}$  (the ratio of back- to forward-scattering cross section), the splash and backscatter could become equal only as the target approached a darkroom wall. This conclusion holds, barring focusing effects which, in the light of our experience with darkrooms of various geometrical shapes, seems highly unlikely.

This result can probably be "explained" on the basis of "non-specular" reflection, but it is not clear that our understanding of darkrooms is very greatly advanced thereby. The reason is that diffuse reflection has a precise definition only in the geometrical optics limit; in Maxwell's Theory there is really no such thing. Conversely, if one insists on using geometrical optics, then deviations from ray propagation may often be thought of as "non-specular" reflection.

In scattering theory, it is known that in Maxwell's Theory there is no such thing as a "black body,"<sup>1</sup> which is again a geometrical-optics concept. Is there then a "black" cavity? Presumably not; the real problem is to determine the true modes of propagation within absorbent-material-lined cavities and their dependence on size and geometry of cavity and the properties of the absorbent material. This latter is not trivial, for these properties may play a different role in

the cavity than they do in free space.

Adopting this viewpoint, we have studied a case in which deviations from free space propagation should be marked, readily discernible, and amenable to theoretical calculation--the case of the tunnel-like darkroom with cross-sectional dimensions not too large in free space wavelengths. This study is not entirely academic since several low frequency darkrooms of this general type have been proposed and/or built in recent years. The remainder of this paper is a brief description of this study.

## II. PROPAGATION IN TUNNEL-LIKE DARKROOMS

The simplest case to treat theoretically is that of propagation between parallel plate absorbers of high index of refraction. Both symmetric and antisymmetric, TE and TM, modes exist. As the propagation constants for all behave similarly, we will consider here only the symmetric TM mode. For this mode (see Figure 3):

$$\begin{aligned} E_z &= \sin k_y y e^{jk_z z} \\ E_y &= j \frac{k_z}{k_y} \cos k_y y e^{jk_z z} \\ H_x &= j \frac{\omega \epsilon_0}{k_y} \cos k_y y e^{jk_z z} \end{aligned} \quad (1)$$

in the region between the absorbers. If  $d$  is the distance between the absorbers,  $R_i$  the imaginary part of the plane wave voltage reflection coefficient at normal incidence for the absorbers, and if

$(k_0 d)^2 \gg 1$ ,  $R_i \ll 1$  and with  $ky = k_r + jk_i$  and  $\frac{d}{2} = a$

$$k_r a (k_r a + \tan k_r a) \approx (k_0 a)^2 \quad (2)$$

$$k_i a \approx \frac{k_r}{k_0} + \frac{2R_i (k_r a)}{(k_0 a)^2 - (k_{ra})^2} \quad (3)$$

$$k_z = k_0 - \frac{k_r^2 - k_i^2}{2k_0} - j \frac{k_r k_i}{k_0} \quad (4)$$

For the lower order modes, when  $k_0 a$  is sufficiently large,

$$k_r \approx \frac{n\pi}{d} \quad n \text{ odd} \quad (5)$$

For perfectly matched absorbing walls  $R_i = 0$ , the attenuation for a given mode depends only on the geometry of the tunnel and the field falls to  $\frac{1}{e}$  of its value in a distance proportioned to

$$d \left( \frac{d}{\lambda_0} \right)^2$$

For imperfectly matched walls the attenuation is greater.

The measurements to be described below were made in square tunnels inasmuch as this is a more characteristic dark-room configuration. Since Equation (3) is the same for both TE and TM modes, we will assume that it applies to  $k_x$  and  $k_y$  for the square tunnel modes. Then if (5) holds for both  $k_x$  and  $k_y$  separately and

$$(k_r a)^2 \ll (k_0 a)^2$$

$$k_z \approx k_0 - \frac{(n^2 + m^2)\pi}{4d^2/\lambda_0} - j \frac{(n^2 + m^2)}{2} \left[ \frac{\lambda_0^2}{d^3} \right] \left[ 1 + \frac{16R_i}{k_0 d} \right] \quad (6)$$

$n, m \text{ odd}$

### III. MEASUREMENTS IN SQUARE TUNNELS

Phase and amplitude measurements have been made at X-band in 3-inch and 6-inch square tunnels lined with a resonant absorber and a foam pyramid absorber. The fields were probed both with a small dipole probe and by measuring the backscattering from small metal spheres. The measurements by dipole probe are consistent with those by backscattering and both are consistent with theory if it is assumed that, with linear detection, one detects a signal proportional to the field with the dipole probe and proportional to the square of the field with backscattering.

Figure 4 shows the result of a backscattering type measurement of the field along the axis of a 3-inch square tunnel lined with resonant absorber. The maximum and minimum at short ranges can be explained, as will be seen below, as the interference between modes. At long ranges, the field falls off exponentially. If  $\frac{1}{a}$  is the distance in which the field falls to  $1/e$  of its value, then we get from Figure 4,  $1/a = 39$  cm. The resonant absorber is of the "perfect match" type, but due to variations in thickness and composition,  $R_1$  is undoubtedly not precisely zero. Since  $1R_1^2 \approx 10^{-2}$ , then in any case  $0 \leq R_1 < 10^{-1}$ . From Equation (6) we compute for  $\frac{1}{a_{11}}$  the attenuation constant for the first mode,  $37 \text{ cm} < \frac{1}{a_{11}} < 41 \text{ cm}$ .

Figure 5 shows the results of a similar measurement in a 6-inch square tunnel lined with a resonant absorber. The open circles have been computed from the mode theory assuming the existence of only the first order mode and the two lowest order symmetrical modes. The theoretical values for attenuation constant are  $300 \text{ cm} < \frac{1}{a_{11}} < 330 \text{ cm}$  and  $60 \text{ cm} < \frac{1}{a_{13}} = \frac{1}{a_{31}} < 66 \text{ cm}$ . The experimental values of 250 cm and 55 cm, respectively, are considered to be in satisfactory agreement with the computed values.

Figure 6 gives field profiles at the ranges of the first major minimum and maximum in Figure 5. The open circles are again computed from the mode theory. The computed values at the minimum are, of course, rather critically dependent on the precise values of the parameters chosen. A better fit at the minimum could be forced by small changes in the parameters. This, however, would be largely an exercise in curve-fitting and would not really any better demonstrate the applicability of the mode theory. Figure 7 gives a profile of the phase at the range of the second major minimum. The extremely uniform phase is, of course, a characteristic of the tunnel modes. The deviation at the sides of the tunnel is very likely a failure in the measuring technique.

Figures 8, 9, and 10 show the, by now, familiar type data for a 6-inch tunnel lined with foam pyramid absorber. We have not so far devised an approximate boundary condition, accurate enough to make detailed mode calculations for this material useful. The experimental data at large range show the typical profiles for the fundamental tunnel mode with a very small field in the plane of the tips of the pyramids. The attenuation of this fundamental mode is, however, apparently even less than that calculated for the perfectly matched case. At the range of



approximately  $d^2/\lambda_0$ , the pyramided tunnel exhibits a minimum rather than a maximum as was the case for the resonant absorber. Furthermore, the profiles at this range reveal a near maximum at the pyramid tips. This shows that, in addition to the tunnel modes previously described, there exist modes which have a considerable penetration into the walls and suffer, in consequence, a greater attenuation. This then may explain the fact that the total energy, which has been transferred into the fundamental tunnel mode, is (for the same size transmitter) about 10 db less in the pyramid-lined tunnel than in the tunnel lined with resonant material.

So far we have treated the absorbent-lined tunnel more or less as a curiosity to be studied as an aid to understanding actual darkrooms, but it can also be a useful tool. Figure 11 shows the pattern of a "dipole in a cavity" antenna with a 3-inch square ground plane taken at a range of about  $2/3 \frac{d^2}{\lambda_0}$  in a 6-inch square pyramid

lined tunnel. The open circles are measurements made on a free-space range. Note that differences between the two appear only at a power level 15 - 20 db below the peak in the pattern. This agreement is probably the result of the uniform amplitude and phase across the tunnel.

#### IV. CONCLUSIONS

We have demonstrated the existence of unique modes of propagation in absorbent lined tunnels and elucidated some of their properties. We need now to obtain a theoretical description of the modes in pyramid lined tunnels and to investigate the ways in which these modes are excited. We should then be able to determine the importance of these modes in actual darkroom practice.

#### REFERENCES

1. Van de Hulst, H. C., "Light Scattering by Small Particles," p. 269 (book), John Wiley and Sons, Inc., New York (1957).

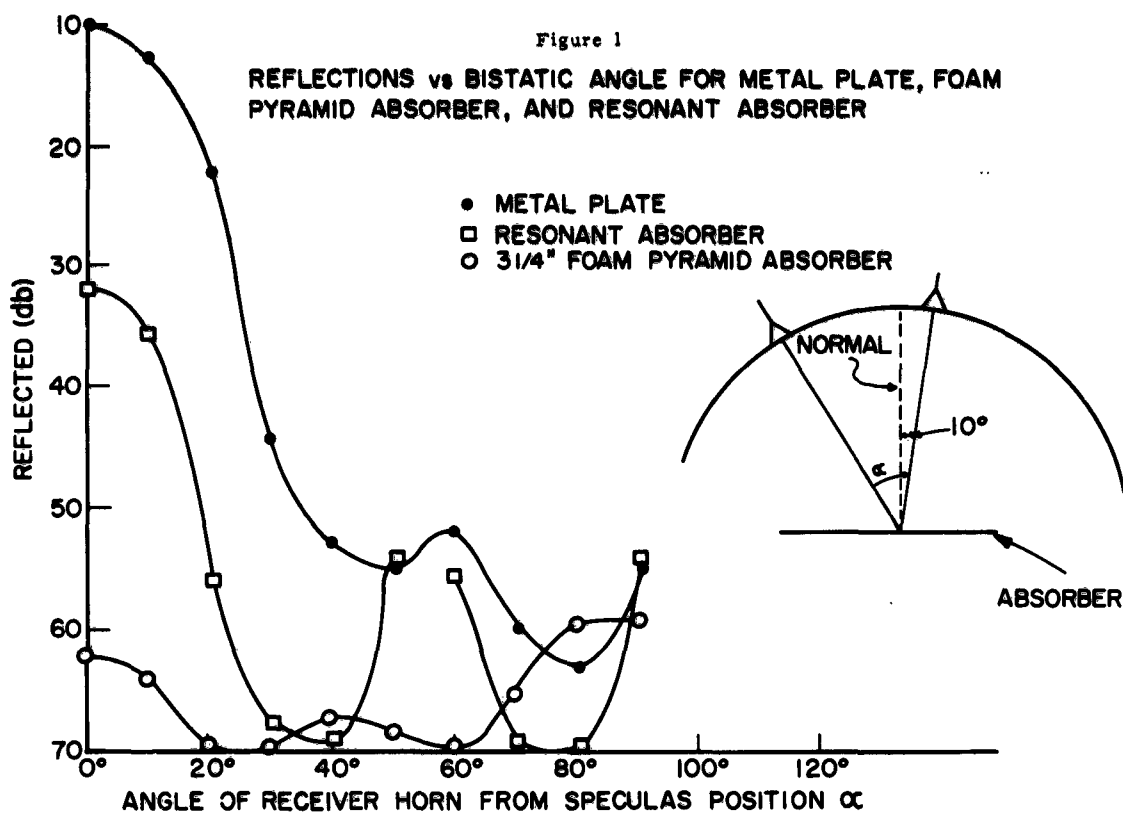


Figure 2

**BACK SCATTERING MEASUREMENT IN AN  
EXPONENTIAL SPIRAL DARKROOM**

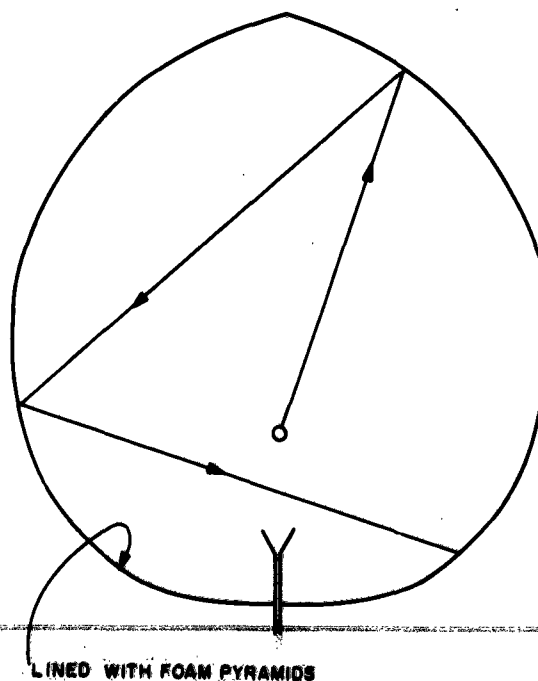


Figure 4  
BACK SCATTERING MEASUREMENT OF THE FIELD ON  
THE AXIS OF A 3" SQUARE TUNNEL LINED WITH  
RESONANT ABSORBER

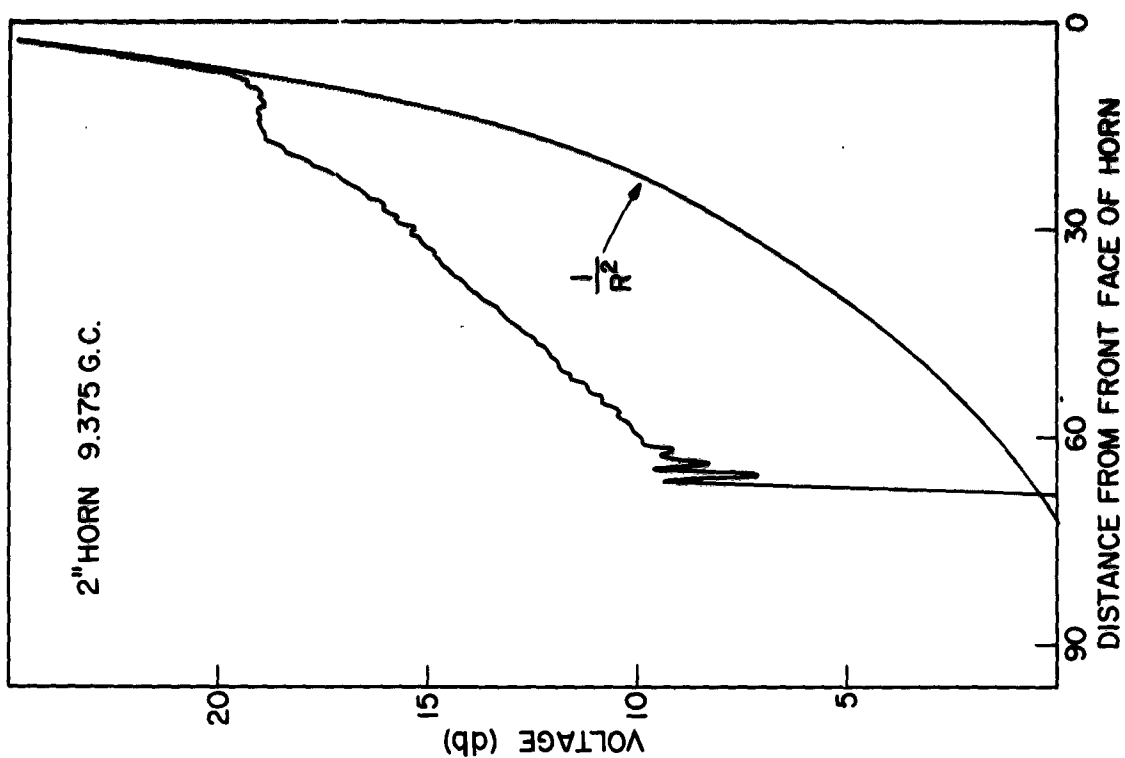


Figure 3  
T-M MODE BETWEEN PARALLEL PLATE ABSORBERS

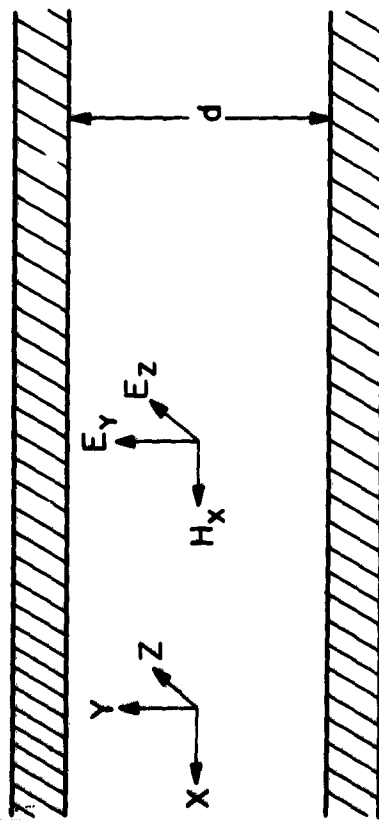


Figure 5

BACK SCATTERING MEASUREMENT OF THE FIELD ON THE AXIS OF A  
6" SQUARE TUNNEL LINED WITH RESONANT ABSORBER

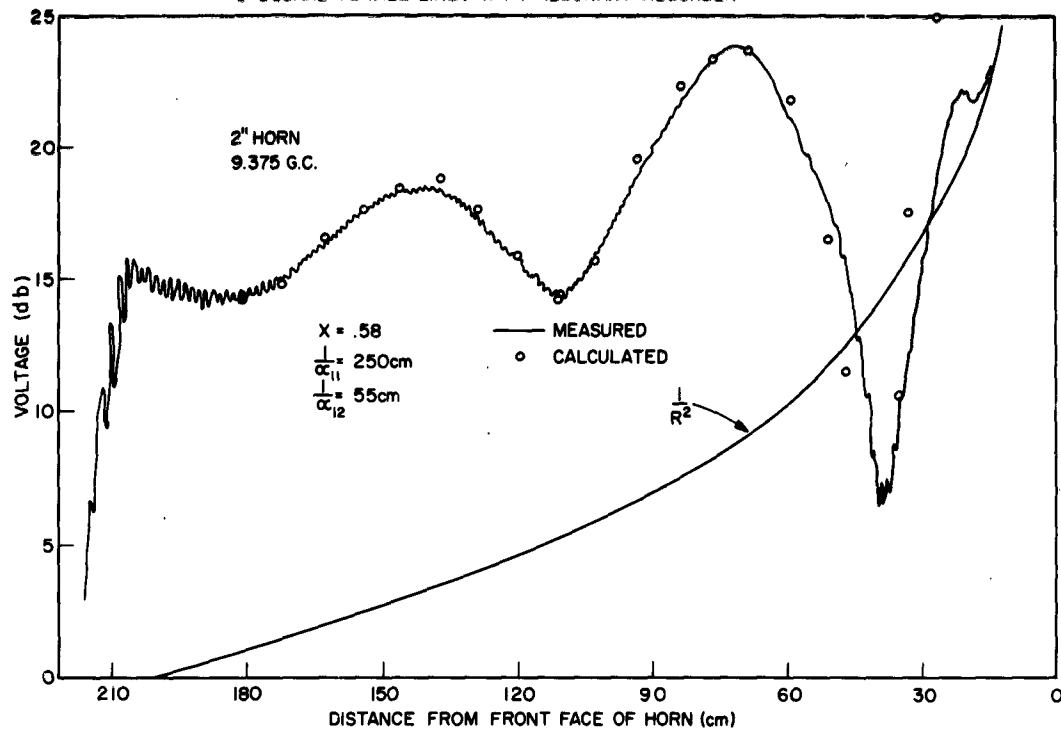


Figure 6

PROFILES OF THE FIELD IN A 6" SQUARE TUNNEL LINED WITH RESONANT  
ABSORBER AT RANGES OF 35 AND 70cm.

2" HORN 9.375 G.C.

ARROW (↑) INDICATES WALL

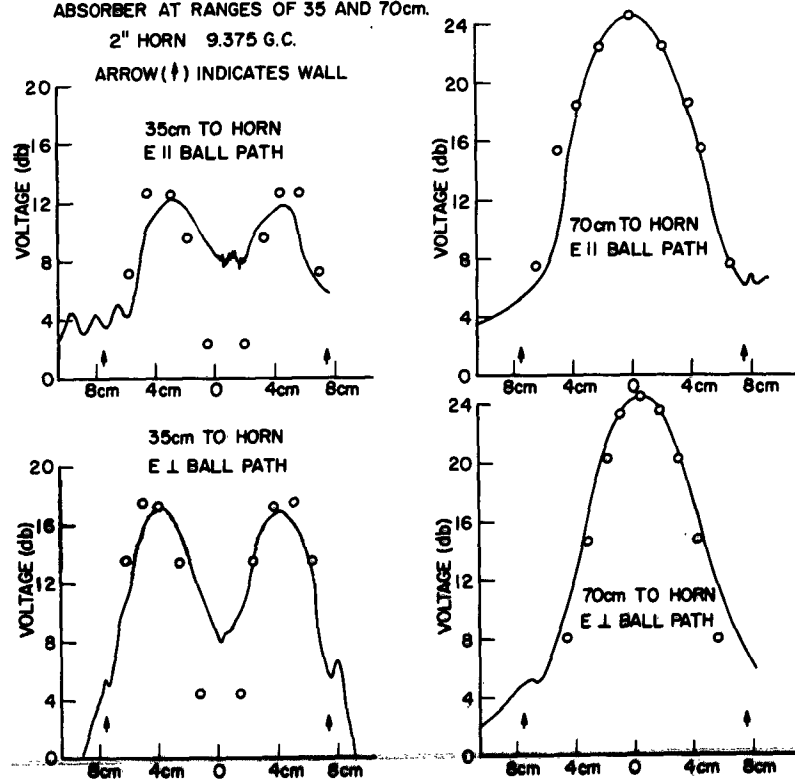


Figure 7

PROFILE OF THE PHASE OF THE FIELD  
IN A 6" SQUARE TUNNEL LINED WITH  
RESONANT ABSORBER

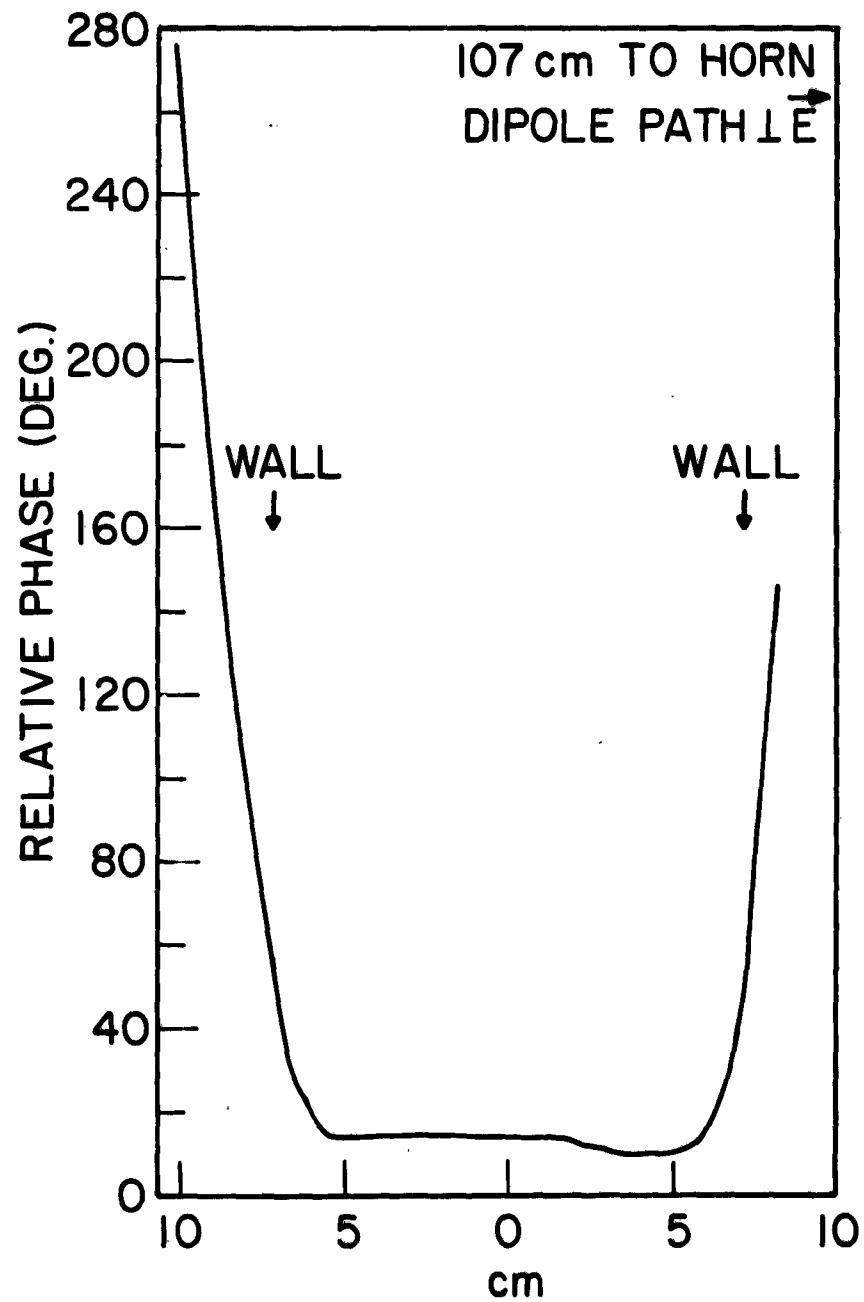


Figure 8

BACK SCATTERING MEASUREMENT OF THE FIELD ON THE AXIS OF A  
6" SQUARE TUNNEL LINED WITH RESONANT ABSORBER

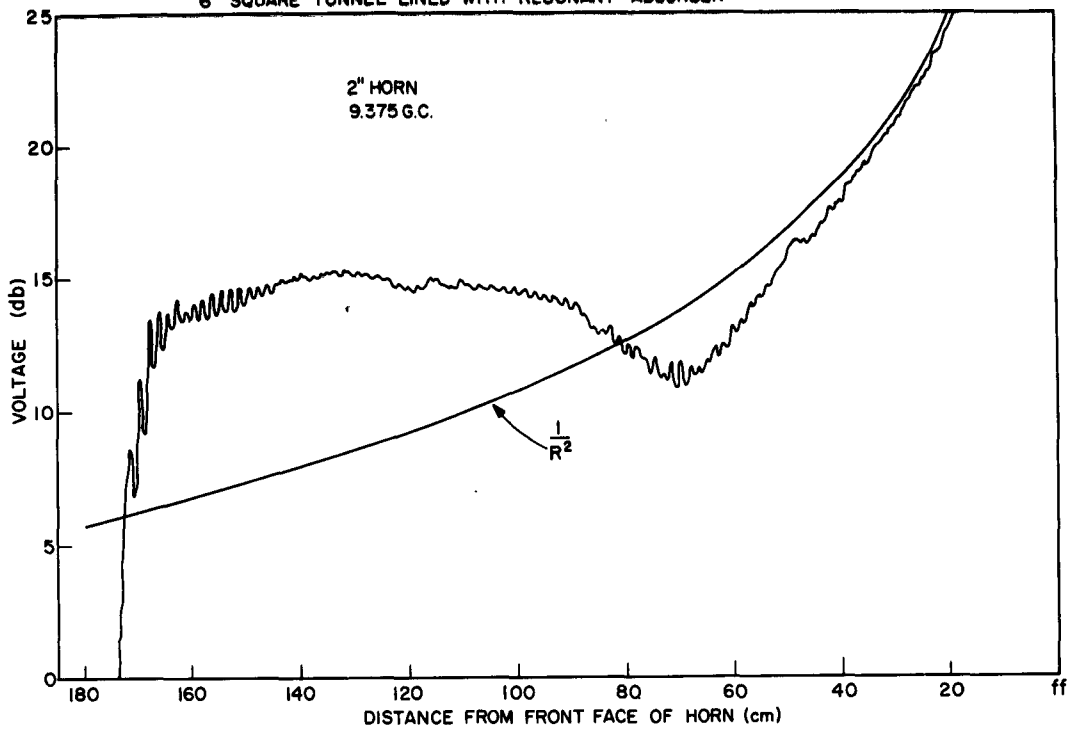
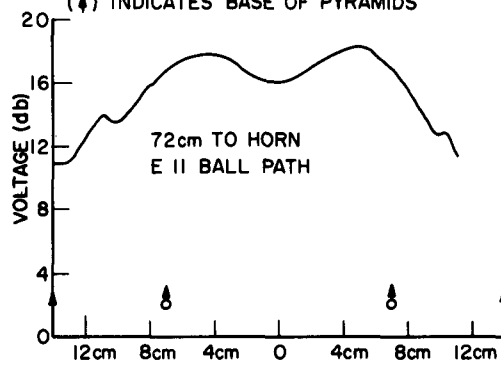


Figure 9

PROFILES OF THE FIELD IN A 6" SQUARE TUNNEL LINED WITH FOAM PYRAMID ABSORBER  
1" HORN 9.375 G.C.

(↑) INDICATES BASE OF PYRAMIDS



(↑) INDICATES POINTS OF PYRAMIDS

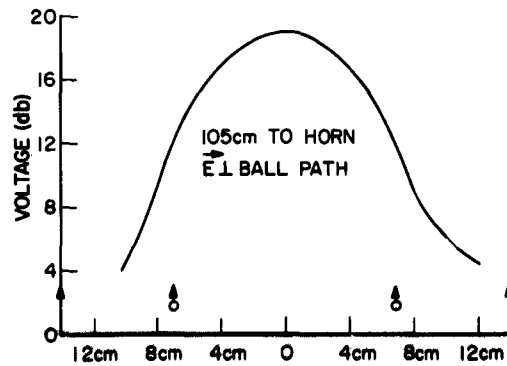
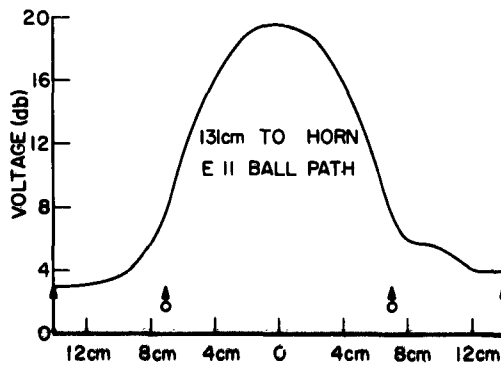
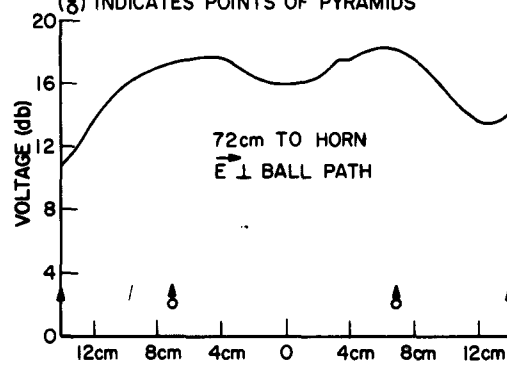


Figure 10

PROFILE OF THE PHASE OF THE FIELD IN A 6" SQUARE TUNNEL  
LINED WITH FOAM PYRAMID ABSORBER

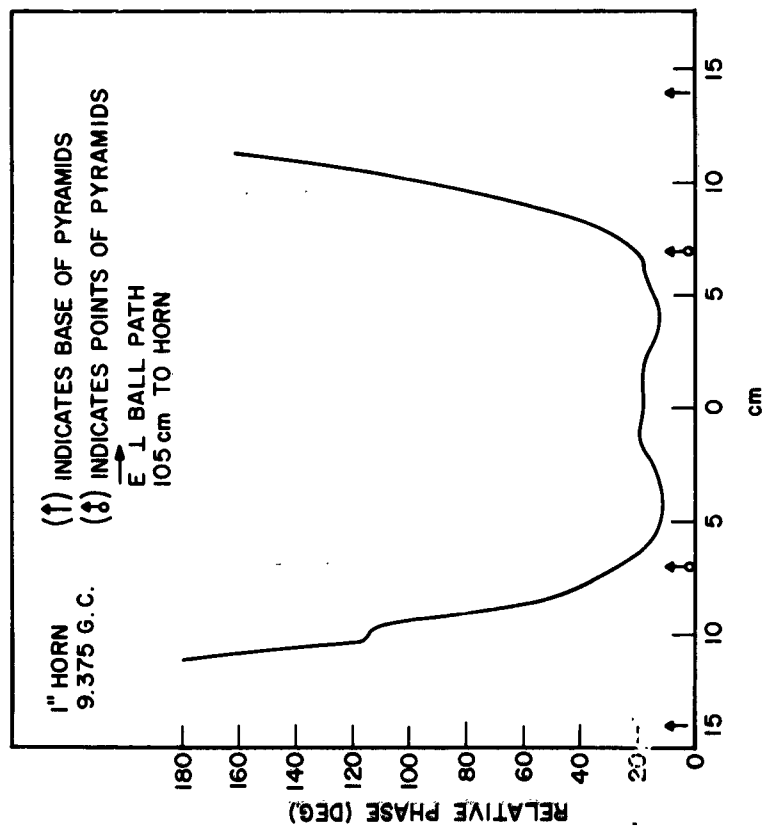
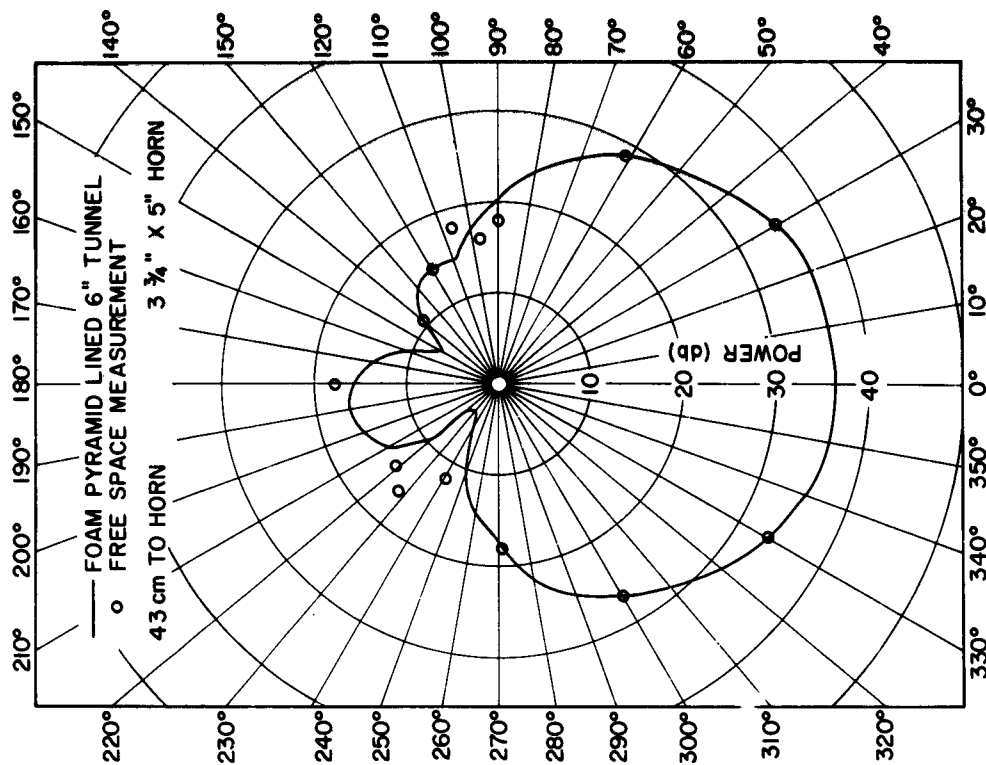


Figure 11

PATTERN OF A "DIPOLE IN A CAVITY ANTENNA"



## A SPECTRUM ANALYZER WITH 2 GC DISPLAY

A. Fong, H. L. Halverson,  
G. C. Jung and R. W. Anderson  
Hewlett-Packard Company - Microwave Lab  
Palo Alto, California

Abstract. - Frequency spectrums up to 2 gc wide can be displayed in a spectrum analyzer using a 2 gc IF amplifier and 2-4 gc backward wave local oscillator. For displays 10 mc to 2 gc wide, the stability of the BWO is sufficient to allow use of resolutions 10 kc to 1 mc. For much narrower displays of 100 kc to 10 mc where narrower resolution is desired, the BWO can be phase locked to a harmonic of a very stable low frequency reference oscillator. Frequency spectrums within the range of 10 mc to 40 gc can be analyzed.

### I. INTRODUCTION

Requirements for a wide sweep spectrum analyzer for simultaneous viewing of many signals have existed for some time. This analyzer should be capable of locating and identifying signals over a wide frequency spectrum. It should be able to magnify the spectrum for more thorough analyzing with stable calibrated sweeps and filters. It should be relatively free of spurious signals and have flat response with wide dynamic range.

### II. DESIGN CONSIDERATIONS

A block diagram is shown in Fig. 1. The RF tuning unit contains the input attenuator, mixers, BWO, sweeping power supply, 180 and 1800 mc local oscillators, 2 gc IF amplifier, 200 mc IF amplifier, and 20 mc IF output. The RF conversion is accomplished by a crystal mixer, a 2 gc IF amplifier and a BWO local oscillator operating over the range of 2-4 gc. The 2 gc IF signals are amplified and mixed with the 1.8 gc source to a second IF of 200 mc. The 200 mc IF signal is amplified and mixed with a 180 mc local oscillator to give a final IF signal of 20 mc. Note that the 1.8 gc source is derived from the 10th harmonic of the 180 mc local oscillator.

As an alternative, one can use the 200 mc IF amplifier following the input mixer. This allows signals near 2 gc to be analyzed. It also offers 5 to 10 db more sensitivity because of the lower noise figure of the 200 mc IF amplifier. The limitation in using the 200 mc IF amplifier is that the images are only 400 mc apart and each signal will appear twice on wide sweep displays.

The display unit contains the IF attenuator, bandpass filters, vertical display shapers, 20 mc IF amplifier, detector,



video amplifier and a 5" cathode ray tube. This unit is designed with solid state components, except for the CRT. The input consists of a 0-80 db attenuator with 1 db steps. The bandpass filters controlling the resolution follow. These have accurately controlled bandwidths of 1 kc, 3 kc, 10 kc, 100 kc and 1 mc. They can be operated automatically during search operations; a switching logic chooses the optimum filter depending on the sweep rate and sweep width giving an automatic resolution control. Manual selection of the filters is available for special application.

Three 6 cm vertical displays are available; linear, logarithmic and power. The log and power displays are formed by the shaping of a feedback network which drive a current controlled PIN diode attenuator. The accuracy of the log display is about  $\pm 1$  to 2 db over a 60 db dynamic range.

A 5" cathode ray tube with internal graticule displays the information with excellent linearity.

### III. RF TUNING RANGE

The input coaxial mixer is sensitive to all signals between 10 mc and 12.4 gc, when no preselection is used. Looking at Fig. 2 for example, when the LO is sweeping through 3 gc, signals at 1, 4, 5, 7, 8, 10, 11 and 13 will appear on the same point of the CRT display. By the use of an external 2 gc low-pass filter all signals below 2 gc can be seen without interference. With a 2-4 gc bandpass filter, signals between 2-4 gc can be seen without interference. The heavy lines indicate bands of frequencies where external filters can be used to obtain interference free bands.

With signals larger than -30 dbm, the higher order images can be generated within the mixer. The most serious set is the one caused by

$$f_o - f_s = \pm f_{if}/d$$

where the beat frequency is a sub-harmonic of the IF and the non-linearity of the mixer generates a signal frequency equal to the IF. Figure 3 is identical to Fig. 2 with several sets of higher order images indicated. With proper design of the input mixer and proper assignment of gain in the successive stages these responses can be held to a minimum. Typically, for 1 milliwatt into the mixer these responses are -42 db for  $d = 2$ , -48 db for  $d = 3$ , -52 db for  $d = 4$ . Therefore, with 1 mw input, a 40 db dynamic range can be easily achieved. These responses decrease rapidly as the input power level is decreased. For inputs less than -30 dbm these spurious responses are more than 60 db below the main response, therefore, a 60 db dynamic range is easily achieved.

A sketch of the coaxial mixer for input frequencies up

to 10 gc is shown in Fig. 4. Its response is typically flat to  $\pm 3$  db over a 2 gc range or  $\pm 1$  db over a 200 mc range, under the condition that the detection is done within the same harmonic of the local oscillator. This mixer is contained within the analyzer and is preceded by a 0 to 60 db resistive coaxial attenuator. The insertion loss of the attenuator at zero db is small, so that direct input to mixer is accomplished through it. Separate connectors or patch cables are not necessary for attenuator operation.

A waveguide X-band mixer has been developed to cover 8.2 to 12.4 gc. Fig. 5 shows it connected to the analyzer with a single coaxial cable for convenience. The LO power is delivered through cable to the mixer, and the IF signal is fed back to the analyzer in the same cable. Selective filtering separates the two signals inside the analyzer. The external mixer has the advantage of being able to operate remotely. In general, it is much easier to connect with coax cable rather than with waveguide.

A wide band waveguide mixer was developed for the 12.4 to 40 gc range. This covers 3 waveguide bands, 12.4-18, 18-26, 26-40 gc. The basic mixer is in ridged waveguide, while three transitions are used to adapt to the different waveguide sizes. It also connects to the analyzer through the same cable as described for the X-band mixer.

#### IV. SIGNAL IDENTIFIER

When an operator uses this analyzer or any other analyzers with a direct mixer input, it is often difficult to determine the frequency of input signals. As shown in Fig. 2 for one BWO frequency setting, many signals could appear on the CRT display. To simplify the problem of identification, a signal identifier has been built into this analyzer. (See Fig. 6) The method involves shifting the second LO for a predetermined displacement of the signal on the CRT display. The shift is proportional to the harmonic of the BWO; therefore, a dial which tunes the second LO can be calibrated in harmonic numbers.

In operation one would center the signal on the CRT graticule and turn the second LO dial for a given frequency displacement as marked on the CRT graticule. The dial would give the harmonic number of the BWO with which the signal is mixing. A shift of the signal to the higher frequency would indicate it is the higher image. Next, the operator would select the appropriate dial range for that harmonic. Both images are calibrated, so he chooses the correct scale and reads the indicated frequency. Finally, he may select and attach the proper input filter for the frequency range where he is working to eliminate the unwanted image and other responses.

## V. SPECTRUM DISPLAY

The spectrum scan rates are variable from 0 to 30 cps. They are accurately calibrated from 1 sec/cm to 3 ms/cm in 1, 3, 10 --- steps, which make it useful for measuring pulse time intervals.

Spectrum widths are calibrated at 100 kc, 300 kc, 1 mc, 3 mc, etc., up to 2 gc. The sweeps are very linear, so that a signal on the center of the screen will remain centered as the spectrum width is reduced for closer examination.

The sweep voltage for the BWO is furnished by a stable, low ripple, power supply. Frequency stability of the BWO is better than 10 kc which is sufficient for use with resolutions of 10 kc to 1 mc for fundamental mixing. At 40 gc where the 10th harmonic of the BWO is used, the 100 kc filter would be the narrowest usable filter. When maximum resolution is desired, the frequency of the BWO may be phase locked to a harmonic of a stable low frequency reference oscillator. In this case the residual FM of the BWO is in the order of several hundred cycles, thus allowing use of the 3 kc and 1 kc resolution filter.

Figure 7 shows the 2-4 gc BWO being phase locked to a stable 10 mc reference oscillator. The locking covers the 200th to 400th harmonic of the reference oscillator. A ramp potentiometer tunes the reference oscillator over the narrow range of each harmonic, and it is geared to the main tuning potentiometer which tunes the BWO over the entire 2-4 gc range. Each turn of the ramp pot tunes the reference oscillator by 10 mc/n while the main tuning has changed to 10 mc. ( $n = 200$  at 2 gc and 400 at 4 gc.) The phase locking is entirely automatic and the jump in locking from one harmonic to the next is hardly perceptible. Thus continuous phase locking is accomplished.

## VI. CALIBRATED RESOLUTION FILTERS

The use of accurately fixed IF resolution bandwidths gives the operator the ability to determine the peak amplitude of pulsed RF signals when the pulse repetition frequency is much less than the resolution bandwidth used. As KAMM (Rad Lab Vol. 11) points out, the displayed spectrum of a pulsed carrier is attenuated from that of a c.w. signal with equal peak amplitude by a factor of  $K\tau\Delta F$  where  $\tau$  is the effective pulse width,  $\Delta F$  is the resolution bandwidth, and  $K$  is a constant dependent on the resolution band shape. Thus by comparing the pulse amplitude with a c.w. signal from a signal generator, determining  $\tau$  from the spectral presentation and knowing  $K\Delta F$ , an instrument constant, the peak power of a pulsed carrier can be determined.

## VII. APPLICATIONS

Aside from the usual application of the Spectrum Analyzer,

such as adjustment of signal sources, detecting spurious signals, observing side bands, calibrating attenuator, wavemeter and so on, the wide spectrum displays have created new applications.

It is especially useful in spectrum signature work where the multiple responses can be eliminated by passive filters as pre-selectors. Fig. 8 shows the entire FM and TV band, the sweep is from 10 mc to 200 mc. A 2 gc low pass filter is used. Fig. 9 shows the channel 7 and an FM multiplex station. Note the video and audio components of the TV station, and the 19 kc sidebands of the FM station. (The signal at 30 kc below the carrier is an external interfering signal not associated with the station or the analyzer.)

In some applications, electronically tunable band-pass filters may be tracked in conjunction with the sweeping BWO. YIG tunable filters are now available in octave ranges from 2 to 12.4 gc. This will provide the preselection necessary for EMC-RFI work.

Harmonic generators are often used in frequency synthesizer and also with reference oscillators for phase locking, frequency locking, frequency counting and frequency calibration. Figure 10 shows the spectrum generated by a step recovery diode driving a shorted transmission line. In the application of this device, it was necessary to get a spectrum which was fairly uniform. With the wide sweep and flat response of this analyzer it was easy to see and adjust for discontinuities in the spectrum.

Very short video pulses have been difficult to analyze in the frequency domain due to restricted sweep widths and narrow resolving bandwidths of present analyzers. The wide sweep widths in conjunction with the 1 mc IF bandwidth incorporated in this instrument allows more spectrum and better dynamic range. Figure 11 shows the spectrum of a 10 ns video pulse.

Another interesting application has come from a paramp manufacturer. In adjusting a paramp it is extremely useful to be able to see the output, pump, idler and upper sideband frequencies simultaneously. Figure 12a shows the relative spectral location of these frequencies. Figure 12b shows how these frequencies appear on the spectrum analyzer. The 500 mc output is mixed with the analyzer local oscillator at 2500. The pump signal (9.6 gc), the upper sideband (10.1 gc) and idler frequency (9.1 gc) are mixed with the 3rd harmonic of the analyzer local oscillator. Now adjustments can be made to maximize the idler and output signal and minimize the upper sideband. Any other interfering spurious signals are also seen so steps can be taken to eliminate them.

#### VIII. SUMMARY

This Analyzer has increased usefulness because of its wide sweep, increased stability, fewer spurious responses, flat

sensitivity, and wide dynamic range. It can display a wide spectrum. If a signal requires more investigation, the scan can be quickly reduced to magnify the spectrum so that one can examine or identify its amplitude, modulation, and other distinctive character. Calibrated sweep widths, calibrated resolution, and calibrated sweep rates and calibrated amplitudes make the analyzer easy to use in duplicating a spectral presentation and re-establishing old data. It can be very useful in EMC-RFI analysis because it will simultaneously display functional signals as well as interfering signal.

#### ACKNOWLEDGEMENT

This development was performed at the Microwave Laboratory of the Hewlett-Packard Company. Others in the development team included R. H. Bauhaus, J. D. Cardon, G. J. Eiler, and R. F. Rauskolb. We give particular credit to our product designers R. C. Given, W. R. Hanisch, J. M. Hedquist, and E. C. Hurd. We also acknowledge E. H. Phillips, J. L. Boortz, and D. R. Veteran, for their contribution in the mechanical design. Our appreciation is also extended to A. E. Inhelder for the industrial design, and to Dr. H. C. Poulter for his advice and encouragement.

#### Reference:

Massachusetts Institute of Technology, Radiation Laboratory Series Vol. 11, Chapter 7.

Microwaves, April 1963, p. 56, Introduction to Spectrum Analyzers by Murray Feigenbaum.

Electronic, June 21, 1963, p. 44, RFI Measurement and Instrumentation by Sy Vogel.

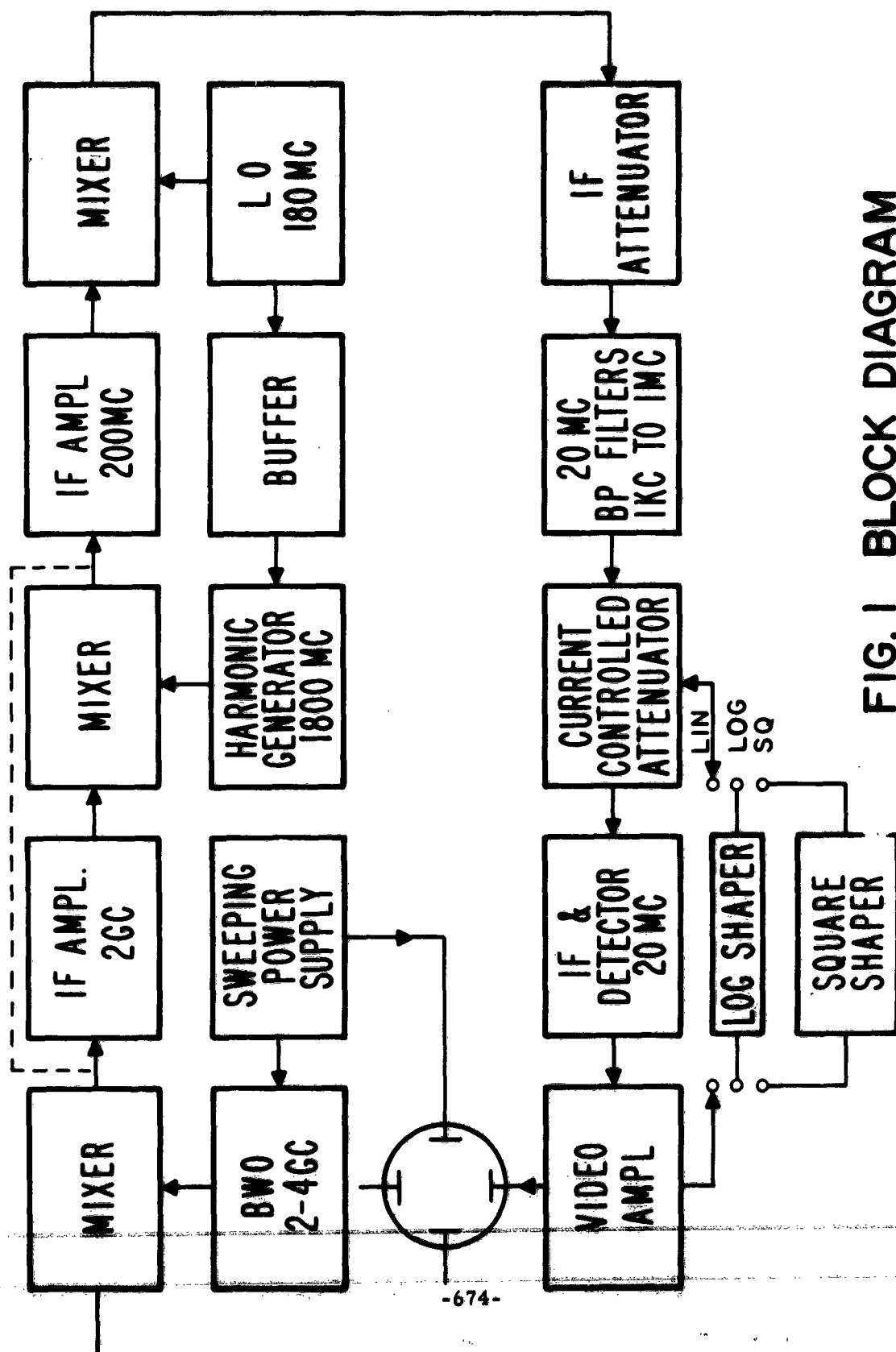


FIG. 1 BLOCK DIAGRAM

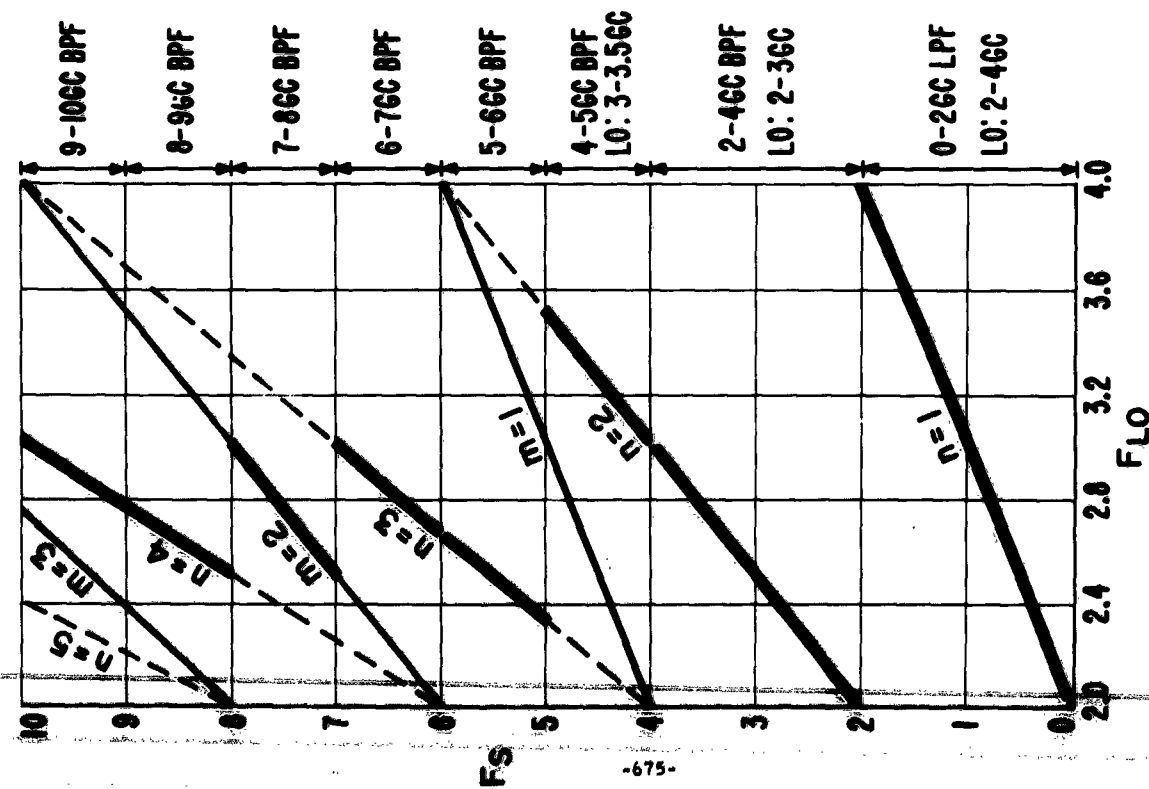


FIG. 2 RF TUNING RANGE

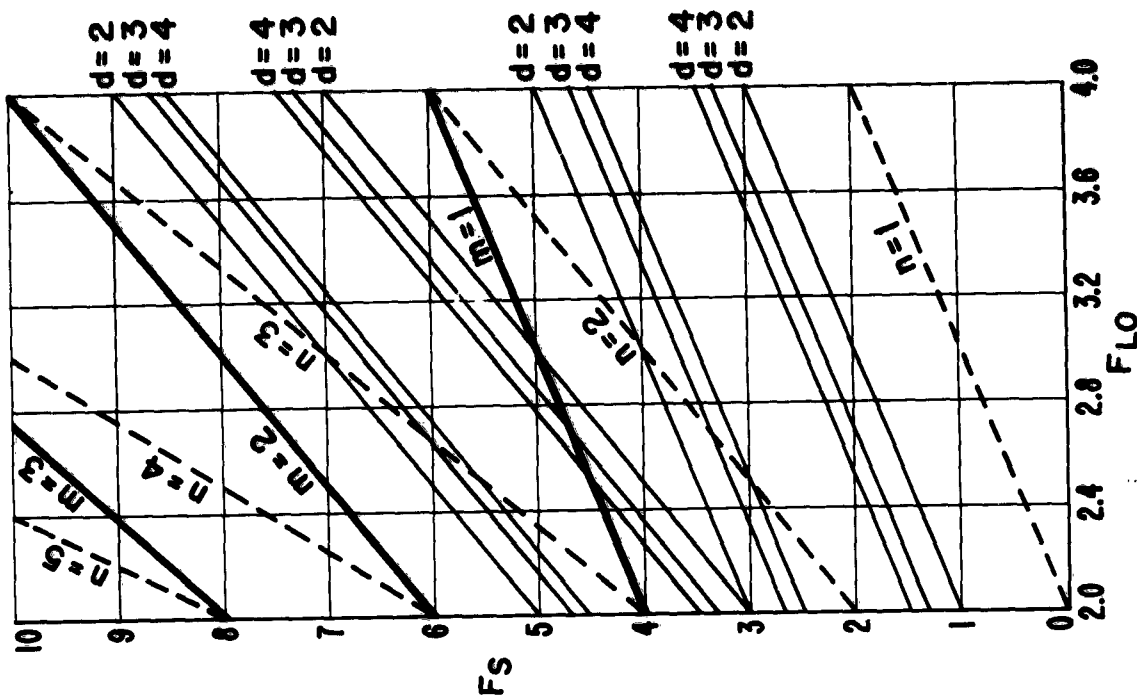
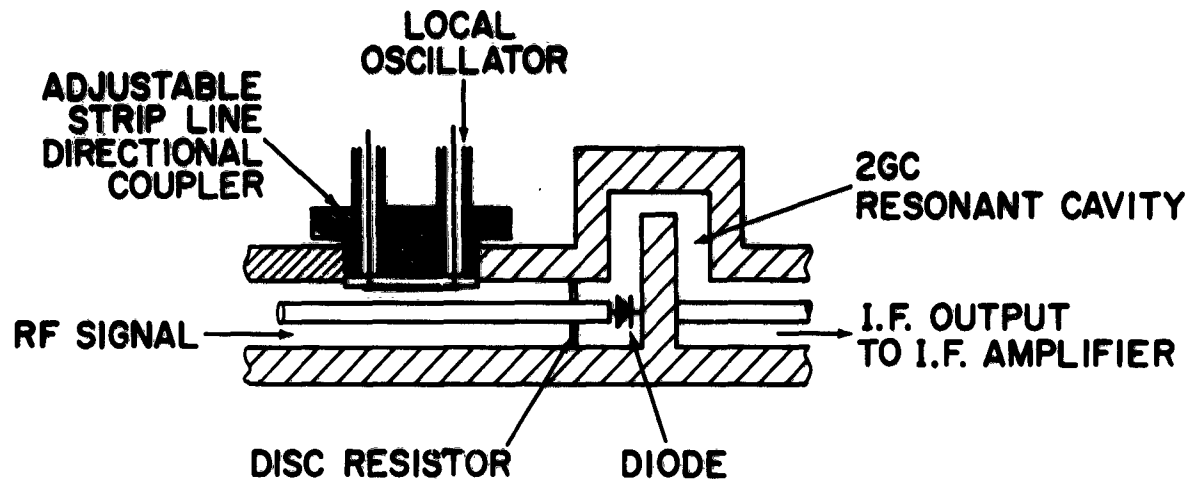
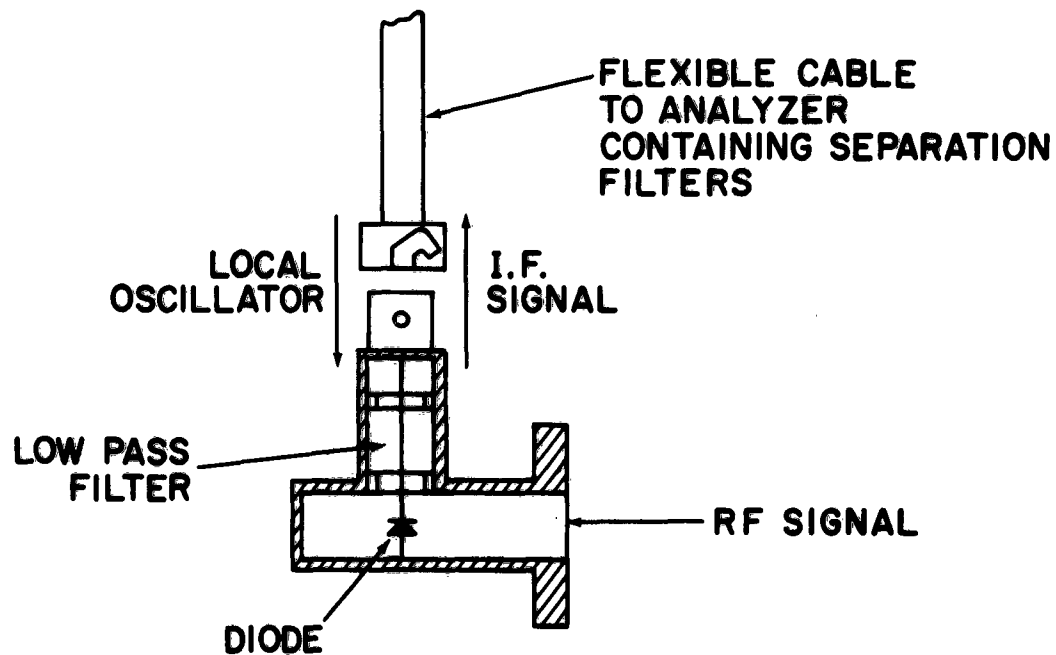


FIG. 3 SPURIOUS SIGNALS GENERATED BY OVERDRIVING FIRST MIXER

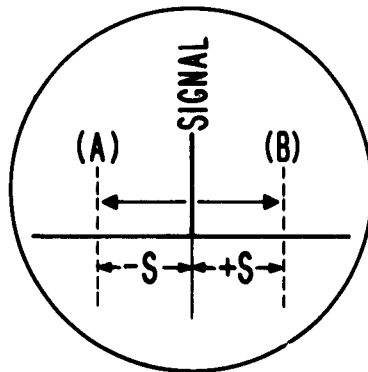
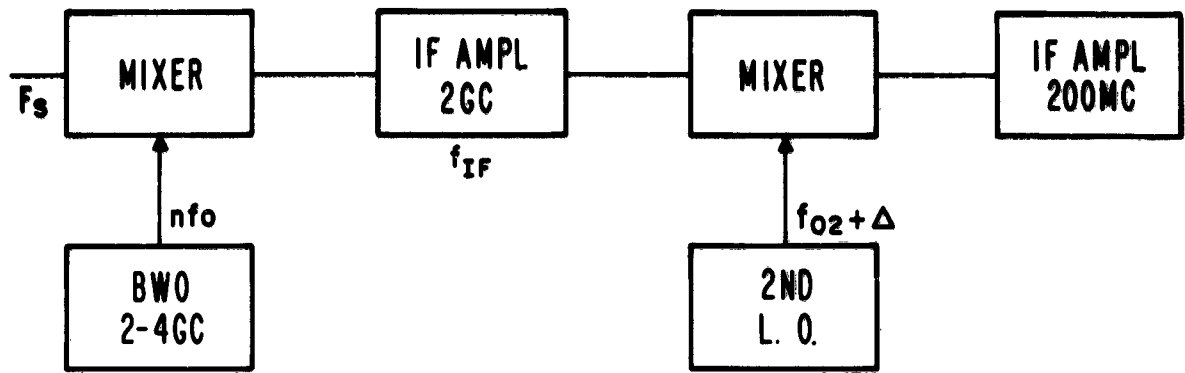


**FIG. 4 COAXIAL MIXER**



**FIG. 5 SINGLE CABLE WAVEGUIDE MIXER**





CHANGE  $f_{o2}$  BY  $\Delta$

SIGNAL SHIFT TO LEFT (A) THEN  $f_s = nfo + f_{IF}$

SIGNAL SHIFTS TO RIGHT (B) THEN  $f_s = nfo - f_{IF}$

$$n = \frac{\Delta}{S}$$

FIG. 6 HARMONIC IDENTIFIER

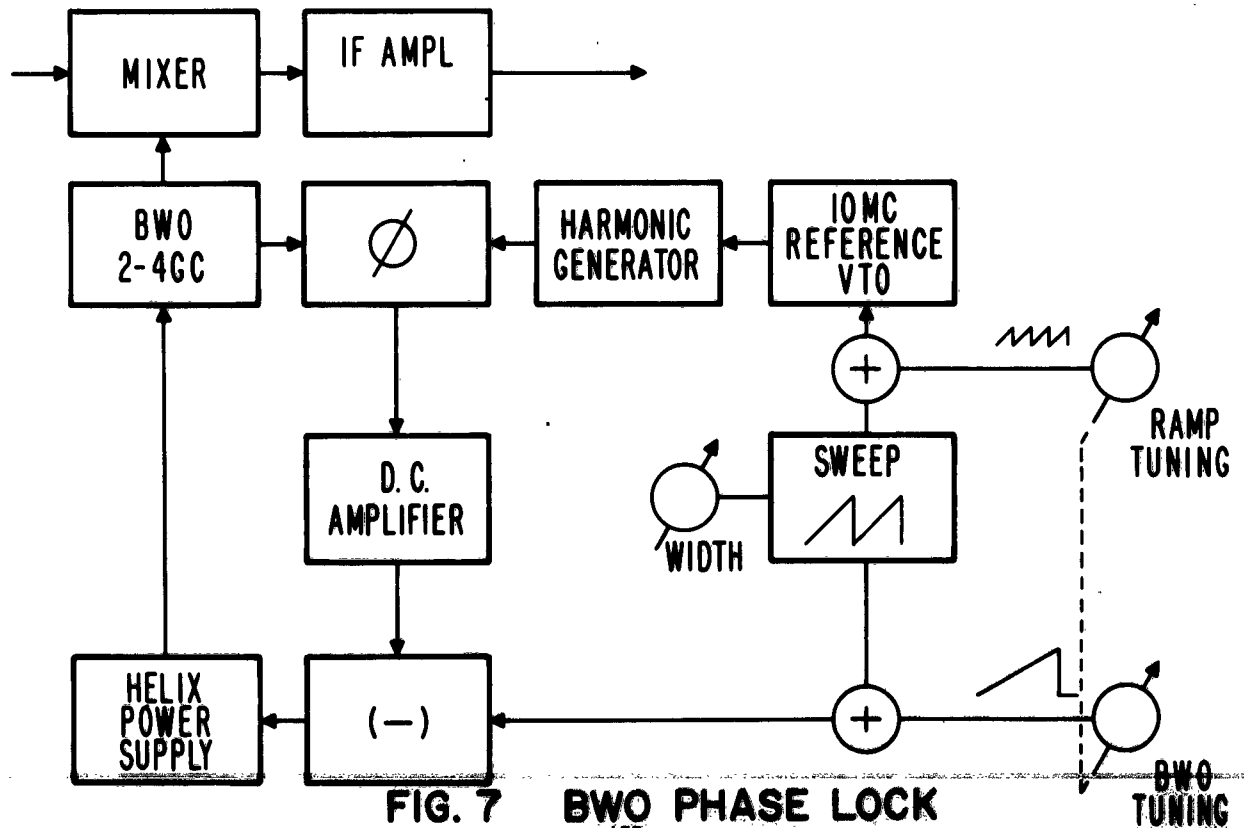
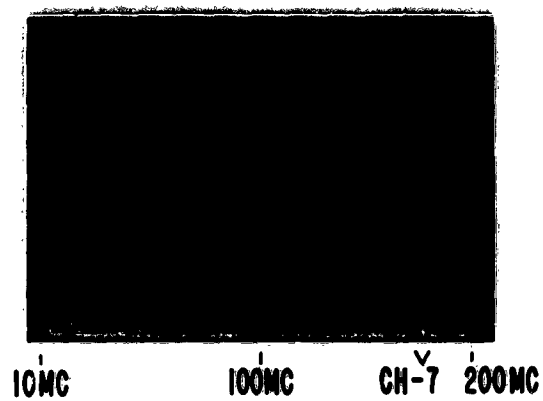
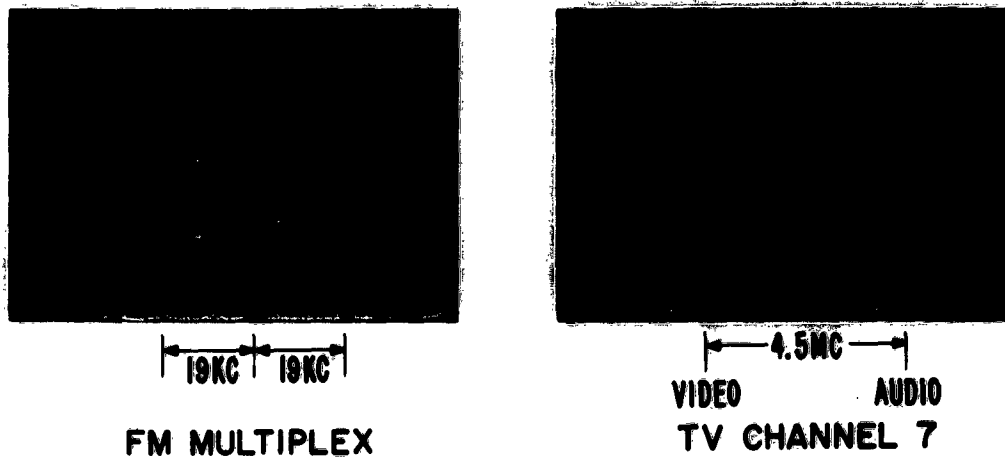


FIG. 7 BWO PHASE LOCK



**FIG. 8 FM & TV BANDS**



**FIG. 9 TYPICAL BROADCAST SPECTRUMS**

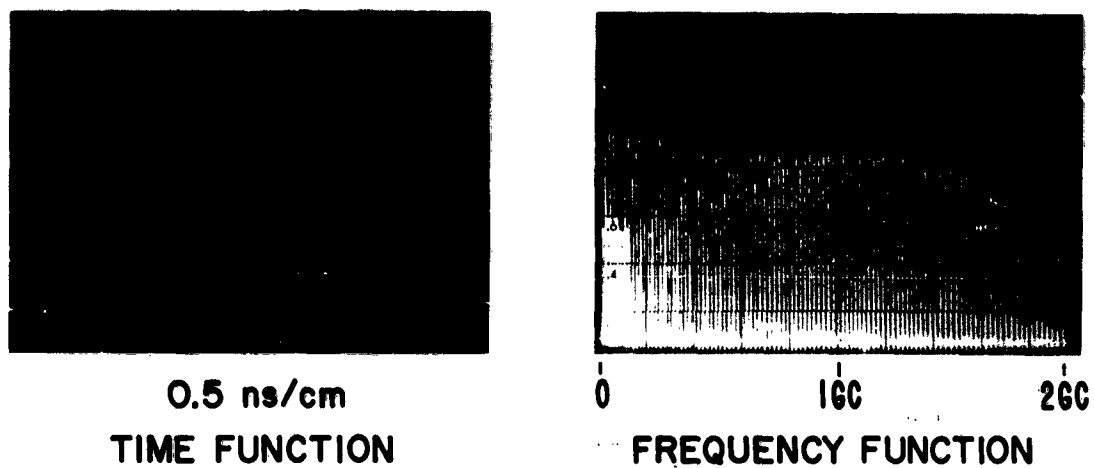


FIG. 10 SPECTRUM OF A BOFF STEP RECOVERY DIODE

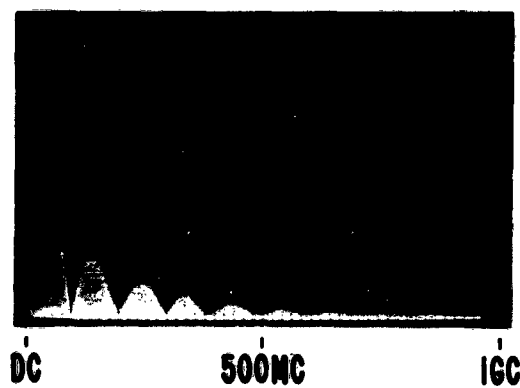
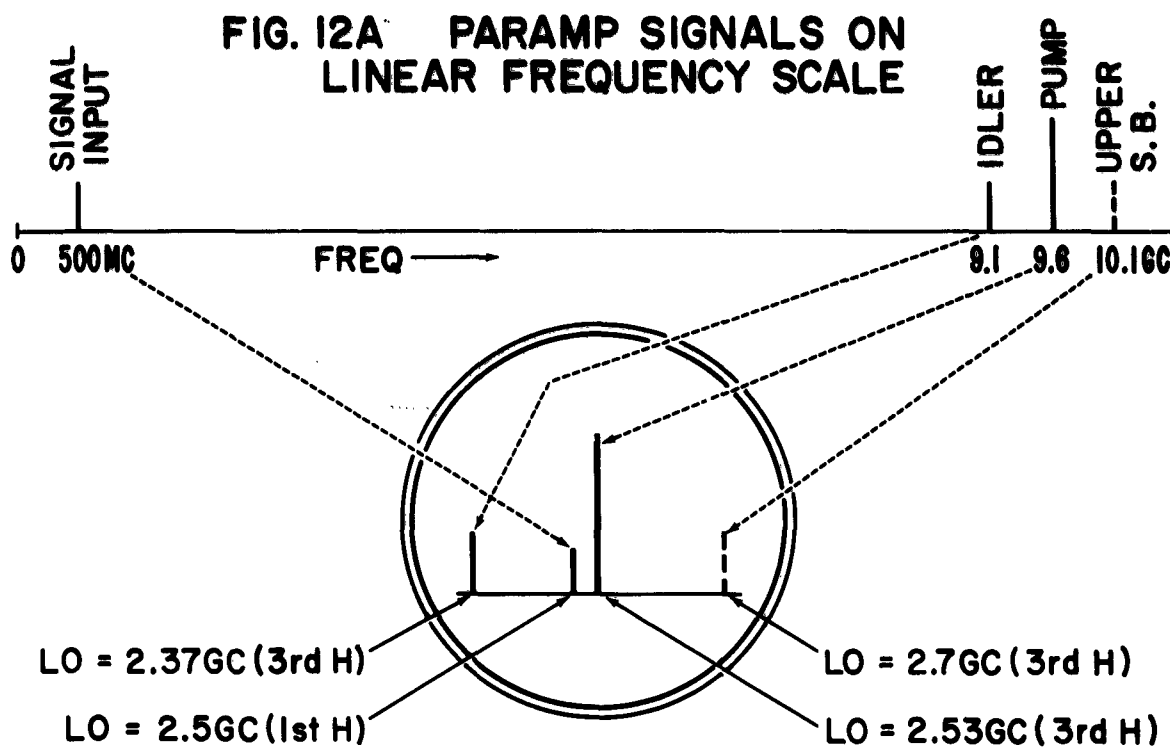
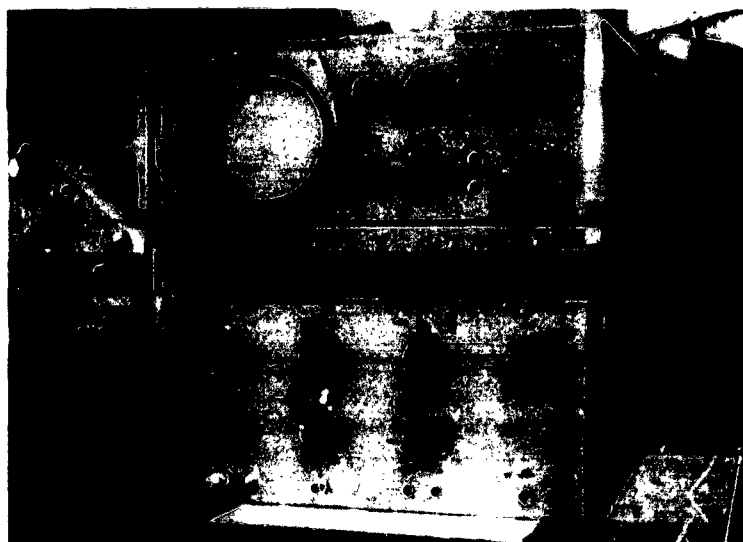


FIG. 11 SPECTRUM OF A 10ns  
PULSE FROM 215A



**FIG. 12B PARAMP SIGNALS ON SPECTRUM ANALYZER**



**FIG. 13 SPECTRUM ANALYZER PROTOTYPE**

## INTERFERENCE SPECTRUM ANALYZER WITH AUTOMATIC FREQUENCY SCANNING AND DATA RECORDING

L. Valcik, J. E. Batz, and J. N. Faraone  
IIT Research Institute  
Chicago 16, Illinois

D. Rees  
Avionics Laboratory  
Wright-Patterson AFB, Ohio

**Abstract.** - A broadband electronically-tuned spectrum analyzer for pulsed interference signals has been developed. Sweeping at the uniform rate of 500 mc each second the unit scans portions of the UHF and SHF bands in approximately one-half minute. With a receiver bandwidth of 10 mc, data are read out and recorded every 20 milliseconds, corresponding to a 10 mc frequency increment.

For each 10 mc frequency increment individual incoming pulses are first quantized on an amplitude basis, with seven amplitude bins each about 12 db apart. Next, for each amplitude bin the pulses are counted, and the pulse count is quantized into seven bins. Data are expressed in terms of three-digit binary numbers which are recorded on three tracks of magnetic tape. The analyzer repetitively scans the four microwave bands until the entire four-hour tape recording capacity has been utilized, at which time the unit turns itself off.

For data readout the recording tape is played back at a high rate into auxiliary equipment which converts the data to a standard IBM format on another tape. This new tape is then used with the IBM 1401, the IBM 7090, and a suitable program for decoding the recorded data and obtaining a data print out. Data are sorted by frequency, with the result of each successive sweep listed sequentially. The chronological changes in signal environment over the four-hour period for each 10 mc increment are thus available.

### I. INTRODUCTION

The primary objective of a recently completed program was the development of techniques applicable for instrumentation to measure high-altitude man-made electromagnetic interference in portions of the UHF and SHF bands. A flyable breadboard covering these bands and demonstrating these techniques was constructed.

The system utilizes four sequentially operated receivers, each electronically swept 500 mc during each second, using separate backward-wave oscillators as local-oscillator sources. The amplitude of pulse signals is measured using a successive-detection type of IF amplifier in conjunction with appropriate pulse processing circuitry. Each incoming pulse is assigned an amplitude bin; the pulses within each such bin are counted, and the count is quantized. For each amplitude bin the quantized count numbers are

recorded digitally on three tracks of magnetic tape. After the system's four-hour recording capacity has been used the system is automatically turned off.

For data reduction the magnetic tape is played back in conjunction with a Ground Station Chassis constructed for this purpose. The outputs are applied to a Data Converter to convert the data-recording format to the IBM format. Data display consists of a print out of the information in tabular form using the IBM 7090 and 1401 computer equipments.

## II. SYSTEM DESCRIPTION

### A. General

A block diagram of the flyable breadboard is given in Figure 1, and exterior views of the equipment are given in Figure 2. Overall panel height in each cabinet is 21 inches. Input requirements for the flyable breadboard consist of 110 v, 60 cps for powering two small blowers, and 28 v dc for the main system power from which all the necessary operating voltages are derived using converters.

Separate signal input connectors are provided for each of the four receivers. For the two lower-frequency receivers Type N coaxial connectors are provided; for the two higher-frequency receivers waveguide inputs are used.

Backward-wave oscillators are used as the local oscillators in order to provide rapid (electronic) tuning over the large bandwidths. Balanced mixers are used so as to minimize the effects of local-oscillator noise. The four receiver front ends are operated sequentially, each BWO being gated on for the proper time interval. The four individual preamplifier stages are gated concurrently with the associated BWO. The preamplifier stages, operating at 60 mc, supply the signal to the IF subsystem. A bandwidth of 10 mc was selected for the wideband IF amplifier to accommodate pulse widths down to about 0.1 microsecond.

A continuous frequency scan (rather than a step scan) is used. The measured data derived from the signal are recorded after the receiver scans across each frequency aperture (taken as 10 mc to correspond with the 10 mc receiver bandwidth). A time interval of 20 milliseconds is allotted to scan 10 mc; the pulse receiver thus scans 10 mc in 20 milliseconds, or 500 mc in each second. Altogether, a total spectrum width of 12,100 mc is swept. The total time for the sequential operation of the four receivers is 24.2 seconds for the actual frequency scanning, plus seven seconds for the four receiver switching operations (during which time identification codes are generated). Table I shows the time sequence.

The block diagram of Figure 1 indicates a second conversion to an intermediate frequency of 10 mc, with the outputs of a narrowband IF amplifier used for driving seven flip-flops. This circuitry was intended to provide a means for detection and amplitude measurement of narrowband signals in an earlier version of the system. It is not included in the flyable breadboard, however.

Measurements of the incoming pulse signals are accomplished by assigning to each incoming pulse one of seven Amplitude Bins. Amplitude quantization of each individual pulse is made possible by the successive-detection characteristic of the IF amplifier, in conjunction with a threshold circuit. The data chassis accepts these seven detector outputs and -- during each 20 millisecond observation period -- counts the pulses within each amplitude quantization bin. The pulse counts for each of the seven amplitude bins are quantized by separate analog-to-digital converters, and the pulse count rates (PRF) are then recorded on three tracks of a magnetic tape. First the nature and performance of the IF amplifier will be described. Then the data recording format will be indicated.

#### B. Successive-Detection IF Amplifier

The technique used for measuring the amplitude of an incoming signal is that of amplifying the signal by different amounts, with each output applied to a threshold detector. A quantized measure of the signal amplitude can thus be determined by noting which of the threshold circuits have been triggered. To provide the different amounts of gain a seven-stage successive-detection IF Amplifier is used. Each stage, except the last, performs two functions: (1) Provides signal drive to the next amplifier stage, and (2) provides a video output pulse which can be applied to a threshold circuit.

A close-up view of the wideband amplifier, showing its one 60 mc input and its seven video outputs is given in Figure 3.

Oscillograms showing typical successive detection and limiting characteristics are given in Figure 4 for a one-microsecond input pulse. For this example stages 7 and 6 are in hard limiting, stage 5 is not in limiting but is producing an appreciable signal, stage 4 has a signal output just barely visible, and stages 3, 2, and 1 have no signal output. Outputs from stages 7 and 6 would trigger threshold circuits, while outputs from stages 4, 3, 2, and 1 would not. Stage 5 output may or may not trigger an output circuit, depending upon the level at which the threshold is set.

Graphs of 60 mc input signal power vs. magnitude of video output pulse are given in Figure 5 for six of the seven stages of the amplifier. (Sufficient output was not available from the signal generator to obtain data on the first amplifier stage.) From Figure 5 can be noted (1) the limiting characteristic (at about 14 volts peak), and (2) the gain separations between stages (about 12 to 14 db). This set of transfer characteristics was obtained using one microsecond IF pulses, but the characteristics are almost constant for pulse widths in the range from 0.1 to 10  $\mu$ seconds.

The output pulses from the seven stage outputs are used as inputs to the data processing circuits.

#### C. Data Processing

Figure 6 shows an idealized arrangement of amplitude and PRF quantization bins. It is termed "idealized" because not all of the actual quantization bins are equal as indicated in Figure 6. Ideally, any pulse with received power greater than about -80 dbm but less than -70 dbm will fall in the lowest-level amplitude bin, Bin No. 1. Those between -70 dbm and -60 dbm

fall within Amplitude Bin No. 2; etc. Pulses greater than about -20 dbm are in the highest amplitude bin, Bin No. 7.

Pulses within each Amplitude Bin are then counted and the counts quantized as shown along the vertical axis in Figure 6. If less than four pulses are received in the 20 millisecond interval -- corresponding to less than 200 pulses per second -- the PRF is assigned Bin No. 0. If at least four pulses but less than eight pulses have been received, corresponding to a PRF between 200 and 400 per second, PRF Bin No. 1 is assigned, etc. If more than 68 pulses are received, corresponding to a PRF in excess of 3400, PRF Bin No. 6 is assigned.

Figure 7 is a simplified block diagram of the electronics required to perform these functions, while Figure 8 is an expanded diagram. Output signals from each of the seven stages of the Wideband IF Amplifier are applied to a Level Detector, or Threshold Circuit, which triggers a Pulse Standardizer. The output of the Pulse Standardizer for Stage 7 -- which will be triggered by all pulses sufficiently above receiver noise level -- triggers a Gate Generator, used for sampling the outputs of the various Inhibit circuits. An Inhibit circuit will pass every pulse received from its associated Pulse Standardizer except if the Pulse Standardizer from the previous stage also produces an output pulse, thereby causing inhibit action. This inhibit feature permits the amplitude quantization to be based on a pulse level exceeding one value, but being less than a second value, as outlined previously.

Pulses from each "And" gate are counted, with the states of three Flip-Flops determined by the number of pulses counted during the 20 millisecond observation period. The three Flip-Flop states are used for triggering three Record Multivibrators.

Figure 9 shows the data recording format. The basic recorded data word consists of three parallel tracks, each having ten 2-millisecond-long bits, giving an overall word length of 20 milliseconds. Data accumulated in the amplitude and PRF quantization circuits during one 20-millisecond observation period are put into temporary storage and are then sequentially recorded during the next 20-millisecond period while new data are being accumulated in the quantization circuits. As indicated in Figure 9, the data from each amplitude bin are recorded using three parallel bits. The chart at the left side of Figure 9 indicates the binary form of the data for any of the seven PRF Bin numbers (0 to 6) which could be recorded in each of the seven Amplitude Bin time slots.

As indicated previously receivers are scanned at a constant rate of 10 mc every 20 milliseconds, with one 20-millisecond data word generated for every 10 mc frequency increment swept. After each of the four receiver bands is scanned, a certain recovery time is allotted for transients to subside, and also for recording a series of Scan Identification (I. D.) code words -- indicating which of the four receivers has just been scanned. Table I showed the time sequence of data words and I. D. code words during the basic frame time of 31.2 seconds. The chart on the right side of Figure 9 shows the I. D. codes. Figure 10 is an example of the format for a small portion of the three recorder tracks.



Frequency data is not recorded directly, but instead is derived during data playback by noting the specific ten-character words which have signal indications. Frequency scan vs. time is linear, so that linear interpolation (by counting the ten-character words) can be used to determine frequency.

Overall timing for receiver switching and sweeping is performed by the "Programmer". A 50 cps clock signal drives an eleven-stage binary counter and a diode matrix, with the matrix configuration arranged so that output pulses are produced at the proper times for triggering the various switching and gating circuits. In addition to the preamplifier and BWO gating previously mentioned, gates control the data code or the scan identification code used in each word. The data code, represented by a 0, 0, 0 on the three recorder tracks, is used as one of the characters in every ten-character data word, no matter which of the four receivers is being scanned. A receiver identification code designating which of the four receivers has just completed its scan is generated in place of the data code during the time interval between the turning off of one receiver and the turning on of the next receiver.

Another purpose of the diode matrix is to drive the Nonlinear-Ramp Generator used for deriving the series of four nonlinear ramps needed to obtain linear frequency-vs-time scanning of the four BWO's. The desired ramps are approximated by a series of straight-line segments. The straight-line segments are obtained digitally, with the breakpoints determined by the times of occurrence of additional output pulses from the diode matrix. These output pulses control four current gates. The slope of the curve between breakpoints thus depends upon which of the current gates are on during that interval. An oscillogram of the series of four ramps is given in Figure 11.

The BWO High-Voltage Power Supply is a power-and voltage-amplifier, amplifying by a factor of 150 the nonlinear ramp voltage applied to its input. It is a regulated, all-solid-state supply capable of outputs up to 1500 volts.

Recording is accomplished using a miniature three-track recorder having a recording capacity of four hours. System operation can be terminated either automatically by an end-of-tape sensing circuit activated at the end of the four-hour recording period, or manually at any time by a front-panel push-button. If the system is operated merely for preliminary testing or alignment and recording is not desired, the recorder can be turned off by another front-panel switch.

Performance of the receivers and a portion of the processing circuits can be monitored using a commercial oscilloscope in conjunction with a sweep input signal, vertical deflection signal, and intensity modulation signal available from the Data Chassis.

For recorder playback and data reduction the Recorder, Matrix Chassis is removed from its Flyable Breadboard cabinet and operated in the laboratory together with a Ground Station Chassis, suitable laboratory power supplies, and a Data Converter. The Data Converter is required in order to convert the three-track recording format to the seven-track IBM format. The converted tape is then used with the IBM 7090 and 1401 computer equipments

to obtain data print-out in tabular form. The computer programs furnished provide for two types of data print-out: (1) a summary sheet listing the number of times that a signal was received in each of the 10 mc frequency increments, and (2) a detailed listing for every 10 mc frequency increment, showing the PRF Bin numbers for each of the seven Amplitude Bins, in chronological order.

### III. SUMMARY OF EXPERIMENTAL OPERATION

#### A. Receiver Sensitivities

With the BWO's swept over their desired frequency ranges, the BWO grid bias and the l.o. attenuators were adjusted so as to produce a current of approximately one to one and one-half ma in each mixer crystal. As an indication of receiver sensitivity, the minimum discernible signal was measured at several spot frequencies in the different bands using an oscilloscope to give the conventional A-scope presentation. With r-f input pulses 2  $\mu$ sec wide at a rate of 4000/second, the minimum discernible signal was approximately -94 dbm, when observing the video output of Stage 7 of the Wideband IF Amplifier. The noise level was approximately constant across each band. With an input power approximately 10 db higher, i. e., -84 dbm, the video pulse output was about 4 volts. As observed on the scope, only occasionally did noise spikes cross the 4 volt level. The threshold levels were therefore set to about 4 volts.

#### B. Spurious Responses

As expected with no r-f preselection, the image response is equal to the signal response. The signal response is taken to be the response obtained with the local oscillator 60 mc above the signal. Therefore, if the receiver output is observed on a scope, the image response occurs at an indicated frequency about 120 mc below the signal response. Although comprehensive tests for other spurious responses was not conducted, one receiver was checked for other responses when tuned to a fixed frequency. Table II shows the input signal levels required to produce a reference-level output from the receiver. The two spurious responses 40 db below the signal response are assumed due to the mixing of third harmonics of signal generator and local oscillator frequencies. No low-pass filters were used.

#### C. Frequency Errors

Receiver alignment was performed using HP signal generators as sources. With the available resolution in adjusting the individual ramp functions for sweeping the BWO's, the errors due to the resolution limitations are estimated to be as follows: For Receiver 1: 10 mc; Receiver 2: 20 mc; Receiver 3 and 4: 50 mc. To these errors must be added errors in signal generator frequency calibration and errors due to drift (thermal and aging) of the receiving equipment. A thermal drift problem was previously encountered which caused approximately a 100 mc shift in Receiver 2 and corresponding shifts in the other bands. This has subsequently been corrected.

#### D. Test Recording

A 2-hour test recording was made with the entire receiving system operating\* and with r-f signals injected into Receivers 1 and 2. The approximate input frequencies and PRF's were read from the signal generator dials. After the test the recorded tape was played into the IITRI Data Converter in conjunction with the Ground Station Chassis, and the data were converted to a Univac tape. Portions of the Univac tape were printed out directly for visual examination. It was found that parts of the converted output were correct, and parts obviously had errors. The errors are believed due to noise (probably recorder motor noise) causing erroneous triggerings of the output flip-flop during data playback.

A sample portion of some of the data apparently not affected by this source of error is shown in Table III. Several things of interest can be seen apart from the apparent frequency error of about 50 mc. The signal and image frequencies are indicated to be spaced by about 100 mc, instead of their actual 120 mc spacing. This may be due to the resolution limitations in adjusting the ramps, as previously discussed. Of greater interest, however, are the PRF Bin Numbers indicated\*\*. Signals are indicated to be within three successive 10-mc increments, even though they were fairly narrow band -- due to 4  $\mu$ sec pulses. The spread into three 10-mc bands is evidently due to the skirt response of the IF passband. As a last point, even though the input pulses were of constant amplitude, pulses are indicated in several Amplitude Bins even within one 10-mc increment. This is attributed primarily to the fact that as the signal is swept through the IF passband the magnitudes of the video signals applied to the threshold circuits will change. When the signal is near the center of the passband, the threshold for Amplitude Bin 4 may be triggered, while only the threshold circuit for Amplitude Bin 3 may be triggered when the signal is detuned by a few megacycles from band center. It can be noted that the (maximum) total pulse rate at the signal frequency appears to be satisfactory: For PRF Bins 2, 3, and 4 the quantized ranges are 400 to 900, 900 to 1400, and 1400 to 2400, respectively. This gives a total indication of 2700 to 4700 pulses per second for the 2040-2050 mc increment, which encompasses the approximate value of 4000 pulses per second actually used.

#### ACKNOWLEDGEMENT

This work was performed under Contract AF 33(616)-8428 for the Avionics Laboratory, Air Force Systems Command, United States Air Force.

---

\* This test was made prior to elimination of the frequency drift previously mentioned.

\*\* See Figure 6 for the actual PRF ranges associated with each PRF Bin Bin Number.

**TABLE I**  
**TIME SEQUENCE OF EVENTS DURING AIRBORNE RECORDING**  
**(Cycle Repeated Every 31.2 Seconds)**

		<u>Time Interval</u>	<u>Number of 20-Millisecond Words</u>
Receiver No. 1	Data	1.2 sec	60
Receiver No. 1	I. D. Code	1.0	50
Receiver No. 2	Data	4.0	200
Receiver No. 2	I. D. Code	2.0	100
Receiver No. 3	Data	9.0	450
Receiver No. 3	I. D. Code	2.0	100
Receiver No. 4	Data	10.0	500
Receiver No. 4	I. D. Code	2.0	100
<b>Totals</b>		<u>31.2</u>	<u>1560</u>

**TABLE II**  
**INPUT SIGNAL LEVELS WHICH PRODUCED**  
**A REFERENCE-LEVEL OUTPUT**

10,530 Mc	-72 dbm	signal
10,570	-33	spurious
10,610	-32	spurious
10,650	-72	image

**TABLE III**  
**DECODED DATA DERIVED FROM PORTION**  
**OF TEST RECORDING (For One Scan of One Receiver)**

Input Frequency = 2100 mc (approx)  
PRF = 4000 (approx); Pulse Width = 4  $\mu$ sec  
Tabulated Values are PRF Bin Numbers

Decoded Frequency	1	2	Amplitude Bin		5	6	7	
			3	4				
-----								
1920-1930 mc	-	-	-	-	-	-	-	
1930-1940	2	3	-	-	-	-	-	
1940-1950	-	-	2	5	-	-	-	(Image)
1950-1960	2	2	2	-	-	-	-	
1960-1970	-	-	-	-	-	-	-	
1970-1980	-	-	-	-	-	-	-	
1980-1990	-	-	-	-	-	-	-	
1990-2000	-	-	-	-	-	-	-	
2000-2010	-	-	-	-	-	-	-	
2010-2020	-	-	-	-	-	-	-	
2020-2030	-	-	-	-	-	-	-	
2030-2040	2	2	3	-	-	-	-	
2040-2050	-	2	4	3	-	-	-	(Signal)
2050-2060	2	-	-	-	-	-	-	
2060-2070	-	-	-	-	-	-	-	
-----								



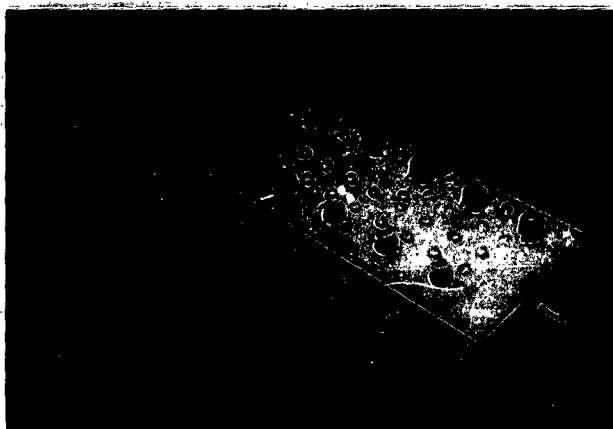
**FIG. 1 BLOCK DIAGRAM OF ELECTRONICS FOR MEASUREMENTS IN UHF AND SHF BANDS  
(FLYABLE BREADBOARD)**



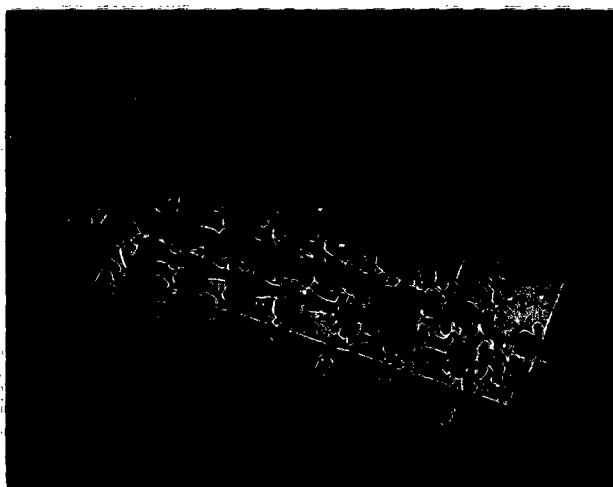
FIG. 2(a) FLYABLE BREADBOARD (FRONT VIEW)



FIG. 2(b) FLYABLE BREADBOARD (REAR VIEW)



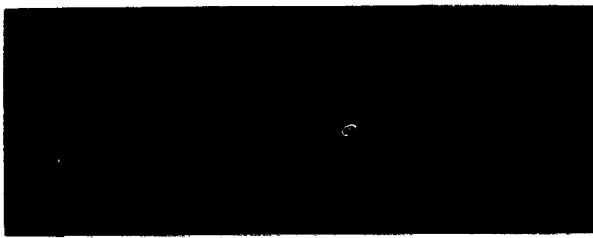
a.) Top View



b.) Bottom view showing internal layout

**FIG. 3 60 MC WIDEBAND I. F. AMPLIFIER**

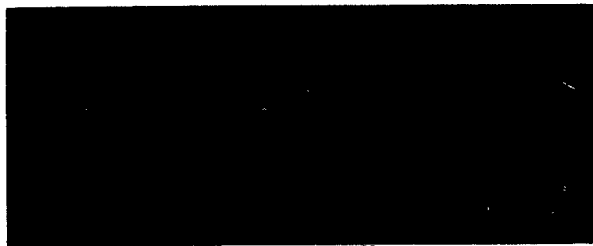




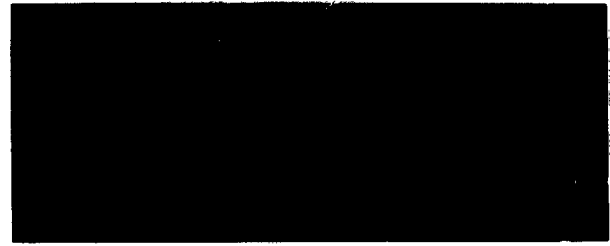
**a) Stage 1 Video Output**



**b) Stage 2 Video Output**



**c) Stage 3 Video Output**



**d) Stage 4 Video Output**



**e) Stage 5 Video Output**



**f) Stage 6 Video Output**



**g) Stage 7 Video Output**

**FIG. 4 - OSCILLOGRAMS OF WIDEBAND IF AMPLIFIER  
SUCCESSIVE DETECTION AND LIMITING  
CHARACTERISTICS**

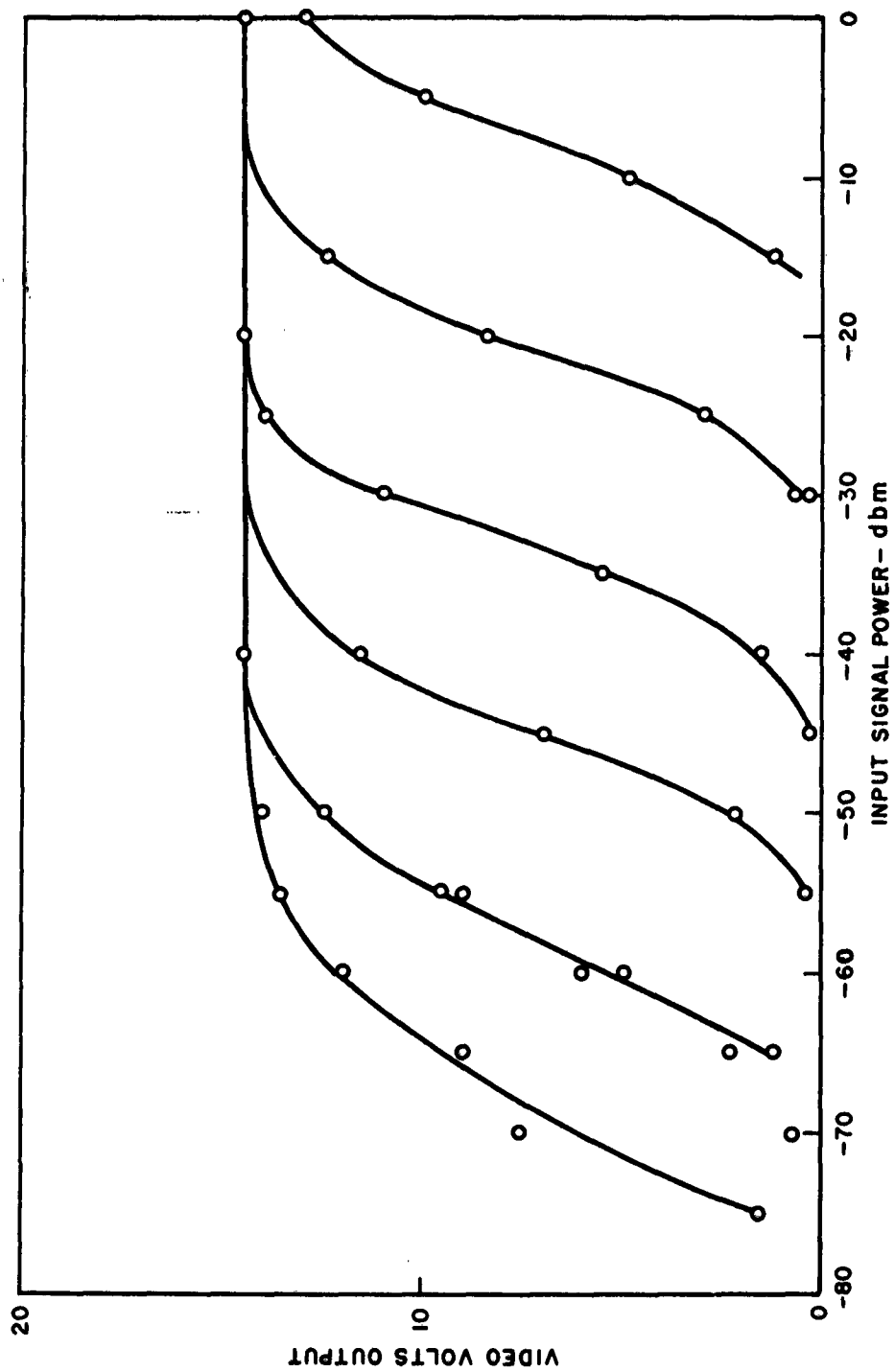


FIG. 5 SUCCESSIVE DETECTION AND LIMITING CHARACTERISTICS OF  
WIDE BAND IF AMPLIFIER - 2nd MODEL

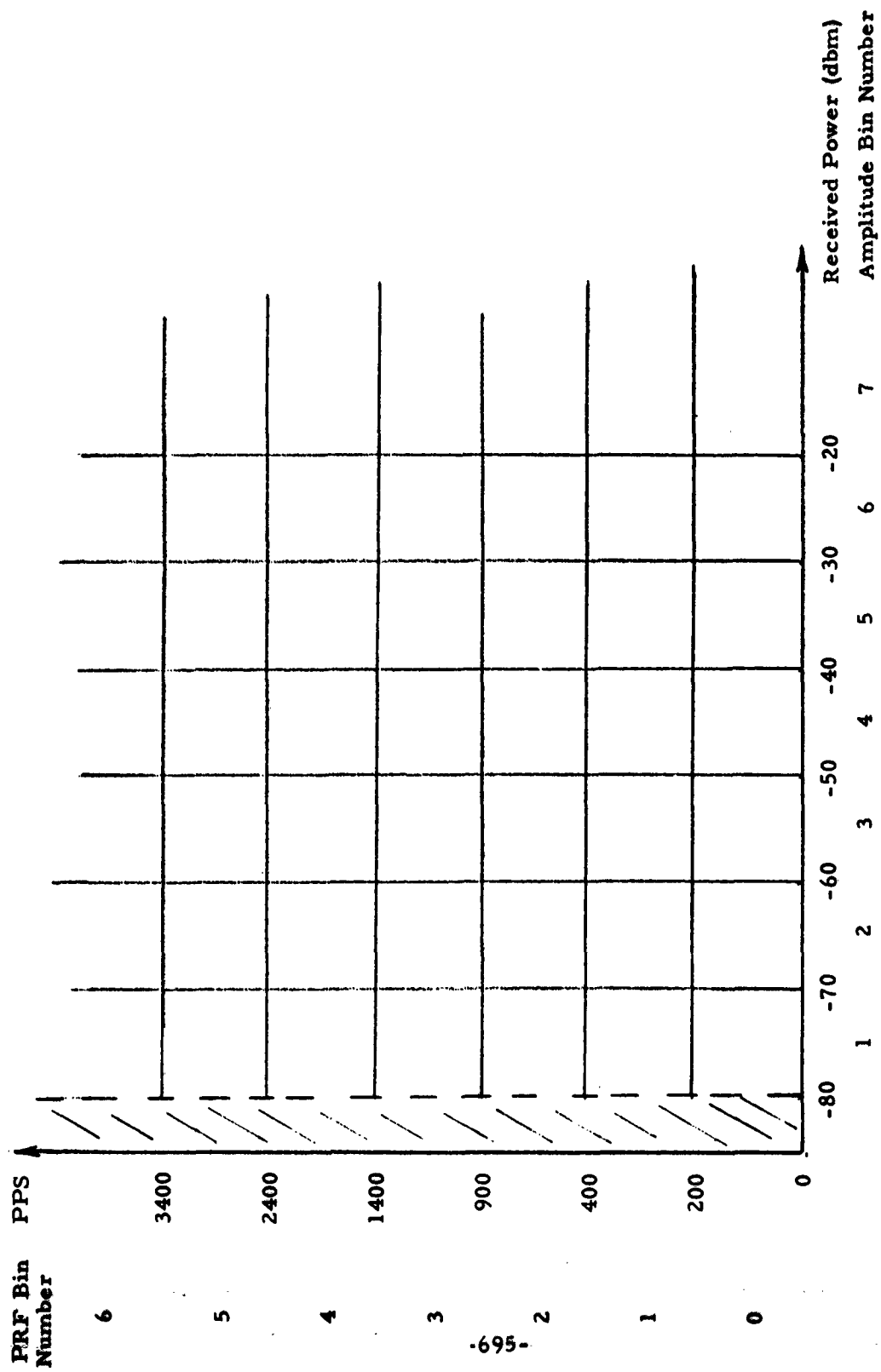


FIG. 6 IDEALIZED AMPLITUDE AND PRF QUANTIZATION BINS

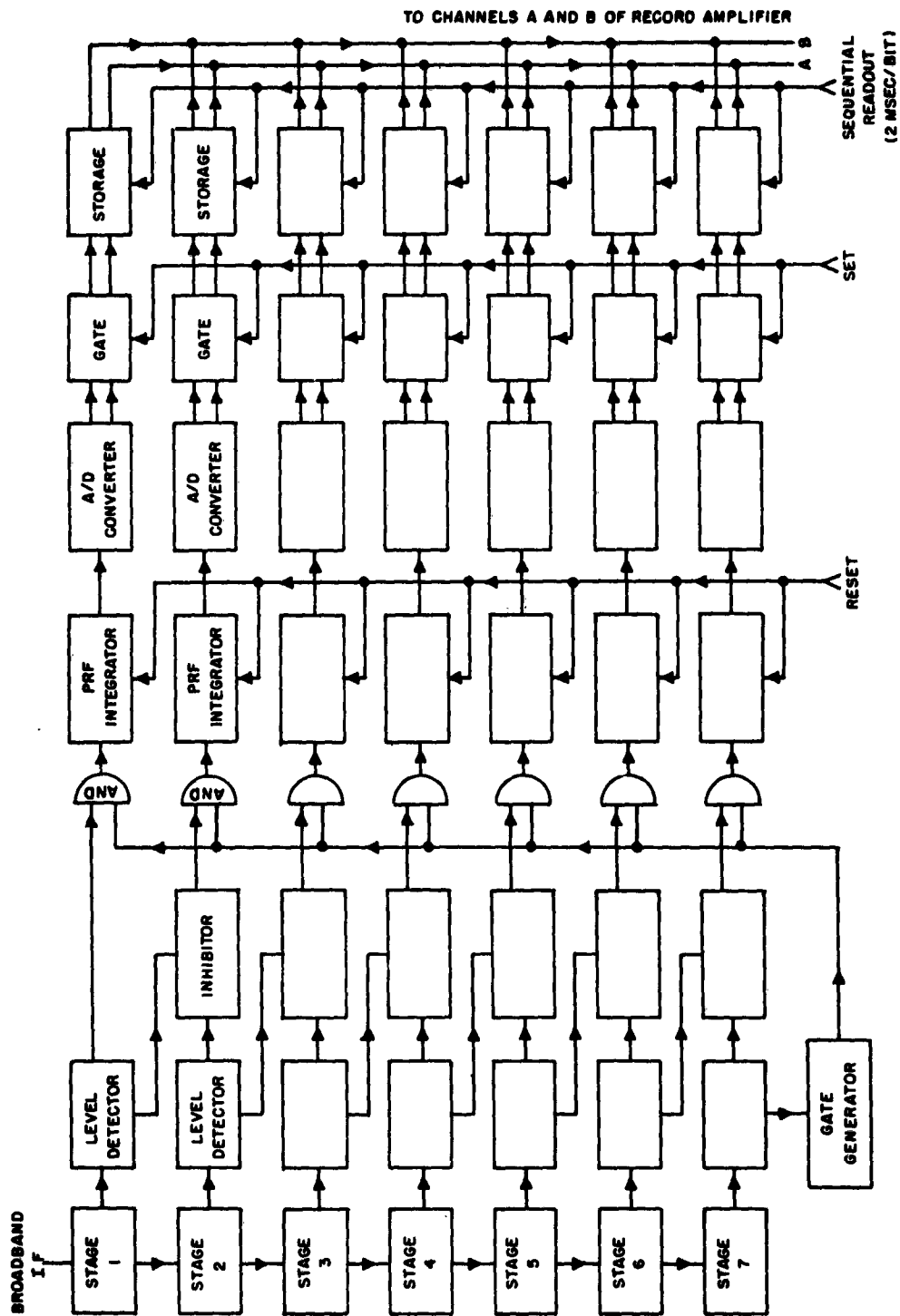


FIG. 7 SIMPLIFIED BLOCK DIAGRAM OF ELECTRONICS FOR PROVIDING PRF READOUT FROM EACH OF SEVEN DETECTORS

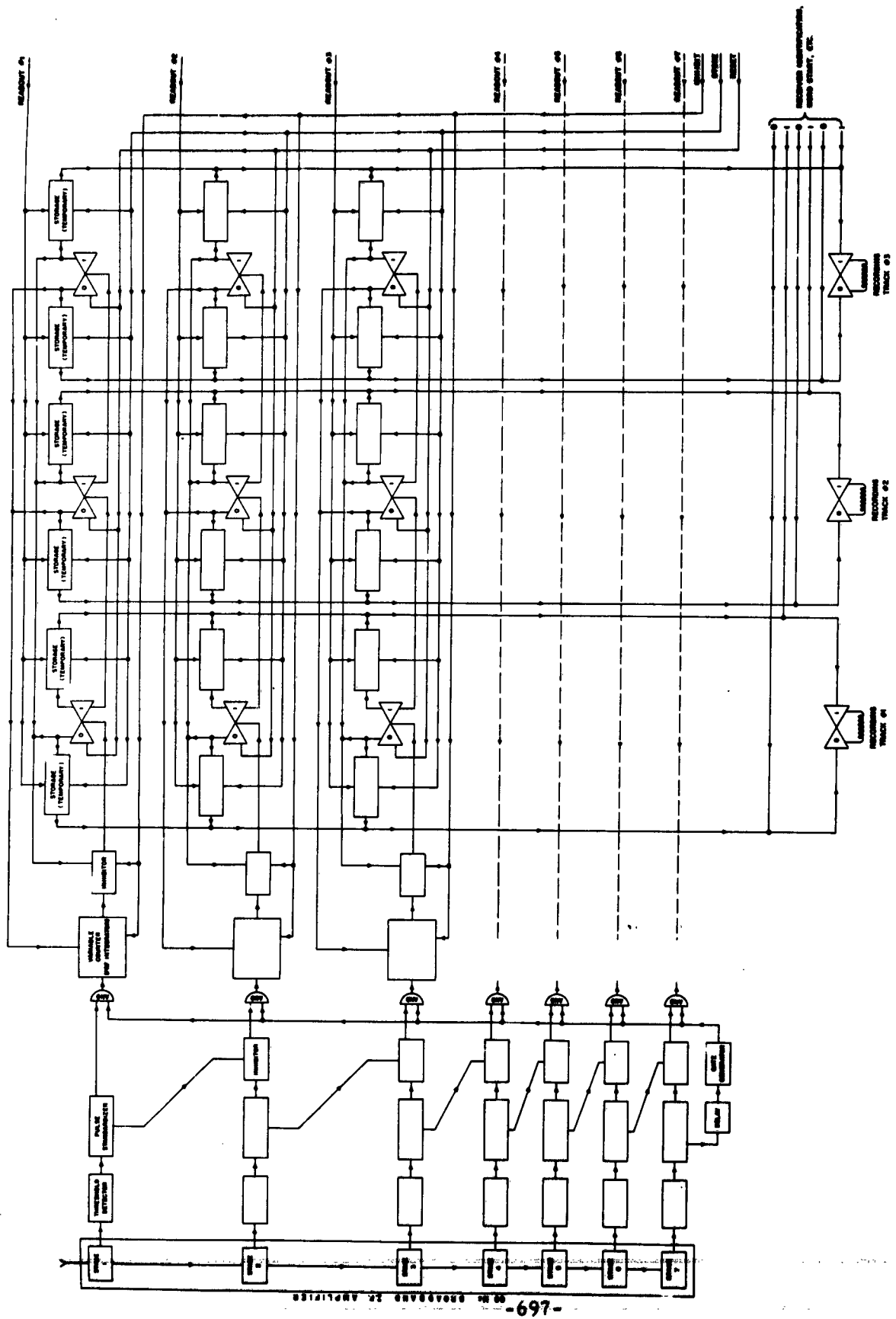
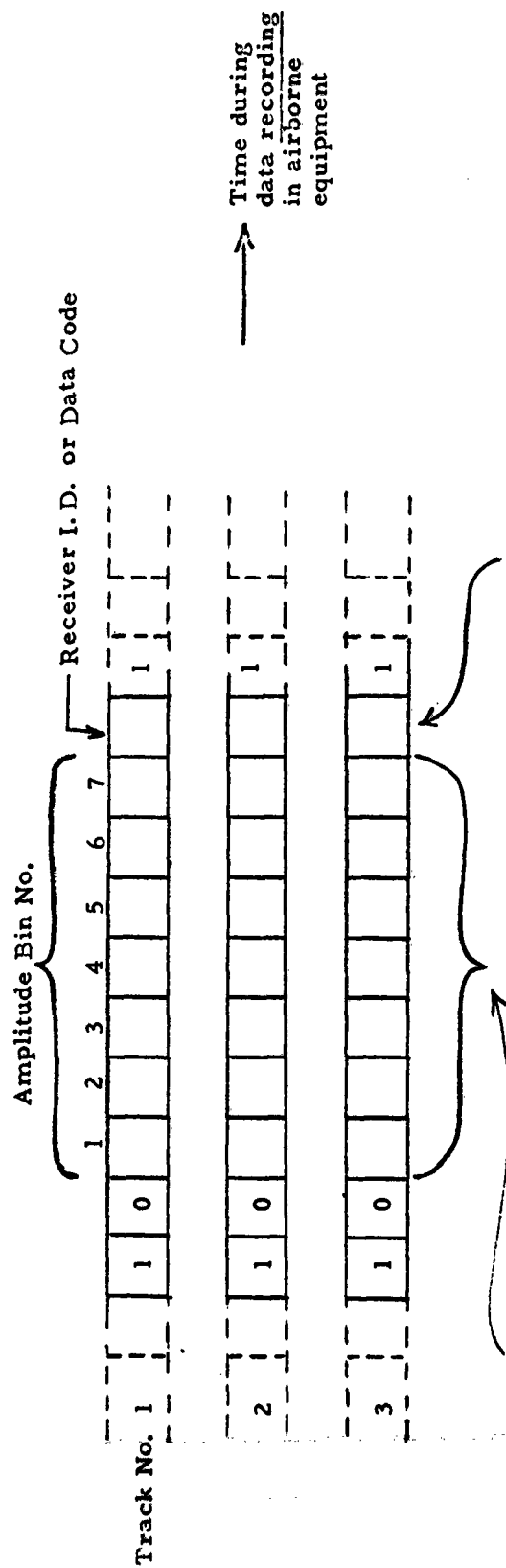


FIG. 8 EXPANDED BLOCK DIAGRAM OF REVISED MEASUREMENT CIRCUITRY



PRF Bin No.	Track No. 1	Track No. 2	Track No. 3
0	0	0	0
1	1	0	0
2	0	1	0
3	1	1	0
4	0	0	1
5	1	0	1
6	0	1	1

Function	Track No. 1	Track No. 2	Track No. 3
Data	0	0	0
I. D. Code No. 1	1	0	0
I. D. Code No. 2	0	1	0
I. D. Code No. 3	1	1	0
I. D. Code No. 4	0	0	1

FIG. 9 DATA RECORDING FORMAT FOR ONE WORD

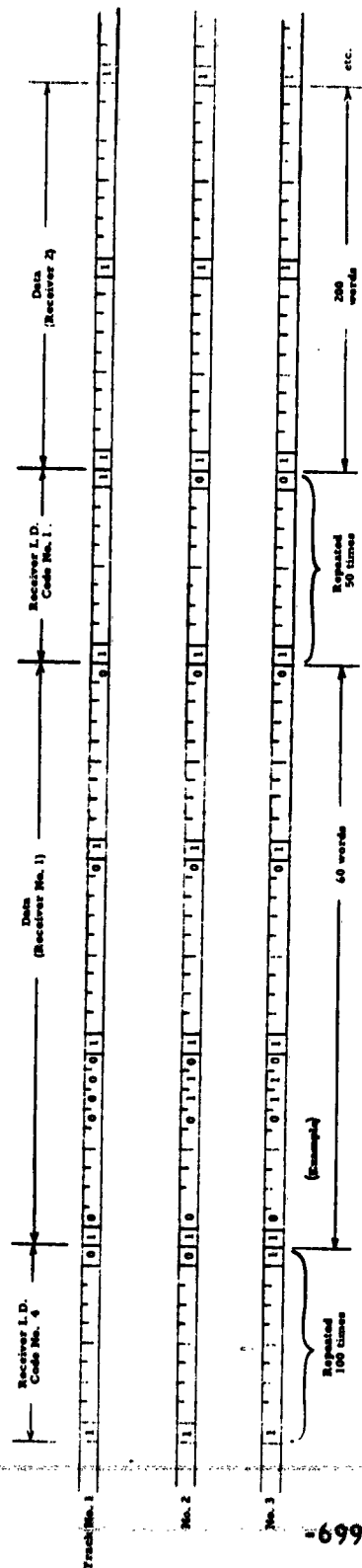
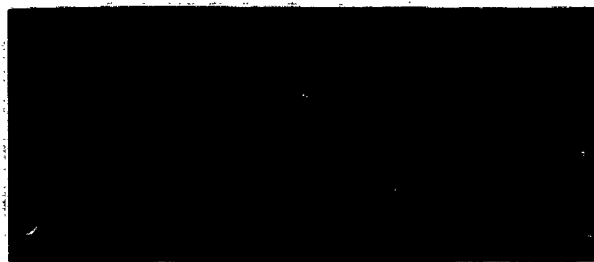


FIG. 10 EXAMPLE OF PORTION OF RECORDS D MAGNETIC TAPE TRACKS



**FIG. 11 RAMP OUTPUT OF SWEEP GENERATOR**  
(Vert. Sens. Approx. 2 v/cm;  
Hor. Sens. Approx. 3.1 sec/cm)



## MEASUREMENTS TECHNIQUES WITH A SPECTRUM SIGNATURE MONITOR

M. Feigenbaum and R. Sandstrom  
Polarad Electronic Instruments  
Long Island City, New York

Abstract. - This paper describes the use of a Spectrum Signature Monitor in conjunction with a field intensity receiver for interference measurements. Its use speeds measurements and provides for rapid identification of modulated signals. The greater resolving capabilities due to its narrow bandwidth allow for the measurement of low level spurious signals close to the desired signal.

### I. INTRODUCTION

The application of spectral analysis techniques in making field intensity measurements is not basically a new concept. The well equipped interference measurement group has been using spectrum analyzers in conjunction with field intensity measurement equipment for many years. In using a separate spectrum analyzer however, the inherent lack of preselection makes quantitative measurements difficult, and the cost of an analyzer with preselection in addition to the field intensity receiver is prohibitive. The newer sophistication in measurement techniques and the requirements for spectrum signature monitoring by the newly proposed military specifications have led to the development of a Spectrum Signature Monitor, the DM-1/2 by Polarad Electronic Instruments.

### II. DESCRIPTION

The Spectrum Signature Monitor consists of a swept I.F. and display unit which is loosely coupled into the I.F. system of a field intensity meter. The R.F. tuning unit therefore becomes a function of the field intensity meter and the spectrum analyzer and the need for a secondary tuning unit is eliminated. The desired preselection is obtained from the field intensity meter, and the loose I.F. coupling does not interfere with the measurement capability of the field intensity meter. Since the R.F. tuning unit is common, the display on the screen of the monitor is that of the quantity being measured.

Figure 1 is a simplified block diagram of the Spectrum Signature Monitor, presented for a quick review of the spectrum analyzer concept. The sampled I.F. input is amplified and then heterodyned with a swept oscillator into a narrow band I.F. amplifier, the output is detected and presented to the vertical plates of a CRT in synchronism with the sawtooth modulating the swept oscillator. The resultant display on the CRT is then narrow band energy vs. frequency. The ability to vary the bandwidth of the narrow band amplifier from 1 to 80 kc is of particular importance in this application, as is the logarithmic display. The use of these controls will be discussed in their application to field intensity measurements.

Figure 2 is a photograph showing the interconnection and operational setup of the Spectrum Signature Monitor used in conjunction with a Polarad Model CFI Field Intensity Meter. The coupling box can be seen in front of the CFI tuning unit across the I.F. jumper connections standardly provided on the CFI for this purpose.

Figure 3 is the schematic of the coupling box which, as can be seen, is a simple resistive attenuator.

### III. MEASUREMENT TECHNIQUES

The visual display of the Spectrum Signature Monitor gives the operator the ability to scan through the tuning range of the receiver much more rapidly than by the normal method of watching the indicating meter of the field intensity receiver. The speed of location of signals is improved by several orders of magnitude, and is most improved by allowing the operator to scan using the peak detector position of the receiver. In this position, the detector has a time constant of approximately one second, and to tune through a typical band of from 7 to 10 gc. using a 5 megacycle receiver bandwidth would normally take an operator approximately ten minutes. Using the display of the Spectrum Signature Monitor, signal location time is reduced to approximately one minute. Both these times are of course modified by the skill of the operator, but the ratio of one to ten in time holds fairly well.

The ability of the operator to recognize the nature of the received signal rapidly is again greatly enhanced by the visual display of the Spectrum Signature Monitor. Figure 4 gives respectively the characteristic display of a frequency modulated signal, a pulsed signal, and two closely spaced continuous signals. The ease of photographing the display is obvious and the picture plus the quantitative measurement provide the complete identification of the signal.

Being able to resolve signals spaced within the bandpass of the field intensity meter is of extreme importance in the laboratory when using the meter, as it should be used, during the design phases of a new equipment. The increasing popularity of varactor multiplier chains for stable microwave sources results in the presence of spurious signals in close proximity to the desired output. The detection and elimination of these spurious signals is a design and not a field function. The increased resolving power of the Spectrum Signature Monitor allows rapid detection and measurement of these unwanted signals.

The resolving power of the Spectrum Signature Monitor is a function of several variables. The I.F. bandwidth of the Spectrum Signature Monitor is variable from one to eighty kilocycles. Theoretically one could resolve two signals spaced one kilocycle apart, however, the incidental frequency modulation of the existing field intensity meter tuning units is normally higher than one kilocycle and typically on the order of ten kilocycles. This is a definite limiting factor in the resolving power of the system, but provisions can be optionally made for

the introduction of phase locking techniques for the tuning unit. Using these techniques, resolutions of better than one kilocycle are possible.

The use of the variable resolution capability of the DM-1 offers the advantage of increased system sensitivity, in the CW case, without the need for expensive and limited dynamic range low noise pre-amplifiers. Theoretically the improvement in sensitivity of the system over that of the receiver alone is the ratio of the noise bandwidth of the system without the monitor to the bandwidth of the system with the monitor. In practice, the limiting factor is once again the incidental frequency modulation presented by the local oscillator of the tuning unit. For the equipment shown in Figure 2, the measured sensitivity improvement was fifteen db. This correlates well with the ten kc of frequency modulation present in the tuning unit. The presence of this frequency modulation is not normally noticeable in the meter function of the field intensity receiver since the minimum bandwidth is one megacycle. A further improvement of an additional eight db was noted with the use of a Dymec phase lock system to stabilize the local oscillator. The phase lock system for improved CW sensitivity is only applicable in measurements where the operator has advance knowledge of the frequency of the incoming signal. A photograph of a signal made with the phase locked system is presented in Figure 5.

The application of the DM-1 to a pulsed R.F. signal allows rapid identification of the pulse spectra. By the use of gating techniques available at the I.F. jumper provided on the CFI and in conjunction with a multipulse spectrum selector Polarad Model SD-1, the measurement of multipulsed signals may be made and viewed. The width of a pulse may be readily determined by using the variable marker of the Monitor. Figure 6 is a photo of a pulse display showing the marker.

For pulsed signal applications, there is no improvement in system sensitivity using the Monitor. In this case the narrow bandwidth of the Monitor using its maximum position of eighty kc does not allow a fast enough charge time to respond to the peak amplitude of the pulse. For pulses narrower than eight microseconds there is a loss in sensitivity corresponding to the ratio of pulse width to bandwidth of the Monitor. This loss assumes the function;

$$a_s = \frac{3}{2} \beta \tau$$

$a_s$  = Sensitivity loss

$\beta$  = 3 db I.F. bandwidth in cycles

$\tau$  = pulse width in seconds

Figure 7 is the nomograph presenting this function in a simple form for rapid reference.

The logarithmic display function of the DM-1 allows the measurement of the relative amplitude of signals on the display of 36 db. By using the peak reading of the field intensity meter at a calibrated level, the display can be calibrated giving an additional dynamic range to the system of this 36 db. The accuracy of measurement made this way is certainly within the accuracy of the complete system and allows the measurement of signal levels into the noise level of the system.

#### REFERENCES

1. Polarad Electronics Corporation, Spectrum Analyser Techniques Handbook.

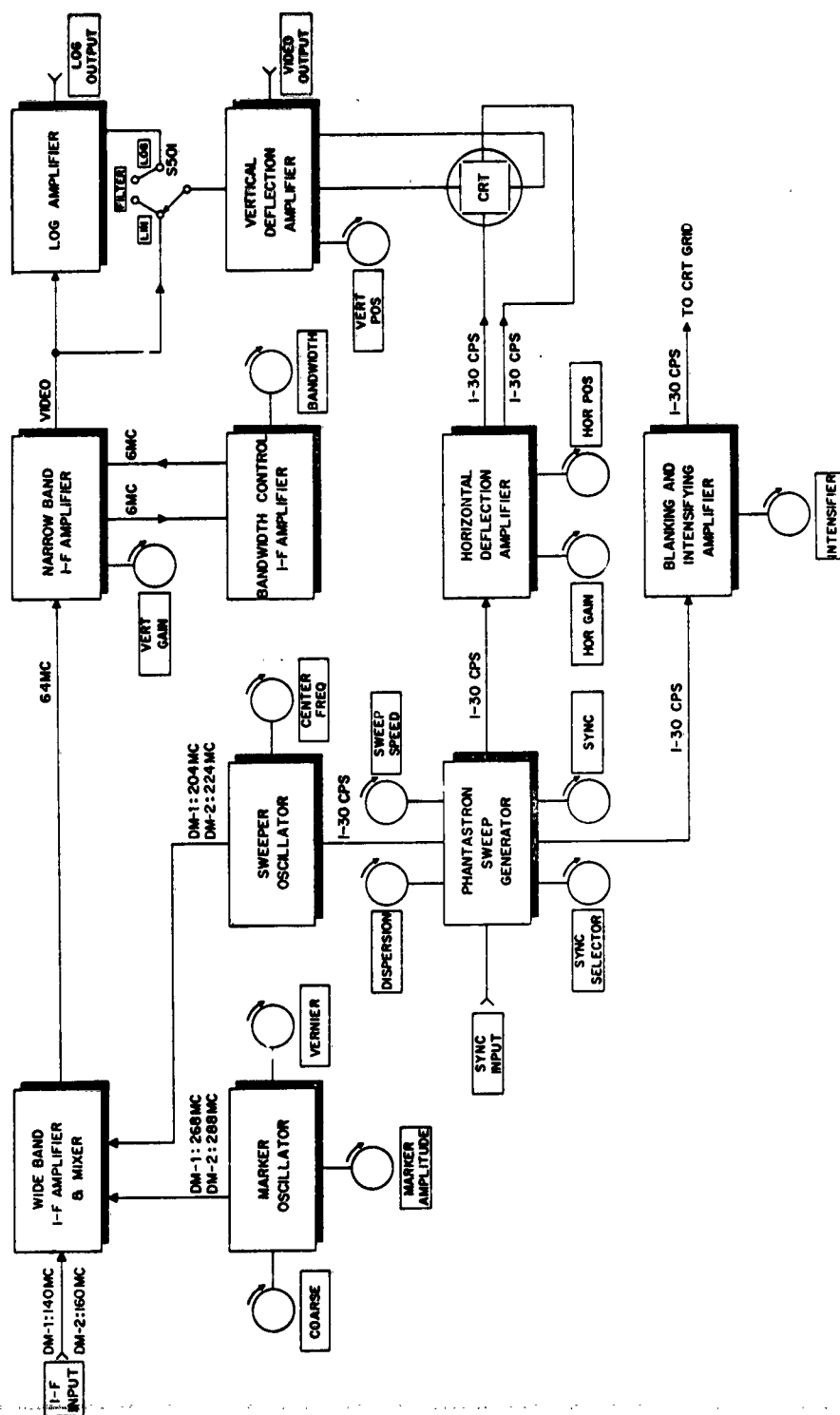


Figure 1. Simplified Block Diagram, Model DM-1 or DM-2

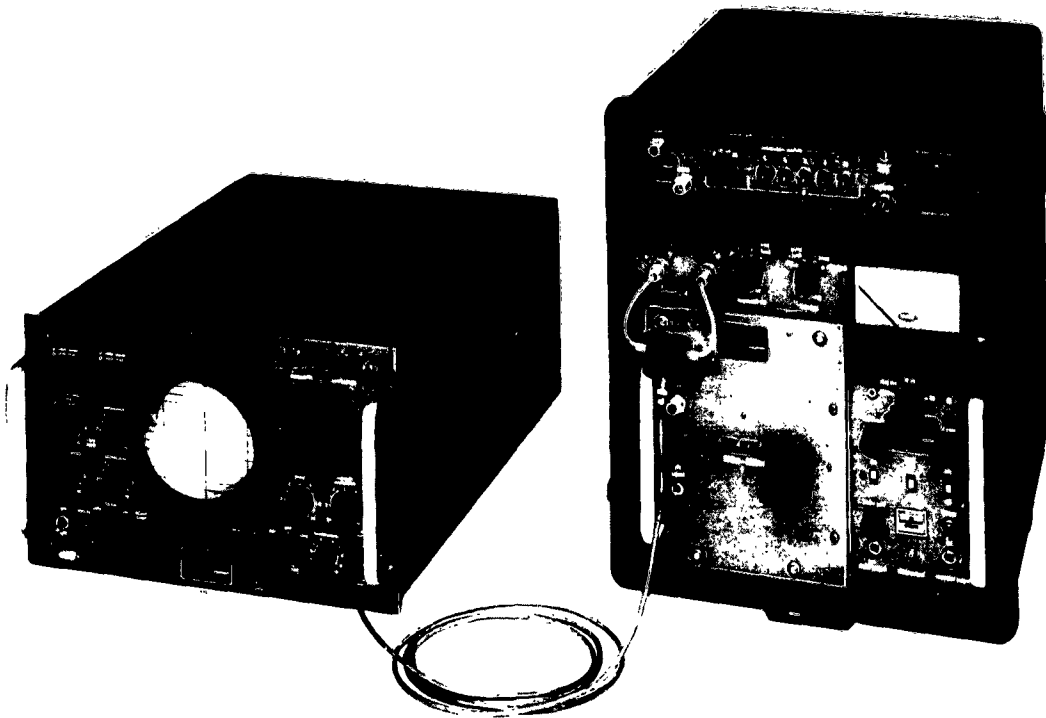


Figure 2. Operational Setup of Model DM-1 or DM-2 with Polarad Model CFI Receiver and Field Intensity Meter

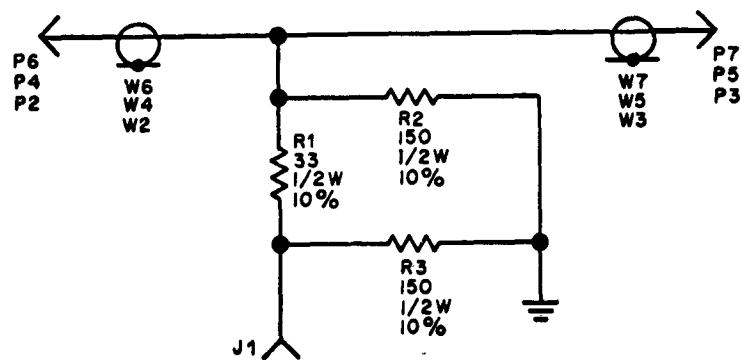
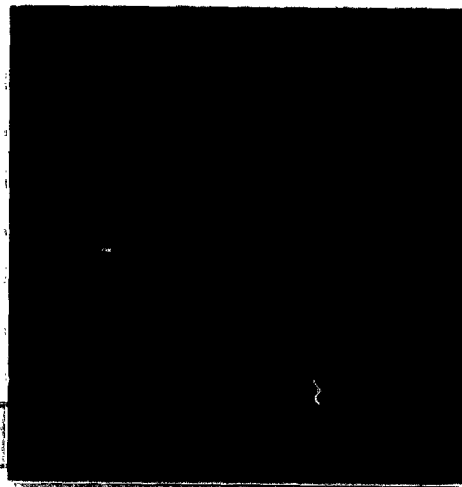


Figure 3. Coupling Box, Schematic Diagram



(a) Display of a Pulsed Signal



(b) FM Analysis



(c) Two CW Signals

-707-

Figure 4.

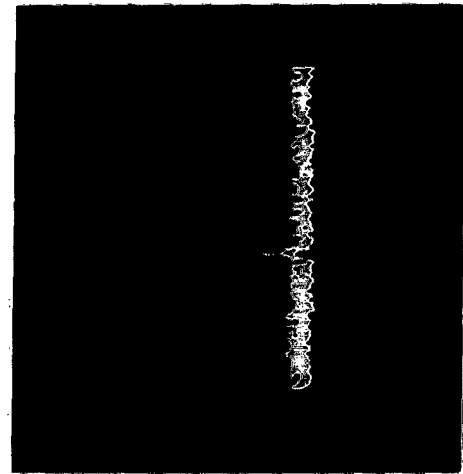


Figure 5. Signal Plus Noise = 2X Noise

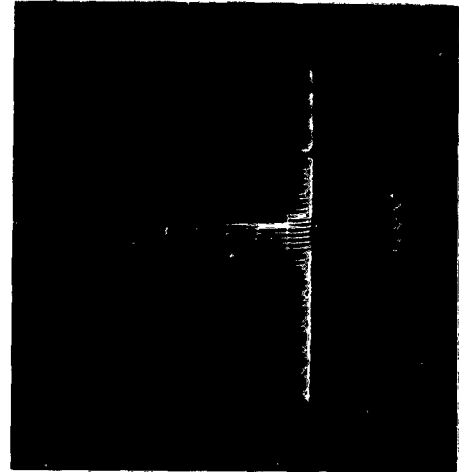


Figure 6. Pulse Display with Marker

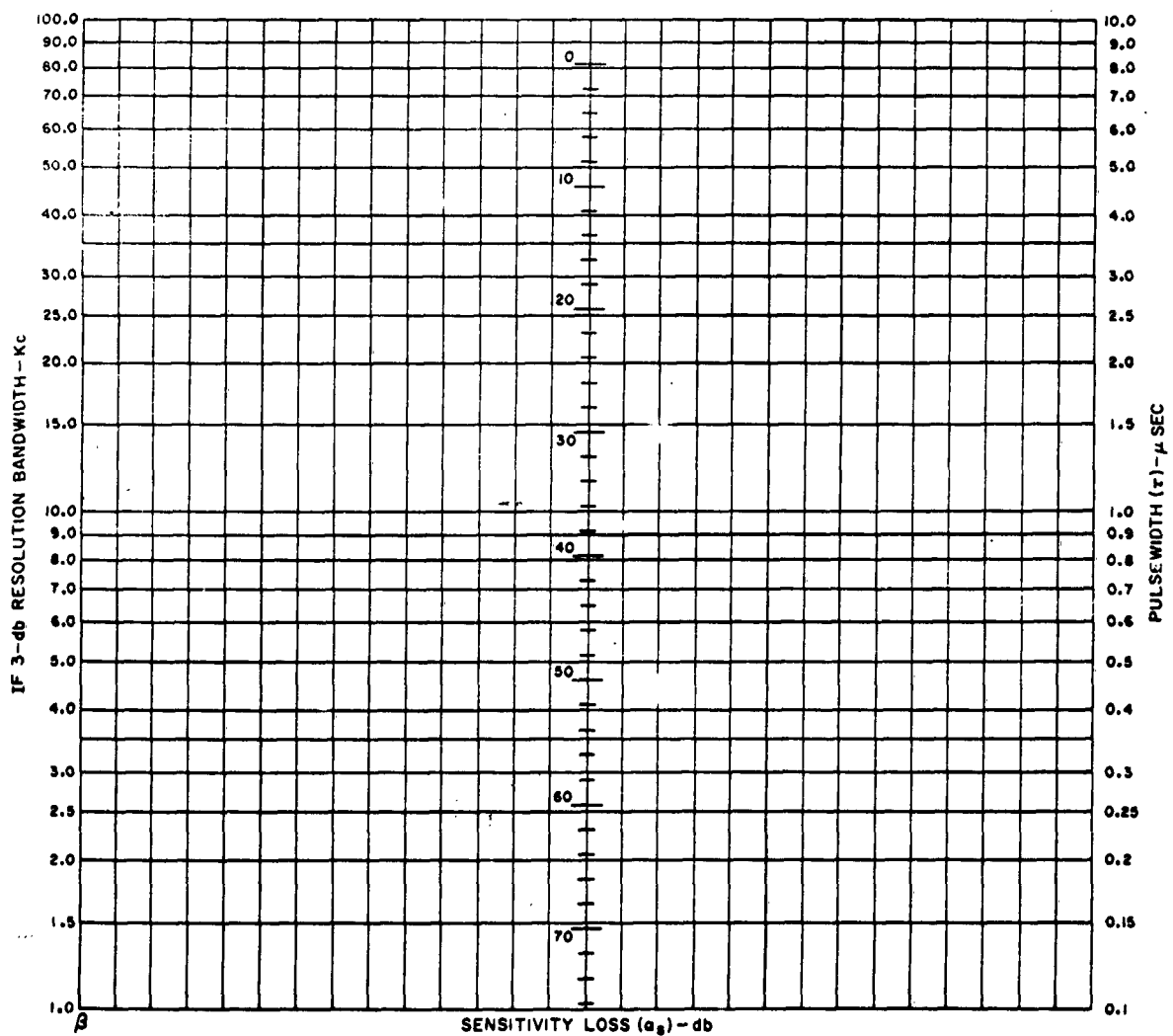


Figure 7. Sensitivity Loss as a Function of Signal Pulse Width and Bandwidth



## **ELECTROMAGNETIC COMPATIBILITY PROGRAM FOR THE MCDONNELL RF-4C, PHANTOM II AIRCRAFT**

**W. D. McKerchar  
McDonnell Aircraft Corporation  
Aircraft Systems Engineering Division  
St. Louis, Mo.**

**Abstract.** – The RF-4C aircraft involves a high density installation of electronic, electrical and electro-optical subsystems, integrated to perform a tactical reconnaissance mission.

Successful integration of individual subsystems in aircraft weapon systems depends significantly on the effects of interconnecting wiring and the associated grounding techniques. Inter- and intra-cable crosstalk among power, control and signal circuits may be high. Irradiation of cables by high power cw and pulsed energy, and the high level coupling which may result may cause serious data degradation and system malfunction, and may also pose the threat of premature ignition of on-board ordnance devices.

McDonnell has directed major effort toward Electromagnetic Compatibility of the aircraft system electrical and electronic devices, equipments and subsystems by careful attention to cable selection, routing and related grounding.

### **I. INTRODUCTION**

The Electromagnetic Compatibility program being conducted by McDonnell Aircraft Corporation for the United States Air Force RF-4C aircraft provides a wide variety of interference problems for the Electromagnetic Compatibility Manager. The RF-4C aircraft involves a high density installation of electronic, electrical and electro-optical subsystems, integrated to perform tactical reconnaissance missions. Early recognition of potential Electromagnetic Interference problems by McDonnell and the Air Force resulted in a strict Electromagnetic Compatibility control program involving five interdependent and concurrent phases:

- a. Equipment Requirements
- b. Design and Development
- c. Integration and Interface Considerations
- d. Preliminary Testing
- e. Aircraft Qualification.

To date, phases a and b have reached program planning milestones with a satisfactory confidence factor. The Equipment Requirements and the Design and Development phases include: Design Procedures; Contractor and Government Furnished Airborne Equipment considerations; Aerospace Ground Equipment; Subsystem testing; Quality Assurance provisions; Engineering

Design Techniques, and new manufacturing processes and methods. The requirements of MIL-I-26600 or MIL-I-6181D have been imposed on all subsystems. Interface and interconnection aspects are continually assessed to achieve a high confidence level for Weapon System compatibility.

## **II. DESIGN AND DEVELOPMENT**

All RF-4C weapon system subcontractors are required to submit Interference Control plans. Careful control is exercised by McDonnell management in cases where deviations are requested because of extreme costs or design compromise so that over-all system compatibility is not degraded. In some cases, preliminary reviews established design requirements exceeding existing Electromagnetic Compatibility and Interference Specifications. McDonnell had the responsibility of anticipating these needs and directing attention to them as early as practical in the design and development time period.

### **Subcontractor Interference Control Plans**

A critical factor often overlooked by many Prime contractors is the usefulness of the Subcontractor Interference Control Plan. McDonnell has highlighted the Interference Control Plan in its Vendor Technical Data Requirements document. Further, the EMI group in the Aircraft Systems Engineering Division assists vendors by advising them of the intent and the detailed information that should be in, an Interference Control Plan. An Electromagnetic Interference Control Plan advises the procuring activity of the effort a vendor will exercise to preclude the possibility that his product will adversely affect, or be affected by, other equipments located in close proximity to his installation. Adherence to this plan also serves to assure that the vendor's product is unlikely to be affected by stray external interference signals from other equipments.

It is recommended that the following control plan topics be discussed by the vendor in as much detail as possible:

- a. Circuits to be shielded.
- b. Circuits to be filtered.
- c. Method of selecting interference free components.
- d. Methods of obtaining continuous shielding in equipment housing and enclosures, including access doors, and other apertures.
- e. Definition of the frequency range for which the shielding is designed to preclude interference signals from affecting his equipment, and the attenuation to be expected.
- f. Protective finishes to be employed on mating surfaces, and methods for maintaining good electrical conductivity when protective coatings are applied.

- g. Suggested methods of bonding shock mounted units to the aircraft structure.
- h. Methods for selecting ground points for circuits and suppression components to minimize stray couplings caused by common ground impedances and circulatory currents in the chassis.
- i. Precautions to be taken to prevent susceptibility, spurious emanations, responses, and unwanted resonances.
- j. Good engineering practices in suppression techniques, such as filtering, shielding, bonding, grounding and isolation.
- k. Suppression measures that will be incorporated as an integral part of his system.
- l. Facilities available for testing to EMI specification and requirements.
- m. Administration of the vendor's EMI control plan, including:
  - 1. The number and qualifications of personnel assigned to the program.
  - 2. The company policy and the level of authority for influencing design to eliminate causes of interference.
  - 3. The vendor's designee for EMI liaison with the customer.

Upon review of the vendor's control plan, the EMI control group can, in many instances, determine the areas that may present interference situations causing system incompatibility in the completed vehicle. The EMI control group may then act to avert such situations by assisting the vendor in design "fix" efforts and/or by providing for cable separation, shielding or shading within the aircraft. Thus, the vendor's EMI control plan is a useful tool in McDonnell's program for insuring that aircraft electromagnetic compatibility requirements can be met.

The plan is used to expose problem areas in advance, to act to eliminate or suppress them, to provide further EMI liaison efforts with the vendor or between vendors and thereby to improve the product.

#### McDonnell Interference Control Plan

The McDonnell interference control plan for the RF-4C weapon system, a formal document submitted to the Air Force, describes a multi-phased program for analyzing, predicting, controlling and monitoring potential audio and radio frequency interference within the RF-4C aircraft to achieve electromagnetic compatibility of the weapon system.

The primary objective is that no undesirable response, malfunction or degradation of performance due to electromagnetic interference will occur in, or be produced by, electrical or electronic equipment installed in the RF-4C. Maximum feasible system and subsystem operational compatibility and over-all weapon system effectiveness obtained by competent interference design techniques constitute the acceptable performance criteria of this plan.

### **III. ENGINEERING DESIGN TECHNIQUES**

To provide reasonable assurance that the requirements of the weapon system compatibility specification will be met, the following engineering design techniques are employed as applicable.

#### **Basic Installation Planning**

In the early phases of weapon system design, there is relative freedom of choice of equipment, location and cabling. Once the system is committed to a specific configuration, the level of electromagnetic interference has been essentially established, and changes and improvements become difficult to effect. The minimum change, minimum cost concept of the RF-4C aircraft made careful planning essential for optimum results in interference control. The initial work phase utilized all known system parameters in the following categories:

- a. Susceptibilities and paths of entry of interference for each component of the aircraft system.
- b. Interference producing capabilities of each component part of the aircraft system.
- c. Limits on the flexibility of component location and orientation imposed by structural and environmental considerations.
- d. Possible alternate antenna installation locations on the aircraft causing the least reduction of performance of installed equipments.

#### **Installation Considerations**

Consideration was given to installation techniques of:

- a. Physical Isolation
- b. Equipment Grouping
- c. Use of Interference Reduction Components
- d. Structure Shielding and Shading
- e. Equipment Shielding
- f. Aircraft Interconnect Wiring.

In common with most complex weapon systems, the RF-4C is an example of high density packaging. Physical isolation is difficult to achieve, as equipment grouping is dictated principally by reconnaissance requirements. If required, suppression components are added later. Shielding and shading afforded by structure can be used only within weight and practicable limitations. Therefore, major installation considerations pursued were in equipment (case) shielding and in the heart of weapon system compatibility, aircraft interconnect wiring.

### Equipment Shielding

Inasmuch as shielding for the containment of radio frequency energy furnishes the most important element in the reduction of radiated interference, vendor design techniques for equipment housing were carefully evaluated. An ideal shield has extremely high conductivity, great thickness, high permeability, and is virtually watertight with no openings or discontinuities. Practical shields usually represent compromises dictated by weight and space limitations.

### Equipment Housing

The following design criteria were evaluated:

- a. Thickness
- b. Conductivity
- c. Permeability
- d. Minimum-access openings
- e. Joint construction
- f. Contact area
- g. Contact pressure.

### Discontinuity Considerations

Equipment housing design was reviewed to evaluate possible discontinuities in housing construction. The following considerations were applied. Mechanical discontinuities were required to be minimum; joints and flat metal seams be electrically continuous across the interface; surfaces of joints be mechanically smooth (highly conductive and use noncorrosive materials), joints welded wherever possible. Where bolts, rivets, or other fasteners are employed, fastener spacing must be consistent with the amount of energy to be confined. Where bolts or screws are used, the necessity of RF gasketing or RF "weather stripping" was investigated. Bolts, screws, or any metal projections which pass through the equipment housing were particularly scrutinized for being RF "tight."

### Ventilation

Where relatively large "holes" for air flow openings are provided, the need for covering by well bonded metallic tubing or conduit having the high pass filter characteristics of a wave guide was evaluated.

### Bonding

Shock mounted chassis were provided with bonding to the aircraft structure with a bond strap of length not greater than five times its width, where practicable. Bond straps were specified to be accessible for maintenance.

### Flexible Conduit

Flexible conduit consists of metallic interlocking spiral hose with an outer covering of tightly woven metal braid. Without the outer braid, the flexible conduit offers good reflection characteristics, but is likely to leak at the junctions between spiral turns. This leakage can be quite serious at high frequencies. The outer braid reduces the tendency to leakage. At low frequencies, the single braid outer covering yields about 50 db additional attenuation over that of the flexible hose.

Due to space, weight, and maintainability considerations, the use of flexible conduit was avoided where possible; however, severe electromagnetic compatibility situations dictated its use in certain cases. In these instances, McDonnell employed conduit recommended by the military services (e.g., MS25067-( ) with MS25065-( ) ferrules and MS25066-( ) nuts).

### Aircraft Interconnect Wiring

Successful integration of individual subsystems in an aircraft weapons system depends to a great extent on the effects of interconnecting wiring and its associated grounding philosophy. In a small, dense, aircraft complex such as the RF-4C, the possibility of inter- and intra-cable crosstalk among power, control, and signal circuits is high. In addition, irradiation of cables by high power cw and pulsed energy, with the possibility of high level coupling, may not only cause serious data degradation and system malfunction, but may also pose the threat of premature ignition of on-board ordnance devices.

The peculiarities of varying grounding philosophies in connection with interconnecting wiring compound the problem and often control the limiting factors in precluding malfunctions.

Major effort was directed toward electromagnetic compatibility of the aircraft system electrical and electronic devices, equipments, and subsystems by careful attention to cable selection, routing, and related grounding. Extensive guidance was given to both McDonnell and subcontractor engineering personnel in the employment of proven interference control techniques and to establish the aircraft interconnect design objectives. A unique aircraft wiring concept, the "COMPACT WIRE HARNESS", developed by McDonnell, posed additional problems in effecting required objectives.

To resolve the several problems outlined above, close liaison was maintained with cognizant design engineers on each equipment, and the current, voltage, impedance, signal types, susceptibility, and sensitivity of each interconnect circuit were established. These data, combined with knowledge of lengths of interconnect cables and equipment locations, provided information for an analysis of electrostatic and electromagnetic coupling. The results of the analysis were used in establishing effective, realistic, EMI wiring criteria for new system installations in the RF-4C aircraft. The coordination effort, thus accomplished, permitted the guidance necessary in the aircraft interconnect installation consideration.

### McDonnell Compact Wiring Harness

Due to increasing complexities of electronic equipments and electrical wiring, problems arose because of the increase in wiring and the smaller areas in which it had to be placed. For example, the Phantom aircraft of 1946 had 18,000 feet of wire compared to 54,000 feet in today's Phantom II.

To solve a high density wiring problem, McDonnell Aircraft Corporation, in May of 1959, established a program called "Project Wire," to study and investigate the state of the art concepts and techniques for improving aircraft wire installations. The primary objective of this program was to decrease the harness diameter, improve reliability and improve appearance. From this program evolved a wiring method called the compact wire harness. The compact wire harness, capable of withstanding 300°F for prolonged periods of time, generally consists of a harness made from teflon insulated hook-up wire designed for the internal wiring of electrical and electronic equipment instead of airframe wire, and protected by a coated dacron braided outer cover. Figure 1 provides a good comparison as to the difference in size of a conventional harness fabricated with airframe wire and that of a compact wire harness. Other than the approximate one-third decrease in the harness diameter, the compact wire harness is appreciably lighter, more flexible, offers increased abrasion resistance, has a better appearance (Fig. 2) and cuts installation time in half compared to conventional airframe wire harnesses. Also, our records at McDonnell Aircraft Corporation indicate that since the advent of the compact wire harness on the F-4B aircraft, damage because of fabrication and installation is approximately one-half or less, than when conventional airframe wire harnesses were used.

### McDonnell Shielded Compact Wiring Harness

In the initial cable analysis, it was evident that completely shielded wiring harness would be necessary.

These needs were not as severe as requiring flexible conduit, but dictated more stringent shielding than afforded by conventional shielded wiring.

In relation to solving the problem of shielding the compact wire harnesses, the RF-4C aircraft project in January 1963 requested the Material & Process Development Department to investigate and determine the best method of providing shielding for a complete harness of wires. The objectives set up for this investigation were as follows:

- a. To keep the harness diameter as small as possible and withstand 300°F without sacrificing performance or reliability.
- b. To determine the best method for providing a shield able to provide a minimum coverage of 85% as defined in MIL-C-27500.

- c. To obtain a good electrical bond between the shielding braid and the connector.
- d. To derive a method to feed a shielded harness through a potted pressure-sealed bushing.
- e. To fabricate a harness that could be repaired in the field.

The investigation indicated that the best and easiest way for McDonnell Aircraft Corporation to provide the shielding of a harness was basically to fabricate the harness, using our compact harness methods and braid tin coated copper wire over it.

The first objective, that of keeping the bundle diameter to a minimum, was solved by fabrication of the bundle using the same basic methods employed in the compact wire harness. This generally employs the use of MIL-E-16878, Type E, polytetrafluoroethylene insulated wire in place of airframe wire. While this wire lacks in the physical properties of airframe wire, it has the same electrical properties. To provide the necessary protection from possible physical damage due to the braiding of the shielding over the wires, a heat shrinkable polyolefin sleeving is applied over the bundle (Fig. 3). Then, after the shielding braid is applied, the harness is dacron braided and Kel-F coated.

The next objective, that of providing a shield medium over the harness (Fig. 3), was solved by the use of braided tin coated copper wire. This braid is applied by the use of a 24 carrier braiding machine equipped with an overhead sheave capstan. The machine, in general, is the type used in the manufacturing of shielded or coaxial cable. The machine permits the use of various sizes of braid wire, and by control of the number of wire ends per spool and capstan speed, enables one to obtain a minimum of 85% coverage as defined in MIL-D-27500 on bundles 1/4 to 1 inch in diameter.

The third objective, which was to obtain a good electrical bond between the shielding braid and the connector, was achieved by the use of a straight 90 degree strain relief clamp (Fig. 4). Before the shield braiding is started, a metal sleeve is positioned on the harness under the clamp. This is done to prevent the crushing of the metal braid into the harness when the strain relief clamp is tightened on the braid. The process also provides a good mechanical and electrical bond between the shielding braid and the connector shell. A maximum bond resistance of .0025 ohms is required. In practice, the measured resistance is approximately .0001 ohm.

Fourth, the objective of deriving a method to feed a shielded harness through a potted pressure sealed bushing was achieved by prepotting the wires prior to metal braiding. After the braiding is completed, the harness is again potted in the bushing (Fig. 5).



The fifth objective, that of obtaining maximum shielding effectiveness for internal shielded and coaxial cables, was achieved by: one, limiting the distance between the shield termination and the connector; two, by the use of a "solder ring" (Fig. 4). Because of the limited space created by restricting the shield termination in the connector's strain relief clamp, a new polyolefin heat shrinkable solder termination was used. This type of shield termination reduces the bundle diameter at terminations approximately 20 per cent compared to other commonly known methods and allows the shield termination to be within 1/4 to 1 inch from the connector. These shields are then jumpered together by the use of a "solder ring", consisting of a number 16 gage non-insulated copper wire which is wrapped around the harness in the connector adapter. The shield jumpers are soldered to the solder ring and a ground lead is then attached to a connector contact and the solder ring; thus, the shields are grounded through the connector. To isolate these grounds from the bundle's external shielding, the connector's strain relief clamp is then potted. The potting's primary purpose is to waterproof the backside of the connector and to support the wires, but, as one can see, it serves a secondary purpose, that of isolating the internal shields from external shields.

Figure 6 shows the detail of shield coverage at a harness branch. Figure 7 depicts shield termination at a junction box assembly.

The last objective, that of a repairable shielded bundle, has not been achieved to the extent that we had hoped. While limited repair can be done, it can only be done in a fairly well equipped shop. The main problem lies in the connector's strain relief clamp which we are presently using.

Areas in which we are investigating methods of improving our shielded compact wire harness in relation to weight, size and shielding effectiveness are as follows:

- a. Evaluation of newer wire insulations for resistance to abrasion and cut-through to determine if insulation thickness can be reduced.
- b. Evaluation of higher strength conductor to determine if the use of a smaller gage wire is feasible.
- c. Evaluation of methods of lowering the density of potting compounds.
- d. Evaluation of different material to be used as a barrier between the wire and outer shield.
- e. Evaluation of other methods and materials to outer shield the harness.
- f. Evaluation of a connector adapter to increase reparability of the harness.

The objectives have been met to keep the harness diameter as small as possible without sacrificing reliability or performance, to maintain flexibility and decrease possible physical damage, and to provide a minimum shield coverage of 85%.

By meeting the above requirements, we have limited the use of flexible conduit to only severe interference situations; reduced maintainability and installation problems; achieved savings in weight, and have provided shielding adequate to preclude the possibility of undesirable interference situations.

#### Electrostatic and Electromagnetic Coupling

Electrostatic and Electromagnetic Coupling analysis involved these factors: voltage, current, receiver circuit parallel impedance, receiving circuit sensitivity (voltage and waveform), length of cable run and physical separation of source and receiver wiring.

Equipment location had to be considered from the standpoint of flight missions of the aircraft, as well as the weight reduction that could be achieved from minimum cable lengths. This approach resulted in numerous coupling and crosstalk problem possibilities, in that the designs of most equipments were not as yet firm and therefore interconnect wiring characteristics were unknown. In some instances, highly susceptible cables were required to be routed necessarily long and adjacent to "offenders", compounding interference situations. During electrostatic and electromagnetic coupling analysis, cable lengths were considered, but could not be changed. Further, cross-sectional area for cable routing was limited; this, coupled with the large number of interconnect cables, prevented wiring separation for a complete run. Both the above restrictions affected electrostatic coupling. Thus, if a wire length could have been decreased by a 10 to 1 factor, the voltage induced into the receiving wire would also have decreased by the same ratio, or 20 db.

In view of the above, the alternatives remaining for EMI design engineering included interference control from the standpoints of impedances, circuit susceptibility (both level and waveform) and the generally accepted twisting and shielding of interconnect wiring. To provide a wiring configuration guideline, graphs were made which aided in the determination of coupling between source and receiver wiring. Extensive coordination with vendors and other McDonnell departments permitted design changes which could be accomplished to further preclude interference problems.

### Grounding

The grounding philosophy for use on the RF-4C aircraft interconnecting wiring, as well as vendor equipment, was established after a careful review of the state-of-the-art objectives and available information concerning:

- a. transients,
- b. ambient electromagnetic fields,
- c. sensitivities,
- d. cable pickup,
- e. frequency data, and
- f. impedance data.

The above review resulted in guidelines to be used by the EMI group in determining system grounding. The following rules were applied to the extent possible within the vendor's equipment as well as aircraft wiring:

#### Signal Ground

Signal ground is the low side of circuits of whose susceptibility characteristics are best described as low level (less than one volt), low frequency (up to and including the high audio frequency range).

The grounding (to aircraft structure) technique used on the RF-4C for signal ground is a modified single point ground in that no single point within the aircraft was used for signal ground, but rather each subsystem or black box contains its own signal ground that in turn was tied to aircraft ground as close as possible at its point of emerging from the subsystem.

Transformers and other isolation devices were used to the extent possible to decrease the length of run necessary for each signal ground.

#### Signal Shield Ground

Signal shield ground refers to the grounding (to aircraft structure) technique utilized for shields covering wires that are susceptible to low level, low frequency pickup. Signal shields are grounded at one end only.

### **RF Interference Shield Ground**

RF interference shield ground refers to the grounding (to aircraft structure) technique of shields utilized to protect leads susceptible to RF fields or carrying RF energy. RF interference shields are grounded to the aircraft structure at both ends and at all breaks in the run.

### **Chassis Ground**

Chassis ground refers to the metal structure utilized to support electrical or electronic components. Chassis ground requirements are an extension of the aircraft structure ground in that the bonding resistance shall not exceed .0025 ohms at DC.

### **Schematic Coding**

Schematic coding on each interconnect drawing was devised to explicitly show the method of shield termination, i.e., ground at one end only, ground at both ends, etc.

## **IV. CONCLUSIONS**

The Equipment Requirements and Design & Development phases are now complete. The Interface and Integration, as well as Preliminary Testing phases, currently in progress, favorably indicate that a satisfactory confidence factor has been realized. Aircraft qualification tests will provide the measure of the effectiveness of the EMI control program which is being pursued by McDonnell.

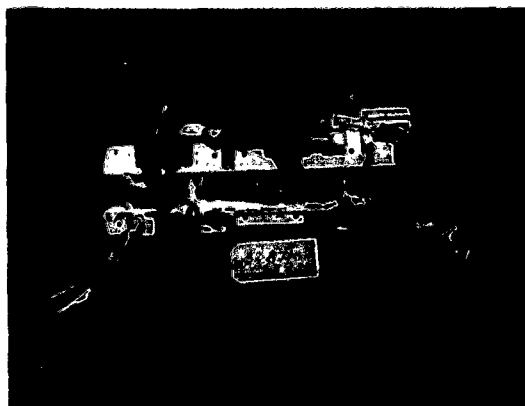
## **ACKNOWLEDGEMENTS**

The work described in this paper was performed for the United States of America, under contract NOW 62-0383-i.

Appreciation is expressed to R.A. Fischer of McDonnell Material and Process Development department and to C.J. Lamont of Sprague Electric Co. for their contributions to this effort.



**FIGURE 1 COMPARISON OF CONVENTIONAL/COMPACT/SHIELDED COMPACT**



**COMPACT WIRE HARNESS**



**CONVENTIONAL WIRE HARNESS**

**FIGURE 2. COMPARISON - BUNDLE ASSEMBLIES**

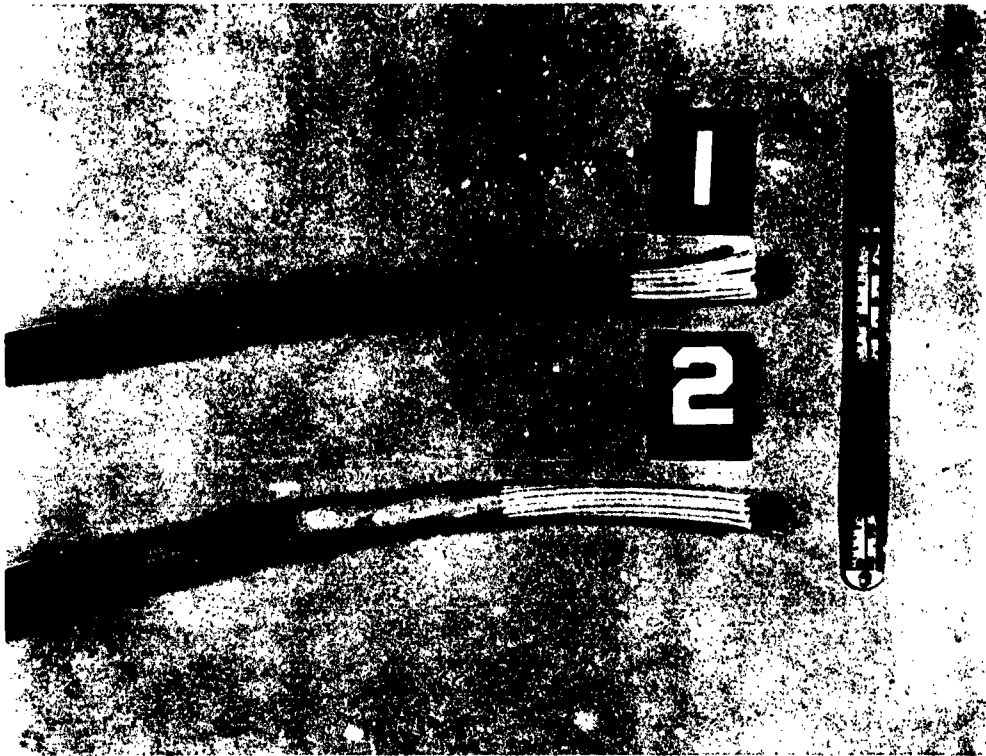


FIGURE 3 COMPARISON COMPACT/SHIELDED COMPACT WIRE HARNESS

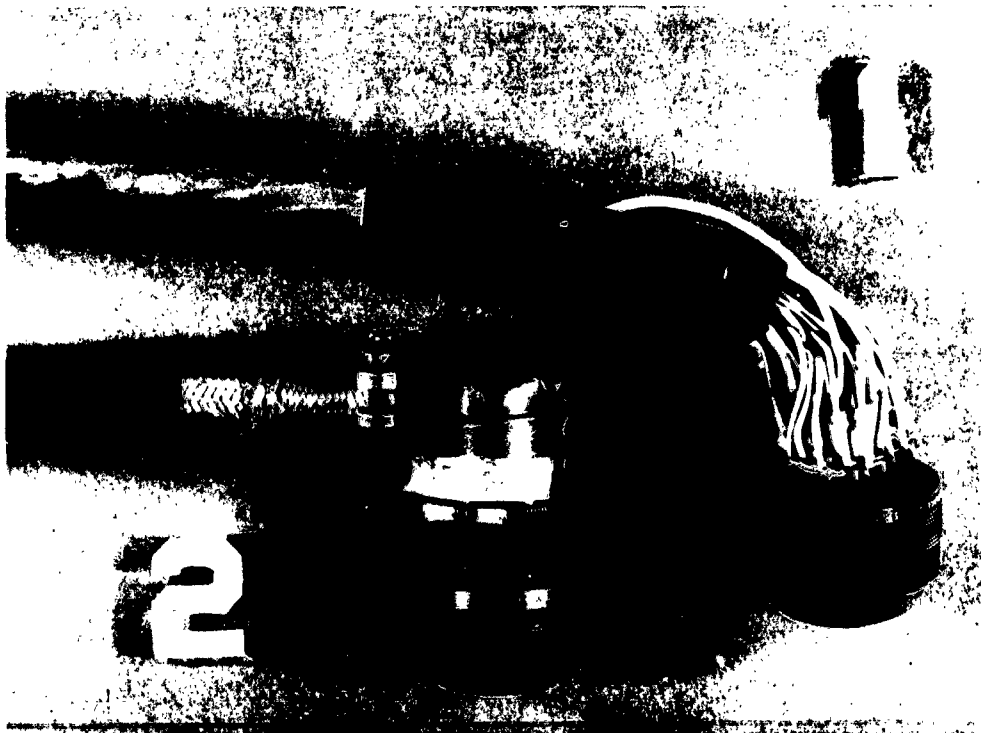
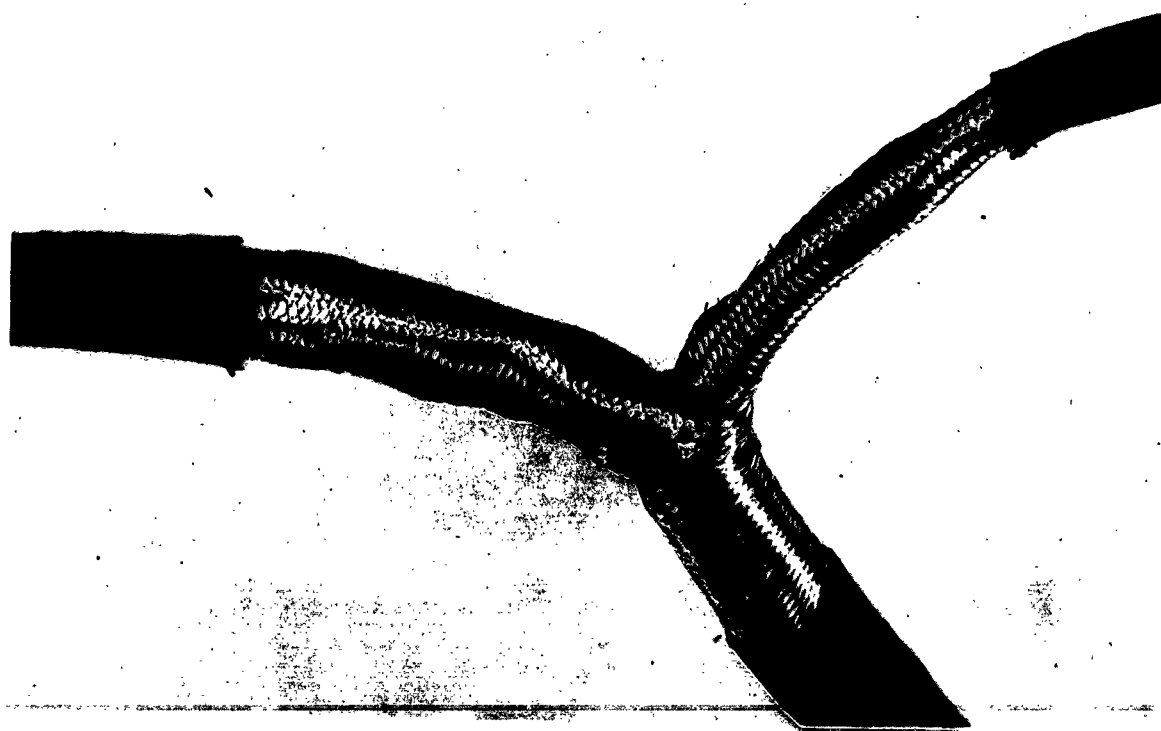


FIGURE 4 DETAIL OF CONNECTOR ASSEMBLY



**FIGURE 5 HARNESS FABRICATION FOR PRESSURE BULKHEAD**



**FIGURE 6 SHIELDED COMPACT WIRE HARNESS - BRANCH DETAIL**



FIGURE 7 SHIELDED COMPACT HARNESS - JUNCTION BOX TERMINATION DETAIL



## A METHOD FOR PERFORMING TRANSIENT SUSCEPTIBILITY TESTS ON PRIMARY POWER LEADS

R. F. Kantner  
Westinghouse Electric Corporation  
Air Arm Division  
Baltimore, Maryland

**Abstract.** - This paper describes a method for performing audio frequency susceptibility tests on primary power leads using square waves, triangular shaped pulses, exponentials, and most other types of functions.

On D.C. power leads this can be accomplished using well-known methods such as transformer coupling, series modulators, etc.

To vary the RMS voltage on A.C. power leads in some functional manner, use is made of the result that occurs when an A.C. signal at a frequency close to or at the power line frequency is transformer coupled onto the power line.

When the injected frequency is exactly the same as the power line frequency and both are in phase, the RMS voltage at the load is increased by an amount equal to the injected voltage. When the injected voltage is at exactly the same frequency and both are out of phase, the RMS voltage at the load is decreased by an amount equal to the injected voltage. When the frequency is slightly below or above the power line frequency, the RMS voltage at the load varies in a sine wave fashion at a frequency equal to the difference frequency between the power line and the injected voltage. The instantaneous voltage at the load is in all cases equal to the vector sum of the instantaneous power line voltage and the injected voltage.

Use can be made of the above results to vary the RMS of the power line voltage in step functions, exponential functions, exponential sine functions, or using many other common functions.

### I. INTRODUCTION

From time to time, requirements exist to determine the performance of an equipment while subjecting it to transient disturbances applied to its primary power leads. The transient disturbances are of a nature likely to exist during field use and in general are the same as required by MIL-STD-704. Very little has been written on this type of testing and those MIL specs which require testing of this type (Such as MIL-STD-704) do not prescribe a method for producing these transient disturbances. Therefore, test methods must be devised. The test methods presented in this paper presents in some respects an interesting approach to this problem.

## II. Types of Transient Disturbances

Figures 1 thru 4 show the basic types of transient disturbances most commonly found to exist on primary power leads. On DC power leads the transients are in general exponentials or exponentially decaying sinusoids. On AC power leads the disturbance is of the same nature as DC leads in that the RMS of the line voltage fluctuates in an exponential decaying sinusoidal fashion. In some cases the transient disturbances exceed one half second in duration.

Less common transient type disturbances found on both AC and DC power leads include square waves, triangular shaped waves and less describable functions.

Except for the magnitude of the transient disturbance, this then defines the testing requirements for this type of test. The test method, as a minimum, should be capable of providing the most common type transient disturbances and if possible should be capable of providing some of the less common types. The amplitude of the transient disturbance should be variable up to at least 6 db greater than the transient disturbance known or expected to exist during field use.

## III. Transient Disturbances on DC Lines

Two methods were used to produce transient disturbances as described above on DC power leads. One method involves transformer coupling the transient onto the power lead (Series Induction) and the other involves the use of a Series Regulator.

### Series Induction Method.

Figure 5 shows the test set-up for producing transient disturbances by series induction. The test set-up is that prescribed in MIL-I-6181 and MIL-I-26600 for performing audio susceptibility tests except that the signal source is a transient or function generator.

The transient generator takes on various forms depending on the type of transient disturbance being generated. For exponential transients, an RC network such as that shown in Figure 6 was used. Exponentially decaying sinusoids can be generated by modulating the output of an oscillator with an exponential function. Often, however, it is difficult to decouple the desired modulated signal out of the modulator from the modulating function, particularly when there is not an appreciable difference between the frequencies contained in the modulating function and the output of the oscillator. The circuit shown in Figure 7 has been useful in avoiding this problem. A photocell connected in a bridge circuit is taped to the face of an oscilloscope. The oscilloscope is triggered and the beam allowed to sweep across the photocell resulting in a function across the bridge such as that shown in figure 8. The duration of the transient can be varied by varying the sweep speed and can be made repetitive by allowing the sweep to free run.

Figure 9 is useful for determining the amplifier power requirements as a function of the amplitude of the desired transient disturbance and the impedance of the load. This is based on the amplifier output impedance being matched to the impedance of the line.

When it is desired to simulate very low frequency transient disturbances, that is transient disturbances that contain very low frequencies, it becomes impractical to design a transformer to efficiently pass these frequencies. In those cases series regulators were used to produce the desired disturbance.

#### Series Regulators.

An example of a simple series regulator is shown in figure 10. The circuit was designed to produce transient disturbances on 28 VDC lines that draw a nearly constant load current. A 35 VDC power supply was used and the voltage was dropped down to 28 VDC by the series transistor. The desired transient was then applied across the emitter base circuit of the transistor.

The supply voltage must be at least equal to the peak voltage desired during the transient disturbance and the transistor must be capable of dissipating power equal to the difference between the supply voltage and the quiescent line voltage times the load current.

The transient generators were used with the series regulator as were used for the series induction method.

#### IV. Transient Disturbances on AC Power Leads

The method chosen for producing transient disturbances on AC power leads, like the Series Induction method used on DC power leads, also involves transformer coupling AC signals onto the power line, however, the transient disturbance was produced in a slightly different manner than on DC leads.

Consider the circuit in figure 11. The transformer can be considered as another generator in series with the power source. Then the voltage across the load is the vector sum of the voltages out of the two generators. When the voltages out of the two generators are of the same frequency and in phase, the voltage across the load is the algebraic sum of the voltages out of the two generators. When the voltages out of the two generators are of the same frequency and exactly 180 degrees out of phase, the voltage across the load is the algebraic difference between the outputs of the two generators. When the output of the two generators are at a slightly different frequency, the vector sum is an oscillating function, being a maximum when the generators are in phase, a minimum when the generators are out of phase and oscillating between minimum and maximum at a frequency equal to the difference between the frequencies of the two generators.

By varying the amplitude of the signal injected onto the power line and by proper selection of its frequency and phase, the voltage across the load can be made to vary in a manner very similar to the common disturbances found to exist on AC power leads. For example, the signal in figure 12 was injected onto a 400 cps power lead and the voltage shown in figure 13 resulted across the load. The waveform shown in figure 12 was generated by applying the 400 cps line voltage across the bridge circuit shown in figure 14. This insures that the signal will be of exactly the same frequency as the line. The photocell in the bridge circuit was taped to the face of an oscilloscope and the oscilloscope trace was allowed to sweep across the photocell. The injected signal was at the same frequency as the line and exactly in phase. The voltage across the load rises rather sharply from 115 VRMS to 160 VRMS and decays approximately exponentially back to its quiescent level of 115 VRMS.

Figure 15 shows the voltage across the load under the same conditions as above except that the injected signal was 180 degrees out of phase with the line voltage. The voltage across the load drops rather sharply from 115 VRMS to 70 VRMS and increases approximately exponentially back to its quiescent level of 115 VRMS.

Figure 16 shows the voltage across the load under the same conditions as above except that the excitation for the bridge in the transient generator was fed from an audio oscillator and was set at 385 cps. Note the 15 cps oscillation on the voltage applied to the load, 15 cps being the difference between the line frequency and the injected signal frequency. The voltage across the load varies sinusoidally from 70 VRMS to 160 VRMS, the variation decaying approximately exponentially back to its quiescent level of 115 VRMS. One of the chief advantages of using this method for producing transient disturbances on AC power leads is the relative ease in producing this type of transient disturbance.

Other methods considered for use in producing transient disturbances of these types include varying the field current of a rotary generator and modulating the output of an electronic power supply. The output of rotary supplies generally cannot be varied rapidly because of the high reluctance of the field. A method for generating transient disturbances using an electronic supply was previously presented by R. C. Dyer.<sup>1</sup>

The transformer method of producing transient disturbances also has some disadvantages, however, these are not major problems for most testing at subsystem level. The output impedance of the transient source must be sufficiently low to avoid absorbing excessive power from the power line. Normally the output impedance of the generator is kept below 1 ohm and the power absorbed from the line by the transient source is limited to 25% of the rated output of the power amplifier used in the transient generator.

<sup>1</sup> MIL-I-006051B Audio-Transient Generator, R. C. Dyer, Proceedings, 7th Conference on Radio Interference Reduction and Electronic Compatibility.

Figure 17 is a graph of amplifier power vs amplitude of transient for various output impedances of the transient source. Since the output impedance level of the transient source must be kept low, the power requirements are high for generating high transient levels on the line.

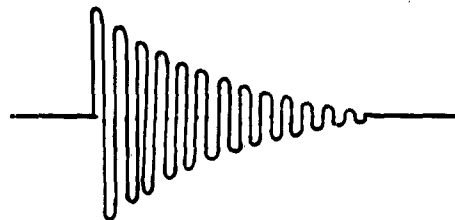
The shape of the transient disturbance is a function of the injected signal and the number of shapes that can be applied is limited only by the ability to generate these forms in the transient generator. Work is progressing as time permits in developing an improved transient generator for generating the many less common transient disturbances.

#### ACKNOWLEDGEMENTS

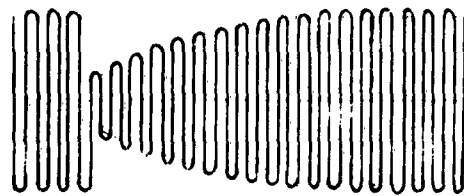
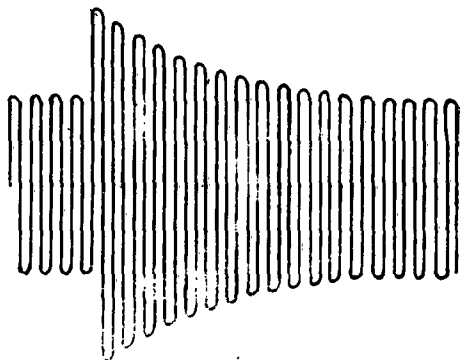
The author expresses appreciation to G. A. Bickerstaff for his assistance in the laboratory and to W. W. Hill for his encouragement and time spent in reviewing this paper.



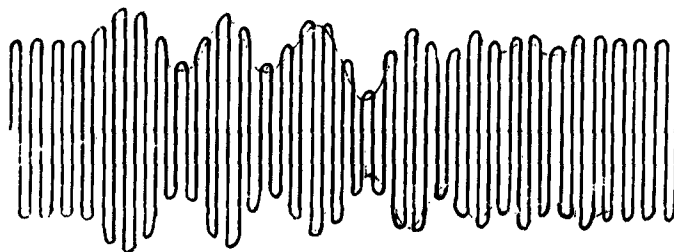
Exponential Transient - DC Power Lead  
Figure 1



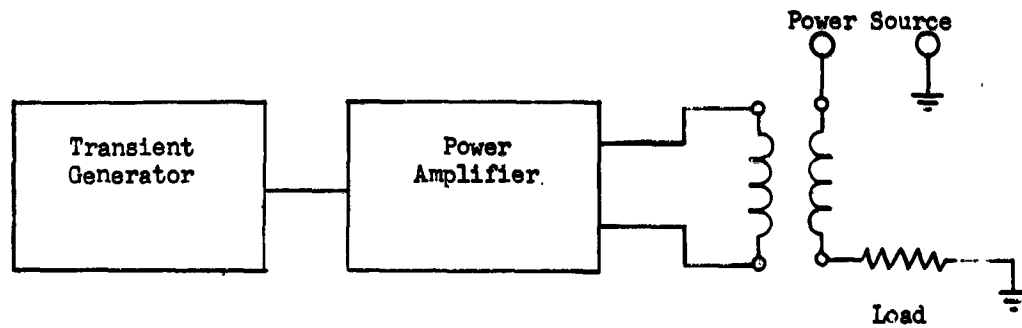
Exponential Sinusoid - DC Power Lead  
Figure 2



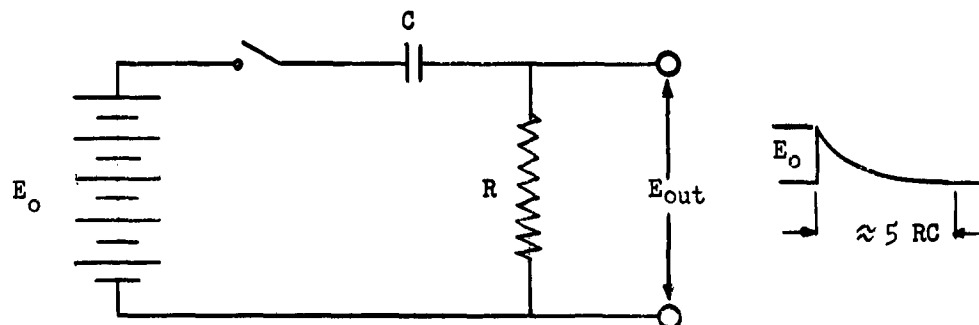
Exponential Transients - AC Power Leads  
Figure 3



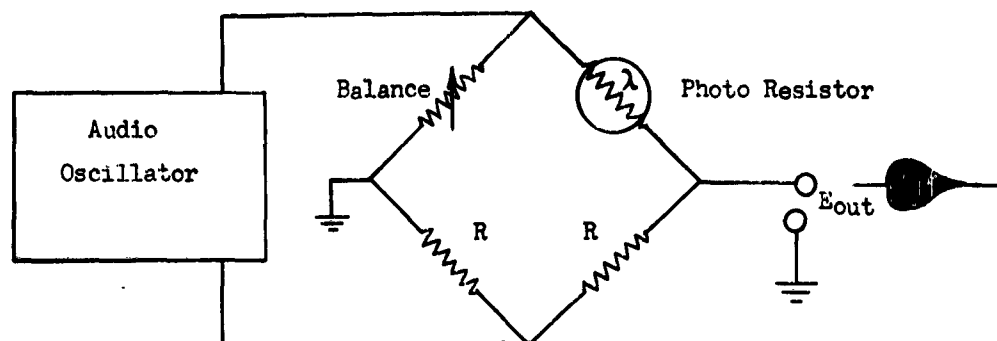
Exponential Sinusoid - AC Power Leads  
Figure 4



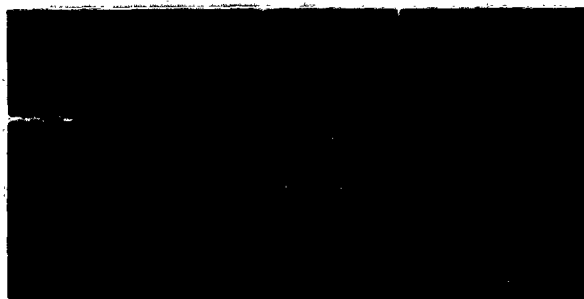
Test Set-up - DC Power Line Transient  
Figure 5



Simple Transient Generator  
Figure 6

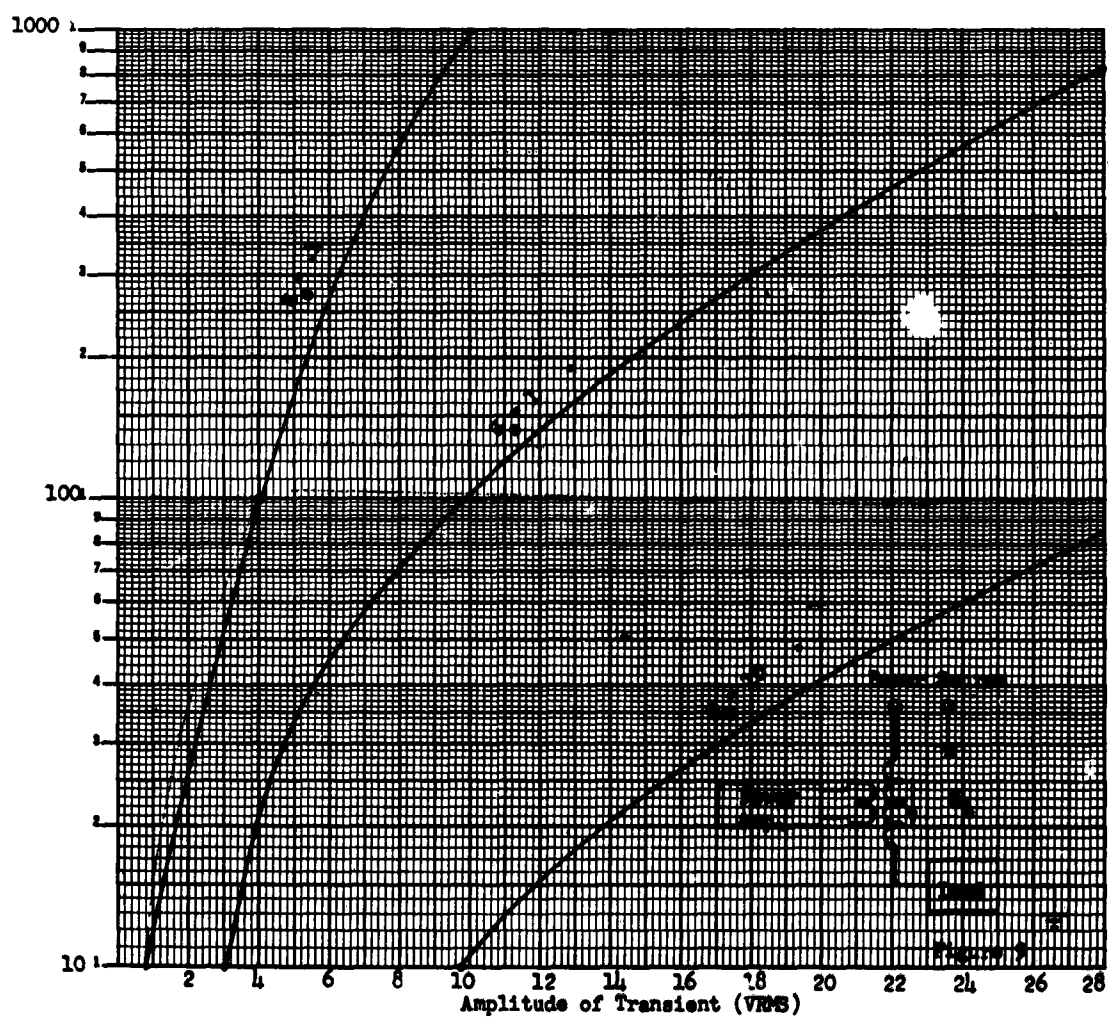


Transient Generator (See Text)  
Figure 7



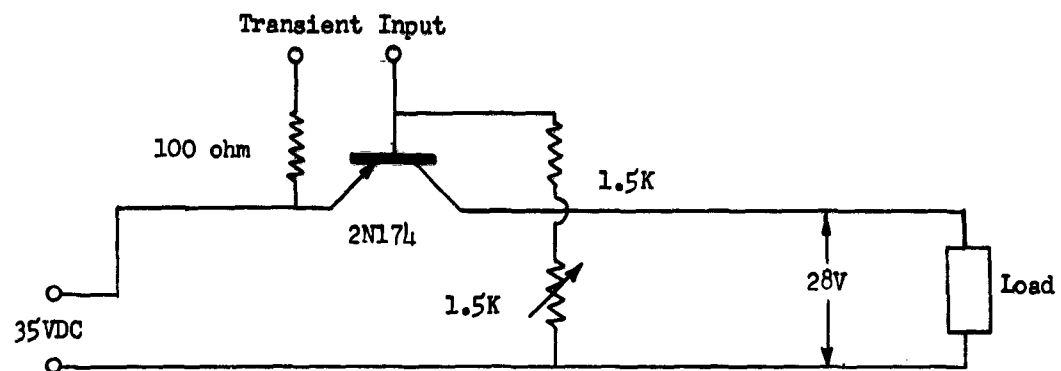
Bridge Output

Figure 8

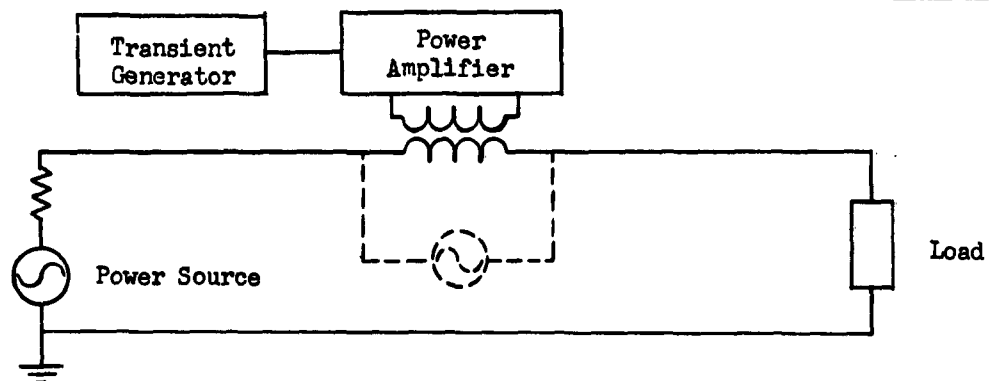


Amplifier Power Requirements - DC Power Leads  
-732-





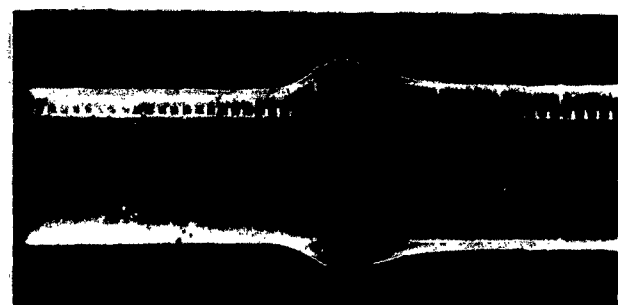
Series Regulator  
Figure 10



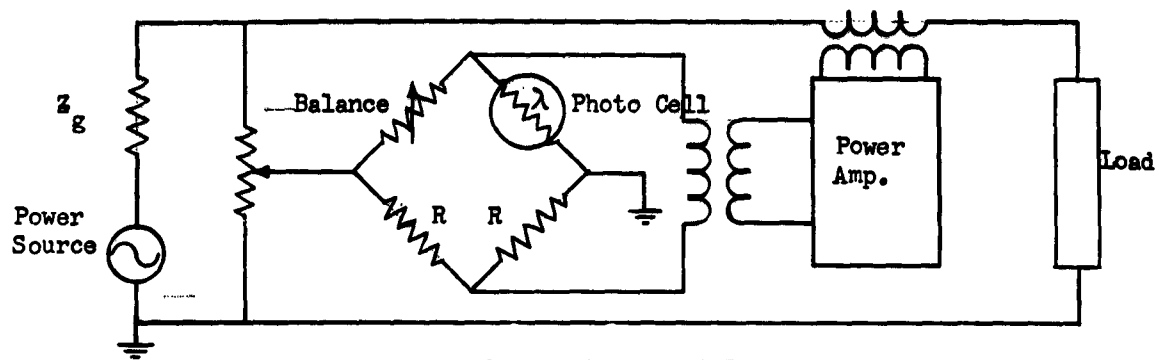
Test Set-up - AC Power Leads  
Figure 11



Horizontal .2 sec/cm  
Power Amplifier Input  
Figure 12



Horizontal .2 sec/cm  
Disturbance on 115V, 400 cps  
Power Line  
Figure 13



Test Set-up - AC Power Lead  
Figure 14



Horizontal .2 sec/cm  
Disturbance on 115V,  
400 cps Power Line

Figure 15



Horizontal .2 sec/cm  
Disturbance on 115V,  
400 cps Power Line

Figure 16

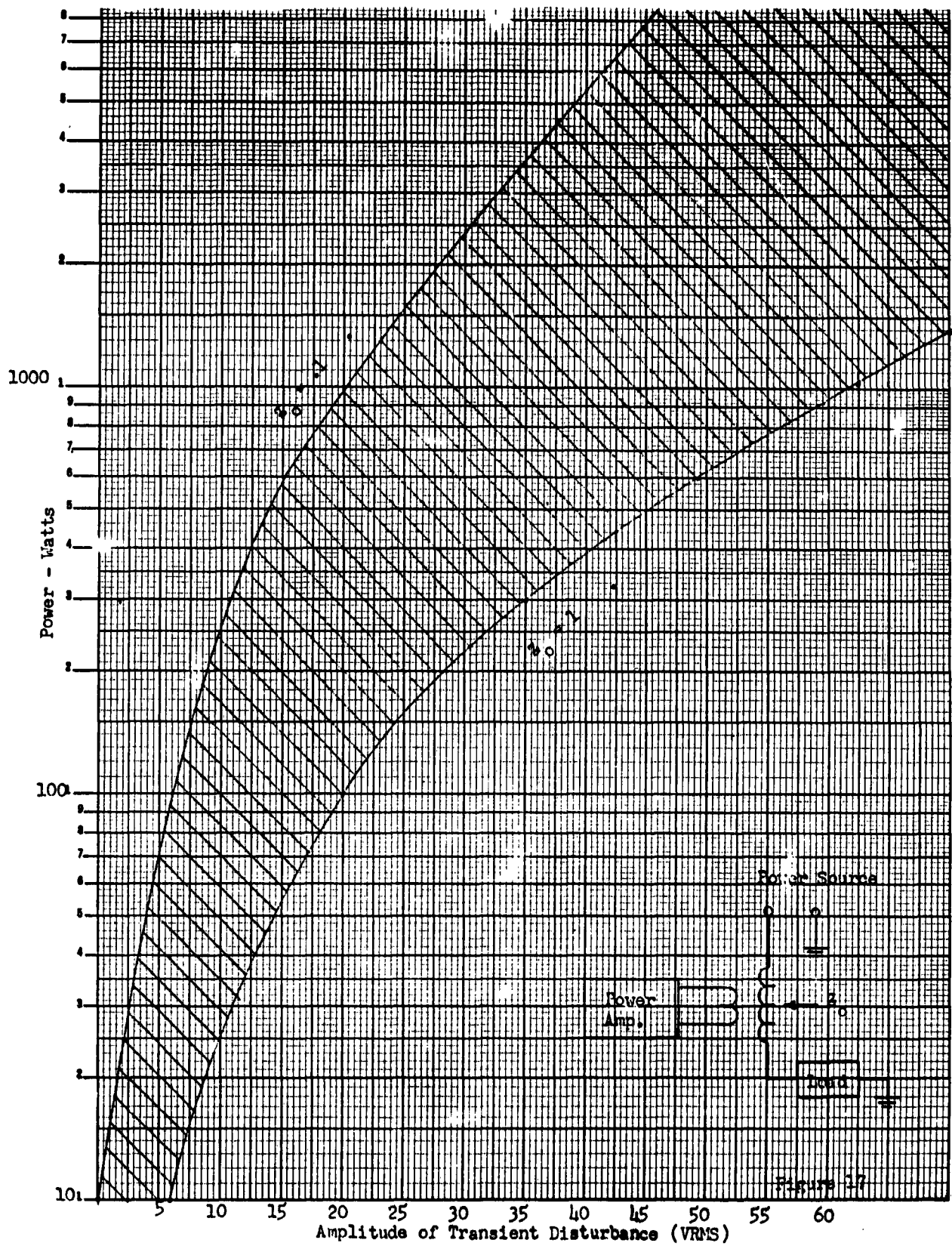


Fig. 17 Amplifier Power Requirements - AC Power Leads  
-735-

## MIL-E-6051 ELECTROMAGNETIC COMPATIBILITY TESTING CONCEPTS AND TECHNIQUES

W. A. Taylor  
Nortronics Division Northrop Corp.  
Hawthorne, Calif.

Abstract. - This paper discusses MIL-E-6051 electromagnetic compatibility testing concepts and instrumentation techniques necessary to implement the tests. For Compatibility tests to be realistic, the test procedures and implementing instrumentation must be designed to compliment and be compatible with both the test specimen system and data requirements of the test program. Procedures and monitoring equipment must permit the system to be operated as an integrated system through an operational sequence that faithfully reflects the intended tactical operation insofar as is practicable. AGE and other use site facilities capable of contributing to the total EMI environment must be considered a part of the system under test.

### I. INTRODUCTION

Specification MIL-E-6051 establishes the compatibility requirements for a weapon system, based primarily on unacceptable response, no malfunction, and margin of safety criteria. Unlike other MIL specifications dealing with control of electromagnetic interferences, the test procedures and instrumentation necessary to conduct realistic electromagnetic compatibility tests are not defined by the specification, instead are the responsibility of the system contractor. There are three basic approaches that may be followed in setting up compatibility demonstration tests. These basic approaches, which may be used singly or collectively, are:

1. Injecting interference at critical system points at a level 6db higher than predetermined system levels. Appropriate system points are then monitored for malfunction.
2. Sensitizing the system so as to raise its susceptibility level to interference by 6db while monitoring for malfunctions.
3. Measuring the susceptibility of key subsystem and system circuits for comparison to existing interference levels to determine if a 6db margin exists.

### II. CONCEPTS AND TECHNIQUES

The electromagnetic compatibility requirements of MIL-E-6051 are essentially that all elements of a weapon system operate properly, individually, and collectively, with a signal to noise ratio of 2 to 1 in the electromagnetic interference environment resulting from the operation of the total operating system. The signal to noise ratio is herein defined as the

ratio of the desired signal level required to produce a desired action to the level resulting from the summation of all extraneous undesired electromagnetic effects.

Any and all elements of the system must operate as designed with twice the noise level that actually exists within the system regardless of its frequency, duration, modulation, waveform, repetition rate, duty cycle, sequence, time, or amplitude, or any other characteristic or set of characteristic that may be used to define noise. The primary concern is how it effects the operation of the system. It is entirely reasonable to expect a given element of a complex system to see (be affected by) a burst of noise differently than would a voltmeter, a noise meter, or other measurement devices. It is also entirely reasonable to presume that the susceptibility characteristics (sensitivity, bandwidth, etc.) of a weapon system element would change as a function of time, signal level, or other programmed change so that the effect of noise would not be constant. These effects may or may not have a synchronous relation; transients may, or may not coincide with clock pulses. Random transients would, therefore, find random coincidence with periodic ON gates for example. Other, and numerous cases could be cited to illustrate the many differences between the value placed upon any given type of noise by measurement devices and by elements, circuits, or subsystems within a weapon system. Electromagnetic Compatibility Instrumentation, therefore, should be capable of evaluating existing noise levels in terms of how the system under test would see the noise. In many cases this can be accomplished by measuring the effect of noise upon functional elements and loops within the system.

The total weapon system noise level, a summation of all the electromagnetic effects created by the system, and the systems detail sensitivity to this noise both vary as a function of time, and as a function of the operational profile of the weapon in its use environment. Therefore, to determine by test whether or not the weapon system can indeed operate as designed with the required safety margin will require test methods and instrumentation that will permit close and accurate time and event correlation of all the quantities measured. Other equally important test methods and procedures are:

1. Instrumentation must include the capability to measure the effects of noise on critical elements and subsystems.
2. It must be possible to analyze all data on a time and event basis.
3. Test procedures must include system support equipment where the support equipment is capable of contributing to the electromagnetic environment. Many items of AGE have this capability and must be tested along with the primary system.
4. Test procedures must encompass the total operational profile of the weapon system and ensure that all loops and subsystems are exercised thru their total dynamic range.

Due consideration of the preceding four basic requirements has led to the formulation of the following guidelines, found to be useful in writing compatibility test procedures and instrumentation specifications.

1. All elements of the system under test must be on and operating in a manner approximately normal tactical usage to the extent possible.
2. The use of AGE as items of test instrumentation is to be avoided, instead AGE is regarded as an element of the test specimen.
3. Test instrumentation should be capable of monitoring all critical circuits simultaneously, and of accepting event and time correlation inputs as required to properly identify and correlate the resulting test data.
4. Because of the importance of noise transients in systems using digital devices, all data channels must be full time. Time shaving to reduce test equipment complexity is not permitted.
5. Monitor those equipments and circuits capable of showing the effects of system noise, thereby, in effect, using elements of the system as noise measuring devices.

Due consideration of the above guidelines dictates the use of multi-channel oscillograph recorders as the basic element of the test instrumentation setup. Various types of recorders are available, however, the type using light beam galvanometers provide the widest range of galvanometer selection and provide widest range of record speed and run time capability.

The most significant problem encountered in using the recording oscillograph is the upper frequency limit of the galvanometer. The response of the highest frequency galvanometer is approximately 5000 cps at the upper 5% down point. This limit would seem, at least initially, to severely limit the usefulness of the recording oscillograph in modern system testing. This is especially true when one considers the fact that the useful direct writing frequency is further limited by resolution of the recorded line. High record velocity is required to fully utilize the 5 KC galvanometers capability. For example a record velocity of 100 inches per second is required to resolve a 5 KC sine wave, as can be seen, slower record speeds are highly desirable, and indeed are necessary to make the recording approach practical.

However, when considered as a voltmeter that automatically and continuously records its readings, rather than as a cathode ray oscilloscope to display waveforms, the range of application of the recording oscillograph becomes greatly enlarged. In most applications the galvanometer need not be capable of directly recording a high frequency AC or RF signal, instead it need only follow the rate of change of the information conveyed by the AC signal. Using this technique, the relatively low frequency galvanometer can

be used to advantage, and the problem then becomes one of providing the proper signal conditioning.

The signal conditioning devices required to make the oscillograph galvanometer compatible with the wide variety and frequency range of the signal sources encountered in weapon system instrumentation have been developed to cover a wide range of signal types. The following table lists 9 types that may be considered as typical, but by no means a complete listing.

1. Convert RF to a DC analog
2. Convert AC voltage and current to a DC analog
3. Convert AC of complex waveform to a DC analog of the true RMS value
4. Converts mechanical position to a DC analog
5. Convert temperature levels to a DC analog
6. Convert light intensity to DC analog
7. Subtract a predetermined voltage from the total signal voltage so that the remainder is recorded in an expanded scale type of presentation.
8. Provide for line to line voltage recording where both lines are above ground.
9. Enable separated signal recording where the desired quantity is:
  - a. Noise component on a DC voltage
  - b. Noise and harmonics on AC power lines

Signal conditioning units are self contained and miniaturized to facilitate mounting at the signal source. Mounting the signal conditioning unit at the source allows extremely short signal input leads thereby eliminating much of the signal transfer problem. The long cable run, signal conditioning unit to recorder, carries the DC analog voltage only, and therefore is not critical. In practice the cable may vary from 10 to 100 ft. in length without requiring recalibration of the channel involved.

A relatively wide frequency range is practical through use of the technique of placing the signal conditioning circuit at the point of signal origin as noted above, and by utilizing passive detection circuits which avoids the use of amplifiers and their attendant drift, noise and bandwidth problems. The high sensitivity of the light beam galvanometer combined with high efficiency detection circuits makes possible usable deflections with as little as 25 millivolts of signal using completely passive circuitry. Response up to 400 mc has been obtained through the use of high speed diodes and optimized layout geometry.

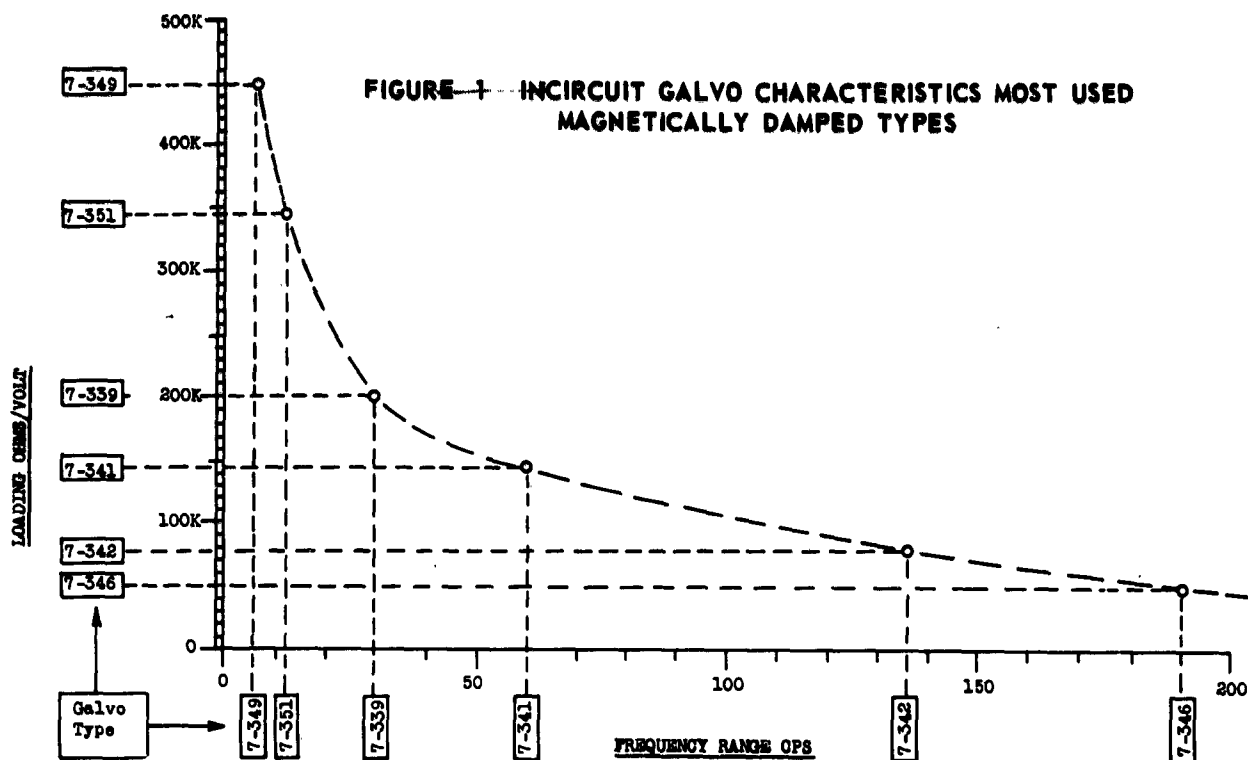
### III. CONCLUSIONS

Electromagnetic compatibility testing, as in any other form of system testing, must be meaningful. Compatibility testing probably presents more pitfalls in this regard than do, for example, MIL-I-6181 tests. Compatibility test methods and procedures require a high degree of compatibility between test procedures and instrumentation and the system under test. The procedure, for example, must faithfully reflect the tactical operational profile, and for similar reasons monitoring instrumentation should weigh noise in the system as would subsystems within the weapon system. Preferably, at least in some cases, system elements would be monitored for the effects of noise, rather than the noise itself, thereby in effect using system elements as noise detectors thus achieving maximum realism and minimum disturbance to the system under test by the addition of measurement devices.

The importance of precise event identification and time correlation is difficult to overstress, and is necessary for the cause and effect studies that result when incompatibilities within the weapon system are detected.

The multichannel recording oscillograph coupled with suitable signal conditioning units represents a very satisfactory means of implementing electromagnetic compatibility tests when combined with step by step procedures which reflect the weapon systems operational profile.





PAPER SPEED INCHES PER SECOND	HIGHEST READABLE FREQUENCY CYCLES PER SECOND	RUNNING TIME
0.10	5.0	15 hr
0.16	8.0	9 hr 23 min
0.25	12.5	6 hr
0.40	20.0	3 hr 45 min
0.63	31.5	2 hr 22 min
1.0	50.0	1 hr 30 min
1.6	80.0	56 min 15 sec
2.5	125.0	36 min
4.0	200.0	22 min 30 sec
6.3	315.0	14 min 15 sec
10.0	500.0	9 min
16.0	800.0	5 min 36 sec
25.0	1250.0	3 min 36 sec
40.0	2000.0	2 min 12 sec
63.0	3150.0	1 min 24 sec
100.0	5000.0	54 sec

**FIGURE II CHART-PAPER-SPEED-RESOLUTION-RUNNING TIME, BASED ON  
LINE RESOLUTION 0.02 INCHES - 450 FT ROLLS OF RECORDING PAPER**

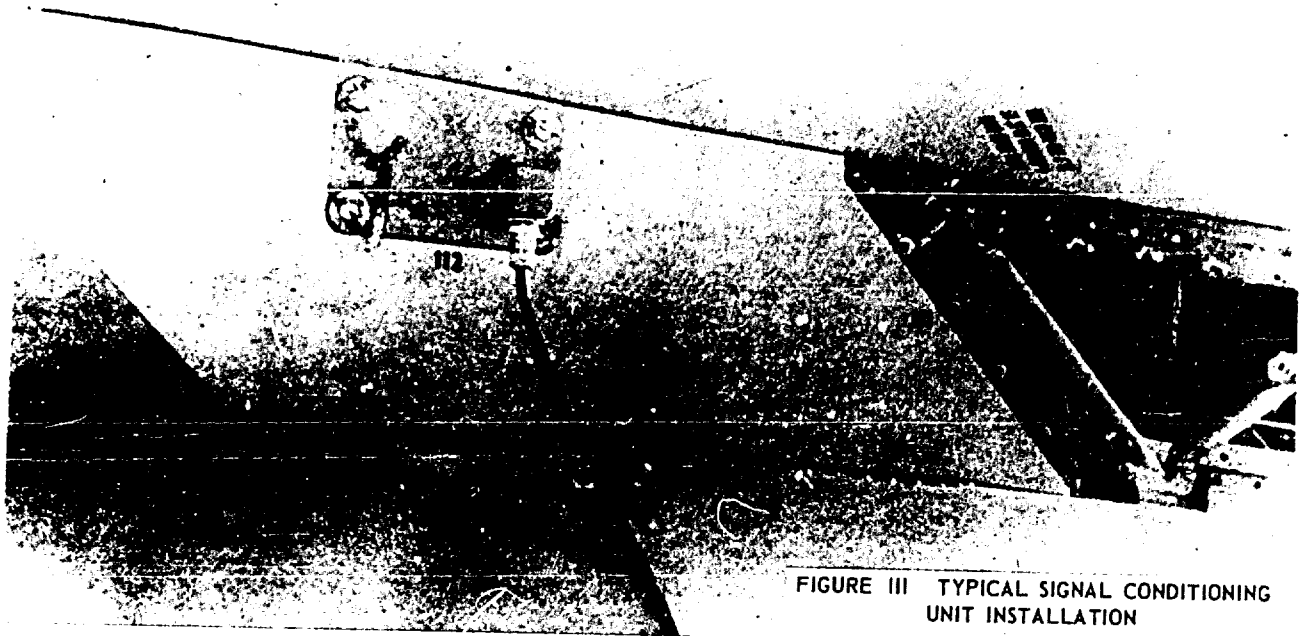


FIGURE III TYPICAL SIGNAL CONDITIONING UNIT INSTALLATION

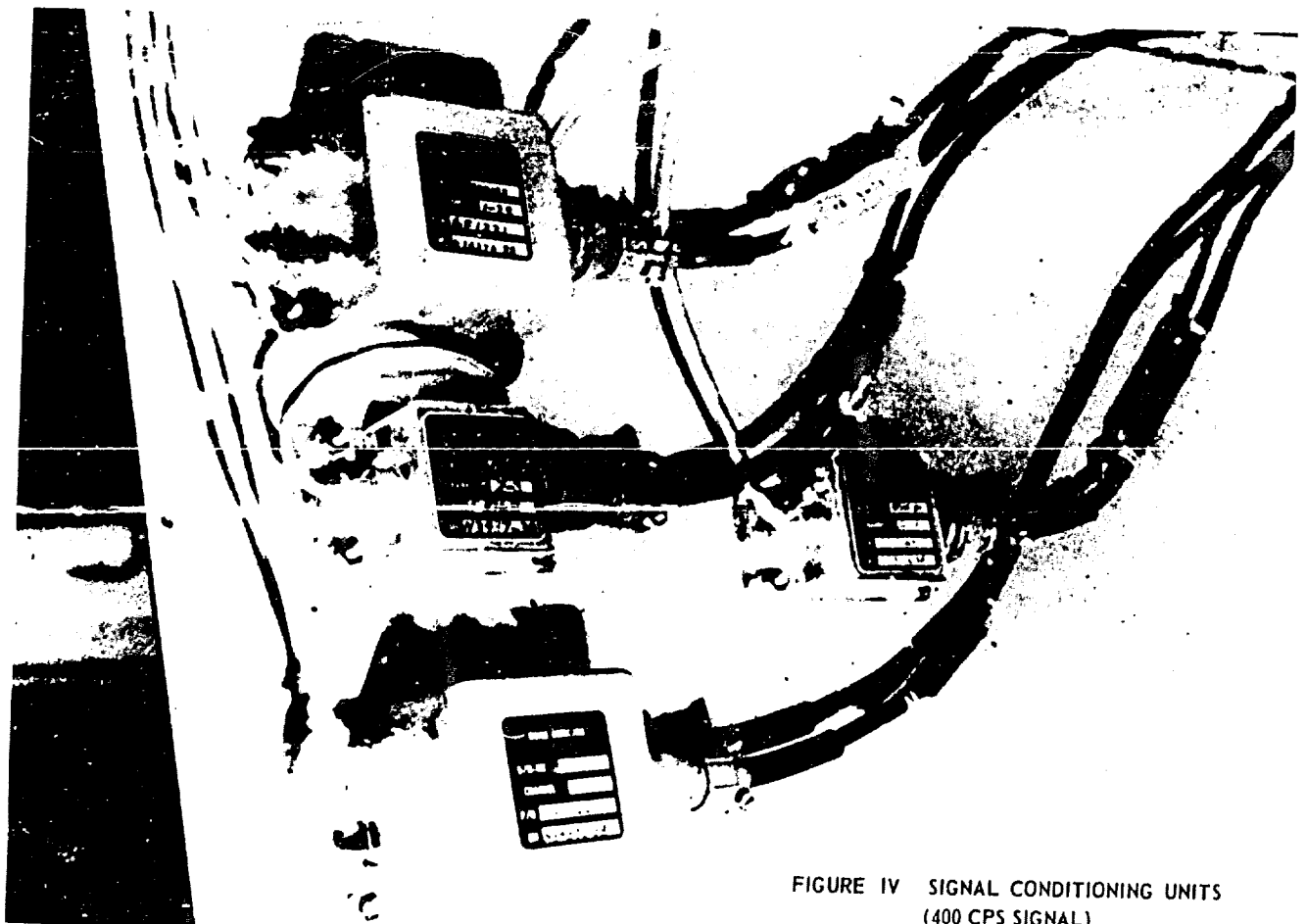
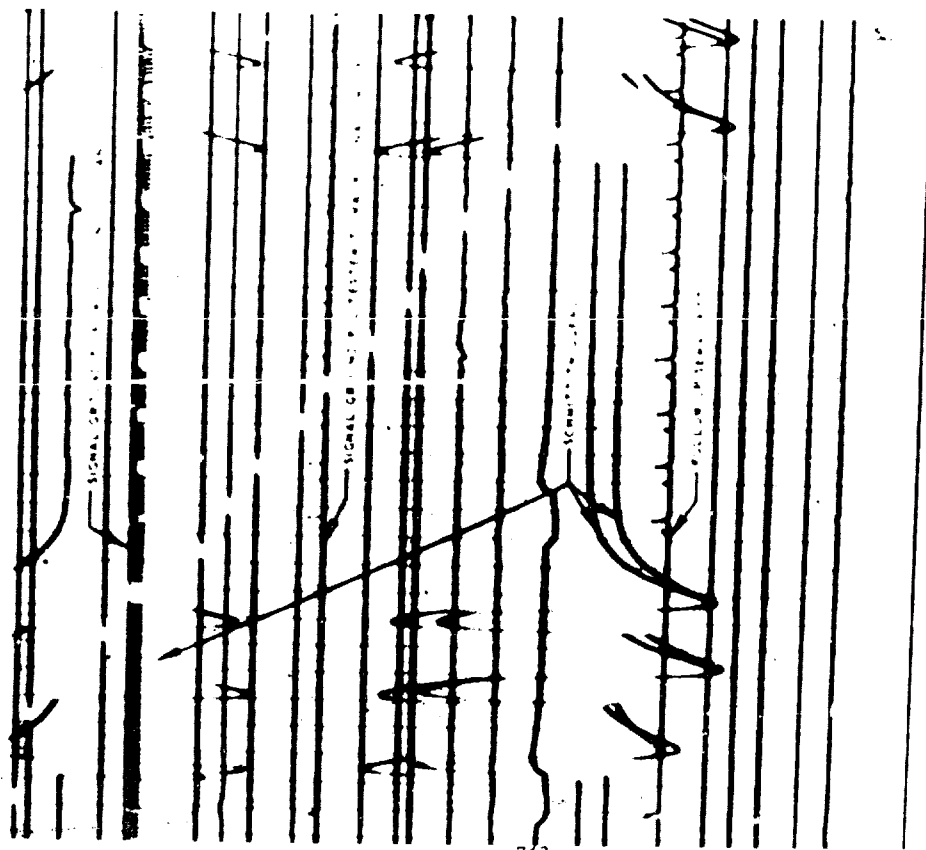
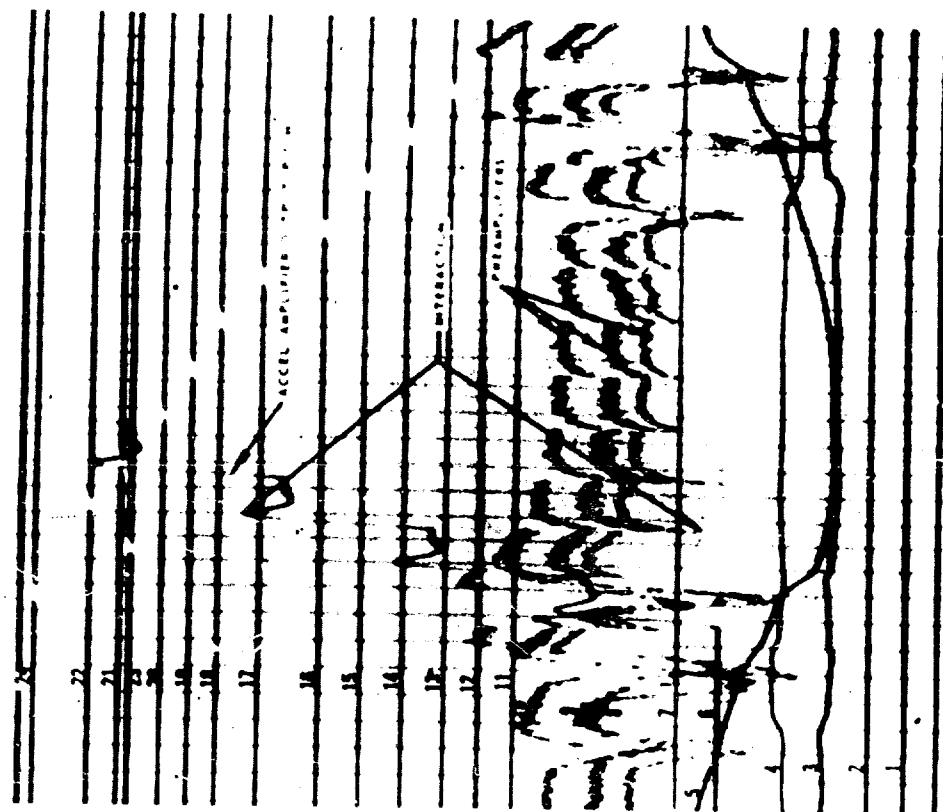


FIGURE IV SIGNAL CONDITIONING UNITS  
(400 CPS SIGNAL)



OSCILLOGRAPH NO. 3 - TRAJECTORY CONTROL TEST OF GUIDANCE SYSTEM

FIGURE V OSCILLOGRAMS



OSCILLOGRAPH NO. 2 - TRAJECTORY CONTROL TEST OF GUIDANCE SYSTEM

FIGURE VI OSCILLOGRAMS TYPICAL ASTRONAUTICAL GUIDANCE SYSTEM RECORDINGS

# NORTHROP MODEL 101 ELECTROMAGNETIC INTERFERENCE TEST CONSOLE

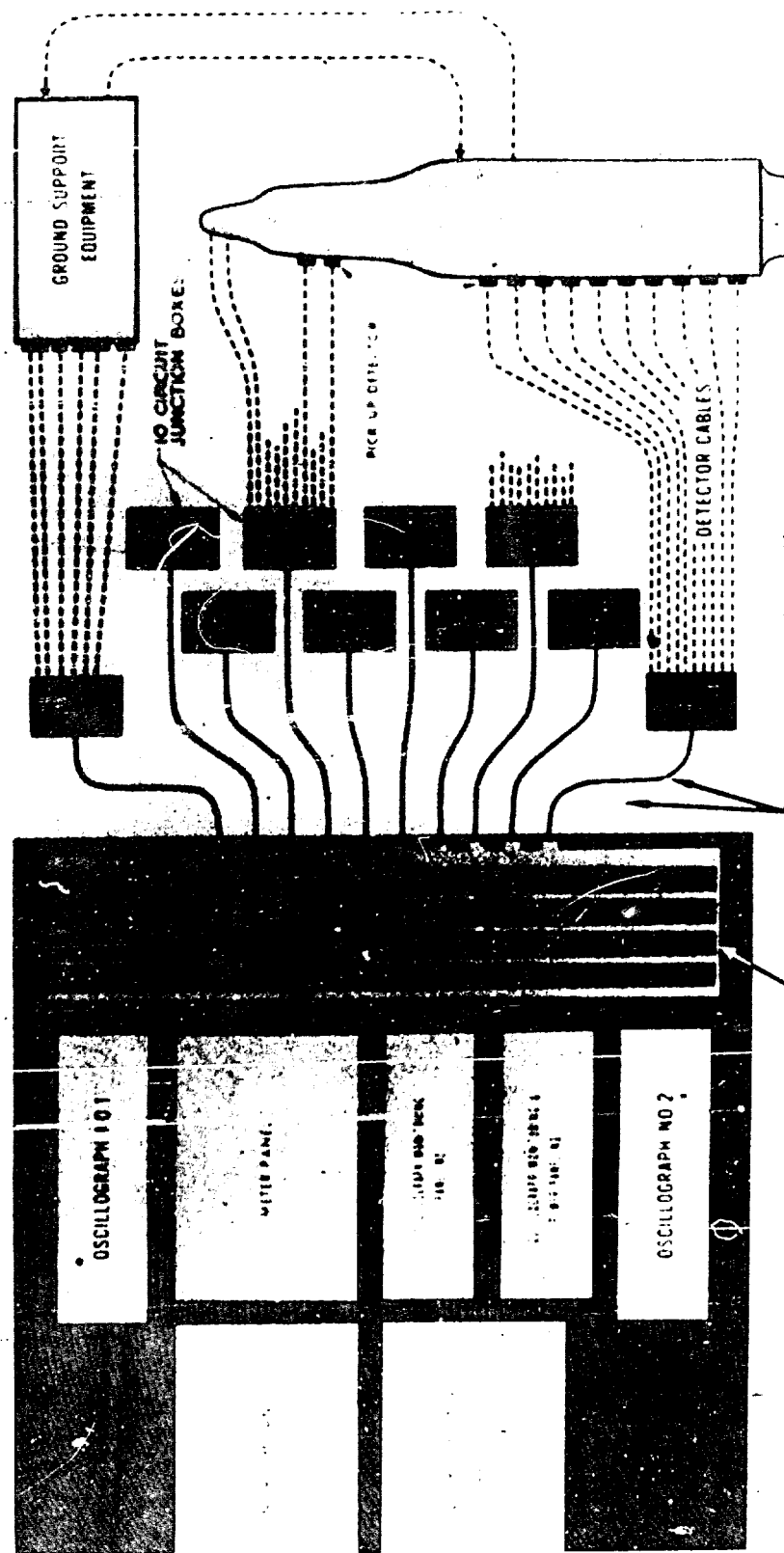


FIGURE VII SYSTEM TEST PICTORIAL SCHEMATIC

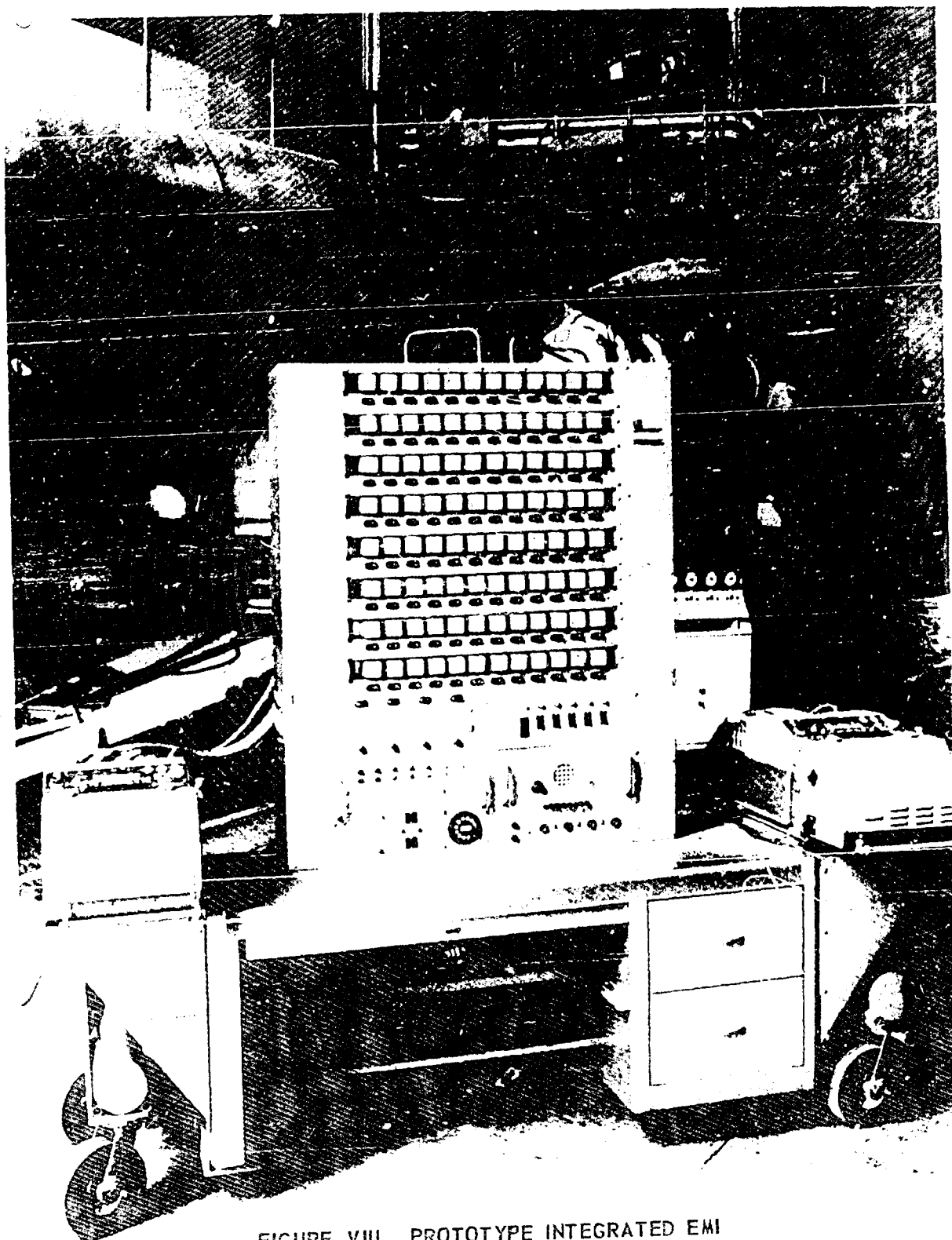


FIGURE VIII PROTOTYPE INTEGRATED EMI  
INSTRUMENTATION CONSOLE

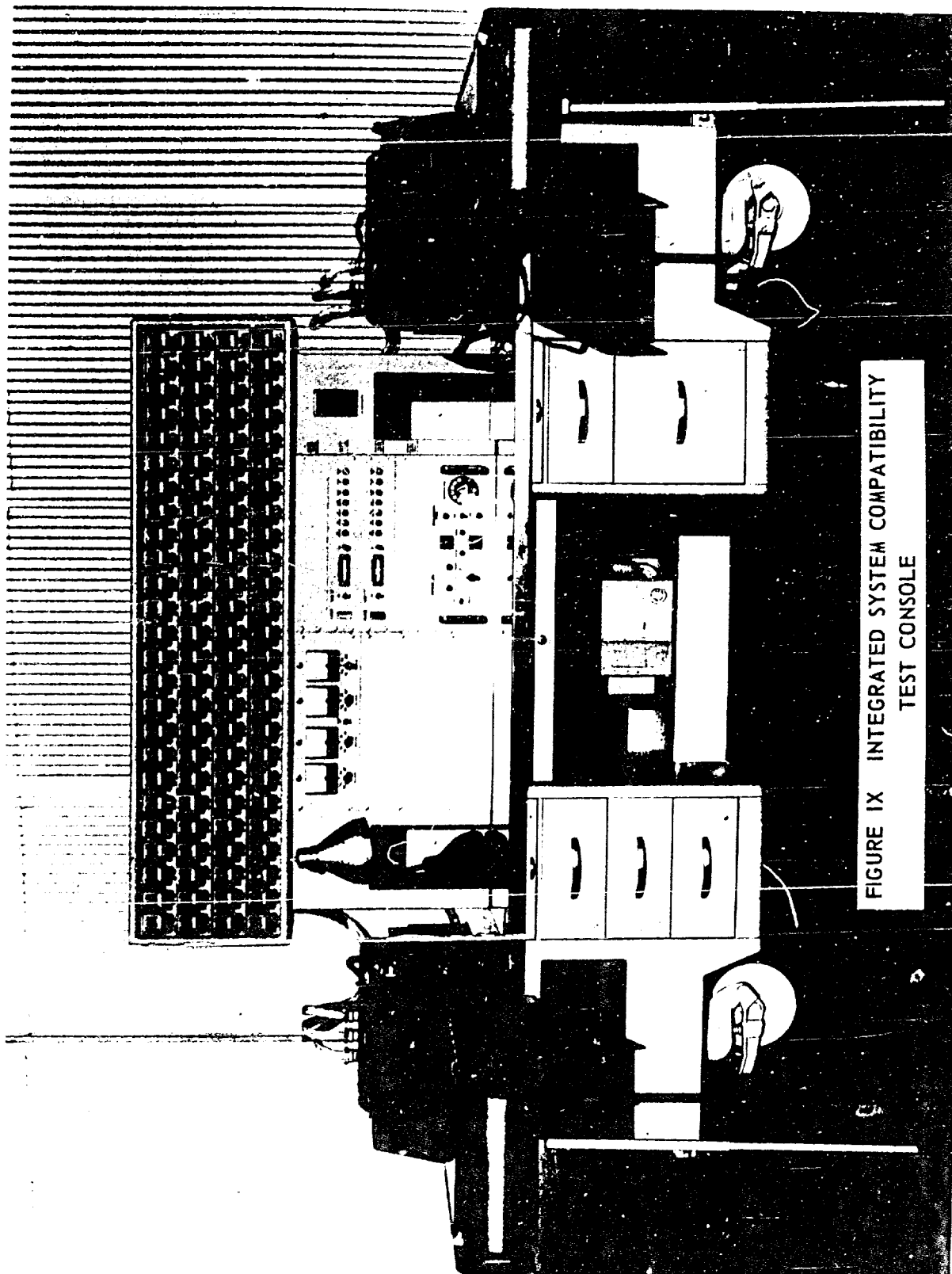


FIGURE IX INTEGRATED SYSTEM COMPATIBILITY  
TEST CONSOLE

## ANALYSIS OF THE HIGH IMPEDANCE FIELD IN SUSCEPTIBILITY TESTS

W. A. Stirrat

U.S. Army Electronics Research and Development Laboratories  
Fort Monmouth, New Jersey

**Abstract.** - The susceptibility test requiring that equipment be immersed in strong vertically polarized high impedance 14 kc - 20 mc fields introduces difficulties, most of which are minimized by minimizing the space Y between the driven vertical monopole antenna of height H and the item of height Z under test. If at Y the field is permitted to be 6 db lower at Z above ground level, then the minimum Y is  $2/\sqrt{3}$  for  $H/Z > 5.5$ , is  $8Z/3$  for  $H/Z < 1.2$ , and approximately  $3.2Z^2/H$  for  $1.2 < H/Z < 5.5$ . For fields at ground level, curves of the monopole driving voltage to produce one volt per meter and the width over which the field will fall off 6 db are plotted vs Y for specific monopoles. The theory is developed. Also discussed are experimental verification, impedance matching transformers for the monopole, mutual impedance considerations, and application to receiving antennas.

### I. INTRODUCTION

The test for susceptibility to the vertical component of the electric field applied with a vertical monopole in the frequency range of 14 kc to 20 mc has been difficult to perform. First there is the problem of driving the monopole with sufficient voltage: if an adequate source can be obtained, that voltage may be the order of 1000 volts. Measurement of the field is another problem: experimental data from independent workers has not been in agreement and that of each worker has failed to show proper consistency. A theoretical analysis is necessary to determine what experimental results should be expected and why there has been lack of agreement in the experimental results. Once a theory has been developed, it can be used in place of considerable experimental work to determine the best procedure for setting up the field.

### II. THEORY

a. From the reference, Equation 1 has been obtained for  $E_z$ , the vertical component of the electric field at P, shown in Figure 1.

$$E_z = \frac{-jI_0\beta}{4\pi\epsilon(\sin\beta H)} \left[ \frac{(\exp-j\beta r_1)}{r_1} + \frac{(\exp-j\beta r_2)}{r_2} - \frac{2(\exp-j\beta r_0)\cos\beta H}{r_0} \right] \quad (1),$$

where  $\beta = 2\pi/\lambda$

$\epsilon$  = dielectric constant

$\lambda$  = wavelength

$\omega = 2\pi f$

$j = \sqrt{-1}$

$f$  = frequency

$I_0$  = current applied at monopole base

$$r_1 = \sqrt{\rho^2 + (H-z)^2} \quad (1a)$$

$$r_2 = \sqrt{\rho^2 + (H+z)^2} \quad (1b)$$

$$r_0 = \sqrt{\rho^2 + z^2} \quad (1c).$$

Using a series expansion,

$$\begin{aligned} & \left[ \frac{(\exp - j\beta r_1)}{r_1} + \frac{(\exp - j\beta r_2)}{r_2} - \frac{2(\exp - j\beta r_0) \cos \beta H}{r_0} \right] = \\ & \quad 1/r_1 - j\beta - \beta^2 r_1/2 + \dots \\ & \quad + 1/r_2 - j\beta - \beta^2 r_2/2 + \dots \\ & \quad - 2 \left[ 1 - (\beta H)^2/2 + (\beta H)^4/4! + \dots \right] \left[ 1/r_0 - j\beta - \beta^2 r_0/2 + \dots \right] \\ & = \left[ 1/r_1 + 1/r_2 - 2/r_0 \right] - \beta^2/2 \left[ r_1 + r_2 - 2r_0 - 2H^2/r_0 \right] \\ & \quad + \text{terms containing higher powers of } \beta. \end{aligned}$$



At the low frequencies of concern, terms containing  $\beta^2$  and higher powers of  $\beta$  are neglected and  $\sin \beta H$  is approximated by  $\beta H$ . Using

$$\frac{\beta I_0}{4\pi\epsilon\omega\sin\beta H} = \frac{I_0}{4\pi\epsilon\omega H} = \frac{V_0 C_{ant}}{4\pi\epsilon H},$$

where  $C_{ant}$  is the capacity of the monopole and  $V_0 = I_0/\omega C_{ant}$  is the voltage applied to the antenna, Equation 2 is thus obtained with independence from frequency.

$$E_z = (-jV_0 C_{ant}/4\pi\epsilon H)(1/r_1 + 1/r_2 - 2/r_0) \quad (2)$$

b. To determine how  $E_z$  varies with  $z$  and  $\rho$ , let

$$r_1 = \rho \sqrt{1 + (H/\rho)^2 (1 - z/H)^2} = \rho \sqrt{1 + (a_1 H/\rho)^2} \text{ where } a_1 = 1 - z/H \quad (3a),$$

$$r_2 = \rho \sqrt{1 + (H/\rho)^2 (1 + z/H)^2} = \rho \sqrt{1 + (a_2 H/\rho)^2} \text{ where } a_2 = 1 + z/H \quad (3b),$$

$$r_0 = \rho \sqrt{1 + (H/\rho)^2 (z/H)^2} = \rho \sqrt{1 + (a_0 H/\rho)^2} \text{ where } a_0 = z/H \quad (3c).$$

Each  $\frac{1}{r}$  is expressed in the form

$$1/\sqrt{1 + \tan^2 \theta} = \cos \theta$$

where if  $\tan \theta$  is given, the corresponding  $\cos \theta$  can (to much greater than sliderule accuracy) be found from tables.

If, for example,  $H/\rho = 1/2$  and  $z/H = 2$ , then

$$a_1 = -1, \quad a_1 H/\rho = -1/2 = \tan \theta, \text{ and } \cos \theta = .8944;$$

$$a_2 = 3, \quad a_2 H/\rho = 3/2 = \tan \theta, \text{ and } \cos \theta = .5547;$$

$$a_0 = 2, \quad a_0 H/\rho = 1 = \tan \theta, \text{ and } \cos \theta = .7071;$$

so that  $(1/r_1 + 1/r_2 - 2/r_0) = (1/\rho)(.8944 + .5547 - 1.4142) = .0349/\rho$ .

For a range of  $z/H$  and  $H/\rho$  values,  $\rho(1/r_1 + 1/r_2 - 2/r_0)$  has been found to be as tabulated in Table 1.

TABLE 1

z/H	at H/ $\rho$ =						
	1/8	1/4	1/2	1	2	4	8
0	-.0154	-.0596	-.2112	-.5858	-1.1054	-1.5150	-1.7519
1/8	-.0154	-.0595	-.2082	-.5678	-1.0382	-1.2972	-1.1624
1/4	-.0154	-.0587	-.2002	-.5147	-.8627	-.9011	-.6307
1/2	-.0152	-.0557	-.1702	-.3397	-.3908	-.2829	-.1589
1	-.0144	-.0460	-.0818	.0333	.3479	.6390	
2	-.0115	-.0186	.0349	.1286	.1267	.0775	
4	-.0044	.0107	.0315	.0273	.0158	.0082	

Plots of the ratio of  $E_z$  at  $z$  to  $E_z$  at  $z = 0$  are made in Figures 8a and 8b for specific values of  $H/\rho$ .

From Appendix 1, for  $\rho/H \rightarrow \infty$ , Equation 2 becomes

$$E_z = (-jV_0 C_{ant}/4\pi\epsilon H)(-H^2/r_0^3)(1 - 3z^2/r_0^2) \quad (2a)$$

which agrees with the field of an infinitesimal antenna.

From inspection of Figure 1 it is obvious that for  $\rho/H \rightarrow 0$ , Equation 2 becomes for  $z \approx \rho$

$$E_z = (-jV_0 C_{ant}/4\pi\epsilon H)(-2/r_0) \quad (2b)$$

From (2a), (2b), and Table 1,  $E_z$  at  $z = 0$  is approximated to better than 5% by

$$E_z = (jV_0 C_{ant}/4\pi\epsilon H) / (\rho/2H + 0.3\rho^2/H^2 + \rho^3/H^3) \quad (2c)$$

which is exact at  $(\rho/H) \rightarrow \infty$  and  $(\rho/H) \rightarrow 0$ .

c. To determine for a particular value of  $\rho/H$  that value of  $z/H$  where  $E_z$  falls 6 db below its value at  $z = 0$ , Figures 8a and 8b are used. A recomputation of the ratio of  $E_z$  at  $z$  to  $E_z$  at  $z = 0$  is made at those values of  $z/H$  where the initial plot shows the ratio to be 0.5. If a recomputation failed to yield a ratio of 0.5, a re-plot and a second recalculation was made. The results of the recalculations are as shown in Table 1a.

TABLE 1a

$H/\rho$	final recalculation		first recalculation		$\rho/z$
	$Z/H$	ratio	$z/H$	ratio	
1/8	3.09	.500	3.06	.507	2.59
1/4	1.59	.500			2.51
1/2	.87	.500			2.30
1	.557	.500	.566	.487	1.765
2	.417	.500			1.200
4	.298	.500	.310	.480	.840
8	.181	.500	.190	.481	.692

From Appendix 2, for  $H/\rho \rightarrow 0$ ,

$$z/\rho = .385 \quad (4a),$$

where  $Z$  is that value of  $z$  where  $E_z$  is 6 db below its value at  $z = 0$ .

From Equation 2b it is obvious that for  $H/\rho \rightarrow \infty$ ,

$$z/\rho = \sqrt{3} \quad (4b).$$

From Equations 4a and 4b,

$$\rho/Z = 1/\sqrt{3} + 2.022/(1 + .14H^3/Z^3) \quad (4c)$$

is accurate to better than 7%. This equation is used to determine, for a monopole of height  $H$ , the spacing  $\rho$  necessary to obtain at height  $Z$  an  $E_z$  field 6 db below  $E_z$  at the ground (see Figure 2). Note that a simpler equation

$$\rho/Z = 1/\sqrt{3} + 2/(1 + H^3/Z^3)$$

is good to 5% for  $n = 4$  and  $H/Z \leq 3.4$  but is accurate to 13% at  $H/Z = 5.53$ . For  $n = 3$  the simpler equation approximates Equation 4c.

Using data from Table 1a,  $\rho/Z$  has been calculated. The results have been tabulated in Table 1a.

d. There is at  $z = 0$  along the  $x$  axis shown in Figure 2 a point  $X$  where the  $E_z$  field falls 6 db below its value at  $x = 0$ ,  $z = 0$ , and  $\rho = Y$ . The field falls off along the  $x$  dimension because of the increase of  $\rho$  with  $x$ . From Equation 2 rewritten as

$$E_z = (-jV_0 C_{ant} / 4\pi\epsilon H^2) (H/\rho) [\rho(1/r_1 + 1/r_2 - 2/r_0)] \quad (2d)$$

and the data in Table 1, the db of change in  $E_z$  with a 2:1 increase of  $\rho$  has been determined. The results are tabulated in Table 2. For example, at  $H/\rho = 1/4$ ,

$$\Delta \text{ db} = 20 \log(1/4)(.0596)/(1/8)(.0134) = 17.76 \text{ db}$$

From  $H/\rho = 1/8$  to  $H/\rho = 1/16$  it is assumed that  $E_z$  is proportional to  $1/\rho^3$  in accordance with Equation 2a.

Using the tabulated values of  $\Delta$  db for a 2:1 increase in  $\rho/Y$ , the ratio  $\rho/Y$  for a 6 db change has been calculated using Equation 5a (below).

$$20 \log (\rho/Y)^m = 6 \text{ db}$$

where  $m$  is determined from

$$20 \log 2^m = \text{the tabulated } \Delta \text{ db,}$$

$$\rho/Y = \log^{-1}(6\text{db}/20)(20 \log 2)/(\Delta \text{ db}) = \log^{-1}(1.8/\Delta \text{ db}) \quad (5a).$$

The results are tabulated in Table 2.

$H/\rho$	$\Delta$ db for 2:1 increase	$\frac{\rho}{Y}$ for 6 db	$X/Y$	$X/Z$	$Z/H$
1/8	18.0	1.260	.77	1.97	3.09
1/4	17.8	1.265	.77	1.91	1.59
1/2	16.6	1.285	.80	1.85	.87
1	15.4	1.31	.85	1.52	.557
2	11.6	1.42	1.01	1.21	.417
4	8.8	1.60	1.25	1.03	.298
8	7.3	1.77	1.46	1.005	.181

From the tabulated data of  $\rho/Y$  for 6 db and from Equation 5b,

$$X = Y \sqrt{(\rho/Y \text{ for 6 db})^2 - 1} \quad (5b),$$

the value of  $x = X$  at which  $E_z$  is 6 db lower than at  $x = 0$  has been calculated. The results are tabulated in Table 2.

From  $X/Y$  in Table 2,  $Z/H$  in Table 1a, and the corresponding values of  $H/Y$  the ratio of  $X/Z$  has been calculated from

$$(X/Y)(Y/H)(H/Z) = X/Z$$

The value of  $Z/H$  is also tabulated in Table 2.

From Appendix 3,

$$X/Y = .766 \text{ for } H/Y \rightarrow 0 \quad (5c)$$

$$\text{and } X/Y = \sqrt{3} \text{ for } H/Y \rightarrow \infty \quad (5d)$$

which in combination with Equations 4a and 4b lead to Equation 5e which approximates to better than 4% the data in Table 2.

$$X/Z = 1 + 1/[1 + (H/\sqrt{3} Z)^4] \quad (5e)$$

e. The factor  $C_{ant}/4\pi\epsilon H^2$  in Equation 2c receives its value from

$$1/4\pi\epsilon = (36\pi \times 10^9 / 4\pi) \text{ (meters/farad)}$$

and from Appendix 4,

$$C_{ant} = - \frac{H \text{ farads/meter}}{9 \times 10^9 (2 - 2 \ln H/a)} \quad (6a)$$

where  $a$  is the radius of the antenna cross section. Using Equation 6a,

$$C_{ant}/4\pi\epsilon H^2 = \frac{(1/H)/[2 \ln \frac{H}{a} - 2]}{\text{per meter}} \quad (6b)$$

For a typical antenna:  $H = 9 \text{ feet} = 2.74 \text{ meters}$   
 $a = 3/16 \text{ inch}$

$C_{ant} = 27 \text{ uuf}$  by Equation 6a and by measurement

$$C_{ant}/(4\pi\epsilon H^2) = 1/(30.4 \text{ meter}).$$

For the same antenna reduced to  $H = 5' = 1.52 \text{ meters}$ ,

$C_{ant} = 18 \text{ uuf}$  by (6a)

$$C_{ant} = 1/(14.5 \text{ meter}).$$

For an antenna of

$$C_{\text{ant}} = 10 \text{ uuf by design}$$

$$H = 41" = 1.04 \text{ meter}$$

$$\frac{C_{\text{ant}}}{4\pi\epsilon H^2} = 1/(12 \text{ meter}).$$

For these antennas, the following approximations,

$$C_{\text{ant}} \approx (10 \text{ uuf})H/(1 \text{ meter}), \quad (6c)$$

$$C_{\text{ant}}/4\pi\epsilon H^2 \approx 9 \times 10^{-2}/H \quad (6d)$$

apply well.

Combining (2d) modified

$$E_z Z/V_0 = (-jC_{\text{ant}}/4\pi\epsilon H)(Z/Y) [Y(1/r_1 + 1/r_2 - 2/r_0)]$$

with (6b) produces

$$E_z Z/V_0 = [j/(2 - 2 \ln \frac{H}{a})](Z/Y) [Y(1/r_1 + 1/r_2 - 2/r_0)] \quad (7)$$

Using the approximations of (6c) and (6d) in (7) produces

$$E_z Z/V_0 \approx -j(.09)(Z/Y)[Y(1/r_1 + 1/r_2 - 2/r_0)] \quad (7a).$$

The data tabulated in Table 3 is calculated by (7a) from data of Tables 1 and 1a. Note  $(Z/Y) = (Z/H)(H/Y)$ .

TABLE 3

Z/H	$E_z Z/V_0$	db below 0.312
.181	.228	2.7
.298	.163	5.6
.417	$8.30 \times 10^{-2}$	11.5
.557	$2.94 \times 10^{-2}$	20.5
.870	$8.27 \times 10^{-3}$	31.5
1.59	$2.13 \times 10^{-3}$	43.3
3.09	$5.35 \times 10^{-4}$	55.3

When  $Z/H \rightarrow 0$  : by (4b),  $Z \rightarrow \sqrt{3} Y$  and  $Y/H \rightarrow 0$  ;

$$\text{by (2b), } E_z = (jV_0 C_{\text{ant}} / 4\pi \epsilon H^2) (2H/Y) ;$$

$$\text{by (6d), } E_z = j18 \times 10^{-2} V_0 / Y ;$$

$$\text{by (4b), } E_z = j18 \times 10^{-2} V_0 (\sqrt{3}/Z) ;$$

$$\text{and } E_z Z / V_0 = j0.312 \quad (7b)$$

The db by which  $E_z Z / V_0$  is below .312 is tabulated in Table 3.

When  $Z/H \rightarrow \infty$  :

$$\text{by (4a), } Z \rightarrow .385 Y \text{ and } Y/H \rightarrow \infty ;$$

$$\text{by (2a), } E_z = (jV_0 C_{\text{ant}} / 4\pi \epsilon H^2) (H/Y)^3 ;$$

$$\text{by (6d), } E_z = j9 \times 10^{-2} V_0 H^2 / Y^3 ;$$

$$\text{by (4a), } E_z = j9 \times 10^{-2} V_0 (H^2/Z^3) (.385)^3 ;$$

$$\text{and } E_z Z / V_0 = j5.14 \times 10^{-3} (H/Z)^2 \quad (7c)$$

For greater exactness, the value of  $E_z Z / V_0$  can always be corrected by the factor  $\frac{1}{18 \times 10^{-2} \left[ \left( \ln \frac{H}{a} \right) - 2 \right]}$  or  $\frac{C_{\text{ant meter}}}{10 \text{ uuf } H}$ .

f. The effect of  $Z/H$  on the important parameters is shown in Figure 9. Using data in Table 1a,  $Y/Z$  is plotted against  $Z/H$ . Using data in Table 2,  $X/Z$  is plotted against  $Z/H$ . Using data in Table 3,  $E_z Z / V_0$  is plotted against  $Z/H$ .

Figure 9 indicates the voltage  $V_0$  that must be applied to a monopole of length  $H$  to obtain a field of from  $\frac{1}{2}E_z$  to  $E_z$  over a plane of height  $Z$  and width  $2X$ . If  $V_0$  is obtained by a transformer step-up from a 50 ohm source, the voltage step-up ratio in matching 50 ohms to the magnitude of the antenna reactance, is proportional to  $\sqrt{1/C_{\text{ant}}}$  or by (6c) to  $\sqrt{1/H}$ . Assuming that a particular  $Z$  must be covered, the disadvantage of using a small  $H$  is decreased by the added transformer gain. A correction of  $20 \log \sqrt{Z/.16H}$  relative to the transformer gain at  $\frac{Z}{H} = .161$  has been

added to the curves.

### III. EXPERIMENTAL VERIFICATION

Experimental work conducted prior to development of the theory was re-performed partly to check the theory and partly to determine the problems of the experimental work. Standard equipment consisting of two BB-105 ground planes, a 9' whip, a 41" whip, two VA-205SC matching transformers (or equivalent), two tripods, two 30' double cables, and a shielded test van containing instrumentation were used as shown in Figure 4.

For a 9 foot radiator,  $Z/H$  is 1.0 for a pickup antenna of 9' and  $Z/H$  is 0.38 for a pickup antenna of 41". Also, using the  $Y/Z$  vs  $Z/H$  plot in Figure 9, a minimum  $Y$  of 3.85' can be used with a 41" pickup antenna and a minimum  $Y$  of 21.4' can be used with a 9' pickup antenna. The use of too large a pickup antenna for the distance  $Y$  used accounts for some of the past experimental errors.

When the test was first performed after development of the theory, the ground planes were placed at ground level with holes dug in the ground to accommodate the matching transformers. The ground planes were later raised to 2' above ground with no apparent change in experimental results. They were raised to the 2' level for all the data given. The 2' level is preferred for convenience and for keeping the equipment free of dirt.

The 10 db pad was used to properly terminate the driving signal generator.

The voltage applied to the 9' whip was determined by measuring the voltage at terminal 2. This voltage equals 5.71 times the antenna current. The antenna current times the antenna reactance equals the voltage applied to the antenna. Correction is made for distributed capacity.

The field at the 41" pickup antenna is determined by measuring the voltage that must be applied to terminal 2 to produce at terminal 1 the same output voltage as is produced by the voltage that  $E_z$  induces in the antenna. With correction for distributed capacity, the voltage substituted at 2 equals the voltage induced in the antenna. The voltage induced in the antenna is  $E_z$  times the effective length (.52 meters) the 41" rod.

For the same drive on the 9' antenna, the 41" antenna pickup at  $Y$  relative to that at  $Y=4'$  is tabulated in Table 4 and plotted in Figure 10. The relative pickup is determined at several frequencies. The results are compared to the theory developed here. The results at 30 mc are compared to radiation field theory not developed here.



TABLE 4

Y in feet	Relative db of Pickup								Theory (Radiation Field)
	Theory	Experiment							
		.15 mc	.36 mc	.87 mc	2.1 mc	5.2 mc	12.7 mc	30 mc	
4	0	2	2	2	2	2	2	2	0
8	11	11	11	9	8	5	3	3	6
12	19	19	18	13	10	5	4	8	9.5
16	25	24	20	14	12	5	5	9	12
20	30	30	21	15	13	5	5	11	14
24	35	34	21	15	13	5	6	15	15.5

The theory is based on Equation (2d), except at  $\frac{H}{Y} \rightarrow 0$  and  $\frac{H}{Y} \rightarrow \infty$  where (2c) is applied using  $\rho = Y$ .

$$E_z = (-jV_0 C_{ant} / 4\pi \epsilon H^2) (H/Y) \left[ Y \left( 1/r_1 + 1/r_2 - 2/r_0 \right) \right] \quad (2d)$$

The quantity  $\left(\frac{H}{Y}\right)Y \left(\frac{1}{r_1} + \frac{1}{r_2} - \frac{2}{r_0}\right)$  is calculated from the data in Table 1 for  $z = 0$ . Using the equations developed in (e) of theory,  $C_{ant}/4\pi \epsilon H^2$  is (1/30.4) per meter for the 9' whip, 1/(14.5 meter) for the 5' whip, and 1/(12.0 meter) for the 41" whip. The  $V_0$  in db above 1 volt required to produce a field of 1 volt/meter at Y, as tabulated in Table 5 and plotted in Figure 11, is calculated as follows:

$$V_0 = (-4\pi \epsilon H^2 / C_{ant}) (E_z) / \left[ (H/Y)(Y) \left( 1/r_1 + 1/r_2 - 2/r_0 \right) \right]$$

For 1 volt/meter at  $H/Y = 1/8$

$$\frac{V_0}{1 \text{ volt}} = \frac{-30.4}{-.001927} = 1.585 \times 10^4 \text{ or } 84 \text{ db for } H=9',$$

$$\frac{V_0}{1 \text{ volt}} = \frac{-14.5}{-.001927} = 7.54 \times 10^3 \text{ or } 77.5 \text{ db for } H=5',$$

$$\frac{V_0}{1 \text{ volt}} = \frac{-12.0}{-.001927} = 6.23 \times 10^3 \text{ or } 75.9 \text{ db for } H=41''.$$

For other values of  $H/Y$  the relative db is obtained from Table 5.

TABLA 5

H/Y	$\frac{H}{Y} Y \left( \frac{1}{r_1} + \frac{1}{r_2} - \frac{2}{r_0} \right)$		Y in Feet		
	Value	Relative db	H = 9'	H = 5'	H = 41"
1/8	$-1.927 \times 10^{-3}$	0	72	40	27.3
1/4	$-1.490 \times 10^{-2}$	17.8	36	20	13.64
1/2	-.1006	34.4	18	10	6.82
1	-.586	49.6	9	5	3.41
2	-2.2108	61.2	4.5	2.5	1.71
4	-6.060	69.9	2.25	1.25	0.855
8	-14.02	77.2	1.125	0.625	0.427
→ 0	$-(H/Y)^3$				
→ ∞	$-2 H/Y$				

From Figure 10 it can be seen that good agreement is obtained at 150 kc. At frequencies above 150 kc experiment departs from theory until a complete departure is made at 5.2 mc. At frequencies above 5.2 mc experiment tends toward agreement with theory, especially of the radiation field at 30 mc. The disagreement between theory and experiment does not result from failure of the theory to hold at frequencies above 150 kc. At .36 mc for Y = 15', part a of the theory, which shows the first order correction to be in  $\theta^2$ , produces a first order correction of  $< 4\%$  which is considerably less than the 7 db of departure. That results at 5.2 mc were not produced by the field was evident when it was found that the same "pick-up" was obtained with the 41" rod shielded from the 9' whip.

The results at 5.2 mc are explained by Figure 5. When  $V_0$  is applied to the 9' whip a current  $I_0$  flows up the 9' whip and an equal current  $I_0$  in the opposite, or ground, direction. The ground current flows along ground lines to the ground plane of the 41" rod, through the input impedance  $Z'$  of VA - 205 SC matching network, and to the tip of the 41" rod where it is reflected. A standing wave exists on the ground side of the 9' whip as though it were one side of an unsymmetrical dipole. That current flowing through  $Z'$  produces a voltage across  $Z'$  that is independent of Y and antenna orientation provided Y is great enough for the field to have negligible effect. The influence of this current is greatest at those frequencies where  $\lambda$  is somewhere between 4 times and 2 times the 70.4 feet of ground current path. It was found that conditions could be altered by altering the length of this path.

The effect at 5.2 mc could be minimized by driving the 9' whip with a battery operated generator or using a battery operated receiver at the 41" rod to isolate at least one end from ground. An alternate method would be to provide a ground current "sink" between the grounds of the two antennas. Any equipment to which a field is applied could be subject to this effect.

#### IV. OTHER CONSIDERATIONS

##### a. Impedance Matching Transformers

Impedance matching transformers used to match the antenna to a 50 ohm receiver input can be used in reverse to match a 50 ohm signal source to the antenna. A transformer designed for receiving purposes must not, of course, be driven by too large a voltage when being used to set up a field.

The design of an impedance matching transformer can only be approximately predicted. Assume the turns ratio  $N$  provides a match of 50 ohms to a reactance  $1/\omega_0 C_0$  where  $C_0$  is a specific capacity and  $\omega_0$  is  $2\pi$  times a specific frequency.

$$N^2 = 1/\omega_0 C_0 50.$$

If this transformer is used to couple a capacity  $C$  at a frequency  $f$ , where  $\omega = 2\pi f$ , to a 50 ohm source that would produce a voltage  $V$  across a 50 ohm load, the voltage appearing across  $C$  would be

$$2NV/\sqrt{1 - (\omega C/\omega_0 C_0)^2}.$$

If the coupling is in the opposite direction, the voltage across a 50 ohm load as the result of a voltage  $V'$  in series with  $C$  is

$$(V'/N)/\sqrt{1 - (\omega_0 C_0/\omega C)^2}.$$

If  $C = C_{ant} + C$  distributed (see Figure 4) and  $V'$  is in series with  $C_{ant}$ , the voltage across a 50 ohm load becomes

$$(V' C_{ant}/NC)/\sqrt{1 - (\omega_0 C_0/\omega C)^2}.$$

For  $\omega_0 C_0 = \omega C$  the step-up voltage ratio, not effected by  $C$  distributed, becomes

$$\sqrt{2} N$$

and the step-down voltage ratio becomes

$$\sqrt{2} N \left[ 1 + \frac{C_{distributed}}{C_{ant}} \right]$$

The step up ratio, within limitations, can be estimated from the step-down ratio.

An estimate of  $N = 1/\omega_0 C_0 50$  for a 9 ft. whip of  $C_0 = 27$  uuf matched to 50 ohms, assuming no distributed capacity ( $C_{dist.} = 0$  and  $C_{ant} = C_0$ ), appears in Table 6. The ratio  $N$  for a 41" rod would be 8.5 db less and for a 5' whip would be 3.5 db less.

TABLE 6

$f_o$	N in db	Comment
48.5 kc	38	(30 - 40 db over 15 kc to 150 kc)
232 kc	30	
560 kc	27	
1.35 mc	23	
3.3 mc	19	
8.12 mc	15	
19.5 mc	11	

The above theory assumes the transformer to be ideal. If the transformer is designed to cover too large a frequency range, the transformer does not act ideally at the lower frequencies of the range because the primary and secondary reactances become too low.

Although only one distributed capacity is shown in Figure 4, there is a second distributed capacity across the transformer winding from the antenna to the junction of the 5 and 45 ohm resistors. In Figure 4, only that shown is of concern. In the above analysis the distributed capacity includes both.

#### b. Mutual Impedance Considerations

The theory developed herein permits a degree of flexibility in the height and position of the antenna. To exploit this flexibility it becomes necessary to know how close the antenna can be moved to a metallic ceiling or wall without appreciably altering its functions or characteristics.

Moving close to a metallic surface must not appreciably alter the antenna self impedance. As long as the mutual capacity between the antenna and its image produced by the surface is considerably larger than the capacity of the antenna, the effect of the surface on the antenna capacity can be neglected. In Appendix 4 two equations, one for mutual capacity with an image produced by a wall and one for mutual capacity produced by a ceiling, are developed. Mutual capacities  $C_m$  calculated by these equations for particular spacings from metallic surfaces are tabulated in Table 7.

TABLE 7

Distance from antenna to Parallel Wall or from Tip of Antenna to Ceiling		$C_m/H$ in uuf/meter	
		Wall	Ceiling
$\frac{1}{16}$	H	44.2	525
$\frac{1}{8}$	H	75.1	714
$\frac{1}{4}$	H	165	1140
$\frac{1}{2}$	H	528	2310
	H	2520	

In e. of the Theory  $C_{ant}$  is approximated by

$$\frac{C_{ant}}{H} = \frac{10 \text{ uuf}}{\text{meter}}$$

which can be used to estimate the ratio of  $C_{ant}/C_m$ .

#### c. Application to Receiving Antennas

Since an antenna has the same pattern and impedance when receiving as when transmitting, the theory developed here can be applied to a receiving monopole.

The effects of nearby metallic ceilings and walls are more easily visualized when a receiving antenna is considered. The image produced by the metallic surface acts as a receiving antenna and the voltage induced in this image antenna adds directly to the voltage induced in the antenna. The voltage contribution by the image should be negligible. It is made negligible by keeping the image sufficiently far away from the source. To determine where the image can be placed in this consideration is beyond the scope of this paper; however, the techniques and information provided herein can be applied to determine the pickup by an image at any particular location.

#### V. RECAPITULATION

The work in this paper primarily applies to radiation susceptibility tests in the range of 14 kc to 150 kc. Any field intensity discussed is that at the bottom center of the item receiving the test: at Point A in Figure 3. The bottom of the item under test is assumed to rest on (or to be at the same level as) the ground plane of the antenna used to produce the field. The

vertically polarized electric field produced by a vertical monopole is the only field discussed.

When the radiation susceptibility test is performed it is assumed that on the item under test the field at the top and center (Point D in Figure 3) and the field at the bottom corners (Points B and C of Figure 3) is each within 6 db of the field at the bottom center (Point A in Figure 3). It is further assumed that either the field at the top center (for an item of height Z) or the field at the bottom corners (for an item of width 2X) is exactly 6 db below the field at the bottom center. (Using the data supplied here the 6 db down points can, if desired, be made to fall at points E and F of Figure 3.)

The electric field of concern has not been defined as a near field or as a far field. All of the characteristics are asymptotic to two conditions. One condition is when the distance to the antenna is small relative to the height of the antenna. The second condition is when the distance to the antenna is large compared to the height of the antenna. References to near and far field involving distances relative to a wavelength are dropped in a. of Theory. All dimensions used are assumed to be small compared to a wavelength; however, first order corrections involving  $\beta^2$  can be made using an equation found in a. of Theory.

The experimental techniques require refinement. It is not known that the refinements suggested here will be adequate, because they have not been tried; however, the explanation of the faults of the techniques already used have been verified.

The entire analysis can be applied when measuring radiation from an item under test. The data supplied here can also be used to modify limits to fit a change of antenna or test distance. Moving into a screened room can require considerable work by the person preparing the test plan.

This paper does not intend to specify antennas, test distances, and other test conditions. It is meant to relate these factors so that conditions may be optimized for any purpose.

As stated in the title, the field of concern is a high impedance field since the ratio in ohms of the electric field to the magnetic field is much higher than the free space impedance. A field intensity meter using a loop for an antenna will not properly indicate the intensity of this electric field.

Equations which approximate the curves and are usually stated to be accurate within some percentage are derived from the asymptotes of the curves but otherwise are fitted on a "cut-and-try" basis.

As the theory is developed, a transition is made from cylindrical coordinates which fit the monopole to rectangular coordinates which fit most items to which the field is applied. The dimension Y is measured from the base of the monopole to point A on the item as shown in Figure 9.

Figure 9 replaces a plot of X vs Y for specific monopoles.

In Figure 5 when dimensions are the order of  $\lambda$ , the current standing wave is better represented by

$$I_0 [\sin \beta (9' + l)] / \sin \beta 9' \text{ on the left and}$$

$$I_0 [\sin \beta (70.4' - l)] / \sin \beta 70.4' \text{ on the right}$$

where  $+l$  is measured to the right and  $-l$  to the left of the terminals where  $V_0$  is applied.

#### ACKNOWLEDGEMENTS

This work was performed during 1963 at the Interference Control Section, USAELRDL. The experimental work presented in this paper was performed with the assistance of Walter Stepien and John Forston. The experimental data was reduced primarily by Walter Stepien.

#### REFERENCE

E. C. Jordan, "Electromagnetic Waves and Radiating Systems" Prentice-Hall, Inc: 1950; Chapters 10, 11, 13.

# APPENDIX 1

$E_z$  for  $(\rho/H) \rightarrow \infty$ :

From 1a, 1b, and 1c

$$r_1 = \sqrt{r_0^2 + H^2 - 2Hz}$$

$$r_2 = \sqrt{r_0^2 + H^2 + 2Hz}$$

By expansion into series,

$$\begin{aligned} \left[ 1/r_1 + 1/r_2 - 2/r_0 \right] &= (1/r_0) \left[ 1 - (1/2)(H^2 - 2Hz)/r_0^2 + \right. \\ &\quad \left. (3/8)(H^2 - 2Hz)^2/r_0^4 + \dots \right. \\ &\quad \left. + 1 - (1/2)(H^2 + 2Hz)/r_0^2 + \right. \\ &\quad \left. (3/8)(H^2 + 2Hz)^2/r_0^4 + \dots - 2 \right] \\ &\simeq (1/r_0) \left[ -H^2/r_0^2 + (3/4)(H^4 + 4H^2z^2)/r_0^4 \right] \\ &\simeq (-H^2/r_0^3) \left[ 1 - 3z^2/r_0^2 - \underbrace{3H^2/4r_0^2}_{\text{neglect, since } (r_0/H) \rightarrow \infty} \right] \end{aligned}$$

# APPENDIX 2

$z/\rho$  for  $(\rho/H) \rightarrow \infty$ :

From 1c:  $r_0 = \sqrt{\rho^2 + z^2} = \rho \sqrt{1 + (z/\rho)^2}$

From 2a:  $(1/r_0^3) [1 - 3z^2/r_0^2] = (1/r_0^3) [1 - 3z^2/(\rho^2 + z^2)] =$   
 $(1/r_0^3) [-2 + 3\rho^2/(\rho^2 + z^2)] = (1/\rho^3) \left[ -2/[1 + (z/\rho)^2] + 3/[1 + (z/\rho)^2]^{5/2} \right]$   
 $= 1/2\rho^3$  at  $z$ .

Then  $-2/[1 + (z/\rho)^2] + 3/[1 + (z/\rho)^2]^{5/2} = 1/2$

First approximation:  $1/2 \simeq -2[1 - (3/2)(z/\rho)^2] + 3[1 - (5/2)(z/\rho)^2]$

$$z/\rho \simeq 1/3$$

Second approximation: let  $z/\rho = 1/3 + \Delta$

$$1 + (z/\rho)^2 \simeq 10/9 + 2\Delta/3 = 10/9 [1 + 3\Delta/5]$$

$$1/2 \simeq 2(.9)^{3/2} [1 - (3/2)(3/5)\Delta] + 3(.9)^{5/2} [1 - (5/2)(3/5)\Delta]$$

Yields  $\Delta = .054$  and  $z/\rho = .387$ ; however,  $z/\rho = .385$  is closer approx.



### APPENDIX 3

Determination of  $X/Y$  at  $(Y/H) \rightarrow \infty$  and  $z=0$ :

$$\text{From Equation 2a, } (E_z \text{ at } x=0)/(E_z \text{ at } x=X) = 2 = (1/Y^3)/[1/(X^2+Y^2)^{3/2}] = [1+(X/Y)^2]^{3/2} = 2. \quad \text{Then } (X/Y) = \sqrt{4^{1/3}-1} = .766$$

Determination of  $X/Y$  at  $(Y/H) \rightarrow 0$  and  $z=0$ :

$$\text{From Equation 2b, } (E_z \text{ at } x=0)/(E_z \text{ at } x=X) = 2 = (1/Y)/[1/(X^2+Y^2)] = \sqrt{1+(X/Y)^2} = 2. \quad \text{Then } (X/Y) = \sqrt{3}.$$

### APPENDIX 4

#### MUTUAL AND SELF IMPEDANCES

The first antenna is that shown in Figure 1. The mutual impedances are formulated for

Case 1: Between the first antenna and its image created by a flat vertical metal wall or between the first antenna and a second antenna equivalent to the image.

Case 2: Between the first antenna and its image created by a flat metal ceiling or a second antenna equivalent to the image.

The techniques used are those of Chapter 11 of the reference. For  $E_z$ , Equation 2 (modified) developed in this paper is used.

Case 1 The terminal open circuit voltage  $V_{oc}$  induced in the image by the terminal current  $I_0$  in the first antenna (see Fig. 6) is

$$V_{oc} = - \int_0^H (E_z / \sin \beta H) \sin \beta (H-z) dz \\ = (j\beta I_0 / 4\pi\epsilon\omega \sin^2 \beta H) \int_0^H (1/r_1 + 1/r_2 - 2/r_0) \sin \beta (H-z) dz.$$

For  $\beta H$  small

$$V_{oc} = (jI_0 / 4\pi\epsilon\omega) \int_0^1 (1/r_1 + 1/r_2 - 2/r_0) (1-z/H) d(z/H).$$

The mutual capacity  $C_m = I_0 / j\omega V_{oc}$ , then

$$1/C_m = -(1/4\pi\epsilon) \int_0^1 (1/r_1 + 1/r_2 - 2/r_0) (1-z/H) d(z/H).$$

Using

$$r_1 = [1 + (H/Y)^2 (1 - z/H)^2]^{1/2} \\ r_2 = [1 + (H/Y)^2 (1 + z/H)^2]^{1/2} \\ r_0 = [1 + (H/Y)^2 (z/H)^2]^{1/2},$$

integrals of two forms can be obtained:

$$\text{Form A} \quad \int \frac{p}{\sqrt{1+(H/Y)^2 p^2}} dp = (Y/H)^2 \sqrt{1+(H/Y)^2 p^2}$$

$$\text{Form B} \quad \int \frac{1}{\sqrt{1+(H/Y)^2 p^2}} dp = (Y/H) \ln \left[ (H/Y)p + \sqrt{1+(H/Y)^2 p^2} \right]$$

After integration

$$(1/C_m) = -(1/4\pi\epsilon) \left[ 2 \ln \left[ 2(H/Y) + \sqrt{1+(2H/Y)^2} \right] - 2 \ln \left[ (H/Y) + \sqrt{1+(H/Y)^2} \right] \right]^2 + (Y/H) \left[ 4 \sqrt{1+(H/Y)^2} - 3 - \sqrt{1+(2H/Y)^2} \right]$$

For the special case of  $(Y/H) \rightarrow 0$  and  $Y=a$ =radius of a cylindrical antenna

$$(1/C_m) = (1/C_{ant}) = -(1/4\pi\epsilon H) \left[ -2 \ln(H/a) + 2 \right].$$

Case 2 The terminal open circuit voltage induced in the image by the terminal current  $I_0$  in the antenna (see Fig. 7) is

$$V_{oc} = - \int_0^H (E_z / \sin \beta H) \sin \beta (H - z_2) dz_2 - \int_0^H (E_z / \sin \beta H) \sin \beta (H + z_2) dz_2.$$

Using  $C_m = 2I_0 / j\omega V_{oc}$  for the monopole half of the image and making the  $\beta H$  approximations of Case 1,

$$(1/C_m) = -(1/8\pi\epsilon H^2) \left[ \int_0^H (1/r_1 + 1/r_2 - 2/r_0)(1 - z_2) dz_2 - \int_0^H (1/r_1 + 1/r_2 - 2/r_0)(1 + z_2) dz_2 \right].$$

$$\text{Using} \quad r_1 = z_2 + S - H$$

$$r_2 = z_2 + S + H$$

$$r_0 = z_2 + S$$

and simplification of the form  $z_2/(b - z) = 1 - b/(b + z_2)$

yields integrals of the form  $\int [1/(b+p)] dp = \ln(p+b)$ .

After integration

$$(1/C_m) = -(1/8\pi\epsilon H) \left[ 6(S/H) \ln(S/H) - 4[(S/H)-1] \ln[(S/H)-1] + [(S/H)+2] \ln[(S/H)+2] - 4[(S/H)+1] \ln[(S/H)+1] - [(S/H)-2] \ln[(S/H)-2] \right].$$

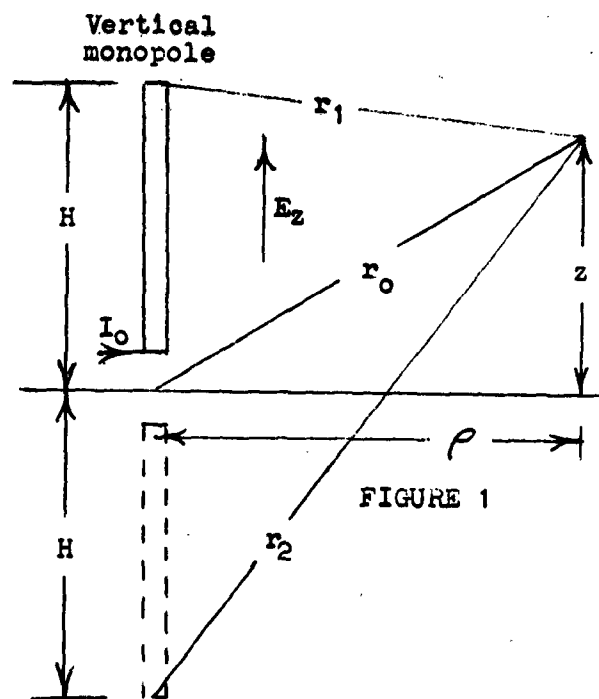


FIGURE 1

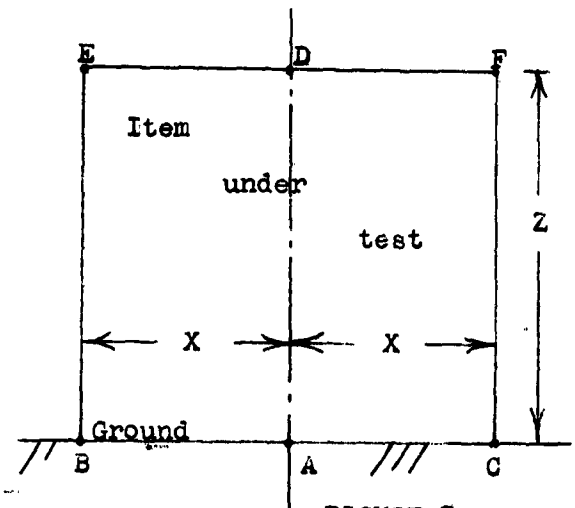


FIGURE 3

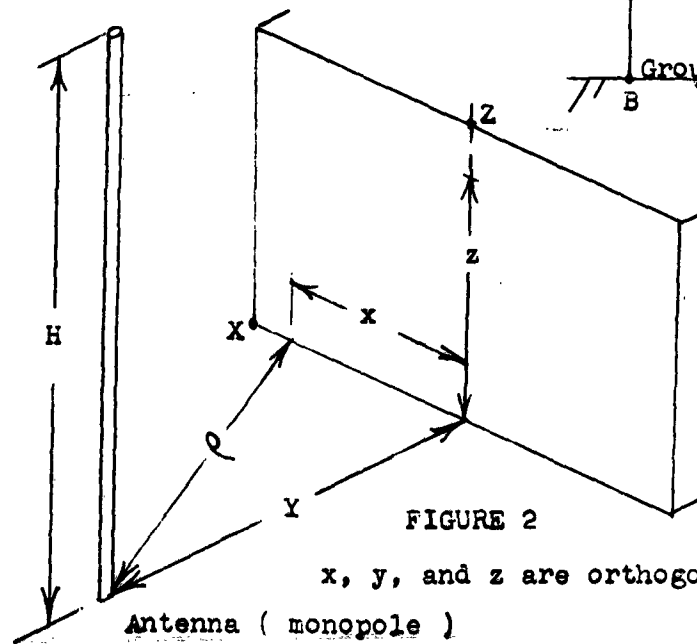
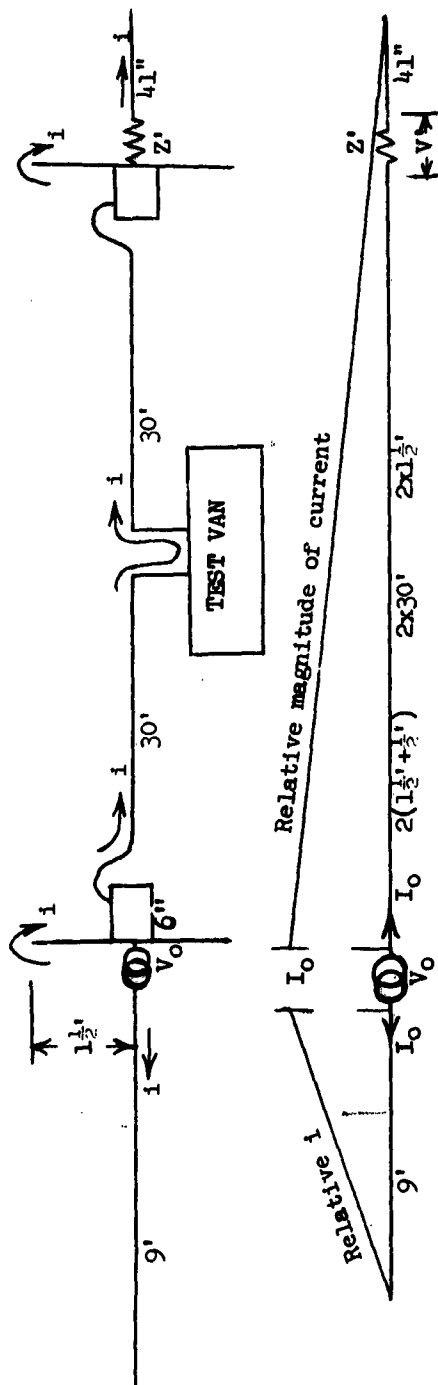


FIGURE 2

$x$ ,  $y$ , and  $z$  are orthogonal



$$V' = 41'' Z_0 I_0 / (41'' + 67')$$

FIGURE 5

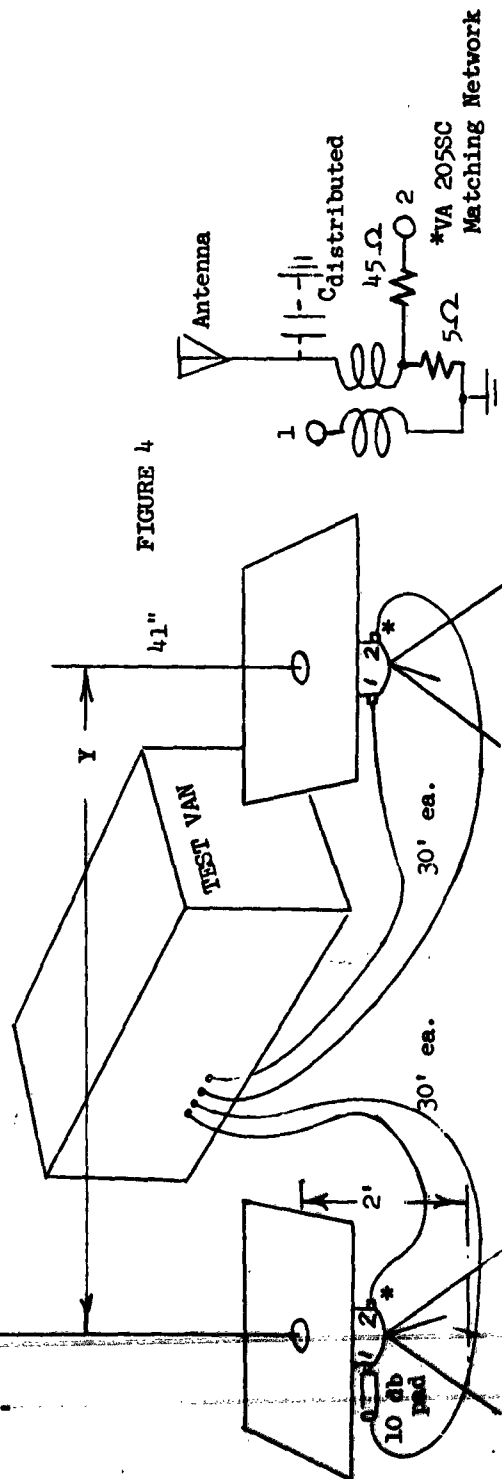


FIGURE 4

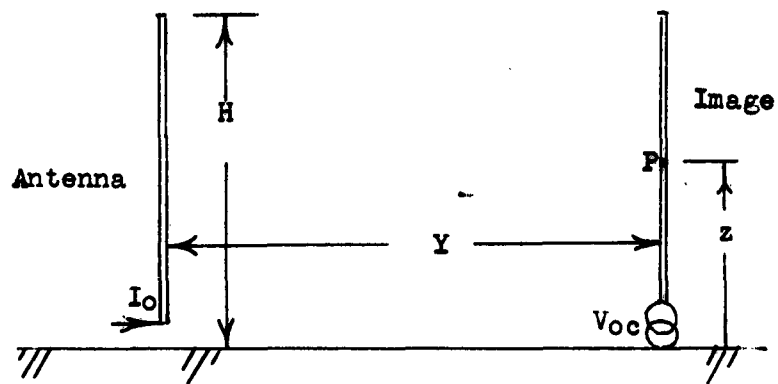


FIGURE 6

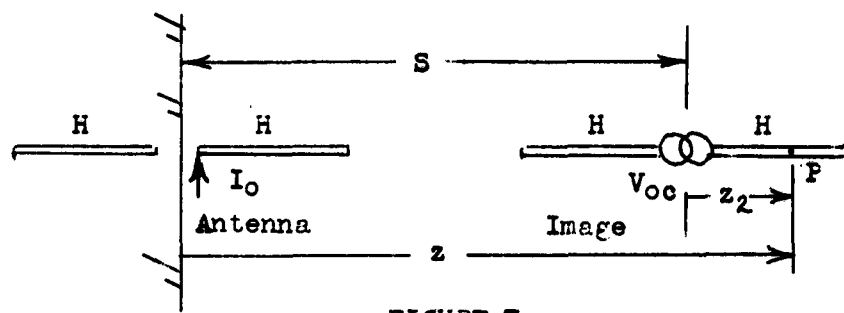


FIGURE 7

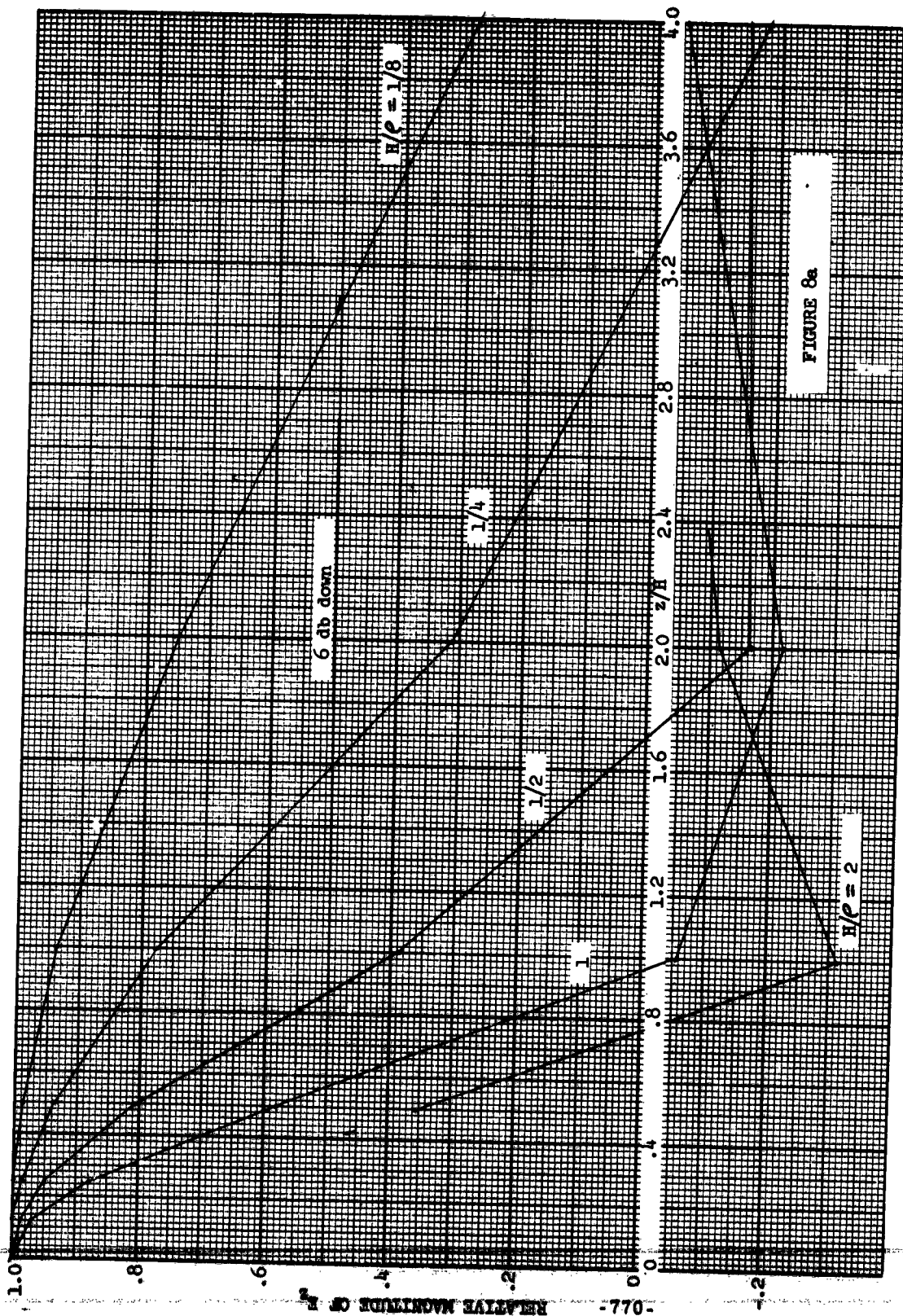


FIGURE 8a

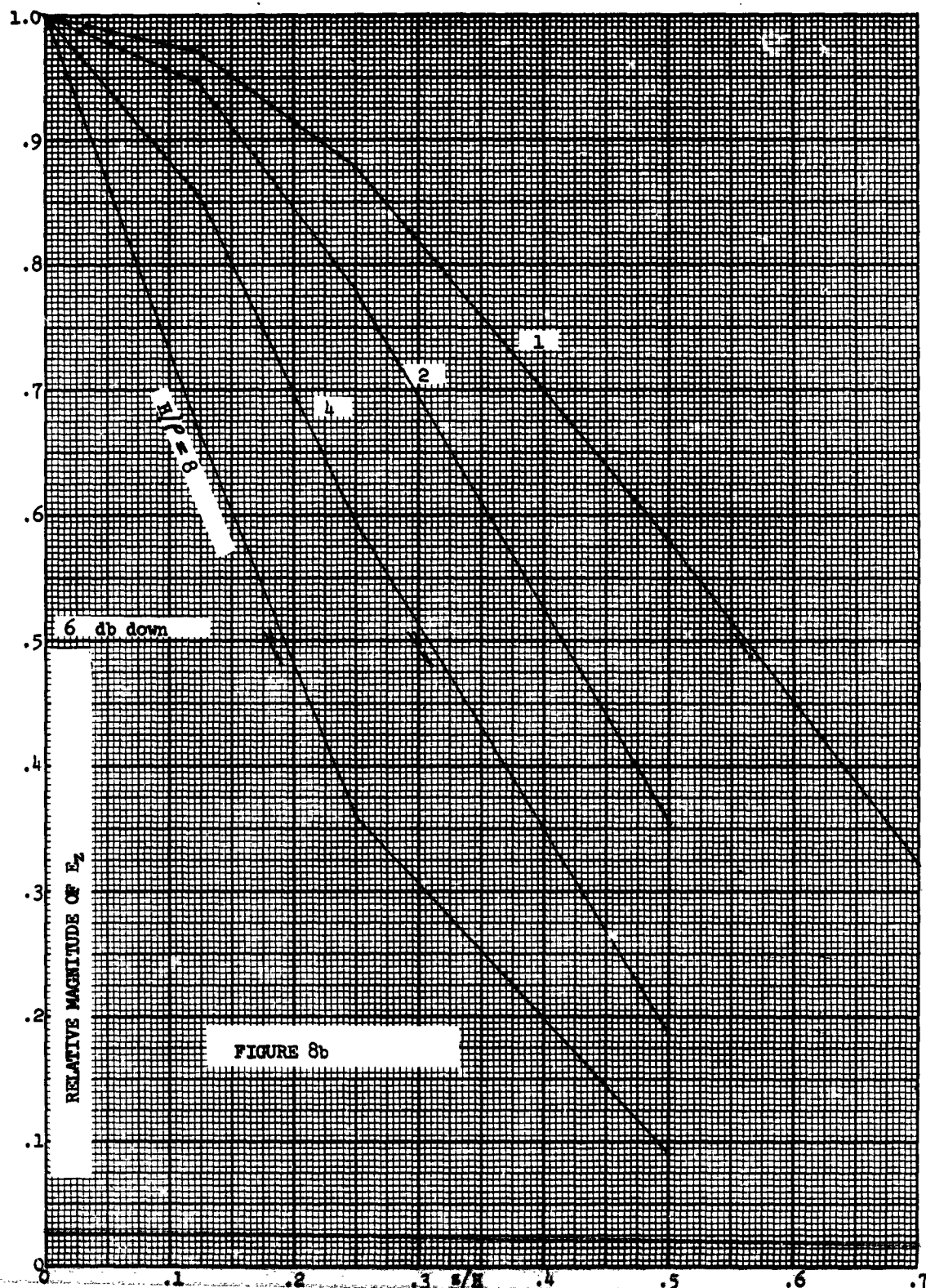
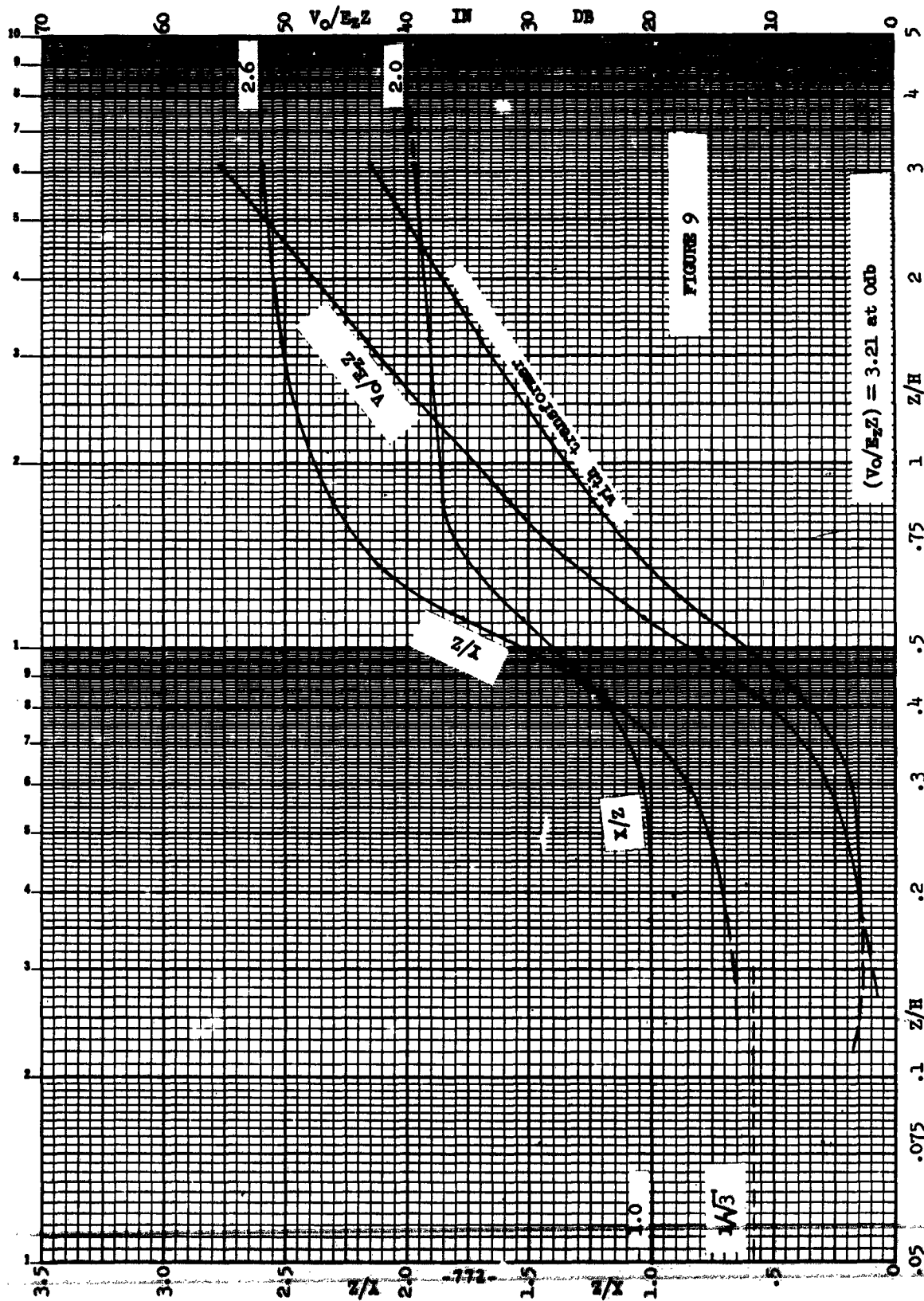


FIGURE 8b





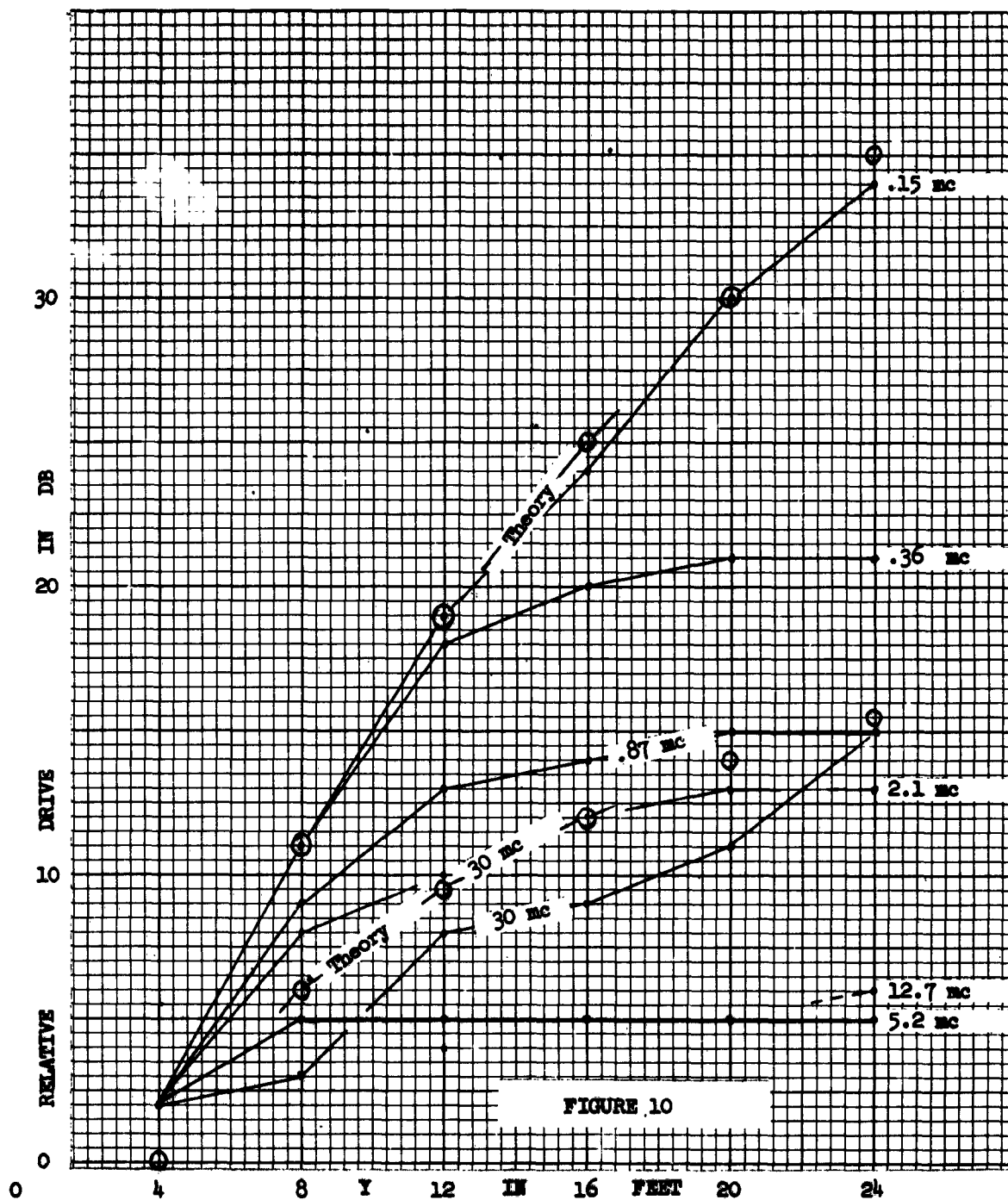


FIGURE 10

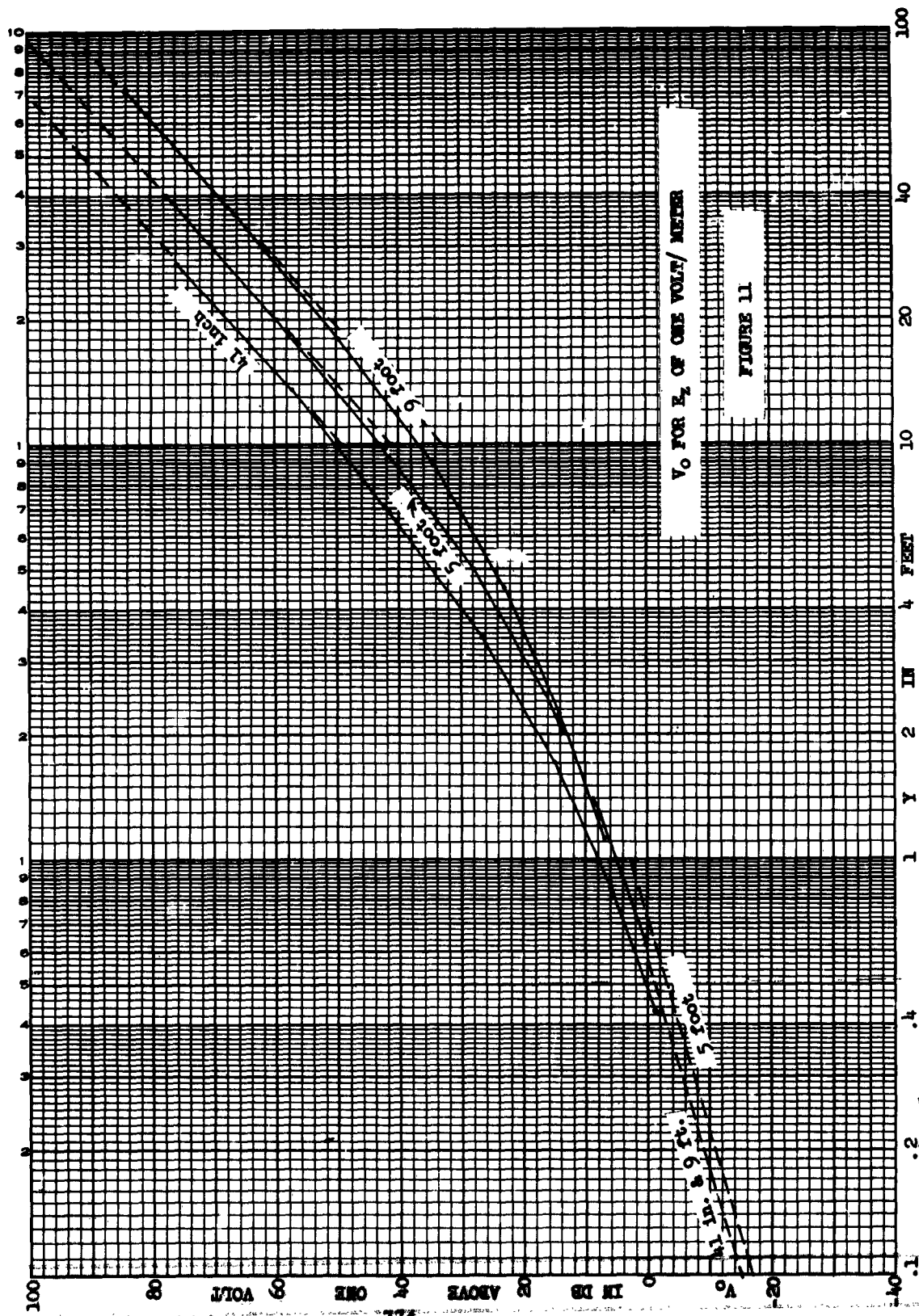


FIGURE 11

$V_0$  FOR  $E_2$  OF ONE VOLT/ METER

RADIO NOISE CONSIDERATIONS FOR EXTRA HIGH VOLTAGE TRANSMISSION,  
345 TO 1000 KILOVOLTS

E. R. Taylor and W. E. Pakala  
Westinghouse Electric Corporation  
Pittsburgh, Pa.

**Abstract.** - This paper discusses several aspects of radio noise from extra high voltage (EHV) transmission lines. Specifically it discusses radio noise generation and the effects of weather, the principal type of radio noise meter detector used for measurements, the relations of the line radio noise measurements to the AM broadcast station signal levels, the methods of making measurements in the field and the effect of various transmission line parameters on the radio noise field strength in the vicinity of the line. The possible sources of radio noise generation will be discussed and the need for measurements on existing lines and short test lines in order to make predictions for new and higher voltage lines.

I. INTRODUCTION

The radio noise level of a transmission line depends on many factors such as weather and conductor surface conditions, and the relative effect of some of these factors is not accurately known so that the composite effect must be considered, more or less, on a statistical basis. Even the measurement, definition, and assessment of radio noise are complex and the complexity, expense and planning required in the field of power transmission is not generally appreciated. In fact, there are very few simple solutions in the field of radio noise, and the problems of electro-magnetic compatibility are becoming more numerous, extensive, and difficult. Two reasons for this are the expanding use of the frequency spectrum, and the electro-magnetic compatibility environment which is expanding into the universe.

With respect to EHV lines it is necessary to consider radio noise generation due to conductor corona as well as generation by the line components. The frequency spectrum of EHV line radio noise is, under normal conditions, such that consideration of interference is important mainly in the AM broadcast frequency range. Interference to the higher frequencies, such as TV or FM is usually caused by loose hardware or improper line components. Because of the variation in strength and number of broadcast signals along a long line and because of possible differences in population density for lines, the same radio noise design limit is not justified for all lines. It is necessary to obtain the most economical line design consistent with the actual requirements along the line.

The line design for tolerable radio noise level is by necessity, because of the present limitations in knowledge of the corona pulse, based on comparisons and experience with existing EHV lines for which the radio noise level and the significant parameters are known. This comparative method is necessary because the radio noise generation by conductor corona and other means, cannot be calculated by means of theoretical considerations. In order to obtain a better grip on this problem a great deal of experimental work and analysis has been done, and is being done, in the radio noise field by the electric utilities and electrical manufacturers on EHV lines and short test lines in U.S.A., Canada, and Europe. This work was essentially started about sixteen years ago by engineers of the Westinghouse Electric Corporation at the 500 Kv Tidd Project.<sup>1</sup> This project was originated to obtain data for proposed EHV transmission lines. About the same time, measurement and analysis was also started in Europe,

especially in Germany, France, and Sweden, and several 400 Kv lines were subsequently constructed. Most of this and later work is published in the technical literature of the power generation, distribution, and transmission fields. Regardless of this extensive work, it is not too well known in the electronic and communications fields, and this is the basis for having this paper at the Ninth Tri-Service Conference on Electromagnetic Compatibility.

## II. ELECTRICAL CHARACTERISTICS OF THE CORONA DISCHARGE

The generation of radio noise by conductor corona is by means of the electrical discharge, usually called corona, occurring at or near the conductor surface. Fig. 3 shows how intense conductor corona can be at excessive gradients. Corona is defined<sup>2</sup> as "a luminous discharge due to ionization of the air surrounding a conductor around which exists a voltage gradient exceeding a certain critical value." Many aspects of corona discharges especially in non-uniform fields such as exists on lines are unknown, undefined, and a quantitative analysis, at least for the conductor diameters used for EHV lines, is not possible with the present state of knowledge. For the purposes of this paper a short resume of the known processes for the case of a conductor will be given.

The basic physical process is that of electron multiplication or avalanche formation. The electric gradient in the vicinity of the line conductor is the highest gradient, and if this gradient or electric stress is sufficiently high, any electrons in the air around the conductor will ionize the gas molecules, and electrons produced by this ionization will produce an avalanche. If an additional electron is formed in this gradient by some process from the original electron avalanche, a new avalanche is formed by this secondary process and a self-maintaining discharge is developed. Fig. 1 shows how the efficiency of this process increases with the electric gradient. In the case of the transmission line conductor, it is believed that the important secondary process is the ejection of electrons from gas molecules by high energy ultra-violet light (photoionization) generated by the original avalanche. It has been found by several investigators that the radio noise generated when the conductor is at positive potential is significantly greater, at the gradients generally used for line conductors, than it is with the conductor at negative potential. In the case of a positive line conductor, the cathode is so far away that cathode emission is of no consequence, and so stated before, the only secondary process existing in this case is photoionization of the gas. The positive corona which causes radio interference is of the streamer type; that is, a compact and bright filament starting from the conductor and extending out and ending in a tree-like discharge array. This type of discharge can be heard by ear directly and readily photographed at night. Sharp current pulses occur and radio noise is produced. Some aspects of this streamer corona are known. These streamers propagate at very high velocities  $2 \times 10^7$  to over  $10^8$  cm. per sec.<sup>3</sup> Also because of the electric field intensification by the streamer itself, it propagates into fields which are below the critical breakdown as based on the non-uniform field around the conductor with no ionization. Near the conductor surface, however, an opposite effect occurs in that the field is reduced which effect tends to inhibit the streamer. The current pulse formed is of the form  $i = te^{-at}$ . The pulse form and the frequency spectrum of the positive corona pulse for a 5 cm. advance of streamer at a velocity of  $5 \times 10^7$  cm./sec., (rise time of  $10^{-7}$  seconds) is shown in Fig. 2. This spectrum is similar to the spectrum measured (see Fig. 2) near a transmission line with a radio noise meter having a quasi-peak detector. When the conductor is at sufficiently high negative potential ionization occurs. In this case, the cathode emission process prevails, and since this process is more efficient than the gas photoemission process with conductor positive, it is expected that negative corona starts at lower conductor gradients than does positive corona. The current pulses have longer rise times and their peak values will not reach the magnitude of

the positive pulses and with the quasi-peak detector the negative corona pulses will give considerably lower readings as has been found by measurement using an oscilloscope in the radio noise meter peak detector.

When streamer corona forms at a "point" on the conductor two pulse fields will exist. Near the streamer a localized or direct field is formed, and along the line the indirect field is developed due to the pulses traveling down the line. For design of EHV lines only the indirect field is considered and the most significant measurements are made at some distance from the streamer location.

### III. DEFINITIONS

We have found that the radio noise field, the radio noise voltage, and the signal to noise ratio are best expressed in decibels (db). The db scale gives an almost linear relation of radio noise to line voltage and conductor gradient over the range of voltages and gradients presently used on lines. This greatly simplifies any analytical expressions used relating radio noise to gradient. The radio noise field strength is then expressed in db above 1 microvolt per meter and the radio noise voltage in db above 1 microvolt.

### IV. INSTRUMENTATION

Instrumentation for radio noise measurements has been improved considerably since line radio noise became a line design factor. The older instruments have several drawbacks; such as bandwidth and calibration variation with the frequency. The response of several meters has been compared on a 345 Kv line by the IEEE Sub-committee on Radio Noise, a sub-committee of the Transmission and Distribution Committee. By means of accurate calibration using sine wave signal generators and accurately calibrated voltmeters (+ 5%) with separate attenuators or with micropot voltmeters (+ 1%), several meters having essentially the same bandwidth will read within + 2.35 db on the quasi-peak detector. This result was obtained with six meters compared<sup>4</sup> on line noise with six operators. Considering the variation in the meter pointer with line noise, this result is quite good. In one test a meter was read 12 times by one operator and the results varied by 1.8 db (average reading 41 db). In another test, one operator read 12 meters in succession. The total variation in readings was 2.5 db (average reading was 42 db).

For most line comparisons and line design the results with a quasi-peak detector have been used, and the instruments used and recommended essentially meet ASA Standard C63.2.<sup>5</sup> Four types of detectors have been proposed and used for obtaining quantitative values for the assessment of radio interference and, in some cases, for other purposes. These four types of detectors are average, rms, quasi-peak and peak. Historically, the quasi-peak detector was one of the first used and it was originally intended to measure interference effect or nuisance value of various types of interference on amplitude modulated broadcast signals.<sup>6</sup> The peak detector is valuable in obtaining by visual means the peak value of corona pulses on any phase conductor. This is possible since the corona pulses occur at different times on a three phase line.<sup>4</sup> The rms detector has the advantage that random noise average energy can be determined and this method will result in "better correlating between theoretical, laboratory and field data."<sup>7</sup>

The radio noise meter has been used to measure field strengths near lines with both the vertical antenna and the loop antenna. It has been used as a voltmeter for conducted measurements on EHV lines. It has also been used to measure the radio noise current due to corona in the phase conductor by means of a special clamp-on current transformer. This is done by means of

a lift truck with an insulated boom. (See Figure 4) The meter, current transformer, and operator are connected to the energized conductor and all readings are made from the insulated bucket. This method has been used on a line energized at 775,000 volts three phase. This method is of considerable help in determining the relative RI generation of the phase conductors and in calculating the resultant field strengths.

Radio noise may be generated by the formation of corona at burrs and scratches on the conductor surface. Since radio noise may be caused by particles, such as raindrops, snow, aerosols, dirt, and insects, that may pass within the near field of the conductor or be on the surface of the conductor, radio noise generation becomes variable and useful determination of the radio noise level must be based on statistical methods. In order, therefore, to evaluate the performance of a given line conductor at a given voltage (gradient) within a given environment, long time statistical data are required. Present research on transmission-line radio noise, therefore, has incorporated small scale data logging facilities. This method of data accumulation has been a new instrumentation to the transmission engineer since the data storage may be of such form that modern high speed, high capacity digital computers can be used to evaluate the data. Simultaneous measurements of parameters believed to affect the radio noise levels can be used for establishing correlation factors by such data accumulation methods.

#### V. DISCUSSION OF FACTORS IN THE PREDICTION OF EHV LINE RADIO NOISE

Transmission Line Gradient Calculations. - Conductor gradient calculations are necessary since the conductor gradient so greatly affects the radio noise generation. In general, and if conductor corona exists and predominates, an increase in the conductor gradient of about 10 per cent will double the radio noise level of a line. Also it is interesting to note that EHV line conductor gradients as obtained from calculations for smooth conductors are considerably below the critical gradient for this smooth conductor and yet corona exists along the conductor in service.

The tedious calculation of multi-conductor systems such as on the EHV lines presently used is now by-passed by the use of digital-computer calculations of the surface voltage gradients. Simple calculations of the surface voltage gradient are based on electrostatic principles, assuming the ground plain to be a perfect conductor. Some recent work has been done in evaluating the effect of this assumption.<sup>8</sup>

Propagation of Radio Noise. - In order to better predict line noise, it is helpful to know the manner or modes of propagation of the corona pulses so that the resulting radio noise field strengths and lateral patterns in the vicinity of the line can be calculated for existing lines and comparisons made with new lines. Digital computers are used to calculate the propagation characteristics and the lateral radio noise field strength patterns for the EHV line conductor configuration under consideration. The calculation of the propagation characteristics of EHV lines has been attacked by several authors in recent publications.<sup>9,10,11,12,13,14,15</sup> The digital computer provides a tool to handle the matrix manipulations to perform the calculations. Some such analyses determine the natural modes associated with the matrix representing the transmission line as a multi-coupled circuit, with some modifications made to the matrix based on such factors as those of Carson's ground effect. Physical significance is given to the Eigen values and Eigen roots of the associated matrix by the results of tests on short transmission test lines. For example, lateral field profiles on short lines or with single sources of radio noise generation are calculable using the modal approach to the multi-conductor circuit. Other authors have approached the same problem using a

different breakdown of modes or parts associated with the propagation of the corona energy along the wire. For example, the propagation may be broken down into line components and ground components with the line components being of different magnitudes while the ground components for each wire are of an equal magnitude.<sup>12</sup> Each of these modes or parts whether considered as Eigen vectors or line and ground components are characterized by different propagation velocities and attenuation constants. In the case of long lines, the evidence appears to indicate that for conductor in corona uniformly along the line, the ground mode or component is the most important one although it has the highest attenuation. However, further research is desirable to verify this result. As an interesting side light to these calculations, the method of modal components has recently been applied to carrier applications.<sup>15</sup>

Experimental Lines or Test Lines have been built and tests made to help find the effect of various factors and to help in the overall analysis of the problem. It should be realized that test lines are of course built to obtain other engineering data than just that required for line design with respect to radio noise.

Short test lines have the advantage of exhibiting the various modal components more readily than do long lines. However, test lines are all separated from other parts of a test facility by some "trap" means, such as coils and other means specially tuned to exhibit high impedance in the broadcast band. These means may affect the response exhibited by the test line conductors over the frequency range of interest. For example, an open-ended test line trapped at the station end may exhibit a shift in electrical centers for the frequency range and a peculiar modal breakdown. Obviously, the best test line would be the actual transmission line, but economics prohibit such experimentation and many short test lines have therefore been built to evaluate the performance of a long line with similar configuration of conductors. Short test lines are provided with variable voltage sources so that measurements may be made at different voltage levels. This is not the case for an operating transmission line since the voltage is more narrowly fixed. The prediction of long line radio noise from measurements on short test lines is quite complicated due to the frequency characteristics of the short line. However, a "first approximation," based on theoretical work such as that of Helstrom,<sup>16</sup> can be made by considering the geometric mean between the peaks and the minimum points in the standing wave pattern of the frequency spectrum for the short lines. However, in the case of a multi-conductor system, the frequency spectrum may not be as simple as that considered by Helstrom and others, and this is the area in which the complications in analysis occur. In order to circumvent this complicating factor associated with short test lines, some investigations have been made to terminate the test line in such a manner as to make it appear to be a long line for radio frequencies.<sup>17</sup> However, just because of the physical dimensions of the apparatus necessary to terminate EHV lines, the problem is quite difficult and has not been completely solved.

The AM Broadcast Station Field Strengths along the right-of-way of a transmission line are measured and considered in any thorough analyses. Because transmission lines are so long, the signal levels and station coverage varies along the line and over the country from place to place. Because of this, it does not seem realistic to specify the same radio noise limit for all EHV lines in service or for new lines. This means that the number of conductors per phase and their diameters and therefore the conductor gradients will not necessarily be the same for all lines. With respect to the signal to noise ratio, a value of 24 db (based on the quasi-peak detector as used in American meters and according to ASA C63.2<sup>18</sup>) has been used.

We believe that the design of EHV lines with respect to radio noise is as highly developed from an experimental and analytical standpoint as any system we know of where broadband noise is considered.

#### REFERENCES

1. Radio Influence Tests in Field and Laboratory - 500 Kv Test Project of AG&E Co., G. D. Lippert, W. E. Pakala, S. C. Bartlett, C. D. Fahrnkopf. AIEE Transactions, vol. 70, pt. I, 1951, pp. 251-269.
2. American Standard Definition of Electrical Terms. ASA C42-1941.
3. M. R. Amin, Journal of Applied Physics, vol. 25, pp. 210, 358, 627 (three articles).
4. Experimental Comparisons of Radio Influence Fields from Short and Long Transmission Lines, C. R. Bond, W. E. Pakala, R. E. Graham, J. E. O'Neil. AIEE Transactions Paper 62-1406.
5. American Standard Specifications for Radio Noise and Field Strength Meters, 0.015 to 30 Megacycles per Second. ASA-C63.2.
6. Evaluation of Radio Noise Meter Performance in Terms of Listening Experience, C. M. Burrill, Proc. of IRE, October, 1942.
7. Development of a Square Law Radio Noise Meter, F. J. Trebby, AIEE Transactions Paper 59-79.
8. Capacitive Correction Factors for Transmission Lines to Include Finite Conductivity and Dielectric Constant of the Earth, A. Arismunandar, IEEE Transactions Paper 63-1030.
9. The Calculation of the Radio Interference Level of Transmission Lines Caused by Corona Discharges, G. E. Adams, AIEE Transactions, pt. III, Power Apparatus and Systems, vol. 75, June 1956, pp. 417-19.
10. The Calculation of Attenuation Constants for Radio Noise Analysis of Overhead Lines, G. E. Adams, L. O. Barthold, AIEE Transactions Paper 60-848.
11. Propagation of Switching-Surge Wavefronts on EHV Transmission Line, A. J. McElroy, H. M. Smith, IEEE Transactions Paper 62-1101, Power Apparatus and Systems, February 1963, pp. 983-998.
12. Traveling Waves on Power Transmission Lines with Special Emphasis on Radio Noise, C. F. Wagner, IEEE Transactions Paper No. 63-1020.
13. Analysis of Radio Noise from High Voltage Lines Part I Meter Response to Corona Pulses, O. Nigol, IEEE Transactions Paper No. 63-1022.
14. Analysis of Radio Noise from High Voltage Lines Part II Propagation Theory, O. Nigol, IEEE Transactions Paper No. 63-1023.
15. Natural Modes of Power Line Carrier on Horizontal Three Phase Lines, M. C. Perz, IEEE Transactions Paper 63-936.
16. The Spectrum of Corona Near a Transmission Line, C. W. Helstrom, AIEE Transactions, pt. III, Power Apparatus and Systems, vol. 80, December 1961, pp. 831-37.



17. Decoupling of Transmission Lines to Radio-Influence Voltages, S. B. Griscom, D. F. Shankle, R. H. Schlomann, E. R. Taylor, Jr. AIEE Transactions, February 1961, pp. 1066-1073.

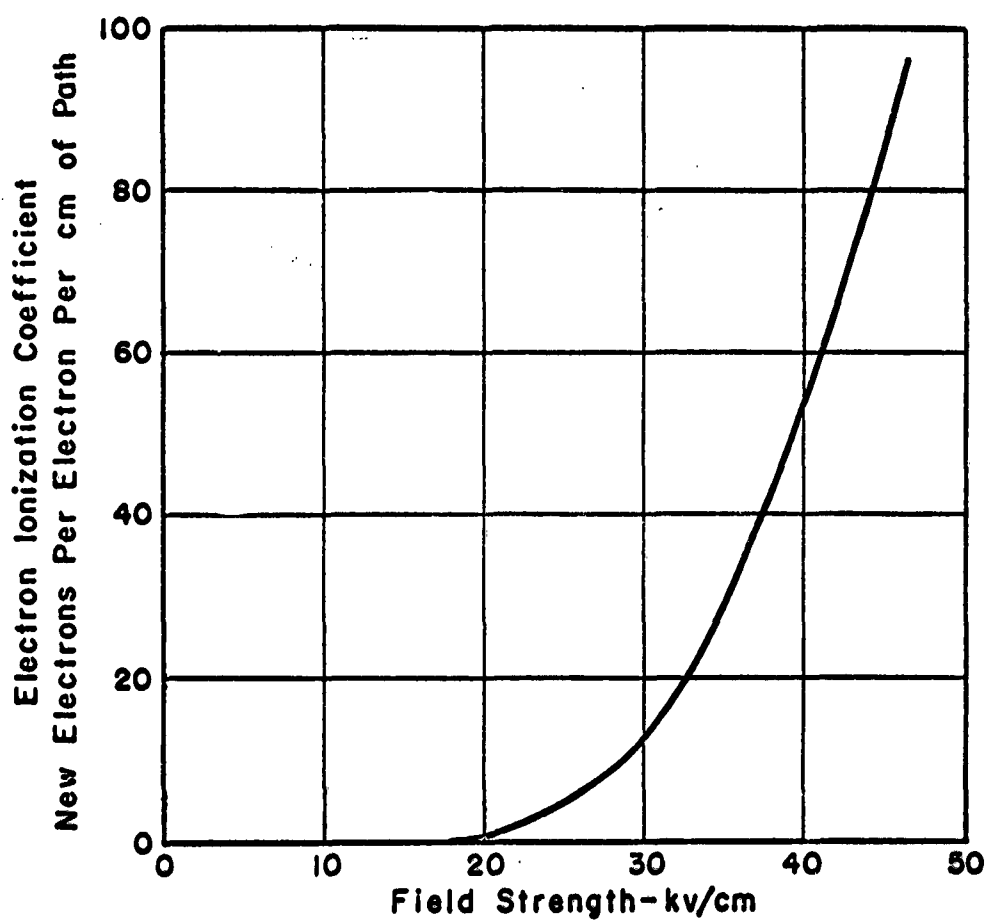


**Fig.1-Ionization by collision  
(Electrons in air at atmospheric pressure)**

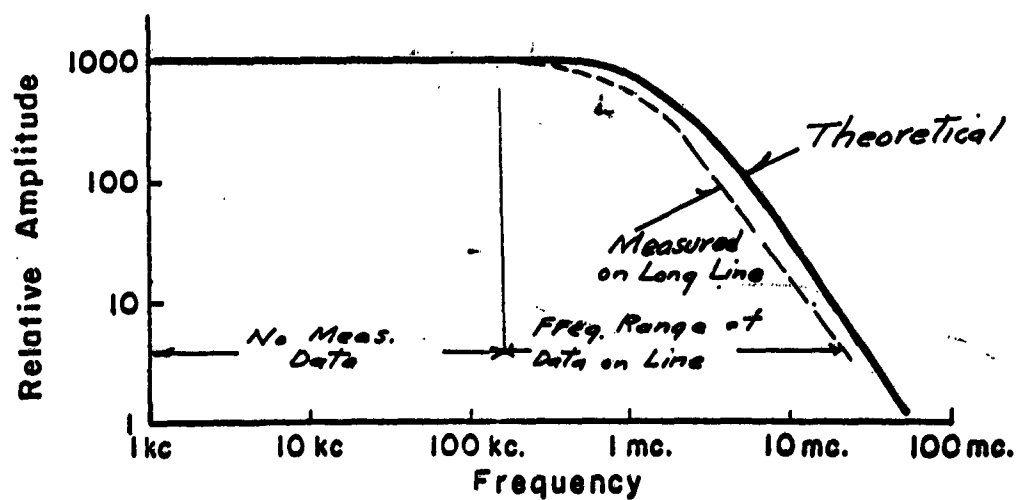
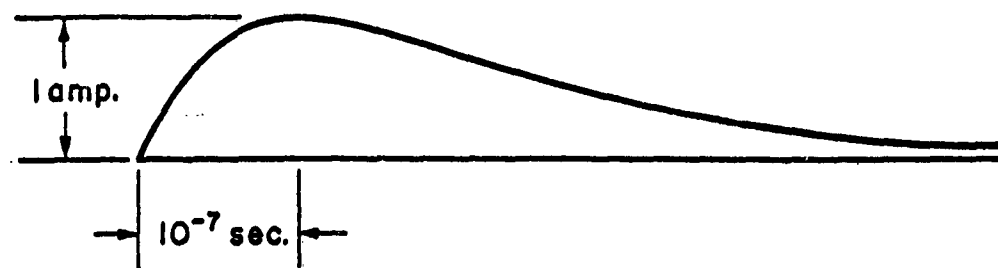


Fig.2- Positive corona pulse and frequency spectrum

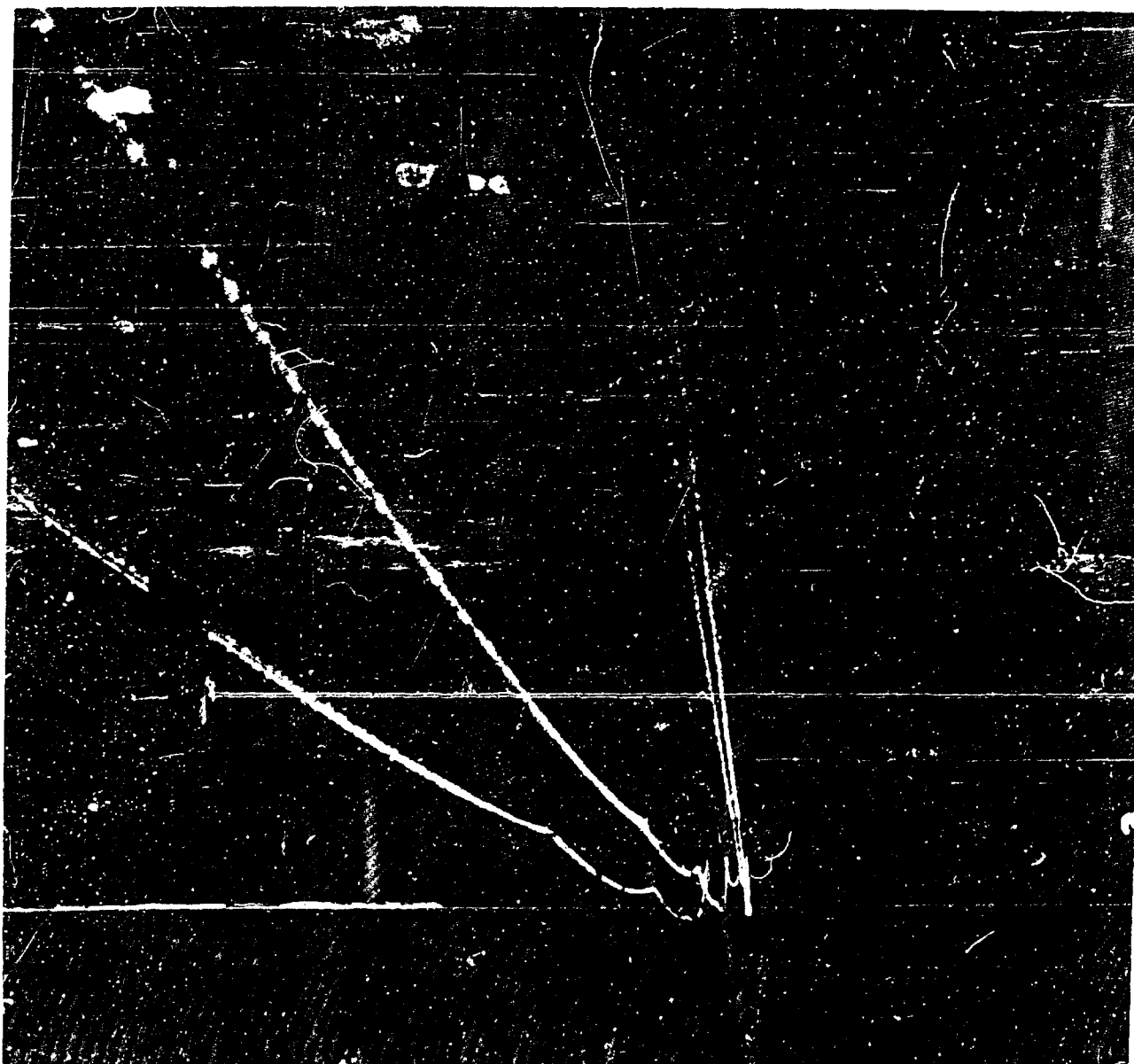


Fig. 3 Corona on high voltage conductors and the ground wires on a test line at 10,700 foot altitudes.



Fig. 4 Radio noise current measurements on an extra high voltage line conductor.

Best Available Copy